

Quantum Chemistry and Spectroscopy 4e

Thomas Engel





PHYSICAL CHEMISTRY

Quantum Chemistry and Spectroscopy

FOURTH EDITION

Thomas Engel

University of Washington

Chapter 15, "Computational Chemistry,"
was contributed by

Warren Hehre

CEO, Wavefunction, Inc.

Chapter 17, "Nuclear Magnetic Resonance Spectroscopy,"
was coauthored by

Alex Angerhofer

University of Florida



Pearson

Director, Courseware Portfolio Management: Jeanne Zalesky
Product Manager: Elizabeth Bell
Courseware Director, Content Development: Jennifer Hart
Courseware Analyst: Spencer Cotkin
Managing Producer, Science: Kristen Flathman
Content Producer, Science: Beth Sweeten
Rich Media Content Producer: Nicole Constantino
Production Management and Composition: Cenveo Publishing Services
Design Manager: Mark Ong
Interior/Cover Designer: Preston Thomas
Illustrators: Imagineering, Inc.
Manager, Rights & Permissions: Ben Ferrini
Photo Research Project Manager: Cenveo Publishing Services
Senior Procurement Specialist: Stacey Weinberger

Credits and acknowledgments borrowed from other sources and reproduced, with permission, in this textbook appear on the appropriate page within the text or on pages 521–522.

Copyright © 2019, 2013, 2010 Pearson Education, Inc. All Rights Reserved. Printed in the United States of America. This publication is protected by copyright, and permission should be obtained from the publisher prior to any prohibited reproduction, storage in a retrieval system, or transmission in any form or by any means, electronic, mechanical, photocopying, recording, or otherwise. For information regarding permissions, request forms and the appropriate contacts within the Pearson Education Global Rights & Permissions department, please visit www.pearsoned.com/permissions/.

Unless otherwise indicated herein, any third-party trademarks that may appear in this work are the property of their respective owners and any references to third-party trademarks, logos or other trade dress are for demonstrative or descriptive purposes only. Such references are not intended to imply any sponsorship, endorsement, authorization, or promotion of Pearson's products by the owners of such marks, or any relationship between the owner and Pearson Education, Inc. or its affiliates, authors, licensees or distributors.

Library of Congress Cataloging-in-Publication Data

Names: Engel, Thomas, 1942- author. | Hehre, Warren, author. | Angerhofer, Alex, 1957- author. | Engel, Thomas, 1942- Physical chemistry.
Title: Physical chemistry, quantum chemistry, and spectroscopy / Thomas Engel (University of Washington), Warren Hehre (CEO, Wavefunction, Inc.), Alex Angerhofer (University of Florida).
Description: Fourth edition. | New York : Pearson Education, Inc., [2019] | Chapter 15, Computational chemistry, was contributed by Warren Hehre, CEO, Wavefunction, Inc. Chapter 17, Nuclear magnetic resonance spectroscopy, was contributed by Alex Angerhofer, University of Florida. | Previous edition: Physical chemistry / Thomas Engel (Boston : Pearson, 2013). | Includes index.
Identifiers: LCCN 2017046193 | ISBN 9780134804590
Subjects: LCSH: Chemistry, Physical and theoretical--Textbooks. | Quantum chemistry--Textbooks. | Spectrum analysis--Textbooks.
Classification: LCC QD453.3 .E55 2019 | DDC 541/.28--dc23
LC record available at <https://lccn.loc.gov/2017046193>



To Walter and Juliane,
my first teachers,
and to Gloria,
Alex,
Gabrielle, and Amelie.

Brief Contents

QUANTUM CHEMISTRY AND SPECTROSCOPY

- 1** From Classical to Quantum Mechanics 19
 - 2** The Schrödinger Equation 45
 - 3** The Quantum-Mechanical Postulates 67
 - 4** Applying Quantum-Mechanical Principles to Simple Systems 77
 - 5** Applying the Particle in the Box Model to Real-World Topics 95
 - 6** Commuting and Noncommuting Operators and the Surprising Consequences of Entanglement 119
 - 7** A Quantum-Mechanical Model for the Vibration and Rotation of Molecules 143
 - 8** Vibrational and Rotational Spectroscopy of Diatomic Molecules 171
 - 9** The Hydrogen Atom 209
 - 10** Many-Electron Atoms 233
 - 11** Quantum States for Many-Electron Atoms and Atomic Spectroscopy 257
 - 12** The Chemical Bond in Diatomic Molecules 285
 - 13** Molecular Structure and Energy Levels for Polyatomic Molecules 315
 - 14** Electronic Spectroscopy 349
 - 15** Computational Chemistry 377
 - 16** Molecular Symmetry and an Introduction to Group Theory 439
 - 17** Nuclear Magnetic Resonance Spectroscopy 467
- APPENDIX A Point Group Character Tables** 513
- Credits** 521
- Index** 523

Detailed Contents

QUANTUM CHEMISTRY AND SPECTROSCOPY

Preface ix

Math Essential 1 Units, Significant Figures, and Solving End of Chapter Problems

Math Essential 2 Differentiation and Integration

Math Essential 3 Partial Derivatives

Math Essential 4 Infinite Series

1 From Classical to Quantum Mechanics 19

- 1.1 Why Study Quantum Mechanics? 19
- 1.2 Quantum Mechanics Arose out of the Interplay of Experiments and Theory 20
- 1.3 Blackbody Radiation 21
- 1.4 The Photoelectric Effect 22
- 1.5 Particles Exhibit Wave-Like Behavior 24
- 1.6 Diffraction by a Double Slit 26
- 1.7 Atomic Spectra and the Bohr Model of the Hydrogen Atom 29

Math Essential 5 Differential Equations

Math Essential 6 Complex Numbers and Functions

2 The Schrödinger Equation 45

- 2.1 What Determines If a System Needs to Be Described Using Quantum Mechanics? 45
- 2.2 Classical Waves and the Nondispersive Wave Equation 49
- 2.3 Quantum-Mechanical Waves and the Schrödinger Equation 54
- 2.4 Solving the Schrödinger Equation: Operators, Observables, Eigenfunctions, and Eigenvalues 55
- 2.5 The Eigenfunctions of a Quantum-Mechanical Operator Are Orthogonal 57
- 2.6 The Eigenfunctions of a Quantum-Mechanical Operator Form a Complete Set 59
- 2.7 Summarizing the New Concepts 61

3 The Quantum-Mechanical Postulates 67

- 3.1 The Physical Meaning Associated with the Wave Function is Probability 67

3.2 Every Observable Has a Corresponding Operator 69

3.3 The Result of an Individual Measurement 69

3.4 The Expectation Value 70

3.5 The Evolution in Time of a Quantum-Mechanical System 73

4 Applying Quantum-Mechanical Principles to Simple Systems 77

- 4.1 The Free Particle 77
- 4.2 The Case of the Particle in a One-Dimensional Box 79
- 4.3 Two- and Three-Dimensional Boxes 83
- 4.4 Using the Postulates to Understand the Particle in the Box and Vice Versa 84

5 Applying the Particle in the Box Model to Real-World Topics 95

- 5.1 The Particle in the Finite Depth Box 95
- 5.2 Differences in Overlap between Core and Valence Electrons 96
- 5.3 Pi Electrons in Conjugated Molecules Can Be Treated as Moving Freely in a Box 97
- 5.4 Understanding Conductors, Insulators, and Semiconductors Using the Particle in a Box Model 98
- 5.5 Traveling Waves and Potential Energy Barriers 100
- 5.6 Tunneling through a Barrier 103
- 5.7 The Scanning Tunneling Microscope and the Atomic Force Microscope 104
- 5.8 Tunneling in Chemical Reactions 109
- 5.9 Quantum Wells and Quantum Dots 110

6 Commuting and Noncommuting Operators and the Surprising Consequences of Entanglement 119

- 6.1 Commutation Relations 119
- 6.2 The Stern–Gerlach Experiment 121
- 6.3 The Heisenberg Uncertainty Principle 124

- 6.4 The Heisenberg Uncertainty Principle Expressed in Terms of Standard Deviations 128
- 6.5 A Thought Experiment Using a Particle in a Three-Dimensional Box 130
- 6.6 Entangled States, Teleportation, and Quantum Computers 132

Math Essential 7 Vectors

Math Essential 8 Polar and Spherical Coordinates

7 A Quantum-Mechanical Model for the Vibration and Rotation of Molecules 143

- 7.1 The Classical Harmonic Oscillator 143
- 7.2 Angular Motion and the Classical Rigid Rotor 147
- 7.3 The Quantum-Mechanical Harmonic Oscillator 149
- 7.4 Quantum-Mechanical Rotation in Two Dimensions 154
- 7.5 Quantum-Mechanical Rotation in Three Dimensions 157
- 7.6 Quantization of Angular Momentum 159
- 7.7 Spherical Harmonic Functions 161
- 7.8 Spatial Quantization 164

8 Vibrational and Rotational Spectroscopy of Diatomic Molecules 171

- 8.1 An Introduction to Spectroscopy 171
- 8.2 Absorption, Spontaneous Emission, and Stimulated Emission 174
- 8.3 An Introduction to Vibrational Spectroscopy 175
- 8.4 The Origin of Selection Rules 178
- 8.5 Infrared Absorption Spectroscopy 180
- 8.6 Rotational Spectroscopy 184
- 8.7 Fourier Transform Infrared Spectroscopy 190
- 8.8 Raman Spectroscopy 194
- 8.9 How Does the Transition Rate between States Depend on Frequency? 196

9 The Hydrogen Atom 209

- 9.1 Formulating the Schrödinger Equation 209
- 9.2 Solving the Schrödinger Equation for the Hydrogen Atom 210
- 9.3 Eigenvalues and Eigenfunctions for the Total Energy 211
- 9.4 Hydrogen Atom Orbitals 217

- 9.5 The Radial Probability Distribution Function 219
- 9.6 Validity of the Shell Model of an Atom 224

Math Essential 9 Working with Determinants

10 Many-Electron Atoms 233

- 10.1 Helium: The Smallest Many-Electron Atom 233
- 10.2 Introducing Electron Spin 235
- 10.3 Wave Functions Must Reflect the Indistinguishability of Electrons 236
- 10.4 Using the Variational Method to Solve the Schrödinger Equation 239
- 10.5 The Hartree–Fock Self-Consistent Field Model 240
- 10.6 Understanding Trends in the Periodic Table from Hartree–Fock Calculations 247

11 Quantum States for Many-Electron Atoms and Atomic Spectroscopy 257

- 11.1 Good Quantum Numbers, Terms, Levels, and States 257
- 11.2 The Energy of a Configuration Depends on Both Orbital and Spin Angular Momentum 259
- 11.3 Spin–Orbit Coupling Splits a Term into Levels 266
- 11.4 The Essentials of Atomic Spectroscopy 267
- 11.5 Analytical Techniques Based on Atomic Spectroscopy 269
- 11.6 The Doppler Effect 272
- 11.7 The Helium–Neon Laser 273
- 11.8 Auger Electron Spectroscopy and X-Ray Photoelectron Spectroscopy 277

12 The Chemical Bond in Diatomic Molecules 285

- 12.1 Generating Molecular Orbitals from Atomic Orbitals 285
- 12.2 The Simplest One-Electron Molecule: H₂⁺ 289
- 12.3 Energy Corresponding to the H₂⁺ Molecular Wave Functions ψ_g and ψ_u 291
- 12.4 A Closer Look at the H₂⁺ Molecular Wave Functions ψ_g and ψ_u 294
- 12.5 Homonuclear Diatomic Molecules 297
- 12.6 Electronic Structure of Many-Electron Molecules 299
- 12.7 Bond Order, Bond Energy, and Bond Length 302
- 12.8 Heteronuclear Diatomic Molecules 304
- 12.9 The Molecular Electrostatic Potential 307

13 Molecular Structure and Energy Levels for Polyatomic Molecules 315

- 13.1 Lewis Structures and the VSEPR Model 315
- 13.2 Describing Localized Bonds Using Hybridization for Methane, Ethene, and Ethyne 318
- 13.3 Constructing Hybrid Orbitals for Nonequivalent Ligands 321
- 13.4 Using Hybridization to Describe Chemical Bonding 324
- 13.5 Predicting Molecular Structure Using Qualitative Molecular Orbital Theory 326
- 13.6 How Different Are Localized and Delocalized Bonding Models? 329
- 13.7 Molecular Structure and Energy Levels from Computational Chemistry 332
- 13.8 Qualitative Molecular Orbital Theory for Conjugated and Aromatic Molecules: The Hückel Model 334
- 13.9 From Molecules to Solids 340
- 13.10 Making Semiconductors Conductive at Room Temperature 342

14 Electronic Spectroscopy 349

- 14.1 The Energy of Electronic Transitions 349
- 14.2 Molecular Term Symbols 350
- 14.3 Transitions between Electronic States of Diatomic Molecules 353
- 14.4 The Vibrational Fine Structure of Electronic Transitions in Diatomic Molecules 354
- 14.5 UV-Visible Light Absorption in Polyatomic Molecules 356
- 14.6 Transitions among the Ground and Excited States 359
- 14.7 Singlet–Singlet Transitions: Absorption and Fluorescence 360
- 14.8 Intersystem Crossing and Phosphorescence 361
- 14.9 Fluorescence Spectroscopy and Analytical Chemistry 362
- 14.10 Ultraviolet Photoelectron Spectroscopy 363
- 14.11 Single-Molecule Spectroscopy 365
- 14.12 Fluorescent Resonance Energy Transfer 366
- 14.13 Linear and Circular Dichroism 368
- 14.14 Assigning + and – to Σ Terms of Diatomic Molecules 371

15 Computational Chemistry 377

- 15.1 The Promise of Computational Chemistry 377
- 15.2 Potential Energy Surfaces 378

- 15.3 Hartree–Fock Molecular Orbital Theory: A Direct Descendant of the Schrödinger Equation 382
- 15.4 Properties of Limiting Hartree–Fock Models 384
- 15.5 Theoretical Models and Theoretical Model Chemistry 389
- 15.6 Moving Beyond Hartree–Fock Theory 390
- 15.7 Gaussian Basis Sets 395
- 15.8 Selection of a Theoretical Model 398
- 15.9 Graphical Models 412
- 15.10 Conclusion 420

Math Essential 10 Working with Matrices

16 Molecular Symmetry and an Introduction to Group Theory 439

- 16.1 Symmetry Elements, Symmetry Operations, and Point Groups 439
- 16.2 Assigning Molecules to Point Groups 441
- 16.3 The H_2O Molecule and the C_{2v} Point Group 443
- 16.4 Representations of Symmetry Operators, Bases for Representations, and the Character Table 448
- 16.5 The Dimension of a Representation 450
- 16.6 Using the C_{2v} Representations to Construct Molecular Orbitals for H_2O 454
- 16.7 Symmetries of the Normal Modes of Vibration of Molecules 456
- 16.8 Selection Rules and Infrared versus Raman Activity 460
- 16.9 Using the Projection Operator Method to Generate MOs That Are Bases for Irreducible Representations 461

17 Nuclear Magnetic Resonance Spectroscopy 467

- 17.1 Intrinsic Nuclear Angular Momentum and Magnetic Moment 467
- 17.2 The Nuclear Zeeman Effect 470
- 17.3 The Chemical Shift 473
- 17.4 Spin–Spin Coupling and Multiplet Splittings 476
- 17.5 Spin Dynamics 484
- 17.6 Pulsed NMR Spectroscopy 491
- 17.7 Two-Dimensional NMR 498
- 17.8 Solid-State NMR 503
- 17.9 Dynamic Nuclear Polarization 505
- 17.10 Magnetic Resonance Imaging 507

APPENDIX A Point Group Character Tables 513

Credits 521

Index 523

About the Author



THOMAS ENGEL taught chemistry at the University of Washington for more than 20 years, where he is currently professor emeritus of chemistry. Professor Engel received his bachelor's and master's degrees in chemistry from the Johns Hopkins University and his Ph.D. in chemistry from the University of Chicago. He then spent 11 years as a researcher in Germany and Switzerland, during which time he received the Dr. rer. nat. habil. degree from the Ludwig Maximilians University in Munich. In 1980, he left the IBM research laboratory in Zurich to become a faculty member at the University of Washington.

Professor Engel has published more than 80 articles and book chapters in the area of surface chemistry. He has received the Surface Chemistry or Colloids Award from the American Chemical Society and a Senior Humboldt Research Award from the Alexander von Humboldt Foundation. Other than this textbook, his current primary science interests are in energy policy and energy conservation. He serves on the citizen's advisory board of his local electrical utility, and his energy-efficient house could be heated in winter using only a hand-held hair dryer. He currently drives a hybrid vehicle and plans to transition to an electric vehicle soon to further reduce his carbon footprint.

Preface

The fourth edition of *Quantum Chemistry and Spectroscopy* includes many changes to the presentation and content at both a global and chapter level. These updates have been made to enhance the student learning experience and update the discussion of research areas. At the global level, changes that readers will see throughout the textbook include:

- **Review of relevant mathematics skills.** One of the primary reasons that students experience physical chemistry as a challenging course is that they find it difficult to transfer skills previously acquired in a mathematics course to their physical chemistry course. To address this issue, contents of the third edition Math Supplement have been expanded and split into 11 two- to five-page Math Essentials, which are inserted at appropriate places throughout this book, as well as in the companion volume *Thermodynamics, Statistical Thermodynamics, and Kinetics*, just before the math skills are required. Our intent in doing so is to provide “just-in-time” math help and to enable students to refresh math skills specifically needed in the following chapter.
- **Concept and Connection.** A new Concept and Connection feature has been added to each chapter to present students with a quick visual summary of the most important ideas within the chapter. In each chapter, approximately 10–15 of the most important concepts and/or connections are highlighted in the margins.
- **End-of-Chapter Problems.** Numerical Problems are now organized by section number within chapters to make it easier for instructors to create assignments for specific parts of each chapter. Furthermore, a number of new Conceptual Questions and Numerical Problems have been added to the book. Numerical Problems from the previous edition have been revised.
- **Introductory chapter materials.** Introductory paragraphs of all chapters have been replaced by a set of three questions plus responses to those questions. This new feature makes the importance of the chapter clear to students at the outset.
- **Figures.** All figures have been revised to improve clarity. Also, for many figures additional annotation has been included to help tie concepts to the visual program.
- **Key Equations.** An end-of-chapter table that summarizes Key Equations has been added to allow students to focus on the most important of the many equations in each chapter. Equations in this table are set in red type where they appear in the body of the chapter.
- **Further Reading.** A section on Further Reading has been added to each chapter to provide references for students and instructors who would like a deeper understanding of various aspects of the chapter material.
- **Guided Practice and Interactivity**
 - **MasteringTM Chemistry**, with a new enhanced eBook, has been significantly expanded to include a wealth of new end-of-chapter problems from the fourth edition, new self-guided, adaptive Dynamic Study Modules with wrong answer feedback and remediation, and the new Pearson eBook, which is mobile friendly. Students who solve homework problems using MasteringTM Chemistry obtain immediate feedback, which greatly enhances learning associated with solving homework problems. This platform can also be used for pre-class reading quizzes linked directly to the eText that are useful in ensuring students remain current in their studies and in flipping the classroom.
 - **NEW! Pearson eText, optimized for mobile** gives students access to their textbook anytime, anywhere.
 - Pearson eText mobile app offers offline access and can be downloaded for most iOS and Android phones/tablets from the Apple App Store or Google Play
 - Configurable reading settings, including resizable type and night-reading mode
 - Instructor and student note-taking, highlighting, bookmarking, and search functionalities

- **NEW! 66 Dynamic Study Modules** help students study effectively on their own by continuously assessing their activity and performance in real time.
- Students complete a set of questions with a unique answer format that also asks them to indicate their confidence level. Questions repeat until the student can answer them all correctly and confidently. These are available as graded assignments prior to class and are accessible on smartphones, tablets, and computers.
- **Topics** include key math skills, as well as a refresher of general chemistry concepts such as understanding matter, chemical reactions, and the periodic table and atomic structure. Topics can be added or removed to match your coverage.

In terms of chapter and section content, many changes were made. The most significant of these changes are:

- Chapter 17, on nuclear magnetic resonance (NMR), has been completely rewritten and expanded with the significant contribution of co-author Alex Angerhofer. This chapter now covers the nuclear Overhauser effect and dynamic nuclear polarization, and presents an extensive discussion of how two-dimensional NMR techniques are used to determine the structure of macromolecules in solution.
- Section 5.4 has been revised and expanded to better explain conduction in solids.
- Section 6.6 has been extensively revised to take advances in quantum computing into account.
- Section 8.4, on the origin of selection rules, has been revised and expanded to enhance student learning.
- Sections 14.5, 14.7, and 14.10 have been extensively revised and reformulated to relate electronic transitions to molecular orbitals of the initial and final states.
- Section 14.12 has been revised to reflect advances in the application of FRET to problems of chemical interest.

For those not familiar with the third edition of *Quantum Chemistry and Spectroscopy*, our approach to teaching physical chemistry begins with our target audience, undergraduate students majoring in chemistry, biochemistry, and chemical engineering, as well as many students majoring in the atmospheric sciences and the biological sciences. The following objectives outline our approach to teaching physical chemistry.

- **Focus on teaching core concepts.** The central principles of physical chemistry are explored by focusing on core ideas and then extending these ideas to a variety of problems. The goal is to build a solid foundation of student understanding in a limited number of areas rather than to provide a condensed encyclopedia of physical chemistry. We believe this approach teaches students how to learn and enables them to apply their newly acquired skills to master related fields.
- **Illustrate the relevance of physical chemistry to the world around us.** Physical chemistry becomes more relevant to a student if it is connected to the world around us. Therefore, example problems and specific topics are tied together to help the student develop this connection. For example, topics such as scanning tunneling microscopy, quantum dots, and quantum computing are discussed and illustrated with examples from the recent chemistry literature. Every attempt is made to connect fundamental ideas to applications that could be of interest to the student.
- **Link the macroscopic and atomic-level worlds.** The manifestation of quantum mechanics in the macroscopic world is illustrated by discussions of the band structure of solids, atomic force microscopy, quantum mechanical calculations of thermodynamic state functions, and NMR imaging.
- **Present exciting new science in the field of physical chemistry.** Physical chemistry lies at the forefront of many emerging areas of modern chemical research. Heterogeneous catalysis has benefited greatly from mechanistic studies carried out using the techniques of modern surface science. Quantum computing, using the principles of superposition and entanglement, is on the verge of being a viable technology. The role of physical chemistry in these and other emerging areas is highlighted throughout the text.

- **Provide a versatile online homework program with tutorials.** Students who submit homework problems using MasteringTM Chemistry obtain immediate feedback, a feature that greatly enhances learning. Also, tutorials with wrong answer feedback offer students a self-paced learning environment.
- **Use web-based simulations to illustrate the concepts being explored and avoid math overload.** Mathematics is central to physical chemistry; however, the mathematics can distract the student from “seeing” the underlying concepts. To circumvent this problem, web-based simulations have been incorporated as end-of-chapter problems in several chapters so that the student can focus on the science and avoid a math overload. These web-based simulations can also be used by instructors during lecture. An important feature of the simulations is that each problem has been designed as an assignable exercise with a printable answer sheet that the student can submit to the instructor. Simulations, animations, and homework problem worksheets can be accessed at www.pearsonhighered.com/advchemistry.

Effective use of *Quantum Chemistry and Spectroscopy* does not require proceeding sequentially through the chapters or including all sections. Some topics are discussed in supplemental sections, which can be omitted if they are not viewed as essential to the course. Also, many sections are sufficiently self-contained that they can be readily omitted if they do not serve the needs of the instructor and students. This textbook is constructed to be flexible to your needs. I welcome the comments of both students and instructors on how the material was used and how the presentation can be improved.

Thomas Engel
University of Washington

ACKNOWLEDGMENTS

Many individuals have helped me to bring the text into its current form. Students have provided me with feedback directly and through the questions they have asked, which has helped me to understand how they learn. Many colleagues, including Peter Armentrout, Doug Doren, Gary Drobny, Alex Engel, Graeme Henkelman, Lewis Johnson, Tom Pratum, Bill Reinhardt, Peter Rosky, George Schatz, Michael Schick, Gabrielle Varani, and especially Wes Borden and Bruce Robinson, have been invaluable in advising me. I am also fortunate to have access to some end-of-chapter problems that were originally presented in *Physical Chemistry*, 3rd edition, by Joseph H. Noggle and in *Physical Chemistry*, 3rd edition, by Gilbert W. Castellan. The reviewers, who are listed separately, have made many suggestions for improvement, for which I am very grateful. All those involved in the production process have helped to make this book a reality through their efforts. Special thanks are due to Jim Smith, who guided the first edition, to the current editor Jeanne Zalesky, to the developmental editor Spencer Cotkin, and to Jennifer Hart and Beth Sweeten at Pearson, who have led the production process.

4TH EDITION MANUSCRIPT REVIEWERS

David Coker, <i>Boston University</i>	George Papadantonakis, <i>University of Illinois, Chicago</i>
Yingbin Ge, <i>Central Washington University</i>	Stefan Stoll, <i>University of Washington</i>
Eric Gislason, <i>University of Illinois, Chicago</i>	Liliya Yatsunyk, <i>Swarthmore College</i>
Nathan Hammer, <i>University of Mississippi</i>	

4TH EDITION ACCURACY REVIEWERS

Garry Crosson, <i>University of Dayton</i>	Andrea Munro, <i>Pacific Lutheran University</i>
Benjamin Huddle, <i>Roanoke College</i>	

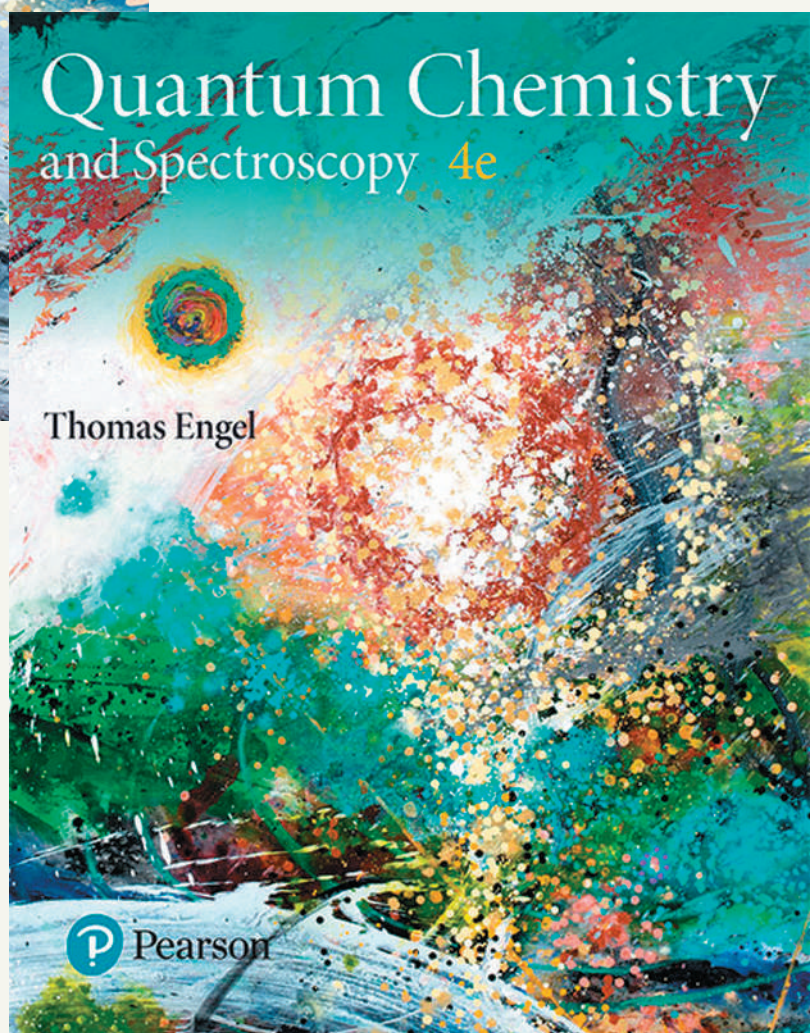
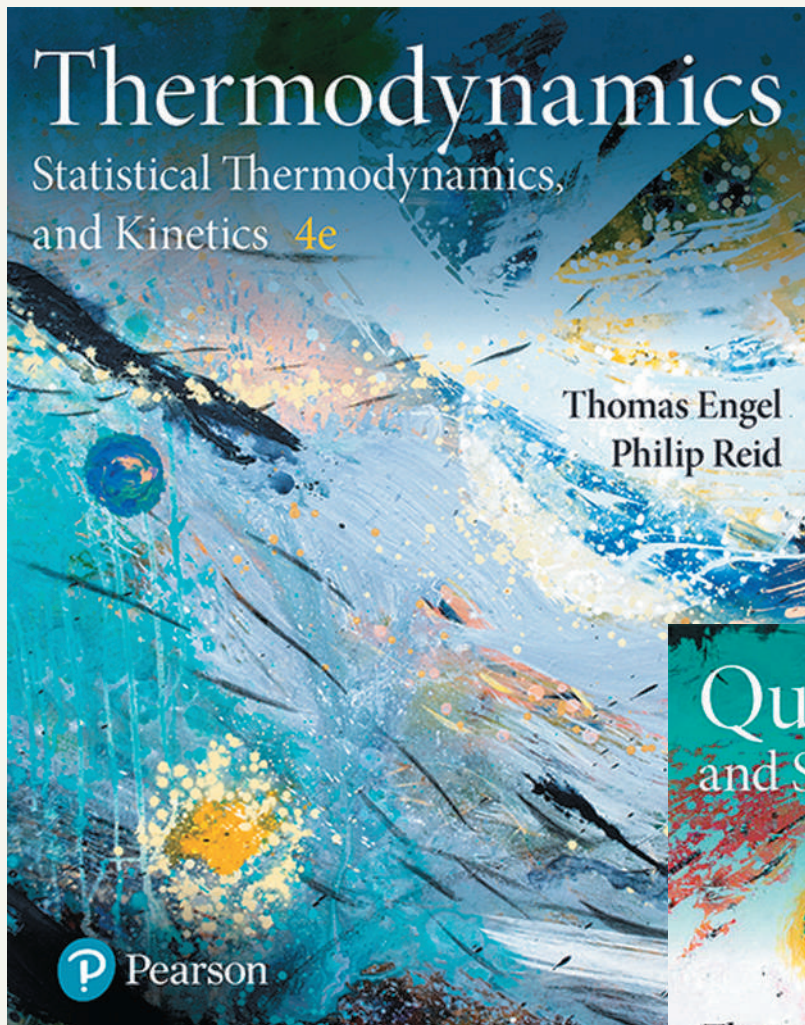
4TH EDITION PRESCRIPTIVE REVIEWERS

Joseph Alia, <i>University of Minnesota, Morris</i>	Richard Mabbs, <i>Washington University, St. Louis</i>
Herbert Axelrod, <i>California State University, Fullerton</i>	Vicki Moravec, <i>Trine University</i>
Timothy Brewer, <i>Eastern Michigan University</i>	Andrew Petit, <i>California State University, Fullerton</i>
Paul Cooper, <i>George Mason University</i>	Richard Schwenz, <i>University of Northern Colorado</i>
Bridget DePrince, <i>Florida State University</i>	Ronald Terry, <i>Western Illinois University</i>
Patrick Fleming, <i>California State University, East Bay</i>	Dunwei Wang, <i>Boston College</i>
Gerard Harbison, <i>University of Nebraska, Lincoln</i>	

PREVIOUS EDITION REVIEWERS

Alexander Angerhofer, <i>University of Florida</i>	Cynthia Hartzell, <i>Northern Arizona University</i>
Clayton Baum, <i>Florida Institute of Technology</i>	Geoffrey Hutchinson, <i>University of Pittsburgh</i>
Martha Bruch, <i>State University of New York at Oswego</i>	John M. Jean, <i>Regis University</i>
David L. Cedeño, <i>Illinois State University</i>	Martina Kaledin, <i>Kennesaw State University</i>
Rosemarie Chinni, <i>Alvernia College</i>	George Kaminski, <i>Worcester Polytechnic Institute</i>
Allen Clabo, <i>Francis Marion University</i>	Daniel Lawson, <i>University of Michigan, Dearborn</i>
Lorrie Comeford, <i>Salem State College</i>	William Lester, <i>University of California, Berkeley</i>
Stephen Cooke, <i>University of North Texas</i>	Dmitrii E. Makarov, <i>University of Texas at Austin</i>
Douglas English, <i>University of Maryland, College Park</i>	Herve Marand, <i>Virginia Polytechnic Institute and State University</i>
Sophya Garashchuk, <i>University of South Carolina</i>	Thomas Mason, <i>University of California, Los Angeles</i>
Leon Gerber, <i>St. John's University</i>	Jennifer Mihalik, <i>University of Wisconsin, Oshkosh</i>
Nathan Hammer, <i>The University of Mississippi</i>	Enrique Peacock-López, <i>Williams College</i>

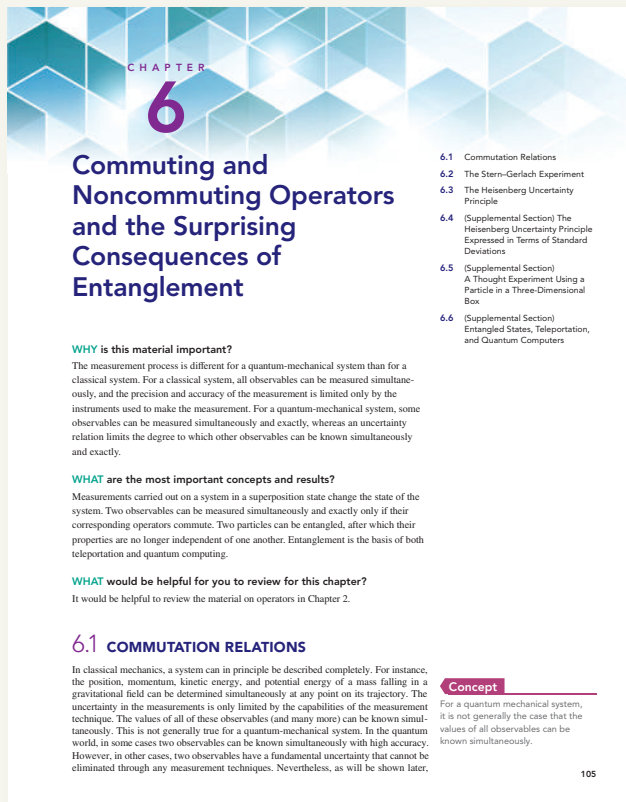
A Visual, Conceptual, and Contemporary Approach to Physical Chemistry



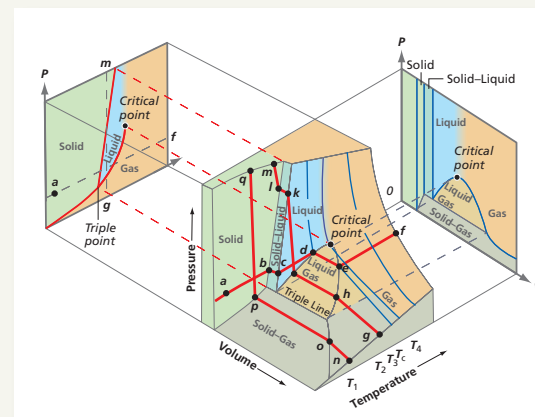
A Visual, Conceptual, and Contemporary Approach to Physical Chemistry

NEW! Math Essentials provide a review of relevant math skills, offer “just in time” math help, and enable students to refresh math skills specifically needed in the chapter that follows.

UPDATED! Introductory paragraphs of all chapters have been replaced by a set of three questions plus responses to those questions making the relevance of the chapter clear at the outset.



UPDATED! All figures have been revised to improve clarity and for many figures, additional annotation has been included to help tie concepts to the visual program.



MATH ESSENTIAL 2: Differentiation and Integration

Differential and integral calculus is used extensively in physical chemistry. In this unit we review the most relevant aspects of calculus needed to understand the chapter discussions and to solve the end-of-chapter problems.

ME2.1 THE DEFINITION AND PROPERTIES OF A FUNCTION

A function f is a rule that generates a value y from the value of a variable x . Mathematically, we write this as $y = f(x)$. The set of values x over which f is defined is the domain of the function. Single-valued functions have a single value of y for a given value of x . Most functions that we will deal with in physical chemistry are single valued. However, inverse trigonometric functions and $\sqrt[3]{\cdot}$ are examples of common functions that are multivalued. A function is continuous if it satisfies these three conditions:

- ME2.1** The Definition and Properties of a Function
 - ME2.2** The First Derivative of a Function
 - ME2.3** The Chain Rule
 - ME2.4** The Sum and Product Rules
 - ME2.5** The Reciprocal Rule and the Quotient Rule
 - ME2.6** Higher-Order Derivatives: Maxima, Minima, and Inflection Points
 - ME2.7** Definite and Indefinite Integrals

$$\begin{aligned}f(x) &\text{ is defined at } a \\ \lim_{x \rightarrow a} f(x) &\text{ exists} \\ \lim_{x \rightarrow a} f(x) &= f(a)\end{aligned}\quad (\text{ME2.1})$$

ME2.2 THE FIRST DERIVATIVE OF A FUNCTION

The first derivative of a function has as its physical interpretation the slope of the function evaluated at the point of interest. In order for the first derivative to exist at a point a , the function must be continuous at $x = a$, and the slope of the function at $x = a$ must be the same when approaching a from $x < a$ and $x > a$. For example, the slope of the function $y = x^2$ at the point $x = 1.5$ is indicated by the line tangent to the curve shown in Figure ME2.1.

Mathematically, the first derivative of a function $f(x)$ is denoted $df(x)/dx$. It is defined by

$$\frac{f(x) - f(x-h)}{2h} = \lim_{h \rightarrow 0} \frac{f(x+h) - f(x)}{h} \quad (\text{ME2.2})$$

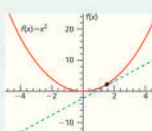


Figure ME2.1
The function $y = x^2$ plotted as a function of x . The dashed line is the tangent to the curve at $x = 1.5$.

In order for $df(x)/dx$ to be defined over an interval in x , $f(x)$ must be continuous over the interval. Next, we present rules for differentiating simple functions. Some of these functions and their derivatives are as follows:

$$\frac{d(ax^n)}{dx} = anx^{n-1}, \quad \text{where } a \text{ is a constant and } n \text{ is any real number} \quad (\text{ME2.4})$$

$$\frac{d(ae^x)}{dx} = ae^x, \quad \text{where } a \text{ is a constant} \quad (\text{ME2-5})$$

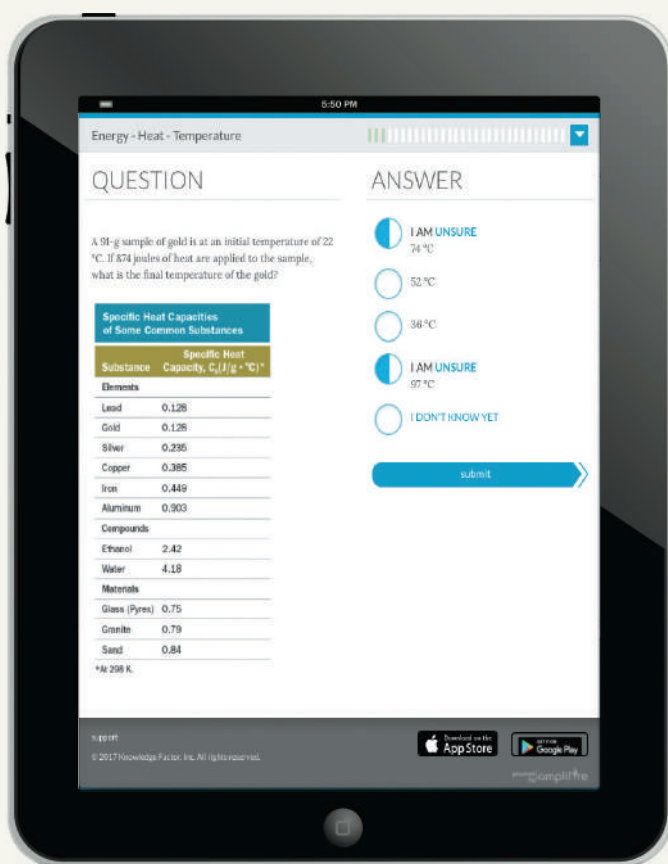
$$\frac{d \ln x}{dx} = \frac{1}{x} \quad (\text{ME2-6})$$

$$\frac{dx}{dt} = -x \quad (NDEq1)$$

NEW! Concept and Connection features in each chapter present students with quick visual summaries of the core concepts within the chapter, highlighting key take aways and providing students with an easy way to review the material.

Figure 8.15
A P - V - T phase diagram for a substance that expands upon melting. The indicated processes are discussed in the text.

Continuous Learning Before, During, and After Class



Mastering™ Chemistry

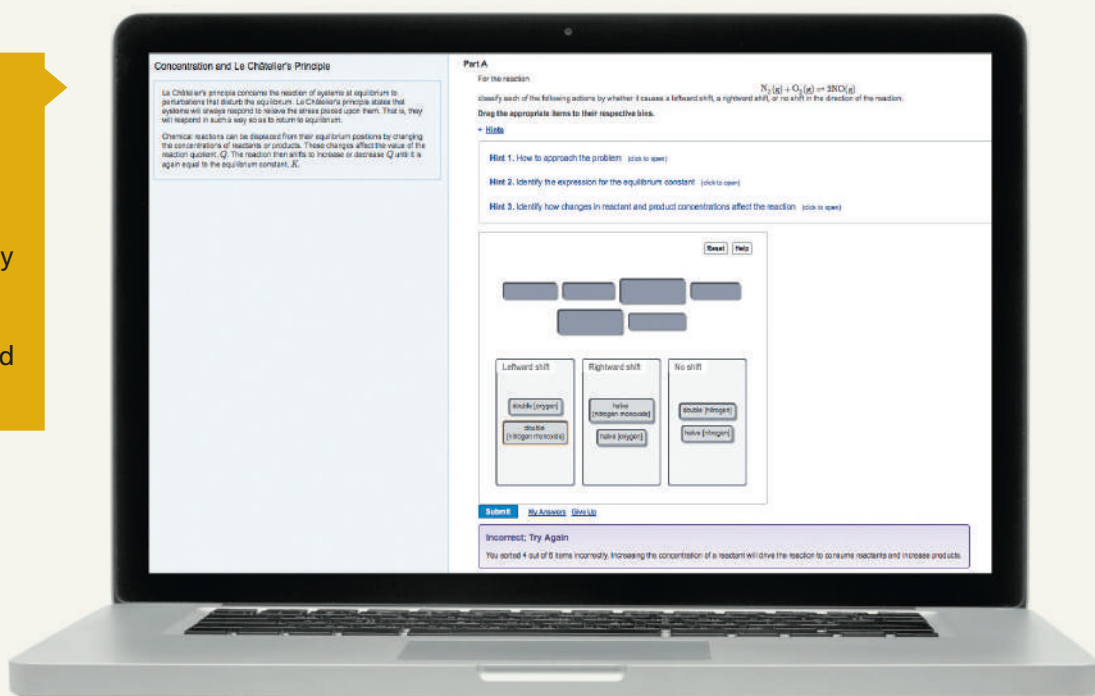
NEW! 66 Dynamic Study Modules

help students study effectively on their own by continuously assessing their activity and performance in real time.

Students complete a set of questions with a unique answer format that also asks them to indicate their confidence level. Questions repeat until the student can answer them all correctly and confidently. These are available as graded assignments prior to class and are accessible on smartphones, tablets, and computers.

Topics include key math skills as well as a refresher of general chemistry concepts such as understanding matter, chemical reactions, and understanding the periodic table & atomic structure. Topics can be added or removed to match your coverage.

NEW! Enhanced End-of-Chapter and Tutorial Problems offer students the chance to practice what they have learned while receiving answer-specific feedback and guidance.



Pearson eText

NEW! Pearson eText, optimized for mobile gives students access to their textbook anytime, anywhere.

Pearson eText is a mobile app which offers offline access and can be downloaded for most iOS and Android phones/tablets from the Apple App Store or Google Play:

- Configurable reading settings, including resizable type and night-reading mode
 - Instructor and student note-taking, highlighting, bookmarking, and search functionalities



MATH ESSENTIAL 1: Units, Significant Figures, and Solving End of Chapter Problems

ME1.1 UNITS

Quantities of interest in physical chemistry such as pressure, volume, or temperature are characterized by their magnitude and their units. In this textbook, we use the SI (from the French *Le Système international d'unités*) system of units. All physical quantities can be defined in terms of the seven base units listed in Table ME1.1. For more details, see <http://physics.nist.gov/cuu/Units/units.html>. The definition of temperature is based on the coexistence of the solid, gaseous, and liquid phases of water at a pressure of 1 bar.

- ME1.1** Units
- ME1.2** Uncertainty and Significant Figures
- ME1.3** Solving End-of-Chapter Problems

TABLE ME1.1 Base SI Units

Base Unit	Unit	Definition of Unit
Unit of length	meter (m)	The meter is the length of the path traveled by light in vacuum during a time interval of $1/299,792,458$ of a second.
Unit of mass	kilogram (kg)	The kilogram is the unit of mass; it is equal to the mass of the platinum iridium international prototype of the kilogram kept at the International Bureau of Weights and Measures.
Unit of time	second (s)	The second is the duration of $9,192,631,770$ periods of the radiation corresponding to the transition between the two hyperfine levels of the ground state of the cesium 133 atom.
Unit of electric current	ampere (A)	The ampere is the constant current that, if maintained in two straight parallel conductors of infinite length, is of negligible circular cross section, and if placed 1 meter apart in a vacuum would produce between these conductors a force equal to 2×10^{-7} kg m s ⁻² per meter of length. In this definition, 2 is an exact number.
Unit of thermodynamic temperature	kelvin (K)	The Kelvin is the unit of thermodynamic temperature. It is the fraction $1/273.16$ of the thermodynamic temperature of the triple point of water.
Unit of amount of substance	mole (mol)	The mole is the amount of substance of a system that contains as many elementary entities as there are atoms in 0.012 kilogram of carbon 12 where 0.012 is an exact number. When the mole is used, the elementary entities must be specified and may be atoms, molecules, ions, electrons, other particles, or specified groups of such particles.
Unit of luminous intensity	candela (cd)	The candela is the luminous intensity, in a given direction, of a source that emits monochromatic radiation of frequency 540×10^{12} hertz and that has a radiant intensity in that direction of $1/683$ watt per steradian.

Quantities of interest other than the seven base quantities can be expressed in terms of the units meter, kilogram, second, ampere, kelvin, mole, and candela. The most important of these derived units, some of which have special names as indicated, are listed in Table ME1.2. A more inclusive list of derived units can be found at <http://physics.nist.gov/cuu/Units/units.html>.

TABLE ME1.2 Derived Units

Unit	Definition	Relation to Base Units	Special Name	Abbreviation
Area	Size of a surface	m^2		m^2
Volume	Amount of three-dimensional space an object occupies	m^3		m^3
Velocity	Measure of the rate of motion	m s^{-1}		m s^{-1}
Acceleration	Rate of change of velocity	m s^{-2}		m s^{-2}
Linear momentum	Product of mass and linear velocity of an object	kg m s^{-1}		kg m s^{-1}
Angular momentum	Product of the moment of inertia of a body about an axis and its <i>angular</i> velocity with respect to the same axis	$\text{kg m}^2 \text{s}^{-1}$		$\text{kg m}^2 \text{s}^{-1}$
Force	Any interaction that, when unopposed, will change the motion of an object	kg m s^{-2}	newton	N
Pressure	Force acting per unit area	$\text{kg m}^{-1} \text{s}^{-2}$ N m^{-2}	pascal	Pa
Work	Product of force on an object and movement along the direction of the force	$\text{kg m}^2 \text{s}^{-2}$	joule	J
Kinetic energy	Energy an object possesses because of its motion	$\text{kg m}^2 \text{s}^{-2}$	joule	J
Potential energy	Energy an object possesses because of its position or condition	$\text{kg m}^2 \text{s}^{-2}$	joule	J
Power	Rate at which energy is produced or consumed	$\text{kg m}^2 \text{s}^{-3}$	watt	W
Mass density	Mass per unit volume	kg m^{-3}		kg m^{-3}
Radian	Angle at the center of a circle whose arc is equal in length to the radius	$\text{m/m} = 1$		$\text{m/m} = 1$
Steradian	Angle at the center of a sphere subtended by a part of the surface equal in area to the square of the radius	$\text{m}^2/\text{m}^2 = 1$		$\text{m}^2/\text{m}^2 = 1$
Frequency	Number of repeat units of a wave per unit time	s^{-1}	hertz	Hz
Electrical charge	Physical property of matter that causes it to experience an electrostatic force	A s	coulomb	C
Electrical potential	Work done in moving a unit positive charge from infinity to that point	$\text{kg m}^2 \text{s}^{-3}/\text{A}$ W/A	volt	V
Electrical resistance	Ratio of the voltage to the electric current that flows through a conductive material	$\text{kg m}^2 \text{s}^{-3}/\text{A}^2 \text{W/A}^2$	ohm	Ω

If SI units are used throughout the calculation of a quantity, the result will have SI units. For example, consider a unit analysis of the electrostatic force between two charges:

$$\begin{aligned}
 F &= \frac{q_1 q_2}{8\pi\epsilon_0 r^2} = \frac{\text{C}^2}{8\pi \times \text{kg}^{-1}\text{s}^4\text{A}^2\text{m}^{-3} \times \text{m}^2} = \frac{\text{A}^2\text{s}^2}{8\pi \times \text{kg}^{-1}\text{s}^4\text{A}^2\text{m}^{-3} \times \text{m}^2} \\
 &= \frac{1}{8\pi} \text{kg m s}^{-2} = \frac{1}{8\pi} \text{N}
 \end{aligned}$$

Therefore, in carrying out a calculation, it is only necessary to make sure that all quantities are expressed in SI units rather than carrying out a detailed unit analysis of the entire calculation.

ME1.2 UNCERTAINTY AND SIGNIFICANT FIGURES

In carrying out a calculation, it is important to take into account the uncertainty of the individual quantities that go into the calculation. The uncertainty is indicated by the number of significant figures. For example, the mass 1.356 g has four significant figures. The mass 0.003 g has one significant figure, and the mass 0.01200 g has four significant figures. By convention, the uncertainty of a number is ± 1 in the rightmost digit. A zero at the end of a number that is not to the right of a decimal point is not significant. For example, 150 has two significant figures, but 150. has three significant figures. Some numbers are exact and have no uncertainty. For example, 1.00×10^6 has three significant figures because the 10 and 6 are exact numbers. By definition, the mass of one atom of ^{12}C is exactly 12 atomic mass units.

If a calculation involves quantities with a different number of significant figures, the following rules regarding the number of significant figures in the result apply:

- In addition and subtraction, the result has the number of digits to the right of the decimal point corresponding to the number that has the smallest number of digits to the right of the decimal point. For example $101 + 24.56 = 126$ and $0.523 + 0.10 = 0.62$.
- In multiplication or division, the result has the number of significant figures corresponding to the number with the smallest number of significant figures. For example, $3.0 \times 16.00 = 48$ and $0.05 \times 100. = 5$.

It is good practice to carry forward a sufficiently large number of significant figures in different parts of the calculation and to round off to the appropriate number of significant figures at the end.

ME1.3 SOLVING END-OF-CHAPTER PROBLEMS

Because calculations in physical chemistry often involve multiple inputs, it is useful to carry out calculations in a manner that they can be reviewed and easily corrected. For example, the input and output for the calculation of the pressure exerted by gaseous benzene with a molar volume of 2.00 L at a temperature of 595 K using the Redlich–Kwong equation of state $P = \frac{RT}{V_m - b} - \frac{a}{\sqrt{T}} \frac{1}{V_m(V_m + b)}$ in Mathematica is shown below. The statement in the first line clears the previous values of all listed quantities, and the semicolon after each input value suppresses its appearance in the output.

```
In[36]:= Clear[r, t, vm, a, b, prk]
r = 8.314 * 10^-2;
t = 595;
vm = 2.00;
a = 452;
b = .08271;
prk =  $\frac{rt}{vm - b} - \frac{a}{\sqrt{t}} \frac{1}{vm(vm + b)}$ 
out[42]= 21.3526
```

Invoking the rules for significant figures, the final answer is $P = 21.4$ bar.

The same problem can be solved using Microsoft Excel as shown in the following table.

	A	B	C	D	E	F
1	R	T	V_m	a	b	$=((A2*B2)/(C2-E2))-(D2/SQRT(B2))*(1/(C2*(C2+E2)))$
2	0.08314	595	2	452	0.08271	21.35257941

This page intentionally left blank

MATH ESSENTIAL 2: Differentiation and Integration

Differential and integral calculus is used extensively in physical chemistry. In this unit we review the most relevant aspects of calculus needed to understand the chapter discussions and to solve the end-of-chapter problems.

ME2.1 THE DEFINITION AND PROPERTIES OF A FUNCTION

A function f is a rule that generates a value y from the value of a variable x . Mathematically, we write this as $y = f(x)$. The set of values x over which f is defined is the domain of the function. Single-valued functions have a single value of y for a given value of x . Most functions that we will deal with in physical chemistry are single valued. However, inverse trigonometric functions and $\sqrt{}$ are examples of common functions that are multivalued. A function is continuous if it satisfies these three conditions:

$$\begin{aligned}f(x) &\text{ is defined at } a \\ \lim_{x \rightarrow a} f(x) &\text{ exists} \\ \lim_{x \rightarrow a} f(x) &= f(a)\end{aligned}\quad (\text{ME2.1})$$

ME2.2 THE FIRST DERIVATIVE OF A FUNCTION

The first derivative of a function has as its physical interpretation the slope of the function evaluated at the point of interest. In order for the first derivative to exist at a point a , the function must be continuous at $x = a$, and the slope of the function at $x = a$ must be the same when approaching a from $x < a$ and $x > a$. For example, the slope of the function $y = x^2$ at the point $x = 1.5$ is indicated by the line tangent to the curve shown in Figure ME2.1.

Mathematically, the first derivative of a function $f(x)$ is denoted $df(x)/dx$. It is defined by

$$\frac{df(x)}{dx} = \lim_{h \rightarrow 0} \frac{f(x + h) - f(x)}{h} \quad (\text{ME2.2})$$

The symbol $f'(x)$ is often used in place of $df(x)/dx$. For the function of interest,

$$\frac{df(x)}{dx} = \lim_{h \rightarrow 0} \frac{(x + h)^2 - (x)^2}{h} = \lim_{h \rightarrow 0} \frac{2hx + h^2}{h} = \lim_{h \rightarrow 0} 2x + h = 2x \quad (\text{ME2.3})$$

In order for $df(x)/dx$ to be defined over an interval in x , $f(x)$ must be continuous over the interval. Next, we present rules for differentiating simple functions. Some of these functions and their derivatives are as follows:

$$\frac{d(ax^n)}{dx} = anx^{n-1}, \quad \text{where } a \text{ is a constant and } n \text{ is any real number} \quad (\text{ME2.4})$$

$$\frac{d(ae^x)}{dx} = ae^x, \quad \text{where } a \text{ is a constant} \quad (\text{ME2.5})$$

$$\frac{d \ln x}{dx} = \frac{1}{x} \quad (\text{ME2.6})$$

- ME2.1** The Definition and Properties of a Function
- ME2.2** The First Derivative of a Function
- ME2.3** The Chain Rule
- ME2.4** The Sum and Product Rules
- ME2.5** The Reciprocal Rule and the Quotient Rule
- ME2.6** Higher-Order Derivatives: Maxima, Minima, and Inflection Points
- ME2.7** Definite and Indefinite Integrals

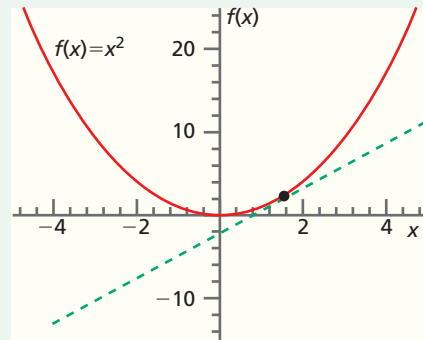


Figure ME2.1
The function $y = x^2$ plotted as a function of x . The dashed line is the tangent to the curve at $x = 1.5$.

$$\frac{d(a \sin x)}{dx} = a \cos x, \quad \text{where } a \text{ is a constant} \quad (\text{ME2.7})$$

$$\frac{d(a \cos x)}{dx} = -a \sin x, \quad \text{where } a \text{ is a constant} \quad (\text{ME2.8})$$

ME2.3 THE CHAIN RULE

In this section, we deal with the differentiation of more complicated functions. Suppose that $y = f(u)$ and $u = g(x)$. From the previous section, we know how to calculate $df(u)/du$. But how do we calculate $df(u)/dx$? The answer to this question is stated as the chain rule:

$$\frac{df(u)}{dx} = \frac{df(u)}{du} \frac{du}{dx} \quad (\text{ME2.9})$$

Several examples illustrating the chain rule follow:

$$\frac{d \sin(3x)}{dx} = \frac{d \sin(3x)}{d(3x)} \frac{d(3x)}{dx} = 3 \cos(3x) \quad (\text{ME2.10})$$

$$\frac{d \ln(x^2)}{dx} = \frac{d \ln(x^2)}{d(x^2)} \frac{d(x^2)}{dx} = \frac{2x}{x^2} = \frac{2}{x} \quad (\text{ME2.11})$$

$$\frac{d\left(x + \frac{1}{x}\right)^{-4}}{dx} = \frac{d\left(x + \frac{1}{x}\right)^{-4}}{d\left(x + \frac{1}{x}\right)} \frac{d\left(x + \frac{1}{x}\right)}{dx} = -4\left(x + \frac{1}{x}\right)^{-5} \left(1 - \frac{1}{x^2}\right) \quad (\text{ME2.12})$$

$$\frac{d \exp(ax^2)}{dx} = \frac{d \exp(ax^2)}{d(ax^2)} \frac{d(ax^2)}{dx} = 2ax \exp(ax^2), \quad \text{where } a \text{ is a constant} \quad (\text{ME2.13})$$

Additional examples of use of the chain rule include:

$$d(\sqrt[3]{x^{4/3}})/dx = (4/3)\sqrt[3]{x^{1/3}} \quad (\text{ME2.14})$$

$$d(5e^{3\sqrt{2x}})/dx = 15\sqrt{2}e^{3\sqrt{2x}} \quad (\text{ME2.15})$$

$$\frac{d(4 \sin kx)}{dx} = 4k \cos x, \quad \text{where } k \text{ is a constant}$$

$$\frac{d(\sqrt{3} \cos 2\pi x)}{dx} = -2\sqrt{3}\pi \sin 2\pi x \quad (\text{ME2.16})$$

ME2.4 THE SUM AND PRODUCT RULES

Two useful rules in evaluating the derivative of a function that is itself the sum or product of two functions are as follows:

$$\frac{d[f(x) + g(x)]}{dx} = \frac{df(x)}{dx} + \frac{dg(x)}{dx} \quad (\text{ME2.17})$$

For example,

$$\frac{d(x^3 + \sin x)}{dx} = \frac{dx^3}{dx} + \frac{d \sin x}{dx} = 3x^2 + \cos x \quad (\text{ME2.18})$$

$$\frac{d[f(x)g(x)]}{dx} = g(x)\frac{df(x)}{dx} + f(x)\frac{dg(x)}{dx} \quad (\text{ME2.19})$$

For example,

$$\begin{aligned}\frac{d[\sin(x)\cos(x)]}{dx} &= \cos(x)\frac{d\sin(x)}{dx} + \sin(x)\frac{d\cos(x)}{dx} \\ &= \cos^2x - \sin^2x\end{aligned} \quad (\text{ME2.20})$$

ME2.5 THE RECIPROCAL RULE AND THE QUOTIENT RULE

How is the first derivative calculated if the function to be differentiated does not have a simple form such as those listed in the preceding section? In many cases, the derivative is found by using the product rule and the quotient rule given by

$$\frac{d\left(\frac{1}{f(x)}\right)}{dx} = -\frac{1}{[f(x)]^2} \frac{df(x)}{dx} \quad (\text{ME2.21})$$

For example,

$$\frac{d\left(\frac{1}{\sin x}\right)}{dx} = -\frac{1}{\sin^2 x} \frac{d\sin x}{dx} = \frac{-\cos x}{\sin^2 x} \quad (\text{ME2.22})$$

$$\frac{d\left[\frac{f(x)}{g(x)}\right]}{dx} = \frac{g(x)\frac{df(x)}{dx} - f(x)\frac{dg(x)}{dx}}{[g(x)]^2} \quad (\text{ME2.23})$$

For example,

$$\frac{d\left(\frac{x^2}{\sin x}\right)}{dx} = \frac{2x \sin x - x^2 \cos x}{\sin^2 x} \quad (\text{ME2.24})$$

ME2.6 HIGHER-ORDER DERIVATIVES: MAXIMA, MINIMA, AND INFLECTION POINTS

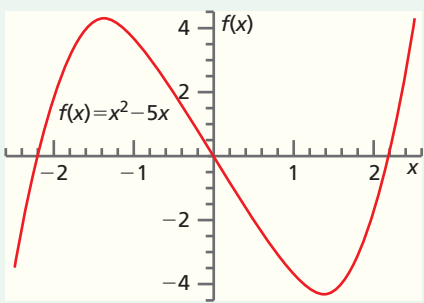
A function $f(x)$ can have higher-order derivatives in addition to the first derivative. The second derivative of a function is the slope of a graph of the slope of the function versus the variable. In order for the second derivative to exist, the first derivative must be continuous at the point of interest. Mathematically,

$$\frac{d^2f(x)}{dx^2} = \frac{d}{dx}\left(\frac{df(x)}{dx}\right) \quad (\text{ME2.25})$$

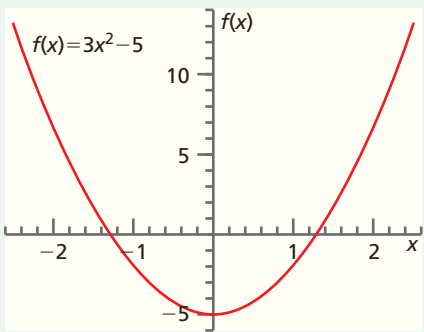
For example,

$$\begin{aligned}\frac{d^2 \exp(ax^2)}{dx^2} &= \frac{d}{dx}\left[\frac{d \exp(ax^2)}{dx}\right] = \frac{d[2ax \exp(ax^2)]}{dx} \\ &= 2a \exp(ax^2) + 4a^2x^2 \exp(ax^2), \quad \text{where } a \text{ is a constant}\end{aligned} \quad (\text{ME2.26})$$

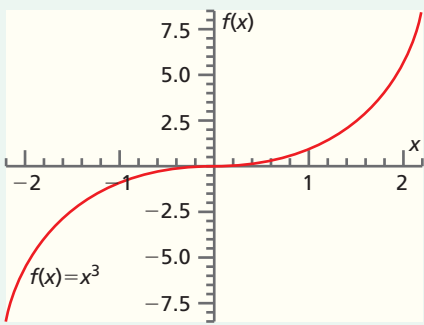
The symbol $f''(x)$ is often used in place of $d^2f(x)/dx^2$. If a function $f(x)$ has a concave upward shape (\cup) at the point of interest, its first derivative is increasing with x and therefore $f''(x) > 0$. If a function $f(x)$ has a concave downward shape (\cap) at the point of interest, $f''(x) < 0$.

**Figure ME2.2**

$f(x) = x^3 - 5x$ plotted as a function of x . Note that it has a maximum and a minimum in the range shown.

**Figure ME2.3**

The first derivative of the function shown in the previous figure as a function of x .

**Figure ME2.4**

$f(x) = x^3$ plotted as a function of x .

The value of x at which the tangent to the curve is horizontal is called an inflection point.

The second derivative is useful in identifying where a function has its minimum or maximum value within a range of the variable, as shown next. Because the first derivative is zero at a local maximum or minimum, $df(x)/dx = 0$ at the values x_{\max} and x_{\min} . Consider the function $f(x) = x^3 - 5x$ shown in Figure ME2.2 over the range $-2.5 \leq x \leq 2.5$.

By taking the derivative of this function and setting it equal to zero, we find the minima and maxima of this function in the range

$$\frac{d(x^3 - 5x)}{dx} = 3x^2 - 5 = 0, \text{ which has the solutions } x = \pm \sqrt{\frac{5}{3}} = 1.291$$

The maxima and minima can also be determined by graphing the derivative and finding the zero crossings, as shown in Figure ME2.3.

Graphing the function clearly shows that the function has one maximum and one minimum in the range specified. Which criterion can be used to distinguish between these extrema if the function is not graphed? The sign of the second derivative, evaluated at the point for which the first derivative is zero, can be used to distinguish between a maximum and a minimum:

$$\begin{aligned} \frac{d^2f(x)}{dx^2} &= \frac{d}{dx} \left[\frac{df(x)}{dx} \right] < 0 && \text{for a maximum} \\ \frac{d^2f(x)}{dx^2} &= \frac{d}{dx} \left[\frac{df(x)}{dx} \right] > 0 && \text{for a minimum} \end{aligned} \quad (\text{ME2.27})$$

We return to the function graphed earlier and calculate the second derivative:

$$\frac{d^2(x^3 - 5x)}{dx^2} = \frac{d}{dx} \left[\frac{d(x^3 - 5x)}{dx} \right] = \frac{d(3x^2 - 5)}{dx} = 6x \quad (\text{ME2.28})$$

By evaluating

$$\frac{d^2f(x)}{dx^2} \text{ at } x = \pm \sqrt{\frac{5}{3}} = \pm 1.291 \quad (\text{ME2.29})$$

we see that $x = 1.291$ corresponds to the minimum, and $x = -1.291$ corresponds to the maximum.

If a function has an inflection point in the interval of interest, then

$$\frac{df(x)}{dx} = 0 \quad \text{and} \quad \frac{d^2f(x)}{dx^2} = 0 \quad (\text{ME2.30})$$

An example for an inflection point is $x = 0$ for $f(x) = x^3$. A graph of this function in the interval $-2 \leq x \leq 2$ is shown in Figure ME2.4. In this case,

$$\frac{dx^3}{dx} = 3x^2 = 0 \quad \text{at } x = 0 \quad \text{and} \quad \frac{d^2(x^3)}{dx^2} = 6x = 0 \quad \text{at } x = 0 \quad (\text{ME2.31})$$

ME2.7 DEFINITE AND INDEFINITE INTEGRALS

In many areas of physical chemistry, the property of interest is the integral of a function over an interval in the variable of interest. For example, the work done in expanding an ideal gas from the initial volume V_i to the final volume V_f is the integral of the external pressure P_{ext} over the volume

$$w = - \int_{x_i}^{x_f} P_{\text{external}} Adx = - \int_{V_i}^{V_f} P_{\text{external}} dV \quad (\text{ME2.32})$$

Equation ME2.13 defines a definite integral in which the lower and upper limits of integration are given. Geometrically, the integral of a function over an interval is the area

under the curve describing the function. For example, the integral $\int_{-2.3}^{2.3} (x^3 - 5x)dx$ is the sum of the areas of the individual rectangles in Figure ME2.5 in the limit within which the width of the rectangles approaches zero. If the rectangles lie below the zero line, the incremental area is negative; if the rectangles lie above the zero line, the incremental area is positive. In this case, the total area is zero because the total negative area equals the total positive area.

The integral can also be understood as an antiderivative. From this point of view, the integral symbol is defined by the relation

$$f(x) = \int \frac{df(x)}{dx} dx \quad (\text{ME2.33})$$

and the function that appears under the integral sign is called the integrand. Interpreting the integral in terms of area, we evaluate a definite integral, and the interval over which the integration occurs is specified. The interval is not specified for an indefinite integral.

The geometrical interpretation is often useful in obtaining the value of a definite integral from experimental data when the functional form of the integrand is not known. For our purposes, the interpretation of the integral as an antiderivative is more useful. The value of the indefinite integral $\int (x^3 - 5x)dx$ is that function which, when differentiated, gives the integrand. Using the rules for differentiation discussed earlier, you can verify that

$$\int (x^3 - 5x)dx = \frac{x^4}{4} - \frac{5x^2}{2} + C \quad (\text{ME2.34})$$

Note the constant that appears in the evaluation of every indefinite integral. By differentiating the function obtained upon integration, you should convince yourself that any constant will lead to the same integrand. In contrast, a definite integral has no constant of integration. If we evaluate the definite integral

$$\int_{-2.3}^{2.3} (x^3 - 5x)dx = \left(\frac{x^4}{4} - \frac{5x^2}{2} + C \right)_{x=2.3} - \left(\frac{x^4}{4} - \frac{5x^2}{2} + C \right)_{x=-2.3} \quad (\text{ME2.35})$$

we see that the constant of integration cancels. The function obtained upon integration is an even function of x , and $\int_{-2.3}^{2.3} (x^3 - 5x)dx = 0$, just as we saw in the geometric interpretation of the integral.

Some indefinite integrals are encountered so often by students of physical chemistry that they become second nature and are recalled at will. These integrals are directly related to the derivatives discussed in Sections ME2.2–ME2.5 and include the following:

$$\int df(x) = f(x) + C$$

$$\int x^n dx = \frac{x^{n+1}}{n+1} + C$$

$$\int \frac{dx}{x} = \ln x + C \quad (\text{ME2.36})$$

$$\int e^{ax} dx = \frac{e^{ax}}{a} + C, \quad \text{where } a \text{ is a constant} \quad (\text{ME2.37})$$

$$\int \sin x dx = -\cos x + C \quad (\text{ME2.38})$$

$$\int \cos x dx = \sin x + C \quad (\text{ME2.39})$$

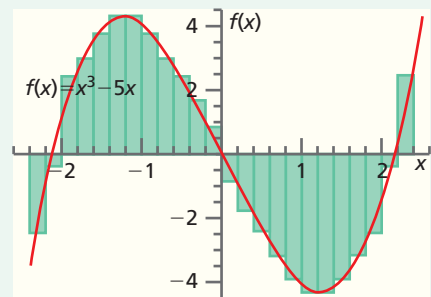


Figure ME2.5

The integral of a function over a given range corresponds to the area under the curve. The area under the curve is shown approximately by the green rectangles.

Although students will no doubt be able to recall the most commonly used integrals, the primary tool for the physical chemist in evaluating integrals is a good set of integral tables. Some commonly encountered integrals are listed below. The first group presents indefinite integrals.

$$\int (\sin ax)dx = -\frac{1}{a} \cos ax + C \quad (\text{ME2.40})$$

$$\int (\cos ax)dx = \frac{1}{a} \sin ax + C \quad (\text{ME2.41})$$

$$\int (\sin^2 ax)dx = \frac{1}{2}x - \frac{1}{4a} \sin 2ax + C \quad (\text{ME2.42})$$

$$\int (\cos^2 ax)dx = \frac{1}{2}x + \frac{1}{4a} \sin 2ax + C \quad (\text{ME2.43})$$

$$\int x \sin^2 bxdx = \frac{x^2}{4} - \frac{\cos 2bx}{8b^2} - \frac{x \sin 2bx}{4b} + C \quad (\text{ME2.44})$$

$$\int x \cos^2 bxdx = \frac{x^2}{4} + \frac{\cos 2bx}{8b^2} + \frac{x \sin 2bx}{4b} + C \quad (\text{ME2.45})$$

$$\int (x^2 \sin^2 ax)dx = \frac{1}{6}x^3 - \left(\frac{1}{4a}x^2 - \frac{1}{8a^3} \right) \sin 2ax - \frac{1}{4a^2}x \cos 2ax + C \quad (\text{ME2.46})$$

$$\int (x^2 \cos^2 ax)dx = \frac{1}{6}x^3 + \left(\frac{1}{4a}x^2 - \frac{1}{8a^3} \right) \sin 2ax + \frac{1}{4a^2}x \cos 2ax + C \quad (\text{ME2.47})$$

$$\int (\sin^3 ax)dx = -\frac{3 \cos ax}{4a} + \frac{\cos 3ax}{12a} + C \quad (\text{ME2.48})$$

$$\int (x^2 \sin ax)dx = \frac{(a^2 x^2 - 2) \cos ax}{a^3} + \frac{2x \sin ax}{a^2} + C \quad (\text{ME2.49})$$

$$\int (x^2 \cos ax)dx = \frac{(a^2 x^2 - 2) \sin ax}{a^3} + \frac{2x \cos ax}{a^2} + C \quad (\text{ME2.50})$$

$$\int x^m e^{ax} dx = \frac{x^m e^{ax}}{a} - \frac{m}{a} \int x^{m-1} e^{ax} dx + C \quad (\text{ME2.51})$$

$$\int \frac{e^{ax}}{x^m} dx = -\frac{1}{m-1} \frac{e^{ax}}{x^{m-1}} + \frac{a}{m-1} \int \frac{e^{ax}}{x^{m-1}} dx + C \quad (\text{ME2.52})$$

$$\int r^2 e^{-ar} dr = -\frac{e^{-ar}}{a^3} (a^2 r^2 + 2ar + 2) + C \quad (\text{ME2.53})$$

The following group includes definite integrals.

$$\int_0^a \sin\left(\frac{n\pi x}{a}\right) \times \sin\left(\frac{m\pi x}{a}\right) dx = \int_0^a \cos\left(\frac{n\pi x}{a}\right) \times \cos\left(\frac{m\pi x}{a}\right) dx = \frac{a}{2} \delta_{mn}$$

$$\text{where } \delta_{mn} \text{ is one if } m = n \text{ and 0 if } m \neq n \quad (\text{ME2.54})$$

$$\int_0^a \left[\sin\left(\frac{n\pi x}{a}\right) \right] \times \left[\cos\left(\frac{n\pi x}{a}\right) \right] dx = 0 \quad (\text{ME2.55})$$

$$\int_0^{\pi} \sin^2 mx \, dx = \int_0^{\pi} \cos^2 mx \, dx = \frac{\pi}{2} \quad (\text{ME2.56})$$

$$\int_0^{\infty} \frac{\sin x}{\sqrt{x}} \, dx = \int_0^{\infty} \frac{\cos x}{\sqrt{x}} \, dx = \sqrt{\frac{\pi}{2}} \quad (\text{ME2.57})$$

$$\int_0^{\infty} x^n e^{-ax} \, dx = \frac{n!}{a^{n+1}} \quad (a > 0, n \text{ positive integer}) \quad (\text{ME2.58})$$

$$\int_0^{\infty} x^{2n} e^{-ax^2} \, dx = \frac{1 \cdot 3 \cdot 5 \cdots (2n-1)}{2^{n+1} a^n} \sqrt{\frac{\pi}{a}} \quad (a > 0, n \text{ positive integer}) \quad (\text{ME2.59})$$

$$\int_0^{\infty} x^{2n+1} e^{-ax^2} \, dx = \frac{n!}{2 a^{n+1}} \quad (a > 0, n \text{ positive integer}) \quad (\text{ME2.60})$$

$$\int_0^{\infty} e^{-ax^2} \, dx = \left(\frac{\pi}{4a} \right)^{1/2} \quad (\text{ME2.61})$$

Commercially available software such as MathematicaTM, MapleTM, MatlabTM, and MathCadTM can evaluate both definite and indefinite integrals.

This page intentionally left blank

MATH ESSENTIAL 3:

Partial Derivatives

Many quantities that we will encounter in physical chemistry are functions of several variables. In that case, we have to reformulate differential calculus to take several variables into account. We define the partial derivative with respect to a specific variable just as we did in Section ME2.2 by treating all other variables indicated by subscripts as constants. For example, consider 1 mol of an ideal gas for which

$$P = f(V, T) = \frac{RT}{V} \quad (\text{ME3.1})$$

Note that P can be written as a function of the two variables V and T . The change in P resulting from a change in V or T is proportional to the following **partial derivatives**:

$$\begin{aligned} \left(\frac{\partial P}{\partial V}\right)_T &= \lim_{\Delta V \rightarrow 0} \frac{P(V + \Delta V, T) - P(V, T)}{\Delta V} = \lim_{\Delta V \rightarrow 0} \frac{R}{\Delta V} \left(\frac{1}{V + \Delta V} - \frac{1}{V} \right) \\ &= \lim_{\Delta V \rightarrow 0} \frac{R}{\Delta V} \left(\frac{-\Delta V}{V^2 + V\Delta V} \right) = -\frac{RT}{V^2} \\ \left(\frac{\partial P}{\partial T}\right)_V &= \lim_{\Delta T \rightarrow 0} \frac{P(V, T + \Delta T) - P(V, T)}{\Delta T} = \lim_{\Delta T \rightarrow 0} \frac{1}{\Delta T} \left[\frac{R(T + \Delta T)}{V} - \frac{RT}{V} \right] \\ &= \frac{R}{V} \end{aligned} \quad (\text{ME3.2})$$

The subscript y in $(\partial f / \partial x)_y$ indicates that y is being held constant in the differentiation of the function f with respect to x . The partial derivatives in Equation (ME3.2) allow one to determine how a function changes when all of the variables change. For example, what is the change in P if the values of T and V both change? In this case, P changes to $P + dP$ where

$$dP = \left(\frac{\partial P}{\partial T}\right)_V dT + \left(\frac{\partial P}{\partial V}\right)_T dV = \frac{R}{V}dT - \frac{RT}{V^2}dV \quad (\text{ME3.3})$$

Consider the following practical illustration of Equation (ME3.3). You are on a hill and have determined your altitude above sea level. How much will the altitude (denoted z) change if you move a small distance east (denoted by x) and north (denoted by y)? The change in z as you move east is the slope of the hill in that direction, $(\partial z / \partial x)_y$, multiplied by the distance dx that you move. A similar expression can be written for the change in altitude as you move north. Therefore, the total change in altitude is the sum of these two changes or

$$dz = \left(\frac{\partial z}{\partial x}\right)_y dx + \left(\frac{\partial z}{\partial y}\right)_x dy \quad (\text{ME3.4})$$

The first term is the slope of the hill in the x direction, and the second term is the slope in the y direction. These changes in the height z as you move first along the x direction and then along the y direction are illustrated in Figure ME3.1. Because the slope of the hill is a function of x and y , this expression for dz is only valid for small changes dx and dy . Otherwise, higher-order derivatives need to be considered.

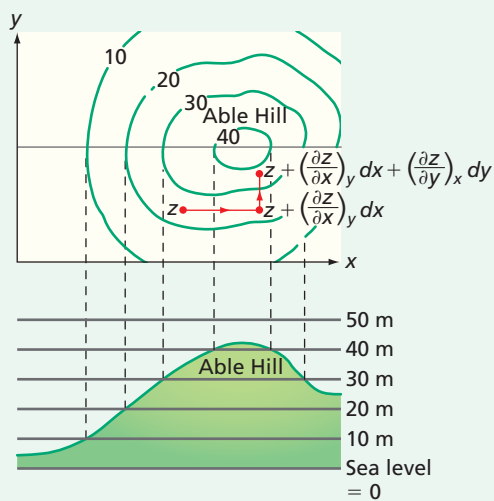


Figure ME3.1

Able Hill contour plot and cross section. The cross section (bottom) is constructed from the contour map (top). Starting at the point labeled z on the hill, you first move in the positive x direction and then along the y direction. If dx and dy are sufficiently small, the change in height dz is given by $dz = \left(\frac{\partial z}{\partial x}\right)_y dx + \left(\frac{\partial z}{\partial y}\right)_x dy$.

Second or higher derivatives with respect to either variable can also be taken. The mixed second partial derivatives are of particular interest. Consider the two mixed second partial derivatives of P :

$$\left(\frac{\partial}{\partial T} \left(\frac{\partial P}{\partial V} \right)_T \right)_V = \frac{\partial^2 P}{\partial T \partial V} = \left(\partial \left(\frac{\partial \left[\frac{RT}{V} \right]}{\partial V} \right)_T \right) \Bigg/ \partial T \Bigg|_V = \left(\partial \left[-\frac{RT}{V^2} \right] \right) \Bigg/ \partial T \Bigg|_V = -\frac{R}{V^2}$$

$$\left(\frac{\partial}{\partial V} \left(\frac{\partial P}{\partial T} \right)_V \right)_T = \frac{\partial^2 P}{\partial T \partial V} = \left(\partial \left(\frac{\partial \left[\frac{RT}{V} \right]}{\partial T} \right)_V \right) \Bigg/ \partial V \Bigg|_T = \left(\partial \left[\frac{R}{V} \right] \right) \Bigg/ \partial V \Bigg|_T = -\frac{R}{V^2}$$
(ME3.5)

For all state functions f and for the specific case of P , the order in which the function is doubly differentiated does not affect the outcome, and we conclude that

$$\left(\frac{\partial}{\partial T} \left(\frac{\partial f(V, T)}{\partial V} \right)_T \right)_V = \left(\frac{\partial}{\partial V} \left(\frac{\partial f(V, T)}{\partial T} \right)_V \right)_T$$
(ME3.6)

Because Equation (ME3.5) is only satisfied by state functions f , it can be used to determine if a function f is a state function. If f is a state function, one can write $\Delta f = \int_i^f df = f_{final} - f_{initial}$. This equation states that f can be expressed as an infinitesimal quantity, df , that, when integrated, depends only on the initial and final states; df is called an exact differential.

We can illustrate these concepts with the following calculation.

PROBLEM

- a. Calculate

$$\left(\frac{\partial f}{\partial x} \right)_y, \left(\frac{\partial f}{\partial y} \right)_x, \left(\frac{\partial^2 f}{\partial x^2} \right)_y, \left(\frac{\partial^2 f}{\partial y^2} \right)_x, \left(\frac{\partial \left(\frac{\partial f}{\partial x} \right)_y}{\partial y} \right)_x, \text{ and } \left(\frac{\partial \left(\frac{\partial f}{\partial y} \right)_x}{\partial x} \right)_y$$

for the function $f(x, y) = ye^x + xy + x \ln y$.

- b. Determine if $f(x, y)$ is a state function of the variables x and y .

- c. If $f(x, y)$ is a state function of the variables x and y , what is the total differential df ?

Solution

$$\mathbf{a.} \quad \left(\frac{\partial f}{\partial x} \right)_y = ye^x + y + \ln y, \quad \left(\frac{\partial f}{\partial y} \right)_x = e^x + x + \frac{x}{y}$$

$$\left(\frac{\partial^2 f}{\partial x^2} \right)_y = ye^x, \quad \left(\frac{\partial^2 f}{\partial y^2} \right)_x = -\frac{x}{y^2}$$

$$\left(\frac{\partial \left(\frac{\partial f}{\partial x} \right)_y}{\partial y} \right)_x = e^x + 1 + \frac{1}{y}, \quad \left(\frac{\partial \left(\frac{\partial f}{\partial y} \right)_x}{\partial x} \right)_y = e^x + 1 + \frac{1}{y}$$

- b.** Because we have shown that

$$\left(\frac{\partial \left(\frac{\partial f}{\partial x} \right)_y}{\partial y} \right)_x = \left(\frac{\partial \left(\frac{\partial f}{\partial y} \right)_x}{\partial x} \right)_y$$

$f(x, y)$ is a state function of the variables x and y . Generalizing this result, any well-behaved function that can be expressed in analytical form is a state function.

- c.** The total differential is given by

$$\begin{aligned} df &= \left(\frac{\partial f}{\partial x} \right)_y dx + \left(\frac{\partial f}{\partial y} \right)_x dy \\ &= (ye^x + y + \ln y)dx + \left(e^x + x + \frac{x}{y} \right)dy \end{aligned}$$

MATH ESSENTIAL 4: Infinite Series

ME4.1 INTRODUCTION TO INFINITE SERIES

An infinite series expresses a function as a sum of terms such as

$$f(x) = b_0 + b_1x + b_2x^2 + b_3x^3 + b_4x^4 + b_5x^5 + \dots \quad (\text{ME4.1})$$

The three dots at the end of the series signify an ellipsis and indicate that the number of terms is infinite. The sum of the first n terms of an infinite series is called the n th partial sum. If as $n \rightarrow \infty$ the n th partial sum approaches a definite finite value, we say that the series converges. If this criterion is not satisfied, we say that the series diverges. For example, consider the following infinite series in which x is a positive integer

$$\sum_{n=1}^{\infty} \frac{1}{x(x+1)} = \frac{1}{2} + \frac{1}{6} + \frac{1}{12} + \frac{1}{20} + \dots \quad (\text{ME4.2})$$

The first four partial sums of this series are

$$S_1 = \frac{1}{2}, \quad S_2 = \frac{2}{3}, \quad S_3 = \frac{3}{4}, \quad S_4 = \frac{4}{5} \quad (\text{ME4.3})$$

We can see from this sequence of partial sums that the n th partial sum and its limit as $n \rightarrow \infty$ are given by

$$S_n = \frac{n}{n+1}, \quad \text{and} \quad \lim_{n \rightarrow \infty} S_n = 1 \quad (\text{ME4.4})$$

Because $\lim_{n \rightarrow \infty} S_n = 1$, the series converges.

Another test of convergence for a series is the ratio test. If the ratio of two consecutive terms in the series is less than one, the series converges. For the series in Equation (ME4.2)

$$\frac{1}{(x+1)(x+2)} / \frac{1}{x(x+1)} = \frac{x(x+1)}{(x+1)(x+2)} < 1 \quad (\text{ME4.5})$$

and therefore this series converges.

ME4.2 POWER SERIES

The power series is a particularly important type of series that is frequently used to fit experimental data to a functional form. It has the form

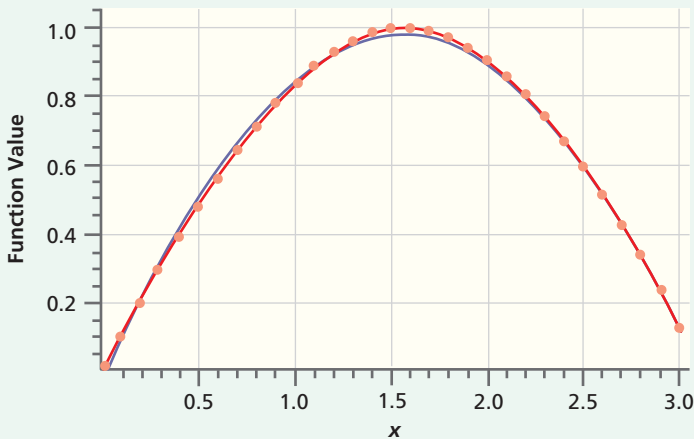
$$a_0 + a_1x + a_2x^2 + a_3x^3 + a_4x^4 + \dots = \sum_{n=0}^{\infty} a_n x^n \quad (\text{ME4.6})$$

This series converges if $x < 1$. Fitting a data set to a series with a large number of terms is impractical, and to be useful, the series should contain as few terms as possible to satisfy the desired accuracy. For example, the data points shown in Figure ME4.1 were fit to a power series over the interval $0 \leq x \leq 3.0$, including three and six terms. The best fit series are as follows.

$$\sin x = -0.03418 + 1.2611x - 0.3889x^2$$

$$\sin x = 0.00003281 + 0.9988x + 0.006823x^2 - 0.1803x^3 + 0.01178x^4 + 0.004321x^5 \quad (\text{ME4.7})$$

- ME4.1** Introduction to Infinite Series
- ME4.2** Power Series
- ME4.3** Taylor–Maclaurin Series
- ME4.4** Fourier Sine and Cosine Series

**Figure ME4.1**

Data points and the best fit power series given by Equation ME4.2. The circles are data points for the function $\sin x$. The blue curve is generated by the three term series in Equation (ME4.7). The orange curve is generated by the six term series in Equation (ME4.7). Small deviations from the data can be seen for the three-term expansion. The deviations of the six-term expansion from the data are too small to be seen.

The coefficients in Equation ME4.7 have been determined using a least squares fitting routine. The first series includes terms in x to x^2 and is accurate to within 4% over the interval. The second series includes terms to x^5 and is accurate to within 0.06% over the interval. In general, including more terms in a series will increase accuracy.

ME4.3 TAYLOR–MACLAURIN SERIES

If the functional form of $f(x)$ is known, it can be expanded about a point of interest $x = a$ using the Taylor–Maclaurin expansion, a special form of a power series, given by

$$\begin{aligned} f(x) &= f(a) + \left(\frac{df(x)}{dx} \right)_{x=a} (x - a) + \frac{1}{2!} \left(\frac{d^2f(x)}{dx^2} \right)_{x=a} (x - a)^2 \\ &\quad + \frac{1}{3!} \left(\frac{d^3f(x)}{dx^3} \right)_{x=a} (x - a)^3 + \dots \end{aligned} \quad (\text{ME4.8})$$

For example, consider the expansion of $f(x) = e^x$ about $x = 0$. Because $(d^n e^x / dx^n)_{x=0} = 1$ for all values of n , the Taylor–Maclaurin expansion for e^x about $a = 0$ is

$$f(x) = 1 + x + \frac{1}{2!}x^2 + \frac{1}{3!}x^3 + \dots \quad (\text{ME4.9})$$

Similarly, the Taylor–Maclaurin expansion for $\ln(1 + x)$ is found by obtaining the derivatives in turn:

$$\begin{aligned} \frac{d \ln(1 + x)}{dx} &= \frac{1}{1 + x} \\ \frac{d^2 \ln(1 + x)}{dx^2} &= \frac{d}{dx} \frac{1}{(1 + x)} = -\frac{1}{(1 + x)^2} \\ \frac{d^3 \ln(1 + x)}{dx^3} &= -\frac{d}{dx} \frac{1}{(1 + x)^2} = \frac{2}{(1 + x)^3} \\ \frac{d^4 \ln(1 + x)}{dx^4} &= \frac{d}{dx} \frac{2}{(1 + x)^3} = \frac{-6}{(1 + x)^4} \end{aligned} \quad (\text{ME4.10})$$

Each of these derivatives must be evaluated at $x = 0$.

TABLE ME4.1 Values for Series Expansion of $\ln(1 + x)$ compared with Exact Values

Number of Terms in Series	$x = 0$	$x = 0.05$	$x = 0.10$	$x = 0.15$	$x = 0.20$	$x = 0.25$	$x = 0.30$	$x = 0.35$	$x = 0.40$	$x = 0.45$	$x = 0.50$
two	0	0.0488	0.0950	0.139	0.180	0.219	0.255	0.289	0.320	0.349	0.375
four	0	0.0488	0.0953	0.140	0.182	0.223	0.262	0.300	0.335	0.369	0.401
exact	0	0.0488	0.0953	0.140	0.182	0.223	0.262	0.300	0.336	0.372	0.405

Using these results, we find that the Taylor–Maclaurin expansion for $\ln(1 + x)$ about $x = 0$ is

$$f(x) = x - \frac{x^2}{2!} + \frac{2x^3}{3!} - \frac{6x^4}{4!} + \dots = x - \frac{x^2}{2} + \frac{x^3}{3} - \frac{x^4}{4} + \dots \quad (\text{ME4.11})$$

The number of terms that must be included to adequately represent the function depends on the function and value of x . Table ME4.1 shows the value obtained for the series expansion of $\ln(1 + x)$, including only the first two terms and the first four terms for different values of x , together with the exact value. It is seen that for $x < 0.25$, the two-term expansion gives good results. For $x = 0.50$, the relative error defined as $\frac{|f(x)_{\text{exact}} - f(x)_{\text{series}}|}{f(x)_{\text{exact}}}$ of the two- and four-term expansion is 7% and 1%, respectively.

Taylor–Maclaurin expansions for other commonly encountered functions about $x = 0$ are as follows.

$$\begin{aligned} \frac{1}{1+x} &= -x + x^2 - x^3 + x^4 + \dots \\ e^x &= 1 + x + \frac{x^2}{2!} + \frac{x^3}{3!} + \frac{x^4}{4!} + \dots \\ e^{ix} &= 1 + ix - \frac{x^2}{2!} - i\frac{x^3}{3!} + \frac{x^4}{4!} + i\frac{x^5}{5!} \dots \quad (\text{ME4.12}) \\ \sin x &= x - \frac{x^3}{3!} + \frac{x^5}{5!} - \frac{x^7}{7!} + \dots \\ \cos x &= 1 - \frac{x^2}{2!} + \frac{x^4}{4!} - \frac{x^6}{6!} + \dots \end{aligned}$$

Note that the sine and cosine functions have the appropriate symmetry; namely, $\sin(-x) = -\sin x$ and $\cos(-x) = \cos x$. Comparing the last three equations, we see that

$$e^{ix} = \cos x + i \sin x \quad (\text{ME4.13})$$

This equation, which will be used frequently, is known as Euler's formula or the Euler relation.

ME4.4 FOURIER SINE AND COSINE SERIES

The Fourier sine and cosine series has the form

$$f(x) = d_0 + \sum_{n=1}^m \left[c_n \sin\left(\frac{n\pi x}{b}\right) + d_n \cos\left(\frac{n\pi x}{b}\right) \right]$$

This series will be discussed in more detail in Section 2.6.

This page intentionally left blank

From Classical to Quantum Mechanics

WHY is this material important?

In this chapter, we will discuss a series of experiments carried out in the first part of the 20th century that overturned many assumptions held by physicists. At the time, physicists assumed that waves and particles were distinct and separate. However, the new round of experiments demonstrated that at the atomic level waves and particles are two manifestations of the same phenomenon. The concept of wave–particle duality was the first step in the formulation of quantum mechanics, which became, and still is, the conceptual model for understanding the properties of atoms and molecules.

WHAT are the most important concepts and results?

Atoms consist of a small, positively charged nucleus surrounded by a diffuse cloud of negatively charged electrons. The energy of atoms and molecules is restricted to a discrete set of energy levels. Waves can manifest as particles and particles as waves. The act of measurement influences the outcome of an experiment.

WHAT would be helpful for you to review for this chapter?

It would be helpful to review the material on series in Math Essential 4.

1.1 WHY STUDY QUANTUM MECHANICS?

Imagine how difficult it would be for humans to function in a world governed by underlying principles without knowing what they were. If we could not calculate the trajectory of a projectile, we could not launch a satellite. Without understanding how energy is transformed into work, we could not design an automobile that gets more mileage for a given amount of fuel. Technology arises from an understanding of matter and energy, which argues for a broad understanding of scientific principles.

Chemistry is a molecular science; the goal of chemists is to understand macroscopic behavior in terms of the properties of individual atoms and molecules. In the first decade of the 20th century, scientists learned that an atom consisted of a small, positively charged nucleus surrounded by a diffuse electron cloud. However, this structure was not compatible with classical physics (the physics of pre-1900), which predicted that the electrons would follow a spiral trajectory and end in the nucleus. Classical physics was also unable to explain why graphite conducts electricity and diamond does not or why the light emitted by a hydrogen discharge lamp appears at only a small number of wavelengths.

These deficiencies in classical physics made it clear that another physical model was needed to describe matter at the microscopic scale of atoms and molecules. During a period of about 20 years, quantum mechanics was developed, and scientists found

- 1.1 Why Study Quantum Mechanics?
- 1.2 Quantum Mechanics Arose out of the Interplay of Experiments and Theory
- 1.3 Blackbody Radiation
- 1.4 The Photoelectric Effect
- 1.5 Particles Exhibit Wave-Like Behavior
- 1.6 Diffraction by a Double Slit
- 1.7 Atomic Spectra and the Bohr Model for the Hydrogen Atom

Concept

The central foundation of quantum mechanics is wave-particle duality.

that the puzzling phenomena just cited can be explained using this new science. The central feature that distinguishes quantum from classical mechanics is wave–particle duality. At the atomic level, electrons, protons, and light all behave as wave–particles as opposed to waves or particles. It is the experiment that determines whether wave or particle behavior will be observed.

Although few people may realize it, we are already users of quantum mechanics. We take for granted the stability of the atom with its central positively charged nucleus and surrounding electron cloud, the laser in our BluRay players, the integrated circuit in our computers, and the chemical bonds that link atoms in a molecule. We know that infrared spectroscopy provides a useful way to identify chemical compounds and that nuclear magnetic resonance spectroscopy provides a powerful tool to image internal organs. However, these different types of spectroscopy would not be possible if atoms and molecules could have *any* value of energy as is predicted by classical physics. Quantum mechanics predicts that atoms and molecules can only have discrete energies and provides a common basis for understanding all spectroscopic techniques.

Many areas of modern technology such as integrated circuits in electronics were developed based on an understanding of quantum mechanics. Quantum mechanical calculations of the chemical properties of pharmaceutical molecules are now sufficiently accurate that in many cases molecules are designed for a specific application before they are tested at the laboratory bench. Quantum computing, in which a logic state can be described by zero *and* one rather than zero *or* one, is a very active area of research. When quantum computers are realized, they will be much more powerful than current computers. As many sciences such as biology become increasingly focused on the molecular level, more scientists will need to be able to think in terms of quantum-mechanical models. Therefore, a basic understanding of quantum mechanics is an essential part of the chemist’s knowledge base.

1.2 QUANTUM MECHANICS AROSE OUT OF THE INTERPLAY OF EXPERIMENTS AND THEORY

Scientific theories gain acceptance if they help us to understand the world around us. A key feature of validating theories is to compare the result of new experiments with the prediction of currently accepted theories. If the experiment and the theory agree, we gain confidence in the model underlying the theory; if not, the model needs to be modified. At the end of the 19th century, Maxwell’s electromagnetic theory unified existing knowledge in the areas of electricity, magnetism, and waves. This theory, combined with the well-established field of Newtonian mechanics, ushered in a new era of maturity for the physical sciences. Many scientists of that era believed that there was little left in the natural sciences to learn. However, the growing ability of scientists to probe natural phenomena at an atomic level soon showed that this presumption was incorrect. The field of quantum mechanics arose in the early 1900s as scientists became able to investigate natural phenomena at the newly accessible atomic level. A number of key experiments showed that the predictions of classical physics were inconsistent with certain experimental outcomes. Several of these experiments are described in more detail in this chapter in order to show the important role that experiments have had—and continue to have—in stimulating the development of theories to describe the natural world.

The rest of this chapter presents experimental evidence for two key properties that have come to distinguish classical and quantum physics. The first of these is **quantization**. Energy at the atomic level is not a continuous variable but occurs in discrete packets called *quanta*. The second key property is **wave–particle duality**. At the atomic level, light waves have particle-like properties, and atoms, as well as subatomic particles such as electrons, have wave-like properties. Neither quantization nor wave–particle duality was a recognized concept until the experiments described in Sections 1.3 through 1.7 were conducted.

Concept

At the atomic level, energy is quantized rather than continuous, which is the case for macroscopic scale phenomena.

1.3 BLACKBODY RADIATION

Think of the heat that a person feels from the embers of a fire. The energy that the body absorbs is radiated from the glowing coals. An idealization of this system that is more amenable to theoretical study is a red-hot block of metal with a spherical cavity in its interior. The cavity can be observed through a hole small enough that the conditions inside the block are not perturbed. An ideal blackbody absorbs all radiation falling on it, at all wavelengths. When a blackbody is at a uniform temperature, its emission has a characteristic frequency distribution that depends only on its temperature. A schematic depiction of blackbody radiation is shown in Figure 1.1. Under the condition of equilibrium between the radiation field inside the cavity and the glowing piece of matter, classical electromagnetic theory can predict what frequencies ν of light are radiated in the form of **blackbody radiation** and their relative magnitudes. The resulting expression is

$$\rho(\nu, T) d\nu = \frac{8\pi\nu^2}{c^3} \bar{E}_{osc} d\nu \quad (1.1)$$

In this equation, ρ is the **spectral density**, which has the units of energy \times (volume) $^{-1}$ \times (frequency) $^{-1}$. The spectral density is a function of temperature T and frequency ν . The speed of light is c , and \bar{E}_{osc} is the average energy of an oscillating dipole in the solid. In words, the spectral density is the energy stored in the electromagnetic field of the blackbody radiator at frequency ν per unit volume and unit frequency.

The factor $d\nu$ is used on both sides of this equation because we are asking for the energy density observed within the frequency interval of width $d\nu$ centered at the frequency ν . Classical theory further predicts that the average energy of an oscillator is simply related to the temperature by

$$\bar{E}_{osc} = k_B T \quad (1.2)$$

in which k is the Boltzmann constant. Combining these two equations results in an expression for $\rho(\nu, T) d\nu$, the amount of energy per unit volume in the frequency range between ν and $\nu + d\nu$ in equilibrium with a blackbody at temperature T :

$$\rho(\nu, T) d\nu = \frac{8\pi k_B T \nu^2}{c^3} d\nu \quad (1.3)$$

It is possible to measure the spectral density of the radiation emitted by a blackbody. The results are shown in Figure 1.2 for several temperatures, together with a result predicted by classical theory. The experimental curves have a common behavior. The spectral density is peaked in a broad maximum and falls off at both lower and higher frequencies. The shift of the maxima to higher frequencies with increasing temperatures is consistent with our experience that if more power is put into an electrical heater, its color will change from dull red to yellow (increasing frequency).

The comparison of the spectral density distribution predicted by classical theory with that observed experimentally for $T = 6000$. K is particularly instructive. The two curves show similar behavior at low frequencies, but the theoretical curve continues to increase with frequency as Equation (1.3) predicts. Because the area under the $\rho(\nu, T)$ versus ν curves gives the total energy per unit volume of the field of the blackbody, classical theory predicts that a blackbody will emit an infinite amount of energy at all temperatures greater than absolute zero! It is clear that this prediction is incorrect, but scientists at the beginning of the 20th century were greatly puzzled about where the theory went wrong.

In considering data such as that shown in Figure 1.2, the German physicist Max Planck (1858–1947) was able to develop important insights that ultimately led to an understanding of blackbody radiation. It was understood at the time that the origin of blackbody radiation was the vibration of electric dipoles, formed by atomic nuclei and their associated electrons, that emit radiation at the frequency at which they oscillate. Planck saw that the discrepancy between experiment and classical theory occurred at high, but not at low, frequencies. The absence of high-frequency radiation at low temperatures showed that the high-frequency dipole oscillators emitted

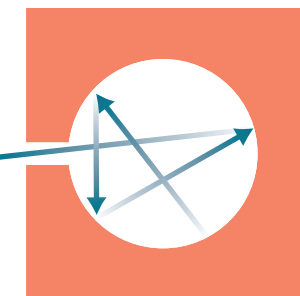


Figure 1.1

An idealized blackbody. A solid metal at a high temperature emits light from an interior spherical surface. The light reflects several times within the solid before emerging through a narrow channel. The reflections ensure that the radiation is in thermal equilibrium with the solid.

Concept

Planck explained the dependence of spectral density on frequency for blackbody radiation by assuming that the energy radiated was quantized.

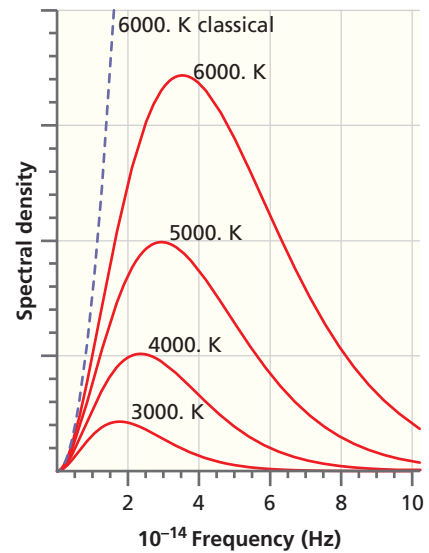
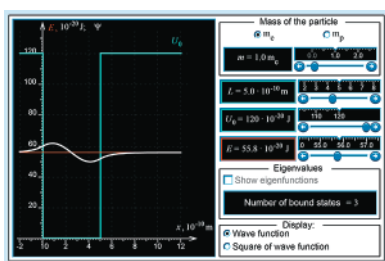


Figure 1.2

Spectral density of radiation emitted by a blackbody at several temperatures. The red curves indicate the light intensity emitted from an ideal blackbody as a function of the frequency for 3000., 4000., 5000., and 6000. K. The dashed curve is that predicted from classical theory for $T = 6000$. K.



W1.1 Blackbody radiation 1
W1.2 Blackbody radiation 2

radiation only at high temperatures. Unless a large amount of energy is put into the blackbody (high temperature), it is not possible to excite the high-energy (high-frequency) oscillators.

Planck found that he could obtain agreement between theory and experiment only if he assumed that the energy radiated by the blackbody was related to the frequency by

$$E = nhv \quad (1.4)$$

The **Planck constant** h was initially an unknown proportionality constant, and n is a positive integer ($n = 1, 2, \dots$). The frequency v is continuous, but for a given v , the energy is *quantized*. Equation (1.4) was a radical departure from classical theory in which the energy stored in electromagnetic waves is proportional to the square of the amplitude but independent of the frequency. This relationship between energy and frequency ushered in a new era of physics. Energy in classical theory is a *continuous* quantity, which means that it can take on all values. Equation (1.4) states that the energy radiated by a blackbody can take on only a set of *discrete* values for each frequency. Its main justification was that agreement between theory and experiment could be obtained. Using Equation (1.4) and some classical physics, Planck obtained the following relationship:

$$\bar{E}_{osc} = \frac{hv}{e^{hv/k_B T} - 1} \quad (1.5)$$

It is useful to obtain an approximate value for \bar{E}_{osc} from this equation in two limits: at high temperatures, where $hv/k_B T \ll 1$, and at low temperatures, where $hv/k_B T > 1$. At high temperatures, the exponential function in Equation (1.5) can be expanded in a Taylor–Maclaurin series, as discussed in Math Essential 4, giving

$$\bar{E}_{osc} = \frac{hv}{(1 + hv/k_B T + \dots) - 1} \approx k_B T \quad (1.6)$$

just as classical theory had predicted. However, for low temperatures corresponding to $hv/k_B T > 1$ the denominator in Equation (1.5) becomes very large, and \bar{E}_{osc} approaches zero. The high-frequency oscillators do not contribute to the radiated energy at low and moderate temperatures.

Using Equation (1.5), in 1901 Planck obtained the following general formula for the spectral radiation density from a blackbody:

$$\rho(v, T)dv = \frac{8\pi hv^3}{c^3} \frac{1}{e^{hv/k_B T} - 1} dv \quad (1.7)$$

The value of the constant h was not known, and Planck used it as a parameter to fit the data. He was able to reproduce the experimental data at all temperatures with the single adjustable parameter h , which through more accurate measurements, currently has the value $h = 6.626070040 \times 10^{-34}$ J s. In calculations in this book, we use only four significant figures. Obtaining this degree of agreement using a single adjustable parameter was a remarkable achievement. However, Planck's explanation, which relied on the assumption that the energy of the radiation came in discrete packets or quanta, was not accepted initially. Soon afterward, Einstein's explanation of the photoelectric effect gave support to Planck's hypothesis.

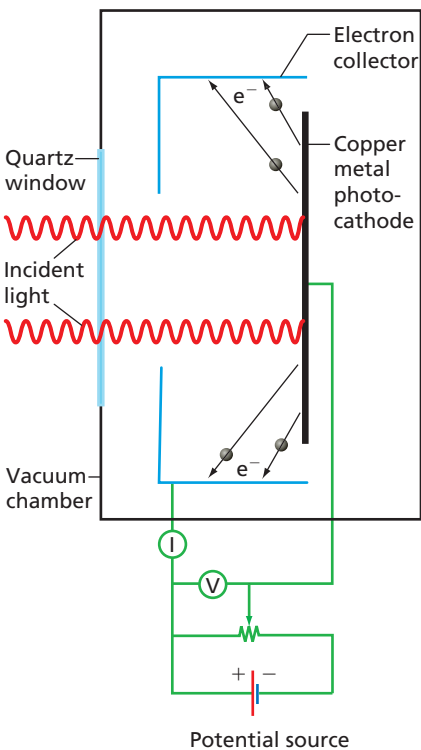


Figure 1.3
Schematic illustration of the photoelectric effect experiment. The electrons emitted by the surface upon illumination are incident on the collector, which is at an appropriate electrical potential to attract them. The experiment is carried out in a vacuum chamber to avoid collisions and capture of electrons by gas molecules.

1.4 THE PHOTOELECTRIC EFFECT

Figure 1.3 schematically depicts an experiment that demonstrates the photoelectric effect. Light is incident on a copper plate in a vacuum system, which we refer to as the photocathode. Some of the light is absorbed, leading to the excitation of electrons in the copper plate to higher energies. Sufficient energy can be transferred to the electrons such that some leave the metal and are ejected into the vacuum. The emitted electrons can be collected by another electrode in the vacuum system, called the collector.

This process of electron ejection by light is called the **photoelectric effect**. The absorbed light energy is equal to the sum of the energy required to eject an electron and the kinetic energy of the emitted electrons because energy is conserved. Classical theory makes the following predictions:

- Light is incident as a plane wave over the whole copper plate. Therefore, the light is absorbed by many electrons in the solid. Any one electron can absorb only a small fraction of the incident light.
- Electrons are emitted to the collector for all light frequencies, provided that the light is sufficiently intense.
- The kinetic energy per emitted electron increases with the light intensity.

The results of the experiment are summarized as follows:

- The number of emitted electrons is proportional to the light intensity, but their kinetic energy is independent of the light intensity.
- No electrons are emitted unless the light frequency ν is above a threshold frequency ν_0 , even for large light intensities.
- The kinetic energy of the emitted electrons depends on the light frequency in the manner depicted in Figure 1.4.
- Electrons are emitted even at such low light intensities that the light absorbed by the entire copper plate is barely enough to eject a single electron, based on energy conservation considerations.

Just as for blackbody radiation, the inability of classical theory to correctly predict experimental results stimulated a new theory. In 1905, Albert Einstein hypothesized that light could be thought of as a stream of particle-like **photons** and that the energy of a photon was proportional to its frequency:

$$E = \beta\nu \quad (1.8)$$

where β is a constant to be determined. This is a marked departure from classical electrodynamics, in which the energy of a light wave and its frequency are independent. Invoking energy conservation, the energy of the ejected electron E_e is related to the energy of the incident photon by

$$E_e = \beta\nu - \phi \quad (1.9)$$

The binding energy of the electron in the solid, which is analogous to the ionization energy of an atom, is designated by ϕ in this equation and is called the **work function**. In words, this equation states that the kinetic energy of the photoelectron that has escaped from the solid is smaller than the photon energy by the amount with which the electron is bound to the solid. Einstein's theory gives a prediction of the dependence of the kinetic energy of the photoelectrons as a function of the light frequency that can be compared directly with experiment. Because ϕ can be determined independently, only β is unknown. It can be obtained by fitting the data points in Figure 1.4 to Equation (1.9). The results shown by the red line in Figure 1.4 not only reproduce the data very well, but they yield the striking result that β , the slope of the line, is identical to the Planck constant h . The equation that relates the energy of light to its frequency

$$E = h\nu \quad (1.10)$$

is one of the most widely used equations in quantum mechanics and earned Albert Einstein a Nobel Prize in physics. A calculation involving the photoelectric effect is carried out in Example Problem 1.1.

The agreement between the theoretical prediction and the experimental data validates Einstein's fundamental assumption that the energy of light is proportional to its frequency. This result also suggested that h is a *universal constant* that appears in seemingly unrelated phenomena. Its appearance in this context gained greater acceptance for the assumptions Planck used to explain blackbody radiation.

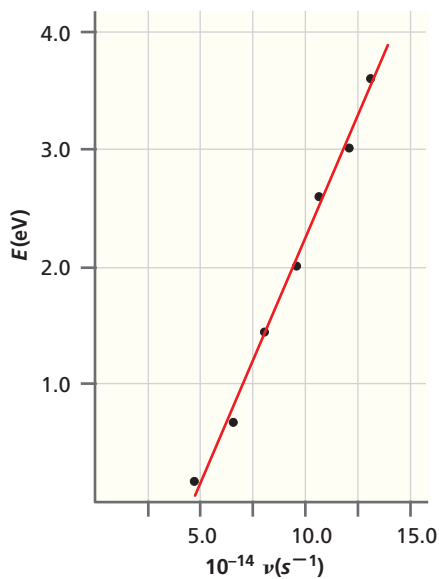


Figure 1.4

Graphical confirmation of the photoelectric effect and determination of the Planck constant. The energy of photoejected electrons is shown as a function of the light frequency. The individual data points are well fit by a straight line, as shown.

Concept

Experiments to elucidate the photoelectric effect provided the first evidence of wave-particle duality for light.

EXAMPLE PROBLEM 1.1

Light with a wavelength of 300. nm is incident on a potassium surface for which the work function ϕ is 2.26 eV. Calculate the kinetic energy and speed of the ejected electrons.

Solution

Using Equation (1.9), we write $E_e = h\nu - \phi = (hc/\lambda) - \phi$ and convert the units of ϕ from electron-volts to joules: $\phi = (2.26\text{eV})(1.602 \times 10^{-19}\text{J/eV}) = 3.62 \times 10^{-19}\text{J}$. Electrons will only be ejected if the photon energy $h\nu$ is greater than ϕ . The photon energy is calculated to be

$$\frac{hc}{\lambda} = \frac{(6.626 \times 10^{-34}\text{J s})(2.998 \times 10^8\text{ m s}^{-1})}{300. \times 10^{-9}\text{m}} = 6.62 \times 10^{-19}\text{ J}$$

which is sufficient to eject electrons.

Using Equation (1.9), we obtain $E_e = (hc/\lambda) - \phi = 3.00 \times 10^{-19}\text{J}$. Using $E_e = 1/2 mv^2$, we calculate that

$$v = \sqrt{\frac{2E_e}{m}} = \sqrt{\frac{2(3.00 \times 10^{-19}\text{J})}{9.109 \times 10^{-31}\text{kg}}} = 8.12 \times 10^5\text{ m s}^{-1}$$

Another important conclusion can be drawn from the observation that electrons are emitted from the solid in the photoelectric experiment even at very low intensities. That is, even with intensities so small that all energy incident on the solid surface is only slightly greater than the threshold energy required to yield a single photoelectron, an electron can be emitted. This observation indicates that the light that liberates the photoelectron is not uniformly distributed over the surface. If such uniformity were the case, no individual electron could receive enough energy to escape into the vacuum. The experiment shows that all incident light energy can be concentrated in a single electron excitation. This observation supports the hypothesis that light can be described as a spatially localized packet or photon as well as a wave. Because this spatial localization is characteristic of particles, the conclusion that light can exhibit particle-like behavior under some circumstances is inescapable.

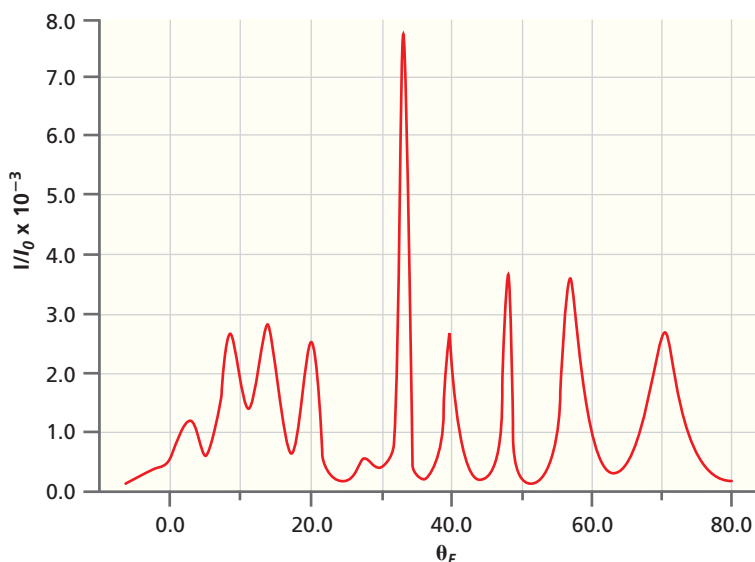
Many experiments have shown that light exhibits wave-like behavior. It has long been recognized that light can be diffracted by an aperture or slit. However, the photon in the photoelectric effect that exhibits particle-like properties and the photon in a diffraction experiment that exhibits wave-like properties are one and the same. We conclude that light is a wave-particle, and depending on the experiment, it can manifest as a wave or as a particle. This important recognition leads us to the third fundamental experiment to be described: the diffraction of electrons by a crystalline solid. Because diffraction is proof of wave-like behavior, if particles such as electrons can be diffracted, they exhibit a particle-wave duality just as light does.

1.5 PARTICLES EXHIBIT WAVE-LIKE BEHAVIOR

In 1924, Louis de Broglie suggested that a relationship that had previously been derived to relate momentum and wavelength for light should also apply to particles. The **de Broglie relation** states that

$$\lambda = \frac{h}{p} \quad (1.11)$$

in which h is the by now familiar Planck constant and p is the particle momentum given by $p = mv$, in which momentum is expressed in terms of the particle mass

**Figure 1.5**

Diffraction produced by a beam of He atoms impinging on a crystal of nickel. The diffraction scan in which I/I_0 is the intensity and θ_f is the diffraction angle was obtained by rotating a mass spectrometer around a nickel single-crystal surface on which a collimated He beam was incident. Each peak corresponds to a different diffraction maximum.

Source: Adapted from D. S. Kaufman et al., *The Journal of Chemical Physics*, Vol. 86, 3682 (1987).

and velocity. This proposed relation was confirmed in 1927 by Clinton Davisson and Lester Germer, who carried out a diffraction experiment. Diffraction is a phenomenon in which the directions and intensities of waves change after passing through an aperture or reflecting from a grating whose characteristic size is approximately the same as the wavelength of the waves. Putting numbers in Equation (1.11) will demonstrate that it is difficult to obtain wavelengths much longer than 1 nm even with particles as light as the electron, as shown in Example Problem 1.2. Therefore, diffraction requires a grating with atomic dimensions, and an ideal candidate is a crystalline solid. Davisson and Germer observed diffraction of electrons from crystalline NiO in their classic experiment to verify the de Broglie relation. The de Broglie relation suggests that diffraction of light atoms should also be possible. Figure 1.5 shows a scan through a diffraction pattern obtained by diffracting a beam of He atoms from a crystal surface of nickel.

EXAMPLE PROBLEM 1.2

Electrons are used to determine the structure of crystal surfaces. To produce diffraction, the wavelength λ of the electrons should be on the order of the lattice constant, which is typically 0.30 nm. What energy do such electrons have, expressed in electron-volts and joules?

Solution

Using Equation (1.11) and the expression $E = p^2/2m$ for the kinetic energy, we obtain

$$\begin{aligned} E &= \frac{p^2}{2m} = \frac{h^2}{2m\lambda^2} = \frac{(6.626 \times 10^{-34} \text{ J s})^2}{2(9.109 \times 10^{-31} \text{ kg})(3.0 \times 10^{-10} \text{ m})^2} \\ &= 2.7 \times 10^{-18} \text{ J or } 17 \text{ eV} \end{aligned}$$

Concept

Diffraction by solid crystals verified wave-particle duality for electrons and light atoms.

The Davisson–Germer experiment was critical in the development of quantum mechanics because it showed that particles exhibit wave behavior. As a consequence, there must be a wave equation that relates the spatial and time dependencies of the wave amplitude for the (wave-like) particle. This equation could be used to describe an atomic-scale system rather than Newton's second law $F = ma$. It was Erwin Schrödinger (1887–1961) who formulated this wave equation, which will be discussed in Chapter 2.

1.6 DIFFRACTION BY A DOUBLE SLIT

Probably no single experiment exhibits the surprising nature of quantum mechanics as well as the diffraction of particles by a double slit. An idealized version of this experiment is described next, but everything in the description has been confirmed by experiments carried out with particles such as neutrons, electrons, and He atoms.

Diffraction is a phenomenon that is widely exploited in science. For example, the atomic-level structure of DNA was determined by analyzing the diffraction of X rays from crystalline DNA samples. Figure 1.6 illustrates diffraction of light from a thin slit in an otherwise opaque wall.

The analysis of this problem is simpler if the screen on which the image is projected is far away from the slit. Mathematically, this requires that $b \gg a$ (see a and b in Figure 1.6). Assuming classical ray optics, the light incident on the slit from the left in Figure 1.6 will generate a sharp image of the slit on the screen. In this case, parallel light is assumed to be incident on the slit and, therefore, the image and slit dimensions are identical. The expected intensity pattern is that shown by the blue curve in the figure. Instead, an intensity distribution akin to that shown by the red curve is observed if the light wavelength is comparable in magnitude to the slit width.

The origin of this pattern of alternating maxima and minima (which lies well outside the profile expected from classical ray optics) is wave interference. Its origin can be understood by treating each point in the plane of the slit as a source of cylindrical waves (Huygens's construction). Maxima and minima arise as a result of a path difference between the sources of the cylindrical waves and the screen, as shown in Figure 1.7. The condition that the minima satisfy is

$$\sin \theta = \frac{n\lambda}{a}, \quad n = \pm 1, \pm 2, \pm 3, \pm \dots \quad (1.12)$$

This equation helps us understand under what conditions we might observe diffraction. The wavelength of light in the middle of the visible spectrum is about 600 nm or 6.00×10^{-4} mm. If this light is allowed to pass through a 1.00-mm-wide slit and the angle calculated at which the first minimum will appear, the result is $\theta = 0.03^\circ$ for $n = 1$. This minimum is not easily observable because it lies so close to the maximum, and we expect to see a sharp image of the slit on our screen, just as in ray optics. However, if the slit width is decreased to 1.00×10^{-2} mm, then $\theta = 3.4^\circ$. This minimum is easily observable, and successive bands of light and darkness will be observed instead of a sharp image. Note that there is no clear demarcation between ray optics and diffraction. The crossover between the two is continuous and depends on the resolution of the experimental techniques. The same behavior is observed if a beam of particles is incident on the slit. If the slit is much wider than the wavelength, diffraction by particles will not be observed, and ray optics holds.

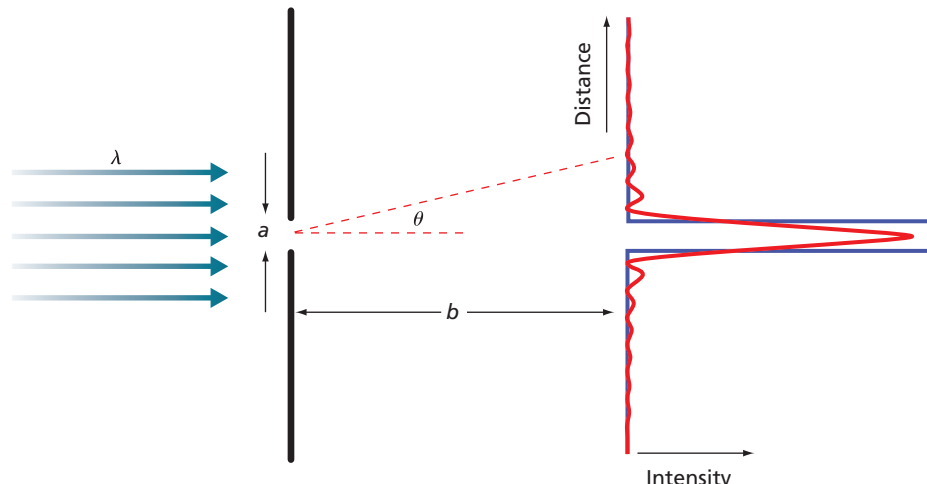
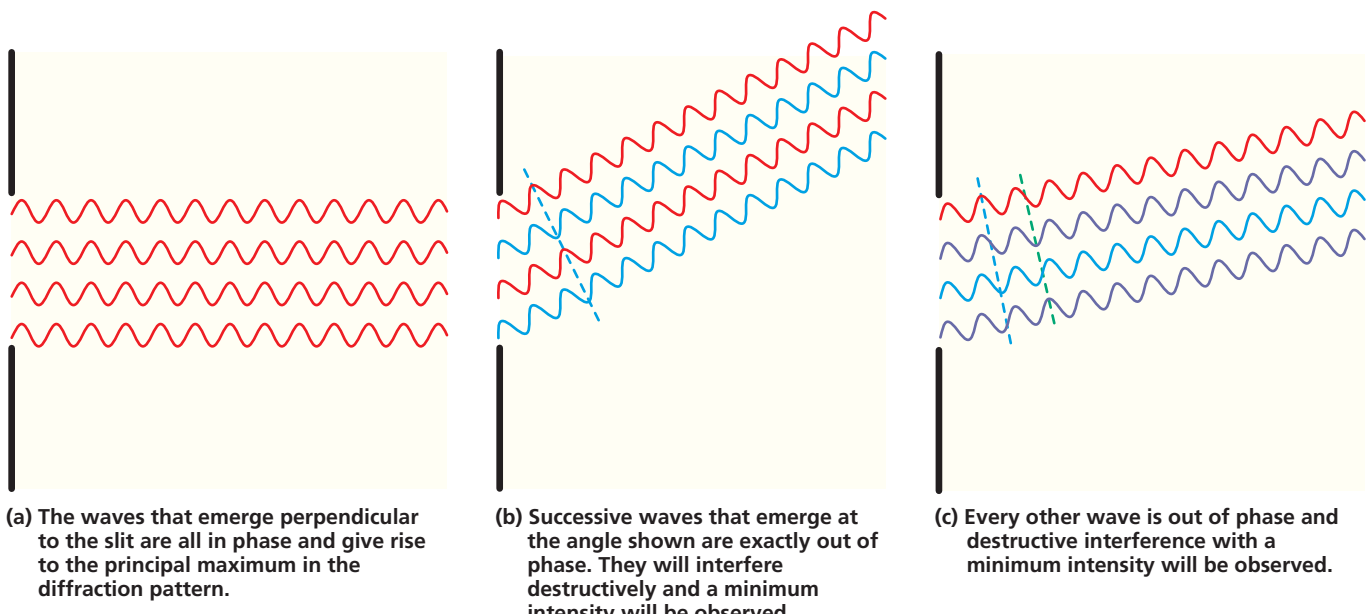


Figure 1.6

Diffraction of light of wavelength λ by a slit. The long axis of the slit is perpendicular to the page. The arrows from the left indicate parallel rays of light incident on an opaque plate containing the slit. Instead of a sharp image of the slit on the screen (blue curve), a diffraction pattern is produced (red curve). This is schematically indicated in a plot of intensity versus distance. In the absence of diffraction, the intensity versus distance indicated by the blue curve would be observed.



Consider the experimental setup designed to detect the diffraction of particles shown in Figure 1.8. The essential feature of the apparatus is a metal plate in which two rectangular slits of width a have been cut. The long axis of the rectangles is perpendicular to the plane of the page. Why two slits? Rather than detecting the diffraction from the individual slits, the apparatus is designed to detect diffraction from the *combination of the two slits*. Diffraction will only be observed when both slits are open (case 2) if the particle passes through both slits simultaneously, which is difficult to imagine from the vantage point of classical physics.

First, we need a source of particles, for instance, an electron gun. By controlling the energy of the electron, the wavelength is varied. Each electron has a **random phase angle** with respect to every other electron. Consequently, two electrons can never interfere with one another to produce a diffraction pattern. One electron gives rise to the diffraction pattern, but many electrons are needed to amplify the signal so that we can see the pattern. A more exact way to make this statement is to say that the intensities of the electron waves—rather than the amplitudes—add together.

Figure 1.7

Wave diffraction, interference, and intensity maximum and minimum. Waves propagate from left to right, through the slit, where waves appear to bend as diffraction occurs. Each segment of a slit through which light is diffracted can be viewed as a source of waves that interfere with one another. (a) All waves in phase. (b) Every other wave out of phase. (c) Successive waves out of phase. The wavelength and slit width are not drawn to scale.

Concept

The outcome of the double slit experiment is consistent with a single particle passing through both slits simultaneously.

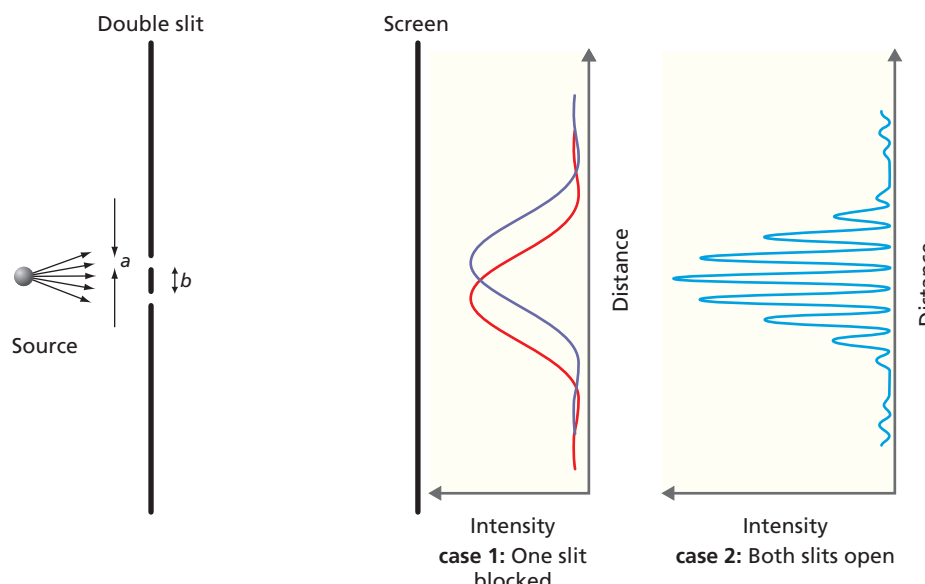


Figure 1.8

The double-slit diffraction experiment. On the left, electrons propagate toward a plate with two slits. Case 1 describes the outcome of the diffraction when one of the slits is blocked. Case 2 describes the outcome when both slits are open.

A phosphorescent screen that lights up when energy from an incident wave or particle is absorbed is mounted behind the plate with the slits. The electron energy is adjusted so that diffraction by a single slit of width a results in broad maxima with the first intensity minimum at a large diffraction angle. The distance between the two slits, b , has been chosen such that we will observe a number of intensity oscillations for small diffraction angles. The diffraction patterns in Figure 1.8 (case 2) were calculated for the ratio $b/a = 5$.

Now let us consider the results and significance of the experiment depicted in Figure 1.8. If one slit is closed and an observer looks at the screen, he or she will see the broad intensity versus distance pattern shown as case 1 in Figure 1.8. (1) Depending on which slit has been closed, the observer sees one of the two diffraction patterns shown and concludes that the electron acts like a wave. (2) If the observer measures the electron current, he or she finds that exactly 50% of electrons impinge on the screen and 50% on the device that blocks one slit for a large number of electrons. (3) When working with very sensitive phosphors, the arrival of each individual electron at the screen is detected by a flash of light localized to a small area of a screen. Which of these three results is consistent with both wave *and* particle behavior, and which is only consistent with wave *or* particle behavior?

In the next experiment, both slits are left open. The result of this experiment is shown in Figure 1.8 as case 2. For very small electron currents, the observer again sees individual light flashes localized to small areas of the screen in a random pattern, which looks like particle behavior. Figure 1.9 shows what the observer would see if the results of a number of these individual electron experiments are stored. However, unmistakable diffraction features in the form of intensity maxima and minima are seen if we accumulate the results of many individual light flashes. These diffraction features demonstrate that a wave (a single electron) is incident on *both* slits simultaneously.

How can the results of this experiment be understood? The fact that diffraction is seen from a single slit as well as from the double slit shows the wave-like behavior of the electron. Yet, individual light flashes are observed on the screen, which is what we expect from particle trajectories. To add to the complexity, the spatial distribution of the individual flashes on the screen is what we expect from waves rather than from particles. The measurement of the electron current to the slit blocker seems to indicate that the electron went *either* through one slit *or* through the other.

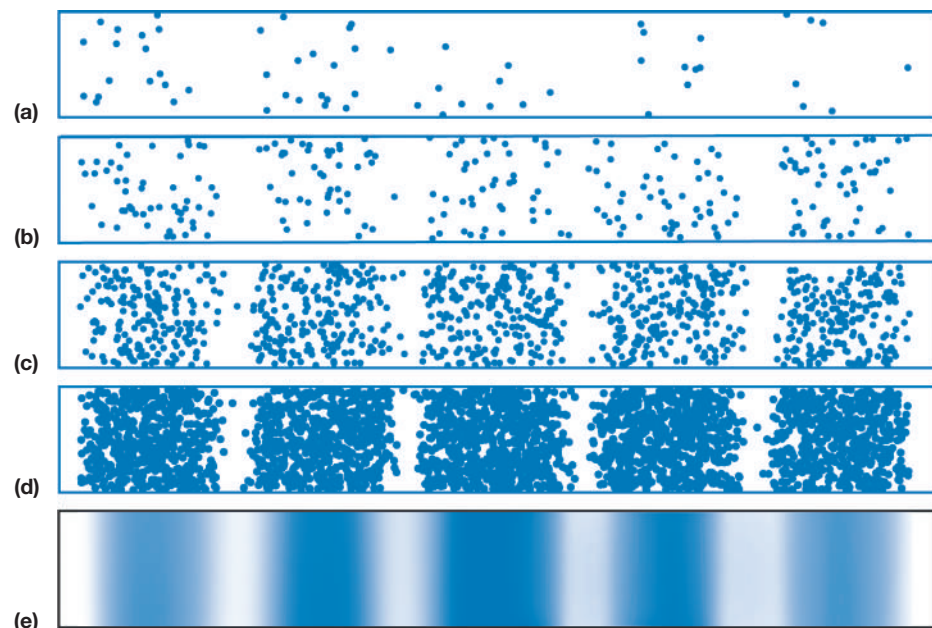


Figure 1.9

Simulation of the diffraction pattern observed in the double-slit experiment. From top to bottom the number of particles is (a) 60, (b) 250, (c) 1000, and (d) 3000. The panel in (e) shows what would be expected for a wave incident on the apparatus. Blue corresponds to high intensity, and white corresponds to low intensity. Note that the diffraction pattern only becomes obvious after a large number of particles have passed through the apparatus, although intensity minima are evident even for 60 incident particles.

However, this conclusion is inconsistent with the appearance of a diffraction pattern because a diffraction pattern only arises if one and the same electron goes through both slits!

Regardless of how we turn these results around, we will find that all the results are inconsistent with the logic of classical physics; namely, the electron passes through one slit or the other. This either/or logic cannot explain the results. In a quantum-mechanical description, the electron wave function is a superposition of wave functions that pass through the top slit and the bottom slit, which is equivalent to saying that the electron can go through both slits. We will have much more to say about wave functions in the next few chapters. The act of measurement, such as blocking one slit, changes the wave function such that the electron passes through either the top slit or the bottom one. The results represent a mixture of particle and wave behavior. That is, individual electrons move through the slits and generate points of light on the screen. This behavior is particle-like. However, the location of the points of light on the screen is not what is expected from classical trajectories; rather, the locations are governed by the diffraction pattern. This behavior is wave-like. Whereas in classical mechanics the operative word concerning several possible modes of behavior is *or*, in quantum mechanics it is *and*. If all of this seems strange at first sight, welcome to the crowd! Although particle diffraction has been observed directly only for atomic and molecular masses up to 20 amu (neon), the de Broglie relation has been verified for molecules as heavy as tetraphenylporphyrin, which has a molecular mass of 614 amu.

1.7 ATOMIC SPECTRA AND THE BOHR MODEL OF THE HYDROGEN ATOM

The most direct evidence of energy quantization comes from analysis of the light emitted from highly excited atoms in a plasma. The structure of the atom was not known until fundamental studies that used the scattering of alpha particles were carried out in Ernest Rutherford's laboratory beginning in 1910. These experiments showed that the positive and negative charges in an atom were separated. The positive charge is contained in the nucleus, whereas the negative charge of the electrons occupies a much greater volume than the nucleus, and the electron volume is centered at the nucleus. In analogy to our solar system, the first picture of the atom that emerged was that of electrons orbiting the nucleus.

However, this picture of the atom is inconsistent with classical electrodynamic theory. An electron orbiting the nucleus is constantly accelerating and must therefore radiate energy. In a classical picture, the electron would continually radiate away its kinetic energy and eventually fall into the nucleus, as depicted in Figure 1.10.

Clearly, electrons were not falling into nuclei. But why not? We will answer this question when we discuss the hydrogen atom in Chapter 9. Even before Rutherford's experiments, it was known that if an electrical arc is placed across a vacuum tube containing a small pressure of hydrogen, light is emitted. Our current picture of this phenomenon is that the atom absorbs energy from the electromagnetic field and makes a transition to an excited state. The excited state has a limited lifetime, and when the transition to a state of lower energy occurs, light is emitted. An apparatus used to obtain atomic spectra, together with a typical spectrum, are shown schematically in Figure 1.11.

How did scientists working in the 1890s explain these spectra? The most important experimental observation they made was that, over a wide range of wavelengths, light emitted from atoms is only observed at certain discrete wavelengths; that is, it is quantized. This result was not understandable on the basis of classical theory because in classical physics, energy is a continuous variable. Even more baffling to these first spectroscopists was their ability to derive a simple relationship to explain all of the frequencies that appeared in the hydrogen emission spectrum. For the emission spectrum

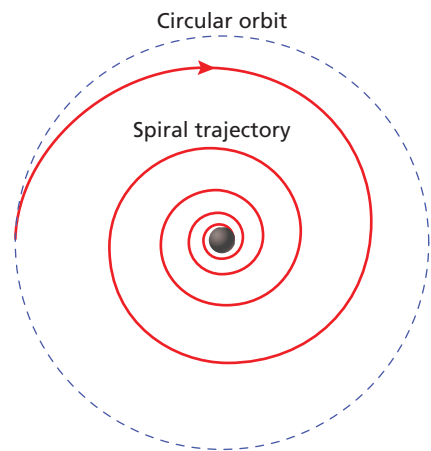
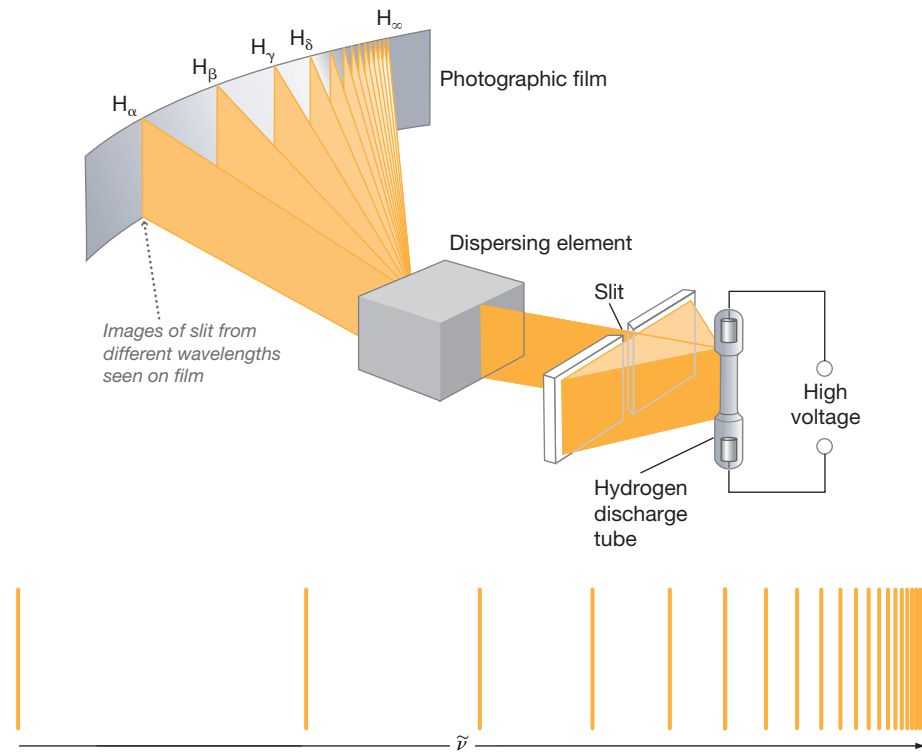


Figure 1.10

Classical physics representation of the electron falling into the nucleus. Classical, particle-based physics predicts that an electron in a circular orbit will lose energy by radiation and spiral into the nucleus.

Figure 1.11

Schematic depiction of a spectrometer and a typical spectrum. Light emitted from a hydrogen discharge lamp is passed through a narrow slit and separated into its component wavelengths by a dispersing element. As a result, multiple images of the slit, each corresponding to a different wavelength, are seen on the photographic film. One of the different series of spectral lines for H is shown at the bottom of the diagram. $\tilde{\nu}$ represents the inverse wavelength [see Equation (1.13)].



observed, the inverse of the wavelength $1/\lambda = \tilde{\nu}$ of all lines in an atomic hydrogen spectrum is given by the following equation

$$\tilde{\nu}(\text{cm}^{-1}) = R_H(\text{cm}^{-1}) \times \left(\frac{1}{n_1^2} - \frac{1}{n^2} \right), n > n_1 \quad (1.13)$$

Concept

The stability of atoms cannot be explained using classical physics.

in which the parameters R_H and n_1 appear. In this equation, n is an integer that takes on the values $n_1 + 1, n_1 + 2, n_1 + 3, \dots$, and R_H is called the **Rydberg constant**, which has the value $109,677.581 \text{ cm}^{-1}$. The experimentalists who derived this equation had no explanation for the relationship between $\tilde{\nu}$ and n .

In 1911 Niels Bohr, who played a seminal role in the development of quantum mechanics, proposed a model for the hydrogen atom that explained its emission spectrum. Even though Bohr's model was superseded by the Schrödinger model described in Chapter 9, it offered the first explanation of how quantized energy levels arise in atoms as a result of wave–particle duality. Bohr assumed a simple model of the hydrogen atom in which an electron revolved around the nucleus in a circular orbit. The orbiting electron experiences two forces: a coulombic attraction to the nucleus and a centrifugal force that is opposite in direction. In a stable orbit, these two forces are equal.

$$\frac{e^2}{4\pi\epsilon_0 r^2} = \frac{m_e v^2}{r} \quad (1.14)$$

In Equation (1.14), e is the charge on the electron, m_e and v are its mass and speed, and r is the orbit radius.

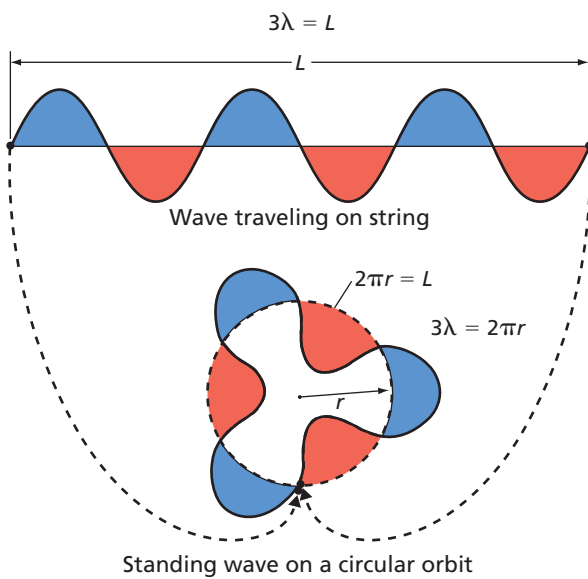
Bohr next introduced wave–particle duality by asserting that the electron had the de Broglie wavelength $\lambda = h/p$. Bohr made a new assumption that the length of an orbit had to be an integral number of wavelengths.

$$2\pi r = n\lambda = n\frac{h}{p} \quad (1.15)$$

which leads to the condition

$$m_e v r = n\hbar, \text{ where } n = 1, 2, 3 \dots \quad (1.16)$$

We have introduced the symbol \hbar for $h/2\pi$. The rationale for Equation (1.15) is shown in Figure 1.12.

**Figure 1.12**

Bohr's rationale for the wave behavior of an electron in his model of the atom. In analogy to a wave on a string (upper image), Bohr postulated a standing wave on a circular orbit (lower image). Unless the circumference of the orbit is an integral number of wavelengths, the wave will cancel itself out.

Bohr reasoned that unless the orbit length is an integral number of wavelengths, the wave will destructively interfere with itself, and the amplitude will decrease to zero in a few orbits. The assertion that there is a stable orbit for the electron contradicts classical physics, which predicts the behavior shown in Figure 1.10.

Solving Equation (1.16) for v and substituting the result in Equation (1.14) yield the following expression for the orbit radius r :

$$r = \frac{\varepsilon_0 h^2 n^2}{\pi m_e e^2} = \frac{4\pi \varepsilon_0 \hbar^2 n^2}{m_e e^2} \quad (1.17)$$

Equation (1.17) shows that an electron can only have certain discrete values for the orbit radii, each corresponding to a different value of n . We next show that the discrete set of orbit radii gives rise to a discrete set of energy levels in Example Problem 1.3.

EXAMPLE PROBLEM 1.3

Calculate the radius of the electron in the hydrogen atom in its lowest energy state, corresponding to $n = 1$.

Solution

$$\begin{aligned} r &= \frac{4\pi \varepsilon_0 \hbar^2 n^2}{m_e e^2} \\ &= \frac{4\pi \times 8.85419 \times 10^{-12} \text{ C}^2 \text{ N}^{-1} \text{ m}^{-2} \times (1.0545 \times 10^{-34} \text{ J s})^2 \times 1^2}{9.109 \times 10^{-31} \text{ kg} \times (1.6022 \times 10^{-19} \text{ C})^2} \\ &= 5.292 \times 10^{-11} \text{ m} \end{aligned}$$

The total energy of the electron in the hydrogen atom is the sum of its kinetic and potential energies.

$$E_{total} = E_{kinetic} + E_{potential} = \frac{1}{2} m_e v^2 - \frac{e^2}{4\pi \varepsilon_0 r} \quad (1.18)$$

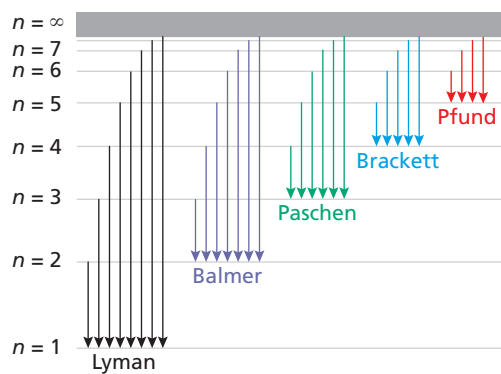
We transform Equation (1.18) into a more useful form by first eliminating v using Equation (1.14).

$$E_{total} = \frac{1}{2} \left(\frac{e^2}{4\pi \varepsilon_0 r} \right) - \left(\frac{e^2}{4\pi \varepsilon_0 r} \right) = -\frac{e^2}{8\pi \varepsilon_0 r} \quad (1.19)$$

Figure 1.13

Electron transitions in the Bohr model and the light emission series they produce.

The series differ in the quantum number of the final state. The shaded bar at the top of the lower portion of the diagram, where $n = \infty$, refers to the ionized atom for which the energy spectrum is continuous.



We next eliminate r using Equation (1.17), obtaining Equation (1.20), which shows that the energy levels in the Bohr model are discrete.

$$E_n = -\frac{m_e e^4}{8\epsilon_0^2 h^2 n^2} \quad n = 1, 2, 3, \dots \quad (1.20)$$

All energy values have negative values because the zero of energy, which is arbitrary, is chosen to correspond to $n \rightarrow \infty$, or to a proton and an electron at infinite separation. The ground state energy, which is the lowest energy that a hydrogen atom can have, corresponds to $n = 1$.

Because the energy of the electron can have only certain discrete values, the light emitted when an electron makes a transition from a higher- to a lower-energy level has a discrete set of frequencies:

$$\nu_{n_2 \rightarrow n_1} = \frac{m_e e^4}{8\epsilon_0^2 h^3} \left(\frac{1}{n_1^2} - \frac{1}{n_2^2} \right) \quad n_2 > n_1 \quad (1.21)$$

Equation (1.21) provides a rationale for the empirical formula given by Equation (1.13). Calculated and measured frequencies for the hydrogen atom are in quantitative agreement with Equation (1.21). This agreement between theory and experiment appears to justify the assumptions made in the Bohr model. A number of possible energy transitions in the Bohr model are shown in Figure 1.13.

Although the Bohr model predicts the absorption and emission frequencies observed in the hydrogen atom, it does not give quantitative agreement with spectra observed for any atom containing more than one electron, for reasons that will become clear in Chapters 10 and 11. There is also a fundamental flaw in the Bohr model that was discovered by Werner Heisenberg (1901–1976) 14 years after the model was introduced. Heisenberg showed that it is not possible to simultaneously know the electron orbit radius and its momentum as Bohr had assumed. We discuss Heisenberg's work on the uncertainty principle in Chapter 6.

VOCABULARY

blackbody

blackbody radiation

de Broglie relation

photoelectric effect

photon

Planck constant

quantization

random phase angle

Rydberg constant

spectral density

wave–particle duality

work function

KEY EQUATIONS

Equation	Significance of Equation	Equation Number
$\rho(v, T) dv = \frac{8\pi k_B T v^2}{c^3} dv$	Classical physics formula for spectral density of blackbody radiation	1.3
$\bar{E}_{osc} = \frac{hv}{e^{hv/k_B T} - 1}$	Energy of oscillators emitting blackbody radiation	1.5
$\rho(v, T) dv = \frac{8\pi h v^3}{c^3} \frac{1}{e^{hv/k_B T} - 1} dv$	Planck formula for spectral density of blackbody radiation	1.7
$E = hv$	Relationship between light frequency and energy of a photon	1.10
$\lambda = \frac{h}{p}$	de Broglie relation between momentum of a particle and its wavelength	1.11
$\tilde{v}(\text{cm}^{-1}) = R_H(\text{cm}^{-1}) \times \left(\frac{1}{n_1^2} - \frac{1}{n_2^2} \right), n > n_1$	Empirical formula for allowed transitions between energy levels of hydrogen atom.	1.13
$v_{n_2 \rightarrow n_1} = \frac{m_e e^4}{8\epsilon_0^2 h^3} \left(\frac{1}{n_1^2} - \frac{1}{n_2^2} \right) n_2 > n_1$	Formula for allowed transitions in hydrogen atom derived from the Bohr model	1.21

CONCEPTUAL PROBLEMS

Q1.1 Why is there an upper limit to the photon energy that can be observed in the emission spectrum of the hydrogen atom?

Q1.2 Why were investigations at the atomic and subatomic levels required to detect the wave nature of particles?

Q1.3 Classical physics predicts that there is no stable orbit for an electron moving around a proton. What criterion did Niels Bohr use to define special orbits that he assumed were stable?

Q1.4 You observe light passing through a slit of width a as lambda decreases from $\lambda \gg a$ to $\lambda \ll a$. Will you observe a sharp transition between ray optics and diffraction? Explain why or why not.

Q1.5 Which of the experimental results for the photoelectric effect suggests that light can display particle-like behavior?

Q1.6 Is the intensity observed from the diffraction experiment depicted in Figure 1.7 the same for the angles shown in parts (b) and (c)?

Q1.7 What feature of the distribution depicted as case 1 in Figure 1.8 tells you that the broad distribution arises from diffraction?

Q1.8 Why does the analysis of the photoelectric effect based on classical physics predict that the kinetic energy of electrons will increase with increasing light intensity?

Q1.9 In the double-slit experiment, researchers found that an equal amount of energy passes through each slit. Does this result allow you to distinguish between purely particle-like and purely wave-like behavior?

Q1.10 The inability of classical theory to explain the spectral density distribution of a blackbody was called the *ultraviolet catastrophe*. Why is this name appropriate?

Q1.11 In the diffraction of electrons by crystals, the depth sampled by the diffracting electrons is on the order of 3 to 10 atomic layers. If He atoms are incident on the surface, only the topmost atomic layer is sampled. Can you explain this difference?

Q1.12 Why is a diffraction pattern generated by an electron gun formed by electrons interfering with themselves rather than with one another?

Q1.13 What did Einstein postulate to explain that the kinetic energy of the emitted electrons in the photoelectric effect depends on the frequency? How does this postulate differ from the predictions of classical physics?

Q1.14 How did Planck conclude that the discrepancy between experiments and classical theory for blackbody radiation was at high and not low frequencies?

Q1.15 Write down formulas relating the wave number with the frequency, wavelength, and energy of a photon.

NUMERICAL PROBLEMS

Section 1.3

P1.1 A more accurate expression for \bar{E}_{osc} would be obtained by including additional terms in the Taylor–Maclaurin series. The Taylor–Maclaurin series expansion of $f(x)$ in the vicinity of x_0 (see Math Essential 4) is given by

$$\begin{aligned} f(x) &= f(x_0) + \left(\frac{df(x)}{dx}\right)_{x=x_0}(x - x_0) \\ &\quad + \frac{1}{2!}\left(\frac{d^2f(x)}{dx^2}\right)_{x=x_0}(x - x_0)^2 \\ &\quad + \frac{1}{3!}\left(\frac{d^3f(x)}{dx^3}\right)_{x=x_0}(x - x_0)^3 + \dots \end{aligned}$$

Use this formalism to better approximate \bar{E}_{osc} by expanding $\frac{h\nu}{e^{h\nu/kT}}$ in powers of $h\nu/kT$ to $(h\nu/kT)^3$ in the vicinity of

$h\nu/kT = 0$. Calculate the relative error, $\frac{\bar{E}_{osc} - kT}{\bar{E}_{osc}}$, that

results without the additional terms for $\nu = 9.00 \times 10^{11} \text{ s}^{-1}$ at temperatures of 1000., 600., and 200. K. Explain the trend you see.

P1.2 Show that the energy density radiated by a blackbody

$$\frac{E_{total}(T)}{V} = \int_0^\infty \rho(\nu, T) d\nu = \int_0^\infty \frac{8\pi h\nu^3}{c^3} \frac{1}{e^{h\nu/kT} - 1} d\nu$$

depends on the temperature as T^4 . (*Hint:* Make the substitution of variables $x = h\nu/kT$.) Use the definite integral $\int_0^\infty [x^3/(e^x - 1)] dx = \pi^4/15$. Using your result, calculate the energy density radiated by a blackbody at 1100. K and 6000. K.

P1.3 In the discussion of blackbody radiation, the average energy of an oscillator $\bar{E}_{osc} = h\nu/(e^{h\nu/kT} - 1)$ was approximated as $\bar{E}_{osc} = h\nu/[(1 + h\nu/kT) - 1] = kT$ for $h\nu/kT \ll 1$. Calculate the relative error $= (E - E_{approx})/E$ in making this approximation for $\nu = 7.50 \times 10^{12} \text{ s}^{-1}$ at temperatures of 5000., 1500., and 300. K. Can you predict what the sign of the relative error will be without a detailed calculation?

P1.4 The distribution in wavelengths of the light emitted from a radiating blackbody is a sensitive function of the temperature. This dependence is used to measure the temperature of hot objects (for example, lava flowing down the slopes of Kilauea Volcano), without making physical contact with those objects, in a technique called *optical pyrometry*. In the limit $(hc/\lambda kT) \gg 1$, the maximum in a plot of $\rho(\lambda, T)$ versus λ is given by $\lambda_{max} = hc/5kT$. At what wavelength does the maximum in $\rho(\lambda, T)$ occur for $T = 675$, 1150., and 6200. K?

P1.5 The power (energy per unit time) radiated by a blackbody per unit area of surface expressed in units of W m^{-2} is given by $P = \sigma T^4$, with $\sigma = 5.67 \times 10^{-8} \text{ W m}^{-2} \text{ K}^{-4}$. The radius of the sun is $6.95 \times 10^5 \text{ km}$, and the surface temperature is 5800. K. Calculate the total energy radiated per second by the sun. Assume ideal blackbody behavior.

P1.6 The power per unit area emitted by a blackbody is given by $P = \sigma T^4$ with $\sigma = 5.67 \times 10^{-8} \text{ W m}^{-2} \text{ K}^{-4}$. Calculate the power radiated by a spherical blackbody of radius 0.500 m at 925 K. What would be the radius of a blackbody at 3000. K if it emitted the same energy as the spherical blackbody of radius 0.500 m at 925 K?

Section 1.4

P1.7 What is the maximum number of electrons that can be emitted from a potassium surface of work function 2.40 eV that absorbs $5.00 \times 10^{-3} \text{ J}$ of radiation at a wavelength of 325 nm? What are the kinetic energy and velocity of the emitted electrons?

P1.8 The following data were observed in an experiment on the photoelectric effect of potassium:

10¹⁹ Kinetic Energy (J)	4.49	3.09	1.89	1.34	0.700	0.311
Wavelength (nm)	250.	300.	350.	400.	450.	500.

Graphically evaluate these data to obtain values for the work function and Planck's constant.

P1.9 The work function of palladium is 5.22 eV. (a) What is the minimum frequency of light required to observe the photoelectric effect on W? (b) If light with a 200. nm wavelength is absorbed by the surface, what is the velocity of the emitted electrons?

Section 1.5

P1.10 When a molecule absorbs a photon, both the energy and momentum are conserved. (a) If a H₂ molecule at 500. K absorbs an ultraviolet photon of wavelength 175 nm, what is the change in its velocity Δv ? (b) Given that its average speed is $v_{rms} = \sqrt{3kT/m}$, what is $\Delta v/v_{rms}$?

P1.11 Calculate the speed of a gas-phase fluorine molecule if it has the same energy as an infrared photon ($\lambda = 1.00 \times 10^4 \text{ nm}$), a visible photon ($\lambda = 500. \text{ nm}$), an ultraviolet photon ($\lambda = 100. \text{ nm}$), and an X-ray photon ($\lambda = 0.100 \text{ nm}$). What temperature will the gas have if it has the same energy as each of these photons? Use the root mean square speed, $v_{rms} = \langle v^2 \rangle^{1/2} = \sqrt{3kT/m}$, for this calculation.

P1.12 What speed does a F₂ molecule have if it has the same momentum as a photon of wavelength 225 nm?

P1.13 A newly developed substance that emits 250. W of photons with a wavelength of 325 nm is mounted in a small rocket initially at rest in outer space such that all of the radiation is released in the same direction. Because momentum is conserved, the rocket will be accelerated in the opposite direction. If the total mass of the rocket is 14.2 kg, how fast will it be traveling at the end of 30.0 days in the absence of frictional forces?

P1.14 Using the root mean square speed, $v_{rms} = \langle v^2 \rangle^{1/2} = \sqrt{3kT/m}$, calculate the gas temperatures of He and Ar for which $\lambda = 0.25$ nm, a typical value needed to resolve diffraction from the surface of a metal crystal. On the basis of your result, explain why Ar atomic beams are not suitable for atomic diffraction experiments.

P1.15 Electrons have been used to determine molecular structure by diffraction. Calculate the speed and kinetic energy of an electron for which the wavelength is equal to a typical bond length, namely, 0.125 nm.

P1.16 For a monatomic gas, one measure of the *average speed* of the atoms is the root mean square speed, $v_{rms} = \langle v^2 \rangle^{1/2} = \sqrt{3kT/m}$, in which m is the molecular mass and k is the Boltzmann constant. Using this formula, calculate the de Broglie wavelength for H₂ and Ar at 200. and at 900. K.

P1.17 A beam of electrons with a speed of 5.25×10^4 m/s is incident on a slit of width 200. nm. The distance to the detector plane is chosen such that the distance between the central maximum of the diffraction pattern and the first diffraction minimum is 0.300 cm. How far is the detector plane from the slit?

P1.18 If an electron passes through an electrical potential difference of 1 V, it has an energy of 1 electron-volt. What potential difference must it pass through in order to have a wavelength of 0.300 nm?

P1.19 X-rays can be generated by accelerating electrons in a vacuum and letting them impact atoms in a metal surface. If the 1250. eV kinetic energy of the electrons is completely converted to the photon energy, what is the wavelength of the X-rays produced? If the electron current is 3.50×10^{-5} A, how many photons are produced per second?

P1.20 Assume that water absorbs light of wavelength 4.20×10^{-6} m with 100% efficiency. How many photons are

required to heat 5.75 g of water by 1.00 K? The heat capacity of water is $75.3 \text{ J mol}^{-1} \text{ K}^{-1}$.

P1.21 A 1000. W gas discharge lamp emits 4.50 W of ultraviolet radiation in a narrow range centered near 275 nm. How many photons of this wavelength are emitted per second?

P1.22 Pulsed lasers are powerful sources of nearly monochromatic radiation. Lasers that emit photons in a pulse of 5.00 ns duration with a total energy in the pulse of 0.175 J at 875 nm are commercially available.

- What is the average power (energy per unit time) in units of watts ($1 \text{ W} = 1 \text{ J/s}$) associated with such a pulse?
- How many 875-nm photons are emitted in such a pulse?

Section 1.7

P1.23 The observed lines in the emission spectrum of atomic hydrogen are given by

$$\tilde{\nu}(\text{cm}^{-1}) = R_H(\text{cm}^{-1}) \left(\frac{1}{n_1^2} - \frac{1}{n^2} \right) \text{cm}^{-1}, n > n_1$$

In the notation favored by spectroscopists, $\tilde{\nu} = 1/\lambda = E/hc$ and $R_H = 109,737 \text{ cm}^{-1}$. The Lyman, Balmer, and Paschen series refer to $n_1 = 1, 2$, and 3 , respectively, for emission from atomic hydrogen. What is the highest value of $\tilde{\nu}$ and E in each of these series?

P1.24 Calculate the highest possible energy of a photon that can be observed in the emission spectrum of H.

P1.25 Calculate the longest and the shortest wavelength observed in the Balmer series.

P1.26 Calculate the longest and the shortest wavelength observed in the Lyman series.

P1.27 A ground state H atom absorbs a photon and makes a transition to the $n = 4$ energy level. It then emits a photon of frequency $1.598 \times 10^{14} \text{ s}^{-1}$. What are the final energy and n value of the atom?

WEB-BASED SIMULATIONS, ANIMATIONS, AND PROBLEMS

Simulations, animations, and homework problem worksheets can be accessed at www.pearsonhighered.com/advchemistry

W1.1 The maximum in a plot of the spectral density of blackbody radiation versus T is determined for a number of values of T using numerical methods. Using these results, we can test the validity of the approximation $\lambda_{\max} = hc/5k_BT$ graphically.

W1.2 The total radiated energy of blackbody radiation is calculated numerically for the temperatures of W1.1. Using these results, we can determine the exponent in the relation $E = CT^\alpha$.

FURTHER READING

Bemstein, J., and Shaik, S. S. "The Wave-Particle Duality: Teaching via a Visual Metaphor." *Journal of Chemical Education* 65 (1988): 339–340.

Haendler, Blanca L. "Presenting the Bohr Atom." *Journal of Chemical Education* 59 (1982): 372–376.

Larsen, Russell D. "The Planck Radiation Functions." *Journal of Chemical Education* 62 (1985): 199–202.

This page intentionally left blank

MATH ESSENTIAL 5: Differential Equations

ME5.1 GENERAL COMMENTS ON DIFFERENTIAL EQUATIONS

Many widely used equations in chemistry and physics such as the Schrödinger equation are differential equations. A differential equation is one that includes a function $f(x)$ as well as its derivatives. The highest order of differentiation is called the order of the equation. A differential equation of n th order has n linearly independent solutions. As equations of order higher than two rarely occur in the physical sciences, we will restrict this discussion to differential equations that have the general form

$$\frac{d^2f(x)}{dx^2} + A(x)\frac{df(x)}{dx} + B(x)f(x) = C(x) \quad (\text{ME5.1})$$

For first-order equations, the first term is absent. Because all of the differential equations that we will encounter have the additional properties that A and B are constants and $C = 0$, we consider only solutions for first- and second-order differential equations which have the form

$$\begin{aligned} \frac{df(x)}{dx} + Af(x) &= 0 \quad \text{and} \\ \frac{d^2f(x)}{dx^2} + B\frac{df(x)}{dx} + Cf(x) &= 0 \end{aligned} \quad (\text{ME5.2})$$

Differential equations of the form in Equation (ME5.2) in which zero appears on the right-hand side are called linear differential equations and have the property that if $u(x)$ and $v(x)$ are solutions of the differential equation, then a linear combination of these solutions, $w(x)$, where a and b are constants, is also a solution.

$$w(x) = au(x) + bv(x) \quad (\text{ME5.3})$$

ME5.2 SOLVING FIRST-ORDER LINEAR DIFFERENTIAL EQUATIONS WITH CONSTANT COEFFICIENTS

First-order ordinary differential equations can be solved by direct integration. For example, consider a chemical reaction in which the rate at which $[A]$ decreases in a unimolecular reaction. The rate equation has the form

$$\frac{d[A(t)]}{dt} = -k[A(t)] \quad (\text{ME5.4})$$

where k is the rate constant. We separate the function A and the variable t on different sides of the equation giving

$$\frac{d[A(t)]}{[A(t)]} = -kdt \quad (\text{ME5.5})$$

- ME5.1** General Comments on Differential Equations
- ME5.2** Solving First-Order Linear Differential Equations with Constant Coefficients
- ME5.3** Solving Second-Order Linear Differential Equations with Constant Coefficients
- ME5.4** Partial Differential Equations

Integrating both sides gives

$$\int \frac{d[A(t)]}{[A(t)]} = -k \int dt \quad (\text{ME5.6})$$

Evaluating the integrals, we obtain

$$\ln[A(t)] = -kt + C \quad (\text{ME5.7})$$

where C is a constant of integration which can be evaluated using boundary conditions. For example, if $[A(t)]$ at $t = 0$ is $[A]_0$,

$$\begin{aligned} \ln[A(t)] &= -kt + [A]_0 \\ A(t) &= [A]_0 e^{-kt} \end{aligned} \quad (\text{ME5.8})$$

ME5.3 SOLVING SECOND-ORDER LINEAR DIFFERENTIAL EQUATIONS WITH CONSTANT COEFFICIENTS

We will consider two methods to solve linear differential equations with constant coefficients. In the first method, we guess the general form of the solution and refine the guess. In the equation

$$\frac{d^2f(x)}{dx^2} + B\frac{df(x)}{dx} + Cf(x) = 0 \quad (\text{ME5.9})$$

we are seeking a solution whereby the second and first derivatives, each multiplied by constants, are added to the solution give zero. This suggests that $f(x)$ has the form $f(x) = e^{mx}$ because we know that $d^n f(x)/dx^n = m^n e^{mx}$. Substituting this guess into Equation (ME5.9), we obtain

$$\begin{aligned} \frac{d^2e^{mx}}{dx^2} + B\frac{de^{mx}}{dx} + Ce^{mx} &= 0 \\ m^2e^{mx} + Bme^{mx} + Ce^{mx} &= 0 \end{aligned} \quad (\text{ME5.10})$$

Canceling the exponential function in each term leaves the quadratic equation

$$m^2 + Bm + C = 0 \quad (\text{ME5.11})$$

We solve the quadratic equation and obtain the condition that m must satisfy to be a solution of the differential equation, namely

$$m = \frac{-B \pm \sqrt{B^2 - 4C}}{2} \quad (\text{ME5.12})$$

The constant m can be real, imaginary, or complex depending on the values of B and C . For example, if $B = 3$ and $C = 2$, m is real and has the values -1 and -2 . The particular solutions to the differential equation are e^{-x} and e^{-2x} , and the general solution is

$$f(x) = c_1 e^{-x} + c_2 e^{-2x} \quad (\text{ME5.13})$$

where c_1 and c_2 are arbitrary constants that can be evaluated from boundary conditions. If $B = 2$ and $C = 2$, m is complex and has the values $-1 + i$ and $-1 - i$. The particular solutions to the differential equation are $e^{-x}e^{ix}$ and $e^{-x}e^{-ix}$, and the general solution is

$$f(x) = c_1 e^{-x}e^{ix} + c_2 e^{-x}e^{-ix} \quad (\text{ME5.14})$$

If $B = 0$ and $C = 2$, m is imaginary and has the values $i\sqrt{2}$ and $-i\sqrt{2}$. The particular solutions to the differential equation are $e^{i\sqrt{2}x}$ and $e^{-i\sqrt{2}x}$, and the general solution is

$$f(x) = c_1 e^{i\sqrt{2}x} + c_2 e^{-i\sqrt{2}x} \quad (\text{ME5.15})$$

The second method for solving linear differential equations involves expressing the solution as a power series in x . We present the method here for completeness, although it is not necessary to use the method in this textbook. To demonstrate this second method, we will apply it to the simple second-order differential equation

$$\frac{d^2f(x)}{dx^2} + f(x) = 0 \quad (\text{ME5.16})$$

and assume that $f(x)$ can be written as the following power series:

$$f(x) = \sum_{n=0}^{\infty} a_n x^n \quad (\text{ME5.17})$$

Substituting this series into Equation (ME5.16), we obtain

$$\sum_{n=2}^{\infty} n(n-1)a_n x^{n-2} + \sum_{n=0}^{\infty} a_n x^n = 0 \quad (\text{ME5.18})$$

We have started the summation in the first expression with $n = 2$ because the expression $n(n-1) = 0$ for $n = 0$ and $n = 1$. We can combine the two summations with the same starting index by rewriting $n(n-1)a_n x^{n-2}$ as $(n+2)(n+1)a_{n+2}x^n$. Convince yourself that the first expression evaluated for $n = 2$ is identical to the second expression evaluated for $n = 0$. Equation (ME5.18) now has the form

$$\sum_{n=0}^{\infty} (n+2)(n+1)a_{n+2}x^n + \sum_{n=0}^{\infty} a_n x^n = \sum_{n=0}^{\infty} \left[\overbrace{(n+2)(n+1)a_{n+2} + a_n}^{=0} \right] x^n = 0 \quad (\text{ME5.19})$$

For the equality to hold, the coefficient in front of x^n in the rightmost summation must be equal to zero for each value of n separately.

$$a_{n+2} = -\frac{a_n}{(n+2)(n+1)} \quad n = 0, 1, 2, 3, \dots \quad (\text{ME5.20})$$

The previous equation gives us a recursion formula for calculating a_{n+2} from a_n . Starting from a_0 , we obtain the values for the higher even-valued coefficients

$$a_2 = -\frac{a_0}{2 \times 1} \quad a_4 = -\frac{a_2}{4 \times 3} = \frac{a_0}{4 \times 3 \times 2 \times 1} = \frac{a_0}{4!} \quad a_6 = -\frac{a_4}{6 \times 5} = -\frac{a_0}{6!} \quad (\text{ME5.21})$$

The general formula for all even coefficients in terms of a_0 is

$$a_{2n} = -\frac{(-1)^n}{(2n)!} a_0 \quad n = 0, 1, 2, 3, \dots \quad (\text{ME5.22})$$

To obtain the odd coefficients, we follow the same procedure starting with $n = 1$ and obtain

$$a_3 = -\frac{a_1}{3 \times 2} \quad a_5 = -\frac{a_3}{5 \times 4} = \frac{a_1}{5!} \quad a_7 = -\frac{a_5}{7 \times 6} = -\frac{a_1}{7!} \quad (\text{ME5.23})$$

and the general formula for odd coefficients

$$a_{2n+1} = -\frac{(-1)^n}{(2n+1)!} a_1 \quad n = 0, 1, 2, 3, \dots \quad (\text{ME5.24})$$

Substituting the general formulas for the coefficients into Equation (ME5.19), we obtain the final result

$$f(x) = a_0 \sum_{n=0}^{\infty} \frac{(-1)^n}{(2n)!} x^{2n} + a_1 \sum_{n=0}^{\infty} \frac{(-1)^n}{(2n+1)!} x^{2n+1} \quad (\text{ME5.25})$$

ME5.4 PARTIAL DIFFERENTIAL EQUATIONS

In previous sections, we have assumed that the function f depends only on a single variable. However, for atoms, the Schrödinger equation has to be formulated in three dimensions as will be discussed in Chapter 9. In this case, partial derivatives rather than simple derivatives appear in the differential equation to be solved. The simplest approach to solving partial differential equations is the separation of variables, in which we assume that the function of several variables can be written as a product of single variable functions. We illustrate this method for a function of two variables. This method suffices for the differential equations explored in this textbook, and partial differential equations that cannot be solved this way often need to be solved using numerical methods.

Consider the partial differential equation

$$\frac{\partial^2 f(x, y)}{\partial x^2} + \frac{\partial^2 f(x, y)}{\partial y^2} + f(x, y) = 0 \quad (\text{ME5.26})$$

We assume that $f(x, y) = g(x)h(y)$. Substituting this expression in the previous equation, we obtain

$$h(y) \frac{d^2 g(x)}{dx^2} + g(x) \frac{d^2 h(y)}{dy^2} + g(x)h(y) = 0 \quad (\text{ME5.27})$$

because in each term one of the functions g and h is constant with respect to the derivative. Dividing by $g(x)h(y)$ gives

$$\begin{aligned} \frac{1}{g(x)} \frac{d^2 g(x)}{dx^2} + \frac{1}{h(y)} \frac{d^2 h(y)}{dy^2} + 1 &= 0 \quad \text{or} \\ -\frac{1}{g(x)} \frac{d^2 g(x)}{dx^2} &= \frac{1}{h(y)} \frac{d^2 h(y)}{dy^2} \end{aligned} \quad (\text{ME5.28})$$

For the last equation to hold for all values of x and y , it must be true that

$$\begin{aligned} \frac{1}{g(x)} \frac{d^2 g(x)}{dx^2} &= c_1 \quad \text{and} \\ \frac{1}{h(y)} \frac{d^2 h(y)}{dy^2} &= c_2 \quad \text{with} \quad c_1 + c_2 = -1 \end{aligned} \quad (\text{ME5.29})$$

where c_1 and c_2 are arbitrary constants.

We see that the original partial differential equation has been reduced to two ordinary differential equations that can be solved by the methods described in previous sections.

MATH ESSENTIAL 6:

Complex Numbers and Functions

ME6.1 WORKING WITH COMPLEX NUMBERS

Complex numbers can be written in the form

$$z = a + ib \quad (\text{ME6.1})$$

where a and b are real numbers and $i = \sqrt{-1}$. The complex conjugate of a complex number z is designated by z^* and is obtained by changing the sign of i , wherever it appears in the complex number. The magnitude of a complex number is defined by $\sqrt{zz^*}$ and is always a real number.

It is useful to represent complex numbers in the complex plane shown in Figure ME6.1. The vertical and horizontal axes correspond to the imaginary and real parts of z , respectively. As shown in Figure ME6.1, a complex number corresponds to a point in the complex plane. Note the similarity to the polar coordinate system. Because of this analogy, a complex number can be represented either as the pair (a, b) or by the radius vector r and the angle θ . From Figure ME6.1, it can be seen that

$$r = \sqrt{a^2 + b^2} \quad \text{and} \quad \phi = \arctan \frac{b}{a} \quad (\text{ME6.2})$$

Using the relations between a , b , and r as well as the Euler relation $e^{i\phi} = \cos \phi + i \sin \phi$, we can represent a complex number in one of four equivalent ways:

$$a + ib = r \cos \phi + ir \sin \phi = re^{i\phi} = \sqrt{a^2 + b^2} \exp [i \arctan(b/a)] \quad (\text{ME6.3})$$

When calculating ϕ on a hand-held calculator, a problem arises in that the calculator cannot distinguish between $-b/a$ and $b/(-a)$ as well as b/a and $(-b)/(-a)$ because only the sign of the ratio b/a can be entered. Programs such as Mathematica allow

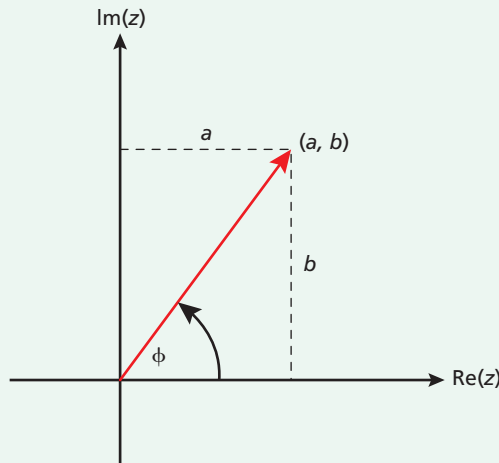


Figure ME6.1

ME6.1 Working with Complex Numbers

ME6.2 Working with Complex Functions

a and b to be entered separately and do not have this problem. Additionally, most handheld calculators output ϕ values between $-\pi/2$ and $\pi/2$, whereas in polar coordinates ϕ is defined between 0 and 2π . The following table is useful in correcting for values obtained on a calculator for which the signs of a and b cannot be entered separately and for which the output values are in the range $-\pi/2$ to $\pi/2$.

a	b	quadrant	ϕ
positive	positive	1 $0 \leq \phi < \pi/2$	$\phi = \left(\arctan \frac{b}{a} \right)_{calculator}$
negative	positive	2 $\pi/2 \leq \phi < \pi$	$\phi = \pi + \left(\arctan \frac{b}{a} \right)_{calculator}$
negative	negative	3 $\pi \leq \phi < 3\pi/2$	$\phi = \pi + \left(\arctan \frac{b}{a} \right)_{calculator}$
positive	negative	4 $3\pi/2 \leq \phi < 2\pi$	$\phi = 2\pi + \left(\arctan \frac{b}{a} \right)_{calculator}$

If a complex number is represented in one way, it can easily be converted to the other way.

Example 1

Express the complex number $6 - 7i$ in the form $re^{i\phi}$.

The magnitude of the radius vector r is given by $\sqrt{6^2 + 7^2} = \sqrt{85}$. The phase is given by $\tan \phi = [(-7)/6]$ or $\phi = \arctan[(-7)/6]$. Therefore, we can write $6 - 7i$ as $\sqrt{85} \exp(i \arctan[(-7)/6]) = \sqrt{85} \exp(-0.862i)$. The phase angle is expressed in radians, which are dimensionless. Because by definition (see Math Essential 1) 2π radians are equivalent to 360° , one radian is equivalent to 57.30° .

This phase was calculated with Mathematica, which outputs ϕ values between $-\pi/2$ and $\pi/2$. To bring this value in accord with polar coordinates for which ϕ lies between 0 and 2π , we add 2π to the calculated value, giving a phase angle of 5.42 radians, which is consistent with the point $(6, -7i)$ being in the fourth quadrant of the complex plane.

Example 2

Convert the complex number $2e^{i\pi/2}$ to the $a + ib$ notation.

Using Euler's formula $e^{i\alpha} = \exp(i\alpha) = \cos \alpha + i \sin \alpha$, we can write $2e^{i\pi/2}$ as

$$2\left(\cos \frac{\pi}{2} + i \sin \frac{\pi}{2}\right) = 2(0 + i) = 2i.$$

Example 3

The complex conjugate of a complex number z is designated by z^* and is obtained by changing the sign of i , wherever it appears in the complex number. For example, if $z = (3 - \sqrt{5}i)e^{i\sqrt{2}\phi}$, then $z^* = (3 + \sqrt{5}i)e^{-i\sqrt{2}\phi}$. The magnitude of a complex number is defined by $\sqrt{zz^*}$ and is always a real number. Determine the magnitude of the following complex numbers:

a. $(1 + i)(\sqrt{2} + 5i)$

c. $\frac{e^{\sqrt{2}i\pi} e^{-3i\pi}}{4e^{i\pi/4}}$

b. $\frac{1 + \sqrt{3}i}{11 - 2i}$

d. $\frac{1 + 6i}{i}$

The magnitude of a complex number or function f is $\sqrt{f^* f}$. The magnitude of a complex number is always a real number.

a. $\sqrt{(1+i)(\sqrt{2}+5i)(1-i)(\sqrt{2}-5i)} = 3\sqrt{6}$

b. $\sqrt{\frac{1+\sqrt{3}i}{11-2i} \frac{1-\sqrt{3}i}{11+2i}} = \frac{2}{5\sqrt{5}}$

c. $\sqrt{\frac{e^{\sqrt{2}i\pi} e^{-3i\pi}}{4e^{i\pi/4}} \frac{e^{-\sqrt{2}i\pi} e^{+3i\pi}}{4e^{-i\pi/4}}} = \frac{1}{4}$

d. $\sqrt{\frac{1+6i}{i} \frac{1-6i}{-i}} = \sqrt{37}$

Complex numbers can be added, multiplied, and divided just like real numbers. A few examples follow:

$$(3 + \sqrt{2}i) + (1 - \sqrt{3}i) = [4 + (\sqrt{2} - \sqrt{3})i]$$

$$\begin{aligned}(3 + \sqrt{2}i)(1 - \sqrt{3}i) &= 3 - 3\sqrt{3}i + \sqrt{2}i - \sqrt{6}i^2 \\ &= (3 + \sqrt{6}) + (\sqrt{2} - 3\sqrt{3})i\end{aligned}$$

$$\begin{aligned}\frac{(3 + \sqrt{2}i)}{(1 - \sqrt{3}i)} &= \frac{(3 + \sqrt{2}i)(1 + \sqrt{3}i)}{(1 - \sqrt{3}i)(1 + \sqrt{3}i)} = \frac{3 + 3\sqrt{3}i + \sqrt{2}i + \sqrt{6}i^2}{4} \\ &= \frac{(3 - \sqrt{6}) + (3\sqrt{3} + \sqrt{2})i}{4} \quad (\text{ME6.4})\end{aligned}$$

ME6.2 WORKING WITH COMPLEX FUNCTIONS

Functions can depend on a complex variable. As is discussed in Chapter 2, a wave traveling in the positive x direction can be described by the function

$$\begin{aligned}\Psi(x, t) &= A \sin(kx - \omega t + \phi) = A \cos(kx - \omega t + \phi - \pi/2) \\ &= A \cos(kx - \omega t + \phi') \quad (\text{ME6.5})\end{aligned}$$

where $\phi' = \phi - \pi/2$. Using the Euler relation, $e^{i\alpha} = \exp(i\alpha) = \cos \alpha + i \sin \alpha$, we can write Equation (ME6.5) as

$$\begin{aligned}\Psi(x, t) &= \operatorname{Re}(Ae^{i(kx - \omega t + \phi')}) \\ &= \operatorname{Re}(A \exp i(kx - \omega t + \phi')) \quad (\text{ME6.6})\end{aligned}$$

in which the notation Re indicates that we are considering only the real part of the complex function that follows. Working with only the real part of the functions makes some of the mathematical treatment more cumbersome, so that it is easier to work with the whole complex function knowing that we can always extract the real part if we wish to do so. For the complex function $f(x, t) = Ae^{i(kx - \omega t)}$, $z\bar{z}^* = \psi(x, t)\psi^*(x, t) = Ae^{i(kx - \omega t)}A^*e^{-i(kx - \omega t)} = AA^*$, so that the magnitude of the function is a constant and does not depend on t or x .

The mathematics of dealing with wave functions is much simpler if they are represented as complex functions. For example, if $z_1 = r_1 e^{i\phi_1}$ and $z_2 = r_2 e^{i\phi_2}$,

$$\begin{aligned}z_1 z_2 &= r_1 r_2 e^{i(\phi_1 + \phi_2)} \\ z_1/z_2 &= (r_1/r_2) e^{i(\phi_1 - \phi_2)} \\ \sqrt{z_1} &= \sqrt{r_1} e^{i\phi_1/2} \quad (\text{ME6.7})\end{aligned}$$

We work with the complex form rather than the real form of a function because calculations such as differentiation and integration can be carried out more easily that way. Waves in classical physics have real amplitudes because their amplitudes are linked directly to observables. For example, the amplitude of a sound wave is the local pressure that arises from the expansion or compression of the medium through which the wave passes. However, in quantum mechanics, observables are related to $|\psi(x, t)|^2$ rather than $\psi(x, t)$. Because $|\psi(x, t)|^2$ is always real, even though $\psi(x, t)$ can be complex, and the observables associated with the wave function are still real.

When working with waves expressed as sine or cosine functions, we find the following trigonometric identities useful

$$\sin(x \pm y) = \sin x \cos y \pm \cos x \sin y$$

$$\cos(x \pm y) = \cos x \cos y \mp \sin x \sin y$$

$$\sin 2x = 2 \sin x \cos x$$

$$\cos 2x = \cos^2 x - \sin^2 x$$

$$\sin(x/2) = \sqrt{\frac{1 - \cos x}{2}}$$

$$\cos(x/2) = \sqrt{\frac{1 + \cos x}{2}}$$

(ME6.8)

2

The Schrödinger Equation

WHY is this material important?

The key to understanding why classical mechanics is not an appropriate framework for understanding phenomena at the atomic level is the recognition that wave–particle duality needs to be integrated into the operative model of physics. Rather than solving Newton’s equations of motion for a particle, an appropriate wave equation needs to be solved for the wave particle. Erwin Schrödinger was the first to formulate such an equation successfully.

WHAT are the most important concepts and results?

Operators, eigenfunctions, wave functions, and eigenvalues are key concepts that arise in a viable framework to solve quantum-mechanical wave equations. The eigenvalues correspond to the possible values of measured results, or observables, in an experiment.

WHAT would be helpful for you to review for this chapter?

It would be helpful to review the material in Math Essential 5 and 6 on differential equations and complex numbers and functions. The material in Chapter 1 serves as a launching point for this chapter and should be reviewed.

2.1 WHAT DETERMINES IF A SYSTEM NEEDS TO BE DESCRIBED USING QUANTUM MECHANICS?

Quantum mechanics was viewed as a radically different way of looking at matter at the molecular, atomic, and subatomic levels in the 1920s. However, the historical distance we have from what was a revolution at the time makes the quantum view much more familiar today. It is important to realize that classical and quantum mechanics are not two competing ways to describe the world around us. Each has its usefulness in a different regime of physical properties that describe reality. Quantum mechanics merges seamlessly into classical mechanics in moving from atoms to masses the size of baseballs. Classical mechanics can be derived from quantum mechanics in the limit that allowed energy values to become continuous rather than discrete. Some of these complexities will require a different way of thinking about physics as you gain an understanding of quantum mechanics. For instance, it is not correct to say that in dealing with atoms, a quantum-mechanical description must always be used.

To illustrate the point that a quantum-mechanical description is not always necessary when dealing with atoms, consider a container filled with argon gas at a low pressure. At the atomic level, the origin of pressure is the collision of rapidly and randomly moving argon atoms with the container walls. Classical mechanics gives a perfectly good description of the origin of pressure in this case. However, if we pass ultraviolet light through hydrogen gas and ask how much energy can be absorbed by an H_2 molecule,

- 2.1** What Determines If a System Needs to Be Described Using Quantum Mechanics?
- 2.2** Classical Waves and the Nondispersing Wave Equation
- 2.3** Quantum-Mechanical Waves and the Schrödinger Equation
- 2.4** Solving the Schrödinger Equation: Operators, Observables, Eigenfunctions, and Eigenvalues
- 2.5** The Eigenfunctions of a Quantum-Mechanical Operator Are Orthogonal
- 2.6** The Eigenfunctions of a Quantum-Mechanical Operator Form a Complete Set
- 2.7** Summarizing the New Concepts

we must use a quantum-mechanical description. At first, this seems puzzling—why do we need quantum mechanics in one case but not the other? On further consideration, we discover that a small number of important relationships govern whether a classical description suffices in a given case. We will now discuss these relationships in order to develop an understanding of when to use a classical description and when to use a quantum description for a given system.

Concept

Quantum mechanics must be used if the wavelength of the particle is similar to the dimension of the problem.

The essence of quantum mechanics is that particles and waves are not entirely separate and distinct entities. Waves can show particle-like behavior, as illustrated by the photoelectric effect. Particles can also show wave-like properties, as shown by diffraction of atomic beams from surfaces. How can we develop criteria that tell us when a particle description (classical) of an atomic or molecular system is sufficient and when we need to use a wave description (quantum mechanical)? Two criteria are used: the magnitude of the wavelength of the particle relative to the dimensions of the problem and the degree to which the allowed energy values form a continuous energy spectrum.

A good starting point is to think about diffraction of light of wavelength λ passing through a slit of width a . Ray optics is a good description as long as $\lambda \ll a$. Diffraction is only observed when the wavelength is comparable to the slit width. What is the magnitude of the wavelength of a molecule? Of a macroscopic mass such as a baseball? By putting numbers into Equation (1.11), we find that the wavelength for a room temperature H₂ molecule is about 10⁻¹⁰ m, and that for a baseball is about 10⁻³⁴ m. Keep in mind that because p rather than v appears in the denominator of Equation (1.11), which defines the wavelength of a particle, the wavelength of a toluene molecule with the same velocity as an H₂ molecule is approximately a factor of 50 smaller. As we learned in discussing the Davisson–Germer experiment in Chapter 1, crystalline solids have regular spacings between atoms that are appropriate for the diffraction of electrons, as well as low-atomic mass atoms and molecules. Particle diffraction is a demonstration of wave–particle duality. To see the wave character of a baseball, we would need to design a diffraction experiment in which a baseball is diffracted in passing through a slit of width $\sim 1 \times 10^{-34}$ m. This does not mean that wave–particle duality breaks down for macroscopic masses; it simply means that the wave character of a baseball does not manifest. There is no sharp boundary such that for values of momentum greater than a critical value we are dealing with a particle and for values less than that we are dealing with a wave. The degree to which each of these properties is exhibited flows smoothly from one extreme to the other. Consider the second example cited earlier. Adding energy to hydrogen molecules using UV light cannot be treated classically because the localization of the electrons to a small volume around the nuclei brings out their wave-like character, and therefore the process must be described using quantum mechanics.

Concept

Quantum mechanics must be used if the problem exhibits a discrete energy spectrum.

We next discuss the second criterion for determining when we need a quantum-mechanical description of a system. It is based on the energy spectrum of the system. Because all values of the energy are allowed for a classical system, it is said to have a **continuous energy spectrum**. In a bounded quantum-mechanical system, only certain values of the energy are allowed, and such a system has a **discrete energy spectrum**. To make this criterion quantitative, we need to discuss the Boltzmann distribution.

In this chapter we will attempt to show that Boltzmann's most important result is plausible, so that we can apply it in our study of quantum mechanics. Consider a one-liter container filled with an ideal atomic gas at the standard conditions of 1 bar and a temperature of 298.15 K. Because the atoms have no rotational or vibrational degrees of freedom, all of their energy is in the form of translational kinetic energy. At equilibrium, not all of the atoms have the same kinetic energy. In fact, the atoms exhibit a broad range of energies. To define the distribution of atoms having a given energy, descriptors such as the mean, the median, or the root mean square energy per atom are used. For the atoms in a gas, the root mean square energy is simply related to the absolute temperature T by

$$E_{rms} = \frac{3}{2}k_B T \quad (2.1)$$

The Boltzmann constant k_B is the familiar ideal gas law constant R divided by Avogadro's number.

As we have said, there is a broad distribution of kinetic energy in the gas for the individual atoms. What governs the probability of observing one value of the energy as opposed to another? This question led Ludwig Boltzmann (1844–1906) to one of the most important equations in physics and chemistry. With regard specifically to our case, it relates the number of atoms n_i that have energy ε_i to the number of atoms n_j that have energy ε_j by the equation

$$\frac{n_i}{n_j} = \frac{g_i}{g_j} e^{-[\varepsilon_i - \varepsilon_j]/k_B T} \quad (2.2)$$

This formula is called the **Boltzmann distribution**. An important concept to keep in mind is that a formula is just a shorthand way of describing phenomena that occur in the real world. It is critical to understand what lies behind the formula. Take a closer look at this equation. It states that the ratio of the number of atoms having the energy ε_i to the number having the energy ε_j depends on several quantities. It depends exponentially on the difference in the energies and the reciprocal of the temperature. This means that this ratio varies rapidly with the variables temperature and $\varepsilon_i - \varepsilon_j$. The equation also states that it is the ratio of the energy difference to $k_B T$ that is important. What is $k_B T$? It has the units of energy and is approximately the average energy that an atom has at temperature T . This exponential term informs us that the larger the temperature, the closer the ratio n_i/n_j will be to unity; the probability of an atom having a given energy decreases exponentially with increasing energy.

The third variable that influences the ratio n_i/n_j is the ratio g_i/g_j . The quantities g_i and g_j are the degeneracies of the energy levels i and j . The **degeneracy** of an energy level counts the number of ways that an atom can have an energy ε within the interval $\varepsilon_i - \Delta\varepsilon < \varepsilon < \varepsilon_i + \Delta\varepsilon$. The degeneracy can depend on the energy. In our example, degeneracy can be illustrated as follows. The energy of an atom $\varepsilon_i = \frac{1}{2}mv_i^2$ is determined by $v_i^2 = v_{xi}^2 + v_{yi}^2 + v_{zi}^2$. We have explicitly written that the energy depends only on the speed of the atom and not on its individual velocity components. For a fixed value of $\Delta\varepsilon$, there are many more ways of combining different individual velocity components to give the same speed at large values of speed than there are for small values of speed. Therefore, the degeneracy corresponding to a particular energy ε_i increases with speed.

The importance of these considerations will become clearer as we continue to apply quantum mechanics to atoms and molecules. As already stated, a quantum-mechanical system has a discrete rather than a continuous energy spectrum. On the one hand, if $k_B T$ is small compared to the spacing between allowed energies, the distribution of states in energy will be very different from a classical system, which has a continuous energy spectrum. On the other hand, if $k_B T$ is much larger than the energy spacing, classical and quantum mechanics will give the same result for the relative numbers of atoms or molecules of different energy. This scenario occurs in either of two limits: large T or small $\varepsilon_i - \varepsilon_j$, illustrating how a continuous transition between classical and quantum mechanics is possible. A large increase in T could cause a system that exhibited quantum behavior at low temperatures to exhibit classical behavior at high temperatures. A calculation using the Boltzmann distribution for a two-level system is carried out in Example Problem 2.1.

Concept

The Boltzmann distribution can be used to calculate the relative population of two energy levels.

EXAMPLE PROBLEM 2.1

Consider a system of 1000 particles that can only have two energies, ε_1 and ε_2 , with $\varepsilon_2 > \varepsilon_1$. The difference in the energy between these two values is $\Delta\varepsilon = \varepsilon_2 - \varepsilon_1$. Assume that $g_1 = g_2 = 1$.

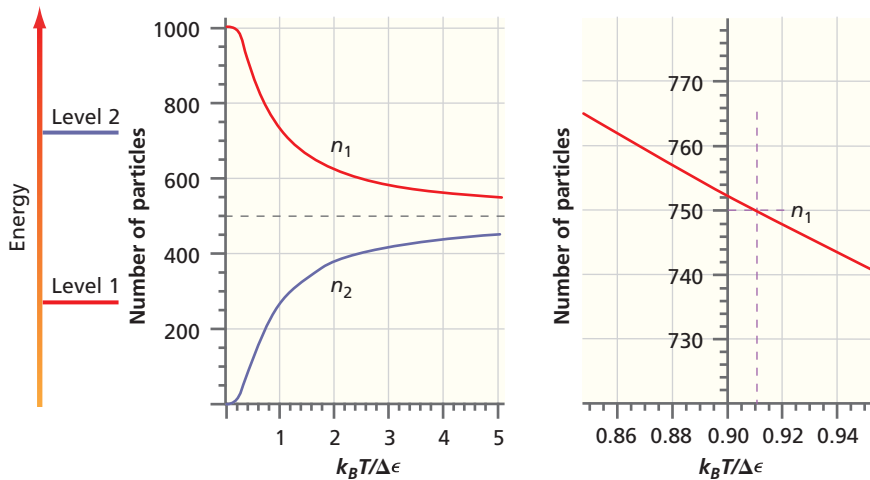
- Graph the number of particles, n_1 and n_2 , in states ε_1 and ε_2 as a function of $k_B T/\Delta\varepsilon$. Explain your result.
- At what value of $k_B T/\Delta\varepsilon$ do 750 of the particles have the energy ε_1 ?

Solution

Using information from the problem and Equation (2.2), we can write the following two equations: $n_2/n_1 = e^{-\Delta\varepsilon/k_B T}$ and $n_1 + n_2 = 1000$. We solve these two equations for n_2 and n_1 to obtain

$$n_2 = \frac{1000 \cdot e^{-\Delta\varepsilon/k_B T}}{1 + e^{-\Delta\varepsilon/k_B T}} \quad \text{and} \quad n_1 = \frac{1000}{1 + e^{-\Delta\varepsilon/k_B T}}$$

If these functions are plotted as a function of $k_B T/\Delta\varepsilon$, the following graphs result:



We see from the left graph that as long as $k_B T/\Delta\varepsilon$ is small, the vast majority of the particles have the lower-energy value. How can we interpret this result? As long as the thermal energy of the particle, which is approximately $k_B T$, is much less than the difference in energy between the two allowed values, the particles with the lower energy are unable to gain energy through collisions with other particles. However, as $k_B T/\Delta\varepsilon$ increases (which is equivalent to a temperature increase for a fixed-energy difference between the two values), the random thermal energy available to the particles enables some of them to jump to the higher-energy value. Therefore, n_1 decreases and n_2 increases. For all finite temperatures, $n_1 > n_2$. As T approaches infinity, n_1 becomes equal to n_2 .

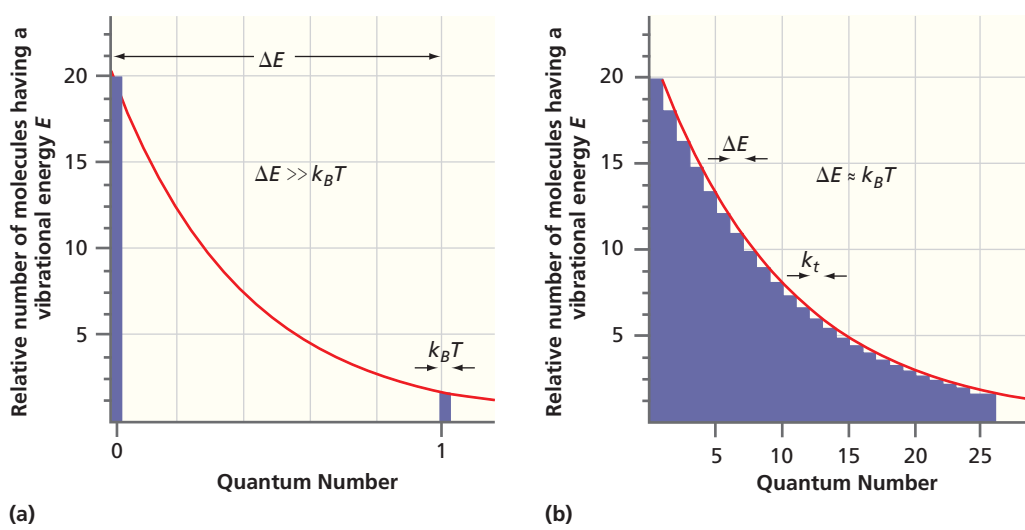
Part (b) is solved graphically. n_1 is shown as a function of $k_B T/\Delta\varepsilon$ on an expanded scale on the right side of the preceding graphs, and we see that $n_1 = 750$ for $k_B T/\Delta\varepsilon = 0.91$.

Example Problem 2.1 shows that the population of states associated with the energy values ε_i and ε_j are very different if

$$\frac{(\varepsilon_i - \varepsilon_j)}{k_B T} \gg 1 \quad (2.3)$$

and very similar if the inequality is reversed. What are the consequences of this result?

Consider a quantum-mechanical system, which, unlike a classical system, has a discrete energy spectrum. The allowed values of energy are called **energy levels**. Anticipating a system that we will deal with in Chapter 7, we refer specifically to the vibrational energy levels of a molecule. The allowed levels are equally spaced with an interval ΔE . These discrete energy levels are numbered with integers, beginning with zero. Under what conditions will this quantum-mechanical system *appear* to follow classical behavior? It will do so if the discrete energy spectrum *appears* to be continuous. How can this occur? In a gas at equilibrium, the total energy of an individual molecule fluctuates within a range $\Delta E \approx k_B T$ through collisions of molecules with one another. Therefore, the energy of a molecule with a particular vibrational quantum number fluctuates within a range of width $k_B T$ centered at the particular energy level. A plot of the relative number of molecules having a vibrational energy E as a function



of E is shown in Figure 2.1 for sharp energy levels and for the two indicated limits, $\Delta E \approx k_B T$ and $\Delta E \gg k_B T$. The curve is generated using the Boltzmann distribution.

For $\Delta E \approx k_B T$, each discrete energy level is sufficiently broadened by energy fluctuations that adjacent energy levels can no longer be distinguished. This is indicated by the overlap of the purple bars representing individual states shown in Figure 2.1b. In this limit, any energy that we choose in the range shown lies in the purple area. It corresponds to an allowed value, and therefore the discrete energy spectrum *appears* to be continuous. Classical behavior will be observed under these conditions. However, if $\Delta E \gg k_B T$, an arbitrarily chosen energy in the range lies outside the purple bars with high probability because the purple bars of width $k_B T$ are widely separated. The range between the two purple bars corresponds to forbidden energies; therefore, the discontinuous nature of the energy spectrum is observable. Quantum-mechanical behavior is observed under these conditions.

In summary, if the allowed energies form a continuum, classical mechanics is sufficient to describe *that feature* of the system. If the allowed energies are discrete, a quantum-mechanical description is needed. The words *that feature* require emphasis. The pressure exerted by the H_2 molecules in the box arises from momentum transfer governed by the translational energy spectrum of the molecules, which *appears* to be continuous, as we will learn in Chapter 4. Therefore, we do not need quantum mechanics to discuss the pressure in the box. However, if we discuss light absorption by the same H_2 molecules, a quantum-mechanical description of light absorption is required. This is so because light absorption involves an electronic excitation of the molecule, with electronic energy-level spacings much larger than $k_B T$. Therefore, these levels remain discrete at all reasonable temperatures.

2.2 CLASSICAL WAVES AND THE NONDISPERSIVE WAVE EQUATION

In Chapter 1, we learned that particles exhibit wave character under certain conditions. This suggests that a wave equation should be used to describe particles. This equation is called the Schrödinger equation, and it is the fundamental equation used to describe atoms and molecules. However, before discussing this equation, we briefly review classical waves and the classical wave equation.

What characteristics differentiate waves and particles? Think about the collision between two billiard balls. We can treat the balls as point masses (any pool player will recognize this as an idealization) and apply Newton's laws of motion to calculate trajectories, momenta, and energies as a function of time if we know all the forces acting on the balls. Now think of a person shouting. Often there is an echo. What is happening here? The vocal cords create a local compression of the air in the larynx. This compression

Figure 2.1
Relative population in different energy levels plotted as a function of vibrational quantum number at constant T . (a) The width of an energy level, $k_B T$, is small compared to the energy-level spacing ΔE , $\Delta E \gg k_B T$; (b) The width of an energy level, $k_B T$, is comparable to the energy-level spacing ΔE . In parts (a) and (b), the Boltzmann distribution correctly describes the relative populations. However, only if $\Delta E \approx k_B T$ or if $\Delta E < k_B T$ does the system behave as if it has a continuous energy spectrum.

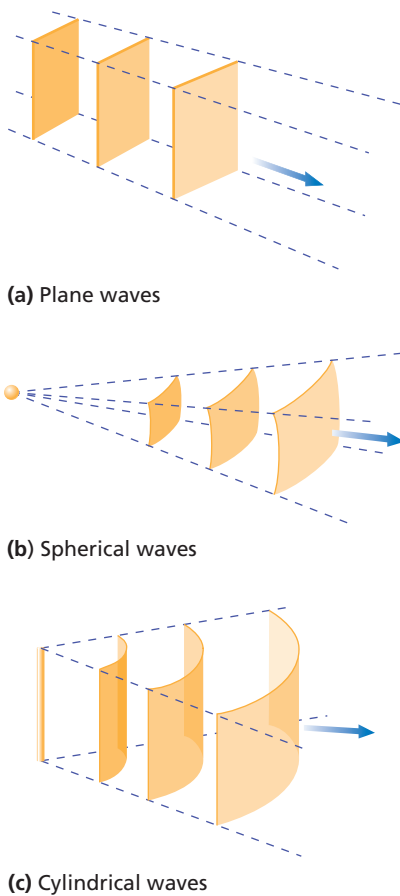
**Figure 2.2**

Illustration of wave fronts for various wave types. Waves can be represented by a succession of surfaces over which the amplitude of the wave has its maximum or minimum value. The distance between successive surfaces is the wavelength. Representative surfaces are shown for (a) plane waves, (b) spherical waves, and (c) cylindrical waves. The direction of propagation of the waves is perpendicular to the surfaces, as indicated by the blue arrows.

zone propagates away from its source as a wave with the speed of sound. The louder the sound, the larger the pressure is in the compressed zone. The pressure variation is the amplitude of the wave, and the energy contained in this wave is proportional to the square of the amplitude. The sound reflects from a surface and returns as a weakened local compression of the air. When the wave is incident on the eardrum, a signal that we recognize as sound is generated. Note that the energy associated with the sound wave is only localized at its origin in the larynx. Unlike billiard balls, waves are not just located at a single point in space. A further important characteristic of a wave is that it has a characteristic velocity and frequency with which it propagates. The velocity and frequency govern the variation of the amplitude of the wave with time.

Types of waves are illustrated in Figure 2.2. A wave can be represented pictorially by a succession of **wave fronts**, corresponding to surfaces over which the amplitude of the wave has a maximum or minimum value. A point source emits energy in all directions and produces **spherical waves**, as shown in Figure 2.2b. Light passing through a rectangular slit can be represented by cylindrical waves, as shown in Figure 2.2c. Waves that originate from a faraway source such as the sun when viewed from Earth are spherical waves with such little curvature that they can be represented as **plane waves**, as shown in Figure 2.2a. Plane waves have parallel, planar wave fronts that are normal to the direction of propagation of the wave.

Mathematically, the amplitude of a wave can be described by a **wave function**. The wave function describes how the amplitude of the wave depends on the variables x and t . The variable x is measured along the direction of propagation. For convenience, only sinusoidal waves of **wavelength** λ and the single **frequency** $v = 1/T$, where T is the **period**, are considered. The velocity v , frequency v , and wavelength λ , are related by $v = \lambda v$. The peak-to-peak amplitude of the wave is $2A$:

$$\Psi(x, t) = A \sin 2\pi \left(\frac{x}{\lambda} - \frac{t}{T} \right) \quad (2.4)$$

In this equation, we have arbitrarily chosen our zero of time and distance such that $\Psi(0, 0) = 0$. This equation represents a wave that is moving in the direction of positive x . We can prove this by considering how a specific feature of this wave changes with time. The wave amplitude is zero for

$$2\pi \left(\frac{x}{\lambda} - \frac{t}{T} \right) = n\pi \quad (2.5)$$

where n is an integer. Solving for x , the location of the nodes is given by

$$x = \lambda \left(\frac{n}{2} + \frac{t}{T} \right) \quad (2.6)$$

Note that x increases as t increases, showing that the wave is moving in the direction of positive x . Figure 2.3 shows a graph of the wave function given in Equation (2.4). To graph this function in two dimensions, one of the variables x or t is kept constant.

The functional form in Equation (2.4) appears so often that it is convenient to combine some of the constants and variables to write the wave amplitude as

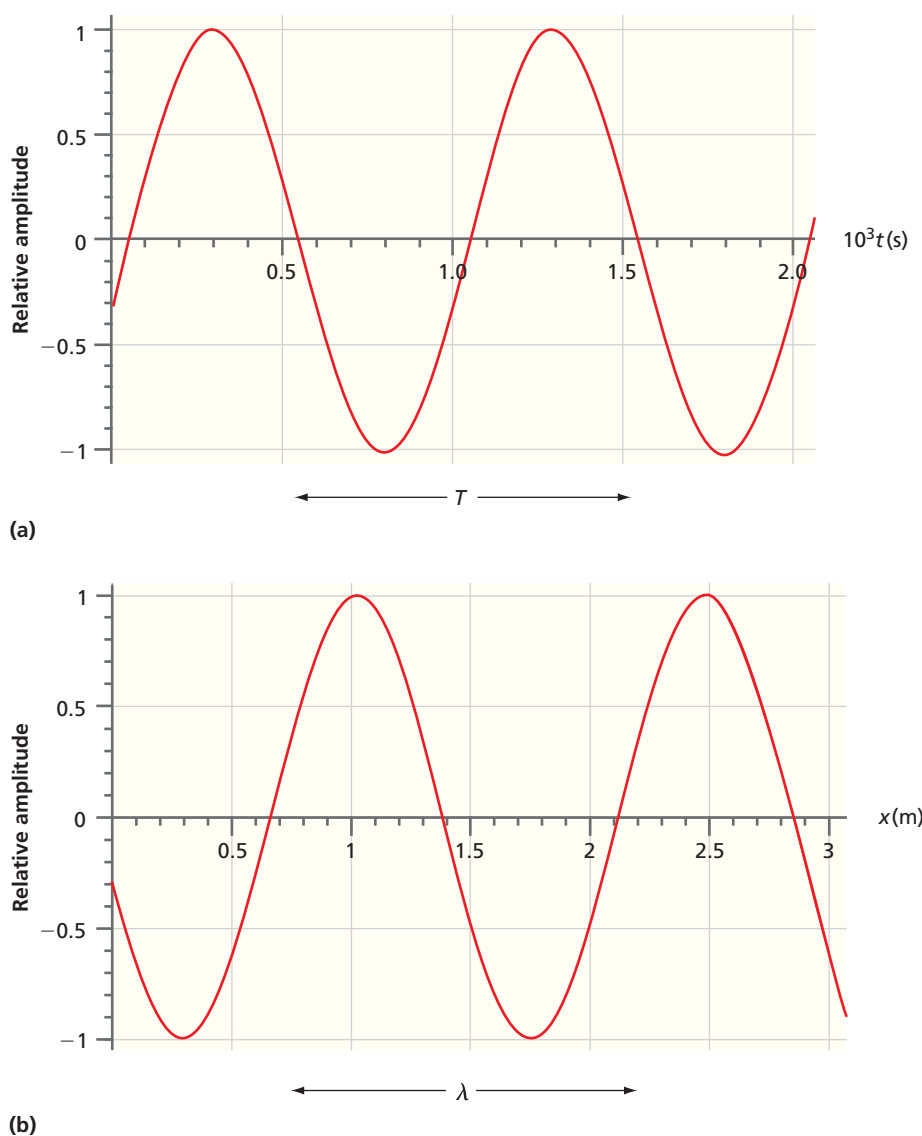
$$\Psi(x, t) = A \sin(kx - \omega t) \quad (2.7)$$

The quantity k is called the **wave vector** and is defined by $k = 2\pi/\lambda$. The quantity $\omega = 2\pi v$ is called the **angular frequency**.

Because the wave amplitude is a simple sine function in our case, it has the same value as the argument changes by 2π . The choice of a zero in position or time is arbitrary and is chosen at our convenience. As an illustration, consider Equation (2.7) rewritten in the form

$$\Psi(x, t) = A \sin(kx - \omega t + \phi) \quad (2.8)$$

in which the quantity ϕ has been added to the argument of the sine function. This is appropriate when $\Psi(0, 0) \neq 0$. The argument of the wave function is called the **phase**, and a change in the initial phase ϕ shifts the wave function to the right or left relative to the horizontal axes in Figure 2.3, depending on the sign of ϕ .

**Figure 2.3**

Graph of wave equation given by Equation (2.4). (a) Wave amplitude as a function of time at a fixed point. The wave is completely defined by the period, the maximum amplitude, and the amplitude at $t = 0$. (b) The analogous information as in (a) when the wave amplitude is plotted as a function of distance at a fixed time. $\lambda = 1.46 \text{ m}$ and $T = 1.00 \times 10^{-3} \text{ s}$.

When two or more waves are present in the same region of space, their time-dependent amplitudes add together, and the waves are said to interfere with one another. The **interference** between two waves produces an enhancement in a region of space if the wave amplitudes are both positive or both negative, which is referred to as **constructive interference**. It can also lead to a cancellation of the wave amplitude in a region of space if the wave amplitudes are opposite in sign which is referred to as **destructive interference**. At the constructive interference condition, maxima of the waves from the two sources align (constructive interference) because the phases of the two waves are the same within an integral multiple of 2π . Likewise, they are out of phase at the destructive interference condition where the phases differ by $(2n + 1)\pi$, where n is an integer.

One special consequence of interference, is that when two or more traveling waves interfere, they may form a standing wave. A standing wave has spatially fixed nodes where the amplitude is zero at all times. Consider the superposition of two waves of the same frequency and amplitude that are moving in opposite directions. The resultant wave amplitude is the sum of the individual amplitudes:

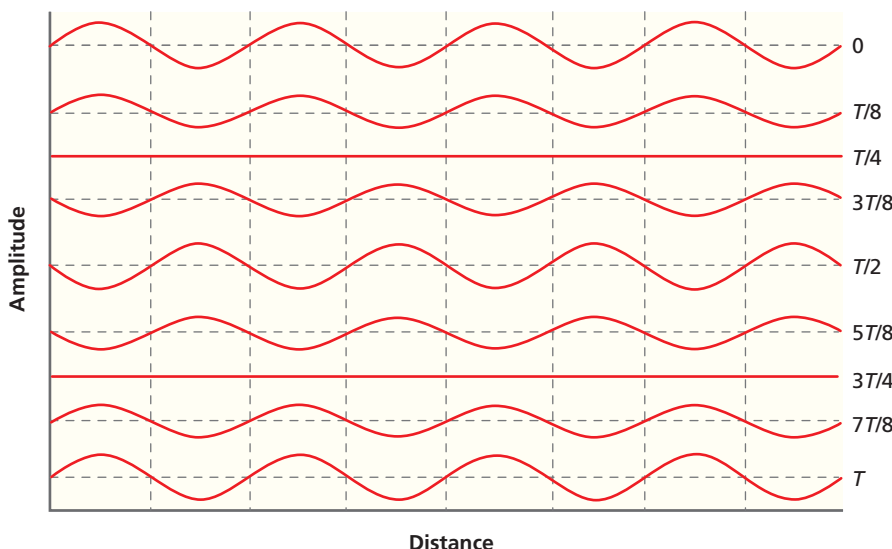
$$\Psi(x, t) = A [\sin(kx - \omega t) + \sin(kx + \omega t)] \quad (2.9)$$

Using the standard trigonometric identity $\sin(\alpha \pm \beta) = \sin \alpha \cos \beta \pm \cos \alpha \sin \beta$, Equation (2.9) can be simplified to

$$\Psi(x, t) = 2A \sin kx \cos \omega t = \psi(x) \cos \omega t \quad (2.10)$$

Concept

Unlike particles, waves can interfere, either decreasing or increasing the resulting amplitude.



Concept

For standing waves, the nodes always appear at the same positions. For traveling waves, the whole waveform, including the nodes, moves with time.

Figure 2.4

Time evolution of a standing wave at a fixed point. The time intervals are shown as a function of the period T . The vertical lines indicate the nodal positions x_0 . Note that the wave function has temporal nodes for $t = T/4$ and $3T/4$.

This function of x and t is a product of two functions, each of which depends on only one of the variables. Therefore, the position of the nodes, which is determined by $\sin kx = 0$, is the same at all times. This property distinguishes **standing waves** from **traveling waves**, in which the whole wave, including the nodes, propagates at the same velocity.

The form that the standing wave amplitudes take at different times is shown in Figure 2.4. Standing waves arise if the space in which the waves can propagate is bounded. For instance, plucking a guitar string gives rise to a standing wave because the string is fixed at both ends. Standing waves play an important role in quantum mechanics because, as demonstrated later, they represent **stationary states**, which are states of the system in which the measurable properties of the system do not change with time.

We return to the functional dependencies of the wave amplitude on time and distance for a traveling wave. For wave propagation in a medium for which all frequencies move with the same velocity (a nondispersive medium), the variation of amplitude with time and distance is related by

$$\frac{\partial^2 \Psi(x, t)}{\partial x^2} = \frac{1}{v^2} \frac{\partial^2 \Psi(x, t)}{\partial t^2} \quad (2.11)$$

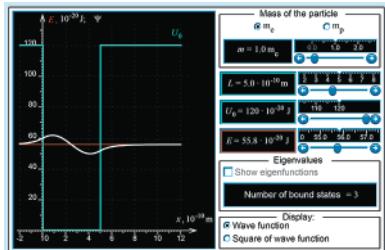
Equation (2.11) is known as the **classical nondispersive wave equation**, and v designates the velocity at which the wave propagates. This equation provides a starting point in justifying the Schrödinger equation, which is the fundamental quantum-mechanical wave equation. (See Math Essential 3 for a discussion of partial differentiation.) Example Problem 2.2 demonstrates that the traveling wave of Equation (2.8) is a solution of the nondispersive wave equation.

EXAMPLE PROBLEM 2.2

The nondispersive wave equation in one dimension is given by

$$\frac{\partial^2 \Psi(x, t)}{\partial x^2} = \frac{1}{v^2} \frac{\partial^2 \Psi(x, t)}{\partial t^2}$$

Show that the traveling wave $\Psi(x, t) = A \sin(kx - \omega t + \phi)$ is a solution of the nondispersive wave equation. How is the velocity of the wave related to k and ω in this case?



- W2.1 Combining traveling waves
- W2.2 Combining standing waves

Solution

$$\frac{\partial^2 \Psi(x, t)}{\partial x^2} = \frac{1}{v^2} \frac{\partial^2 \Psi(x, t)}{\partial t^2}$$

$$\frac{\partial^2 A \sin(kx - \omega t + \phi)}{\partial x^2} = -k^2 A \sin(kx - \omega t + \phi)$$

$$\frac{1}{v^2} \frac{\partial^2 A \sin(kx - \omega t + \phi)}{\partial t^2} = \frac{-\omega^2}{v^2} A \sin(kx - \omega t + \phi)$$

Because $v = \omega/k$, the nondispersive wave equation is obeyed.

The mathematics of wave functions is much simpler if they are represented in the complex number plane. As discussed, a wave traveling in the positive x direction can be described by the function

$$\begin{aligned}\Psi(x, t) &= A \sin(kx - \omega t + \phi) = A \cos(kx - \omega t + \phi - \pi/2) \\ &= A \cos(kx - \omega t + \phi')\end{aligned}\tag{2.12}$$

where $\phi' = \phi - \pi/2$. Using the **Euler relation**, $e^{i\alpha} = \exp(i\alpha) = \cos \alpha + i \sin \alpha$, we can write Equation (2.12) as

$$\begin{aligned}\Psi(x, t) &= \operatorname{Re}(Ae^{i(kx-\omega t+\phi')}) \\ &= \operatorname{Re}(A \exp i(kx - \omega t + \phi'))\end{aligned}\tag{2.13}$$

in which the notation Re indicates that we are considering only the real part of the complex function that follows.

Whereas the wave functions considered previously (for example, sound waves) have only real amplitudes, quantum-mechanical wave functions can also have complex amplitudes. Working with only the real part of the functions makes some of the mathematical treatment more cumbersome, so it is easier to work with the whole complex function knowing that we can always extract the real part if we wish to do so.

The wave function of Equation (2.13) can then be written in the form

$$\Psi(x, t) = A \exp i(kx - \omega t + \phi')\tag{2.14}$$

where the amplitude A is a constant. All quantities that fully characterize the wave, namely, the maximum amplitude, the wavelength, the period of oscillation, and the phase angle for $t = 0$ and $x = 0$, are contained in Equation (2.14). Operations such as differentiation, integration, and adding two waves to form a superposition are generally easier when working with complex exponential notation than with real trigonometric wave functions, as shown in Example Problem 2.3.

Concept

The Euler relation allows a conversion of complex numbers between exponential and trigonometric forms.

EXAMPLE PROBLEM 2.3

Perform the following calculations by expressing the complex function in exponential form using the Euler relation.

- Simplify the ratio $\frac{\cos 5x + i \sin 5x}{\cos 2x + i \sin 2x}$.
- Form the derivative $d\left[\frac{\cos 5x + i \sin 5x}{\cos 2x + i \sin 2x}\right]/dx$
- Evaluate the integral $\int_0^{\pi/2} e^x (\cos x + i \sin x) dx$

Solution

- $$\frac{\cos 5x + i \sin 5x}{\cos 2x + i \sin 2x} = e^{i5x} e^{-2ix} = e^{i3x} = \cos 3x - i \sin 3x$$

$$\begin{aligned}
 \mathbf{b.} \quad & d\left[\frac{\cos 5x + i \sin 5x}{\cos 2x + i \sin 2x}\right] / dx = \frac{de^{i3x}}{dx} = 3ie^{i3x} = 3i \cos 3x - 3 \sin 3x \\
 \mathbf{c.} \quad & \int_0^{\pi/2} e^x (\cos x + i \sin x) dx = \int_0^{\pi/2} e^x e^{ix} dx = \int_0^{\pi/2} e^{x(1+i)} dx = \frac{e^{x(1+i)}}{1+i} \Big|_0^{\pi/2} \\
 & = \frac{e^{(\pi/2)(1+i)} - 1}{1+i} = \frac{e^{(\pi/2)e^{i\pi/2}} - 1}{1+i} = \frac{e^{(\pi/2)} - 1}{1+i}
 \end{aligned}$$

We have used the Euler relation in the first and the final step of part (c).

2.3 QUANTUM-MECHANICAL WAVES AND THE SCHRÖDINGER EQUATION

In this section, we justify the time-independent Schrödinger equation by combining the classical nondispersive wave equation [Equation (2.11)] and the de Broglie relation [Equation (1.11)]. For classical standing waves, in Equation (2.10) we showed that the wave function is a product of two functions, one of which depends only on spatial coordinates and the other only on time:

$$\Psi(x, t) = \psi(x) \cos \omega t \quad (2.15)$$

If this function is substituted in Equation (2.11), we obtain

$$\frac{d^2\psi(x)}{dx^2} + \frac{\omega^2}{v^2} \psi(x) = 0 \quad (2.16)$$

The time-dependent part $\cos \omega t$ cancels because it appears on both sides of the equation after the derivative with respect to time is taken. Using the relations $\omega = 2\pi v$ and $v\lambda = v$, we see that Equation (2.16) becomes

$$\frac{d^2\psi(x)}{dx^2} + \frac{4\pi^2}{\lambda^2} \psi(x) = 0 \quad (2.17)$$

To this point in this section, all of the expressions are consistent with a classical wave. Next, we will turn our attention to quantum mechanics.

To derive a wave equation appropriate for quantum mechanics, we will use the de Broglie relation, $\lambda = h/p$, for the wavelength. The momentum is related to the total energy E and the potential energy $V(x)$ by

$$\frac{p^2}{2m} = E - V(x) \quad \text{or} \quad p^2 = 2m(E - V(x)) \quad (2.18)$$

Introducing this expression for momentum into the de Broglie relation and substituting the expression obtained for λ into Equation (2.17), we obtain

$$\frac{d^2\psi(x)}{dx^2} + \frac{8\pi^2 m}{h^2} [E - V(x)] \psi(x) = 0 \quad (2.19)$$

Using the abbreviation $\hbar = h/2\pi$ and rewriting Equation (2.19), we obtain the **time-independent Schrödinger equation** in one dimension:

$$-\frac{\hbar^2}{2m} \frac{d^2\psi(x)}{dx^2} + V(x)\psi(x) = E\psi(x) \quad (2.20)$$

This is the fundamental equation used to study the stationary states of quantum-mechanical systems. The familiar $1s$ and $2p_z$ orbitals of the hydrogen atom are examples of stationary states obtained from the time-independent Schrödinger equation.

Concept

The solutions to the time independent Schrödinger equation are standing waves that correspond to stationary states.

There is an analogous quantum-mechanical form of the time-dependent classical nondispersive wave equation. It is called the **time-dependent Schrödinger equation** and has the following form:

$$-\frac{\hbar^2}{2m} \frac{\partial^2 \Psi(x, t)}{\partial x^2} + V(x, t)\Psi(x, t) = i\hbar \frac{\partial \Psi(x, t)}{\partial t} \quad (2.21)$$

Equation (2.21) relates the temporal and spatial derivatives of $\Psi(x, t)$ with the potential energy function $V(x, t)$. It is applied in systems in which the energy changes with time. For example, the time-dependent equation is used to model transitions in which the energy of a molecule changes as it absorbs a photon.

Equations (2.20) and (2.21) were both formulated by Schrödinger and are the basis of all quantum-mechanical calculations. Their validity has been confirmed by countless experiments carried out during the last 90 years. The equations look very different from Newton's equations of motion. The mass of the particle appears in both forms of the Schrödinger equation, but what meaning can be attached to $\Psi(x, t)$ and $\psi(x)$? This question will be discussed in some detail in Chapter 3. For now, we consider $\Psi(x, t)$ and $\psi(x)$ to represent the amplitude of the wave that describes the particle or system of particles under consideration. To keep the notation simple, we have considered a one-dimensional system, but, in general, the spatial part of Ψ , denoted ψ , depends on all spatial coordinates.

Our main focus is on the stationary states of a quantum-mechanical system. For these states, both the time-dependent and time-independent Schrödinger equations are satisfied. In this case,

$$i\hbar \frac{\partial \Psi(x, t)}{\partial t} = E\Psi(x, t) \quad (2.22)$$

For stationary states, $\Psi(x, t) = \psi(x)f(t)$, as was discussed in Section 2.2. Substituting this expression in Equation (2.22) gives

$$i\hbar \frac{df(t)}{dt} = Ef(t) \quad \text{or} \quad \frac{df(t)}{dt} = -i\frac{E}{\hbar}f(t) \quad (2.23)$$

Solving this equation, we obtain $f(t) = e^{-i(E/\hbar)t}$. We have shown that wave functions that describe states whose energy is independent of time have the form

$$\Psi(x, t) = \psi(x)e^{-i(E/\hbar)t} \quad (2.24)$$

Note that $\Psi(x, t)$ is the product of two functions, each of which depends on only one variable. We conclude that stationary states in quantum mechanics are represented by standing waves.

2.4 SOLVING THE SCHRÖDINGER EQUATION: OPERATORS, OBSERVABLES, EIGENFUNCTIONS, AND EIGENVALUES

Now that we have introduced the quantum-mechanical wave equation, we need to learn how to work with it. In this section, we develop this topic by introducing the language used in solving the Schrödinger equation. The key concepts introduced are those of *operators*, *observables*, *eigenfunctions*, and *eigenvalues*. These terms are defined later in this section. A good understanding of these concepts is necessary to understand the quantum-mechanical postulates in Chapter 3.

Both forms of the Schrödinger equation are differential equations whose solutions depend on the potential energy $V(x)$. Our emphasis in the next chapters will be on using the solutions of the time-independent equation for various problems such as the harmonic oscillator or the H atom to enhance our understanding of chemistry. We will not focus on methods to solve differential equations. However, it is very useful to develop a general understanding of the formalism used to solve the time-independent

Concept

The time-dependent Schrödinger equation is used to model transitions in which the energy changes with time.

Concept

The process of solving the Schrödinger equation can be described in terms of operators, eigenfunctions, and eigenvalues.

Schrödinger equation. This initial introduction is brief because our primary goal in this chapter is to provide a broad overview of the language of quantum mechanics. As we work with these new concepts in successive chapters, they will become more familiar.

We begin by illustrating the meaning of the term *operator* in the context of classical mechanics. Think about how we would describe the time evolution of a system consisting of a particle on which a force is acting. The velocity at time t_1 is known, and we wish to know the velocity at a later time t_2 . We write down Newton's second law

$$m \frac{d^2x}{dt^2} = F(x, t) \quad (2.25)$$

and integrate it to give

$$v(t_2) = v(t_1) + \frac{1}{m} \int_{t_1}^{t_2} F(x, t) dt \quad (2.26)$$

In words, one could describe this process as the series of operations:

- Integrate the force acting on the particle over the interval t_1 to t_2 .
- Multiply by the inverse of the mass.
- Add this quantity to the velocity at time t_1 .

These actions have the names *integrate*, *form the inverse*, *multiply*, and *add*, and they are all called operators. Note that we started at the right-hand side of the equation and worked our way to the left.

How are operators used in quantum mechanics? To every measurable quantity (**observable**), such as energy, momentum, or position, there is a corresponding **operator** in quantum mechanics. Quantum-mechanical operators usually involve differentiation with respect to a variable such as x , or multiplication by x , or a function of the energy such as $V(x)$. Operators are denoted by a caret, as in: \hat{O} . If two operators act on a wave function as indicated by $\hat{A}\hat{B} f(x)$, it is important to carry out the operations in succession, with the first operation being that nearest to the function. Mathematically, $\hat{A}\hat{B} f(x) = \hat{A}(\hat{B} f(x))$ and $\hat{A}^2 f(x) = \hat{A}(\hat{A} f(x))$.

Just as a differential equation has a set of solutions, an operator \hat{O} has a set of eigenfunctions and eigenvalues. This means that there is a set of wave functions ψ_n with the index n such that

$$\hat{O}\psi_n = a_n\psi_n \quad (2.27)$$

The operator acting on these special wave functions returns the wave function multiplied by a number. These special functions are called the **eigenfunctions** of the operator, and the values a_n are called the **eigenvalues**. The eigenvalues for quantum-mechanical operators are always real numbers because they correspond to the values of observables that are measured in an experiment. There are in general an infinite number of eigenfunctions for a given operator for the specific system under consideration. For example, the eigenfunctions for the total energy operator (kinetic plus potential energy) for the hydrogen atom are the wave functions that describe the orbitals that we know as $1s, 2s, 2p_x, \dots$. The set of these eigenfunctions is infinite in size. The corresponding eigenvalues are the $1s, 2s, 2p_x, \dots$ orbital energies.

We can now recognize that the time-independent Schrödinger equation is an eigenvalue equation for the total energy, E

$$\left\{ -\frac{\hbar^2}{2m} \frac{\partial^2}{\partial x^2} + V(x) \right\} \psi_n(x) = E_n \psi_n(x) \quad (2.28)$$

where the expression in the curly brackets $\{ \}$ is the total energy operator. This operator is given the symbol \hat{H} in quantum mechanics and is called the Hamiltonian for historical reasons. With this notation, Equation (2.28) can be written in the form

$$\hat{H}\psi_n(x) = E_n\psi_n(x) \quad (2.29)$$

The operator acting on one of its eigenfunctions returns the eigenfunction multiplied by the corresponding eigenvalue. In Example Problem 2.4, this formalism is applied for two operators. Solving the time-independent Schrödinger equation is equivalent to finding the set of eigenfunctions and eigenvalues that are the solutions to the eigenvalue problem of Equation (2.29). In this chapter, we consider only a single operator acting on a function. In Chapter 6, we will show that the outcome of two sequential operations on a wave function can depend on the order in which the operations occur. This fact has important implications for the measurement process in quantum mechanics.

EXAMPLE PROBLEM 2.4

Consider the operators d/dx and d^2/dx^2 . Is $\psi(x) = Ae^{ikx} + Be^{-ikx}$ an eigenfunction of these operators? If so, what are the eigenvalues? A , B , and k are real numbers.

Solution

To test if a function is an eigenfunction of an operator, we carry out the operation and see if the result is the same function multiplied by a constant:

$$\frac{d(Ae^{ikx} + Be^{-ikx})}{dx} = ik Ae^{ikx} - ik Be^{-ikx} = ik(Ae^{ikx} - Be^{-ikx})$$

In this case, the result is not $\psi(x)$ multiplied by a constant, so $\psi(x)$ is not an eigenfunction of the operator d/dx unless either A or B is zero. We consider the second operator.

$$\begin{aligned}\frac{d^2(Ae^{ikx} + Be^{-ikx})}{dx^2} &= (ik)^2 Ae^{ikx} + (-ik)^2 Be^{-ikx} \\ &= -k^2(Ae^{ikx} + Be^{-ikx}) = -k^2\psi(x)\end{aligned}$$

This result shows that $\psi(x)$ is an eigenfunction of the operator d^2/dx^2 with the eigenvalue $-k^2$.

In general, a quantum-mechanical operator such as \hat{H} has an infinite number of eigenfunctions. How are the eigenfunctions of a quantum-mechanical operator related to one another? In the next sections we discuss two of the most important properties, *orthogonality* and *completeness*.

2.5 THE EIGENFUNCTIONS OF A QUANTUM-MECHANICAL OPERATOR ARE ORTHOGONAL

We are familiar with the concept of orthogonal vectors. For example, orthogonality in three-dimensional Cartesian coordinate space is defined by

$$\mathbf{x} \cdot \mathbf{y} = \mathbf{x} \cdot \mathbf{z} = \mathbf{y} \cdot \mathbf{z} = 0 \quad (2.30)$$

in which the scalar product between the unit vectors along the x , y , and z axes is zero. In function space, the analogous expression that defines **orthogonality** between the eigenfunctions $\psi_i(x)$ and $\psi_j(x)$ of a quantum-mechanical operator is

$$\int_{-\infty}^{\infty} \psi_i^*(x) \psi_j(x) dx = 0 \quad \text{unless } i = j \quad (2.31)$$

Example Problem 2.5 shows that graphical methods can be used to determine if two functions are orthogonal.

Concept

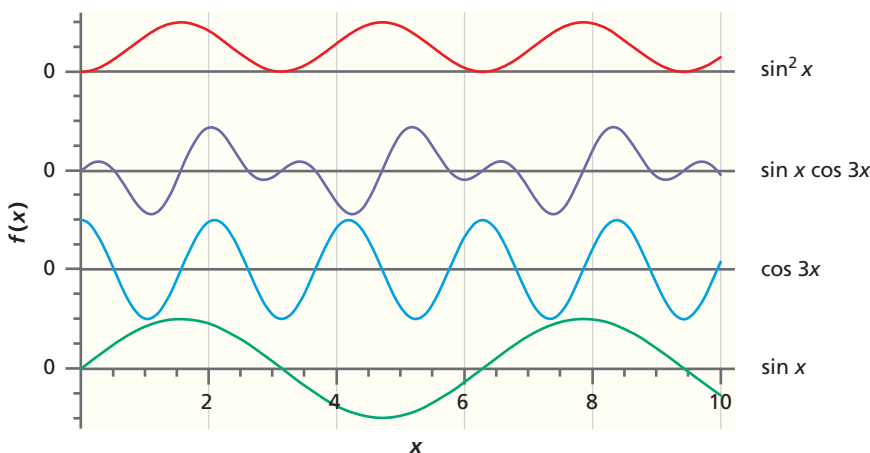
The eigenfunctions of a quantum mechanical operator are orthogonal.

EXAMPLE PROBLEM 2.5

Show graphically that $\sin x$ and $\cos 3x$ are orthogonal functions over the interval $[-2j\pi, 2j\pi]$ where for the purposes of our discussion j is a very large integer. Also show graphically that $\int_{-2j\pi}^{2j\pi} (\sin mx)(\sin nx)dx \neq 0$ for $n = m = 1$.

Solution

The functions are shown in the following graphs. The vertical axes have been offset to avoid overlap, and the horizontal line indicates the zero for each plot. Because the functions are periodic, we can draw conclusions about their behavior in a very large interval that is an integral multiple of 2π by considering their behavior in any interval that is an integral multiple of the period.



The integral of these functions equals the sum of the areas between the curves and the zero line. Areas above and below the line contribute with positive and negative signs, respectively, and indicate that $\int_{-\infty}^{\infty} \sin x \cos 3x dx = 0$ and $\int_{-\infty}^{\infty} \sin x \sin x dx > 0$. By similar means, we could show that any two functions of the type $\sin mx$ and $\sin nx$ or $\cos mx$ and $\cos nx$ are orthogonal unless $n = m$. Are the functions $\cos mx$ and $\sin mx$ ($m = n$) orthogonal?

Concept

Quantum mechanical wave functions can be complex functions of space and time.

As shown in Math Essential 6, the superscript * on a function indicates the **complex conjugate**. The product $\psi_i^*(x)\psi_j(x)$ rather than $\psi_i(x)\psi_j(x)$ occurs in Equation (2.31) because wave functions in quantum mechanics can be complex functions of x and t . If in addition to Equation (2.31) the integral has the value one for $i = j$, we say that the functions are **normalized** and form an **orthonormal** set. As we will see in Chapter 3, wave functions must be normalized so that they can be used to calculate probabilities. We show how to normalize wave functions in Example Problem 2.6.

EXAMPLE PROBLEM 2.6

Normalize the function $a(a - x)$ over the interval $0 \leq x \leq a$.

Solution

To normalize a function $\psi(x)$ over the given interval, we multiply it and $\psi^*(x)$ by a constant N and then calculate N from the equation $N^2 \int_0^a \psi^*(x)\psi(x) dx = 1$.

In this particular case,

$$\begin{aligned} N^2 \int_0^a [a(a-x)]^2 dx &= 1 \\ N^2 a^2 \int_0^a [a^2 - 2ax + x^2] dx &= 1 \\ N^2 \left(a^4 x - a^3 x^2 + a^2 \frac{x^3}{3} \right)_0^a &= 1 \\ N^2 \frac{a^5}{3} = 1 &\quad \text{so that } N = \sqrt{\frac{3}{a^5}} \end{aligned}$$

The normalized wave function is $\sqrt{\frac{3}{a^5}} a(a-x)$

2.6 THE EIGENFUNCTIONS OF A QUANTUM-MECHANICAL OPERATOR FORM A COMPLETE SET

The eigenfunctions of a quantum-mechanical operator have another important property that we will use frequently in later chapters, namely, that the eigenfunctions of a quantum-mechanical operator form a **complete set**. The idea of a complete set is familiar from the three-dimensional Cartesian coordinate system. Because any three-dimensional vector can be expressed as a linear combination of the three mutually perpendicular unit vectors **x**, **y**, and **z**, we say that these three unit vectors form a complete set.

Completeness is also an important concept in function space. To say that the eigenfunctions of any quantum-mechanical vector form a complete set means that any well-behaved wave function $f(x)$ can be expanded in the eigenfunctions $\phi_n(x)$ of any of the quantum-mechanical operators of interest to us defined in the same space, x in this case:

$$\psi(x) = \sum_{n=1}^{\infty} b_n \phi_n(x) \quad (2.32)$$

Before we expand wave functions in a complete set of eigenfunctions in later chapters, we will first illustrate how to expand an arbitrary function, in this case the simple sawtooth function, in a **Fourier sine and cosine series**. We approximate the sawtooth function shown in Figure 2.5 by a linear combination of the mutually orthogonal functions $\sin(n\pi x/b)$ and $\cos(n\pi x/b)$. These functions form an infinitely large complete set for $n = 1, 2, 3, \dots, \infty$. Because this function set is complete only as $n \rightarrow \infty$, the approximation only becomes exact as $n \rightarrow \infty$. The degree to which the approximation approaches the exact function depends on how many terms we include in the sum. We approximate the sawtooth function by the finite sum in Equation (2.33), and evaluate how good the approximation is for different values of m .

$$f(x) = d_0 + \sum_{n=1}^m \left[c_n \sin\left(\frac{n\pi x}{b}\right) + d_n \cos\left(\frac{n\pi x}{b}\right) \right] \quad (2.33)$$

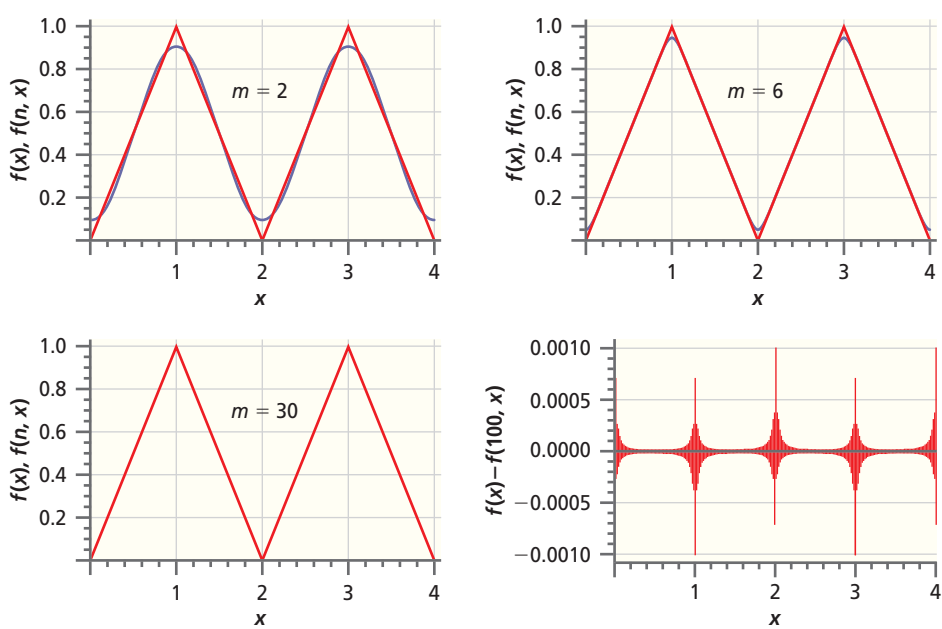
We first need a way to calculate the coefficients d_0 , c_m , and d_m . In our case, the function is even, $f(x) = f(-x)$, so that all the coefficients c_m are identically zero. For the Fourier series, the values for the d_m are easily obtained using the mutual orthogonality property of the sine and cosine functions demonstrated in Example Problem 2.5.

Concept

The eigenfunctions of any quantum mechanical operator form a complete set, allowing a series expansion of any well behaved function in terms of the eigenfunctions.

Figure 2.5

The sawtooth function compared with a finite Fourier series. The sawtooth function curves are shown in red, and the finite Fourier series curves are shown in blue. The Fourier series are defined by Equation (2.33) and contain m terms for $m = 2, 6$, and 30 . The difference between the sawtooth function and the finite Fourier series for $m = 100$ is shown in the bottom right panel as a function of x .



To obtain d_m , we multiply both sides of Equation (2.33) by one of the expansion functions, for example, $\cos(m\pi x/b)$, and integrate over the interval $-b, b$:

$$\begin{aligned} \int_{-b}^b f(x) \cos\left(\frac{m\pi x}{b}\right) dx &= \int_{-b}^b \cos\left(\frac{m\pi x}{b}\right) \\ &\quad \times \left(d_0 + \sum_n d_n \cos\left(\frac{n\pi x}{b}\right)\right) dx \\ &= \int_{-b}^b \left(\cos\left(\frac{m\pi x}{b}\right)\right) d_m \cos\left(\frac{m\pi x}{b}\right) dx = bd_m \end{aligned}$$

Only one term in the summation within the integral gives a nonzero contribution because all cosine functions for which $m \neq n$ are orthogonal. We have used one of the standard integrals listed in Math Essential 2 to obtain this result. We conclude that the optimal values for the coefficients are given by

$$\begin{aligned} d_m &= \frac{1}{b} \int_{-b}^b f(x) \cos\left(\frac{m\pi x}{b}\right) dx, \quad m \neq 0 \quad \text{and} \\ d_0 &= \frac{1}{2b} \int_{-b}^b f(x) dx \end{aligned}$$

Using these equations to obtain the optimal coefficients will make the finite sum of Equation (2.33) nearly exact if enough terms can be included in the sum. How good is the approximation if m is finite? This question is answered in Figure 2.5, which shows that the sawtooth function can be described reasonably well for $m < 30$. To make this statement more quantitative, we graph $f(x) - \left(d_0 + \sum_{n=1}^{100} \left[c_n \sin\left(\frac{n\pi x}{b}\right) + d_n \cos\left(\frac{n\pi x}{b}\right)\right]\right)$ versus x in Figure 2.5 for a 101 term series. We see that the difference is less than 0.1% of the maximum amplitude for the sawtooth function. Generalizing the results shown in Figure 2.5 to other expansions, we find that the maximum error occurs at the points for which the function or the slope of the function is discontinuous.

2.7 SUMMARIZING THE NEW CONCEPTS

In this chapter we introduced a number of the key tools of quantum mechanics that are used to solve the Schrödinger equation. The time-dependent and time-independent Schrödinger equations play the role in solving quantum-mechanical problems that Newton's laws play in classical mechanics. Operators, eigenfunctions, and observables form the framework for solving the time-independent Schrödinger equation. All of these concepts will be applied to problems of chemical interest in the next few chapters. However, we will first introduce and discuss the five postulates of quantum mechanics in Chapter 3.

VOCABULARY

angular frequency	eigenvalue	phase
Boltzmann distribution	energy levels	plane wave
classical nondispersive wave equation	Euler relation	spherical wave
complete set	Fourier sine and cosine series	standing wave
completeness	frequency	stationary state
complex conjugate	interference	time-dependent Schrödinger equation
constructive interference	normalized	time-independent Schrödinger equation
continuous energy spectrum	observable	traveling wave
degeneracy	operator	wave front
destructive interference	orthogonality	wave function
discrete energy spectrum	orthonormal	wave vector
eigenfunction	period	wavelength

KEY EQUATIONS

Equation	Significance of Equation	Equation Number
$\frac{n_i}{n_j} = \frac{g_i}{g_j} e^{-[E_i - E_j]/k_B T}$	Boltzmann distribution gives the relative population of different energy levels	2.2
$\Psi(x, t) = A \sin 2\pi \left(\frac{x}{\lambda} - \frac{t}{T} \right)$	Wave function for traveling plane wave	2.4
$\frac{\partial^2 \Psi(x, t)}{\partial x^2} = \frac{1}{v^2} \frac{\partial^2 \Psi(x, t)}{\partial t^2}$	Classical nondispersive wave equation	2.11
$-\frac{\hbar^2}{2m} \frac{d^2 \psi(x)}{dx^2} + V(x) \psi(x) = E \psi(x)$	Time-independent Schrödinger equation in one dimension	2.20
$-\frac{\hbar^2}{2m} \frac{\partial^2 \Psi(x, t)}{\partial x^2} + V(x, t) \Psi(x, t) = i\hbar \frac{\partial \Psi(x, t)}{\partial t}$	Time-dependent Schrödinger equation in one dimension	2.21
$\Psi(x, t) = \psi(x) e^{-i(E/\hbar)t}$	Wave function for stationary states	2.24
$\hat{H}\psi_n(x) = E_n \psi_n(x)$	Schrödinger equation written as operator equation for total energy	2.29
$\int_{-\infty}^{\infty} \psi_i^*(x) \psi_j(x) dx = 0 \quad \text{unless } i = j$	Definition of orthogonality of eigenfunctions	2.31
$\psi(x) = \sum_{n=1}^{\infty} b_n \phi_n(x)$	Definition of completeness of set of eigenfunctions	2.32
$f(x) = d_0 + \sum_{n=1}^m \left[c_n \sin\left(\frac{n\pi x}{b}\right) + d_n \cos\left(\frac{n\pi x}{b}\right) \right]$	Expansion of function in Fourier sine and cosine series	2.33

CONCEPTUAL PROBLEMS

Q2.1 One source emits spherical waves, and another emits plane waves. For which source does the intensity measured by a detector of fixed size fall off more rapidly with distance? Why?

Q2.2 What is the relationship between evaluating an integral and graphing the integrand?

Q2.3 A traveling wave with arbitrary phase ϕ can be written as $\psi(x, t) = A \sin(kx - \omega t + \phi)$. What are the units of ϕ ? Show that ϕ could be used to represent a shift in the origin of time or distance.

Q2.4 Why is it true for any quantum-mechanical problem that the set of wave functions is larger than the set of eigenfunctions?

Q2.5 By discussing the diffraction of a beam of particles by a single slit, justify the statement that there is no sharp boundary between particle-like and wave-like behavior.

Q2.6 Redraw Figure 2.2 to show surfaces corresponding to both minimum and maximum values of the amplitude.

Q2.7 Is it correct to say that because the de Broglie wavelength of a H₂ molecule at 300 K is on the order of atomic dimensions that all properties of H₂ are quantized?

Q2.8 If $\psi(x, t) = A \sin(kx - \omega t)$ describes a wave traveling in the plus x direction, how would you describe a wave moving in the minus x direction?

Q2.9 In Figure 2.5 the extent to which the approximate and true functions agree was judged visually. How could you quantify the quality of the fit?

Q2.10 Why does a quantum-mechanical system with discrete vibrational energy levels behave as if it has a continuous energy spectrum if the energy difference between vibrational energy levels ΔE satisfies the relationship?

Q2.11 Distinguish between the following terms applied to a set of functions: orthogonal and normalized.

Q2.12 Why can we conclude that the wave function $\psi(x, t) = \psi(x)e^{-i(E/\hbar)t}$ represents a standing wave?

Q2.13 What is the usefulness of a complete set of functions?

Q2.14 Can the function $\sin kx$ be normalized over the interval $-\infty < x < \infty$? Explain your answer.

Q2.15 A linear operator satisfies the condition $A(f(x) + g(x)) = \hat{A}f(x) + \hat{A}g(x)$. Are \hat{A} or \hat{B} linear operators if $\hat{A}f(x) = (f(x))^2$ and $\hat{B}f(x) = df(x)/dx$?

Q2.16 Is \hat{A} a linear operator if $\hat{A}f(x) = d^2f(x)/dx^2 + xf(x)$?

Q2.17 Two operators can be applied to a function in succession. By definition, $\hat{A}\hat{B}f(x) = \hat{A}[\hat{B}f(x)]$. Evaluate $\hat{A}\hat{B}f(x)$ if $\hat{A} = d/dx$, $\hat{B} = x$, and $f(x) = \cos x$.

Q2.18 Is $\cos x$ an eigenfunction of the operator \hat{A} if $\hat{A}f(x) = xf(x)$?

Q2.19 Which of the following functions are eigenfunctions of the operator \hat{B} if $\hat{B}f(x) = d^2f(x)/dx^2$: x^2 , $\cos x$, e^{-3ix} . State the eigenvalue if applicable.

NUMERICAL PROBLEMS

Section 2.2

P2.1 A wave traveling in the z direction is described by the wave function $\Psi(z, t) = A_1 \mathbf{x} \sin(kz - \omega t + \phi_1) + A_2 \mathbf{y} \sin(kz - \omega t + \phi_2)$, where \mathbf{x} and \mathbf{y} are vectors of unit length along the x and y axes, respectively. Because the amplitude is perpendicular to the propagation direction, $\Psi(z, t)$ represents a transverse wave.

- a. What requirements must A_1 and A_2 satisfy for a plane polarized wave in the x - z plane? The amplitude of a plane polarized wave is nonzero only in one plane.
- b. What requirements must A_1 and A_2 satisfy for a plane polarized wave in the y - z plane?
- c. What requirements must A_1 and A_2 and ϕ_1 and ϕ_2 satisfy for a plane polarized wave in a plane oriented at 45° to the y - z plane?
- d. What requirements must A_1 and A_2 and ϕ_1 and ϕ_2 satisfy for a circularly polarized wave? The phases of the two components of a circularly polarized wave differ by $\pi/2$.

P2.2 Does the superposition $\psi(x, t) = A \sin(kx - \omega t) + 2A \sin(kx + \omega t)$ generate a standing wave? Answer this question by using trigonometric identities to combine the two terms.

P2.3 To plot $\Psi(x, t) = A \sin(kx - \omega t)$ as a function of one of the variables x and t , the other variable needs to be set at a fixed value, x_0 or t_0 . If $\Psi(x_0, 0)/\Psi_{\max} = -0.280$, what is the constant value of x_0 in the upper panel of Figure 2.3? If $\Psi(0, t_0)/\Psi_{\max} = -0.309$, what is the constant value of t_0 in the lower panel of Figure 2.3? (Hint: The inverse sine function has two solutions within an interval of 2π . Make sure that you choose the correct one.)

P2.4 Using the exponential representation of the sine and cosine functions, $\cos \theta = \frac{1}{2}(e^{i\theta} + e^{-i\theta})$ and $\sin \theta = \frac{1}{2i}(e^{i\theta} - e^{-i\theta})$, $\cos \theta = \frac{1}{2}(e^{i\theta} + e^{-i\theta})$ and $\sin \theta = \frac{1}{2i}(e^{i\theta} - e^{-i\theta})$, show that

- a. $\cos^2 \theta + \sin^2 \theta = 1$
- b. $d(\cos \theta)/d\theta = -\sin \theta$
- c. $\sin\left(\theta + \frac{\pi}{2}\right) = \cos \theta$

Section 2.3

P2.5 Show that

$$\frac{a+ib}{c+id} = \frac{ac+bd+i(bc-ad)}{c^2+d^2}$$

P2.6 Express the following complex numbers in the form $re^{i\theta}$.

- a. $3 - 2i$
- b. 4
- c. $\frac{3-i}{4+2i}$
- d. $5i$
- e. $2 - 4i$

P2.7 Express the following complex numbers in the form $a + ib$ if they are in the form $re^{i\theta}$ or vice versa.

- a. $3e^{1.333i}$
- b. $2\sqrt{2}e^{0.500i}$
- c. $3 - 4i$
- d. $2 + 3i$

Section 2.4

P2.8 Determine in each of the following cases if the function in the first column is an eigenfunction of the operator in the second column. If so, what is the eigenvalue?

- a. $5y^5$
- b. $yx^7 - xy^{-7}$
- c. $\sin\theta \cos 3\phi$
- $y^2 d^2/dy^2$
- $x^3(\partial^3/\partial x^3) + y^3(\partial^3/\partial y^3)$
- $\partial^2/\partial\theta^2 + \partial^2/\partial\phi^2$

P2.9 If two operators act on a wave function as indicated by $\hat{A}\hat{B} f(x)$, it is important to carry out the operations in succession, with the first operation being that nearest to the function. Mathematically, $\hat{A}\hat{B} f(x) = \hat{A}(\hat{B} f(x))$ and $\hat{A}^2 f(x) = \hat{A}(\hat{A} f(x))$. Evaluate the following successive operations $\hat{A}\hat{B} f(x)$. The operators \hat{A} and \hat{B} are listed in the first two columns and $f(x)$ is listed in the third column.

- a. $\frac{d}{dx}$
- b. x^2
- c. $\frac{d^2}{d\theta^2}$
- d. $\frac{d}{d\theta}$
- x^2
- $\frac{d}{dx}$
- $\frac{d}{d\theta}$
- $\frac{d^2}{d\theta^2}$
- e^{-ikx}
- e^{-ikx}
- $3 \cos^2\theta - 1$
- $3 \cos^2\theta - 1$

Are your answers to parts (a) and (b) identical? Are your answers to parts (c) and (d) identical? As we will learn in Chapter 6, the fact that switching the order of the operators x and d/dx changes the outcome of the operation $\hat{A}\hat{B} f(x)$ is the basis for the Heisenberg uncertainty principle.

P2.10 Let $(1, 0)$ and $(0, 1)$ represent the unit vectors along the x and y directions, respectively. The operator

$$\begin{pmatrix} \cos\theta & -\sin\theta \\ \sin\theta & \cos\theta \end{pmatrix}$$

effects a rotation in the x - y plane. Show that the length of an arbitrary vector

$$\begin{pmatrix} a \\ b \end{pmatrix} = a \begin{pmatrix} 1 \\ 0 \end{pmatrix} + b \begin{pmatrix} 0 \\ 1 \end{pmatrix}$$

which is defined as $\sqrt{a^2 + b^2}$, is unchanged by this rotation. See Math Essential 10 for a discussion of matrices.

P2.11 Operators can also be expressed as matrices and wave functions as column vectors. The operator matrix

$$\begin{pmatrix} \alpha & \beta \\ \delta & \varepsilon \end{pmatrix}$$

acts on the wave function $\begin{pmatrix} a \\ b \end{pmatrix}$ according to the rule

$$\begin{pmatrix} \alpha & \beta \\ \delta & \varepsilon \end{pmatrix} \begin{pmatrix} a \\ b \end{pmatrix} = \begin{pmatrix} \alpha a + \beta b \\ \delta a + \varepsilon b \end{pmatrix}$$

In words, the 2×2 matrix operator acting on the two-element column wave function generates another two-element column wave function. If the wave function generated by the operation is the original wave function multiplied by a constant, the wave function is an eigenfunction of the operator. What is the effect of the operator

$$\begin{pmatrix} 0 & 1 \\ 1 & 0 \end{pmatrix}$$

on the column vectors $(1, 0)$, $(0, 1)$, $(1, 1)$, and $(-1, 1)$? Are these wave functions eigenfunctions of the operator? See Math Essential 10 for a discussion of matrices.

P2.12 Operate with (a) $\frac{\partial}{\partial x} + \frac{\partial}{\partial y} + \frac{\partial}{\partial z}$ and (b) $\frac{\partial^2}{\partial x^2} + \frac{\partial^2}{\partial y^2} + \frac{\partial^2}{\partial z^2}$ on the function $Ae^{-ik_1x}e^{-ik_2y}e^{-ik_3z}$. Is the function an eigenfunction of either operator? If so, what is the eigenvalue?

P2.13 Determine in each of the following cases if the function in the first column is an eigenfunction of the operator in the second column. If so, what is the eigenvalue?

- a. $\cos\theta$
- b. e^{4ix}
- c. $\cos^2\theta$
- $\frac{1}{\sin\theta} \frac{d}{d\theta} \left(\sin\theta \frac{d}{d\theta} \right)$
- $\frac{d^2}{dx^2} + \frac{d}{dx} - 4i$
- $\frac{\cos\theta}{\sin\theta} \frac{d^2}{d\theta^2}$

P2.14 Determine in each of the following cases if the function in the first column is an eigenfunction of the operator in the second column. If so, what is the eigenvalue?

- a. $e^{2i(3x+y^2)}$
- b. $\sin^2 a\theta$
- c. $\cos 5\theta + \sin 5\theta$
- $\frac{\partial^2}{\partial x^2}$
- $\frac{d^2}{d\theta^2} - 2a^2 \cos^2\theta$
- $\frac{d^2}{d\theta^2}$

P2.15 Assume that a system has a very large number of energy levels given by the formula $\varepsilon_l = \varepsilon_0 l^2$ with $\varepsilon_0 = 1.25 \times 10^{-22}$ J, where l takes on the integral values 1, 2, 3, Assume further that the degeneracy of a level is given by $g_l = 2l$. Calculate the ratios n_{12}/n_1 and n_{12}/n_1 for $T = 220$ K and $T = 875$ K.

P2.16 Is the function x^4y^5 an eigenfunction of the operator $xd/dx + yd/dy$? If so, what is the eigenvalue?

P2.17 Find the result of operating with $d^2/dx^2 - 3x^2$ on the function e^{-2ax^2} . What must the value of a be to make this function an eigenfunction of the operator?

P2.18 Determine in each of the following cases if the function in the first column is an eigenfunction of the operator in the second column. If so, what is the eigenvalue?

a. $\sin^4 \theta$ $-\tan \theta d/d\theta$

b. $e^{-5x^2/\sqrt{2}}$ $(1/x)d/dx$

c. $\sqrt{1+x^2}$ $\frac{1+x^2}{x} d/dx$

P2.19 Find the result of operating with $x^2 d^2/dx^2 + y^2 d^2/dy^2 + z^2 d^2/dz^2$ on the function $x^5 + y^5 + z^5$.

Is this function an eigenfunction of the operator?

P2.20 If two operators act on a wave function as indicated by $\hat{A}\hat{B} f(x)$, it is important to carry out the operations in succession, with the first operation being that nearest to the function. Mathematically, $\hat{A}\hat{B} f(x) = \hat{A}(\hat{B} f(x))$ and $\hat{A}^2 f(x) = \hat{A}(\hat{A} f(x))$. Evaluate the following successive operations $\hat{A}\hat{B} f(x)$. The operators \hat{A} and \hat{B} are listed in the first and second columns, and $f(x)$ is listed in the third column.

a. $\frac{d}{dx}$ x $e^{5ix} - 1$

b. x $\frac{d}{dx}$ $e^{5ix} - 1$

c. $\frac{d^2}{dy^2}$ y^2 $1+y$

d. y^2 $\frac{d^2}{dy^2}$ $1+y$

P2.21 Consider a two-level system with

$\varepsilon_1 = 1.75 \times 10^{-22}$ J and $\varepsilon_2 = 3.50 \times 10^{-21}$ J. If $g_2 = 2g_1$, what value of T is required to obtain $n_2/n_1 = 0.150$? What value of T is required to obtain $n_2/n_1 = 0.900$?

P2.22 Find the result of operating with

$(1/r^2)(d/dr)(r^2 d/dr) + 2/r$ on the function Ae^{-4ibr} . What must the values of A and b be to make this function an eigenfunction of the operator?

P2.23 Operate with (a) $\frac{\partial}{\partial x} + \frac{\partial}{\partial y} + \frac{\partial}{\partial z}$ and (b) $\frac{\partial^2}{\partial x^2} + \frac{\partial^2}{\partial y^2} + \frac{\partial^2}{\partial z^2}$

on the function $A e^{-ik_1 x} e^{-ik_2 y} e^{-ik_3 z}$. Is the function an eigenfunction of either operator? If so, what is the eigenvalue?

P2.24 Form the operator \hat{A}^2 if $\hat{A} = y + 2d/dy$. Be sure to include an arbitrary function on which the operator acts.

P2.25 Is the function e^{-4ix^2} an eigenfunction of the operator $d^2/dx^2 + 64x^2$? If so, what is the eigenvalue?

P2.26 Which of the following wave functions are eigenfunctions of the operator d/dx ? If they are eigenfunctions, what is the eigenvalue?

a. e^{-5ix} b. e^{-5x^2} c. $e^{\sin 5ax}$

P2.27 Form the operator \hat{A}^2 if $\hat{A} = d^2/dy^2 - 5$. Be sure to include an arbitrary function on which the operator acts.

P2.28 Which of the following wave functions are eigenfunctions of the operator d^2/dx^2 ? If they are eigenfunctions, what is the eigenvalue?

a. $e^{-3\sqrt{5}x}$ b. $e^{2\sqrt{7}ix}$

c. $\cos \frac{3\sqrt{2}}{5}x$ d. e^{-ax^2}

e. $\frac{e^{-2x}}{4} + \frac{e^{-2ix}}{4}$

Section 2.6

P2.29 Because $\int_{-d}^d \cos(n\pi x/d) \cos(m\pi x/d) dx = 0$, $m \neq n$, the functions $\cos(n\pi x/d)$ for $n = 1, 2, 3, \dots$ form an orthogonal set. What constant must these functions be multiplied by to form an orthonormal set?

P2.30 Carry out the following coordinate transformations:

a. Express the point $x = 2$, $y = 3$, and $z = 1$ in spherical coordinates.

b. Express the point $r = 6$, $\theta = 0.785$ radians, and $\phi = 1.047$ radians in Cartesian coordinates.

P2.31 Show that the set of functions $\phi_n(\theta) = e^{in\theta}$, $0 \leq \theta \leq 2\pi$, is orthogonal if n and m are integers. To do so, you need to show that the integral $\int_0^{2\pi} \phi_m^*(\theta) \phi_n(\theta) d\theta = 0$ for $m \neq n$ if n and m are integers.

P2.32 Show by carrying out the integration that $\sin(m\pi x/a)$ and $\cos(m\pi x/a)$, where m is an integer, are orthogonal over the interval $0 \leq x \leq a$. Would you get the same result if you used the interval $0 \leq x \leq 3a/4$? Explain your result.

P2.33 Make the three polynomial functions a_0 , $a_1 + b_1 x$, and $a_2 + b_2 x + c_2 x^2$ orthonormal in the interval $-1 \leq x \leq +1$ by determining appropriate values for the constants a_0 , a_1 , b_1 , a_2 , b_2 , and c_2 .

P2.34 Normalize the set of functions $\phi_n(\theta) = e^{in\theta}$, $0 \leq \theta \leq 2\pi$. To do so, you need to multiply the functions by a so-called normalization constant N so that the integral $NN^* \int_0^{2\pi} \phi_m^*(\theta) \phi_n(\theta) d\theta = 1$ for $m = n$.

P2.35 In normalizing wave functions, the integration is over all space in which the wave function is defined. Normalize the wave function $x(a-x)y(b-y)$ over the range $0 \leq x \leq a$, $0 \leq y \leq b$. The element of area in two-dimensional Cartesian coordinates is $dx dy$; a and b are constants.

P2.36 Show that the following pair of wave functions is orthogonal over the indicated range. $e^{-\alpha x^2}$ and $x(x^2 - 1)e^{-\alpha x^2}$, $-\infty \leq x < \infty$ where α is a constant that is greater than zero.

Section 2.7

P2.37 Use a Fourier series expansion to express the function $f(y) = y^2$, $-a \leq y \leq a$, in the form

$$f(y) = d_0 + \sum_{n=1}^m c_n \sin\left(\frac{n\pi y}{a}\right) + d_n \cos\left(\frac{n\pi y}{a}\right)$$

Obtain d_0 and the first five coefficients c_n and d_n .

WEB-BASED SIMULATIONS, ANIMATIONS, AND PROBLEMS

Simulations, animations, and homework problem worksheets can be accessed at www.pearsonhighered.com/advchemistry

W2.1 Two waves of the same frequency traveling in opposite directions are combined. The relative amplitude is changed with sliders, and the relative phase of the waves is varied. The effect of these changes on the superposition wave is investigated.

W2.2 Two waves, both of which are standing waves, are combined. The effect of varying the wavelength, period, and phase of the waves on the resulting wave using sliders is investigated.

FURTHER READING

Barrante, J. R. *Applied Mathematics for Physical Chemistry* (3rd edition). Upper Saddle River, NJ: Pearson, 2004, Chapters 6 and 10.

McQuarrie, D. A. "Mathematical Methods for Scientists and Engineers." Sausalito, CA: University Science Books, 2003, Chapters 4, 11, and 15.

This page intentionally left blank

The Quantum-Mechanical Postulates

WHY is this material important?

To understand the properties of atoms and molecules, it is necessary to be familiar with the principles of quantum mechanics and the postulates on which quantum mechanics is based. In this chapter, we discuss the postulates and give examples of their application.

WHAT are the most important concepts and results?

A quantum-mechanical system is fully described by its wave function. In quantum mechanics, for every measurable property of a system, such as position, momentum, and energy (which we refer to as observables), there exists a corresponding operator. In any single measurement of the observable that corresponds to the operator \hat{A} , the only values that will ever be measured are the eigenvalues of that operator. In classical mechanics, knowledge of the present state of a system and the forces acting on it determine a future state of the system. By contrast, quantum mechanics is inherently probabilistic. In general, we can only predict the probability of obtaining a particular result in an experiment.

WHAT would be helpful for you to review for this chapter?

It would be useful to be familiar with the discussion of the Schrödinger equation, operators, observables, eigenfunctions, and eigenvalues in Chapter 2.

3.1 THE PHYSICAL MEANING ASSOCIATED WITH THE WAVE FUNCTION IS PROBABILITY

Quantum mechanics can be formulated in terms of six postulates. A **postulate** is a claim or an assumption of truth, especially as a basis for reasoning. Postulates cannot be proven, but they can be tested. The five postulates discussed in this chapter provide a framework for summarizing the basic concepts of quantum mechanics. The quantum-mechanical postulates have been extensively tested since they were proposed in the early 1930s. No case has been found in which they predict an outcome that conflicts with the result of an experiment. The sixth postulate will be introduced in Chapter 10.

- 3.1 The Physical Meaning Associated with the Wave Function Is Probability
- 3.2 Every Observable Has a Corresponding Operator
- 3.3 The Result of an Individual Measurement
- 3.4 The Expectation Value
- 3.5 The Evolution in Time of a Quantum-Mechanical System

POSTULATE 1

The state of a quantum-mechanical particle is completely specified by a wave function $\Psi(x, t)$. To simplify the notation, only one spatial coordinate is considered. The probability that the particle will be found at time t_0 in a spatial interval of width dx centered at x_0 is given by $\Psi^*(x_0, t_0)\Psi(x_0, t_0)dx$.

Concept

Quantum mechanics is based on six postulates, which have been extensively tested and confirmed by experiments.

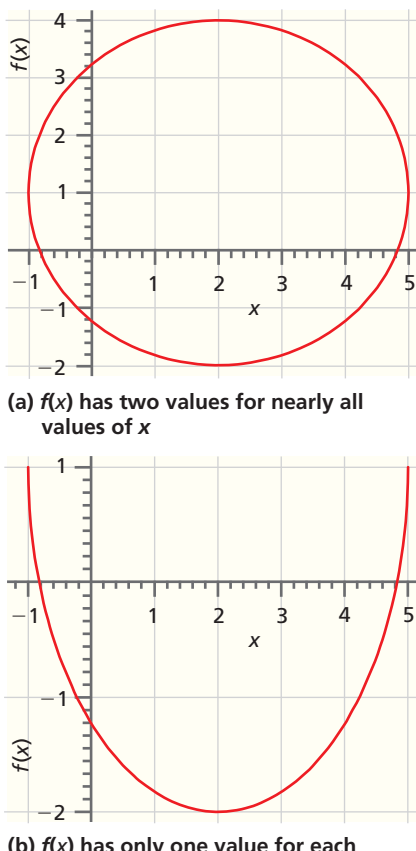


Figure 3.1

Multiple- and single-valued functions of the spatial coordinate x . Examples of (a) a multi-valued function and (b) a single-valued function.

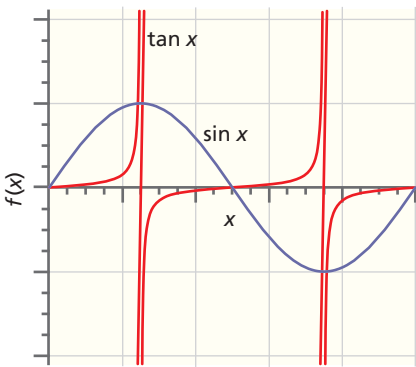


Figure 3.2

Examples of continuous and discontinuous functions.

For a sound wave, the wave function $\Psi(x, t)$ is the pressure at time t and position x . For a water wave, $\Psi(x, t)$ is the height of the wave as a function of position and time. What physical meaning can we associate with $\Psi(x, t)$ for quantum systems? For a particle, which also has wave character, the probability $P(x_0, t_0)dx$ of finding the particle at position x_0 at time t_0 within an interval dx is

$$P(x_0, t_0) dx = \Psi^*(x_0, t_0)\Psi(x_0, t_0) dx = |\Psi(x_0, t_0)|^2 dx \quad (3.1)$$

Unlike classical waves such as sound waves, the wave amplitude $\Psi(x, t)$ itself has no direct physical meaning in quantum mechanics. Because the probability is related to the *square of the magnitude* of $\Psi(x, t)$, given by $\Psi^*(x, t)\Psi(x, t)$, the wave function can be complex or negative and still be associated with a probability that lies between zero and one. The wave amplitude $\Psi(x, t)$ can be multiplied by -1 , or its phase can be changed by multiplying it by a complex function of magnitude such as $e^{i\theta(x,t)}$, without changing $\Psi^*(x, t)\Psi(x, t)$. Therefore, all wave functions that are identical except for a phase angle $\theta(x, t)$ are indistinguishable in that they generate the same observables. The wave function is a complete description of the system in that any measurable property (observable) can be obtained from the wave function, as will be described later.

The association of the wave function with the probability places an important requirement on a wave function called **normalization**. The probability that the particle is found in an interval of width dx centered at the position x must lie between zero and one. The sum of the probabilities over all intervals accessible to the particle is one because the particle is somewhere in its range. Consider a particle that is confined to a one-dimensional space of infinite extent. The requirement that the particle is somewhere in the interval leads to the following normalization condition:

$$\int_{-\infty}^{\infty} \Psi^*(x, t)\Psi(x, t) dx = 1 \quad (3.2)$$

Such a definition is obviously meaningless if the integral does not exist. Therefore, $\Psi(x, t)$ must satisfy several mathematical conditions to ensure that it represents a possible physical state. These conditions are as follows:

- The wave function must be a **single-valued function** of the spatial coordinates. If this were not the case, a particle would have more than one probability of being found in the same interval. For example, for the ellipse depicted in Figure 3.1a, $f(x)$ has two values for each value of x except the two points at which the tangent line is vertical. If only the part of the ellipse is considered for which $f(x) < 1$, as in Figure 3.1b, $f(x)$ has only one value for each value of x .
- The wave function and its first derivative must be continuous over the interval in which it is defined. Otherwise the second derivative is not well defined. As shown in Figure 3.2, $\sin x$ is a **continuous function** of x . A function $f(x)$ is continuous at the point a if the following conditions hold:¹
 - $f(x)$ is defined at a .
 - $\lim_{x \rightarrow a} f(x)$ exists and has the same value when $x \rightarrow a$ from values greater than or less than a .
 - $\lim_{x \rightarrow a} f(x) = f(a)$

The function $\tan x$ is not continuous at $x = \pi/2$ because $\tan \pi/2$ has different values when approached from $x > \pi/2$ and $x < \pi/2$.

- The wave function cannot have an infinite amplitude within the interval. If this is the case, the wave function cannot be normalized. As an example, the function

$$\Psi(x, t) = e^{-i(E/\hbar)t} \frac{1}{x^2} \sin \frac{2\pi x}{a}, \quad 0 \leq x \leq a \text{ cannot be normalized.}$$

¹We will encounter an exception to this rule in Chapter 4. If the potential energy abruptly increases to infinity, the wave function will have a kink at that point; therefore, the slope of the first derivative will be discontinuous.

3.2 EVERY OBSERVABLE HAS A CORRESPONDING OPERATOR

POSTULATE 2

For every measurable property of a system such as position, momentum, and energy, there exists a corresponding operator in quantum mechanics. An experiment in the laboratory to measure a value for such an observable is simulated in quantum mechanics by operating on the wave function of the system with the corresponding operator.

All quantum-mechanical operators belong to a mathematical class called **Hermitian operators** that have real eigenvalues. The most important observables in classical mechanics, the corresponding quantum-mechanical operators, and the symbols for these operators are listed in Table 3.1. To simplify the notation, only one spatial coordinate is considered, except for angular momentum. Partial derivatives have been retained because the wave function depends on both position and time. The total energy operator, called the Hamiltonian, is given the symbol \hat{H} . For the position and potential energy operators, the operation is “multiply on the left by the position or potential energy.” Operators act on a wave function from the left, and the order of operation is important. For example, the result of the operation $\hat{p}_x \hat{x}$ on $\sin x$ is $-i\hbar(\sin x + x \cos x)$, whereas $\hat{x} \hat{p}_x$ operating on the same wave function results in $-i\hbar x \cos x$. As discussed in Chapter 6, operators for which the interchanging of the order does not change the result have a particular role in quantum mechanics.

TABLE 3.1 Observables and Their Quantum-Mechanical Operators

Observable	Operator	Symbol for Operator
Momentum	$-i\hbar \frac{\partial}{\partial x}$	\hat{p}_x
Kinetic energy	$-\frac{\hbar^2}{2m} \frac{\partial^2}{\partial x^2}$	$\hat{E}_{kinetic} = \frac{1}{2m} (\hat{p}_x)(\hat{p}_x)$
Position	x	\hat{x}
Potential energy	$V(x)$	$\hat{E}_{potential}$
Total energy	$-\frac{\hbar^2}{2m} \frac{\partial^2}{\partial x^2} + V(x)$	\hat{H}
Angular momentum	$-i\hbar \left(y \frac{\partial}{\partial z} - z \frac{\partial}{\partial y} \right)$ $-i\hbar \left(z \frac{\partial}{\partial x} - x \frac{\partial}{\partial z} \right)$ $-i\hbar \left(x \frac{\partial}{\partial y} - y \frac{\partial}{\partial x} \right)$	\hat{l}_x \hat{l}_y \hat{l}_z

Concept

The physical interpretation of the wave function is that $\Psi^*(x_0, t_0)\Psi(x_0, t_0)$ is related to the probability of finding the particle in a small region centered at x_0 at time t_0 .

Concept

Analyzing the results of an experiment using quantum mechanics can be modeled in terms of an operator acting on a wave function.

Concept

Operators involve an action, which is usually multiplication by a function or differentiation with respect to a variable.

3.3 THE RESULT OF AN INDIVIDUAL MEASUREMENT

POSTULATE 3

In any single measurement of the observable that corresponds to the operator \hat{A} , the only values that will ever be measured are the eigenvalues of that operator.

Concept

The only possible outcome of a measurement is one of the eigenvalues of the corresponding operator.

This postulate states, for example, that if the energy of the hydrogen atom is measured, the only values obtained are the energies that are the eigenvalues E_n of the time-independent Schrödinger equation:

$$\hat{H}\Psi_n(x, t) = E_n\Psi_n(x, t) \quad (3.3)$$

This makes sense because the energy levels of the hydrogen atom are discrete and, therefore, only those energies are allowed. What gives pause for thought is that the wave function need not be an eigenfunction of \hat{H} because the eigenfunctions are a subset of the infinite number of functions that satisfy all the requirements to be an acceptable wave function. We address this issue in the following postulate.

3.4 THE EXPECTATION VALUE

Concept

The measurement process in quantum mechanics is inherently probabilistic. However, the average of a measurement on a large number of identically prepared systems can be predicted and is given by Equation (3.4).

POSTULATE 4

If the system is in a state described by the wave function $\Psi(x, t)$, and the value of the observable a is measured once on each of many identically prepared systems, the average value (also called the **expectation value**) of all of these measurements is given by

$$\langle a \rangle = \frac{\int_{-\infty}^{\infty} \Psi^*(x, t)\hat{A}\Psi(x, t) dx}{\int_{-\infty}^{\infty} \Psi^*(x, t)\Psi(x, t) dx} \quad (3.4)$$

For the case in which $\Psi(x, t)$ is normalized, the denominator in this expression has the value 1. Wave functions are usually normalized, and in Equations (3.5) through (3.8), this is assumed to be the case. This postulate requires some explanation. As we know, two cases apply with regard to $\Psi(x, t)$: it either is or is not an eigenfunction of the operator \hat{A} . These two cases need to be examined separately.

In the first case, $\Psi(x, t)$ is a normalized eigenfunction of \hat{A} —for example, $\phi_j(x, t)$. Because $\hat{A}\phi_j(x, t) = a_j\phi_j(x, t)$,

$$\begin{aligned} \langle a \rangle &= \int_{-\infty}^{\infty} \phi_j^*(x, t)\hat{A}\phi_j(x, t)dx = a_j \int_{-\infty}^{\infty} \phi_j^*(x, t)\phi_j(x, t) dx \\ &= a_j \end{aligned} \quad (3.5)$$

If $\Psi(x, t)$ is $\phi_j(x, t)$, all measurements will give the same answer, namely, a_j .

Now consider the second case, in which $\Psi(x, t)$ is not an eigenfunction of the operator \hat{A} . Because the eigenfunctions of \hat{A} form a complete set, $\Psi(x, t)$ can be expanded in terms of these eigenfunctions:

$$\Psi(x, t) = \sum_n b_n \phi_n(x, t) \quad (3.6)$$

Because $\Psi(x, t)$ is normalized, $\sum_m b_m^* b_m = \sum_m |b_m|^2 = 1$. The expression for $\Psi(x, t)$ in Equation (3.6) can be inserted in Equation (3.4), giving

$$\begin{aligned} \langle a \rangle &= \int \Psi^*(x, t)\hat{A}\Psi(x, t)dx \\ &= \int_{-\infty}^{\infty} \left[\sum_{m=1}^{\infty} b_m^* \phi_m^*(x, t) \right] \left[\sum_{n=1}^{\infty} a_n b_n \phi_n(x, t) \right] dx \\ &= \sum_{m=1}^{\infty} \sum_{n=1}^{\infty} b_m^* b_n a_n \int_{-\infty}^{\infty} \phi_m^*(x, t) \phi_n(x, t) dx \end{aligned} \quad (3.7)$$

This expression can be greatly simplified by making use of the property that the eigenfunctions of a quantum-mechanical operator are orthogonal. Because the eigenfunctions of \hat{A} form an **orthonormal set**, the only terms in this double sum for which the integral is nonzero are those for which $m = n$. The integral has the value 1 for these terms because the eigenfunctions of \hat{A} are normalized. Therefore,

$$\langle a \rangle = \sum_{m=1}^{\infty} a_m b_m^* b_m = \sum_{m=1}^{\infty} |b_m|^2 a_m \quad (3.8)$$

How do we interpret the coefficients b_m ? They are the **expansion coefficients** of the wave function in the complete set of the eigenfunctions of the operator \hat{A} . The coefficient b_m is a measure of the extent to which the wave function “looks like” the m th eigenfunction of the operator \hat{A} . To illustrate this point, consider the case in which $\Psi(x, t) = \phi_n(x, t)$. In this case, all of the b_m except the one value corresponding to $m = n$ are zero, $b_n = 1$, and $\langle a \rangle = a_n$. So, if $\phi(x, t)$ is one of the eigenfunctions of \hat{A} , only one of the coefficients is nonzero, and the average value is just the eigenvalue corresponding to that eigenfunction. If only three of the coefficients are nonzero, for example, b_2 , b_8 , and b_{11} , then $b_2^2 + b_8^2 + b_{11}^2 = 1$, and $\langle a \rangle$ is given by

$$\langle a \rangle = |b_2|^2 a_2 + |b_8|^2 a_8 + |b_{11}|^2 a_{11} \quad (3.9)$$

Note that $\langle a \rangle$ is not simply an average of these three eigenvalues; instead, it is a **weighted average**. The weighting factor $|b_m|^2$ is directly related to the contribution of the m th eigenfunction to the wave function $\Psi(x, t)$.

The fourth postulate allows us to calculate the result of many measurements, each carried out only once on a large number of identically prepared systems. What will be measured in each of these individual measurements? The third postulate states that the only possible result of a single measurement is one of the eigenvalues a_n . However, it does not tell us which of the a_n will be measured. The answer is that there is no way of knowing the outcome of an **individual measurement** and that the outcomes from identically prepared systems are not the same. This is a sharp break with the predictability we have come to depend on in classical mechanics.

Consider a hypothetical example. Suppose that a single hydrogen atom could be isolated in a box and the electronic wave function prepared such that it is in a superposition of the ground state, in which the electron is in the $1s$ orbital, and the excited states, in which the electron is in the $2s$, $2p_x$, and $3s$ orbitals. Assume that the wave function for this **superposition state** is

$$\Psi_{\text{electronic}} = b_1 \Psi_{1s} + b_2 \Psi_{2s} + b_3 \Psi_{2p_x} + b_4 \Psi_{3s} \quad (3.10)$$

We now prepare a large number of these systems, each of which is identical and has the same wave function, and carry out a measurement of the total energy of the atom. The results that would be obtained are illustrated in Figure 3.3. Even though the systems are identical, the same value is not obtained for the energy of the atom in each system.

More generally, the particular value observed in one measurement will be any one of the eigenvalues a_n for which the corresponding b_n is nonzero. This is a

Concept

Any well behaved function can be expanded in the eigenfunctions of a quantum mechanical operator because they form a complete orthonormal set.

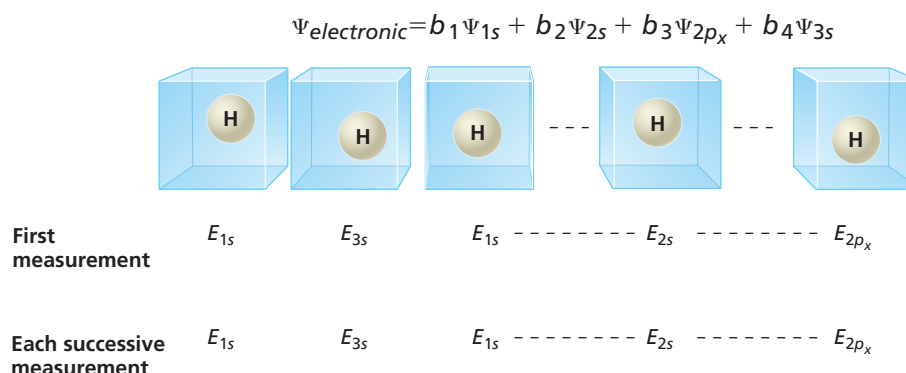


Figure 3.3

A large number of identically prepared systems consist of a single hydrogen atom in a three-dimensional box. The atom is described by the superposition state $\Psi_{\text{electronic}} = b_1 \Psi_{1s} + b_2 \Psi_{2s} + b_3 \Psi_{2p_x} + b_4 \Psi_{3s}$. Consider a hypothetical experiment that measures the total energy and is completed in such a short time that transitions to the ground state can be neglected. The result of the first measurement on each system is probabilistic, whereas successive measurements are deterministic.

probabilistic outcome, similar to asking what the chance is of rolling a six with one throw of a die. In this more familiar case, there is no way to predict the outcome of a single throw. However, if the die is thrown many times, the six will land facing up a proportion of times that approaches 1/6. The equivalent case to the die for the wave function is that all of the coefficients b_m have the same value. In the particular case under consideration, we have only four nonzero coefficients; therefore, we will only measure one of the values E_{1s} , E_{2s} , E_{2p} , or E_{3s} in an individual measurement, but we have no way of knowing which of these values we will obtain. The certainty that we are familiar with from classical mechanics—that identically prepared systems all have the same outcomes in a measurement—is replaced in quantum mechanics by the probabilistic outcome just described.

More can be said about the outcome of a large number of measurements than about the outcome of a single measurement. Consider the more general result stated in Equation (3.8): the average value of a large number of measurements carried out once on identically prepared systems is given by a sum containing the possible eigenvalues of the operator weighted by $|b_m|^2$, the square of the expansion coefficient. The bigger the contribution of an eigenfunction $\phi_m(x, t)$ of \hat{A} to $\Psi(x, t)$ (larger $|b_m|^2$), the more probable it is that the outcome of an individual measurement will be a_m and the more a_m will influence the average value $\langle a \rangle$. There is no way to predict which of the a_m will be found in an individual measurement. However, if this same experiment is repeated many times on identical systems, the average value can be predicted with very high precision. It is important to realize that this is not a shortcoming of how the “identical” systems were prepared. These systems are identical in every way, and there is no reason to believe that we have left something out that resulted in this probabilistic result.

To illustrate the preceding discussion, consider the three different normalized superposition wave functions shown in Figure 3.4. They are made of the normalized eigenfunctions $\phi_1(x)$, $\phi_2(x)$, and $\phi_3(x)$ of the operator \hat{A} with eigenvalues a_1 , $4a_1$, and $9a_1$, respectively. The superposition wave functions are the following combinations of $\phi_1(x)$, $\phi_2(x)$, and $\phi_3(x)$:

$$\begin{aligned}\psi_1(x) &= \frac{\sqrt{11}}{4} \phi_1(x) + \frac{1}{4} \phi_2(x) + \frac{1}{2} \phi_3(x) \\ \psi_2(x) &= \frac{1}{2} \phi_1(x) + \frac{1}{4} \phi_2(x) + \frac{\sqrt{11}}{4} \phi_3(x) \\ \psi_3(x) &= \frac{1}{2} \phi_1(x) + \frac{\sqrt{11}}{4} \phi_2(x) + \frac{1}{4} \phi_3(x)\end{aligned}\quad (3.11)$$

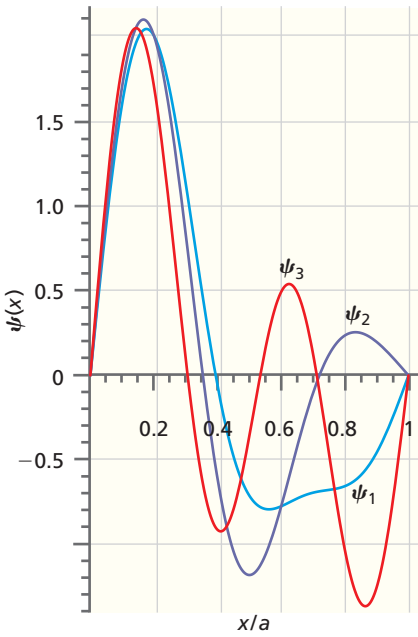


Figure 3.4

Plot of three normalized wave functions. The three normalized wave functions $\psi_1(x)$, $\psi_2(x)$, and $\psi_3(x)$ (blue, purple, and red curves, respectively) are defined over the interval $0 \leq x \leq a$. The amplitude of the wave functions is zero at both ends of the interval.

Concept

The act of measurement on a superposition state changes the wave function into an eigenfunction of the corresponding operator.

An individual measurement of the observable a gives only one of the values a_1 , $4a_1$, and $9a_1$ regardless of which wave function describes the system. However, the probability of observing these values depends on the system wave function. For example, the probability of observing the value $9a_1$ is given by the square of the magnitude of the coefficient of $\phi_3(x)$ and is $1/4$, $11/16$, and $1/16$, respectively, depending on whether the state is described by $\psi_1(x)$, $\psi_2(x)$, or $\psi_3(x)$.

Notice that the postulate specified that the measurement was to be carried out only once on each of a large number of identically prepared systems. What lies behind this requirement? We have just learned that the first measurement will give one of the eigenvalues of the operator corresponding to the observable being measured. We have also learned that we have no way to predict the outcome of a single measurement. What is expected if a second measurement of the same observable were to be carried out on the same system? The experimentally established answer to this question is illustrated in Figure 3.3. In successive measurements on the same system, exactly the same result will be obtained that was obtained in the first experiment. If further successive measurements are carried out, all of the results will be the same. The probabilistic result is obtained only on the first measurement; after that, the result is deterministic.

How can this transition from a probabilistic to a **deterministic outcome** be understood? Note that the second and all successive results are exactly what would be expected if the system were in a particular eigenstate of the operator for which only one coefficient b_m is nonzero, namely, Ψ_{1s} , or Ψ_{2s} , or Ψ_{2p_z} , or Ψ_{3s} , and not in the

original superposition state $\Psi_{\text{electronic}} = b_1\Psi_{1s} + b_2\Psi_{2s} + b_3\Psi_{2p_x} + b_4\Psi_{3s}$. In fact, this is the key to understanding this very puzzling result. The act of carrying out a quantum-mechanical measurement appears to collapse the wave function of a system to an eigenfunction of the operator corresponding to the measured quantity! We are accustomed to thinking of our role in carrying out a measurement in classical mechanics as being passive. We simply note what the system is doing, and it is not influenced by us. The **measurement process** in quantum mechanics is radically different. In fact, the standard interpretation of quantum mechanics, attributed to the school of Niels Bohr, gives the measurement process a central role in the outcome of the experiment. This has vexed many scientists, most notably Albert Einstein. Applying this reasoning to the macroscopic world, he remarked to a colleague, “Do you really think that the moon is not there when we are not looking at it?” However strange this may all seem, no one has devised an experiment to show that the view of the measurement process in quantum mechanics stated in this postulate is incorrect.

Although the concept of superposition and the collapse of the superposition wave function by the act of measurement in quantum mechanics is unfamiliar, it is analogous to interpreting the optical illusion shown in Figure 3.5. This image can be interpreted as depicting either a young woman or an old woman. Therefore, we can describe it as a superposition of the two images. When the brain interprets it in what we can call a measurement, the result is either the young woman or the old woman. Just as in the quantum-mechanics experiment described earlier, the result of observation is one of the elements of the superposition, and the act of measurement generates the outcome from one of several possibilities. However, unlike the quantum-mechanics experiment, a second viewing of the image in Figure 3.5 need not give the same result as the first viewing.



Figure 3.5

The image can be interpreted as either a young woman or an old woman.

3.5 THE EVOLUTION IN TIME OF A QUANTUM-MECHANICAL SYSTEM

POSTULATE 5

The evolution in time of a quantum-mechanical system is governed by the time-dependent Schrödinger equation:

$$\hat{H}\Psi(x, t) = i\hbar \frac{\partial\Psi(x, t)}{\partial t} \quad (3.12)$$

In one dimension, the total energy operator is given by $\hat{H} = (-\hbar^2/2m)(\partial^2/\partial x^2) + V(x, t)$. This looks like more familiar territory in that the equation has a unique solution for a set of given initial conditions. We call this behavior *deterministic* (like Newton's second law) in contrast to the probabilistic nature of Postulate 4. The fourth and fifth postulates are not contradictory. If a measurement is carried out at time t_0 , Postulate 4 applies. If we ask what state the system will be in for a time $t_1 > t_0$, *without carrying out a measurement in this time interval*, Postulate 5 applies. If at time t_1 we carry out a measurement again, Postulate 4 will apply.

Note that for wave functions that are solutions of the time-independent Schrödinger equation, $\Psi(x, t) = \psi(x)e^{-i(E/\hbar)t}$. In this case, in solving the eigenvalue equation for any operator \hat{A} that is not a function of time, we can write

$$\begin{aligned} \hat{A}(x)\Psi_n(x, t) &= a_n\Psi_n(x, t) \\ \hat{A}(x)\psi_n(x)e^{-i(E/\hbar)t} &= a_n\psi_n(x)e^{-i(E/\hbar)t} \quad \text{or} \\ \hat{A}(x)\psi_n(x) &= a_n\psi_n(x) \end{aligned} \quad (3.13)$$

This means that eigenvalue equations can be written for $\hat{A}(x)$ using only the spatial part of the wave function $\psi(x)$, knowing that $\psi(x)$ and $\Psi(x, t)$ are related by $\Psi(x, t) = \psi(x)e^{-i(E/\hbar)t}$.

Concept

A system undergoing change is not in a stationary state. Its behavior is described by the time dependent Schrödinger equation.

VOCABULARY

continuous function	Hermitian operator	orthonormal set	superposition state
deterministic outcome	individual measurement	postulate	weighted average
expansion coefficient	measurement process	probabilistic outcome	
expectation value	normalization	single-valued function	

KEY EQUATIONS

Equation	Significance of Equation	Equation Number
$P(x_0, t_0) dx = \Psi^*(x_0, t_0)\Psi(x_0, t_0) dx = \Psi(x_0, t_0) ^2 dx$	Probability $P(x_0, t_0)$ of finding the particle at position x_0 at time t_0 within an interval dx	3.1
$\int_{-\infty}^{\infty} \Psi^*(x, t)\Psi(x, t) dx = 1$	Definition of normalization	3.2
$\langle a \rangle = \frac{\int_{-\infty}^{\infty} \Psi^*(x, t)\hat{A}\Psi(x, t) dx}{\int_{-\infty}^{\infty} \Psi^*(x, t)\Psi(x, t) dx}$	Definition of expectation value	3.4
$\Psi(x, t) = \sum_n b_n \phi_n(x, t)$	Expansion of a wave function in terms of a complete set	3.6
$\Psi_{electronic} = b_1\Psi_{1s} + b_2\Psi_{2s} + b_3\Psi_{2p_x} + b_4\Psi_{3s}$	Example of a wave function for a superposition state	3.10
$\hat{H}\Psi(x, t) = i\hbar \frac{\partial\Psi(x, t)}{\partial t}$	Evolution in time of a quantum mechanical system	3.12

CONCEPTUAL PROBLEMS

Q3.1 The amplitude of a wave function that represents a moving particle can change from positive to negative values in the domain $(0, a)$ over which the wave function is defined. It must therefore pass through zero at some value x_0 , where $0 < x_0 < a$. Therefore, the probability of the particle being at x_0 is zero, and the particle cannot get from a position $x < x_0$ to a position $x > x_0$. Is this reasoning correct?

Q3.2 Postulate 3 states that in any single measurement of the total energy, the only values that will ever be measured are the eigenvalues of the total energy operator. Apart from the discrete energy values characteristic of a quantum-mechanical system, is the result of an individual measurement of the total energy identical to the result obtained on a classical system?

Q3.3 Why must an acceptable wave function be single-valued?

Q3.4 Why must the first derivative of an acceptable wave function be continuous?

Q3.5 Why must a quantum-mechanical operator \hat{A} satisfy the relation $\int \psi^*(x)[\hat{A}\psi(x)] dx = \int \psi(x)[\hat{A}\psi(x)]^* dx$?

Q3.6 If you flip a coin, what prediction can you make about it coming up heads in a single event?

Q3.7 If you flip a coin 1000 times, what prediction can you make about the number of times it comes up heads?

Q3.8 A superposition wave function can be expanded in the eigenfunctions of the operator corresponding to an observable to be measured. In analogy to rolling a single die, each of the infinite number of eigenvalues of the operator is equally likely to be measured. Is this statement correct?

Q3.9 If a system is in an eigenstate of the operator of interest, the wave function of the system can be determined. Explain this assertion. How could you know that the system is in an eigenstate of the operator of interest?

Q3.10 If the wave function for a system is a superposition wave function, the wave function of the system cannot be determined. Explain this assertion.

Q3.11 If hair color were a quantum-mechanical observable, you would not have a hair color until you looked in the mirror or someone else looked at you. Is this reasoning consistent with the discussion of quantum mechanics in this chapter?

Q3.12 What did Einstein mean in his famous remark “Do you really think that the moon is not there when we are not looking at it?”

NUMERICAL PROBLEMS

Section 3.1

P3.1 Which of the following functions are single-valued functions of the variable x ?

- a. x^2
- b. \sqrt{x}
- c. $\sqrt{x} + 3x$
- d. $\cos^{-1}\frac{2\pi x}{a}$

P3.2 Which of the following functions are single-valued functions of the variable x ?

- a. $\sin\frac{2\pi x}{a}$
- b. $e^{3\sqrt{x}}$
- c. $1 - 3 \sin^2 x$
- d. $e^{2\pi ix}$

P3.3 Graph $f(x) = \begin{cases} x^2 + 1 & -1 \leq x \leq 1 \text{ except } x = 0 \\ 0 & x = 0 \end{cases}$

over the interval $-1 \leq x \leq 1$. Is $f(x)$ a continuous function of x ?

P3.4 Graph $f(x) = |x|$ over the interval $-4 \leq x \leq 4$. Are $f(x)$ and $df(x)/dx$ continuous functions of x ?

P3.5 Is the function $(x^2 - 1)/(x - 1)$ continuous at $x = 1$? Answer this question by evaluating $f(1)$ and $\lim_{x \rightarrow 1} f(x)$.

P3.6 Is the function $1/(1 - x)^2$ continuous at $x = 1$?

Answer this question using the criteria listed in Section 3.1.

P3.7 Consider the function $f(x) = \sin \pi x/2$, $-1 < x < 1$.

Graph $f(x)$, $\frac{df}{dx}$, and $\frac{d^2f}{dx^2}$ over the interval $-1 < x < 1$.

Which, if any, of these functions exist and are continuous over the interval?

P3.8 Consider the function $f(x) = |x| - x$, $-1 \leq x \leq 1$.

Graph $f(x)$, $\frac{df}{dx}$, and $\frac{d^2f}{dx^2}$ over the interval $-1 < x < 1$.

Which, if any, of these functions exist and are continuous over the interval?

P3.9 Which of the following functions are acceptable wave functions over the indicated interval?

- a. e^{-x} $0 < x < \infty$
- b. e^{-x} $-\infty < x < \infty$
- c. $e^{-2\pi ix}$ $-100 < x < 100$
- d. $\frac{1}{x}$ $0 < x < \infty$

Explain your answers.

P3.10 Which of the following functions are acceptable wave functions over the indicated interval?

- a. $e^{-x^2/2}$ $-\infty < x < \infty$
- b. e^{-ix} $0 < x < 2\pi$
- c. $x^2 e^{-2\pi ix}$ $0 < x < \infty$
- d. xe^{-x} $1 < x < \infty$

Explain your answers.

P3.11 Show that the three wave functions in Equation (3.11) are normalized.

P3.12 Is $\psi(x) = x(a - x)$ an acceptable wave function over the interval $0 \leq x \leq a$? Answer this question by determining if the function is single valued and by evaluating the properties of the first and second derivatives with respect to x .

P3.13 Normalize $\psi(x) = x(a - x)$ defined over the interval $0 \leq x \leq a$ by multiplying $\psi(x)$ by a constant N and determining N using Equation (3.2).

Section 3.2

P3.14 In combining operators sequentially, it is useful to insert an arbitrary function after the operator to avoid errors. For example, if the operators \hat{A} and \hat{B} are x and d/dx , then $\hat{A}\hat{B}$ is $x df(x)/dx$ and $\hat{B}\hat{A}$ is $d[xf(x)]/dx$. Derive the operator for kinetic energy using the classical relation $\text{kinetic energy} = p^2/2m$ and the operator for linear momentum listed in Table 3.1.

P3.15 For a Hermitian operator \hat{A} , $\int \psi^*(x)[\hat{A}\psi(x)] dx = \int \psi(x)[\hat{A}\psi(x)]^* dx$. Assume that $\hat{A}f(x) = (a + ib)f(x)$ where a and b are constants. Show that if \hat{A} is a Hermitian operator, $b = 0$, so that the eigenvalues of $f(x)$ are real.

P3.16 Is the relation $(\hat{A}f(x))/f(x) = \hat{A}$ always obeyed? If not, give an example to support your conclusion.

P3.17 Is the relation $\hat{A}[f(x) + g(x)] = \hat{A}f(x) + \hat{A}g(x)$ always obeyed? If not, give an example to support your conclusion.

P3.18 In classical mechanics, the angular momentum vector \mathbf{L} is defined by $\mathbf{L} = \mathbf{r} \times \mathbf{p}$. Determine the components of \mathbf{L} . Substitute quantum-mechanical operators for the components of \mathbf{r} and \mathbf{p} to prove that $\hat{l}_x = -i\hbar\left(y\frac{\partial}{\partial z} - z\frac{\partial}{\partial y}\right)$.

Section 3.3

P3.19 Show that if $\psi_n(x)$ and $\psi_m(x)$ are solutions of the time-independent Schrödinger equation, $\Psi(x, t) = \psi_n(x)e^{\frac{-iE_n t}{\hbar}} + \psi_m(x)e^{\frac{-iE_m t}{\hbar}}$ is a solution of the time-dependent Schrödinger equation.

Section 3.4

P3.20 Use Equation (3.4) with the appropriate interval values to determine the expectation value of x for $\psi(x) = x(a - x)$ over the interval $0 \leq x \leq a$.

P3.21 Use Equation (3.4) with the appropriate interval values to determine the expectation value of p_x for $\psi(x) = x(a - x)$ over the interval $0 \leq x \leq a$.

P3.22 Suppose that the wave function for a system can be written as

$$\psi(x) = \frac{\sqrt{2}}{4}\phi_1(x) + \frac{1}{\sqrt{2}}\phi_2(x) + \frac{2 + \sqrt{2}i}{4}\phi_3(x)$$

and that $\phi_1(x)$, $\phi_2(x)$, and $\phi_3(x)$ are normalized eigenfunctions of the operator $\hat{E}_{kinetic}$ with eigenvalues E_1 , $2E_1$, and $4E_1$, respectively.

- a. Verify that $\psi(x)$ is normalized.
- b. What are the possible values that you could obtain in measuring the kinetic energy on identically prepared systems?
- c. What is the probability of measuring each of these eigenvalues?
- d. What is the average value of $E_{kinetic}$ that you would obtain from a large number of measurements?

FURTHER READING

Chow, Tai L. "A Note on the Schrödinger Representation of the Momentum and Energy Operators." *Journal of Chemical Education* 69 (1992): 537–538.

McQuarrie, D. A. *Quantum Chemistry* (2nd Edition). Sausalito, CA: University Science Books, 2008, Chapter 4.

Teixeira-Dias, Jose J. C. "How to Teach the Postulates of Quantum Mechanics without Enigma." *Journal of Chemical Education* 60 (1983): 963–965.

Applying Quantum-Mechanical Principles to Simple Systems

- 4.1 The Free Particle
- 4.2 The Case of the Particle in a One-Dimensional Box
- 4.3 Two- and Three-Dimensional Boxes
- 4.4 Using the Postulates to Understand the Particle in the Box and Vice Versa

WHY is this material important?

In this chapter, we begin to apply the Schrödinger equation to simple problems and discuss how to use the postulates discussed in Chapter 3. This will allow you to gain facility in applying the framework of quantum mechanics to problems of chemical interest.

WHAT are the most important concepts and results?

A discrete energy spectrum arises when a wave particle is confined in space with a length scale of atomic and molecular dimensions. A discrete energy spectrum that consists of energy levels is characterized by a quantum number, n . As $n \rightarrow \infty$, quantum mechanics merges into classical mechanics. The Schrödinger equation in two or three dimensions can be solved by the separation of variables.

WHAT would be helpful for you to review for this chapter?

It would be useful to review the postulates introduced in Chapter 3.

4.1 THE FREE PARTICLE

The simplest classical system imaginable is the free particle in one dimension; that is, a particle in a one-dimensional space on which no forces are acting. We begin with

$$F = ma = m \frac{d^2x}{dt^2} = 0 \quad (4.1)$$

This differential equation can be solved to obtain

$$x = x_0 + v_0 t \quad (4.2)$$

Verify that this is a solution by substitution in Equation (4.1). We can calculate the position at any time if the boundary conditions of the problem, namely, the initial position and velocity, are known.

How do we calculate the position of the wave particle using quantum mechanics? The condition that no forces can be acting on the particle means that the potential

energy is constant and independent of x and t . Therefore, we use the time-independent Schrödinger equation in one dimension,

$$-\frac{\hbar^2}{2m} \frac{d^2\psi(x)}{dx^2} + V(x)\psi(x) = E\psi(x) \quad (4.3)$$

to solve for the dependence of the wave function $\psi(x)$ on x . Whenever the potential energy $V(x)$ is constant, we can choose to make it zero because there is no fixed reference point for the zero of potential energy, and only changes in this quantity are measurable. The Schrödinger equation for this problem reduces to

$$\frac{d^2\psi(x)}{dx^2} = -\frac{2m}{\hbar^2} E\psi(x) \quad (4.4)$$

In words, $\psi(x)$ is a function that when differentiated twice returns the same function multiplied by a constant. Equation (4.4) has two linearly independent solutions that can be written either in terms of trigonometric functions or complex exponential functions as discussed in Math Essential 6. The most appropriate form of these solutions for our purposes is

$$\begin{aligned}\psi^+(x) &= A_+ e^{i\sqrt{(2mE/\hbar^2)x}} = A_+ e^{ikx} \\ \psi^-(x) &= A_- e^{-i\sqrt{(2mE/\hbar^2)x}} = A_- e^{-ikx}\end{aligned} \quad (4.5)$$

in which the constants in the exponent have been combined using

$$k = 2\pi/\lambda = \sqrt{2mE/\hbar^2} \quad (4.6)$$

Note that the last equality is consistent with the definition of classical kinetic energy, $E = 1/2 mv^2$, using the de Broglie relation [Equation (1.11)]. We have been working with $\psi(x)$ rather than $\Psi(x, t)$. To obtain $\Psi(x, t)$, these two solutions are multiplied by $e^{-i(E/\hbar)t}$ or equivalently $e^{-i\omega t}$, where the relation $E = \hbar\omega$ has been used.

Concept

A free particle has a continuous energy spectrum.

These solutions are plane waves, one moving to the right (positive x direction), the other moving to the left (negative x direction). The eigenvalues for the total energy can be found by substituting the wave functions of Equation (4.5) into Equation (4.4). For both solutions, $E = \hbar^2 k^2 / 2m$. Because k is a constant, these wave functions represent waves moving at a constant velocity determined by their initial velocity. Therefore, the quantum-mechanical solution of this problem contains the same information as the classical problem; namely, motion with a constant velocity. One other important similarity between the classical and quantum-mechanical free particle is that both can take on all values of energy because k is a continuous variable. The quantum-mechanical free particle has a continuous energy spectrum. Why is this the case? We will learn the answer to this question in Section 4.2.

Because a plane wave is not localized in space, we cannot speak of its position as we did for the particle. However, the probability of finding the particle in an interval of length dx can be calculated. The free-particle wave functions cannot be normalized over the interval $-\infty < x < \infty$, but if x is restricted to the interval $-L \leq x \leq L$, where L can be very large, the probability of finding the particle described by $\psi^+(x)$ at position x in the interval dx is

$$P(x) dx = \frac{\psi^{+*}(x) \psi^+(x) dx}{\int_{-L}^L \psi^{+*}(x) \psi^+(x) dx} = \frac{A_+^* A_+ e^{-ikx} e^{ikx} dx}{A_+^* A_+ \int_{-L}^L e^{-ikx} e^{ikx} dx} = \frac{dx}{2L} \quad (4.7)$$

Concept

A free particle is equally likely to be found anywhere.

The same result is found for $\psi^-(x)$. The coefficient A_+ cancels because it appears in both the numerator and the denominator. We find that $P(x) dx$ is independent of x , which means that the particle is equally likely to be anywhere in the interval. This result is equivalent to saying that nothing is known about the position of the particle. As will be shown in Chapter 6, this result is linked to the fact that the momentum of the particle has been precisely specified to have the values $\hbar k$ and $-\hbar k$ for the wave functions $\psi^+(x)$ and $\psi^-(x)$, respectively. We can verify that the eigenfunctions of the total energy operator are also eigenfunctions of the momentum operator by applying the momentum operator to these total energy eigenfunctions.

4.2 THE CASE OF THE PARTICLE IN A ONE-DIMENSIONAL BOX

The next case to be considered is the **particle in a box**. To keep the mathematics simple, the box is one dimensional; that is, it is the one-dimensional analogue of a single atom moving freely in a cube that has impenetrable walls. Two- and three-dimensional boxes are dealt with in Section 4.3 and in the problems at the end of this chapter. The impenetrable walls are modeled by making the potential energy infinite outside of a region of width a . The potential is depicted in Figure 4.1.

$$\begin{aligned} V(x) &= 0, \quad \text{for } a \geq x \geq 0 \\ V(x) &= \infty, \quad \text{for } x > a, x < 0 \end{aligned} \quad (4.8)$$

How does this change in potential energy affect the eigenfunctions that were obtained for the free particle? To answer this question, the Schrödinger equation is written in the following form:

$$\frac{d^2\psi(x)}{dx^2} = \frac{2m}{\hbar^2} [V(x) - E] \psi(x) \quad (4.9)$$

Outside of the box, where the potential energy is infinite, the second derivative of the wave function would be infinite if $\psi(x)$ were not zero for all x values outside the box. Because $d^2\psi(x)/dx^2$ must exist and be well behaved, $\psi(x)$ must be zero everywhere outside of the box. Because the wave function must be continuous, $\psi(x)$ must be zero as well at $x = 0$ and $x = a$.

$$\psi(0) = \psi(a) = 0, \psi(x) = 0 \quad \text{for } x > a, x < 0 \quad (4.10)$$

Equation (4.10) lists **boundary conditions** that any well-behaved wave function for the one-dimensional box must satisfy.

Inside the box, where $V(x) = 0$, the Schrödinger equation is identical to that for a free particle [Equation (4.4)], so the solutions must be the same. For ease in applying the boundary conditions, the solution is written as a linear combination of the two solutions in a trigonometric form equivalent to that of Equation (4.5):

$$\psi(x) = A \sin kx + B \cos kx \quad (4.11)$$

Now the boundary conditions given by Equation (4.10) are applied. Putting the values $x = 0$ and $x = a$ in Equation (4.11), we obtain

$$\begin{aligned} \psi(0) &= 0 + B = 0 \\ \psi(a) &= A \sin ka = 0 \end{aligned} \quad (4.12)$$

The first condition can only be satisfied by the condition that $B = 0$. The second condition can be satisfied if either $A = 0$ or $ka = n\pi$ with n being an integer. Setting A equal to zero would mean that the wave function is always zero, which is unacceptable because then there is no particle in the box. Therefore, we conclude that

$$\psi_n(x) = A \sin\left(\frac{n\pi x}{a}\right), \quad \text{for } n = 1, 2, 3, 4, \dots \quad (4.13)$$

The requirement that $ka = n\pi$ will turn out to have important consequences for the energy spectrum of the particle in the box. Each different value of n corresponds to a different eigenfunction. To use operator language, we have found the infinite set of eigenfunctions of the total energy operator for the potential energy defined by Equation (4.8).

Note the undefined constant A in these equations. This constant can be determined by normalization; that is, by realizing that $\psi^*(x)\psi(x) dx$ represents the probability of finding the particle in the interval of width dx centered at x . Because the probability of finding the particle somewhere in the entire interval is 1,

$$\int_0^a \psi^*(x)\psi(x) dx = A^*A \int_0^a \sin^2\left(\frac{n\pi x}{a}\right) dx = 1 \quad (4.14)$$

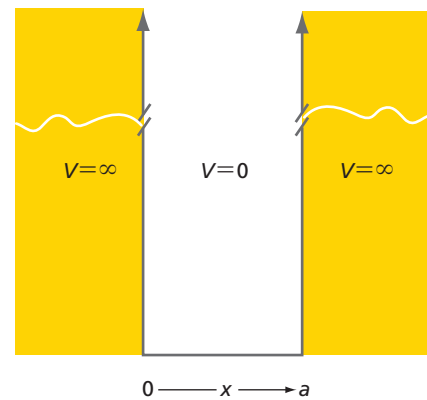
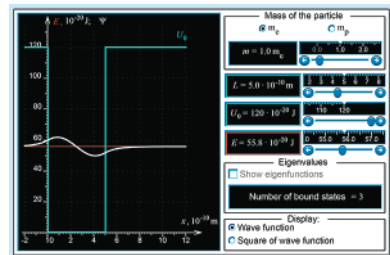


Figure 4.1

Potential of a particle inside and outside a one-dimensional box. The potential described by Equation (4.8) is depicted. Because the particle is confined to the range $0 \leq x \leq a$, we say that it is confined to a one-dimensional box.

Concept

Boundary conditions play an important role in solving the Schrödinger equation.



W4.1 Energy levels for the quantum mechanical particle in an infinitely deep box

This integral is evaluated using the standard integral

$$\int \sin^2(by) dy = \frac{y}{2} - \frac{\sin(2by)}{4b}$$

resulting in $A = \sqrt{2/a}$, so the normalized eigenfunctions are

$$\psi_n(x) = \sqrt{\frac{2}{a}} \sin\left(\frac{n\pi x}{a}\right) \quad (4.15)$$

Concept

Wave functions must be normalized to allow probability calculations.

Concept

The particle in the infinitely deep box has a discrete energy spectrum and a zero point energy.

What are the energy eigenvalues that go with these eigenfunctions? Applying the total energy operator to the eigenfunctions will give back the eigenfunction multiplied by the eigenvalue. We find that

$$-\frac{\hbar^2}{2m} \frac{d^2\psi_n(x)}{dx^2} = \frac{\hbar^2}{2m} \left(\frac{n\pi}{a}\right)^2 \sqrt{\frac{2}{a}} \sin\left(\frac{n\pi x}{a}\right) \quad (4.16)$$

Because

$$-\frac{\hbar^2}{2m} \frac{d^2\psi_n(x)}{dx^2} = E_n \psi_n(x)$$

the following result is obtained:

$$E_n = \frac{\hbar^2}{2m} \left(\frac{n\pi}{a}\right)^2 = \frac{\hbar^2 n^2}{8ma^2}, \quad \text{for } n = 1, 2, 3, \dots \quad (4.17)$$

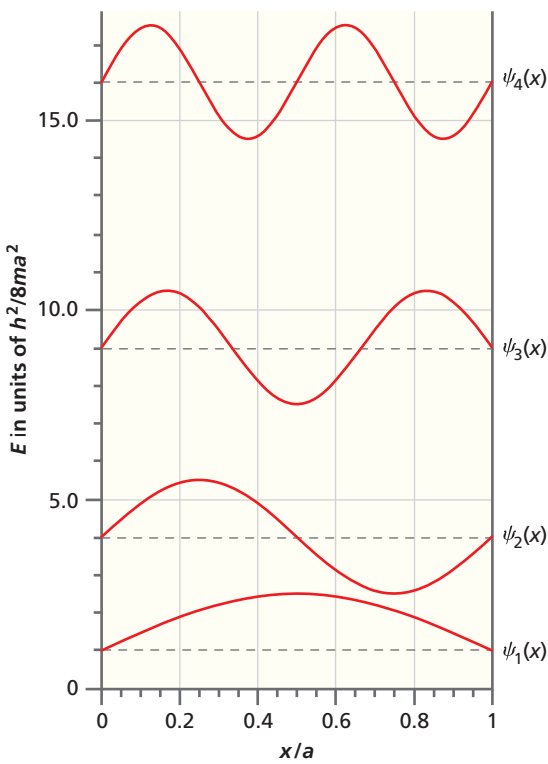


Figure 4.2

First four eigenfunctions for the particle in a box with the corresponding energy eigenvalues. The energy scale is shown on the left. The wave function amplitude inside the box is shown on the right, with the zero for each level indicated by the dashed line. Outside the box, the amplitude of the wave function is zero everywhere. Note that at $x = 0$ and $x = a$, the wave function is continuous, but the first derivative of the wave function is discontinuous. The discontinuity occurs because $V(x)$ changes abruptly from zero to infinity at $x = 0$ and $x = a$.

If this result is compared to that obtained for the free particle, an important difference is seen. The energy for the particle in the box can only take on discrete values. We say that the energy of the particle in the box is **quantized** and the integer n is a **quantum number**. Another important result of this calculation is that the lowest allowed energy is greater than zero. The particle has a nonzero minimum energy, known as a **zero point energy**.

Why are quite different results obtained for the free and the confined particle? A comparison of these two problems reveals that quantization entered through the confinement of the particle. Because the particle is confined to the box, the amplitude of all allowed wave functions must be zero everywhere outside the box. By considering the limit $a \rightarrow \infty$, the confinement condition is removed. Example Problem 4.1 shows that the discrete energy spectrum becomes continuous in this limit.

The lowest four energy levels for the particle in the box are shown in Figure 4.2 superimposed on an energy-versus-distance diagram. The eigenfunctions are also shown in this figure. Keep in mind that the time-independent part of the wave function is graphed. The full wave function is obtained by multiplying the wave functions shown in Figure 4.2 by $e^{-i(E/\hbar)t}$. If this is done, the variation of the total wave function with time is exactly what was shown in Figure 2.4 for a standing wave, if the real and imaginary parts of $\Psi(x, t)$ are considered separately. This result turns out to be general: the wave function for a state whose energy is independent of time is a standing and not a traveling wave. A standing wave has **nodes** that are at fixed distances independent of time, whereas the nodes move in time for a traveling wave. For this reason, the boundary conditions of Equation (4.10) cannot be satisfied for a traveling wave. A node is a point where a wave function passes through zero. An end point is not a node.

The particle in the box is also useful for showing that the quantization of energy ultimately has its origin in the coupling of wave properties and boundary conditions. In moving from $\psi_n(x)$ to $\psi_{n+1}(x)$, the number of half-wavelengths, and therefore the number of nodes, has been increased by one. There is no way to add anything other than an integral number of half-wavelengths and still have $\psi_n(x) = 0$ at the ends of the box.

Therefore, the **wave vector** k will increase in discrete increments rather than continuously in successive stationary states. Because

$$k = \frac{2\pi}{\lambda} = \frac{p}{\hbar} = \frac{\sqrt{2mE}}{\hbar}$$

the allowed energies E also increase in jumps rather than in a continuous fashion as in classical mechanics. Thinking in this way also helps in understanding the origin of the zero point energy. Because $E = h^2/2m\lambda^2$, zero energy corresponds to an infinite wavelength, but the longest wavelength for which $\psi_n(x) = 0$ at the ends of the box is $\lambda = 2a$. Substituting this value in the equation for E yields exactly the zero point energy. Note that the zero point energy approaches zero as a approaches infinity. In this limit, the particle becomes free.

Considering Equation (4.17), which shows the dependence of the total energy eigenvalues on the quantum number n , it is not immediately obvious that the energy spectrum will become continuous in the **classical limit** of very large n because the spacing between adjacent levels increases with n . This issue is addressed in Example Problem 4.1.

The total energy is one example of an observable that can be calculated once the eigenfunctions of the time-independent Schrödinger equation are known. Another observable that comes directly from solving this equation is the quantum-mechanical analogue of position. Recall that the probability of finding the particle in any interval of width dx in the one-dimensional box is given by $\psi^*(x)\psi(x) dx$. The **probability density** $\psi^*(x)\psi(x)$ at a given point is shown in Figure 4.3 for the first few eigenfunctions.

How can these results be understood? Looking back at the discussion of waves in Chapter 2, recall that to ask for the position of a wave is not meaningful because the wave is not localized at a point. Wave-particle duality modifies the classical picture of being able to specify the location of a particle. Figure 4.3 shows the probability density of finding the particle in the vicinity of a given value of x rather than the position of that particle. We see that the probability of finding the particle outside of the box is zero, but that the probability of finding the particle within an interval dx in the box depends on the position and the quantum number. Although $|\psi(x)|^2$ can be zero at nodal positions, $\int_{x-\Delta x}^{x+\Delta x} \psi^*(x')\psi(x') dx'$ is never zero for a finite interval $2\Delta x$ inside the box. This means that there is no finite length interval inside the box in which the particle is not found. For the ground state, it is much more likely that the particle is found near the center of the box than at the edges. A classical particle would be found with the same probability everywhere. Does this mean that quantum mechanics and classical mechanics are in conflict? No, because we need to consider large values of n to compare with the classical limit. A feature in Figure 4.3 that appears hard to understand is the oscillations in $\psi^2(x)$. They will not disappear for large n ; they will just be spaced more closely together. Because there are no such oscillations for the classical case, we need to make the quantum oscillations disappear for very large n .

The way to understand the convergence to the classical limit is to consider the measurement process. Any measurement has a certain resolution that averages data over the resolution range. What effect will the limited resolution have on a measurement such as probability? The result is shown in Figure 4.4. The probability density $\psi^2(x)$ is shown for the 1st, 30th, and 50th eigenstates of the particle in the box for three different limits of resolution. The probability density for the ground state is unaffected by including a resolution limit. However, as the resolution of the measurement decreases, we see that the probability density for the 50th state is beginning to approach the classical behavior of a constant probability everywhere. The classical limit is closer to $n = 1 \times 10^{10}$ rather than 50 for $E \approx kT$ at realistic temperatures and box dimensions on the order of centimeters. The difference between the quantum and classical results disappears as n becomes large. This is a general result known as the **correspondence principle**.

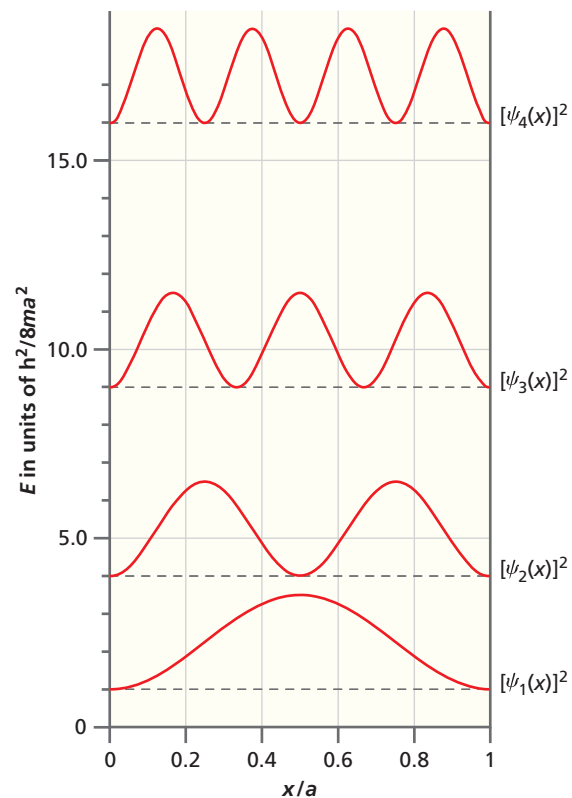
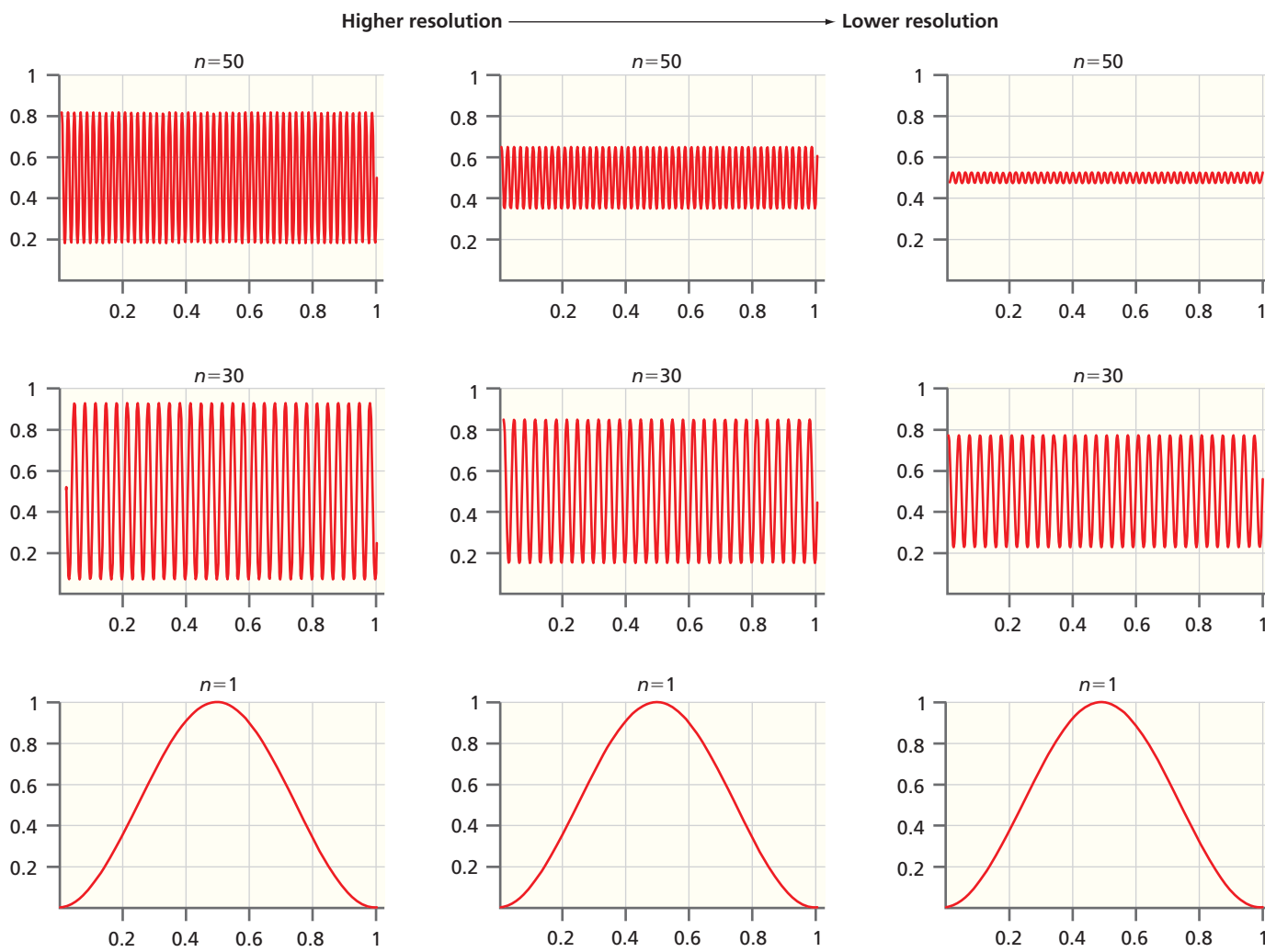


Figure 4.3

Probability density at a given point for the first few eigenfunctions. The square of the magnitude of the wave function, or probability density, is shown as a function of position together with the corresponding energy eigenvalues. The energy scale is shown on the left. The square of the wave function amplitude is shown on the right, with the zero for each level indicated by the dashed line.

Concept

The probability density for the particle in the infinitely deep box depends on the position and the quantum number.

**Figure 4.4**

Probability density for selected eigenstates for three limits of resolution. The three columns in this figure each show $\psi_n^2(x)/[\psi_1^2(x)]_{\text{max}}$ as a function of x/a for $n = 1, 30$, and 50 (from bottom to top). In moving from left to right, the data have been convoluted with an instrument function that averages the data over an increasingly wider range. Note that the probability of finding the particle in an interval dx becomes increasingly independent of position as n increases and as resolution decreases.

Concept

The correspondence principle states that the difference between the quantum and classical results disappears as the quantum number n becomes large.

This first attempt to apply quantum rather than classical mechanics to two familiar problems has led to several useful insights. By representing a wave particle as a wave, familiar questions that can be asked in classical mechanics become inappropriate. An example is “Where is the particle at time t_0 ?” The appropriate question in quantum mechanics is “What is the probability of finding the particle at time t_0 in an interval of length dx centered at the position x_0 ?” For the free particle, we found that the relationship between momentum and energy is the same as in classical mechanics and that there are no restrictions on the allowed energy. Restricting the motion of a particle to a finite region on the order of its wavelength has a significant effect on many observables associated with the particle. We saw that the origin of the effect is the requirement that the amplitude of the wave function be zero at the ends of the box for all times. This requirement changes the eigenfunctions of the Schrödinger equation from the traveling waves of the free particle to standing waves. Only discrete values of the particle momentum are allowed because of the condition $ka = n\pi$, $n = 1, 2, 3, \dots$. Because $E = h^2n^2/8ma^2$, the particle can only have certain values for the energy, and these values are determined by the length of the box. Wave–particle duality also leads to a nonuniform probability for finding the particle in the box.

EXAMPLE PROBLEM 4.1

From the formula given for the energy levels for the particle in the box, $E_n = \frac{\hbar^2 n^2}{8ma^2}$ for $n = 1, 2, 3, \dots$, we can see that the spacing between adjacent levels increases with n . This appears to indicate that the energy spectrum does not become continuous for large n , which must be the case for the quantum-mechanical result to be identical to the classical result in the high-energy limit. A better way to look at the spacing between levels is to consider the ratio $(E_{n+1} - E_n)/E_n$. Form this ratio and show that $\Delta E/E$ becomes a smaller fraction of the energy as $n \rightarrow \infty$. This result shows that the energy spectrum becomes continuous for large n .

Solution

$$\frac{E_{n+1} - E_n}{E_n} = \left(\frac{\hbar^2 [(n+1)^2 - n^2]}{h^2 n^2 / 8ma^2} \right) = \frac{2n+1}{n^2}$$

which approaches zero as $n \rightarrow \infty$. Both the level spacing and the energy increase with n , but the energy increases faster (as n^2), making the energy spectrum appear to be continuous as $n \rightarrow \infty$. This is another example of the correspondence principle.

4.3 TWO- AND THREE-DIMENSIONAL BOXES

The one-dimensional box is a useful model system because the conceptual simplicity allows the focus to be on the quantum mechanics rather than on the mathematics. The extension of the formalism developed for the one-dimensional problem to two and three dimensions has several aspects that are of use in understanding topics such as the rotation of molecules and the electronic structure of atoms, which cannot be reduced to one-dimensional problems.

Our focus here is on the three-dimensional box because the reduction in dimensionality from three to two is straightforward. The potential energy is given by

$$\begin{aligned} V(x, y, z) &= 0 \quad \text{for } 0 \leq x \leq a; \quad 0 \leq y \leq b; \quad 0 \leq z \leq c \\ &= \infty \quad \text{otherwise} \end{aligned} \tag{4.18}$$

As before, the amplitude of the eigenfunctions of the total energy operator is identically zero outside the box. Inside the box, the Schrödinger equation can be written as

$$-\frac{\hbar^2}{2m} \left(\frac{\partial^2}{\partial x^2} + \frac{\partial^2}{\partial y^2} + \frac{\partial^2}{\partial z^2} \right) \psi(x, y, z) = E\psi(x, y, z) \tag{4.19}$$

This differential equation is solved assuming that $\psi(x, y, z)$ has the form

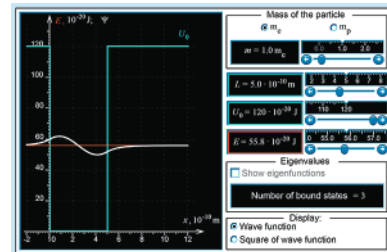
$$\psi(x, y, z) = X(x)Y(y)Z(z) \tag{4.20}$$

in which $\psi(x, y, z)$ is the product of three functions, each of which depends on only one of the variables. The assumption is valid in this case because $V(x, y, z)$ is independent of x , y , and z inside the box. This process is referred to as a **separation of variables**. It is also valid for a potential of the form $V(x, y, z) = V_x(x) + V_y(y) + V_z(z)$. Substituting Equation (4.20) in Equation (4.19), we obtain

$$\begin{aligned} -\frac{\hbar^2}{2m} \left(Y(y)Z(z) \frac{d^2X(x)}{dx^2} + X(x)Z(z) \frac{d^2Y(y)}{dy^2} + X(x)Y(y) \frac{d^2Z(z)}{dz^2} \right) \\ = EX(x)Y(y)Z(z) \end{aligned} \tag{4.21}$$

Note that Equation (4.21) no longer contains partial derivatives because each of the three functions X , Y , and Z depends on only one variable. Dividing by the product $X(x)Y(y)Z(z)$ results in

$$-\frac{\hbar^2}{2m} \left[\frac{1}{X(x)} \frac{d^2X(x)}{dx^2} + \frac{1}{Y(y)} \frac{d^2Y(y)}{dy^2} + \frac{1}{Z(z)} \frac{d^2Z(z)}{dz^2} \right] = E \tag{4.22}$$



W.2 Eigenfunctions for the two-dimensional box

Concept

The Schrödinger equation is solved for two- and three-dimensional boxes using the separation of variables method.

The form of this equation shows that E can be viewed as having independent contributions from the three coordinates, $E = E_x + E_y + E_z$, and the original differential equation in three variables reduces to three differential equations, each in one variable:

$$-\frac{\hbar^2}{2m} \frac{d^2X(x)}{dx^2} = E_x X(x); \quad -\frac{\hbar^2}{2m} \frac{d^2Y(y)}{dy^2} = E_y Y(y); \quad -\frac{\hbar^2}{2m} \frac{d^2Z(z)}{dz^2} = E_z Z(z) \quad (4.23)$$

Each of these equations has the same form as the equation that was solved for the one-dimensional problem. Therefore, the total energy eigenfunctions have the form

$$\psi_{n_x n_y n_z}(x, y, z) = N \sin \frac{n_x \pi x}{a} \sin \frac{n_y \pi y}{b} \sin \frac{n_z \pi z}{c} \quad (4.24)$$

and the total energy has the form

$$E = \frac{\hbar^2}{8m} \left(\frac{n_x^2}{a^2} + \frac{n_y^2}{b^2} + \frac{n_z^2}{c^2} \right) \quad (4.25)$$

This is a general result. *If the total energy can be written as a sum of independent terms corresponding to different degrees of freedom, then the wave function is a product of individual terms, each corresponding to one of the degrees of freedom.*

Because this is a three-dimensional problem, the eigenfunctions depend on three quantum numbers. Because more than one set of the three quantum numbers may have the same energy [for example, $(1, 2, 1)$, $(2, 1, 1)$, and $(1, 1, 2)$ if $a = b = c$], several distinct eigenfunctions of the total energy operator may have the same energy. In this case, we say that the energy level is **degenerate**, and the number of states, each represented by a distinct eigenfunction, that have the same energy is the degeneracy of the level.

What form do ψ and E take for the two-dimensional box? How many quantum numbers are needed to characterize ψ and E for the two-dimensional problem? Additional issues related to the functional form, degeneracy, and normalization of the total energy eigenfunctions are covered in the end-of-chapter problems.

Because the particle in the box model is very useful in understanding properties that can be measured for real systems, we have made a considerable effort to understand it. Some of these real systems will be discussed in Chapter 5. However, now that the Schrödinger equation has been solved for an interesting system, we first return to the postulates introduced in Chapter 3.

4.4 USING THE POSTULATES TO UNDERSTAND THE PARTICLE IN THE BOX AND VICE VERSA

Because of its simplicity, the particle in a box is an excellent teaching tool for learning how to apply quantum mechanics to a specific system. In this section, each of the postulates is applied to this problem using the eigenvalues and eigenfunctions calculated earlier. We begin with the first postulate.

POSTULATE 1

The state of a quantum-mechanical system is completely specified by a wave function $\Psi(x, t)$. The probability that a particle will be found at time t in a spatial interval of width dx centered at x_0 is given by $\Psi^*(x_0, t)\Psi(x_0, t) dx$.

This postulate states that all the information that can ever be obtained about the system is contained in the wave function. At this point, it is useful to review the distinction between a wave function and an eigenfunction. A wave function is any mathematically well-behaved function that satisfies the boundary conditions and that can be normalized to allow a meaningful definition of probability. An eigenfunction must satisfy

these and one more criterion. A wave function is an eigenfunction of an operator \hat{A} only if it satisfies the relationship $\hat{A}\psi_n(x) = a_n\psi_n(x)$. These criteria are implemented in Example Problem 4.2.

EXAMPLE PROBLEM 4.2

Consider the superposition wave function $\psi(x) = c \sin(\pi x/a) + d \sin(2\pi x/a)$.

- Is $\psi(x)$ an acceptable wave function for the particle in the box?
- Is $\psi(x)$ an eigenfunction of the total energy operator \hat{H} ?
- Is $\psi(x)$ normalized?

Solution

- If $\psi(x)$ is to be an acceptable wave function, it must satisfy the boundary conditions $\psi(x) = 0$ at $x = 0$ and $x = a$. The first and second derivatives of $\psi(x)$ must also be well-behaved functions between $x = 0$ and $x = a$. This is the case for $\psi(x)$. We conclude that $\psi(x) = c \sin(\pi x/a) + d \sin(2\pi x/a)$ is an acceptable wave function for the particle in the box.
- Although $\psi(x) = c \sin(\pi x/a) + d \sin(2\pi x/a)$ may be an acceptable wave function, it need not be an eigenfunction of a given operator. To see if $\psi(x)$ is an eigenfunction of the total energy operator, the operator is applied to the wave function:

$$\begin{aligned} & -\frac{\hbar^2}{2m} \frac{d^2}{dx^2} \left(c \sin\left(\frac{\pi x}{a}\right) + d \sin\left(\frac{2\pi x}{a}\right) \right) \\ &= \frac{\hbar^2 \pi^2}{2ma^2} \left(c \sin\left(\frac{\pi x}{a}\right) + 4d \sin\left(\frac{2\pi x}{a}\right) \right) \end{aligned}$$

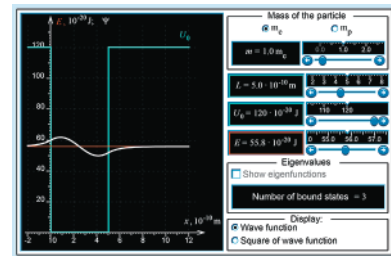
The result of this operation is not $\psi(x)$ multiplied by a constant. Therefore, $\psi(x)$ is not an eigenfunction of the total energy operator.

- To see if $\psi(x)$ is normalized, the following integral is evaluated:

$$\begin{aligned} & \int_0^a \left| c \sin\left(\frac{\pi x}{a}\right) + d \sin\left(\frac{2\pi x}{a}\right) \right|^2 dx \\ &= \int_0^a \left[c^* c \sin^2\left(\frac{\pi x}{a}\right) + d^* d \sin^2\left(\frac{2\pi x}{a}\right) + (cd^* + c^* d) \sin\left(\frac{\pi x}{a}\right) \sin\left(\frac{2\pi x}{a}\right) \right] dx \\ &= \int_0^a |c|^2 \sin^2\left(\frac{\pi x}{a}\right) dx + \int_0^a |d|^2 \sin^2\left(\frac{2\pi x}{a}\right) dx \\ & \quad + \int_0^a (cd^* + c^* d) \sin\left(\frac{\pi x}{a}\right) \sin\left(\frac{2\pi x}{a}\right) dx \end{aligned}$$

Using the standard integral $\int \sin^2(by) dy = y/2 - (1/4b)\sin(2by)$ and recognizing that the third integral is zero because all $\sin nx$ functions with different n are orthogonal,

$$\begin{aligned} & \int_0^a \left[|c|^2 \sin^2\left(\frac{\pi x}{a}\right) + |d|^2 \sin^2\left(\frac{2\pi x}{a}\right) \right] dx \\ &= |c|^2 \left[\frac{a}{2} - \frac{a(\sin 2\pi - \sin 0)}{4\pi} \right] + |d|^2 \left[\frac{a}{2} - \frac{a(\sin 4\pi - \sin 0)}{8\pi} \right] \\ &= \frac{a}{2} (|c|^2 + |d|^2) \end{aligned}$$

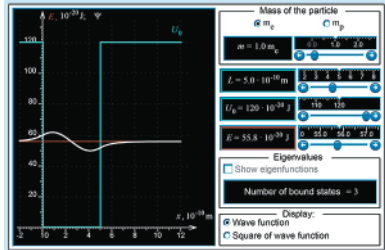


W4.3 Acceptable wave functions for the particle in an infinitely deep box

Therefore, $\psi(x)$ is not normalized in general, but the wave function

$$\sqrt{\frac{2}{a}} \left[c \sin\left(\frac{\pi x}{a}\right) + d \sin\left(\frac{2\pi x}{a}\right) \right]$$

is normalized for the condition that $|c|^2 + |d|^2 = 1$.



W4.4 Expectation values for a superposition wave function

Note that a superposition wave function has a more complicated dependence on time than does an eigenfunction of the total energy operator. For instance, $\psi(x, t)$ for the wave function under consideration is given by

$$\Psi(x, t) = \sqrt{\frac{2}{a}} \left[ce^{-iE_1 t/\hbar} \sin\left(\frac{\pi x}{a}\right) + de^{-iE_2 t/\hbar} \sin\left(\frac{2\pi x}{a}\right) \right] \neq \psi(x)f(t)$$

This wave function cannot be written as a product of a function of x and a function of t . It is not a standing wave, and it does not describe a state whose properties are, in general, independent of time.

All of the particles in the box eigenfunctions, $\psi_n(x) = \sqrt{2/a} \sin(n\pi x/a)$, for $n = 1, 2, 3, \dots$, are normalized, meaning that the total probability of finding the particle somewhere between $x = 0$ and $x = a$ is one. In other words, the particle is somewhere in the box. We cannot predict with certainty the outcome of a single measurement in which the position of the particle is determined, because these eigenfunctions of the total energy operator are not eigenfunctions of the position operator. In Chapter 6, we will discuss why the eigenvalues of \hat{H} and \hat{x} cannot be determined simultaneously. We can, however, predict the average value determined in a large number of independent measurements of the particle position. This is equivalent to asking for the probability density of finding the particle at a given position. The formula for calculating this probability is stated in the first postulate. The total probability of finding the particle in a finite length interval is obtained by integrating the probability density, as shown in Example Problem 4.3.

EXAMPLE PROBLEM 4.3

What is the probability P of finding the particle in the central third of the box if it is in its ground state?

Solution

For the ground state, $\psi_1(x) = \sqrt{2/a} \sin(\pi x/a)$. From the postulate, P is the sum of all the probabilities of finding the particle in intervals of width dx within the central third of the box. This probability is given by the integral

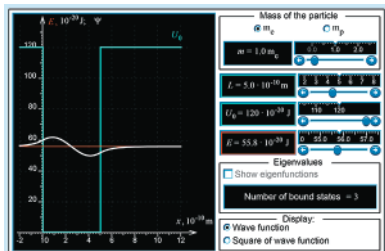
$$P = \frac{2}{a} \int_{a/3}^{2a/3} \sin^2\left(\frac{\pi x}{a}\right) dx$$

Solving this integral as in Example Problem 4.2,

$$P = \frac{2}{a} \left[\frac{a}{6} - \frac{a}{4\pi} \left(\sin \frac{4\pi}{3} - \sin \frac{2\pi}{3} \right) \right] = 0.609$$

Although we cannot predict the outcome of a single measurement, we can predict that for 60.9% of a large number of individual measurements, the particle is found in the central third of the box. What is the probability of finding a classical particle in this interval?

Postulate 2 is a recipe for associating classical observables with quantum-mechanical operators and need not be considered further. Postulates 3 and 4 are best understood by considering them together.



W4.5 Probability of finding the particle in a given interval

POSTULATE 3

In any single measurement of the observable that corresponds to the operator \hat{A} , the only values that will ever be measured are the eigenvalues of that operator.

POSTULATE 4

If the system is in a state described by the wave function $\Psi(x, t)$, and the value of the observable a is measured once each on many identically prepared systems, the average value of all of these measurements is given by

$$\langle a \rangle = \frac{\int_{-\infty}^{\infty} \Psi^*(x, t) \hat{A} \Psi(x, t) dx}{\int_{-\infty}^{\infty} \Psi^*(x, t) \Psi(x, t) dx} \quad (4.26)$$

The wave function for a particle in its ground state is $\psi(x) = \sqrt{2/a} \sin(\pi x/a)$, which is a normalized eigenfunction of the total energy operator. Applying the operator to this wave function returns the function multiplied by the constant. This is the value of the energy that is determined in any single measurement; therefore, it is also the average of all values for the energy that are measured on many particles prepared in the same state.

Now consider a measurement of the total energy for a case in which the wave function of the system is not an eigenfunction of this operator. As you convinced yourself in Example Problem 4.2, the normalized superposition wave function

$$\psi(x) = \sqrt{\frac{2}{a}} \left(c \sin \frac{\pi x}{a} + d \sin \frac{2\pi x}{a} \right)$$

where $|c|^2 + |d|^2 = 1$ is not an eigenfunction of \hat{H} . Postulate 4 states that the average value of the energy for a large number of identical measurements on a system whose state is described by a normalized wave function is

$$\langle E \rangle = \int_0^a \psi^*(x) \left[-\frac{\hbar^2}{2m} \frac{d^2}{dx^2} + V(x) \right] \psi(x) dx \quad (4.27)$$

We now substitute the expression for $\psi(x)$ into Equation (4.27):

$$\langle E \rangle = \frac{2}{a} \int_0^a \left(c^* \sin \frac{\pi x}{a} + d^* \sin \frac{2\pi x}{a} \right) \left[-\frac{\hbar^2}{2m} \frac{d^2}{dx^2} \right] \left(c \sin \frac{\pi x}{a} + d \sin \frac{2\pi x}{a} \right) dx \quad (4.28)$$

Multiplying out the terms in the brackets, and recognizing that each of the individual terms in the parentheses is an eigenfunction of the operator, $\langle E \rangle$ reduces to

$$\begin{aligned} \langle E \rangle &= \frac{2}{a} \left[|c|^2 E_1 \int_0^a \sin^2 \frac{\pi x}{a} dx + |d|^2 E_2 \int_0^a \sin^2 \frac{2\pi x}{a} dx \right] \\ &\quad + \frac{2}{a} \left[c^* d E_2 \int_0^a \sin \frac{\pi x}{a} \sin \frac{2\pi x}{a} dx + d^* c E_1 \int_0^a \sin \frac{\pi x}{a} \sin \frac{2\pi x}{a} dx \right] \end{aligned} \quad (4.29)$$

From our efforts to normalize the functions, we know that the value of each of the first two integrals is $a/2$. Each of the last two integrals is identically zero because the sine functions with different arguments are mutually orthogonal. Therefore, the result of these calculations is

$$\langle E \rangle = |c|^2 E_1 + |d|^2 E_2 \quad (4.30)$$

where $E_n = n^2 \hbar^2 / 8ma^2$. Because $|c|^2 + |d|^2 = 1$, $\langle E \rangle$ is a weighted average of E_1 and E_2 . As seen in Example Problem 4.2, the superposition wave function does not describe a stationary state, and the average values of observables such as $\langle p \rangle$ and $\langle x \rangle$

are functions of time as shown in Problem W4.6. However, the average energy is independent of time because the energy is conserved.

Note that this result is exactly what was derived for a more general case in discussing Postulate 4 (see Chapter 3). We will next discuss in more detail what will be obtained for an individual measurement of the total energy and relate it to the result that was just derived for the average of many individual measurements. Postulate 3 states that in an individual measurement, only one of the eigenvalues of the operator can be measured. In this case, it means that only one of the infinite set of E_n given by $E_n = n^2\hbar^2/8ma^2$, $n = 1, 2, 3, \dots$, is a possible result of an individual measurement. What is the likelihood that the value E_2 will be measured? Postulate 4 gives a recipe for answering this question. It instructs us to expand the system wave function in the complete set of functions that are the eigenfunctions of the operator of interest. The probability that an individual measurement will give E_n is given by the square of the expansion coefficient of that eigenfunction in the expression for the wave function. In the particular case under consideration, the wave function can be written as follows:

$$\psi(x) = c\psi_1(x) + d\psi_2(x) + 0 \times (\psi_3(x) + \dots + \psi_n(x) + \dots) \quad (4.31)$$

in which it has been made explicit that the coefficients of all the eigenfunctions other than $\psi_1(x)$ and $\psi_2(x)$ are zero. Therefore, given the wave function for the system, individual measurements on identically prepared systems will never yield anything other than E_1 or E_2 . The probability of obtaining E_1 is c^2 , and the probability of obtaining E_2 is d^2 . From this result, it is clear that the average value for the energy determined from a large number of measurements is $c^2E_1 + d^2E_2$.

A more detailed discussion of causality in quantum mechanics would lead us to a number of conclusions that differ significantly from our experience with classical mechanics. For instance, it is not possible to predict whether E_1 or E_2 would be measured in an individual measurement any more than the outcome of a single throw of a die can be predicted. However, if the energy is measured again on the same system (rather than carrying out a second measurement on an identically prepared system), the same result will be obtained as in the initial measurement. This conclusion also holds for all subsequent measurements. This last result is particularly intriguing because it suggests that through the measurement process, the system has been forced into an eigenfunction of the operator corresponding to the quantity being measured.

Now consider a measurement of the momentum or the position. As shown earlier, we need to know the wave function that describes the system to carry out such a calculation. For this calculation, assume that the system is in one of the eigenfunctions of the total energy operator, for which $\psi_n(x) = \sqrt{2/a} \sin(n\pi x/a)$. From the second postulate and Table 3.1, the quantum-mechanical operator associated with momentum is $-i\hbar(d/dx)$. Although $\psi(x)$ is an eigenfunction of the total energy operator, it is not clear if it is an eigenfunction of the momentum operator. Verify that it is not an eigenfunction of this operator by operating on the wave function with the momentum operator. We will return to the significance of this result in Chapter 6, but we first proceed in applying the postulates. Postulate 4 defines how the average value of the momentum obtained in a large number of individual measurements on an identically prepared system can be calculated. The result is given by

$$\begin{aligned} \langle p \rangle &= \int_0^a \psi^*(x) \hat{p} \psi(x) dx \\ &= \frac{2}{a} \int_0^a \sin\left(\frac{n\pi x}{a}\right) \left[-i\hbar \frac{d}{dx} \sin\left(\frac{n\pi x}{a}\right) \right] dx \\ &= \frac{-2i\hbar n\pi}{a^2} \int_0^a \sin\left(\frac{n\pi x}{a}\right) \cos\left(\frac{n\pi x}{a}\right) dx = \frac{-i\hbar}{a} [\sin^2 n\pi - \sin^2 0] = 0 \end{aligned} \quad (4.32)$$

Note that the result is the same for all values of n . We know that the energy of the lowest state is greater than zero and that all the energy is in the form of kinetic energy.

Because $E = p^2/2m \neq 0$, the magnitude of p must be greater than zero for an individual measurement. How can the result that the average value of the momentum is zero be understood?

Keep in mind that, classically, the particle is bouncing back and forth between the two walls of the one-dimensional box with a constant velocity. Therefore, it is equally likely that the particle is moving in the $+x$ and $-x$ directions and that its momentum is positive or negative. For this reason, the average momentum is zero. This result holds up in a quantum-mechanical picture. However, a major difference exists between the quantum and classical pictures. In classical mechanics, the magnitude of the momentum of the particle is known to be $\sqrt{2m E_{kin}}$ exactly. In quantum mechanics, a consequence of confining the particle to a box of length a is that an uncertainty has been introduced in its momentum that is proportional to $1/a$. This issue will be discussed in depth in Chapter 6. The calculation for the average value of position is carried out in Example Problem 4.4.

EXAMPLE PROBLEM 4.4

Assume that a particle is confined to a box of length a and that the system wave function is $\psi(x) = \sqrt{2/a} \sin(\pi x/a)$.

- Is this state an eigenfunction of the position operator?
- Calculate the average value of the position $\langle x \rangle$ that would be obtained for a large number of measurements. Explain your result.

Solution

- The position operator $\hat{x} = x$. Because $x\psi(x) = \sqrt{2/a} x \sin(\pi x/a) \neq c\psi(x)$, where c is a constant, the wave function is not an eigenfunction of the position operator.
- The expectation value is calculated using the fourth postulate:

$$\langle x \rangle = \frac{2}{a} \int_0^a \left\{ \sin\left(\frac{\pi x}{a}\right) \right\} x \sin\left(\frac{\pi x}{a}\right) dx = \frac{2}{a} \int_0^a x \left\{ \sin\left(\frac{\pi x}{a}\right) \right\}^2 dx$$

Using the standard integral $\int x(\sin bx)^2 dx = \frac{x^2}{4} - \frac{\cos 2bx}{8b^2} - \frac{x \sin 2bx}{4b}$

$$\begin{aligned} \langle x \rangle &= \frac{2}{a} \left[\frac{x^2}{4} - \frac{\cos\left(\frac{2\pi x}{a}\right)}{8\left(\frac{\pi}{a}\right)^2} - \frac{x \sin\left(\frac{2\pi x}{a}\right)}{4\left(\frac{\pi}{a}\right)} \right]_0^a \\ &= \frac{2}{a} \left[\left(\frac{a^2}{4} - \frac{a^2}{8\pi^2} - 0 \right) + \frac{a^2}{8\pi^2} \right] = \frac{a}{2} \end{aligned}$$

The average position is midway in the box. This is exactly what we would expect because the particle is equally likely to be in each half of the box.

VOCABULARY

boundary condition

degenerate

probability density

separation of variables

classical limit

node

quantized

wave vector

correspondence principle

particle in a box

quantum number

zero point energy

KEY EQUATIONS

Equation	Significance of Equation	Equation Number
$-\frac{\hbar^2}{2m} \frac{d^2\psi(x)}{dx^2} + V(x)\psi(x) = E\psi(x)$	Time-independent Schrödinger equation in one dimension	4.3
$\psi^+(x) = A_+ e^{+i\sqrt{(2mE/\hbar^2)x}} = A_+ e^{+ikx}$ $\psi^-(x) = A_- e^{-i\sqrt{(2mE/\hbar^2)x}} = A_- e^{-ikx}$	Two linearly independent solutions of Schrödinger equation for free particle in one dimension	4.5
$\psi_n(x) = \sqrt{\frac{2}{a}} \sin\left(\frac{n\pi x}{a}\right), \quad \text{for } n = 1, 2, 3, 4, \dots$	Total energy eigenfunctions of Schrödinger equation for particle in one-dimensional box of infinite depth	4.13
$E_n = \frac{\hbar^2 n^2}{8ma^2}, \quad \text{for } n = 1, 2, 3, \dots$	Total energy eigenvalues for particle in one-dimensional box of infinite depth	4.17
$\psi_{n_x n_y n_z}(x, y, z) = N \sin\frac{n_x \pi x}{a} \sin\frac{n_y \pi y}{b} \sin\frac{n_z \pi z}{c}$	Total energy eigenfunctions of Schrödinger equation for particle in three-dimensional box of infinite depth	4.24
$E = \frac{\hbar^2}{8m} \left(\frac{n_x^2}{a^2} + \frac{n_y^2}{b^2} + \frac{n_z^2}{c^2} \right)$	Total energy eigenvalues for particle in three-dimensional box of infinite depth	4.25

CONCEPTUAL PROBLEMS

Q4.1 We set the potential energy in the particle in the box equal to zero and justified it by stating that there is no absolute scale for potential energy. Is this also true for kinetic energy?

Q4.2 Discuss why a quantum-mechanical particle in a box has a zero point energy in terms of its wavelength.

Q4.3 How does an expectation value for an observable differ from an average of all possible eigenvalues?

Q4.4 Is the probability distribution for a free particle consistent with a purely particle picture, a purely wave picture, or both?

Q4.5 Why is it not possible to normalize the free-particle wave functions over the whole range of motion of the particle?

Q4.6 The probability density for a particle in a box is an oscillatory function even for very large energies. Explain how the classical limit of a constant probability density that is independent of position is achieved.

Q4.7 Explain using words, rather than equations, why if $V(x, y, z) \neq V_x(x) + V_y(y) + V_z(z)$, the total energy eigenfunctions cannot be written in the form $\psi(x, y, z) = X(x)Y(y)Z(z)$.

Q4.8 Can a guitar string be in a superposition of states, or is such a superposition only possible for a quantum-mechanical system?

Q4.9 Show that for the particle in the box total energy eigenfunctions, $\psi_n(x) = \sqrt{2/a} \sin(n\pi x/a)$, $\psi(x)$ is a continuous function at the edges of the box. Is $d\psi/dx$ a continuous function of x at the edges of the box?

Q4.10 Why are standing-wave solutions for the free particle not compatible with the classical result $x = x_0 + v_0 t$?

Q4.11 What is the difference between probability and probability density?

Q4.12 Why are traveling-wave solutions for the particle in the box not compatible with the boundary conditions?

Q4.13 Can the particles in a one-dimensional box, a square two-dimensional box, and a cubic three-dimensional box all have degenerate energy levels?

Q4.14 Invoke wave-particle duality to address the following question: How does a particle get through a node in a wave function to get to the other side of the box?

Q4.15 Why is the zero point energy lower for a He atom in a box than for an electron?

Q4.16 What are the units of the probability density for the particle in a one-dimensional box?

Q4.17 What are the units of the probability density for the particle in a three-dimensional box?

Q4.18 What is the relationship between the zero point energy for a H atom and a H₂ molecule in a one-dimensional box?

Q4.19 Show that the correct energy eigenvalues for the particle in a one-dimensional box are obtained even if the total energy eigenfunctions are not normalized.

NUMERICAL PROBLEMS

Section 4.1

P4.1 Consider a free particle moving in one dimension whose probability of moving in the negative x direction is three times that for moving in the positive x direction. Give as much information as you can about the wave function of the particle.

P4.2 Show that the energy eigenvalues for the free particle, $E = \hbar^2 k^2 / 2m$, are consistent with the classical result $E = (1/2)mv^2$.

P4.3 Show by examining the position of the nodes that $\text{Re}[A_+e^{i(kx-\omega t)}]$ and $\text{Re}[A_-e^{i(-kx-\omega t)}]$ represent plane waves moving in the positive and negative x directions, respectively. The notation $\text{Re}[\cdot]$ refers to the real part of the function in the brackets.

Section 4.2

P4.4 Evaluate the normalization integral for the eigenfunctions of \hat{H} for the particle in the box $\psi_n(x) = A \sin(n\pi x/a)$ using the trigonometric identity $\sin^2 y = (1 - \cos 2y)/2$.

P4.5 Is the function $\psi(x) = A(y/b)\left[1 - \left(\frac{y}{b}\right)^2\right]$ an accept-

able wave function for the particle in the one-dimensional infinite depth box of length b ? Calculate the normalization constant A and the expectation values $\langle y \rangle$ and $\langle y^2 \rangle$. Does $\langle y \rangle$ have the same value as for the total energy eigenfunctions for this problem? If not, why not? It may be useful to plot the wave function to answer this question.

P4.6 Derive an equation for the probability that a particle characterized by the quantum number n is in the first 25% ($0 \leq x \leq a/4$) of an infinite depth box. Show that this probability approaches the classical limit as $n \rightarrow \infty$.

P4.7 It is useful to consider the result for the energy eigenvalues for the one-dimensional box $E_n = \hbar^2 n^2 / 8ma^2$, $n = 1, 2, 3, \dots$ as a function of n , m , and a .

- a.** By what factor do you need to change the box length to decrease the zero point energy by a factor of 35 for a fixed value of m ?
- b.** For what value of n is the energy greater than the zero point energy by a factor of 250 for fixed values of a and m ?
- c.** By what factor would you have to change a to have the zero point energies of a He atom be equal to the zero point energy of a hydrogen atom in the box?

Q4.20 What are the possible results for the energy that would be obtained in a measurement on the particle in a one-dimensional box if the wave function is $\psi_n(x) = \sqrt{2/a} \sin(7\pi x/a)$?

P4.8 Calculate the wavelength of the light emitted when an electron in a one-dimensional box of length 5.0 nm makes a transition from the $n = 8$ state to the $n = 7$ state.

P4.9 A bowling ball has a weight of 12 lb, and the length of the lane is approximately 60 ft. Treat the ball in the lane as a one-dimensional box. What quantum number corresponds to a velocity of 6.25 miles per hour?

P4.10 Calculate (a) the zero point energy of a hydrogen molecule in a one-dimensional box of length 1.00 cm and (b) the ratio of the zero point energy to $k_B T$ at 300.K.

P4.11 The smallest observed frequency for a transition between states of an electron in a one-dimensional box is $1.3 \times 10^{13} \text{ s}^{-1}$. What is the length of the box?

P4.12 Use the eigenfunction $\psi(x) = A'e^{+ikx} + B'e^{-ikx}$ rather than $\psi(x) = A \sin kx + B \cos kx$ to apply the boundary conditions for the particle in the box.

- a.** How do the boundary conditions restrict the acceptable choices for A' and B' and for k ?
- b.** Do these two functions give different probability densities if each is normalized?

P4.13 Consider a particle in a one-dimensional box defined by $V(x) = 0$, $a > x > 0$ and $V(x) = \infty$, $x \geq a$, $x \leq 0$. Explain why each of the following unnormalized functions is or is not an acceptable wave function based on criteria such as being consistent with the boundary conditions and with the association of $\psi^*(x)\psi(x)dx$ with probability. All constants are nonzero.

- a.** $A \cos \frac{n\pi x}{a} + B \sin \frac{n\pi x}{a}$
- b.** $C\left(1 - \cos \frac{n\pi x}{a}\right)$
- c.** $Be^{\frac{-x}{a}}$
- d.** $B(x + x^2)$
- e.** $\frac{E}{\cos(n\pi x/a)}$

P4.14 Calculate the probability that a particle in a one-dimensional box of length a is found between $0.28a$ and $0.32a$ when it is described by the following wave functions:

- a.** $\sqrt{\frac{2}{a}} \sin\left(\frac{\pi x}{a}\right)$
- b.** $\sqrt{\frac{2}{a}} \sin\left(\frac{3\pi x}{a}\right)$

What would you expect for a classical particle? Compare your results in the two cases with the classical result.

P4.15 What are the solutions to the Schrödinger equation for the particle in the infinitely deep box of

length a if (a) $V(x) = 0$, for $\frac{a}{2} > x > -\frac{a}{2}$ and

(b) $V(x) = \infty$, for $\frac{a}{2} \leq x \leq -\frac{a}{2}$?

P4.16 Is the function $\psi(x) = A(y/b)[1 - y/b]$ an acceptable wave function for the particle in the one-dimensional infinite depth box of length b ? Calculate the normalization constant A and the expectation values for the total energy and the linear momentum. How does your calculated value of $\langle E \rangle$ compare with the lowest eigenvalue for the one-dimensional infinite depth box?

Section 4.3

P4.17 This problem explores the conditions under which the classical limit is reached for a macroscopic cubic box of edge length a . An oxygen molecule of average translational energy $3/2 k_B T$ is confined in a cubic box of volume $V = 1.250 \text{ m}^3$ at 298 K. Use the result from Equation (4.25) for the dependence of the energy levels on a and on the quantum numbers n_x , n_y , and n_z .

- What is the value of the “reduced quantum number” $\alpha = \sqrt{n_x^2 + n_y^2 + n_z^2}$ for $T = 298 \text{ K}$?
- What is the energy separation between the levels α and $\alpha + 1$? (*Hint:* Subtract $E_{\alpha+1}$ from E_α before plugging in numbers.)
- Calculate the ratio $(E_{\alpha+1} - E_\alpha)/kT$ and use your result to conclude whether a classical or quantum-mechanical description is appropriate for the particle.

P4.18 Normalize the total energy eigenfunctions for the three-dimensional box in the interval $0 \leq x \leq a$, $0 \leq y \leq b$, $0 \leq z \leq c$.

P4.19 a. Show by substitution into Equation (4.19) that the eigenfunctions of \hat{H} for a box with lengths along the x , y , and z directions of a , b , and c , respectively, are

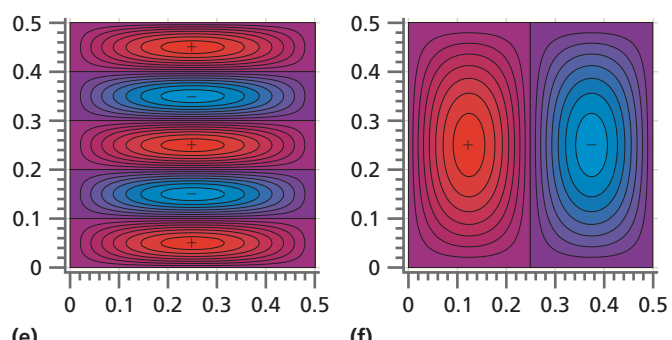
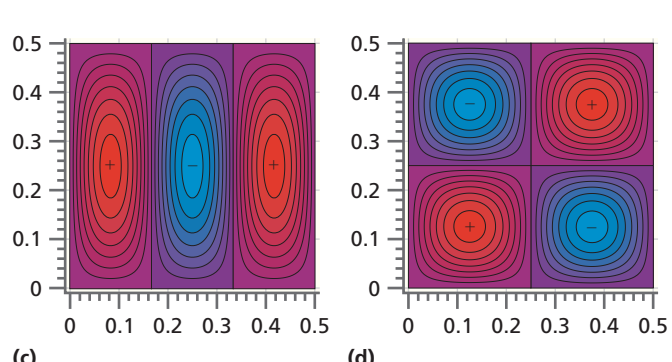
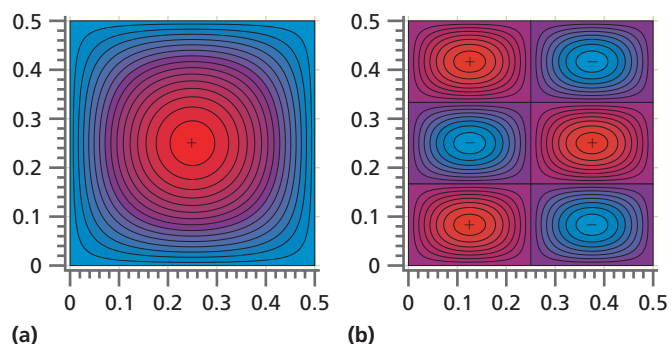
$$\psi_{n_x, n_y, n_z}(x, y, z) = N \sin\left(\frac{n_x \pi x}{a}\right) \sin\left(\frac{n_y \pi y}{b}\right) \sin\left(\frac{n_z \pi z}{c}\right).$$

- Obtain an expression for E_{n_x, n_y, n_z} in terms of n_x , n_y , n_z , and a , b , and c .

P4.20 For a particle in a two-dimensional box, the total energy eigenfunctions are $\psi_{n_x, n_y}(x, y) = N \sin\left(\frac{n_x \pi x}{a}\right) \sin\left(\frac{n_y \pi y}{b}\right)$.

- Obtain an expression for E_{n_x, n_y} in terms of n_x , n_y , a , and b by substituting this wave function into the two-dimensional analogue of Equation (4.19).

b. Contour plots of several eigenfunctions are shown here. The x and y directions of the box lie along the horizontal and vertical directions, respectively. The amplitude has been displayed as a gradation in colors. Regions of positive and negative amplitude are indicated. Identify the values of the quantum numbers n_x and n_y for plots a–f.



P4.21 Consider the contour plots of Problem P4.20.

- What are the most likely area or areas $\Delta x \Delta y$ to find the particle for each of the eigenfunctions of \hat{H} depicted in plots a–f?
- For the one-dimensional box, the nodes are points. What form do the nodes take for the two-dimensional box? Where are the nodes located in plots a–f? How many nodes are there in each contour plot?

P4.22 Using your result from P4.20, list the energy levels and corresponding quantum numbers for a particle of mass m in a two-dimensional square box of edge length b with $E \leq 35h^2/8mb^2$. What is the degeneracy of each level?

P4.23 Normalize the total energy eigenfunction for the rectangular two-dimensional box,

$$\psi_{n_x, n_y}(x, y) = N \sin\left(\frac{n_x \pi x}{a}\right) \sin\left(\frac{n_y \pi y}{b}\right)$$

in the interval $0 \leq x \leq a$, $0 \leq y \leq b$.

P4.24 Generally, the quantization of translational motion is not significant for atoms because of their mass. However, this conclusion depends on the dimensions of the space to which they are confined. Zeolites are structures with small pores that we describe by a cube with edge length 1.00 nm. Calculate the energy of a H₂ molecule with $n_x = n_y = n_z = 10$. Compare this energy to $k_B T$ at $T = 300$ K. Is a classical or a quantum description appropriate?

P4.25 What are the energies of the lowest eight energy levels in a three-dimensional box with $a = b = c$? What is the degeneracy of each level?

P4.26 In discussing the Boltzmann distribution in Chapter 2, we used the symbols g_i and g_j to indicate the degeneracies of the energy levels i and j . By degeneracy, we mean the number of distinct quantum states (different quantum numbers), all of which have the same energy.

- a. Using your answer to Problem P4.22, what is the degeneracy of the energy level $5\hbar^2/2ma^2$ for the square two-dimensional box of edge length a ?
- b. Using your answer to Problem P4.19, what is the degeneracy of the energy level $29\hbar^2/8ma^2$ for a three-dimensional cubic box of edge length a ?

P4.27 Use your result from P4.20 and make an energy-level diagram for the first five energy levels of a square two-dimensional box of edge length b . Indicate which of the energy levels are degenerate and the degeneracy of these levels.

Section 4.4

P4.28 Calculate the expectation value $\langle x^2 \rangle$ for a particle in the state $n = 6$, moving in a one-dimensional box of length 3.25×10^{-10} m. Is $\langle x^2 \rangle = \langle x \rangle^2$? Explain your answer.

P4.29 Is the superposition wave function for the free particle an eigenfunction of the momentum operator? Is it an eigenfunction of the total energy operator? Explain your result.

P4.30 Suppose that the wave function for a system can be written as

$$\psi(x) = \frac{\sqrt{2}}{4} \phi_1(x) + \frac{1}{\sqrt{2}} \phi_2(x) + \frac{2 + \sqrt{2}i}{4} \phi_3(x)$$

and that $\phi_1(x)$, $\phi_2(x)$, and $\phi_3(x)$ are orthonormal eigenfunctions of the operator $\hat{E}_{kinetic}$ with eigenvalues E_1 , $2E_1$, and $4E_1$, respectively.

- a. Verify that $\psi(x)$ is normalized.
- b. What are the possible values that you could obtain in measuring the kinetic energy on identically prepared systems?

c. What is the probability of measuring each of these eigenvalues?

d. What is the average value of $E_{kinetic}$ that you would obtain from a large number of measurements?

P4.31 Are the eigenfunctions of \hat{H} for the particle in the one-dimensional box also eigenfunctions of the momentum operator \hat{p}_x ? Calculate the average value of p_x for the case $n = 2$. Repeat your calculation for $n = 4$ and, from these two results, suggest an expression valid for all values of n . How does your result compare with the prediction based on classical physics?

P4.32 What is the solution of the time-dependent Schrödinger equation for the total energy eigenfunction $\psi_4(x) = \sqrt{2/a} \sin(4\pi x/a)$ for an electron in a one-dimensional box of length 2.00×10^{-10} m.? Write the solution explicitly in terms of the parameters of the problem. Give numerical values for the angular frequency ω and the wavelength of the particle.

P4.33 Are the eigenfunctions of \hat{H} for the particle in the one-dimensional box also eigenfunctions of the position operator \hat{x} ? Calculate the average value of x for the case where $n = 3$. Explain your result by comparing it with what you would expect for a classical particle. Repeat your calculation for $n = 5$ and, from these two results, suggest an expression valid for all values of n . How does your result compare with the prediction based on classical physics?

P4.34 Two wave functions are distinguishable if they lead to a different probability density. Which of the following wave functions are distinguishable from $\sin kx$?

- a. $(e^{ikx} - e^{-ikx})/2$
- b. $e^{i\theta} \sin kx$, θ a constant
- c. $\cos(kx - \pi/2)$
- d. $i \cos(kx + \pi/2)(\sin \theta + i \cos \theta)\left(-\frac{\sqrt{2}}{2} + i \frac{\sqrt{2}}{2}\right)$

P4.35 Is the superposition wave function

$\psi(x) = \sqrt{2/a} [\sin(n\pi x/a) + \sin(m\pi x/a)]$ an eigenfunction of the total energy operator for the particle in the box?

P4.36 Are the total energy eigenfunctions for the free particle in one dimension, $\psi^+(x) = A_+ e^{+i\sqrt{(2mE/\hbar^2)}x}$ and $\psi^-(x) = A_- e^{-i\sqrt{(2mE/\hbar^2)}x}$, eigenfunctions of the one-dimensional linear momentum operator? If so, what are the eigenvalues?

WEB-BASED SIMULATIONS, ANIMATIONS, AND PROBLEMS

Simulations, animations, and homework problem worksheets can be accessed at www.pearsonhighered.com/advchemistry

W4.1 Wave functions for $n = 1 - 5$ are shown for the particle in the infinite depth box, and the energy levels are calculated. Sliders are used to vary the box length and the mass of the particle. The student is asked questions that clarify the relationship between the level energy, the mass, and the box length.

W4.2 Contour plots are generated for the total energy eigenfunctions of the particle in the two-dimensional infinite depth box,

$$\psi_{n_x n_y}(x, y) = N \sin \frac{n_x \pi x}{a} \sin \frac{n_y \pi y}{b}$$

The student is asked questions about the nodal structure of these eigenfunctions and instructed to assign quantum numbers n_x and n_y to each contour plot.

W4.3 The student is asked to determine if the normalized wave function

$$\psi(x) = \sqrt{\frac{105}{a^7}} x^2(x - a)^2$$

is an acceptable wave function for the particle in the infinite depth box based on graphs of $\psi(x)$ and $d\psi(x)/dx$ as a function of x . The wave function $\psi(x)$ is expanded in eigenfunctions of the total energy operator. The student is asked to determine the probability of observing certain values of the total energy in a measurement on the system.

W4.4 The normalized wave function,

$$\Psi(x, t) = \sqrt{\frac{2}{a}} \left[c e^{-iE_1 t/\hbar} \sin\left(\frac{\pi x}{a}\right) + d e^{-iE_2 t/\hbar} \sin\left(\frac{2\pi x}{a}\right) \right]$$

with $|c|^2 + |d|^2 = 1$ is a superposition of the ground state and first excited state for the particle in the infinite depth box. Simulations are carried out to determine if $\langle E \rangle$, $\langle p \rangle$, and $\langle x \rangle$ are independent of time for this superposition state.

W4.5 The probability is calculated for finding a particle in the infinite depth box in the interval $0 \rightarrow 0.1a$, $0.1a \rightarrow 0.2a$, ..., $0.9a \rightarrow 1.0a$ for $n = 1$, $n = 2$, and $n = 50$. The student is asked to explain these results.

FURTHER READING

Chow, Tai L. "The Two-Dimensional Particle in a Box." *Journal of Chemical Education* 67 (1990): 866–867.

Jinks, K. M. "A Particle in a Chemical Box." *Journal of Chemical Education* 52 (1975): 312–313.

Liang, Ying Q., Zhang, Hong, and Dardenne, Yves X. "Momentum Distributions for a Particle in a Box." *Journal of Chemical Education* 72 (1995): 148–151.

Applying the Particle in the Box Model to Real-World Topics

WHY is this material important?

To this point in this book, the formal aspects of quantum mechanics have been introduced. In this chapter, we show how selected molecular-level chemical properties and behavior can be explained by quantum mechanics.

WHAT are the most important concepts and results?

The finite depth particle in the box is a useful model because it can be used to explain why metals conduct electricity and insulators do not. It can also explain the electronic energy levels of π -electrons in conjugated organic molecules and quantum dots.

WHAT would be helpful for you to review for this chapter?

It would be helpful to review the material on the infinite depth particle in the box model in Chapter 4.

5.1 THE PARTICLE IN THE FINITE DEPTH BOX

Before applying the particle in a box model to the “real world,” the box must be modified to make it more realistic. This is done by letting the box have a finite depth, which allows the particle to escape. This modification is necessary to model problems such as the ionization of an atom. The potential is defined by

$$V(x) = 0, \quad \text{for } -a/2 \leq x \leq a/2 \\ V(x) = V_0, \quad \text{for } x > a/2, x < -a/2 \quad (5.1)$$

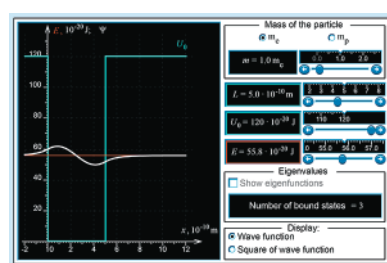
The origin of the x coordinate has been changed from one end of the box (as in Chapter 4) to the center of the box to simplify the mathematics of solving the Schrödinger equation. The shift of the origin changes the functional form of the total energy eigenfunctions, as you will see in the end-of-chapter problems. However, it has no physical consequences in that eigenvalues and graphs of the eigenfunctions superimposed on the potential are identical for both choices of the origin.

How do the eigenfunctions and eigenvalues for the Schrödinger equation for the **finite depth box** differ from those for the infinitely deep potential? Inside the box, the eigenfunctions have the oscillatory behavior that was exhibited for the infinitely deep box. However, because $V_0 < \infty$, the reasoning following Equation (4.10) no longer holds; the amplitude of the eigenfunctions need not be zero at the ends of the box. For $E < V(x)$ (outside of the box), the eigenfunctions decay exponentially with distance

- 5.1** The Particle in the Finite Depth Box
- 5.2** Differences in Overlap between Core and Valence Electrons
- 5.3** Pi Electrons in Conjugated Molecules Can Be Treated as Moving Freely in a Box
- 5.4** Understanding Conductors, Insulators, and Semiconductors Using the Particle in a Box Model
- 5.5** Traveling Waves and Potential Energy Barriers
- 5.6** Tunneling through a Barrier
- 5.7** The Scanning Tunneling Microscope and the Atomic Force Microscope
- 5.8** Tunneling in Chemical Reactions
- 5.9** (Supplemental Section) Quantum Wells and Quantum Dots

Concept

A finite depth box is more realistic than an infinitely deep box.



W5.1 Energy Eigenfunctions and Eigenvalues for a Finite Depth Box

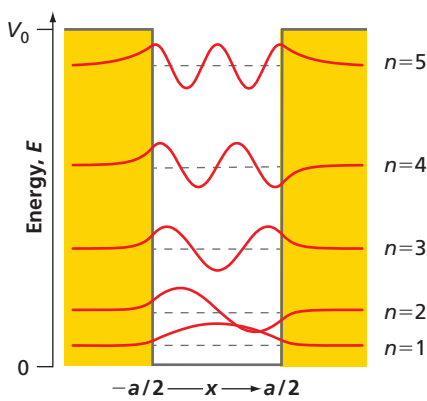


Figure 5.1

Allowed energy levels and corresponding eigenfunctions for a finite depth box. These results are for an electron in a well of depth $V_0 = 1.20 \times 10^{-18}$ J and width $a = 1.00 \times 10^{-9}$ m. The yellow areas correspond to the classically forbidden regions for which $E_{\text{potential}} > E_{\text{total}}$.

Concept

The energy eigenfunctions for a finite depth box extend into the classically forbidden region.

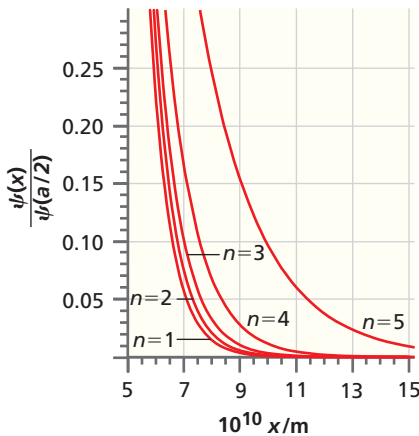


Figure 5.2

Decrease of the amplitude of the eigenfunctions as a function of distance from the center of the box. All eigenfunctions have been normalized to the value one at $x = 5.00 \times 10^{-10}$ m for purposes of comparison.

from the box, as we will show next. The regions inside and outside the box are considered separately. Inside the box, $V(x) = 0$, and

$$\frac{d^2\psi(x)}{dx^2} = -\frac{2mE}{\hbar^2}\psi(x) \quad (5.2)$$

Outside the box, the Schrödinger equation has the form

$$\frac{d^2\psi(x)}{dx^2} = \frac{2m(V_0 - E)}{\hbar^2}\psi(x) \quad (5.3)$$

The difference in sign on the right-hand side of Equation (5.3) makes a big difference in the eigenfunctions! Inside the box, the solutions have the same general form as discussed in Chapter 4, but outside the box, they have the form

$$\begin{aligned} \psi(x) &= A e^{-\kappa x} + B e^{+\kappa x} && \text{for } \infty \geq x > a/2 \quad \text{and} \\ \psi(x) &= A' e^{-\kappa x} + B' e^{+\kappa x} && \text{for } -\infty \leq x < -a/2 \\ \text{where } \kappa &= \sqrt{\frac{2m(V_0 - E)}{\hbar^2}} \end{aligned} \quad (5.4)$$

The coefficients (A, B and A', B') are yet to be determined. Because $\psi(x)$ must remain finite for very large positive and negative values of x , $B = A' = 0$. We require that $\psi(x)$ and $d\psi(x)/dx$ are continuous at the box boundaries. If $\psi(x)$ were not continuous at the boundaries, the probability density would have two different values at the same point, which makes no sense. If $d\psi(x)/dx$ were not continuous at the boundaries, $d^2\psi(x)/dx^2$ would not exist and we could not solve the Schrödinger equation. We also impose a normalization condition so that we can associate $\psi^*(x)\psi(x)$ with a probability density. We solve the Schrödinger equation with these conditions to determine the coefficients A and B' , as well as total energy eigenfunctions and eigenvalues in the potential for given values of m , a , and V_0 . The details of the solution are left to the end-of-chapter problems.

The allowed energy levels and the corresponding eigenfunctions for a finite depth potential are shown in Figure 5.1. The yellow areas correspond to the region for which $E_{\text{potential}} > E_{\text{total}}$. Because $E_{\text{total}} = E_{\text{kinetic}} + E_{\text{potential}}$, $E_{\text{kinetic}} < 0$ in this region. For a particle, $E_{\text{kinetic}} = p^2/2m$, and a negative value for E_{kinetic} implies that the momentum is imaginary. For this reason, $E_{\text{kinetic}} < 0$ defines what is called the **classically forbidden region**.

Two major differences in the solutions between the finite and the infinite depth box are immediately apparent. First, the potential has only a finite number of total energy eigenvalues, which correspond to bound states. The number depends on m , a , and V_0 . Second, the amplitude of the wave function does not go to zero at the edge of the box. We explore the consequences of this second difference when discussing tunneling in Section 5.6. As seen in Figure 5.2, the falloff of the wave function outside of the box is not the same for all eigenfunctions: $\psi(x)$ falls off most rapidly with distance for the most strongly bound state ($V_0 \gg E$) in the potential and most slowly for the least strongly bound state in the potential ($V_0 \sim E$). Equation (5.4) predicts this trend.

5.2 DIFFERENCES IN OVERLAP BETWEEN CORE AND VALENCE ELECTRONS

Figure 5.2 shows that weakly bound states have wave functions that penetrate quite far into the region outside of the box. What are the consequences of this behavior? Interpret this potential as a crude model for electrons in an atom. Strongly bound levels correspond to **core electrons**, and weakly bound levels correspond to **valence electrons**. What happens when a second atom is placed close enough to the first atom that a chemical

bond is formed? The results in Figure 5.3 show that the falloff of the wave functions for the weakly bound states in the box is gradual enough that both wave functions have a nonzero amplitude in the region between the wells. *These wave functions have a significant overlap.* Note that this is not the case for the strongly bound levels; these energy eigenfunctions have a small overlap.

We conclude that a correlation exists between the nonzero overlap required for chemical bond formation and the position of the energy level in the potential. This is our first application of the particle in the box model. It provides an understanding of why chemical bonds involve the least strongly bound, or valence, electrons and not the more strongly bound, or core, electrons. We will have more to say on this topic when chemical bonds are discussed in Chapter 12.

5.3 PI ELECTRONS IN CONJUGATED MOLECULES CAN BE TREATED AS MOVING FREELY IN A BOX

The absorption of light in the visible and ultraviolet (UV) part of the electromagnetic spectrum in molecules is a result of the excitation of electrons from occupied to unoccupied energy levels. If the electrons are delocalized as in an organic molecule with a **π -bonded network**, the maximum in the absorption spectrum shifts from the UV into the visible range. The greater the degree of **delocalization**, the more the absorption maximum shifts toward the red end of the visible spectrum. The energy levels for such a conjugated system can be described quite well with a one-dimensional particle in a box model. The series of molecules 1,4-diphenyl-1,3-butadiene, 1,6-diphenyl-1,3,5-hexatriene, and 1,8-diphenyl-1,3,5,7-octatetraene consist of a planar backbone of alternating C—C and C=C bonds and have phenyl groups attached to the ends. The phenyl groups serve the purpose of decreasing the volatility of the compound. The π -bonded network does not include the phenyl groups, but it does include the terminal carbon–phenyl group bond length. Only the π -bonded electrons are modeled using the particle in the box. Because each energy level can be occupied by two electrons, the highest occupied energy level corresponds to $n = 2, 3$, and 4 for the series of molecules considered.

The longest wavelength at which light is absorbed occurs when one of the electrons in the highest occupied energy level is promoted to the lowest lying unoccupied level. As Equation (4.17) shows, the energy-level spacing depends on the length of the π -bonded network. For 1,4-diphenyl-1,3-butadiene, 1,6-diphenyl-1,3,5-hexatriene, and 1,8-diphenyl-1,3,5,7-octatetraene, the maximum wavelength at which absorption occurs is 345, 375, and 390 nm, respectively. From these data, and taking into account the quantum numbers corresponding to the highest occupied and lowest unoccupied levels, the apparent network length can be calculated. The calculation for 1,6-diphenyl-1,3,5-hexatriene, for which the transition corresponds to $n_i = 3 \rightarrow n_f = 4$, as indicated in Figure 5.4, is as follows:

$$\begin{aligned} a &= \sqrt{\frac{(n_f^2 - n_i^2)h^2}{8m\Delta E}} = \sqrt{\frac{(n_f^2 - n_i^2)h\lambda_{\max}}{8mc}} \\ &= \sqrt{\frac{(4^2 - 3^2)(6.626 \times 10^{-34} \text{ J s})(375 \times 10^{-9} \text{ m})}{8(9.109 \times 10^{-31} \text{ kg})(2.998 \times 10^8 \text{ ms}^{-1})}} \\ &= 892 \text{ pm} \end{aligned} \quad (5.5)$$

The apparent and calculated network lengths are shown and compared in Table 5.1 for each of the three molecules. For more information, see the citation to Anderson (1997) in Further Reading. The agreement is reasonably good, given the simplicity of the model. Most importantly, the model correctly predicts that because λ is proportional to a^2 , shorter π -bonded networks show absorption at smaller wavelengths. This trend is confirmed by experiment.

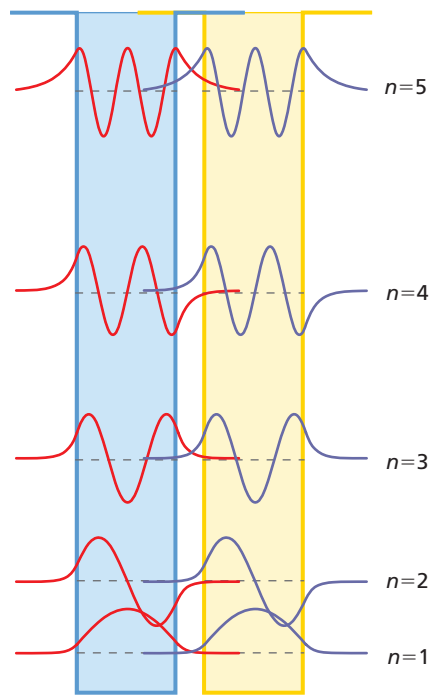


Figure 5.3
Overlap of wave functions from two closely spaced finite depth wells. Each box and its wave functions represent an atom capable of forming a chemical bond. The vertical scale has been expanded relative to Figure 5.1 to better display the overlap.

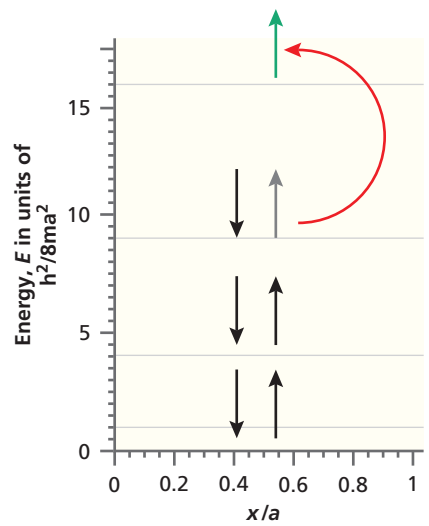


Figure 5.4
Example of the transition from the highest occupied energy level to the lowest unoccupied energy level. The transition is shown for the particle in the box model of the π electrons in 1,6-diphenyl-1,3,5-hexatriene.

TABLE 5.1 Calculated Network Length for Conjugated Molecules

Compound	Apparent Network Length (pm)	Calculated Network Length (pm)
1,4-diphenyl-1,3-butadiene	723	695
1,6-diphenyl-1,3,5-hexatriene	892	973
1,8-diphenyl-1,3,5,7-octatetraene	1030	1251

Concept

Electrons in π -bonded networks are delocalized and their absorption spectrum can be understood using the particle in the box model.

For 1,6-diphenyl-1,3,5-hexatriene in the **ground state**, which is the lowest energy state, the highest occupied energy level corresponds to $n = 3$. Does this mean that in a large number of molecules there will be very few molecules for which the $n = 4$ level is occupied at 300. K? This question can be answered with the help of the Boltzmann distribution.

The energy difference between the $n = 3$ and $n = 4$ levels is given by

$$\Delta E = \frac{h^2(n_f^2 - n_i^2)}{8ma^2} = \frac{7 \times (6.626 \times 10^{-34} \text{ J s})^2}{8 \times 9.109 \times 10^{-31} \text{ kg} \times (973 \times 10^{-12} \text{ m})^2} \\ = 4.45 \times 10^{-19} \text{ J} \quad (5.6)$$

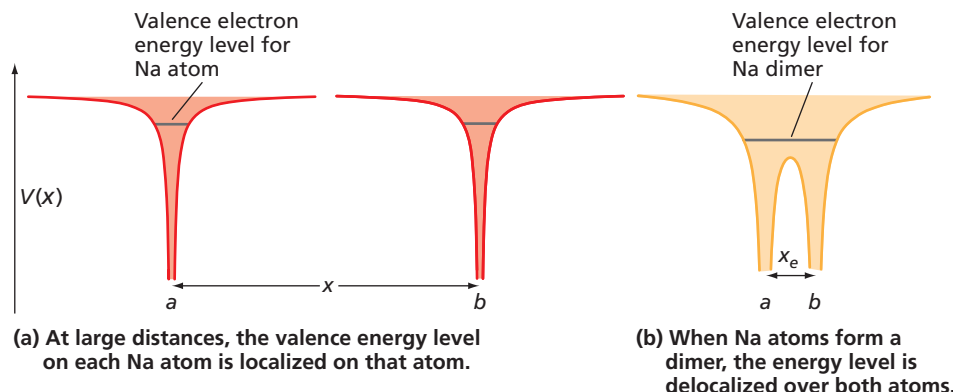
Because there are two quantum states for each value of n , $g_4 = g_3 = 2$. The ratio of the population in the $n = 4$ level to that in the $n = 3$ level is given by

$$\frac{n_4}{n_3} = \frac{g_4}{g_3} e^{-\Delta E/k_B T} = \exp\left[-\frac{4.45 \times 10^{-19} \text{ J}}{1.381 \times 10^{-23} \text{ J K}^{-1} \times 300. \text{ K}}\right] \\ = 2.0 \times 10^{-47} \quad (5.7)$$

Therefore, the $n = 3 \rightarrow n = 4$ transition cannot be achieved by the exchange of translational energy in the collision between molecules at 300. K, and essentially all molecules are in their electronic ground state.

5.4 UNDERSTANDING CONDUCTORS, INSULATORS, AND SEMICONDUCTORS USING THE PARTICLE IN A BOX MODEL

As discussed in Section 5.3, valence electrons on adjacent atoms in a molecule or a solid can have an appreciable overlap of their wave functions. This means that the electrons can “hop” from one atom to the next. Consider Na, which has one valence electron per atom. If two Na atoms are bonded to form a dimer, the valence level that was localized on each atom will be delocalized over both atoms, as is illustrated in Figure 5.5. Note that delocalization leads to a lower energy level for the dimer than for individual atoms.



Now add additional Na atoms to form a one-dimensional Na crystal. A crystalline metal can be thought of as a box with a periodic corrugated potential at the bottom. To illustrate the relationship to a particle in a box model, the potential of a one-dimensional periodic array of Na^+ potentials arising from the atomic cores at lattice sites is shown in Figure 5.6. Because the Na 3s valence electrons can be found with equal probability at any Na atom, one electron per atom is delocalized over the whole metal sample. This is exactly the model of the particle in the box.

The potential energy diagram of Figure 5.6 can be idealized as a box, as shown in Figure 5.7. This box differs from the simple boxes discussed earlier in an essential way. There are many atoms in the atomic chain under consideration (large a), such that the energy levels for the delocalized electrons are very closely spaced, as we show next. About 2×10^7 Na atoms will fit into a 1.00-cm-long box. The energy difference between adjacent levels is given by

$$\begin{aligned} E_{n+1} - E_n &= \frac{(n+1)^2 h^2}{8ma^2} - \frac{n^2 h^2}{8ma^2} = \frac{h^2}{8ma^2}(2n+1) \\ &= (2n+1)(6.02 \times 10^{-34} \text{ J}) \end{aligned} \quad (5.8)$$

The spacing between unoccupied energy levels for which $n > 10^7$ is only $\approx 10^{-13} k_B T$ for $T = 300$ K. Therefore, the energy levels are continuous, and we refer to the range of continuous energy levels as an **energy band**.

An electrical **conductor** is a material that allows the flow of electricity under the influence of an electrical potential. In contrast, an **insulator** is a material that impedes the flow of electricity under these conditions. A **semiconductor** is a material that allows the flow of electricity at elevated temperatures. Conductors, insulators, and semiconductors all have energy bands rather than energy levels that can be resolved, but these three categories of materials differ significantly in their **band structure**, which shows how the bands are occupied and spaced in energy as shown in Figure 5.7. The core electrons form a **valence band**, which is completely filled because the core levels in the atoms are fully occupied. The valence electrons in each atom form a **conduction band**,

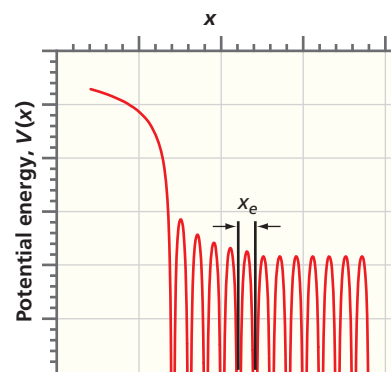


Figure 5.6

The potential energy resulting from a one-dimensional periodic array of Na^+ ions. One valence electron per Na is delocalized over this box. The quantity x_e represents the lattice spacing. Only the left end of the box is shown.

Concept

Metals, semiconductors, and insulators exhibit bands of continuous energy levels separated by band gaps.

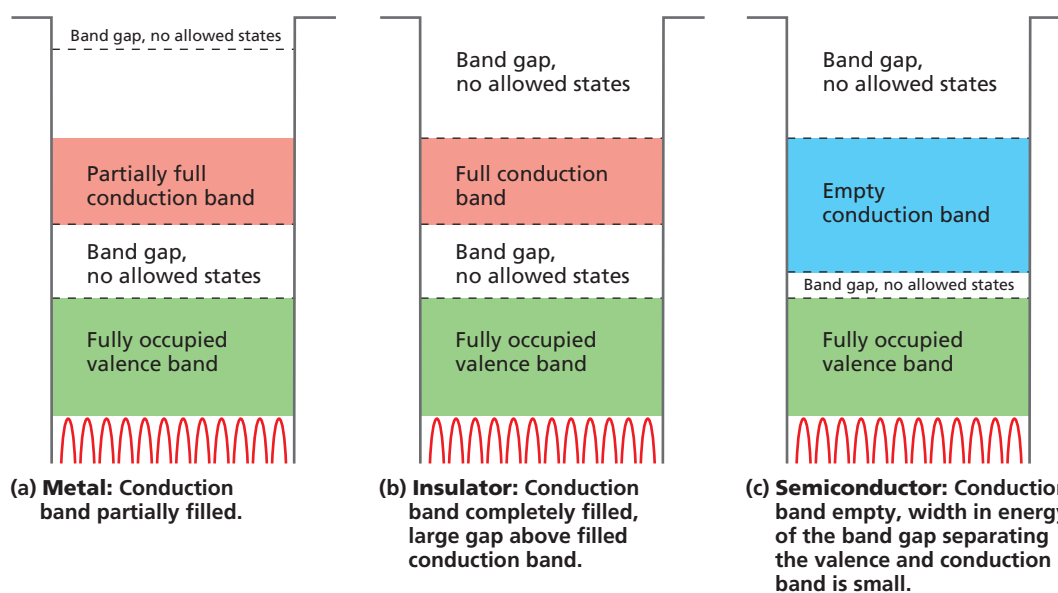


Figure 5.7

Band structures differ for metals, insulators, and semiconductors. All three categories of material have a valence band and a conduction band separated by a band gap. The diagrams are for (a) a metal, (b) an insulator, and (c) a semiconductor. The dashed lines define the energy width of the bands and band gaps. The horizontal scale is greatly expanded to show the periodic potential. Actually, more than 10^7 Na atoms will fit into a 1-cm-long box. The energy of the bands is not to scale.

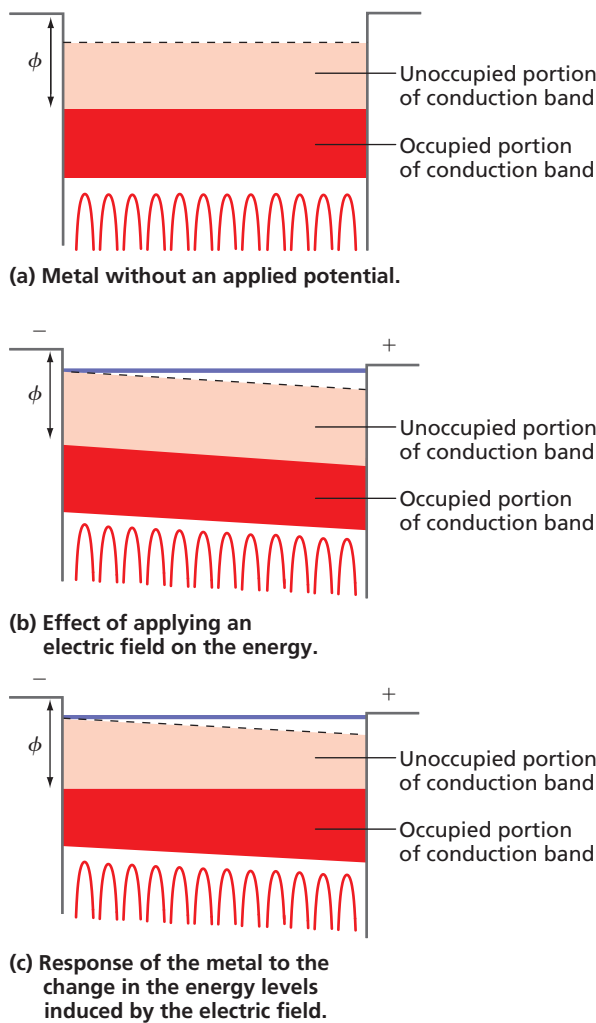


Figure 5.8

Idealization of a metal in the particle in the box model.

For simplicity, the valence band shown in Figure 5.7 has been omitted. The red-shaded conduction band shows the range of energies filled by the valence electrons of the individual atoms. The highest energy level that can be occupied in this band is indicated by the dashed line. The energy required to remove an electron from the highest occupied state is the work function, ϕ , discussed in Chapter 1. The thin solid purple line at the top of the band in parts (b) and (c) indicates where the energy of the highest level would lie in the absence of an electric field.

Concept

A metal conducts electricity because the conduction band is not completely filled.

which is separated by an **energy gap** from the valence band. The energy levels in the valence and conduction bands are continuous, and there are no allowed states in the **band gaps**. In this nomenclature which comes from physics, the states of the valence electrons generate the conduction band, and the states of the core electrons generate the valence band.

In a metal, the conduction band is only partially filled, producing continuous energy levels accessible to excited electrons. In an insulator, both valence and conduction bands are completely filled so that there are no low-lying accessible states available to excited electrons. In a semiconductor, the conduction band is empty, but the energy gap between it and the valence band is small, so that thermal excitation of electrons from the filled valence band to the empty conduction band is possible at elevated temperatures. We next discuss why the band structure of metals allows electrical conduction.

What happens when an electrical potential is applied between the two ends of the box? The electric field produces a gradient of potential energy along the box superimposed on the original potential, as shown in Figure 5.8b. The unoccupied states on the side of the metal with the more positive electrical potential have a lower energy than the occupied states with the more negative electrical potential. This makes it energetically favorable for the electrons to move toward the end of the box with the more positive voltage, as shown in Figure 5.8c. This flow of electrons is the current that flows through the metal. Current flow is possible because of the **overlap of wave functions** on adjacent atoms, which allows delocalization of the electrons over the entire box. Because the unoccupied energy levels are continuous in energy with the filled levels, no activation energy is required to move the electrons along the box.

From the preceding discussion and reference to Figure 5.8, we can now understand what makes a substance such as diamond an insulator. In diamond, the valence band is completely filled. In Figure 5.8, this corresponds to extending the red area up to the dashed line at which the band gap begins. This means that, although we could draw diagrams just like the upper two panels of Figure 5.8 for diamond, the system cannot respond as shown in the lower panel because the band is completely filled. There are no unoccupied states in the valence band that can be used to transport electrons through the crystal. Therefore, diamond is an insulator and will not conduct electricity. Semiconductors are intermediate between metals and insulators in conducting electricity. The band gap is smaller than for insulators, allowing excitation of electrons from the filled valence band to the empty conduction band to occur at elevated temperatures. The excited electrons can be transported along the box, as shown in Figure 5.8c. The band structure of solids is discussed in more detail in Chapter 13.

5.5 TRAVELING WAVES AND POTENTIAL ENERGY BARRIERS

In the previous sections, we focused on the energy of bound states for a finite depth box. Next, we will investigate how a traveling wave particle is affected by a sudden change in the potential energy in the form of a step potential in order to develop a framework for discussing quantum-mechanical tunneling in Section 5.6.

Figure 5.9a shows an electron that moves from a region in which there is no electric field to a region within a parallel plate capacitor in which the electric field opposes

the motion of the particle. An energy diagram for this event is shown in Figure 5.9b. Because energy is conserved in this event, the electron is slowed down abruptly as it enters the region of higher potential energy. The increase in the potential energy at the step leads to a decrease in kinetic energy. Classically, we expect that the probability that the electron passes the step is one for $E > V_0$, and zero if $E < V_0$.

To solve this problem quantum mechanically, we need to solve the time-independent Schrödinger equation for the following potential:

$$V(x) = \begin{cases} 0, & x < 0 \\ V_0, & x \geq 0 \end{cases} \quad (5.9)$$

Just as we did for the free particle in Section 4.1, we write the Schrödinger equation in the form

$$\frac{d^2\psi(x)}{dx^2} = \left[\frac{2m(V(x) - E)}{\hbar^2} \right] \psi(x) \quad (5.10)$$

and solve it in the two separate regions for $x < 0$ and $x > 0$ that we refer to as regions 1 and 2, respectively. We then combine these two solutions while requiring the continuity of $\psi(x)$ and $d\psi(x)/dx$ at $x = 0$ where the electron passes from one region to the other. We consider only the case $E > V_0$.

In the region $x < 0$, we consider the possibility that the electron will be reflected by the sudden change in the potential energy. Classically, reflection would not occur for $E > V_0$, but we know that light waves incident on an interface between two materials of differing refractive index can either be reflected or transmitted. An appropriate wave function for the electron that includes reflection is

$$\psi(x) = Ae^{+ik_1x} + Be^{-ik_1x}, \quad x < 0 \quad (5.11)$$

where the first term is the wave incident on the barrier, moving to the right, and the second term is the reflected wave, moving to the left. The wave vector k_1 is related to the kinetic energy by

$$k_1 = \sqrt{\frac{2mE_{kinetic1}}{\hbar^2}} \quad (5.12)$$

In the region for $x > 0$, we write the wave function in the form

$$\psi(x) = Ce^{+ik_2x}, \quad x > 0 \quad \text{where} \quad k_2 = \sqrt{\frac{2mE_{kinetic2}}{\hbar^2}} \quad (5.13)$$

There is no wave moving in the direction of decreasing x values in this region because the electron experiences no forces that could turn it around.

We next require that $\psi(x)$ and $d\psi(x)/dx$ in the two regions have the same values at $x = 0$. If the wave functions did not have the same value, the probability density at $x = 0$ would have two different values at the same point, which makes no sense. If $d\psi(x)/dx$ for the two regions did not have the same value at $x = 0$, $d^2\psi(x)/dx^2$ would not exist and we could not solve the Schrödinger equation. Applying the continuity condition on $\psi(x)$, we obtain

$$\begin{aligned} Ae^{+ik_10} + Be^{-ik_10} &= Ce^{+ik_20} \\ A + B &= C \end{aligned} \quad (5.14)$$

Applying the continuity condition on $d\psi(x)/dx$, we obtain

$$\begin{aligned} ik_1Ae^{+ik_10} - ik_1Be^{-ik_10} &= ik_2Ce^{+ik_20} \\ k_1(A - B) &= k_2C \end{aligned} \quad (5.15)$$

To obtain the probabilities for reflection and transmission, we must take the speeds of the particle in the two regions into account. The number of particles reflected or

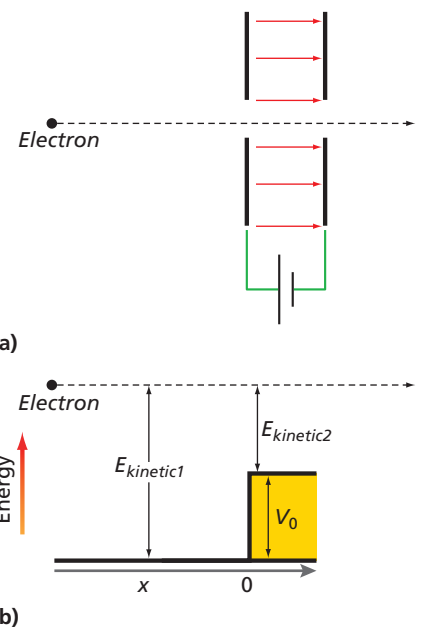


Figure 5.9

Effect on electron as it enters an electric field. (a) An electron moves from left to right from a field-free region into a parallel plate capacitor in which it is slowed down. (b) The energetics of the electron is shown in the regions before entering the capacitor and in the capacitor.

transmitted per unit time is given by the product of the probability density and the speed. The units of this product are probability/length \times length/time = probability/time as required. Because the speed and the wave vector k are proportional, we can substitute k for speed. The transmission probability T and the reflection probability R are given by Equation (5.16).

$$R = \frac{\text{number reflected/unit time}}{\text{number incident/unit time}} = \frac{B^* B \times k_1}{A^* A \times k_1} = \frac{B^* B}{A^* A}$$

$$T = \frac{\text{number transmitted/unit time}}{\text{number incident/unit time}} = \frac{C^* C \times k_2}{A^* A \times k_1} \quad (5.16)$$

We can use Equations (5.14) and (5.15) to express B in terms of A to calculate R and to express C in terms of A to calculate T . The results are

$$R = \frac{\left(\frac{k_1 - k_2}{k_1 + k_2} A\right)^* \left(\frac{k_1 - k_2}{k_1 + k_2} A\right)}{A^* A} = \left(\frac{k_1 - k_2}{k_1 + k_2}\right)^2$$

$$T = \frac{\left(\frac{2k_1}{k_1 + k_2} A\right)^* \left(\frac{2k_1}{k_1 + k_2} A\right)}{A^* A} \times \frac{k_2}{k_1} = \frac{4k_1 k_2}{(k_1 + k_2)^2} \quad (5.17)$$

These results can be expressed in terms of E and V_0 where $E = E_{\text{kinetic}}$.

$$R = \frac{(\sqrt{E} - \sqrt{E - V_0})^2}{(\sqrt{E} + \sqrt{E - V_0})^2}$$

$$T = \frac{4\sqrt{E(E - V_0)}}{(\sqrt{E} + \sqrt{E - V_0})^2} \quad (5.18)$$

Note that we are only considering energies for which $E > V_0$. The probabilities for reflection and transmission as a function of the dimensionless parameter E/V_0 are shown in Figure 5.10. Classical physics would predict that $T = 1$ and $R = 0$ for $E > V_0$ and that $T = 0$ and $R = 1$ for $E < V_0$. Quantum mechanics predicts that $R \rightarrow 1$ as $E \rightarrow V_0$, but R only approaches zero asymptotically for $E \gg V_0$. We will discuss the quantum-mechanical solution for $E < V_0$ in the next section.

Concept

Reflection and transmission of a wave-particle at a step potential are not accurately described by classical physics.

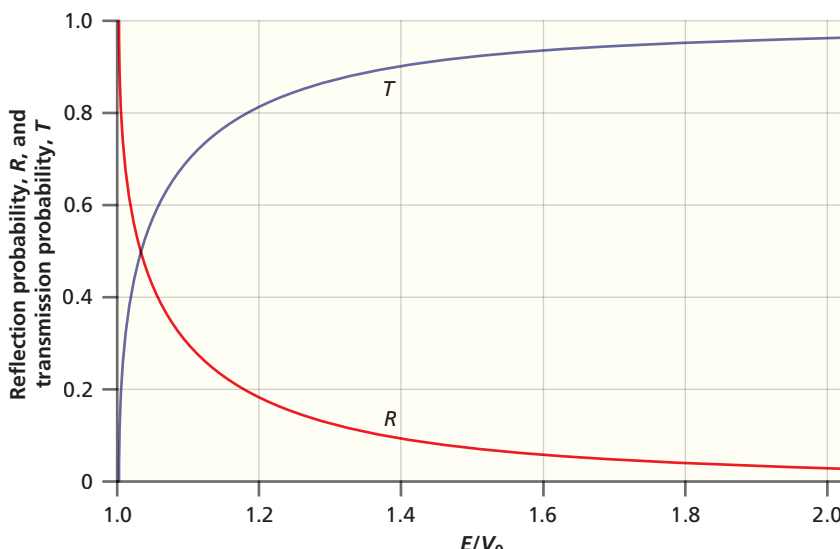


Figure 5.10

Probability for reflection R and transmission T from a step potential of height V_0 plotted as a function of the ratio E/V_0 .

5.6 TUNNELING THROUGH A BARRIER

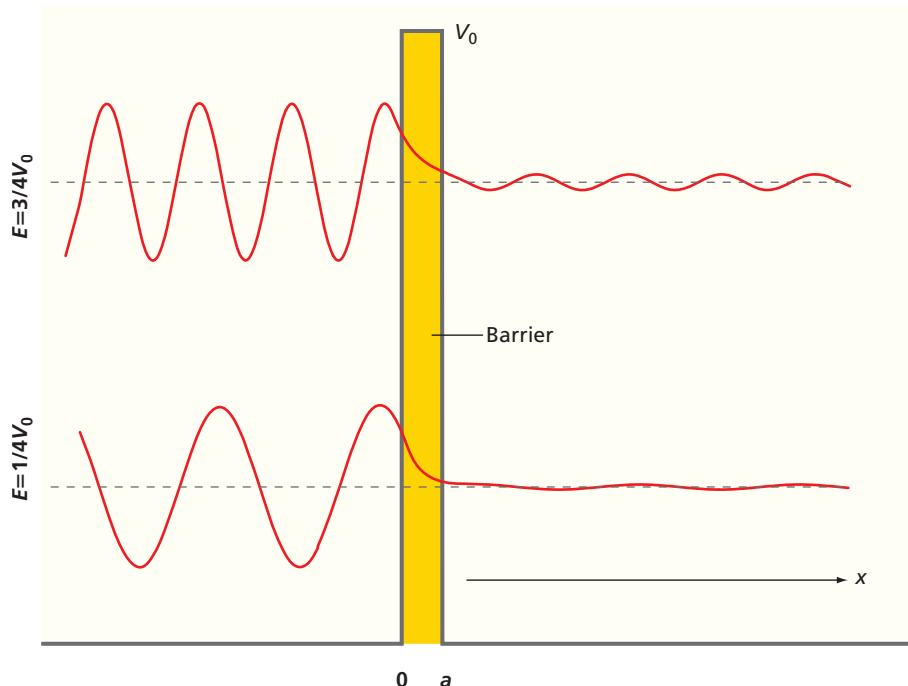
In the preceding section, we saw that a wave particle approaching a step potential can be reflected even if its energy is greater than the barrier height. For the step potential, the barrier is present for all positive values of x . We next consider a barrier of finite width for a particle of energy such that $V_0 > E$. Classically, the particle will not pass the barrier region because it has insufficient energy to get over the barrier. This situation is quite different in quantum mechanics. As we saw for the finite depth box in Section 5.1, the wave function for the particle can penetrate into the classically forbidden barrier region. For the infinitely thick barrier presented by the step potential, the amplitude of the wave function decays rapidly to a negligibly small value. However, something surprising happens if the barrier is thin, meaning that $V_0 > E$ only over a distance comparable to the particle wavelength. The particle can escape *through* the barrier even though it does not have sufficient energy to go *over* the barrier. This process, depicted in Figure 5.11, is known as **tunneling**.

To investigate tunneling, we modify the step potential as shown in Equation (5.19). The potential is now described by

$$\begin{aligned} V(x) &= 0, \quad \text{for } x < 0 \\ V(x) &= V_0, \quad \text{for } 0 \leq x \leq a \\ V(x) &= 0, \quad \text{for } x > a \end{aligned} \tag{5.19}$$

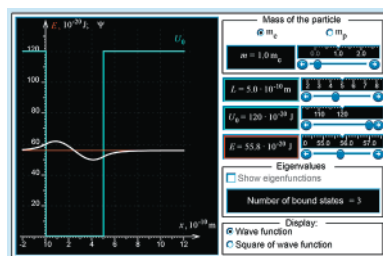
The oscillating wave function for two incident particle energies is shown to the left of the barrier where $E > V_0$ in Figure 5.11. Inside the barrier where $E < V_0$, the wave function decays exponentially with distance. If the **barrier width** a is small enough that $\psi(x)$ has not decayed to a negligibly small value by the time it arrives at the end of the barrier at $x = a$, the wave function in the region $x > a$ will have a finite amplitude. Because $V(x) = 0$ for $x > a$, the wave function in this region is again a traveling wave. If the amplitude is greater than zero for $x > a$, the particle has a finite probability of passing through the barrier, even though its energy is less than the height of the barrier.

Figure 5.12 shows that tunneling is much more likely for particles with energies near the top of the barrier. This is due to the degree to which the wave function in the barrier falls off with distance as $e^{-\kappa x}$, in which the **decay length** $1/\kappa$ is given by



Concept

Tunneling, in which a wave-particle can pass through an energy barrier, has no analog in classical physics.



W5.2 Tunneling Through a Barrier

Figure 5.11

Depiction of tunneling. Wave-particles corresponding to the indicated energy are incident from the left on a barrier of height $V_0 = 1.60 \times 10^{-19} \text{ J}$ and width $9.00 \times 10^{-10} \text{ m}$. The exponentially decaying wave function is shown inside the barrier, and the incident and transmitted wave functions are shown for $x < a$ and $x > a$, respectively.

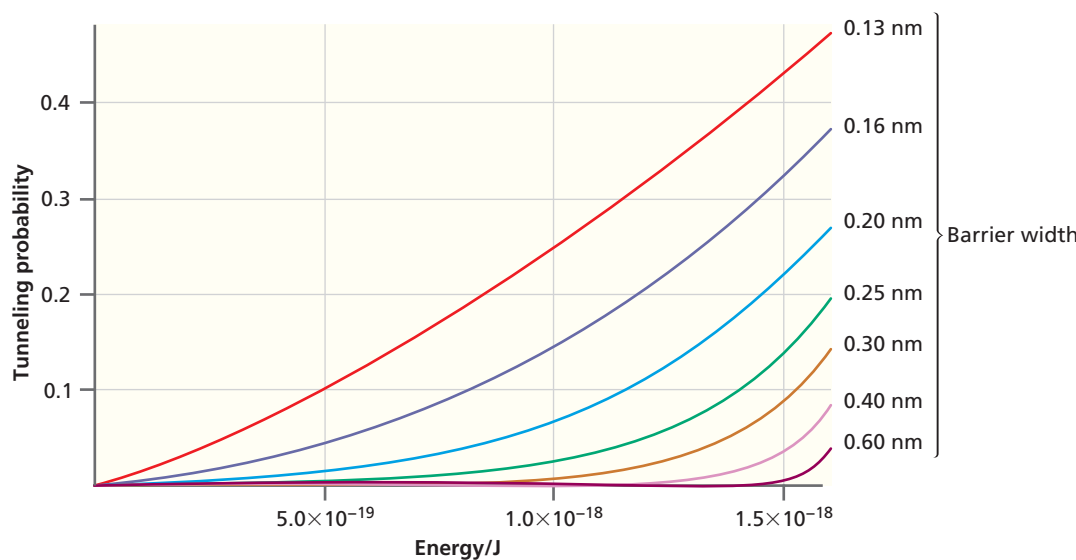


Figure 5.12

Tunneling probability for an electron for various barrier widths as a function of the particle energy for various barrier heights. The tunneling probability for an electron is shown for seven barrier widths as a function of the particle energy for a barrier height of 1.6×10^{-18} J. $E = V_0$ for $E = 1.6 \times 10^{-18}$ J.

$\sqrt{\hbar^2/2m(V_0 - E)}$. Because the wave function decays more slowly as $E \rightarrow V_0$, the amplitude of the wave function at $x = a$ is greater and tunneling is more likely to occur.

Rather than derive expressions for R and T as for the step potential, we leave the details of the calculations related to tunneling for the end-of-chapter problems. To illustrate the extreme sensitivity of the tunneling probability on the barrier width and particle energy, the results of a calculation for electron tunneling through a barrier of height 10. eV are shown in Figure 5.12. Note that for the narrowest barrier, the tunneling probability approaches 0.5 as $E \rightarrow V_0$ and that for wide barriers, the tunneling probability is very small unless $E \rightarrow V_0$.

5.7 THE SCANNING TUNNELING MICROSCOPE AND THE ATOMIC FORCE MICROSCOPE

That particles could tunnel through a barrier was unknown until the advent of quantum mechanics. In the early 1980s, the tunneling of electrons between two solids was used to develop an atomic resolution microscope. Gerd Binnig and Heinrich Rohrer received a Nobel Prize for the invention of the **scanning tunneling microscope (STM)** in 1986.

The STM allows the imaging of solid surfaces with atomic resolution with surprisingly simple instrumentation. The STM and a closely related device called the **atomic force microscope (AFM)** have been successfully used to study phenomena at atomic and near atomic resolution in a wide variety of areas, including chemistry, physics, mineralogy, biology, and engineering. The invention of the STM and AFM played a significant role in enabling the development of nanotechnology. The essential elements of an STM are a sharp metallic tip and a conducting sample over which the tip is scanned to create an image of the sample surface. In an STM, the barrier between these two conductors is usually a vacuum, and electrons are induced to tunnel through this barrier, as discussed later in this chapter. As might be expected, the barrier width needs to be on the order of atomic dimensions to observe tunneling. The barrier height V_0 in a metal is called the **work function**. The decay length $\sqrt{\hbar^2/2m(V_0 - E)}$ for a tunneling electron in a vacuum barrier is generally in the range 0.1–0.5 nm. Therefore,

Concept

Scanning tunneling and atomic force microscopy have enabled the imaging of solid surfaces at an atomic scale and have helped establish the field of nanotechnology.

if the tip and sample are brought to within a nanometer of one another, electron tunneling can be observed between them.

How does a scanning tunneling microscope work? We will address this question first in principle and then from a practical point of view. Because the particle in a box is a good model for electrons in the metal solid, the tip and surface can be represented by boxes, as shown in Figure 5.13. For convenience, only the conduction band has been included, and only the part of the box immediately adjacent to the tip-sample gap is shown. The tip and sample in general have different work functions, as indicated. If they are not connected in an external circuit, their energy diagrams line up as in Figure 5.13a. When they are connected in an external circuit, charge flows between the tip and sample until the highest occupied level is the same everywhere, as shown in Figure 5.13b.

Tunneling takes place at constant energy, which in Figure 5.13 corresponds to a horizontal line (dashed in the figure). However, for the configuration shown in Figure 5.13b, there is no empty state on the sample into which an electron from the tip can tunnel. To allow tunneling to occur, a small (0.01–2 V) electrical potential is placed between the two metals. This raises the highest filled energy level of the tip relative to that of the sample. Now tunneling of electrons can take place from tip to sample, resulting in a net current flow.

Up until now, we have discussed a tunneling junction, not a microscope. Figure 5.14 shows how an STM functions in an imaging mode. A radius of curvature of 100 nm at the apex of the tip is routinely achievable by electrochemically etching a metal wire. The sample could be a single crystal whose structure is to be investigated at an atomic scale. This junction is shown on an atomic scale in the bottom part of Figure 5.14. No matter how blunt the tip is, one atom is closer to the surface than all the others. At a tunneling gap distance of about 0.5 nm, the tunneling current decreases by an order of magnitude for every 0.1 nm that the gap is increased. Therefore, the next atoms farther back from the apex of the tip make a negligible contribution to the tunneling current, and the whole tip acts like a single atom for tunneling.

The tip is mounted on a segmented tubular scanner made of a piezoelectric material that changes its length in response to an applied voltage. In this way, the tip can be brought close to the surface by applying a voltage to the piezoelectric tube. Assume that we have managed to bring the tip within tunneling range of the surface. On the magnified scale shown in Figure 5.14, the individual atoms in the tip and surface are seen at a tip–surface spacing of about 0.5 nm. Keep in mind that the wave functions for the tunneling electrons in the tip decay rapidly in the region between tip and sample, as shown earlier in Figure 5.2. If the tip is directly over a surface atom, the amplitude of the wave function is large at the surface atom and the tunneling current is high. If the tip is between surface atoms, the amplitude of the wave functions is smaller and the tunneling current will be lower. To scan over the surface, different voltages are applied to the four segmented electrodes on the piezoelectric tube, which causes the tube to bend. For a large bending radius, this corresponds to a translation of the tip parallel to the surface. In this way, a topographical image of the surface is obtained. Because the tunneling current varies exponentially with the tip–surface distance, the microscope provides a very high sensitivity to changes in the height of the surface that occur on an atomic scale.

In this abbreviated description, some details have been glossed over. The current is usually kept constant as the tip is scanned over the surface using a feedback circuit to keep the tip–surface distance constant. This is done by changing the voltage to the piezoelectric tube electrodes as the tip scans over the surface. Additionally, a vibrational isolation system is required for the STM to prevent the tip from crashing into the surface as a result of vibrations, which are always present in a laboratory.

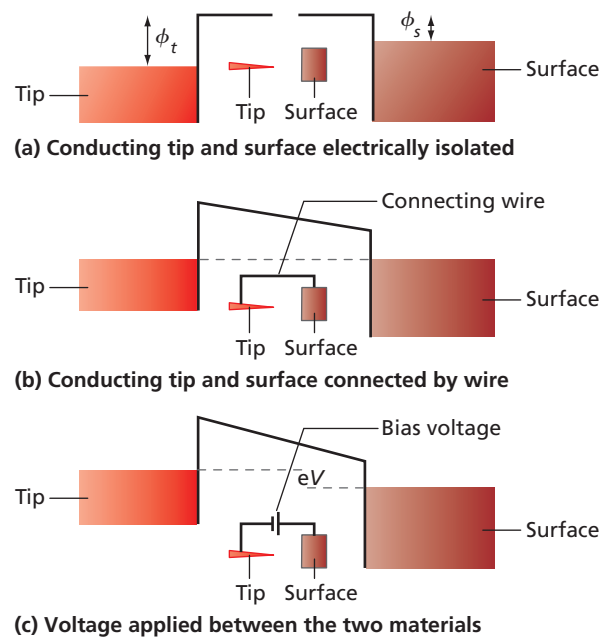


Figure 5.13

Schematic diagram of a scanning tunneling microscope. The conduction band of the STM tip is on the left (orange box) and that of the conducting sample on the right (brown box). ϕ is the work function. The subscripts t and s refer to tip and surface. (a) If the conducting tip and surface are electrically isolated from one another, their energy diagrams line up. (b) If they are connected by a wire in an external circuit, charge flows from the lower work function material into the higher work function material until the highest occupied states have the same energy in both materials. (c) By applying a voltage V between the two materials, the highest occupied levels have an offset of energy eV . This allows tunneling to occur from left to right.

Figure 5.14

Schematic representation of a scanning tunneling microscope.

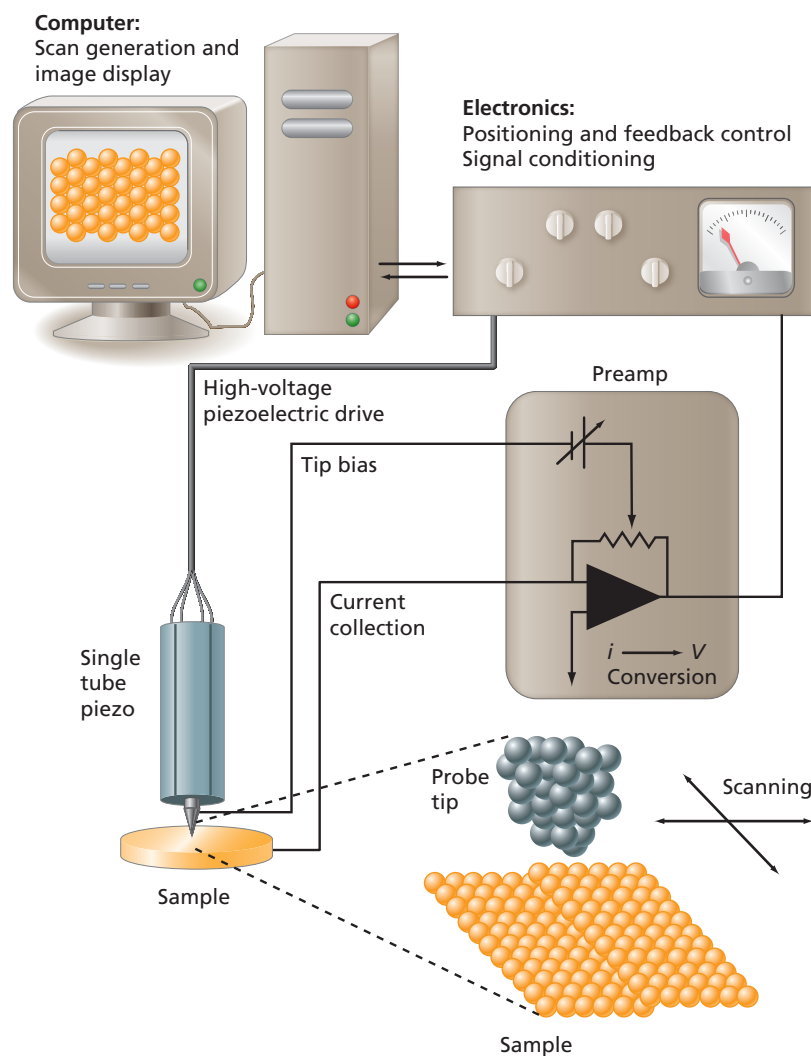
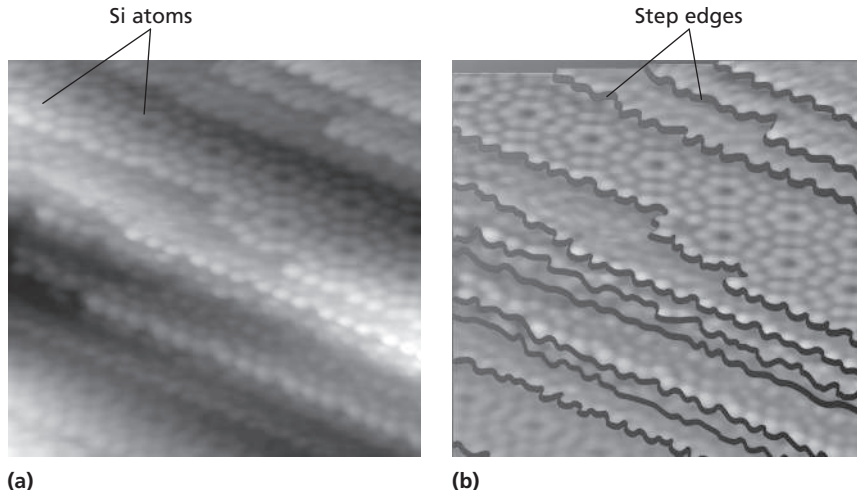


Figure 5.15 provides an example of the detail that can be seen with a scanning tunneling microscope. The individual planes, which are stacked together to make the silicon crystal, and the 0.3 nm height change between planes are clearly seen. Defects in the crystal structure are also clearly resolved. Researchers are using this microscope in many new applications aimed at understanding the structure of solid surfaces and modifying surfaces atom by atom.

**Figure 5.15**

STM images of the (111) surface of Si.

(a) The image shows a 200. × 200. nm region with a high density of atomic steps. The light dots correspond to individual Si atoms. (b) The image emphasizes the structure of parallel crystal planes separated by steps of one atom height. The step edges are shown as dark ribbons.

EXAMPLE PROBLEM 16.1

As was found for the finite depth well, the wave function amplitude decays in the barrier according to $\psi(x) = A \exp[-\sqrt{2m(V_0 - E)/\hbar^2}x]$. This result will be used to calculate the sensitivity of the scanning tunneling microscope. Assume that the tunneling current through a barrier of width a is proportional to $\psi(x)^2$ or $|A|^2 \exp[-2\sqrt{2m(V_0 - E)/\hbar^2}a]$.

- If $V_0 - E$ is 4.50 eV, by what factor would the current be greater for a barrier width of 0.20 nm than for 0.30 nm?
- A friend suggests to you that a proton tunneling microscope would be equally effective as an electron tunneling microscope. For a 0.20 nm barrier width, by what factor is the tunneling current changed if protons are used instead of electrons?

Solution

- Putting the numbers into the formula given, we obtain

$$\begin{aligned} \frac{I(a = 2.0 \times 10^{-10} \text{ m})}{I(a = 3.0 \times 10^{-10} \text{ m})} &= \exp \left[-2 \sqrt{\frac{2m(V_0 - E)}{\hbar^2}} \right. \\ &\quad \left. \times (2.0 \times 10^{-10} \text{ m} - 3.0 \times 10^{-10} \text{ m}) \right] \\ &= \exp \left[-2 \sqrt{\frac{2 \times 9.109 \times 10^{-31} \text{ kg} \times 4.50 \text{ eV} \times 1.602 \times 10^{-19} \text{ J/eV}}{(1.055 \times 10^{-34} \text{ J s})^2}} \right. \\ &\quad \left. \times (-1.0 \times 10^{-10} \text{ m}) \right] \\ &= 8.8 \end{aligned}$$

Even a small distance change results in a substantial change in the tunneling current.

- We find that the tunneling current for protons is appreciably smaller than that for electrons.

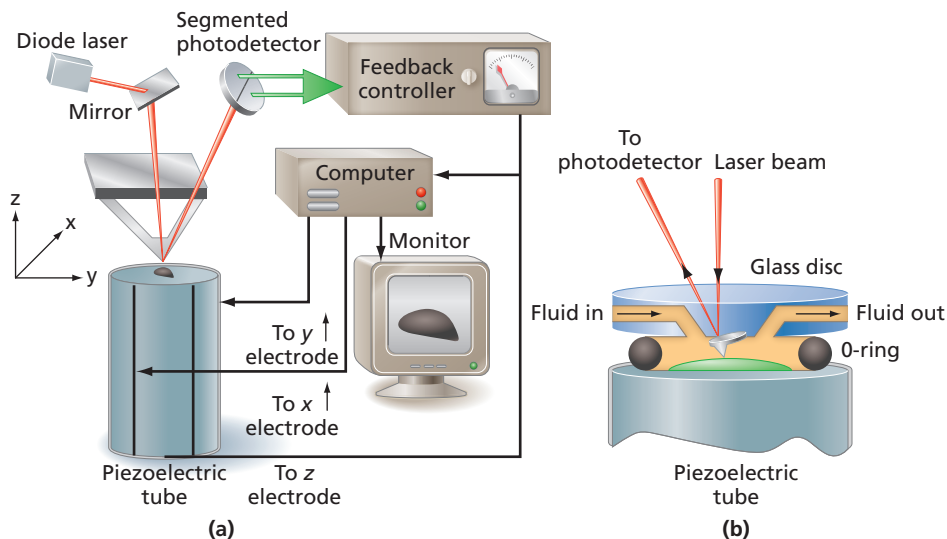
$$\begin{aligned} \frac{I(\text{proton})}{I(\text{electron})} &= \frac{\exp \left[-2 \sqrt{\frac{2m_{\text{proton}}(V_0 - E)}{\hbar^2}} a \right]}{\exp \left[-2 \sqrt{\frac{2m_{\text{electron}}(V_0 - E)}{\hbar^2}} a \right]} \\ &= \exp \left[-2 \sqrt{\frac{2(V_0 - E)}{\hbar^2}} (\sqrt{m_{\text{proton}}} - \sqrt{m_{\text{electron}}}) a \right] \\ &= \exp \left[-2 \sqrt{\frac{2 \times 4.50 \text{ eV} \times 1.602 \times 10^{-19} \text{ J/eV}}{(1.055 \times 10^{-34} \text{ J s})^2}} \times \left(\frac{\sqrt{1.67 \times 10^{-27} \text{ kg}}}{-\sqrt{9.11 \times 10^{-31} \text{ kg}}} \right) \right. \\ &\quad \left. \times 2.0 \times 10^{-10} \text{ m} \right] \\ &= 1.2 \times 10^{-79} \end{aligned}$$

This result does not make the proton tunneling microscope look very promising.

The STM is limited to studies on conductive surfaces because although the tunneling current is small, the current density is very high. The AFM extends the range of the STM by allowing studies to be carried out on nonconductive surfaces. It does so by probing the force between the tip and the surface without any current passing across the junction. Although the AFM is not based on tunneling, we discuss it here because the atomic force microscope and the scanning tunneling microscope complement one another in structural studies of solid surfaces at the molecular and atomic level, as we show later. The German physicist Gerd Binnig is a co-inventor of the AFM as well as the STM.

Figure 5.16

Schematic diagram of an atomic force microscope. (a) A tip mounted on a microfabricated cantilever is scanned over a surface in the x - y plane by applying dc voltages to a segmented piezoelectric tube. If the tip experiences an attractive or repulsive force from the surface, the cantilever is deflected from its horizontal position. As a result, the laser light reflected from the back of the cantilever onto a segmented photodetector is differently distributed on the segments, giving rise to a difference current that is the input to a feedback controller. The controller changes the length of the piezoelectric tube in such a way as to keep the cantilever deflection constant as the tip scans across the surface. Therefore, the surface image obtained corresponds to a constant force that can be varied using the feedback circuit. (b) The AFM can be modified to allow measurements in a liquid or controlled atmosphere using an O-ring seal mounted on the piezoelectric tube.



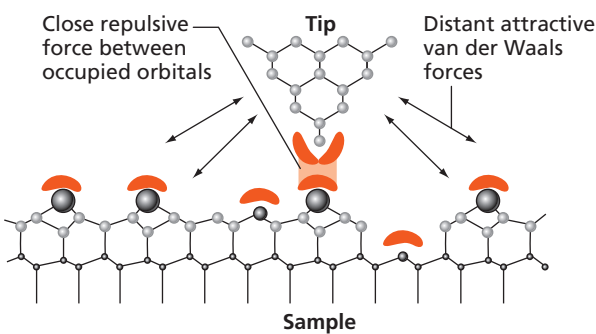
In an AFM, a tip attached to a flexible cantilever is scanned over the surface of a sample using the same feedback circuitry as for an STM, as shown in Figure 5.16. The tip and cantilever are generally microfabricated from Si, and the deflection of the cantilever from its horizontal position is given by

$$x = -\frac{F}{k} \quad (5.20)$$

where F is the force exerted on the cantilever and k is its spring constant, which can have values in the range $0.01\text{--}100\text{ N m}^{-1}$, depending on the application. The tip has a radius of curvature of $\sim 10\text{--}20\text{ nm}$, and the force of interaction between the tip and the surface is primarily determined by those few atoms on the tip closest to the surface. The force is attractive and van der Waals in nature except for very small tip–surface distances, in which case repulsive electron–electron forces dominate. The deflection of the cantilever is measured using a laser similar to that in a CD player. The light reflected from the back of the cantilever is incident on a segmented photodetector, and the deflection of the cantilever can be determined by comparing the signal from the segments of the photodetector. The feedback circuit keeps the cantilever deflection, and therefore the tip–surface force, constant as the tip is scanned across the surface.

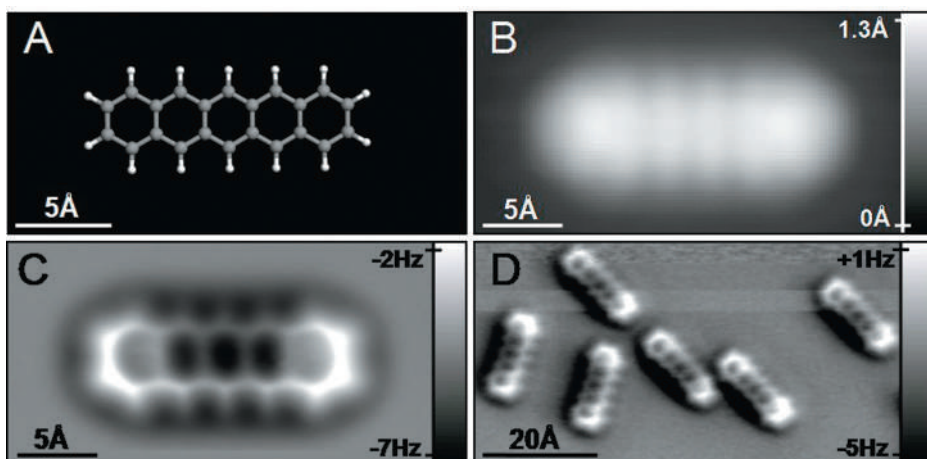
Whereas in an STM, an image corresponds to a surface contour at constant tunneling current, in an AFM, an image corresponds to a surface contour at constant force. Image acquisition is sufficiently fast that many kinetic processes can be imaged in real time.

The AFM design described is suitable for high-resolution work in a controlled environment, including liquids. To obtain ultrahigh molecular and atomic resolution, the device must be operated in an ultrahigh vacuum in order to avoid contamination of the surface under study. The highest resolution images have been obtained in microscopes cooled to a temperature of $\sim 5\text{ K}$ to minimize drifts in the area being scanned by thermal gradients. For atomic-resolution studies, the tip must be scanned close enough to the surface that the repulsive rather than the attractive forces between the tip and the surface are sensed, as shown in Figure 5.17. The cantilever is oscillated at a resonant frequency determined by its geometry at an amplitude of $\sim 1\text{ nm}$. The repulsive interaction between the tip and the surface leads to small shifts in the cantilever eigenfrequency that can be used as the feedback parameter to keep the force constant as the tip is scanned over the surface. If the tip and surface are conductive, both STM and AFM images of the surface can be obtained with the same instrument. With an appropriate choice of cantilever and tip, AFM can be used to measure friction, conductivity, temperature,

**Figure 5.17**

Imaging modes of an atomic force microscope. If an AFM tip is scanned over the surface in the more distant attractive part of the tip–surface potential that probes van der Waals forces, the atomic-scale structure is averaged because the tip senses many atoms, as indicated by the double headed arrows. If the tip is sufficiently close to the surface, the repulsive force between the occupied orbitals at the end of the tip and the occupied orbitals of the surface atoms (shown in orange) is probed. Because these forces are very localized, atomic resolution is possible.

Source: Adapted from Giessibl, *Reviews of Modern Physics* 75 (2003): 949.



and variations of chemical composition on surfaces with high resolution. For more details, see the references to Giessibl (2003) and Gross et al. (2009) in Further Reading.

Figure 5.18 shows images of pentacene molecules bound to a metal surface obtained using both STM and AFM modes of operation. The STM image arises from tunneling out of the highest filled molecular orbitals of the molecule, which are delocalized over the molecule. For this reason, atomic-scale resolution is not obtained. Note the nodal structure seen in the image. The AFM image in Figure 5.18c arises from the repulsive electrostatic force between the filled orbitals on CO and the electron density in the pentacene molecule. The enhanced density due to bonding between the carbon atoms of the benzene rings as well as the electron density in the C-H bonds can be seen clearly. This example shows both how tunneling can be used to image the structure of molecular orbitals directly (see also Section 13.6) and how the electron density in chemical bonds can be imaged directly using atomic force microscopy. For more details, see Gross et al. (2009).

Figure 5.18

STM and AFM imaging of pentacene on a copper surface. The tip has been prepared with a CO molecule at the apex, with the oxygen atom pointing to the surface being scanned. (a) Ball-and-stick model of the pentacene molecule. (b) Constant-current STM image of a single pentacene molecule. The scale on the right shows the correspondence between the gray scale and the height within the molecule. (c) Constant-height AFM image of a single pentacene molecule. The scale on the right shows the correspondence between the gray scale and the frequency shift observed in scanning over the molecule. (d) Constant-height AFM image showing six pentacene molecules. The scale on the right is the same as in (c).

Source: Adapted from Gross et al., *Science* 325 (2009): 1110.

5.8 TUNNELING IN CHEMICAL REACTIONS

Most chemical reactions are thermally activated; they proceed faster as the temperature of the reaction mixture is increased. This behavior is typical of reactions for which an energy barrier must be overcome in order to transform reactants into products. This barrier is referred to as the **activation energy** for the reaction. By increasing the temperature of the reactants, the fraction of reactants with an energy that exceeds the activation energy is increased, allowing the reaction to proceed.

Tunneling provides another mechanism to convert reactants to products that does not require an increase in energy of the reactants for the reaction to proceed. It is well known that hydrogen transfer reactions can involve tunneling. An example is the reaction $R_1OH + R_2O^- \rightarrow R_2OH + R_1O^-$, where R_1 and R_2 are two different organic groups. The test for tunneling in this case is to substitute deuterium for hydrogen. If the reaction is thermally activated, the change in reaction rate is small and can be attributed to the different ground-state vibrational frequency of $-OH$ and $-OD$ bonds (see Chapter 8). However, if tunneling occurs, the rate decreases greatly because the tunneling rate depends exponentially on the decay length $\sqrt{\hbar^2/2m(V_0 - E)}$. It is not widely appreciated that tunneling can be important for heavier atoms such as C and O. It has been shown that the rate of the ring expansion reaction depicted in Figure 5.19 is faster than the predicted thermally activated rate by the factor 10^{152} at 10 K! For more detail, see the reference to Zuev et al. (2003) in Further Reading. This increase is due to the tunneling pathway. Because the tunneling rate depends exponentially on $\sqrt{\hbar^2/2m(V_0 - E)}$, heavier atom tunneling is only appreciable if $(V_0 - E)$ is very small. However, in a number of reactions, particularly in the fields of chemical catalysis and enzymology, this condition is met.

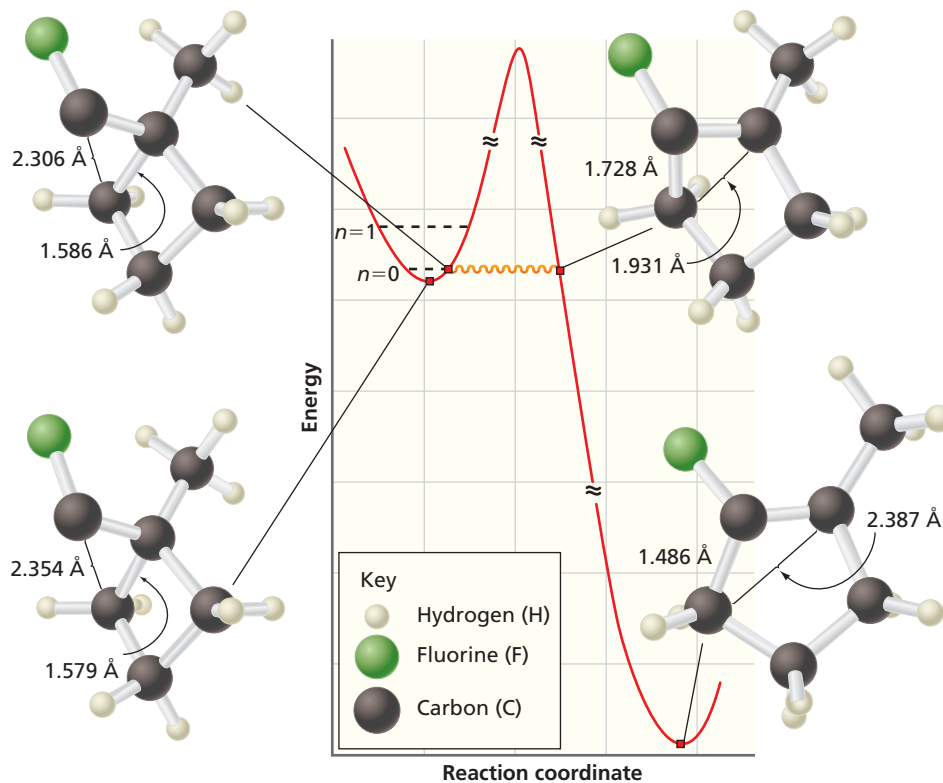
Concept

Tunneling of atoms also plays a role in chemical reactions.

Figure 5.19

Example of reaction facilitated by tunneling. The structures of four species and the reaction path from reactant to product are shown, together with a schematic energy diagram. The reaction occurs not by surmounting the barrier but by tunneling through the barrier at the energy indicated by the wavy line.

Source: Adapted from Zuev et al., *Science* 299 (2003): 867–870.



SUPPLEMENTAL SECTION

5.9 QUANTUM WELLS AND QUANTUM DOTS

Just as all atoms do not have the same ionization energy, all solids do not have the same work function. The width and energetic position of the bands of allowed states are also not the same. These facts can be used to design some very useful devices. One good example is a device called a **quantum well structure**. Gallium arsenide is a widely used semiconductor in microelectronic applications. $\text{Al}_\alpha\text{Ga}_{1-\alpha}\text{As}$ is a substitutional alloy in which some of the Ga atoms are replaced by Al atoms. It can be combined with GaAs to form a crystalline **heterostructure** that consists of alternating layers of GaAs and $\text{Al}_\alpha\text{Ga}_{1-\alpha}\text{As}$. Both substances are semiconductors that have a fully occupied valence band, as discussed in Section 5.4. As the energy increases, a band gap with no allowed states is found, followed by an empty conduction band. However, at 300 K there are only enough electrons in the electrically neutral crystal to fill the valence band. This is analogous to an H atom in which the 1s state is occupied and the 2s state is empty. The band structures for GaAs and $\text{Al}_\alpha\text{Ga}_{1-\alpha}\text{As}$ are shown in Figure 5.20.

Using the **molecular beam epitaxy** (MBE) technique, materials are slowly evaporated onto a growing crystal in an ultrahigh vacuum. A crystalline structure can be created in which a 0.1 to 1 nm layer of GaAs is sandwiched between two macroscopically thick (several micrometers) $\text{Al}_\alpha\text{Ga}_{1-\alpha}\text{As}$ layers. Such a heterostructure is depicted in Figure 5.21a. When this GaAs layer is considered as a three-dimensional (3D) box, it has energy levels that depend on three quantum numbers because of the 3D geometry:

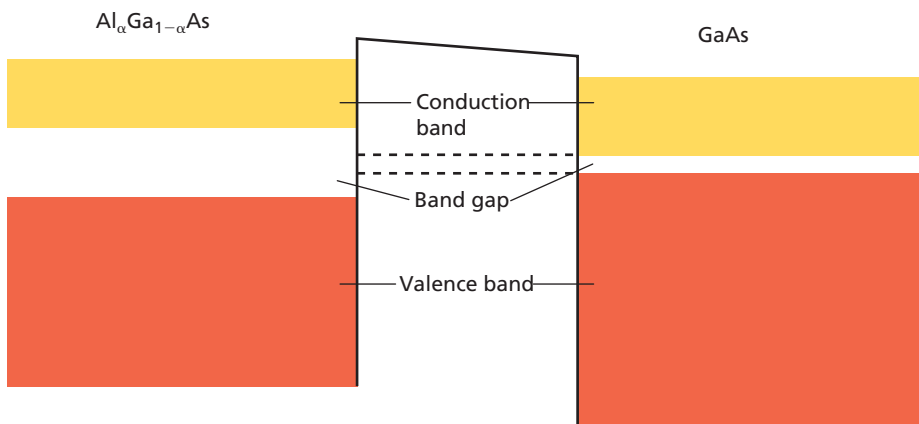
$$E_{n_x n_y n_z} = \frac{\hbar^2}{8m} \left(\frac{n_z^2 + n_y^2}{b^2} + \frac{n_x^2}{a^2} \right) \quad (5.21)$$

The length b is on the order of 1000 nm, whereas a is 0.1 to 1.0 nm. Therefore, the energy spectrum is essentially continuous in n_z and n_y but discrete in n_x . What does the band-gap region in such an alternating layer structure look like? This can be deduced from Figure 5.20 and is shown in Figure 5.21.

In this very thin layer of GaAs, the empty conduction band has lower-energy states in the GaAs region than elsewhere in the heterostructure. The $\text{Al}_\alpha\text{Ga}_{1-\alpha}\text{As}$ layers have

Concept

Quantum wells exhibit continuous energy levels in two dimensions and discrete energy levels in the third dimension.

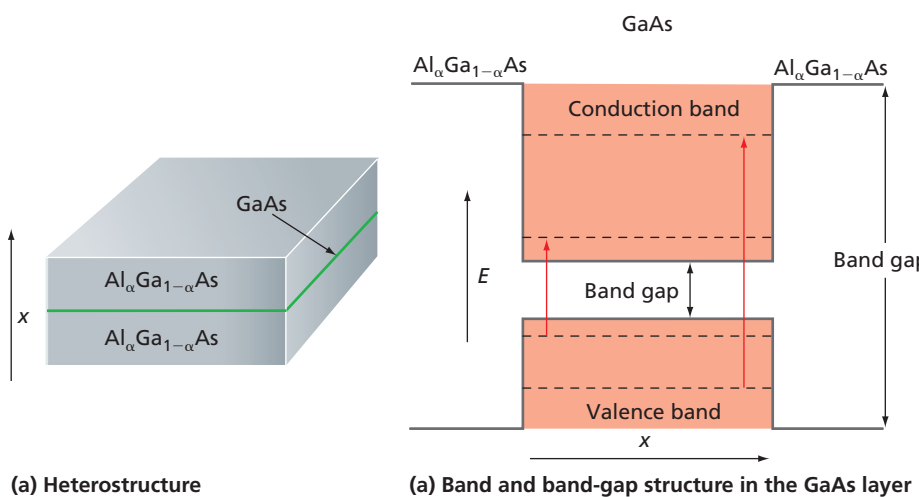
**Figure 5.20**

Schematic representation of relative positions of bands in GaAs and $\text{Al}_{\alpha}\text{Ga}_{1-\alpha}\text{As}$ connected in an external circuit. See Figure 5.13b for an example of an external circuit. Note that the center of the smaller band gap in GaAs lines up with the center of the larger band gap in $\text{Al}_{\alpha}\text{Ga}_{1-\alpha}\text{As}$. The bands are not to scale.

macroscopic dimensions in all three directions, so that the particle in the box states form continuous energy bands. By contrast, the GaAs layer has relatively large dimensions parallel to the layer, but atomic-scale dimensions along the x direction perpendicular to the interface between the substances. Along this direction, the quantization conditions are those expected from a particle in a finite well, leading to discrete energy levels, as shown in Figure 5.21. Along the other two directions, the energy-level spectrum is continuous. By choosing this unusual geometry for the box, the system has a continuous energy spectrum along the y and z directions and a discrete energy spectrum along the x direction. The discrete energy levels can be changed by varying the thickness of the GaAs layer.

The $\text{Al}_{\alpha}\text{Ga}_{1-\alpha}\text{As}$ -GaAs structure is a novel and useful structure. It is useful because it can be made to function as an efficient and energy-selective photodetector. In the ground state, the valence band is fully occupied and the conduction band is empty. The lowest energy excitations are the promotion of an electron from the valence band into the conduction band of the GaAs layer by absorption of a photon, as indicated by the two red arrows in Figure 5.21. These events lead to an increase in the electrical conductivity of the heterostructure for photon absorption at the specific frequencies $v = \Delta E/h$, which can be varied by changing the thickness of the GaAs layer. Devices based on the principles outlined here are called **quantum well devices**.

Molecular beam epitaxy is the technique used to manufacture heterostructures such as the $\text{Al}_{\alpha}\text{Ga}_{1-\alpha}\text{As}$ -GaAs structure just discussed. Because the materials must be deposited in a very high vacuum, MBE is an expensive technique. Techniques involving size-controlled crystallization in solution offer a less expensive way to synthesize nanoscale particles. Such techniques can produce crystalline spherical particles of compound semiconductors such as CdSe with uniform diameters in the range of 1 to 10 nm, which produces energy levels quantized in all three directions. Such size-controlled particles are called **quantum dots**. Quantum dots have a band-gap energy that strongly depends on their diameter for the reasons discussed earlier.

**Figure 5.21**

Schematic depiction of the $\text{Al}_{\alpha}\text{Ga}_{1-\alpha}\text{As}$ -GaAs device structure and the energy band diagram. (a) Heterostructure and (b) the energy band diagram in the GaAs layer. The discrete energy levels below the band gap are for the positively charged holes left behind when an excited electron occupies the conduction band. These holes can move by electrons tunneling into them from adjacent atoms and therefore contribute to electrical conductivity. Because the holes are positively charged, the energy in this part of the diagram increases downward rather than upward, as is the case in the rest of the diagram. Two possible transitions generated by photon absorption are shown by red arrows. Not to scale.

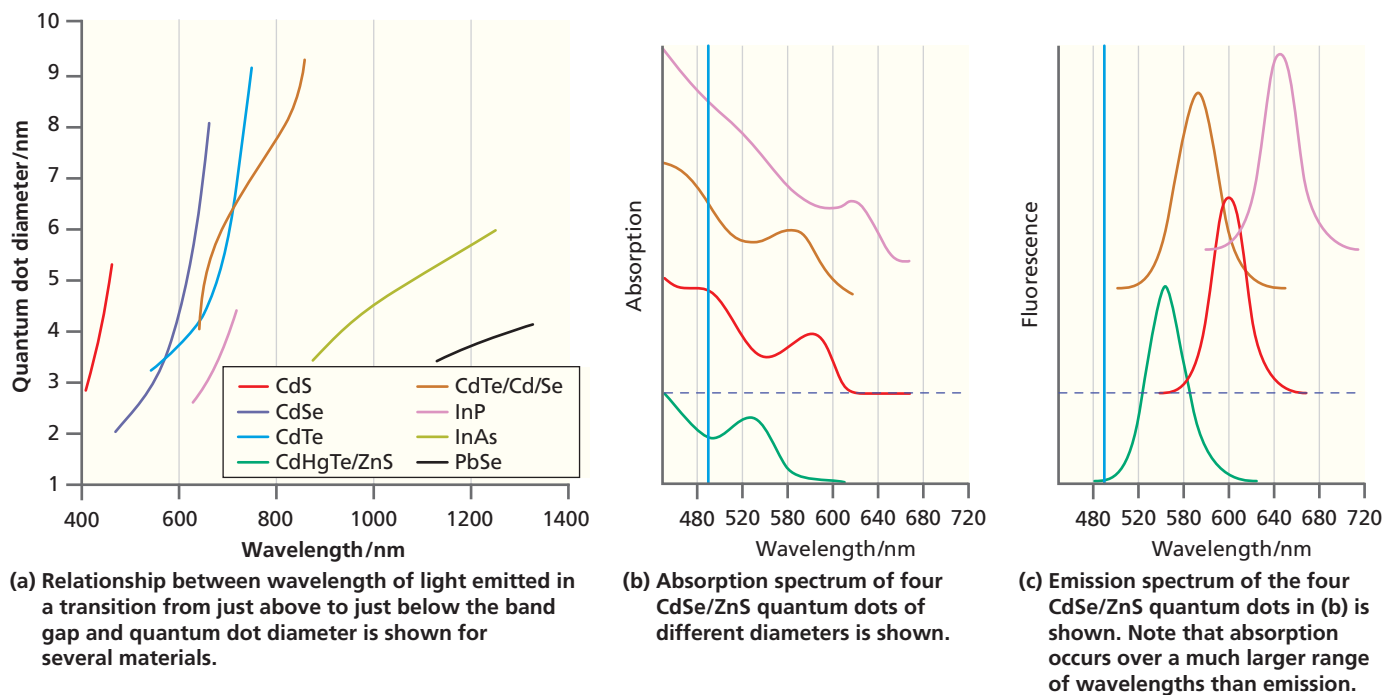


Figure 5.22

Absorption and emission by quantum dots. (a) Dependence of wavelength of light emitted in a transition from just above to just below the band gap is shown as a function of quantum dot diameter for several materials. (b) Absorption spectrum of four CdSe/ZnS quantum dots of different diameters is shown. (c) The corresponding emission spectrum of the four CdSe/ZnS quantum dots is shown. Note that absorption occurs over a much larger range of wavelengths than emission. The vertical bar indicates the wavelength of a 488 nm argon ion laser that can be used to excite electrons from below to above the band gap for all four diameters. Using this laser ensures that absorption and emission occur at distinctly different wavelengths.

Source: Adapted from Michalat et al., *Science* 307 (2005): 538.

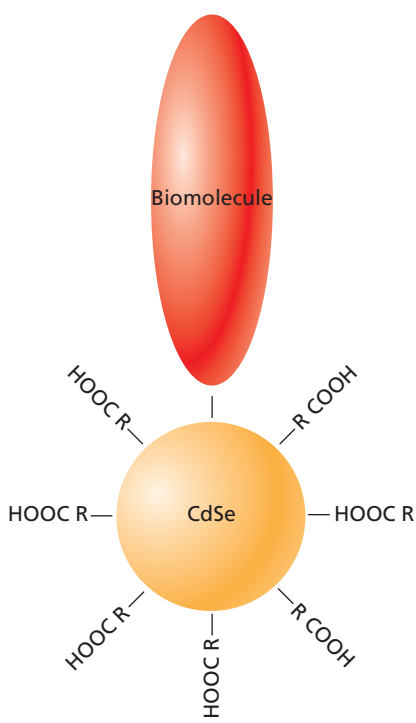


Figure 5.23

Utility of a CdSe quantum dot. A quantum dot is soluble in an aqueous solution when coated with a single molecular layer of an organic acid. When tethered to a biomolecule of interest, it can be used as a fluorescent tag to locate the biomolecule when the biomolecule is bound to a receptor in a heterogeneous environment such as a cell.

All valence band states are filled, and all conduction band states are empty in the ground state of the quantum dot. Electrons can be promoted from energy levels below to those above the band gap through absorption of visible light. Subsequently, the electron in the excited state can rapidly lose energy and transition to a state just above the band gap. From there, it can drop to an empty state below the band gap, emitting a photon in a process called **fluorescence** with a wavelength $\lambda = hc/E_{bg}$. Because the energy levels and the band gap energy depend on the nanocrystal diameter b , λ also depends on b . This property is illustrated in Figure 5.22a. For CdSe quantum dots, the emission wavelength increases from 450 nm (blue light) to 650 nm (red light) as the dot diameter increases from 2 to 8 nm. Figure 5.22c shows another important property of quantum dots. Although they absorb light over a wide range of wavelengths, they emit light in a much smaller range of wavelengths. This occurs because electrons excited from occupied states just below the band gap to states well above the band gap by absorbing light rapidly lose energy and relax to states just above the band gap. Therefore, the light emitted in fluorescence is in a narrow frequency range determined by the band-gap energy of the semiconducting quantum dot. For more details, see the reference to Michalat et al. (2005) in Further Reading.

Quantum dots are currently being used in bioanalytical methods. The usefulness of these quantum dots is their ability to act as tags for biologically interesting substrates such as proteins, as shown in Figure 5.23. By functionalizing such quantum dots with an appropriate molecular layer, they can be made soluble in aqueous solutions and tethered to the protein of interest.

The following example illustrates the usefulness of a protein with a fluorescent label. After letting the tagged proteins enter a cell and attach to their receptors, the cell is illuminated with light and the quantum dots act as point sources of fluorescent light whose location can be imaged using optical microscopy. Because the light used for excitation and the fluorescent light have different wavelengths, it is easy to distinguish between the excitation and fluorescence light using optical filters. The same excitation

wavelength can be used for quantum dots of different size, so that several different ligand–receptor combinations can be probed simultaneously if the individual ligands are tethered to quantum dots of differing diameter. It might appear that the number of possible different fluorescent tags is limited by overlap in the wavelengths at which they fluoresce. However, one can also tether various combinations of a few different quantum dots to a protein, creating a barcode. For instance, the intensity versus wavelength distribution of the fluorescent signal from a tagged protein to which two 1 nm, one 3 nm, and two 5 nm quantum dots have been attached is different from all other distinct possible permutations of five quantum dots. This analysis method, which is based on size quantization, offers new analytical techniques for measuring the spatial distribution of molecules in inherently heterogeneous biological environments.

Because a quantum dot absorbs strongly over a wide range of wavelengths but emits in a narrow range of wavelengths, it can be used as an internal light source for imaging the interior of semitransparent specimens. Figure 5.24 shows an image obtained by projecting onto a plane the capillary structure of adipose tissue in a 250- μm -thick specimen surrounding a surgically exposed ovary of a living mouse. In another example, the rate of blood flow and the differences in systolic and diastolic pressure can be directly observed in these experiments. For more details, see the reference to Larson et al. (2003) in Further Reading. It is not possible to obtain such images with X-ray-based techniques because there is no appropriate contrast mechanism.

The usefulness of quantum dots in imaging tissues *in vivo* has significant potential applications in surgery, provided that toxicity issues currently associated with quantum dots can be resolved. Figure 5.25 shows images obtained with a near-infrared camera resulting from the injection of quantum dots emitting in the near-infrared region (840–860 nm) into a mouse. The quantum dots had a \sim 15 nm diameter, including the functionalization layer, which is a suitable diameter for trapping in lymph nodes. Fluorescence from the quantum dots allows the lymph node to be imaged through the overlying tissue layers. Because near-infrared light is invisible to the human eye and visible light is not registered by the camera, the mouse can be simultaneously illuminated with both types of light. A comparison of images obtained with near-infrared and visible light can be used to guide the surgeon in the removal of tumors and to verify that all affected tissues have been removed. Near-infrared light is also useful because this wavelength minimizes the absorption of light by overlying tissues, allowing tissues containing quantum dots to be imaged through an overlying tissue layer of 6–10 cm. For more details, see Kim et al. (2004).

Quantum dots have several applications that are in developmental stages. It may be possible to use them to couple electrical signal amplification, currently based on charge carrier conduction in semiconductors, with light amplification, in an application known as **optoelectronics**. Additionally, the reduced dimensions of quantum dots utilized as wavelength-tunable lasers allow them to be integrated into conventional silicon-based microelectronics.

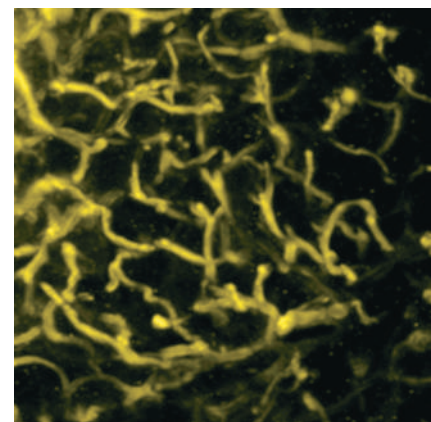
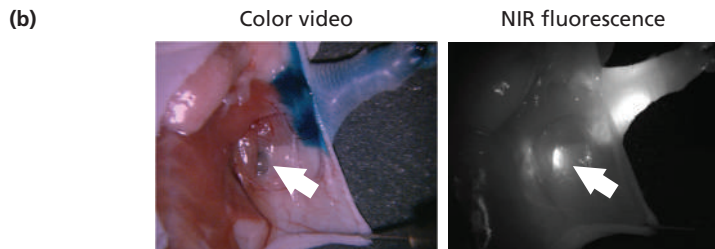
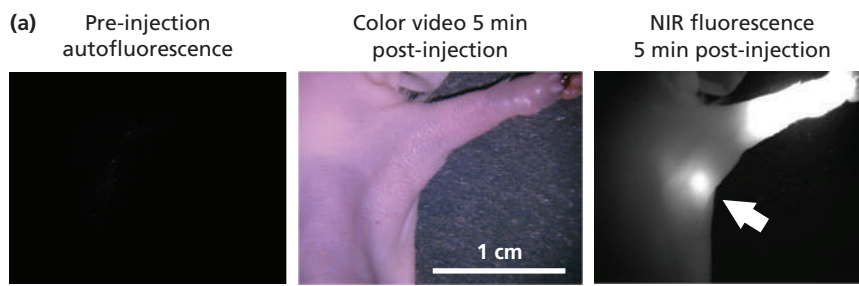


Figure 5.24

Image of adipose tissue in the skin of a living mouse using CdSe quantum dots that fluoresce at 550 nm. The image is $160 \times 160 \mu\text{m}$ and was obtained by projecting the capillary structure in a 250- μm -thick specimen of adipose tissue on a plane.

Source: Adapted from Larson et al., *Science* 300 (2003): 1434.

Concept

Quantum dots have an important role in fields as diverse as digital displays, optoelectronics, and the early detection of malignant tumors.

Figure 5.25

Images of mouse tissue undergoing surgery injected with quantum dots.

(a) The middle panel shows a video image taken 5 minutes after the quantum dots were introduced. The right panel is a fluorescence image that shows localization of the quantum dots in the lymph node. The left panel shows that without the quantum dots, no fluorescence is observed. (b) Surgery after injection of a chemical mapping agent that is known to localize in lymph nodes confirms that the quantum dots are localized in the lymph nodes.

Source: Adapted from Kim et al., *Nature Biotechnology* 22 (2004): 93.

VOCABULARY

activation energy	energy band	quantum dot
atomic force microscope (AFM)	energy gap	quantum well device
band gap	finite depth box	quantum well structure
band structure	fluorescence	scanning tunneling microscope (STM)
barrier width	ground state	semiconductor
classically forbidden region	heterostructure	tunneling
conduction band	insulator	valence band
conductor	molecular beam epitaxy	valence electrons
core electrons	optoelectronics	work function
decay length	overlap of wave functions	
delocalization	π -bonded network	

KEY EQUATIONS

Equation	Significance of Equation	Equation Number
$\psi(x) = A e^{-\kappa x} + B e^{+\kappa x}$ for $\infty \geq x > a/2$ and $\psi(x) = A' e^{-\kappa x} + B' e^{+\kappa x}$ for $-\infty \leq x < -a/2$ where $\kappa = \sqrt{\frac{2m(V_0 - E)}{\hbar^2}}$	Solutions of Schrödinger equation for particle in finite depth box	5.4
$R = \frac{(\sqrt{E} - \sqrt{E - V_0})^2}{(\sqrt{E} + \sqrt{E - V_0})^2}$ $T = \frac{4\sqrt{E(E - V_0)}}{(\sqrt{E} + \sqrt{E - V_0})^2}$	Reflection and transmission probabilities for a step potential	5.18
$E_{n_x n_y n_z} = \frac{\hbar^2}{8m} \left(\frac{n_z^2 + n_y^2}{b^2} + \frac{n_x^2}{a^2} \right)$	Energy levels for a heterostructure that is very large in two dimensions and has atomic-scale dimensions in the third direction	5.21

CONCEPTUAL PROBLEMS

Q5.1 Why is it necessary to apply a bias voltage between the tip and surface in a scanning tunneling microscope?

Q5.2 The amplitude of the wave on the right side of the barrier in Figure 5.11 is much smaller than that of the wave incident on the barrier. What happened to the “rest of the wave”?

Q5.3 Why is a tunneling current not observed in an STM when the tip and the surface are 1 mm apart?

Q5.4 Redraw Figure 5.8 for an insulator.

Q5.5 Explain how it is possible to create a three-dimensional electron conductor that has a continuous energy spectrum in two dimensions and a discrete energy spectrum in the third dimension.

Q5.6 Explain, without using equations, why tunneling is more likely for the particle with $E = 3/4V_0$ than for $E = 1/4V_0$ in Figure 5.11.

Q5.7 What is the advantage of using quantum dots that fluoresce in the near infrared for surgical applications?

Q5.8 The overlap between wave functions can either be constructive or destructive, just as for waves. Can you distinguish between constructive and destructive overlap for the various energy levels in Figure 5.3?

Q5.9 Explain how you can use size-quantized quantum dots to create a protein with a barcode that can be read using light.

Q5.10 A STM can also be operated in a mode in which electrons tunnel from the surface into the tip. Use Figure 5.13 to explain how you would change the experimental setup to reverse the tunneling current.

Q5.11 For CdSe quantum dots, the emission wavelength increases from 450. nm to 650. nm as the dot diameter increases from 2 to 8 nm. Calculate the band-gap energy for these two particle diameters.

Q5.12 Why is it necessary to functionalize CdSe quantum dots with groups such as organic acids to make them useful in bioanalytical applications?

Q5.13 Why must the amplitudes of the first derivatives of the energy eigenfunctions in the finite depth box and in the adjoining barrier regions have the same value at the boundary?

Q5.14 Why must the amplitudes of the energy eigenfunctions in the finite depth box and in the adjoining barrier regions have the same value at the boundary?

Q5.15 Explain how a quantum dot can absorb light over a range of wavelengths and emit light over a much smaller range of wavelengths.

Q5.16 Explain why the speed of the particle needs to be taken into account in calculating the probability for transmission over a step potential.

Q5.17 The reflection probability from a step potential was calculated for $E > V_0$ in Section 5.5. Is Equation (5.18) valid for $E < V_0$? What information can you extract from Figure 5.1 that will allow you to state the value of R for a step potential if $E < V_0$?

Q5.18 Figure 5.17 shows that atomic-level resolution with an AFM is only attainable in the repulsive portion of the tip–surface potential. What does this tell you about the range of the attractive and repulsive parts of the potential?

Q5.19 Why is atomic-level resolution obtained on pentacene in the AFM mode as shown in Figure 5.18, but not in the STM mode?

Q5.20 Why were quantum dots emitting in the near-infrared region used for the surgery experiment shown in Figure 5.25?

NUMERICAL PROBLEMS

Section 5.1

P5.1 Calculate the energy levels of the π -network in butadiene, C_4H_6 , using the particle in the box model. To calculate the box length, assume that the molecule is linear and use the values 135 and 154 pm for C=C and C–C bonds. What is the wavelength of light required to induce a transition from the ground state to the first excited state? How does this compare with the experimentally observed value of 290 nm? What does the comparison suggest to you about estimating the length of the π -network by adding bond lengths for this molecule?

P5.2 Calculate the energy levels of the π -network in octatetraene, C_8H_{10} , using the particle in the box model. To calculate the box length, assume that the molecule is linear and use the values 135 and 154 pm for C=C and C–C bonds. What is the wavelength of light required to induce a transition from the ground state to the first excited state?

P5.3 In this problem, you will solve for the total energy eigenfunctions and eigenvalues for an electron in a finite depth box. We first go through the calculation for the box parameters used in Figure 5.1. You will then carry out the calculation for a different set of parameters.

We describe the potential in this way:

$$V(x) = V_0 \quad \text{for } x \leq -\frac{a}{2} \quad \text{Region I}$$

$$V(x) = 0 \quad \text{for } -\frac{a}{2} < x < \frac{a}{2} \quad \text{Region II}$$

$$V(x) = V_0 \quad \text{for } x \geq \frac{a}{2} \quad \text{Region III}$$

The eigenfunctions must have the following form in these three regions:

$$\begin{aligned} \psi(x) &= B \exp\left[+\sqrt{\frac{2m(V_0 - E)}{\hbar^2}}x \right] \\ &\quad + B' \exp\left[-\sqrt{\frac{2m(V_0 - E)}{\hbar^2}}x \right] \\ &= Be^{+\kappa x} + B'e^{-\kappa x} \end{aligned} \quad \text{Region I}$$

$$\begin{aligned} \psi(x) &= C \sin\sqrt{\frac{2mE}{\hbar^2}}x + D \cos\sqrt{\frac{2mE}{\hbar^2}}x \\ &= C \sin kx + D \cos kx \end{aligned} \quad \text{Region II}$$

$$\begin{aligned} \psi(x) &= A \exp\left[-\sqrt{\frac{2m(V_0 - E)}{\hbar^2}}x \right] \\ &\quad + A' \exp\left[+\sqrt{\frac{2m(V_0 - E)}{\hbar^2}}x \right] \\ &= A e^{-\kappa x} + A' e^{+\kappa x} \end{aligned} \quad \text{Region III}$$

so that the wave functions remain finite at large positive and negative values of x , $A' = B' = 0$. An additional condition must also be satisfied. To arrive at physically meaningful solutions for the eigenfunctions, the wave functions in the separate regions must have the same amplitude and derivatives at the values of $x = a/2$ and $x = -a/2$ bounding the regions. This restricts the possible values for the coefficients

A, B, C, and D. Show that applying these conditions gives the following equations:

$$\text{at } x = -a/2 \quad B e^{-\kappa(a/2)} = -C \sin k \frac{a}{2} + D \cos k \frac{a}{2}$$

$$\text{at } x = -a/2 \quad B \kappa e^{-\kappa(a/2)} = C k \cos k \frac{a}{2} + D k \sin k \frac{a}{2}$$

$$\text{at } x = a/2 \quad A e^{-\kappa(a/2)} = C \sin k \frac{a}{2} + D \cos k \frac{a}{2}$$

$$\text{at } x = a/2 \quad -A \kappa e^{-\kappa(a/2)} = C k \cos k \frac{a}{2} - D k \sin k \frac{a}{2}$$

These two pairs of equations differ on the right side only by the sign of one term. We can obtain a set of equations that contain fewer coefficients by adding and subtracting the equations for amplitude and derivative to give

$$(A + B)e^{-\kappa(a/2)} = 2D \cos\left(k \frac{a}{2}\right)$$

$$(A - B)e^{-\kappa(a/2)} = 2C \sin\left(k \frac{a}{2}\right)$$

$$(A + B)\kappa e^{-\kappa(a/2)} = 2Dk \sin\left(k \frac{a}{2}\right)$$

$$-(A - B)\kappa e^{-\kappa(a/2)} = 2Ck \cos\left(k \frac{a}{2}\right)$$

At this point we notice that by dividing the equations in each pair, the coefficients can be eliminated to give

$$\kappa = k \tan\left(k \frac{a}{2}\right) \text{ or } \sqrt{\frac{2m(V_0 - E)}{\hbar^2}}$$

$$= \sqrt{\frac{2mE}{\hbar^2}} \tan\left(\sqrt{\frac{2mE}{\hbar^2}} \frac{a}{2}\right) \text{ and}$$

$$-\kappa = k \cot\left(k \frac{a}{2}\right) \text{ or } -\sqrt{\frac{2m(V_0 - E)}{\hbar^2}}$$

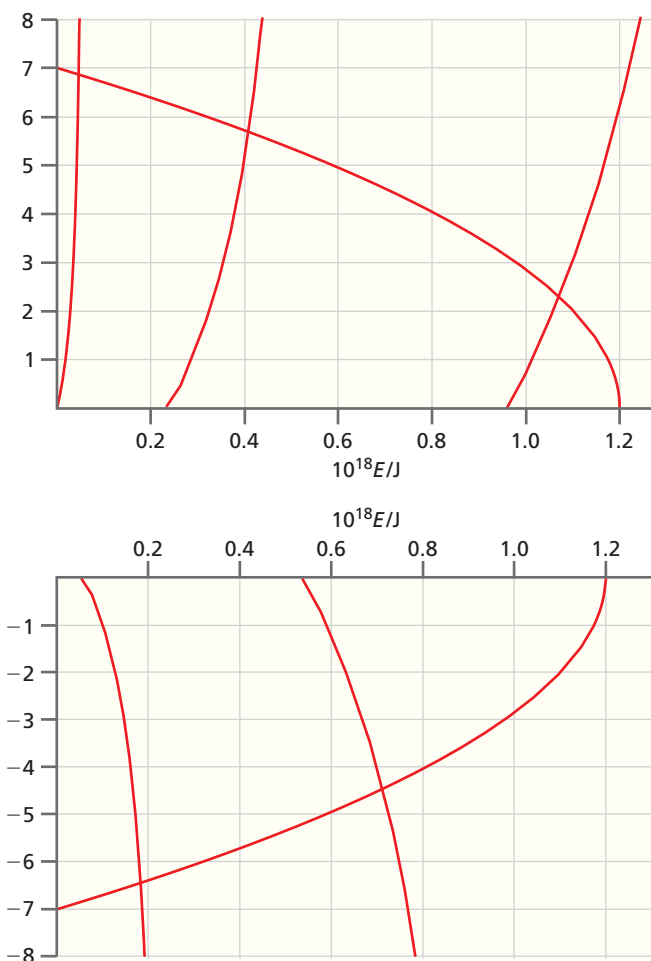
$$= \sqrt{\frac{2mE}{\hbar^2}} \cot\left(\sqrt{\frac{2mE}{\hbar^2}} \frac{a}{2}\right)$$

Multiplying these equations on both sides by $a/2$ gives dimensionless parameters, and the final equations are

$$\sqrt{\frac{m(V_0 - E)a^2}{2\hbar^2}} = \sqrt{\frac{mEa^2}{2\hbar^2}} \tan\sqrt{\frac{mEa^2}{2\hbar^2}} \text{ and}$$

$$-\sqrt{\frac{m(V_0 - E)a^2}{2\hbar^2}} = \sqrt{\frac{mEa^2}{2\hbar^2}} \cot\sqrt{\frac{mEa^2}{2\hbar^2}}$$

The allowed energy values E must satisfy these equations. They can be obtained by graphing the two sides of each equation against E . The intersections of the two curves are the allowed energy eigenvalues. For the parameters in the caption of Figure 5.1, $V_0 = 1.20 \times 10^{-18}$ J and $a = 1.00 \times 10^{-9}$ m, the following two graphs are obtained:



The five allowed energy levels are at 4.61×10^{-20} , 4.09×10^{-19} , and 1.07×10^{-18} J (top figure), and 1.84×10^{-19} and 7.13×10^{-19} J (bottom figure).

- Given these values, calculate λ for each energy level. Is the relation $\lambda = 2a/n$ (for n an integer), which arose from the calculations on the infinitely deep box, still valid? Compare the values with the corresponding energy level in the infinitely deep box. Explain why the differences arise.
- Repeat this calculation for $V_0 = 5.00 \times 10^{-19}$ J and $a = 0.900 \times 10^{-9}$ m. Do you think that there will be fewer or more bound states than for the problem just worked out? How many allowed energy levels are there for this well depth, and what is the energy corresponding to each level?

Section 5.4

P5.4 Semiconductors can become conductive if their temperature is raised sufficiently to populate the (empty) conduction band from the highest filled levels in the valence band. The ratio of the populations in the lowest level of the conduction band to that of the highest level in the valence band is

$$\frac{n_{\text{conduction}}}{n_{\text{valence}}} = \frac{g_{\text{conduction}}}{g_{\text{valence}}} e^{-\Delta E/kT}$$

where ΔE is the band gap, which is 1.12 eV for Si and 5.5 eV for diamond. Assume for simplicity that the ratio of

the degeneracies is one and that the semiconductor becomes sufficiently conductive when

$$\frac{n_{conduction}}{n_{valence}} = 3.1 \times 10^{-7}$$

At what temperatures will silicon and diamond become sufficiently conductive? Given diamond sublimates near 3000 K, could you heat diamond enough to make it conductive and not sublime it?

P5.5 For the π -network of β -carotene modeled with the particle in the box approach, the position-dependent probability density of finding 1 of the 22 electrons is given by

$$P_n(x) = |\psi_n(x)|^2 = \frac{2}{a} \sin^2\left(\frac{n\pi x}{a}\right)$$

The quantum number n in this equation is determined by the energy level of the electron under consideration. As we saw in Chapter 4, this function is strongly position dependent.

The question addressed in this problem is as follows: Would you also expect the total probability density defined by

$P_{total}(x) = \sum_n |\psi_n(x)|^2$ to be strongly position dependent? The sum is over all the electrons in the π -network.

- a. Calculate the total probability density $P_{total}(x) = \sum_n |\psi_n(x)|^2$ using the box length $a = 2.90$ nm and plot your results as a function of x . Does $P_{total}(x)$ have the same value near the ends and at the middle of the molecule?
- b. Determine $\Delta P_{total}(x) / \langle P_{total}(x) \rangle$, where $\Delta P_{total}(x)$ is the peak-to-peak amplitude of $P_{total}(x)$ in the interval between 1.20 and 1.60 nm.
- c. Compare the result of part (b) with what you would obtain for an electron in the highest occupied energy level.
- d. What value would you expect for $P_{total}(x)$ if the electrons were uniformly distributed over the molecule? How does this value compare with your result from part (a)?

Section 5.5

P5.6 An electron of energy 4.0 eV approaches a step potential of height 3.0 eV. Calculate the probabilities that the electron will be reflected and transmitted.

Section 5.6

P5.7 The maximum safe current in a copper wire with a diameter of 3.0 mm is about 20 amperes. In a STM, a current of 8.0×10^{-10} A passes from the tip to the surface in a filament of diameter ~ 1.0 nm. Compare the current density in the copper wire with that in the STM.

Section 5.7

P5.8 In this problem, you will calculate the transmission probability through the barrier illustrated in Figure 5.11. First go through the mathematics leading to the solution. You will then carry out further calculations.

The domain in which the calculation is carried out is divided into three regions for which the potentials are

$$\begin{aligned} V(x) &= 0 & \text{for } x \leq 0 & \text{Region I} \\ V(x) &= V_0 & \text{for } 0 < x < a & \text{Region II} \\ V(x) &= 0 & \text{for } x \geq a & \text{Region III} \end{aligned}$$

The wave functions must have the following form in the three regions if $E < V_0$:

$$\begin{aligned} \psi(x) &= A \exp\left[+i\sqrt{\frac{2mE}{\hbar^2}}x\right] + B \exp\left[-i\sqrt{\frac{2mE}{\hbar^2}}x\right] \\ &= Ae^{+ikx} + Be^{-ikx} \end{aligned} \quad \text{Region I}$$

$$\begin{aligned} \psi(x) &= C \exp\left[-\sqrt{\frac{2m(V_0 - E)}{\hbar^2}}x\right] \\ &\quad + D \exp\left[+\sqrt{\frac{2m(V_0 - E)}{\hbar^2}}x\right] \\ &= Ce^{-\kappa x} + De^{+\kappa x} \end{aligned} \quad \text{Region II}$$

$$\begin{aligned} \psi(x) &= F \exp\left[+i\sqrt{\frac{2mE}{\hbar^2}}x\right] + G \exp\left[-i\sqrt{\frac{2mE}{\hbar^2}}x\right] \\ &= Fe^{+ikx} + Ge^{-ikx} \end{aligned} \quad \text{Region III}$$

Assume that the wave approaches the barrier from the negative x direction. The coefficient B cannot be set equal to zero because $Be^{+i\sqrt{(2mE/\hbar^2)}x}$ represents reflection from the barrier. However, G can be set equal to zero because there is no wave incident on the barrier from the positive x direction.

- a. The wave functions and their derivatives must be continuous at $x = 0$ and $x = a$. Show that the coefficients must satisfy the following conditions:

$$\begin{aligned} A + B &= C + D & Ce^{-\kappa a} + De^{+\kappa a} &= Fe^{+ika} \\ A - B &= -\frac{i\kappa}{k}(-C + D) & -Ce^{-\kappa a} + De^{+\kappa a} &= \frac{i\kappa}{\kappa}Fe^{+ika} \end{aligned}$$

- b. Because the transmission probability is given by $|F/A|^2$, it is useful to manipulate these equations to get a relationship between F and A . By adding and subtracting the first pair of equations, A and B can be expressed in terms of C and D . The second pair of equations can be solved individually to give equations for D and C in terms of F . Show that

$$\begin{aligned} D &= \frac{i\kappa e^{+ika} + \kappa e^{+ika}}{2\kappa e^{+\kappa a}} F \\ C &= \frac{-i\kappa e^{+ika} + \kappa e^{+ika}}{2\kappa e^{-\kappa a}} F, \quad \text{and} \\ A &= \frac{(ik - \kappa)C + (ik + \kappa)D}{2ik} \end{aligned}$$

- c. Substitute these results for C and D in terms of F into

$$A = \frac{(ik - \kappa)C + (ik + \kappa)D}{2ik}$$

to relate A and F . Show that

$$\begin{aligned} 2ikA &= \frac{e^{+ika}}{2\kappa} [(ik - \kappa)(-ik + \kappa)e^{+\kappa a} \\ &\quad + (ik + \kappa)(ik + \kappa)e^{-\kappa a}] F \end{aligned}$$

d. Using the hyperbolic trigonometric functions

$$\sinh x = \frac{e^x - e^{-x}}{2} \quad \text{and} \quad \cosh x = \frac{e^x + e^{-x}}{2}$$

and the relationship $\cosh^2 x - \sinh^2 x = 1$, show that

$$\begin{aligned} \left| \frac{F}{A} \right|^2 &= \frac{16(\kappa k)^2}{16(\kappa k)^2 + (4(k^2 - \kappa^2)^2 + 16(\kappa k)^2) \sinh^2(\kappa a)} \\ &= \frac{1}{1 + [(k^2 + \kappa^2)^2 \sinh^2(\kappa a)] / 4(\kappa k)^2} \end{aligned}$$

- e.** Plot the transmission probability for an electron as a function of energy for $V_0 = 1.6 \times 10^{-19}$ J and $a = 9.0 \times 10^{-10}$ m up to an energy of 8×10^{-19} J. At what energy is the tunneling probability 0.1? At what energy is the tunneling probability 0.02?

- f.** Plot the transmission probability for an electron of energy 0.50×10^{-19} J as a function of the barrier width for $V_0 = 1.6 \times 10^{-19}$ J between 2×10^{-10} and 8×10^{-10} m. At what barrier width is the transmission probability 0.2?

COMPUTATIONAL PROBLEMS

More detailed instructions on carrying out these calculations using Spartan Physical Chemistry are found at:
<https://www.pearsonhighered.com/chemistryresources/>

C5.1 Build (a) ethylene, (b) the trans conformation for 1,3 butadiene, and (c) all trans hexatriene and calculate the ground-state (singlet) energy of these molecules using the B3LYP method with the 6-311+G** basis set. Repeat your calculation for the triplet state, which corresponds to the

excitation of a π electron from the highest filled energy level to the lowest unoccupied energy level. Use a nonplanar input geometry for the triplet states. Compare the energy difference from these calculations to literature values of the maximum in the UV-visible absorption spectrum.

WEB-BASED SIMULATIONS, ANIMATIONS, AND PROBLEMS

Simulations, animations, and homework problem worksheets can be accessed at www.pearsonhighered.com/advchemistry

W5.1 The Schrödinger equation is solved numerically for the particle in the finite height box. Using the condition that the wave function must approach zero amplitude in the classically forbidden region, the energy levels are determined for a fixed particle mass, box depth, and box length. The particle mass and energy and the box depth and length are varied with sliders to demonstrate how the number of bound states varies with these parameters.

W5.2 The Schrödinger equation is solved numerically to calculate the tunneling probability for a particle through a thin finite barrier. Sliders are used to vary the barrier width and height and the particle energy and mass. The dependence of the tunneling probability on these variables is investigated.

FURTHER READING

- Anderson, B. D. "Alternative Compounds for the Particle in a Box Experiment." *Journal of Chemical Education* 74 (1997): 985.
- Giessibl, F. J. "Advances in Atomic Force Microscopy." *Reviews in Modern Physics* 75 (2003): 949–983.
- Gross, L., Mohn, F., Moll, N., Liljeroth, P., and Meyer, G. "The Chemical Structure of a Molecule Resolved by Atomic Force Microscopy." *Science* 325 (2009): 1110–1115.
- Kim, S., Lim, Y. T., Soltesz, E. G., DeGrand, A. M., Lee, J., A. Nakayama, A., Frangioni, J. V. "Near-Infrared Fluorescent Type II Quantum Dots for Sentinel Lymph Node Mapping." *Nature Biotechnology* 22 (2004): 93–97.

- Larson, D. R., Zipfel, W. R., Williams, R. M., Clark, S. W., Bruchez, M. P., Wise, F. W., and Webb, W. W. "Water-Soluble Quantum Dots for Multiphoton Fluorescence Imaging in Vivo." *Science* 300 (2003): 1434.
- Michalat, X., Pinuad, F. F., Bentolla, L. A., Tsay, J. M., Doose, S., Li, J. J., Weiss, S. "Quantum Dots for Live Cells, in Vivo Imaging, and Diagnostics." *Science* 307 (2005): 538–544.
- Zuev, P. S., Sheridan, R. S., Albu, T. V., Truhlar, D. G., Hrovat, D. A., and Borden, W. T. "Carbon Tunneling from a Single Quantum State." *Science* 299 (2003): 867–870.

Commuting and Noncommuting Operators and the Surprising Consequences of Entanglement

WHY is this material important?

The measurement process is different for a quantum-mechanical system than for a classical system. For a classical system, all observables can be measured simultaneously, and the precision and accuracy of the measurement is limited only by the instruments used to make the measurement. For a quantum-mechanical system, some observables can be measured simultaneously and exactly, whereas an uncertainty relation limits the degree to which other observables can be known simultaneously and exactly.

WHAT are the most important concepts and results?

Measurements carried out on a system in a superposition state change the state of the system. Two observables can be measured simultaneously and exactly only if their corresponding operators commute. Two particles can be entangled, after which their properties are no longer independent of one another. Entanglement is the basis of both teleportation and quantum computing.

WHAT would be helpful for you to review for this chapter?

It would be helpful to review the material on operators in Chapter 2.

6.1 COMMUTATION RELATIONS

In classical mechanics, a system can in principle be described completely. For instance, the position, momentum, kinetic energy, and potential energy of a mass falling in a gravitational field can be determined simultaneously at any point on its trajectory. The uncertainty in the measurements is only limited by the capabilities of the measurement technique. The values of all of these observables (and many more) can be known simultaneously. This is not generally true for a quantum-mechanical system. In the quantum world, in some cases two observables can be known simultaneously with high accuracy. However, in other cases, two observables have a fundamental uncertainty that cannot be eliminated through any measurement techniques. Nevertheless, as will be shown later,

- 6.1 Commutation Relations
- 6.2 The Stern–Gerlach Experiment
- 6.3 The Heisenberg Uncertainty Principle
- 6.4 (Supplemental Section) The Heisenberg Uncertainty Principle Expressed in Terms of Standard Deviations
- 6.5 (Supplemental Section) A Thought Experiment Using a Particle in a Three-Dimensional Box
- 6.6 (Supplemental Section) Entangled States, Teleportation, and Quantum Computers

Concept

For a quantum mechanical system, it is not generally the case that the values of all observables can be known simultaneously.

in the classical limit of very large quantum numbers, the fundamental uncertainty for such observables is less than the uncertainty associated with experimental techniques. Therefore, quantum mechanics is consistent with classical mechanics for large quantum numbers.

In quantum mechanics, the values of two different observables a and b , which correspond to the operators \hat{A} and \hat{B} , can be simultaneously determined only if the measurement process does not change the state of the system. Otherwise, the system on which the second measurement is carried out is not the same as for the first measurement. Let $\psi_n(x)$ be the wave function that characterizes the system. How can the measurements of the observables corresponding to the operators \hat{A} and \hat{B} be described? Carrying out a measurement of the observables corresponding first to the operator \hat{A} and subsequently to the operator \hat{B} is equivalent to evaluating $\hat{B}[\hat{A}\psi_n(x)]$. If $\psi_n(x)$ is an eigenfunction of \hat{A} , then $\hat{B}[\hat{A}\psi_n(x)] = \alpha_n\hat{B}\psi_n(x)$. The only case in which the second measurement does not change the state of the system is if $\psi_n(x)$ is also an eigenfunction of \hat{B} . In this particular case, $\hat{B}[\hat{A}\psi_n(x)] = \beta_n\alpha_n\psi_n(x)$. Reversing the order of the two operations gives $\hat{A}[\hat{B}\psi_n(x)] = \alpha_n\beta_n\psi_n(x)$. Because the eigenvalues β_n and α_n are simply constants, $\beta_n\alpha_n\psi_n(x) = \alpha_n\beta_n\psi_n(x)$ and, therefore, $\hat{B}[\hat{A}\psi_n(x)] = \hat{A}[\hat{B}\psi_n(x)]$.

Concept

If the value of the commutator of two operators is equal to zero, the values of the corresponding observables can be known simultaneously.

We have just shown that the act of measurement does not change the state of the system if the system wave function is an eigenfunction of the two different operators. Therefore, this is a condition for being able to simultaneously know the values of the observables corresponding to these operators. How can one know if two operators have a common set of eigenfunctions? The example just discussed suggests a simple test that can be applied. Only if

$$\hat{A}[\hat{B}f(x)] - \hat{B}[\hat{A}f(x)] = 0 \quad (6.1)$$

for $f(x)$, an arbitrary function, will \hat{A} and \hat{B} have a common set of eigenfunctions, and only then can the corresponding observables be known simultaneously as shown in Example Problem 6.1.

If two operators have a common set of eigenfunctions, we say that they **commute**. The difference $\hat{A}[\hat{B}f(x)] - \hat{B}[\hat{A}f(x)]$ is abbreviated $[\hat{A}, \hat{B}]f(x)$, and the expression in the square brackets is called the **commutator** of the operators \hat{A} and \hat{B} . If the value of the commutator is not zero for an arbitrary function $f(x)$, the corresponding observables cannot be determined simultaneously and exactly. We will have more to say about what is meant by *exactly* later in this chapter.

EXAMPLE PROBLEM 6.1

Determine whether the momentum and (a) the kinetic energy and (b) the total energy of a quantum-mechanical system can be known simultaneously and exactly.

Solution

We determine if two operators \hat{A} and \hat{B} commute by evaluating the commutator $\hat{A}[\hat{B}f(x)] - \hat{B}[\hat{A}f(x)]$. If the commutator is zero, the two observables can be determined simultaneously and exactly.

- a. We use the operators for momentum and kinetic energy in Table 3.1 to evaluate the commutator

$$-i\hbar \frac{d}{dx} \left(-\frac{\hbar^2}{2m} \frac{d^2}{dx^2} \right) f(x) - \left(-\frac{\hbar^2}{2m} \frac{d^2}{dx^2} \right) \left(-i\hbar \frac{d}{dx} \right) f(x) = 0$$

In calculating the third derivative, it does not matter if the function is first differentiated twice and then once or the other way around. Therefore, the momentum and the kinetic energy can be determined simultaneously and exactly.

- b. For momentum and total energy, we evaluate

$$-i\hbar \frac{d}{dx} \left(-\frac{\hbar^2}{2m} \frac{d^2}{dx^2} + V(x) \right) f(x) - \left(-\frac{\hbar^2}{2m} \frac{d^2}{dx^2} + V(x) \right) \left(-i\hbar \frac{d}{dx} \right) f(x)$$

Because the kinetic energy and momentum operators commute, per part (a), this expression is equal to

$$\begin{aligned} & -i\hbar \frac{d}{dx}(V(x)f(x)) + i\hbar V(x) \frac{d}{dx}f(x) \\ &= -i\hbar V(x) \frac{d}{dx}f(x) - i\hbar f(x) \frac{d}{dx}V(x) + i\hbar V(x) \frac{d}{dx}f(x) \\ &= -i\hbar f(x) \frac{d}{dx}V(x) \end{aligned}$$

We conclude the following:

$$\left[V(x), -i\hbar \frac{d}{dx} \right] = -i\hbar \frac{d}{dx} V(x) \neq 0$$

Therefore, the momentum and the total energy cannot be known simultaneously and exactly. Note that the arbitrary function $f(x)$ is not present in the final expression for the commutator. Note also that the momentum and the total energy can be known simultaneously if $[dV(x)]/dx = 0$. This corresponds to a constant potential energy for all values of x ; in other words, the free particle of Section 4.1.

Now apply the formalism just discussed to the particle in the box in its lowest energy state. In Chapter 4, we found that although the wave function for this state is an eigenfunction of the total energy operator, it is not an eigenfunction of the momentum operator. Therefore, these two operators do not commute. If the total energy of the particle is measured, the value $E = \hbar^2/8ma^2$ is obtained. If the average momentum is subsequently determined from a number of individual measurements, the result is $\langle p_x \rangle = 0$. This result merely states that it is equally likely that positive and negative values will be obtained. There is no way of knowing what the magnitude and sign of the momentum will be for an individual measurement. Because the energy is known precisely, nothing is known about the momentum. This result is consistent with the fact that the two operators do not commute.

6.2 THE STERN-GERLACH EXPERIMENT

Next, let us consider a real experiment in a simple quantum-mechanical framework that illustrates some of the concepts discussed in the preceding section in more concrete terms. This experiment also illustrates how quantum-mechanical concepts of measurement arose out of analyzing results obtained in laboratories. In this experiment, a beam of silver atoms with a well-defined direction passes through a magnetic field that has a gradient along the z coordinate, which is chosen to be perpendicular to the path of the atoms. An atomic beam of silver atoms can be made in a vacuum system by heating solid silver in an oven to a temperature at which the vapor pressure of Ag is in the range of 10^{-2} Torr. Letting the atoms escape through a series of collimating apertures in the wall of the oven results in a beam of Ag atoms, all traveling in the same direction, which is chosen to be the y direction. The atoms pass through the magnetic field and are detected some distance beyond the magnet. The forces acting on the magnetic dipoles representing individual Ag atoms are depicted in Figure 6.1, and the **Stern-Gerlach experiment** is shown schematically in Figure 6.2.

Before describing the consequences of the Stern-Gerlach experiment, we should note several aspects of silver atoms. (View the remarks in the balance of this paragraph as an aside because none of this was known at the time the Stern-Gerlach experiment was conducted.) Silver atoms have a single unpaired electron that has an intrinsic

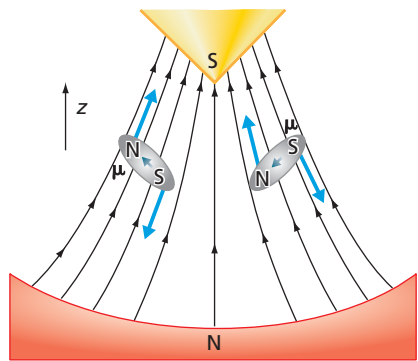
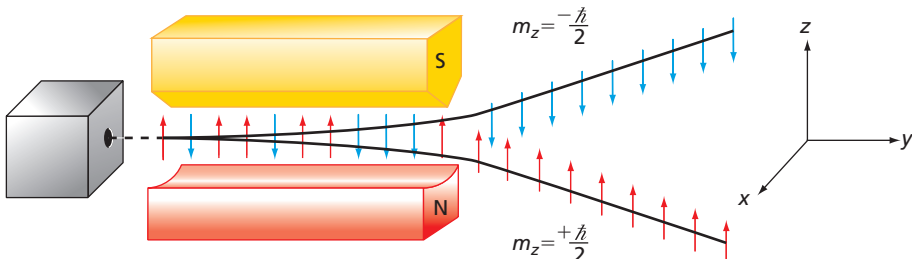


FIGURE 6.1
Forces acting on magnetic dipoles of individual Ag atoms. The effect of an inhomogeneous magnetic field on magnetic dipoles is to orient and deflect them in opposite directions, depending on the sign of the component of the magnetic moment along the z direction.

FIGURE 6.2

Schematic representation of the Stern–Gerlach experiment. The inhomogeneous magnetic field separates the silver beam into two, and only two, components.



magnetic moment. The magnetic moment is associated with what is called the *electron spin*. Although the picture of a spherical electron spinning around an axis through its center is incorrect, it turns out that the spin emerges naturally in relativistic quantum mechanics.

Because each atom has a magnetic moment associated with the unpaired electron, the atom is deflected in the z direction as it passes through the inhomogeneous magnetic field. The atom is not deflected along the x and y directions because the magnetic field has no gradient along these directions. What outcome is expected in this experiment? Consider the classical system of a beam of magnetic dipoles. We expect that the magnetic dipoles are randomly oriented in space and that only their z component is affected by the magnet. Because the z component takes on all possible values between $+|\mu|$ and $-|\mu|$, where μ is the magnetic moment of the atom, the silver atoms will be equally distributed along a range of z values at the detector. The z values can be predicted from the geometry of the experiment and the strength of the field gradient if the magnetic moment is known.

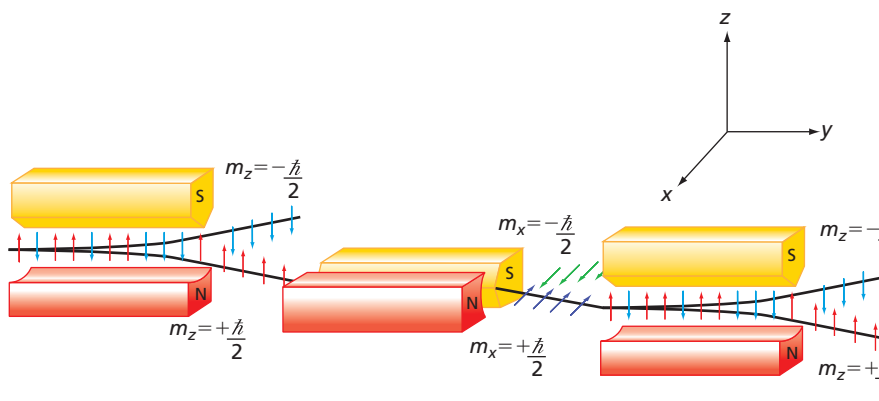
6.2.1 Results of the Stern–Gerlach Experiment

What are the results of the experiment? Silver atoms are deflected only in the z direction as expected, but only two z values are observed. One corresponds to an upward deflection and the other to a downward deflection of the same magnitude. *What conclusions can be drawn from this experiment?* We conclude that the operator called “measure the z component of the magnetic moment,” denoted by \hat{A} , has only two eigenfunctions, with eigenvalues that are equal in magnitude but opposite in sign. We call the two eigenfunctions α and β and assume that they are normalized. Because the experiment shows that these two eigenfunctions form a complete set (only two deflection angles are observed), any acceptable wave function can be written as a linear combination of α and β . Therefore, the initial normalized wave function that describes a single silver atom is

$$\psi = c_1\alpha + c_2\beta \quad \text{with} \quad |c_1|^2 + |c_2|^2 = 1 \quad (6.2)$$

We cannot specify the values of c_1 and c_2 because they refer to individual measurements, and only the total number of silver atoms in the two deflected beams at the detector is measured. However, the relative number of Ag atoms that was deflected upward and downward can be measured for a large number of atoms. This ratio is one, and therefore $|c_1|_{\text{average}}^2 = |c_2|_{\text{average}}^2 = 1/2$. The average is over all the atoms that have landed on the detector.

The Stern–Gerlach experiment has one additional step. We follow the path of the downwardly deflected atoms, which have the wave function $\psi = \alpha$ and deflect them once again. However, this time the magnet has been turned 90° , so that the magnetic field gradient is in the x direction. Note that now there is an inhomogeneity in the x direction, such that the atoms are separated along this direction. The operator is now “measure the x component of the magnetic moment,” which is denoted \hat{B} . The experiment shows that this operator also has two and only two eigenfunctions, which we call δ and γ . They have the same eigenvalues as α and β , respectively. If the relative number of Ag atoms deflected in the $+x$ and $-x$ directions is measured, the ratio is

**FIGURE 6.3**

Three-magnet configuration of the Stern-Gerlach experiment. One of the beams exiting from the first magnet has been passed through a second magnet rotated by 90°. The beam is again split into two components. The third magnet gives a result that is different from what would have been expected from classical physics.

determined to be one. We conclude that the wave function prior to entering the second magnet was

$$\psi = c_3\delta + c_4\gamma \quad \text{with} \quad |c_3|^2 + |c_4|^2 = 1 \quad (6.3)$$

As before, $|c_3|_{\text{average}}^2 = |c_4|_{\text{average}}^2 = 1/2$.

Now comes the punch line. We ask the question “Do the operators \hat{A} and \hat{B} commute?” This question is answered by repeating the first measurement to see if the state of the system has been changed by carrying out the second measurement. Experimentally, a third magnet that has the same alignment as the first magnet is added. This third magnet acts on one of the two separated beams that have emerged from the second magnet, as shown in Figure 6.3.

If the operators commute, a single downwardly deflected beam of Ag atoms corresponding to $\psi = \alpha$ will be observed. If they do not commute, the wave function for the atoms entering the third magnet will no longer be an eigenfunction of \hat{A} , and two beams will be observed. Why is this? If the wave function that describes the Ag atom emerging from the second magnet is not an eigenfunction of \hat{A} , it still can be represented as a linear combination of the two eigenfunctions of \hat{A} . A state whose wave function is a linear combination of α and β will give rise to two deflected beams of Ag atoms.

The result of the experiment with the third magnet is that two beams emerge, just as was seen from the first magnet! *We conclude that the operators \hat{A} , “measure the z component of the magnetic moment,” and \hat{B} , “measure the x component of the magnetic moment,” do not commute.* This means that a silver atom does not simultaneously have well-defined values for both μ_z and μ_x . This is, of course, not the conclusion reached by applying classical mechanics to a classical magnetic moment. The experiment is a good illustration of how the quantum-mechanical postulates arose from consideration of the outcomes of experiments.

Because the magnetic moment and the angular momentum of a charged particle differ only by a multiplicative constant, we have also shown that the operators for the individual components of the angular momentum vector do not commute. The consequences of this result will be discussed in Chapter 7.

Concept

Stern and Gerlach created an experiment that is equivalent to evaluating a commutator.

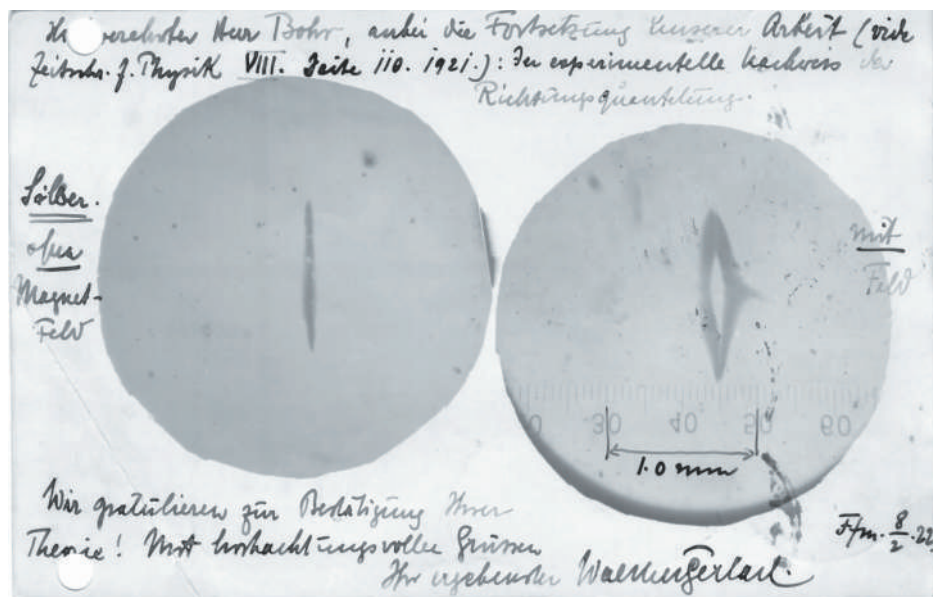
6.2.2 History of the Stern-Gerlach Experiment

This classic experiment, carried out in 1921, was designed to test the quantum-mechanical model of the atom proposed by Niels Bohr. A silver beam generated by an oven in a vacuum chamber was collimated by two narrow slits of 0.03 mm width. The beam passed through an inhomogeneous magnet 3.5 cm in length and impinged on a glass plate. After about an hour of operation, the plate was removed and examined visually. Only about one atomic layer of Ag was deposited on the plate in this time, making the detection of the spatial distribution of the silver atoms very difficult. The key to their successful detection was that both Stern and Gerlach smoked cheap cigars with a high sulfur content. The sulfur-containing smoke reacted with the Ag atoms, producing Ag_2S , which was clearly visible under a microscope, even though the amount deposited

FIGURE 6.4

Result of the Stern–Gerlach experiment.

The postcard shows the result obtained without the magnetic field (left) and with the magnetic field (right). The splitting of the beam with the magnetic field into two distinct components is clearly visible. The handwritten notes explain the experiment and congratulate Bohr, saying that the results confirmed his theory.



was less than 10^{-7} mol. Upon successful completion of the experiment, Gerlach sent Bohr the postcard shown in Figure 6.4.

The agreement with the Bohr model turned out to be fortuitous. Several years later, researchers discovered that the electron has an intrinsic angular momentum (spin). The magnetic moment arising from this angular momentum—and not a magnetic moment produced by electrons orbiting around the nucleus—is the basis for the observed deflection. A more detailed account of this experiment appears in the article by Friedrich and Herschbach (2003) cited in Further Reading.

6.3 THE HEISENBERG UNCERTAINTY PRINCIPLE

The best-known case of noncommuting operators concerns position and momentum and is associated with the **Heisenberg uncertainty principle**. This principle quantifies the uncertainty in the position and momentum of a quantum mechanical particle that arises from the fact that $[\hat{x}, \hat{p}_x] \neq 0$.

The uncertainty principle can be nicely illustrated using the free particle as an example. As discussed in Chapter 2, the free-particle total energy eigenfunctions have the form $\Psi(x, t) = A \exp i(kx - \omega t - \phi)$. What can be said about the position and momentum of states described by this wave function? It is convenient to set $\phi = 0$ and $t = 0$, so that we can focus on the spatial variation of $\psi(x)$.

By operating on this wave function with the momentum operator, it can be easily shown that it is an eigenfunction of the momentum operator with the eigenvalue $\hbar k = \hbar k/2\pi$. To discuss probability, this wave function must be normalized. As shown in Section 4.1, a plane wave cannot be normalized over an interval that is infinite, but it can be normalized over the finite interval $-L \leq x \leq L$:

$$\int_{-L}^L \Psi^*(x)\Psi(x) dx = 1$$

$$A^* A \int_{-L}^L e^{-ikx} e^{ikx} dx = 1 \quad (6.4)$$

$$|A| = \frac{1}{\sqrt{2L}}$$

Now that the function is normalized, we calculate the probability of finding the particle near an arbitrary point $x = x_0$:

$$P(x_0)dx = \psi^*(x_0)\psi(x_0)dx = dx/2L \quad (6.5)$$

We see that the probability is independent of position. This means that it is equally probable that the particle will be found anywhere. Now let the interval length L become arbitrarily large. The probability of finding the particle within the interval dx centered at $x = x_0$ approaches zero! We conclude that if a particle is prepared in a state in which the momentum is exactly known, then its position is completely unknown. It turns out that if a particle is prepared such that its position is exactly known (the wave function is an eigenfunction of the position operator), then its momentum is completely unknown.

This result is completely at variance with expectations based on classical mechanics because simultaneous knowledge of position and momentum is essential to calculating trajectories of particles subject to forces. How can this counterintuitive result be understood?

The total uncertainty in position arises because the momentum is precisely known. Is it possible to construct a wave function for which the momentum is known to be within a certain range of values? Will such a wave function give more information about the position of the particle than the plane wave $\Psi(x, t) = A \exp i(kx - \omega t - \phi)$ does? These questions can be answered by constructing a wave function that is a superposition of several plane waves and then examining its properties. Consider the superposition of plane waves of very similar wave vectors given by

$$\psi(x) = \frac{1}{2}Ae^{ik_0x} + \frac{1}{2}A \sum_{n=-m}^m e^{i(k_0+n\Delta k)x}, \quad \text{with } \Delta k \ll k \quad (6.6)$$

This superposition wave function is not an eigenfunction of the momentum operator, although each individual term in the sum is an eigenfunction of the momentum operator. The upper portion of Figure 6.5 shows the real part of each of the 51 individual terms about an arbitrarily chosen zero of distance for $m = 25$.

How does the amplitude of $\psi(x)$ vary over the interval? At $x = 0$, all 51 waves constructively interfere, but they undergo destructive interference at smaller and larger distances. Consequently, the superposition wave function in Equation (6.6) has a maximum amplitude at $x = 0$; the amplitude rapidly decays to small values at smaller and larger distances. How does the probability density vary over the interval? Evaluating Equation (6.6) for $m = 25$ and forming $|\psi(x)|^2$, the function shown as the red curve in Figure 6.5 is obtained. Because $|\psi(x)|^2$ is strongly peaked at the center of the interval, by superposing these 51 waves we see that the particle has been localized. The oscillations in $|\psi(x)|^2$ result from having taken only a small number of terms in the superposition.

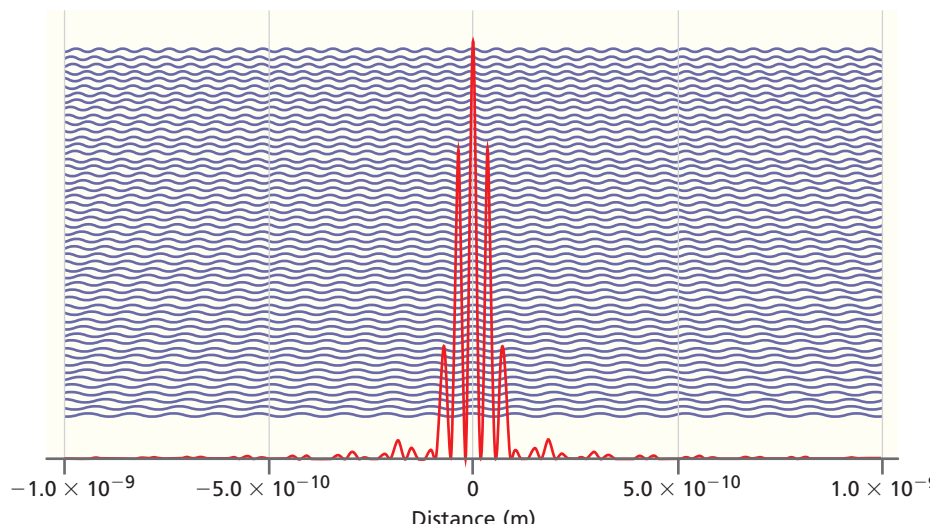


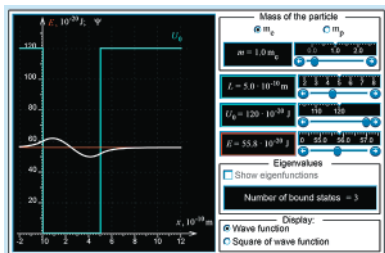
FIGURE 6.5
Superposition of momentum eigenfunctions leads to localization. The top part of the figure shows the real part of 51 plane waves that have been displaced vertically for purposes of display. The wave vectors lie between $6.00 \times 10^{10} \text{ m}^{-1}$ and $11.00 \times 10^{10} \text{ m}^{-1}$. The red curve shows the probability density $\psi^*(x)\psi(x)$ resulting from adding all 51 waves.

What does this calculation show? Because 51 waves of differing momentum have been superposed to construct the wave function, the momentum is no longer exactly known. Can we make this statement more quantitative? An individual measurement of the momentum for a state described by $\psi(x)$ will give values in the following range:

$$\hbar(k_0 - 25\Delta k) \leq p \leq \hbar(k_0 + 25\Delta k) \quad (6.7)$$

Concept

The position and momentum of a particle cannot both be known exactly and simultaneously.



W6.1 Wave Packets and the Uncertainty Principle

In going from a single plane wave to the superposition function $\psi(x)$, the uncertainty in momentum has increased from zero to $50\hbar\Delta k$. As the curve for $|\psi(x)|^2$ in Figure 6.5 shows, increasing the uncertainty in momentum has decreased the uncertainty in position from ∞ to $\sim 6 \times 10^{-10}$ m. The superposition wave function of Equation (6.6) is referred to as a **wave packet** because it has wave character but is localized to a finite interval.

Comparing the results just obtained for the superposition wave function of Equation (6.6) with those for a single plane wave of precisely determined momentum allows the following conclusion to be made: *As a result of the superposition of many plane waves, the position of the particle is no longer completely unknown, and the momentum of the particle is no longer exactly known.* Figure 6.5 shows that the approximate position of the particle can be known as long as an uncertainty in its momentum can be tolerated. The lesson of this discussion is that both position and momentum cannot be known *exactly and simultaneously* in quantum mechanics. We must accept a trade-off between the uncertainty in p and that of x . This result was quantified by Heisenberg in his famous uncertainty principle:

$$\Delta p \Delta x \geq \frac{\hbar}{2} \quad (6.8)$$

EXAMPLE PROBLEM 6.2

Assume that the double-slit experiment could be carried out with electrons using a slit spacing of $b = 10.0$ nm. To be able to observe diffraction, we choose $\lambda = b$, and because diffraction requires reasonably monochromatic radiation, we choose $\Delta p/p = 0.0100$. Show that, with these parameters, the uncertainty in the position of the electron is greater than the slit spacing b .

Solution

Using the de Broglie relation, we see that the average momentum of an electron is given by

$$\langle p \rangle = \frac{h}{\lambda} = \frac{6.626 \times 10^{-34} \text{ J s}}{1.00 \times 10^{-8} \text{ m}} = 6.626 \times 10^{-26} \text{ kg m s}^{-1}$$

and $\Delta p = 6.626 \times 10^{-28} \text{ kg m s}^{-1}$. The minimum uncertainty in position is given by

$$\Delta x = \frac{\hbar}{2\Delta p} = \frac{1.055 \times 10^{-34} \text{ J s}}{2 \times 6.626 \times 10^{-28} \text{ kg m s}^{-1}} = 7.96 \times 10^{-8} \text{ m}$$

which is greater than the slit spacing. Note that the concept of an electron trajectory is not well defined under these conditions. This offers an explanation for the observation that the electron appears to go through both slits simultaneously!

As shown in Example Problem 6.2, the trajectory of a particle for which the momentum and energy are exactly known is not a well-defined concept in quantum mechanics. However, a good approximation for a “trajectory” in quantum-mechanical systems is obtained by using wave packets.

What is the practical effect of the uncertainty principle? Does this mean that we have no idea what trajectories the electrons in a TV picture tube will follow or where a baseball thrown by a pitcher will pass a waiting batter? As mentioned earlier, this issue gets down to what is meant by *exact*. An exact trajectory could be calculated if \hbar were equal to zero, rather than being a small number. Because \hbar is a very small number,

the uncertainty principle does not affect the calculation of the trajectories of baseballs, rockets, or other macroscopic objects. Although the uncertainty principle holds for both electrons and baseballs, the effect is so small that it is not detectable for large masses. The uncertainty principle need not play a role for electron trajectories as shown in Example Problem 6.3 and does not have an effect on the trajectories of macroscopic objects as shown in Example Problem 6.4.

EXAMPLE PROBLEM 6.3

The electrons in a television picture tube have an energy of about 1.00×10^4 eV. If $\Delta p/p = 0.010$ in the direction of the electron trajectory for this case, calculate the minimum uncertainty in the position that defines where the electrons land on the phosphor in the picture tube.

Solution

Using the relation $\langle p \rangle = \sqrt{2 m E}$, we calculate the momentum as follows:

$$\begin{aligned}\langle p \rangle &= \sqrt{2 \times 9.109 \times 10^{-31} \text{ kg} \times 1.00 \times 10^4 \text{ eV} \times 1.602 \times 10^{-19} \text{ J/eV}} \\ &= 5.41 \times 10^{-23} \text{ kg m s}^{-1}\end{aligned}$$

Proceeding as in Example Problem 6.2,

$$\Delta x = \frac{\hbar}{2\Delta p} = \frac{1.055 \times 10^{-34} \text{ J s}}{2 \times 5.41 \times 10^{-25} \text{ kg m s}^{-1}} = 9.8 \times 10^{-11} \text{ m}$$

This distance is much smaller than could be measured and, therefore, the uncertainty principle has no effect in this instance.

EXAMPLE PROBLEM 6.4

An (over)educated baseball player tries to convince his manager that he cannot hit a 100-mile-per-hour (44.7 m s^{-1}) baseball that has a mass of 140. g and a relative momentum uncertainty of 1.00% because the uncertainty principle does not allow him to estimate its position within 0.1 mm. Is his argument valid?

Solution

The momentum is calculated using the following equation:

$$p = mv = 0.140 \text{ kg} \times 44.7 \text{ m s}^{-1} = 6.26 \text{ kg m s}^{-1}, \text{ and } \Delta p = 0.0626 \text{ kg m s}^{-1}$$

Substituting in the uncertainty principle,

$$\Delta x = \frac{\hbar}{2\Delta p} = \frac{1.055 \times 10^{-34} \text{ J s}}{2 \times 0.0626 \text{ kg m s}^{-1}} = 8.43 \times 10^{-34} \text{ m}$$

The uncertainty is not zero, but it is well below the experimental sensitivity. Sorry, back to the minor leagues.

This result—that it is not possible to know the exact values of two observables simultaneously—is not restricted to position and momentum. It applies to any two observables whose corresponding operators do not commute. Energy and time are another example of two observables that are linked by an uncertainty principle. The energy of the H atom with the electron in the 1s state can only be known to high accuracy because it has a very long lifetime. This is the case because there is no lower state to which it can decay. Excited states that rapidly decay to the ground state have an uncertainty in their energy. Evaluation of the commutator is the means used to test whether any two observables can be determined simultaneously and exactly.

SUPPLEMENTAL SECTION

6.4 THE HEISENBERG UNCERTAINTY PRINCIPLE EXPRESSED IN TERMS OF STANDARD DEVIATIONS

This section addresses the topic of how to use the Heisenberg uncertainty principle in a quantitative fashion. The Heisenberg uncertainty principle can be written in terms of standard deviations. This inequality can be written in the form

$$\sigma_x \sigma_p \geq \frac{\hbar}{2} \quad (6.9)$$

In this equation, σ_p and σ_x are the standard deviations that would be obtained by analyzing the distribution of a large number of measured values of position and momentum. The **standard deviations**, σ_p and σ_x , are related to observables by the relations

$$\sigma_p^2 = \langle p^2 \rangle - \langle p \rangle^2 \quad \text{and} \quad \sigma_x^2 = \langle x^2 \rangle - \langle x \rangle^2 \quad (6.10)$$

where σ_p^2 is called the variance in the momentum. The variance in the position is calculated in Example Problem 6.5.

EXAMPLE PROBLEM 6.5

Starting with the definition for the standard deviation in position, $\sigma_x = \sqrt{(1/N) \sum_{i=1}^N (x_i - \langle x \rangle)^2}$, derive the expression for σ_x^2 in Equation (6.10).

Solution

$$\begin{aligned} \sigma_x^2 &= \frac{1}{N} \sum_{i=1}^N (x_i - \langle x \rangle)^2 = \frac{1}{N} \sum_{i=1}^N (x_i^2 - 2x_i \langle x \rangle + \langle x \rangle^2) \\ &= \langle x^2 \rangle - 2\langle x \rangle \langle x \rangle + \langle x \rangle^2 \\ &= \langle x^2 \rangle - \langle x \rangle^2 \end{aligned}$$

The fourth postulate of quantum mechanics expresses how to calculate the observables in Equation (6.10) from the normalized wave functions:

$$\langle p^2 \rangle = \int \psi^*(x) \hat{p}^2 \psi(x) dx \quad \text{and}$$

$$\langle p \rangle^2 = \left(\int \psi^*(x) \hat{p} \psi(x) dx \right)^2$$

Similarly,

$$\langle x^2 \rangle = \int \psi^*(x) \hat{x}^2 \psi(x) dx \quad \text{and}$$

$$\langle x \rangle^2 = \left(\int \psi^*(x) \hat{x} \psi(x) dx \right)^2 \quad (6.11)$$

We next carry out a calculation for σ_p and σ_x using the particle in the box as an example. The normalized wave functions are given by $\psi_n(x) = \sqrt{2/a} \sin(n\pi x/a)$ and the operators needed are $\hat{p} = -i\hbar(d/dx)$ and $\hat{x} = x$.

Using the standard integrals

$$\int x \sin^2 bx dx = \frac{x^2}{4} - \frac{1}{4b}x \sin 2bx - \frac{1}{8b^2} \cos 2bx \quad \text{and}$$

$$\int x^2 \sin^2 bx dx = \frac{1}{6}x^3 - \left(\frac{1}{4b}x^2 - \frac{1}{8b^3} \right) \sin 2bx - \frac{1}{4b^2}x \cos 2bx$$

we find that

$$\begin{aligned}\langle x \rangle &= \int_0^a \sqrt{\frac{2}{a}} \sin\left(\frac{n\pi x}{a}\right) x \sqrt{\frac{2}{a}} \sin\left(\frac{n\pi x}{a}\right) dx = \frac{2}{a} \int_0^a x \sin^2\left(\frac{n\pi x}{a}\right) dx = \frac{1}{2}a \\ \langle x^2 \rangle &= \int_0^a \sqrt{\frac{2}{a}} \sin\left(\frac{n\pi x}{a}\right) x^2 \sqrt{\frac{2}{a}} \sin\left(\frac{n\pi x}{a}\right) dx = \frac{2}{a} \int_0^a x^2 \sin^2\left(\frac{n\pi x}{a}\right) dx \\ &= a^2 \left(\frac{1}{3} - \frac{1}{2\pi^2 n^2} \right) \\ \langle p \rangle &= \int_0^a \sqrt{\frac{2}{a}} \sin\left(\frac{n\pi x}{a}\right) \left(-i\hbar \frac{\partial}{\partial x} \sqrt{\frac{2}{a}} \sin\left(\frac{n\pi x}{a}\right) \right) dx \\ &= -i\hbar \frac{2\pi n}{a^2} \int_0^a \sin\left(\frac{n\pi x}{a}\right) \cos\left(\frac{n\pi x}{a}\right) dx = 0 \\ \langle p^2 \rangle &= \int_0^a \sqrt{\frac{2}{a}} \sin\left(\frac{n\pi x}{a}\right) \left(-\hbar^2 \frac{\partial^2}{\partial x^2} \sqrt{\frac{2}{a}} \sin\left(\frac{n\pi x}{a}\right) \right) dx \\ &= \frac{2\pi^2 n^2 \hbar^2}{a^3} \int_0^a \sin^2\left(\frac{n\pi x}{a}\right) dx = \frac{n^2 \pi^2 \hbar^2}{a^2}\end{aligned}$$

With these results, σ_p becomes

$$\sigma_p = \sqrt{\frac{n^2 \pi^2 \hbar^2}{a^2}} = \frac{n\pi\hbar}{a} \quad \text{and} \quad \sigma_x = a\sqrt{\left(\frac{1}{12} - \frac{1}{2\pi^2 n^2}\right)} \quad (6.12)$$

Next, these results are verified as being compatible with the uncertainty principle for $n = 1$:

$$\begin{aligned}\sigma_p \sigma_x &= \frac{n\pi\hbar}{a} \sqrt{a^2 \left(\frac{1}{12} - \frac{1}{2\pi^2 n^2} \right)} = \hbar \sqrt{\left(\frac{\pi^2 n^2}{12} - \frac{1}{2} \right)} \\ &= 0.57\hbar > \frac{\hbar}{2} \quad \text{for } n = 1\end{aligned} \quad (6.13)$$

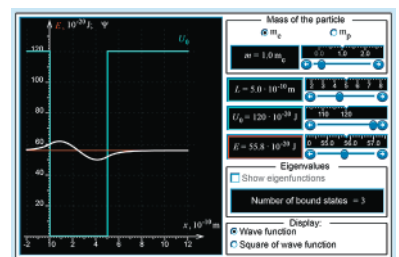
Because this function has its minimum value for $n = 1$, the uncertainty principle is satisfied for all values of n .

In evaluating a quantum-mechanical result, it is useful to make sure that it converges to the classical result as $n \rightarrow \infty$. To do so, the relative uncertainties in x and p are evaluated. The quantity $\sqrt{\langle p^2 \rangle}$ rather than $\langle p \rangle$ is used for this calculation because $\langle p \rangle = 0$. The following result is obtained:

$$\frac{\sigma_x}{\langle x \rangle} = \frac{a\sqrt{\left(\frac{1}{12} - \frac{1}{2\pi^2 n^2}\right)}}{a/2} = \sqrt{\frac{1}{3} - \frac{2}{\pi^2 n^2}} \quad \text{and} \quad \frac{\sigma_p}{\sqrt{\langle p^2 \rangle}} = \frac{n\pi\hbar/a}{n\pi\hbar/a} = 1 \quad (6.14)$$

Note that the relative uncertainty $\sigma_x/\langle x \rangle$ increases as $n \rightarrow \infty$. How can this result be understood? Looking back at the probability density in Figure 4.4, we see that the particle is most likely to be found near the center of the box for $n = 1$, whereas it is equally likely to be anywhere in the box for large n . The fact that the ground-state particle is more confined than the classical particle is at first surprising, but it is consistent with the discussion in Chapter 4.

The result that the relative uncertainty in momentum is independent of momentum is counterintuitive because in the classical limit, the uncertainty in the momentum is



W6.2 Expanding the Total Energy Eigenfunctions in Eigenfunctions of the Momentum Operator

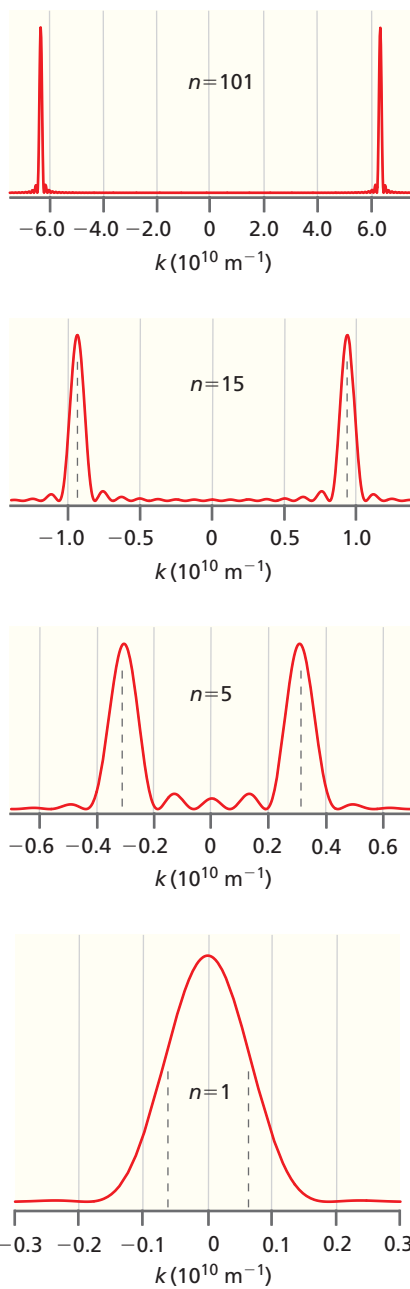


FIGURE 6.6

Probability density of measuring a given momentum. The relative probability density of observing a particular value of k , $A_k^* A_k$ (vertical axis), is graphed versus k for a 5.00-nm-long box for several values of n . The dashed vertical lines for $n = 1, 5$, and 15 show the classically expected values $p = \pm\sqrt{2mE}$.

expected to be negligible. It turns out that the result for $\sigma_p/\sqrt{\langle p^2 \rangle}$ in Equation (6.14) is misleading because there are two values of p for a given value of p^2 . The variance calculated earlier is characteristic of the set of the two p values, and what we want to know is $\sigma_p/\sqrt{\langle p^2 \rangle}$ for each value of p individually. How can the desired result be obtained?

The result is obtained by expanding the eigenfunctions $\psi_n(x)$ in the eigenfunctions of the momentum operator. We need to determine what values of k and what relative amplitudes A_k are required to represent the wave functions

$$\begin{aligned}\psi_n(x) &= \sqrt{\frac{2}{a}} \sin\left(\frac{n\pi x}{a}\right), \quad \text{for } n = 1, 2, 3, 4, \dots \quad a > x > 0 \quad \text{and} \\ \psi_n(x) &= 0, \quad \text{for } 0 \geq x, \quad x \geq a\end{aligned}\quad (6.15)$$

in the form

$$\psi_n(x) = \sum_{k=-\infty}^{\infty} A_k e^{ikx} \quad (6.16)$$

Expressing the particle in the box eigenfunctions in terms of the complete set of momentum eigenfunctions allows the probability of observing a particular value of p for a particle to be calculated. As outlined in the discussion of the fourth postulate in Chapter 3, the probability density of measuring a given momentum is proportional to $A_k^* A_k$. This quantity is shown as a function of k for several values of n in Figure 6.6. For $n = 101$, the result looks quite classical in that the probability is sharply peaked at the two classically predicted values $p = \pm\sqrt{2mE}$. However, as n becomes smaller, quantum effects become apparent. The most probable values of p are still given by $p = \pm\sqrt{2mE}$ for $n = 5$ and 15 , but subsidiary maxima are seen, and the width of the peaks (which is a measure of the uncertainty in p) is substantial. For $n = 1$, the distribution is peaked at $p = 0$, rather than the classical values. For this lowest energy state, quantum and classical mechanics give very different results.

Figure 6.6 demonstrates that the relative uncertainty $\sigma_p/\sqrt{\langle p^2 \rangle}$ decreases as p increases if only one of the two possible values of momentum is considered. You will explore this issue more quantitatively in the end-of-chapter problems. The counterintuitive result of Equation (6.14)—that the relative uncertainty in momentum is constant—is an artifact of characterizing the distribution consisting of two widely separated peaks by one variance, rather than looking at each of the peaks individually.

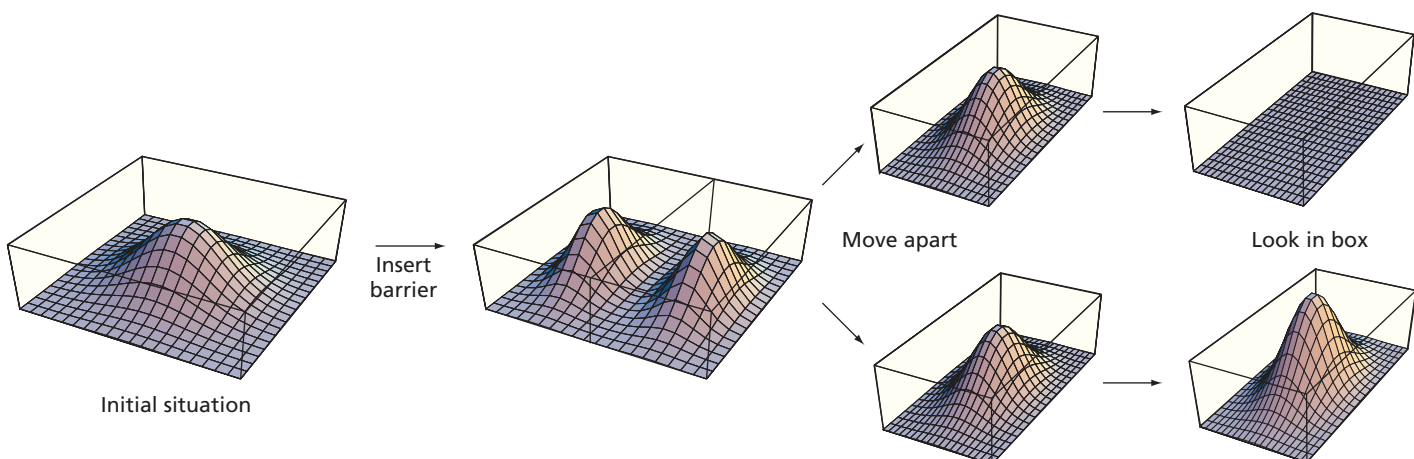
SUPPLEMENTAL SECTION

6.5 A THOUGHT EXPERIMENT USING A PARTICLE IN A THREE-DIMENSIONAL BOX

Consider the following experiment: one particle is put in an opaque box, and the top is securely fastened. From the outside, a partition is slid into the box, dividing it into two equal leak-tight volumes. This partition allows the initial box to be separated into two separate leak-tight boxes, each with half the volume. These two boxes are separated by sending one of them to the moon. Finally, an observer opens one of the boxes. The observer finds that the box he has opened is either empty or contains the particle. From the viewpoint of classical mechanics, this is a straightforward experiment. If the box that was opened is empty, then that half of the box was empty when the partition was initially inserted. What does this problem look like from a quantum-mechanical point of view? The individual steps are illustrated in Figure 6.7.

Initially, we know only that the particle is somewhere in the box before the partition is inserted. Because it exhibits wave-particle duality, the position of the particle cannot be determined exactly. If two eigenstates of the position operator, ψ_{left} and ψ_{right} , are defined, then the initial wave function is given by

$$\psi = a\psi_{left} + b\psi_{right}, \quad \text{with} \quad |a|^2 + |b|^2 = 1 \quad (6.17)$$

**FIGURE 6.7**

Thought experiment using a particle in a box. The square of the magnitude of the wave function is plotted along the x and y coordinates of the box.

In the figure, it has been assumed that $a = b$. The square of the wave function is non-zero everywhere in the box and goes to zero at the walls. When the partition is inserted, the characterization that was just given is again true, except that now the wave function also goes to zero along the partition. Classically, the particle is in either the left- or the right-hand side of the combined box, although it is not known which of these possibilities applies.

From a quantum-mechanical perspective, such a definitive statement cannot be made. We can merely say that there is an equal probability of finding the particle in each of the two parts of the original box. Therefore, when the two halves of the box are separated, the integral of the square of the wave function is one-half in each of the smaller boxes.

Now the box is opened. This is equivalent to applying the position operator to the wave function of Equation (6.17). According to the discussion in Chapter 3, the wave function becomes either ψ_{left} or ψ_{right} . We do not know which of these will be the final wave function of the system, but we do know that in a large number of measurements, the probability of finding it on the left is a^2 . Assume the particle is indeed found in the lower box, which is the case depicted in Figure 6.7. *In that case, the integral of the square of the wave function in that box instantaneously changes from 0.5 to 1.0 at the moment we look into the box, and the integral of the square of the wave function in the other box drops from 0.5 to zero!* Because this result does not depend on the distance of separation between the boxes, this distance can be made large enough that the boxes are not coupled by a physical force. Even so, the one box “knows” instantaneously what has been learned about the other box. This is the interpretation of quantum mechanics attributed to the Copenhagen school of Niels Bohr, which gives the act of measurement a central role in the outcome of an experiment. Nearly 80 years after the formulation of quantum theory, the search for an “observer-free” theory has not yet led to a widely accepted alternative to the Copenhagen school’s interpretation.

Before dismissing this scenario as unrealistic, and accepting the classical view that the particle really is in one part of the box *or* the other, have another look at Figure 3.3. The results shown there demonstrate clearly that the outcome of an experiment on *identically prepared* quantum-mechanical systems is inherently probabilistic. Therefore, the wave function for an individual system must be formulated in such a way that it includes all possible outcomes of an experiment. This means that, in general, it describes a superposition state. The result that measurements on identically prepared systems lead to different outcomes has been amply documented by experiments at the atomic level; this precludes the certainty in the classical assertion that the particle really is in one part of the box *or* the other. Where does the classical limit appear in this case? For instance, one might ask why the motion of a human being is successfully described by Newton’s second law rather than by the Schrödinger equation if every atom in our body is described

Concept

The act of measurement collapses a superposition wave function into an eigenfunction of the operator corresponding to the measurement.

by quantum mechanics. The answer is that the superposition wave function of a macroscopic system is unstable because of interactions with the environment, so that it decays very rapidly to a single term. This decay has the consequence that the strange behavior characteristic of quantum-mechanical superposition states is no longer observed in large classical systems.

S U P P L E M E N T A L S E C T I O N

6.6 ENTANGLED STATES, TELEPORTATION, AND QUANTUM COMPUTERS

Concept

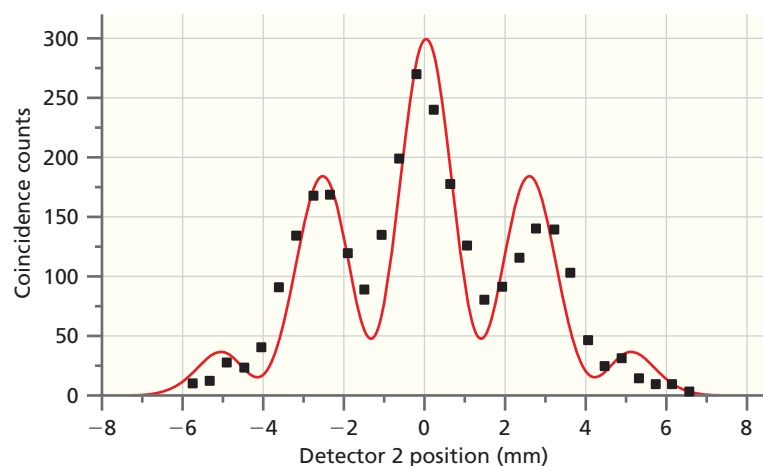
Entanglement couples the properties of two wave-particles regardless of how far apart they may be.

Erwin Schrödinger first noted a prediction of quantum mechanics that was very much at variance with classical physics. It is that two quantum particles can be coupled in such a way that their properties are no longer independent of one another, no matter how far apart they may be. We say that the particles are **entangled**. Einstein referred to this consequence of entanglement as “spooky action at a distance” to indicate what he believed to be a serious flaw in quantum mechanics. Definitive experiments to determine whether entanglement could be observed were not possible until the 1970s, when it was shown that Einstein was wrong in this instance.

Consider the following example of entanglement. A particle with no magnetic moment decays, giving two identical particles whose z component of the magnetic moment (which we call m_z) can take on the values $\pm 1/2$. Each of these particles is sent through a Stern–Gerlach analyzer, as described in Section 6.2. A series of measurements of m_z for particle one gives $\pm 1/2$ in a random pattern; it is not possible to predict the outcome of a single measurement. However, because angular momentum is conserved, the net magnetic moment of the two particles must be zero. If one of the particles is found to have m_z equal to $+1/2(\uparrow)$, the other must have $m_z = -1/2(\downarrow)$. There are only two possibilities for the two particles, $\uparrow\downarrow$ or $\downarrow\uparrow$; the left arrow in each case indicates m_z for particle one. Because the combinations $\uparrow\downarrow$ or $\downarrow\uparrow$ occur with equal probability, the two particles must be described by a single superposition wave function, which we write schematically as $\uparrow\downarrow + \downarrow\uparrow$. Note that neither particle can be described by its own wave function as a result of the entanglement.

This result implies that the second particle has no well-defined value of m_z until a measurement is carried out on the first particle. Because the roles of particles one and two can be reversed, the principles of quantum mechanics indicate that neither of the particles has a well-defined value of m_z until a measurement is carried out. This result violates a basic principle of classical physics called local realism. **Local realism** asserts that (1) measured results correspond to elements of reality. For example, if an observation determines that a person’s hair is black, according to local realism, that person’s hair was black before the measurement was made and is black regardless of whether a measurement is ever made. (2) Measured results are independent of any action that might be taken at a distant location at the same time. If a person has an identical twin on the other side of the planet, a measurement of the twin’s hair color has no influence on a measurement of the other twin’s hair color made at the same time.

The experiment just described shows that local realism is not valid because there is no value for m_z for the particles until a measurement is carried out and because the m_z values of the two particles remain coupled no matter how far apart they are when the first measurement is made. The outcome of an experiment that illustrates this surprising result is depicted in Figure 6.8. Two entangled photons are passed through separate optical fibers to locations spaced 10 km apart. Photon 1 is passed through a double slit and exhibits a diffraction pattern. If the profile of the light intensity corresponding to photon 2 is subsequently scanned, it corresponds to that of a photon that has passed through a double slit, which is what happened to the other photon! If a person and his or her identical twin were quantum mechanically entangled, neither twin’s hair color would be known before a measurement was made. Any possible hair color would be equally likely to be determined for one twin in a measurement, and the other twin would subsequently be found to have the same hair color.

**FIGURE 6.8**

Experimental demonstration of entanglement. The spatial distribution of the light intensity for photon 2 (see text discussion) shows a diffraction pattern (black squares), even though it has not passed through a slit. This result arises because photons 1 and 2 are entangled. The red curve is the diffraction pattern calculated using experimental parameters. For more details see the reference below.

Source: Adapted from D. V. Strekalov et al., *Physical Review Letters* 74 (1995): 3600–3603. Copyright 1995 by the American Physical Society. <http://link.aps.org/doi/10.1103/PhysRevLett.74.3600>

Does entanglement suggest that information can be transmitted instantaneously over an arbitrarily large distance? To answer this question, we examine how information about a system is transmitted to a distant location, first for a classical system and then for a quantum-mechanical system. Classically, a copy of the original object is created at the distant location while the original object remains in place. For example, a three-dimensional object is scanned at one location, and the data file is transmitted via the Internet to a distant location where a 3D printer creates a copy of the original object. A classical system can be copied as often as desired, and the accuracy of the copy is limited only by the quality of the tools used. In principle, the copies can be so well made that they are indistinguishable from the original. The speed with which information is transferred is limited by the speed of light.

By contrast, the information needed to make a copy of a single quantum-mechanical system cannot be obtained because it is impossible to determine the state of the system exactly by measurement. If the system wave function is given by

$$\psi = \sum_m b_m \phi_m \quad (6.18)$$

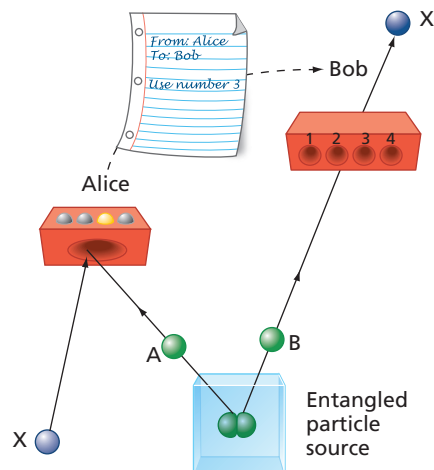
in which the ϕ_m are the eigenfunctions of an appropriate quantum-mechanical operator, an experiment can only determine the absolute magnitudes $|b_m|^2$. This is not enough information to determine the wave function. Therefore, the information needed to make a copy is not available. Making a copy of a quantum-mechanical system is also in violation of the Heisenberg uncertainty principle. If a copy could be made, one could easily measure the momentum of one of the copies and measure the position of the other copy. If this were possible, both the momentum and position could be known simultaneously.

Given this limited knowledge of quantum-mechanical systems, how can a quantum-mechanical state be transported? The answer is to use **teleportation**—the transfer of matter from one location to another without traversing the distance between the locations. The distinction between copying and teleportation is that the original object is no longer found at the initial location after teleportation has occurred. Consider the following experiment in which a photon at one location was teleported to a second location. For more details, see the reference to Zeilinger (2000) in Further Reading. Although photons were used in this experiment, there is no reason in principle why atoms or molecules could not be moved from one location to another in the same way.

Bob and Alice are at distant locations and share an entangled photon pair, of which Bob has photon B and Alice has photon A, as shown in Figure 6.9. Each of them carefully stores his or her photon to avoid interactions with the environment, so that the entanglement is maintained. At a later time, Alice has another photon that we call X, which she would like to teleport to Bob. How can this be done? A photon of a given energy is completely described by its polarization state, which can only take one of two possible values, horizontal or vertical. The states corresponding to horizontal and vertical polarization are orthogonal. She cannot measure the polarization state of photon X directly because the act of measurement would change the state of the photon. Instead, she entangles X and A. The two photons in the entangled state have different polarizations.

Concept

A quantum mechanical system cannot be copied.

**FIGURE 6.9**

Teleportation of photon X from Alice to Bob. Note the classical communication channel that Alice uses to communicate the outcome of her measurement on A and X to Bob.

What are the consequences of the entanglement of A and X on A and B? We know that whatever state X has, A must have the orthogonal state. If X is vertically polarized, then A must be horizontally polarized. Likewise, if X is horizontally polarized, then A must be vertically polarized. However, the same logic must apply to A and B because they are also entangled. Whatever state A has, B must have the orthogonal state. If the state of B is orthogonal to that of A and the state of A is orthogonal to that of X, *then the states of B and X must be identical*. This follows from the fact that there are only two possible eigenfunctions of the polarization operator.

What has been accomplished by this experiment? Photon B acquires the original polarization of Alice's photon X and is therefore identical in every way to the original state of X. In order to know that photons A and X have been successfully entangled, Alice has to pass both her photons through a detector. Therefore, the properties of X have been changed at Alice's location, which is equivalent to saying that photon X no longer exists at Alice's location. Consequently, we can say that photon X has been successfully teleported from Alice to Bob. Note that the uncertainty principle has not been violated because the photon has been teleported rather than copied.

Maintaining the entanglement of pairs A and B and A and X is the crucial ingredient of teleportation. Neither Bob nor Alice knows the state of X at the start or the end of the experiment. This is the case because neither of them has measured the state of X directly. Had they done so, the state of the photon would have been irreversibly changed. It is only because they did not determine the state of X that teleportation was possible.

If the preceding outcome were the only possible outcome of Alice's entanglement of A and X, the transmission of information from Alice to Bob would be instantaneous, regardless of the distance between them. Therefore, it would be faster than the speed of light. Unfortunately, it turns out that Alice's entanglement of A and X has four possible outcomes, which we will not discuss other than to say that each is equally probable. Although there is no way to predict which of the four outcomes will occur, Alice has detectors that will tell her after the fact which outcome occurred.

In each of these outcomes, the entanglement of A and X is transferred to B, but in three of the four, Bob must carry out an operation on B, such as to rotate its polarization by a fixed angle, in order to make B identical to X. Only if Alice sends him the result of her measurement does Bob know what he must do to B to make it indistinguishable from X. It is the need for this additional information that limits the speed of quantum information transfer through teleportation. Although the state of Bob's photon B is instantaneously transformed as Alice entangles A and X, he cannot interpret his results without additional information from her. Because Alice's information can only be sent to Bob using conventional methods such as phone, fax, or e-mail, the information transmitted in teleportation is limited by the speed of light. Although the state of entangled particles changes instantaneously, information transmission utilizing entanglement cannot proceed faster than the speed of light.

In principle, the same technique could be used to teleport an atom or a molecule. The primary requirement is that it must be possible to create entangled pairs of the object to be teleported. The initial experiment was carried out with photons because experimental methods to entangle photons are available. As discussed earlier, entangled states are fragile and can decay rapidly through interactions with the environment to a single eigenfunction of the operator corresponding to the interaction. Such a decay occurs rapidly for systems containing a large number of atoms, making it unlikely that it will ever be possible to teleport a person.

Entanglement has a further interesting application. It provides the basis for the **quantum computer**, which is currently in a rapid state of development. Such a computer would be far more powerful than the largest supercomputers currently available. Quantum computers could deliver solutions to important problems where patterns cannot be found and the number of possibilities that are needed to explore to get to the answer are too enormous ever to be processed by conventional computers. How does a quantum computer differ from a conventional computer? In a conventional computer, information is stored in bits. A **bit** generally takes the form of a macroscopic object like a wire or a memory element that can be described in terms of a property such as voltage. For example, two different ranges of voltage are used to represent the numbers

Concept

Teleportation is the quantum mechanical analog of copying but recreates the original at a distant location.

0 and 1. Within this binary system, an n bit memory can have 2^n possible states that range between 00000...00 and 11111...11. A three-bit memory can have the eight states 100, 010, 001, 110, 101, 011, 111, and 000. Information such as text and images can be stored in the form of such states. Mathematical or logical operations can be represented as transformations between such states. Logic gates operate on binary strings to carry out mathematical operations. Software provides an instruction set to route the data through the logic gates that are the heart of the computer hardware. This is the basis on which conventional computers operate.

The quantum analog of the bit, in which two numbers characterize the entity, is the **qubit**, which through superposition is *simultaneously* a linear combination of 0 and 1, rather than being either 1 or 0. Qubits can be entangled with one another in such a way that the processing capability of a quantum computer doubles with each additional entangled qubit. Five entangled qubits can do 2^5 or 32 parallel computations simultaneously, whereas in a conventional computer the calculations would have to be done sequentially. Not all applications would benefit from the ability to carry out parallel calculations. One of the most interesting applications of quantum computing is data encryption, which is essential to monetary transactions on the Internet. Shor's algorithm, which allows the rapid factorization of very large numbers, would allow modest-sized quantum computers to outperform the largest conventional supercomputers in the area of data encryption.

As discussed earlier, quantum superposition and entanglement states are easily destroyed by interactions with the surroundings. The main challenge in building viable quantum computers is to create addressable superposition and entangled states in an array of entangled qubits, with state lifetimes sufficiently long to carry out the desired calculations. Leading candidates for qubits include superconducting loops at temperatures near zero Kelvin and individual ions trapped in electromagnetic fields. Superposition state lifetimes are typically 10^3 s in trapped ions and only 5×10^{-5} s in superconducting loops. However, creating superposition states in trapped ions requires multiple tuned lasers, whereas creating superposition states in superconducting loops is easily accomplished using microwave signals. The most viable building blocks for successful quantum computers must satisfy a set of competing demands. For a discussion of technologies that are currently being investigated for quantum computers, see the reference to Popkin (2016) in Further Reading.

Connection

IBM has made a real 5-qubit quantum computer and a quantum computer simulator available for public use. For more information, see www.research.ibm.com/ibm-q/

VOCABULARY

bit	Heisenberg uncertainty principle	standard deviation
commutator	local realism	Stern–Gerlach experiment
commute	quantum computer	teleportation
entangled	qubit	wave packet

KEY EQUATIONS

Equation	Significance of Equation	Equation Number
$\hat{A}[\hat{B}f(x)] - \hat{B}[\hat{A}f(x)] = 0$	Condition that observables of two operators can be determined simultaneously and exactly	6.1
$\psi(x) = \frac{1}{2}Ae^{ik_0x} + \frac{1}{2}A \sum_{n=-m}^m e^{i(k_0+n\Delta k)x}$, with $\Delta k \ll k$	Wave packet expressed as series in eigenfunctions of momentum operator	6.6
$\Delta p \Delta x \geq \frac{\hbar}{2}$	Heisenberg uncertainty principle	6.8
$\sigma_x \sigma_p \geq \frac{\hbar}{2}$	Heisenberg uncertainty principle in terms of standard deviations	6.9
$\sigma_p^2 = \langle p^2 \rangle - \langle p \rangle^2$ and $\sigma_x^2 = \langle x^2 \rangle - \langle x \rangle^2$	Definition of standard deviations of position and momentum	6.10

CONCEPTUAL PROBLEMS

Q6.1 Why does the Stern–Gerlach experiment show that the operator “measure the z component of the magnetic moment of an Ag atom” and has only two eigenfunctions with eigenvalues that have the same magnitude and opposite sign?

Q6.2 Have a closer look at Equation (6.6) and Figure 6.5. How would Figure 6.5 change if m increases? Generalize your conclusion to make a statement of how well the momentum is known if the position is known exactly.

Q6.3 Why is maintaining the entanglement of pairs A and B and A and X considered the crucial ingredient of teleportation?

Q6.4 Why is it not possible to reconstruct the wave function of a quantum-mechanical superposition state from experiments?

Q6.5 Why does the relative uncertainty in x for the particle in the box increase as $n \rightarrow \infty$?

Q6.6 Why is the statistical concept of variance a good measure of uncertainty in a quantum-mechanical measurement?

Q6.7 Derive a relationship between $[\hat{A}, \hat{B}]$ and $[\hat{B}, \hat{A}]$.

Q6.8 How does our study of the eigenfunctions for the particle in the box let us conclude that the position uncertainty has its minimum value for $n = 1$?

Q6.9 What is the difference between a bit and a qubit?

Q6.10 How does the Heisenberg uncertainty principle allow us to conclude that it is not possible to make exact copies of quantum mechanical objects?

Q6.11 Which result of the Stern–Gerlach experiment allows us to conclude that the operators for the z and x components of the magnetic moment do not commute?

Q6.12 Why is the motion of a human being successfully described by Newton’s second law rather than by the Schrödinger equation if every atom in our body is described by quantum mechanics?

Q6.13 Explain the following statement: if $\hbar = 0$, it would be possible to measure the position and momentum of a particle exactly and simultaneously.

Q6.14 Why is $\sqrt{\langle p^2 \rangle}$ rather than $\langle p \rangle$ used to calculate the relative uncertainty for the particle in the box?

Q6.15 How would the results of the Stern and Gerlach experiment be different if they had used a Mg beam instead of an Ag beam?

Q6.16 How would the results of the Stern and Gerlach experiment be different if they had used a homogeneous magnetic field instead of an inhomogeneous field?

Q6.17 Discuss whether the results shown in Figure 6.8 are consistent with local realism.

Q6.18 An electron and an He atom have the same uncertainty in their speed. What can you say about the relative uncertainty in position for the two particles?

Q6.19 Describe the trends in Figure 6.6 as the quantum number n increases.

NUMERICAL PROBLEMS

Section 6.1

P6.1 Evaluate the commutator $[d/dx, 1/x]$ by applying the operators to an arbitrary function $f(x)$.

P6.2 a) Show that $\psi(x) = e^{-x^2/2}$ is an eigenfunction of $\hat{A} = x^2 - \partial^2/\partial x^2$. Show that $\hat{B}\psi(x)$ where $\hat{B} = x - \partial/\partial x$ is another eigenfunction of \hat{A} .

P6.3 Evaluate the commutator $[y(\partial/\partial y), x(\partial/\partial x)]$ by applying the operators to an arbitrary function $f(x, y)$.

P6.4 Evaluate $[\hat{A}, \hat{B}]$ if $\hat{A} = x + xd/dx$ and $\hat{B} = x - xd/dx$.

P6.5 Evaluate the commutator $[\hat{p}_x, \hat{x}^2]$ by applying the operators to an arbitrary function $f(x)$.

P6.6 Evaluate the commutator $[y^2, \partial^2/\partial x^2 + \partial^2/\partial y^2]$ by applying the operators to an arbitrary function $f(x, y)$.

P6.7 Evaluate the commutator $[(d^2/dy^2), y]$ by applying the operators to an arbitrary function $f(y)$.

P6.8 Evaluate the commutator $[d/dx, 1/x^2]$ by applying the operators to an arbitrary function $f(x)$.

P6.9 Evaluate the commutator $[\hat{x}, \hat{p}_x]$ by applying the operators to an arbitrary function $f(x)$. What value does the commutator $[\hat{p}_x, \hat{x}]$ have?

P6.10 Evaluate the commutator $[(d^2/dy^2) - y, (d^2/dy^2) + y]$ by applying the operators to an arbitrary function $f(y)$.

P6.11 Evaluate the commutator $[\hat{x}, \hat{p}_x^2]$ by applying the operators to an arbitrary function $f(x)$.

P6.12 What is wrong with the following argument? We know that the functions $\psi_n(x) = \sqrt{2/a} \sin(n\pi x/a)$ are eigenfunctions of the total energy operator for the particle in the infinitely deep box. We also know that in the box,

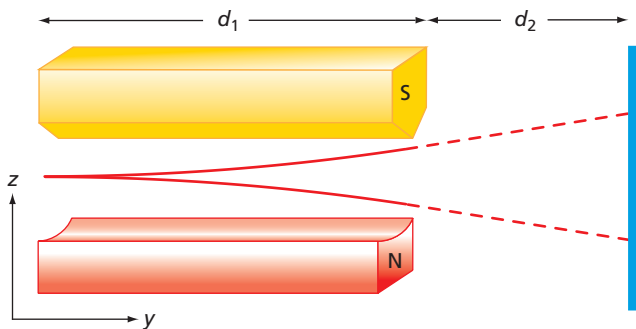
$E = \frac{p_x^2}{2m} + V(x) = \frac{p_x^2}{2m}$ because $V(x) = 0$. Therefore, the operator for E is proportional to the operator for p_x^2 . Because the operators for p_x^2 and p_x commute as you can easily demonstrate, the functions $\psi_n(x) = \sqrt{2/a} \sin(n\pi x/a)$ are eigenfunctions of both the total energy and momentum operators.

P6.13 For linear operators A , B , and C , show that $[\hat{A}, \hat{B} \hat{C}] = [\hat{A}, \hat{B}] \hat{C} + \hat{B} [\hat{A}, \hat{C}]$.

Section 6.2

P6.14 In this problem, you will carry out the calculations that describe the Stern–Gerlach experiment shown in Figure 6.2. Classically, a magnetic dipole μ has the potential energy $E = -\mu \cdot \mathbf{B}$. If the field has a gradient in the z direction, the magnetic moment will experience a force, leading it to be deflected in the z direction. Because classically μ can take on any value in the range $-|\mu| \leq \mu_z \leq |\mu|$, a continuous range of positive and negative z deflections of a beam along the y direction will be observed. From a quantum-mechanical perspective, the forces are the same as those in the classical picture, but μ_z can only take on a discrete set of values. Therefore, the incident beam will be split into a discrete set of beams that have different deflections in the z direction.

- a. The geometry of the experiment is shown here. In the region of the magnet indicated by d_1 , the Ag atom experiences a constant force. It continues its motion in the force-free region indicated by d_2 .



If the force inside the magnet is F_z , show that $|z| = 1/2(F_z/m_{Ag})t_1^2 + t_2 v_z(t_1)$. The times t_1 and t_2 correspond to the regions d_1 and d_2 .

- b. Show that assuming a small deflection,

$$|z| = F_z \left(\frac{d_1 d_2 + \frac{1}{2} d_1^2}{m_{Ag} v_y^2} \right)$$

- c. The magnetic moment of the electron is given by $|\mu| = g_S \mu_B / 2$. In this equation, μ_B is the Bohr magneton and has the value $9.274 \times 10^{-24} \text{ J/T}$. The gyromagnetic ratio of the electron g_S has the value 2.00231. If $\partial B_z / \partial z = 600 \text{ T m}^{-1}$, and d_1 and d_2 are 0.250 and 0.175 m, respectively, and $v_y = 300 \text{ m s}^{-1}$, what values of z will be observed?

Section 6.3

P6.15 Consider the results of Figure 6.5 more quantitatively. Describe the values of x and k by $x \pm \Delta x$ and $k_0 \pm \Delta k$. Evaluate Δx from the zero of distance to the point at which the envelope of $\psi^*(x)\psi(x)$ is reduced to one-half of its peak value. Evaluate Δk from $\Delta k = |1/2(k_0 - k_{min})|$ where k_0 is the average wave vector of the set of 51 waves (26th of 51) and k_{min} corresponds to the 51st of the 51 waves. Is your estimated value of $\Delta p \Delta x = \hbar \Delta k \Delta x$ in reasonable agreement with the Heisenberg uncertainty principle?

P6.16 Another important uncertainty principle is encountered in time-dependent systems. It relates the lifetime of a state Δt with the measured spread in the photon energy ΔE associated with the decay of this state to a stationary state of the system. “Derive” the relation $\Delta E \Delta t \geq \hbar/2$ in the following steps.

- Starting from $E = p_x^2/2m$ and $\Delta E = (dp_x/dp_x)\Delta p_x$, show that $\Delta E = v_x \Delta p_x$.
- Using $v_x = \Delta x / \Delta t$, show that $\Delta E \Delta t = \Delta p_x \Delta x \geq \hbar/2$.
- Estimate the width of a spectral line originating from the decay of a state of lifetime $5.0 \times 10^{-10} \text{ s}$ and $7.5 \times 10^{-11} \text{ s}$ in inverse seconds and inverse centimeters.

P6.17 Revisit the double-slit experiment of Example Problem 6.2. Using the same geometry and relative uncertainty in the momentum, what electron momentum would give a position uncertainty of $1.45 \times 10^{-10} \text{ m}$? What is the ratio of the wavelength and the slit spacing for this momentum? Would you expect a pronounced diffraction effect for this wavelength?

P6.18 Revisit the television picture tube of Example Problem 6.3. Keeping all other parameters the same, what electron energy would result in a position uncertainty of $4.25 \times 10^{-9} \text{ m}$?

P6.19 Apply the Heisenberg uncertainty principle to estimate the zero point energy for the particle in the box.

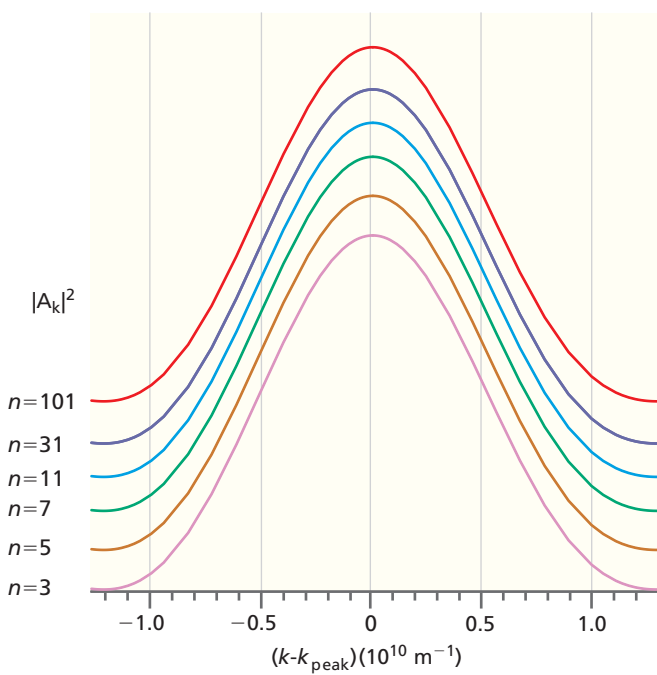
- First justify the assumption that $\Delta x \leq a$ and, as a result, that $\Delta p \geq \hbar/2a$. Justify the statement that, if $\Delta p \geq 0$, we cannot know that $E = p^2/2m$ is identically zero.
- Make this application more quantitative. Assume that $\Delta x = 0.25a$ and $\Delta p = 0.25p$ where p is the momentum in the lowest energy state. Calculate the total energy of this state based on these assumptions and compare your result with the ground-state energy for the particle in the box.
- Compare your estimates for Δp and Δx with the more rigorously derived uncertainties σ_p and σ_x of Equation (6.12).

P6.20 The muzzle velocity of a rifle bullet is 725 m s^{-1} . If the bullet weighs 25.0 g and the uncertainty in its momentum is 0.150%, how accurately can the position of the bullet be measured along the direction of motion?

P6.21 In this problem, we consider in more detail the calculations for σ_p and σ_x for the particle in the box shown in Figure 6.6. In particular, we want to determine how the absolute uncertainty Δp_x and the relative uncertainty $\Delta p_x/p_x$ of a single peak corresponding to either the most probable positive or negative momentum depend on the quantum number n .

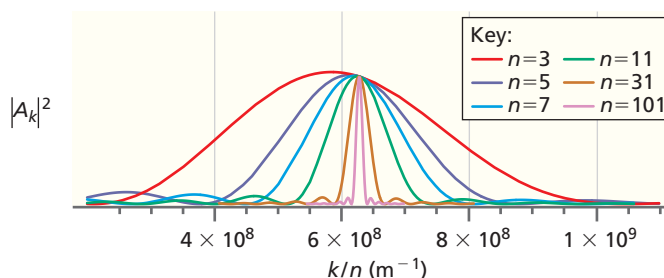
- First, we must relate k and p_x . From $E = p_x^2/2m$ and $E = n^2 h^2 / 8ma^2$, show that $p_x = nh/2a$.
- Use the result from part (a) together with the relation linking the length of the box and the allowed wavelengths to obtain $p_x = \hbar k$.
- Relate Δp_x and $\Delta p_x/p_x$ with k and Δk .
- The following graph shows $|A_k|^2$ versus $k-k_{peak}$. By plotting the results of Figure 6.6 in this way, all peaks appear at the same value of the abscissa. Successive curves have been shifted upward to avoid overlap. Use the width of the

$|A_k|^2$ peak at half height as a measure of Δk . What can you conclude from this graph about the dependence of Δp_x on n ?



- e. The following graph shows $|A_k|^2$ versus k/n for $n = 3, n = 5, n = 7, n = 11, n = 31$, and $n = 101$. Plotting the data in this way allows all principal peaks to be viewed simultaneously. Use the width of the $|A_k|^2$ peak at half height as a measure of $\Delta k/n$. Using this graph and the graph in part (d), determine the dependence of $\Delta p_x/p_x$ on n . One way to do this is to assume that the width depends on n , such as $(\Delta p_x/p_x) = n^\alpha$, where α is a constant to be determined.

If this relationship holds, a plot of $\ln(\Delta p_x/p_x)$ versus $\ln n$ will be linear and the slope will give the constant α .



P6.22 If the wave function describing a system is not an eigenfunction of the operator \hat{B} , measurements on identically prepared systems will give different results. The variance of this set of results is defined in error analysis as $\sigma_B^2 = \langle (B - \langle B \rangle)^2 \rangle$, where B is the value of the observable in a single measurement and $\langle B \rangle$ is the average of all measurements. Using the definition of average value from the quantum-mechanical postulates, $\langle A \rangle = \int \psi^*(x) \hat{A} \psi(x) dx$, show that $\sigma_B^2 = \langle B^2 \rangle - \langle B \rangle^2$.

P6.23 Consider the entangled wave function for two photons,

$$\psi_{12} = \frac{1}{\sqrt{2}} (\psi_1(H)\psi_2(V) + \psi_1(V)\psi_2(H))$$

Assume that the polarization operator \hat{P}_i has the properties $\hat{P}_i \psi_i(H) = -\psi_i(H)$ and $\hat{P}_i \psi_i(V) = +\psi_i(V)$ where $i = 1$ or $i = 2$.

- a. Show that ψ_{12} is not an eigenfunction of \hat{P}_1 or \hat{P}_2 .
- b. Show that each of the two terms in ψ_{12} is an eigenfunction of the polarization operator \hat{P}_1 .
- c. What is the average value of the polarization P_1 that you will measure on identically prepared systems? It is not necessary do a calculation to answer this question.

WEB-BASED SIMULATIONS, ANIMATIONS, AND PROBLEMS

Simulations, animations, and homework problem worksheets can be accessed at www.pearsonhighered.com/advchemistry

W6.1 The simulation of particle diffraction from a single slit is used to illustrate the dependence between the uncertainty in the position and momentum. The slit width and particle velocity are varied using sliders.

W6.2 The uncertainty in momentum will be determined for the total energy eigenfunctions for the particle in the infinite depth box for several values of the quantum number n . The function describing the distribution in k ,

$$g_n(k) = \frac{1}{\sqrt{2\pi}} \int_{-\infty}^{\infty} f_n(x) e^{-ikx} dx = \frac{1}{\sqrt{2\pi}} \int_0^a \sin \frac{n\pi x}{a} e^{-ikx} dx$$

will be determined. The values of k for which this function has maxima will be compared with that expected for a classical particle of momentum $p = \sqrt{2mE}$. The width in k of the function $g_n(k)$ on n will be investigated.

FURTHER READING

Friedrich, B., and Herschbach, D. "Stern and Gerlach: How a Bad Cigar Helped Reorient Atomic Physics." *Physics Today* (December 2003): 53.

Popkin, G. "Quest for Qubits." *Science* 354 (2016): 1091–1093.

Strelkov, D. V., et al. "Observation of Two-Photon 'Ghost' Interference and Diffraction." *Physical Review Letters* 74, (1995): 3600–3603.

Zeilinger, Anton. "Quantum Teleportation." *Scientific American*, 282 (2000): 50–59.

MATH ESSENTIAL 7:

Vectors

Observables such as temperature, mass, and angular momentum can be divided into two categories: scalars and vectors. Temperature, density, and mass are examples of scalars. Scalars have a numerical value, called the magnitude, but a direction is not associated with them. The value of a scalar can depend on position in space. For example, the density of an inhomogeneous mixture may vary with position. Angular momentum and electric field are examples of vectors, which have both a magnitude and a direction at a specific point in space. As for scalars, the magnitude of a vector can depend on position in space. To differentiate between scalar and vector observables, we use italics for scalars and a bold roman font for vectors.

ME7.1 INTRODUCTION TO VECTORS

In three-dimensional Cartesian coordinates, an arbitrary vector \mathbf{A} can be written in the form

$$\mathbf{A} = A_x \mathbf{i} + A_y \mathbf{j} + A_z \mathbf{k} \quad (\text{ME7.1})$$

To specify its direction where \mathbf{i} , \mathbf{j} , and \mathbf{k} are the mutually perpendicular vectors of unit length along the x , y , and z axes, respectively, and A_x , A_y , and A_z are scalars that are called the components along the x , y , and z axes, respectively. This vector is depicted in a three-dimensional coordinate system in Figure ME7.1.

By definition, the angle θ is measured from the z axis and the angle ϕ is measured in the x - y plane from the x axis. The angles θ and ϕ are related to A_x , A_y , and A_z by

$$\theta = \cos^{-1} \frac{A_z}{\sqrt{A_x^2 + A_y^2 + A_z^2}} \quad \text{and} \quad \phi = \tan^{-1} \frac{A_y}{A_x} \quad (\text{ME7.2})$$

We can see from Figure ME7.1 that A_x , A_y , and A_z are related to the magnitude of \mathbf{A} , which we designate by A

$$\begin{aligned} A_x &= A \sin \theta \cos \phi \\ A_y &= A \sin \theta \sin \phi \\ A_z &= A \cos \theta \end{aligned}$$

As we can also see from Figure ME7.1, the magnitude of vector \mathbf{A} is given by

$$A = |\mathbf{A}| = \sqrt{A_x^2 + A_y^2 + A_z^2} \quad (\text{ME7.3})$$

ME7.2 ADDITION AND SUBTRACTION OF VECTORS

We next consider the addition and subtraction of two vectors. Two vectors $\mathbf{A} = A_x \mathbf{i} + A_y \mathbf{j} + A_z \mathbf{k}$ and $\mathbf{B} = B_x \mathbf{i} + B_y \mathbf{j} + B_z \mathbf{k}$ can be added or subtracted according to the equations

$$\mathbf{A} \pm \mathbf{B} = (A_x \pm B_x) \mathbf{i} + (A_y \pm B_y) \mathbf{j} + (A_z \pm B_z) \mathbf{k} \quad (\text{ME7.4})$$

The addition and subtraction of vectors can also be depicted graphically by connecting their tails while preserving their orientation, as shown in the Figure ME7.2.

- ME7.1** Introduction to Vectors
- ME7.2** Addition and Subtraction of Vectors
- ME7.3** Multiplication of Vectors

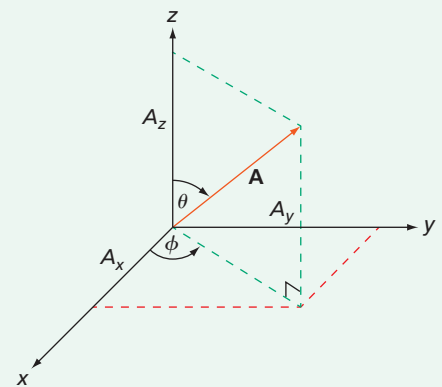


Figure ME7.1
The relationships of the Cartesian axes, the angles θ and ϕ , the vector \mathbf{A} , and the components of vector \mathbf{A} .

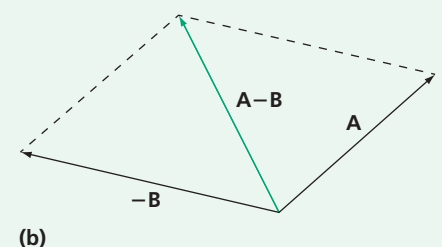
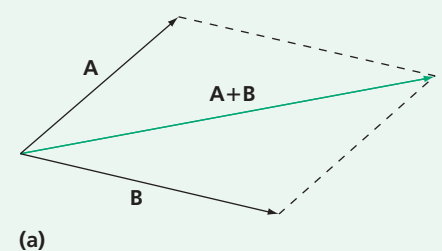


Figure ME7.2
Graphical depiction of vector addition and subtraction. (a) Vector addition and (b) vector subtraction.

ME7.3 MULTIPLICATION OF VECTORS

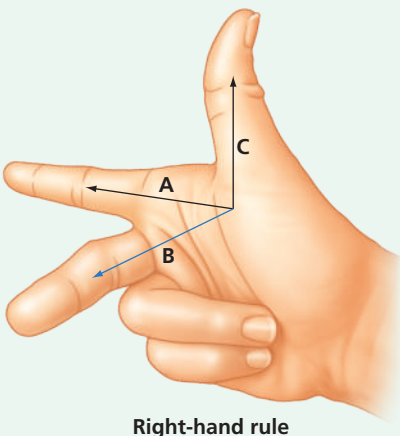


Figure ME7.3

The right-hand rule for Cartesian axes and vectors.

The multiplication of two vectors \mathbf{A} and \mathbf{B} can occur in either of two forms. Scalar multiplication of \mathbf{A} and \mathbf{B} , also called the dot product of \mathbf{A} and \mathbf{B} is defined by

$$\mathbf{A} \cdot \mathbf{B} = |\mathbf{A}| |\mathbf{B}| \cos \alpha \quad (\text{ME7.5})$$

where α is the angle between the vectors. The geometric interpretation of the scalar product is that it is the projection of \mathbf{A} on \mathbf{B} , or vice versa. For example, $\mathbf{A} \cdot \mathbf{k}$ in Figure ME7.1 is the projection of the vector \mathbf{A} on the z axis.

The other form in which vectors are multiplied is the vector product, also called the cross product. The vector multiplication of two vectors results in a vector, whereas the scalar multiplication of two vectors results in a scalar. The cross product is defined by the equation

$$\mathbf{A} \times \mathbf{B} = \mathbf{C} |\mathbf{A}| |\mathbf{B}| \sin \alpha \quad (\text{ME7.6})$$

where \mathbf{C} is a vector that is perpendicular to the plane defined by \mathbf{A} and \mathbf{B} . In forming the cross product, it is important to follow the convention depicted in Figure ME7.3 known as the right-hand rule.

Note that $\mathbf{A} \times \mathbf{B} = -\mathbf{B} \times \mathbf{A}$ using the right-hand rule. By contrast, in forming the scalar product, $\mathbf{A} \cdot \mathbf{B} = \mathbf{B} \cdot \mathbf{A}$.

The right-hand rule is useful in identifying the direction of the vector formed in the cross product. The magnitude of the components of the vector is most easily evaluated using a determinantal formulation of the cross product given by

$$\begin{aligned} \mathbf{A} \times \mathbf{B} &= \begin{vmatrix} \vec{i} & \vec{j} & \vec{k} \\ A_x & A_y & A_z \\ B_x & B_y & B_z \end{vmatrix} = \mathbf{i} \begin{vmatrix} A_y & A_z \\ B_y & B_z \end{vmatrix} - \mathbf{j} \begin{vmatrix} A_x & A_z \\ B_x & B_z \end{vmatrix} + \mathbf{k} \begin{vmatrix} A_x & A_y \\ B_x & B_y \end{vmatrix} \\ &= (A_y B_z - A_z B_y) \mathbf{i} + (A_z B_x - A_x B_z) \mathbf{j} + (A_x B_y - A_y B_x) \mathbf{k} \end{aligned}$$

For a review of working with determinants, see Math Essential 9.

MATH ESSENTIAL 8:

Polar and Spherical Coordinates

In solving integrals in two and three dimensions, it is useful to choose a coordinate system that has the symmetry of the problem. For example, in calculating the area of a circle, the logical choice of a coordinate system is polar coordinates and is shown in Figure ME8.1 and Equation (ME8.1).

For small values of dr and $d\phi$, the area element can be approximated by a rectangle of area $rd\phi$.

$$\text{Area} = \int_0^R dr \int_0^{2\pi} rd\phi = 2\pi \int_0^R rdr = \pi R^2$$

Solving this problem in Cartesian coordinates is more cumbersome, as shown in the following.

$$x^2 + y^2 = R^2, \text{ therefore } x = \pm \sqrt{R^2 - y^2}$$

$$\text{Area} = \int_{-R}^R dy \int_{-\sqrt{R^2 - y^2}}^{\sqrt{R^2 - y^2}} dx = \int_{-R}^R 2\sqrt{R^2 - y^2} dy$$

Using the substitution $y = R \sin \zeta$, $dy = R \cos \zeta d\zeta$

$$\text{Area} = \int_{-\pi/2}^{\pi/2} 2\sqrt{R^2 - R^2 \sin^2 \zeta} R \cos \zeta d\zeta = 2 \int_{-\pi/2}^{\pi/2} R^2 \cos^2 \zeta d\zeta$$

Using the identity $\cos^2 \zeta = \frac{1}{2}(1 + \cos 2\zeta)$

$$\text{Area} = 2 \int_{-\pi/2}^{\pi/2} R^2 \frac{1}{2}(1 + \cos 2\zeta) d\zeta = R^2 \left[\zeta + \frac{1}{2} \sin 2\zeta \right] \Big|_{-\pi/2}^{\pi/2} = \pi R^2$$

The three-dimensional system that will be of most importance to us is the atom. Closed shell atoms are spherically symmetric, so that we might expect that atomic wave functions are best described in spherical coordinates. Therefore, you should become familiar with integrations in this coordinate system. In transforming from spherical coordinates r, θ , and ϕ to Cartesian coordinates x, y , and z , we use the following relationships

$$\begin{aligned} x &= r \sin \theta \cos \phi \\ y &= r \sin \theta \sin \phi \\ z &= r \cos \theta \end{aligned} \tag{ME8.1}$$

In transforming from Cartesian coordinates x, y , and z to the spherical coordinates r, θ , and ϕ , the following relationships are used.

$$r = \sqrt{x^2 + y^2 + z^2}, \theta = \cos^{-1} \frac{z}{\sqrt{x^2 + y^2 + z^2}}, \text{ and } \phi = \tan^{-1} \frac{y}{x} \tag{ME8.2}$$

These relationships are depicted in Figure ME8.2.

For small increments in the variables r, θ , and ϕ , the volume element depicted is a rectangular solid of volume

$$dV = (r \sin \theta d\phi) (dr) (rd\theta) = r^2 \sin \theta dr d\theta d\phi \tag{ME8.3}$$

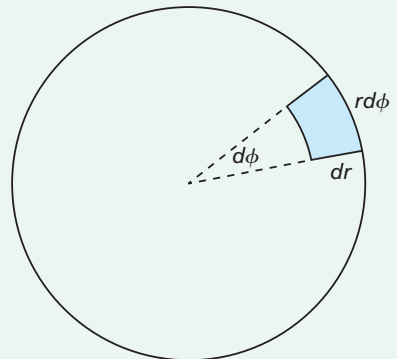
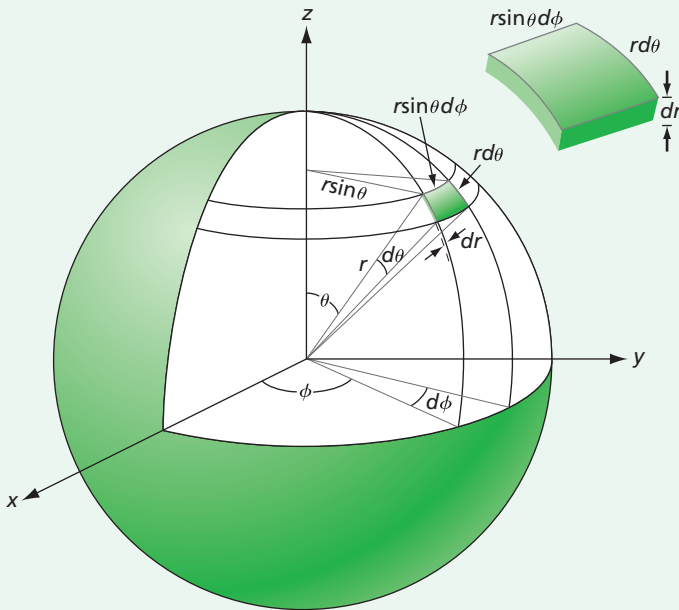


Figure ME8.1

Polar coordinates in which the coordinates are r and ϕ .

Figure ME8.2

Spherical coordinates in which the coordinates are r , θ , and ϕ .



Note in particular that the volume element in spherical coordinates is not $dr d\theta d\phi$ in analogy with the volume element $dxdydz$ in Cartesian coordinates.

What is the appropriate range of variables to integrate over all space in spherical coordinates? If we imagine the radius vector scanning over the range $0 \leq \theta \leq \pi$; $0 \leq \phi \leq 2\pi$, the whole angular space is scanned out. If we combine this range of θ and ϕ with $0 \leq r \leq \infty$, all of the three-dimensional space is scanned out. Note that $r = \sqrt{x^2 + y^2 + z^2}$ is always positive.

To illustrate the process of integration in spherical coordinates, we normalize the function $f(r, \theta) = Ne^{-r} \cos \theta$ over the interval $0 \leq r \leq \infty$; $0 \leq \theta \leq \pi$; $0 \leq \phi \leq 2\pi$

$$N^2 \int_0^{2\pi} d\phi \int_0^\pi \sin \theta d\theta \int_0^\infty (e^{-r} \cos \theta)^2 r^2 dr = N^2 \int_0^{2\pi} d\phi \int_0^\pi \cos^2 \theta \sin \theta d\theta \int_0^\infty r^2 e^{-2r} dr = 1$$

It is most convenient to integrate first over ϕ , giving

$$2\pi N^2 \int_0^\pi \cos^2 \theta \sin \theta d\theta \int_0^\infty r^2 e^{-2r} dr = 1$$

We next integrate over θ , giving

$$2\pi N^2 \left[\frac{-\cos^3 \pi + \cos^3 0}{3} \right] \int_0^\infty r^2 e^{-2r} dr = \frac{4\pi N^2}{3} \int_0^\infty r^2 e^{-2r} dr = 1$$

We finally integrate over r using the standard integral $\int_0^\infty x^n e^{-ax} dx = \frac{n!}{a^{n+1}}$ ($a > 0$, n positive integer). The result is

$$\frac{4\pi N^2}{3} \int_0^\infty r^2 e^{-2r} dr = \frac{4\pi N^2}{3 \times 4} = 1 \quad \text{or} \quad N = \sqrt{\frac{3}{\pi}}$$

We conclude that the normalized wave function is $\sqrt{\frac{3}{\pi}} e^{-r} \cos \theta$.

It is important to keep in mind that $r = \sqrt{x^2 + y^2 + z^2}$ is a function of three variables. Therefore, in normalizing a function such as $f(r) = Ne^{-r}$, the integration must be carried out over all three variables and the interval $0 \leq r \leq \infty$; $0 \leq \theta \leq \pi$; $0 \leq \phi \leq 2\pi$, even though the function does not depend explicitly on θ and ϕ .

A Quantum-Mechanical Model for the Vibration and Rotation of Molecules

WHY is this material important?

A molecule has translational, vibrational, and rotational degrees of freedom. Each of these can be separately described by its own energy spectrum and energy eigenfunctions. As shown in Chapter 4, the particle in the box is a useful model for exploring the translational degree of freedom. In this chapter, quantum-mechanical principles are used to formulate models for the vibration and rotation of a diatomic molecule.

WHAT are the most important concepts and results?

A discussion of classical models for rotation and vibration provides a contrast to quantum-mechanical models. Unlike the classical analogues, the rotation and vibration degrees of freedom are characterized by discrete energy spectra. Because the operators for the three components of angular momentum do not commute, only the magnitude and one component of the angular momentum associated with the angular momentum of a rotating molecule can be known simultaneously and exactly.

WHAT would be helpful for you to review for this chapter?

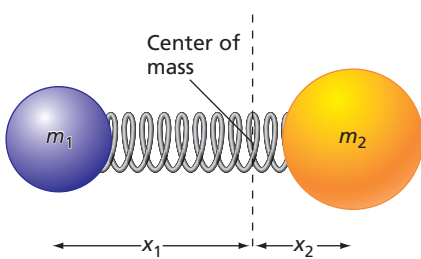
It would be helpful to review the material in Math Essential 7 on vectors and Math Essential 8 on spherical coordinates.

- 7.1 The Classical Harmonic Oscillator
- 7.2 Angular Motion and the Classical Rigid Rotor
- 7.3 The Quantum-Mechanical Harmonic Oscillator
- 7.4 Quantum-Mechanical Rotation in Two Dimensions
- 7.5 Quantum-Mechanical Rotation in Three Dimensions
- 7.6 Quantization of Angular Momentum
- 7.7 Spherical Harmonic Functions
- 7.8 Spatial Quantization

7.1 THE CLASSICAL HARMONIC OSCILLATOR

The particle in the box model that was discussed in Chapter 4 is a good model for the translational degree of freedom for an atom or molecule. In this chapter, we will look at the two further degrees of freedom that are relevant for molecules, namely, vibration and rotation. A good model for the vibration of a diatomic molecule is two masses connected by a spring, which is called a **harmonic oscillator**. In this section, the harmonic oscillator is reviewed from the perspective of classical mechanics. Consider two masses m_1 and m_2 that are connected by a coiled spring. When at rest, the spring is at its equilibrium length. If the masses are pushed together, the spring is compressed, and if the masses are pulled apart, the spring is extended. In each case, the spring resists motion of the masses away from their equilibrium positions. If the deviation of the spacing between the masses from its rest position is denoted by x , then

$$x = [x_{m_1}(t) + x_{m_2}(t)] - [x_{m_1} + x_{m_2}]_{\text{equilibrium}} \quad (7.1)$$

**Figure 7.1**

Two unequal masses connected by a spring of force constant k . The intersection of the vertical line with the spring indicates the center of mass.

Concept

For a harmonic oscillator, the force and displacement are in opposite directions.

Positive and negative values of x correspond to stretching and compression of the spring, respectively, as shown in Figure 7.1. Experimentally, it is found that to double x , the force exerted on the system must be doubled. This means that a linear relationship exists between the force and x given by

$$F = -kx \quad (7.2)$$

In this equation, k is called the **force constant**. The negative sign shows that the force and the displacement are in opposite directions.

Before developing a mathematical model of the harmonic oscillator, it is useful to make a mental image of what happens when the spring is either stretched or compressed and then let go. In either case, the force that the spring exerts on each of the masses will be in the direction opposite that of the applied force. As soon as the spacing of the masses reaches its equilibrium distance, the direction of the force applied by the spring on the masses changes. This causes the direction of motion to reverse; an initial stretch becomes a compression and vice versa. In the absence of dissipative forces, the masses continue through alternate half cycles of being farther apart and closer together than their equilibrium distance. This system exhibits **oscillatory behavior**.

Although the masses move in opposite directions, the magnitudes of their displacements are not equal if their masses are unequal. This makes it difficult to develop a simple picture of the time evolution of this system. However, somewhere between the masses is a point that does not move. This is called the center of mass, and a transformation to **center-of-mass coordinates** gives us a simpler description of the oscillatory motion of the harmonic oscillator.

Before continuing with our discussion, it is useful to summarize what information is needed to describe the harmonic oscillator and what information can be derived using classical mechanics. The oscillator is described by the two masses m_1 and m_2 and the force constant k , which allows the force F acting on each of the masses to be calculated. To solve Newton's second law of motion, two independent pieces of information, such as the value of x and the kinetic energy of the oscillator at a given time, are needed that describe the state of the system at the initial time. From this information, the positions x_1 and x_2 , the velocities v_1 and v_2 , and the kinetic and potential energies of each mass can be determined as a function of time. This is more information than is necessary because we are primarily interested in the potential and kinetic energies associated with the entire oscillator as a unit than with the values for each of the masses separately. This is the main reason for working with the center-of-mass coordinates.

In the center-of-mass coordinates, the physical picture of the system changes from two masses connected by a spring of force constant k to a single mass, called the **reduced mass** μ , connected by a spring of the same force constant to an immovable wall. Why is this transformation used? We do this because only the *relative* motion of these two masses with respect to one another and not their individual motions is of interest. This change of coordinates also reduces the description of the periodic motion to a single coordinate.

The locations of the center of mass x_{cm} and the reduced mass μ are given by the equations

$$x_{cm} = \frac{m_1 x_1 + m_2 x_2}{m_1 + m_2} \quad (7.3)$$

and

$$\mu = \frac{m_1 m_2}{m_1 + m_2} \quad (7.4)$$

We now use Newton's second law of motion to investigate the dynamics of the harmonic oscillator. Because the motion is in one dimension, the scalar magnitude of force and acceleration can be used in what follows. Recall that the variable x denotes the deviation of the spring extension from its equilibrium position. Starting with

$$F = \mu a = \mu \frac{d^2 x}{dt^2} \quad (7.5)$$

where a is the acceleration, and using Equation (7.2) for the force, the differential equation

$$\mu \frac{d^2x}{dt^2} + kx = 0 \quad (7.6)$$

describes the time dependence of the distance between the masses relative to its equilibrium value.

The general solution to this differential equation is

$$x(t) = c_1 e^{+i\sqrt{(k/\mu)t}} + c_2 e^{-i\sqrt{(k/\mu)t}} \quad (7.7)$$

in which c_1 and c_2 are arbitrary coefficients. At this point the *Euler formula*, $re^{\pm i\theta} = r \cos \theta \pm ir \sin \theta$, is used to write Equation (7.7) in the form

$$x(t) = c_1 \left(\cos \sqrt{\frac{k}{\mu}}t + i \sin \sqrt{\frac{k}{\mu}}t \right) + c_2 \left(\cos \sqrt{\frac{k}{\mu}}t - i \sin \sqrt{\frac{k}{\mu}}t \right) \quad (7.8)$$

The last equation can be further simplified to

$$x(t) = b_1 \cos \sqrt{\frac{k}{\mu}}t + b_2 \sin \sqrt{\frac{k}{\mu}}t \quad (7.9)$$

with $b_1 = c_1 + c_2$ and $b_2 = i(c_1 - c_2)$. This is the general solution of the differential equation with no restrictions on b_1 and b_2 . Because the amplitude of oscillation is real, the boundary condition that b_1 and b_2 be real is imposed. The general solution contains two constants of integration that can be determined through the boundary conditions, $x(0)$, and $v(0) = [dx(t)/dt]_{t=0}$. For instance, if $x(0) = 0$ and $v(0) = v_0$, then

$$\begin{aligned} x(0) &= b_1 \cos \left(\sqrt{\frac{k}{\mu}} \times 0 \right) = b_1 = 0 \\ v(0) &= \left(\frac{dx(t)}{dt} \right)_{t=0} = b_2 \sqrt{\frac{k}{\mu}} \cos \left(\sqrt{\frac{k}{\mu}} \times 0 \right) = b_2 \sqrt{\frac{k}{\mu}} \quad \text{and} \\ b_2 &= \sqrt{\frac{\mu}{k}} v_0 \end{aligned} \quad (7.10)$$

The specific solution for these boundary conditions is

$$x(t) = \sqrt{\frac{\mu}{k}} v_0 \sin \sqrt{\frac{k}{\mu}} t \quad (7.11)$$

Note that only the second term in Equation (7.9) remains. This is because we arbitrarily choose $x(0) = 0$ and $v(0) = v_0$. Other boundary conditions could lead to solutions in which both b_1 and b_2 are nonzero.

Because the sine and cosine functions are periodic functions of the variable t , x exhibits oscillatory motion. The period of oscillation T is defined by the relation

$$\sqrt{\frac{k}{\mu}}(t + T) - \sqrt{\frac{k}{\mu}}t = 2\pi \quad (7.12)$$

giving

$$T = 2\pi \sqrt{\frac{\mu}{k}} \quad (7.13)$$

The inverse of T is the frequency v :

$$v = \frac{1}{2\pi} \sqrt{\frac{k}{\mu}} \quad (7.14)$$

These definitions of v and T allow x in Equation (7.9) to be written in the form

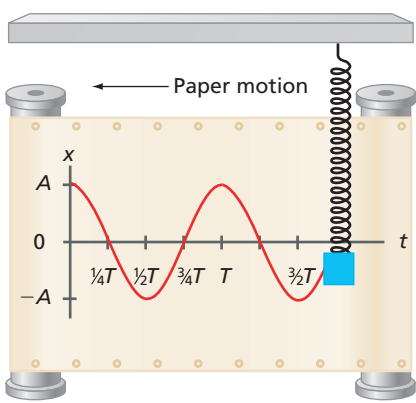
$$x(t) = b_1 \cos 2\pi \frac{t}{T} + b_2 \sin 2\pi \frac{t}{T} \quad (7.15)$$

Concept

Boundary conditions determine the integration constants in solving for $x(t)$.

Concept

The frequency of a harmonic oscillator depends on the force constant and the reduced mass.

**Figure 7.2**

Periodic motion of a harmonic oscillator. The periodic motion of a harmonic oscillator is revealed if the vertical motion is displayed on a moving piece of paper.

Often, the angular frequency, $\omega = 2\pi\nu$, is introduced, giving

$$x(t) = b_1 \cos \omega t + b_2 \sin \omega t, \text{ or equivalently, } x(t) = A \sin(\omega t + \alpha) \quad (7.16)$$

where the phase shift α is explored in Example Problem 7.1. The oscillatory periodic motion of the harmonic oscillator is depicted in Figure 7.2.

With a mathematical description of the motion, our mental picture of the oscillatory behavior can be tested. Because the potential energy $E_{potential}$ and the kinetic energy $E_{kinetic}$ of the oscillator are related to the magnitudes of x and v by the equations

$$E_{potential} = \frac{1}{2}kx^2 \quad \text{and} \quad E_{kinetic} = \frac{1}{2}\mu v^2 \quad (7.17)$$

$E_{potential}$ and $E_{kinetic}$ can be expressed as a function of time, as is done in Example Problem 7.1.

Visualize the harmonic oscillator in terms of the potential and kinetic energies. The energy of a harmonic oscillator at rest can be increased by stretching or compressing the spring. The maximum displacement from the equilibrium position depends on the force constant and the amount of energy taken up. The kinetic and potential energies also oscillate with time. As the amount of injected energy increases, the maximum amplitude of vibration and maximum velocity of the harmonic oscillator increases. Because there are no constraints on what value of the energy is allowed, the classical harmonic oscillator has a **continuous energy spectrum**.

EXAMPLE PROBLEM 7.1

For a harmonic oscillator described by $x(t) = A \sin(\omega t + \alpha)$, $\omega = (k/\mu)^{1/2}$, answer the following questions.

- What are the units of A ? What role does α have in this equation?
- Graph the kinetic and potential energies given by the following equations as a function of time:

$$E_{kinetic} = \frac{1}{2}mv^2 \quad \text{and} \quad E_{potential} = \frac{1}{2}kx^2$$

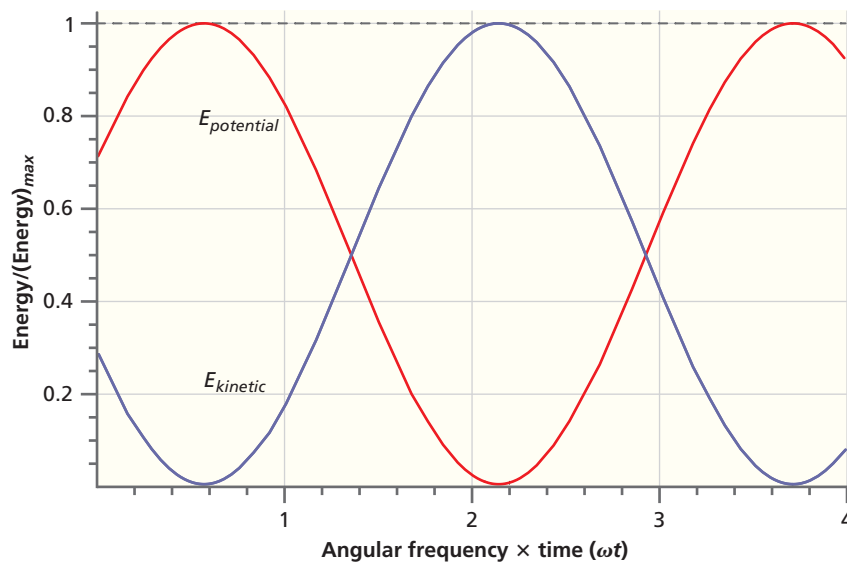
- Show that the sum of the kinetic and potential energies is independent of time.

Solution

- Because $x(t)$ has the units of length and the sine function is dimensionless, A must have the units of length. The quantity α sets the value of x at $t = 0$, because $x(0) = A \sin(\alpha)$.
- We begin by expressing the kinetic and potential energies in terms of $x(t)$:

$$\begin{aligned} E_{kinetic} &= \frac{1}{2}\mu v^2 = \frac{1}{2}\mu \left(\frac{dx}{dt} \right)^2 \\ &= \frac{\mu}{2} (A\omega \cos(\omega t + \alpha))^2 \\ &= \frac{1}{2}\mu\omega^2 A^2 \cos^2(\omega t + \alpha) \\ E_{potential} &= \frac{1}{2}kx^2 = \frac{1}{2}k A^2 \sin^2(\omega t + \alpha) \\ &= \frac{1}{2}\mu\omega^2 A^2 \sin^2(\omega t + \alpha) \text{ because } \omega = \sqrt{\frac{k}{\mu}} \text{ and } k = \mu\omega^2 \end{aligned}$$

In the following figure, the energy is expressed in increments of $(1/2)\mu\omega^2 A^2$, and we have arbitrarily chosen $\alpha = \pi/6$. Note that the kinetic and potential energies are out of phase. Why is this the case?



- c. The dashed line in the preceding figure is the sum of the kinetic and potential energies, which is a constant. This can be verified algebraically by adding the expressions for E_{kinetic} and $E_{\text{potential}}$:

$$\begin{aligned} E_{\text{total}} &= \frac{1}{2}\mu\omega^2 A^2 \cos^2(\omega t + \alpha) + \frac{1}{2}\mu\omega^2 A^2 \sin^2(\omega t + \alpha) \\ &= \frac{1}{2}\mu\omega^2 A^2 [\cos^2(\omega t + \alpha) + \sin^2(\omega t + \alpha)] \\ &= \frac{1}{2}\mu\omega^2 A^2 \end{aligned}$$

Note that the sum of the kinetic and potential energies is independent of time, as must be the case, because no energy is added to the system after the initial stretching of the spring and there is no mechanism such as frictional forces for losing energy.

Concept

In the absence of frictional forces, the energy of a harmonic oscillator is constant in time.

7.2 ANGULAR MOTION AND THE CLASSICAL RIGID ROTOR

The harmonic oscillator is a good example of linear motion. In this system, the vectors for the velocity, momentum, and acceleration are all parallel to the direction of motion. Next, we will discuss rotational motion. Why is rotational motion of interest to chemists? Energy can be taken up by a molecule in any of several ways. The first of these is translational kinetic energy, which is associated with the collective motion of all atoms in the molecule. A second way to store energy, in the form of vibrational energy, was just discussed. Now set the molecule spinning in addition to having it vibrate and undergo translational motion. Additional energy is taken up in this rotational motion. The **rigid rotor** is defined as a three-dimensional rigid object rotating about an axis. It is a good model for thinking about rotation of a diatomic molecule. The term *rigid* stems from the assumption that the rotational motion does not result in a stretching of the bond.

Consider the rigid rotor shown in Figure 7.3. The axis of rotation is perpendicular to the plane of rotation and passes through the center of mass. The distances of the individual masses from the center of mass are indicated. As for the harmonic oscillator, it is convenient to view the motion of the rigid rotor in the center-of-mass coordinates because only the relative motion of the two masses is of interest. In these coordinates,

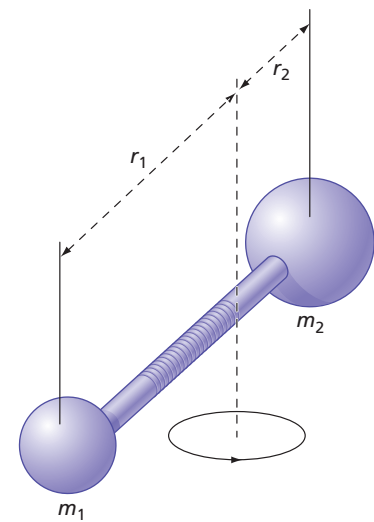
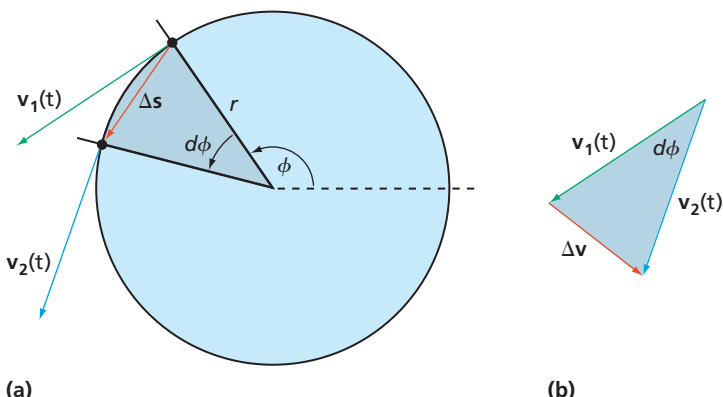


Figure 7.3

Sketch of a rigid rotor. A rigid rotor consisting of two masses is separated by a fixed distance. The dashed vertical line is the axis of rotation and is perpendicular to the plane of rotation and passes through the center of mass.

Figure 7.4

Rigid rotor in center-of-mass coordinates. (a) The rigid rotor in the center-of-mass coordinates is a single particle of reduced mass μ rotating on a circular ring of radius r equal to the bond length. The position and velocity of the reduced mass μ are shown at time t_1 and $t_2 = t_1 + dt$. (b) Vector diagram of \mathbf{v}_1 , \mathbf{v}_2 , and $\Delta\mathbf{v}$ from Figure 7.4a.



the rotor is equivalent to a single mass $\mu = (m_1 m_2)/(m_1 + m_2)$ moving on a circular ring at a distance from a fixed axis equal to the bond length, as shown in Figure 7.4a.

In the rotating system under consideration, no force opposes the rotation. For this reason, potential energy cannot be stored in the motion of the rigid rotor. All energy put into the rigid rotor is kinetic energy that, in the absence of dissipative losses, will be retained indefinitely.

Next, let us discuss the observables that characterize the classical rigid rotor. The force, momentum, velocity, and acceleration vectors have two components that could be chosen to lie along the x and y axes of a fixed coordinate system. However, because of the cylindrical symmetry of the rotation, it is more convenient to consider the two components along the tangential and radial directions. (Math Essential 7 provides additional discussion of vectors.) Because no acceleration occurs along the tangential direction, the magnitude of the velocity is constant in time, $|\mathbf{v}_2| = |\mathbf{v}_1| = |\mathbf{v}|$. However, Figure 7.4b shows that $\Delta\mathbf{v} = \mathbf{v}_2 - \mathbf{v}_1$ is not zero because the direction of the velocity vector changes as the reduced mass rotates on the ring. Because the acceleration is given by $\mathbf{a} = \lim_{\Delta t \rightarrow 0} (\mathbf{v}_2 - \mathbf{v}_1)/\Delta t$, the acceleration is not zero for circular motion.

As can be seen in Figure 7.4b, in the limit that $\Delta t \rightarrow 0$, \mathbf{a} and \mathbf{v} are perpendicular and only the radial component of the acceleration is nonzero. This component is called the **centripetal acceleration** $a_{\text{centripetal}}$.

We calculate $a_{\text{centripetal}}$ realizing that because the angles in the two shaded triangles in Figure 7.4 are the same and the sides are in the same proportion, the two triangles are similar. Therefore

$$\frac{|\Delta\mathbf{v}|}{|\mathbf{v}|} = \frac{|\Delta\mathbf{s}|}{r} \quad \text{or} \quad |\Delta\mathbf{v}| = \frac{|\mathbf{v}|}{r} |\Delta\mathbf{s}| \quad (7.18)$$

The magnitude of the average acceleration is therefore given by

$$|\mathbf{a}_{\text{average}}| = \frac{|\Delta\mathbf{v}|}{\Delta t} = \frac{|\mathbf{v}|}{r} \frac{|\Delta\mathbf{s}|}{\Delta t} \quad (7.19)$$

The instantaneous acceleration is given by

$$|\mathbf{a}_{\text{centripetal}}| = \lim_{\Delta t \rightarrow 0} \frac{|\mathbf{v}|}{r} \frac{|\Delta\mathbf{s}|}{\Delta t} = \frac{|\mathbf{v}|}{r} \lim_{\Delta t \rightarrow 0} \frac{|\Delta\mathbf{s}|}{\Delta t} = \frac{|\mathbf{v}|^2}{r} \quad (7.20)$$

because $\lim_{\Delta t \rightarrow 0} \frac{|\Delta\mathbf{s}|}{\Delta t} = |\mathbf{v}|$.

In circular motion, the total accumulated rotation angle ϕ is analogous to the distance variable in linear motion. The angle is typically measured in **radians**. A radian is the angle for which the arc length is equal to the radius; radians are related to degrees by 2π radians = 360° or one radian $\approx 57.3^\circ$. **Angular velocity** ω and **angular acceleration** α , which are analogous to \mathbf{v} and \mathbf{a} in linear motion, are defined by

$$|\boldsymbol{\omega}| = \frac{d\phi}{dt} \quad \text{and} \quad \alpha = \frac{d|\boldsymbol{\omega}|}{dt} = \frac{d^2\phi}{dt^2} \quad (7.21)$$

Concept

A rigid rotor continually undergoes accelerated motion.

The directions of both ω and α are determined by the right-hand rule and point along the axis of rotation. The application of the right-hand rule in determining the direction of ω is illustrated in Figure 7.5. Keep in mind that ω is a vector perpendicular to the plane of rotation. Because the velocity is also defined by the expression

$$\mathbf{v} = \frac{\Delta \mathbf{s}}{\Delta t} = \frac{\mathbf{r} \Delta \phi}{\Delta t} \quad \text{in the limit as } \Delta t \rightarrow 0, |\mathbf{v}| = \left| \frac{\mathbf{r} d\phi}{dt} \right| = r\omega \quad (7.22)$$

the magnitudes of the angular and linear velocities can be related. The vector \mathbf{r} spans the distance from the rotation axis to the reduced mass and lies in the plane of rotation. In the case under consideration, the acceleration along the direction of motion is zero, and the expression for $d\phi/dt$ in Equation (7.21) can be integrated to obtain

$$\phi = \phi_0 + \omega t \quad (7.23)$$

The kinetic energy can be expressed in the form

$$E_{kinetic} = \frac{1}{2}\mu\mathbf{v}^2 = \frac{1}{2}\mu\mathbf{r}^2\omega^2 = \frac{1}{2}I\omega^2 \quad (7.24)$$

The quantity μr^2 is called the **moment of inertia** and given the symbol I . With this definition, the kinetic energy takes on a form similar to that in linear motion with the moment of inertia and the angular velocity taking on the role of the mass and linear velocity.

Next, we will develop a relationship for angular motion similar to that for linear motion, where $\mathbf{F} = m\mathbf{a} = d\mathbf{p}/dt$. The **angular momentum**, \mathbf{l} , is defined by

$$\mathbf{l} = \mathbf{r} \times \mathbf{p} \quad (7.25)$$

in which \mathbf{p} is the linear momentum and \times indicates the vector cross product between \mathbf{r} and \mathbf{p} . Use of the right-hand rule to determine the orientation of \mathbf{l} relative to \mathbf{r} and \mathbf{p} is shown in Figure 7.6.

The magnitude of \mathbf{l} is given by

$$l = pr \sin \phi = \mu vr \sin \phi \quad (7.26)$$

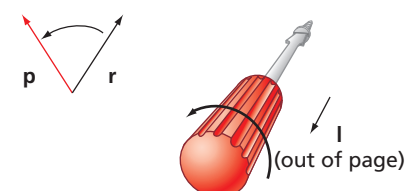
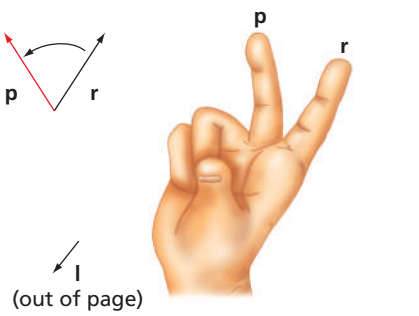
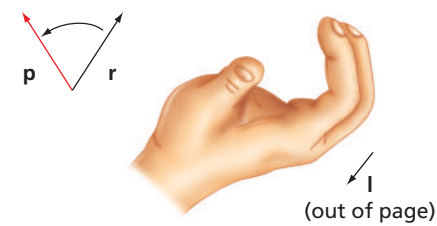
in which ϕ is the angle between the vectors \mathbf{r} and \mathbf{p} . For circular motion, \mathbf{r} and \mathbf{p} are perpendicular so that $l = \mu vr$. The equation $E = p^2/2m$ and the definition of angular momentum can be used to express the kinetic energy in terms of l :

$$E = \frac{p^2}{2\mu} = \frac{l^2}{2\mu r^2} = \frac{l^2}{2I} \quad (7.27)$$

Classical mechanics does not place any restrictions on the direction or magnitude of \mathbf{l} . As for any observable in a classical system, the magnitude of \mathbf{l} can change by an incrementally small amount. Therefore, any amount of energy can be stored in the rigid rotor, and an increase in the energy appears as an increase in the angular frequency. Because the amount of energy can be increased by an infinitesimally small amount, the classical rigid rotor has a continuous energy spectrum, just like the classical harmonic oscillator.



Figure 7.5
Use of the right-hand rule to determine the direction of the angular velocity vector.

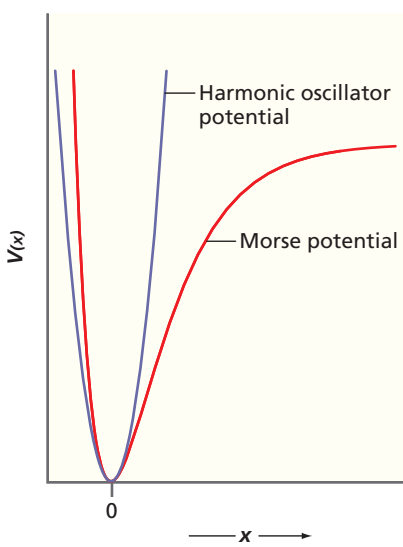


Right hand rule depicted using screwdriver as analogy

7.3 THE QUANTUM-MECHANICAL HARMONIC OSCILLATOR

In this and the next two sections, we will develop quantum-mechanical models for the harmonic oscillator and rigid rotor. The free particle and the particle in the box discussed in Chapters 4 and 5 were useful for understanding how translational motion in various potentials is described in the context of wave-particle duality. In applying quantum mechanics to molecules, two other types of motion that molecules can undergo require discussion: vibration and rotation. The energy needed to stretch the chemical bond can be described by a simple potential function such as that shown

Figure 7.6
Use of the right-hand rule to determine the cross product between two vectors.

**Figure 7.7**

Potential energy $V(x)$ as a function of the displacement x from the equilibrium bond length for a diatomic molecule. The zero of energy is chosen to be the bottom of the potential. The red curve depicts a realistic potential in which the molecule dissociates for large values of x . The purple curve shows a harmonic potential, $V(x) = (1/2)kx^2$, which is a good approximation to the realistic potential near the bottom of the well.

in Figure 7.7. The existence of a stable chemical bond implies that a minimum energy exists at the equilibrium bond length. The position of atoms in a molecule is dynamic rather than static. Think of the chemical bond as a spring rather than a rigid bar connecting the two atoms. Thermal energy increases the vibrational amplitude of the atoms about their equilibrium positions but does not change the vibrational frequency to a good approximation. The potential becomes steeply repulsive at short distances as the electron clouds of the atoms interpenetrate. It levels out at large distances because the overlap of electrons between the atoms required for chemical bond formation falls to zero.

The exact form of $V(x)$ as a function of x depends on the molecule under consideration. However, as will be shown in Chapter 8, only the lowest few vibrational energy levels are occupied for most molecules for $T \sim 300$ K. Therefore, it is a good approximation to say that the functional form of the potential energy near the equilibrium bond length can be approximated by the harmonic potential

$$V(x) = \frac{1}{2}kx^2 \quad (7.28)$$

In Equation (7.28), k is the force constant. For weakly bound molecules or high temperatures, the more realistic Morse potential (red curve in Figure 7.7) discussed in Section 8.3 should be used.

We expect the wave particle of mass μ vibrating around its equilibrium distance to be described by a set of wave functions $\psi_n(x)$. To find these wave functions and the corresponding allowed vibrational energies, the Schrödinger equation with the appropriate potential energy function must be solved:

$$-\frac{\hbar^2}{2\mu} \frac{d^2\psi_n(x)}{dx^2} + \frac{kx^2}{2}\psi_n(x) = E_n\psi_n(x) \quad (7.29)$$

The solution of this second-order differential equation was well known in the mathematical literature from other contexts well before the development of quantum mechanics. We simply state that the normalized wave functions are

$$\psi_n(x) = A_n H_n(\alpha^{1/2} x) e^{-\alpha x^2/2}, \text{ for } n = 0, 1, 2, \dots \quad (7.30)$$

The solution is written in this manner because the set of functions $H_n(\alpha^{1/2} x)$ is well established in mathematics and are known as **Hermite polynomials**. The first few eigenfunctions $\psi_n(x)$ are given by

$$\begin{aligned} \psi_0(x) &= \left(\frac{\alpha}{\pi}\right)^{1/4} e^{-(1/2)\alpha x^2} \\ \psi_1(x) &= \left(\frac{4\alpha^3}{\pi}\right)^{1/4} x e^{-(1/2)\alpha x^2} \\ \psi_2(x) &= \left(\frac{\alpha}{4\pi}\right)^{1/4} (2\alpha x^2 - 1) e^{-(1/2)\alpha x^2} \\ \psi_3(x) &= \left(\frac{\alpha^3}{9\pi}\right)^{1/4} (2\alpha x^3 - 3x) e^{-(1/2)\alpha x^2} \end{aligned} \quad (7.31)$$

A harmonic potential is a good approximation for a vibrating diatomic molecule for small vibrational energies.

Concept

$\psi_0, \psi_2, \psi_4, \dots$ are even functions of x , [$\psi(x) = \psi(-x)$], whereas $\psi_1, \psi_3, \psi_5, \dots$ are odd functions of x [$\psi(x) = -\psi(-x)$]. It is shown in Example Problem 7.2 that these functions are solutions of the Schrödinger equation and in Example Problem 7.3 that they are not solutions of the kinetic energy operator.

EXAMPLE PROBLEM 7.2

Show that the function $e^{-\beta x^2}$ satisfies the Schrödinger equation for the quantum harmonic oscillator. What conditions does this place on β ? What is E ?

Solution

$$\begin{aligned} -\frac{\hbar^2}{2\mu} \frac{d^2\psi_n(x)}{dx^2} + V(x)\psi_n(x) &= E_n\psi_n(x) \\ -\frac{\hbar^2}{2\mu} \frac{d^2(e^{-\beta x^2})}{dx^2} + V(x)(e^{-\beta x^2}) &= -\frac{\hbar^2}{2\mu} \frac{d(-2\beta xe^{-\beta x^2})}{dx} + \frac{1}{2}kx^2(e^{-\beta x^2}) \\ &= -\frac{\hbar^2}{2\mu}(-2\beta e^{-\beta x^2}) + \frac{\hbar^2}{2\mu}(-4\beta^2 x^2 e^{-\beta x^2}) \\ &\quad + \frac{1}{2}kx^2(e^{-\beta x^2}) \end{aligned}$$

The function is an eigenfunction of the total energy operator only if the last two terms cancel:

$$\hat{H}_{total} e^{-\beta x^2} = \frac{\hbar^2 \beta}{\mu} e^{-\beta x^2} \text{ if } \beta^2 = \frac{1}{4} \frac{k\mu}{\hbar^2}$$

$$\text{Finally, } E = \frac{\hbar^2 \beta}{\mu} = \frac{\hbar^2}{\mu} \sqrt{\frac{1}{4} \frac{k\mu}{\hbar^2}} = \frac{\hbar}{2} \sqrt{\frac{k}{\mu}}$$


In the preceding equation, several constants have been combined to give $\alpha = \sqrt{k\mu/\hbar^2}$, and the normalization constant A_n is given by

$$A_n = \frac{1}{\sqrt{2^n n!}} \left(\frac{\alpha}{\pi} \right)^{1/4} \quad (7.32)$$

A necessary boundary condition is that the amplitude of the wave functions remains finite at large values of x . As for the particle in the box, this boundary condition gives rise to quantization. It can be shown that the amplitude of the wave functions approaches zero for large x values only if the following condition is met:

$$E_n = \hbar \sqrt{\frac{k}{\mu}} \left(n + \frac{1}{2} \right) = \hbar v \left(n + \frac{1}{2} \right) \text{ with } n = 0, 1, 2, 3, \dots \quad (7.33)$$

For a more detailed discussion of the solution of the Schrödinger equation for the quantum harmonic oscillator, see the reference to Levine (2014) in Further Reading.

Once again, we see that the imposition of boundary conditions has led to a discrete energy spectrum. Unlike the classical analogue, the energy stored in the quantum-mechanical harmonic oscillator can only take on discrete values. As for the particle in the box, the lowest state accessible to the system still has an energy greater than zero, referred to as a *zero point energy*. The **frequency of oscillation** is given by

$$v = \frac{1}{2\pi} \sqrt{\frac{k}{\mu}} \quad (7.34)$$

just as for the classical harmonic oscillator.

Connection

Dependence of the frequency of vibration for a quantum harmonic oscillator on k and μ is identical to that for a classical harmonic oscillator.

EXAMPLE PROBLEM 7.3

- Is $\psi_1(x) = (4\alpha^3/\pi)^{1/4} x e^{-(1/2)\alpha x^2}$ an eigenfunction of the kinetic energy operator? Is it an eigenfunction of the potential energy operator?
- What are the average values of the kinetic and potential energies for a quantum-mechanical oscillator in this state?

Solution

- As discussed in Chapter 6, neither the potential energy operator nor the kinetic energy operator commutes with the total energy operator. Therefore, because $\psi_1(x) = (4\alpha^3/\pi)^{1/4} x e^{-(1/2)\alpha x^2}$ is an eigenfunction of the total energy operator, it is not an eigenfunction of the potential or kinetic energy operators.

- b.** The fourth postulate states how the average value of an observable can be calculated. Because

$$\hat{E}_{\text{potential}}(x) = V(x) \quad \text{and} \quad \hat{E}_{\text{kinetic}}(x) = -\frac{\hbar^2}{2\mu} \frac{d^2}{dx^2}$$

then

$$\begin{aligned}\langle E_{\text{potential}} \rangle &= \int \psi_1^*(x) V(x) \psi_1(x) dx \\ &= \int_{-\infty}^{\infty} \left(\frac{4\alpha^3}{\pi}\right)^{1/4} x e^{-(1/2)\alpha x^2} \left(\frac{1}{2} k x^2\right) \left(\frac{4\alpha^3}{\pi}\right)^{1/4} x e^{-(1/2)\alpha x^2} dx \\ &= \frac{1}{2} k \left(\frac{4\alpha^3}{\pi}\right)^{1/2} \int_{-\infty}^{\infty} x^4 e^{-\alpha x^2} dx = k \left(\frac{4\alpha^3}{\pi}\right)^{1/2} \int_0^{\infty} x^4 e^{-\alpha x^2} dx\end{aligned}$$

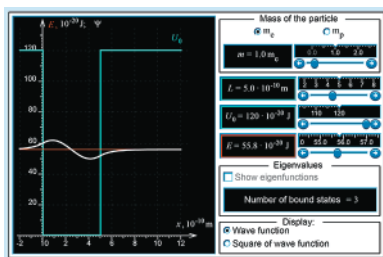
The limits can be changed as indicated in the last integral because the integrand is an even function of x . To obtain the solution, the following standard integral found in the Math Essential 2 is used:

$$\int_0^{\infty} x^{2n} e^{-ax^2} dx = \frac{1 \times 3 \times 5 \cdots (2n-1)}{2^{n+1} a^n} \sqrt{\frac{\pi}{a}}$$

The calculated values for the average potential and kinetic energy are

$$\begin{aligned}\langle E_{\text{potential}} \rangle &= \frac{1}{2} k \left(\frac{4\alpha^3}{\pi}\right)^{1/2} \left(\sqrt{\frac{\pi}{\alpha}}\right) \frac{3}{4\alpha^2} \\ &= \frac{3k}{4\alpha} = \frac{3}{4} \hbar \sqrt{\frac{k}{\mu}}\end{aligned}$$

$$\begin{aligned}\langle E_{\text{kinetic}} \rangle &= \int \psi_1^*(x) \left(-\frac{\hbar^2}{2\mu} \frac{d^2}{dx^2}\right) \psi_1(x) dx \\ &= \int_{-\infty}^{\infty} \left(\frac{4\alpha^3}{\pi}\right)^{1/4} x e^{-(1/2)\alpha x^2} \left(-\frac{\hbar^2}{2\mu} \frac{d^2}{dx^2}\right) \left(\frac{4\alpha^3}{\pi}\right)^{1/4} x e^{-(1/2)\alpha x^2} dx \\ &= -\frac{\hbar^2}{2\mu} \left(\frac{4\alpha^3}{\pi}\right)^{1/2} \int_{-\infty}^{\infty} (\alpha^2 x^4 - 3\alpha x^2) e^{-\alpha x^2} dx \\ &= -\frac{\hbar^2}{\mu} \left(\frac{4\alpha^3}{\pi}\right)^{1/2} \int_0^{\infty} (\alpha^2 x^4 - 3\alpha x^2) e^{-\alpha x^2} dx \\ &= -\frac{\hbar^2}{\mu} \left(\frac{4\alpha^3}{\pi}\right)^{1/2} \left(\alpha^2 \left[\sqrt{\frac{\pi}{\alpha}} \frac{3}{4\alpha^2}\right] - 3\alpha \left[\sqrt{\frac{\pi}{\alpha}} \frac{1}{2\alpha}\right]\right) \\ &= \frac{3}{4} \frac{\hbar^2 \alpha}{\mu} = \frac{3}{4} \hbar \sqrt{\frac{k}{\mu}}\end{aligned}$$

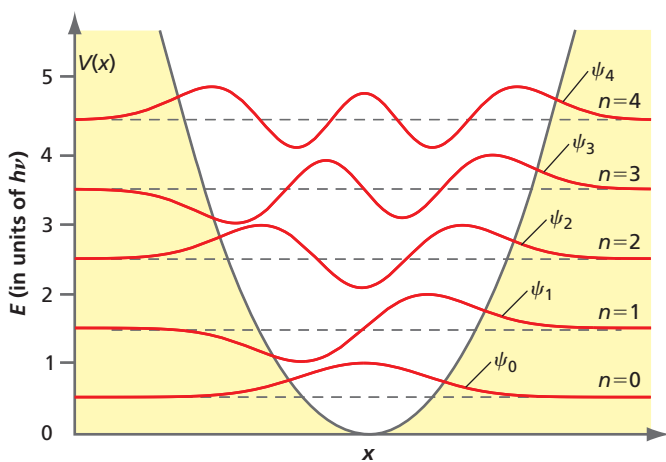


W7.1 Energy levels for the quantum harmonic oscillator

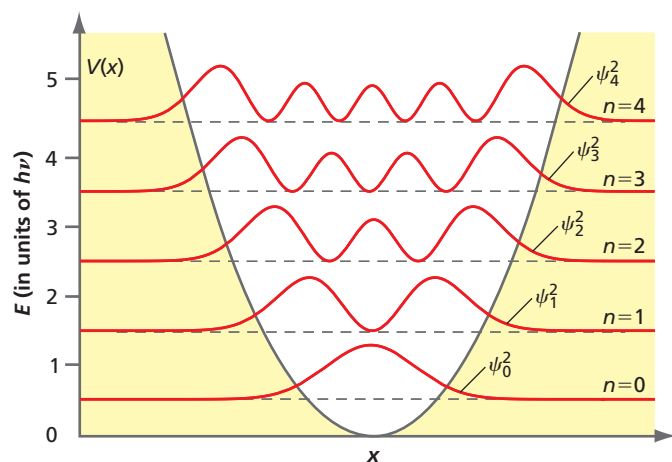


Note that just as for the classical harmonic oscillator discussed in Section 7.1, the average values of the kinetic and potential energies are equal. When the kinetic energy has its maximum value, the potential energy is zero and vice versa. In general, we find that for the n th state,

$$\langle E_{\text{kinetic},n} \rangle = \langle E_{\text{potential},n} \rangle = \frac{\hbar}{2} \sqrt{\frac{k}{\mu}} \left(n + \frac{1}{2}\right)$$

**Figure 7.8**

The first few eigenfunctions of the quantum-mechanical harmonic oscillator shown with the potential function. The amplitude of the corresponding eigenfunction is shown superimposed on each energy level, with the zero of amplitude for the eigenfunctions indicated by the dashed lines. The yellow area indicates the classically forbidden region for which $E < V$.

**Figure 7.9**

The square of the first few eigenfunctions of the quantum-mechanical harmonic oscillator (the probability density) superimposed on the energy spectrum shown with the potential function. The yellow area indicates the classically forbidden region.

As was done for the particle in the box, it is useful to plot $\psi(x)$ and $\psi^2(x)$ against x . These plots are shown superimposed on the potential energy function in Figures 7.8 and 7.9.

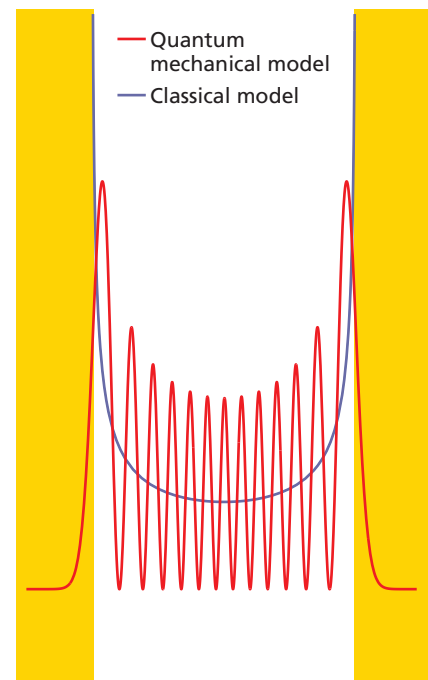
It is instructive to compare the quantum mechanical with the classical results. In quantum mechanics the value of x cannot be known if the system is in an eigenstate of the total energy operator because these two operators do not commute. This issue arose earlier in considering the particle in the box. What can one say about x , the amplitude of the vibration?

Only the probability of the vibrational amplitude having a particular value of x within an interval dx can be calculated, and this probability is given by $\psi^2(x) dx$. For the classical harmonic oscillator, the probability of the vibrational amplitude having a particular value of x within the interval dx can also be calculated. Because the probability density varies inversely with the velocity, the maximum values are found at the turning points and its minimum value is found at $x = 0$. To visualize this behavior, imagine a frictionless ball rolling on a parabolic track under the influence of gravity. The ball moves fastest at the lowest point on the track and stops momentarily as it reverses its direction at the highest points on either side of the track. Figure 7.10 shows a comparison of $\psi_{12}^2(x)$ and the probability density of finding a particular amplitude for a classical oscillator with the same total energy as a function of x . A large quantum number has been used for comparison because in the limit of high energies (very large quantum numbers), classical and quantum mechanics give the same result as required by the correspondence principle.

The main difference between the classical and quantum-mechanical results is the behavior in the classically forbidden region and for the oscillations in $\psi_{12}^2(x)$, which are absent in the classical result. In calculating the probability of finding the value x for the oscillation amplitude in the interval Δx , it is necessary to evaluate

$$\int_{-\Delta x/2}^{\Delta x/2} \psi^2(x) dx \quad (7.35)$$

rather than the probability density $\psi^2(x)$. For large quantum numbers, Δx is large in comparison to the distance between neighboring oscillations in $\psi^2(x)$. Therefore, the oscillations in the probability density $\psi^2(x)$ are averaged out in performing the integration, so that the quantum and classical results agree well if the finite resolution of the measurement is taken into account. The argument is the same as that used in calculating the results for the particle in the box shown in Figure 4.4.

**Figure 7.10**

Calculated probability density for the vibrational amplitude for the 12th eigenstate of the quantum-mechanical oscillator. The quantum-mechanical oscillator result is shown by the red curve, and the classical result is shown by the purple curve. The yellow areas indicate the classically forbidden region.

Concept

The most probable amplitudes of vibration for classical and quantum harmonic oscillators correspond to the turning points.

We have been working with the time-independent Schrödinger equation, whose eigenfunctions allow the probability density to be calculated. To describe the time dependence of the oscillation amplitude, the total wave function, $\psi_n(x, t) = e^{-i\omega t}\psi_n(x)$, is constructed. The spatial amplitude shown in Figure 7.8 is modulated by the factor $e^{-i\omega t}$, which has a frequency given by $\omega = \sqrt{k/\mu}$. Because $\psi_n(x, t)$ is a standing wave, the nodal positions shown in Figures 7.8 and 7.9 do not move with time.

In looking at Figures 7.8 and 7.9, several similarities are seen with Figures 4.2 and 4.3, in which the equivalent results were shown for the particle in the box. The eigenfunctions are again standing waves, but they are now in a box with a more complicated shape. Successive eigenfunctions add one more oscillation within the “box,” and the amplitude of the wave function is small at the edge of the “box.” The reason why it is small rather than zero follows the same lines as the discussion of the particle in the finite depth box in Chapter 5. The quantum-mechanical harmonic oscillator also has a zero point energy, meaning that the lowest possible energy state still has vibrational energy. The origin of this zero point energy is similar to that for the particle in the box. By attaching a spring to the particle, its motion has been constrained. As the spring is made stiffer (larger k), the particle is more constrained and the zero point energy increases. This is the same trend observed for the particle in the box as the length is decreased.

Note, however, that important differences exist in the two systems that are a result of the more complicated shape of the harmonic oscillator “box.” Although the harmonic oscillator wave functions show oscillatory behavior, they are no longer represented by simple sine functions because the classical probability density is greatest at the classical turning points. The energy spacing is the same between adjacent energy levels; that is, it does not increase with the quantum number, as was the case for the particle in the box. These differences show the sensitivity of the eigenfunctions and eigenvalues to the functional form of the potential.

7.4 QUANTUM-MECHANICAL ROTATION IN TWO DIMENSIONS

Quantum-mechanical models were developed for translation in Chapter 4 and for vibration in Section 7.3. We now consider rotation to complete the description of the fundamental types of motion available to a molecule. To a good approximation, the three types of motion—translation, vibration, and rotation—can be dealt with independently. This treatment is exact rather than approximate if the following conditions are met: (1) if the translational part of the total energy operator depends only on the translational coordinates of the center of mass, (2) if the rotational part depends only on the angular coordinates of the center of mass, and (3) if the vibrational part depends only on the internal coordinates of the molecule. This condition cannot be exactly satisfied for real molecules because the types of motion are not totally decoupled. For example, the average bond length of a rapidly rotating molecule is slightly longer than for a molecule that is not rotating because of the centrifugal forces acting on the atoms. However, although the coupling between the types of motion can be measured using sensitive spectroscopic techniques, it is small for most molecules.

Neglecting this coupling, the total energy operator can be written as a sum of individual operators for the types of motion for the molecule:

$$\hat{H}_{total} = \hat{H}_{trans}(r_{cm}) + \hat{H}_{vib}(\tau_{internal}) + \hat{H}_{rot}(\theta_{cm}, \phi_{cm}) \quad (7.36)$$

In this equation, r_{cm} , θ_{cm} , and ϕ_{cm} refer to the spatial coordinates of the center of mass in spherical coordinates (see Math Essential 8). The symbol $\tau_{internal}$ refers collectively to the vibrational amplitudes of all atoms in the molecule around their equilibrium position. Because different variables appear in $\hat{H}_{trans}(r_{cm})$, $\hat{H}_{vib}(\tau_{internal})$, and $\hat{H}_{rot}(\theta_{cm}, \phi_{cm})$, it is possible to solve the Schrödinger equation for each type of motion separately. In this approximation, the total energy is given by the sum of the individual contributions,

$$E_{total} = E_{trans}(r_{cm}) + E_{vib}(\tau_{internal}) + E_{rot}(\theta_{cm}, \phi_{cm}) \quad (7.37)$$

and the system wave function is a product of the eigenfunctions for the three types of motion:

$$\psi_{total} = \psi_{trans}(r_{cm})\psi_{vib}(\tau_{internal})\psi_{rot}(\theta_{cm}, \phi_{cm}) \quad (7.38)$$

Because the wave function is a product of individual terms that depend on different variables, what has been accomplished in Equations (7.37) and (7.38) is a **separation of variables**.

Whereas for a diatomic molecule, translation can be considered in one to three independent dimensions and vibration in one dimension, rotation requires at least a two-dimensional description. We restrict our considerations to diatomic molecules because the motion is easy to visualize. However, the process outlined next can be generalized to any molecule if several angular coordinates are included. Rotation in a two-dimensional space is discussed first because the mathematical formalism needed to describe such a problem is less complicated. The formalism is extended in Section 7.5 to rotation in three dimensions.

Rotation in two dimensions occurs only in a constrained geometry. An example is a molecule adsorbed on a smooth surface. Consider a diatomic molecule with masses m_1 and m_2 and a fixed bond length r_0 freely rotating in the xy plane. Because the bond length is assumed to remain constant as the molecule rotates, this model is often referred to as the rigid rotor. By transforming to the center-of-mass coordinate system, this problem becomes equivalent to a single reduced mass $\mu = (m_1 m_2)/(m_1 + m_2)$ rotating in the xy plane on a ring of radius r_0 , just as for the classical rigid rotor. It is shown in Example Problem 7.4 how to calculate the center of mass in a diatomic molecule.

EXAMPLE PROBLEM 7.4

The bond length for H^{19}F is 91.68×10^{-12} m. Where does the axis of rotation intersect the molecular axis?

Solution

The position of the center of mass is given by $x_{cm} = (m_H x_H + m_F x_F)/(m_H + m_F)$. We choose the origin of our coordinate system to be at the F atom, so $x_F = 0$ and $x_H = 91.68 \times 10^{-12}$ m. Substituting $m_F = 18.9984$ amu and $m_H = 1.008$ amu, we find that $x_{cm} = 4.62 \times 10^{-12}$ m. Therefore, $x_F = 4.62 \times 10^{-12}$ m and $x_H = 87.06 \times 10^{-12}$ m. We see that the axis of rotation is very close to the F atom. This effect is even more pronounced for HI or HCl.

Because it has been assumed that the particle experiences no hindrance to rotation, the potential energy is constant everywhere. Therefore, we can conveniently set $V(x, y) = 0$ everywhere without affecting the eigenfunctions of the total energy operator. The Schrödinger equation in Cartesian coordinates for this problem is

$$-\frac{\hbar^2}{2\mu} \left(\frac{\partial^2 \psi(x, y)}{\partial x^2} + \frac{\partial^2 \psi(x, y)}{\partial y^2} \right)_{r=r_0} = E\psi(x, y) \quad (7.39)$$

The subscript after the bracket makes it clear that the radius is constant. Although Equation (7.39) is correct, it is always best to choose a coordinate system that reflects the symmetry of the system being considered. In this case, two-dimensional polar coordinates with the variables r and ϕ are the logical choice. In these coordinates, with r fixed at r_0 , the operator $(\partial^2/\partial x^2) + (\partial^2/\partial y^2)$ becomes $(1/r_0^2)(\partial^2/\partial \phi^2)$. Therefore, the Schrödinger equation takes the simple form

$$-\frac{\hbar^2}{2\mu r_0^2} \frac{d^2 \Phi(\phi)}{d\phi^2} = E\Phi(\phi) \quad (7.40)$$

and the eigenfunction $\Phi(\phi)$ depends only on the angle ϕ . We have changed the symbol for the wave function from ψ to Φ to emphasize the change in the variables. This equation has the same form as the Schrödinger equation for a free particle, which was

solved in Chapter 4. You should verify that the two linearly independent solutions to this equation are

$$\Phi_+(\phi) = A_{+\phi} e^{im_l \phi} \quad \text{and} \quad \Phi_-(\phi) = A_{-\phi} e^{-im_l \phi} \quad (7.41)$$

The two solutions correspond to counterclockwise and clockwise rotation. It is shown in Example Problem 7.5 how to calculate the normalization constants $A_{\pm\phi}$.

EXAMPLE PROBLEM 7.5

Determine the normalization constant in Equation (7.41).

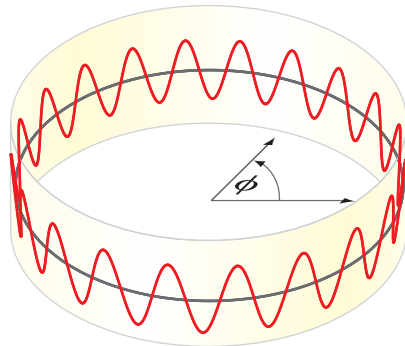
Solution

The variable ϕ can take on values between 0 and 2π . The following result is obtained:

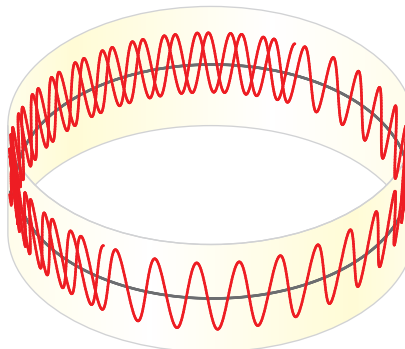
Concept

The boundary condition for the two-dimensional quantum rigid rotor arises from the requirement that the probability density is single valued.

$$\begin{aligned} \int_0^{2\pi} \Phi_{m_l}^*(\phi) \Phi_{m_l}(\phi) d\phi &= 1 \\ (A_{\pm\phi})^2 \int_0^{2\pi} e^{\mp im_l \phi} e^{\pm im_l \phi} d\phi &= (A_{\pm\phi})^2 \int_0^{2\pi} d\phi = 1 \\ A_{\pm\phi} &= \frac{1}{\sqrt{2\pi}} \end{aligned}$$



(a) $m_l = \pm$ integer



(b) $m_l \neq \pm$ integer

Figure 7.11

Justification of the boundary condition

$m_l = \text{integer}$. If the condition $m_l = \text{integer}$ is not met, the wave function does not have the same value for $\phi + 2\pi$ as for ϕ . The real part of the wave function is plotted as a function of ϕ in each case. The diagrams are for the conditions (a) m_l is an integer and (b) m_l is not an integer.

To obtain solutions of the Schrödinger equation that describe this physical problem, it is necessary to introduce the boundary condition $\Phi(\phi + 2\pi) = \Phi(\phi)$. This condition states that there is no way to distinguish the particle that has rotated n times around the circle from one that has rotated $n + 1$ times around the circle. Without this condition, the probability density would have multiple values for ϕ and $\phi + 2n\pi$, as shown in Figure 7.11, which is unacceptable. Applying the single-value condition to the eigenfunction, $e^{im_l[\phi+2\pi]} = e^{im_l\phi}$ or $e^{2\pi im_l} = 1$. Using Euler's relation, this expression is equivalent to

$$\cos 2\pi m_l + i \sin 2\pi m_l = 1 \quad (7.42)$$

To satisfy this condition, m_l must equal $0, \pm 1, \pm 2, \pm 3, \dots$. We see that the boundary condition generates the quantization rules for the quantum number m_l . The motivation for using the subscript l on the quantum number m will become clear when rotation in three dimensions is considered.

What do these eigenfunctions look like? Because they are complex functions of the angle ϕ , only the real part of the function is shown in Figure 7.12. The imaginary part is identical in shape but is shifted in phase by the angle $\pi/2$. Note that, as for the particle in the box and the harmonic oscillator, the lowest energy state has no nodes, and the number of nodes, which is twice the quantum number, increases with m_l .

Putting the eigenfunctions back into Equation (7.40) allows the corresponding eigenvalues E_{m_l} to be calculated. The energy-level spectrum is discrete and is given by

$$E_{m_l} = \frac{\hbar^2 m_l^2}{2\mu r_0^2} = \frac{\hbar^2 m_l^2}{2I} \quad \text{for } m_l = 0, \pm 1, \pm 2, \pm 3, \dots \quad (7.43)$$

In Equation (7.43), $I = \mu r_0^2$ is the moment of inertia. Note that states with $+m_l$ and $-m_l$ have the same energy, although the wave functions corresponding to these states are orthogonal to one another. We say that the energy levels with $m_l \neq 0$ are *twofold degenerate*.

The origin of the energy quantization is again a boundary condition. In this case, imagine the ring as a box of length 2π defined by the variable ϕ . The boundary condition given in Equation (7.42) states that an integral number of wavelengths must fit into this "box." For a classical rigid rotor,

$$E = \frac{|\mathbf{I}|^2}{2\mu r_0^2} = \frac{|\mathbf{I}|^2}{2I} = \frac{1}{2} I \omega^2 \quad (7.44)$$

where, throughout this chapter, the symbol \mathbf{l} is used for the angular momentum vector, $|\mathbf{l}|$ for its magnitude, and \hat{l} for the angular momentum operator. Equation (7.44) also holds for the quantum-mechanical rigid rotor, with the association $\omega = m_l \hbar / I$. Therefore, the quantization of energy means that only a discrete set of rotational frequencies is allowed.

One aspect of the eigenvalues for free rotation in two dimensions is different from what was encountered with the particle in the box or the harmonic oscillator: no zero point energy is associated with free rotational motion; $E_{m_l} = 0$ when $m_l = 0$. Why is this the case? A zero point energy appears only if the potential confines the motion to a limited region. In free rotation, there is no confinement and no zero point energy. Of course, a gas-phase diatomic molecule also moves and vibrates. Therefore, the rotating molecule has a zero point energy associated with these degrees of freedom.

The angular momentum can also be calculated for the two-dimensional rigid rotor. For rotation in the xy plane, the angular momentum vector lies on the z axis. The angular momentum operator in these coordinates takes the simple form $\hat{l}_z = -i\hbar(\partial/\partial\phi)$. Applying this operator to an eigenfunction,

$$\hat{l}_z \Phi_{\pm}(\phi) = \frac{-i\hbar}{\sqrt{2\pi}} \frac{d e^{\pm im_l \phi}}{d\phi} = \frac{\pm m_l \hbar}{\sqrt{2\pi}} e^{\pm im_l \phi} = \pm m_l \hbar \Phi_{\pm}(\phi) \quad (7.45)$$

This result shows that the angular momentum is quantized. We see that $\Phi_+(\phi)$ and $\Phi_-(\phi)$ are eigenfunctions of both the total energy and the angular momentum operators for the two-dimensional rigid rotor. As we will see, this is not the case for rotation in three dimensions. Because the angular momentum has the values $+\hbar m_l$ and $-\hbar m_l$, Equation (7.43) can be written in the form

$$E_{m_l} = \frac{\hbar^2 m_l^2}{2I} = \frac{|\mathbf{l}|^2}{2I} \quad (7.46)$$

just as in classical mechanics.

What can be said about the value of the rotation angle with respect to a fixed direction in the xy plane? We know that the probability of finding a particular angle ϕ in the interval $d\phi$ is

$$P(\phi) d\phi = \Phi^*(\phi)\Phi(\phi) d\phi = \left(\frac{1}{\sqrt{2\pi}}\right)^2 e^{\pm im_l \phi} e^{\mp im_l \phi} d\phi = \frac{d\phi}{2\pi} \quad (7.47)$$

The probability of finding the particle in a given interval $d\phi$ is the same for all values of ϕ . Just as for the position of a free particle whose linear momentum is precisely defined, nothing is known about the angular position of the molecule whose angular momentum is precisely defined. The origin of this result is that the operators $\hat{\phi}$ and \hat{l}_z do not commute, just as \hat{x} and \hat{p}_x do not commute.

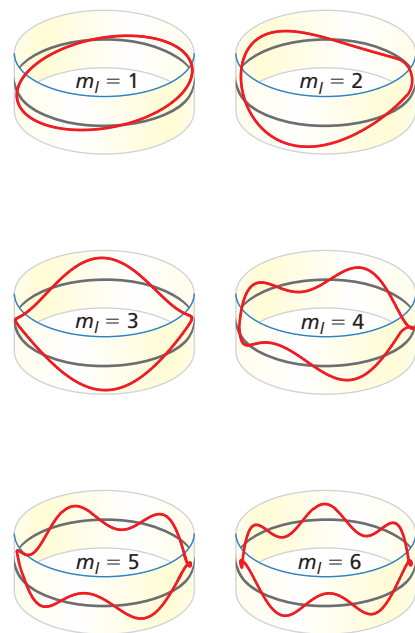


Figure 7.12

The real part of the second through seventh eigenfunctions for the rigid rotor with rotation confined to a plane plotted as a function of ϕ . In the center-of-mass coordinates, this problem is equivalent to the particle on a ring. What does the first eigenfunction look like?

7.5 QUANTUM-MECHANICAL ROTATION IN THREE DIMENSIONS

In the case just considered, the motion has been constrained to two dimensions. Now imagine the more familiar case of a molecule freely rotating in three-dimensional space. This problem is not more difficult, but the mathematics is more cumbersome than the two-dimensional case. Again, we transform to the center-of-mass coordinate system, and the rotational motion is transformed to the motion of a particle on the surface of a sphere of radius r_0 . As before, it is advantageous to express the kinetic and potential energy operators in an appropriate coordinate system, which in this case is spherical coordinates. Because there is no hindrance to rotation, the potential energy is constant and can be set equal to zero. In the spherical coordinate system, the Schrödinger equation is

$$-\frac{\hbar^2}{2\mu r_0^2} \left[\frac{1}{\sin\theta} \frac{\partial}{\partial\theta} \left(\sin\theta \frac{\partial Y(\theta, \phi)}{\partial\theta} \right) + \frac{1}{\sin^2\theta} \frac{\partial^2 Y(\theta, \phi)}{\partial\phi^2} \right] = EY(\theta, \phi) \quad (7.48)$$

The relationship between x , y , and z in Cartesian coordinates, and r , θ , and ϕ in spherical coordinates is discussed in Math Essential 8.

Our task is to find the eigenfunctions $Y(\theta, \phi)$ and the corresponding eigenvalues that are the solutions of this equation. Although the solution of this partial differential equation is not discussed in detail here, the first few steps are outlined because they provide some important physical insights. For a more detailed discussion of the solution of the Schrödinger equation for rotation in three dimensions, see the reference to Levine (2014) in Further Reading. Combining constants in the form

$$\beta = \frac{2\mu r_0^2 E}{\hbar^2} \quad (7.49)$$

multiplying both sides by $\sin^2 \theta$, and rearranging terms results in the following equation:

$$\sin \theta \frac{\partial}{\partial \theta} \left(\sin \theta \frac{\partial Y(\theta, \phi)}{\partial \theta} \right) + [\beta \sin^2 \theta] Y(\theta, \phi) = -\frac{\partial^2 Y(\theta, \phi)}{\partial \phi^2} \quad (7.50)$$

On the right side of Equation (7.50), the differentiation is with respect to ϕ only. On the left side of the equation, the differentiation is with respect to θ only. If this equality is to hold for all ϕ and θ , $Y(\theta, \phi)$ must be the product of two functions, each of which depends on only one of the two independent variables:

$$Y(\theta, \phi) = \Theta(\theta)\Phi(\phi) \quad (7.51)$$

This separation of variables leads to a major simplification in solving the Schrödinger equation (Equation (7.48)).

The functions $Y(\theta, \phi)$ are known as the **spherical harmonic functions** and are discussed in detail later in this chapter. Substituting Equation (7.51) into Equation (7.50) and dividing through by $\Theta(\theta)\Phi(\phi)$, we obtain

$$\frac{1}{\Theta(\theta)} \sin \theta \frac{d}{d\theta} \left(\sin \theta \frac{d\Theta(\theta)}{d\theta} \right) + \beta \sin^2 \theta = -\frac{1}{\Phi(\phi)} \frac{d^2 \Phi(\phi)}{d\phi^2} \quad (7.52)$$

Note that this equation no longer contains partial derivatives. Because each side of the equation depends on only one of the variables and the equality exists for all values of the variables, it must be true that both sides of the equation are equal to the same constant:

$$\begin{aligned} \frac{1}{\Theta(\theta)} \sin \theta \frac{d}{d\theta} \left(\sin \theta \frac{d\Theta(\theta)}{d\theta} \right) + \beta \sin^2 \theta &= m_l^2 \quad \text{and} \\ \frac{1}{\Phi(\phi)} \frac{d^2 \Phi(\phi)}{d\phi^2} &= -m_l^2 \end{aligned} \quad (7.53)$$

To emphasize the separation of variables, the spherical harmonic functions are written in the form

$$Y(\theta, \phi) = Y_l^{m_l}(\theta, \phi) = \Theta_l^{m_l}(\theta)\Phi_{m_l}(\phi) \quad (7.54)$$

The function $\Theta_l^{m_l}(\theta)$ is associated with both quantum numbers l and m_l , and the function $\Phi_{m_l}(\phi)$ is associated only with the quantum number m_l . For a given value of l , there are $2l + 1$ different values of m_l ranging from $-l$ to $+l$. We will next consider the origin of these quantum numbers more closely.

Looking back at the differential equation for rotation in two dimensions, we clearly see why the constant m_l is written in this way. The solutions for the second equation in Equation (7.53) can be obtained immediately because the same equation was solved for the molecule rotating in two dimensions:

$$\Phi_+(\phi) = A_{+\phi} e^{im_l\phi} \quad \text{and} \quad \Phi_-(\phi) = A_{-\phi} e^{-im_l\phi}, \quad \text{for } m_l = 0, 1, 2, 3, \dots \quad (7.55)$$

where the part of $Y(\theta, \phi)$ that depends on ϕ is associated with the quantum number m_l .

The first equation in Equation (7.53) allows the part of $Y(\theta, \phi)$ that depends on θ to be determined. It can be solved to give a set of eigenfunctions and their corresponding eigenvalues. Rather than work through the solution, the results are summarized with a

focus on the eigenvalues. A discussion of the spherical harmonics is postponed until Section 7.7. Two boundary conditions must be satisfied to solve Equation (7.53). To ensure that the functions $Y(\theta, \phi)$ are single-valued functions of θ and ϕ and that the amplitude of these functions remains finite everywhere, the following conditions must be met. We state rather than derive these conditions:

$$\begin{aligned}\beta &= l(l + 1), \text{ for } l = 0, 1, 2, 3, \dots \quad \text{and} \\ m_l &= -l, -(l - 1), -(l - 2), \dots, 0, \dots, (l - 2), (l - 1), l\end{aligned}\quad (7.56)$$

Both l and m_l must be integers. Note that l and m_l are the quantum numbers for the three-dimensional rigid rotor.

Why are there two quantum numbers for rotation in three dimensions, whereas there is only one for rotation in two dimensions? The answer is related to the dimensionality of the problem. For rotation in two dimensions, r was held constant. Therefore, ϕ is the only variable in the problem and there is only one boundary condition. For rotation in three dimensions, r is again held constant and, therefore, only the two boundary conditions on θ and ϕ generate quantum numbers. Similarly, the particle in the one-dimensional box is characterized by a single quantum number, whereas three quantum numbers are required to characterize the particle in the three-dimensional box.

What observables of the rotating molecule are associated with the quantum numbers l and m_l ? From the equation

$$\beta = \frac{2\mu r_0^2 E}{\hbar^2} = \frac{2I}{\hbar^2} E = l(l + 1)$$

the energy eigenvalues for rotation in three dimensions can be obtained. This shows that the quantum number l is associated with the total energy observable,

$$E_l = \frac{\hbar^2}{2I} l(l + 1), \quad \text{for } l = 0, 1, 2, 3, \dots \quad (7.57)$$

and that the total energy eigenfunctions $Y_l^{m_l}(\theta, \phi)$ satisfy the eigenvalue equation

$$\hat{H}_{total} Y_l^{m_l}(\theta, \phi) = \frac{\hbar^2}{2I} l(l + 1) Y_l^{m_l}(\theta, \phi), \quad \text{for } l = 0, 1, 2, 3, \dots \quad (7.58)$$

Note that the rotational energy values are quantized and that, once again, the quantization arises through a boundary condition. We see that the energy levels depend differently on the quantum number than the energy levels for rotation in two dimensions for which

$$E_{m_l} = \frac{\hbar^2 m_l^2}{2\mu r_0^2} = \frac{\hbar^2 m_l^2}{2I}, \quad \text{for } m_l = 0, \pm 1, \pm 2, \pm 3, \dots \quad (7.59)$$

For rotation in three dimensions, the energy depends on the quantum number l but not on m_l . Why is this the case? As will be shown in Section 7.7, the quantum number m_l determines the z component of the vector \mathbf{l} . Because $E_{total} = |\mathbf{l}|^2 / 2\mu r_0^2$, the energy of rotation depends only on the magnitude of the angular momentum and not its direction. Therefore, all $2l + 1$ total energy eigenfunctions that have the same l value but different m_l values have the same energy. This means that the degeneracy of each energy level is $2l + 1$. Recall that for rotation in two dimensions, the degeneracy of each energy level is two, except for the $m_l = 0$ level, which is nondegenerate.

Concept

Two boundary conditions arise in solving the Schrödinger equation for rotation in three dimensions.

Concept

The quantum number l together with the moment of inertia determine the rotational energy of a molecule. The quantum number m_l determines the z component of the angular momentum.

7.6 QUANTIZATION OF ANGULAR MOMENTUM

Now we will continue our discussion of three-dimensional rotation, although now it is discussed in the context of angular momentum rather than energy as was done earlier. Why is angular momentum important in quantum chemistry? Consider a familiar example from introductory chemistry, namely, the *s*, *p*, and *d* **orbitals** associated with atoms of the periodic table. This notation will be discussed in more detail in Chapter 9. We know that the bonding behavior of *s*, *p*, and *d* electrons is quite different.

Why is an s orbital spherically symmetrical, whereas a p orbital has a dumbbell structure? Why are three energetically degenerate p orbitals directed along the x , y , and z directions? The origin of these chemically important properties is the particular value of l and m_l associated with these orbitals.

As discussed earlier, the spherical harmonic functions $Y_l^{m_l}(\theta, \phi)$ are eigenfunctions of the total energy operator for a molecule that rotates freely in three dimensions. Are these functions also eigenfunctions of other operators of interest to us? Because the potential energy is zero for a free rotor, the total energy stored in rotational motion is given by the kinetic energy $E_{total} = |\mathbf{I}|^2/2I$, in which \mathbf{I} is the angular momentum and $I = \mu r_0^2$. Note that E_{total} and $|\mathbf{I}|^2$ differ only by the constant $1/2I$. Therefore, the corresponding operators \hat{H}_{total} and \hat{l}^2 also satisfy this relationship. Because they differ only by a multiplicative constant, these two operators commute with one another and have a common set of eigenfunctions. Furthermore, because E_{total} is quantized, it can be concluded that $|\mathbf{I}|^2$ is also quantized. Using the proportionality of E_{total} and $|\mathbf{I}|^2$, we can immediately write the eigenvalue equation for the operator \hat{l}^2 from Equation (7.58):

$$\hat{l}^2 Y_l^{m_l}(\theta, \phi) = \hbar^2 l(l+1) Y_l^{m_l}(\theta, \phi) \quad (7.60)$$

The notation explicitly shows that the quantum numbers l and m_l are defining indices for the eigenfunctions of \hat{H}_{total} and \hat{l}^2 . Because the eigenvalues for \hat{l}^2 are given by $\hbar^2 l(l+1)$, the magnitude of the angular momentum takes on the quantized values $|\mathbf{I}| = \hbar\sqrt{l(l+1)}$.

Note that it is \hat{l}^2 and not \hat{l} that commutes with \hat{H}_{total} . We now focus our attention on the angular momentum \mathbf{I} and the corresponding operator \hat{l} . How many components does \mathbf{I} have? For rotation in the xy plane, the angular momentum vector has only a single component that lies on the z axis. For rotation in three dimensions, the angular momentum vector has the three components l_x , l_y , and l_z , which are obtained from the vector cross product $\mathbf{I} = \mathbf{r} \times \mathbf{p}$. See Math Essential 7 for a more detailed discussion of the cross product and angular motion. As expected from the discussion of the Stern-Gerlach experiment in Chapter 6, the operators \hat{l}_x , \hat{l}_y , and \hat{l}_z do not commute.

As you will see when working the end-of-chapter problems, the operators \hat{l}_x , \hat{l}_y , and \hat{l}_z have the following form in Cartesian coordinates:

$$\begin{aligned}\hat{l}_x &= -i\hbar\left(y\frac{\partial}{\partial z} - z\frac{\partial}{\partial y}\right) \\ \hat{l}_y &= -i\hbar\left(z\frac{\partial}{\partial x} - x\frac{\partial}{\partial z}\right) \\ \hat{l}_z &= -i\hbar\left(x\frac{\partial}{\partial y} - y\frac{\partial}{\partial x}\right)\end{aligned}\quad (7.61)$$

Although not derived here, the operators have the following form in spherical coordinates:

$$\begin{aligned}\hat{l}_x &= -i\hbar\left(-\sin\phi\frac{\partial}{\partial\theta} - \cot\theta\cos\phi\frac{\partial}{\partial\phi}\right) \\ \hat{l}_y &= -i\hbar\left(\cos\phi\frac{\partial}{\partial\theta} - \cot\theta\sin\phi\frac{\partial}{\partial\phi}\right) \\ \hat{l}_z &= -i\hbar\left(\frac{\partial}{\partial\phi}\right)\end{aligned}\quad (7.62)$$

As you will verify in the end-of-chapter problems for the operators in Cartesian coordinates, the commutators relating the operators \hat{l}_x , \hat{l}_y , and \hat{l}_z are given by

$$\begin{aligned}[\hat{l}_x, \hat{l}_y] &= i\hbar\hat{l}_z \\ [\hat{l}_y, \hat{l}_z] &= i\hbar\hat{l}_x \\ [\hat{l}_z, \hat{l}_x] &= i\hbar\hat{l}_y\end{aligned}\quad (7.63)$$

Note that the order of the commutator is important; that is, $[\hat{l}_x, \hat{l}_y] = -[\hat{l}_y, \hat{l}_x]$.

What are the consequences of the fact that the operators corresponding to the components of the angular momentum do not commute with one another? Because the commutators are not zero, the direction of the angular momentum vector cannot be specified for rotation in three dimensions. To do so, it would be necessary to know all three components simultaneously, which would require that the three commutators in Equation (7.63) are zero. Given that \hat{l}_x , \hat{l}_y , and \hat{l}_z do not commute, what can be known about the components of the angular momentum for a rotating molecule?

To answer this question, we look more closely at the operators for the individual components of the angular momentum. In spherical coordinates, \hat{l}_x and \hat{l}_y depend on both θ and ϕ , but as Equation (7.62) shows, \hat{l}_z depends only on ϕ . As shown earlier, the spherical harmonics, $Y_l^{m_l}(\theta, \phi) = \Theta_l^m(\theta)\Phi_{m_l}(\phi)$, are eigenfunctions of the total energy operator and of \hat{l}^2 . We now show that the spherical harmonics are also eigenfunctions of \hat{l}_z . Applying \hat{l}_z to the functions $Y_l^{m_l}(\theta, \phi)$, we obtain

$$\hat{l}_z(Y_l^{m_l}(\theta, \phi)) = \Theta_l^m(\theta) \left[-i\hbar \frac{\partial}{\partial \phi} \left(\frac{1}{\sqrt{2\pi}} e^{im_l\phi} \right) \right] = m_l \hbar \Theta_l^m(\theta) \Phi_{m_l}(\phi),$$

for $m_l = 0, \pm 1, \pm 2, \pm 3, \dots, \pm l$ (7.64)

showing that $Y_l^{m_l}(\theta, \phi)$ are eigenfunctions of \hat{l}_z . What can we conclude from Equation (7.64)? Because the spherical harmonics are eigenfunctions of both \hat{l}^2 and \hat{l}_z , both the magnitude of $|\mathbf{l}|$ and its z component can be known simultaneously. In other words, one can know the length of the vector \mathbf{l} and one of its components, but it is not possible to simultaneously know the other two components of \mathbf{l} .

Why has \hat{l}_z rather than \hat{l}_x or \hat{l}_y been singled out, and what makes the z component special? There is nothing special about the z direction, and one could have just as easily chosen another direction. The way in which the variables are defined in spherical coordinates makes \hat{l}_z take on a simple form. Therefore, when a direction is chosen, it is convenient to make it the z direction. The essence of the preceding discussion is that one can know the magnitude of \mathbf{l} and only one of its components simultaneously. The consequences of the different commutation relations among \hat{H} , \hat{l}^2 , \hat{l}_x , \hat{l}_y , and \hat{l}_z are explored in Section 7.8, which deals with spatial quantization.

7.7 SPHERICAL HARMONIC FUNCTIONS

Until now, only the eigenvalues for \hat{l}^2 , \hat{H} , and \hat{l}_z for rotation in three dimensions have been discussed. We now discuss the spherical harmonic functions, $Y_l^{m_l}(\theta, \phi)$, which are the eigenfunctions common to these three operators. Although we have mentioned and utilized spherical harmonic functions earlier in this chapter, now we will approach them in a more formal manner. They are listed here for the first few values of l and m_l :

$$\begin{aligned} Y_0^0(\theta, \phi) &= \frac{1}{(4\pi)^{1/2}} \\ Y_1^0(\theta, \phi) &= \left(\frac{3}{4\pi} \right)^{1/2} \cos \theta \\ Y_1^{\pm 1}(\theta, \phi) &= \mp \left(\frac{3}{8\pi} \right)^{1/2} \sin \theta e^{\pm i\phi} \\ Y_2^0(\theta, \phi) &= \left(\frac{5}{16\pi} \right)^{1/2} (3 \cos^2 \theta - 1) \\ Y_2^{\pm 1}(\theta, \phi) &= \mp \left(\frac{15}{8\pi} \right)^{1/2} \sin \theta \cos \theta e^{\pm i\phi} \\ Y_2^{\pm 2}(\theta, \phi) &= \left(\frac{15}{32\pi} \right)^{1/2} \sin^2 \theta e^{\pm 2i\phi} \end{aligned} \quad (7.65)$$

As seen earlier in Equation (7.55), the ϕ dependence is a simple exponential function. The θ dependence enters as a polynomial in $\sin\theta$ and $\cos\theta$. The numerical factor in front of these functions ensures that they are normalized over the intervals $0 \leq \theta \leq \pi$ and $0 \leq \phi \leq 2\pi$. Because the spherical harmonics are eigenfunctions of the time-independent Schrödinger equation, they represent standing waves on the surface of a sphere in which the nodal positions are independent of time.

For $l = 0$, the eigenfunction is equal to a constant determined by the normalization condition. What does this mean? Remember that the square of the wave function gives the probability density for finding the particle at the coordinates θ and ϕ within the interval $d\theta$ and $d\phi$. These coordinates specify the angle defining the internuclear axis in a diatomic molecule. If the wave function is independent of θ and ϕ , any orientation of the internuclear axis in the rotation of a molecule is equally likely. This is the case for a state in which the angular momentum is zero.

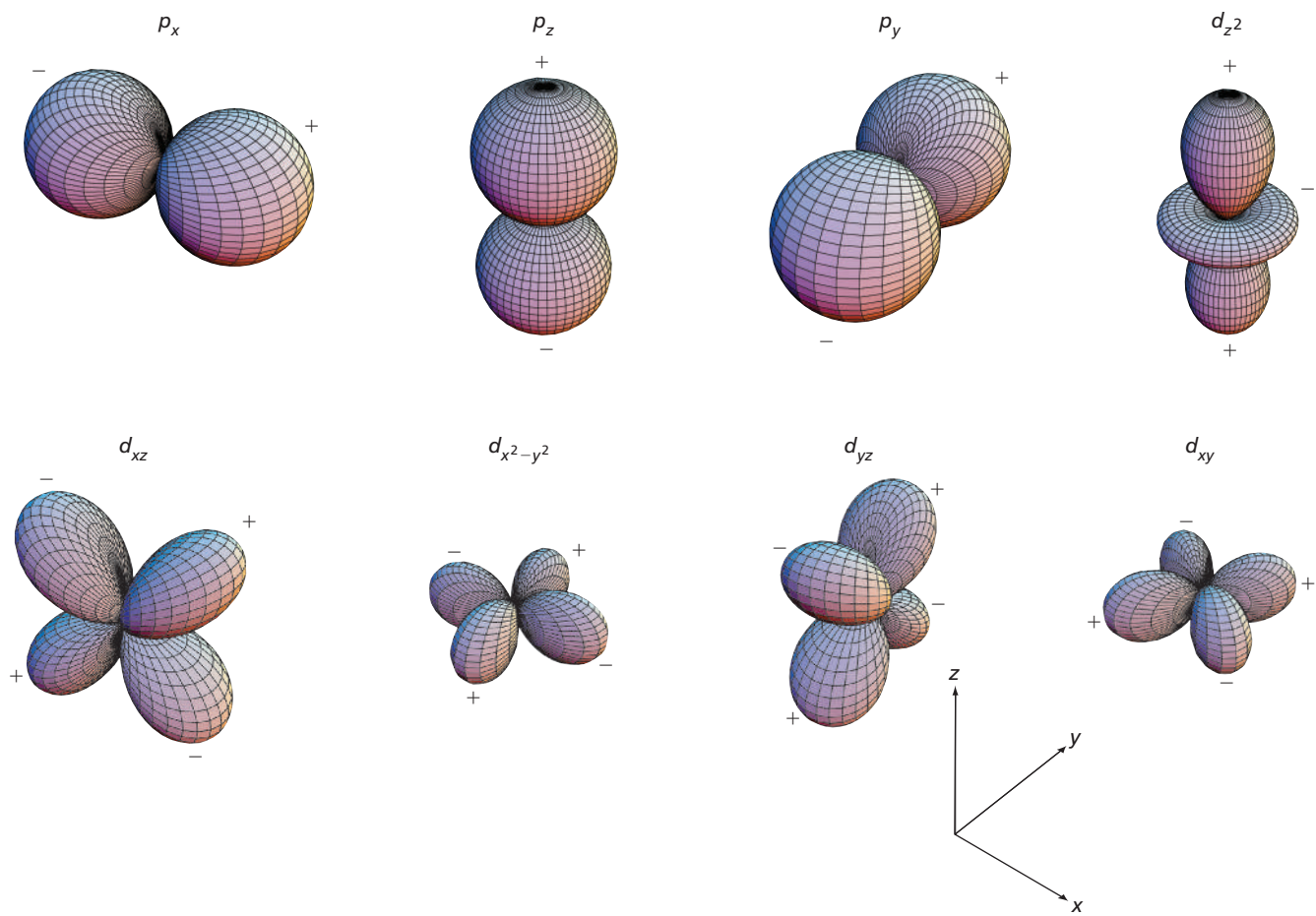
The spherical harmonics are complex functions unless $m_l = 0$. Graphing complex functions requires double the number of dimensions as for real functions, so that it is customary to form appropriate linear combinations of the $Y_l^{m_l}(\theta, \phi)$ and their complex conjugates to generate real functions for graphing purposes. These functions, which still form an orthonormal set, are given in the following equations. Equation (7.66) lists the p functions, and Equation (7.67) lists the d functions.

$$\begin{aligned} p_x &= \frac{-1}{\sqrt{2}}(Y_1^1 - Y_1^{-1}) = \sqrt{\frac{3}{4\pi}} \sin\theta \cos\phi \\ p_y &= \frac{-1}{\sqrt{2}i}(Y_1^1 + Y_1^{-1}) = \sqrt{\frac{3}{4\pi}} \sin\theta \sin\phi \\ p_z &= Y_1^0 = \sqrt{\frac{3}{4\pi}} \cos\theta \end{aligned} \quad (7.66)$$

$$\begin{aligned} d_{z^2} &= Y_2^1 = \sqrt{\frac{5}{16\pi}}(3 \cos^2\theta - 1) \\ d_{xz} &= \frac{-1}{\sqrt{2}}(Y_2^1 - Y_2^{-1}) = \sqrt{\frac{15}{4\pi}} \sin\theta \cos\theta \cos\phi \\ d_{yz} &= \frac{-1}{\sqrt{2}i}(Y_2^1 + Y_2^{-1}) = \sqrt{\frac{15}{4\pi}} \sin\theta \cos\theta \sin\phi \\ d_{x^2-y^2} &= \frac{1}{\sqrt{2}}(Y_2^2 + Y_2^{-2}) = \sqrt{\frac{15}{16\pi}} \sin^2\theta \cos 2\phi \\ d_{xy} &= \frac{1}{\sqrt{2}i}(Y_2^2 - Y_2^{-2}) = \sqrt{\frac{15}{16\pi}} \sin^2\theta \sin 2\phi \end{aligned} \quad (7.67)$$

We recognize the abbreviations in these two sets of equations in connection with the orbital designations for the hydrogen atom. As shown in Chapter 9, the functions shown in Figures 7.13 and 7.14 appear in the solutions of the Schrödinger equation for the hydrogen atom. Consequently, they merit more discussion. The functions in Equations (7.66) and (7.67) depend on two variables, θ and ϕ , and the way in which they are named refers them back to Cartesian coordinates. In graphing the functions, spherical coordinates have been used, whereby the radial coordinate is used to display the value of the amplitude. All the functions generate lobular patterns in which the amplitude of the function in a lobe is either positive or negative. The signs of the lobes are indicated in the plots.

The p functions form a set of three mutually perpendicular dumbbell structures. The wave function has the same amplitude but a different sign in the two lobes of each p function, and each function has a nodal plane passing through the origin. Four of the five d functions have a more complex four-lobed shape, with nodal planes separating

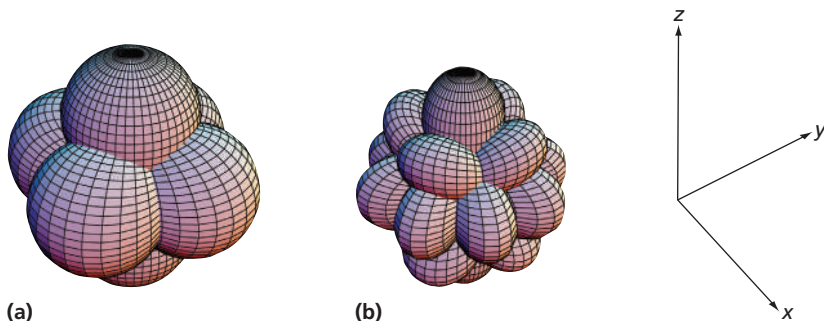
**Figure 7.13****Three-dimensional perspective plots of p and d linear combinations of spherical harmonics.**

The plots show three-dimensional surfaces in which the relationship of the angles θ and ϕ to the Cartesian axes is defined in Math Essential 8. The distance from the origin to a point on the surface (θ, ϕ) represents the absolute magnitude of the functions defined by Equations (7.66) and (7.67). The sign of the functions in the different lobes is indicated by plus and minus signs.

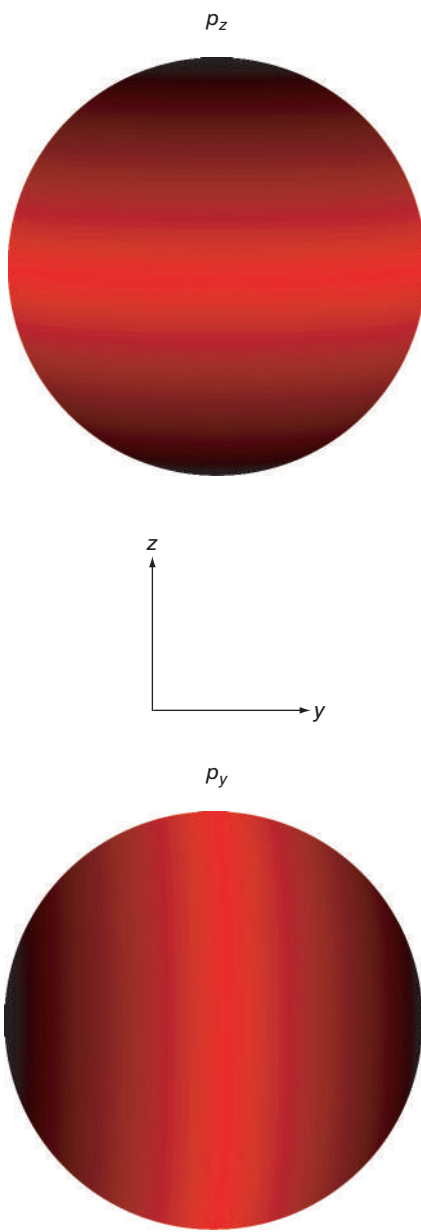
lobes in which the function has opposite signs. Because l is larger for the d than for the p functions, more nodes are seen in both angles. As for the particle in the box wave functions, an increase in the number of nodes corresponds to an increase in the energy of the quantum state. For the particle in the box, an increase in the number of nodes over a fixed interval corresponds to a shorter wavelength and, through the de Broglie relation, to a higher linear momentum. For the rigid rotor, an increase in the number of nodes over a fixed interval corresponds to a higher angular momentum. We will return to the spherical harmonic functions when discussing the orbitals for the H atom in Chapter 9.

Concept

The spherical harmonic functions determine the angular dependence of atomic orbitals.

**Figure 7.14**

Three-dimensional superimposed perspective plots of (a) three p and (b) five d linear combinations of the spherical harmonics. The convention used in displaying the functions is explained in the text and in the caption for Figure 7.13.

**Figure 7.15**

Absolute magnitude of the amplitude of p_z and p_y functions plotted on the surface of a unit sphere. Black and red regions correspond to high- and low-probability densities, respectively.

Concept

Because l_z is quantized, only discrete orientations of the angular momentum vector for a molecule rotating in three dimensions are allowed.

Up to this point, questions have been asked about the energy and the momentum. What can be learned about the angular orientation of the internuclear axis for the rotating molecule? This information is given by the probability density, defined by the first postulate as the square of the magnitude of the wave function. The probability density for the p and d functions is very similar in shape to the wave function amplitude shown in Figure 7.13, although the amplitude in all lobes is positive. Taking the p_z plot as an example, Figure 7.13 shows that the maximum amplitude of $|Y_1^0|^2$ is found along the positive and negative z axis, corresponding to a higher probability for finding the molecular axis parallel to the z axis.

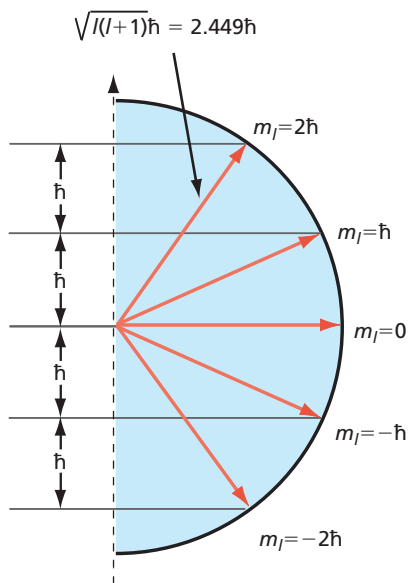
An alternate graphical representation can be used that recognizes that spherical harmonics can be used to represent waves on the surface of a sphere. This can be done by displaying the amplitude of the desired function on the sphere at the location θ, ϕ using a color scale. This is done in Figure 7.15, where the square of the amplitude of the p_z and p_y functions is plotted as a color scale on the surface of a sphere. Black and red regions correspond to high- and low-probability densities, respectively. For the p_z function, there is a much higher probability density of finding the particle near the z axis than in the $z = 0$ plane. This means that the molecular axis is much more likely to be parallel to the z axis than to lie in the xy plane. For a state whose wave function is p_y , the internuclear axis is much more likely to be parallel to the y axis than to lie in the $y = 0$ plane. This is consistent with the angular orientation of the maxima of these functions shown in Figure 7.13. Why is the probability density not more sharply peaked in a small angular region near the z or y axis? If the wave function is the p_z function, $E_{total}, |\mathbf{I}^2|$, and l_z are well defined. However, the operators for the angular coordinates ϕ and θ do not commute with the operators for $E_{total}, |\mathbf{I}^2|$, and l_z . As a consequence, the angular position coordinates are not known exactly, and only average values can be determined for these observables.

7.8 SPATIAL QUANTIZATION

The fact that the operators \hat{H} , \hat{l}^2 , and \hat{l}_z commute with one another, but \hat{l}_x , \hat{l}_y , and \hat{l}_z do not commute with one another, implies that the energy, the magnitude of the angular momentum vector, and the value of any one of its components can be known simultaneously, whereas the other two components of angular momentum cannot be known. Contrast this with classical mechanics in which all three components of an angular momentum vector can be specified simultaneously. In the classical mechanical case, both the length of the vector and its direction can be known.

We summarize what can be known about the angular momentum vector associated with a molecule rotating in three dimensions pictorially. In doing so, classical and quantum-mechanical descriptions are mixed. For this reason, the following is a **semiclassical** description. The one component that is known is chosen to be along the z direction. In Figure 7.16, we show what can be known about \mathbf{I} and l_z . The magnitude of \mathbf{I} is $\sqrt{l(l+1)}\hbar$ and that of $l_z = m_l\hbar$. The vector \mathbf{I} cannot lie on the z axis because $|\sqrt{m_l(m_l+1)}| \geq |m_l|$, from which we conclude that $|m_l| \leq l$. From another point of view, \mathbf{I} cannot lie on the z axis because the commutators in Equation (7.63) are not zero. If \mathbf{I} did lie on the z axis, then l_x and l_y would both be zero and, therefore, all three components of the vector \mathbf{I} could be known simultaneously.

Although the picture in Figure 7.16 is useful, it does not depict \mathbf{I} as a three-dimensional vector. We modify this figure to take the three-dimensional nature of \mathbf{I} into account in Figure 7.17 for the case where $l = 2$ and $m_l = 2$. The vector \mathbf{I} is depicted as a line on the surface of the cone beginning at its apex. The magnitude of \mathbf{I} and its projection on the z axis are known exactly and can be determined from the figure. However, the components of the angular momentum vector along the x and y axes, l_x and l_y , cannot be known exactly and simultaneously. All that is knowable about them is that $l^2 - l_z^2 = l_x^2 + l_y^2 = l(l+1)\hbar^2 - m_l^2\hbar^2$. This equation defines the circle terminating the cone at its open end. Figure 7.17 depicts all that can be known simultaneously about the components of the angular momentum. To give a more physical picture to Figure 7.17, a classical rigid rotor for which the z component of the angular momentum

**Figure 7.16**

Possible orientations of an angular momentum vector. The angular momentum vector shown is $|I| = \sqrt{l(l + 1)} \hbar$ and $l_z = m_l \hbar$, $l \geq |m_l|$ for $l = 2$.

vector is the same as for the quantum-mechanical case is also shown. Do not take this comparison literally because the rotor can be depicted as shown only because all three components of angular momentum can be known simultaneously. Such a depiction is not possible for a quantum-mechanical rigid rotor.

Figure 7.18 combines the information about all possible values of m_l consistent with $l = 2$ in one figure. Such a depiction is often referred to as a **vector model of angular momentum**. Only the orientations of \mathbf{I} for which the vector lies on one of the cones are allowed. A surprising result emerges from these considerations. Not only are the possible magnitudes of the angular momentum quantized, but the vector can only have certain orientations in space! This result is referred to as **spatial quantization**.

What is the analogous situation in classical mechanics? Because l_x , l_y , and l_z can be known simultaneously for a classical system and because their values are not quantized, the possible orientations of \mathbf{I} map out a continuous spherical surface. The contrast between classical and quantum-mechanical behavior is clearly evident! It is also apparent how quantum and classical results merge for high energies (large quantum numbers) as required by the correspondence principle. For a given l value, there are $2l + 1$ conical surfaces on a vector diagram like that shown in Figure 7.18. For large values of l , the individual cones are so close together that they merge into a sphere, and the angular momentum vector no longer seems to exhibit spatial quantization. It is shown in Example Problem 7.6 how to calculate the number of conical surfaces for a given value of l .

EXAMPLE PROBLEM 7.6

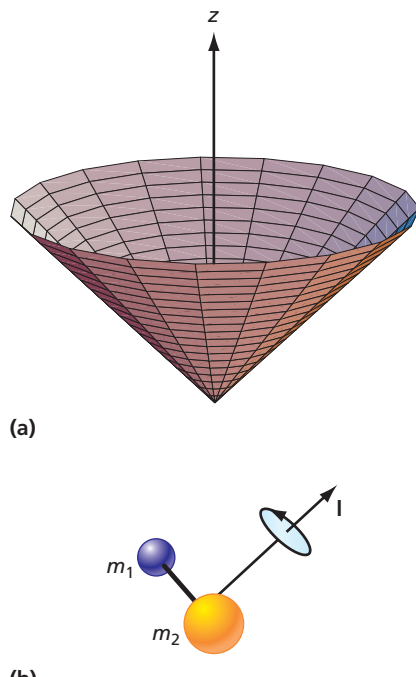
How many cones of the type shown in Figure 7.18 will there be for $l = 1000$? What is the closest allowed angle between \mathbf{I} and the z axis?

Solution

There will be $2l + 1$ or 2001 cones. The smallest allowed angle is for $l_z = 1000\hbar$, and is given by

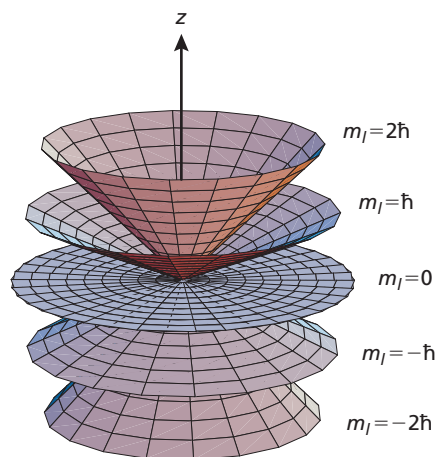
$$\cos \phi = \frac{l}{\sqrt{l(l+1)}} = \frac{1000}{1000.50}$$

$$\phi = 0.03 \text{ radians} = 1.7^\circ$$

**Figure 7.17**

Depiction of angular momentum vector.

(a) An angular momentum vector for which only l^2 , l_z , and $l_x^2 + l_y^2$ are known. In this case, $l = 2$ and $m_l = +2$. (b) Illustration of a classical rigid rotor for which the angular momentum vector has the same l_z component.

**Figure 7.18**

All possible orientations of an angular momentum vector with $l = 2$. The z component of the angular momentum is also shown.

VOCABULARY

angular acceleration	frequency of oscillation	reduced mass
angular momentum	harmonic oscillator	rigid rotor
angular velocity	Hermite polynomial	semiclassical
center-of-mass coordinates	moment of inertia	separation of variables
centripetal acceleration	orbital	spatial quantization
continuous energy spectrum	oscillatory behavior	spherical harmonic functions
force constant	radian	vector model of angular momentum

KEY EQUATIONS

Equation	Significance of Equation	Equation Number
$x_{cm} = \frac{m_1x_1 + m_2x_2}{m_1 + m_2}$	Defines center of mass for diatomic molecule	7.3 and 7.4
$\mu = \frac{m_1m_2}{m_1 + m_2}$		
$x(t) = c_1 e^{+i\sqrt{(k/\mu)t}} + c_2 e^{-i\sqrt{(k/\mu)t}}$	Time dependence of extension of classical harmonic oscillator	7.7
$E_{kinetic} = \frac{1}{2}\mu v^2 = \frac{1}{2}\mu r^2\omega^2 = \frac{1}{2}I\omega^2$	Kinetic and total energy of classical rigid rotor	7.24
$\mathbf{l} = \mathbf{r} \times \mathbf{p}$	Definition of angular momentum	7.25
$V(x) = \frac{1}{2}kx^2$	Potential energy function for classical and quantum harmonic oscillator	7.28
$\psi_n(x) = A_n H_n(\alpha^{1/2}x)e^{-\alpha x^2/2}$, for $n = 0, 1, 2, \dots$	Total energy eigenfunctions for quantum harmonic oscillator	7.30
$E_n = \hbar\sqrt{\frac{k}{\mu}}\left(n + \frac{1}{2}\right) = \hbar\nu\left(n + \frac{1}{2}\right)$ with $n = 0, 1, 2, 3, \dots$	Total energy eigenvalues for quantum harmonic oscillator	7.33
$\nu = \frac{1}{2\pi}\sqrt{\frac{k}{\mu}}$	Vibrational frequency for quantum harmonic oscillator	7.34
$\Phi_+(\phi) = A_{+\phi} e^{i m_l \phi}$ and $\Phi_-(\phi) = A_{-\phi} e^{-i m_l \phi}$	Total energy eigenfunctions for 2-D rigid rotor	7.41
$E_{m_l} = \frac{\hbar^2 m_l^2}{2\mu r_0^2} = \frac{\hbar^2 m_l^2}{2I}$ for $m_l = 0, \pm 1, \pm 2, \pm 3, \dots$	Energy eigenvalues for rotation in two dimensions	7.43
$\hat{l}_z \Phi_{\pm}(\phi) = \frac{-i\hbar}{\sqrt{2\pi}} \frac{de^{\pm im_l\phi}}{d\phi} = \frac{\pm m_l \hbar}{\sqrt{2\pi}} e^{\pm im_l\phi} = \pm m_l \hbar \Phi_{\pm}(\phi)$	Angular momentum eigenvalues for rotation in two dimensions	7.45
$Y(\theta, \phi) = Y_l^m(\theta, \phi) = \Theta_l^m(\theta)\Phi_{m_l}(\phi)$	Spherical harmonic functions are total and kinetic energy eigenfunctions of 3-D rigid rotor	7.54
$E_l = \frac{\hbar^2}{2I} l(l+1)$, for $l = 0, 1, 2, 3, \dots$	Total and kinetic energy eigenvalues for 3-D quantum rigid rotor	7.57
$[\hat{l}_x, \hat{l}_y] = i\hbar \hat{l}_z$	Commutators for angular momentum operators	7.63
$[\hat{l}_y, \hat{l}_z] = i\hbar \hat{l}_x$		
$[\hat{l}_z, \hat{l}_x] = i\hbar \hat{l}_y$		

CONCEPTUAL PROBLEMS

Q7.1 Why is the probability of finding a harmonic oscillator at its maximum extension or compression larger than that for finding it at its rest position?

Q7.2 Why does the energy of a rotating molecule depend on l but not on m_l ?

Q7.3 Are the real functions listed in Equations (7.66) and (7.67) eigenfunctions of \hat{l}_z ? Justify your answer.

Q7.4 Spatial quantization was discussed in Section 7.8.

Suppose that we have a gas consisting of atoms and each atom has a nonzero angular momentum. Are all of their angular momentum vectors aligned?

Q7.5 Does the average length of a harmonic oscillator depend on its energy? Answer this question by referring to Figure 7.7. The average length is the midpoint of the horizontal line connecting the two parts of $V(x)$.

Q7.6 Why can the angular momentum vector lie on the z axis for two-dimensional rotation in the x - y plane but not for rotation in three-dimensional space?

Q7.7 What is the functional dependence of the total energy of the quantum harmonic oscillator on the position variable x ?

Q7.8 Explain in words why the amplitude of the total energy eigenfunctions for the quantum-mechanical harmonic oscillator increases with $|x|$ as shown in Figure 7.10.

Q7.9 Why is it possible to write the total energy eigenfunctions for rotation in three dimensions in the form $Y(\theta, \phi) = \Theta(\theta)\Phi(\phi)$?

Q7.10 The two linearly independent total energy eigenfunctions for rotation in two dimensions are

$$\Phi_+(\phi) = \frac{1}{\sqrt{2\pi}} e^{im_l\phi} \quad \text{and} \quad \Phi_-(\phi) = \frac{1}{\sqrt{2\pi}} e^{-im_l\phi}$$

What is the difference in motion for these two solutions? Explain your answer.

Q7.11 Why is only one quantum number needed to characterize the eigenfunctions for rotation in two dimensions, whereas two quantum numbers are needed to characterize the eigenfunctions for rotation in three dimensions?

Q7.12 What makes the z direction special such that \hat{l}^2, \hat{H} , and \hat{l}_z commute, whereas \hat{l}^2, \hat{H} , and \hat{l}_x do not commute?

Q7.13 How are the spherical harmonics combined to form real p and d functions? What is the advantage in doing so?

Q7.14 Does the bond length of a real molecule depend on its energy? Answer this question by referring to Figure 7.7. The bond length is the midpoint of the horizontal line connecting the two parts of $V(x)$.

Q7.15 The zero point energy of the particle in the box goes to zero as the length of the box approaches infinity. What is the appropriate analogue for the quantum harmonic oscillator?

Q7.16 Figure 7.12 shows the solutions to the time-independent Schrödinger equation for the rigid rotor in two dimensions. Describe the corresponding solutions for the time-dependent Schrödinger equation.

Q7.17 Use the anharmonic Morse potential function in Figure 7.7 to demonstrate that rotation and vibration are not separable degrees of freedom for large quantum numbers.

Q7.18 Conservation of energy requires that the variation of the potential and kinetic energies with oscillator extension be exactly out of phase. Explain this statement.

Q7.19 What is the degeneracy of the energy levels for the rigid rotor in two dimensions? If it is different from one, explain why.

Q7.20 Consider a two-dimensional harmonic oscillator, $V(x, y) = k_x x^2 + k_y y^2$. Write an expression for the energy levels of such an oscillator in terms of k_x and k_y .

NUMERICAL PROBLEMS

Section 7.1

P7.1 Two 2.75-g masses are attached by a spring with a force constant of $k = 325 \text{ kg s}^{-2}$. Calculate the zero point energy of the system and compare it with the thermal energy $k_B T$ at 298 K. If the zero point energy were converted to translational energy, what would be the speed of the masses?

P7.2 Calculate the position of the center of mass of (a) ${}^1\text{H}{}^{35}\text{Cl}$, which has a bond length of 127.5 pm, and (b) CO, which has a bond length of 112.8 pm.

P7.3 Calculate the constants b_1 and b_2 in Equation 7.9 for the condition $x(0) = x_{max}$, the maximum extension of the oscillator. What is $v(0)$ for this condition?

Section 7.3

P7.4 ${}^1\text{H}{}^{35}\text{Cl}$ has a force constant of 516 N m^{-1} and a bond length of 127.5 pm. Calculate the frequency of the light corresponding to the lowest energy pure vibrational and pure rotational transitions. In what regions of the electromagnetic spectrum do the transitions lie?

P7.5 The vibrational frequency for N_2 expressed in wave numbers is 2358 cm^{-1} . What is the force constant associated with the N_2 bond? How much would a classical spring with this force constant be elongated if a mass of 1.75 kg were attached to it? Use the gravitational acceleration on Earth at sea level for this problem.

P7.6 Evaluate the average of the square of the linear momentum of the quantum harmonic oscillator, $\langle p_x^2 \rangle$, for the ground state ($n = 0$) and first two excited states ($n = 1$ and $n = 2$).

Hint: In evaluating integrals of this type, $\int_{-\infty}^{\infty} f(x) dx = 0$ if $f(x)$ is an odd function of x and $\int_{-\infty}^{\infty} f(x) dx = 2 \int_0^{\infty} f(x) dx$ if $f(x)$ is an even function of x .

P7.7 Show, by carrying out the appropriate integration, that the total energy eigenfunctions for the harmonic oscillator $\psi_0(x) = (\alpha/\pi)^{1/4} e^{-(1/2)\alpha x^2}$ and $\psi_2(x) = (\alpha/4\pi)^{1/4}(2\alpha x^2 - 1)e^{-(1/2)\alpha x^2}$ are orthogonal over the interval $-\infty < x < \infty$ and that $\psi_2(x)$ is normalized over the same interval. Use the hint about evaluating integrals in Problem P7.6.

P7.8 Calculate the frequency and wavelength of the radiation absorbed when a quantum harmonic oscillator with a frequency of $1.75 \times 10^{13} \text{ s}^{-1}$ makes a transition from the $n = 1$ to the $n = 2$ state.

P7.9 Evaluate the average kinetic and potential energies, $\langle E_{\text{kinetic}} \rangle$ and $\langle E_{\text{potential}} \rangle$, for the ground state ($n = 0$) of the harmonic oscillator by carrying out the appropriate integrations.

P7.10 The vibrational frequency of ${}^1\text{H}{}^{35}\text{Cl}$ is $8.97 \times 10^{13} \text{ s}^{-1}$. Calculate the force constant of the molecule. How large a mass would be required to stretch a classical spring with this force constant by 3.75 cm? Use the gravitational acceleration on Earth at sea level for this problem.

P7.11 Evaluate the average of the square of the vibrational amplitude of the quantum harmonic oscillator about its equilibrium value, $\langle x^2 \rangle$, for the ground state ($n = 0$) and first two excited states ($n = 1$ and $n = 2$). Use the hint about evaluating integrals in Problem P7.6.

P7.12 A coin with a mass of 6.21 g suspended on a rubber band has a vibrational frequency of 3.00 s^{-1} . Calculate (a) the force constant of the rubber band; (b) the zero point energy; (c) the total vibrational energy if the maximum displacement is 0.450 cm; and (d) the vibrational quantum number corresponding to the energy in part (c).

P7.13 The force constant for the ${}^1\text{H}{}^{35}\text{Cl}$ molecule is 516 N m^{-1} . Calculate the vibrational zero point energy of this molecule. If this amount of energy were converted to translational energy, how fast would the molecule be moving? Compare this speed to the root mean square speed from the kinetic gas theory, $|\mathbf{v}|_{\text{rms}} = \sqrt{3kT/m}$, for $T = 300 \text{ K}$.

P7.14 The force constant for a ${}^1\text{H}{}^{19}\text{F}$ molecule is 966 N m^{-1} .

- Calculate the zero point vibrational energy for this molecule for a harmonic potential.
- Calculate the light frequency needed to excite this molecule from the ground state to the first excited state.

P7.15 At 300 K, most molecules are in their ground vibrational state. Calculate $N_{n=1}/N_{n=0}$ and $N_{n=2}/N_{n=0}$ for the ${}^{79}\text{Br}_2$ molecule where n is the vibrational quantum number. The force constant is 325.3 N m^{-1} . At what temperature is $N_{n=2}/N_{n=0} = 0.400$? Repeat the calculation for D_2 for which

the force constant is 577 N m^{-1} and explain the difference in the results.

P7.16 Verify that $\psi_1(x)$ in Equation 7.31 is a solution of the Schrödinger equation for the quantum harmonic oscillator. Determine the energy eigenvalue.

P7.17 Evaluate the average kinetic and potential energies, $\langle E_{\text{kinetic}} \rangle$ and $\langle E_{\text{potential}} \rangle$, for the second excited state ($n = 2$) of the harmonic oscillator by carrying out the appropriate integrations.

P7.18 By substituting in the Schrödinger equation for the harmonic oscillator, show that the ground state vibrational wave function is an eigenfunction of the total energy operator. Determine the energy eigenvalue.

P7.19 Evaluate the average linear momentum of the quantum harmonic oscillator, $\langle p_x \rangle$, for the ground state ($n = 0$) and first two excited states ($n = 1$ and $n = 2$). Use the hint about evaluating integrals in Problem P7.6.

P7.20 Use $\sqrt{\langle x^2 \rangle}$ as calculated in Problem P7.11 as a measure of the vibrational amplitude for a molecule. What fraction is $\sqrt{\langle x^2 \rangle}$ of the 228.1-pm bond length of the ${}^{79}\text{Br}_2$ molecule for $n = 0, 1$, and 2 ? The force constant for ${}^{79}\text{Br}_2$ is 246 N m^{-1} .

P7.21 Evaluate $\langle x \rangle$, for the ground state ($n = 0$) and first two excited states ($n = 1$ and $n = 2$) of the quantum harmonic oscillator. Use the hint about evaluating integrals given in Problem P7.6.

P7.22 Using your results for Problems P7.6, P7.11, P7.19, and P7.21, calculate the uncertainties in the position and momentum $\sigma_p^2 = \langle p^2 \rangle - \langle p \rangle^2$ and $\sigma_x^2 = \langle x^2 \rangle - \langle x \rangle^2$ for the ground state ($n = 0$) and first two excited states ($n = 1$ and $n = 2$) of the quantum harmonic oscillator. Compare your results with the predictions of the Heisenberg uncertainty principle.

P7.23 A ${}^1\text{H}{}^{35}\text{Cl}$ molecule has the rotational quantum number $J = 8$ and vibrational quantum number $n = 0$. The data needed for the following calculations can be found in Table 8.3.

- Calculate the rotational and vibrational energy of the molecule. Compare each of these energies with $k_B T$ at 300 K.
- Calculate the period for vibration and rotation. How many times does the molecule rotate during one vibrational period?

P7.24 (a) Calculate the extensions that the quantum harmonic oscillator is most likely to be found from its equilibrium value for $n = 1$ in terms of the reduced distance $\alpha = \sqrt{k\mu/\hbar^2}$. (b) Calculate numerical values of the most probable extensions for ${}^1\text{H}{}^{35}\text{Cl}$. (c) What fraction is the extension of the bond length?

Section 7.4

P7.25 Show by carrying out the necessary integration that the eigenfunctions of the Schrödinger equation for rotation in two dimensions, $\frac{1}{\sqrt{2\pi}}e^{im_l\phi}$ and $\frac{1}{\sqrt{2\pi}}e^{-in_l\phi}$, $m_l \neq n_l$, are orthogonal.

P7.26 Is it possible to simultaneously know the angular orientation of a molecule rotating in a two-dimensional space and its angular momentum? Answer this question by evaluating the commutator $[\phi, -i\hbar(\partial/\partial\phi)]$.

P7.27 A $^{12}\text{C}^{16}\text{O}$ molecule, with a bond length of 112.8 pm, adsorbed on a surface rotates in two dimensions.

- Calculate the zero point energy associated with this rotation.
- What is the smallest quantum of energy that can be absorbed by this molecule in a rotational excitation?
- Calculate the ratio of the energy calculated in part (b) to $k_B T$ at 300. K.

Section 7.5

P7.28 A gas-phase $^1\text{H}^{19}\text{F}$ molecule, with a bond length of 91.7 pm, rotates in a three-dimensional space.

- Calculate the zero point energy associated with this rotation.
- What is the smallest quantum of energy that can be absorbed by this molecule in a rotational excitation?

P7.29 In discussing molecular rotation, the quantum number J is used rather than l . Using the Boltzmann distribution, calculate n_J/n_0 for $^1\text{H}^{19}\text{F}$ for $J = 0, 5, 10$, and 20 at $T = 800$. K. Does n_J/n_0 go through a maximum as J increases? If so, what can you say about the value of J corresponding to the maximum?

P7.30 In discussing molecular rotation, the quantum number J is used rather than l . Calculate E_{rot}/kT for $^1\text{H}^{19}\text{F}$ for $J = 0, 5, 10$, and 20 at 450. K. For which of these values of J is $E_{rot}/k_B T > 5$?

P7.31 By substituting in the Schrödinger equation for rotation in three dimensions, show that the rotational wave function $(5/16\pi)^{1/2}(3 \cos^2\theta - 1)$ is an eigenfunction of the total energy operator. Determine the energy eigenvalue.

P7.32 Calculate the first five energy levels for a $^{12}\text{C}^{16}\text{O}$ molecule that has a bond length of 112.8 pm if it (a) rotates freely in three dimensions and (b) if it is adsorbed on a surface and forced to rotate in two dimensions.

P7.33 Calculate reduced mass, moment of inertia, angular momentum, and energy in the $J = 2$ rotational level for $^1\text{H}^{35}\text{Cl}$, which has a bond length of 127.5 pm.

Section 7.6

P7.34 In this problem, you will derive the commutator $[\hat{l}_x, \hat{l}_y] = i\hbar\hat{l}_z$.

- The angular momentum vector in three dimensions has the form $\mathbf{l} = \mathbf{i}l_x + \mathbf{j}l_y + \mathbf{k}l_z$, where the unit vectors in the x , y , and z directions are denoted by \mathbf{i} , \mathbf{j} , and \mathbf{k} . Determine l_x , l_y , and l_z by expanding the 3×3 cross product $\mathbf{l} = \mathbf{r} \times \mathbf{p}$. The vectors \mathbf{r} and \mathbf{p} are given by $\mathbf{r} = \mathbf{i}x + \mathbf{j}y + \mathbf{k}z$ and $\mathbf{p} = \mathbf{i}p_x + \mathbf{j}p_y + \mathbf{k}p_z$.
- Substitute the operators for position and momentum in your expressions for l_x and l_y . Always write the position operator to the left of the momentum operator in a simple product of the two.
- Show that $[\hat{l}_x, \hat{l}_y] = i\hbar\hat{l}_z$.

Section 7.7

P7.35 The wave functions p_x and d_{xz} are linear combinations of the spherical harmonic functions, which are eigenfunctions of the operators \hat{H} , \hat{l}^2 , and \hat{l}_z for rotation in three dimensions. The combinations have been chosen to yield real functions. Are these functions still eigenfunctions of \hat{l}_z ? Answer this question by applying the operator to the functions.

P7.36 At what values of θ does $Y_2^0(\theta, \phi) = (5/16\pi)^{1/2}(3 \cos^2\theta - 1)$ have nodes? Are the nodes points, lines, planes, or other surfaces?

P7.37 Show that the function $Y_2^0(\theta, \phi) = (5/16\pi)^{1/2}(3 \cos^2\theta - 1)$ is normalized over the interval $0 \leq \theta \leq \pi$ and $0 \leq \phi \leq 2\pi$.

Section 7.8

P7.38 Draw a picture (to scale) showing all angular momentum cones consistent with $l = 5$. Calculate the half angles for each of the cones.

WEB-BASED SIMULATIONS, ANIMATIONS, AND PROBLEMS

Simulations, animations, and homework problem worksheets can be accessed at www.pearsonhighered.com/advchemistry

W7.1 The allowed energy levels for the quantum harmonic oscillator are determined by numerical integration of the Schrödinger equation, starting in the classically forbidden region to the left of the potential. The criterion that the energy is an eigenvalue for the problem is that the wave function

decays to zero in the classically forbidden region to the right of the potential. The zero point energy is determined for different values of k . The results are graphed to obtain a functional relationship between the zero point energy and k .

FURTHER READING

Levine, I. N. *Quantum Chemistry* (7th ed.). New York: Pearson, 2014.

McQuarrie, D. S. *Mathematical Methods for Scientists and Engineers*. Sausalito, CA: University Science Books, 2003.

Teichmann, T., Wenderoth, M., Prüser, H., Pierz, K., Schumacher, H., and Ulbrich, R. “Harmonic Oscillator

Wavefunctions of a Self-Assembled InAs Quantum Dot Measured by Scanning Tunneling Microscopy.” *Nano Letters* 13 (2013): 3571–3575.

Pye, C. “On the Solution of the Quantum Rigid Rotor.” *Journal of Chemical Education* 83 (2006): 460–463.

Vibrational and Rotational Spectroscopy of Diatomic Molecules

WHY is this material important?

Chemists have a wide range of spectroscopic techniques available to them. With these methods, unknown molecules can be identified, bond lengths can be measured, the force constants associated with chemical bonds can be determined, and the presence of functional groups in molecules, such as carbonyls, can be detected.

WHAT are the most important concepts and results?

Spectroscopic techniques are based on transitions that occur between different energy eigenstates of molecules when the molecules interact with electromagnetic radiation. Selection rules determine which of many possible transitions occur. The absorption of electromagnetic radiation in the infrared and microwave regions of the spectrum induces transitions between eigenstates of vibrational and rotational energy.

WHAT would be helpful for you to review for this chapter?

It would be helpful to review the material in Chapter 7 on the harmonic oscillator and the rigid rotor.

8.1 AN INTRODUCTION TO SPECTROSCOPY

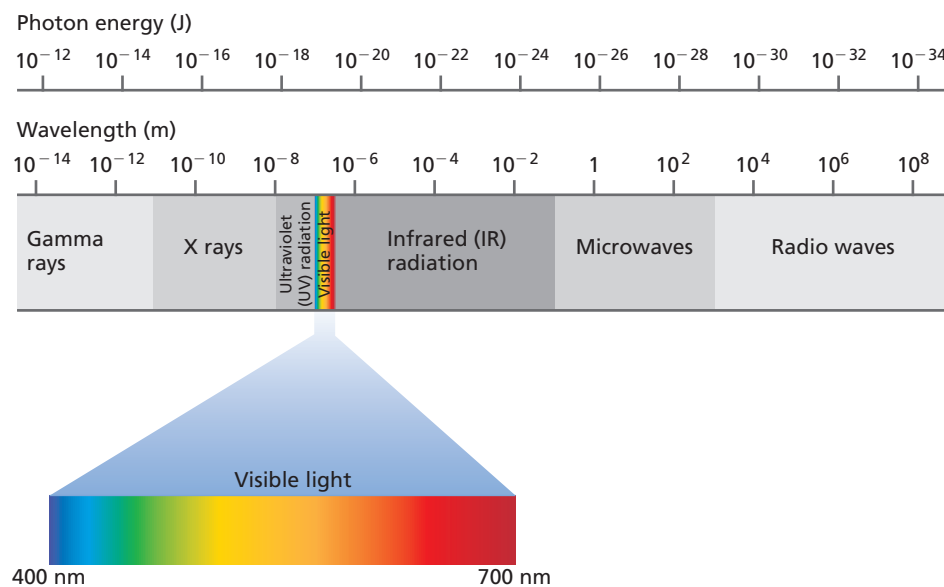
Spectroscopy is the study of the interaction between matter and electromagnetic radiation. In most types of spectroscopy, atoms or molecules absorb or emit electromagnetic radiation and undergo transitions between allowed quantum states. The various forms of spectroscopy are among the most powerful tools that chemists have at their disposal to probe the world at an atomic and molecular level. In this chapter, we begin a discussion of molecular spectroscopy that will be continued in later chapters. Atomic spectroscopy will be discussed separately in Chapter 11. The information that is accessible through molecular spectroscopy includes bond lengths (rotational spectroscopy) and the vibrational frequencies of molecules (vibrational spectroscopy). Allowed energy levels for electrons in molecules can be determined with electronic spectroscopy, which is discussed in Chapter 14. This spectroscopic information is crucial for a deeper understanding of the chemical bonding and the reactivity of molecules.

In a simple spectroscopy experiment, light of a fixed wavelength is incident on a sample of matter. The intensity of the light is reduced as atoms or molecules in the sample absorb the light and undergo transitions to higher-energy levels. This experiment is repeated at different wavelengths. The results are combined to generate an absorption spectrum in which the intensity of the transmitted light is graphed against

- 8.1 An Introduction to Spectroscopy
- 8.2 Absorption, Spontaneous Emission, and Stimulated Emission
- 8.3 An Introduction to Vibrational Spectroscopy
- 8.4 The Origin of Selection Rules
- 8.5 Infrared Absorption Spectroscopy
- 8.6 Rotational Spectroscopy
- 8.7 (Supplemental Section) Fourier Transform Infrared Spectroscopy
- 8.8 (Supplemental Section) Raman Spectroscopy
- 8.9 (Supplemental Section) How Does the Transition Rate between States Depend on Frequency?

Figure 8.1

The electromagnetic spectrum depicted on a logarithmic wavelength scale.



Concept

The photon energy corresponding to absorption or emission is directly related to the energy levels involved in the transition.

the wavelength or frequency. Because quantum-mechanical systems have a discrete energy spectrum, an absorption or emission spectrum consists of individual peaks, each of which is associated with a transition between two allowed energy levels of the system. As we show later in Supplemental Section 8.9, the frequency at which energy is absorbed or emitted is related to the energy levels involved in the transitions by

$$h\nu = |E_2 - E_1| \quad (8.1)$$

The photon energy that is used in chemical spectroscopies spans more than 16 orders of magnitude from the radio frequency to the X-ray region. This is an indication of the very different energy-level spacings probed by these techniques. The energy-level spacing is smallest in nuclear magnetic resonance (NMR) spectroscopy, which is discussed in Chapter 17, and largest for electronic spectroscopy. Transitions between rotational and vibrational energy levels are intermediate between these two extremes, with rotational energy levels being more closely spaced in energy than vibrational energy levels. The electromagnetic spectrum is depicted schematically in Figure 8.1. Note that visible light is a very small part of this spectrum.

The spectral regions associated with various types of spectroscopy are shown in Table 8.1. Spectroscopists—scientists who utilize and interpret spectrographic information as part of their research—commonly use the quantity **wave number** $\tilde{\nu} = 1/\lambda$, which has units of inverse centimeters, rather than the wavelength λ or frequency ν , to designate spectral transitions for historical reasons. The relationship between ν and $\tilde{\nu}$ is given by $\nu = \tilde{\nu}c$, where c is the speed of light. It is important to use consistent units when calculating the energy difference between states associated with a frequency in units of inverse seconds and wave numbers in units of inverse centimeters. Equation (8.1) expressed for both units is $|E_2 - E_1| = h\nu = hc\tilde{\nu}$.

TABLE 8.1 Important Types of Spectroscopy and Their Associated Spectral Ranges

Spectral Range	λ (m)	ν (Hz)	$\tilde{\nu}$ (cm^{-1})	Energy (J)	Spectroscopy
Radio	>0.1	$<3 \times 10^9$	>0.1	$<2 \times 10^{-24}$	NMR
Microwave	$0.001 - 0.1$	$3 \times 10^9 - 3 \times 10^{11}$	$0.1 - 10$	$2 \times 10^{-24} - 2 \times 10^{-22}$	Rotational
Infrared	$7 \times 10^{-7} - 1 \times 10^{-3}$	$3 \times 10^{11} - 4 \times 10^{14}$	$10 - 1 \times 10^4$	$2 \times 10^{-22} - 3 \times 10^{-19}$	Vibrational
Visible	$4 \times 10^{-7} - 7 \times 10^{-7}$	$4 \times 10^{14} - 7 \times 10^{14}$	$1 \times 10^4 - 3 \times 10^4$	$3 \times 10^{-19} - 5 \times 10^{-19}$	Electronic
Ultraviolet	$1 \times 10^{-8} - 4 \times 10^{-7}$	$7 \times 10^{14} - 3 \times 10^{16}$	$3 \times 10^4 - 1 \times 10^6$	$5 \times 10^{-19} - 2 \times 10^{-17}$	Electronic

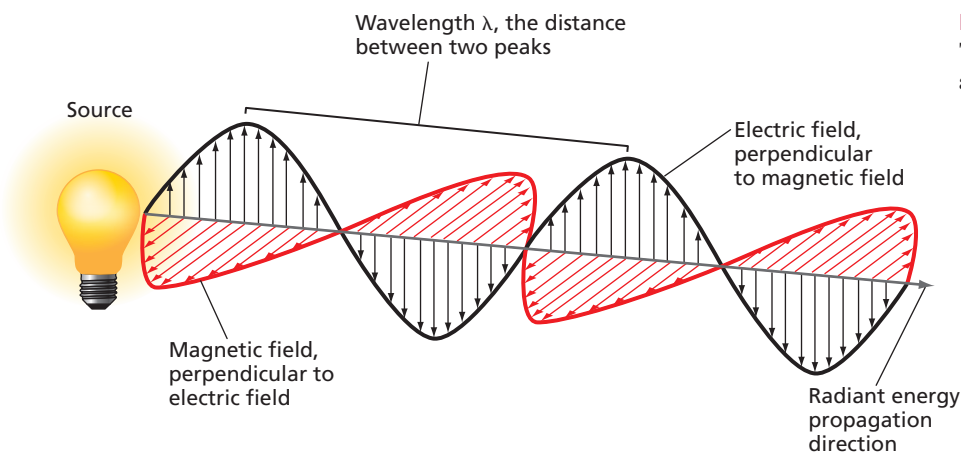


Figure 8.2
The electric and magnetic fields associated with a traveling light wave.

The fact that atoms and molecules possess a set of discrete energy levels is an essential feature of all types of spectroscopy. If molecules had a continuous energy spectrum, it would be very difficult to distinguish specific species on the basis of their absorption spectra. However, as discussed in Section 8.4, not all transitions between arbitrarily chosen states occur. **Selection rules** tell us which transitions will be experimentally observed. Because spectroscopy involves transitions between quantum states, we must first describe how electromagnetic radiation interacts with molecules.

We begin with a qualitative description of energy transfer from the electromagnetic field to a molecule leading to vibrational excitation. Light is a traveling electromagnetic wave that has magnetic and electric field components that are perpendicular to the propagation direction, as shown in Figure 8.2. Consider the effect of a time-dependent electric field on a classical dipolar diatomic “molecule” constrained to move in one dimension. Such a molecule is depicted in Figure 8.3. If the spring were replaced by a rigid rod, the molecule could not take up energy from the field. However, the spring allows the two masses to oscillate about their equilibrium distance, thereby generating a periodically varying dipole moment. If the electric field and oscillation of the dipole moment have the same frequency, the molecule can absorb energy from the field. For a classical “molecule,” any amount of energy can be taken up and the absorption spectrum is continuous.

For a real quantum-mechanical molecule, the interaction with the electromagnetic field is similar. The electric field acts on a dipole moment within the molecule that can be of two types: permanent and dynamic. Polar molecules like HCl have a **permanent dipole moment**. As molecules vibrate, an additional induced **dynamic dipole moment** can be generated. How does the dynamic dipole arise? The magnitude of the dipole moment depends on the bond length and the degree to which charge is transferred from one atom to another. In turn, the charge transfer depends on the overlap of the electron densities of the atoms, which in turn depends on the internuclear distances. As the molecule vibrates, its dipole moment changes because of these effects, generating a dynamic dipole moment. Because the vibrational amplitude is a small fraction of the bond distance, the dynamic dipole moment is generally small compared to the permanent dipole moment.

As we will discuss in the next section, the dynamic rather than the permanent dipole moment determines if a molecule will absorb energy in the infrared region. By contrast, the permanent dipole moment determines if a molecule will undergo rotational transitions by absorbing energy in the microwave region. Homonuclear diatomic molecules have neither permanent nor dynamic dipole moments and cannot absorb infrared radiation. However, vibrational spectroscopy can be carried out on these molecules using either the Raman effect, as discussed in Section 8.8, or electronic spectroscopy, as will be discussed in Chapter 14.

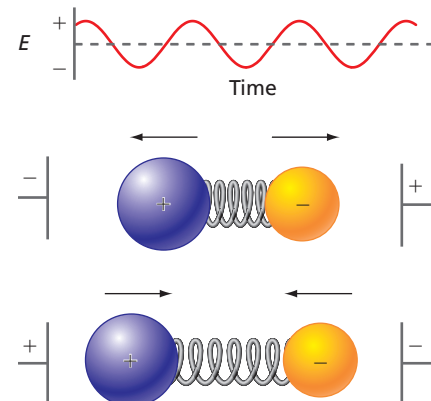


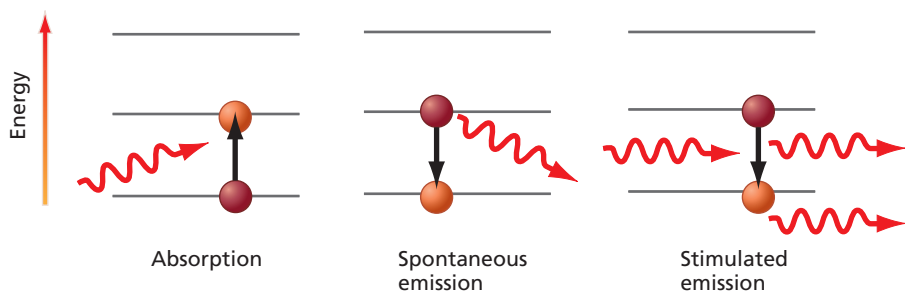
Figure 8.3
Schematic diagram of a classical harmonic oscillator constrained to move in one dimension under the influence of an electric field. The sinusoidally varying electric field shown at the top of the figure is applied between a pair of capacitor plates. The arrows indicate the direction of force on each of the two charged masses. If the phases of the field and vibration are as shown and the frequencies are equal, the oscillator will absorb energy in both the stretching and compression half cycles.

Concept

A molecule can have a permanent and a dynamic dipole moment.

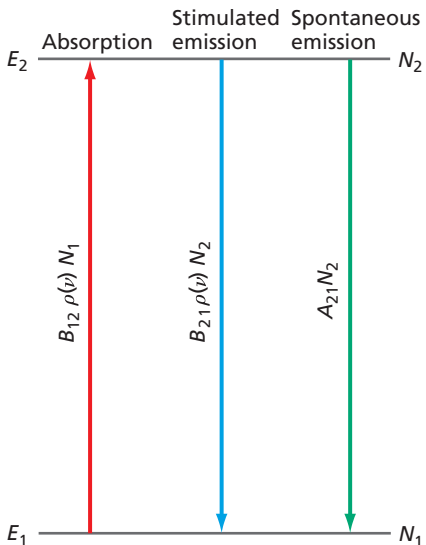
Figure 8.4

The three basic processes by which photon-assisted transitions occur. Orange- and red-filled circles indicate final and initial levels, respectively.



Concept

Photon-assisted transitions can be characterized by absorption, spontaneous emission, and stimulated emission.

**Figure 8.5**

Schematic illustration of the rate at which transitions occur between two levels. In each case, the rate is proportional to the product of the appropriate rate coefficient, A_{21} , B_{12} , or B_{21} , for the process and the population in the originating state, N_1 or N_2 . For absorption and stimulated emission, the rate is also proportional to the radiation density $\rho(\nu)$.

8.2 ABSORPTION, SPONTANEOUS EMISSION, AND STIMULATED EMISSION

We now move from a classical picture to a quantum-mechanical description involving discrete energy levels. The basic processes by which photon-assisted transitions of electrons between energy levels occur are **absorption**, **spontaneous emission**, and **stimulated emission**. For simplicity, only transitions in a two-level system are considered, as shown in Figure 8.4.

In absorption, the incident photon is absorbed and induces a transition of an electron to a higher level, and in emission, a photon is emitted as an excited state relaxes to one of lower energy. Absorption and stimulated emission are initiated by a photon incident on the molecule of interest. As the name implies, spontaneous emission is a random event, and its rate is related to the lifetime of the excited state. These three processes are not independent in a system at equilibrium, as can be seen by considering Figure 8.5. At equilibrium, the overall transition rate from level 1 to 2 must be the same as that from level 2 to 1. This means that

$$B_{12}\rho(\nu)N_1 = B_{21}\rho(\nu)N_2 + A_{21}N_2 \quad (8.2)$$

The proportionality constants for the three processes are A_{21} for spontaneous emission, B_{12} for absorption, and B_{21} for stimulated emission. Whereas spontaneous emission is independent of the radiation density at a given frequency $\rho(\nu)$, the rates of absorption and stimulated emission are directly proportional to $\rho(\nu)$. Each of these rates is directly proportional to the number of molecules (N_1 or N_2) in the state from which the transition originates. This means that unless the lower state is populated, absorption cannot occur. Similarly, unless the upper state is populated, emission cannot occur.

The appropriate function to use for $\rho(\nu)$ in Equation (8.2) is the blackbody spectral density function of Equation (1.7), because $\rho(\nu)$ is the distribution of frequencies at equilibrium for a given temperature. Following this reasoning, Einstein concluded that

$$B_{12} = B_{21} \quad \text{and} \quad \frac{A_{21}}{B_{21}} = \frac{16\pi^2\hbar\nu^3}{c^3} \quad (8.3)$$

This result is derived in Example Problem 8.1.

EXAMPLE PROBLEM 8.1

Derive the equations $B_{12} = B_{21}$ and $A_{21}/B_{21} = 16\pi^2\hbar\nu^3/c^3$ using these two pieces of information: (1) the overall rate of transition between levels 1 and 2 (see Figure 8.5) is zero at equilibrium, and (2) the ratio of N_2 to N_1 is governed by the Boltzmann distribution.

Solution

The rate of transitions from level 1 to level 2 is equal and opposite to the rate of transitions from level 2 to level 1. This gives the equation $B_{12}\rho(\nu)N_1 = B_{21}\rho(\nu)N_2 + A_{21}N_2$. The Boltzmann distribution function states that

$$\frac{N_2}{N_1} = \frac{g_2}{g_1} e^{-\hbar\nu/k_B T}$$

In this case, $g_2 = g_1$. These two equations can be solved for $\rho(\nu)$, giving $\rho(\nu) = A_{21}/(B_{12} e^{h\nu/k_B T} - B_{21})$. As Planck showed, $\rho(\nu)$ has the form shown in Equation (1.7) so that

$$\rho(\nu) = \frac{A_{21}}{B_{12} e^{h\nu/k_B T} - B_{21}} = \frac{8\pi h\nu^3}{c^3} \frac{1}{e^{h\nu/k_B T} - 1}$$

For these two expressions to be equal, $B_{12} = B_{21}$ and $A_{21}/B_{21} = 8\pi h\nu^3/c^3 = 16\pi^2 \hbar\nu^3/c^3$.

Spontaneous emission and stimulated emission differ in an important respect. Spontaneous emission is a completely random process, and the emitted photons are *incoherent*, by which we mean that their phases are random. In stimulated emission, the phase and direction of propagation are the same as those of the incident photon. This is referred to as coherent photon emission. A light bulb is an **incoherent photon source**. The phase relation between individual photons is random, and because the propagation direction of the photons is also random, the intensity of the source falls off as the square of the distance. A laser is a **coherent source** of radiation. All photons are in phase, and because they have the same propagation direction, the divergence of the beam is very small. This explains why a laser beam that is reflected from the moon still has a measurable intensity when it returns to Earth. We will have more to say about lasers when atomic spectroscopy is discussed in Chapter 11.

Concept

Light sources can emit coherent or incoherent photons.

8.3 AN INTRODUCTION TO VIBRATIONAL SPECTROSCOPY

We now have a framework with which we can discuss spectroscopy as a chemical tool. Two features have enabled vibrational spectroscopy to achieve the importance that it has as a tool in chemistry. The first is that the vibrational frequency depends primarily on the identity of the two vibrating atoms on either end of the bond and to a much lesser degree on the presence of atoms farther away from the bond. This property generates characteristic frequencies for atoms joined by a bond known as **group frequencies**. We will discuss group frequencies further in Section 8.5. The second feature is that a particular vibrational mode in a molecule has only one characteristic frequency of appreciable intensity. We discuss this feature next.

In all types of spectroscopy, transitions occur from one energy level to another. As discussed in Section 8.2, the energy level from which the transition originates must be occupied in order to generate a spectral signal. Which of the infinite set of vibrational levels has a substantial probability of being occupied? Table 8.2 shows the number of diatomic molecules in the first excited vibrational state (N_1) relative to those in the ground state (N_0) at 300. and 1000. K. The calculations have been carried out using the Boltzmann distribution. We see that nearly all the molecules in a macroscopic sample are in their ground vibrational state at room temperature because $N_1/N_0 \ll 1$. Even at 1000. K, N_1/N_0 is very small except for Br₂. This means that for these molecules, absorption of light at the characteristic frequency will occur from molecules in the $n = 0$ state. What final states are possible? As shown in the next section, for

Concept

Group frequencies are important in identifying which molecules contribute to a vibrational spectrum.

TABLE 8.2 Vibrational State Populations for Selected Diatomic Molecules

Molecule	$\tilde{\nu}$ (cm ⁻¹)	ν (s ⁻¹)	N_1/N_0 for 300. K	N_1/N_0 for 1000. K
H–H	4400	1.32×10^{14}	6.78×10^{-10}	1.78×10^{-3}
H–F	4138	1.24×10^{14}	2.44×10^{-9}	2.60×10^{-3}
H–Br	2649	7.94×10^{13}	3.05×10^{-6}	2.21×10^{-2}
N–N	2358	7.07×10^{13}	1.23×10^{-5}	3.36×10^{-2}
C–O	2170	6.51×10^{13}	3.01×10^{-5}	4.40×10^{-2}
Br–Br	323	9.68×10^{12}	0.213	0.628

Concept

In most cases, an observed vibrational transition will be generated by a $n = 0 \rightarrow n = 1$ transition.

absorption by a quantum-mechanical harmonic oscillator, $\Delta n = n_{final} - n_{initial} = +1$. Because only the $n = 0$ state has an appreciable population, with few exceptions only the $n = 0 \rightarrow n = 1$ transition is observed in vibrational spectroscopy.

EXAMPLE PROBLEM 8.2

A strong absorption of infrared radiation is observed for $^1\text{H}^{35}\text{Cl}$ at 2991 cm^{-1} .

- Calculate the force constant k for this molecule.
- By what factor do you expect this frequency to shift if deuterium is substituted for hydrogen in this molecule? The force constant is unaffected by this substitution.

Solution

a. We first write $\Delta E = h\nu = hc/\lambda = \hbar\sqrt{k/\mu}$. Solving for k ,

$$\begin{aligned} k &= 4\pi^2 \left(\frac{c}{\lambda}\right)^2 \mu \\ &= 4\pi^2 (2.998 \times 10^8 \text{ m s}^{-1})^2 \left(\frac{2991}{\text{cm}} \times \frac{100 \text{ cm}}{1 \text{ m}}\right)^2 \frac{(1.008)(34.969) \text{ amu}}{35.977} \\ &\quad \times \left(\frac{1.661 \times 10^{-27} \text{ kg}}{1 \text{ amu}}\right) \\ &= 516.3 \text{ N m}^{-1} \end{aligned}$$

$$\begin{aligned} \text{b. } \frac{\nu_{DCl}}{\nu_{HCl}} &= \sqrt{\frac{\mu_{HCl}}{\mu_{DCl}}} = \sqrt{\frac{m_H m_{Cl} (m_D + m_{Cl})}{m_D m_{Cl} (m_H + m_{Cl})}} = \sqrt{\left(\frac{1.0078}{2.0140}\right) \left(\frac{36.983}{35.977}\right)} \\ &= 0.717 \end{aligned}$$

Concept

Isotope effects in vibrational spectroscopy are an important tool in identifying molecules.

The vibrational frequency for DCl is lower by a substantial amount. Would the shift be as great if ^{37}Cl were substituted for ^{35}Cl ? The fact that vibrational frequencies are so strongly shifted by isotopic substitution of deuterium for hydrogen makes infrared spectroscopy a valuable tool for determining the presence of hydrogen atoms in molecules.

Note that the high sensitivity available in modern instrumentation to carry out vibrational spectroscopy makes it possible in favorable cases to see vibrational transitions originating from the $n = 0$ state for which $\Delta n = +2, +3, \dots$. These **overtone** transitions are much weaker than the $\Delta n = +1$ absorption but are possible because the selection rule $\Delta n = +1$ is not rigorously obeyed for an anharmonic potential. This more advanced topic is explored in Problem P8.21 at the end of the chapter.

The overtone transitions are useful because they allow us to determine the degree to which real molecular potentials differ from the simple **harmonic potential**, $V(x) = (1/2)kx^2$. It is shown in Example Problem 8.2 how to calculate the force constant from an observed vibrational frequency. To a good approximation, a realistic **anharmonic potential** can be described in analytical form by the **Morse potential**:

$$V(x) = D_e [1 - e^{-\alpha(x-x_e)}]^2 \quad (8.4)$$

in which D_e is the dissociation energy relative to the bottom of the potential and $\alpha = \sqrt{k/(2D_e)}$. The force constant k for the Morse potential is defined by $k = (d^2V/dx^2)_{x=x_e}$ just as for the harmonic potential. The **bond energy** D_0 is defined with respect to the lowest allowed level, rather than to the bottom of the potential, as shown in Figure 8.6.

The energy levels for the Morse potential are given by

$$E_n = \hbar\nu \left(n + \frac{1}{2}\right) - \frac{(\hbar\nu)^2}{4D_e} \left(n + \frac{1}{2}\right)^2 \quad (8.5)$$

The second term gives the anharmonic correction to the energy levels. Measurements of the frequencies of the overtone vibrations allow the parameter D_e in the Morse

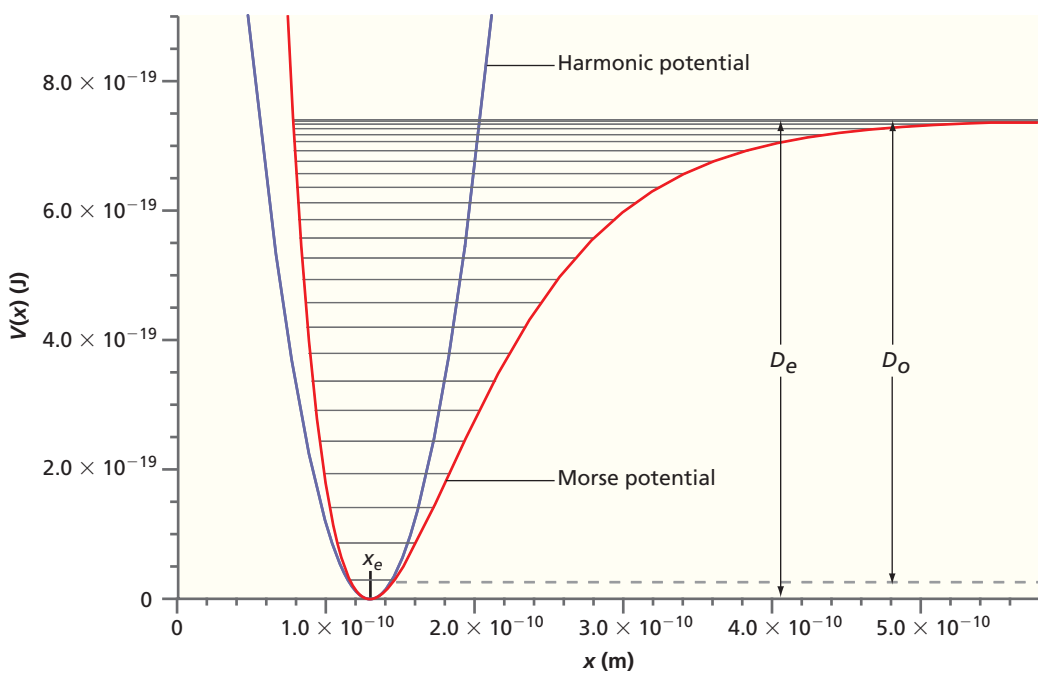


Figure 8.6
Morse potential energy as a function of the bond length x for HCl. The Morse potential, $V(x)$, shown in the red curve, was calculated using the parameters from Example Problem 8.3. The zero of energy is chosen to be the bottom of the potential. The purple curve shows a harmonic potential, which is a good approximation to the Morse potential near the bottom of the well. The horizontal lines indicate allowed energy levels in the Morse potential. D_e and D_0 represent the bond energies defined with respect to the bottom of the potential and the lowest state, respectively, and x_e is the equilibrium bond length.

potential to be determined for a specific molecule. This provides a useful method for determining the details of the interaction potential in a molecule. CO is an example of a diatomic molecule for which overtone vibrations are easily observed.

EXAMPLE PROBLEM 8.3

The Morse potential can be used to model dissociation as illustrated in this example. The ${}^1\text{H}{}^{35}\text{Cl}$ molecule can be described by a Morse potential with $D_e = 7.41 \times 10^{-19}$ J. The force constant k for this molecule is 516.3 N m^{-1} and $\nu = 8.97 \times 10^{13} \text{ s}^{-1}$. Calculate the number of allowed vibrational states in this potential and the bond energy for the ${}^1\text{H}{}^{35}\text{Cl}$ molecule.

Solution

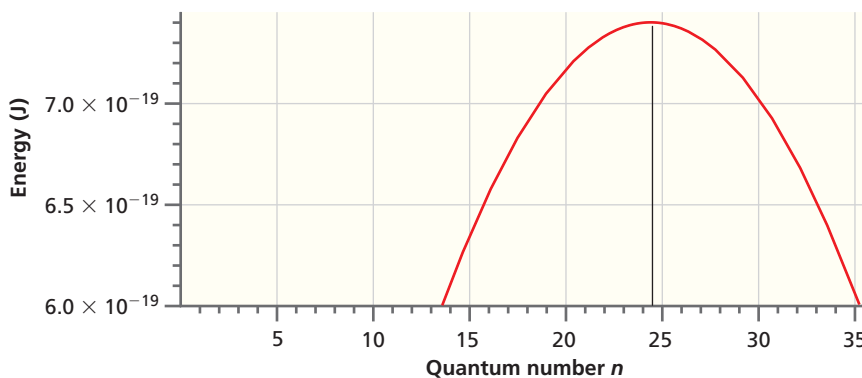
We solve the equation

$$E_n = h\nu\left(n + \frac{1}{2}\right) - \frac{(h\nu)^2}{4D_e}\left(n + \frac{1}{2}\right)^2 = D_e$$

to obtain the highest value of n consistent with the potential. Using the parameters given earlier, we obtain the following equation for n :

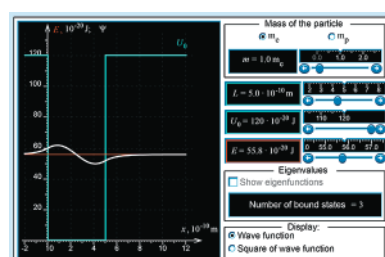
$$-1.1918 \times 10^{-21} n^2 + 5.8243 \times 10^{-20} n + 2.942 \times 10^{-20} = 7.41 \times 10^{-19}$$

Both solutions to this quadratic equation give $n = 24.4$, so we conclude that the potential has 24 allowed levels. If the left side of the equation is graphed versus n , we obtain the results shown in the following figure.



Concept

The Morse potential is a more realistic potential than a harmonic potential in modeling vibrations.



W8.1 Energy levels for a Morse potential

TABLE 8.3 Values of Molecular Constants for Selected Diatomic Molecules

	$\tilde{\nu}$ (cm $^{-1}$)	$\tilde{\nu}$ (s $^{-1}$)	x_e (pm)	k (Nm $^{-1}$)	B (cm $^{-1}$)	D_0 (kJ mol $^{-1}$)	D_0 (J molecule $^{-1}$)
H ₂	4401	1.32×10^{14}	74.14	575	60.853	436	7.24×10^{-19}
D ₂	3115	9.33×10^{13}	74.15	577	30.444	443	7.36×10^{-19}
$^1\text{H}^{81}\text{Br}$	2649	7.94×10^{13}	141.4	412	8.4649	366	6.08×10^{-19}
$^1\text{H}^{35}\text{Cl}$	2991	8.97×10^{13}	127.5	516	10.5934	432	7.17×10^{-19}
$^1\text{H}^{19}\text{F}$	4138	1.24×10^{14}	91.68	966	20.9557	570	9.46×10^{-19}
$^1\text{H}^{127}\text{I}$	2309	6.92×10^{13}	160.92	314	6.4264	298	4.95×10^{-19}
$^{35}\text{Cl}_2$	559.7	1.68×10^{13}	198.8	323	0.2440	243	4.03×10^{-19}
$^{79}\text{Br}_2$	325.3	9.75×10^{12}	228.1	246	0.082107	194	3.22×10^{-19}
$^{19}\text{F}_2$	916.6	2.75×10^{13}	141.2	470	0.89019	159	2.64×10^{-19}
$^{127}\text{I}_2$	214.5	6.43×10^{12}	266.6	172	0.03737	152	2.52×10^{-19}
$^{14}\text{N}_2$	2359	7.07×10^{13}	109.8	2295	1.99824	945	1.57×10^{-18}
$^{16}\text{O}_2$	1580.	4.74×10^{13}	120.8	1177	1.44563	498	8.27×10^{-19}
$^{12}\text{C}^{16}\text{O}$	2170.	6.51×10^{13}	112.8	1902	1.9313	1076	1.79×10^{-18}

Source: Lide, D. R., ed. *CRC Handbook of Chemistry and Physics*. 83rd ed. Boca Raton, FL: CRC Press, 2003.

Note that E_n decreases for $n > 25$. This is mathematically correct, but unphysical because for $n > 24$, the molecule has a continuous energy spectrum and Equation (8.5) is no longer valid.

The bond energy D_0 is not D_e but $D_e - E_0$, where

$$E_0 = \frac{hv}{2} - \frac{(hv)^2}{16D_e}$$

from Equation (8.5), because the molecule has a zero point vibrational energy. Using the parameters given earlier, the bond energy is 7.11×10^{-19} J. The Morse and harmonic potentials as well as the allowed energy levels for this molecule are shown in Figure 8.6.

The material-dependent parameters that determine the frequencies observed in vibrational spectroscopy for diatomic molecules are the force constant k and the reduced mass μ . The corresponding parameters for rotational spectroscopy (see Section 8.6) are the rotational constant $B = h/(8\pi^2 c \mu r_0^2)$ in which the bond length, r_0 or x_e , and the reduced mass μ appear. These parameters, along with the bond energy D_0 , are listed in Table 8.3 for selected molecules. The quantities B and $\tilde{\nu}$ are expressed in units of inverse centimeters.

8.4 THE ORIGIN OF SELECTION RULES

Every type of spectroscopy has selection rules that govern the transitions that can occur between different states of a system. This greatly simplifies the interpretation of spectra because far fewer transitions occur than if there were no selection rules. To illustrate how selection rules arise, we next derive the selection rules for vibrational spectroscopy based on the quantum-mechanical harmonic oscillator.

As discussed later in Supplemental Section 8.9, the transition probability from state n to state m is only nonzero if the **transition dipole moment** μ_x^{mn} satisfies the following condition:

$$\mu_x^{mn} = \int \psi_m^*(x)\mu_x(x_e + x)\psi_n(x) dx \neq 0 \quad (8.6)$$

In this equation, x is the vibrational amplitude and μ_x is the dipole moment along the electric field direction, which we take to be the x axis.

In the following discussion, we show how selection rules for vibrational excitation arise from Equation (8.6). As discussed in Section 8.1, the dipole moment μ_x will change slightly as the molecule vibrates. Because the amplitude of vibration x is an oscillatory function of t , the molecule has a time-dependent dynamic dipole moment. We take this into account by expanding μ_x in a Taylor series about the equilibrium bond length. Because x is the amplitude of vibration, the equilibrium bond length x_e corresponds to $x = 0$:

$$\mu_x(x_e + x(t)) = \mu_{0x} + x(t) \left(\frac{d\mu_x}{dx} \right)_{x=0} + \dots \quad (8.7)$$

in which the values of μ_{0x} and $(d\mu_x/dx)_{x=0}$ depend on the molecule under consideration. Note that because $x = x(t)$, $\mu_x(x_e + x(t))$ is a function of time. The first term in Equation (8.7) is the permanent dipole moment at the equilibrium position, and the second term is the dynamic dipole moment. As we saw earlier, for absorption experiments, it is reasonable to assume that only the $n = 0$ state is populated. Using Equation (7.29), which gives explicit expressions for the eigenfunctions m ,

$$\begin{aligned} \mu_x^{m0} &= A_m A_0 \mu_{0x} \int_{-\infty}^{\infty} H_m(\alpha^{1/2}x) H_0(\alpha^{1/2}x) e^{-\alpha x^2} dx \\ &\quad + A_m A_0 \left[\left(\frac{d\mu_x}{dx} \right)_{x=0} \right] \int_{-\infty}^{\infty} H_m(\alpha^{1/2}x) x H_0(\alpha^{1/2}x) e^{-\alpha x^2} dx \end{aligned} \quad (8.8)$$

The first integral is zero because different eigenfunctions are orthogonal. To solve the second integral, we need to use the specific functional form of $H_m(\alpha^{1/2}x)$. However, because the integration is over the symmetric interval $-\infty < x < \infty$, this integral is zero if the integrand is an odd function of x . As Equation (7.31) shows, the Hermite polynomials $H_m(\alpha^{1/2}x)$ are odd functions of x if m is odd and even functions of x if m is even. The term $x H_0(\alpha^{1/2}x) e^{-\alpha x^2}$ in the integrand is an odd function of x , and, therefore, μ_x^{m0} is zero if $H_m(\alpha^{1/2}x)$ is even. This simplifies the problem because only transitions of the type

$$n = 0 \rightarrow m = 2b + 1, \quad \text{for } b = 0, 1, 2, \dots \quad (8.9)$$

can have nonzero values for μ_x^{m0} .

Do all the transitions indicated in Equation (8.9) lead to nonzero values of μ_x^{m0} ? To answer this question, the integrand $H_m(\alpha^{1/2}x)x H_0(\alpha^{1/2}x) e^{-\alpha x^2}$ is graphed against x for the transitions $n = 0 \rightarrow m = 1$, $n = 0 \rightarrow m = 3$, and $n = 0 \rightarrow m = 5$ in Figure 8.7. Whereas the integrand is positive everywhere for the $n = 0 \rightarrow n = 1$ transition, the areas above the dashed line exactly cancel those below the line for the $n = 0 \rightarrow m = 3$ and $n = 0 \rightarrow m = 5$ transitions, showing that $\mu_0^{mn} = 0$. Therefore, $\mu_x^{m0} \neq 0$ only for the first of the three transitions shown and $\mu_0^{mn} = 0$ for $\Delta n \neq +1$. It can be shown more generally that in the **dipole approximation**, in which only the first two terms in Equation (8.7) are retained, the selection rule for absorption is, $\Delta n = +1$ and for emission it is $\Delta n = -1$. Selection rules are different for different types of spectroscopy. However, within the dipole approximation, the selection rules for any type of spectroscopy are calculated using Equation (8.6) and the appropriate total energy eigenfunctions.

Note that because we found that the first integral in Equation (8.8) was zero, the absence or presence of a permanent dipole moment μ_{0x} is not relevant for the absorption of infrared radiation. For vibrational excitation to occur, the dynamic dipole moment must be nonzero. Because of this condition, homonuclear diatomic molecules do not absorb light in infrared wavelengths. This has important consequences for our environment. The temperature of Earth is determined primarily by an energy balance between visible and ultraviolet (UV) radiation absorbed from the sun and infrared radiation emitted by the planet. The molecules N₂, O₂, and H₂, which have no permanent or transient dipole moment, together with the rare gases make up 99.93% of the atmosphere.

Concept

Selection rules determine which transitions will actually be observed.

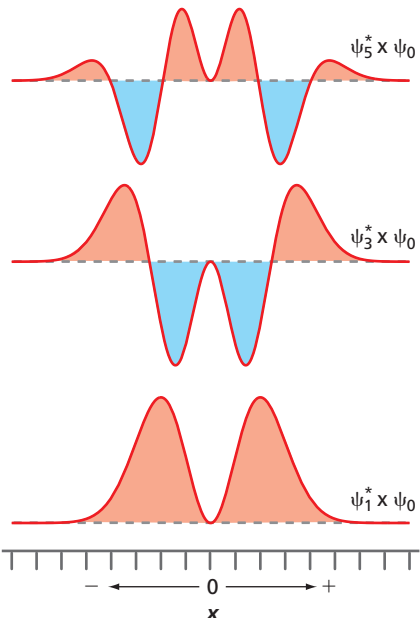
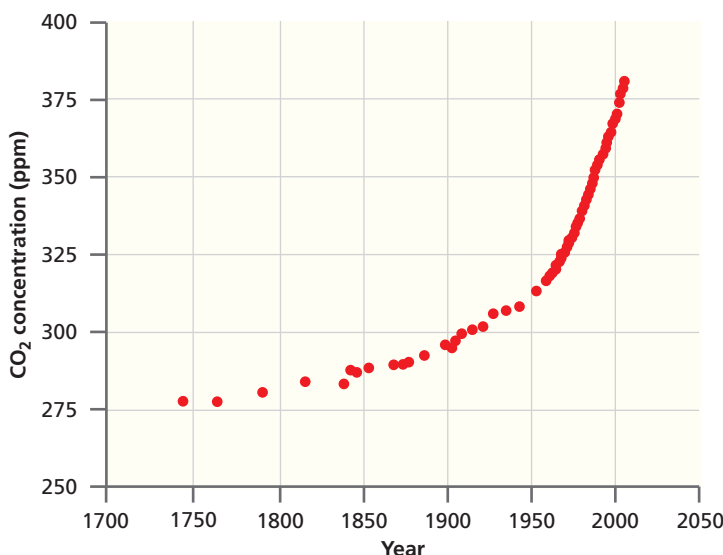


Figure 8.7

The integrand $H_m(\alpha^{1/2}x) \times H_0(\alpha^{1/2}x) e^{-\alpha x^2}$ graphed as a function of x for the transitions $n = 0 \rightarrow m = 1$, $n = 0 \rightarrow m = 3$, and $n = 0 \rightarrow m = 5$. The dashed line shows the zero level for each graph.

Figure 8.8

Atmospheric CO₂ concentration and the CO₂ equivalent of other greenhouse gases plotted as a function of time since the beginning of the industrial revolution.



Concept

Only 0.07% of the gases in Earth's atmosphere contribute to global warming.

These gases do not absorb the infrared radiation emitted by Earth. Therefore, almost all of the Earth's emitted infrared radiation passes through the atmosphere and escapes into space. By contrast, greenhouse gases such as CO₂, NO_x, H₂O, and hydrocarbons absorb the infrared radiation emitted by Earth and radiate a portion of it back to Earth. The concentration of CO₂ in the atmosphere together with the CO₂ equivalent of other greenhouse gases has risen significantly since the beginning of the industrial revolution, as shown in Figure 8.8. The current level is higher than it has been at any time in more than one million years. The result is an increase in Earth's temperature and global warming.

8.5 INFRARED ABSORPTION SPECTROSCOPY

The most basic result of quantum mechanics is that atoms and molecules possess a discrete energy spectrum and that energy can only be absorbed or emitted in amounts that correspond to the difference between two energy levels. Because the energy spectrum for each chemical species is unique, the allowed transitions between these levels provide a “fingerprint” for that species. Using such a fingerprint to identify and quantify the species is a primary role of all chemical spectroscopic techniques. For a molecule of known composition, the vibrational spectrum can also be used to determine the symmetry of the molecule and the force constants associated with the characteristic vibrations.

In absorption spectroscopy in general, electromagnetic radiation from a source of the appropriate wavelength is incident on a sample that is confined in a cell. The chemical species in the sample undergo transitions that are allowed by the appropriate selection rules among rotational, vibrational, or electronic states. The attenuation of light is related to the properties of the material it passes through by the **Beer–Lambert law**, which in differential form is

$$dI(\lambda) = -\varepsilon(\lambda)M I_0(\lambda) dl \quad (8.10)$$

In Equation (8.10), the incident light of intensity $I_0(\lambda)$ is attenuated in passing a distance dl through the sample; M is the concentration of the absorber, and $I(\lambda)$ is the intensity of the transmitted light leaving the cell. Units of moles per liter are commonly used for M in liquid solutions, and partial pressure is used for gas mixtures. Equation (8.10) can be integrated to give

$$\frac{I(\lambda)}{I_0(\lambda)} = e^{-\varepsilon(\lambda)M l} \quad (8.11)$$

The information on the discrete energy spectrum of the chemical species in the cell is contained in the wavelength dependence of the **molar absorption coefficient** $\varepsilon(\lambda)$. It is evident that the strength of the absorption is proportional to $I_0(\lambda)/I(\lambda)$, which increases with $\varepsilon(\lambda)$, M , and with path length l . Because $\varepsilon(\lambda)$ is a function of the

wavelength, absorption spectroscopy experiments typically consist of the elements shown in Figure 8.9. It is shown in Example Problem 8.4 how to use the Beer-Lambert law. In the most basic form of this spectroscopy, a **monochromator** is used to separate the broadband radiation from the source into its constituent wavelengths. After passing through the sample, the transmitted light impinges on the detector. With this setup, only one wavelength can be measured at a time. This form of absorption spectroscopy is unnecessarily time consuming in comparison with Fourier transform techniques, which are discussed in Supplemental Section 8.7.

EXAMPLE PROBLEM 8.4

The molar absorption coefficient $\varepsilon(\lambda)$ for ethane is 40. $(\text{cm bar})^{-1}$ at a wavelength of 12 μm . Calculate $I(\lambda)/I_0(\lambda)$ in a 1.0-cm-long absorption cell if ethane is present at a contamination level of 2.0 ppm in one bar of air. What cell length is required to make $I(\lambda)/I_0(\lambda) = 0.90$?

Solution

$$\text{Using } \frac{I(\lambda)}{I_0(\lambda)} = e^{-\varepsilon(\lambda)ML}$$

$$\frac{I(\lambda)}{I_0(\lambda)} = \exp \left\{ - [40.(\text{cm bar})^{-1} (2.0 \times 10^{-6} \text{ bar}) (1.0 \text{ cm})] \right\} = 0.9992 \approx 1.0$$

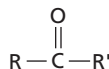
This result shows that for this cell length, light absorption is difficult to detect.

Rearranging the Beer-Lambert equation, we have

$$\begin{aligned} l &= -\frac{1}{M\varepsilon(\lambda)} \ln \left(\frac{I(\lambda)}{I_0(\lambda)} \right) = -\frac{1}{40.(\text{cm bar})^{-1}(2.0 \times 10^{-6} \text{ bar})} \ln(0.90) \\ &= 1.3 \times 10^3 \text{ cm} \end{aligned}$$

Path lengths of this order are possible in sample cells in which the light undergoes multiple reflections from mirrors outside of the cell. Even longer path lengths are possible in *cavity ringdown spectroscopy*. In this method, the absorption cell is mounted between two highly focusing mirrors with a reflectivity greater than 99.99%. Because of the many reflections that take place between the mirrors without appreciable attenuation of the light, the effective length of the cell is very large. The detection sensitivity to molecules such as NO_2 is less than 10 parts per billion using this technique.

How does $\varepsilon(\lambda)$ depend on the wavelength or frequency? We know that for a harmonic oscillator, $\nu = (1/2\pi)\sqrt{k/\mu}$, so that the masses of the atoms and the force constant of the bond determine the resonant frequency. Now consider a molecule such as



The vibrational frequency of the C and O atoms in the carbonyl group is determined by the force constant for the $\text{C}=\text{O}$ bond. This force constant is primarily determined by the chemical bond between these atoms and to a much lesser degree by the adjacent R and R' groups. For this reason, the carbonyl group has a characteristic frequency at which it absorbs infrared radiation that varies in a narrow range for different molecules. These group frequencies are valuable in determining the structure of molecules, and an illustrative set is shown in Table 8.4.

We have shown that a diatomic molecule has a single vibrational peak of appreciable intensity because the overtone frequencies have very low intensities. How many vibrational peaks are observed for larger molecules in an infrared absorption experiment? A molecule consisting of n atoms has three translational degrees of freedom and two or three rotational degrees of freedom depending on whether it is a linear or nonlinear molecule. The remaining $3n - 6$ (nonlinear molecule) or $3n - 5$ (linear)

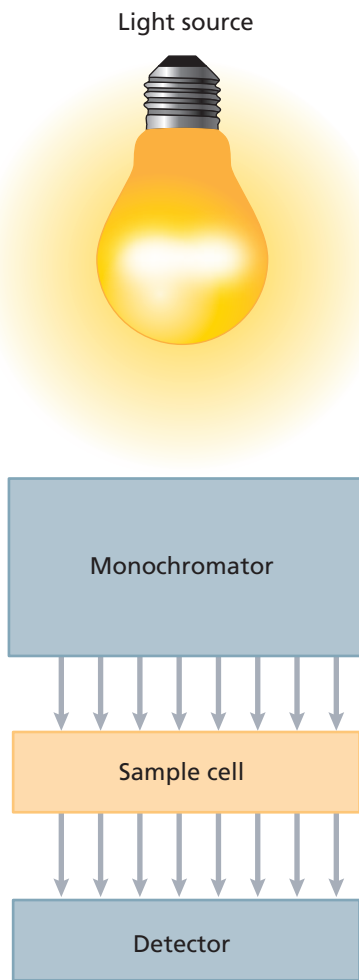


Figure 8.9

Chief elements of a spectroscopy experiment. In an absorption experiment, the dependence of the sample absorption on wavelength is determined. A monochromator is used to filter out a particular wavelength from the broadband light source.

Concept

The Beer-Lambert law allows quantitative measurement of concentrations in a mixture using vibrational spectroscopy.

TABLE 8.4 Selected Group Frequencies

Group	Frequency (cm^{-1})	Group	Frequency (cm^{-1})
O—H stretch	3450–3650	C=O stretch	1650–1750
N—H stretch	3300–3500	C=C stretch	1620–1680
C—H stretch	2800–3000	C—C stretch	1200–1300
C—H bend	1450–1480	C—Cl stretch	600–800

degrees of freedom are vibrational modes. For example, benzene has 30 vibrational modes. However, some of these modes have the same frequency (they are degenerate in energy), so that benzene has only 20 distinct vibrational frequencies.

Let us now examine some experimental data. Vibrational spectra for gas-phase CO and CH_4 are shown in Figure 8.10. Because CO and CH_4 are linear and nonlinear molecules, we expect one and nine vibrational modes, respectively. However, the spectrum for CH_4 shows two rather than nine peaks that we might associate with vibrational transitions. We also see several unexpected broad peaks in the CH_4 spectrum. The single peak in the CO spectrum is much broader than would be expected for a vibrational peak, and it has a deep minimum at the central frequency.

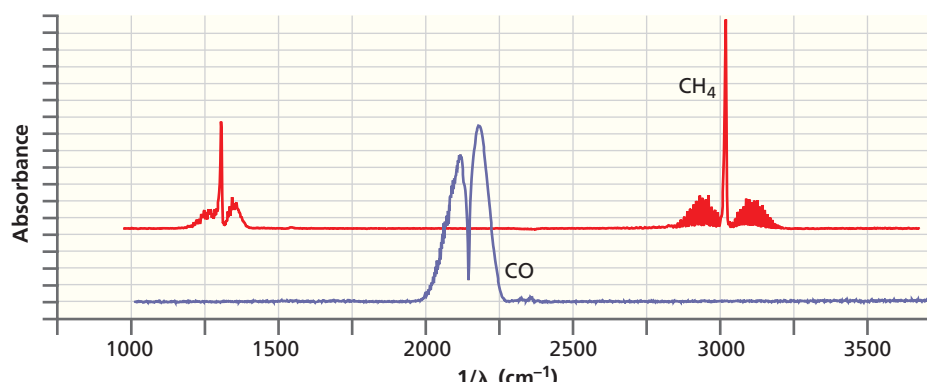
These spectra look different than expected for two reasons. The broadening in the CO absorption peak and the broad envelopes of additional peaks for CH_4 result from transitions between different rotational energy states that occur simultaneously with the $n = 0 \rightarrow n = 1$ transition between vibrational energy levels. We will discuss transitions between rotational energy levels and analyze a high-resolution infrared absorption spectrum for a diatomic molecule in some detail in Section 8.6. At this point, we simply note that absorption of infrared radiation results in both rotational and vibrational, rather than just vibrational, transitions.

The second unexpected feature in Figure 8.10 is that two and not nine peaks are observed in the CH_4 spectrum. Why is this? To discuss the vibrational modes of polyatomic species in more detail, the information about molecular symmetry and group theory discussed in Chapter 16 is needed. For now, we simply state the results. In applying group theory to the CH_4 molecule, the 1306 cm^{-1} peak can be associated with three degenerate C—H bending modes, and the 3020 cm^{-1} peak can be associated with three degenerate C—H stretching modes. This still leaves three vibrational modes unaccounted for. Again, applying group theory to the CH_4 molecule, one finds that these modes are symmetric and do not satisfy the condition $d\mu_x/dx \neq 0$. Therefore, they are infrared inactive. However, the stretching mode for CO and all modes for CH_4 are active in Raman spectroscopy, which we will discuss in Supplemental Section 8.8.

Of the 30 vibrational modes for benzene, four peaks (corresponding to 7 of the 30 modes) are observed in infrared spectroscopy, and seven peaks (corresponding to 12 of the 30 modes) are observed in Raman spectroscopy. None of the frequencies is observed in both Raman and infrared spectroscopy. Eleven vibrational modes are neither infrared nor Raman active.

Concept

Some vibrational modes can be observed using infrared spectroscopy whereas other modes are observed using Raman spectroscopy.

**Figure 8.10**

Infrared absorption spectra of gaseous CO and CH_4 . The curves for the two molecules are offset vertically for clarity.

Although the discussion to this point might lead us to believe that each bonded pair of atoms in a molecule vibrates independently of the others, this is not the case. For example, we might think that the linear CO_2 molecule has a single $\text{C}=\text{O}$ stretching frequency because the two $\text{C}=\text{O}$ bonds are equivalent. However, experiments show that this molecule has two distinct $\text{C}=\text{O}$ stretching frequencies. Why is this the case? When one $\text{C}=\text{O}$ bond vibrates, the atomic positions and electron distribution throughout the molecule are changed, thereby influencing the other $\text{C}=\text{O}$ bond. In other words, we can view the CO_2 molecule as consisting of two coupled harmonic oscillators that undergo concerted vibrations known as *normal modes*. Normal modes have the following characteristics: (1) A normal mode is a concerted motion of all atoms such that all atoms oscillate about their equilibrium positions in phase and pass through their maximum and minimum amplitudes at the same time. (2) The center of mass of the molecule does not move in the vibration. (3) Each normal mode acts like a single harmonic oscillator with a characteristic frequency and the normal modes do not mix with one another.

We next use a simplified argument to derive the $3n - 5 = 4$ normal modes of the linear CO_2 molecule. For this derivation and a more detailed discussion of normal modes, see the reference to Berry et al. in Further Reading. We know that the CO_2 molecule is linear and that the two $\text{C}=\text{O}$ bond lengths are equal, as shown in Figure 8.11.

We also know that all three components of both the total linear and angular momentum of the vibrating molecule are equal to zero because the molecule is neither in translational nor in rotational motion. Therefore

$$p_x = \sum_{i=1}^3 m_i v_{xi} = 0; \quad p_y = \sum_{i=1}^3 m_i v_{yi} = 0; \quad p_z = \sum_{i=1}^3 m_i v_{zi} = 0; \quad (8.12)$$

$$l_y = \sum_{i=1}^3 \pm R_0 m_i v_{zi} = 0; \quad l_z = \sum_{i=1}^3 \pm R_0 m_i v_{yi} = 0 \quad (8.13)$$

The signs in Equation (8.13) are determined by using the right-hand rule for the direction of the angular momentum (see Math Essential 7). The component l_x is negligibly small because displacements perpendicular to the molecular axis are very small.

The x component of linear momentum of atom i is $m_i v_i = m_i(dx_i/dt)$. At this point, we take advantage of the fact that for an oscillation, the functional dependence of each coordinate x_i with time is a sine function. Therefore, the variation of v_i with time is a cosine function, which is simply the sine function one-quarter period later. Furthermore, we can substitute the coordinate x_i for v_i in Equation (8.12) because x_i and v_i are simply related by a phase shift. Because oxygen occurs at both ends of the molecule, we obtain the three equations

$$\begin{aligned} m_O(x_1 + x_3) + m_C x_2 &= 0 \\ m_O(y_1 + y_3) + m_C y_2 &= 0 \\ m_O(z_1 + z_3) + m_C z_2 &= 0 \end{aligned} \quad (8.14)$$

In calculating angular momentum, only the oxygen atoms at the ends of the molecule contribute. We again substitute the position coordinate for velocity and obtain

$$\begin{aligned} m_O R_0(z_1 - z_3) &= 0 \\ m_O R_0(y_3 - y_1) &= 0 \end{aligned} \quad (8.15)$$

Equation (8.15) immediately gives $z_1 = z_3$ and $y_3 = y_1$ as solutions. Substituting these results into Equation (8.14) gives the displacements for two normal modes

$$y_1 = y_3; \quad y_2 = -\frac{2m_O}{m_C} y_1 \quad \text{and} \quad (8.16)$$

$$z_1 = z_3; \quad y_2 = -\frac{2m_O}{m_C} z_1 \quad (8.17)$$

For the x coordinate, rearranging the first entry in Equation (8.14) gives

$$x_2 = -\frac{m_O}{m_C}(x_1 - x_3) \quad (8.18)$$

Concept

Frequencies observed in vibrational spectra correspond to normal modes, which are collective vibrations of the whole molecule.

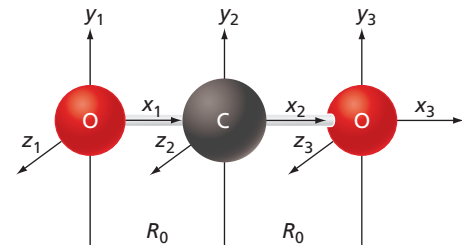
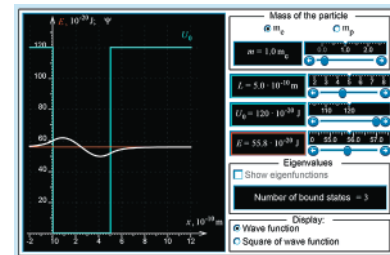
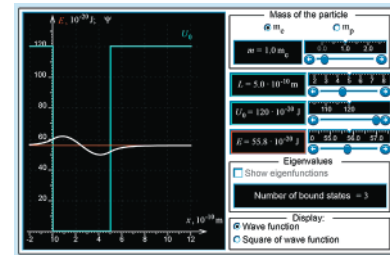


Figure 8.11

The coordinates of each of the atoms in CO_2 that are used to derive the normal modes of vibration.



W8.2 Normal modes for H_2O
W8.3 Normal modes for CO_2

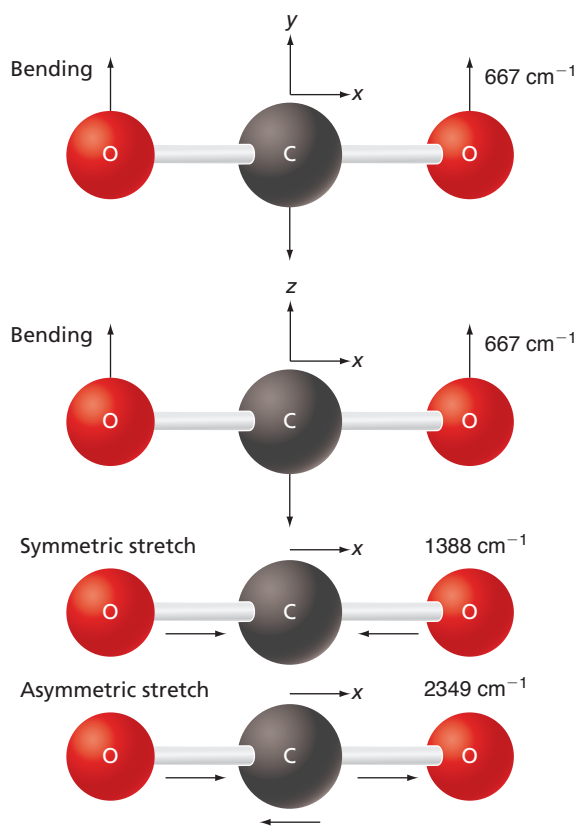


W8.4 Normal modes for NH_3
W8.5 Normal modes for formaldehyde

Figure 8.12

Normal modes for vibration of CO₂.

The experimentally observed vibrational frequencies for C¹²O₂¹⁶ are shown.



Two relationships between x_1 and x_3 are consistent with the fact that the two O atoms are indistinguishable, namely, $x_1 = x_3$ and $x_1 = -x_3$. The displacements for these two normal modes are given by

$$x_1 = x_3; \quad x_2 = -\frac{2m_O}{m_C}x_1 \quad \text{and} \quad (8.19)$$

$$x_1 = -x_3; \quad x_2 = 0 \quad (8.20)$$

The displacements of the atoms in CO₂ from their equilibrium positions for these four normal modes are shown in Figure 8.12.

In order to estimate the relative vibrational frequencies of these normal modes of CO₂, the force constants must be known. Because bending changes the nearest-neighbor spacing less than motion along the internuclear axis, we expect that the two bending modes will have the lowest frequencies. As these bending modes differ only in the orientation of the molecule, the frequencies will be the same. In the symmetric stretch, only the oxygen atoms are moving, whereas in the asymmetric stretch, the carbon displacement is larger than the oxygen displacement. The vibrational frequency of a harmonic oscillator depends inversely on $\sqrt{\mu}$. We therefore expect the frequency of the asymmetric mode to be greater than the symmetric mode because the C atom is lighter than the O atom. These conclusions are consistent with experimental observations on C¹²O₂¹⁶, as shown in Figure 8.12.

8.6 ROTATIONAL SPECTROSCOPY

As for the harmonic oscillator, a selection rule governs the absorption of electromagnetic energy for a molecule to change its rotational energy, namely, $\Delta J = J_{final} - J_{initial} = \pm 1$. Although we do not derive this selection rule, Example Problem 8.5 shows that it holds for a specific case.

Note that we have just changed the symbol for the angular momentum quantum number from l to J . The quantum number l is usually used for orbital angular momentum (for example, the electron orbiting around the nucleus), and J is usually used for rotating molecules.

EXAMPLE PROBLEM 8.5

Using the following total energy eigenfunctions for the three-dimensional rigid rotor, show that the $J = 0 \rightarrow J = 1$ transition is allowed and that the $J = 0 \rightarrow J = 2$ transition is forbidden:

$$Y_0^0(\theta, \phi) = \frac{1}{(4\pi)^{1/2}}$$

$$Y_1^0(\theta, \phi) = \left(\frac{3}{4\pi}\right)^{1/2} \cos\theta$$

$$Y_2^0(\theta, \phi) = \left(\frac{5}{16\pi}\right)^{1/2} (3 \cos^2\theta - 1)$$

The notation $Y_J^{M_J}$ is used for the preceding functions.

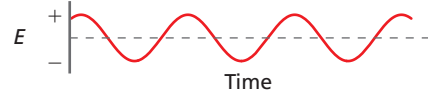
Solution

Assuming the electromagnetic field to lie along the z axis, $\mu_z = \mu \cos\theta$, and the transition dipole moment takes the form

$$\mu_z^{J_0} = \mu \int_0^{2\pi} d\phi \int_0^\pi Y_J^0(\theta, \phi) (\cos\theta) Y_0^0(\theta, \phi) \sin\theta d\theta$$

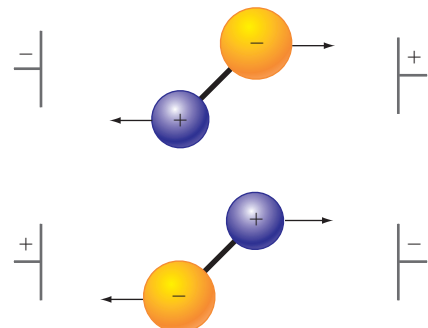
For the $J = 0 \rightarrow J = 1$ transition,

$$\mu_z^{10} = \mu \frac{\sqrt{3}}{4\pi} \int_0^{2\pi} d\phi \int_0^\pi \cos^2\theta \sin\theta d\theta = \frac{\mu\sqrt{3}}{2} \left[-\frac{\cos^3\theta}{3} \right]_{\theta=0}^{\theta=\pi} = \frac{\mu\sqrt{3}}{3} \neq 0$$



For the $J = 0 \rightarrow J = 2$ transition,

$$\begin{aligned} \mu_z^{20} &= \mu \frac{\sqrt{5}}{8\pi} \int_0^{2\pi} d\phi \int_0^\pi (3 \cos^2\theta - 1) \cos\theta \sin\theta d\theta \\ &= \mu \frac{\sqrt{5}}{4} \left[-\frac{3 \cos^4\theta}{4} + \frac{\cos^2\theta}{2} \right]_{\theta=0}^{\theta=\pi} \\ &= \mu \frac{\sqrt{5}}{4} \left[-\frac{1}{4} + \frac{1}{4} \right] = 0 \end{aligned}$$

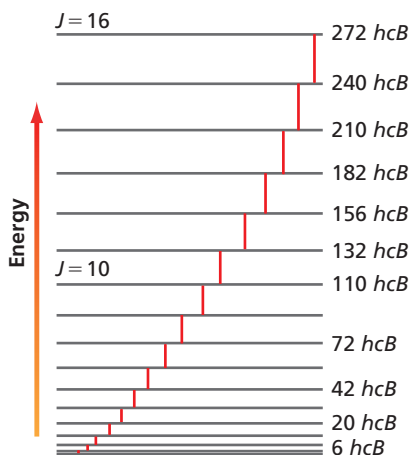


The preceding calculations show that the $J = 0 \rightarrow J = 1$ transition is allowed and that the $J = 0 \rightarrow J = 2$ transition is forbidden.

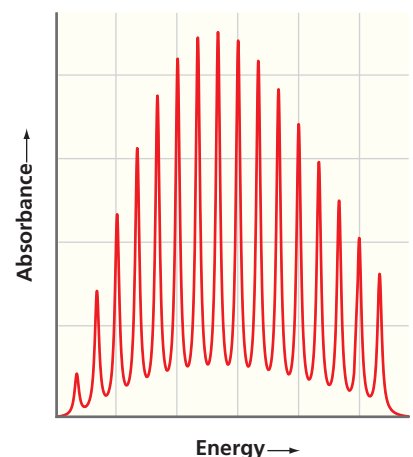
In discussing vibrational spectroscopy, we learned that a molecule must have a nonzero dynamic dipole moment to absorb infrared radiation. By contrast, a molecule must have a permanent dipole moment to absorb energy in the microwave frequency range in which rotational transitions occur. As was the case for vibrational spectroscopy, the dominant interaction with the electric field is through the dipole moment. This is shown schematically in Figure 8.13.

Figure 8.13

The interaction of a rigid rotor with an electric field. Imagine the sinusoidally varying electric field shown at the top of the figure applied between a pair of capacitor plates. The arrows indicate the direction of force on each of the two charged masses. If the frequencies of the field and rotation are equal, the rotor will absorb energy from, or emit energy into, the electric field.



(a) Energy levels for a rigid rotor.



(b) Spectrum observed through absorption of microwave radiation.

Figure 8.14

Transitions allowed by the selection rule $\Delta J = J_{final} - J_{initial} = +1$ and a simulated rotational spectrum. The allowed transitions between levels are shown as vertical bars.

Concept

In contrast to vibrational spectra, many transitions are observed in rotational spectra.

As shown in Section 7.5, the dependence of the rotational energy on the quantum number is given by

$$E_J = \frac{\hbar^2}{2\mu r_0^2} J(J+1) = \frac{\hbar^2}{8\pi^2 \mu c r_0^2} J(J+1) = hcBJ(J+1) \quad (8.21)$$

In this equation, the constants specific to a molecule are combined in the so-called **rotational constant** $B = h/(8\pi^2 c \mu r_0^2)$. The factor c is included in B so that it has the units of inverse centimeters rather than inverse seconds. The energy levels and transitions allowed by the selection rule $\Delta J = J_{final} - J_{initial} = \pm 1$ as well as a simulated rotational spectrum are shown in Figure 8.14.

We can calculate the energy corresponding to rotational transitions for $\Delta J = +1$ and $\Delta J = -1$ originating from energy level J . $\Delta J = +1$ corresponds to absorption and $\Delta J = -1$ corresponds to emission of a photon. In the following equations, J is the quantum number of the state from which the transition occurs.

$$\Delta E = E(J_{final}) - E(J_{initial})$$

for $\Delta J = +1$

$$\begin{aligned} \Delta E_+ &= \frac{\hbar^2}{2\mu r_0^2} (J+1)(J+2) - \frac{\hbar^2}{2\mu r_0^2} J(J+1) \\ &= \frac{\hbar^2}{2\mu r_0^2} [(J^2 + 3J + 2) - (J^2 + J)] = \frac{\hbar^2}{\mu r_0^2} (J+1) \\ &= 2hcB(J+1) \end{aligned}$$

for $\Delta J = -1$

$$\begin{aligned} \Delta E_- &= \frac{\hbar^2}{2\mu r_0^2} (J-1)J - \frac{\hbar^2}{2\mu r_0^2} J(J+1) \\ &= \frac{\hbar^2}{2\mu r_0^2} [(J^2 - J) - (J^2 + J)] = -\frac{\hbar^2}{\mu r_0^2} J = -2hcBJ \quad (8.22) \end{aligned}$$

Note that $|\Delta E_+| \neq |\Delta E_-|$ because the energy levels are not equally spaced. We see that the larger the J value of the originating energy level, the more energetic the photon must be to promote excitation to the next highest energy level. Because the rotational energy does not depend on m_J , each energy level is $(2J+1)$ -fold degenerate.

EXAMPLE PROBLEM 8.6

Because of the very high precision of frequency measurements, bond lengths can be determined with a correspondingly high precision, as illustrated in this example. From the rotational microwave spectrum of ${}^1\text{H}{}^{35}\text{Cl}$, we find that $B = 10.59342 \text{ cm}^{-1}$. Given that the masses of ${}^1\text{H}$ and ${}^{35}\text{Cl}$ are 1.0078250 and 34.9688527 amu, respectively, determine the bond length of the ${}^1\text{H}{}^{35}\text{Cl}$ molecule.

Solution

$$B = \frac{h}{8\pi^2 \mu c r_0^2}$$

$$r_0 = \sqrt{\frac{h}{8\pi^2 \mu c B}}$$

$$\begin{aligned} &= \sqrt{\frac{6.62606957 \times 10^{-34} \text{ J s}}{8\pi^2 c \left(\frac{(1.0078250)(34.9688527) \text{ amu}}{1.0078250 + 34.9688527} \right) (1.66054 \times 10^{-27} \text{ kg amu}^{-1}) (10.59342 \text{ cm}^{-1})}} \\ &= 1.274551 \times 10^{-10} \text{ m} \end{aligned}$$

TABLE 8.5 Rotational Frequencies, $\Delta(\Delta\nu)$ and $\Delta E/k_B T$ at 300. K for $^1\text{H}^{35}\text{Cl}$

$J \rightarrow J'$	$\Delta\nu$	$\Delta\nu \text{ HCl/s}^{-1}$	$\Delta(\Delta\nu)$	$\Delta(\Delta\nu) \text{ HCl/s}^{-1}$	$\Delta E/k_B T$ at 300. K
$0 \rightarrow 1$	$2cB$	6.3158×10^{11}	$2cB$	6.3158×10^{11}	0.102
$1 \rightarrow 2$	$4cB$	1.27036×10^{12}	$2cB$	6.3158×10^{11}	0.203
$2 \rightarrow 3$	$6cB$	1.90554×10^{12}	$2cB$	6.3158×10^{11}	0.305
$3 \rightarrow 4$	$8cB$	2.54072×10^{12}	$2cB$	6.3158×10^{11}	0.406
$4 \rightarrow 5$	$10cB$	3.1759×10^{12}	$2cB$	6.3158×10^{11}	0.508

The structure of a rotational spectrum becomes more apparent when we consider the energy-level spacing in more detail. Table 8.5 shows the frequencies needed to excite various transitions consistent with the selection rule $\Delta J = J_{final} - J_{initial} = +1$ in general as well as for $^1\text{H}^{35}\text{Cl}$. Each of these transitions can lead to absorption of electromagnetic radiation. We see that for successive initial values of J , the ΔE associated with the transition increases in such a way that the difference between these $\Delta\nu$, which we call $\Delta(\Delta\nu)$, is constant. This means that the spectrum for a molecule immersed in a microwave field with a broad range of frequencies shows a series of equally spaced lines, separated in frequency by $2cB$, as seen in Figure 8.14. It is shown in Example Problem 8.6 how to obtain the bond length of a diatomic molecule from a rotational spectrum.

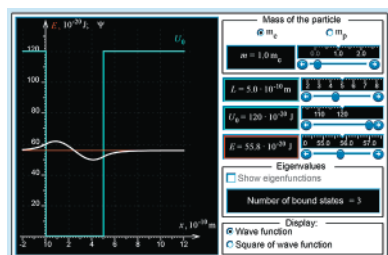
How many absorption peaks will be observed? For vibrational spectroscopy, we expect only one intense peak for the following reasons. The energy-level spacing between adjacent levels is the same for all values of the quantum number in the harmonic approximation so that, given the selection rule $\Delta n = +1$, all transitions have the same frequency. Also, in general only the $n = 0$ energy level has a significant population so that even taking anharmonicity into account will not generate additional peaks originating from peaks with $n > 0$. However, the situation is different for rotational transitions. Note that because the rotational energy levels are not equally spaced in energy, different transitions give rise to separate peaks. Additionally, $\Delta E_{rotation} < k_B T$ under most conditions so that many rotational energy levels will be populated. Therefore, many peaks are generally observed in a rotational spectrum.

Up to this point, we have considered rotation and vibration separately. In the microwave region of the electromagnetic spectrum, the photon energy is sufficient to excite rotational transitions but not to excite vibrational transitions. However, this is not the case for infrared radiation. Diatomic molecules that absorb infrared radiation can make transitions in which both n and J change according to the selection rules $\Delta n = +1$ and $\Delta J = \pm 1$. Therefore, an infrared absorption spectrum contains both vibrational and rotational transitions. What does a rotational-vibrational spectrum look like? To answer this question, first consider the relative photon energies associated with rotational and vibrational excitation. The energy levels for both degrees of freedom are indicated schematically in Figure 8.15. The ratio of the smallest value of ΔE in a rotational transition to that in a vibrational transition is

$$\frac{\Delta E_{rot}}{\Delta E_{vib}} = \frac{\hbar^2/\mu r_0^2}{\hbar\sqrt{k/\mu}} = \frac{\hbar}{r_0^2\sqrt{k\mu}} \quad (8.23)$$

This ratio is molecule specific, but we consider two extremes. For H_2 and I_2 , $\Delta E_{rot}/\Delta E_{vib}$ is 0.028 and 0.00034, respectively, where ΔE_{rot} is for the $J = 0 \rightarrow J = 1$ transition. In both cases, there are many rotational levels between adjacent vibrational levels. Large moments of inertia (large atomic masses and/or long bonds) and large force constants (strong bonds) lead to a smaller value of $\Delta E_{rot}/\Delta E_{vib}$. It is largely the difference in the moment of inertia $I = \mu r_0^2$ that makes the ratio so different for I_2 and H_2 .

On the basis of the previous discussion, what will be seen in an infrared absorption experiment on a diatomic molecule in which both rotational and vibrational transitions



W8.6 Rotational spectra

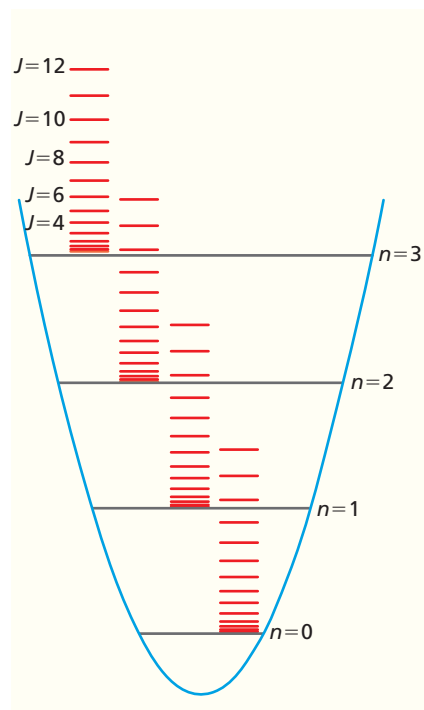


Figure 8.15

Schematic representation of rotational and vibrational levels. Each vibrational level has a set of rotational levels associated with it. Therefore, vibrational transitions usually also involve rotational transitions. The rotational levels are shown on an expanded energy scale and are much more closely spaced for real molecules.

occur? As discussed in Section 8.3, the dominant vibrational transition is $n = 0 \rightarrow n = 1$. All transitions must now satisfy two selection rules, $\Delta n = +1$ and $\Delta J = \pm 1$. As discussed earlier, a vibrational-rotational spectrum will exhibit many different rotational transitions. What can one predict about the relative intensities of the peaks? Recall that the intensity of a spectral line in an absorption experiment is determined by the number of molecules in the energy level from which the transition originates. (This rule holds as long as the upper state population is small compared to the lower state population.) How many molecules are there in states for a given value of J relative to the number in the ground state for which $J = 0$? This ratio can be calculated using the Boltzmann distribution:

$$\frac{n_J}{n_0} = \frac{g_J}{g_0} e^{-(E_J - E_0)/k_B T} = (2J + 1) e^{-\hbar^2 J(J+1)/2Ik_B T} \quad (8.24)$$

The term g_J/g_0 in the middle expression in Equation (8.24) is the ratio of the degeneracy of the energy level J to that for $J = 0$. It generally dominates n_J/n_0 for small J and sufficiently large T . However, as J increases, the exponential term causes n_J/n_0 to decrease rapidly with increasing J . For molecules with a large moment of inertia, the exponential term does not dominate until J is quite large. As a result, many rotational energy levels are occupied; this behavior is seen for CO in Figure 8.16. Because many levels are occupied, a large number of peaks are observed in a rotational spectrum. For a molecule with a small moment of inertia, the rotational levels can be far enough apart that few rotational states are populated. This behavior is shown in Figure 8.16 for HD. At 100. K, only the $J = 0, 1$, and 2 states have an appreciable population. Increasing the temperature raises this upper value of J to approximately 4 and 7 for 300. and 700. K, respectively. The corresponding J values for CO are 13, 23, and 33.

Therefore, as long as n_J/n_0 increases with J , the intensity of the spectral peaks originating from states with those J values will increase. Beyond the J values for which n_J/n_0 increases, the intensity of the peaks decreases.

A simulated rotational-vibrational infrared absorption spectrum for HCl is shown in Figure 8.17. Such a spectrum consists of two nearly symmetric parts. The higher frequency part of the spectrum corresponds to transitions in which $\Delta J = +1$ and is called the **R branch**. The lower frequency part of the spectrum corresponds to transitions in which $\Delta J = -1$ and is called the **P branch**. Note that the gap in the center of the spectrum corresponds to $\Delta J = 0$, which is a forbidden transition in the dipole approximation for a linear molecule. Without going into more detail, note that Raman spectroscopy (see Supplemental Section 8.8) also shows both rotational and vibrational transitions. However, the selection rules are different. For rotational Raman spectra,

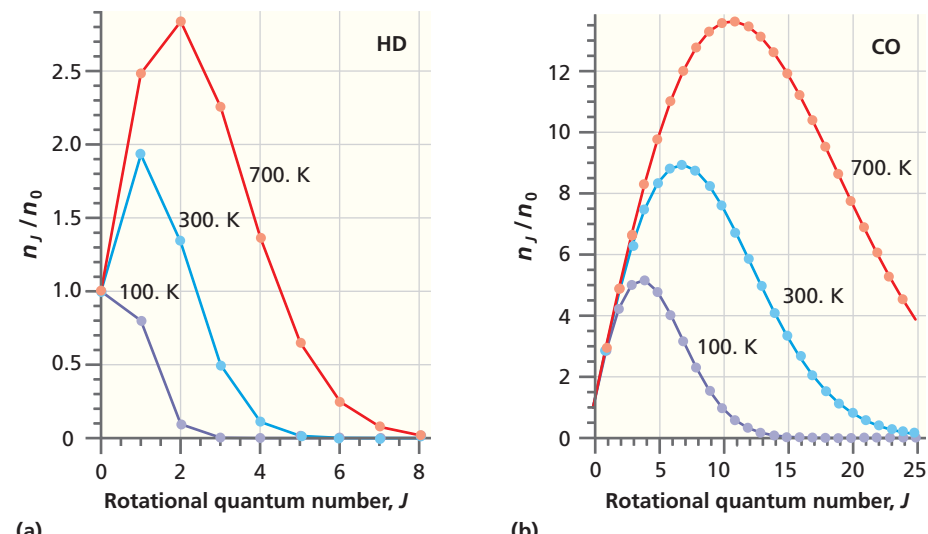
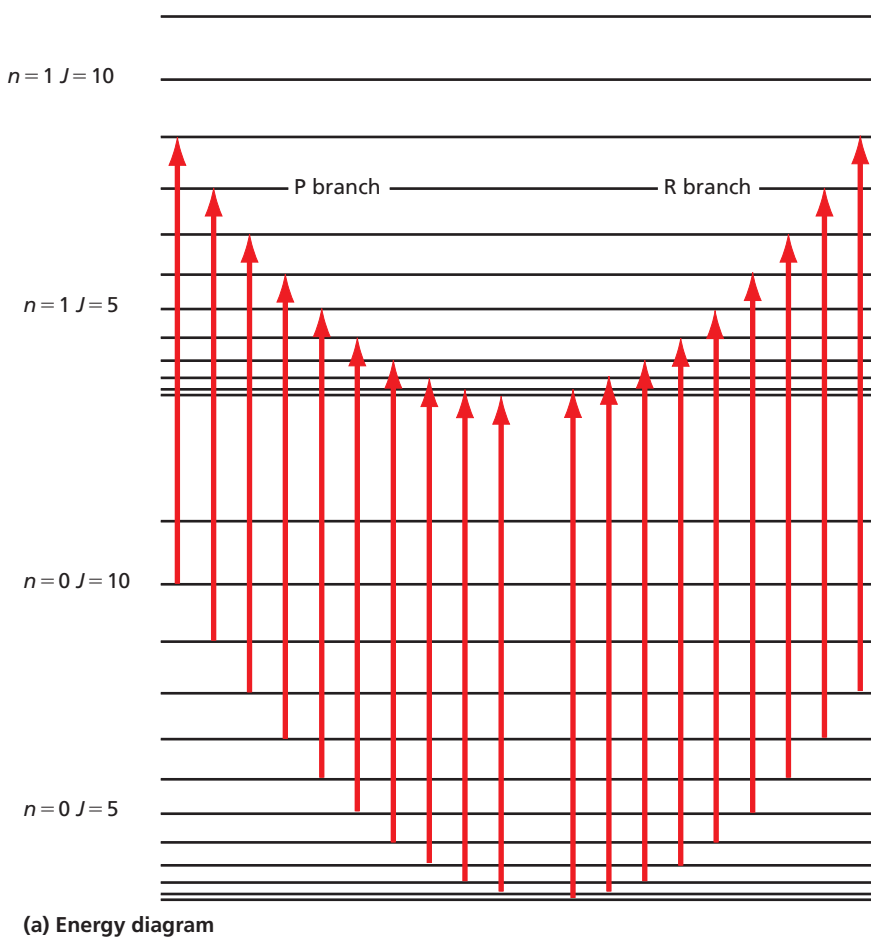
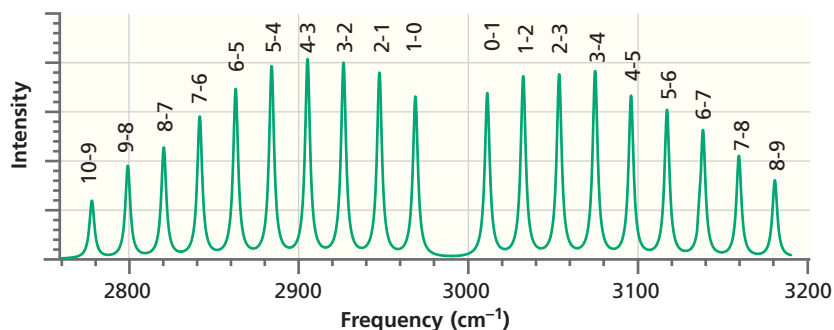


Figure 8.16

Number of molecules in energy levels corresponding to the quantum number J relative to the number in the ground state as a function of J . The ratios are shown at three different temperatures for (a) HD and (b) CO.



(a) Energy diagram



(b) Absorption spectrum

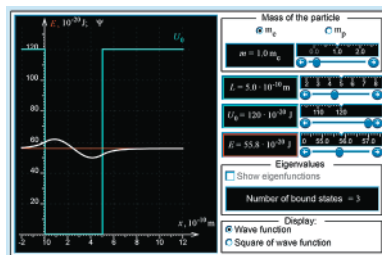
Figure 8.17

Simulated energy diagram and 300. K infrared absorption spectrum for $H^{35}Cl$.

(a) Energy diagram and (b) absorption spectrum. The two indices above the peak refer to the initial (first) and final (second) J values. The region of the spectrum with $\Delta J = +1$ (higher frequency) is called the R branch, and the region of the spectrum with $\Delta J = -1$ (lower frequency) is called the P branch. The energy levels in (a) are not drawn to scale.

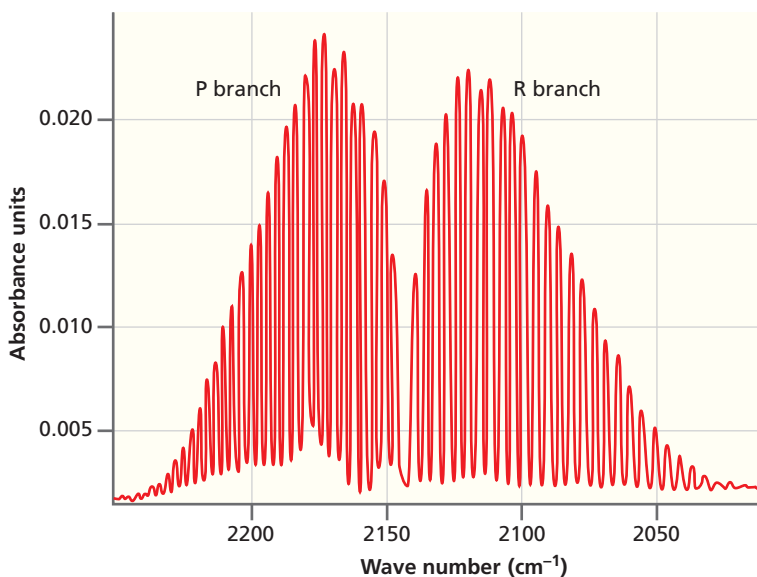
Concept

Infrared absorption spectra will exhibit peaks corresponding to both vibrational and rotational transitions.


W8.7 Vibrational-rotational spectra

the selection rule is $\Delta J = 0, \pm 2$, and not $\Delta J = \pm 1$ as it is for absorption spectra in the infrared or microwave ranges.

Based on this discussion of rotational-vibrational spectroscopy and the results shown in Figures 8.16 and 8.17, it is useful to revisit the infrared spectra of CO and CH_4 shown in Figure 8.10. The broad unresolved peaks between 2000 and 2250 cm^{-1} for CO are the P and R branches corresponding to rotational-vibrational excitations. The minimum near 2150 cm^{-1} corresponds to the forbidden $\Delta J = 0$ transition. The broad and only partially resolved peaks for CH_4 seen around the sharp peaks centered near 1300 and 3000 cm^{-1} are again the P and R branches. The $\Delta J = 0$ transition is allowed for methane and is the reason the sharp central peaks are observed in the methane spectrum visible in Figure 8.10. To demonstrate the origin of the broad CO peaks in Figure 8.10, a high-resolution infrared absorption spectrum for this molecule is shown in Figure 8.18. It is apparent that the envelopes of the P and R branches in this figure correspond to the broad unresolved peaks in Figure 8.10.

**Figure 8.18**

A high-resolution spectrum for CO. The *P* and *R* branches are resolved into the individual rotational transitions.

S U P P L E M E N T A L S E C T I O N

8.7 FOURIER TRANSFORM INFRARED SPECTROSCOPY

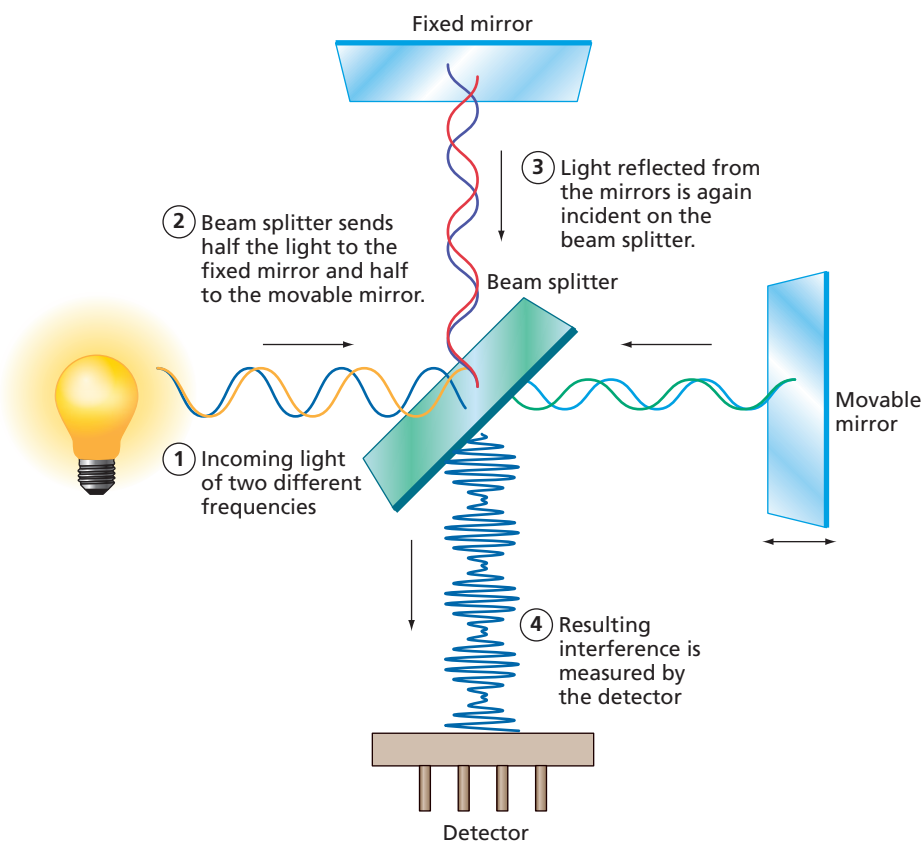
To investigate how infrared absorption spectra are obtained in practice, we now turn to a discussion of Fourier transform infrared (FTIR) spectroscopy, which is the most widely used technique for obtaining vibrational absorption spectra. **FTIR spectroscopy** improves on the schematic absorption experiment shown in Figure 8.9 by eliminating the monochromator and analyzing light of all frequencies simultaneously. By doing so, it achieves a **multiplex advantage** that is equivalent to carrying out many single-wavelength experiments simultaneously. This technique allows a spectrum to be obtained in a short time and therefore has become the experimental method of choice for absorption vibrational spectroscopy. We describe how FTIR spectroscopy works in this section.

The multiplex advantage in FTIR is gained by using a **Michelson interferometer** to determine the frequencies at which radiation is absorbed by molecules. A schematic drawing of this instrument is shown in Figure 8.19. The most important components of the interferometer are a beam splitter that both transmits and reflects 50% of the incident light, a fixed mirror, a movable mirror, and the detector. The functioning of a Michelson interferometer is first explained by analyzing its effect on monochromatic radiation. An incoming traveling plane wave of amplitude $A_0 \exp\{i(kx - \omega t)\}$ impinges on the beam splitter from the left. Fifty percent of the light is reflected to the movable mirror, and 50% to the fixed mirror. Each of these two waves is reflected from the mirrors and travels back to the beam splitter. The wave that is reflected back from the movable mirror and reflected by the beam splitter interferes with the wave that is reflected from the fixed mirror and transmitted by the beam splitter. The recombined wave resulting from this interference travels in the negative y direction and has an amplitude at the detector plane $y = y_D$ given by

$$\begin{aligned} A(t) &= \frac{A_0}{\sqrt{2}} [\exp\{i(ky_D - \omega t)\} + \exp\{i(k[y_D + \Delta d(t)] - \omega t)\}] \\ &= \frac{A_0}{\sqrt{2}} (1 + e^{i\delta(t)}) \exp\{i(ky_D - \omega t)\} \end{aligned} \quad (8.25)$$

Concept

FTIR spectroscopy is equivalent to obtaining many single wavelength spectra simultaneously.

**Figure 8.19**

Schematic diagram of a Michelson interferometer. Light of two different frequencies enters from the left and is incident on a beam splitter that sends half the light to the fixed mirror at the top and half to the movable mirror on the right. The light reflected from the mirrors is again incident on the beam splitter, and the resulting interference is measured by the detector. The light reflected from the mirrors, but not the light incident on the mirrors, is shown.

The two interfering waves have a phase difference $\delta(t)$ that results from the path difference Δd that the two interfering waves have traveled. It arises because the two mirrors are not equidistant from the beam splitter. The path difference is given by

$$\delta(t) = \frac{2\pi}{\lambda} \Delta d(t) = \frac{2\pi}{\lambda} 2vt = \frac{2v}{c} \omega t \quad (8.26)$$

In this equation, v is the speed at which the mirror is moved, and ω is related to the wavelength and frequency of the entering light by $\omega = 2\pi c/\lambda = 2\pi\nu$. The intensity of the resultant wave at the detector plane I is proportional to the product $A(t)A^*(t)$:

$$I(y_D, t) = \frac{I_0}{2}(1 + \cos \delta(t)) = \frac{I_0}{2} \left(1 + \cos \left[\frac{2v}{c} \omega t\right]\right) \quad (8.27)$$

where $I_0 = A_0^2$. The intensity varies with distance as the movable mirror travels toward the beam splitter. Whenever $\Delta d = n\lambda$, the interference is constructive, and the maximum intensity is transmitted to the detector. Whenever $\Delta d = (2n + 1)(\lambda/2)$, the interference is destructive and no intensity is transmitted to the detector. This result is depicted in Figure 8.20a. For the more general case of light of several frequencies, j , incident on the interferometer, Equation (8.27) becomes

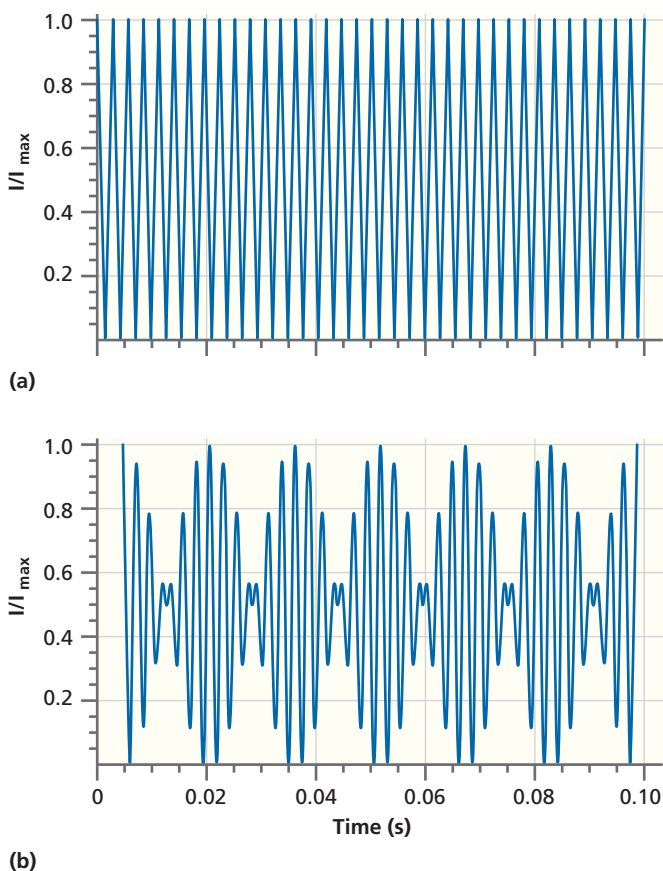
$$I(y_D, t) = \sum_j I(\omega_j) \left(1 + \cos \left[\frac{2v}{c} \omega_j t\right]\right) \quad (8.28)$$

The signal $I(y_D, t)$ measured by the detector is called an **interferogram** because it results from the interference of the two waves. For incoming light of a single frequency, the interferogram is a sine wave, as shown in Figure 8.20a. For light of two closely spaced frequencies, a more complex interferogram, including a beat frequency, is observed, as shown in Figure 8.20b.

To this point we have considered only light for which the frequency is exactly known. A more realistic case is assigning a frequency width to a vibrational transition. This is equivalent to saying that a peak in the spectrum is a superposition of closely

Figure 8.20

Examples of interferograms. Interferograms calculated for (a) a single frequency of $\omega = 5.65 \times 10^{13} \text{ s}^{-1}$ and for (b) light of equal intensity and frequencies of $\omega = 5.65 \times 10^{13} \text{ s}^{-1}$ and $6.60 \times 10^{13} \text{ s}^{-1}$. The mirror speed is $v = 0.600 \text{ cm s}^{-1}$. The vertical axis shows the intensity relative to the maximum value.



Concept

A spectrum is obtained from an interferogram using the Fourier transform.

spaced frequencies. In this case, the interferogram decays to a low amplitude outside of the center that corresponds to $\Delta d(t) = 0$, as shown in Figure 8.21. By comparing the different parts of Figure 8.21, one can conclude that the interferogram is sensitive to both the light frequency and the relative amplitude of the different frequencies.

The experimental result of a FTIR measurement is the interferogram. To learn what frequencies gave rise to a particular interferogram, we make use of the **Fourier transform**, which is closely related to the Fourier sine and cosine series discussed in Section 2.7. Consider the periodic function of time shown in Figure 8.22 with period τ . Recall from Section 2.7 that such a function can be represented by a Fourier series of sine and cosine functions.

We let the period of the function, τ , approach infinity by increasing the length of the region in which the function is zero, so that the function consists of very widely spaced peaks. The frequencies of the individual sine and cosine terms such as $\cos(2\pi nt/\tau)$ in the series depend inversely on the period length and therefore become so closely spaced that we can replace the sum of sine and cosine terms in the Fourier series by an integral over time. In that case, the sum over discrete frequencies in the complex representation of the Fourier series becomes the integral

$$f(\omega) = \sum_{n=-\infty}^{\infty} c_n e^{-2\pi i n(t/\tau)} \Rightarrow \int_{-\infty}^{\infty} g(t) e^{-i\omega t} dt \quad (8.29)$$

and we can relate the time and frequency description of the function by

$$f(\omega) = \int_{-\infty}^{\infty} g(t) e^{-i\omega t} dt \quad (8.30)$$

which defines the Fourier transform. The inverse Fourier transform, which expresses the time domain function in terms of an integral of the frequency domain function is given by

$$g(t) = \frac{1}{2\pi} \int_{-\infty}^{\infty} f(\omega) e^{i\omega t} d\omega \quad (8.31)$$

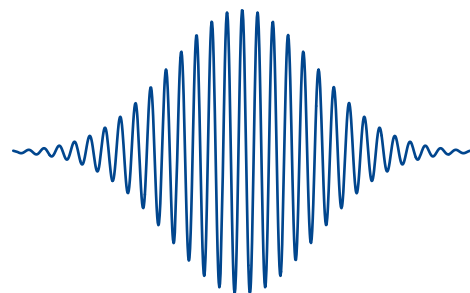
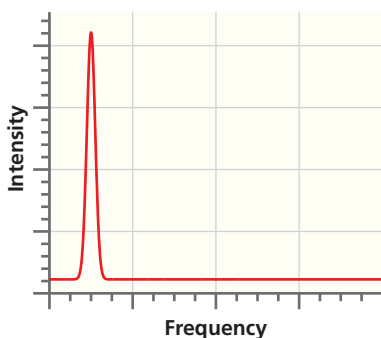
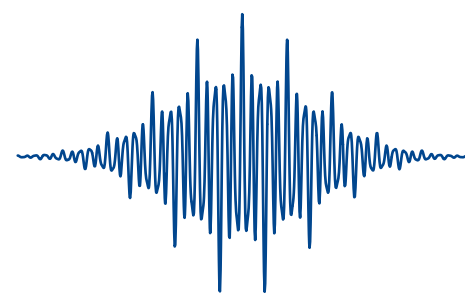
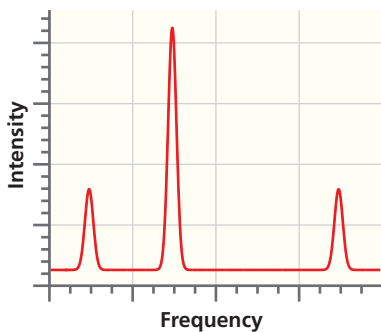
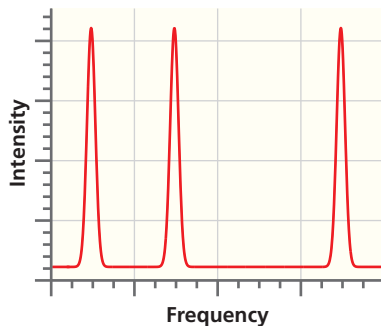


Figure 8.21
Spectra and resulting interferograms.



(a) Simulated sample spectra with finite line width

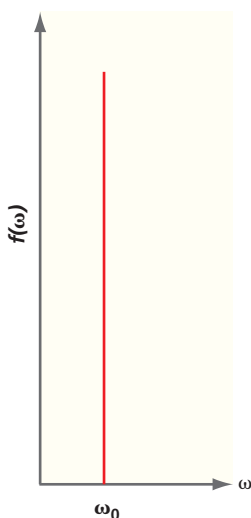
(b) Resulting calculated interferograms

We apply Equation (8.31) to our specific issue by associating $g(t)$ with the interferogram and $f(\omega)$ with the unknown vibrational spectrum. To demonstrate this association, we calculate the Fourier transform of the sinusoidal interferogram shown in Figure 8.20a. We then write $g(t)$ as

$$g(t) = \cos \omega_0 t \quad (8.32)$$



Figure 8.22
A periodic function of time with period τ consisting of widely spaced peaks.

**Figure 8.23**

Frequency distribution that generated the interferogram of Figure 8.20a.

Concept

Raman spectroscopy differs from infrared absorption spectroscopy in that a photon is scattered from, rather than absorbed by, a molecule.

Substituting in Equation (8.30),

$$\begin{aligned} f(\omega) &= \int_{-\infty}^{\infty} (\cos \omega_0 t) e^{-i\omega t} dt = \int_{-\infty}^{\infty} \left(\frac{e^{i\omega_0 t} + e^{-i\omega_0 t}}{2} \right) e^{-i\omega t} dt \\ &= \frac{1}{2} \int_{-\infty}^{\infty} e^{i(\omega_0 - \omega)t} dt + \frac{1}{2} \int_{-\infty}^{\infty} \exp^{-i(\omega_0 + \omega)t} dt \end{aligned} \quad (8.33)$$

The integrands in Equation (8.33) are rapidly oscillating functions that integrate to zero unless $\omega = \pm \omega_0$. Only the positive frequency corresponds to a physically meaningful solution. Therefore, a graph of $f(\omega)$ consists of a single sharp peak, as shown in Figure 8.23.

We see that the absorption spectrum $f(\omega)$ consists of a single frequency, which is exactly what we used to generate the interferogram. Generalizing this result, we have demonstrated that the frequency dependence of the incoming light, which is the absorption spectrum, is given by the Fourier transform of the interferogram generated by the Michelson interferometer.

SUPPLEMENTAL SECTION

8.8 RAMAN SPECTROSCOPY

As discussed in the previous sections, absorption of light in the infrared portion of the spectrum can lead to transitions between eigenstates of the vibrational-rotational energy. Another interaction between a molecule and an electromagnetic field can also lead to vibrational and rotational excitation. It is called the **Raman effect** after its discoverer, C. V. Raman (1888–1970), and involves scattering of a photon by a molecule. We can think of scattering as the collision between a molecule and a photon in which energy and momentum are transferred between the two collision partners. Raman spectroscopy complements infrared absorption spectroscopy because it obeys different selection rules. For instance, the stretching mode in a homonuclear diatomic molecule is Raman active but infrared inactive. The reasons for this difference will become clear in the discussion that follows.

Consider a molecule with a characteristic vibrational frequency ν_{vib} in an electromagnetic field that has a time-dependent electric field given by

$$E = E_0 \cos(2\pi\nu t) \quad (8.34)$$

The electric field distorts the molecule slightly because the negatively charged valence electrons and the positive nuclei and their tightly bound core electrons experience forces in opposite directions. This induces a time-dependent dipole moment of magnitude $\mu_{induced}(t)$ in the molecule of the same frequency as the field. The dipole moment is linearly proportional to the magnitude of the electric field, and the proportionality constant is the **polarizability** α . The polarizability is an anisotropic quantity, and its value depends on the direction of the electric field relative to the molecular axes:

$$\mu_{induced}(t) = \alpha E_0 \cos(2\pi\nu t) \quad (8.35)$$

The polarizability also depends on the bond length $x_e + x(t)$, where x_e is the equilibrium value and can be expanded in a Taylor–Maclaurin series (see Math Essential 4) in which terms beyond the first order have been neglected:

$$\alpha(x_e + x) = \alpha(x_e) + x \left(\frac{d\alpha}{dx} \right)_{x=x_e} + \dots \quad (8.36)$$

Because of the vibration of the molecule, $x(t)$ is time dependent and is given by

$$x(t) = x_{max} \cos(2\pi\nu_{vib} t) \quad (8.37)$$

Combining this result with Equation (8.36), we can rewrite Equation (8.35) in the form

$$\mu_{induced}(t) = \alpha E = E_0 \cos(2\pi\nu t) \left[\alpha(x_e) + \left\{ \left(\frac{d\alpha}{dx} \right)_{x=x_e} \right\} x_{max} \cos(2\pi\nu_{vib} t) \right] \quad (8.38)$$

Equation (8.38) can be simplified using the trigonometric identity $\cos x \cos y = \frac{1}{2}[\cos(x - y) + \cos(x + y)]$ to

$$\begin{aligned}\mu_{induced}(t) &= \alpha(x_e)E_0 \cos(2\pi\nu t) \\ &+ \left[\left(\frac{d\alpha}{dx} \right)_{x=x_e} \right] x_{\max} E_0 [\cos\{2\pi(\nu + \nu_{vib})t\} + \cos\{2\pi(\nu - \nu_{vib})t\}] \quad (8.39)\end{aligned}$$

Three different frequencies appear in this equation for $\mu_{induced}(t)$. Therefore, the time-varying dipole moment radiates light of the same frequency as the dipole moment and at the frequencies ν , $(\nu - \nu_{vib})$, and $(\nu + \nu_{vib})$. These three frequencies are referred to as the **Rayleigh, Stokes, and anti-Stokes frequencies**, respectively. We see that in addition to scattered light at the incident frequency, light will also be scattered at frequencies corresponding to vibrational excitation and de-excitation. Higher-order terms in the expansion for the polarizability [Equation (8.36)] also lead to scattered light at the frequencies $\nu \pm 2\nu_{vib}$, $\nu \pm 3\nu_{vib}$, . . . , but the scattered intensity is much weaker at these frequencies than at the primary frequencies.

The preceding discussion showed that the intensity of the Stokes and anti-Stokes peaks is zero unless $d\alpha/dx \neq 0$. We conclude that for vibrational modes to be Raman active, the polarizability of the molecule must change as it vibrates. This condition is satisfied for many vibrational modes, and, in particular, it is satisfied for the stretching vibration of a homonuclear molecule, although $d\mu_x/dx = 0$ for these molecules, which makes them infrared inactive. Not all vibrational modes that are infrared active are Raman active and vice versa. This is why infrared and Raman spectroscopies provide a valuable complement to one another.

A schematic picture of the scattering event in Raman spectroscopy on an energy scale is shown in Figure 8.24. This diagram is quite different from that considered earlier in depicting a transition between two states. The initial and final states are the $n = 0$ and $n = 1$ states at the bottom of the figure. To visualize the interaction of the molecule with the photon of energy $h\nu$, which is much greater than the vibrational energy spacing, we imagine the scattered photon to be “absorbed” by the molecule, resulting in a much higher intermediate energy “virtual state.” This very short-lived “virtual state” quickly decays to the final state. Whereas the initial and final states are eigenfunctions of the time-independent Schrödinger equation, the upper “virtual state” in this energy diagram need not satisfy this condition. For this reason, it is referred to as a virtual state.

Are the intensities of the Stokes and anti-Stokes peaks equal? We know that their relative intensity is governed by the relative number of molecules in the originating states. For the Stokes line, the transition originates from the $n = 0$ state, whereas for the anti-Stokes line, the transition originates from the $n = 1$ state. Therefore, the relative intensity of the Stokes and anti-Stokes peaks can be calculated using the Boltzmann distribution:

$$\frac{I_{anti-Stokes}}{I_{Stokes}} = \frac{n_{excited}}{n_{ground}} = \frac{e^{-3h\nu/2k_BT}}{e^{-h\nu/2k_BT}} = e^{-h\nu/k_BT} \quad (8.40)$$

For vibrations for which $\tilde{\nu}$ is in the range of 1000 to 3000 cm^{-1} , $\frac{I_{anti-Stokes}}{I_{Stokes}}$ ranges between 8×10^{-3} and 5×10^{-7} at 300 K. This calculation shows that the intensities of the Stokes and anti-Stokes peaks will be quite different. In this discussion of the Raman effect, we have only considered vibrational transitions. However, just as for infrared absorption spectra, Raman spectra show peaks originating from both vibrational and rotational transitions.

Raman and infrared spectroscopy are complementary, and both can be used to study the vibrations of molecules. Both techniques can be used to determine the identities of molecules in a complex mixture by comparing the observed spectral peaks with characteristic group frequencies. The most significant difference between these two spectroscopies is the light source needed to implement the technique. For infrared absorption spectroscopy, the light source is in the infrared range. Because Raman spectroscopy is a scattering technique, the frequency of the light used need not match the frequency of the transition being studied. Therefore, a source in the visible part of the spectrum is generally used to study rotational and vibrational modes. This has several advantages over infrared sources. By shifting the vibrational spectrum from

Concept

A normal mode is Raman active if the polarizability changes as the molecule vibrates.

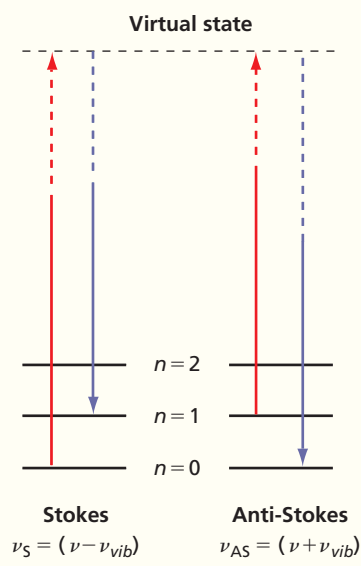


Figure 8.24

Schematic depiction of the Raman scattering event. The spectral peak resulting in vibrational excitation is called the Stokes peak, and the spectral peak originating from vibrational de-excitation is called the anti-Stokes peak.

Concept

Because the light source in Raman spectroscopy can be in the visible region, interference from species in the mixture that are not of interest, such as the solvent, can be minimized.

the infrared into the visible part of the spectrum, commonly available lasers can be used to obtain Raman spectra. Intense lasers are necessary because the probability for Raman scattering is generally on the order of 10^{-6} or less. Furthermore, shifting the frequency of the source from the infrared into the visible part of the spectrum can reduce interference with absorbing species that are not of primary interest. For instance, infrared spectra of aqueous solutions always contain strong water peaks that may mask other peaks of interest. By shifting the source frequency to the visible part of the spectrum, such interferences can be eliminated.

Another interesting application of the Raman effect is the Raman microscope or microprobe. Because Raman spectroscopy is undertaken in the visible part of the light spectrum, it can be combined with optical microscopy to obtain spectroscopic information with a spatial resolution of better than 0.01 mm. An area in which this technique has proven particularly useful is as a nondestructive probe of the composition of gas inclusions such as CH₄, CO, H₂S, N₂, and O₂ in mineral samples. Raman microscopy has also been used in biopsies to identify mineral particles in the lung tissues of silicosis victims and to analyze the composition of gallstones.

SUPPLEMENTAL SECTION

8.9 HOW DOES THE TRANSITION RATE BETWEEN STATES DEPEND ON FREQUENCY?

Now that we have some familiarity with the terms *absorption*, *spontaneous emission*, and *stimulated emission*, the frequency dependence of the interaction of molecules with light can be examined. Until now, we have only dealt with potential energy functions that are independent of time. In any spectroscopic method, transitions occur from one state to another. Transitions cannot be induced by a time-independent potential because the eigenfunctions of the time-independent Schrödinger equation are stationary states and have a constant energy. We now outline how a time-dependent electromagnetic field of light incident on molecules with a discrete set of energy levels can induce transitions between these levels. To make the mathematics more tractable, we consider a two-state system in which the states are denoted by 1 and 2 and the normalized solutions to the time-independent Schrödinger equation are $\psi_1(x)$ and $\psi_2(x)$ with eigenvalues E_1 and E_2 , respectively. We assume that $E_2 > E_1$. The corresponding wave functions including the time dependence are $\Psi_1 = \psi_1(x)e^{-i(E_1/\hbar)t}$ and $\Psi_2 = \psi_2(x)e^{-i(E_2/\hbar)t}$. We also assume that the system is in the ground state (state 1) at time $t = 0$.

When the light is turned on, the molecule interacts with the electric field of the light through its permanent or induced dipole moment, and the time-dependent potential energy is given by

$$\hat{H}_{\text{field}}(t) = -\boldsymbol{\mu} \cdot \mathbf{E} = -\mu_x E_0 \cos(2\pi\nu t) = -\frac{\mu_x E_0}{2}(e^{2\pi i\nu t} + e^{-2\pi i\nu t}) \quad (8.41)$$

We have assumed that the electric field E_0 lies along the x axis. Writing the operator $\hat{H}_{\text{field}}(t)$ in this way is called the dipole approximation because much smaller terms involving higher-order multipoles are neglected. What change will the system undergo under the influence of the light? We can expect transitions from the ground state to the first excited state to occur.

Because this is a time-dependent system, we must solve the time-dependent Schrödinger equation $(\hat{H}_0 + \hat{H}_{\text{field}})\Phi(x, t) = i\hbar(\partial\Phi(x, t)/\partial t)$. In this two-level system, Ψ_1 and Ψ_2 form a complete set, and therefore the eigenfunctions of the operator $\hat{H}_0 + \hat{H}_{\text{field}}$ must be a linear combination of Ψ_1 and Ψ_2 :

$$\Phi(x, t) = a_1(t)\Psi_1 + a_2(t)\Psi_2 \quad (8.42)$$

a_1^* and a_2^* are the probabilities that the state is in level 1 and 2, respectively. At $t = 0$, $a_1^*a_1 = 1$ and $a_2^*a_2 = 0$. At later times, $a_1^*a_1 < 1$ and $a_2^*a_2 > 0$ as the transition to state 2 occurs. Our goals are to derive an expression for $a_2^*(t)a_2(t)$ and to determine how it depends on the frequency of the electric field.

Substituting Equation (8.42) in the time-dependent Schrödinger equation, we obtain

$$\begin{aligned} a_1(t)\hat{H}_0\Psi_1 + a_2(t)\hat{H}_0\Psi_2 + a_1(t)\hat{H}_{field}\Psi_1 + a_2(t)\hat{H}_{field}\Psi_2 \\ = i\hbar\Psi_1 \frac{da_1(t)}{dt} + i\hbar\Psi_2 \frac{da_2(t)}{dt} + i\hbar a_1(t) \frac{d\Psi_1(t)}{dt} + i\hbar a_2(t) \frac{d\Psi_2(t)}{dt} \end{aligned} \quad (8.43)$$

This equation can be simplified by evaluating $i\hbar a_1(t) \frac{d\Psi_1(t)}{dt} + i\hbar a_2(t) \frac{d\Psi_2(t)}{dt}$:

$$\begin{aligned} i\hbar a_1(t) \frac{d\Psi_1(t)}{dt} + i\hbar a_2(t) \frac{d\Psi_2(t)}{dt} &= i\hbar a_1(t)\psi_1(x) \frac{de^{-i(E_1/\hbar)t}}{dt} + i\hbar a_2(t)\psi_2(x) \frac{de^{-i(E_2/\hbar)t}}{dt} \\ &= a_1(t)E_1\Psi_1(x) + a_2(t)E_2\Psi_2(x) \end{aligned} \quad (8.44)$$

Because $\hat{H}_0\Psi_1 = E_1\Psi_1$ and $\hat{H}_0\Psi_2 = E_2\Psi_2$, $i\hbar a_1(t) \frac{d\Psi_1(t)}{dt} + i\hbar a_2(t) \frac{d\Psi_2(t)}{dt}$ cancels out $a_1(t)\hat{H}_0\Psi_1 + a_2(t)\hat{H}_0\Psi_2$ on the left side of Equation (8.43) and Equation (8.44) takes the simpler form

$$a_1(t)\hat{H}_{field}\Psi_1 + a_2(t)\hat{H}_{field}\Psi_2 = i\hbar\Psi_1 \frac{da_1(t)}{dt} + i\hbar\Psi_2 \frac{da_2(t)}{dt} \quad (8.45)$$

In order to obtain an equation for $da_2(t)/dt$, we next multiply Equation (8.45) on both sides by Ψ_2^* and integrate over the spatial coordinate x to obtain

$$\begin{aligned} a_1(t) \int \Psi_2^* \hat{H}_{field} \Psi_1 dx + a_2(t) \int \Psi_2^* \hat{H}_{field} \Psi_2 dx \\ = i\hbar \frac{da_1(t)}{dt} \int \Psi_2^* \Psi_1 dx + i\hbar \frac{da_2(t)}{dt} \int \Psi_2^* \Psi_2 dx \end{aligned} \quad (8.46)$$

Because Ψ_1 and Ψ_2 are orthonormal, the last two integrals can be evaluated to be 0 and 1, respectively and Equation (8.46) can be simplified to

$$i\hbar \frac{da_2(t)}{dt} = a_1(t) \int \Psi_2^* \hat{H}_{field} \Psi_1 dx + a_2(t) \int \Psi_2^* \hat{H}_{field} \Psi_2 dx \quad (8.47)$$

Equation (8.47) can be simplified further if only changes in the coefficients $a_1(t)$ and $a_2(t)$ for small values of t are considered. In this limit, we can replace $a_1(t)$ and $a_2(t)$ on the right side of this equation by their initial values, $a_1(t) = 1$ and $a_2(t) = 0$. Therefore, only one term remains on the right side of Equation (8.47). It turns out that imposing this limit does not affect the general conclusions drawn next. We also replace Ψ_1 and Ψ_2 by the complete form $\Psi_1 = \psi_1(x)e^{-i(E_1/\hbar)t}$ and $\Psi_2 = \psi_2(x)e^{-i(E_2/\hbar)t}$. After doing so, the following equations are obtained:

$$\begin{aligned} i\hbar \frac{da_2(t)}{dt} &= \exp\left[\frac{i}{\hbar}(E_2 - E_1)t\right] \int \psi_2^*(x) \hat{H}_{field} \psi_1(x) dx \\ &= -\frac{E_0}{2} \exp\left[\frac{i}{\hbar}(E_2 - E_1)t\right] (\exp[2\pi i\nu t] + \exp[-2\pi i\nu t]) \\ &\quad \times \int \psi_2^*(x) \mu_x \psi_1(x) dx \\ &= -\frac{E_0}{2} \left(\exp\left[\frac{i}{\hbar}(E_2 - E_1 + h\nu)t\right] + \exp\left[\frac{i}{\hbar}(E_2 - E_1 - h\nu)t\right] \right) \\ &\quad \times \int \psi_2^*(x) \mu_x \psi_1(x) dx \\ i\hbar \frac{da_2(t)}{dt} &= -\mu_x^{21} \frac{E_0}{2} \left(\exp\left[\frac{i}{\hbar}(E_2 - E_1 + h\nu)t\right] + \exp\left[\frac{i}{\hbar}(E_2 - E_1 - h\nu)t\right] \right) \end{aligned} \quad (8.48)$$

In the last equation, we introduced the transition dipole moment μ_x^{21} defined in Equation (8.6) by $\mu_x^{mn} = \int \psi_m^*(x)\mu_x(x_e + x)\psi_n(x)dx$. The transition dipole moment is important because it generates the selection rules for any spectroscopy, as discussed in Section 8.4. Next, Equation (8.48) is integrated with respect to time, using the dummy variable t' to obtain $a_2(t)$:

$$a_2(t) = \frac{i}{\hbar}\mu_x^{21}\frac{E_0}{2}\int_0^t \left(e^{\frac{i}{\hbar}(E_2 - E_1 + h\nu)t'} + e^{\frac{i}{\hbar}(E_2 - E_1 - h\nu)t'} \right) dt' \quad (8.49)$$

$$= \mu_x^{21}\frac{E_0}{2} \left(\frac{-1 + e^{\frac{i}{\hbar}(E_2 - E_1 + h\nu)t}}{E_2 - E_1 + h\nu} + \frac{-1 + e^{-\frac{i}{\hbar}(E_2 - E_1 - h\nu)t}}{E_2 - E_1 - h\nu} \right) \quad (8.50)$$

This expression for $a_2(t)$ looks complicated, but it contains a great deal of useful information that can be extracted fairly easily. Most importantly, it is seen that $a_2(t) = 0$ for all times unless the transition dipole moment $\mu_z^{21} \neq 0$. Next, we look at the terms in the parentheses. The numerator in each of the terms is an oscillating function of time. The period of oscillation approaches zero in the first and second terms as $E_1 - E_2 \rightarrow h\nu$ and $E_2 - E_1 \rightarrow h\nu$, respectively. In these limits, the denominator approaches zero. These are the conditions that lead a_2 to grow rapidly with time. The second term corresponds to absorption of a photon because we have chosen $E_2 > E_1$. The first term corresponds to stimulated emission of a photon. Stimulated emission is of importance in understanding lasers; this process is discussed in more detail in Chapter 11. However, because the current topic is absorption, we focus on the narrow range of energy around $E_2 - E_1 = h\nu$ in which only the absorption peak appears. The behavior of $a_2(t)$ at the resonance condition $E_2 - E_1 = h\nu$ is not easy to discern because $\lim a_2(t) = 0/0$ as $E_2 - E_1 \rightarrow h\nu$. We use L'Hôpital's rule,

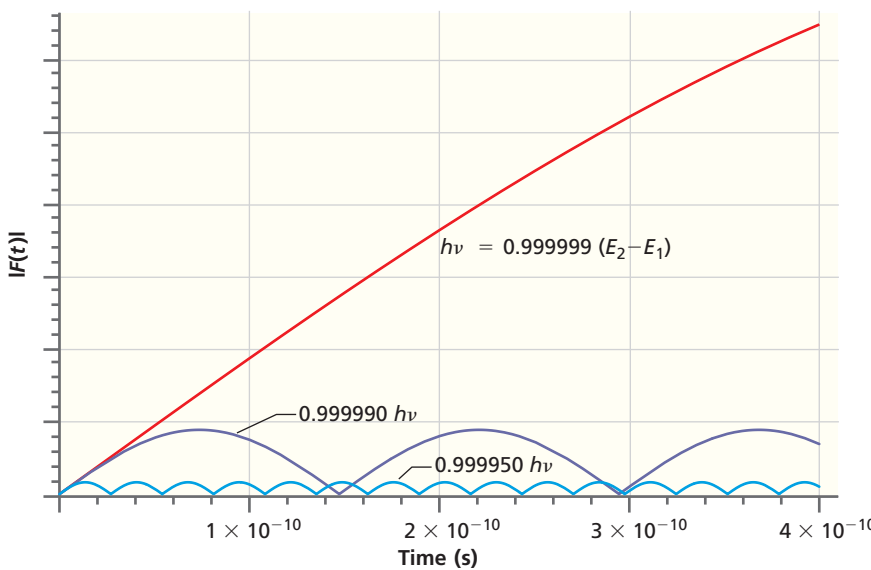
$$\lim \left[\frac{f(x)}{g(x)} \right]_{x \rightarrow 0} = \lim \left[\frac{df(x)/dx}{dg(x)/dx} \right]_{x \rightarrow 0} \quad (8.51)$$

which in this case takes the form

$$\begin{aligned} F(t) &= \lim_{E_2 - E_1 - h\nu \rightarrow 0} \left[\frac{-1 + \exp \left[-\frac{i}{\hbar}(E_2 - E_1 - h\nu)t \right]}{(E_2 - E_1 - h\nu)} \right] \\ &= \lim_{E_2 - E_1 - h\nu \rightarrow 0} \left[\frac{d \left[\left(-1 + \exp \left[-\frac{i}{\hbar}(E_2 - E_1 - h\nu)t \right] \right) \right] / d(E_2 - E_1 - h\nu)}{d(E_2 - E_1 - h\nu) / d(E_2 - E_1 - h\nu)} \right] \\ &= -\frac{it}{\hbar} \left[\exp \left(\frac{-i}{\hbar}[E_2 - E_1 - h\nu]t \right) \right]_{E_2 - E_1 - h\nu = 0} = -\frac{it}{\hbar} \end{aligned} \quad (8.52)$$

The important result that emerges from this calculation is that at the resonance condition $E_2 - E_1 = h\nu$, the magnitude of $a_2(t)$ increases linearly with t . How does $a_2(t)$ change with t close to but not at the resonance condition? We can get this information if $a_2(t)$ is graphed versus t for the $h\nu$ values near the resonance, as shown in Figure 8.25.

Figure 8.25 shows that $|F(t)|$ and therefore $|a_2(t)|$ increase nearly linearly with time for small values of t if $E_2 - E_1$ is extremely close to $h\nu$. This means that the probability of finding the atom or molecule in the excited state increases with time. However, for photon energies that deviate even by 1 ppm from this limit, $|a_2(t)|$ will oscillate and remain small. The oscillations will be more frequent and smaller in amplitude the more $h\nu$ differs from $E_2 - E_1$. The probability of finding an atom or molecule in the excited state remains small if $h\nu$ differs even slightly from $E_2 - E_1$ and if an atom

**Figure 8.25**

Graph of $|F(t)|$ versus t for the $h\nu$ values near the resonance condition. The change in the magnitude of $|F(t)|$ with time for the three photon energies indicated. The curves are calculated for $E_2 - E_1 = 5.00 \times 10^{-19}$ J.

or molecule is unable to take up energy from the electromagnetic field. We conclude that the rate of transition from the ground to the excited state is appreciable only if $h\nu$ is equal to $E_2 - E_1$.

Our final goal is to find an expression for $a_2^*(t)a_2(t)$ that represents the probability of finding the molecule in the excited state with energy E_2 after it has been exposed to the light for the time t . We leave this part of the derivation for the end-of-chapter problems and simply state the result here:

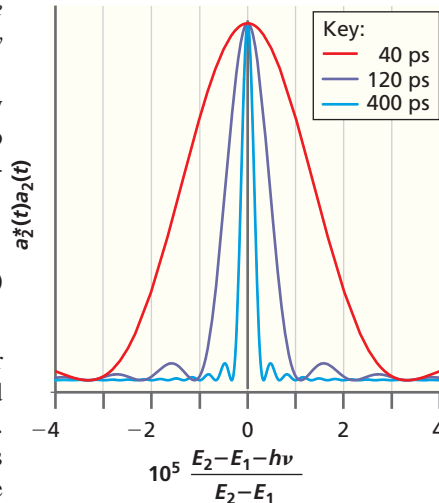
$$a_2^*(t)a_2(t) = E_0^2 [\mu_x^{21}]^2 \frac{\sin^2[(E_2 - E_1 - h\nu)t/2\hbar]}{(E_2 - E_1 - h\nu)^2} \quad (8.53)$$

Figure 8.26 shows a graph of $a_2^*(t)a_2(t)$ plotted against $(E_2 - E_1 - h\nu)/(E_2 - E_1)$ for 40, 120, and 400 ps. As expected, the probability of finding the molecule in the excited state is sharply peaked if the photon energy satisfies the condition $E_2 - E_1 = h\nu$. Because $|a_2(t)|$ increases linearly with time for $E_2 - E_1 = h\nu$, $a_2^*(t)a_2(t)$ increases as t^2 at resonance. The different curves in Figure 8.26 have been normalized to the same maximum value to allow a direct comparison of their widths in energy. The relative amplitudes of $a_2^*(t)a_2(t)$ at resonance for 40, 120, and 400 ps are 1, 9, and 100, respectively. Because the peak height varies with time as t^2 and the width decreases as a function of $1/t$, the total area under the resonance varies with t . This shows that the probability of finding the molecule in the upper state increases linearly with time.

As Figure 8.26 shows, the photon energy range over which absorption occurs becomes narrower as the time t increases. What is the origin of this effect? Small values of t are equivalent to short light pulses. If the time profile of the pulse is expanded as a Fourier series in the frequency, the 40 ps pulse contains a broader range of frequencies than the 400 ps pulse. For this reason, the range of energy over which energy is taken up by the system is larger for the 40 ps pulse than for the 400 ps pulse.

The probability density $a_2^*(t)a_2(t)$ is closely related to the intensity observed in an absorption spectrum. How is the broadening that was just discussed related to the linewidth observed in an experimentally determined spectrum? To answer this question, we must distinguish between an intrinsic and a measured linewidth. By intrinsic linewidth, we mean the linewidth that would be measured if the spectrometer was flawless and produced only “perfect” results. However, a real spectrometer is defined by an instrument function, which is the output of the spectrometer for a very narrow spectral peak. The observed spectrum results from the convolution of the instrument function with the intrinsic linewidth.

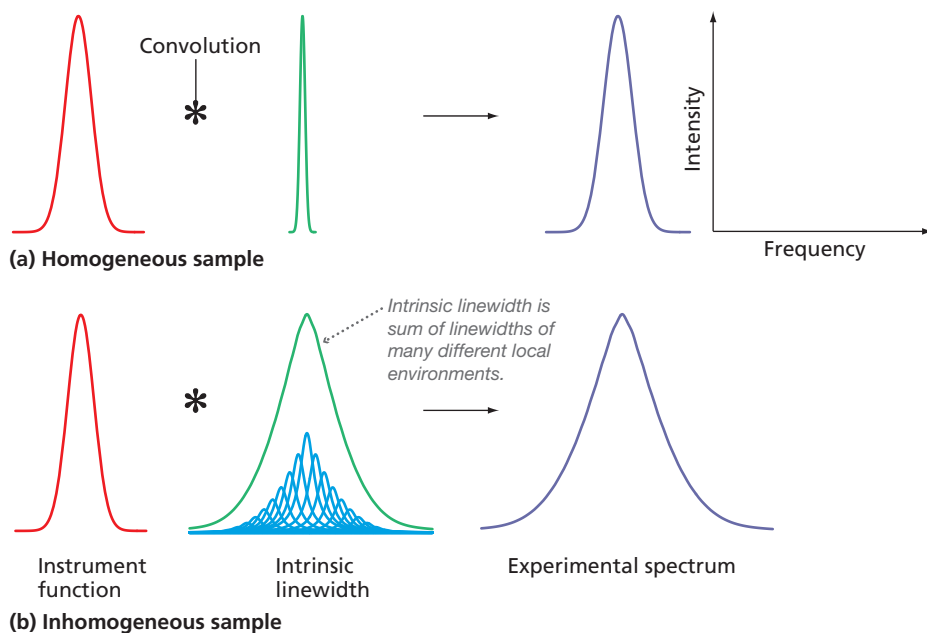
Based on theoretical calculations, the intrinsic linewidth for vibrational spectra is less than $\sim 10^{-3}$ cm⁻¹. This is very small compared with the resolution of conventional

**Figure 8.26**

Graph of $a_2^*(t)a_2(t)$ plotted against $(E_2 - E_1 - h\nu)/(E_2 - E_1)$. In the calculations $E_2 - E_1 = 5.00 \times 10^{-19}$ J. The range of $E_2 - E_1 - h\nu$ shown in the graph is only 80 parts per million of $E_2 - E_1$. The broadest and narrowst resonances are observed for $t = 40$ and 400 ps, respectively. The intermediate resonance is for $t = 120$ ps. All curves have been normalized to the same amplitude to allow peak widths to be directly compared.

Figure 8.27

Convolution of instrument function and intrinsic linewidth. An experimental spectrum (purple curve) arises from the convolution (indicated by the symbol $*$) of the instrument function (red curve) and the intrinsic linewidth of the transition (green curve). The figure shows schematically the case for (a) a homogeneous sample and (b) an inhomogeneous sample. For a homogeneous sample, such as that in (a), the width of the spectrum is often determined by the instrument function. For the inhomogeneous sample, such as that shown in (b), the intrinsic linewidth is the sum of the linewidths of the many different local environments. For inhomogeneous samples, the width of the spectrum can be determined by the intrinsic linewidth rather than the instrument function.



Concept

An observed spectral lineshape arises from a convolution of the instrument function with the true spectral lineshape.

infrared spectrometers, which is typically no better than 0.1 cm^{-1} . Therefore, the width of peaks in a spectrum is generally determined by the instrumental function as shown in the top panel of Figure 8.27 and provides no information about the intrinsic linewidth. However, peaks that are broader than the instrument function are obtained if a sample contains many different local environments for the entity generating the peak. For example, the O—H stretching region in an infrared spectrum in liquid water is very broad. This is the case because of the many different local geometries that arise from hydrogen bonding between H_2O molecules, and each of them gives rise to a slightly different O—H stretching frequency. This effect is referred to as **inhomogeneous broadening** and is illustrated in the bottom panel of Figure 8.27.

VOCABULARY

absorption	incoherent photon source	R branch
anharmonic potential	inhomogeneous broadening	Raman effect
anti-Stokes frequency	interferogram	Rayleigh frequency
Beer–Lambert law	Michelson interferometer	rotational constant
bond energy	molar absorption coefficient	selection rule
coherent source	monochromator	spectroscopy
dipole approximation	Morse potential	spontaneous emission
dynamic dipole moment	multiplex advantage	stimulated emission
Fourier transform	overtone	Stokes frequency
FTIR spectroscopy	P branch	transition dipole moment
group frequencies	permanent dipole moment	wave number
harmonic potential	polarizability	

KEY EQUATIONS

Equation	Significance of Equation	Equation Number
$h\nu = E_2 - E_1 $	Relationship between the frequency at which energy is absorbed or emitted and the energy levels involved in the transitions	8.1
$B_{12} = B_{21}$ and $\frac{A_{21}}{B_{21}} = \frac{16\pi^2\hbar\nu^3}{c^3}$	Relative rates of absorption, stimulated emission, and spontaneous emission	8.3
$E_n = h\nu\left(n + \frac{1}{2}\right) - \frac{(h\nu)^2}{4D_e}\left(n + \frac{1}{2}\right)^2$	Energy levels of the Morse potential	8.5
$\mu_x^{mn} = \int \psi_m^*(x)\mu_x(x_e + x)\psi_n(x) dx \neq 0$	Definition of transition dipole moment	8.6
$\frac{I(\lambda)}{I_0(\lambda)} = e^{-\epsilon(\lambda)Ml}$	Beer–Lambert law, which describes attenuation of incident light by substance	8.11
$E_J = \frac{\hbar^2}{2\mu r_0^2}J(J+1) = \frac{\hbar^2}{8\pi^2\mu r_0^2}J(J+1) = hcBJ(J+1)$	Dependence of rotational energy on quantum number	8.21
$\frac{n_J}{n_0} = \frac{g_J}{g_0}e^{-(E_J-E_0)/k_B T} = (2J+1)e^{-\hbar^2 J(J+1)/2Ik_B T}$	Relative population of different rotational states	8.24
$i\hbar \frac{da_2(t)}{dt} = -\mu_x^{21} \frac{E_0}{2} \left(\exp\left[\frac{i}{\hbar}(E_2 - E_1 + h\nu)t\right] + \exp\left[\frac{i}{\hbar}(E_2 - E_1 - h\nu)t\right] \right)$	Time dependent transitions	8.48

CONCEPTUAL PROBLEMS

Q8.1 Why would you observe a pure rotational spectrum in the microwave region but a rotational-vibrational spectrum in the infrared region?

Q8.2 Solids generally expand as the temperature increases. Such an expansion results from an increase in the bond length between adjacent atoms as the vibrational amplitude increases. Will a harmonic potential lead to thermal expansion? Will a Morse potential lead to thermal expansion?

Q8.3 How can you observe vibrational transitions in Raman spectroscopy using visible light lasers where the photon energy is much larger than the vibrational energy spacing?

Q8.4 A molecule in an excited state can decay to the ground state by either stimulated emission or spontaneous emission. Use the Einstein coefficients to predict how the relative probability of these processes changes as the frequency of the transition doubles.

Q8.5 In Figure 8.16, n_J/n_0 increases initially with J for all three temperatures for CO but for only the two highest temperatures for HD. Explain this difference.

Q8.6 What is the difference between the transition dipole moment and the dynamic dipole moment?

Q8.7 Nitrogen and oxygen do not absorb infrared radiation and are therefore not greenhouse gases. Explain why this is the case.

Q8.8 Does the excitation in Raman spectroscopy take place from the initial state to a stationary state of the system? Explain your answer.

Q8.9 What feature of the Morse potential makes it suitable for modeling dissociation of a diatomic molecule?

Q8.10 If the rotational levels of a diatomic molecule were equally spaced and the selection rule remained unchanged, how would the appearance of the rotational-vibrational spectrum in Figure 8.17 change?

Q8.11 If a spectral peak is broadened, can you always conclude that the excited state has a short lifetime?

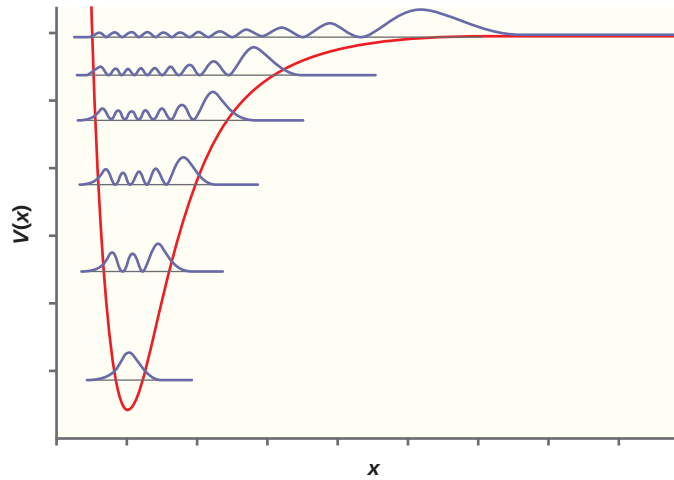
Q8.12 What is the difference between a permanent and a dynamic dipole moment?

Q8.13 What is the explanation for the absence of a peak in the rotational-vibrational spectrum near 3000 cm^{-1} in Figure 8.17?

Q8.14 What is the advantage in acquiring a vibrational spectrum using a FTIR spectrometer over a spectrometer in which the absorption is measured separately at each wavelength?

Q8.15 The number of molecules in a given energy level is proportional to $e^{-\Delta E/kT}$ where ΔE is the difference in energy between the level in question and the ground state. How is it possible that a higher lying rotational energy level can have a higher population than the ground state?

Q8.16 The square of a number of vibrational energy eigenfunctions is shown superimposed on a Morse potential in the accompanying figure. Assign quantum numbers to the levels shown. Explain the differences in the shape of the eigenfunctions compared to those for a harmonic potential.



Q8.17 As a diatomic molecule rotates, the centrifugal force leads to a small change in the bond length. Do you expect the bond length to increase or decrease? Do you expect the difference between adjacent rotational energy peaks $\Delta(\Delta\nu)$ to increase or decrease?

Q8.18 For a harmonic potential, the vibrational force constant is both independent of the quantum number n and independent of $x - x_e$ for the molecule. Do you expect the same behavior for a Morse potential?

NUMERICAL PROBLEMS

Section 8.3

P8.1 The $^1\text{H}^{19}\text{F}$ molecule can be described by a Morse potential with $D_e = 9.05 \times 10^{-19} \text{ J}$. The force constant k for this molecule is 966 N m^{-1} and $\nu = 1.24 \times 10^{14} \text{ s}^{-1}$.

a. Calculate the lowest four energy levels for a Morse potential using the formula

$$E_n = \hbar\nu \left(n + \frac{1}{2} \right) - \frac{(\hbar\nu)^2}{4D_e} \left(n + \frac{1}{2} \right)^2$$

b. Calculate the fundamental frequency ν_0 corresponding to the transition $n = 0 \rightarrow n = 1$ and the frequencies of the first two overtone vibrations. How large would the relative error be if you assume that the first two overtone frequencies are $2\nu_0$ and $3\nu_0$?

P8.2 The infrared spectrum of $^{127}\text{I}^{79}\text{Br}$ has an intense line at 268.4 cm^{-1} . Calculate the force constant and period of vibration of this molecule.

P8.3 Calculate the zero point energies for $^1\text{H}_2$ and $^2\text{D}_2$ assuming a harmonic potential using the data in Table 8.3. Compare the difference in the zero point energies to kT at 298. K.

P8.4 The force constants for $^1\text{H}_2$ and $^{79}\text{Br}_2$ are 575 and 246 N m^{-1} , respectively. Calculate the ratio of the vibrational state populations n_1/n_0 and n_2/n_0 at $T = 250$ and at 1250 . K.

Q8.19 Use your answer from Q8.18 to compare the force constants for compression and stretching at the classical turning points for the levels shown in Q8.16. What trend do you see as n increases?

Q8.20 How many vibrational degrees of freedom does each of the following molecules have: NH_3 , HCN , C_2H_6 , C_{60} ?

Q8.21 Consider a vibrational energy state for a diatomic molecule described by the potential energy function $V(x) = k(x - x_e)^2/2$. The distance between the two classical turning points where the horizontal line representing the energy level intersects the potential energy function is a measure of the vibrational amplitude. State how this vibrational amplitude varies if

- a. The equilibrium bond length x_e is increased while the quantum number n and the reduced mass, μ , of the molecule remain constant.
- b. The quantum number n is increased while the equilibrium bond length x_e and the reduced mass, μ , of the molecule remain constant.
- c. The reduced mass, μ , of the molecule is increased while the quantum number n and equilibrium bond length x_e remain constant.

Q8.22 Put the following molecules in increasing order from lowest to highest vibrational energy level: H_2 , HD , D_2 . Explain your reasoning.

Q8.23 Put the following molecules in increasing order from lowest to highest rotational energy level: H_2 , HD , D_2 . Explain your reasoning.

P8.5 Show that the Morse potential approaches the harmonic potential for small values of the vibrational amplitude.
(Hint: Expand the Morse potential in a Taylor-Maclaurin series.)

P8.6 The fundamental vibrational frequency for $^{79}\text{Br}_2$ is 325.3 cm^{-1} and that for D_0 is $3.22 \times 10^{-19} \text{ J}$. Using this information, calculate D_e .

P8.7 Isotopic substitution is used to identify characteristic groups in an unknown compound using vibrational spectroscopy. Consider the C=C bond in ethene ($^{12}\text{C}_2^{14}\text{H}_4$). By what factor would the frequency change if deuterium were substituted for all the hydrogen atoms? Treat the H and D atoms as being rigidly attached to the carbon atoms.

P8.8 The force constant to $^{23}\text{Na}_2$ is 17.0 N m^{-1} . Calculate the vibrational frequency and zero point energy of this molecule.

P8.9 A strong absorption band in the infrared region of the electromagnetic spectrum is observed at $\tilde{\nu} = 378 \text{ cm}^{-1}$ for $^{27}\text{Al}^{79}\text{Br}$. Assuming that the harmonic potential applies, calculate the fundamental frequency ν in units of inverse seconds, the vibrational period in seconds, and the zero point energy for the molecule in joules and electron-volts.

P8.10 A measurement of the vibrational energy levels of $^{12}\text{C}^{16}\text{O}$ gives the relationship

$$\tilde{\nu}(n) = 2170.21 \left(n + \frac{1}{2} \right) \text{ cm}^{-1} - 13.461 \left(n + \frac{1}{2} \right)^2 \text{ cm}^{-1}$$

where n is the vibrational quantum number. The fundamental vibrational frequency is $\tilde{\nu}_0 = 2170.21 \text{ cm}^{-1}$. From these data, calculate the depth D_e of the Morse potential for $^{12}\text{C}^{16}\text{O}$. Calculate the bond energy of the molecule.

P8.11 Using the formula for the energy levels for the Morse potential,

$$E_n = h\nu \left(n + \frac{1}{2} \right) - \frac{(h\nu)^2}{4D_e} \left(n + \frac{1}{2} \right)^2$$

show that the energy spacing between adjacent levels is given by

$$E_{n+1} - E_n = h\nu - \frac{(h\nu)^2}{2D_e}(n + 1)$$

P8.12 Use your results from P8.11 and solve the following problem. For $^1\text{H}_2$, $D_e = 6.80 \times 10^{-19} \text{ J}$ and $\nu = 1.32 \times 10^{14} \text{ s}^{-1}$. As n increases, the energy difference between adjacent vibrational levels decreases and approaches zero, corresponding to dissociation. Assuming a Morse potential, calculate all discrete vibrational energy eigen values for $^1\text{H}_2$. What value of n corresponds to dissociation?

P8.13 If the vibrational potential is not harmonic, the force constant is not independent of degree of stretching or compression of a molecule. Using the relation $k_{\text{effective}} = (d^2V(x)/dx^2)$, derive an expression for the vibrational force constant for a Morse potential as a function of $x - x_e$. Using the parameters for HCl from Table 8.3, plot $k_{\text{effective}}$ as a function of x over a $\pm 5.0 \text{ pm}$ range from x_e . What is the variation of $k_{\text{effective}}$ over this range of x ?

P8.14 Consider a vibrational energy state for a diatomic molecule described by the potential energy function $V(x) = k(x - x_e)^2/2$. The distance between the two classical turning points where the horizontal line representing the energy level intersects is a measure of the vibrational amplitude. (a) Derive an expression for the distance between the classical turning points in terms of the force constant k , the quantum number n , and the reduced mass μ . (b) State how this distance varies if each of these three variables is varied in turn, keeping the other two constant.

P8.15 Show that a harmonic oscillator described by the Morse potential, $V(x) = D_e [1 - \exp(-\sqrt{k/(2D_e)}(x - x_e))]^2$, has an equilibrium length x_e and the depth D_e .

P8.16 Calculate the probability of finding the vibrational amplitude of the HCl molecule within $\pm 1.00 \text{ pm}$ of its equilibrium distance for the lowest energy state. (a) Rather than

evaluating the integral $\int_{-\Delta x}^{\Delta x} \psi^2(x) dx$, use the approximation $\int_{-\Delta x}^{\Delta x} \psi^2(x) dx \approx 2\Delta x \psi^2(x_e)$, which is valid if the integrand is

nearly constant over this interval. (b) Verify that this approximation is valid by calculating the value of the integrand at the middle and one end of the interval.

Section 8.4

P8.17 Show that the selection rule for the two-dimensional rotor in the dipole approximation is $\Delta m_l = \pm 1$. Use $A_{+\phi} e^{im_1\phi}$ and $A_{+\phi} e^{im_2\phi}$ for the initial and final states of the rotor and $\mu \cos \phi$ as the dipole moment element.

P8.18 Following Example Problem 8.5, show that the $J = 1 \rightarrow J = 2$ rotational transition is allowed.

P8.19 Selection rules in the dipole approximation are determined by the integral $\mu_x^{mn} = \int \psi_m^*(\tau) \mu_x(\tau) \psi_n(\tau) d\tau$. If this integral is nonzero, the transition will be observed in an absorption spectrum. If the integral is zero, the transition is “forbidden” in the dipole approximation. It actually occurs with low probability because the dipole approximation is not exact. Consider the particle in the one-dimensional box and set $\mu_x = -ex$.

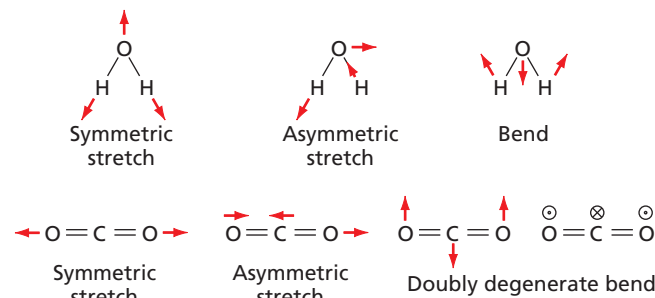
- a. Calculate μ_x^{12} and μ_x^{13} in the dipole approximation. Can you see a pattern and discern a selection rule? You may need to evaluate a few more integrals of the type μ_x^{lm} . The standard integral

$$\begin{aligned} & \int x \sin \frac{\pi x}{a} \sin \frac{n\pi x}{a} dx \\ &= \frac{1}{2} \left(\frac{a^2 \cos \frac{(n-1)\pi x}{a}}{(n-1)^2 \pi^2} + \frac{ax \sin \frac{(n-1)\pi x}{a}}{(n-1)\pi} \right) \\ & \quad - \frac{1}{2} \left(\frac{a^2 \cos \frac{(n+1)\pi x}{a}}{(n+1)^2 \pi^2} + \frac{ax \sin \frac{(n+1)\pi x}{a}}{(n+1)\pi} \right) \end{aligned}$$

is useful for solving this problem.

- b. Determine the ratio μ_x^{12}/μ_x^{14} . On the basis of your result, would you modify the selection rule that you determined in part (a)?

P8.20 Calculating the motion of individual atoms in the vibrational modes of molecules (called normal modes) is an advanced topic. Given the normal modes shown in the following figure, decide which of the normal modes of CO_2 and H_2O have a nonzero dynamical dipole moment and are therefore infrared active. The motion of the atoms in the second of the two doubly degenerate bend modes for CO_2 is identical to the first but is perpendicular to the plane of the page.



P8.21 Overtone transitions in vibrational absorption spectra for which $\Delta n = +2, +3, \dots$ are forbidden for the harmonic potential $V = (1/2)kx^2$ because $\mu_x^{mn} = 0$ for $|m - n| \neq 1$, as shown in Section 8.4. However, overtone transitions are allowed for the more realistic anharmonic potential. In this problem, you will explore how the selection rule is modified by including anharmonic terms in the potential. We do so in an indirect manner by including additional terms in the expansion of the dipole moment $\mu_x(x) = \mu_{0x} + x(d\mu_x/dx)_{r_e} + \dots$, but assuming that the harmonic oscillator total energy eigenfunctions are still valid. This approximation is valid if the anharmonic correction to the harmonic potential is small. You will show that including the next term in the expansion of the dipole moment, which is proportional to x^2 , makes the transitions $\Delta n = \pm 2$ allowed.

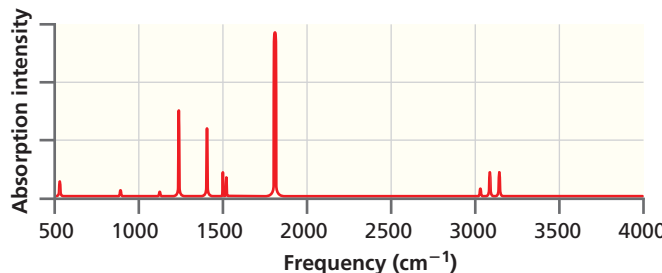
- a. Show that Equation (8.8) becomes

$$\begin{aligned}\mu_x^{m0} &= A_m A_0 \mu_{0x} \int_{-\infty}^{\infty} H_m(\alpha^{1/2}x) H_0(\alpha^{1/2}x) e^{-\alpha x^2} dx \\ &+ A_m A_0 \left(\frac{d\mu_x}{dx} \right)_{x=0} \int_{-\infty}^{\infty} H_m(\alpha^{1/2}x)x H_0(\alpha^{1/2}x) e^{-\alpha x^2} dx \\ &+ \frac{A_m A_0}{2!} \left(\frac{d^2\mu_x}{dx^2} \right)_{x=0} \int_{-\infty}^{\infty} H_m(\alpha^{1/2}x)x^2 H_0(\alpha^{1/2}x) e^{-\alpha x^2} dx\end{aligned}$$

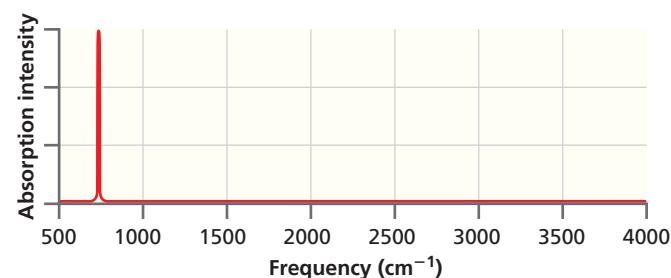
- b. Evaluate the effect of adding the third term of the equation in part (a) to μ_x^{mn} . You will need the recursion relationship $\alpha^{1/2}x H_n(\alpha^{1/2}x) = n H_{n-1}(\alpha^{1/2}x) + \frac{1}{2} H_{n+1}(\alpha^{1/2}x)$.
c. Show that both the transitions $n = 0 \rightarrow n = 1$ and $n = 0 \rightarrow n = 2$ are allowed in the case presented in part (c).

Section 8.5

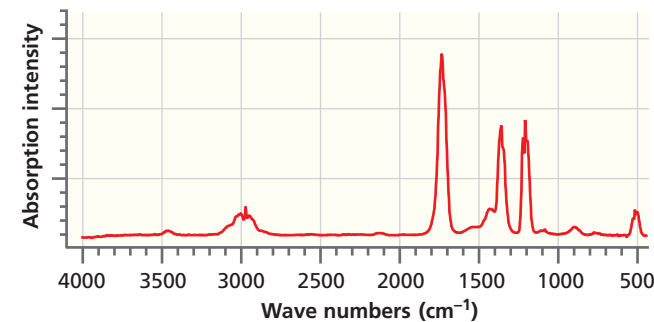
P8.22 A simulated infrared absorption spectrum of a gas-phase organic compound is shown in the following figure. Use the characteristic group frequencies listed in Section 8.5 to decide whether this compound is more likely to be CCl_4 , $(\text{CH}_3)_2\text{CO}$, CH_3OH , CH_3CN , C_3H_8 , CH_3COOH , or Cl_2CO . Explain your reasoning.



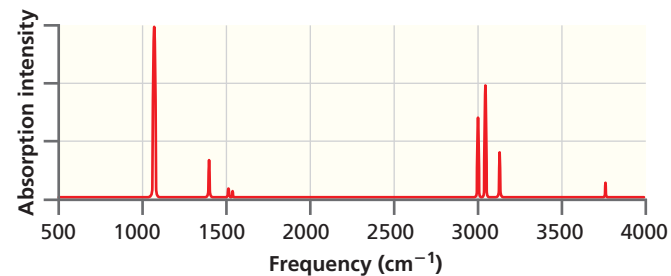
P8.23 A simulated infrared absorption spectrum of a gas-phase organic compound is shown in the following figure. Use the characteristic group frequencies listed in Section 8.5 to decide whether this compound is more likely to be CCl_4 , $(\text{CH}_3)_2\text{CO}$, CH_3OH , CH_3CN , C_3H_8 , CH_3COOH , or Cl_2CO . Explain your reasoning.



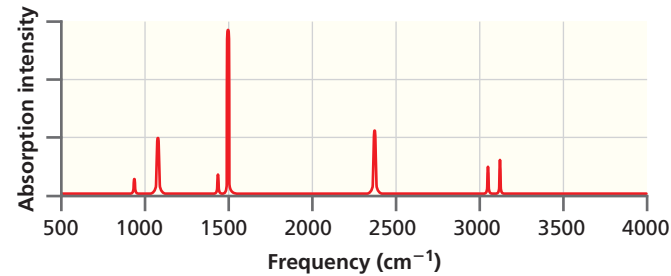
P8.24 An infrared absorption spectrum of an organic compound is shown in the following figure. Use the characteristic group frequencies listed in Section 8.5 to decide whether this compound is more likely to be ethyl amine, pentanol, or acetone.



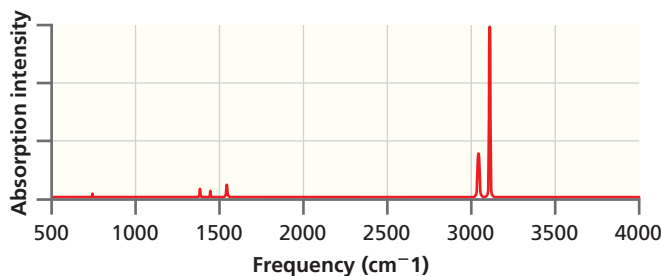
P8.25 A simulated infrared absorption spectrum of a gas-phase organic compound is shown in the following figure. Use the characteristic group frequencies listed in Section 8.5 to decide whether this compound is more likely to be CCl_4 , $(\text{CH}_3)_2\text{CO}$, CH_3OH , CH_3CN , C_3H_8 , CH_3COOH , or Cl_2CO . Explain your reasoning.



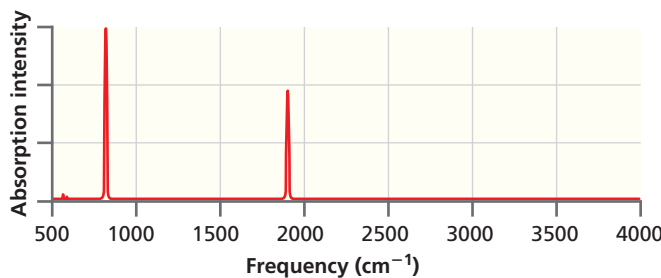
P8.26 A simulated infrared absorption spectrum of a gas-phase organic compound is shown in the following figure. Use the characteristic group frequencies listed in Section 8.5 to decide whether this compound is more likely to be CCl_4 , $(\text{CH}_3)_2\text{CO}$, CH_3OH , CH_3CN , C_3H_8 , CH_3COOH , or Cl_2CO . Explain your reasoning.



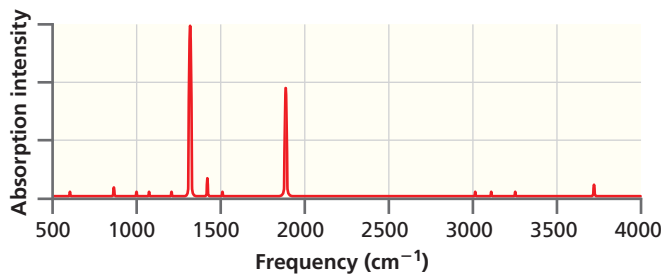
P8.27 A simulated infrared absorption spectrum of a gas-phase organic compound is shown in the following figure. Use the characteristic group frequencies listed in Section 8.5 to decide whether this compound is more likely to be CCl_4 , $(\text{CH}_3)_2\text{CO}$, CH_3OH , CH_3CN , C_3H_8 , CH_3COOH , or Cl_2CO . Explain your reasoning.



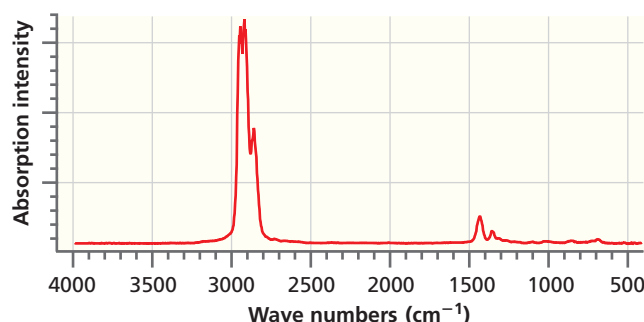
P8.28 A simulated infrared absorption spectrum of a gas-phase organic compound is shown in the following figure. Use the characteristic group frequencies listed in Section 8.5 to decide whether this compound is more likely to be CCl_4 , $(\text{CH}_3)_2\text{CO}$, CH_3OH , CH_3CN , C_3H_8 , CH_3COOH , or Cl_2CO . Explain your reasoning.



P8.29 A simulated infrared absorption spectrum of a gas-phase organic compound is shown in the following figure. Use the characteristic group frequencies listed in Section 8.5 to decide whether this compound is more likely to be CCl_4 , $(\text{CH}_3)_2\text{CO}$, CH_3OH , CH_3CN , C_3H_8 , CH_3COOH , or Cl_2CO . Explain your reasoning.



P8.30 An infrared absorption spectrum of an organic compound is shown in the following figure. Use the characteristic group frequencies listed in Section 8.5 to decide whether this compound is more likely to be hexene, hexane, or hexanol. Explain your reasoning.



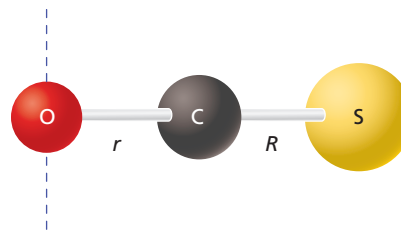
P8.31 Purification of water for drinking using UV light is a viable way to provide potable water in many areas of the world. Experimentally, the decrease in UV light of wavelength 250 nm follows the empirical relation $I/I_0 = e^{-\varepsilon' l}$, where l is the distance that light passed through the water and ε' is an effective absorption coefficient. $\varepsilon' = 0.070 \text{ cm}^{-1}$ for pure water and 0.30 cm^{-1} for water exiting a waste-water treatment plant. What distance corresponds to a decrease in I of 20.% from its incident value for (a) pure water and (b) waste water?

P8.32 50.% of the light incident on a 15.0-mm-thick piece of fused silica quartz glass passes through the glass. What percentage of the light will pass through a 35.0-mm-thick piece of the same glass?

P8.33 Greenhouse gases generated from human activity absorb infrared radiation from the Earth and keep it from being dispersed outside our atmosphere. This is a major cause of global warming. Compare the path length required to absorb 85% of the Earth's radiation near a wavelength of $7 \mu\text{m}$ for CH_3CCl_3 [$\varepsilon(\lambda) = 1.8 \text{ (cm atm)}^{-1}$] and the chlorofluorocarbon CFC-14 [$\varepsilon(\lambda) = 4.1 \times 10^3 \text{ (cm atm)}^{-1}$], assuming that each of these gases has a partial pressure of $2.25 \times 10^{-6} \text{ atm}$.

Section 8.6

P8.34 The molecules $^{16}\text{O}^{12}\text{C}^{32}\text{S}$ and $^{16}\text{O}^{12}\text{C}^{34}\text{S}$ have values for $h/8\pi^2 I$ of $6081.490 \times 10^6 \text{ s}^{-1}$ and $5932.816 \times 10^6 \text{ s}^{-1}$, respectively. Calculate the C-O and C-S bond distances. The molecule is pictured here.



P8.35 The rotational constant for $^{127}\text{I}^{35}\text{Cl}$ determined from microwave spectroscopy is $0.1141619 \text{ cm}^{-1}$. Calculate the bond length in $^{127}\text{I}^{35}\text{Cl}$ to the maximum number of significant figures consistent with this information.

P8.36 Write an expression for the moment of inertia of the acetylene molecule in terms of the bond distances. Does this molecule have a pure rotational spectrum?

P8.37 The bond length of $^{23}\text{Na}^{19}\text{F}$ is 192.6 pm. Calculate the value of B and the spacing between lines in the pure rotational spectrum of this molecule in units of s^{-1} .

P8.38 The rigid rotor model can be improved by recognizing that in a realistic anharmonic potential, the bond length increases with the vibrational quantum number n . Therefore, the rotational constant depends on n , and it can be shown that $B_n = B - (n + 1/2)\alpha$, where B is the rigid rotor value. The constant α can be obtained from experimental spectra. For $^1\text{H}^{35}\text{Cl}$, $B = 10.5909 \text{ cm}^{-1}$ and $\alpha = 0.3019 \text{ cm}^{-1}$. Using this more accurate formula for B_n , calculate the bond length for $^1\text{H}^{35}\text{Cl}$ in the ground state and for $n = 3$. Compare your answer with that obtained neglecting the dependence of B on n .

P8.39 Because the intensity of a transition to first order is proportional to the population of the originating state, the J value for which the maximum intensity is observed in a rotational-vibrational spectrum is not generally $J = 0$. Treat J in the equation

$$\frac{n_J}{n_0} = \frac{g_J}{g_0} e^{-(\varepsilon_J - \varepsilon_0)/kT} = (2J + 1) e^{-\hbar^2 J(J+1)/2IkT}$$

as a continuous variable.

a. Show that

$$\frac{d\left(\frac{n_J}{n_0}\right)}{dJ} = 2e^{-\hbar^2 J(J+1)/2IkT} - \frac{(2J + 1)^2 \hbar^2}{2IkT} e^{-\hbar^2 J(J+1)/2IkT}$$

b. Show that setting $d(n_J/n_0)/dJ = 0$ yields the equation

$$2 - \frac{(2J_{\max} + 1)^2 \hbar^2}{2IkT} = 0$$

c. Show that the solution of this quadratic equation is

$$J_{\max} = \frac{1}{2} \left[\sqrt{\frac{4IkT}{\hbar^2}} - 1 \right]$$

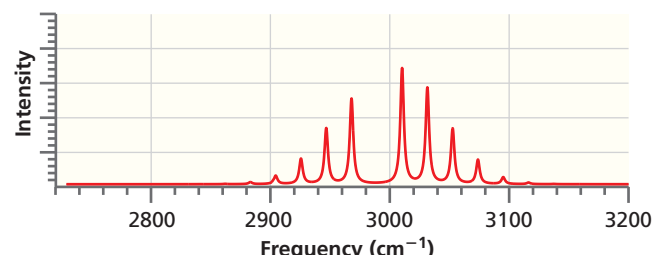
P8.40 The spacing between lines in the pure rotational spectrum of $^7\text{Li}^1\text{H}$ is $4.505 \times 10^{11} \text{ s}^{-1}$. Calculate the bond length of this molecule.

P8.41 Calculate the moment of inertia, the magnitude of the rotational angular momentum, and the energy in the $J = 6$ rotational state for $^{14}\text{N}_2$. Compare the energy to $k_B T$ at 298 K.

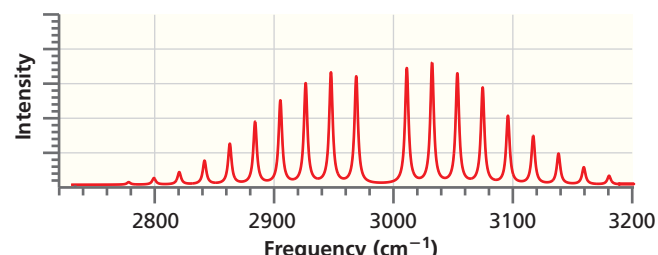
P8.42 In Problem P8.39, you obtained the result

$$J_{\max} = 1/2 \left[\sqrt{4IkT/\hbar^2} - 1 \right]$$

Using this result, estimate T for the simulated $^1\text{H}^{35}\text{Cl}$ rotational spectra shown in parts a and b of the following figure. Give realistic estimates of the precision with which you can determine T from the spectra. In generating the simulation, we assumed that the intensity of the individual peaks is determined solely by the population in the originating state and that it does not depend on the initial and final J values.



(a)



(b)

P8.43 The moment of inertia of $^{14}\text{N}_2$ is $1.402 \times 10^{-46} \text{ kg m}^2$. Calculate the bond length of the molecule.

P8.44 Calculate the angular momentum of $^7\text{Li}_2$ in the $J = 7$ state.

P8.45 The rotational energy of $^{14}\text{N}_2$ in the $J = 7$ state is $2.223 \times 10^{-21} \text{ J}$. Calculate the bond length of the molecule.

Section 8.7

P8.46 In this problem, you will derive the equations used to explain the Michelson interferometer for incident light of a single frequency.

a. Show that the expression

$$A(t) = \frac{A_0}{\sqrt{2}} (1 + e^{i\delta(t)}) \exp i(ky_D - \omega t)$$

represents the sum of two waves of the form

$(A_0/\sqrt{2}) \exp i(kx - \omega t)$, one of which is phase shifted by the amount $\delta(t)$ evaluated at the position y_D .

b. Using the definition $I(t) = A(t)A^*(t)$, show that

$$I(t) = I_0/2(1 + \cos \delta(t)).$$

c. Expressing $\delta(t)$ in terms of $\Delta d(t)$, show that

$$I(t) = \frac{I_0}{2} \left(1 + \cos \frac{2\pi \Delta d(t)}{\lambda} \right)$$

d. Expressing $\Delta d(t)$ in terms of the mirror velocity v , show that

$$I(t) = \frac{I_0}{2} \left(1 + \cos \frac{2v}{c} \omega t \right)$$

Section 8.9

P8.47 Fill in the missing step in the derivation that led to the calculation of the spectral line shape in Figure 8.26. Starting from

$$a_2(t) = \mu_x^{21} \frac{E_0}{2} \left(\frac{1 - e^{\frac{i}{\hbar}(E_2 - E_1 + h\nu)t}}{E_2 - E_1 + h\nu} + \frac{1 - e^{-\frac{i}{\hbar}(E_2 - E_1 - h\nu)t}}{E_2 - E_1 - h\nu} \right)$$

and neglecting the first term in the parentheses, show that

$$a_2^*(t)a_2(t) = E_0^2 [\mu_x^{21}]^2 \frac{\sin^2 [(E_2 - E_1 - h\nu)t/2\hbar]}{(E_2 - E_1 - h\nu)^2}$$

COMPUTATIONAL PROBLEMS

More detailed instructions on carrying out these calculations using Spartan Physical Chemistry are found at: www.pearsonhighered.com/chemistryresources/.

C8.1 Build structures for the gas-phase (a) hydrogen fluoride (${}^1\text{H}{}^{19}\text{F}$), (b) hydrogen chloride (${}^1\text{H}{}^{35}\text{Cl}$), (c) carbon monoxide (${}^{12}\text{C}{}^{16}\text{O}$), and (d) sodium chloride (${}^{23}\text{Na}{}^{35}\text{Cl}$) molecules. Calculate the equilibrium geometry and the infrared spectrum using the B3LYP method with the 6–311+G^{**} basis set.

- a. Compare your result for the vibrational frequency with the experimental value listed in Table 8.3. What is the relative error in the calculation?
- b. Calculate the force constant from the vibrational frequency and reduced mass. Determine the relative error using the experimental value in Table 8.3.
- c. Calculate the values for the rotational constant *B* using the calculated bond length. Determine the relative error using the experimental value in Table 8.3.

C8.2 Calculate the bond energy in gaseous (a) hydrogen fluoride (${}^1\text{H}{}^{19}\text{F}$), (b) hydrogen chloride (${}^1\text{H}{}^{35}\text{Cl}$), (c) carbon monoxide (${}^{12}\text{C}{}^{16}\text{O}$), and (d) sodium chloride (${}^{23}\text{Na}{}^{35}\text{Cl}$) molecules by comparing the total energies of the species in the dissociation reactions [e.g., $\text{HF(g)} \rightarrow \text{H(g)} + \text{F(g)}$]. Use the B3LYP method with the 6–31G^{*} basis set. Determine the relative error of the calculation using the experimental value in Table 8.3.

C8.3 Build structures for the gas-phase (a) NF^3 , (b) PCl_3 , and (c) SO_3 molecules. Calculate the equilibrium geometry and the IR spectrum using the B3LYP method with the 6–31G^{*} basis set. Animate the vibrational normal modes and classify them as symmetrical stretch, symmetrical deformation, degenerate stretch, and degenerate deformation.

C8.4 Build structures for the gas-phase (a) F_2CO , (b) Cl_2CO , and (c) O_2NF molecules of the structural form X_2YZ . Calculate the equilibrium geometry and the IR spectrum using the B3LYP method with the 6–311+G^{**} basis set.

Animate the vibrational normal modes and classify them as Y-Z stretch, YX_2 scissors, antisymmetric X-Y stretch, YX_2 rock, and Y-X₂ wag.

C8.5 Build structures for the bent gas-phase (a) HOF , (b) ClOO , and (c) HSO molecules of the structural form XYZ . Calculate the equilibrium geometry and the IR spectrum using the B3LYP method with the 6–31G^{*} basis set. Animate the vibrational normal modes and classify them as Y-Z stretch, X-Y stretch, and X-Y-Z bend.

WEB-BASED SIMULATIONS, ANIMATIONS, AND PROBLEMS

Simulations, animations, and homework problem worksheets can be accessed at www.pearsonhighered.com/advchemistry

W8.1 The number of allowed energy levels in a Morse potential is determined for variable values of the vibrational frequency and the well depth.

W8.2 The normal modes for H_2O are animated. Each normal mode is associated with a local motion from a list displayed in the simulation.

W8.3 The normal modes for CO_2 are animated. Each normal mode is associated with a local motion from a list displayed in the simulation.

W8.4 The normal modes for NH_3 are animated. Each normal mode is associated with a local motion from a list displayed in the simulation.

W8.5 The normal modes for formaldehyde are animated. Each normal mode is associated with a local motion from a list displayed in the simulation.

W8.6 Simulated rotational (microwave) spectra are generated for one or more of the diatomic molecules $^{12}\text{C}^{16}\text{O}$, $^1\text{H}^{19}\text{F}$, $^1\text{H}^{35}\text{Cl}$, $^1\text{H}^{79}\text{Br}$, and $^1\text{H}^{127}\text{I}$. Using a slider, the temperature is varied. The J value corresponding to the maximum intensity peak is determined and compared with the prediction from the formula

$$J_{\max} = \frac{1}{2} \left[\sqrt{\frac{4Ik_B T}{\hbar^2}} - 1 \right]$$

The number of peaks that have an intensity greater than half of that for the largest peak is determined at different temperatures. The frequencies of the peaks are then used to generate the rotational constants B and α_e .

W8.7 Simulated rotational-vibrational (infrared) spectra are generated for one or more diatomic molecules including $^{12}\text{C}^{16}\text{O}$, $^1\text{H}^{19}\text{F}$, $^1\text{H}^{35}\text{Cl}$, $^1\text{H}^{79}\text{Br}$, $^1\text{H}^{127}\text{I}$ for predetermined temperatures. The frequencies of the peaks are then used to generate the rotational constants B and α_e , and the force constant k .

FURTHER READING

- Antonio, K. A., and Schultz, Z. D. “Advances in Biomedical Raman Microscopy.” *Analytical Chemistry* 86 (2014): 30–46.
- Berry, R. S., Rice, S. A., and Ross, J., *Physical Chemistry*, 2nd edition, Oxford, New York, 2000.
- Elrod, Matthew. “Greenhouse Warming Potentials from the Infrared Spectroscopy of Atmospheric Gases.” *Journal of Chemical Education* 76 (1999): 1702–1705.

- Fedor, A. M., and Toda, M. J. “Investigating Hydrogen Bonding in Phenol Using Infrared Spectroscopy and Computational Chemistry.” *Journal of Chemical Education* 91 (2014): 2191–2194.
- Woods, R., and Henderson, G. “FTIR Rotational Spectroscopy.” *Journal of Chemical Education* 64 (1987): 921–924.

The Hydrogen Atom

WHY is this material important?

The hydrogen atom, consisting of a single proton and electron, is the simplest atom. Many of the insights about eigenvalues and eigenfunctions of the Schrödinger equation of the H atom developed in this chapter can be applied to atoms with many electrons discussed in Chapter 10.

WHAT are the most important concepts and results?

The Schrödinger equation is best solved in spherical coordinates. Because potential energy does not depend on angular coordinates, the angular parts of the total energy eigenfunctions are the spherical harmonic functions developed in Chapter 7. Quantization of energy arises through boundary equations in the radial equation. The radial distribution function is developed to calculate the probability of finding the electron at a given distance from the nucleus. The electron distribution in an H atom can best be described by a modified shell model.

WHAT would be helpful for you to review for this chapter?

It would be helpful to review the material in Math Essential 8 on spherical coordinates and in Chapter 7 on spherical harmonic functions.

9.1 FORMULATING THE SCHRÖDINGER EQUATION

After having applied quantum-mechanical principles to a number of simple problems, we turn to one of the triumphs of quantum mechanics: the understanding of atomic structure and spectroscopy. As will be discussed in Chapter 10, for atoms with more than one electron, the Schrödinger equation can only be solved numerically. However, for the hydrogen atom, the Schrödinger equation can be solved exactly, and many of the results we obtain from that solution can be generalized to many electron atoms.

To set the stage historically, experiments by Ernest Rutherford had established that the positive charge associated with an atom was localized at the center of the atom and that the electrons were spread out over a large volume (relative to nuclear dimensions) centered at the nucleus. This result led to the formulation of the **shell model** of the atom in which the electrons are confined in spherical shells centered at the nucleus. However, this model has a major flaw when viewed from the vantage point of classical physics. An electron orbiting around the nucleus undergoes accelerated motion and radiates energy. Therefore, it will eventually fall into the nucleus. Atoms are not stable according to classical mechanics. The challenge for quantum mechanics was to provide a framework within which the stability of atoms could be understood.

- 9.1 Formulating the Schrödinger Equation
- 9.2 Solving the Schrödinger Equation for the Hydrogen Atom
- 9.3 Eigenvalues and Eigenfunctions for the Total Energy
- 9.4 Hydrogen Atom Orbitals
- 9.5 The Radial Probability Distribution Function
- 9.6 Validity of the Shell Model of an Atom

Concept

Classical physics predicts that atoms in which electrons orbit the nucleus are unstable.

We model the hydrogen atom as consisting of an electron moving about a proton located at the origin of the coordinate system. The two particles attract one another, and the interaction potential is given by a simple Coulomb potential:

$$V(\mathbf{r}) = -\frac{e^2}{4\pi\epsilon_0|\mathbf{r}|} = -\frac{e^2}{4\pi\epsilon_0 r} \quad (9.1)$$

In this equation, e is the electron charge, and ϵ_0 is the permittivity of free space. In the text that follows, we abbreviate the magnitude of the vector \mathbf{r} as r , the distance between the nucleus and the electron. Because the potential is spherically symmetrical, we choose spherical coordinates (r, θ, ϕ) (see Math Essential 8) to formulate the Schrödinger equation for this problem. In doing so, it takes on the formidable form

$$\begin{aligned} & -\frac{\hbar^2}{2m_e} \left[\frac{1}{r^2} \frac{\partial}{\partial r} \left(r^2 \frac{\partial \psi(r, \theta, \phi)}{\partial r} \right) + \frac{1}{r^2 \sin \theta} \frac{\partial}{\partial \theta} \left(\sin \theta \frac{\partial \psi(r, \theta, \phi)}{\partial \theta} \right) \right. \\ & \left. + \frac{1}{r^2 \sin^2 \theta} \frac{\partial^2 \psi(r, \theta, \phi)}{\partial \phi^2} \right] \\ & -\frac{e^2}{4\pi\epsilon_0 r} \psi(r, \theta, \phi) = E\psi(r, \theta, \phi) \end{aligned} \quad (9.2)$$

In this equation m_e is the electron mass.

9.2 SOLVING THE SCHRÖDINGER EQUATION FOR THE HYDROGEN ATOM

Because $V(r)$ depends only on r and not on the angles θ and ϕ , we can achieve a separation of variables, as discussed in Sections 4.3 and 7.4, and write the wave function as a product of three functions, each of which depends on only one of the variables:

$$\psi(r, \theta, \phi) = R(r)\Theta(\theta)\Phi(\phi) \quad (9.3)$$

This greatly simplifies the solution of the partial differential equation. We also recognize that, apart from constants, the angular part of Equation (9.2), the last two terms in the brackets, is the operator \hat{l}^2 discussed in Section 7.6. Therefore, the angular part of $\psi(r, \theta, \phi)$ is the product $\Theta(\theta)\Phi(\phi)$ that we encountered in solving the Schrödinger equation for the rigid rotor—namely, the normalized spherical harmonic functions $Y_l^m(\theta, \phi)$. Therefore, the only part of $\psi(r, \theta, \phi)$ that remains unknown is the radial function $R(r)$.

Equation (9.2) can be reduced to a differential equation involving only the variable r in the following way. Substituting the product function $\psi(r, \theta, \phi) = R(r)\Theta(\theta)\Phi(\phi)$ into Equation (9.2) and moving those parts not affected by the partial derivative in front of each term, we obtain

$$\begin{aligned} & -\frac{\hbar^2}{2m_e r^2} \Theta(\theta)\Phi(\phi) \frac{d}{dr} \left[r^2 \frac{dR(r)}{dr} \right] + \frac{1}{2m_e r^2} R(r) \hat{l}^2 \Theta(\theta)\Phi(\phi) \\ & -\Theta(\theta)\Phi(\phi) \left[\frac{e^2}{4\pi\epsilon_0 r} \right] R(r) = ER(r)\Theta(\theta)\Phi(\phi) \end{aligned} \quad (9.4)$$

We know that $\hat{l}^2\Theta(\theta)\Phi(\phi) = \hbar^2 l(l+1)\Theta(\theta)\Phi(\phi)$. Putting this result into Equation (9.4) and canceling the product $\Theta(\theta)\Phi(\phi)$ that appears in each term, the following differential equation is obtained for $R(r)$:

$$-\frac{\hbar^2}{2m_e r^2} \frac{d}{dr} \left[r^2 \frac{dR(r)}{dr} \right] + \left[\frac{\hbar^2 l(l+1)}{2m_e r^2} - \frac{e^2}{4\pi\epsilon_0 r} \right] R(r) = ER(r) \quad (9.5)$$

Before continuing, we summarize the preceding discussion. The Schrödinger equation was formulated for the hydrogen atom. It differs from the rigid rotor problem, where r has a fixed value, in that the potential energy is not zero but rather depends inversely on r . Because the potential is not dependent on the angular coordinates, a separation of variables is possible, and the solutions to the Schrödinger equation for θ and ϕ are the same as those obtained for the rigid rotor. We have been able to separate the dependence of the wave function on the radial coordinate r from that on the angles θ and ϕ . We now take a closer look at the eigenvalues and eigenfunctions for Equation (9.5).

Note that the second term on the left-hand side of Equation (9.5) can be viewed as an **effective potential**, $V_{\text{eff}}(r)$. The effective potential consists of the **centrifugal potential**, which varies as $+1/r^2$, and the **Coulomb potential**, which varies as $-1/r$:

$$V_{\text{eff}}(r) = \frac{\hbar^2 l(l+1)}{2m_e r^2} - \frac{e^2}{4\pi\epsilon_0 r} \quad (9.6)$$

Each of the terms that contribute to $V_{\text{eff}}(r)$ and their sums are graphed as a function of distance in Figure 9.1.

Because the first term is repulsive and varies more rapidly with r than the Coulomb potential, it dominates at small distances if $l \neq 0$. Both terms approach zero for large values of r . The resultant potential is repulsive at short distances for $l > 0$ and is more repulsive the greater the value of l . The net result of this repulsive centrifugal potential is to force the electrons in orbitals with $l > 0$ (looking ahead, p , d , and f electrons) on average farther from the nucleus than s electrons for which $l = 0$.

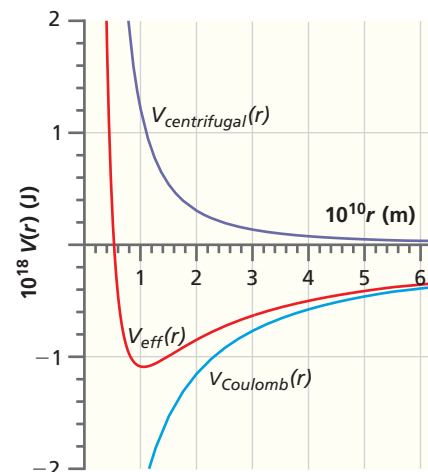


Figure 9.1

Individual contributions to the effective potential and their sum plotted as a function of distance. The centrifugal potential used is for $l = 1$; larger values of l make the effective potential more repulsive at small r .

Concept

The effective potential for the electron in a H atom has coulombic and centripetal contributions.

9.3 EIGENVALUES AND EIGENFUNCTIONS FOR THE TOTAL ENERGY

Equation (9.5) can be solved using standard mathematical methods. For a more detailed discussion of the solution, see the reference to Levine in Further Reading. Here we concern ourselves only with the results. Note that the energy E only appears in the radial equation and not in the angular equation. Because only one variable is involved in this equation, the energy is expected to depend on a single quantum number. The quantization condition that results from the restriction that $R(r)$ be well behaved at large values of r [$R(r) \rightarrow 0$ as $r \rightarrow \infty$] is

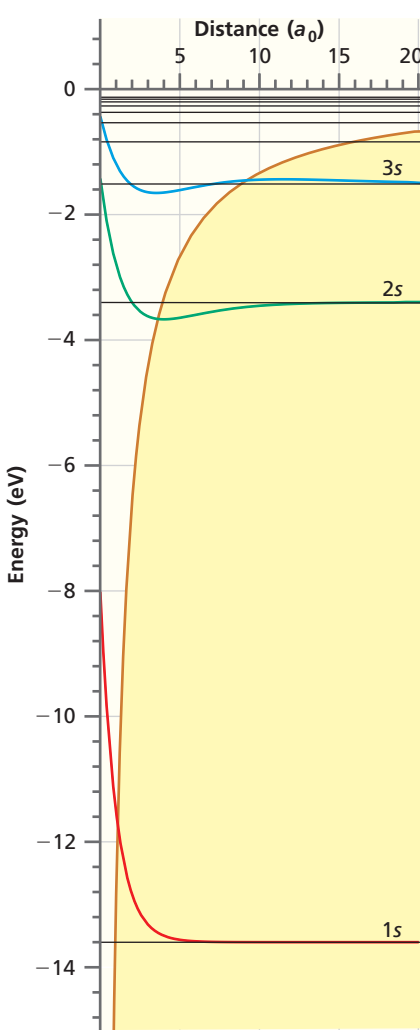
$$E_n = -\frac{m_e e^4}{8\epsilon_0^2 h^2 n^2}, \quad \text{for } n = 1, 2, 3, 4, \dots \quad (9.7)$$

This formula is usually simplified by combining a number of constants in the form $a_0 = \epsilon_0 h^2 / \pi m_e e^2$. The quantity a_0 has the value 0.529×10^{-10} m and is called the **Bohr radius**. Use of this definition leads to the following formula:

$$E_n = -\frac{e^2}{8\pi\epsilon_0 a_0 n^2} = -\frac{2.179 \times 10^{-18} \text{ J}}{n^2} = -\frac{13.60 \text{ eV}}{n^2}, \quad \text{for } n = 1, 2, 3, 4, \dots \quad (9.8)$$

Note that E_n goes to zero as $n \rightarrow \infty$. As previously emphasized, the zero of energy is a matter of convention and cannot be determined uniquely. As n approaches infinity, the electron is on average farther and farther from the nucleus, and the convention that we will use is that the zero of energy corresponds to the electron at infinite separation from the nucleus. With this choice, all negative energies correspond to bound states of the electron in the Coulomb potential, and positive energies correspond to states in which the atom is ionized.

As was done previously for the particle in the box and the harmonic oscillator, the energy eigenvalues can be superimposed on a potential energy diagram. In Figure 9.2, this is shown for the hydrogen atom. The potential forms a “box” that acts to confine

**Figure 9.2**

Energy eigenvalues superimposed on a potential energy diagram for the hydrogen atom. The border of the classically forbidden region, shown in yellow, is the Coulomb potential, which is shown together with E_n for $n = 1$ through $n = 10$. We use the nomenclature, discussed later in this text, that $n = 1, 2$, and 3 correspond to the $1s$, $2s$, and $3s$ wave functions.

Concept

The energy eigenfunctions for the H atom are associated with three quantum numbers.

the particle. This box has a peculiar form in that it is infinitely deep at the center of the atom, and the depth falls off inversely with distance from the proton. Figure 9.2 shows that the two lowest energy levels have an appreciable separation in energy and that the separation for adjacent energy levels becomes rapidly smaller as $n \rightarrow \infty$. All states for which $5 < n < \infty$ have energies in the narrow range between $\sim -1 \times 10^{-19}$ J and zero. Although this seems strange at first, it is exactly what is expected based on the results for the particle in the box. Because of the shape of the potential, the H atom “box” is very narrow for the first few energy eigenstates but becomes very wide for large n . The particle in the box formula [Equation (4.17)] predicts that the energy spacing varies as the inverse of the square of box length. This is the trend seen in Figure 9.2. Note also that the wave functions penetrate into the classically forbidden region just as for the particle in the finite depth box and the harmonic oscillator.

Although the energy depends on a single quantum number n , the total energy eigenfunctions $\psi(r, \theta, \phi)$ are associated with three quantum numbers because three boundary conditions arise in a three-dimensional problem. In addition to n , the other two quantum numbers are l and m_l , which arise from the angular coordinates. As was the case for the rigid rotor, these quantum numbers are not independent. Their relationship is given by

$$\begin{aligned} n &= 1, 2, 3, 4, \dots \\ l &= 0, 1, 2, 3, \dots, n - 1 \\ m_l &= 0, \pm 1, \pm 2, \pm 3, \dots, \pm l \end{aligned} \quad (9.9)$$

The relationship between l and m_l was discussed in Section 7.3. Although we do not present a justification of the relationship between n and l here, all the conditions in Equation (9.9) emerge naturally out of the boundary conditions in the solution of the differential equations.

The radial functions $R(r)$ are products of an exponential function with a polynomial in the dimensionless variable r/a_0 . Their functional form depends on the quantum numbers n and l . The first few normalized radial functions $R_{nl}(r)$ are as follows:

$$\begin{aligned} n = 1, l = 0 \quad R_{10}(r) &= 2\left(\frac{1}{a_0}\right)^{3/2} e^{-r/a_0} \\ n = 2, l = 0 \quad R_{20}(r) &= \frac{1}{\sqrt{8}}\left(\frac{1}{a_0}\right)^{3/2}\left(2 - \frac{r}{a_0}\right)e^{-r/2a_0} \\ n = 2, l = 1 \quad R_{21}(r) &= \frac{1}{\sqrt{24}}\left(\frac{1}{a_0}\right)^{3/2}\frac{r}{a_0}e^{-r/2a_0} \\ n = 3, l = 0 \quad R_{30}(r) &= \frac{2}{81\sqrt{3}}\left(\frac{1}{a_0}\right)^{3/2}\left(27 - 18\frac{r}{a_0} + 2\frac{r^2}{a_0^2}\right)e^{-r/3a_0} \\ n = 3, l = 1 \quad R_{31}(r) &= \frac{4}{81\sqrt{6}}\left(\frac{1}{a_0}\right)^{3/2}\left(6\frac{r}{a_0} - \frac{r^2}{a_0^2}\right)e^{-r/3a_0} \\ n = 3, l = 2 \quad R_{32}(r) &= \frac{4}{81\sqrt{30}}\left(\frac{1}{a_0}\right)^{3/2}\frac{r^2}{a_0^2}e^{-r/3a_0} \end{aligned}$$

To form the hydrogen atom eigenfunctions, we combine $R_{nl}(r)$ with the spherical harmonics and list here the first few of the infinite set of normalized wave functions $\psi(r, \theta, \phi) = R(r)\Theta(\theta)\Phi(\phi)$ for the hydrogen atom. Note that, in general, the eigenfunctions depend on r , θ , and ϕ but are not functions of θ and ϕ for $l = 0$. The quantum numbers are associated with the wave functions using the notation ψ_{nlm_l} :

$$\begin{aligned} n = 1, l = 0, m_l = 0 \quad \psi_{100}(r) &= \frac{1}{\sqrt{\pi}}\left(\frac{1}{a_0}\right)^{3/2} e^{-r/a_0} \\ n = 2, l = 0, m_l = 0 \quad \psi_{200}(r) &= \frac{1}{4\sqrt{2\pi}}\left(\frac{1}{a_0}\right)^{3/2}\left(2 - \frac{r}{a_0}\right)e^{-r/2a_0} \end{aligned}$$

$$n = 2, l = 1, m_l = 0 \quad \psi_{210}(r, \theta, \phi) = \frac{1}{4\sqrt{2\pi}} \left(\frac{1}{a_0}\right)^{3/2} \frac{r}{a_0} e^{-r/2a_0} \cos \theta$$

$$n = 2, l = 1, m_l = \pm 1 \quad \psi_{21\pm 1}(r, \theta, \phi) = \mp \frac{1}{8\sqrt{\pi}} \left(\frac{1}{a_0}\right)^{3/2} \frac{r}{a_0} e^{-r/2a_0} \sin \theta e^{\pm i\phi}$$

$$n = 3, l = 0, m_l = 0 \quad \psi_{300}(r) = \frac{1}{81\sqrt{3\pi}} \left(\frac{1}{a_0}\right)^{3/2} \left(27 - 18\frac{r}{a_0} + 2\frac{r^2}{a_0^2}\right) e^{-r/3a_0}$$

$$n = 3, l = 1, m_l = 0 \quad \psi_{310}(r, \theta, \phi) = \frac{1}{81} \left(\frac{2}{\pi}\right)^{1/2} \left(\frac{1}{a_0}\right)^{3/2} \left(6\frac{r}{a_0} - \frac{r^2}{a_0^2}\right) e^{-r/3a_0} \cos \theta$$

$$n = 3, l = 1, m_l = \pm 1 \quad \psi_{31\pm 1}(r, \theta, \phi) = \mp \frac{1}{81\sqrt{\pi}} \left(\frac{1}{a_0}\right)^{3/2} \left(6\frac{r}{a_0} - \frac{r^2}{a_0^2}\right) e^{-r/3a_0} \sin \theta e^{\pm i\phi}$$

$$n = 3, l = 2, m_l = 0 \quad \psi_{320}(r, \theta, \phi) = \frac{1}{81\sqrt{6\pi}} \left(\frac{1}{a_0}\right)^{3/2} \frac{r^2}{a_0^2} e^{-r/3a_0} (3 \cos^2 \theta - 1)$$

$$n = 3, l = 2, m_l = \pm 1 \quad \psi_{32\pm 1}(r, \theta, \phi) = \mp \frac{1}{81\sqrt{\pi}} \left(\frac{1}{a_0}\right)^{3/2} \frac{r^2}{a_0^2} e^{-r/3a_0} \sin \theta \cos \theta e^{\pm i\phi}$$

$$n = 3, l = 2, m_l = \pm 2 \quad \psi_{32\pm 2}(r, \theta, \phi) = \frac{1}{162\sqrt{\pi}} \left(\frac{1}{a_0}\right)^{3/2} \frac{r^2}{a_0^2} e^{-r/3a_0} \sin^2 \theta e^{\pm 2i\phi}$$

These wave functions are referred to both as the H atom eigenfunctions and the H atom **orbitals**. A shorthand notation for the quantum numbers is to give the numerical value of n followed by a symbol indicating the values of l and m_l . The letters s , p , d , and f are used to denote $l = 0, 1, 2$, and 3 , respectively, $\psi_{100}(r)$ is referred to as the 1s orbital or wave function, and all three wave functions with $n = 2$ and $l = 1$ are referred to as $2p$ orbitals. The wave functions are real functions if $m_l = 0$, and complex functions otherwise. The angular and radial portions of the wave functions have nodes that are discussed in more detail later in this chapter. These functions have been normalized in keeping with the association between probability density and $\psi(r, \theta, \phi)$ stated in the first postulate (see Chapter 3). It is demonstrated in Example Problem 9.1 that the wave functions listed above are eigenfunctions of the Schrödinger equation but are not eigenfunctions of the kinetic and potential energy operators. Example Problem 9.2 demonstrates normalization of these wave functions.

EXAMPLE PROBLEM 9.1

Consider an excited state of the H atom with the electron in the $2s$ orbital.

- a. Is the wave function that describes this state,

$$\psi_{200}(r) = \frac{1}{\sqrt{32\pi}} \left(\frac{1}{a_0}\right)^{3/2} \left(2 - \frac{r}{a_0}\right) e^{-r/2a_0}$$

an eigenfunction of the kinetic energy? Of the potential energy?

- b. Calculate the average values of the kinetic and potential energies for an atom described by this wave function.

Solution

- a. We know that this function is an eigenfunction of the total energy operator because it is a solution of the Schrödinger equation. You can convince yourself that the total energy operator does not commute with either the kinetic energy operator or the potential energy operator by extending the discussion of Example Problem 9.1. Therefore, this wave function cannot be an eigenfunction of either of these operators.

b. The average value of the kinetic energy is given by

$$\begin{aligned}
 \langle E_{kinetic} \rangle &= \int \psi^*(\tau) \hat{E}_{kinetic} \psi(\tau) d\tau \\
 &= -\frac{\hbar^2}{2m_e} \frac{1}{32\pi a_0^3} \int_0^{2\pi} d\phi \int_0^\pi \sin\theta \, d\theta \int_0^\infty \left(2 - \frac{r}{a_0}\right) \times \\
 &\quad e^{-r/2a_0} \left(\frac{1}{r^2} \frac{d}{dr} \left[r^2 \frac{d}{dr} \left\{ \left(2 - \frac{r}{a_0}\right) e^{-r/2a_0} \right\} \right] \right) r^2 dr \\
 &= -\frac{\hbar^2}{2m_e} \frac{1}{8a_0^3} \int_0^\infty \left(2 - \frac{r}{a_0}\right) e^{-r/2a_0} \left(-\frac{e^{-r/2a_0}}{4a_0^3 r} \right) (16a_0^2 - 10a_0 r + r^2) r^2 dr \\
 &= -\frac{\hbar^2}{2m_e} \frac{1}{8a_0^3} \left(\frac{9}{a_0^2} \int_0^\infty r^2 e^{-r/a_0} dr - \frac{8}{a_0} \int_0^\infty r e^{-r/a_0} dr - \frac{3}{a_0^3} \int_0^\infty r^3 e^{-r/a_0} dr \right. \\
 &\quad \left. + \frac{1}{4a_0^4} \int_0^\infty r^4 e^{-r/a_0} dr \right)
 \end{aligned}$$

We use the standard integral, $\int_0^\infty x^n e^{-ax} dx = n! / a^{n+1}$:

$$\langle E_{kinetic} \rangle = \hbar^2 / 8m_e a_0^2$$

Using the relationship $a_0 = \epsilon_0 h^2 / \pi m_e e^2$,

$$\langle E_{kinetic} \rangle = \frac{e^2}{32\pi\epsilon_0 a_0} = -E_n, \quad \text{for } n = 2$$

The average potential energy is given by

$$\begin{aligned}
 \langle E_{potential} \rangle &= \int \psi^*(\tau) \hat{E}_{potential} \psi(\tau) d\tau \\
 &= -\frac{e^2}{4\pi\epsilon_0} \frac{1}{32\pi a_0^3} \int_0^{2\pi} d\phi \int_0^\pi \sin\theta \, d\theta \int_0^\infty \left[\left(2 - \frac{r}{a_0}\right) e^{-r/2a_0} \right] \times \\
 &\quad \left(\frac{1}{r} \right) \left[\left(2 - \frac{r}{a_0}\right) e^{-r/2a_0} \right] r^2 dr \\
 &= -\frac{e^2}{4\pi\epsilon_0} \frac{1}{8a_0^3} \left(4 \int_0^\infty r e^{-r/a_0} dr - \frac{4}{a_0} \int_0^\infty r^2 e^{-r/a_0} dr + \frac{1}{a_0^2} \int_0^\infty r^3 e^{-r/a_0} dr \right) \\
 &= -\frac{e^2}{4\pi\epsilon_0} \frac{1}{8a_0^3} (2a_0^2) \\
 &= -\frac{e^2}{16\pi\epsilon_0 a_0} = 2 E_n \quad \text{for } n = 2
 \end{aligned}$$

We see that $\langle E_{potential} \rangle = 2 \langle E_{total} \rangle$ and $\langle E_{potential} \rangle = -2 \langle E_{kinetic} \rangle$. The relationship of the kinetic and potential energies is a specific example of the **virial theorem**.

More generally, the virial theorem is satisfied if the force between any two particles of the system results from a potential energy $V(r) = \alpha r^n$ that is proportional to some power n of the interparticle distance r , where n is an integer.

EXAMPLE PROBLEM 9.2

Normalize the functions $e^{-r/2a_0}$ and $(r/a_0)e^{-r/2a_0} \sin\theta e^{+i\phi}$ in three-dimensional spherical coordinates.

Solution

In general, a wave function $\psi(\tau)$ is normalized by multiplying it by a constant N defined by $N^2 \int \psi^*(\tau)\psi(\tau)d\tau = 1$. In three-dimensional spherical coordinates, $d\tau = r^2 \sin\theta dr d\theta d\phi$, as discussed in Math Essential 8. The normalization integral becomes $N^2 \int_0^\pi \sin\theta d\theta \int_0^{2\pi} d\phi \int_0^\infty \psi^*(r, \theta, \phi)\psi(r, \theta, \phi)r^2 dr = 1$.

For the first function,

$$N^2 \int_0^\pi \sin\theta d\theta \int_0^{2\pi} d\phi \int_0^\infty e^{-r/2a_0} e^{-r/2a_0} r^2 dr = 1$$

We use the standard integral

$$\int_0^\infty x^n e^{-ax} dx = \frac{n!}{a^{n+1}}$$

Integrating over the angles θ and ϕ , we obtain $4\pi N^2 \int_0^\infty e^{-r/2a_0} e^{-r/2a_0} r^2 dr = 1$. Evaluating the integral over r ,

$$4\pi N^2 \frac{2!}{1/a_0^3} = 1 \quad \text{or} \quad N = \frac{1}{2\sqrt{2\pi}} \left(\frac{1}{a_0} \right)^{3/2}$$

For the second function,

$$N^2 \int_0^\pi \sin\theta d\theta \int_0^{2\pi} d\phi \int_0^\infty \left(\frac{r}{a_0} e^{-r/2a_0} \sin\theta e^{-i\phi} \right) \left(\frac{r}{a_0} e^{-r/2a_0} \sin\theta e^{+i\phi} \right) r^2 dr = 1$$

This simplifies to

$$N^2 \int_0^\pi \sin^3\theta d\theta \int_0^{2\pi} d\phi \int_0^\infty \left(\frac{r}{a_0} \right)^2 e^{-r/a_0} r^2 dr = 1$$

Integrating over the angles θ and ϕ using the result $\int_0^\pi \sin^3\theta d\theta = 4/3$, we obtain

$$\frac{8\pi}{3} N^2 \int_0^\infty \left(\frac{r}{a_0} \right)^2 e^{-r/a_0} r^2 dr = 1$$

Using the same standard integral as in the first part of the problem,

$$\frac{8\pi}{3} N^2 \frac{1}{a_0^2} \left(\frac{4!}{1/a_0^5} \right) = 1 \quad \text{or} \quad N = \frac{1}{8\sqrt{\pi}} \left(\frac{1}{a_0} \right)^{3/2}$$

Each eigenfunction listed here describes a separate state of the hydrogen atom. However, as we have seen, the energy depends only on the quantum number n . Therefore, all states with the same value for n , but different values for l and m_l , have the same energy, and we say that the energy levels are degenerate. Using the formulas given in Equation (9.9), we can see that the degeneracy of a given level is n^2 . Therefore, the $n = 2$ level has a fourfold degeneracy, and the $n = 3$ level has a ninefold degeneracy.

The angular part of each hydrogen atom total energy eigenfunction is a spherical harmonic function. As discussed in Section 7.5, these functions are complex unless $m_l = 0$. To facilitate making graphs, it is useful to form combinations of those hydrogen orbitals $\psi_{nlm_l}(r, \theta, \phi)$ for which $m_l \neq 0$ are real functions of r , θ , and ϕ . As discussed in Section 7.5, this is done by forming linear combinations of $\psi_{nlm_l}(r, \theta, \phi)$

and $\psi_{nl-m_l}(r, \theta, \phi)$. The first few of these combinations, resulting in the $2p$, $3p$, and $3d$ orbitals, are shown here:

$$\begin{aligned}\psi_{2p_x}(r, \theta, \phi) &= \frac{1}{4\sqrt{2\pi}} \left(\frac{1}{a_0}\right)^{3/2} \frac{r}{a_0} e^{-r/2a_0} \sin \theta \cos \phi \\ \psi_{2p_y}(r, \theta, \phi) &= \frac{1}{4\sqrt{2\pi}} \left(\frac{1}{a_0}\right)^{3/2} \frac{r}{a_0} e^{-r/2a_0} \sin \theta \sin \phi \\ \psi_{2p_z}(r, \theta, \phi) &= \frac{1}{4\sqrt{2\pi}} \left(\frac{1}{a_0}\right)^{3/2} \frac{r}{a_0} e^{-r/2a_0} \cos \theta \\ \psi_{3p_x}(r, \theta, \phi) &= \frac{\sqrt{2}}{81\sqrt{\pi}} \left(\frac{1}{a_0}\right)^{3/2} \left(6\frac{r}{a_0} - \frac{r^2}{a_0^2}\right) e^{-r/3a_0} \sin \theta \cos \phi \\ \psi_{3p_y}(r, \theta, \phi) &= \frac{\sqrt{2}}{81\sqrt{\pi}} \left(\frac{1}{a_0}\right)^{3/2} \left(6\frac{r}{a_0} - \frac{r^2}{a_0^2}\right) e^{-r/3a_0} \sin \theta \sin \phi \\ \psi_{3p_z}(r, \theta, \phi) &= \frac{\sqrt{2}}{81\sqrt{\pi}} \left(\frac{1}{a_0}\right)^{3/2} \left(6\frac{r}{a_0} - \frac{r^2}{a_0^2}\right) e^{-r/3a_0} \cos \theta \\ \psi_{3d_{z^2}}(r, \theta, \phi) &= \frac{1}{81\sqrt{6\pi}} \left(\frac{1}{a_0}\right)^{3/2} \frac{r^2}{a_0^2} e^{-r/3a_0} (3 \cos^2 \theta - 1) \\ \psi_{3d_{xz}}(r, \theta, \phi) &= \frac{\sqrt{2}}{81\sqrt{\pi}} \left(\frac{1}{a_0}\right)^{3/2} \frac{r^2}{a_0^2} e^{-r/3a_0} \sin \theta \cos \theta \cos \phi \\ \psi_{3d_{yz}}(r, \theta, \phi) &= \frac{\sqrt{2}}{81\sqrt{\pi}} \left(\frac{1}{a_0}\right)^{3/2} \frac{r^2}{a_0^2} e^{-r/3a_0} \sin \theta \cos \theta \sin \phi \\ \psi_{3d_{x^2-y^2}}(r, \theta, \phi) &= \frac{1}{81\sqrt{2\pi}} \left(\frac{1}{a_0}\right)^{3/2} \frac{r^2}{a_0^2} e^{-r/3a_0} \sin^2 \theta \cos 2\phi \\ \psi_{3d_{xy}}(r, \theta, \phi) &= \frac{1}{81\sqrt{2\pi}} \left(\frac{1}{a_0}\right)^{3/2} \frac{r^2}{a_0^2} e^{-r/3a_0} \sin^2 \theta \sin 2\phi\end{aligned}$$

The real functions are more useful in visualizing chemical bonds and will generally be used throughout this book. However, both the real and complex representations are useful in different applications, and we note that although the real functions are eigenfunctions of \hat{H} and \hat{l}^2 , they are not eigenfunctions of \hat{l}_z .

The challenge we posed for quantum mechanics at the beginning of this chapter was to provide an understanding for the stability of atoms. By verifying that there is a set of eigenfunctions and eigenvalues of the time-independent Schrödinger equation for a system consisting of a proton and an electron, we have demonstrated that there are states whose energy is independent of time. Because the energy eigenvalues are all negative numbers, all of these states are more stable than the reference state of zero energy that corresponds to the proton and electron separated by an infinite distance. Because $n \geq 1$, the energy cannot approach $-\infty$, corresponding to the electron falling into the nucleus. These results show that when the wave nature of the electron is taken into account, the H atom is stable.

As with any new theory, the true test is consistency with experimental data. Although the wave functions are not directly observable, we know that the spectral lines from a hydrogen arc lamp (measured as early as 1885) must involve transitions between two stable states of the hydrogen atom. Therefore, the frequencies measured by the early experimentalists in emission spectra are related to the energy of the states involved in the transition by

$$v = \left| \frac{1}{h} (E_{initial} - E_{final}) \right| \quad (9.10)$$

In a more exact treatment, the origin of the coordinate system describing the H atom is placed at the center of mass of the proton and electron rather than at the position of the proton. Using Equation (9.7) with the reduced mass of the atom in place of m_e and Equation (9.10), quantum theory predicts that the frequencies of all the spectral lines are given by

$$\nu = \left| \frac{\mu e^4}{8\epsilon_0^2 h^3} \left(\frac{1}{n_{initial}^2} - \frac{1}{n_{final}^2} \right) \right| \quad (9.11)$$

where $\mu = m_e m_p / (m_e + m_p)$ is the reduced mass of the atom, which is 0.05% less than m_e . Spectroscopists commonly refer to spectral lines in units of wave numbers. Rather than reporting values of ν , they use the units $\tilde{\nu} = \nu/c = 1/\lambda$. The combination of constants $\mu_e e^4 / 8\epsilon_0^2 h^3 c$ is called the **Rydberg constant for hydrogen**. It has the value $109,677.581 \text{ cm}^{-1}$ in quantitative agreement with the experimental value.

Equation (9.11) quantitatively predicts all observed spectral lines for the hydrogen atom. It also correctly predicts the very small shifts in frequency observed for the isotopes of hydrogen, which have slightly different reduced masses. The agreement between theory and experiment verifies that the quantum-mechanical model for the hydrogen atom is valid and accurate. We discuss the selection rules for transitions between electronic states in atoms in Chapter 11. Some of these transitions are shown superimposed on a set of energy levels in Figure 9.3.

9.4 HYDROGEN ATOM ORBITALS

We now turn to the total energy eigenfunctions (or orbitals) of the hydrogen atom. What insight can be gained from evaluating and determining them? Recall the early quantum-mechanics shell model of atoms proposed by Niels Bohr. It depicted electrons orbiting around the nucleus and associated orbits of small radius with more negative energies. Only certain orbits were allowed to give rise to a discrete energy spectrum. This model was discarded because defining orbits exactly is inconsistent with the Heisenberg uncertainty principle. The model postulated by Schrödinger and other pioneers of quantum theory replaced knowledge of the location of the electron in the hydrogen atom with knowledge of the probability of finding it in a small-volume element at a specific location. As we have seen in considering the particle in the box and the harmonic oscillator, this probability is proportional to $\psi^*(r, \theta, \phi)\psi(r, \theta, \phi) d\tau$.

To what extent does the exact quantum-mechanical solution resemble the shell model? To answer this question, information must be extracted from the H atom orbitals. In the following, a new concept, the radial distribution function, is introduced for this purpose. We begin our discussion by focusing on the wave functions $\psi_{nlm_l}(r, \theta, \phi)$. Next, we discuss what can be learned about the probability of finding the electron in a particular region in space, $|\psi_{nlm_l}(r, \theta, \phi)|^2 r^2 \sin\theta dr d\theta d\phi$. Finally, we define the radial distribution function and look at the similarities and differences between quantum-mechanical and shell models of the hydrogen atom.

The initial step is to look at the ground state (lowest energy state) wave function for the hydrogen atom. Next, we need to find a good way to visualize this function. Because

$$\psi_{100}(r) = \frac{1}{\sqrt{\pi}} \left(\frac{1}{a_0} \right)^{3/2} e^{-r/a_0}$$

is a function of the three spatial coordinates x , y , and z , we need a four-dimensional space to plot ψ_{100} as a function of all its variables. Because such a space is not readily available, the number of variables will be reduced. The dimensionality of the representation can be reduced by evaluating $r = \sqrt{x^2 + y^2 + z^2}$ in one of the xy , xz , or yz planes by setting the third coordinate equal to zero. Three common ways of depicting $\psi_{100}(r)$ are shown in Figures 9.4 through 9.6. In Figure 9.4a, a three-dimensional plot of $\psi_{100}(r)$ evaluated in the xy half-plane ($z = 0, y \geq 0$) is shown in perspective.

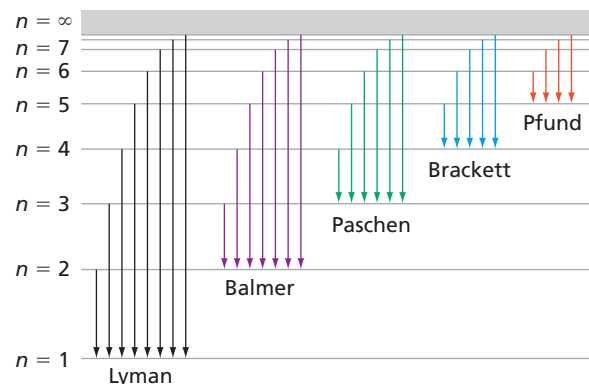
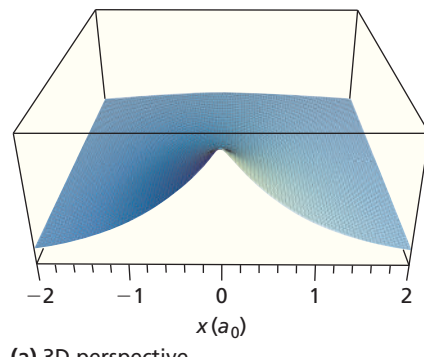
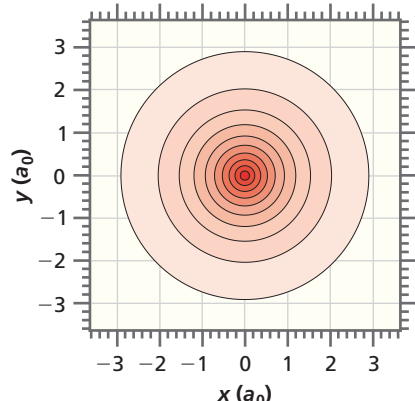


Figure 9.3

Energy-level diagram for the hydrogen atom showing allowed transitions for $n < 8$. Because energy levels are continuous for $E > 0$, the absorption spectrum is continuous above an energy that depends on the initial n value, as indicated by the gray area. The different sets of transitions are named after the scientists who first investigated them.



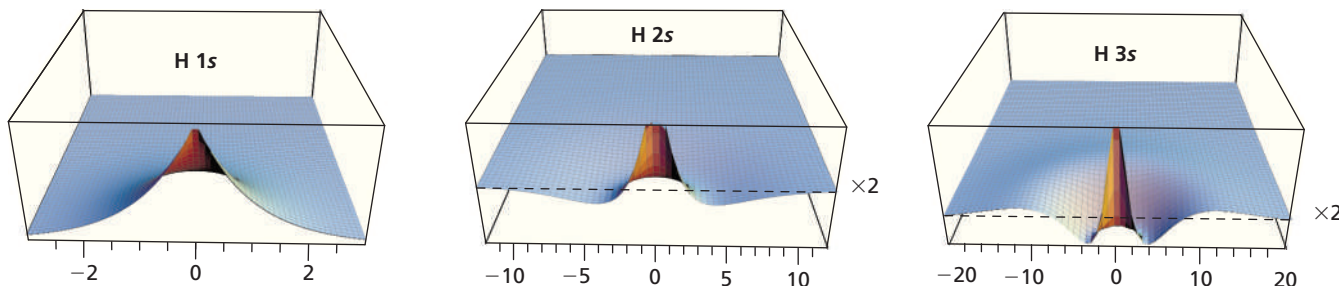
(a) 3D perspective



(b) Contour plot

Figure 9.4

Different images of $\psi_{100}(r)$. Diagrams are a (a) 3D perspective and (b) contour plot of $\psi_{100}(r)$. Darker contour colors indicate larger values for the magnitude of the amplitude.

**Figure 9.5**

Three-dimensional perspective plots of the 1s, 2s, and 3s orbitals. The dashed lines indicate the zero of amplitude for the wave functions. The annotation $\times 2$ refers to the fact that the amplitude of the wave function has been multiplied by 2 to make the subsidiary maxima apparent. The horizontal axis shows radial distance in units of a_0 .

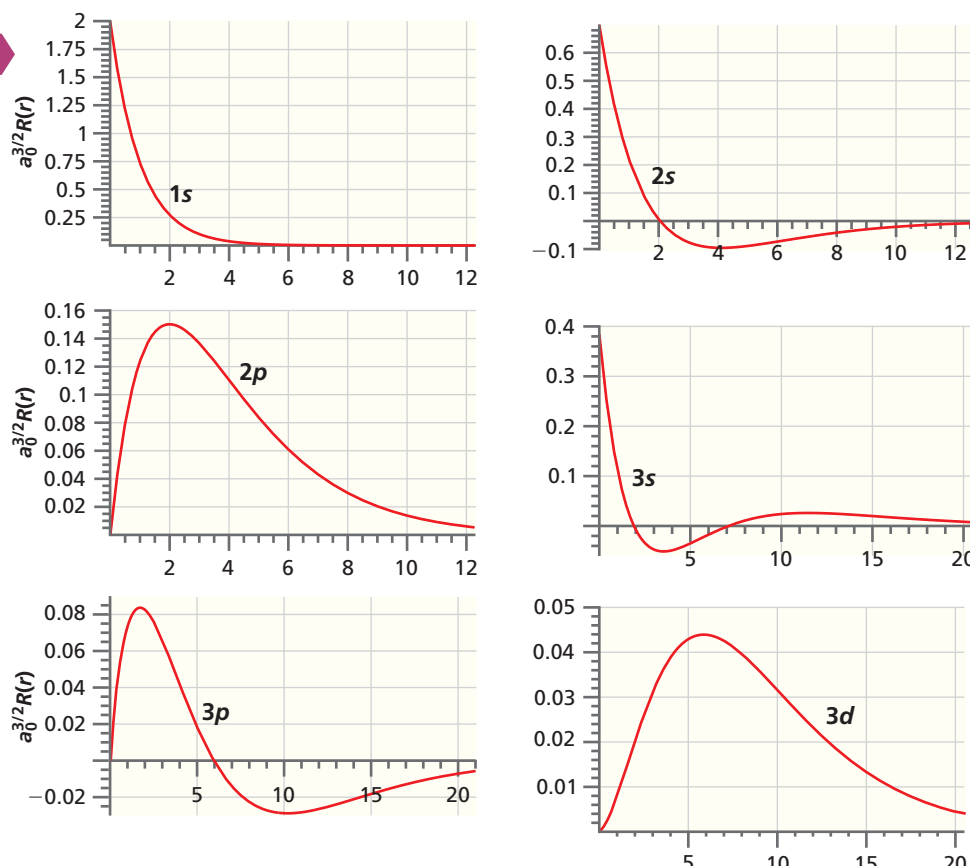
Although it is difficult to extract quantitative information from such a plot directly, it allows a good visualization of the function. We clearly see that the wave function has its maximum value at $r = 0$ (the nuclear position) and that it falls off rapidly with increasing distance from the nucleus.

More quantitative information is available in the contour plot shown in Figure 9.4b in which $\psi_{100}(r)$ is evaluated in the xy plane from a vantage point on the z axis. In this case, the outermost contour represents 10% of the maximum value, and successive contours are spaced at equal intervals. The shading indicates the value of the function, with darker colors representing larger values of the amplitude. This way of depicting $\psi_{100}(r)$ is more quantitative than that of Figure 9.4a in that we can recognize that the contours of constant amplitude are circles and that the contour spacing becomes smaller as r approaches zero. A third useful representation is to show the value of the function with two variables set equal to zero. This represents a cut through $\psi_{100}(r)$ in a plane perpendicular to the $x-y$ plane. Because ψ_{100} is independent of the angular coordinates, the same result is obtained for all planes containing the z axis. As we will see later, this is only true for orbitals for which $l = 0$. This way of depicting $\psi_{100}(r)$ is shown as the front edge of the three-dimensional plot in Figure 9.4a and in Figures 9.5 and 9.6. All of these graphical representations contain exactly the same information.

Because $\psi_{100}(r)$ is a function of the single variable r , the function can be graphed directly. However, it is important to keep in mind that r is a three-dimensional function of

Concept

The energy eigenfunctions for the H atom can have radial and/or angular nodes.

**Figure 9.6**

Plot of $a_0^{3/2}R(r)$ versus r/a_0 for the first few H atomic orbitals.

x , y , and z . For $l = 0$, the wave function does not depend on θ and ϕ . For $l > 0$, the wave function does depend on θ and ϕ , and a plot of the amplitude of a wave function versus r assumes that θ and ϕ are being held constant at values that need to be specified. These values generally correspond to a maximum in the angular part of the wave function.

In Figure 9.6, the radial wave function amplitude $R(r)$ is graphed versus r . What should we expect having solved the particle in the box and harmonic oscillator problems? Because the eigenfunctions of the Schrödinger equation are standing waves, the solutions should be oscillating functions that have nodes. There should be no nodes in the ground state, and the number of nodes should increase as the quantum number increases.

First, consider the eigenfunctions with $l = 0$, namely, the 1s, 2s, and 3s orbitals. From Figure 9.5, we clearly see that ψ_{100} has no nodes as expected. The 2s and 3s orbitals have one and two nodes, respectively. Because these nodes correspond to constant values of r , they are spherical **nodal surfaces**, rather than the nodal points previously encountered for one-dimensional potentials.

Now consider the eigenfunctions with $l > 0$. Why do the 2p and 3d functions in Figure 9.6 appear not to have nodal surfaces? To see the nodes, the angular part of these eigenfunctions must be displayed.

Whereas the spherically symmetric s orbitals are equally well represented by the three forms of graphics described earlier, the p and d orbitals can best be visualized with a contour plot analogous to that of Figure 9.4b. Contour plots for the $2p_y$, $3p_y$, $3d_{xy}$, and $3d_{z^2}$ wave functions are shown in Figure 9.7. This nomenclature was defined in Section 9.3. We can now see that the $2p_y$ wave function has a nodal plane defined by $y = 0$; however, it appears in the angular rather than the radial part of the wave function. It can be shown that the radial part of the energy eigenfunctions has $n - l - 1$ nodal surfaces. There are l nodal surfaces in the angular part of the energy eigenfunctions, making a total of $n - 1$ nodes, just as was obtained for the particle in the box and the harmonic oscillator. As can be seen in Figure 9.7, the $3p_y$ wave function has a second nodal surface in addition to the nodal plane at $y = 0$. This second node comes from the radial part of the energy eigenfunction and is a spherical surface. The d orbitals have a more complex nodal structure that can include spheres, planes, and cones. The $3d_{xy}$ orbital has two nodal planes that intersect in the z axis. The $3d_{z^2}$ orbital has two conical nodal surfaces whose axis of rotation is the z axis. Example Problem 9.3 shows how nodal surfaces are located.

EXAMPLE PROBLEM 9.3

Locate the nodal surfaces in

$$\psi_{310}(r, \theta, \phi) = \frac{1}{81} \left(\frac{2}{\pi} \right)^{1/2} \left(\frac{1}{a_0} \right)^{3/2} \left(6 \frac{r}{a_0} - \frac{r^2}{a_0^2} \right) e^{-r/3a_0} \cos \theta$$

Solution

We consider the angular and radial nodal surfaces separately. The angular part, $\cos \theta$, is zero for $\theta = \pi/2$. In three-dimensional space, this corresponds to the plane $z = 0$. The radial part of the equations is zero for finite values of r/a_0 for $(6r/a_0 - r^2/a_0^2) = 0$. This occurs at $r = 0$, which is not a node because ψ doesn't change sign and at $r = 6a_0$. The first value is a point in three-dimensional space, and the second is a spherical surface. This wave function has one angular and one radial node. In general, an orbital characterized by n and l has l angular nodes and $n - 1 - l$ radial nodes.

9.5 THE RADIAL PROBABILITY DISTRIBUTION FUNCTION

To continue the discussion of the similarities and differences between the quantum-mechanical and shell models of the hydrogen atom, let us see what information can be obtained from $|\psi_{nlm}(r, \theta, \phi)|^2$, which is the probability density of finding the electron at a particular point in space. We again consider the s orbitals and the p and d orbitals

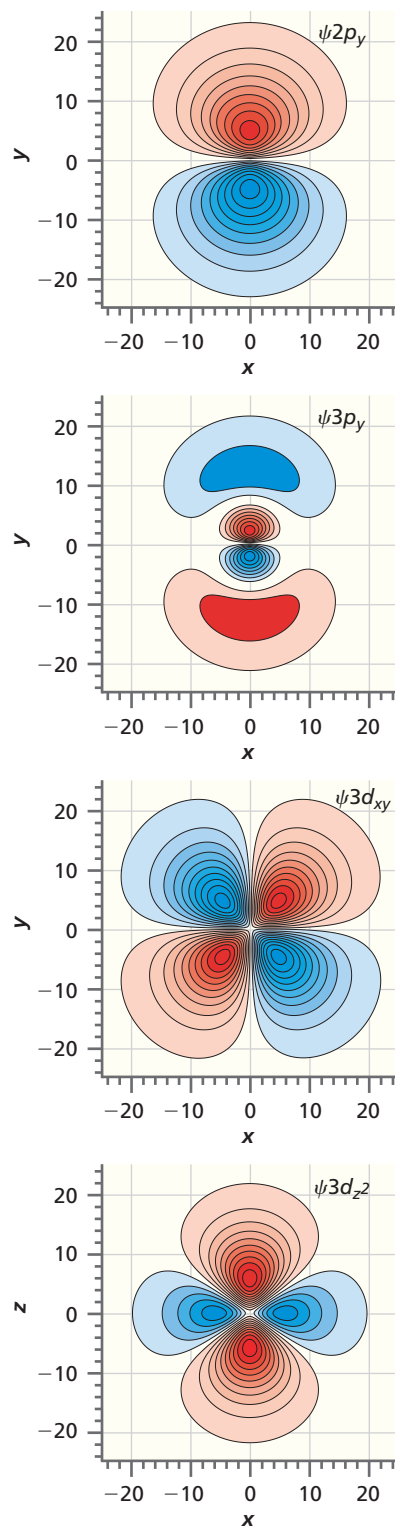
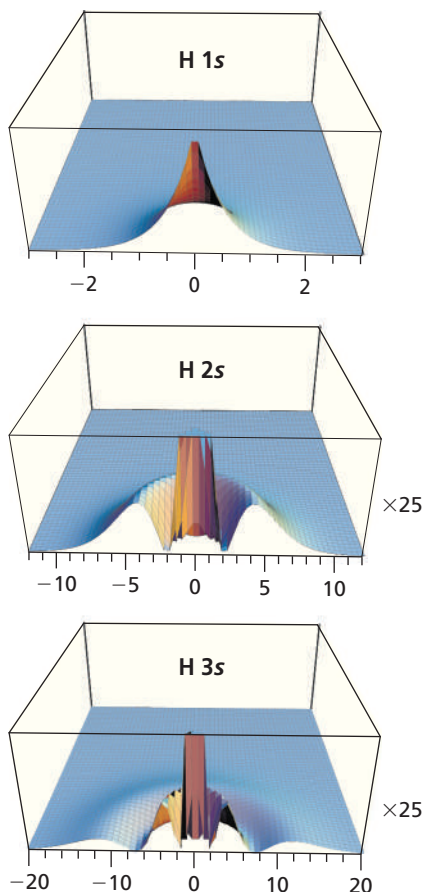


Figure 9.7

Contour plots for the $2p_y$, $3p_y$, $3d_{xy}$, and $3d_{z^2}$ orbitals. Positive and negative amplitudes are shown as red and blue, respectively. Darker colors indicate larger values for the magnitude of the amplitude. Distances are in units of a_0 .

**Figure 9.8**

Three-dimensional perspective plots of the square of the wave functions for the 1s, 2s, and 3s orbitals. The numbers on the axes are in units of a_0 . The annotation $\times 25$ refers to the fact that the amplitude of the wave function has been multiplied by 25 to make the subsidiary maxima apparent.

separately. We first show $\psi_{n00}^2(r, \theta, \phi)$ as a three-dimensional graphic in Figure 9.8 for $n = 1, 2$, and 3 . Subsidiary maxima are seen in addition to the main maximum at $r = 0$. Figure 9.9 shows a graph of $R_{nlm_l}^2(r)$ as a function of r .

Now consider $|\psi_{nlm_l}(r, \theta, \phi)|^2$ for $l > 0$. As expected from the effect of the centrifugal potential (see Figure 9.1), the electron is pushed away from the nucleus, so that $|\psi_{nlm_l}(r, \theta, \phi)|^2$ goes to zero as r approaches zero. Because a nonzero angular momentum is associated with these states, $|\psi_{nlm_l}(r, \theta, \phi)|^2$ is not spherically symmetric. All of this makes sense in terms of our picture of p and d orbitals. Example Problem 9.4 illustrates a calculation of probability density.

EXAMPLE PROBLEM 9.4

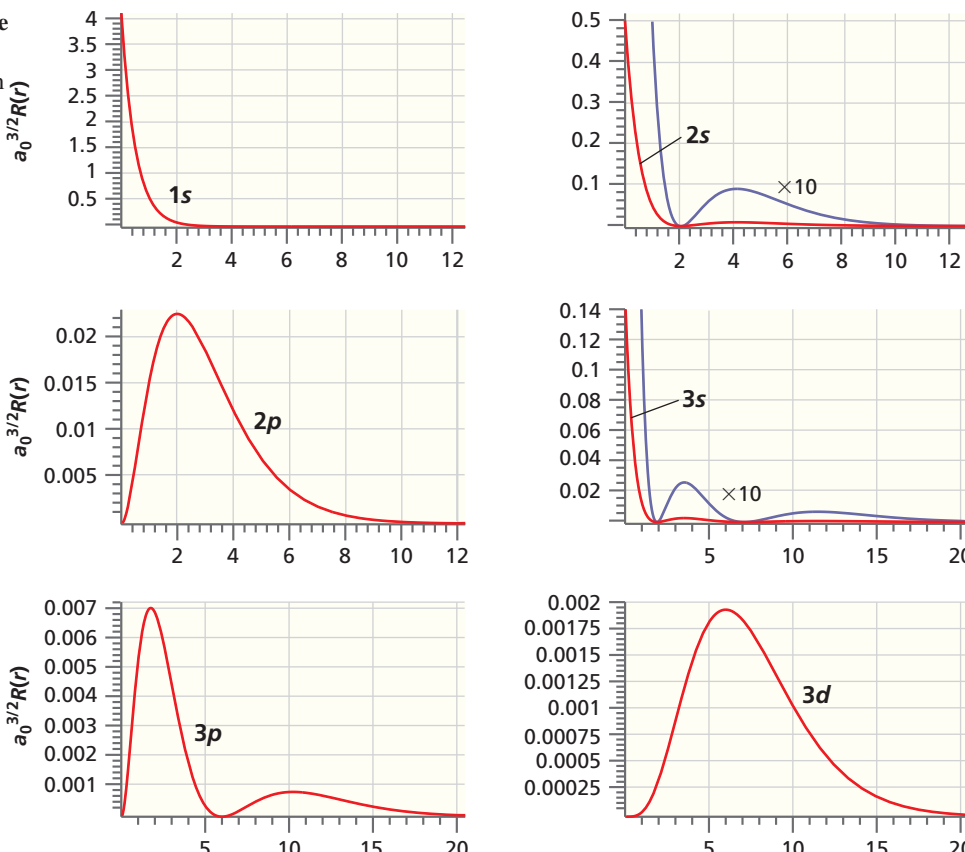
- At what point does the probability density for the electron in a $2s$ orbital have its maximum value?
- Assume that the nuclear diameter for H is 2×10^{-15} m. Using this assumption, calculate the total probability of finding the electron in the nucleus if it occupies the $2s$ orbital.

Solution

- The point at which $\psi^*(\tau)\psi(\tau) d\tau$ and, therefore, $\psi(\tau)$ has its greatest value is found from the wave function:

$$\psi_{200}(r) = \frac{1}{\sqrt{32\pi}} \left(\frac{1}{a_0} \right)^{3/2} \left(2 - \frac{r}{a_0} \right) e^{-r/2a_0}$$

which has its maximum value at $r = 0$, or at the nucleus as seen in Figure 9.6.

**Figure 9.9**

Plot of $a_0^{3/2}R^2(r)$ versus r/a_0 for the first few H atomic orbitals. The numbers on the horizontal axis are in units of a_0 .

- b. The result obtained in part (a) seems unphysical, but it is a consequence of wave-particle duality in describing electrons. It is really a problem only if the total probability of finding the electron within the nucleus is significant. This probability is given by

$$P = \frac{1}{32\pi} \left(\frac{1}{a_0}\right)^3 \int_0^{2\pi} d\phi \int_0^\pi \sin\theta d\theta \int_0^{r_{nucleus}} r^2 \left(2 - \frac{r}{a_0}\right)^2 e^{-r/a_0} dr$$

Because $r_{nucleus} \ll a_0$, we can evaluate the integrand by assuming that $(2 - r/a_0)^2 e^{-r/a_0} \sim 2$ over the interval $0 \leq r \leq r_{nucleus}$:

$$\begin{aligned} P &= \frac{1}{32\pi} \left(\frac{1}{a_0}\right)^3 4\pi \left[\left(2 - \frac{r_{nucleus}}{a_0}\right)^2 e^{-r_{nucleus}/a_0} \right] \int_0^{r_{nucleus}} r^2 dr \\ &= \frac{1}{32\pi} \left(\frac{1}{a_0}\right)^3 \left[\left(2 - \frac{r_{nucleus}}{a_0}\right)^2 e^{-r_{nucleus}/a_0} \right] \frac{4\pi}{3} r_{nucleus}^3 \end{aligned}$$

Because $2 - (r_{nucleus}/a_0) \approx 2$ and $e^{-r_{nucleus}/a_0} \approx 1$,

$$P = \frac{1}{6} \left(\frac{r_{nucleus}}{a_0}\right)^3 = 9.0 \times 10^{-15}$$

Because this probability is vanishingly small, even though the wave function has its maximum amplitude at the nucleus, the probability of finding the electron in the nucleus is essentially zero.

Concept

The radial distribution function is used to calculate the probability of finding an electron at a given distance from the nucleus.

At this point, we ask a different question involving probability. What is the most probable distance from the nucleus at which the electron will be found? For the $1s$, $2s$, and $3s$ orbitals, the maximum probability density is at the nucleus. This result seems to predict that the most likely orbit for the electron has a radius of zero. Clearly, we are missing something because this result is inconsistent with a shell model. It turns out that we are not asking the right question. The probability as calculated from the probability density is correct, but it gives the likelihood of finding the particle in the vicinity of a *particular point* for a given value of r , θ , and ϕ . Why is this not the information we are looking for? Imagine that a planet has a circular orbit and we want to determine the radius of the orbit. To do so, we must find the planet. If we looked at only one point on a spherical shell of a given radius for different values of the radius, we would be unlikely to find the planet. To find the planet, we need to look everywhere on a shell of a given radius simultaneously.

How do we apply this reasoning to finding the electron on the hydrogen atom? The question we need to ask is: What is the probability of finding the electron at a particular value of r , *regardless* of the values of θ and ϕ ? This probability is obtained by integrating the probability density $\psi_{nlm_l}^2(r, \theta, \phi) r^2 \sin\theta dr d\theta d\phi$ over all values of θ and ϕ . This gives the probability of finding the electron in a spherical shell of radius r and thickness dr rather than the probability of finding the electron near a given point on the spherical shell of thickness dr with the particular coordinates r_0, θ_0, ϕ_0 . For example, for the $1s$ orbital the probability of finding the electron in a spherical shell of radius r and thickness dr is

$$\begin{aligned} P_{1s}(r)dr &= \frac{1}{\pi a_0^3} \int_0^{2\pi} d\phi \int_0^\pi \sin\theta d\theta r^2 e^{-2r/a_0} dr \\ &= \frac{4}{a_0^3} r^2 e^{-2r/a_0} dr \end{aligned} \tag{9.12}$$

Example Problem 9.5 illustrates the difference between finding the probability density at a point in space as opposed to the probability density at a given distance from the nucleus.

EXAMPLE PROBLEM 9.5

Consider an excited hydrogen atom with the electron in the 2s orbital.

- Calculate the probability of finding the electron in the volume about a point defined by

$$5.22 \times 10^{-10} \text{ m} \leq r \leq 5.26 \times 10^{-10} \text{ m}, \frac{\pi}{2} - 0.01 \leq \phi \leq \frac{\pi}{2} + 0.01,$$

$$\frac{\pi}{2} - 0.01 \leq \theta \leq \frac{\pi}{2} + 0.01$$

- Calculate the probability of finding the electron in the spherical shell defined by

$$5.22 \times 10^{-10} \text{ m} \leq r \leq 5.26 \times 10^{-10} \text{ m}$$

Solution

- We numerically solve the integral $\iiint \psi^*(r, \theta, \phi) \psi(r, \theta, \phi) r^2 \sin \theta dr d\theta d\phi$. The result is

$$P = \frac{1}{32\pi} \left(\frac{1}{a_0}\right)^3 \int_{\frac{\pi}{2}-0.01}^{\frac{\pi}{2}+0.01} d\phi \int_{\frac{\pi}{2}-0.01}^{\frac{\pi}{2}+0.01} \sin \theta d\theta \int_{5.22 \times 10^{-10}}^{5.26 \times 10^{-10}} r^2 \left(2 - \frac{r}{a_0}\right)^2 e^{-r/a_0} dr \\ = 0.00995 \times 6.76 \times 10^{30} \text{ m}^{-3} \times 0.020 \times 0.0200 \times 3.43 \times 10^{-33} \text{ m}^3 = 9.23 \times 10^{-8}$$

- In this case, we integrate over all values of the angles:

$$P = \frac{1}{32\pi} \left(\frac{1}{a_0}\right)^3 \int_0^{2\pi} d\phi \int_0^\pi \sin \theta d\theta \int_{5.22 \times 10^{-10}}^{5.26 \times 10^{-10}} r^2 \left(2 - \frac{r}{a_0}\right)^2 e^{-r/a_0} dr \\ = 0.00995 \times 6.76 \times 10^{30} \text{ m}^{-3} \times 4\pi \times 3.43 \times 10^{-33} \text{ m}^3 = 2.90 \times 10^{-3}$$

This probability is greater than that calculated in part (a) by a factor of 3.1×10^4 because we have integrated the probability density over the whole spherical shell of thickness $4 \times 10^{-12} \text{ m}$.

Because the integration of the probability density over the angles θ and ϕ amounts to an averaging of $\psi(r, \theta, \phi)^2$ over all angles, it is most meaningful for the s orbitals whose amplitudes are independent of the angular coordinates. However, to arrive at a uniform definition for all orbitals, a new function, the **radial distribution function**, $P_{nl}(r)$, is defined.

$$P_{nl}(r) dr = \left[\int_0^{2\pi} d\phi \int_0^\pi \left(Y_l^{m_l}(\theta, \phi) \right)^* \left(Y_l^{m_l}(\theta, \phi) \right) \sin \theta d\theta \right] r^2 R_{nl}^2(r) dr = r^2 R_{nl}^2(r) dr \quad (9.13)$$

The quantity in square brackets has the value one because the spherical harmonic functions are normalized. The radial distribution function is the probability function of choice to determine the most likely radius to find the electron for a given orbital. Understanding the difference between the radial distribution function $P_{nl}(r) dr$ and the probability density $\psi_{nlm_l}^*(r) \psi_{nlm_l}(r) r^2 \sin \theta dr d\theta d\phi$ is very important in working with the hydrogen atom wave functions. Example Problem 9.6 demonstrates a determination of the maxima in the radial distribution function.

EXAMPLE PROBLEM 9.6

Calculate the maxima in the radial probability distribution for the 2s orbital. What is the most probable distance from the nucleus for an electron in this orbital? Are there subsidiary maxima?

Solution

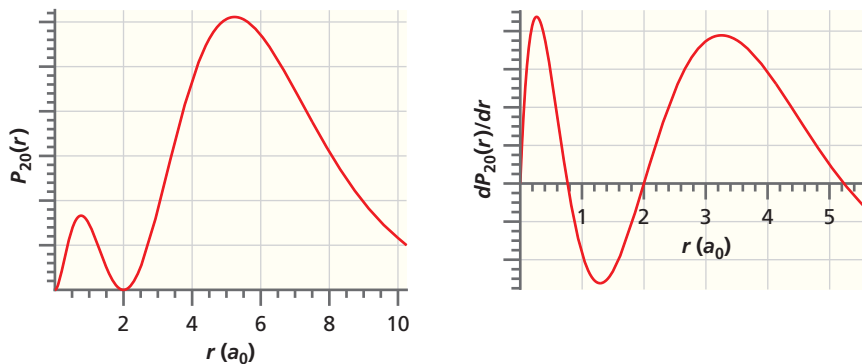
The radial distribution function is

$$P_{20}(r) = r^2 R_{20}^2(r) = \frac{1}{8} \left(\frac{1}{a_0}\right)^3 r^2 \left(2 - \frac{r}{a_0}\right)^2 e^{-r/a_0}$$

To find the maxima, we plot $P(r)$ and

$$\frac{dP_{20}(r)}{dr} = \frac{r}{8a_0^6} (8a_0^3 - 16a_0^2r + 8a_0r^2 - r^3)e^{-r/a_0}$$

versus r/a_0 and look for the nodes in this function. These functions are graphed as a function of r/a_0 in the following plots:



We see that the principal maximum in $P_{20}(r)$ is at $5.24 a_0$. This corresponds to the most probable distance of a $2s$ electron from the nucleus. The subsidiary maximum is at $0.76 a_0$. The minimum is at $2 a_0$ where $P(r)$ changes sign.

The resulting radial distribution function only depends on r , and not on θ and ϕ . Therefore, we can display $P_{nl}(r) dr$ versus r in a graph, as shown in Figure 9.10.

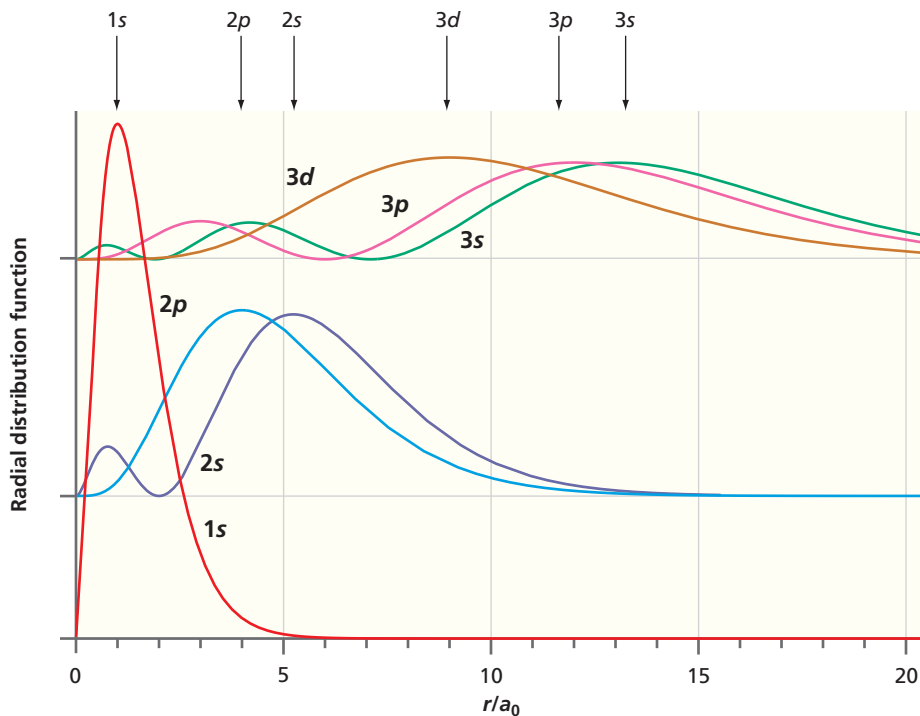


Figure 9.10

Plot of $r^2 R_{nl}^2(r)$ versus r/a_0 for the first few H atomic orbitals. The curves for $n = 2$ and $n = 3$ have been displaced vertically as indicated. The position of the principal maximum for each orbital is indicated by an arrow.

9.6 VALIDITY OF THE SHELL MODEL OF AN ATOM

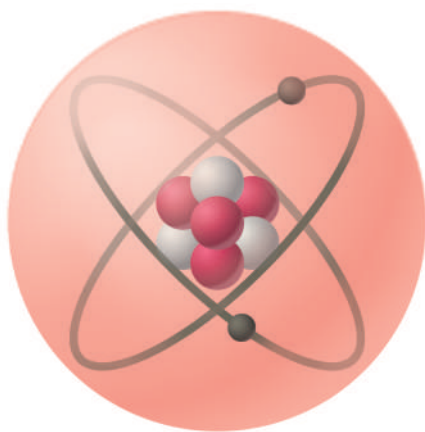


Figure 9.11

A shell model of an atom with electrons moving on spherical shells around the nucleus. Not to scale.

What can we conclude from Figure 9.10 regarding a shell model for the hydrogen atom? By now, we have become accustomed to the idea of wave–particle duality. Waves are not sharply localized, so a shell model like that shown in Figure 9.11 with electrons as point masses orbiting around the nucleus is not viable in quantum mechanics. If there are some remnants of a shell model in the hydrogen atom, it is that there is a greater likelihood of finding the electron at some distance from the nucleus than others.

The quantum-mechanical analogue of the shell model can be generated in the following way. Imagine that three-dimensional images of the shell model for hydrogen with the electron in the 1s, 2s, or 3s levels were obtained at a large number of random times. A section through the resulting images at the $z = 0$ plane would reveal sharply defined circles with a different radius for each orbital. The quantum-mechanical analogue of this process is depicted in Figure 9.12. The principal maxima seen in Figure 9.10 are the source of the darkest rings in each part of Figure 9.12. The rings are broad in comparison to the sharp circle of the classical model. The subsidiary maxima seen in Figure 9.10 appear as less intense rings for the 2s and 3s orbitals.

The radial distribution function gives results that are more in keeping with our intuition and with a shell model than what we saw in the plots for the probability density $\psi^*(r, \theta, \phi)\psi(r, \theta, \phi)$. For the 1s orbital, the radial distribution function is peaked at a value of a_0 . However, the peak has a considerable width, whereas a shell model would give a sharp peak of nearly zero width. This contradiction is reminiscent of our discussion of the double-slit diffraction experiment. Because wave–particle duality is well established, it is not correct to formulate models that are purely particle-like or purely wave-like. The broadening of the orbital shell over what we would expect in a particle picture is a direct manifestation of the wave nature of the electron, and the existence of an orbit is what we would expect in a particle picture. Both aspects of wave–particle duality are evident.

Let us summarize the main features that appear in Figures 9.10 and 9.12 for the radial probability distribution. We see broad maxima that move to greater values of r as n increases. This means that the electron is on average farther away from the nucleus for large n . From Equation (9.8), as n increases, the electron is less strongly bound. Both of these results are consistent with that expected from the Coulomb potential.

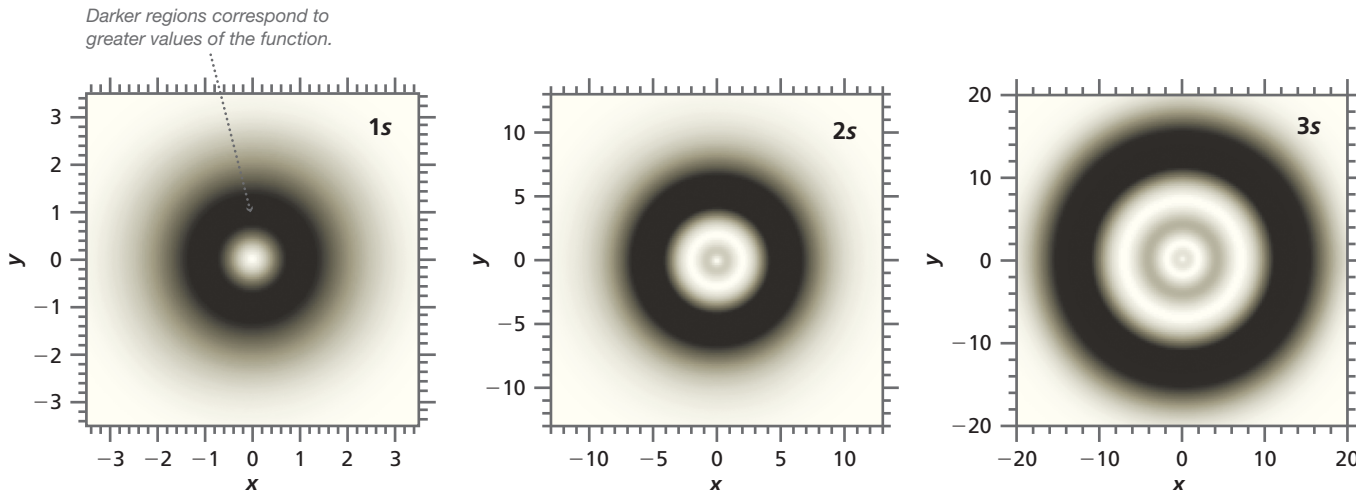


Figure 9.12

The radial probability distribution evaluated for $z = 0$ for the 1s, 2s, and 3s orbitals. The view is in the $x - y$ plane and lengths are in units of a_0 . Darker regions correspond to greater values of the function. The sharp circle in a classical shell model becomes a broad ring in a quantum-mechanical model over which the probability of finding the electron varies. Less intense subsidiary rings are also observed for the 2s and 3s orbitals.

However, we also see nodes and subsidiary maxima in the radial distribution function. How can these features be explained? Nodes are always present in standing waves, and eigenfunctions of the time-independent Schrödinger equation are standing waves. The nodes are directly analogous to the nodes observed for the particle in the box wave functions and are a manifestation of wave–particle duality. The subsidiary maxima are another manifestation of the wave character of the electron and occur whenever wave interference occurs. Recall that such subsidiary maxima are also observed in diffraction experiments. It is tempting to assign orbital radii to the H atomic orbitals with values corresponding to the positions of the principal maxima. The maxima are indicated by arrows in Figure 9.10. However, this amounts to reducing a function to a single number and is unwise.

VOCABULARY

Bohr radius	effective potential	radial distribution function	shell model
centrifugal potential	nodal surface	Rydberg constant for hydrogen	virial theorem
Coulomb potential	orbital		

KEY EQUATIONS

Equation	Significance of Equation	Equation Number
$V(\mathbf{r}) = -\frac{e^2}{4\pi\epsilon_0 \mathbf{r} } = -\frac{e^2}{4\pi\epsilon_0 r}$	Potential energy function for H atom	9.1
$-\frac{\hbar^2}{2m_e} \left[\frac{1}{r^2} \frac{\partial}{\partial r} \left(r^2 \frac{\partial \psi(r, \theta, \phi)}{\partial r} \right) + \frac{1}{r^2 \sin \theta} \frac{\partial}{\partial \theta} \left(\sin \theta \frac{\partial \psi(r, \theta, \phi)}{\partial \theta} \right) + \frac{1}{r^2 \sin^2 \theta} \frac{\partial^2 \psi(r, \theta, \phi)}{\partial \phi^2} \right] - \frac{e^2}{4\pi\epsilon_0 r} \psi(r, \theta, \phi) = E\psi(r, \theta, \phi)$	Schrödinger equation for H atom in spherical coordinates	9.2
$-\frac{\hbar^2}{2m_e r^2} \frac{d}{dr} \left[r^2 \frac{dR(r)}{dr} \right] + \left[\frac{\hbar^2 l(l+1)}{2m_e r^2} - \frac{e^2}{4\pi\epsilon_0 r} \right] R(r) = ER(r)$	Radial equation for H atom	9.5
$V_{eff}(r) = \frac{\hbar^2 l(l+1)}{2m_e r^2} - \frac{e^2}{4\pi\epsilon_0 r}$	Effective potential for H atom	9.6
$E_n = -\frac{e^2}{8\pi\epsilon_0 a_0 n^2} = -\frac{2.179 \times 10^{-18} \text{ J}}{n^2} = -\frac{13.60 \text{ eV}}{n^2} \quad n = 1, 2, 3, 4, \dots$	Energy eigenvalues for H atom	9.8
$n = 1, 2, 3, 4, \dots$ $l = 0, 1, 2, 3, \dots, n-1$ $m_l = 0, \pm 1, \pm 2, \pm 3, \dots, \pm l$	Relations among quantum numbers for H atom	9.9
$\nu = \left \frac{\mu e^4}{8\epsilon_0^2 h^3} \left(\frac{1}{n_{initial}^2} - \frac{1}{n_{final}^2} \right) \right $	Frequencies of allowed transitions in H atom absorption and emission spectrum	9.11
$P_{nl}(r) dr = r^2 R_{nl}^2(r) dr$	Definition of radial distribution function	9.13

CONCEPTUAL PROBLEMS

Q9.1 What possible geometrical forms can the nodes in the angular function for p and d orbitals in the H atom have? What possible geometrical forms can the nodes in the radial function for s , p , and d orbitals in the H atom have?

Q9.2 Which transition gives rise to the highest frequency spectral line in the Lyman series?

Q9.3 Is it always true that the probability of finding the electron in the H atom is greater in the interval $r - dr < r < r + dr$ than in the interval

$$r - dr < r < r + dr \quad \theta - d\theta < \theta < \theta + d\theta \\ \phi - d\phi < \phi < \phi + d\phi?$$

Q9.4 Why are the total energy eigenfunctions for the H atom not eigenfunctions of the kinetic energy?

Q9.5 How do the results shown in Figure 9.10 differ from the predictions of the Bohr model of the H atom?

Q9.6 What effect does the centripetal potential have in determining the maximum in the radial function for the $3s$, $3p$, and $3d$ orbitals?

Q9.7 How does the effective potential differ for p and d electrons?

Q9.8 Why does the centripetal potential dominate the effective potential for small values of r ?

Q9.9 If the probability density of finding the electron in the $1s$ orbital in the H atom has its maximum value for $r = 0$, does this mean that the proton and electron are located at the same point in space?

Q9.10 Explain the different degree to which the $1s$, $2s$, and $3s$ total energy eigenfunctions penetrate into the classically forbidden region.

Q9.11 What are the units of the H atom total energy eigenfunctions? Why is $a_0^{3/2}R(r)$ graphed in Figure 9.6 rather than $R(r)$?

Q9.12 Why is the radial probability function rather than $\psi^*(r)\psi(r)r^2 \sin\theta dr d\theta d\phi$ the best measure of the probability of finding the electron at a distance r from the nucleus?

Q9.13 Use an analogy with the particle in the box to explain why the energy levels for the H atom are more closely spaced as n increases.

Q9.14 Explain why the radial distribution function rather than the square of the magnitude of the wave function should be used to make a comparison with the shell model of the atom.

Q9.15 What is the difference between an angular and a radial node? How can you distinguish the two types of nodes in a contour diagram such as Figure 9.7?

Q9.16 What is the minimum photon energy needed to ionize a hydrogen atom in the ground state?

Q9.17 To which physical state does a hydrogen atom energy of $+1 \times 10^{-19}$ J correspond?

Q9.18 Why does the centrifugal potential force the $3d$ electrons further from the nucleus than the $3s$ electrons?

Q9.19 Why is the radial probability density rather than the probability density used to calculate the most probable distance of the electron from the nucleus?

NUMERICAL PROBLEMS

Section 9.3

P9.1 Calculate the wave number corresponding to the most and least energetic spectral lines in the Lyman, Balmer, and Paschen series for the hydrogen atom.

P9.2 Show that the function $(r/a_0)e^{-r/2a_0}$ is a solution of the differential equation for $R(r)$

$$-\frac{\hbar^2}{2m_e r^2} \frac{d}{dr} \left[r^2 \frac{dR(r)}{dr} \right] + \left[\frac{\hbar^2 l(l+1)}{2\mu r^2} - \frac{e^2}{4\pi\epsilon_0 r} \right] R(r) = ER(r) \text{ for } l = 1$$

What is the eigenvalue? Using this result, what is the value for the principal quantum number n for this function?

P9.3 Calculate the expectation value for the kinetic energy of the H atom with the electron in the $2s$ orbital. Compare your result with the total energy.

P9.4 Ions with a single electron such as He^+ , Li^{2+} , and Be^{3+} are described by the H atom wave functions with Z/a_0 substituted for $1/a_0$, where Z is the nuclear charge. The $1s$ wave function becomes $\psi(r) = 1/\sqrt{\pi(Z/a_0)^{3/2}} e^{-Zr/a_0}$.

Using this result, calculate the total energy for the $1s$ state in H , He^+ , Li^{2+} , and Be^{3+} by substitution in the Schrödinger equation.

P9.5 In this problem, you will calculate the probability of finding an electron within a sphere of radius r for the H atom in its ground state. Use the tabulated integral

$$\int r^2 e^{-ar} dr = -\frac{e^{-ar}}{a^3} (a^2 x^2 + 2ax + 2) \text{ in solving this problem.}$$

- Show that the probability density of finding the electron within a sphere of radius r for the hydrogen atom in its ground state is

$$1 - e^{-2r/a_0} - \frac{2r}{a_0} \left(1 + \frac{r}{a_0} \right) e^{-2r/a_0}$$

- Evaluate this probability density for $r = 0.250 a_0$, $r = 2.25 a_0$, and $r = 5.50 a_0$.

P9.6 In spherical coordinates, $z = r \cos\theta$. Calculate $\langle z \rangle$ and $\langle z^2 \rangle$ for the H atom in its ground state. Without doing the calculation, what would you expect for $\langle x \rangle$ and $\langle y \rangle$, and $\langle x^2 \rangle$ and $\langle y^2 \rangle$? Why?

P9.7 The force acting between the electron and the proton in the H atom is given by $F = -e^2/4\pi\epsilon_0 r^2$. Calculate the expectation value $\langle F \rangle$ for the $1s$ and $2p_z$ states of the H atom in terms of e , ϵ_0 , and a_0 .

P9.8 The d orbitals have the nomenclature d_{z^2} , d_{xy} , d_{xz} , d_{yz} , and $d_{x^2-y^2}$. Show how the d orbital

$$\psi_{3d_{yz}}(r, \theta, \phi) = \frac{\sqrt{2}}{81\sqrt{\pi}} \left(\frac{1}{a_0}\right)^{3/2} \frac{r^2}{a_0^2} e^{-r/3a_0} \sin\theta \cos\theta \sin\phi$$

can be written in the form $yzF(r)$.

P9.9 Calculate the expectation value of the moment of inertia of the H atom in the $2s$ and $2p_z$ states in terms of μ and a_0 .

P9.10 The energy levels for ions with a single electron such as He^+ , Li^{2+} , and Be^{3+} are given by $E_n = -Z^2 e^2 / 8\pi\epsilon_0 a_0 n^2$, $n = 1, 2, 3, 4, \dots$. Calculate the ionization energies of H, He^+ , Li^{2+} , and Be^{3+} in their ground states in units of joules.

P9.11 The total energy eigenvalues for the hydrogen atom are given by $E_n = -e^2 / 8\pi\epsilon_0 a_0 n^2$, $n = 1, 2, 3, 4, \dots$, and the three quantum numbers associated with the total energy eigenfunctions are related by $n = 1, 2, 3, 4, \dots$; $l = 0, 1, 2, 3, \dots, n-1$; and $m_l = 0, \pm 1, \pm 2, \pm 3, \dots, \pm l$. Using the nomenclature ψ_{nlm_l} , list all eigenfunctions that have the following total energy eigenvalues:

a. $E = -\frac{e^2}{32\pi\epsilon_0 a_0}$

b. $E = -\frac{e^2}{72\pi\epsilon_0 a_0}$

c. $E = -\frac{e^2}{128\pi\epsilon_0 a_0}$

d. What is the degeneracy of each of these energy levels?

P9.12 Locate the radial and angular nodes in the H orbitals $\psi_{3p_x}(r, \theta, \phi)$ and $\psi_{3p_z}(r, \theta, \phi)$.

P9.13 Calculate the average value of the kinetic and potential energies for the H atom in its ground state.

P9.14 Show by substitution that $\psi_{100}(r, \theta, \phi) = 1/\sqrt{\pi(1/a_0)^{3/2}} e^{-r/a_0}$ is a solution of

$$\begin{aligned} & -\frac{\hbar^2}{2me} \left[\frac{1}{r^2} \frac{\partial}{\partial r} \left(r^2 \frac{\partial \psi(r, \theta, \phi)}{\partial r} \right) + \frac{1}{r^2 \sin\theta} \frac{\partial}{\partial \theta} \left(\sin\theta \frac{\partial \psi(r, \theta, \phi)}{\partial \theta} \right) \right. \\ & \quad \left. + \frac{1}{r^2 \sin\theta} \frac{\partial^2 \psi(r, \theta, \phi)}{\partial \phi^2} \right] \\ & -\frac{e^2}{4\pi\epsilon_0 r} \psi(r, \theta, \phi) = E\psi(r, \theta, \phi) \end{aligned}$$

What is the eigenvalue for total energy? Use the relation $a_0 = \epsilon_0 h^2 / (\pi m_e e^2)$.

P9.15 Show that the total energy eigenfunctions $\psi_{100}(r)$ and $\psi_{200}(r)$ are orthogonal.

P9.16 As will be discussed in Chapter 10, core electrons shield valence electrons so that they experience an effective nuclear charge Z_{eff} rather than the full nuclear charge. Given that the first ionization energy of Be is 9.32 eV, use the formula in Problem P9.10 to estimate the effective nuclear charge experienced by the $2s$ electron in Be.

P9.17 Is the total energy wave function

$$\psi_{310}(r, \theta, \phi) = \frac{1}{81} \left(\frac{2}{\pi}\right)^{1/2} \left(\frac{1}{a_0}\right)^{3/2} \left(6 \frac{r}{a_0} - \frac{r^2}{a_0^2}\right) e^{-r/3a_0} \cos\theta$$

an eigenfunction of any other operators? If so, which ones? What are the eigenvalues?

P9.18 Show that the total energy eigenfunctions $\psi_{210}(r, \theta, \phi)$ and $\psi_{211}(r, \theta, \phi)$ are orthogonal. Do you have to integrate over all three variables to show that the functions are orthogonal?

P9.19 How many radial and angular nodes are there in the following H orbitals?

a. $\psi_{2p_x}(r, \theta, \phi)$

b. $\psi_{2s}(r)$

c. $\psi_{3d_{xz}}(r, \theta, \phi)$

d. $\psi_{3d_{x^2-y^2}}(r, \theta, \phi)$

P9.20 Show that $\psi_{2p_x}(r, \theta, \phi)$ and $\psi_{2p_y}(r, \theta, \phi)$ can be written in the form $Nxe^{-r/2a_0}$ and $N'ye^{-r/2a_0}$ where N and N' are normalization constants.

P9.21 Calculate the expectation value for the potential energy of the H atom with the electron in the $1s$ orbital. Compare your result with the total energy.

P9.22 Determine the probability of finding the electron in the region for which the ψ_{320} wavefunction is negative (the toroidal region).

Section 9.5

P9.23 Calculate the probability that the $1s$ electron for H will be found between $r = 0$ and $r = a_0$.

P9.24 Calculate the distance from the nucleus for which the radial distribution function for the $2p$ orbital has its main and subsidiary maxima.

P9.25 Calculate the mean value of the radius $\langle r \rangle$ at which you would find the electron if the H atom wave function is $\psi_{100}(r)$.

P9.26 Ions with a single electron such as He^+ , Li^{2+} , and Be^{3+} are described by the H atom wave functions with Z/a_0 substituted for $1/a_0$, where Z is the nuclear charge. The $1s$ wave function becomes $\psi(r) = 1/\sqrt{\pi(Z/a_0)^{3/2}} e^{-Zr/a_0}$. Using this result, compare the mean value of the radius $\langle r \rangle$ at which you would find the $1s$ electron in H, He^+ , Li^{2+} , and Be^{3+} .

P9.27 As the principal quantum number n increases, the electron is more likely to be found far from the nucleus. It can be shown that for H and for ions with only one electron such as H or He^+ ,

$$\langle r \rangle_{nl} = \frac{n^2 a_0}{Z} \left[1 + \frac{1}{2} \left(1 - \frac{l(l+1)}{n^2} \right) \right]$$

where Z is the nuclear charge. Calculate the value of n for an s state in the hydrogen atom such that $\langle r \rangle = 275 a_0$. Round up to the nearest integer. What is the ionization energy of the H atom in this state in electron-volts? Compare your answer with the ionization energy of the H atom in the ground state.

P9.28 The radius of an atom r_{atom} can be defined as that value for which 90% of the electron charge is contained within a sphere of radius r_{atom} . Use the formula in P9.5 to calculate the radius of the H atom.

P9.29 Use the result of P9.28 to

- calculate the mass density of the H atom.
- Compare your answer with the nuclear density assuming a nuclear radius of 1.0×10^{-15} m.
- Calculate the mass density of the H atom outside of the nucleus.

P9.30 Calculate the expectation value $(r - \langle r \rangle)^2$ if the H atom wave function is $\psi_{100}(r)$.

P9.31 Calculate the mean value of the radius $\langle r \rangle$ at which you would find the electron if the H atom wave function is $\psi_{210}(r, \theta, \phi)$.

P9.32 Calculate $\langle r \rangle$ and the most probable value of r for the H atom in its ground state. Explain why they differ with a drawing.

P9.33 Using the result of Problem P9.5, calculate the probability of finding the electron in the $1s$ state outside a sphere of radius $0.50 a_0$, $3.0 a_0$, and $5.0 a_0$.

FURTHER READING

Ball, D. "Do the Series in the Hydrogen Atom Spectrum Ever Overlap?" *Journal of Chemical Education* 83 (2006): 883–884.

Blaise, P., Henri-Rousseau, O., and Merad, N. "Some Further Comments about the Stability of the Hydrogen Atom." *Journal of Chemical Education* 61 (1984): 957–960.

Clark, T., and Chamberlain, J. "Use of a PhET Interactive Simulation in General Chemistry Laboratory: Models of the Hydrogen Atom." *Journal of Chemical Education* 91 (2014): 1198–1202.

Levine, I. N. *Quantum Chemistry*, 7th edition. Boston: Pearson, 2014.

Mak, T., and Li, W.-K. "Probability of Locating the Electron in a Hydrogen Atom." *Journal of Chemical Education* 77 (2000): 490–491.

MATH ESSENTIAL 9:

Working with Determinants

In Chapter 10, it will be shown that wave functions that describe many-electron systems must change sign under the exchange of any two electrons. The simplest way to ensure that this is the case is to express many-electron wave functions in the form of a determinant. In this Math Essential, we discuss how to work with determinants. A determinant of n th order is a square, $n \times n$ array of numbers symbolically enclosed by vertical lines. A 5th-order determinant is shown below with the conventional indexing of the elements of the array with respect to the row (first index) and column (second index) in which they appear.

$$\begin{vmatrix} a_{11} & a_{12} & a_{13} & a_{14} & a_{15} \\ a_{21} & a_{22} & a_{23} & a_{24} & a_{25} \\ a_{31} & a_{32} & a_{33} & a_{34} & a_{35} \\ a_{41} & a_{42} & a_{43} & a_{44} & a_{45} \\ a_{51} & a_{52} & a_{53} & a_{54} & a_{55} \end{vmatrix} \quad (\text{ME9.1})$$

A 2×2 determinant has a value that is defined in Equation (ME9.2). It is obtained by multiplying the elements in the diagonal connected by a line with a negative slope and subtracting from this product the product of the elements in the diagonal connected by a line with a positive slope.

$$\begin{vmatrix} a_{11} & a_{12} \\ a_{21} & a_{22} \end{vmatrix} = a_{11}a_{22} - a_{12}a_{21} \quad (\text{ME9.2})$$

The value of a higher-order determinant is obtained by expanding the determinant in terms of determinants of lower order. This is done using the method of cofactors. We illustrate the use of the method of cofactors by reducing a 3×3 determinant to a sum of 2×2 determinants. Any row or column can be used in the reduction process. We use the first row of the determinant in this reduction. The recipe is spelled out in the following equation.

$$\begin{aligned} \begin{vmatrix} a_{11} & a_{12} & a_{13} \\ a_{21} & a_{22} & a_{23} \\ a_{31} & a_{32} & a_{33} \end{vmatrix} &= (-1)^{1+1} a_{11} \begin{vmatrix} a_{22} & a_{23} \\ a_{32} & a_{33} \end{vmatrix} + (-1)^{1+2} a_{12} \begin{vmatrix} a_{21} & a_{23} \\ a_{31} & a_{33} \end{vmatrix} \\ &\quad + (-1)^{1+3} a_{13} \begin{vmatrix} a_{21} & a_{22} \\ a_{31} & a_{32} \end{vmatrix} \\ &= a_{11} \begin{vmatrix} a_{22} & a_{23} \\ a_{32} & a_{33} \end{vmatrix} - a_{12} \begin{vmatrix} a_{21} & a_{23} \\ a_{31} & a_{33} \end{vmatrix} + a_{13} \begin{vmatrix} a_{21} & a_{22} \\ a_{31} & a_{32} \end{vmatrix} \quad (\text{ME9.3}) \end{aligned}$$

Each term in the sum results from the product of one of the three elements of the first row, $(-1)^{m+n}$, where m and n are the indices of the row and column designating the element, and the 2×2 determinant obtained by omitting the entire row and column to which the element used in the reduction belongs. The product $(-1)^{m+n}$ and the 2×2 determinant are called the cofactor of the element used in the reduction.

To illustrate this process, consider the following 3×3 determinant. We will use the cofactors of the second row. The value of the determinant is obtained as follows:

$$\begin{aligned} \begin{vmatrix} 1 & 3 & 4 \\ 2 & -1 & 6 \\ -1 & 7 & 5 \end{vmatrix} &= (-1)^{2+1} 2 \begin{vmatrix} 3 & 4 \\ 7 & 5 \end{vmatrix} + (-1)^{2+2} (-1) \begin{vmatrix} 1 & 4 \\ -1 & 5 \end{vmatrix} + (-1)^{2+3} 6 \begin{vmatrix} 1 & 3 \\ -1 & 7 \end{vmatrix} \\ &= -1 \times 2 \times (-13) + 1 \times (-1) \times 9 + (-1) \times 6 \times 10 = -43 \end{aligned} \quad (\text{ME9.4})$$

If the initial determinant is of higher order than 3, multiple sequential reductions as outlined earlier will reduce it in order by one in each step until a sum of 2×2 determinants is obtained, each of which can be easily evaluated.

One main use for determinants is in solving a system of linear equations. Such a system of equations is obtained in evaluating the energies of a set of molecular orbitals obtained by combining a set of atomic orbitals in Chapter 11. Before illustrating this method, we list some important properties of determinants. These properties are used to compare localized and delocalized bonding models in Chapter 13.

Property I: The value of a determinant is not altered if each row in turn is made into a column or vice versa as long as the original order is kept. By this we mean that the n^{th} row becomes the n^{th} column. We illustrate this property using 2×2 and 3×3 determinants.

$$\begin{vmatrix} 2 & 1 \\ 3 & -1 \end{vmatrix} = \begin{vmatrix} 2 & 3 \\ 1 & -1 \end{vmatrix} = -5 \quad \text{and} \quad \begin{vmatrix} 1 & 3 & 4 \\ 2 & -1 & 6 \\ -1 & 7 & 5 \end{vmatrix} = \begin{vmatrix} 1 & 2 & -1 \\ 3 & -1 & 7 \\ 4 & 6 & 5 \end{vmatrix} = -43 \quad (\text{ME9.5})$$

Property II: If any two rows or columns are interchanged, the sign of the value of the determinant is changed. For example,

$$\begin{aligned} \begin{vmatrix} 2 & 1 \\ 3 & -1 \end{vmatrix} &= -5, \quad \text{but} \quad \begin{vmatrix} 1 & 2 \\ -1 & 3 \end{vmatrix} = +5 \quad \text{and} \quad \begin{vmatrix} 1 & 3 & 4 \\ 2 & -1 & 6 \\ -1 & 7 & 5 \end{vmatrix} = -43, \\ \text{but} \quad \begin{vmatrix} 2 & -1 & 6 \\ 1 & 3 & 4 \\ -1 & 7 & 5 \end{vmatrix} &= +43 \end{aligned} \quad (\text{ME9.6})$$

Property III: If two rows or columns of a determinant are identical, the value of the determinant is zero. For example,

$$\begin{aligned} \begin{vmatrix} 2 & 1 \\ 2 & 1 \end{vmatrix} &= 2 - 2 = 0 \quad \text{and} \quad \begin{vmatrix} 1 & 1 & 4 \\ 2 & 2 & 6 \\ -1 & -1 & 5 \end{vmatrix} = (-1)^{2+1} 2 \begin{vmatrix} 1 & 4 \\ -1 & 5 \end{vmatrix} \\ &\quad + (-1)^{2+2} 2 \begin{vmatrix} 1 & 4 \\ -1 & 5 \end{vmatrix} + (-1)^{2+3} 6 \begin{vmatrix} 1 & 1 \\ -1 & -1 \end{vmatrix} \\ &= -1 \times 2 \times 9 + 1 \times 2 \times 9 + (-1) \times 6 \times 0 = 0 \end{aligned} \quad (\text{ME9.7})$$

Property IV: If each element of a row or column is multiplied by a constant, the value of the determinant is multiplied by that constant. For example,

$$\begin{aligned} \begin{vmatrix} 2 & 1 \\ 3 & -1 \end{vmatrix} &= -5 \quad \text{and} \quad \begin{vmatrix} 8 & 4 \\ 3 & -1 \end{vmatrix} = -20 \quad \text{and} \quad \begin{vmatrix} 1 & 2 & -1 \\ 3 & -1 & 7 \\ 4 & 6 & 5 \end{vmatrix} = -43 \\ \text{and} \quad \begin{vmatrix} 1 & 3\sqrt{2} & 4 \\ 2 & -\sqrt{2} & 6 \\ -1 & 7\sqrt{2} & 5 \end{vmatrix} &= -43\sqrt{2} \end{aligned} \quad (\text{ME9.8})$$

Property V: The value of a determinant is unchanged if two rows or columns are added to change the array of numbers in a given row or column. For example,

$$\begin{aligned} \begin{vmatrix} 2+1 & 1 \\ 3-1 & -1 \end{vmatrix} &= \begin{vmatrix} 2 & 1 \\ 3 & -1 \end{vmatrix} = -5 \quad \text{and} \quad \begin{vmatrix} 1 & 3 & 4 \\ 2-1 & -1+7 & 6+5 \\ -1 & 7 & 5 \end{vmatrix} \\ &= \begin{vmatrix} 1 & 3 & 4 \\ 2 & -1 & 6 \\ -1 & 7 & 5 \end{vmatrix} = -43 \end{aligned} \tag{ME9.10}$$

Now that the properties of determinants have been discussed, we can turn to the question of how determinants are useful in solving problems in physical chemistry. We answer this question by illustrating how determinants can be used to solve a set of linear equations. Consider the following three linear equations:

$$\begin{aligned} x + y + z &= 10 \\ 3x + 4y - z &= 12 \\ -x + 2y + 5z &= 26 \end{aligned} \tag{ME9.11}$$

One solves this set of equations by first constructing the 3×3 determinant that is the array of the coefficients of x , y , and z .

$$D_{\text{coefficients}} = \begin{vmatrix} 1 & 1 & 1 \\ 3 & 4 & -1 \\ -1 & 2 & 5 \end{vmatrix} \tag{ME9.12}$$

Now imagine that we multiply the first column by x . This changes the value of the determinant as stated in Property IV.

$$\begin{vmatrix} 1x & 1 & 1 \\ 3x & 4 & -1 \\ -1x & 2 & 5 \end{vmatrix} = xD_{\text{coefficients}} \tag{ME9.13}$$

We next add to $xD_{\text{coefficients}}$ the second column of $D_{\text{coefficients}}$ multiplied by y , and the third column multiplied by z . According to the properties IV and V, the value of the determinant is unchanged. Therefore

$$\begin{aligned} D_{c1} &= \begin{vmatrix} 1 & 1 & 1 \\ 3 & 4 & -1 \\ -1 & 2 & 5 \end{vmatrix} = \begin{vmatrix} x+y+z & 1 & 1 \\ 3x+4y-z & 4 & -1 \\ -x+2y+5z & 2 & 5 \end{vmatrix} \\ &= \begin{vmatrix} 10 & 1 & 1 \\ 12 & 4 & -1 \\ 26 & 2 & 5 \end{vmatrix} = xD_{\text{coefficients}} \end{aligned} \tag{ME9.14}$$

To obtain the third determinant in the previous equation, we have used the individual equations in Equation (ME9.11) to substitute the constants for the algebraic expression in the preceding determinants.

From the previous equation, we conclude that

$$x = \frac{D_{c1}}{D_{\text{coefficients}}} = \frac{\begin{vmatrix} 10 & 1 & 1 \\ 12 & 4 & -1 \\ 26 & 2 & 5 \end{vmatrix}}{\begin{vmatrix} 1 & 1 & 1 \\ 3 & 4 & -1 \\ -1 & 2 & 5 \end{vmatrix}} = 3 \tag{ME9.15}$$

We can follow exactly the same procedure, but substituting instead in columns two and three. The first step in each case is to multiply all elements of the second row by y (or the third row by z). If we do so, we obtain the determinants D_{c2} and D_{c3} .

$$D_{c2} = \begin{vmatrix} 1 & 10 & 1 \\ 3 & 12 & -1 \\ -1 & 26 & 5 \end{vmatrix} \quad \text{and} \quad D_{c3} = \begin{vmatrix} 1 & 1 & 10 \\ 3 & 4 & 12 \\ -1 & 2 & 26 \end{vmatrix} \quad (\text{ME9.16})$$

and we conclude that

$$\begin{aligned} y &= \frac{D_{c2}}{D_{\text{coefficients}}} = \frac{\begin{vmatrix} 1 & 10 & 1 \\ 3 & 12 & -1 \\ -1 & 26 & 5 \end{vmatrix}}{\begin{vmatrix} 1 & 1 & 1 \\ 3 & 4 & -1 \\ -1 & 2 & 5 \end{vmatrix}} = 2 \quad \text{and} \quad z = \frac{D_{c3}}{D_{\text{coefficients}}} \\ &= \frac{\begin{vmatrix} 1 & 1 & 10 \\ 3 & 4 & 12 \\ -1 & 2 & 26 \end{vmatrix}}{\begin{vmatrix} 1 & 1 & 1 \\ 3 & 4 & -1 \\ -1 & 2 & 5 \end{vmatrix}} = 5 \end{aligned} \quad (\text{ME9.17})$$

This method of solving a set of simultaneous linear equations is known as Cramer's method.

If the constants in the set of equations are all zero, as in the following set,

$$\begin{aligned} x + y - z &= 0 \\ 3x - 3y + z &= 0 \\ 4x + y - 2z &= 0 \end{aligned} \quad (\text{ME9.18})$$

which can be written as the matrix equation

$$\begin{pmatrix} 1 & 1 & -1 \\ 3 & -3 & 1 \\ 4 & 1 & -2 \end{pmatrix} \begin{pmatrix} x \\ y \\ z \end{pmatrix} = \begin{pmatrix} 0 \\ 0 \\ 0 \end{pmatrix} \quad (\text{ME9.19})$$

the determinants D_{c1} , D_{c2} , and D_{c3} all have the value zero. An obvious set of solutions is $x = 0$, $y = 0$, and $z = 0$. This set of solutions is not physically meaningful and is referred to as the set of trivial solutions. In order for there to be a set of nontrivial solutions, the equation $D_{\text{coefficients}} = 0$ must be satisfied where $D_{\text{coefficients}}$ is the determinant of the 3×3 matrix in Equation (9.19). The equation $D_{\text{coefficients}} = 0$ is used in the Hückel approximation to determine MO energy levels for delocalized π electrons in Chapter 13.

Determinants also offer a convenient way to calculate the cross product of two vectors, as was discussed in Chapter 7. The cross product $\mathbf{a} \times \mathbf{b}$ is evaluated by expanding the 3×3 determinant shown in Equation (ME9.20)

$$\begin{aligned} \mathbf{a} \times \mathbf{b} &= \begin{vmatrix} \mathbf{i} & \mathbf{j} & \mathbf{k} \\ a_x & a_y & a_z \\ b_x & b_y & b_z \end{vmatrix} = \mathbf{i} \begin{vmatrix} a_y & a_z \\ b_y & b_z \end{vmatrix} - \mathbf{j} \begin{vmatrix} a_x & a_z \\ b_x & b_z \end{vmatrix} + \mathbf{k} \begin{vmatrix} a_x & a_y \\ b_x & b_y \end{vmatrix} \\ &= (a_y b_z - a_z b_y) \mathbf{i} + (a_z b_x - a_x b_z) \mathbf{j} + (a_x b_y - a_y b_x) \mathbf{k} \end{aligned} \quad (\text{ME9.20})$$

Note that by referring to Property II, you can show that $\mathbf{b} \times \mathbf{a} = -\mathbf{a} \times \mathbf{b}$.

Many-Electron Atoms

WHY is this material important?

In this chapter, we focus on many-electron atoms. The Schrödinger equation cannot be solved analytically for atoms containing more than one electron because of the electron–electron repulsion term in the potential energy component of the Schrödinger equation. Instead, approximate numerical methods must be used to obtain the eigenfunctions and eigenvalues of the Schrödinger equation for many-electron atoms. Trends found in the periodic table on observables such as atomic radius, ionization energy, and electronegativity emerge naturally from numerical solutions of the Schrödinger equation.

WHAT are the most important concepts and results?

Electron indistinguishability, electron spin, and orbital angular momentum must all be taken into account in assigning electrons to many-electron energy levels. The ability of electrons to shield one another from the nuclear charge has a major influence on energy levels and atomic radii.

WHAT would be helpful for you to review for this chapter?

It would be helpful to review the material in Chapters 2 and 6 on expanding functions in a series of alternate functions.

10.1 HELIUM: THE SMALLEST MANY-ELECTRON ATOM

The Schrödinger equation for the hydrogen atom can be solved analytically to give a solution in functional form because this atom has only one electron. The complexity of solving the Schrödinger equation for systems that have more than one electron can be illustrated using the He atom. Centering the coordinate system at the nucleus, we find that the Schrödinger equation takes the form

$$\left(-\frac{\hbar^2}{2m_e} \nabla_{e1}^2 - \frac{\hbar^2}{2m_e} \nabla_{e2}^2 - \frac{2e^2}{4\pi\epsilon_0 r_1} - \frac{2e^2}{4\pi\epsilon_0 r_2} + \frac{2e^2}{4\pi\epsilon_0 r_{12}} \right) \psi(\mathbf{r}_1, \mathbf{r}_2) = E\psi(\mathbf{r}_1, \mathbf{r}_2) \quad (10.1)$$

In this equation, $r_1 = |\mathbf{r}_1|$ and $r_2 = |\mathbf{r}_2|$ are the distances of electrons 1 and 2 from the nucleus, $r_{12} = |\mathbf{r}_1 - \mathbf{r}_2|$, and ∇_{e1}^2 is shorthand for

$$\frac{1}{r_1^2} \frac{\partial}{\partial r_1} \left(r_1^2 \frac{\partial}{\partial r_1} \right) + \frac{1}{r_1^2 \sin^2 \theta_1} \frac{\partial}{\partial \phi_1^2} + \frac{1}{r_1^2 \sin \theta_1} \frac{\partial}{\partial \theta_1} \left(\sin \theta_1 \frac{\partial}{\partial \theta_1} \right)$$

The previous expression is the part of the operator that is associated with the kinetic energy of electron 1, expressed in spherical coordinates. The last three terms in Equation (10.1) are the potential energy operators for the electron–nucleus

10.1 Helium: The Smallest Many-Electron Atom

10.2 Introducing Electron Spin

10.3 Wave Functions Must Reflect the Indistinguishability of Electrons

10.4 Using the Variational Method to Solve the Schrödinger Equation

10.5 The Hartree–Fock Self-Consistent Field Model

10.6 Understanding Trends in the Periodic Table from Hartree–Fock Calculations

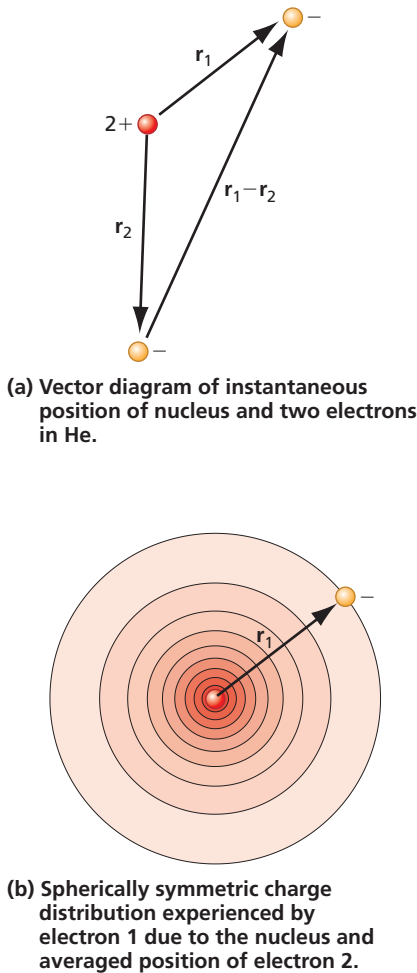


Figure 10.1

Electron-electron correlation in He.

(a) Instantaneous position of the nucleus and two electrons in He are shown. (b) If the position of electron 2 is averaged over its orbit, electron 1 experiences a spherically symmetric charge distribution.

Concept

If electron correlation is neglected, the angular part of the energy eigenfunctions for many-electron atoms is identical to that for the hydrogen atom.

attraction and the electron–electron repulsion. The variables $r_1 = |\mathbf{r}_1|$, $r_2 = |\mathbf{r}_2|$, and $r_{12} = |\mathbf{r}_1 - \mathbf{r}_2|$ are shown in Figure 10.1.

The eigenfunctions of the Schrödinger equation depend on the coordinates of both electrons. If this formalism is applied to argon, each many-electron eigenfunction depends simultaneously on the coordinates of 18 electrons! However, we also know that electrons in different atomic orbitals have quite different properties. For example, valence electrons are involved in chemical bonds, whereas core electrons are not. Therefore, it seems reasonable to express a many-electron eigenfunction in terms of individual electron orbitals, each of which depends only on the coordinates of one electron. This is called the **orbital approximation**, in which the many-electron eigenfunctions of the Schrödinger equation are expressed as a product of one-electron orbitals:

$$\psi(\mathbf{r}_1, \mathbf{r}_2, \dots, \mathbf{r}_n) = \phi_1(\mathbf{r}_1)\phi_2(\mathbf{r}_2) \dots \phi_n(\mathbf{r}_n) \quad (10.2)$$

This is not equivalent to saying that all of the electrons are independent of one another because, as we will see, the functional form for each $\phi_n(\mathbf{r}_n)$ is influenced by all the other electrons. The **one-electron orbitals** $\phi_n(\mathbf{r}_n)$ turn out to be quite similar to the functions $\psi_{nlm}(r, \theta, \phi)$ obtained for the hydrogen atom in Chapter 9, and they are labeled with indices such as $1s$, $2p$, and $3d$. Each of the $\phi_n(\mathbf{r}_n)$ is associated with a one-electron **orbital energy** ε_n .

The orbital approximation allows an n -electron Schrödinger equation to be written as n one-electron Schrödinger equations, one for each electron. However, a further problem arises in solving these n equations. Because of the form of the **electron–electron repulsion term**, $e^2/(4\pi\varepsilon_0 r_{12})$, the potential energy operator no longer has spherical symmetry, so that the potential no longer has the form $V = V(r)$. This is evident from Figure 10.1 because the vector $\mathbf{r}_1 - \mathbf{r}_2$ does not originate at the nucleus. Because of the electron–electron repulsion term, the Schrödinger equation cannot be solved analytically, and numerical methods must be used. For these methods to be effective, further approximations beyond the orbital approximation must be made. Perhaps the most serious of these approximations is that one cannot easily include what electrons do naturally in a many-electron atom, namely, stay out of each other's way by undergoing a correlated motion. Whereas **electron correlation** ensures that the repulsion among electrons is minimized, the numerical methods introduced in this chapter text to solve the Schrödinger equation assume that the electrons move independently of one another. As discussed in Chapter 15, corrections can be introduced in solving the Schrödinger equation and largely eliminate the errors generated through this assumption.

A schematic illustration of how neglect of electron correlation simplifies solving the Schrödinger equation is shown in Figure 10.1 for the He atom. We know from introductory chemistry that both electrons occupy what we call the $1s$ orbital, implying that the wave functions are similar to

$$\frac{1}{\sqrt{\pi}} \left(\frac{\zeta}{a_0} \right)^{3/2} e^{-\zeta r/a_0}$$

In the previous equation, zeta (ζ) is the **effective nuclear charge** of an electron. The importance of ζ in determining chemical properties is discussed later in this chapter. If the assumption is made that the motion of electrons 1 and 2 is uncorrelated, electron 1 can interact with the nucleus and the spatially averaged charge distribution arising from electron 2. This spatially averaged charge distribution is determined by $\phi^*(\mathbf{r}_2)\phi(\mathbf{r}_2)$. Think of electron 2 as being smeared out in a distribution that is spherically symmetrical about the nucleus, with a negative charge in the volume element $d\tau$ proportional to $-e\phi^*(\mathbf{r}_2)\phi(\mathbf{r}_2)d\tau$.

The advantage of this approximation becomes apparent when considering the effective charge distribution that electron 1 experiences. It is spherically symmetrical, as illustrated in Figure 10.1. Because the potential energy V depends only on r , each one-electron wave function can be written as a product of radial and angular functions, $\phi(\mathbf{r}) = \phi(r, \theta, \phi) = R(r)\Theta(\theta)\Phi(\phi)$. Although the radial functions differ from those for the hydrogen atom, the angular functions are the same, so that the s , p , d , f , . . . nomenclature used for the hydrogen atom also applies to many-electron atoms.

This quick look at the helium atom illustrates the approach that we will take in the rest of this chapter. The Schrödinger equation is solved for many-electron atoms by

approximating the true wave function as products of orbitals, each of which depends only on the coordinates of one electron. This approximation reduces the n -electron Schrödinger equation to n one-electron Schrödinger equations. The set of n equations is solved numerically to obtain the one-electron energies and orbitals ϵ_i and ϕ_i . The solutions are approximate because of the orbital approximation and because electron correlation is neglected. However, before this approach is implemented, two important concepts must be introduced; namely, electron spin and the indistinguishability of electrons.

10.2 INTRODUCING ELECTRON SPIN

Electron spin plays an important part in formulating the Schrödinger equation for many-electron atoms. In discussing the Stern–Gerlach experiment in Chapter 6, we focused on commutation relations rather than the other surprising result of this experiment, which is that two and only two deflected beams are observed. In order for a silver atom to be deflected in an inhomogeneous field, it must have a magnetic moment and an associated angular momentum. What is the origin of this moment? An electric current passing through a loop of wire produces a magnetic field, and, therefore, the loop has a magnetic moment. An electron in an orbit around a nucleus for which $l > 0$ has a nonzero angular momentum because of the nonspherical electron charge distribution. However, Ag has a closed-shell configuration plus a single 5s valence electron. A closed shell has a spherical electron charge distribution and no net angular momentum. Therefore, the magnetic moment must be associated with the 5s electron, rather than with orbital angular momentum, because $l = 0$. If this electron has an intrinsic angular momentum, which we call s , it will be split into $2s + 1$ components in passing through the magnet. The fact that two components are observed in the Stern–Gerlach experiment shows that $s = 1/2$. Therefore, there is a z component of angular momentum, $s_z = m_s \hbar = \pm \hbar/2$. This intrinsic electron spin angular momentum is a vector termed \mathbf{s} , and its z component is termed s_z to distinguish it from orbital angular momentum. The term *intrinsic* refers to the fact that the spin is independent of the environment of the electron. Use of the term *spin* implies that the electron is spinning about an axis. Although the nomenclature is appealing, there is no physical basis for this association.

How does the existence of spin change what has been discussed up to now? As we show later, each of the orbitals in a many-electron atom can be doubly occupied; one electron has $m_s = +1/2$, and the other has $m_s = -1/2$. This adds a fourth quantum number to the H atom eigenfunctions that is now labeled $\psi_{nlm_l m_s}(r, \theta, \phi)$. Because electron spin is an intrinsic property of the electron, it does not depend on the spatial variables r , θ , and ϕ .

How can this additional quantum number be incorporated in the formalism described for the hydrogen atom? This can be done by defining spin wave functions called α and β , which are eigenfunctions of the spin angular momentum operators \hat{s}^2 and \hat{s}_z . Because all angular momentum operators have the same properties, the spin operators follow the commutation rules listed in Equation (7.63). As for the orbital angular momentum, only the magnitude of the spin angular momentum and one of its components can be known simultaneously. The spin operators \hat{s}^2 and \hat{s}_z have the following properties:

$$\begin{aligned}\hat{s}^2\alpha &= \hbar^2 s(s+1)\alpha = \frac{\hbar^2}{2}\left(\frac{1}{2} + 1\right)\alpha \\ \hat{s}^2\beta &= \hbar^2 s(s+1)\beta = \frac{\hbar^2}{2}\left(\frac{1}{2} + 1\right)\beta \\ \hat{s}_z\alpha &= m_s \hbar \alpha = \frac{\hbar}{2}\alpha, \quad \hat{s}_z\beta = m_s \hbar \beta = -\frac{\hbar}{2}\beta \\ \int \alpha^* \beta d\sigma &= \int \beta^* \alpha d\sigma = 0 \\ \int \alpha^* \alpha d\sigma &= \int \beta^* \beta d\sigma = 1\end{aligned}\tag{10.3}$$

Concept

Electrons possess an intrinsic angular momentum that is referred to as electron spin.

In these equations, σ is called the spin variable. It is not a spatial variable, and the “integration” over σ exists only formally so that we can define orthogonality. The H atom eigenfunctions are redefined by multiplying them by α and β and including a quantum number for spin. For example, the H atom 1s eigenfunctions take the form

$$\begin{aligned}\psi_{100\frac{1}{2}}(r) &= \frac{1}{\sqrt{\pi}} \left(\frac{1}{a_0}\right)^{3/2} e^{-r/a_0} \alpha \quad \text{and} \\ \psi_{100-\frac{1}{2}}(r) &= \frac{1}{\sqrt{\pi}} \left(\frac{1}{a_0}\right)^{3/2} e^{-r/a_0} \beta\end{aligned}\quad (10.4)$$

The eigenfunctions remain orthonormal because with this formalism

$$\begin{aligned}&\iiint \psi_{100\frac{1}{2}}^*(r, \sigma) \psi_{100-\frac{1}{2}}(r, \sigma) d\tau d\sigma \\ &= \iiint \psi_{100}^*(r) \psi_{100}(r) d\tau \int \alpha^* \beta d\sigma = 0\end{aligned}$$

and

$$\begin{aligned}&\iiint \psi_{100\frac{1}{2}}^*(r, \sigma) \psi_{100\frac{1}{2}}(r, \sigma) d\tau d\sigma \\ &= \iiint \psi_{100}^*(r) \psi_{100}(r) d\tau \int \alpha^* \alpha d\sigma = 1\end{aligned}\quad (10.5)$$

where $d\tau$ is a three-dimensional volume element. These two eigenfunctions have the same energy because the total energy operator of Equation (10.1) does not depend on the spin. Having discussed how to include electron spin in a wave function, we now take on the issue of keeping track of electrons in a many-electron atom.

10.3 WAVE FUNCTIONS MUST REFLECT THE INDISTINGUISHABILITY OF ELECTRONS

In discussing He in Section 10.1, the electrons were numbered 1 and 2. Macroscopic objects can be distinguished from one another, but in an atom we have no way to distinguish between any two electrons. This fact needs to be taken into account in the formulation of a wave function. How can **indistinguishability** be introduced into the orbital approximation? Consider an n -electron wave function written as the product of n one-electron wave functions, which we describe using the notation $\psi(1, 2, \dots, n) = \phi_1(r_1\theta_1\phi_1\sigma_1)\phi_2(r_2\theta_2\phi_2\sigma_2)\dots\phi_n(r_n\theta_n\phi_n\sigma_n)$. The position variables are suppressed in favor of keeping track of the electrons. How does indistinguishability affect how the wave function is written? We know that the wave function itself is not an observable, but the square of the magnitude of the wave function is proportional to the electron density and is an observable. Because the two electrons in He are indistinguishable, no observable of the system can be changed if the electron labels 1 and 2 are interchanged. Therefore, $\psi^2(1, 2) = \psi^2(2, 1)$. This equation can be satisfied either by $\psi(1, 2) = \psi(2, 1)$ or $\psi(1, 2) = -\psi(2, 1)$. We refer to the wave function as being a **symmetric wave function** if $\psi(1, 2) = \psi(2, 1)$ or an **antisymmetric wave function** if $\psi(1, 2) = -\psi(2, 1)$. For a ground state He atom, examples of symmetric and anti-symmetric wave functions are as follows:

$$\begin{aligned}\psi_{\text{symmetric}}(1, 2) &= \phi_{1s}(1)\alpha(1)\phi_{1s}(2)\beta(2) + \phi_{1s}(2)\alpha(2)\phi_{1s}(1)\beta(1) \quad \text{and} \\ \psi_{\text{antisymmetric}}(1, 2) &= \phi_{1s}(1)\alpha(1)\phi_{1s}(2)\beta(2) - \phi_{1s}(2)\alpha(2)\phi_{1s}(1)\beta(1)\end{aligned}\quad (10.6)$$

where $\phi(1) = \phi(\mathbf{r}_1)$. Wolfgang Pauli showed that only an antisymmetric wave function is allowed for electrons, a result that can be formulated as a further fundamental postulate of quantum mechanics.

POSTULATE 6:

Wave functions that describe a many-electron system must change sign (be antisymmetric) under the exchange of any two electrons.

This postulate is also known as the **Pauli principle**. This principle states that different product wave functions of the type $\psi(1, 2, 3, \dots, n) = \phi_1(1)\phi_2(2) \dots \phi_n(n)$ must be combined such that the resulting wave function changes sign when any two electrons are interchanged. A combination of such terms is required because a single-product wave function cannot be made antisymmetric in the interchange of two electrons. For example, $\phi_{1s}(1)\alpha(1)\phi_{1s}(2)\beta(2) \neq -\phi_{1s}(2)\alpha(2)\phi_{1s}(1)\beta(1)$.

How can antisymmetric wave functions be constructed? Fortunately, there is a simple way to do so using determinants. They are known as **Slater determinants** and have the form

$$\psi(1, 2, 3, \dots, n) = \frac{1}{\sqrt{n!}} \begin{vmatrix} \phi_1(1)\alpha(1) & \phi_1(1)\beta(1) & \cdots & \phi_m(1)\beta(1) \\ \phi_1(2)\alpha(2) & \phi_1(2)\beta(2) & \cdots & \phi_m(2)\beta(2) \\ \cdots & \cdots & \cdots & \cdots \\ \phi_1(n)\alpha(n) & \phi_1(n)\beta(n) & \cdots & \phi_m(n)\beta(n) \end{vmatrix} \quad (10.7)$$

where $m = n/2$ if n is even and $m = (n + 1)/2$ if n is odd. The one-electron orbitals in which the n electrons are sequentially filled are listed across each row, with one row for each electron. The factor in front of the determinant accomplishes normalization if the one-electron orbitals are individually normalized. The Slater determinant is simply a recipe for constructing an antisymmetric wave function, and none of the individual entries in the determinant has a separate reality. For the ground state of He, the antisymmetric wave function is the 2×2 determinant:

$$\begin{aligned} \psi(1, 2) &= \frac{1}{\sqrt{2}} \begin{vmatrix} 1s(1)\alpha(1) & 1s(1)\beta(1) \\ 1s(2)\alpha(2) & 1s(2)\beta(2) \end{vmatrix} \\ &= \frac{1}{\sqrt{2}} [1s(1)\alpha(1)1s(2)\beta(2) - 1s(1)\beta(1)1s(2)\alpha(2)] \\ &= \frac{1}{\sqrt{2}} 1s(1)1s(2) [\alpha(1)\beta(2) - \beta(1)\alpha(2)] \end{aligned} \quad (10.8)$$

The shorthand notation $\phi_{1s}(1)\alpha(1) = \phi_{100+\frac{1}{2}}(r_1, \theta_1, \phi_1, \sigma_1) = 1s(1)\alpha(1)$ has been used in the preceding determinant.

Determinants are used in constructing antisymmetric wave functions as shown in Example Problem 10.1 because their value automatically changes sign when two rows (which refer to individual electrons) are interchanged. See Math Essential 9 for more information on working with determinants. Writing the wave function as a determinant also demonstrates another formulation of the Pauli principle. The value of a determinant is zero if two rows are identical. *This is equivalent to stating that the wave function is zero if all quantum numbers of any two electrons are the same.*

For ground state helium, both electrons have the same values of n , l , and m_l , but the values of m_s are $+1/2$ for one electron and $-1/2$ for the other. We now describe the way in which electrons are assigned to orbitals by a configuration. A **configuration** specifies the values of n and l for each electron. For example, the configuration for ground state He is $1s^2$, and that for ground state F is $1s^2 2s^2 2p^5$. The quantum numbers m_l and m_s are not specified in a configuration. Describing the quantum state of an atom requires this additional information, as will be discussed in Chapter 11.

Concept

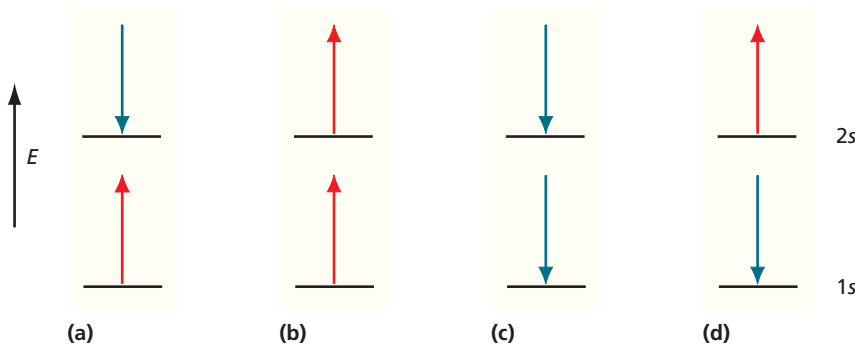
The Pauli principle states that a many-electron wave function must change sign if any two electrons are interchanged.

Concept

Slater determinants provide a convenient way to make many-electron wave functions antisymmetric in the orbital approximation.

EXAMPLE PROBLEM 10.1

This problem illustrates how determinantal wave functions can be associated with α and β spins in a set of orbitals. The first excited state of the helium atom can be described by the configuration $1s^12s^1$. However, four different spin orientations are consistent with this notation, as shown pictorially in the following figure. Do not take these pictures too literally, because they imply that one electron can be distinguished from another.



Keep in mind that the \downarrow and \uparrow notation commonly used for α and β spins is shorthand for the more accurate vector model depiction discussed in Chapter 7 and shown here:



Write determinantal wave functions that correspond to these pictures.

Solution

$$\begin{aligned}
 \text{a) } \psi_1(1, 2) &= \frac{1}{\sqrt{2}} \begin{vmatrix} 1s(1)\alpha(1) & 2s(1)\beta(1) \\ 1s(2)\alpha(2) & 2s(2)\beta(2) \end{vmatrix}; & \text{b) } \psi_2(1, 2) &= \frac{1}{\sqrt{2}} \begin{vmatrix} 1s(1)\alpha(1) & 2s(1)\alpha(1) \\ 1s(2)\alpha(2) & 2s(2)\alpha(2) \end{vmatrix}; \\
 \text{c) } \psi_3(1, 2) &= \frac{1}{\sqrt{2}} \begin{vmatrix} 1s(1)\beta(1) & 2s(1)\beta(1) \\ 1s(2)\beta(2) & 2s(2)\beta(2) \end{vmatrix}; & \text{d) } \psi_4(1, 2) &= \frac{1}{\sqrt{2}} \begin{vmatrix} 1s(1)\beta(1) & 2s(1)\alpha(1) \\ 1s(2)\beta(2) & 2s(2)\alpha(2) \end{vmatrix}
 \end{aligned}$$

Li is the neutral atom that has three electrons. If the third electron is put in the 1s orbital, the determinantal wave function

$$\psi(1, 2, 3) = \frac{1}{\sqrt{3!}} \begin{vmatrix} 1s(1)\alpha(1) & 1s(1)\beta(1) & 1s(1)\alpha(1) \\ 1s(2)\alpha(2) & 1s(2)\beta(2) & 1s(2)\alpha(2) \\ 1s(3)\alpha(3) & 1s(3)\beta(3) & 1s(3)\alpha(3) \end{vmatrix}$$

is obtained, where the third electron can have either α or β spin. However, the first and third columns in this determinant are identical, so that $\psi(1, 2, 3) = 0$. Therefore, the third electron must go into the next higher-energy orbital with $n = 2$. *This example shows that the Pauli exclusion principle requires that each orbital have a maximum occupancy of two electrons.* The configuration of ground-state Li is $1s^22s^1$. For $n = 2$, l can take on the value 0 with the only possible m_l value of 0, or 1 with the possible m_l values of 0, +1, and -1. Each of the possible sets of n , l , and m_l can be combined with $m_s = \pm 1/2$. Therefore, there are eight different sets of quantum numbers for $n = 2$. The set of orbitals with the same values of n and l comprises a **subshell**, and the set of orbitals with the same n value comprises a **shell**. The connotation of a shell is demonstrated pictorially in Figure 9.12.

10.4 USING THE VARIATIONAL METHOD TO SOLVE THE SCHRÖDINGER EQUATION

In Section 10.1, we concluded that electron–electron repulsion terms in the total energy operator for many-electron atoms preclude an analytical solution to the Schrödinger equation. However, numerical methods are available for calculating one-electron energies and the orbitals ε_i and ϕ_i that include electron–electron repulsion. The goal is to obtain as good an approximation as possible to the total energy eigenfunctions and eigenvalues for the many-electron atom. Only one of these methods, the **Hartree–Fock self-consistent field model** combined with the **variational method**, is discussed in this chapter. Several higher-level methods, including those that incorporate the effects of electron correlation, are discussed in Chapter 15.

The variational method is frequently used in computational chemistry calculations. For our purposes, consider a system in its ground state with energy E_0 and the corresponding eigenfunction ψ_0 , which satisfies the equation $\hat{H}\psi_0 = E_0\psi_0$. Multiplying this expression by ψ_0^* and integrating yields the following equation:

$$E_0 = \frac{\int \psi_0^* \hat{H} \psi_0 d\tau}{\int \psi_0^* \psi_0 d\tau} \quad (10.9)$$

The denominator takes into account that the wave function may not be normalized. For a many-electron atom, the total energy operator can be formulated, but the exact total energy eigenfunctions are unknown. How can the energy be calculated in this case? To address this issue, we rely on the variational theorem, which states that regardless of which wave function Φ is substituted for the ground state eigenfunction in Equation (10.9), the energy is always greater than or equal to the true energy. Expressed mathematically, the theorem is written as

$$E = \frac{\int \Phi^* \hat{H} \Phi d\tau}{\int \Phi^* \Phi d\tau} \geq E_0 \quad (10.10)$$

The proof of this theorem is included as an end-of-chapter problem. How can this theorem be implemented in a method to obtain good approximate wave functions and energies? We select and then parameterize a **trial wave function** Φ and find the optimal values for the parameters by minimizing the energy with respect to each parameter. This procedure gives the best energy that can be obtained for that particular choice of a trial wave function. The better the choice made for the trial function, the closer the calculated energy will be to the true energy.

We illustrate this formalism using the particle in the box as a specific example. Any trial wave function used must satisfy a number of general conditions (single-valued, normalizable, the function and its first derivative are continuous) and also satisfy the boundary condition that the wave function approaches zero at the ends of the box. We use the trial function of Equation (10.11) to approximate the ground-state wave function. This wave function satisfies the criteria just listed. This function contains a single parameter α that is used to minimize the energy:

$$\Phi(x) = \left(\frac{x}{a} - \frac{x^3}{a^3} \right) + \alpha \left(\frac{x^5}{a^5} - \frac{1}{2} \left(\frac{x^7}{a^7} + \frac{x^9}{a^9} \right) \right), \quad 0 < x < a \quad (10.11)$$

We first calculate the energy for $\alpha = 0$ and obtain

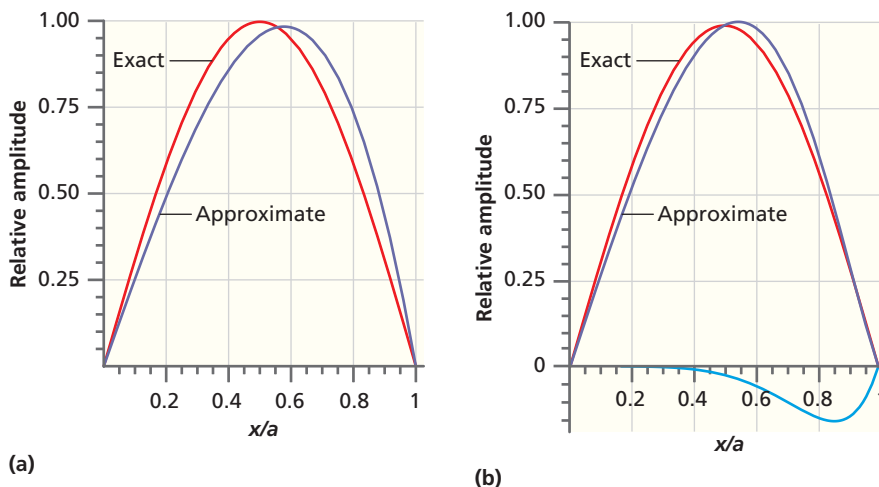
$$E = \frac{-\frac{\hbar^2}{2m} \int_0^a \left(\frac{x}{a} - \frac{x^3}{a^3} \right) \frac{d^2}{dx^2} \left(\frac{x}{a} - \frac{x^3}{a^3} \right) dx}{\int_0^a \left(\frac{x}{a} - \frac{x^3}{a^3} \right)^2 dx} = 0.133 \frac{\hbar^2}{ma^2} \quad (10.12)$$

Concept

The variational method provides a way to minimize the energy of a trial wave function.

Figure 10.2

Exact and approximate wave functions for the ground state of the particle in the box. The exact wave function is shown by the red curve, and the approximate wave function is shown by the purple curve. (a) The approximate wave function contains only the first term in Equation (10.11). (b) The optimal approximate wave function contains both terms of Equation (10.11). The light blue curve shows the contribution of the second term in Equation (10.11) to the approximate wave function.



Because the trial function is not the exact ground state wave function, the energy is higher than the exact value $E_0 = 0.125(\hbar^2/ma^2)$. How similar is the trial function to the ground state eigenfunction? A comparison between the exact solution and the trial function with $\alpha = 0$ is shown in Figure 10.2a.

To find the optimal value for α , E is first expressed in terms of \hbar , m , a , and α , and then minimized with respect to α . The energy E is given by

$$E = \frac{-\frac{\hbar^2}{2m} \int_0^a \left[\left(\frac{x}{a} - \frac{x^3}{a^3} \right) + \alpha \left(\frac{x^5}{a^5} - \frac{1}{2} \left(\frac{x^7}{a^7} + \frac{x^9}{a^9} \right) \right) \right] \times \frac{d^2}{dx^2} \left[\left(\frac{x}{a} - \frac{x^3}{a^3} \right) + \alpha \left(\frac{x^5}{a^5} - \frac{1}{2} \left(\frac{x^7}{a^7} + \frac{x^9}{a^9} \right) \right) \right]}{\int_0^a \left[\left(\frac{x}{a} - \frac{x^3}{a^3} \right) + \alpha \left(\frac{x^5}{a^5} - \frac{1}{2} \left(\frac{x^7}{a^7} + \frac{x^9}{a^9} \right) \right) \right]^2 dx} \quad (10.13)$$

Carrying out this integration gives E in terms of \hbar , m , a , and α :

$$E = \frac{\frac{\hbar^2}{2ma^2} \left(\frac{4}{5} + \frac{116\alpha}{231} + \frac{40247\alpha^2}{109395} \right)}{\left(\frac{8}{105} + \frac{8\alpha}{273} + \frac{1514\alpha^2}{230945} \right)} \quad (10.14)$$

To minimize the energy with respect to the variational parameter, we differentiate this function with respect to α , set the resulting equation equal to zero, and solve for α . The solutions are $\alpha = -5.74$ and $\alpha = -0.345$. The second of these solutions corresponds to the minimum in E . Substituting this value in Equation (10.14) gives $E = 0.127(\hbar^2/ma^2)$, which is very close to the true value of $0.125(\hbar^2/ma^2)$. The optimized trial function is shown in Figure 10.2b. We can see that by choosing the optimal value of α , $E \rightarrow E_0$ and $\Phi \rightarrow \psi_0$. No better value for the energy can be obtained with this particular choice of a trial wave function, and this illustrates a limitation of the variational method. The “best” energy obtained depends on the choice of the trial function. For example, a lower energy is obtained if a function of the type $\Phi(x) = x^\alpha(a - x)^\alpha$ is minimized with respect to α . This example shows how the variational method can be implemented by optimizing approximate solutions to the Schrödinger equation.

10.5 THE HARTREE-FOCK SELF-CONSISTENT FIELD MODEL

We now return to the problem at hand, which is solving the Schrödinger equation for many-electron atoms. The starting point is to use the orbital approximation and to take the Pauli exclusion principle into account. Antisymmetry of the wave function with

respect to electron exchange is accomplished by expressing the wave function as a Slater determinant

$$\psi(1, 2, 3, \dots, n) = \frac{1}{\sqrt{n!}} \begin{vmatrix} \phi_1(1)\alpha(1) & \phi_1(1)\beta(1) & \cdots & \phi_m(1)\beta(1) \\ \phi_1(2)\alpha(2) & \phi_1(2)\beta(2) & \cdots & \phi_m(2)\beta(2) \\ \cdots & \cdots & \cdots & \cdots \\ \phi_1(n)\alpha(n) & \phi_1(n)\beta(n) & \cdots & \phi_m(n)\beta(n) \end{vmatrix} \quad (10.15)$$

in which the individual entries ϕ_j are modified H atom orbitals, as described later. The Hartree–Fock model is a prescription for finding the single Slater determinant that gives the lowest energy for the ground state atom in the absence of electron correlation. (More correctly, configurations with more than one unpaired electron require more than one Slater determinant.)

As for the helium atom discussed in Section 10.1, it is assumed that the electrons are uncorrelated and that a particular electron is affected by the spatially averaged electron charge distribution of the remaining $n - 1$ electrons. These approximations reduce the radial part of the n -electron Schrödinger equation to n one-electron Schrödinger equations that have the form

$$\left(\frac{\hbar^2}{2m} \nabla_i^2 + V_i^{\text{eff}}(r) \right) \phi_i(r) = \varepsilon_i \phi_i(r), \quad i = 1, \dots, n \quad (10.16)$$

in which the effective potential energy experienced by the first electron, $V_i^{\text{eff}}(r)$, takes into account the electron-nuclear attraction and the repulsion between electron 1 and all other electrons. The Hartree–Fock model allows the best (in a variational sense) one-electron orbitals $\phi_i(r)$ and the corresponding orbital energies ε_i to be calculated.

Because of the neglect of electron correlation, the effective potential is spherically symmetrical, and, therefore, the angular part of the wave functions is identical to the solutions for the hydrogen atom. *This means that the s, p, d, ... orbital nomenclature derived for the hydrogen atom remains intact for the one-electron orbitals for all atoms.* What remains to be found are solutions to the radial part of the Schrödinger equation.

To optimize the radial part of the determinantal wave function, the variational method outlined in Section 10.4 is used. What functions should be used for the individual entries $\phi_j(r)$ in the determinant? Each $\phi_j(r)$ is expressed as a linear combination of suitable **basis functions** $f_i(r)$ as shown in Equation (10.17).

$$\phi_j(r) = \sum_{i=1}^m c_i f_i(r) \quad (10.17)$$

What do we mean by a set of suitable functions? Recall that a well-behaved function can be expanded in a Fourier series as a sum of sine and cosine functions, which in this context are basis functions. There are many other choices for individual members of a basis set. The criterion for a “good” basis set is that the number of terms in the sum m representing $\phi_j(r)$ is as small as possible and that the basis functions enable the Hartree–Fock calculations to be carried out rapidly. Two examples of basis set expansions for atomic orbitals are shown in Figures 10.3 and 10.4.

In Figure 10.3, the $2p$ atomic orbital of Ne obtained in a Hartree–Fock calculation is shown together with the individual contributions to Equation (10.17) where each member of the $m = 4$ basis set is of the form $f_i(r) = N_i r \exp[-\zeta_i r/a_0]$ (Slater-type functions) and N_i is a normalization constant. In a second example, the H $1s$ AO, and the contributions of each member of the $m = 3$ basis set to Equation (10.17) are shown in Figure 10.4, where the basis set functions are of the form $f_i(r) = N_i \exp[-\zeta_i r/a_0]^2$ (Gaussian functions). In both cases, the coefficients c_i in Equation (10.17) are used as variational parameters to optimize $\phi_j(r)$ and the ζ_i values are optimized separately. Although the Gaussian functions do not represent the H $1s$ function accurately near the nucleus, they are well suited to Hartree–Fock calculations and are the most widely used basis functions in computational chemistry. (See Chapter 15 for a more detailed discussion of Gaussian basis functions.)

The preceding discussion describes the input to a calculation of the orbital energies, but there is a problem in proceeding with the calculation. To solve the Schrödinger equation for electron 1, $V_1^{\text{eff}}(r)$ must be known, and this means that we must know the

Concept

The Hartree–Fock method allows the best one-electron orbitals and the corresponding orbital energies to be calculated for many-electron atoms if electron correlation is neglected.

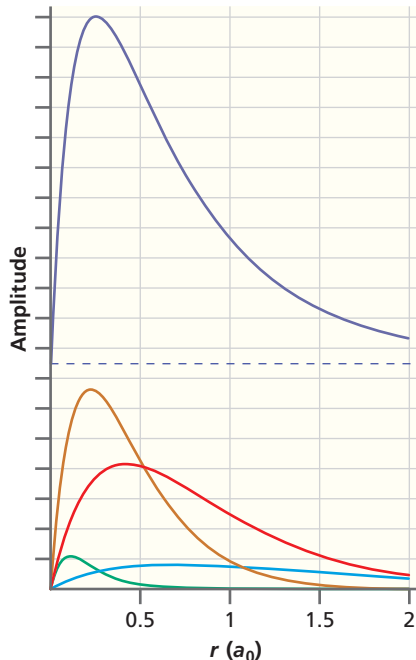
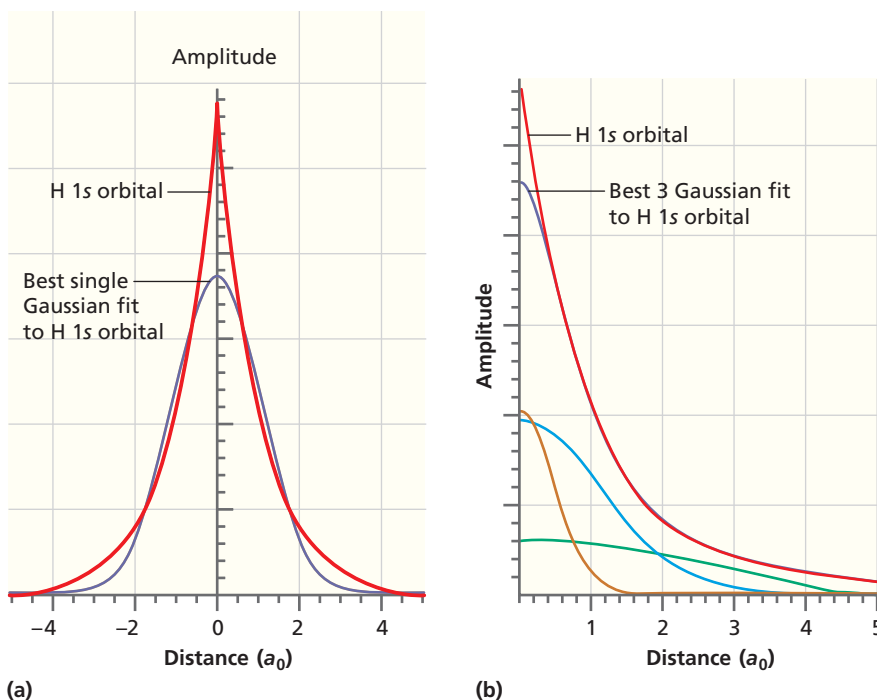


Figure 10.3

Slater-type basis set expansions for atomic orbitals. The top curve shows the radial function for the $2p$ orbital in Ne determined in a Hartree–Fock calculation. It has been shifted upward from the remaining curves for clarity. The lower four curves are the individual terms in the four-element basis set.

Figure 10.4

Gaussian basis set expansions for atomic orbitals. (a) Best fit to a H 1s orbital with a single Gaussian function. Note that the fit is poor. (b) Best fit (purple curve) using a basis set of three Gaussian functions, which are also shown. Except very near the nucleus, the three basis function fit is very good.



functional form of all the other orbitals $\phi_2(\mathbf{r}_2), \phi_3(\mathbf{r}_3), \dots, \phi_n(\mathbf{r}_n)$. This is also the case for the remaining $n - 1$ electrons. In other words, the answers must be known in order to solve the problem.

The way out of this quandary is to use an iterative approach. A reasonable guess is made for an initial set of $\phi_j(r)$. Using these orbitals, we can calculate an effective potential, as well as the energy and improved orbital functions, $\phi'_j(r)$, for each of the n electrons. The $\phi'_j(r)$ are used to calculate a new effective potential, which is used to calculate a further improved set of orbitals, $\phi''_j(r)$. This procedure is repeated for all electrons until the solutions for the energies and orbitals are self-consistent, meaning that they do not change significantly in a further iteration. This procedure, coupled with the variational method in optimizing the parameters in the orbitals, is very effective in giving the best one-electron orbitals and energies available for a many-electron atom in the absence of electron correlation. More accurate calculations that include electron correlation are discussed in Chapter 15.

The accuracy of a Hartree–Fock calculation depends primarily on the size of the basis set. This dependence is illustrated in Table 10.1 in which the calculated total energy of He and the 1s orbital energy are shown for three different basis sets. In each case, $\phi_{1s}(r)$ has the form

$$\phi_{1s}(r) = \sum_{i=1}^m c_i N_i e^{-\zeta_i r/a_0} \quad (10.18)$$

where N_i is a normalization constant for the i th basis function and m is the number of basis functions. It is seen that there is almost no change as the number of basis functions is increased from two to five, which represents the Hartree–Fock limit of a complete basis set in this case. The one element or single zeta basis set yields an energy that differs significantly from the Hartree–Fock limit. We will return to this basis set in discussing the effective nuclear charge later. The He 1s orbital cannot be accurately represented by a single exponential function, as was the case for the hydrogen atom.

One might think that the total energy of an atom is the sum of the orbital energies, or for helium, $\epsilon_{total} = 2\epsilon_{1s}$. As shown in Table 10.1, $\epsilon_{total} - 2\epsilon_{1s} < 0$, and this result can be understood by considering how electron–electron repulsion is treated in a Hartree–Fock calculation. The 1s orbital energy is calculated using an effective potential in which repulsion between the two electrons in the orbital is included. Therefore, the assumption that $\epsilon_{total} = 2\epsilon_{1s}$ counts the repulsion between the two electrons twice and gives a value for ϵ_{total} that is more positive than the true total energy.

Concept

Use of Gaussian basis sets to represent one-electron orbitals minimizes computational time for Hartree–Fock calculations.

TABLE 10.1 Total Energy and 1s Orbital Energy for He for Three Different Basis Sets Used to Represent the 1s Orbital

Number of Basis Functions, m	Exponents, ζ_i	Total Energy of He, ε_{total} (eV)	1s Orbital Energy, ε_{1s} (eV)	$\varepsilon_{total} - 2\varepsilon_{1s}$ (eV)
5	1.41714, 2.37682, 4.39628, 6.52699, 7.94252	-77.8703	-24.9787	-27.9129
2	2.91093, 1.45363	-77.8701	-24.9787	-27.9133
1	1.68750	-77.4887	-24.3945	-28.6998

Source: Data in E. Clementi and C. Roetti. "Roothaan-Hartree-Fock Atomic Wavefunctions: Basis Functions and Their Coefficients for Ground and Certain Excited States of Neutral and Ionized Atoms, $Z \leq 54$." *Atomic Data and Nuclear Data Tables* 14 (1974): 177.

Radial functions for Ar in the Hartree–Fock limit of a large basis set are shown in Figure 10.5. It is seen that they have the same nodal structure as the orbitals for the hydrogen atom.

The Hartree–Fock radial functions can be used to obtain the radial probability distribution for many-electron atoms from

$$P(r) = \sum_i n_i r^2 R_i^2(r) \quad (10.19)$$

where $R_i(r)$ is the radial function corresponding to the i th subshell, for example, 2s, 3p, or 4d, and n_i is the number of electrons in the subshell. $P(r)$ is shown for Ne, Ar, and Kr in Figure 10.6. Note that the radial distribution exhibits a number of maxima, one for each occupied shell, and that the contributions from different shells overlap. The width of $P(r)$ for a given shell increases with n ; it is smallest for $n = 1$ and largest for the largest n value.

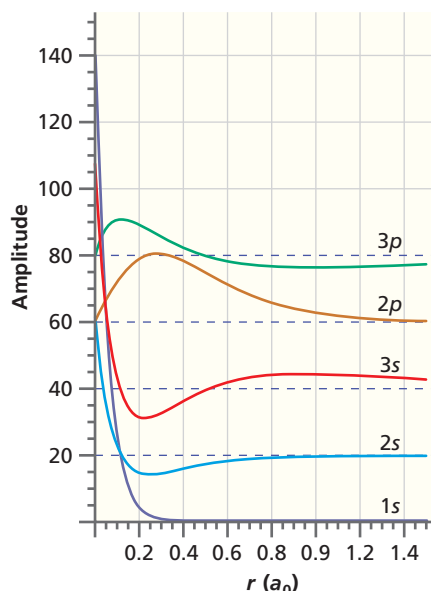


Figure 10.5

Hartree–Fock radial functions for Ar.

The curves are offset vertically to allow individual functions to be compared.

Source: Calculated from data in E. Clementi and C. Roetti. "Roothaan-Hartree-Fock Atomic Wavefunctions: Basis Functions and Their Coefficients for Ground and Certain Excited States of Neutral and Ionized Atoms, $Z \leq 54$." *Atomic Data and Nuclear Data Tables* 14 (1974): 177.

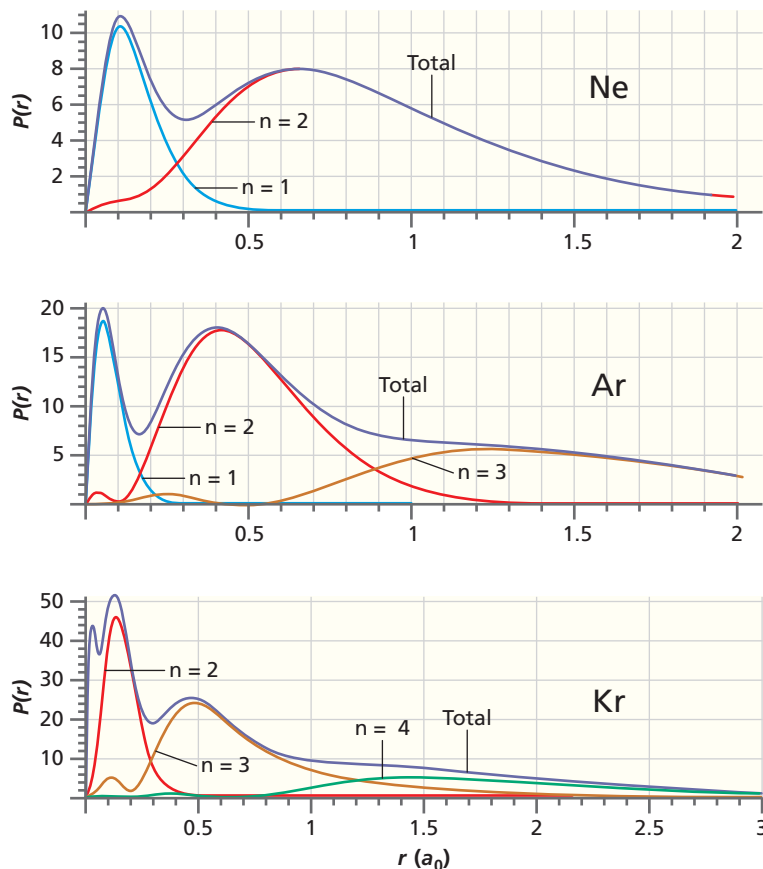


Figure 10.6

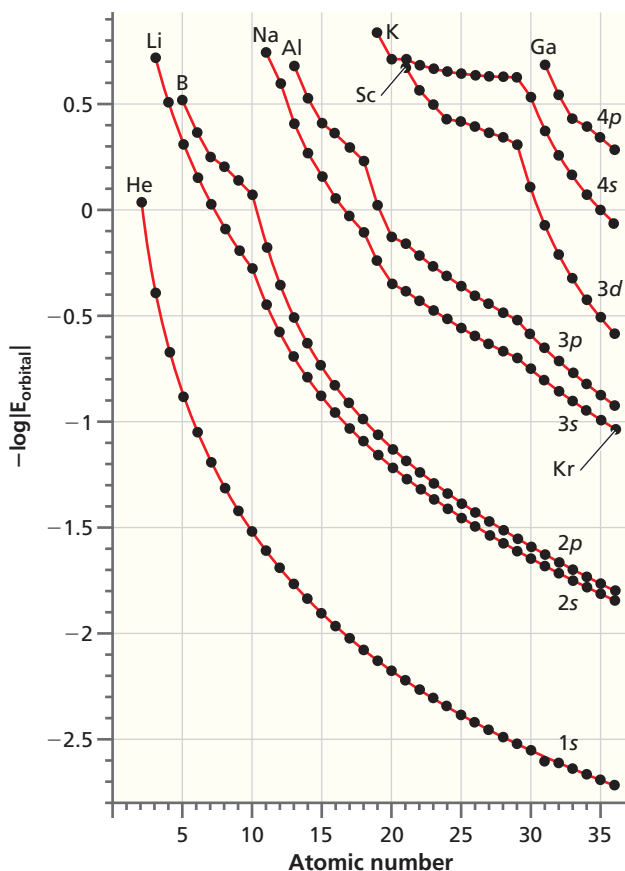
Radial distribution functions calculated from Hartree–Fock wave functions for Ne, Ar, and Kr. The colored curves show the contributions from the individual shells, and the purple curve shows the total radial distribution function. The $n = 1$ curve for Kr is not shown for clarity.

Source: Calculated from data in E. Clementi and C. Roetti. "Roothaan-Hartree-Fock Atomic Wavefunctions: Basis Functions and Their Coefficients for Ground and Certain Excited States of Neutral and Ionized Atoms, $Z \leq 54$." *Atomic Data and Nuclear Data Tables* 14 (1974): 177.

Figure 10.7

One-electron orbital energies obtained from Hartree–Fock calculations for the first 36 elements. Note that the vertical axis has a logarithmic scale.

Source: Calculated from data in E. Clementi and C. Roetti. “Roothaan-Hartree-Fock Atomic Wavefunctions: Basis Functions and Their Coefficients for Ground and Certain Excited States of Neutral and Ionized Atoms, $Z \leq 54$.” *Atomic Data and Nuclear Data Tables* 14 (1974): 177.



Concept

Orbital energies for many-electron atoms depend on both quantum numbers n and l .

Hartree–Fock orbital energies ε_i are shown in Figure 10.7 for the first 36 elements in the periodic table. An important result of these calculations is that the ε_i for many-electron atoms depend on both the principal quantum number n and on the angular momentum quantum number l . This result was not the case for the H atom. Within a shell of principal quantum number n , $\varepsilon_{ns} < \varepsilon_{np} < \varepsilon_{nd} < \dots$. This result can be understood by considering the radial distribution functions for Kr shown in Figure 10.8. As discussed in Chapter 9, this function gives the probability of finding an electron at a given distance from the nucleus. The subsidiary maximum near $r = 0.02 a_0$ in the $3s$ radial distribution function indicates that there is a higher probability of finding the $3s$ electron close to the nucleus than is the case for the $3p$ and $3d$ electrons. The potential energy associated with the attraction between the nucleus and the electron falls off as $1/r$ so that its magnitude increases substantially as the distance of the electron from the nucleus decreases. As a result, the $3s$ electron is bound more strongly to the nucleus, and, therefore, the orbital energy is more negative than for the $3p$ and $3d$ electrons. The same argument can be used to understand why the $3p$ orbital energy is lower than that for the $3d$ orbital. Figure 10.7 shows that the energy of a given orbital decreases strongly with an increase in atomic number. This is a result of the increase in the attractive force between the nucleus and an electron as the charge on the nucleus increases.

Figure 10.8

Contributions of the $3s$, $3p$, and $3d$ subshells to the radial distribution function of krypton obtained from Hartree–Fock calculations.

Source: Calculated from data in E. Clementi and C. Roetti. “Roothaan-Hartree-Fock Atomic Wavefunctions: Basis Functions and Their Coefficients for Ground and Certain Excited States of Neutral and Ionized Atoms $Z \leq 54$.” *Atomic Data and Nuclear Data Tables* 14 (1974): 177.

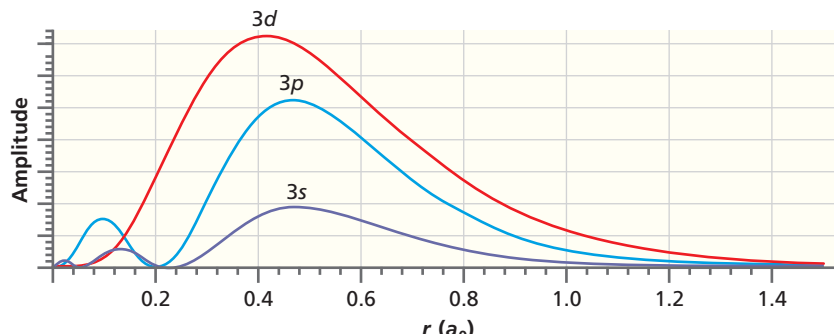


TABLE 10.2 Effective Nuclear Charges for Selected Atoms

H (1)								He (2)
1s	1.00							1.69
	Li (3)	Be (4)	B (5)	C (6)	N (7)	O (8)	F (9)	Ne (10)
1s	2.69	3.68	4.68	5.67	6.66	7.66	8.65	9.64
2s	1.28	1.91	2.58	3.22	3.85	4.49	5.13	5.76
2p			2.42	3.14	3.83	4.45	5.10	5.76

It is important to realize that ε_i for a many-electron atom depends on the electron configuration and on the atomic charge because ε_i is determined in part by the average distribution of all other electrons. For example, the Hartree–Fock limiting value for ε_{1s} is -67.4 eV for neutral Li and -76.0 eV for Li^+ (for Li^+ the 2s electron has been removed).

A further useful result from Hartree–Fock calculations are values for the effective nuclear charge, ζ . The effective nuclear charge takes into account that an electron farther from the nucleus experiences a smaller nuclear charge than that experienced by an inner electron. This can be seen by referring to Figure 10.1. To the electron in question, the nuclear charge appears to have been reduced because of the presence of the other smeared-out electrons. This effect is particularly important for valence electrons, and we say that they are shielded from the full nuclear charge by the core electrons closer to the nucleus. Table 10.2 shows ζ for all occupied orbitals in the first 10 atoms in the periodic table. The zeta values are obtained from a Hartree–Fock calculation using the single-zeta basis set discussed earlier (see Table 10.1). The difference between the true and effective nuclear charge is a direct measure of the shielding. The effective nuclear charge is nearly equal to the nuclear charge for the 1s orbital but falls off quite rapidly for the outermost electron as the principal quantum number increases. Whereas electrons of smaller n value are quite effective in **shielding** electrons with greater n values from the full nuclear charge, those in the same shell are much less effective. Therefore $Z - \zeta$ increases in moving across the periodic table. However, as Example Problem 10.2 shows, some subtle effects are involved.

Concept

The effective nuclear charge is less than the nuclear charge because of shielding.

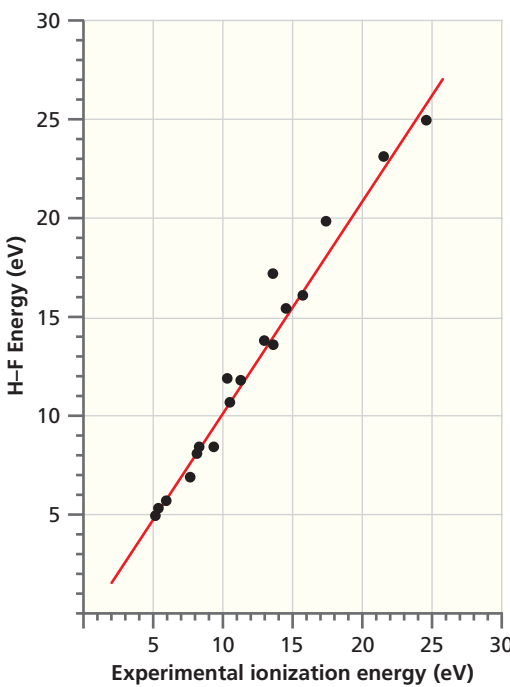
EXAMPLE PROBLEM 10.2

The effective nuclear charge experienced by a 2s electron in Li is 1.28. We might expect this number to be 1.0 rather than 1.28. Why is ζ larger than 1? Similarly, explain the effective nuclear charge seen by a 2s electron in carbon.

Solution

The effective nuclear charge experienced by a 2s electron in Li will be only 1.0 if all the charge associated with the 1s electrons is located between the nucleus and the 2s shell. As Figure 10.1 shows, a significant fraction of the charge is located farther from the nucleus than the 2s shell, and some of the charge is quite close to the nucleus. Therefore, the effective nuclear charge seen by the 2s electrons is reduced by a number smaller than 2. On the basis of the argument presented for Li, we expect the shielding by the 1s electrons in carbon to be incomplete, and we might expect the effective nuclear charge experienced by the 2s electrons in carbon to be more than 4. However, carbon has four electrons in the $n = 2$ shell, and although shielding by electrons in the same shell is less effective than shielding by electrons in inner shells, the total effect of all four $n = 2$ electrons reduces the effective nuclear charge experienced by the 2s electrons to 3.22.

We now turn our attention to the orbital energies ε_i . What observables can be associated with the orbital energies? The most meaningful link of ε_i to physical properties is to the ionization energy. To a reasonable approximation, $-\varepsilon_i$ for the highest

**Figure 10.9**

The negative of the highest occupied Hartree–Fock orbital graphed against experimentally determined first ionization energies of the first 18 elements. If the two values were identical, all points would lie on the red line.

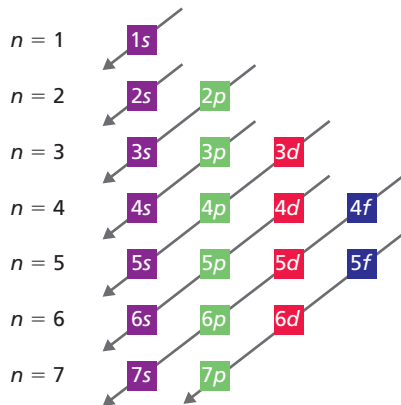
**Figure 10.10**

Illustration of the Aufbau principle.

The order in which orbitals in many-electron atoms are filled for most atoms is described by the gray lines, starting from the top of the figure. Twelve of the forty transition elements show departures from this order.

occupied orbital is the first **ionization energy**. This association is known as **Koopmans' theorem** in the “frozen core” limit, in which it is assumed that the electron distribution in the atom is not affected by the removal of an electron in the ionization event. Figure 10.9 shows that the agreement between the experimentally determined first ionization energy and the highest occupied orbital energy is quite good.

By analogy, $-\varepsilon_i$ for the lowest unoccupied orbital should give the **electron affinity** for a particular atom. However, Hartree–Fock electron affinity calculations are much less accurate than ionization energies. For example, the electron affinity for F based on $-\varepsilon_i$ for the lowest unoccupied orbital is negative. This result predicts that the F^- ion is less stable than the neutral F atom, contrary to experiment. A better estimate of the electron affinity of F is obtained by subtracting the total energies of F^- from that of F. This gives a value for the electron affinity of 0.013 eV, which is still much smaller than the experimental value of 3.34 eV. More accurate calculations, including those that incorporate electron correlation as discussed in Chapter 15, are necessary to obtain accurate results for the electron affinity of atoms.

The electron configuration of most atoms can be obtained by using Figure 10.10, which shows the order in which the atomic orbitals are generally filled based on the orbital energy sequence of Figure 10.7. Filling orbitals in this sequential order is known as the **Aufbau principle**, and it is often asserted that the relative order of orbital energies explains the electron configurations of the atoms in the periodic table. However, this assertion is not always true.

To illustrate exceptions to the Aufbau principle, consider the known configurations of the first transition series shown in Table 10.3. Figure 10.7 shows that the 4s orbital is lower in energy than the 3d orbital for K and Ca but that the order is reversed for higher atomic numbers. Is the order in which the *s* and *d* subshells are filled in the 4th period explained by the relative energy of the orbitals? If this were the case, the configuration $[\text{Ar}]4s^03d^n$ with $n = 3, \dots, 10$ would be predicted for the sequence scandium–nickel where [Ar] is an abbreviation for the configuration of Ar. However, with the exception of Cr and Cu, the experimentally determined configurations are given by $[\text{Ar}]4s^23d^n$, with $n = 1, \dots, 10$ for the sequence scandium–zinc. Cr and Cu have a single 4s electron because a half-filled or filled *d* shell lowers the energy of an atom.

The anomalous configurations for Cr and Cu can be explained if the total energies of the various possible configurations, rather than the orbital energies, are compared. For more details, see the reference to Vanquickenbourne et al. in Further Reading. The difference in the total energy of the anomalous and expected $4s^23d^n$ configurations is determined by two competing factors: the orbital energies and the electrostatic repulsion of the electrons involved in the promotion. ΔE for a $4s^23d^n \rightarrow 4s^13d^{n+1}$ promotion is given by

$$\Delta E(4s \rightarrow 3d) \approx (\varepsilon_{3d} - \varepsilon_{4s}) + [E_{\text{repulsive}}(3d, 3d) - E_{\text{repulsive}}(3d, 4s)] \quad (10.20)$$

The second term in Equation (10.20) represents the difference in the repulsive energies of the two configurations. What is the sign of the second term? Figure 10.6 shows

TABLE 10.3 Configurations for Fourth-Row Atoms

Nuclear Charge	Element	Electron Configuration	Nuclear Charge	Element	Electron Configuration
19	K	$[\text{Ar}]4s^1$	25	Mn	$[\text{Ar}]4s^23d^5$
20	Ca	$[\text{Ar}]4s^2$	26	Fe	$[\text{Ar}]4s^23d^6$
21	Sc	$[\text{Ar}]4s^23d^1$	27	Co	$[\text{Ar}]4s^23d^7$
22	Ti	$[\text{Ar}]4s^23d^2$	28	Ni	$[\text{Ar}]4s^23d^8$
23	V	$[\text{Ar}]4s^23d^3$	29	Cu	$[\text{Ar}]4s^13d^{10}$
24	Cr	$[\text{Ar}]4s^13d^5$	30	Zn	$[\text{Ar}]4s^23d^{10}$

that the distance of the electron from the nucleus corresponding to the principal maxima in the radial probability distribution for a typical many-electron atom follows the order $3s > 3p > 3d$. We conclude that the d electrons are more localized than the s electrons, and therefore the repulsive energies follow the order $E_{repulsive}(3d, 3d) > E_{repulsive}(3d, 4s) > E_{repulsive}(4s, 4s)$. Therefore, the sign of the second term in Equation (10.20) is positive. For this transition metal series, the magnitude of the repulsive term is greater than the magnitude of the difference in the orbital energies. Therefore, even though $(\varepsilon_{3d} - \varepsilon_{4s}) < 0$ for scandium, the promotion $4s^23d^1 \rightarrow 4s^03d^3$ does not occur because $(\varepsilon_{3d} - \varepsilon_{4s}) + [E_{repulsive}(3d, 3d) - E_{repulsive}(3d, 4s)] > 0$. The energy lowering from promotion to the lower orbital energy is more than offset by the energy increase resulting from electron repulsion. Therefore, Sc has the configuration $[\text{Ar}]4s^23d^1$ rather than $[\text{Ar}]4s^03d^3$. For a more detailed discussion, see the reference to Vanquickenbourgh et al. in Further Reading.

These calculations also explain the seemingly anomalous configurations for the doubly charged positive ions in the sequence scandium-zinc, which are $[\text{Ar}]4s^03d^n$ with $n = 1, \dots, 21$. The removal of two electrons significantly increases the effective nuclear charge felt by the remaining electrons. As a result, both ε_{4s} and ε_{3d} are lowered substantially, but ε_{3d} is lowered more. Therefore, $\varepsilon_{3d} - \varepsilon_{4s}$ becomes more negative. For the doubly charged ions, the magnitude of the repulsive term is less than the magnitude of the difference in the orbital energies. As a consequence, the doubly ionized configurations are those that would be predicted by filling the lower lying $3d$ orbital before the $4s$ orbital.

Recall that Hartree–Fock calculations neglect electron correlation. Therefore, the calculated total energy is larger than the true energy by an amount called the **correlation energy**. For example, the correlation energy for He is 110 kJ mol^{-1} . This amount increases somewhat faster than the number of electrons in the atom. Although the correlation energy is a small percentage of the total energy of the atom and decreases with the atomic number (1.4% for He and 0.1% for K), it presents a problem in the application of Hartree–Fock calculations to chemical reactions for the following reason. In chemical reactions, we are not interested in the total energies of the reactants and products but rather in $\Delta_r G$ and $\Delta_r H$. These changes are on the order of 100 kJ mol^{-1} so that errors in quantum chemical calculations resulting from the neglect of the electron correlation can lead to significant errors in thermodynamic calculations. However, the neglect of correlation is often less serious than might be expected. The resulting error in the total energy is often similar for the reactants and products if the number of unpaired electrons is the same for reactants and products. For such reactions, the neglect of electron correlation largely cancels in thermodynamic calculations. Additionally, the coordinated work of many quantum chemists over decades has led to computational methods that go beyond Hartree–Fock by including electron correlation. These advances make it possible to calculate thermodynamic functions and activation energies for many reactions for which it would be very difficult to obtain experimental data. These computational methods will be discussed in Chapter 15.

Concept

Anomalous configurations of transition metal atoms can be explained if electron-electron repulsion is taken into account.

10.6 UNDERSTANDING TRENDS IN THE PERIODIC TABLE FROM HARTREE-FOCK CALCULATIONS

We briefly summarize the main results of Hartree–Fock calculations for atoms:

- The orbital energy depends on both n and l . Within a shell of principal quantum number n , $\varepsilon_{ns} < \varepsilon_{np} < \varepsilon_{nd} < \dots$
- Electrons in a many-electron atom are shielded from the full nuclear charge by other electrons. Shielding can be modeled in terms of an effective nuclear charge. Core electrons are more effective in shielding outer electrons than electrons in the same shell.
- The ground state configuration for an atom results from a balance between orbital energies and electron–electron repulsion.

In addition to the orbital energies, two parameters that can be calculated using the Hartree–Fock method are very useful in understanding chemical trends in the periodic table. They are the atomic radius and the electronegativity. Values for atomic radii are obtained by calculating the radius of the sphere that contains ~90% of the electron charge. This radius is determined by the effective charge felt by valence shell electrons.

The degree to which atoms accept or donate electrons to other atoms in a reaction is closely related to the first ionization energy and the electron affinity, which we associate with the highest occupied and lowest unoccupied orbitals. For example, the energy of these orbitals allows us to predict whether the ionic NaCl species is better described by Na^+Cl^- or Na^-Cl^+ . Formation of Na^+ and Cl^- ions at infinite separation requires

$$\Delta E = E_{\text{ionization}}^{\text{Na}} - E_{\text{electron affinity}}^{\text{Cl}} = 5.14 \text{ eV} - 3.61 \text{ eV} = 1.53 \text{ eV} \quad (10.21)$$

Formation of oppositely charged ions requires

$$\Delta E = E_{\text{ionization}}^{\text{Cl}} - E_{\text{electron affinity}}^{\text{Na}} = 12.97 \text{ eV} - 0.55 \text{ eV} = 12.42 \text{ eV} \quad (10.22)$$

Concept

Electronegativity differences determine the direction of electron transfer between two bonded atoms.

In each case, additional energy is gained by bringing the ions together. Clearly, the formation of Na^+Cl^- is favored over Na^-Cl^+ . The concept of **electronegativity**, which is given the symbol χ , quantifies this tendency of atoms to either accept or donate electrons to another atom in a chemical bond. Because the noble gases in group VIII do not form chemical bonds (with very few exceptions), they are not generally assigned values of χ .

Several definitions of electronegativity (which has no units) exist, but all lead to similar results when scaled to the same numerical range. For instance, χ as defined by the American chemist Robert Mulliken is given by

$$\chi = 0.187(IE + EA) + 0.17 \quad (10.23)$$

where IE is the first ionization energy and EA is the electron affinity. It is basically the average of the first ionization energy and the electron affinity with the parameters 0.187 and 0.17 chosen to optimize the correlation with the earlier electronegativity scale of Pauling, which is based on bond energies. The Mulliken definition of χ can be understood using Figure 10.11.

Assume that an atom with a small ionization energy and electron affinity (A) forms a bond with an atom that has a larger ionization energy and electron affinity (B). Partial charge transfer from A to B lowers the energy of the system and is therefore favored over the reverse process, which increases the energy of the system. Chemical bonds between atoms with large differences in χ have a strong ionic character because significant electron transfer occurs. Chemical bonds between atoms that have similar χ values are largely covalent because the driving force for electron transfer is small, and valence electrons are shared nearly equally by the atoms.

Figure 10.12 compares values for the atomic radius, first ionization energy, and χ as a function of atomic number up to $Z = 55$. This range spans one period in which only the 1s orbital is filled, two short periods in which only s and p orbitals are filled, and two longer periods in which d orbitals are also filled. Beginning with the covalent radius, we

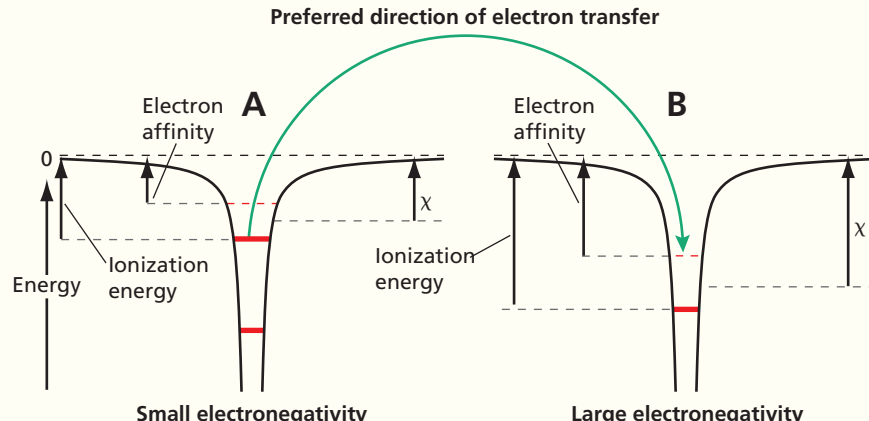
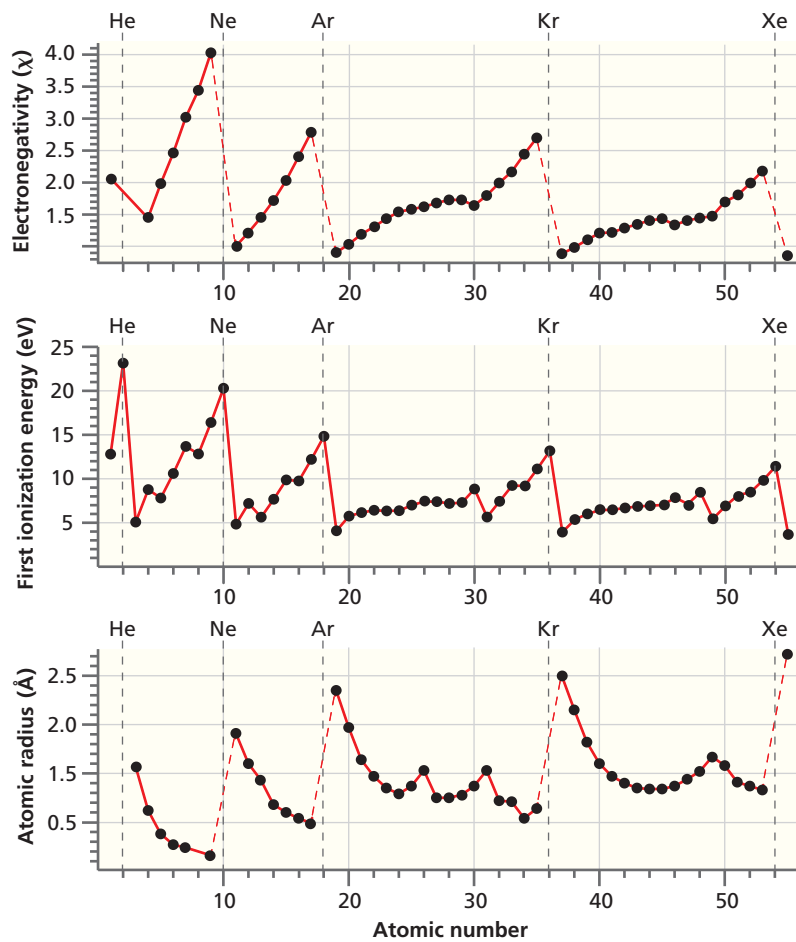


Figure 10.11

Schematic diagram relating electronegativity, ionization energy, and electron transfer. The energy of the molecule AB is lowered if electron charge is transferred from A to B rather than from B to A.

**Figure 10.12**

Electronegativity, first ionization energy, and covalent atomic radius plotted as a function of the atomic number for the first 55 elements. Dashed vertical lines mark the completion of each period.

Concept

Trends in the periodic table for electronegativity, first ionization energy, and atomic radius are determined by corresponding trends in effective nuclear charge.

see the trends predicted from calculated ζ values for the valence electrons that increase across a period and down a group as shown for the main group elements in Figure 10.13.

The radii decrease continuously across a period but increase abruptly as n increases by one in moving to the next period. Moving down a group of the periodic table, the radius increases with n because ζ increases more slowly with the nuclear charge than in moving across a period. Small radii are coupled with large ζ , and this combination leads to a large ionization energy. Therefore, changes in the ionization energy follow the opposite trend to that for the atomic radii. The ionization energy decreases moving down a column because the atomic radius increases more rapidly than ζ increases. The electronegativity follows the same pattern as the ionization energy because in general the ionization energy is larger than the electron affinity.

H 1s 1									He 1s 1.69
Li 2s 1.28	Be 2s 1.91	B 2s 2.58 2p 2.42	C 2s 3.22 2p 3.14	N 2s 3.85 2p 3.83	O 2s 4.49 2p 4.45	F 2s 5.13 2p 5.10	Ne 2s 5.76 2p 5.76		
Na 3s 2.51	Mg 3s 3.31	Al	Si 3s 4.90	P 3s 5.64	S 3s 6.37	Cl 3s 7.07	Ar 3s 7.76		
K 4s 3.50	Ca 4s 4.40	Ga 4s 7.07 4p 6.22	Ge 4s 8.04 4p 6.78	As 4s 8.94 4p 7.45	Se 4s 9.76 4p 8.29	Br 4s 10.55 4p 9.03	Kr 4s 11.32 4p 9.77		
Rb 5s 4.98	Sr 5s 6.07	In 5s 9.51 5p 8.47	Sn 5s 10.63 5p 9.10	Sb 5s 10.61 5p 9.99	Te 5s 12.54 5p 10.81	I 5s 13.40 5p 11.61	Xe 5s 14.22 5p 12.42		

Figure 10.13

Effective nuclear charges for valence shell electrons of main group elements in first five periods of periodic table.

VOCABULARY

antisymmetric wave function	electron correlation	Koopmans' theorem	Slater determinant
Aufbau principle	electron–electron repulsion term	one-electron orbital	subshell
basis functions	electron spin	orbital approximation	symmetric wave function
configuration	electronegativity	orbital energy	trial wave function
correlation energy	Hartree–Fock self-consistent field model	Pauli principle	variational method
effective nuclear charge	indistinguishability	shell	
electron affinity	ionization energy	shielding	

KEY EQUATIONS

Equation	Significance of Equation	Equation Number
$\psi(\mathbf{r}_1, \mathbf{r}_2, \dots, \mathbf{r}_n) = \phi_1(\mathbf{r}_1)\phi_2(\mathbf{r}_2) \dots \phi_n(\mathbf{r}_n)$	Orbital approximation for many-electron wave function	10.2
$\psi(1, 2, 3, \dots, n) = \frac{1}{\sqrt{n!}} \begin{vmatrix} \phi_1(1)\alpha(1) & \phi_1(1)\beta(1) & \dots & \phi_m(1)\beta(1) \\ \phi_1(2)\alpha(2) & \phi_1(2)\beta(2) & \dots & \phi_m(2)\beta(2) \\ \dots & \dots & \dots & \dots \\ \phi_1(n)\alpha(n) & \phi_1(n)\beta(n) & \dots & \phi_m(n)\beta(n) \end{vmatrix}$	Many-electron wave function expressed as Slater determinant	10.7
$E = \frac{\int \Phi^* \hat{H} \Phi \, d\tau}{\int \Phi^* \Phi \, d\tau} \geq E_0$	Variational theorem	10.10
$\left(\frac{\hbar^2}{2m} \nabla_i^2 + V_i^{eff}(r) \right) \phi_i(r) = \varepsilon_i \phi_i(r), \quad i = 1, \dots, n$	n one-electron radial Schrödinger equations to be solved in Hartree–Fock method	10.16
$\phi_j(r) = \sum_{i=1}^m c_i f_i(r)$	Expansion of orbital functions in a basis set	10.17
$\chi = 0.187(IE + EA) + 0.17$	Mulliken definition of electronegativity	10.23

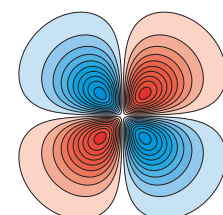
CONCEPTUAL PROBLEMS

Q10.1 Why does the effective nuclear charge ζ for the 1s orbital increase by 0.99 from oxygen to fluorine, but ζ for the 2p orbital only increases by 0.65?

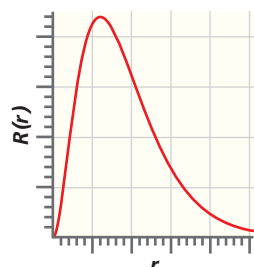
Q10.2 There are more electrons in the $n = 4$ shell than for the $n = 3$ shell in Krypton. However, the peak in the radial distribution in Figure 10.6 is smaller for the $n = 4$ shell than for the $n = 3$ shell. Explain this fact.

Q10.3 How is the effective nuclear charge related to the size of the basis set in a Hartree–Fock calculation?

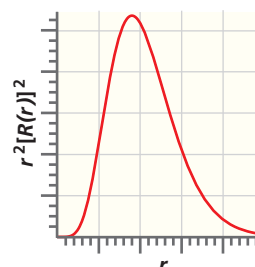
Q10.4 The angular functions, $\Theta(\theta)\Phi(\phi)$, for the one-electron Hartree–Fock orbitals are the same as those for the hydrogen atom, and the radial functions and radial probability functions are similar to those for the hydrogen atom. For this question, assume that the latter two functions are identical to those for the hydrogen atom. The following figure shows (a) a contour plot in the x – y plane, with the y axis being the vertical axis, (b) the radial function, and (c) the radial probability distribution for a one-electron orbital. Identify the orbital ($2s$, $4d_{xz}$, and so on).



(a)



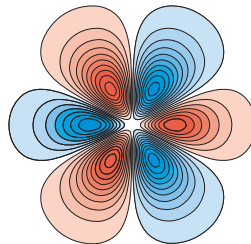
(b)



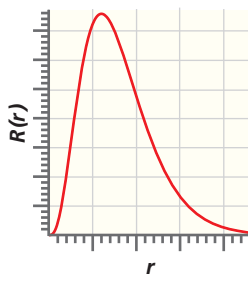
(c)

Q10.5 What is the functional dependence of the $1s$ orbital energy on Z in Figure 10.7? Check your answer against a few data points.

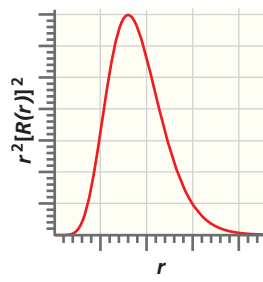
Q10.6 See Question Q10.4 for background information and an explanation of (a), (b), and (c) in the following figures. Identify the orbital.



(a)



(b)



(c)

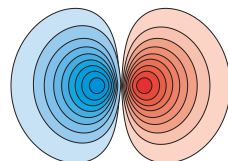
Q10.7 Explain why shielding is more effective by electrons in a shell of lower principal quantum number than by electrons having the same principal quantum number.

Q10.8 Are the elements of a basis set observable in an experiment? Explain your reasoning.

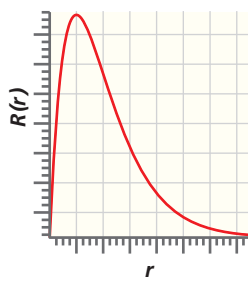
Q10.9 Show with an example that the following two formulations of the Pauli exclusion principle are equivalent:

- Wave functions that describe a many-electron system must change sign under the exchange of any two electrons.
- No two electrons may have the same values for all four quantum numbers.

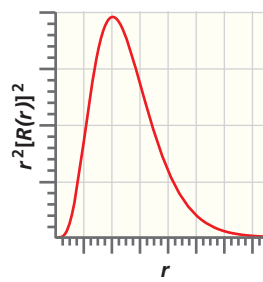
Q10.10 See Question Q10.4 for background information and an explanation of (a), (b), and (c) in the following figures. Identify the orbital.



(a)

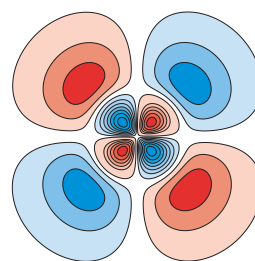


(b)

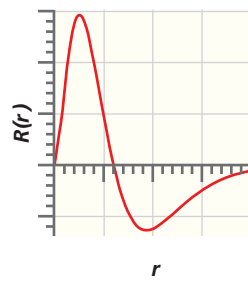


(c)

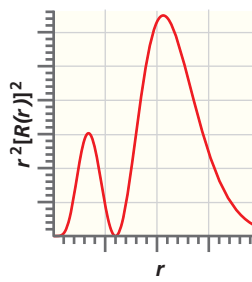
Q10.11 See Question Q10.4 for background information and an explanation of (a), (b), and (c) in the following figures. Identify the orbital.



(a)



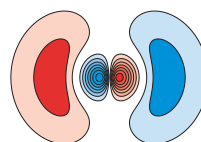
(b)



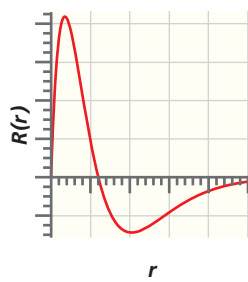
(c)

Q10.12 Why is the total energy of a many-electron atom not equal to the sum of the orbital energies for each electron?

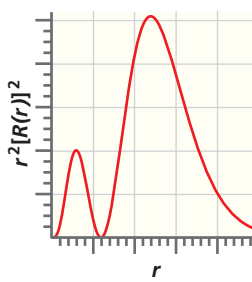
Q10.13 See Question Q10.4 for background information and an explanation of (a), (b), and (c) in the following figures. Identify the orbital.



(a)

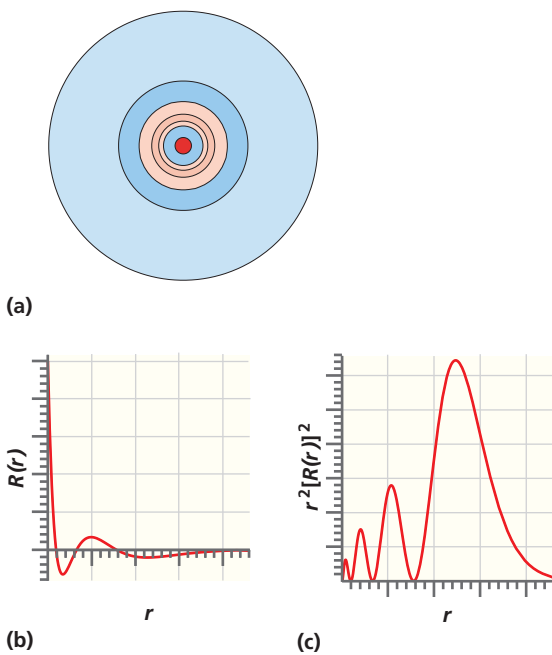


(b)

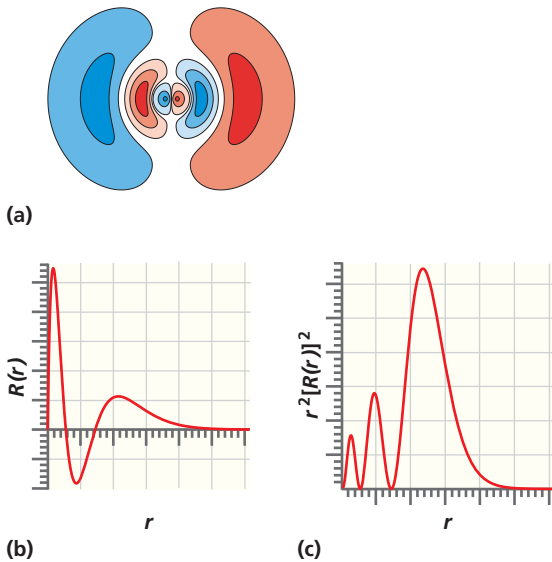


(c)

Q10.14 See Question Q10.4 for background information and an explanation of (a), (b), and (c) in the following figures. Identify the orbital.



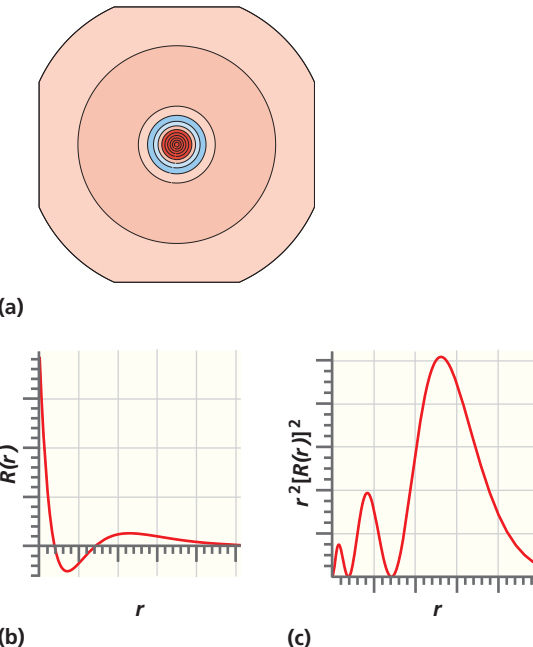
Q10.15 See Question Q10.4 for background information and an explanation of (a), (b), and (c) in the following figures. Identify the orbital.



Q10.16 Show that the Slater determinant formalism automatically incorporates the Pauli exclusion principle by evaluating the He ground state wave function of Equation (10.8), giving both electrons the same quantum numbers.

Q10.17 Is there a physical reality associated with the individual entries of a Slater determinant?

Q10.18 See Question Q10.4 for background information and an explanation of (a), (b), and (c) in the following figures. Identify the orbital.



Q10.19 How can you tell if one basis set is better than another in calculating the total energy of an atom?

Q10.20 Why is the s, p, d, \dots nomenclature derived for the H atom also valid for many-electron atoms?

Q10.21 Would the trial wave function

$$\Phi(x) = \left(\frac{x}{a} - \frac{x^3}{a^3} \right) + \alpha \left(\frac{x^5}{a^5} - \frac{1}{2} \left(\frac{x^7}{a^7} \right) \right), \quad 0 < x < a$$

have been a suitable choice for the calculations carried out in Section 10.4? Justify your answer.

NUMERICAL PROBLEMS

Section 10.1

P10.1 In this problem, you will show that the charge density of the filled $n = 2, l = 1$ subshell is spherically symmetrical. The angular distribution of the electron charge is simply the sum of the squares of the magnitude of the angular part of the wave functions for $l = 1$ and $m_l = -1, 0$, and 1.

- a. Given that the angular part of these wave functions is

$$Y_1^0(\theta, \phi) = \left(\frac{3}{4\pi} \right)^{1/2} \cos \theta$$

$$Y_1^1(\theta, \phi) = \left(\frac{3}{8\pi} \right)^{1/2} \sin \theta e^{i\phi}$$

$$Y_1^{-1}(\theta, \phi) = \left(\frac{3}{8\pi} \right)^{1/2} \sin \theta e^{-i\phi}$$

- write an expression for $|Y_1^0(\theta, \phi)|^2 + |Y_1^1(\theta, \phi)|^2 + |Y_1^{-1}(\theta, \phi)|^2$.
- b.** Show that $|Y_1^0(\theta, \phi)|^2 + |Y_1^1(\theta, \phi)|^2 + |Y_1^{-1}(\theta, \phi)|^2$ does not depend on θ and ϕ .
- c.** Why does the result in part (b) show that the charge density for the filled $n = 2, l = 1$ subshell is spherically symmetrical?

Section 10.2

P10.2 Is $\psi(1, 2) = 1s(1)\alpha(1)1s(2)\beta(2) + 1s(2)\alpha(2)1s(1)\beta(1)$ an eigenfunction of the operator $\hat{S}_z = \hat{S}_{z1} + \hat{S}_{z2}$? If so, what is its eigenvalue M_S ?

P10.3 Calculate the angles that a spin angular momentum vector for an individual electron can make with the z axis.

P10.4 In this problem, we represent the spin eigenfunctions and operators as vectors and matrices. The properties of matrices are discussed in Math Essential 10.

- a.** The spin eigenfunctions are often represented as the column vectors

$$\alpha = \begin{pmatrix} 1 \\ 0 \end{pmatrix} \quad \text{and} \quad \beta = \begin{pmatrix} 0 \\ 1 \end{pmatrix}$$

Show that α and β are orthogonal using this representation.

- b.** If the spin angular momentum operators are represented by the matrices

$$\hat{s}_x = \frac{\hbar}{2} \begin{pmatrix} 0 & 1 \\ 1 & 0 \end{pmatrix}, \hat{s}_y = \frac{\hbar}{2} \begin{pmatrix} 0 & -i \\ i & 0 \end{pmatrix}, \hat{s}_z = \frac{\hbar}{2} \begin{pmatrix} 1 & 0 \\ 0 & -1 \end{pmatrix}$$

show that the commutation rule $[\hat{s}_x, \hat{s}_y] = i\hbar \hat{s}_z$ holds.

- c.** Show that

$$\hat{s}^2 = \hat{s}_x^2 + \hat{s}_y^2 + \hat{s}_z^2 = \frac{\hbar^2}{4} \begin{pmatrix} 3 & 0 \\ 0 & 3 \end{pmatrix}$$

- d.** Show that α and β are eigenfunctions of \hat{s}_z and \hat{s}^2 . What are the eigenvalues?

- e.** Show that α and β are not eigenfunctions of \hat{s}_x and \hat{s}_y .

P10.5 The operator for the square of the total spin of two electrons is $\hat{S}_{total}^2 = (\hat{S}_1 + \hat{S}_2)^2 = \hat{S}_1^2 + \hat{S}_2^2 + 2(\hat{S}_{1x}\hat{S}_{2x} + \hat{S}_{1y}\hat{S}_{2y} + \hat{S}_{1z}\hat{S}_{2z})$. Given that

$$\begin{aligned} \hat{s}_x\alpha &= \frac{\hbar}{2}\beta, & \hat{s}_y\alpha &= \frac{i\hbar}{2}\beta, & \hat{s}_z\alpha &= \frac{\hbar}{2}\alpha, \\ \hat{s}_x\beta &= \frac{\hbar}{2}\alpha, & \hat{s}_y\beta &= -\frac{i\hbar}{2}\alpha, & \hat{s}_z\beta &= -\frac{\hbar}{2}\beta, \end{aligned}$$

show that $\alpha(1)\alpha(2)$ and $\beta(1)\beta(2)$ are eigenfunctions of the operator \hat{S}_{total}^2 . What is the eigenvalue in each case?

- P10.6** Show that the functions $[\alpha(1)\beta(2) + \beta(1)\alpha(2)]/\sqrt{2}$ and $[\alpha(1)\beta(2) - \beta(1)\alpha(2)]/\sqrt{2}$ are eigenfunctions of $\hat{S}_{total}^2 = (\hat{S}_1 + \hat{S}_2)^2 = \hat{S}_1^2 + \hat{S}_2^2 + 2(\hat{S}_{1x}\hat{S}_{2x} + \hat{S}_{1y}\hat{S}_{2y} + \hat{S}_{1z}\hat{S}_{2z})$. What is the eigenvalue in each case?

Section 10.3

P10.7 Classify the following functions as symmetric, anti-symmetric, or neither in the exchange of electrons 1 and 2:

- a.** $[1s(1)2s(2) + 2s(1)1s(2)][\alpha(1)\beta(2) - \beta(1)\alpha(2)]$
- b.** $[1s(1)2s(2) + 2s(1)1s(2)]\alpha(1)\alpha(2)$

- c.** $[1s(1)2s(2) + 2s(1)1s(2)][\alpha(1)\beta(2) + \beta(1)\alpha(2)]$
- d.** $[1s(1)2s(2) - 2s(1)1s(2)][\alpha(1)\beta(2) + \beta(1)\alpha(2)]$
- e.** $[1s(1)2s(2) + 2s(1)1s(2)][\alpha(1)\beta(2) - \beta(1)\alpha(2) + \alpha(1)\alpha(2)]$

P10.8 Write the Slater determinant for the ground state configuration of Be.

Section 10.4

P10.9 In this problem, you will prove that the ground state energy for a system obtained using the variational method is greater than the true energy.

- a.** The approximate wave function Φ can be expanded in the true (but unknown) eigenfunctions ψ_n of the total energy operator in the form $\Phi = \sum_n c_n \psi_n$. Show that by substituting $\Phi = \sum_n c_n \psi_n$ in the equation

$$E = \frac{\int \Phi^* \hat{H} \Phi d\tau}{\int \Phi^* \Phi d\tau}$$

you obtain the result

$$E = \frac{\sum_n \sum_m \int (c_n^* \psi_n^*) \hat{H} (c_m \psi_m) d\tau}{\sum_n \sum_m \int (c_n^* \psi_n^*)(c_m \psi_m) d\tau}$$

- b.** Because the ψ_n are eigenfunctions of \hat{H} , they are orthonormal and $\hat{H}\psi_n = E_n\psi_n$. Show that this information allows us to simplify the expression for D from part (a) to

$$E = \frac{\sum_m E_m c_m^* c_m}{\sum_m c_m^* c_m}$$

- c.** Arrange the terms in the summation such that the first energy is the true ground state energy E_0 and the energy increases with the summation index m . Why can you conclude that $E - E_0 \geq 0$?

P10.10 In this problem, you will use the variational method to find the optimal $1s$ wave function for the hydrogen atom starting from the trial function $\Phi(r) = e^{-\alpha r}$ with α as the variational parameter. You will minimize

$$E(\alpha) = \frac{\int \Phi^* \hat{H} \Phi d\tau}{\int \Phi^* \Phi d\tau}$$

with respect to α .

- a.** Show that

$$\begin{aligned} \hat{H}\Phi &= -\frac{\hbar^2}{2m_e} \frac{1}{r^2} \frac{\partial}{\partial r} \left(r^2 \frac{\partial \Phi(r)}{\partial r} \right) - \frac{e^2}{4\pi\epsilon_0 r} \Phi(r) \\ &= \frac{\alpha\hbar^2}{2m_e r^2} (2r - \alpha r^2) e^{-\alpha r} - \frac{e^2}{4\pi\epsilon_0 r} e^{-\alpha r} \end{aligned}$$

- b.** Obtain the result $\int \Phi^* \hat{H} \Phi d\tau = 4\pi \int_0^\infty r^2 \Phi^* \hat{H} \Phi dr = \pi \hbar^2 / 2m_e \alpha - e^2 / 4\epsilon_0 \alpha^2$ using the standard integrals in Math Essential 2.
- c.** Show that $\int \Phi^* \Phi d\tau = 4\pi \int_0^\infty r^2 \Phi^* \Phi dr = \pi / \alpha^3$ using the standard integrals in Math Essential 2.
- d.** You now have the result $E(\alpha) = \hbar^2 \alpha^2 / 2m_e - e^2 \alpha / 4\pi \epsilon_0$. Minimize this function with respect to α and obtain the optimal value of α .
- e.** Is $E(\alpha_{optimal})$ equal to or greater than the true energy? Why?

P10.11 The exact energy of a ground state He atom is 79.01 eV. Calculate the correlation energy and the ratio of the correlation energy to the total energy for He using the results in Table 10.1.

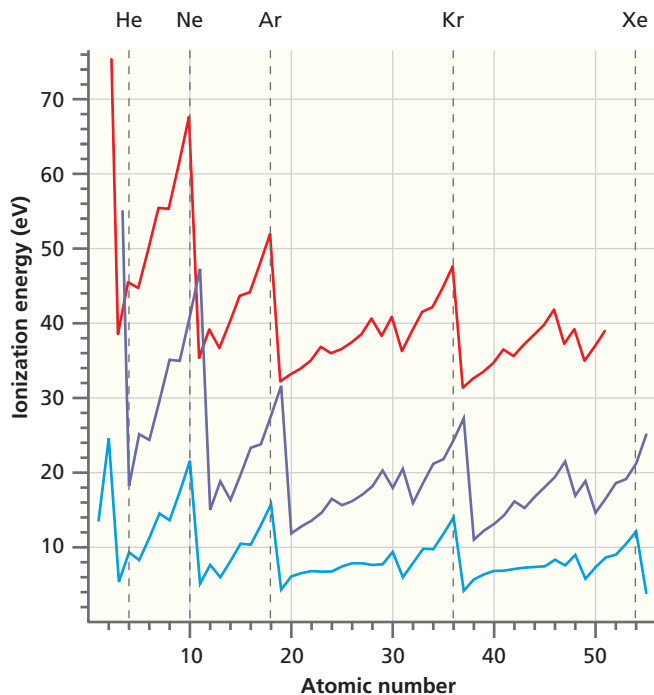
Section 10.5

P10.12 The ground state wave function of Li^{2+} is $\pi^{-1/2} (Z/a_0)^{3/2} e^{-Zr/a_0}$, where Z is the nuclear charge. Calculate the expectation value of the potential energy for Li^{2+} .

P10.13 Calculate the position of the maximum in the radial distribution function for Li^{2+} in its ground state using the wave function in P10.12.

Section 10.6

P10.14 You have commissioned a measurement of the second ionization energy from two independent research teams. You find that they do not agree and decide to plot the data together with known values of the first ionization energy. The results are shown here:



The lowest curve is for the first ionization energy, and the upper two curves are the results for the second ionization energy from the two research teams. The uppermost curve has been shifted vertically to avoid an overlap with the other new data set. On the basis of your knowledge of the periodic table, you suddenly realize (1) which of the two sets of data is correct and (2) the error that one of the teams of researchers made. Which data set is correct? Explain your reasoning.

P10.15–P10.20 refer to the first ionization energies and electron affinities of the first 11 elements (units of eV) shown below.

Element	H	He	Li	Be	B	C	N	O	F	Ne	Na
First ionization energy	13.6	24.6	5.4	9.3	8.3	11.3	14.5	13.6	17.4	21.6	5.1
Electron affinity	0.8	<0	0.6	<0	0.3	1.3	-0.1	1.5	3.4	<0	0.5

P10.15 Why is the magnitude of the electron affinity for a given element smaller than the magnitude of the first ionization energy?

P10.16 The electron affinities of He, Be, and Ne are negative, which means that the negative ion is less stable than the neutral atom. Give an explanation of why this is so for these three elements.

P10.17 Are the effective nuclear charges listed in Figure 10.13 helpful in explaining the trend in the first ionization energy with increasing atomic number? Explain your answer.

P10.18 Are the effective nuclear charges listed in Figure 10.13 helpful in explaining the trend in the electron affinity with increasing atomic number? Explain your answer.

P10.19 Explain why the electron affinity of N is negative.

P10.20 Explain why the first ionization energy and electron affinity for F are larger than for O.

COMPUTATIONAL PROBLEMS

More detailed instructions on carrying out these calculations using Spartan Physical Chemistry are found at: <https://www.pearsonhighered.com/chemistryresources/>. Gaussian basis sets are discussed in Chapter 15.

C10.1 Calculate the total energy and 1s orbital energy for Ne using the Hartree–Fock method and the (a) 3-21G, (b) 6-31G*, and (c) 6-311+G** basis sets. Note the number of basis functions used in the calculations. Calculate the relative error of your result compared with the Hartree–Fock limit of -128.854705 hartree for each basis set. Rank the basis sets in terms of their approach to the Hartree–Fock limit for the total energy. (Note: A hartree is a unit of energy equal to 27.211 eV.)

C10.2 Calculate the total energy and 4s orbital energy for K using the Hartree–Fock method and the (a) 3-21G and (b) 6-31G* basis sets. Note the number of basis functions used in the calculations. Calculate the percentage deviation from the Hartree–Fock limits, which are -16245.7 eV for the total energy and -3.996 eV for the 4s orbital energy. Rank the basis sets in terms of their approach to the Hartree–Fock limit for the total energy. What percentage error in the Hartree–Fock limit to the total energy corresponds to a typical reaction enthalpy change of $100.$ kJ mol $^{-1}$?

C10.3 Calculate the ionization energy for (a) Li, (b) F, (c) S, (d) Cl, and (e) Ne using the Hartree–Fock method and the 6-311+G** basis set. Carry out the calculation in two different ways: (a) Use Koopmans' theorem and (b) compare the total energy of the neutral and singly ionized atom. Compare your answers with literature values.

C10.4 Calculate the electron affinity for (a) Li, (b) F, (c) S, and (d) Cl using the Hartree–Fock method and the 6-311+G** basis set by comparing the total energy of the neutral and singly ionized atom. Compare your answers with literature values.

C10.5 Using your results from C10.3 and C10.4, calculate the Mulliken electronegativity for (a) Li, (b) F, (c) S, and (d) Cl. Compare your results with literature values.

C10.6 To assess the accuracy of the Hartree–Fock method for calculating energy changes in reactions, calculate the total energy change for the reaction $\text{CH}_3\text{OH} \rightarrow \text{CH}_3 + \text{OH}$ by calculating the difference in the total energy of reactants and products (ΔU) using the Hartree–Fock method and the 6-31G* basis set. Compare your result with a calculation using the B3LYP method and the same basis set and with the experimental value of $410.$ kJ mol $^{-1}$. As discussed in Chapter 15, the B3LYP method takes electron correlation into account. What percentage error in the Hartree–Fock total energy for CH_3OH would account for the difference between the calculated and experimental value of (ΔU)?

FURTHER READING

Keepots, D. "Application of the Variational Method to the Particle-in-the-Box Problem." *Journal of Chemical Education* 66 (1989): 314–318.

Sanderson, R. "Principles of Electronegativity Part I. General Nature." *Journal of Chemical Education* 65 (1988): 112–118.

Snow, R., and Bills, J. "The Pauli Principle and Electronic Repulsion in Helium." *Journal of Chemical Education* 51 (1974): 585–586.

Vanquickenbourne, L. G., et al. "Transition Metals and the Aufbau Principle." *Journal of Chemical Education* 71 (1994): 469–471.

Waldron, K., Fehringer, E., Streeb, A., Trosky, J., and Pearson, J. "Screening Percentages Based on Slater Effective Nuclear Charge as a Versatile Tool for Teaching Periodic Trends." *Journal of Chemical Education* 78 (2001): 635–639.

This page intentionally left blank

Quantum States for Many-Electron Atoms and Atomic Spectroscopy

WHY is this material important?

In considering atoms with more than one electron, the indistinguishability of electrons, the electron spin, and the interaction between orbital and spin magnetic moments must be addressed. Taking these issues into consideration leads to a new set of quantum numbers for the states of many-electron atoms. Atomic spectroscopic techniques yield information on the discrete energy levels of atoms and provide the basis for understanding the coupling of individual spin and orbital angular momentum vectors in many-electron atoms.

WHAT are the most important concepts and results?

The indistinguishability of electrons and the electron spin gives rise to the grouping of the hydrogen atom states based on n , l , m_l , and m_s into levels and terms. Because the discrete energy levels for atoms differ, atomic spectroscopic techniques provide information on the identity and concentration of atoms in a sample. For this reason, atomic spectroscopy is widely used in analytical chemistry. The discrete atomic energy levels can be used to construct lasers that provide an intense and coherent source of monochromatic radiation. Atomic spectroscopic techniques can also provide elemental identification specific to the first few atomic layers of a solid, which is crucial in understanding heterogeneous chemical reactions.

WHAT would be helpful for you to review for this chapter?

It would be helpful to review the material in Chapter 7 on angular momentum.

11.1 GOOD QUANTUM NUMBERS, TERMS, LEVELS, AND STATES

How are quantum numbers assigned to many-electron atoms? The quantum numbers n , l , m_l , and m_s that were used to characterize total energy eigenfunctions for the H atom are associated with the eigenvalues of the operators \hat{H} , \hat{l}^2 , \hat{l}_z , and \hat{s}_z . It can be shown that the eigenvalues of a given operator are independent of time only if the operator commutes with \hat{H} . The H atom quantum numbers are **good quantum numbers** because the set of operators \hat{l}^2 , \hat{l}_z , \hat{s}^2 , and \hat{s}_z commutes with the total energy operator \hat{H} . Operators that generate good quantum numbers are of particular interest to us in obtaining the values of time-independent observables for atoms and molecules.

However, n , l , m_l , and m_s are not good quantum numbers for all many-electron atoms or ions. Therefore, another set of quantum numbers whose corresponding

- 11.1 Good Quantum Numbers, Terms, Levels, and States
- 11.2 The Energy of a Configuration Depends on Both Orbital and Spin Angular Momentum
- 11.3 Spin–Orbit Coupling Splits a Term into Levels
- 11.4 The Essentials of Atomic Spectroscopy
- 11.5 Analytical Techniques Based on Atomic Spectroscopy
- 11.6 The Doppler Effect
- 11.7 The Helium–Neon Laser
- 11.8 Auger Electron Spectroscopy and X-Ray Photoelectron Spectroscopy

Concept

n , l , m_l , and m_s are not good quantum numbers for many-electron atoms.

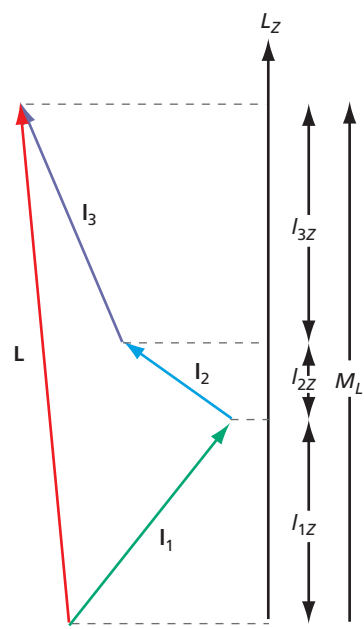


Figure 11.1

Depiction of the three classical angular momentum vectors and their sum.

Whereas it is necessary to know the direction of each vector to calculate \mathbf{L} , this is not necessary to calculate M_L . As discussed in Section 7.8, each angular momentum vector would need to be represented by a cone to be consistent with the commutation relations among \hat{l}_x , \hat{l}_y , and \hat{l}_z .

operators do commute with \hat{H} must be found. Our primary focus is developing a model that adequately describes atoms with $Z < 40$; in Section 11.3 we will explain the reason for this atomic number restriction and also extend this model to atoms for which $Z > 40$. Good quantum numbers are generated by forming vector sums of the electron orbital and spin angular momenta separately, \mathbf{L} and \mathbf{S} , which have the z components M_L and M_S , respectively. Only electrons in unfilled subshells contribute to these sums:

$$\mathbf{L} = \sum_i \mathbf{l}_i, \quad \mathbf{S} = \sum_i \mathbf{s}_i \quad (11.1)$$

where the summation is over the electrons in unfilled subshells. As discussed in Chapter 7 for \mathbf{l} , the magnitudes of \mathbf{L} and \mathbf{S} are $\sqrt{L(L+1)\hbar}$ and $\sqrt{S(S+1)\hbar}$, respectively.

Figure 11.1 illustrates vector addition in classical physics. Note that in order to carry out the vector summations, all three vector components must be known. However, it follows from the commutation rules between \hat{l}_x , \hat{l}_y , and \hat{l}_z [see Equation (7.57)] that only the length of an angular momentum vector and one of its components (which we choose to be on the z axis) can be known in quantum mechanics. This means that the summation shown in Figure 11.1 cannot actually be carried out. By contrast, it is easy to form the sum M_L because the known components l_{zi} add as scalars, $M_L = \sum_i l_{zi}$. As we will see later, it is sufficient to know M_L and M_S in order to determine the good quantum numbers L and S .

We next discuss many-electron atom operators \hat{L}^2 , \hat{L}_z , \hat{S}^2 , and \hat{S}_z , which are formed from one-electron operators. These operators commute with \hat{H} for a many-electron atom with $Z < 40$. The capitalized form of the operators refers to the resultant for all electrons in unfilled subshells of the atom. These operators are defined by

$$\begin{aligned} \hat{S}_z &= \sum_i \hat{s}_{z,i} \quad \text{and} \quad \hat{S}^2 = \left(\sum_i \hat{s}_i \right)^2 \\ \hat{L}_z &= \sum_i \hat{l}_{z,i} \quad \text{and} \quad \hat{L}^2 = \left(\sum_i \hat{l}_i \right)^2 \end{aligned} \quad (11.2)$$

in which the index i refers to the individual electrons in unfilled subshells. The good quantum numbers for many-electron atoms for $Z < 40$ are L , S , M_L , and M_S .

As can be inferred from Equation (11.2), the calculation for \hat{S}^2 is somewhat complex and is not discussed here. By contrast, \hat{S}_z can be calculated easily, as shown in Example Problem 11.1.

Concept

It is sufficient to know M_L and M_S in order to determine the good quantum numbers L and S .

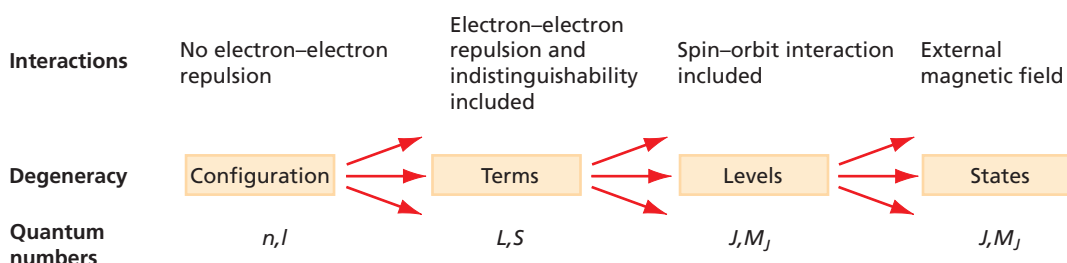
EXAMPLE PROBLEM 11.1

Is $\psi(1, 2) = 1s(1)\alpha(1)1s(2)\beta(2) - 1s(2)\alpha(2)1s(1)\beta(1)$ an eigenfunction of the operator \hat{S}_z ? If so, what is its eigenvalue M_S ?

Solution

$$\begin{aligned} \hat{S}_z &= \hat{s}_z(1) + \hat{s}_z(2) \quad \text{where } \hat{s}_z(i) \text{ acts only on electron } i \\ \hat{S}_z\psi(1, 2) &= (\hat{s}_z(1) + \hat{s}_z(2))\psi(1, 2) \\ &= [\hat{s}_z(1) + \hat{s}_z(2)][1s(1)\alpha(1)1s(2)\beta(2) - 1s(2)\alpha(2)1s(1)\beta(1)] \\ &= (\hat{s}_z(1))[1s(1)\alpha(1)1s(2)\beta(2) - 1s(2)\alpha(2)1s(1)\beta(1)] \\ &\quad + (\hat{s}_z(2))[1s(1)\alpha(1)1s(2)\beta(2) - 1s(2)\alpha(2)1s(1)\beta(1)] \\ &= \frac{\hbar}{2}[1s(1)\alpha(1)1s(2)\beta(2)] + \frac{\hbar}{2}[1s(2)\alpha(2)1s(1)\beta(1)] \\ &\quad - \frac{\hbar}{2}[1s(1)\alpha(1)1s(2)\beta(2)] - \frac{\hbar}{2}[1s(2)\alpha(2)1s(1)\beta(1)] \\ &= \left(\frac{\hbar}{2} - \frac{\hbar}{2}\right)[1s(1)\alpha(1)1s(2)\beta(2) - 1s(2)\alpha(2)1s(1)\beta(1)] = 0 \times \psi(1, 2) \end{aligned}$$

This result shows that the wave function is an eigenfunction of \hat{S}_z with $M_S = 0$.



The occupied orbitals of an atom are specified in a **configuration**. For example, the electron configuration of neon is $1s^2 2s^2 2p^6$. Although a configuration is a very useful way to describe the electronic structure of atoms, it does not completely specify the quantum state of a many-electron atom because it is based on the one-electron quantum numbers n and l . Taking electron–electron repulsion into account and invoking the Pauli exclusion principle splits a configuration into terms, as shown in Figure 11.2. A **term** is a group of states that has the same L and S values. Describing the states of many-electron atoms by terms is appropriate for atoms with a nuclear charge of $Z < 40$ because L and S are “good enough” quantum numbers for these atoms; that is, the difference in energy between quantum states in a term is very small compared to the energy separation of the terms. Levels will be discussed in Section 11.3.

Figure 11.2

Relationship of configurations, terms, levels, and states. The top row of the diagram indicates degree of approximation and type of interaction; the second row shows the group of states that are degenerate in energy; and the bottom row indicates the good quantum numbers in each level of approximation.

Concept

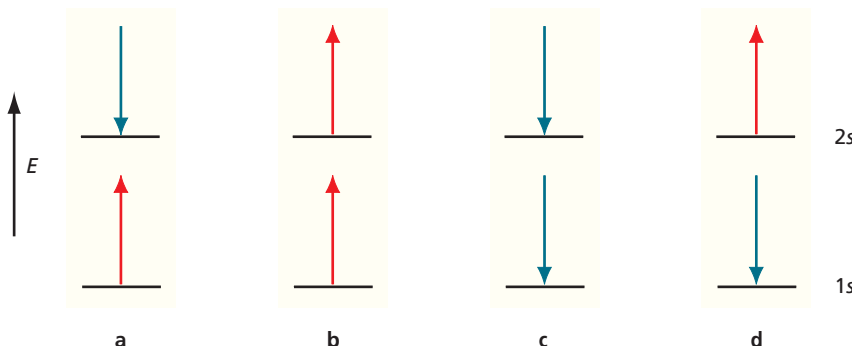
A configuration does not completely specify the quantum state of a many-electron atom.

11.2 THE ENERGY OF A CONFIGURATION DEPENDS ON BOTH ORBITAL AND SPIN ANGULAR MOMENTUM

The energy of an atom depends on the values of the quantum numbers S and L . If an atom has at least two unpaired electrons (electrons in orbitals that are singly occupied), then the atom can have more than one value for S . Consider the excited state of He with the configuration $1s^1 2s^1$. Because both electrons have $l = 0$, $|\mathbf{L}| = 0$. We next show that there are two different values of $|\mathbf{S}|$ consistent with the $1s^1 2s^1$ configuration, and we formulate antisymmetric wave functions for each value of S .

Recall that an individual electron can be characterized by a spin angular momentum vector \mathbf{s} of magnitude $|\mathbf{s}| = \sqrt{s(s+1)}\hbar$, where the quantum number s can only have the single value $s = 1/2$. The vector \mathbf{s} has $2s + 1 = 2$ possible orientations with the z component $s_z = \pm\hbar/2$. Therefore, we say that two spins can only be **parallel**, $\alpha(1)\alpha(2)$ and $\beta(1)\beta(2)$, or **antiparallel**, $\alpha(1)\beta(2)$ and $\beta(1)\alpha(2)$.

Figure 11.3 shows that adding the scalar components m_s for the two electrons in each of the four possible combinations gives the values $M_S = m_{s1} + m_{s2} = 0$ twice, as well as $M_S = m_{s1} + m_{s2} = +1$ and -1 . Surprisingly, the possible values of S for He in the $1s^1 2s^1$ configuration can be deduced using only this information about M_S . We know that $S \geq |M_S|$ because the spin angular momentum follows the same rules as the orbital angular momentum. Because there is no value for $M_S > 1$ among these four possible spin combinations, $M_S = \pm 1$ is only consistent with $S = 1$. Because M_S

**Figure 11.3**

Possible alignment of spins in the He configuration $1s^1 2s^1$. An upward-pointing arrow corresponds to $m_s = +1/2$ and a downward-pointing arrow corresponds to $m_s = -1/2$.

Concept

Singlet and triplet states are associated with paired and unpaired electrons respectively.

takes on all integral values between $+S$ and $-S$, the $S = 1$ group must include $M_S = 0, +1$, and -1 . This accounts for three of the four values of M_S listed earlier. The one remaining combination has $M_S = 0$, which is only consistent with $S = 0$.

We have just shown that three of the four possible spin combinations are characterized by $S = 1$ with $M_S = \pm 1$ and 0 and that the fourth has $S = 0$ with $M_S = 0$. Because of the number of possible M_S values, the $S = 0$ spin combination is called a **singlet** and the $S = 1$ spin combination is called a **triplet**. Singlet and triplet states are encountered frequently in chemistry and are associated with **paired** and **unpaired electrons**, respectively.

Now that we know the S values for the four spin combinations, we can write antisymmetric wave functions for He $1s^12s^1$ that are eigenfunctions of \hat{S}^2 with $S = 0$ and $S = 1$.

$$\begin{aligned} S = 0 \quad \psi_{\text{singlet}} &= \frac{1}{\sqrt{2}} [1s(1)2s(2) + 2s(1)1s(2)] \frac{1}{\sqrt{2}} [\alpha(1)\beta(2) - \beta(1)\alpha(2)] \\ S = 1 \quad \psi_{\text{triplet}} &= \frac{1}{\sqrt{2}} [1s(1)2s(2) - 2s(1)1s(2)] \times \\ &\left. \begin{cases} \alpha(1)\alpha(2) & \text{or} \\ \beta(1)\beta(2) & \text{or} \\ \frac{1}{\sqrt{2}} [\alpha(1)\beta(2) + \beta(1)\alpha(2)] \end{cases} \right\} \end{aligned} \quad (11.3)$$

For the wave functions that describe the three different states for the triplet, $S = 1$, $|\mathbf{S}| = \sqrt{2}\hbar$, and (from top to bottom) $M_S = 1, -1$, and 0. The singlet consists of a single state with $S = 0$ and $M_S = 0$. Note that the antisymmetry of the total wave function is achieved by making the spatial part symmetric and the spin part antisymmetric for the singlet wave function and the other way around for the triplet wave functions.

The vector model of angular momentum introduced in Chapter 7 can be used to depict singlet and triplet states, as shown in Figure 11.4. Although the individual spins cannot be located on the cones, their motion is coupled so that $M_S = 0$ and $S = 0$ for the singlet state. For a triplet state, there is a similar coordinated precession, but in this case the vectors add rather than cancel and $S = 1$. Because $S = 1$, there must be three different cones corresponding to $M_S = -1, 0$, and 1.

We next make it plausible that the total energy for many-electron atoms also depends on $|\mathbf{L}|$. In the Hartree–Fock self-consistent field method, the actual positions of the electrons are approximated by their average positions. This results in a spherically symmetric charge distribution for closed subshells. As discussed in Chapter 10, this approximation greatly simplifies the calculations of orbital energies and wave functions for many-electron atoms. However, by looking at the angular part of the hydrogen atom wave functions (Figure 9.7), we can see that if l is not zero (for example,

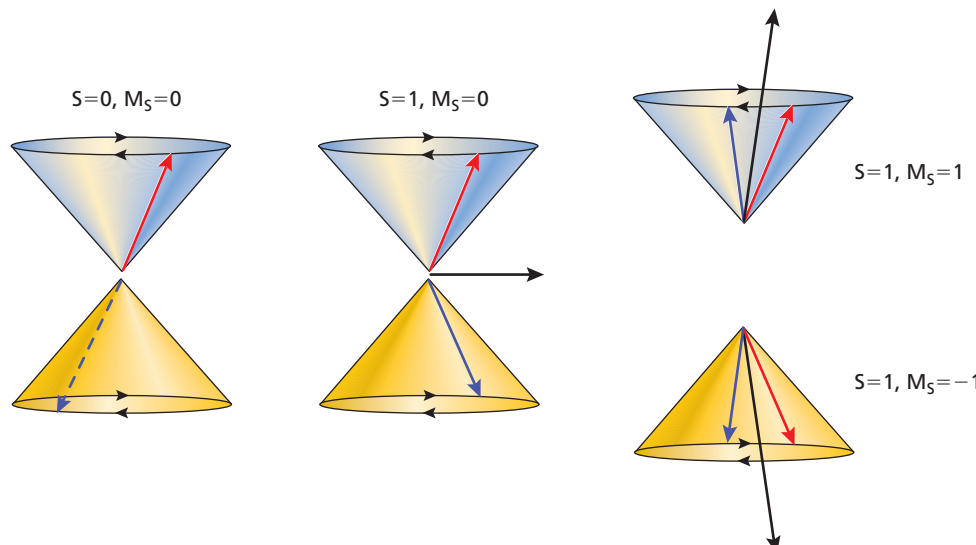


Figure 11.4

Vector model of the singlet and triplet states. The individual spin angular momentum vectors (red and blue arrows) and their vector sum \mathbf{S} (black arrows) are shown for the triplet states. For the singlet state (left image), $|\mathbf{S}| = 0$ and $M_S = 0$. The dashed arrow in the left image indicates that the vector on the yellow cone is on the opposite side of the cone from the vector on the purple cone.

the $2p$ electrons in carbon), the electron probability distribution is not spherically symmetrical. Electrons in states characterized by $l = 1$ that have different values of m_l ($-1, 0$, or $+1$) have different orientations of the same spatial probability distributions. Two such electrons, therefore, have different repulsive interactions depending on their m_l values. By looking at Figure 7.13, we can see that two electrons in the p_x orbital repel each other more strongly than if one of the electrons is in the p_x orbital and the other is in the p_z or p_y orbital.

Because the m_s value constrains the choices for m_l for electrons in the same orbital through the Pauli principle, the repulsive interactions between these electrons are determined by both l and s . Recall that a configuration specifies only the n and l values for the electrons and not the m_l and m_s values. For many atoms, the configuration does not completely define the quantum state. When is this the case, and how does the angular momentum affect the orbital energies of the atom? As you will verify in the end-of-chapter problems, only partially filled subshells contribute to \mathbf{L} and \mathbf{S} . Under what conditions do the values of m_l and m_s for a given configuration lead to different spatial distributions of electrons and therefore to a different electron–electron repulsion? Different spatial distributions occur for cases in which there are at least two electrons in the valence shell and in which multiple possible choices are available in m_l and m_s for these electrons, consistent with the Pauli principle and the configuration. Different spatial distributions do not arise for the ground states of rare gases, alkali metals, alkaline earth metals, group III, and halogens. Atoms in all of these groups have either a filled shell or subshell or only one electron or one electron fewer than the maximum number of electrons in a subshell. None of these atoms has more than one unpaired electron in its ground state, and all are uniquely described by their configuration. However, the ground states for carbon, nitrogen, and oxygen are not completely described by a configuration. Several quantum states, all of which are consistent with the configuration, have significantly different values for the total energy as well as different chemical reactivities.

For atoms with $Z < 40$, the total energy is essentially independent of M_S and M_L . Therefore, a group of different quantum states that have the same values for L and S but different values of M_L and M_S is degenerate in energy. Such a group of states is called a term, and the L and S values for the term are indicated by the **term symbol** $(2S+1)L$. Terms with $L = 0, 1, 2, 3, 4, \dots$ are given the symbols S, P, D, F, G, \dots , respectively. Because there are $2L + 1$ quantum states (different M_L values) for a given value of L and the $2S + 1$ states (different M_S values) for a given value of S , a term will include $(2L + 1)(2S + 1)$ quantum states, all of which have the same energy to a good approximation. Therefore, the **degeneracy of a term** is $(2L + 1)(2S + 1)$. The superscript $2S + 1$ is called the **multiplicity**, and the words *singlet* and *triplet* refer to $2S + 1 = 1$ and 3, respectively. Extending this formalism, $2S + 1 = 2$ and 4 are associated with *doublets* and *quartets*. For a filled subshell or shell,

$$M_L = \sum_i m_{li} = M_S = \sum_i m_{si} = 0 \quad (11.4)$$

and the combination $M_L = 0$ and $M_S = 0$ is only consistent with $L = 0$ and $S = 0$. Therefore, all atoms with no unpaired electrons that have either a filled valence subshell or shell are characterized by the term 1S . Note that the term symbols do not depend on the principal quantum number of the valence shell. Carbon, which has the $1s^22s^22p^2$ configuration, has the same set of terms as silicon, which has the $1s^22s^22p^63s^23p^2$ configuration.

How are terms generated for a given configuration? The simplest case is for a configuration with singly occupied subshells. An example is C $1s^22s^22p^13d^1$, in which an electron has been promoted from the $2p$ to the $3d$ orbital. Only the $2p$ and $3d$ electrons need to be considered because the other electrons are in filled subshells. The possible values of L and S are given by the **Clebsch–Gordan series**. When applied to the two-electron case, allowed L values are given by $|l_1 + l_2|, l_1 + l_2 - 1, l_1 + l_2 - 2, \dots, |l_1 - l_2|$. Using the same rule, the allowed S values are $s_1 - s_2$ and $s_1 + s_2$. For our example, $l_1 = 1, l_2 = 2$, and $s_1 = s_2 = 1/2$. Therefore, L can have the values 3, 2, and 1, and S can have the values 1 and 0. We conclude that the $1s^22s^22p^13d^1$ configuration generates $^3F, ^3D, ^3P, ^3F, ^1D$, and 1P terms. The degeneracy

Concept

The degeneracy of a term is $(2L + 1)(2S + 1)$.

of these terms, $(2L + 1)(2S + 1)$, is 21, 15, 9, 7, 5, and 3, respectively, which corresponds to a total of 60 quantum states. Looking back at the configuration, the $2p$ electron can have $m_l = \pm 1$ and 0 and $m_s = \pm 1/2$. This gives six possible combinations of m_l and m_s . The $3d$ electron can have $m_l = \pm 1, \pm 2$, and 0, and $m_s = \pm 1/2$. This gives 10 possible combinations of m_l and m_s . Because any combination for the $2p$ electron can be used with any combination of the $3d$ electron, there are a total of $6 \times 10 = 60$ combinations of m_l and m_s consistent with the $1s^2 2s^2 2p^1 3d^1$ configuration. These combinations generate the 60 states that belong to the 3F , 3D , 3P , 1F , 1D , and 1P terms.

The same method can be extended to more than two electrons by first calculating L and S for two electrons and adding in the remaining electrons one by one. For example, consider the L values associated with the C $1s^2 2s^1 2p^1 3p^1 3d^1$ configuration. Combining the $2s$ and $2p$ electrons gives only $L = 1$. Combining this L value with the $3p$ electron gives 2, 1, and 0. Combining these values with the $3d$ electron gives possible L values of 4, 3, 2, 1, and 0. The maximum value of S is $n/2$, where n is the number of different singly filled subshells. The minimum value of S is 0 if n is even and $1/2$ if n is odd. For our example, the possible S values are 2, 1, and 0. Which terms are generated by these values of L and S ?

Assigning terms to a configuration is more complicated if subshells contain more than one electron because the Pauli exclusion principle must be obeyed. To illustrate such a case, consider the ground state of carbon, which has the configuration $1s^2 2s^2 2p^2$. We need only consider the $2p$ electrons. Because m_l can have any of the values $-1, 0$, or $+1$, and m_s can have the values $+1/2$ and $-1/2$ for p electrons, six combinations of the quantum numbers m_s and m_l for the first electron are possible. The second electron will have one fewer possible combinations because of the Pauli principle. This appears to give a total of $6 \times 5 = 30$ combinations of quantum numbers for the two electrons. However, this assumes that the electrons are distinguishable, which overcounts the possible number of combinations by a factor of 2. Taking this into account, there are 15 possible quantum states of the carbon atom consistent with the configuration $1s^2 2s^2 2p^2$, which are shown schematically in Figure 11.5.

To determine the possible terms consistent with a p^2 configuration, it is convenient to display the information in Figure 11.5 in tabular form, as shown in Table 11.1. In setting up Table 11.1, we have relied only on the z components m_{si} and m_{li} . Using these components, we can easily calculate $M_S = \sum_i m_{si}$ and $M_L = \sum_i m_{li}$ because no vector addition is involved. To derive terms from this table, it is necessary to determine what values for L and S are consistent with the tabulated M_S and M_L values. How can this be done knowing only M_L and M_S ? This determination of terms requires careful bookkeeping. We first determine which values of L and S are consistent with the entries for M_L and M_S in the table, given that $-S \leq M_S \leq +S$ and $-L \leq M_L \leq +L$. A good way to start is to first look at the largest value for $|M_L|$.

The top and bottom entries in the table have the largest M_L values of -2 and $+2$, respectively. They must belong to a term with $L = 2$ (a D term) because $|M_L|$ can be no greater than L . All states with M_L values of -2 and $+2$ have $M_S = 0$ because the set of quantum numbers for each electron must differ. Stated differently, because $m_{l1} = m_{l2}$, $m_{s1} \neq m_{s2}$, and therefore $M_S = 0$. We conclude that $S = 0$, $2S + 1 = 1$,

m_l												
+1												
0												
-1												
M_S	0	0	0	-1	1	-1	0	0	0	1	-1	0
M_L	-2	-1	-1	-1	-1	0	0	0	0	0	1	1

Figure 11.5

Different ways in which two electrons can be placed in p orbitals. Upward- and downward-pointing arrows correspond to $m_s = +1/2$ and $m_s = -1/2$, respectively, and M_S and M_L are the scalar sums of m_s and m_l , respectively.

TABLE 11.1 States and Terms for the np^2 Configuration

m_{l1}	m_{l2}	$M_L = m_{l1} + m_{l2}$	m_{s1}	m_{s2}	$M_s = m_{s1} + m_{s2}$	Term
-1	-1	-2	1/2	-1/2	0	1D
0	-1	-1	$\begin{cases} -1/2 \\ -1/2 \\ 1/2 \\ 1/2 \end{cases}$	$\begin{cases} -1/2 \\ 1/2 \\ -1/2 \\ 1/2 \end{cases}$	$\begin{cases} -1 \\ 0 \\ 0 \\ 1 \end{cases}$	3P , 1D , 3P
0	0	0	$\begin{cases} 1/2 \\ -1/2 \\ 1/2 \\ -1/2 \\ 1/2 \end{cases}$	$\begin{cases} -1/2 \\ 1/2 \\ -1/2 \\ -1/2 \\ 1/2 \end{cases}$	$\begin{cases} 0 \\ 0 \\ 0 \\ -1 \\ 1 \end{cases}$	1D , 3P , 1S
1	-1	0	$\begin{cases} -1/2 \\ 1/2 \\ 1/2 \\ -1/2 \\ 1/2 \end{cases}$	$\begin{cases} -1/2 \\ 1/2 \\ -1/2 \\ -1/2 \\ 1/2 \end{cases}$	$\begin{cases} -1 \\ 0 \\ 0 \\ 1 \end{cases}$	3P , 3P
1	0	1	$\begin{cases} -1/2 \\ -1/2 \\ 1/2 \\ 1/2 \end{cases}$	$\begin{cases} -1/2 \\ 1/2 \\ -1/2 \\ 1/2 \end{cases}$	$\begin{cases} -1 \\ 0 \\ 0 \\ 1 \end{cases}$	3P , 1D , 3P
1	1	2	1/2	-1/2	0	1D

and the D term must be 1D . This term has $(2S + 1)(2L + 1) = 5$ states associated with it. It includes states with $M_L = -2, -1, 0, +1$, and $+2$, all of which have $M_S = 0$. These 5 states are mentally removed from the table, which leaves us with 10 states. Of those remaining, the next highest value of $|M_L|$ is $+1$, which must belong to a P term. Because there is a combination with $M_L = 1$ and $M_S = 1$, the P term must be 3P . This term has $(2S + 1)(2L + 1) = 9$ states associated with it and by mentally removing these 9 states from the table, a single state is left with $M_L = M_S = 0$. This is a complete 1S term. By a process of elimination, we have found that the 15 combinations of m_l and m_s consistent with the configuration $1s^22s^22p^2$ separate into 1D , 1S , and 3P terms. This conclusion is true for any np^2 configuration. Because the 1D , 1S , and 3P terms have 5, 1, and 9 states associated with them, a total of 15 states are associated with the terms of the $1s^22s^22p^2$ configuration, just as for the classification scheme based on the individual quantum numbers n , l , m_s , and m_l .

Example Problem 11.2 demonstrates how terms are generated from a given configuration.

EXAMPLE PROBLEM 11.2

What terms result from the configuration ns^1nd^1 ? How many quantum states are associated with each term?

Solution

Because the electrons are not in the same subshell, the Pauli principle does not limit the combinations of m_l and m_s . Using the guidelines formulated earlier, $S_{min} = 1/2 - 1/2 = 0$, $S_{max} = 1/2 + 1/2 = 1$, $L_{min} = 2 - 0 = 2$, and $L_{max} = 2 + 0 = 2$. Therefore, the terms that arise from the configuration ns^1d^1 are 3D and 1D . Table 11.2 shows how these terms arise from the individual quantum numbers. In setting up the table, we have relied only on the z components of the vectors m_{si} and m_{li} . Using these components, $M_S = \sum_i m_{si}$ and $M_L = \sum_i m_{li}$ can be easily calculated because no vector addition is involved. Because each term has $(2S + 1)(2L + 1)$ states, the 3D term consists of 15 states, and the 1D term consists of 5 states, as shown in Table 11.2.

TABLE 11.2 States and Terms for the ns^1d^1 Configuration

m_{l1}	m_{l2}	$M_L = m_{l1} + m_{l2}$	m_{s1}	m_{s2}	$M_S = m_{s1} + m_{s2}$	Term
0	-2	-2	$\begin{cases} -1/2 \\ -1/2 \\ 1/2 \\ 1/2 \end{cases}$	$\begin{cases} -1/2 \\ 1/2 \\ -1/2 \\ 1/2 \end{cases}$	$\begin{cases} -1 \\ 0 \\ 0 \\ 1 \end{cases}$	3D
			$\begin{cases} -1/2 \\ 1/2 \\ 1/2 \\ 1/2 \end{cases}$	$\begin{cases} 1/2 \\ -1/2 \\ -1/2 \\ 1/2 \end{cases}$	$\begin{cases} 0 \\ 0 \\ 0 \\ 1 \end{cases}$	${}^1D, {}^3D$
			$\begin{cases} 1/2 \\ 1/2 \\ 1/2 \\ 1/2 \end{cases}$	$\begin{cases} -1/2 \\ 1/2 \\ -1/2 \\ 1/2 \end{cases}$	$\begin{cases} -1 \\ 0 \\ 0 \\ 1 \end{cases}$	3D
			$\begin{cases} 1/2 \\ 1/2 \\ 1/2 \\ 1/2 \end{cases}$	$\begin{cases} -1/2 \\ 1/2 \\ -1/2 \\ 1/2 \end{cases}$	$\begin{cases} -1 \\ 0 \\ 0 \\ 1 \end{cases}$	${}^1D, {}^3D$
0	0	0	$\begin{cases} -1/2 \\ -1/2 \\ 1/2 \\ 1/2 \end{cases}$	$\begin{cases} -1/2 \\ 1/2 \\ -1/2 \\ 1/2 \end{cases}$	$\begin{cases} -1 \\ 0 \\ 0 \\ 1 \end{cases}$	3D
			$\begin{cases} -1/2 \\ 1/2 \\ 1/2 \\ 1/2 \end{cases}$	$\begin{cases} 1/2 \\ -1/2 \\ -1/2 \\ 1/2 \end{cases}$	$\begin{cases} 0 \\ 0 \\ 0 \\ 1 \end{cases}$	${}^1D, {}^3D$
			$\begin{cases} 1/2 \\ 1/2 \\ 1/2 \\ 1/2 \end{cases}$	$\begin{cases} -1/2 \\ 1/2 \\ -1/2 \\ 1/2 \end{cases}$	$\begin{cases} -1 \\ 0 \\ 0 \\ 1 \end{cases}$	3D
			$\begin{cases} 1/2 \\ 1/2 \\ 1/2 \\ 1/2 \end{cases}$	$\begin{cases} -1/2 \\ 1/2 \\ -1/2 \\ 1/2 \end{cases}$	$\begin{cases} -1 \\ 0 \\ 0 \\ 1 \end{cases}$	${}^1D, {}^3D$
0	1	1	$\begin{cases} -1/2 \\ -1/2 \\ 1/2 \\ 1/2 \end{cases}$	$\begin{cases} -1/2 \\ 1/2 \\ -1/2 \\ 1/2 \end{cases}$	$\begin{cases} -1 \\ 0 \\ 0 \\ 1 \end{cases}$	3D
			$\begin{cases} -1/2 \\ 1/2 \\ 1/2 \\ 1/2 \end{cases}$	$\begin{cases} 1/2 \\ -1/2 \\ -1/2 \\ 1/2 \end{cases}$	$\begin{cases} 0 \\ 0 \\ 0 \\ 1 \end{cases}$	${}^1D, {}^3D$
			$\begin{cases} 1/2 \\ 1/2 \\ 1/2 \\ 1/2 \end{cases}$	$\begin{cases} -1/2 \\ 1/2 \\ -1/2 \\ 1/2 \end{cases}$	$\begin{cases} -1 \\ 0 \\ 0 \\ 1 \end{cases}$	3D
			$\begin{cases} 1/2 \\ 1/2 \\ 1/2 \\ 1/2 \end{cases}$	$\begin{cases} -1/2 \\ 1/2 \\ -1/2 \\ 1/2 \end{cases}$	$\begin{cases} -1 \\ 0 \\ 0 \\ 1 \end{cases}$	${}^1D, {}^3D$
0	2	2	$\begin{cases} -1/2 \\ -1/2 \\ 1/2 \\ 1/2 \end{cases}$	$\begin{cases} -1/2 \\ 1/2 \\ -1/2 \\ 1/2 \end{cases}$	$\begin{cases} -1 \\ 0 \\ 0 \\ 1 \end{cases}$	3D
			$\begin{cases} -1/2 \\ 1/2 \\ 1/2 \\ 1/2 \end{cases}$	$\begin{cases} 1/2 \\ -1/2 \\ -1/2 \\ 1/2 \end{cases}$	$\begin{cases} 0 \\ 0 \\ 0 \\ 1 \end{cases}$	${}^1D, {}^3D$
			$\begin{cases} 1/2 \\ 1/2 \\ 1/2 \\ 1/2 \end{cases}$	$\begin{cases} -1/2 \\ 1/2 \\ -1/2 \\ 1/2 \end{cases}$	$\begin{cases} -1 \\ 0 \\ 0 \\ 1 \end{cases}$	3D
			$\begin{cases} 1/2 \\ 1/2 \\ 1/2 \\ 1/2 \end{cases}$	$\begin{cases} -1/2 \\ 1/2 \\ -1/2 \\ 1/2 \end{cases}$	$\begin{cases} -1 \\ 0 \\ 0 \\ 1 \end{cases}$	${}^1D, {}^3D$

The preceding discussion has demonstrated how to generate the terms associated with a particular configuration. The same procedure can be followed for any configuration, and a few examples are shown in Table 11.3 for electrons in the same shell. The numbers in parentheses behind the term symbol indicate the number of different terms of that type that belong to the configuration. A simplifying feature in generating terms is that the same results are obtained for a given number of electrons or “missing electrons” (sometimes called holes) in a subshell. For example, d^1 and d^9 configurations result in the same terms. Note that configurations with a single electron or hole in the unfilled shell or subshell give only a single term as discussed earlier. In filled shells or subshells, $M_L = M_S = 0$ because m_l and m_s take on all possible values between their maximum positive and negative values. For this reason, the term symbol for s^2 , p^6 , and d^{10} is 1S .

Example Problem 11.3 demonstrates how to determine which states are associated with a given configuration.

TABLE 11.3 Possible Terms for Indicated Configurations

Electron Configuration	Term Symbol
s^1	2S
p^1, p^5	2P
p^2, p^4	${}^1S, {}^1D, {}^3P$
p^3	${}^2P, {}^2D, {}^4S$
d^1, d^9	2D
d^2, d^8	${}^1S, {}^1D, {}^1G, {}^3P, {}^3F$
d^3, d^7	${}^4F, {}^4P, {}^2H, {}^2G, {}^2F, {}^2D(2), {}^2P$
d^4, d^6	${}^5D, {}^3H, {}^3G, {}^3F(2), {}^3D, {}^3P(2), {}^1I, {}^1G(2), {}^1F, {}^1D(2), {}^1S(2)$
d^5	${}^6S, {}^4G, {}^4F, {}^4D, {}^4P, {}^2I, {}^2H, {}^2G(2), {}^2F(2), {}^2D(3), {}^2P, {}^2S$

EXAMPLE PROBLEM 11.3

How many states are consistent with a d^2 configuration? What L values result from this configuration?

Solution

The first electron can have any of the m_l values ± 2 , ± 1 , and 0, and either of the m_s values $\pm 1/2$. This gives 10 combinations. The second electron can have 9 combinations, and the total number of combinations for both electrons is $10 \times 9 = 90$. However, because the electrons are not distinguishable, we must divide this number by 2 and obtain 45 states. Using the formula $L = l_1 + l_2, l_1 + l_2 - 1, \dots, |l_1 - l_2|$, we conclude that L values of 4, 3, 2, 1, and 0 are allowed. Therefore, this configuration gives rise to G, F, D, P, and S terms. Table 11.3 shows that the allowed terms for these L values are ^1S , ^1D , ^1G , ^3P , and ^3F . The degeneracy of each term is given by $(2L + 1)(2S + 1)$ and is 1, 5, 9, 9, and 21, respectively. Therefore, the d^2 configuration gives rise to 45 distinct quantum states, just as was calculated based on the possible combinations of m_l and m_s .

The relative energy of the different terms has not been discussed yet. From the examination of a large body of spectroscopic data, Friedrich Hund deduced **Hund's rules**, which state that for a given configuration the following are true:

RULE 1:

The lowest energy term is that which has the greatest spin multiplicity. For example, the ^3P term of an np^2 configuration is lower in energy than the ^1D and ^1S terms.

RULE 2:

For terms that have the same spin multiplicity, the term with the greatest orbital angular momentum lies lowest in energy. For example, the ^1D term of an np^2 configuration is lower in energy than the ^1S term.

Concept

Hund's rules predict the relative energy of different terms arising from the same configuration.

Hund's rules predict that in placing electrons in one-electron orbitals, the number of unpaired electrons should be maximized. For this reason, Cr has the configuration $[\text{Ar}]4s^13d^5$ rather than $[\text{Ar}]4s^23d^4$. Hund's rules imply that the energetic consequences of electron-electron repulsion are greater for spin than for orbital angular momentum. Atoms in quantum states described by different terms can have substantially different chemical reactivity.

Although some care is needed to establish the terms that belong to a particular configuration such as p^n or d^n , it is straightforward to predict the lowest energy term among the possible terms using the following recipe. Create boxes, one for each of the possible values of m_l . Place the electrons specified by the configuration in the boxes in such a way that $M_L = \sum_i m_{li}$ is maximized and that the number of unpaired spins is maximized. L and S for the lowest energy term are given by $L = M_{L,\max}$ and $S = M_{S,\max}$. This procedure is illustrated for the p^2 and d^6 configurations in Example Problem 11.4.

EXAMPLE PROBLEM 11.4

Determine the lowest energy term for the p^2 and d^6 configurations.

Solution

The placement of the electrons is as shown here:

p^2					
m_l	1	0	-1		
	↑	↑			
d^6					
m_l	2	1	0	-1	-2
	↑↓	↑	↑	↑	↑

For the p^2 configuration, $M_{L,\max} = 1$ and $M_{S,\max} = 1$. Therefore, the lowest energy term is 3P . For the d^6 configuration, $M_{L,\max} = 2$ and $M_{S,\max} = 2$. Therefore, the lowest energy term is 5D . It is important to realize that this procedure only provides a recipe for finding the lowest energy term. The picture used in the recipe has no basis in reality because no association of a term with particular values of m_s and m_l can be made.

11.3 SPIN–ORBIT COUPLING SPLITS A TERM INTO LEVELS

Concept

For atoms with $Z > 40$, L and S are no longer good quantum numbers.

Previously, we have assumed that all states in a term have the same energy. This is a good approximation for atoms with $Z < 40$. However, even for these atoms, the terms are split into closely spaced levels. What is the origin of this splitting? We know that electrons have nonzero magnetic moments if $L > 0$ and $S > 0$. The separate spin and orbital magnetic moments can interact through **spin–orbit coupling**, just as two bar magnets interact. As a result of this interaction, the total energy operator contains an extra term proportional to $\mathbf{L} \cdot \mathbf{S}$. Under these conditions, the operators \hat{L}^2 , \hat{L}_z , \hat{S}^2 , and \hat{S}_z no longer commute with \hat{H} , but the operators \hat{J}^2 and \hat{J}_z , where \mathbf{J} is the **total angular momentum** defined by

$$\mathbf{J} = \mathbf{L} + \mathbf{S} \quad (11.5)$$

do commute with \hat{H} . If the coupling is sufficiently large as in atoms for which $Z > 40$, the only good quantum numbers are J and M_J , the projection of J on the z axis. The magnitude of \mathbf{J} can take on all values given by $J = L + S, L + S - 1, L + S - 2, \dots, |L - S|$, and M_J can take on all values between zero and J that differ by one.

For example, the 3P term has J values of 2, 1, and 0. All quantum states with the same J value have the same energy and belong to the same **level**. The additional quantum number J is included in the nomenclature for a level as a subscript in the form $(2S+1)L_J$. In counting states, $2J + 1$ states with different M_J values are associated with each J value. This gives five states associated with 3P_2 , three states associated with 3P_1 , and one state associated with 3P_0 . The total of nine states in the three levels is the same as the number of states in the 3P term, as deduced from the formula $(2L + 1)(2S + 1)$.

Taking spin–orbit coupling into account gives Hund's third rule:

RULE 3:

The order in energy of levels in a term is given by the following:

- If the unfilled subshell is exactly one-half full or more than half full, the level with the highest J value has the lowest energy.
- If the unfilled subshell is less than half full, the level with the lowest J value has the lowest energy.

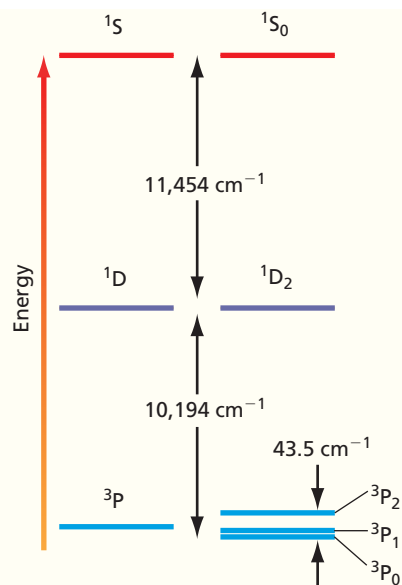


Figure 11.6

Relationship of terms and levels for carbon. For a carbon atom, assuming a spherically symmetric electron distribution, a single energy state is allowed. Considering the dependence of electron repulsion on directions of L and S , the single state is split into terms of different energy, in this case 3P , 1D , and 1S . Further considering the coupling of L and S leads to an additional splitting of the terms into levels according to the J values, in this case 1S_0 , 1D_2 , 3P_2 , 3P_1 , and 3P_0 . The separation of the levels for the 3P term has been multiplied by a factor of 25 to make it visible.

Therefore, the 3P_0 level has the lowest energy for an np^2 configuration. The 3P_2 level has the lowest energy for an np^4 configuration, which describes O.

In a magnetic field, states with the same J , but different M_J , have different energies. For atoms with $Z < 40$, this energy splitting is less than the energy separation between levels, which is in turn less than the energy separation between terms. However, all of these effects are observable with the aid of spectroscopic techniques, as shown for carbon in Figure 11.6. Many of these techniques have practical applications in analytical chemistry. Clearly, the energy levels of many-electron atoms have a greater level of complexity than those for the hydrogen atom. This complexity provides more detailed information about atoms through spectroscopic experiments that can be used to better understand the quantum mechanics of many-electron atoms. Example Problem 11.5 demonstrates how to determine which J values are associated with a given term.

EXAMPLE PROBLEM 11.5

What values of J are consistent with the terms ^2P and ^3D ? How many states with different values of M_J correspond to each?

Solution

The quantum number J can take on all values given by $J = L + S, L + S - 1, L + S - 2, \dots, |L - S|$. For the ^2P term, $L = 1$ and $S = 1/2$. Therefore, J can have the values $3/2$ and $1/2$. There are $2J + 1$ values of M_J , or 4 and 2 states, respectively.

For the ^3D term, $L = 2$ and $S = 1$. Therefore, J can have the values 3, 2, and 1. There are $2J + 1$ values of M_J or 7, 5, and 3 states, respectively.

11.4 THE ESSENTIALS OF ATOMIC SPECTROSCOPY

With an understanding of the quantum states of many-electron atoms, we now turn our attention to atomic spectroscopy. All spectroscopic techniques involve the absorption or emission of electromagnetic radiation that induces transitions between states of a quantum-mechanical system. In this chapter, we will discuss transitions between electronic states in atoms. Whereas the energies involved in rotational and vibrational transitions are on the order of 1 and 10 kJ mol^{-1} , respectively, photon energies associated with electronic transitions are on the order of 200 to 1000 kJ mol^{-1} . Typically, such energies are associated with visible, UV, or X-ray photons.

The information on atomic energy levels discussed in previous sections is derived from atomic spectra. The interpretation of spectra requires knowledge of the selection rules for the spectroscopic method being used. Selection rules, which were introduced in Chapter 8, can be derived by employing the dipole approximation (see Section 8.4). Although transitions that are forbidden in the dipole approximation may be allowed in a higher-level theory, the absorption or emission peaks are very weak. In Chapter 8, the dipole selection rule $\Delta n = \pm 1$ was derived for vibrational transitions, and it was stated without proof that the selection rule for rotational transitions in diatomic molecules is $\Delta J = \pm 1$. What selection rules apply for transitions between atomic levels? If the **L–S** coupling scheme outlined in Section 11.2 applies (atomic numbers < 40), the dipole selection rules for atomic transitions are $\Delta l = \pm 1$, and $\Delta L = 0, \pm 1$, and $\Delta J = 0, \pm 1$. There is an additional selection rule, $\Delta S = 0$, for the spin angular momentum. Note that the first selection rule refers to the angular momentum of an electron involved in the transition, whereas the other rules refer to the vector sums for all electrons in the atom. Keep in mind that aside from the rotational spectroscopy selection rule cited earlier, the quantum number J in this chapter refers to the total electron angular momentum and not to the rotational angular momentum.

Atomic spectroscopy is important in many practical applications of analytical chemistry, including experiments with lasers, which we will discuss in this chapter. At a fundamental level, the relative energy of individual quantum states can be measured to high precision using spectroscopic techniques. An application of such high-precision measurements is the standard for the SI time unit of a second, which is based on a transition between states in the cesium atom that has the frequency $9.192631770 \times 10^9 \text{ s}^{-1}$.

Because the energy levels of the hydrogen atom can be written as

$$E_n = -\frac{\mu e^4}{8\epsilon_0^2 h^2 n^2} \quad (11.6)$$

where n is the principal quantum number, the frequency for absorption lines in the hydrogen spectrum is given by

$$\tilde{v} = \frac{\mu e^4}{8\epsilon_0^2 h^3 c} \left(\frac{1}{n_{\text{initial}}^2} - \frac{1}{n_{\text{final}}^2} \right) = R_H \left(\frac{1}{n_{\text{initial}}^2} - \frac{1}{n_{\text{final}}^2} \right) \quad (11.7)$$

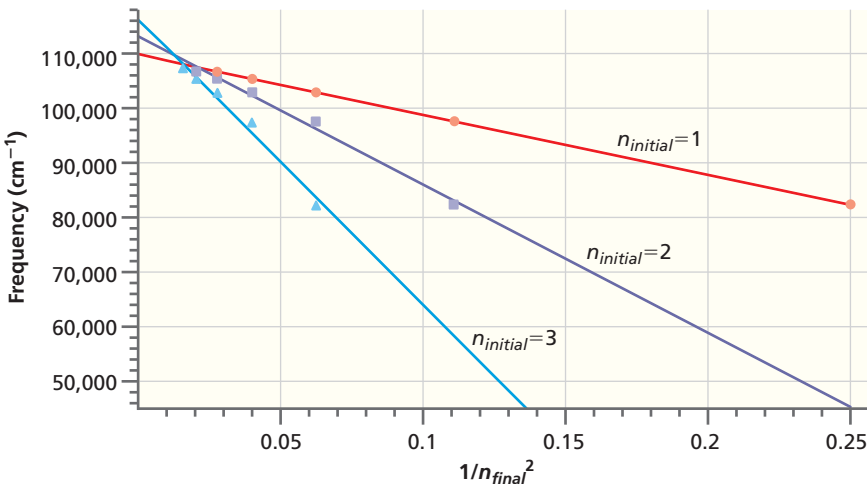
where R_H is the Rydberg constant and μ is the reduced mass of the atom. The derivation of this formula was one of the early major triumphs of quantum mechanics. The Rydberg constant is one of the most precisely known fundamental constants; it has a value of $109677.581 \text{ cm}^{-1}$. The series of spectral lines associated with $n_{\text{initial}} = 1$ is called the Lyman series, and the series associated with $n_{\text{initial}} = 2, 3, 4$, and 5 are called the Balmer, Paschen, Brackett, and Pfund series, respectively, after the spectroscopists who identified them. Example Problem 11.6 demonstrates how to determine which spectral lines are associated with a given series.

EXAMPLE PROBLEM 11.6

The absorption spectrum of the hydrogen atom shows lines at $82,258, 97,491, 102,823, 105,290$, and $106,631 \text{ cm}^{-1}$. There are no lower-frequency lines in the spectrum. Use graphical methods to determine n_{initial} and the ionization energy of the hydrogen atom in this state.

Solution

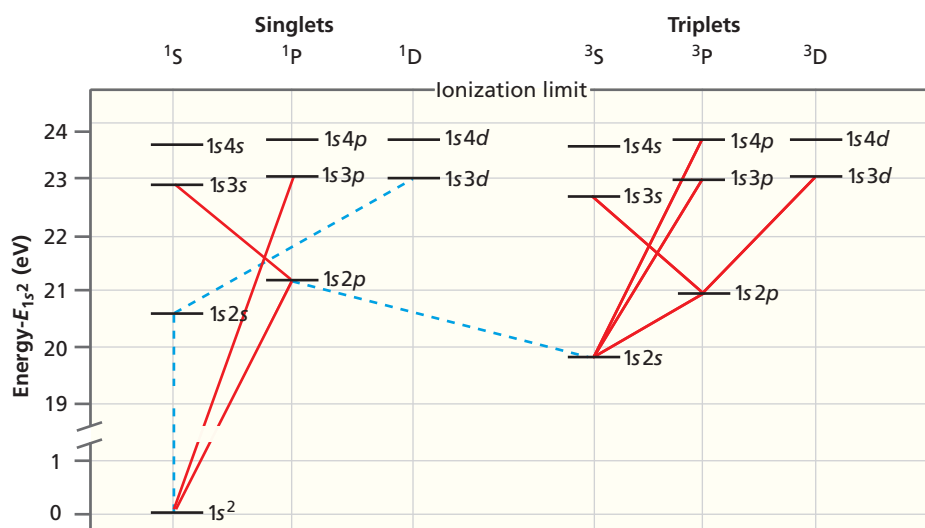
The knowledge that frequencies for transitions follow a formula similar to that of Equation (11.7) allows n_{initial} and the ionization energy to be determined from a limited number of transitions between bound states. The plot of $\tilde{\nu}$ versus assumed values of $1/n_{\text{final}}^2$ has a slope of $-R_H$ and an intercept with the frequency axis of R_H/n_{initial}^2 . However, both n_{initial} and n_{final} are unknown, so that in plotting the data, n_{final} values have to be assigned to the observed frequencies. For the lowest energy transition, n_{final} is $n_{\text{initial}} + 1$. We try different combinations of n_{final} and n_{initial} values to see if the slope and intercept are consistent with the expected values of $-R_H$ and R_H/n_{initial}^2 . In this case, the sequence of spectral lines is assumed to correspond to $n_{\text{final}} = 2, 3, 4, 5$, and 6 for an assumed value of $n_{\text{initial}} = 1$; $n_{\text{final}} = 3, 4, 5, 6$, and 7 for an assumed value of $n_{\text{initial}} = 2$; and $n_{\text{final}} = 4, 5, 6, 7$, and 8 for an assumed value of $n_{\text{initial}} = 3$. The plots are shown in the accompanying figure:



The slopes and intercepts calculated for these assumed values of n_{initial} are

Assumed n_{initial}	Slope (cm^{-1})	Intercept (cm^{-1})
1	-1.10×10^5	1.10×10^5
2	-2.71×10^5	1.13×10^5
3	-5.23×10^5	1.16×10^5

Because for only one of the three assumed values the slope is $-R_H$, we conclude that $n_{\text{initial}} = 1$. The ionization energy of the hydrogen atom in this state is hcR_H , corresponding to $n_{\text{final}} \rightarrow \infty$, or $2.18 \times 10^{-18} \text{ J}$. The appropriate number of significant figures for the slope and intercept is approximate in this example and must be based on an error analysis of the data.

**Figure 11.7**

Grotrian diagram for He atom. The ground state and first few excited states of the He atom are shown on an energy scale. All terms for which $l > 2$ and $n > 4$ have been omitted to simplify the presentation. The top horizontal line indicates the ionization energy of He. Below this energy, all states are discrete. Above this level, the energy spectrum is continuous. Several, but not all, allowed (solid lines) and forbidden (dashed lines) transitions are shown. Which selection rule do the forbidden transitions violate?

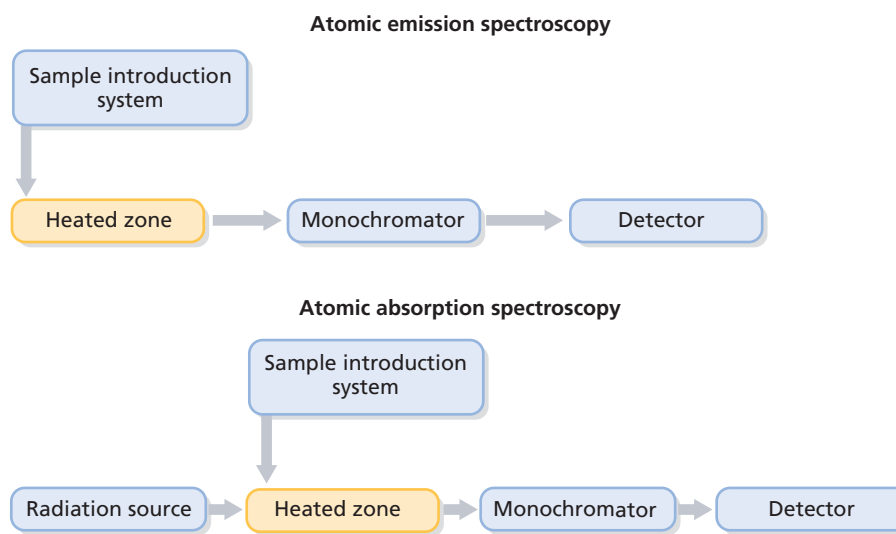
Information from atomic spectra is generally displayed in a standard format called a **Grotrian diagram**. An example is shown in Figure 11.7 for He, for which L–S coupling is a good model. The figure shows the configuration information next to the energy level, and the configurations are arranged according to their energy and term symbols. The triplet and singlet states are shown in separate parts of the diagram because transitions between these states do not occur as a consequence of the $\Delta S = 0$ selection rule. The ${}^3\text{P}$ and ${}^3\text{D}$ He terms are split into levels with different J values, but because the spin–orbit interaction is so small for He, the splitting is not shown in Figure 11.7. For example, the ${}^3\text{P}_0$ and ${}^3\text{P}_2$ levels arising from the $1\text{s}2\text{p}$ configuration differ in energy by only 0.0006%.

Concept

A Grotrian diagram is useful in depicting allowed transitions between energy levels for atoms.

11.5 ANALYTICAL TECHNIQUES BASED ON ATOMIC SPECTROSCOPY

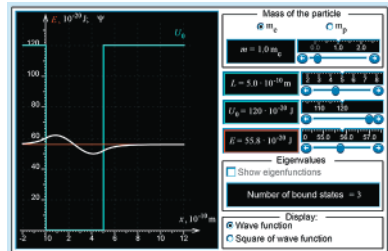
The absorption and emission of light that occurs in transitions between different atomic levels provides a powerful tool for qualitative and quantitative analysis of samples of chemical interest. For example, the concentration of lead in human blood and the presence of toxic metals in drinking water are routinely determined using **atomic emission** and **atomic absorption spectroscopy**. Figure 11.8 illustrates how these

**Figure 11.8**

Flow diagrams of components of atomic emission spectroscopy and atomic absorption spectroscopy.

two spectroscopic techniques are implemented. A sample, ideally in the form of very small droplets ($\sim 1\text{--}10 \mu\text{m}$ in diameter) of a solution or suspension, is injected into the heated zone of the spectrometer. The heated zone may take the form of a flame, an electrically heated graphite furnace, or a plasma arc source. The main requirement of the heated zone is that it must convert a portion of the molecules in the sample of interest into their excited states. We will first discuss atomic emission spectroscopy before turning to atomic absorption spectroscopy.

11.5.1 Atomic Emission Spectroscopy

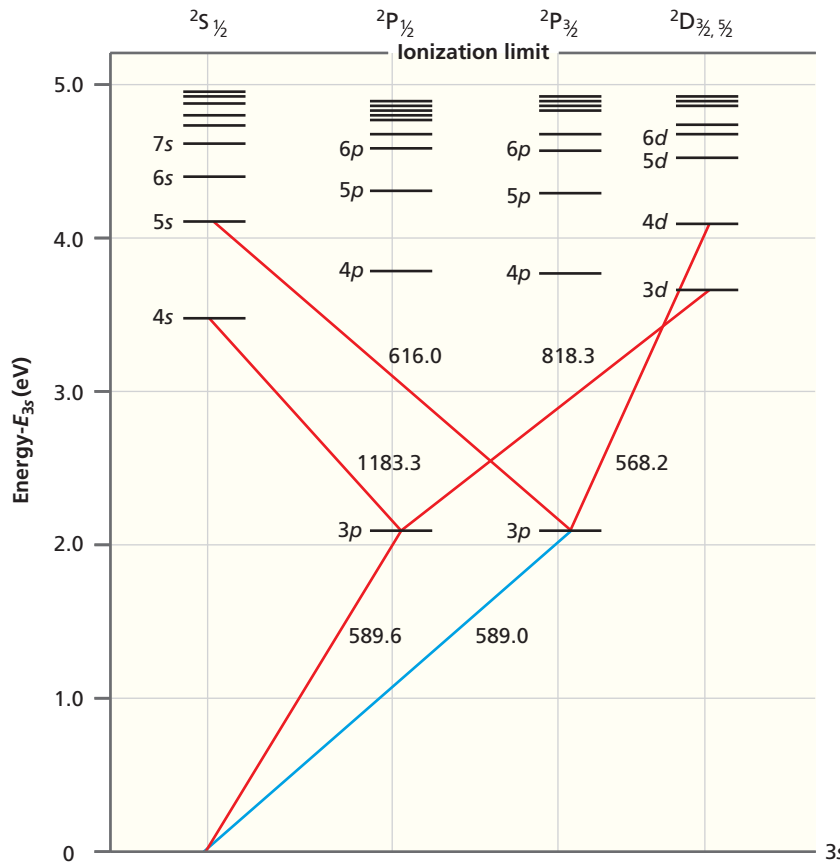


W11.1 Energy levels and emission spectra

In atomic emission spectroscopy, light emitted by excited-state atoms as they undergo transitions back down to the ground state is dispersed into its component wavelengths by a monochromator, and the intensity of the emitted radiation is measured as a function of wavelength. Because the emitted light intensity is proportional to the number of excited-state atoms and because the wavelengths at which emission occurs are characteristic for the atom, the technique can be used for both qualitative and quantitative analysis. Temperatures in the range of 1800 to 3500 K can be achieved in flames and carbon furnaces, and temperatures as high as 10,000 K can be reached in plasma arc sources. These high temperatures are required to produce sufficient excited-state atoms that emit light, as demonstrated in Example Problem 11.7.

EXAMPLE PROBLEM 11.7

The $^2\text{S}_{1/2} \longrightarrow ^2\text{P}_{3/2}$ transition in sodium has a wavelength of 589.0 nm. This is one of the lines characteristic of the sodium vapor lamps used for lighting streets, and it gives the lamps their yellow-orange color. Calculate the ratio of the number of atoms in these two states at 1500., 2500., and 3500. K. The following figure is a Grotrian diagram for Na (not to scale) in which the transition of interest is shown as a blue line.



Solution

The ratio of atoms in the upper and lower levels is given by the Boltzmann distribution:

$$\frac{n_{upper}}{n_{lower}} = \frac{g_{upper}}{g_{lower}} e^{-(\varepsilon_{upper} - \varepsilon_{lower})/k_B T}$$

The degeneracies g are given by $2J + 1$, which is the number of states in each level:

$$g_{upper} = 2 \times \frac{3}{2} + 1 = 4 \text{ and } g_{lower} = 2 \times \frac{1}{2} + 1 = 2$$

From the Boltzmann distribution,

$$\begin{aligned} \frac{n_{upper}}{n_{lower}} &= \frac{g_{upper}}{g_{lower}} \exp(-hc/\lambda_{transition}k_B T) \\ &= \frac{4}{2} \exp\left[-\frac{(6.626 \times 10^{-34} \text{ J s})(2.998 \times 10^8 \text{ m s}^{-1})}{(589.0 \times 10^{-9} \text{ m})(1.381 \times 10^{-23} \text{ J K}^{-1}) \times T}\right] \\ &= 2 \exp\left(-\frac{24420}{T}\right) = 1.699 \times 10^{-7} \text{ at } 1500. \text{ K}, 1.145 \times 10^{-4} \text{ at } 2500. \text{ K}, \\ &\quad \text{and } 1.866 \times 10^{-3} \text{ at } 3500. \text{ K} \end{aligned}$$

As seen in the preceding example problem, the fraction of atoms in the excited state is quite small, but it increases rapidly with temperature. The very high temperature plasma arc sources are widely used because they allow light emission from both more highly excited states and from ions to be observed. This greatly increases the sensitivity of the technique. However, because photons can be detected with very high efficiency, measurements can be obtained from systems for which n_{upper}/n_{lower} is quite small. For instance, a temperature of ~ 3000 K is reached in an oxygen-natural gas flame. If a small amount of NaCl is put into the flame, $n_{upper}/n_{lower} \sim 6 \times 10^{-4}$ for Na, as shown in Example Problem 11.7. Even with this rather low degree of excitation, a bright yellow emission resulting from the 589.0 and 589.6 nm emission lines in the flame is clearly visible with the naked eye. The sensitivity of the technique can be greatly enhanced using photomultipliers, and spectral transitions for which $n_{upper}/n_{lower} < 10^{-10}$ are routinely used in analytical chemistry.

11.5.2 Atomic Absorption Spectroscopy

Atomic absorption spectroscopy differs from atomic emission spectroscopy in that light is passed through the heated zone and the absorption associated with transitions from the lower to the upper state is detected. Because this technique relies on the population of low-lying rather than highly excited atomic states, it has some advantages in sensitivity over atomic emission spectroscopy. It became a very widely used technique when researchers realized that the sensitivity would be greatly enhanced if the light source were nearly monochromatic with a wavelength centered at $\lambda_{transition}$. The advantage of this arrangement can be seen from Figure 11.9.

Only a small fraction of the broadband light that passes through the heated zone is absorbed in the transition of interest. To detect the absorption, the light needs to be dispersed with a grating, and the intensity of the light must be measured as a function of frequency. Because the monochromatic source matches the transition both in frequency and in linewidth, detection is much easier. Only a simple monochromator is needed to remove background light before the light is focused on the detector. The key to implementation of this technique was the development of hollow cathode gas discharge lamps that emit light at the characteristic frequencies of the cathode materials. By using an array of these relatively inexpensive lamps on a single spectrometer, analyses for a number of different elements of interest can be carried out.

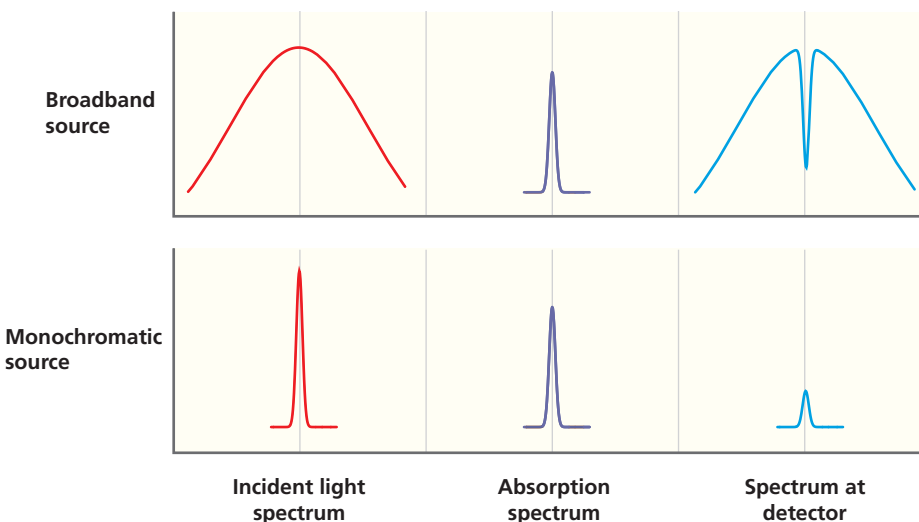
The sensitivity of atomic emission and absorption spectroscopy depends on the element and ranges from $10^{-4} \mu\text{g/mL}$ for Mg to $10^{-2} \mu\text{g/mL}$ for Pt. These techniques

Concept

Atomic absorption spectroscopy and emission spectroscopy are very useful tools in analytical chemistry.

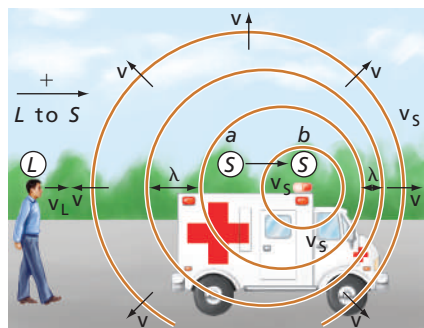
Figure 11.9

Intensity of light as a function of its frequency. The intensity of light is shown at the entrance to the heated zone and at the detector for broadband and monochromatic sources. The absorption spectrum of the atom to be detected is shown in the middle column.



are used in a wide variety of applications including drinking water analysis. The extent of wear on an engine can also be analyzed by detecting trace amounts of abraded metals in the engine's lubricating oil.

11.6 THE DOPPLER EFFECT

**Figure 11.10**

The Doppler effect. The frequency of light or sound at the position of the observer L depends on v_s , the relative velocity of the source S , and the observer L .

An additional application of atomic spectroscopy is a consequence of the Doppler effect. If a source is radiating light and moving relative to an observer, the observer sees a change in the frequency of the light, as shown in Figure 11.10 for sound.

The observed frequency is given by the formula

$$\omega = \omega_0 \sqrt{(1 \pm v_z/c)/(1 \mp v_z/c)} \quad (11.8)$$

In this formula, v_z is the velocity component in the observation direction, c is the speed of light, and ω_0 is the light frequency in the frame in which the source is stationary. The upper and lower signs refer to the object approaching and receding from the observer, respectively. Note that the frequency shift is positive for objects that are approaching (a so-called *blue shift*) and negative for objects that are receding (a so-called *red shift*). The **Doppler shift** is used to measure the speed at which stars and other radiating astronomical objects are moving relative to Earth. Example Problem 11.8 demonstrates how the Doppler effect can be used to determine relative velocities.

EXAMPLE PROBLEM 11.8

A line in the Lyman emission series for atomic hydrogen ($n_{final} = 1$), for which the wavelength is at 121.6 nm for an atom at rest, is seen for a particular quasar at 445.1 nm. Is the source approaching toward or receding from the observer? What is the magnitude of the velocity?

Solution

Because the frequency observed is less than that which would be observed for an atom at rest, the object is receding. The relative velocity is given by

$$\left(\frac{\omega}{\omega_0}\right)^2 = \left(1 - \frac{v_z}{c}\right) / \left(1 + \frac{v_z}{c}\right), \text{ or}$$

$$\frac{v_z}{c} = \frac{1 - (\omega/\omega_0)^2}{1 + (\omega/\omega_0)^2} = \frac{1 - (\lambda_0/\lambda)^2}{1 + (\lambda_0/\lambda)^2}$$

$$= \frac{1 - (121.6/445.1)^2}{1 + (121.6/445.1)^2} = 0.8611; v_z = 2.581 \times 10^8 \text{ m s}^{-1}$$

For source velocities much less than the speed of light, the nonrelativistic formula

$$\omega = \omega_0 \left(1 / \left[1 \mp \frac{v_z}{c} \right] \right) \quad (11.9)$$

applies. This formula is appropriate for a gas of atoms or molecules for which the distribution of speeds is given by the Maxwell–Boltzmann distribution. Because all velocity directions are equally represented for a particular speed, v_z has a large range for a gas at a given temperature, centered at $v_z = 0$. Therefore, the frequency is not shifted by the Doppler effect; instead, the spectral line is broadened. This result is called **Doppler broadening**. Because atomic and molecular velocities are very small compared with the speed of light, the broadening of a line of frequency ω_0 is on the order of 1 part in 10^6 . This effect is not as dramatic as the shift in frequency for the quasar, but it is still of importance in determining the linewidth of a laser, as we will see in the next section.

Concept

The Doppler effect leads to line broadening in gas phase atomic spectra.

11.7 THE HELIUM-NEON LASER

In this section, we will demonstrate the relevance of the basic principles of absorption and emission discussed in Chapter 8 to the functioning of a laser. Specifically, we will focus on the He–Ne laser. Absorption, spontaneous emission, and stimulated emission all obey the same selection rules for an atom: $\Delta l = \pm 1$ for a single electron and $\Delta L = 0$ or ± 1 for the vector sum over all electrons.

Spontaneous and stimulated emission differ in an important respect. Spontaneous emission is a completely random process in time, and the photons that are emitted are incoherent, meaning that their phases are random. An incandescent light bulb is an **incoherent photon source**. Because all propagation directions are equally likely, the intensity of the source falls off as the square of the distance. In stimulated emission, the phase and direction of propagation are the same as those of the incident photon. This is referred to as coherent photon emission and the source of such emission is a **coherent photon source**. An example of a coherent photon source is a **laser**. All photons in a laser beam are in phase, and because they have the same propagation direction, the divergence of the beam is very small. This explains why a laser beam that is reflected from the moon still has a measurable intensity when it returns to Earth. Our discussion makes it clear that a coherent photon source must be based on stimulated rather than spontaneous emission. However, $B_{12} = B_{21}$, as was shown in Section 8.2. Therefore, the rates of absorption and stimulated emission are equal for $N_1 = N_2$. Stimulated emission will only dominate over absorption if $N_2 > N_1$. This condition is called a **population inversion** because for equal level degeneracies, the higher-energy state has the larger population. The key to making a practical laser is to create a stable population inversion. Although a population inversion is not possible under equilibrium conditions, it is possible to maintain such a distribution under steady-state conditions if the relative rates of the transitions between levels are appropriate. This is illustrated in Figure 11.11.

Figure 11.11 can be used to understand how the population inversion between the levels involved in the lasing transition is established and maintained. The lengths of the horizontal lines representing the levels are proportional to the level populations N_1 to N_4 . The initial step involves creating a significant population in level 4 by transitions from level 1. This is accomplished for the He–Ne laser with an electrical discharge in a tube containing the gas mixture. Relaxation to level 3 can occur through spontaneous emission of a photon as indicated by the wavy arrow. Similarly, relaxation from level 2 to level 1 can also occur through spontaneous emission of a photon. If this second relaxation process is fast compared to the first, N_3 will be maintained at a higher level than N_2 . In this way, a population inversion is established between levels two and three. The advantage of having the lasing transition between levels 3 and 2 rather than 2 and 1 is that N_2 can be kept low if relaxation to level 1 from level 2 is fast. It is not possible to keep N_1 at a low level because atoms in the ground state cannot decay to a lower state.

This discussion shows how a population inversion can be established. But how can a continuous lasing transition based on stimulated emission be maintained? This result is accomplished by carrying out the process indicated in Figure 11.11 in an experimental setup known as an optical resonator.

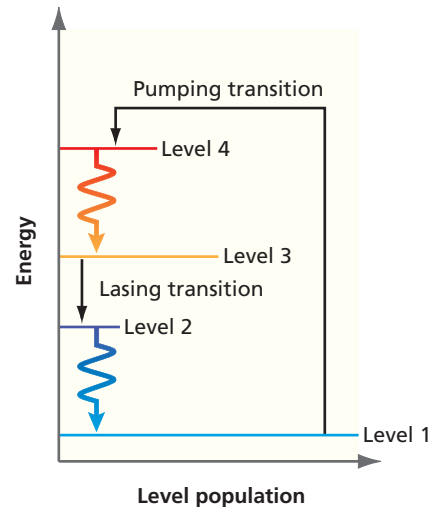


Figure 11.11

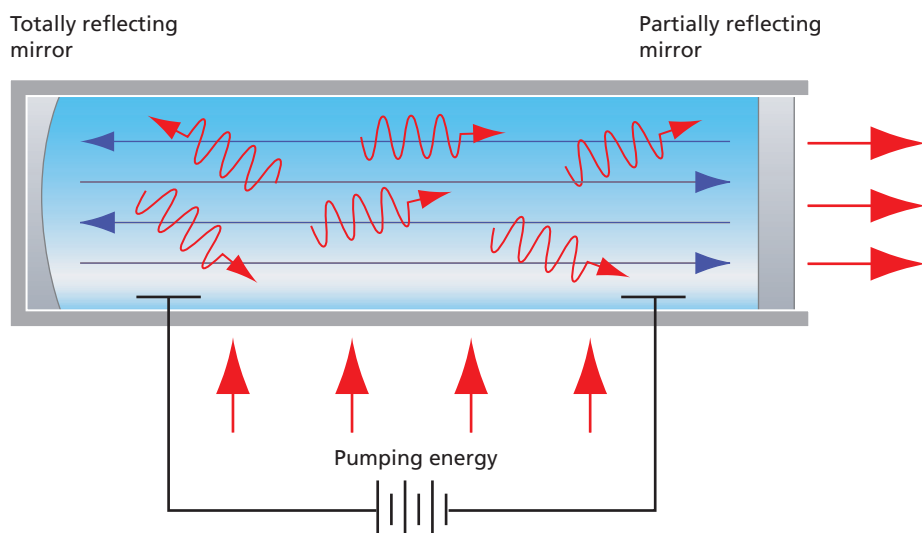
Schematic representation of a four-state laser. The energy is plotted vertically, and the level population is plotted horizontally.

Concept

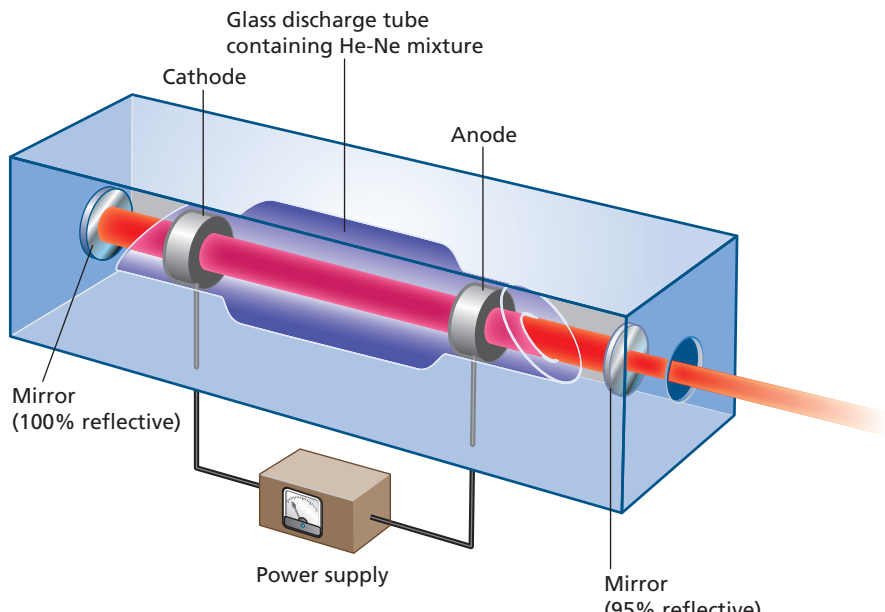
Population inversion and stimulated emission are essential for laser operation.

Figure 11.12

Schematic illustration of a He–Ne laser operated as an optical resonator. The parallel lines in the resonator represent coherent stimulated emission that is amplified by the resonator, and the red waves represent incoherent spontaneous emission events.



An **optical resonator** is shown in Figure 11.12. A He–Ne mixture is placed into a glass tube with carefully aligned parallel mirrors on each end. Electrodes are inserted to maintain the electrical discharge that pumps level 4 from level 1. A schematic diagram of a He–Ne laser, including the anode, cathode, and power supply needed to maintain the electrical discharge as well as the optical resonator, is shown in Figure 11.13. Light reflected back and forth in the optical cavity between the two mirrors interferes constructively only if $n\lambda = n(c/\nu) = 2d$, where d is the distance between mirrors and n is an integer. The next constructive interference occurs when $n \rightarrow n + 1$. The difference in frequency between these two **resonator modes** is $\Delta\nu = c/2d$, which defines the bandwidth of the cavity. At frequencies corresponding to the resonator modes, stimulated emission is greatly amplified by constructive interference and reflection between the mirrors at the ends of the optical cavity. Will a laser emit coherent light at a large number of frequencies, each corresponding to a different resonator mode? The number of resonator modes that contribute to laser action is determined by two factors: the frequencies of the resonator modes and the width in frequency of the stimulated emission transition. The width of the transition is determined by Doppler broadening, which arises through the thermal motion of gas-phase Ne atoms.

**Figure 11.13**

Schematic diagram of a He–Ne laser.

Factors that influence the width in frequency of a lasing transition are depicted in Figure 11.14. In Figure 11.14a, six of the possible resonator modes are indicated. The curve labeled *Doppler linewidth* gives the relative number of atoms in the resonator as a function of the frequency at which they emit light. The product of the Doppler linewidth and the resonator transmission gives the relative intensities of the stimulated emission at the different frequencies supported by the resonator. This product is shown as a function of frequency in Figure 11.14b. Because of losses in the cavity, the number of atoms in level 3 is continuously depleted. A **lasing transition** can only be sustained if enough atoms in the cavity are in the excited state at a supported resonance as indicated by the line labeled *amplification threshold*. In Figure 11.14, only two resonator modes lead to a sufficient intensity to sustain the laser. The main function of the optical resonator is to decrease the width in frequency of the lasing transition to less than the Doppler limit. Example Problem 11.9 shows how the number of supported modes varies with the gas temperature.

EXAMPLE PROBLEM 11.9

The distribution function that describes the probability of finding a particular value of magnitude of the velocity along one dimension v in a gas at temperature T is given by

$$f(v)dv = \sqrt{\frac{m}{2\pi k_B T}} e^{-mv^2/2k_B T} dv$$

This velocity distribution leads to the broadening of a laser line in frequency given by

$$I(\nu)d\nu = \sqrt{\frac{mc^2}{2\pi k_B T \nu_0^2}} \exp\left\{-\frac{mc^2}{2k_B T} \left(\frac{\nu - \nu_0}{\nu_0}\right)^2\right\} d\nu$$

The symbol c stands for the speed of light, and k is the Boltzmann constant. We next calculate the broadening of the 632.8 nm line in the He–Ne laser as a function of T .

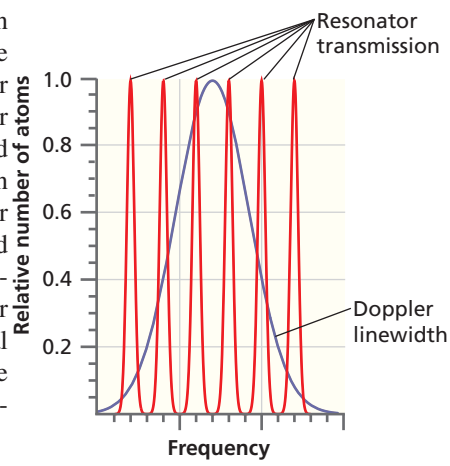
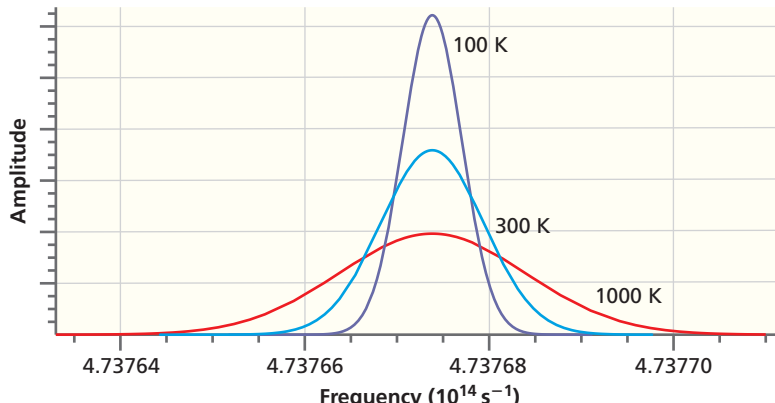
- Plot $I(\nu)$ for $T = 100.0, 300.0$, and 1000.0 K, using the mass appropriate for a Ne atom, and determine the width in frequency at half the maximum amplitude of $I(\nu)$ for each of the three temperatures.
- Assuming that the amplification threshold is 50% of the maximum amplitude, how many modes could lead to amplification in a cavity of length 100. cm?

Solution

- This function is of the form of a normal or Gaussian distribution given by

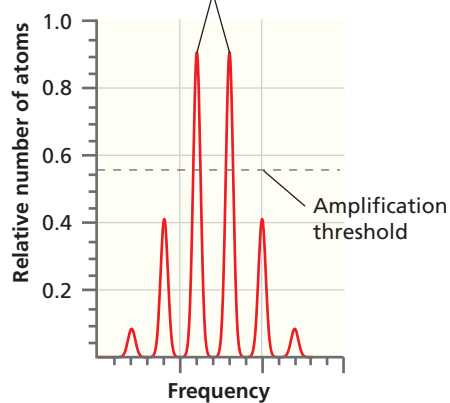
$$f_{v_0, \sigma}(\nu)d\nu = \frac{1}{\sigma\sqrt{2\pi}} e^{-(\nu-\nu_0)/2\sigma^2} d\nu$$

The full width at half height is 2.35σ , or for this case, $2.35\sqrt{k_B T \nu_0^2 / mc^2}$. This gives half widths of 7.554×10^8 s $^{-1}$, 1.308×10^9 s $^{-1}$, and 2.388×10^9 s $^{-1}$ at temperatures of 100.0, 300.0, and 1000.0 K, respectively. The functions $I(\nu)$ are plotted here:



(a)

Only two resonator modes lead to sufficient intensity to sustain the laser.



(b)

Figure 11.14

Factors influencing the width in frequency of a lasing transition. (a) The resonator transmission decreases the linewidth of the lasing transition to less than the Doppler limit. (b) The amplification threshold further reduces the number of frequencies supported by the resonator.

b. The frequency spacing between two modes is given by

$$\Delta\nu = \frac{c}{2d} = \frac{2.998 \times 10^8 \text{ m s}^{-1}}{2 \times 1.00 \text{ m}} = 1.50 \times 10^8 \text{ s}^{-1}$$

The width of the velocity distribution will support 5 modes at 100.0 K, 8 modes at 300.0 K, and 15 modes at 1000. K. The smaller Doppler broadening at low temperatures reduces the number of possible modes considerably.

By adding a further optical filter in the laser tube, it is possible to have only one mode enhanced by multiple reflections in the optical resonator. In addition, all light of the correct frequency but with a propagation direction that is not perpendicular to the mirrors, is not enhanced through multiple reflections. In this way, the resonator establishes a standing wave at the lasing frequency that has a propagation direction aligned along the laser tube axis. This standing wave causes further photons to be emitted from the lasing medium (He–Ne mixture) through stimulated emission. As discussed previously, these photons are exactly in phase with the photons that stimulate the emission and have the same propagation direction. These photons amplify the standing wave, which because of its greater intensity causes even more stimulated emission. Allowing one of the end mirrors to be partially transmitting allows some of the light to escape, and the result is a coherent, well-collimated laser beam.

To this point in our discussion, lasers have been discussed at a schematic level. How does this discussion relate to the atomic energy levels of He and Ne shown schematically in Figure 11.15? The electrical discharge in the laser tube produces electrons and positively charged ions. The electrons are accelerated in the electric field and can excite the He atoms from states in the ${}^1\text{S}$ term of the $1s^2$ configuration to states in the ${}^1\text{S}$ and ${}^3\text{S}$ terms of the $1s2s$ configuration. This is the **pumping transition** in the scheme shown in Figure 11.11. This transition occurs through a collision rather than through the absorption of a photon; therefore, the normal selection rules do not apply. Because the selection rules $\Delta S = 0$ and $\Delta l = \pm 1$ prohibit transitions to the ground state through emission of a photon, these states are long lived. The excited He atoms efficiently transfer their energy through collisions to states in the $2p^55s$ and $2p^54s$ configurations of Ne. This creates a population inversion relative to Ne states in the $2p^54p$ and $2p^53p$ configuration. The corresponding levels are involved in the lasing transition through stimulated emission. Spontaneous emission to states in the $2p^53s$ configuration and collisional deactivation at the inner surface of the optical resonator depopulate the lower state of the lasing transitions and ensure that the population inversion is maintained. The initial excitation is to excited states of He, which consist of a single term. However, the excited-state configurations of Ne give rise to several terms (${}^3\text{P}$ and ${}^1\text{P}$ for $2p^54s$ and $2p^55s$, and ${}^3\text{D}$, ${}^1\text{D}$, ${}^3\text{P}$, ${}^1\text{P}$, ${}^3\text{S}$, and ${}^1\text{S}$ for $2p^53p$ and $2p^54p$). The manifold of these states is indicated in the figure by thicker lines, indicating a range of energies.

Note that a number of wavelengths can lead to lasing transitions. Coating the mirrors in the optical resonator ensures that they are reflective only in the range of interest. The resonator is usually configured to support the 632.8 nm transition in the visible part of the spectrum. This corresponds to the red light characteristic of He–Ne lasers.

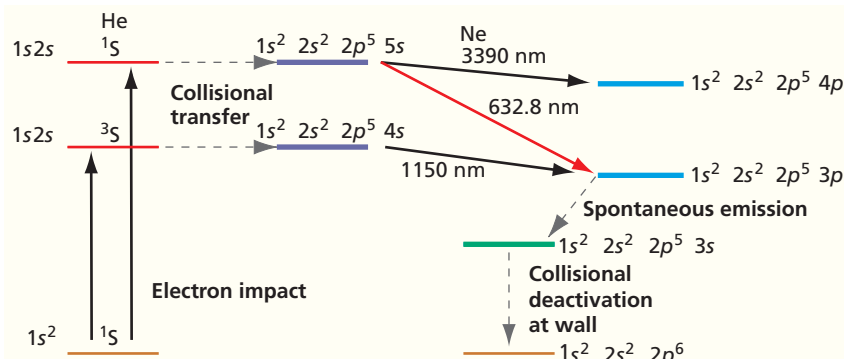


Figure 11.15

Transitions in the He–Ne laser. The inclined solid lines in the upper right side of the figure show three possible lasing transitions

11.8 AUGER ELECTRON SPECTROSCOPY AND X-RAY PHOTOELECTRON SPECTROSCOPY

Most of the atomic spectroscopic techniques that we have discussed have been illustrated with gas-phase examples. Another useful application of spectroscopic methods is in the analysis of the elemental composition of surfaces. This capability is important in such fields as corrosion investigations and heterogeneous catalysis in which a chemical reaction takes place at the interface between a solid phase and a gaseous or liquid phase. Sampling a surface requires methods that analyze only the first few atomic layers of the solid. The two spectroscopic methods described in this section satisfy this requirement, as will be discussed next. These techniques are also applicable to other types of studies, such as gas-phase analysis.

Both of these spectroscopic methods involve the ejection of an electron from individual atoms in a solid and the measurement of the electron energy. To avoid energy losses due to collisions of the ejected electron with gas-phase molecules, the solid sample is examined in a vacuum chamber. If the electron has sufficient energy to escape from the solid into the vacuum, it will have a characteristic energy simply related to the energy level from which it originated. To escape into the vacuum, it must travel from its point of origin to the surface of the solid. This process is analogous to a gas-phase atom traveling through a gas. The atom will travel a certain distance (that depends on the gas pressure) before it collides with another atom. In the collision, it exchanges energy and momentum with its collision partner and thereby loses memory about its previous momentum and energy. Similarly, an electron generated in the solid traveling toward the surface suffers collisions with other electrons and loses memory of the energy levels from which it originated if its path is too long. Only those atoms within one **inelastic mean free path** of the surface eject electrons into the gas phase whose energy is simply related to the atomic energy levels. Electrons emitted from other atoms simply contribute to the background signal. The mean free path for electrons depends on the energy of the electrons but is relatively independent of the surface composition. The mean free path has its minimum value of about 2 atomic layers near 40 eV and increases slowly to about 10 atomic layers at 1000 eV. Electrons in this energy range that have been ejected from atoms can provide information that is highly surface sensitive. Example Problem 11.10 demonstrates the surface sensitivity of these spectroscopic methods.

EXAMPLE PROBLEM 11.10

Upon impingement of X-rays from a laboratory source, titanium atoms near the surface of bulk TiO_2 emit electrons into a vacuum with energy of 790 eV. The finite mean free path of these electrons leads to an attenuation of the signal for Ti atoms beneath the surface according to $[I(d)]/[I(0)] = e^{-d/\lambda}$. In this equation, d is the distance to the surface and λ is the mean free path. If λ is 2.0 nm, what is the sensitivity of Ti atoms 10.0 nm below the surface relative to those at the surface?

Solution

Substituting in the equation $[I(d)]/[I(0)] = e^{-d/\lambda}$, we obtain $\frac{I(10.0)}{I(0)} = e^{-10.0/2.0} = 6.7 \times 10^{-3}$. This result illustrates the surface sensitivity of the technique.

Auger electron spectroscopy (AES or Auger, pronounced *oh-zhe*) is schematically illustrated in Figure 11.16. An electron (or photon) ejects an electron from a low-lying level in an atom (Event I in Figure 11.16). This hole is quickly filled by a transition from a higher state (Event II). This event alone, however, does not conserve energy. Energy conservation is accomplished by the simultaneous ejection of a second electron into the gas phase (Event III). It is the kinetic energy of this electron that is measured. Although three different energy levels are involved in this spectroscopy, the signatures of different atoms are quite easy to distinguish. The main advantage of using electrons

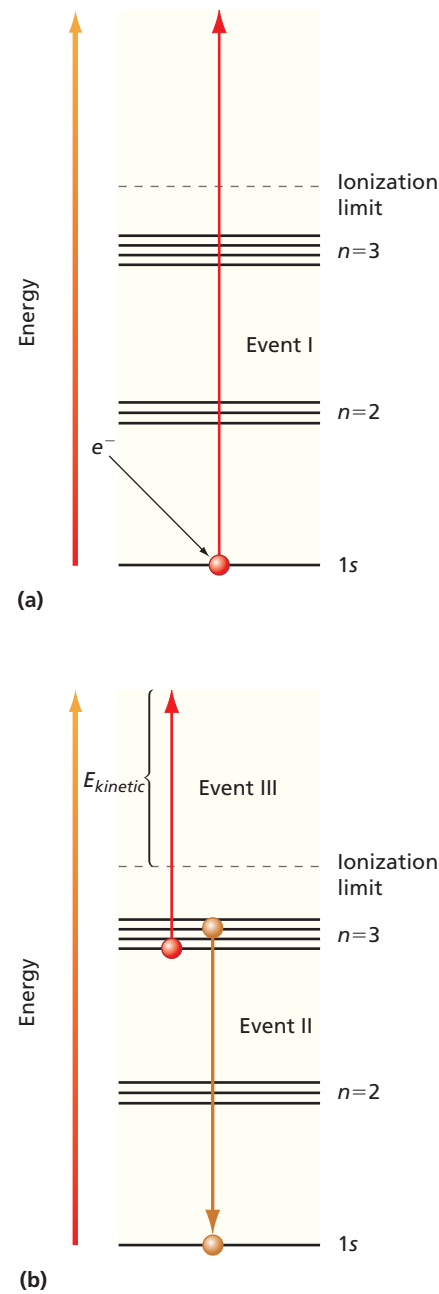
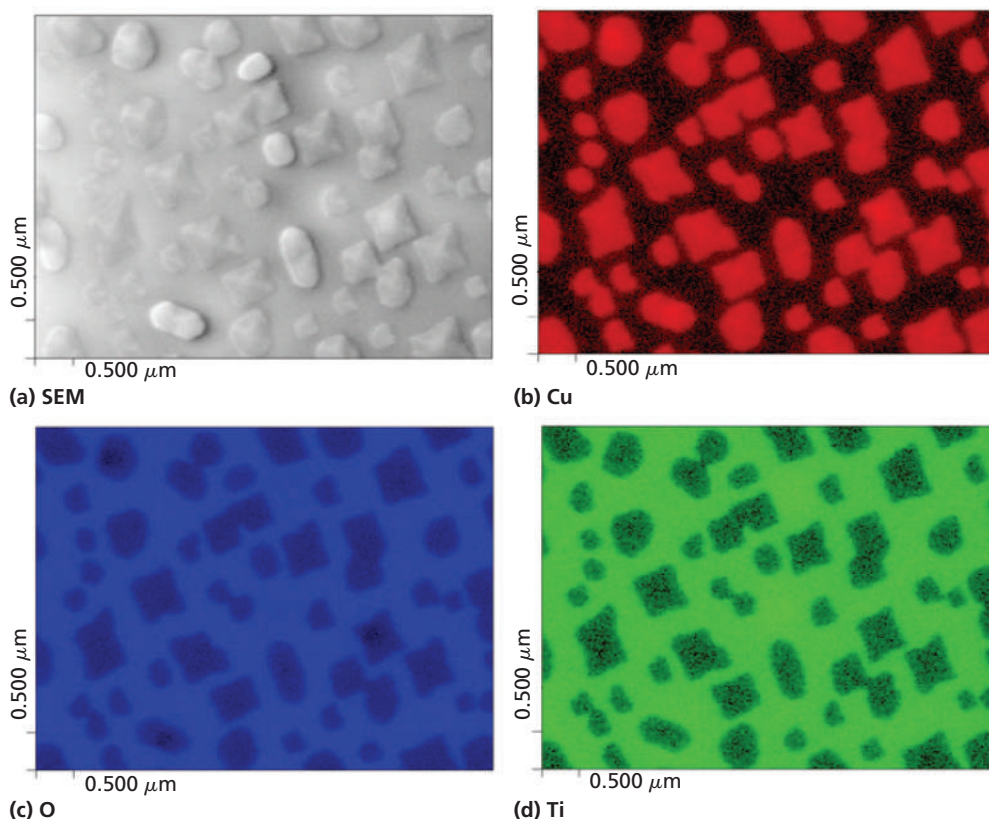


Figure 11.16 Schematic illustration of Auger electron spectroscopy. (a) A core-level hole is formed by energy transfer from an incident photon or electron (Event I). (b) The core hole is filled through relaxation from a higher level (Event II), and a third electron is emitted to conserve energy (Event III). The energy of the emitted electron can be measured and is characteristic of the particular element.

Figure 11.17

Scanning electron microscopy and scanning Auger spectroscopy images for copper, oxygen, and titanium. Images are for a $0.5 \times 0.5\text{-}\mu\text{m}$ area of a SrTiO_3 crystal surface on which Cu_2O nanodots have been deposited by Cu evaporation in an oxygen-containing plasma. (a) The SEM image obtained without energy analysis shows structure but gives no information on the elemental distribution. (b), (c), and (d) are obtained using energy analysis of backscattered electrons. Light and dark areas correspond to high and low values respective of Cu (b), O (c), and Ti (d). An analysis of the data shows that the light areas in (b) contain Cu and O, but no Ti, and that the dark areas in (d) contain no Ti.

Source: Adapted from Liang et al., Electrochemical Society Proceedings 2001-5, 125–133.



rather than photons to create the initial hole is to gain spatial resolution. Electron beams can be focused to a spot size on the order of 10–100 nm. Therefore, Auger spectroscopy with electron excitation is routinely used in many industries to map out elemental distribution at the surfaces of solids with very high lateral resolution.

Results using scanning Auger spectroscopy to study the growth of Cu_2O nanodots on the surface of a SrTiO_3 crystal are shown in Figure 11.17. The scanning electron microscopy (SEM) image in Figure 11.17a shows the structure of the surface but gives no information on the elemental composition. Scanning Auger images of the same area are shown for Cu, O, and Ti (Figure 11.17b, c, and d, respectively). These images show that Cu does not uniformly coat the surface but instead forms three-dimensional crystallites. This conclusion can be drawn from the absence of Cu and the presence of Ti in the areas between the nanodots. The Cu_2O nanodots appear darker (lower O content) than the underlying SrTiO_3 surface in the oxygen image because Cu_2O has only one O for every two Cu cations, whereas the surface has three O in a formula unit containing two cations. These results show that the nanodot deposition process can be understood using a surface-sensitive spectroscopy. For more details, see the reference to Liang et al. in Further Reading.

X-ray photoelectron spectroscopy (XPS) is simpler to understand than AES in that only one level is involved. A photon of energy $h\nu$ is absorbed by an atom, and to conserve energy, an electron is ejected with kinetic energy

$$E_{\text{kinetic}} = h\nu - E_{\text{binding}} \quad (11.10)$$

A small correction term that involves the work functions of the solid (defined in Chapter 1) and the detector has been omitted. A schematic picture of the process that gives rise to an ejected electron is shown in Figure 11.18. Currently, no off-the-shelf X-ray lasers are available, so sources cannot be made with very small bandwidths. However, using monochromatized X-ray sources, we can observe distinctly different peaks for substances in which the same atom is present in chemically nonequivalent environments. This **chemical shift** is also illustrated in Figure 11.18. A positive value for the chemical shift indicates a higher binding energy for the electron in the atom than would be measured for the free atom. The origin of the chemical shift can be understood in a simple model, although accurate calculations require a more detailed treatment.

Consider the different binding environment of the carbon atom in ethyltrifluoroacetate, whose structure is shown in Figure 11.18b. The carbon atom in the CF_3 group experiences a net electron withdrawal to the much more electronegative F atoms. Therefore, the 1s electrons lose some of the shielding effect they had from the 2p electrons, and, as a result, the C 1s electron experiences a slightly greater nuclear charge. This leads to an increase in binding energy or a positive chemical shift. The carbon atom with double and single bonds to oxygen experiences an electron withdrawal, though to a lesser degree. The carbon of the methyl group has little electron transfer, and the methylene carbon experiences electron withdrawal because it is directly bonded to an oxygen. Although these effects are small, they are easily measurable. Therefore, a photoelectron spectrum provides information on the oxidation state as well as on the identity of the element.

An example of the sensitivity of XPS to the oxidation state of elements on the surface is shown in Figure 11.19. The X-ray photon ejects an electron from the 2p level of Cr species near the surface, and the signal is dominated by those species within $\sim 1 \text{ nm}$ of the surface. The spin angular momentum s of the remaining electron in the Cr 2p level couples with its orbital angular momentum \mathbf{l} to form the total angular momentum vector \mathbf{J} with two possible values for the quantum number, $j = 1/2$ and $3/2$. These two states are of different energy, and, therefore, two peaks are observed in the spectrum. The ratio of the measured photoemission signal from these states is given by the ratio of their degeneracy, or

$$\frac{I(2p_{3/2})}{I(2p_{1/2})} = \frac{2 \times \left(\frac{3}{2}\right) + 1}{2 \times \left(\frac{1}{2}\right) + 1} = 2$$

The binding energy corresponding to the Cr peaks clearly shows a pronounced chemical shift that makes it possible to identify the oxidation state of the chromium. For more details, see the reference to Qiao et al. in Further Reading.

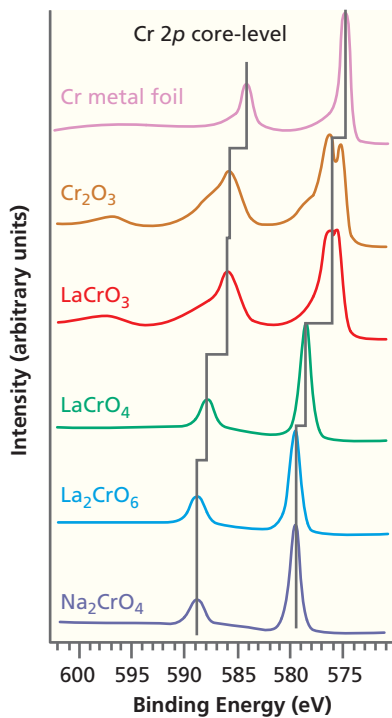


Figure 11.19

XPS spectra for chromium surfaces of different chemical composition. The chemical shift with oxidation state is clearly seen. Note the splitting of the peaks originating from the 2p core level as a result of spin-orbit interaction. The left peak in each spectrum arises from the $\text{Cr } 2p_{1/2}$ level, and the right peak arises from the $\text{Cr } 2p_{3/2}$. Adapted from L. Qiao et al., *Journal of Materials Chemistry C*, 1 (2013) 4527–4535.

Source: Graph courtesy of Scott A. Chambers/Pacific Northwest National Laboratory.

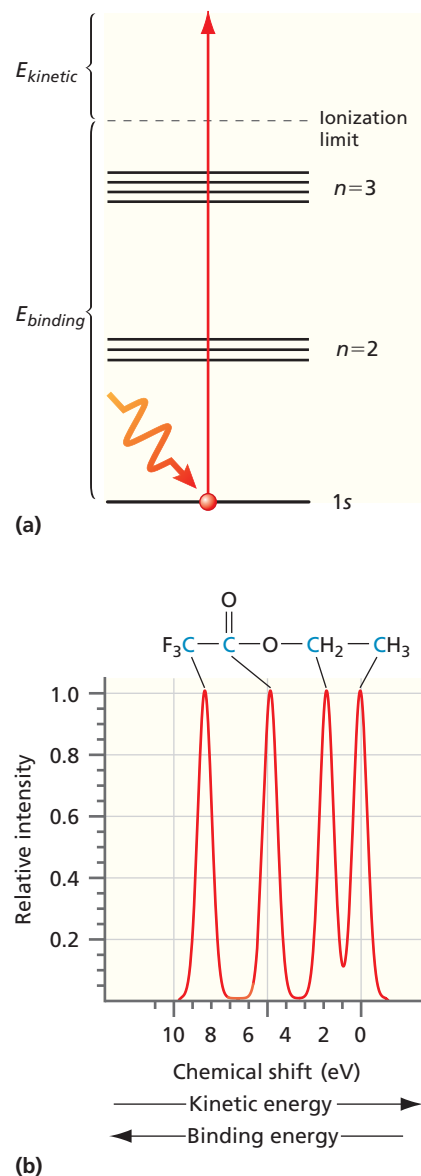


Figure 11.18

Principles and practice of X-ray photoelectron spectroscopy. (a) Depiction of incident photon and ejected electron underlying XPS. (b) An XPS spectrum exhibiting chemical shifts for the carbon 1s level of the ethyltrifluoroacetate molecule.

VOCABULARY

antiparallel spins	Grotian diagram	pumping transition
atomic absorption spectroscopy	Hund's rules	resonator modes
atomic emission spectroscopy	incoherent photon source	singlet
Auger electron spectroscopy	inelastic mean free path	spin-orbit coupling
chemical shift	laser	term
Clebsch-Gordan series	lasing transition	term symbol
coherent photon source	level	total angular momentum
configuration	multiplicity	triplet
degeneracy of a term	optical resonator	unpaired electrons
Doppler broadening	paired electrons	X-ray photoelectron spectroscopy
Doppler shift	parallel spins	
good quantum number	population inversion	

KEY EQUATIONS

Equation	Significance of Equation	Equation Number
$\mathbf{L} = \sum_i \mathbf{l}_i, \quad \mathbf{S} = \sum_i \mathbf{s}_i$	Spin and orbital angular momentum for atom is vector sum over all electrons in unfilled subshells	11.1
$\hat{S}_z = \sum_i \hat{s}_{z,i}$ and $\hat{S}^2 = \left(\sum_i \hat{s}_i \right)^2$	Relations between angular momentum operators for atoms and for individual electrons	11.2
$\hat{L}_z = \sum_i \hat{l}_{z,i}$ and $\hat{L}^2 = \left(\sum_i \hat{l}_i \right)^2$		
$M_L = \sum_i m_{li}, \quad M_S = \sum_i m_{si}$	z component of orbital and spin angular momentum is scalar sum over electrons	11.4
$\mathbf{J} = \mathbf{L} + \mathbf{S}$	Relation between total, spin, and orbital angular momentum	11.5
$\tilde{v} = \frac{\mu e^4}{8\epsilon_0^2 h^3 c} \left(\frac{1}{n_{initial}^2} - \frac{1}{n_{final}^2} \right) = R_H \left(\frac{1}{n_{initial}^2} - \frac{1}{n_{final}^2} \right)$	Frequency of transitions between energy levels of H atom	11.7
$\omega = \omega_0 \left(1 + \left[1 \mp \frac{v_z}{c} \right] \right)$	Nonrelativistic Doppler shift	11.9
$E_{kinetic} = h\nu - E_{binding}$	Kinetic energy of ejected electron in X-ray photoelectron spectroscopy	11.10

CONCEPTUAL PROBLEMS

Q11.1 Without invoking equations, explain why the energy of the triplet state is lower than that of the singlet state for He in the $1s^1 2s^1$ configuration.

Q11.2 How can the width of a laser line be less than that determined by Doppler broadening?

Q11.3 Why is an electronically excited atom more reactive than the same ground state atom?

Q11.4 Why is atomic absorption spectroscopy more sensitive in many applications than atomic emission spectroscopy?

Q11.5 Why does the Doppler effect lead to a shift in the wavelength of the light emitted by a star, but to a broadening of emitted light in a gas?

Q11.6 Why are n , l , m_l , and m_s not good quantum numbers for many electron atoms?

Q11.7 Write an equation giving the relationship between the Rydberg constant for H and for Li^{2+} .

Q11.8 Can the individual states in Table 11.1 be distinguished experimentally?

Q11.9 How is it possible to determine the L and S value of a term knowing only the M_L and M_S values of the states?

Q11.10 What is the origin of the chemical shift in XPS?

Q11.11 Why does one need to put a sample in a vacuum chamber to study it with XPS or AES?

Q11.12 Why is XPS a surface-sensitive technique?

Q11.13 Explain the direction of the chemical shifts for the different chromium containing compounds in Figure 11.19.

NUMERICAL PROBLEMS

Section 11.2

P11.1 Using Table 11.3, which lists the possible terms that arise from a given configuration, and Hund's rules, write the term symbols for the ground state of the atoms H through F in the form $(2S+1)L_J$.

P11.2 Using Table 11.3, which lists the possible terms that arise from a given configuration, and Hund's rules, write the configurations and term symbols for the ground state of the ions F^- and Ca^{2+} in the form $(2S+1)L_J$.

P11.3 How many ways are there to place three electrons into an f subshell? What is the ground-state term for the f^3 configuration, and how many states are associated with this term?

P11.4 List the allowed quantum numbers m_l and m_s for the following subshells and determine the maximum occupancy of the subshells:

- a. $2p$
- b. $3d$
- c. $4f$
- d. $5g$

P11.5 Derive the ground-state term symbols for the following configurations:

- a. d^5
- b. f^3
- c. p^4

P11.6 Calculate the terms that can arise from the configuration $np^1n'p^1$, $n \neq n'$. Compare your results with those derived in the text for np^2 . Which configuration has more terms and why?

P11.7 For a closed-shell atom, an antisymmetric wave function can be represented by a single Slater determinant. For an open-shell atom, more than one determinant is needed. Show that the wave function for the $M_S = 0$ triplet state of He $1s^12s^1$ is a linear combination of two of the Slater determinants of Figure 11.3. Which of the two are needed, and what is the linear combination?

P11.8 Derive the ground-state term symbols for the following atoms or ions:

- a. H
- b. F
- c. F^-
- d. Na
- e. Na^+
- f. P
- g. Sc

P11.9 What atomic terms are possible for the following electron configurations? Which of the possible terms has the lowest energy?

- a. ns^1np^1
- b. ns^1nd^1
- c. ns^2np^1
- d. ns^1np^2

P11.10 List the quantum numbers L and S that are consistent with the following terms:

- a. ^4S
- b. ^4G
- c. ^3P
- d. ^2D

P11.11 A general way to calculate the number of states that arise from a given configuration is as follows. Calculate the combinations of m_l and m_s for the first electron, and call that number n . The number of combinations used is the number of electrons, which we call m . The number of unused combinations is $n - m$. According to probability theory, the number of distinct permutations that arise from distributing the m electrons among the n combinations is $n!/[m!(n-m)!]$. For example, the number of states arising from a p^2 configuration is $6!/[2!4!] = 15$, which is the result obtained in Section 11.2. Using this formula, calculate the number of possible ways to place five electrons in a d^5 subshell. What is the ground state term for the d^5 configuration, and how many states does the term include?

P11.12 The ground state level for the phosphorous atom is $^4\text{S}_{3/2}$. List the possible values of L , M_L , S , M_S , J , and M_J consistent with this level.

P11.13 Derive the ground state term symbols for the following atoms or ions:

- a. F
- b. Na
- c. P

Section 11.3

P11.14 What J values are possible for a ^6H term? Calculate the number of states associated with each level and show that the total number of states is the same as that calculated from $(2S + 1)(2L + 1)$.

P11.15 Consider the $1s np \ ^3\text{P} \rightarrow 1s nd \ ^3\text{D}$ transition in He. Draw an energy-level diagram, taking into account the spin-orbit coupling that splits terms into levels. Into how many levels does each term split? The selection rule for transitions in this case is $\Delta J = 0, \pm 1$. How many transitions will be observed in an absorption spectrum? Show the allowed transitions in your energy diagram.

P11.16 What are the levels that arise from a ^4F term? How many states are there in each level?

P11.17 The spectrum of the hydrogen atom reflects the splitting of the $1s^2\text{S}$ and $2p^2\text{P}$ terms into levels. The energy difference between the levels in each term is much smaller than the difference in energy between the terms. Given this information, how many spectral lines are observed in the $1s^2\text{S} \rightarrow 2p^2\text{P}$ transition? Are the frequencies of these transitions very similar or quite different?

P11.18 Using Table 11.3, which lists the possible terms that arise from a given configuration, and Hund's rules, write the term symbols for the ground state of the atoms K through Cu, excluding Cr, in the form $(^{2S+1})L_J$.

P11.19 Two angular momenta with quantum numbers $j_1 = 3/2$ and $j_2 = 5/2$ are added. What are the possible values of J for the resultant angular momentum states?

P11.20 Derive the ground state term symbols for the following configurations:

- a. d^2
- b. f^9
- c. f^{12}

Section 11.4

P11.21 The absorption spectrum of the hydrogen atom shows lines at 5334, 7804, 9145, 9953, and 10,478 cm^{-1} . There are no lower-frequency lines in the spectrum. Use the graphical methods discussed in Example Problem 11.6 to determine $n_{initial}$ and the ionization energy of the hydrogen atom in this state. Assume values for $n_{initial}$ of 1, 2, and 3.

P11.22 Calculate the transition dipole moment, $\mu_z^{mn} = \int \psi_m^*(\tau) \mu_z \psi_n(\tau) d\tau$ where $\mu_z = -er \cos \theta$ for a transition from the $1s$ level to the $2p_z$ level in H. Show that this transition is allowed. The integration is over r , θ , and ϕ . Use

$$\psi_{210}(r, \theta, \phi) = \frac{1}{\sqrt{32\pi}} \left(\frac{1}{a_0} \right)^{3/2} \frac{r}{a_0} e^{-r/2a_0} \cos \theta$$

for the $2p_z$ wave function.

P11.23 Calculate the wavelengths of the first three lines of the Lyman, Balmer, and Paschen series, and the series limit (the shortest wavelength) for each series.

P11.24 The Lyman series in the hydrogen atom corresponds to transitions that originate from the $n = 1$ level in absorption or that terminate in the $n = 1$ level for emission. Calculate the energy, frequency (in inverse seconds and inverse centimeters), and wavelength of the least and most energetic transition in this series.

P11.25 As discussed in Chapter 9, in a more exact solution of the Schrödinger equation for the hydrogen atom, the coordinate system is placed at the center of mass of the atom rather than at the nucleus. In that case, the energy levels for a one-electron atom or ion of nuclear charge Z are given by

$$E_n = -\frac{Z^2 \mu e^4}{32\pi^2 \epsilon_0^2 \hbar^2 n^2}$$

where μ is the reduced mass of the atom. The masses of an electron, a proton, and a tritium (${}^3\text{H}$ or T) nucleus are given by 9.1094×10^{-31} kg, 1.6726×10^{-27} kg, and 5.0074×10^{-27} kg, respectively. Calculate the frequency of the $n = 1 \rightarrow n = 4$ transition in H and T to five significant figures. Which of the transitions, $1s \rightarrow 4s$, $1s \rightarrow 4p$, or $1s \rightarrow 4d$, could the frequencies correspond to?

P11.26 Calculate the transition dipole moment, $\mu_z^{mn} = \int \psi_m^*(\tau) \mu_z \psi_n(\tau) d\tau$ where $\mu_z = -er \cos \theta$ for a transition from the $1s$ level to the $2s$ level in H. Show that this transition is forbidden. The integration is over r , θ , and ϕ .

P22.27 The first ionization potential of ground state He is 24.6 eV. The wavelength of light associated with the $1s2p$ ^1P term is 58.44 nm. What is the ionization energy of the He atom in this excited state?

P11.28 The Grotrian diagram in Figure 11.7 shows a number of allowed electronic transitions for He. Which of the following transitions shows multiple spectral peaks due to a splitting of terms into levels? How many peaks are observed in each case? Are any of the following transitions between energy levels forbidden by the selection rules?

- a. $1s^2 \ ^1\text{S} \rightarrow 1s2p \ ^1\text{P}$
- b. $1s2p \ ^1\text{P} \rightarrow 1s3s \ ^1\text{S}$
- c. $1s2s \ ^3\text{S} \rightarrow 1s2p \ ^3\text{P}$
- d. $1s2p \ ^3\text{P} \rightarrow 1s3d \ ^3\text{D}$

Section 11.5

P11.29 The principal line in the emission spectrum of sodium is yellow. On close examination, the line is seen to be a doublet with wavelengths of 589.0 and 589.6 nm. Explain the source of this doublet.

P11.30 Atomic emission experiments of a mixture show a calcium line at 422.673 nm corresponding to a $^1\text{P}_1 \rightarrow ^1\text{S}_0$ transition and a doublet due to potassium $^2\text{P}_{3/2} \rightarrow ^2\text{S}_{1/2}$ and $^2\text{P}_{1/2} \rightarrow ^2\text{S}_{1/2}$ transitions at 764.494 and 769.901 nm, respectively.

- a. Calculate the ratio g_{upper}/g_{lower} for each of these transitions.
- b. Calculate n_{upper}/n_{lower} for a temperature of 1600. °C for each transition.

P11.31 Use the transition frequencies shown in Example Problem 11.7 to calculate the energy (in joules and electron-volts) of the six levels relative to the $3s \ ^2\text{S}_{1/2}$ level. State your answers with the correct number of significant figures.

P11.32 The transition Al[Ne] $(3s)^2(3p)^1 \rightarrow$ Al[Ne] $(3s)^2(4s)^1$ has two lines given by $\tilde{\nu} = 25354.8 \text{ cm}^{-1}$ and $\tilde{\nu} = 25242.7 \text{ cm}^{-1}$. The transition Al[Ne] $(3s)^2(3p)^1 \rightarrow$ Al[Ne] $(3s)^2(3d)^1$ has three lines given by $\tilde{\nu} = 32444.8 \text{ cm}^{-1}$, $\tilde{\nu} = 32334.0 \text{ cm}^{-1}$, and $\tilde{\nu} = 32332.7 \text{ cm}^{-1}$. Sketch an energy-level diagram of the states involved and explain the source of all lines. [Hint: The lowest energy levels are P levels and the highest are D levels. The energy spacing between the D levels is greater than for the P levels.]

P11.33 In the Na absorption spectrum, the following transitions are observed:

$$\begin{aligned} 4p \ ^2\text{P} &\rightarrow 3s \ ^2\text{S} \quad \lambda = 330.26 \text{ nm} \\ 3p \ ^2\text{P} &\rightarrow 3s \ ^2\text{S} \quad \lambda = 589.593 \text{ nm}, 588.996 \text{ nm} \\ 5s \ ^2\text{S} &\rightarrow 3p \ ^2\text{P} \quad \lambda = 616.073 \text{ nm}, 615.421 \text{ nm} \end{aligned}$$

Calculate the energies of the $4p \ ^2\text{P}$ and $5s \ ^2\text{S}$ states with respect to the $3s \ ^2\text{S}$ ground state.

P11.34 Given that the levels in the ^3P term for carbon have the relative energies (expressed in wave numbers) of ${}^3\text{P}_1 - {}^3\text{P}_0 = 16.4 \text{ cm}^{-1}$ and ${}^3\text{P}_2 - {}^3\text{P}_1 = 27.1 \text{ cm}^{-1}$, calculate the ratio of the number of C atoms in the ${}^3\text{P}_2$ and ${}^3\text{P}_0$ levels at 200. and 1000. K.

Section 11.7

P11.35 The Doppler broadening in a gas can be expressed as $\Delta\nu = (2\nu_0/c)\sqrt{2k_B T \ln 2/m}$, where m is the molecular mass. For the sodium $3p\ ^2P_{3/2} \rightarrow 3s\ ^2S_{1/2}$ transition, $\nu_0 = 5.0933 \times 10^{14}\text{ s}^{-1}$. Calculate $\Delta\nu$ and $\Delta\nu/\nu_0$ at 500. K.

Section 11.9

P11.36 The inelastic mean free path of electrons in a solid, λ , governs the surface sensitivity of techniques such as AES and XPS. The electrons generated below the surface must make their way to the surface without losing energy in order to give elemental and chemical shift information. An empirical expression for elements that give λ as a function of the kinetic energy of the electron generated in AES or XPS is $\lambda = 538E^{-2} + 0.41(IE)^{0.5}$. The units of λ are monolayers, E is the kinetic energy of the electron, and l is the monolayer thickness in nanometers. Based on this equation, what value

of kinetic energy maximizes the surface sensitivity for a monolayer thickness of 0.3 nm? An equation solver would be helpful in obtaining the answer.

P11.37 The effective path length that an electron travels before being ejected into the vacuum is related to the depth below the surface at which it is generated and the exit angle by $d = \lambda \cos \theta$, where λ is the inelastic mean free path and θ is the angle between the surface normal and the exit direction.

- Justify this equation based on a sketch of the path that an electron travels before exiting into the vacuum.
- The XPS signal from a thin layer on a solid surface is given by $I = I_0(1 - e^{-d/\lambda \cos \theta})$, where I_0 is the signal that would be obtained from an infinitely thick layer, and d and λ are defined in Problem P11.36. Calculate the ratio I/I_0 at $\theta = 0$ for $\lambda = 2d$. Calculate the exit angle required to increase I/I_0 to 0.50.

WEB-BASED SIMULATIONS, ANIMATIONS, AND PROBLEMS

Simulations, animations, and homework problem worksheets can be accessed at www.pearsonhighered.com/advchemistry

W11.1 A pair of emission spectra, one from an unknown (hypothetical) atom and one resulting from the electron energy levels entered using sliders is displayed. The student

adjusts the displayed energy levels in order to replicate the atomic spectrum and determine the actual electron energy levels in the atom.

FURTHER READING

- Harriman, J. "Hund's Rule in Two-Electron Atomic Systems." *Journal of Chemical Education* 85 (2008): 451–452.
- Levine, I. N. *Quantum Chemistry*, 7th ed. Boston: Pearson, 2014.
- Liang, Y., Lea, A. S., McCready, D. E., and Meethunkij, P. *Synthesis and Characterization of Self-Assembled Cu₂O Nano-Dots*. Electrochemical Society Proceedings, 2001-5, 125–133.
- Muñoz-Marquez, M., Zarrabeitia, M., Castillo-Martínez, E., Eguía-Barrio, A., lo Rojo, T., and Casas-Cabanas, M. "Composition and Evolution of the Solid-Electrolyte Interphase in Na₂Ti₃O₇ Electrodes for Na-Ion Batteries:

XPS and Auger Parameter Analysis." *Applied Materials and Interface* 7 (2015): 7801–7808.

Qiao, L., Xiao, H., Heald, S., Bowden, M., Varga, T., Exarhos, G., Biegalski, M., Ivanov, I., Weber, W., Droubay, T., and Chambers, S. "The Impact of Crystal Symmetry on the Electronic Structure and Functional Properties of Complex Lanthanum Chromium Oxides." *Journal of Materials Chemistry C*, 1 (2013): 4527–4535.

Rioux, F. "Hund's Multiplicity Rule Revisited: Some Further Comments about the Stability of the Hydrogen Atom." *Journal of Chemical Education* 84 (2007): 358–360.

This page intentionally left blank

12

The Chemical Bond in Diatomic Molecules

WHY is this material important?

The chemical bond is at the heart of chemistry. In this chapter, we begin a discussion of the chemical bond in the simplest molecules, namely, homonuclear diatomic molecules. Similar to our approach to many-electron atoms, for which we defined a formalism of atomic configurations and atomic orbitals (AOs), our model for molecules is based on molecular configurations and molecular orbitals (MOs), which for valence electrons are delocalized over the entire molecule. The molecular orbital model is very useful in explaining trends in bond order, bond energy, and bond length in homonuclear diatomic molecules.

WHAT are the most important concepts and results?

Two AOs, one localized on each of the atoms in a diatomic molecule, combine to form two delocalized MOs provided that the AOs have a common region in which their amplitudes are nonzero. One of the linear combinations leads to an increased amplitude in the region between the atoms and is denoted as a bonding MO. The other linear combination leads to a decreased amplitude in the region between the atoms and is denoted as an antibonding MO. A larger bond order, defined as $1/2$ [(total number of electrons in bonding MOs) – (total number of electrons in antibonding MOs)] correlates well with an increased bond strength and a shorter bond length.

WHAT would be helpful for you to review for this chapter?

It would be helpful to review the material in Chapter 9 on the hydrogen atom and Chapter 10 on many-electron atoms.

12.1 GENERATING MOLECULAR ORBITALS FROM ATOMIC ORBITALS

Chemists need to have a firm understanding of the theory of the chemical bond because the essence of chemistry is making and breaking bonds between atoms. In this chapter, the origin of the chemical bond is first explored using the H_2^+ molecule as an example. We then discuss chemical bonding in first- and second-row diatomic molecules. In Chapter 13, localized and delocalized bonding models will be used to understand and predict the shape of small molecules. The discussion in this chapter and Chapter 13 is largely qualitative in character. In Chapter 15, numerical quantum chemical calculations on molecules are discussed. It may be useful for you to work on Chapter 15 in parallel with Chapters 12 and 13.

12.1 Generating Molecular Orbitals from Atomic Orbitals

12.2 The Simplest One-Electron Molecule: H_2^+

12.3 Energy Corresponding to the H_2^+ Molecular Wave Functions ψ_g and ψ_u

12.4 A Closer Look at the H_2^+ Molecular Wave Functions ψ_g and ψ_u

12.5 Homonuclear Diatomic Molecules

12.6 Electronic Structure of Many-Electron Molecules

12.7 Bond Order, Bond Energy, and Bond Length

12.8 Heteronuclear Diatomic Molecules

12.9 The Molecular Electrostatic Potential

A chemical bond is formed between two atoms if the total energy of the molecule passes through a minimum at an equilibrium distance that is smaller than the energy of the separated atoms. How does the electron distribution around the nuclei change when a chemical bond is formed? In answering this question, we consider the relative energies of two H atoms compared to the H₂ molecule. Two H atoms are more stable than the four infinitely separated charges by 2624 kJ mol⁻¹. The H₂ molecule is more stable than two infinitely separated H atoms by 436 kJ mol⁻¹. Therefore, the chemical bond lowers the total energy of the two protons and two electrons by 17%. Although appreciable, the **bond energy** is a small fraction of the total energy of the widely separated electrons and nuclei. This result suggests that the charge distribution in a molecule is quite similar to a superposition of the charge distribution of the individual atoms. However, as we will see later, valence electrons that are localized on an individual atom for large internuclear distances are **delocalized** in the molecule, meaning that they have a finite probability of being present anywhere in the molecule. Core electrons generally remain localized on individual atoms.

Concept

Chemical bond formation leads to delocalization of valence electrons.

As discussed in Chapter 10, the introduction of a second electron vastly complicates the task of finding solutions to the Schrödinger equation for atoms. This is also true for molecules. The exact **molecular wave functions** for a molecule with n electrons and m nuclei are functions of the positions of all the electrons and nuclei

$$\psi_i^{\text{molecule}} = \psi(\mathbf{r}_1, \mathbf{r}_2, \dots, \mathbf{r}_n, \mathbf{R}_1, \mathbf{R}_2, \dots, \mathbf{R}_m) \quad (12.1)$$

where the \mathbf{r} and \mathbf{R} are positions of the electrons and nuclei respectively. To solve the Schrödinger equation for a molecule, an approximate wave function with fewer variables is needed. The parts of ψ_i^{molecule} for the motion of the nuclei and the electrons, both of which appear in Equation (12.1), can be separated using the **Born–Oppenheimer approximation**, as follows. Because the electron is lighter than the proton by a factor of nearly 2000, the electron charge quickly rearranges in response to the slower periodic motion of the nuclei in molecular vibrations. Furthermore, because of the very different timescales for nuclear motion and electron motion, the two motions can be decoupled, and we can write Equation (12.1) in the form

$$\psi_i^{\text{molecule}} \approx \psi_{BO}(\mathbf{r}_1, \mathbf{r}_2, \dots, \mathbf{r}_n)\psi_{\text{nuclear}}(\mathbf{R}_1, \mathbf{R}_2, \dots, \mathbf{R}_m) \quad (12.2)$$

ψ_{nuclear} describes the motions of the nuclei in vibration and rotation of the molecule, and ψ_{BO} describes the electron distribution for instantaneous fixed positions of the nuclei. We next formulate the Schrödinger equation for ψ_{BO} and calculate the total energy of the molecule at a fixed set of nuclear positions using additional approximations, as will be discussed later. If this procedure is repeated for many values of $\mathbf{R}_1, \mathbf{R}_2, \dots, \mathbf{R}_m$, we can determine an energy function $E_{\text{total}}(\mathbf{R}_1, \mathbf{R}_2, \dots, \mathbf{R}_m)$. The values for $\mathbf{R}_1, \mathbf{R}_2, \dots, \mathbf{R}_m$ at the minimum in E determine the equilibrium nuclear positions.

The total energy operator for a diatomic molecule in the Born–Oppenheimer approximation is given by

$$\hat{H} = -\frac{\hbar^2}{2m_e} \sum_{i=1}^n \nabla_i^2 - \sum_{i=1}^n \left(\frac{Z_A e^2}{4\pi\epsilon_0 r_{iA}} + \frac{Z_B e^2}{4\pi\epsilon_0 r_{iB}} \right) + \sum_{i=1}^n \sum_{j>i}^n \frac{e^2}{4\pi\epsilon_0 r_{ij}} + \frac{Z_A Z_B e^2}{4\pi\epsilon_0 R_{AB}} \quad (12.3)$$

The first term is the kinetic energy of the electrons, the second term is the Coulomb attraction between the n electrons and two nuclei, the third term is the electron–electron repulsion, and the last term is the nuclear–nuclear repulsion. The restriction $j > i$ on the summation in the third term ensures that the electron–electron repulsion between electrons i and j is not counted twice.

The last term in \hat{H} is a constant because we are assuming that the nuclei do not move. It is convenient to separate out this term and to write an electronic total energy operator

$$\hat{H}_{el} = -\frac{\hbar^2}{2m_e} \sum_{i=1}^n \nabla_i^2 - \sum_{i=1}^n \left(\frac{Z_A e^2}{4\pi\epsilon_0 r_{iA}} + \frac{Z_B e^2}{4\pi\epsilon_0 r_{iB}} \right) + \sum_{i=1}^n \sum_{j>i}^n \frac{e^2}{4\pi\epsilon_0 r_{ij}} \quad (12.4)$$

The eigenvalues for the electronic Schrödinger equation $\hat{H}_{el}\psi_{el} = E_{el}\psi_{el}$ are related to the total energy eigenvalues by

$$E_{total} = E_{el} + \frac{Z_A Z_B e^2}{4\pi\epsilon_0 R_{AB}} \quad (12.5)$$

The reason for separating out the nuclear repulsion term will become clear when we discuss molecular orbital energy diagrams. The energy eigenfunctions are identical for \hat{H}_{el} and \hat{H} . Only the total energy eigenvalues are affected by separating out the nuclear repulsion.

The goal in this chapter is to develop a qualitative model of chemical bonding in diatomic molecules. Quantitative computational chemistry models discussed in Chapter 15 are required to determine accurate bond lengths and bond energies. The qualitative model that we discuss assumes that electrons in molecules occupy **molecular orbitals (MOs)** that extend over the molecule similar to how electrons in an atom occupy atomic orbitals. A given MO, ψ_{el} , can be written as a linear combination (LC) of the **atomic orbitals (AOs)** on individual atoms in the molecule. This is called the **LCAO-MO model**. The justification for this assumption is that the linear combination of AOs is the simplest wave function we can write that leads to the electron delocalization over the molecule. In the rest of this chapter, we drop the subscript *el* to simplify the notation. Keep in mind that we are calculating only the electronic part of $\psi_i^{molecule}$ and that we are doing so at a fixed set of nuclear positions. To simplify the mathematics, we consider only a diatomic molecule AB and assume that each MO is generated by combining only one AO on each atom, ϕ_a and ϕ_b on atoms A and B, respectively. The AOs are the basis functions for the MO (see Chapter 10 for a discussion of basis functions). Such a small basis set is inadequate for quantitative calculations, and in solving the computational problems at the end of the chapter, you will use much larger basis sets.

We next write an approximate MO in terms of the atomic orbitals, $\psi_1 = c_a\phi_a + c_b\phi_b$, and minimize the MO energy with respect to the values of the AO coefficients c_1 and c_2 . The expectation value of the MO energy ϵ for this approximate wave function is given by

$$\begin{aligned} \langle \epsilon \rangle &= \frac{\int \psi_1^* \hat{H}_{el} \psi_1 d\tau}{\int \psi_1^* \psi_1 d\tau} \\ &= \frac{\int (c_a \phi_a + c_b \phi_b)^* \hat{H}_{el} (c_a \phi_a + c_b \phi_b) d\tau}{\int (c_a \phi_a + c_b \phi_b)^* (c_a \phi_a + c_b \phi_b) d\tau} \\ &= \frac{(c_a)^2 \int \phi_a^* \hat{H}_{el} \phi_a d\tau + (c_b)^2 \int \phi_b^* \hat{H}_{el} \phi_b d\tau + 2c_a c_b \int \phi_a^* \hat{H}_{el} \phi_b d\tau}{(c_a)^2 \int \phi_a^* \phi_a d\tau + (c_b)^2 \int \phi_b^* \phi_b d\tau + 2c_a c_b \int \phi_a^* \phi_b d\tau} \quad (12.6) \end{aligned}$$

Because the AOs are normalized, the first two integrals in the denominator of the last line of Equation (12.6) have the value 1.

$$\langle \epsilon \rangle = \frac{(c_a)^2 H_{aa} + (c_b)^2 H_{bb} + 2c_a c_b H_{ab}}{(c_a)^2 + (c_b)^2 + 2c_a c_b S_{ab}} \quad (12.7)$$

In the preceding equation, the symbol H_{ij} is a shorthand notation for the integrals involving \hat{H}_{el} and the AOs *i* and *j*, as follows:

$$H_{ij} = \int \phi_i^*(\tau) \hat{H}_{el} \phi_j(\tau) d\tau \quad (12.8)$$

S_{ab} is called the **overlap integral** and is an abbreviation for $S_{ab} = \int \phi_a^* \phi_b d\tau$. The overlap, which was not encountered in atomic systems, is a new concept. The meaning of S_{ab} is indicated pictorially in Figure 12.1. It is a measure of the degree to which both of the AOs have nonzero values in the same region. S_{ab} can have values between zero and one. It has the value zero for widely separated atoms and increases as the atoms approach one another. As we will see later, in order to have chemical bond formation, it is necessary that $S_{ab} > 0$.

Concept

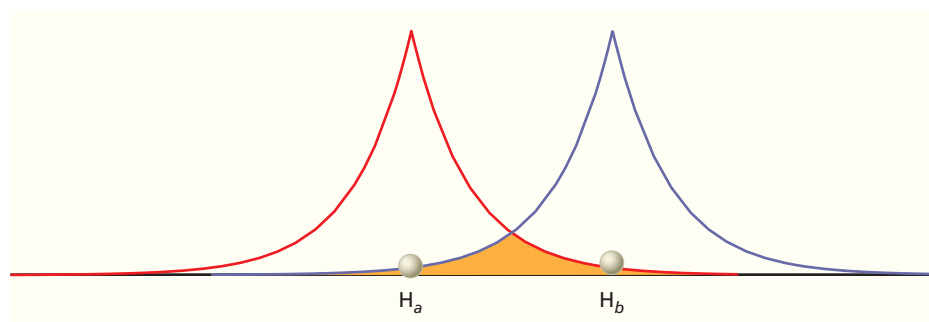
Molecular orbitals (MOs) can be expressed as a linear combination of atomic orbitals (AOs).

Concept

Bond formation requires that the overlap between atomic orbitals is greater than zero.

Figure 12.1

Amplitude of two 1s atomic orbitals shown along an axis connecting the atoms. The overlap is appreciable only for regions in which the amplitude of both AOs is significantly different from zero. Such a region is shown schematically in orange. In reality, the overlap occurs in three-dimensional space.



To minimize ε with respect to the coefficients, ε is first differentiated with respect to c_a and c_b . We then set the two resulting expressions equal to zero and solve for c_a and c_b . By multiplying both sides of the equation by the denominator before differentiating, the following two equations are obtained:

$$(2c_a + 2c_b S_{ab})\varepsilon + \frac{\partial\varepsilon}{\partial c_a}((c_a)^2 + (c_b)^2 + 2c_a c_b S_{ab}) = 2c_a H_{aa} + 2c_b H_{ab} \quad (12.9)$$

$$(2c_b + 2c_a S_{ab})\varepsilon + \frac{\partial\varepsilon}{\partial c_b}((c_a)^2 + (c_b)^2 + 2c_a c_b S_{ab}) = 2c_b H_{bb} + 2c_a H_{ab}$$

Setting $\partial\varepsilon/\partial c_a$ and $\partial\varepsilon/\partial c_b = 0$ and rearranging these two equations, the following two linear equations for c_a and c_b are generated, which are called the **secular equations**:

$$\begin{aligned} c_a(H_{aa} - \varepsilon) + c_b(H_{ab} - \varepsilon S_{ab}) &= 0 \\ c_a(H_{ab} - \varepsilon S_{ab}) + c_b(H_{bb} - \varepsilon) &= 0 \end{aligned} \quad (12.10)$$

These equations have a solution other than $c_a = c_b = 0$ only if the **secular determinant** satisfies the condition

$$\begin{vmatrix} H_{aa} - \varepsilon & H_{ab} - \varepsilon S_{ab} \\ H_{ab} - \varepsilon S_{ab} & H_{bb} - \varepsilon \end{vmatrix} = 0 \quad (12.11)$$

See the reference to McQuarrie in Further Reading for a justification of this assertion. The secular determinant is a 2×2 determinant because the basis set consists of only one AO on each atom.

Expanding the determinant generates a quadratic equation for the MO energy ε . The two solutions are

$$\begin{aligned} \varepsilon &= \frac{1}{2 - 2S_{ab}^2} [H_{aa} + H_{bb} - 2S_{ab}H_{ab}] \pm \frac{1}{2 - 2S_{ab}^2} \\ &\times \left[\sqrt{(H_{aa}^2 + 4H_{ab}^2 + H_{bb}^2 - 4S_{ab}H_{ab}H_{bb} - 2H_{aa}(H_{bb} + 2S_{ab}H_{ab} - 2S_{ab}^2H_{bb}))} \right] \end{aligned} \quad (12.12)$$

For homonuclear diatomic molecules $H_{aa} = H_{bb}$. In this case, Equation (12.12) simplifies to

$$\varepsilon_1 = \frac{H_{aa} + H_{ab}}{1 + S_{ab}} \quad \text{and} \quad \varepsilon_2 = \frac{H_{aa} - H_{ab}}{1 - S_{ab}} \quad (12.13)$$

The relative energies of AOs and MOs and the coefficients of the AOs can be represented in a molecular orbital energy diagram.

Concept

We will return to a discussion of heteronuclear diatomic molecules in Section 12.8. Using the H_2^+ molecule as an example, we will show later that H_{aa} and H_{ab} are both negative and because $S_{ab} > 0$, $\varepsilon_2 > \varepsilon_1$. Substituting ε_1 into Equations (12.10), we find that $c_a = c_b$, whereas if ε_2 is substituted in the same equations, we obtain $c_a = -c_b$.

Figure 12.2 summarizes the following results of this discussion pictorially in a **molecular orbital energy diagram** using H₂ as an example:

- Two localized AOs combine to form two delocalized MOs provided that S_{ab} is nonzero. This is the case if there are regions in space in which the amplitudes of both AOs are nonzero.
- The energy of one MO is lowered and the energy of the other MO is raised relative to the AO energy. The amount by which each MO energy differs from the AO energy depends on H_{ab} and S_{ab}.
- Because S_{ab} > 0, (1 + S_{ab}) > (1 - S_{ab}) and ε₂ is raised relative to the AO energy more than ε₁ is lowered.
- The AO coefficients have the same sign (in-phase) in the lower-energy MO and the opposite sign (out-of-phase) in the higher-energy MO as is shown in Example Problem 12.1.

In a molecular orbital energy diagram, the energy of the orbital rather than the total energy of the molecule is displayed. For this reason, the appropriate energy operator in calculating the MO energy is \hat{H}_{el} rather than \hat{H} .

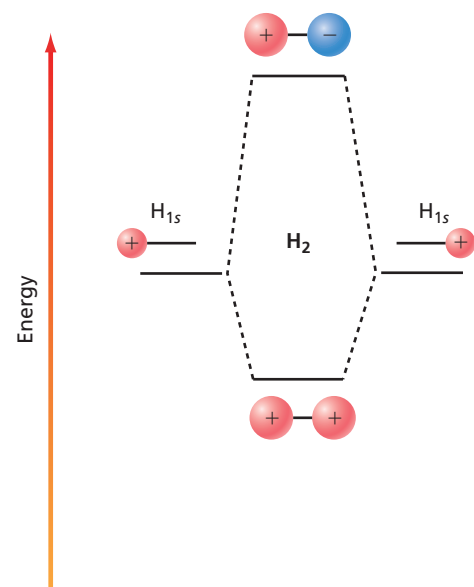


Figure 12.2

Molecular orbital energy diagram displaying a qualitative description of bonding in H₂. Atomic orbitals are shown to the left and right, and molecular orbitals are shown in the middle. Dashed lines connect the MO with the AOs from which it was constructed. Shaded circles have a diameter proportional to the coefficients c_a and c_b. Red and blue shading signifies positive and negative signs of the AO coefficients, respectively. Interchanging red and blue does not generate a different MO.

EXAMPLE PROBLEM 12.1

Show that substituting $\varepsilon_1 = \frac{H_{aa} + H_{ab}}{1 + S_{ab}}$ in Equations (12.10) gives the result c_a = c_b.

Solution

$$\begin{aligned} c_a \left(H_{aa} - \frac{H_{aa} + H_{ab}}{1 + S_{ab}} \right) + c_b \left(H_{ab} - \frac{H_{aa} + H_{ab}}{1 + S_{ab}} S_{ab} \right) &= 0 \\ c_a ([1 + S_{ab}]H_{aa} - [H_{aa} + H_{ab}]) + c_b ([1 + S_{ab}]H_{ab} - [H_{aa} + H_{ab}]S_{ab}) &= 0 \\ c_a (H_{aa} + S_{ab}H_{aa} - H_{aa} - H_{ab}) + c_b (H_{ab} + H_{ab}S_{ab} - H_{aa}S_{ab} - H_{ab}S_{ab}) &= 0 \\ c_a (H_{aa}S_{ab} - H_{ab}) - c_b (H_{aa}S_{ab} - H_{ab}) &= 0 \\ c_a = c_b \end{aligned}$$

Substitution in the second of the two Equations (12.10) gives the same result.

12.2 THE SIMPLEST ONE-ELECTRON MOLECULE: H₂⁺

In the previous section, we outlined a formalism to generate MOs from AOs. We next apply this formalism to the only molecule for which the electronic Schrödinger equation can be solved exactly, the one-electron H₂⁺ molecular ion. Just as for atoms, the Schrödinger equation cannot be solved exactly for any molecule containing more than one electron. Rather than discuss the exact solution, we approach H₂⁺ using the LCAO-MO model, which gives considerable insight into chemical bonding and, more importantly, can be extended easily to many-electron molecules.

We begin by setting up the electronic Schrödinger equation for H₂⁺ in the Born–Oppenheimer approximation. Figure 12.3 shows the relative positions of the two protons and the electron in H₂⁺ at a particular instant in time. The total energy operator for this molecule has the form

$$\hat{H} = -\frac{\hbar^2}{2m_e} \nabla_e^2 - \frac{e^2}{4\pi\varepsilon_0} \left(\frac{1}{r_a} + \frac{1}{r_b} \right) + \frac{e^2}{4\pi\varepsilon_0 R} \quad (12.14)$$

The first term is the electron kinetic energy, the second term is the attractive Coulombic interaction between the electron and each of the nuclei, and the last term

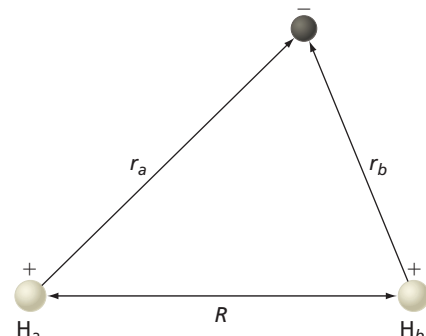
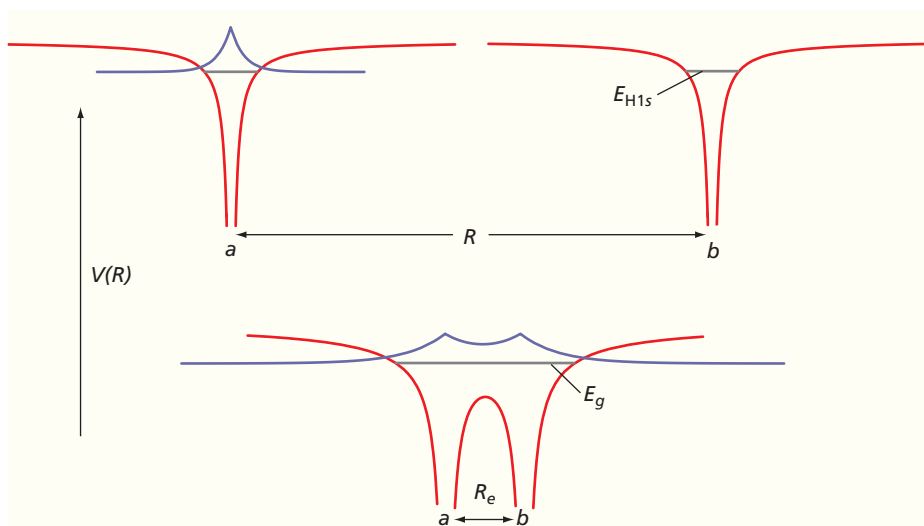


Figure 12.3

Geometric relationship of two protons and the electron in H₂⁺ at one instant in time. The quantities R, r_a, and r_b represent the distances between the charged particles.

Figure 12.4

Potential energy of H_2^+ molecule for two different values of R . Potential energy is shown as the red curves. At large distances, the electron will be localized in a 1s orbital either on nucleus a or b . However, at the equilibrium bond length R_e , the two Coulomb potentials overlap, allowing the electron to be delocalized over the entire molecule. The purple curve represents the amplitude of the atomic (top panel) and molecular (bottom panel) wave functions, and the solid horizontal lines represent the corresponding energy eigenvalues.



is the nuclear–nuclear repulsion. We again separate out the nuclear repulsion term and write an electronic energy operator

$$\hat{H}_{el} = -\frac{\hbar^2}{2m_e} \nabla_e^2 - \frac{e^2}{4\pi\epsilon_0} \left(\frac{1}{r_a} + \frac{1}{r_b} \right) \quad (12.15)$$

From experimental results, we know that H_2^+ is a stable species, so that solving the Schrödinger equation for H_2^+ must give at least one bound state. We define the zero of total energy as an H atom and an H^+ ion that are infinitely separated. Given this choice of the zero, a stable molecule has a negative energy. The energy function $E_{total}(R)$ must have a minimum value for a distance R_e , which is the equilibrium bond length.

Next, we will discuss the approximate wave functions for the H_2^+ molecule in the LCAO-MO model. Imagine slowly bringing together an H atom and an H^+ ion. At infinite separation, the electron is in a 1s orbital on either one nucleus or the other. However, as the internuclear distance approaches R_e , the potential energy wells for the two species overlap, and the barrier between them is lowered. Consequently, the electron can move back and forth between the Coulomb wells on the two nuclei. It is equally likely to be on nucleus a as on nucleus b , so that the molecular wave function looks like the superposition of a 1s orbital on each nucleus, as shown pictorially in Figure 12.4.

The AOs used to form the MOs are the 1s orbitals, ϕ_{H1s} . To allow the electron distribution around each nucleus to change as the bond is formed, a **variational parameter** ζ is inserted in each AO:

$$\phi_{H1s} = \frac{1}{\sqrt{\pi}} \left(\frac{\zeta}{a_0} \right)^{3/2} e^{-\zeta r/a_0} \quad (12.16)$$

This parameter looks like an effective nuclear charge. You will see in the end-of-chapter problems that varying ζ allows the size of the orbital to change.

In the previous section, we showed that $c_a = \pm c_b$. Although the signs of c_a and c_b can differ, the magnitude of the coefficients is the same. Using this result, we find that the two MOs are

$$\begin{aligned} \psi_g &= c_g (\phi_{H1s_a} + \phi_{H1s_b}) \\ \psi_u &= c_u (\phi_{H1s_a} - \phi_{H1s_b}) \end{aligned} \quad (12.17)$$

The wave functions for a homonuclear diatomic molecule are classified as *g* or *u* based on whether they change signs upon undergoing inversion through the center of the molecule. If the origin of the coordinate system is placed at the center of the molecule, inversion corresponds to $\psi(x, y, z) \rightarrow \psi(-x, -y, -z)$. If this operation leaves the wave function unchanged, that is, $\psi(x, y, z) = \psi(-x, -y, -z)$, it has ***g* symmetry**. If $\psi(x, y, z) = -\psi(-x, -y, -z)$, the wave function has ***u* symmetry**. The subscripts *g* and *u* refer to the German words *gerade* and *ungerade*, which can be translated as even

and odd; they are also referred to as **symmetric wave functions** and **antisymmetric wave functions**. See Figures 12.8 and 12.12 for illustrations of g and u MOs. We will see later that only ψ_g describes a stable, chemically bonded H₂⁺ molecule.

The values of c_g and c_u can be determined by normalizing ψ_g and ψ_u . Note that the integrals used in the normalization are over all three spatial coordinates. Normalization requires that

$$\begin{aligned} 1 &= \int c_g^*(\phi_{H1s_a}^* + \phi_{H1s_b}^*)c_g(\phi_{H1s_a} + \phi_{H1s_b})d\tau \\ &= c_g^2 \left(\int \phi_{H1s_a}^* \phi_{H1s_a} d\tau + \int \phi_{H1s_b}^* \phi_{H1s_b} d\tau + 2 \int \phi_{H1s_b}^* \phi_{H1s_a} d\tau \right) \quad (12.18) \end{aligned}$$

The first two integrals in the second line have the value 1 because the H1s orbitals are normalized, and we obtain the result

$$c_g = \frac{1}{\sqrt{2 + 2S_{ab}}} \quad (12.19)$$

S_{ab} is the previously defined overlap integral. The coefficient c_u has a similar form, as you will see in the end-of-chapter problems.

$$c_u = \frac{1}{\sqrt{2 - 2S_{ab}}} \quad (12.20)$$

12.3 ENERGY CORRESPONDING TO THE H₂⁺ MOLECULAR WAVE FUNCTIONS ψ_g AND ψ_u

Keep in mind that the molecular wave functions we are using are approximate rather than exact eigenfunctions of the total energy operator of Equation (12.15). Therefore, we can only calculate the expectation value of the electronic energy for the state corresponding to ψ_g :

$$E_g = \frac{\int \psi_g^* \hat{H}_{el} \psi_g d\tau}{\int \psi_g^* \psi_g d\tau} = \frac{H_{aa} + H_{ab}}{1 + S_{ab}} \quad (12.21)$$

This result was derived in Section 12.1, where we also showed that $E_u = \frac{H_{aa} - H_{ab}}{1 - S_{ab}}$.

Looking ahead, we will find that the total energy corresponding to ψ_g is lower than that corresponding to ψ_u and that only ψ_g describes a stable H₂⁺ molecule. To understand the difference between ψ_g and ψ_u , we must look in more detail at the integrals H_{aa} and H_{ab} .

To evaluate H_{aa} , we use \hat{H}_{el} from Equation (12.15):

$$\begin{aligned} H_{aa} &= \int \phi_{H1s_a}^* \left(-\frac{\hbar^2}{2m} \nabla^2 - \frac{e^2}{4\pi\epsilon_0 r_a} \right) \phi_{H1s_a} d\tau \\ &\quad - \int \phi_{H1s_a}^* \left(\frac{e^2}{4\pi\epsilon_0 r_b} \right) \phi_{H1s_a} d\tau \quad (12.22) \end{aligned}$$

Assume initially that $\zeta = 1$, in which case ϕ_{H1s_a} is an eigenfunction of the operator in parentheses

$$\left(-\frac{\hbar^2}{2m} \nabla^2 - \frac{e^2}{4\pi\epsilon_0 r_a} \right) \phi_{H1s} = E_{1s} \phi_{H1s} \quad (12.23)$$

Because the atomic wave functions are normalized, the first integral in Equation (12.22) is equal to E_{1s} and H_{aa} is given by

$$H_{aa} = E_{1s} - J, \text{ where } J = \int \phi_{H1s_a}^* \left(\frac{e^2}{4\pi\epsilon_0 r_b} \right) \phi_{H1s_a} d\tau \quad (12.24)$$

J represents the energy of interaction of the electron viewed as a negative diffuse charge cloud on atom a with the positively charged nucleus b . This result is exactly what would be calculated in classical electrostatics for a diffuse negative charge of

Concept

Molecular wave functions for homonuclear diatomic molecules have either g or u symmetry.

density $\phi_{H1s_a}^* \phi_{H1s_a}$. What is the physical meaning of the energy H_{aa} ? The quantity H_{aa} represents the total energy of an undisturbed hydrogen atom separated from a bare proton by the distance R excluding the nuclear repulsion. As $R \rightarrow \infty$, $H_{aa} \rightarrow E_{1s}$. What is the sign of H_{aa} ? We know that $E_{1s} < 0$, and because all the terms in the integrand for J are positive, $J > 0$. Therefore, $H_{aa} < 0$.

Next, the energy $H_{ab} = H_{ba}$ is evaluated. Substituting as before, we find that

$$\begin{aligned} H_{ba} = & \int \phi_{H1s_b}^* \left(-\frac{\hbar^2}{2m} \nabla^2 - \frac{e^2}{4\pi\epsilon_0 r_a} \right) \phi_{H1s_a} d\tau \\ & - \int \phi_{H1s_b}^* \left(\frac{e^2}{4\pi\epsilon_0 r_b} \right) \phi_{H1s_a} d\tau \end{aligned} \quad (12.25)$$

Evaluating the first integral gives $S_{ab}E_{1s}$ and

$$H_{ab} = S_{ab}E_{1s} - K \quad \text{where } K = \int \phi_{H1s_b}^* \left(\frac{e^2}{4\pi\epsilon_0 r_b} \right) \phi_{H1s_a} d\tau \quad (12.26)$$

In this model, K plays a central role in lowering the energy that leads to formation of a bond. However, it has no simple physical interpretation. It is a direct consequence of writing the MO as a superposition of two AOs, which leads to an interference term in $\psi_g^* \psi_g$ as seen in Equation (12.18). Both J and K are positive because all terms that appear in the integrals are positive over the entire range of the integration. Quantitative calculations show that near the equilibrium distance $R = R_e$, both H_{aa} and H_{ab} are negative, and $|H_{ab}| > |H_{aa}|$. For many electron atoms, integrals similar to J and K are generated and are referred to as Coulomb and exchange integrals, respectively.

The differences ΔE_g and ΔE_u between the electronic energy of the molecule in the states described by ψ_g and ψ_u and the energy of the H1s AO are calculated in Example Problem 12.2.

EXAMPLE PROBLEM 12.2

Using Equations (12.13), (12.24), and (12.26), express the change in the MO energies resulting from bond formation, $\Delta E_g = E_g - E_{1s}$ and $\Delta E_u = E_u - E_{1s}$, in terms of J , K , and S_{ab} .

Solution

$$\begin{aligned} E_g &= \frac{H_{aa} + H_{ab}}{1 + S_{ab}} = \frac{E_{1s} - J + S_{ab}E_{1s} - K}{1 + S_{ab}} = \frac{(1 + S_{ab})E_{1s} - J - K}{1 + S_{ab}} \\ &= E_{1s} - \frac{J + K}{1 + S_{ab}} \end{aligned}$$

$$\Delta E_g = E_g - E_{1s} = -\frac{J + K}{1 + S_{ab}}$$

$$\begin{aligned} E_u &= \frac{H_{aa} - H_{ab}}{1 - S_{ab}} = \frac{E_{1s} - J - S_{ab}E_{1s} + K}{1 - S_{ab}} = \frac{(1 - S_{ab})E_{1s} - J + K}{1 - S_{ab}} \\ &= E_{1s} - \frac{J - K}{1 - S_{ab}} \end{aligned}$$

$$\Delta E_u = E_u - E_{1s} = -\frac{J - K}{1 - S_{ab}}$$

As discussed earlier, both J and K are positive. Quantitative calculations show that near the equilibrium distance $|K| > |J|$, so that ΔE_u is positive and ΔE_g is negative, meaning that the u state is raised and the g state is lowered in energy with respect to the H1s AO. These calculations also show that $|\Delta E_u| > |\Delta E_g|$ in agreement with Figure 12.2.

To assess the stability of the molecule with respect to its dissociation products, we must include the nuclear repulsion term and calculate E_{total} rather than E_{el} as a function of R . Using the approximate wave function of Equation (12.17), we can obtain an analytical expression for $E_{total}(R, \zeta)$. For details, see the reference to Levine in Further Reading.

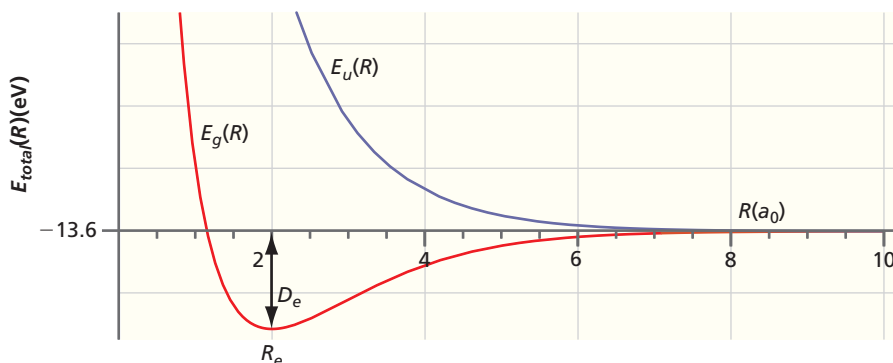


Figure 12.5

Energy functions $E_{total}(R)$ for the g and u states in the approximate solution. See text for discussion. The reference energy (-13.6 eV) corresponds to infinitely separated H and H^+ species E_{1s} , which is the limit of H_{aa} as $R \rightarrow \infty$.

The energy is minimized with respect to ζ at each of the R values in a variational calculation. The resulting $E_{total}(R)$ curves are shown schematically in Figure 12.5. The value of the energy as $R \rightarrow \infty$ is the total energy of a H atom and a proton at infinite separation, or E_{1s} . For the H atom as for any atom, $E_{total} = E_{el}$. The most important conclusions that can be drawn from this figure are that ψ_g describes a stable H_2^+ molecule because the energy has a well-defined minimum at $R = R_e$ and that ψ_u does not describe a bound state of H and H^+ because $E_u(R) > 0$ for all R , which makes the molecule unstable with respect to dissociation. *Therefore, we conclude that only a H_2^+ molecule described by ψ_g is a stable molecule.* The ψ_g and ψ_u wave functions are referred to as **bonding molecular orbitals** and **antibonding molecular orbitals**, respectively, to emphasize their relationship to the chemical bond.

The equilibrium distance R_e and the bond energy D_e are of particular interest and have the values $R_e = 1.98 a_0$ and $D_e = 2.36$ eV. ζ has the value 1.24 for ψ_g and 0.90 for ψ_u at R_e . The result that $\zeta > 1$ for ψ_g shows that the optimal H1s AO to use in constructing ψ_g is contracted relative to a free H atom. This means that the electron in H_2^+ in the ψ_g state is pulled closer to each of the nuclei than it would be in a free hydrogen atom. The opposite is true for the ψ_u state.

Values of E_{total} , E_{el} , and the nuclear repulsion energy $V(R)$ obtained in an exact calculation are shown as a function of R in Figure 12.6. As $R \rightarrow \infty$, $V(R) \rightarrow 0$, and $E_{el} \rightarrow -13.6$ eV, which is the electronic energy (and total energy) of an H atom.

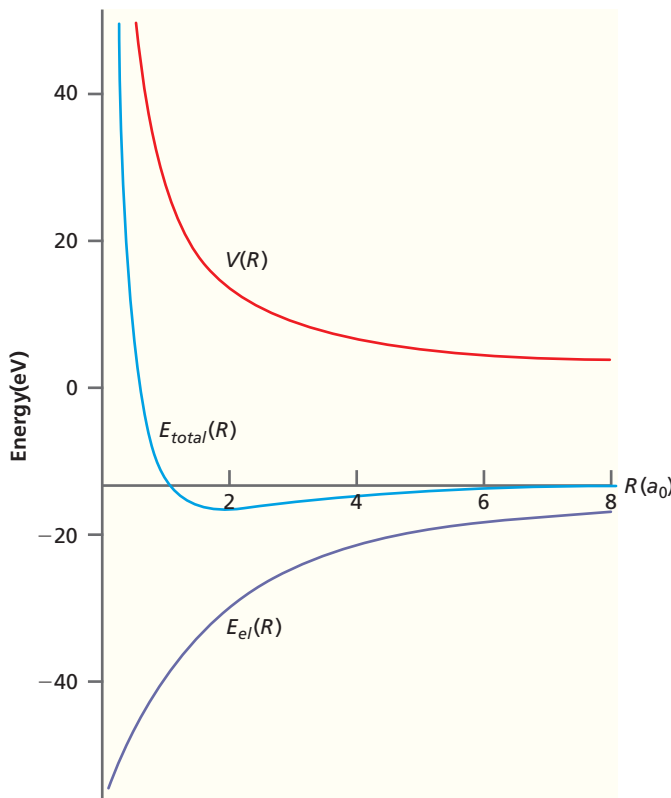
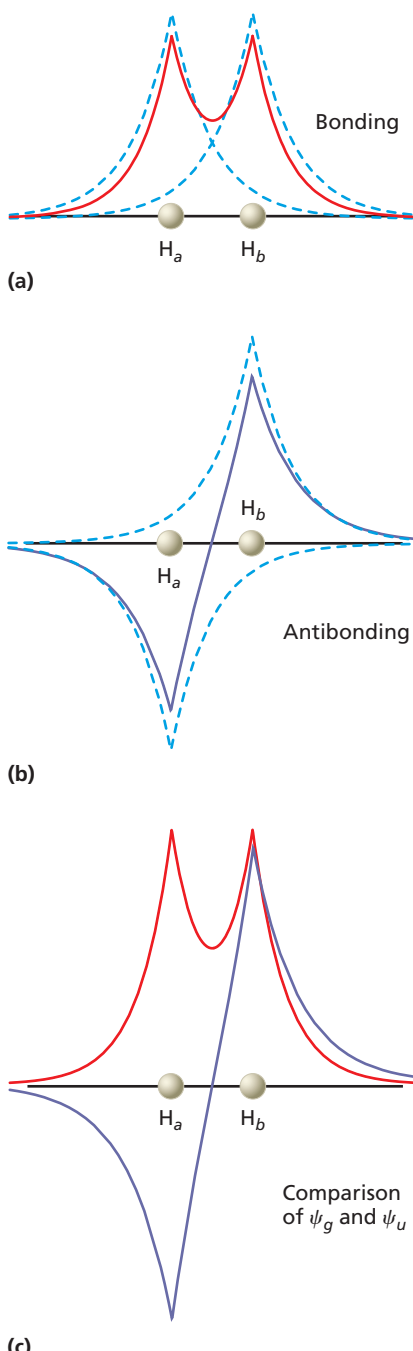


Figure 12.6

E_{total} , E_{el} , and the nuclear repulsion energy $V(R)$ obtained in an exact calculation shown as a function of R . The horizontal line corresponds to -13.6 eV. Source: Based on Wind, *Journal of Chemical Physics* 42 (1965): 2371. For more details, see the reference to Wind in Further Reading.

**Figure 12.7**

Molecular wave functions ψ_g and ψ_u . ψ_g and ψ_u are shown as solid lines evaluated along the internuclear axis for (a) a bonding and (b) an antibonding wave function. The unmodified ($\zeta = 1$) $\text{H}1s$ orbitals from which they were generated are shown as dashed lines. In (c) a direct comparison of ψ_g and ψ_u is shown.

As $R \rightarrow 0$, $E_{el} \rightarrow -54.4 \text{ eV}$, which is the electronic energy of a He^+ ion. At large R values, $E_{total}(R)$ is dominated by $E_{el}(R)$ and is negative. However, at small R values, $E_{total}(R)$ is dominated by $V(R)$ and is positive. This crossover results in a minimum in the total energy at $R = 1.98a_0$ and a bond energy of 2.79 eV or 269 kJ mol^{-1} . The calculated binding energy D_e in the simple model is 2.36 eV, which is reasonably close to the exact value, and the exact and calculated R_e values are both $1.98a_0$. The fact that the approximate values are quite close to the exact values validates the assumption that the exact molecular wave function is quite similar to ψ_g .

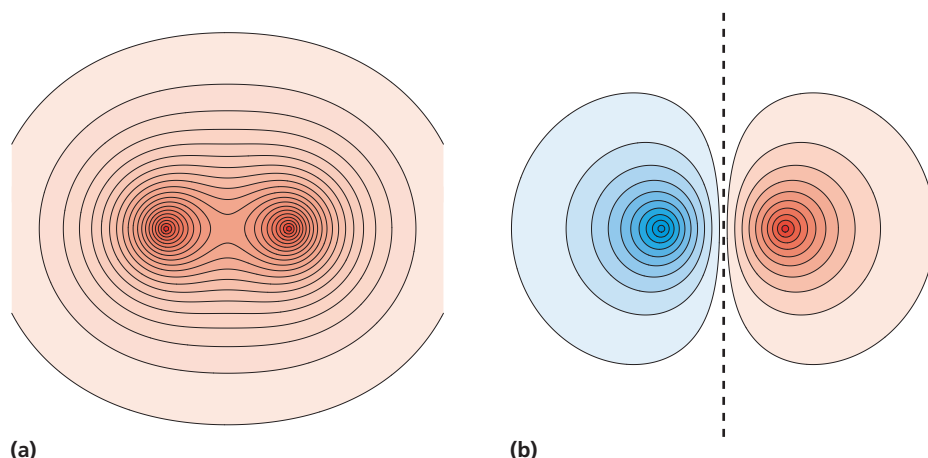
What have we learned so far about the origin of the chemical bond? It is tempting to attribute the binding to H_{ab} or K and, within the LCAO-MO formalism that we have used, this is correct. However, other formalisms for solving the Schrödinger equation for the H_2^+ molecule do not give rise to these integrals. We should, therefore, look for an explanation of chemical binding that is independent of the formalism used. For this reason, we seek the origin of the chemical bond in the differences between ψ_g and ψ_u , as the wave functions are essentially independent of the method used to obtain them.

12.4 A CLOSER LOOK AT THE H_2^+ MOLECULAR WAVE FUNCTIONS ψ_g AND ψ_u

The amplitudes of ψ_g and ψ_u along the molecular axis are shown in Figure 12.7 together with the atomic orbitals from which they are derived. Note that the two wave functions are quite different. The bonding orbital has no nodes, and the amplitude of ψ_g is quite high between the nuclei. The antibonding wave function has a node midway between the nuclei, and ψ_u has its maximum positive and negative amplitudes at the nuclei. Note that the increase in the number of nodes in the wave function with energy is similar to the other quantum-mechanical systems that we have studied to this point. Both wave functions are correctly normalized in three dimensions.

Figure 12.8 shows contour plots of ψ_g and ψ_u evaluated in the $z = 0$ plane. If we compare Figures 12.7 and 12.8, we can see that the node midway between the H atoms in ψ_u corresponds to a nodal plane.

The probability density of finding an electron at various points along the molecular axis is given by the square of the wave function, which is shown in Figure 12.9. For the antibonding and bonding orbitals, the probability density of finding the electron in H_2^+ is compared with the probability density of finding the electron in a hypothetical nonbonded case. For the nonbonded case, the electron is equally likely to be found on

**Figure 12.8**

Contour plots of ψ_g and ψ_u . The plots are for (a) ψ_g and (b) ψ_u . Positive and negative amplitudes are shown as red and blue, respectively. Darker colors indicate larger values for the magnitude of the amplitude. The dashed line indicates the position of the nodal plane in ψ_u .

each nucleus in $\text{H}1s$ AOs and $\zeta = 1$. Two important conclusions can be drawn from this figure. First, for both ψ_g and ψ_u , the volume in which the electron can be found is large compared with the volume accessible to an electron in a hydrogen atom. This tells us that the electron is delocalized over the whole molecule in both the bonding and antibonding orbitals. Second, we see that the probability of finding the electron in the region between the nuclei is quite different for ψ_g and ψ_u . For the antibonding orbital, the probability is zero midway between the two nuclei, but for the bonding orbital, it is quite high. This difference is what makes the g state a bonding state and the u state an antibonding state.

This pronounced difference between ψ_g^2 and ψ_u^2 is explored further in Figure 12.10. The *difference* between the probability density for these orbitals and the hypothetical nonbonding state is shown in this figure. This difference tells us how the electron density would change if we could suddenly switch on the interaction at the equilibrium geometry. We see that for the antibonding state, electron density would move from the region between the two nuclei to the outer regions of the molecule. For the bonding state, electron density would move both to the region between the nuclei and closer to each nucleus. The origin of the density increase between the nuclei for the bonding orbital is the interference term $2\phi_{H1s_a}\phi_{H1s_b}$ in $(\phi_{H1s_a} + \phi_{H1s_b})^2$. The origin of the density increase near each nucleus is the increase in ζ from 1.00 to 1.24 in going from the free atom to the H_2^+ molecule.

The probability density is increased relative to the nonbonding case in the region between the nuclei and decreased by the same amount outside of this region. The opposite is true for ψ_u . Although it may not be apparent in Figures 12.7 to 12.10, the wave functions satisfy this requirement. Only small changes in the probability density outside of the region between the nuclei are needed to balance larger changes in this region because the integration volume outside of the region between the nuclei is much larger. The data shown as a line plot in Figure 12.10 are shown as a contour plot in Figure 12.11. Red and blue correspond to the most positive and negative values for $\Delta\psi_g^2$ and $\Delta\psi_u^2$, respectively. The outermost contour for $\Delta\psi_g^2$ in Figure 12.11 corresponds to a negative value, and it is seen that the corresponding area is large. The product of the small negative charge in $\Delta\psi_g^2$ with the large volume corresponding to the contour area is equal in magnitude and opposite in sign to the increase in $\Delta\psi_g^2$ in the bonding region.

The comparison of the electron charge densities associated with ψ_g and ψ_u helps us to understand the important ingredients in chemical bond formation. For both states, the electronic charge undergoes a **delocalization** over the entire molecule. However,

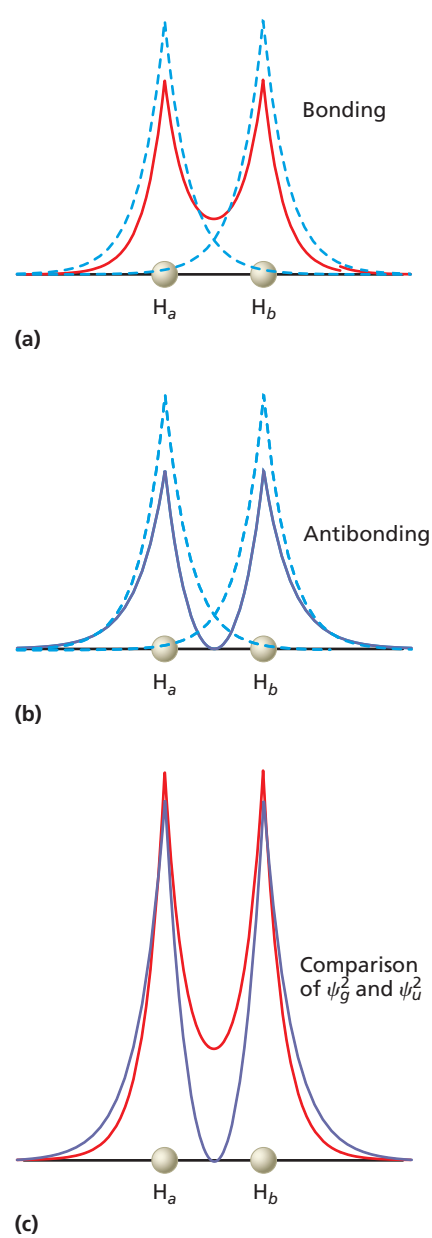


Figure 12.9
Depiction of the probability density of finding an electron along the molecular axis. (a) The probability density ψ_g^2 along the internuclear axis for bonding wave functions. (b) The probability density ψ_u^2 along the internuclear axis for antibonding wave functions. For both (a) and (b) dashed lines indicate $\frac{1}{2}\psi_{H1s_a}^2$ and $\frac{1}{2}\psi_{H1s_b}^2$, which are the probability densities for unmodified ($\zeta = 1$) $\text{H}1s$ orbitals on each nucleus. (c) A direct comparison of ψ_g^2 and ψ_u^2 . Both molecular wave functions are correctly normalized in three dimensions.

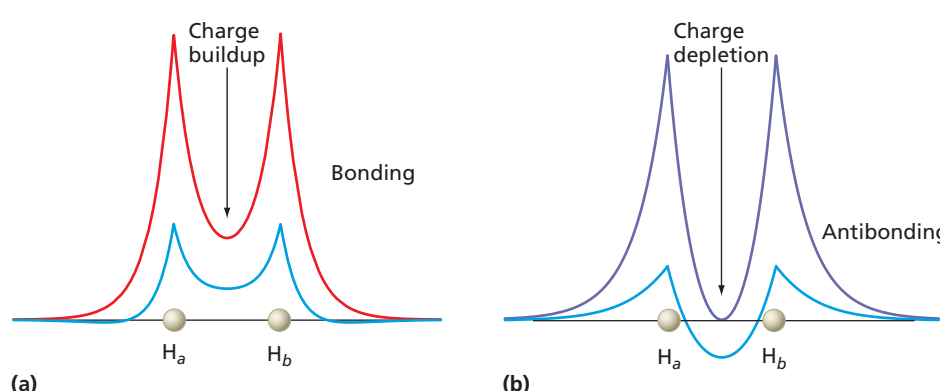
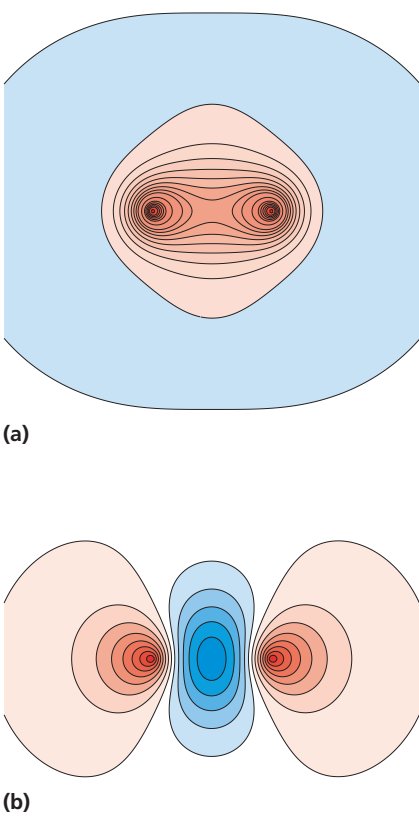


Figure 12.10
Difference between the probability density for ψ_g^2 and ψ_u^2 and the hypothetical nonbonding state. Diagrams for (a) ψ_g^2 and (b) ψ_u^2 . In (a) red curve shows ψ_g^2 and in (b) purple curve shows ψ_u^2 . Light blue curves show the differences $\Delta\psi_g^2 = \psi_g^2 - \frac{1}{2}(\psi_{H1s_a})^2 - \frac{1}{2}(\psi_{H1s_b})^2$ in (a) and $\Delta\psi_u^2 = \psi_u^2 - \frac{1}{2}(\psi_{H1s_a})^2 - \frac{1}{2}(\psi_{H1s_b})^2$ in (b). These differences are a measure of the change in electron density near the nuclei due to bond formation. A charge buildup occurs for the bonding orbital, and a charge depletion occurs for the antibonding orbital in the region between the nuclei.

**Figure 12.11**

Contour plots of $\Delta\psi_g^2$ and $\Delta\psi_u^2$. $\Delta\psi_g^2$ is shown in (a) and $\Delta\psi_u^2$ is shown in (b). Positive and negative amplitudes are shown as red and blue, respectively. Darker colors indicate larger values for the magnitude of the amplitude.

Concept

The dominant driving force for bond formation is electron delocalization.

charge is also localized in the molecular orbitals, and this **localization** is different in the bonding and antibonding states. In the bonding state, the electronic charge redistribution relative to the nonbonded state leads to a charge buildup both near the nuclei and between the nuclei. In the antibonding state, the electronic charge redistribution leads to a charge buildup outside of the region between the nuclei. We conclude that electronic charge buildup between the nuclei is an essential ingredient of a chemical bond.

We now look at how this charge redistribution affects the kinetic and potential energy of the H_2^+ molecule. For a more detailed account, see the reference to Baird in Further Reading. The virial theorem, introduced in Chapter 9, is very helpful in this context. This theorem states that for a Coulomb potential, the average kinetic and potential energies are related by

$$\langle E_{\text{potential}} \rangle = -2 \langle E_{\text{kinetic}} \rangle \quad (12.27)$$

Because $E_{\text{total}} = E_{\text{potential}} + E_{\text{kinetic}}$, it follows that

$$\langle E_{\text{total}} \rangle = -\langle E_{\text{kinetic}} \rangle = \frac{1}{2} \langle E_{\text{potential}} \rangle \quad (12.28)$$

Because Equation (12.28) applies both to the nonbonded case and to the H_2^+ molecule at its equilibrium geometry, the change in total, kinetic, and potential energies associated with bond formation is given by

$$\langle \Delta E_{\text{total}} \rangle = -\langle \Delta E_{\text{kinetic}} \rangle = \frac{1}{2} \langle \Delta E_{\text{potential}} \rangle \quad (12.29)$$

For a molecule to be stable, $\langle \Delta E_{\text{total}} \rangle < 0$ and, therefore, $\langle \Delta E_{\text{kinetic}} \rangle > 0$ and $\langle \Delta E_{\text{potential}} \rangle < 0$. Bond formation must lead to an increase in the kinetic energy and a decrease in the potential energy. How does this result relate to the competing effects of charge localization and delocalization that we saw for ψ_g and ψ_u ?

Imagine that we could break down the change in the electron charge distribution as the bond is formed into two separate steps. First, we bring the proton and H atom to a distance R_e and let them interact, keeping the effective nuclear charge at the value $\zeta = 1$. In this step, the kinetic energy of the electron decreases, and it can be shown that the potential energy changes little. Therefore, the total energy will decrease. Why is the kinetic energy lower? The explanation follows directly from our analysis of the particle in the one-dimensional box: as the box length increases, the kinetic energy decreases. Similarly, as the electron is delocalized over the whole space of the molecule, the kinetic energy decreases. By looking only at this first step, we see that electron delocalization alone will lead to bond formation. However, the total energy of the molecule can be reduced further at the fixed internuclear distance R_e by optimizing ζ . At the optimal value of $\zeta = 1.24$, some of the electron charge is withdrawn from the region between the nuclei and redistributed around the two nuclei. Because the size of the “box” around each atom is decreased, the kinetic energy of the molecule is increased. This increase is sufficiently large that $\langle \Delta E_{\text{kinetic}} \rangle > 0$ for the overall two-step process.

However, increasing ζ from 1.0 to 1.24 decreases the potential energy of the molecule because of the increased Coulombic interaction between the electron and the two protons. The result is that $\langle \Delta E_{\text{potential}} \rangle$ is lowered more than $\langle \Delta E_{\text{kinetic}} \rangle$ is raised. Therefore, the total energy of the molecule decreases further in this second step. Although changes in $\langle \Delta E_{\text{potential}} \rangle$ and $\langle \Delta E_{\text{kinetic}} \rangle$ are both quite large, $\langle \Delta E_{\text{total}} \rangle$ changes very little as ζ increases from 1.0 to 1.24. Although $\langle \Delta E_{\text{kinetic}} \rangle > 0$ for the two step process, the dominant driving force for bond formation is electron delocalization, which is associated with $\langle \Delta E_{\text{kinetic}} \rangle < 0$. This result holds for bond formation in general.

At this point, let us summarize what has been learned about the chemical bond. We have carried out an approximate solution of the Schrödinger equation for the simplest molecule and have developed a formalism based on delocalized molecular orbitals derived from atomic orbitals. In conclusion, both charge delocalization and localization play a role in chemical bond formation. Delocalization promotes bond formation because kinetic energy is lowered as the electron occupies a larger region in the molecule than it would in the atom. However, localization through the contraction of atomic

orbitals and the accumulation of electron density between the atoms in the state described by ψ_g further decreases total energy. Both localization and delocalization play a role in bond formation, and it is this complex interplay between opposites that leads to a strong chemical bond.

12.5 HOMONUCLEAR DIATOMIC MOLECULES

In this section, we develop a picture of the shape and spatial extent of molecular orbitals for the second-row homonuclear diatomic molecules $\text{Li}_2 \rightarrow \text{F}_2$. We do so using Hartree–Fock calculations as discussed in Chapters 10 and 15, but interpret the calculated MOs in terms of $n = 1$ and $n = 2$ H atom-like AOs. Heteronuclear diatomic molecules are discussed in Section 12.8.

All MOs for homonuclear diatomic molecules can be divided into two groups with regard to each of two **symmetry operations**. The first operation is inversion through the center of the molecule. Placing the origin at the center of the molecule, inversion corresponds to $\psi(x, y, z) \rightarrow \psi(-x, -y, -z)$. If this operation leaves the MO unchanged, the MO has g symmetry. If $\psi(x, y, z) \rightarrow -\psi(-x, -y, -z)$, the MO has u symmetry. The second symmetry operation is rotation about the molecular axis, which is taken to be the z axis. If this rotation leaves the MO unchanged, it has no nodes that contain this axis, and the MO has **σ symmetry**. Combining s AOs always gives rise to σ MOs for diatomic molecules. If the MO has one nodal plane containing the molecular axis, the MO has **π symmetry**. All homonuclear diatomic MOs have either σ or π symmetry and either g or u symmetry. Combining p_x or p_y AOs always gives rise to π MOs. Molecular orbitals for H_2^+ of g and u symmetry are shown in Figure 12.12. The nomenclature is described later in this section.

Only atomic orbitals of the same symmetry (σ or π) can combine with one another to form a molecular orbital. We consider only s and p electrons to illustrate this assertion. Figure 12.13 shows that a net nonzero overlap between two atomic orbitals occurs only if both AOs are cylindrically symmetric with respect to the molecular axis (σ AOs) or if both have a common nodal plane that coincides with the molecular axis (π AOs).

Two different notations are commonly used to describe MOs in homonuclear diatomic molecules. In the first, the MOs are classified according to symmetry and increasing energy. For instance, a $2\sigma_g$ orbital has the same symmetry but a higher energy than the $1\sigma_g$ orbital, which is the lowest energy MO of σ symmetry. In the second notation, the integer indicating the relative energy is omitted, and the AOs from which the MOs are generated are listed instead. For instance, the $\sigma_g(2s)$ MO has higher

Concept

All homonuclear diatomic MOs have either σ or π symmetry and either g or u symmetry.

Concept

Only atomic orbitals of the same symmetry (σ or π) can combine with one another to form a molecular orbital.

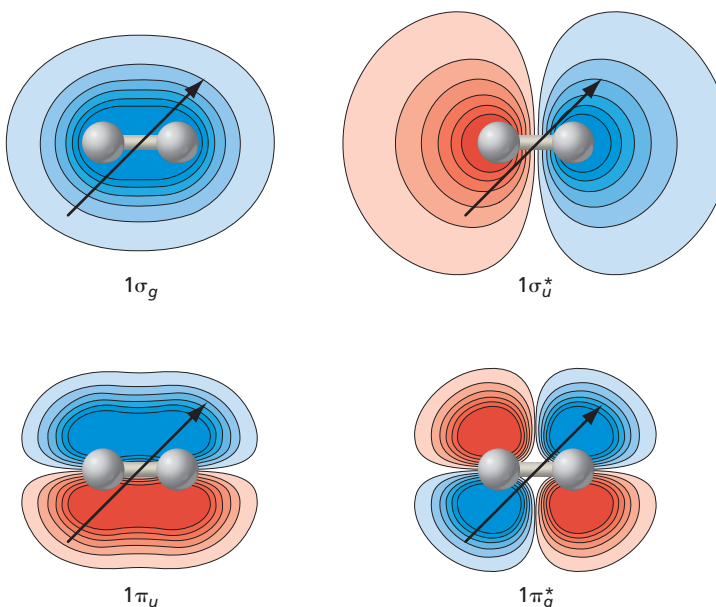
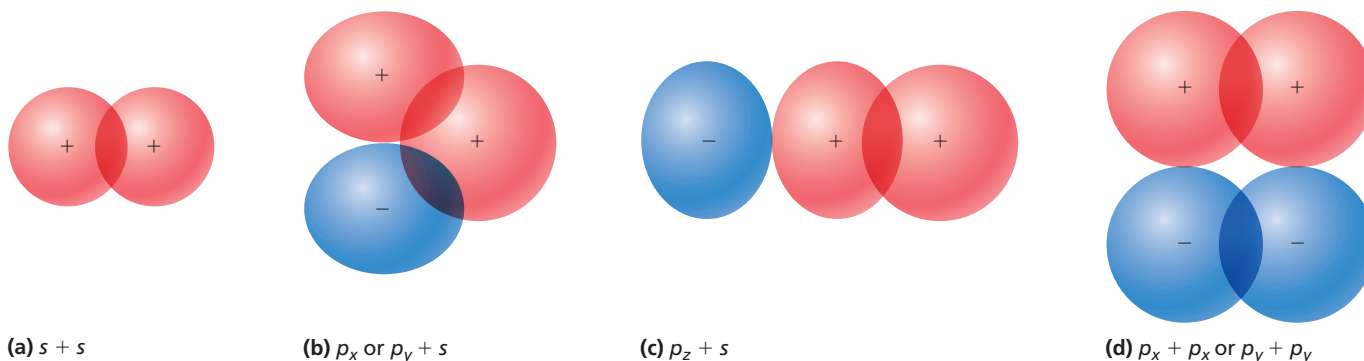


Figure 12.12

Contour plots of several bonding and antibonding orbitals of H_2^+ . Positive and negative amplitudes are shown as red and blue, respectively. Darker colors indicate larger values for the magnitude of the amplitude. The black arrows show the transformation $(x, y, z) \rightarrow (-x, -y, -z)$ for each orbital. If the amplitude of the wave function changes sign under this transformation, it has u symmetry. If it is unchanged, it has g symmetry.

**Figure 12.13****Overlap of various atomic orbitals.**

The illustrations show overlap between (a) two 2s AOs ($\sigma + \sigma$), (b) a 2s and either a $2p_x$ or $2p_y$ AO ($\sigma + \pi$), (c) a 2s and a $2p_z$ AO ($\sigma + \sigma$), and (d) two $2p_x$ or $2p_y$ AOs ($\pi + \pi$). Note that the two shaded areas in (b) have opposite signs, so the net overlap of these two atomic orbitals of different symmetry is zero.

Concept

s–p mixing decreases for the second-row diatomic molecules in the order $\text{Li}_2, \text{B}_2, \dots, \text{O}_2, \text{F}_2$.

energy than the $\sigma_g(1s)$ MO. The superscript * is used to designate antibonding orbitals. As shown in Figure 12.12, $1\sigma_g$ and $1\pi_u$ are bonding MOs, whereas $1\sigma_u^*$ and $1\pi_g^*$ are antibonding MOs, which shows that *u* and *g* cannot be uniquely associated with bonding and antibonding orbitals.

Two types of MOs can be generated by combining $2p$ AOs. If the axis of the $2p$ orbital lies on the intermolecular axis (by convention the *z* axis), two σ MOs are generated. These MOs are called $3\sigma_g$ and $3\sigma_u^*$ depending on the relative phase of the AOs. Adding $2p_x$ (or $2p_y$) orbitals on each atom gives π MOs because of the nodal plane containing the molecular axis. These MOs are called $1\pi_u$ and $1\pi_g^*$ MOs.

In principle, we should use linear combinations of all the basis functions of the same symmetry (either σ or π) when constructing MOs. However, little mixing occurs between AOs of the same symmetry if they have greatly different orbital energies. For example, the mixing between $1s$ and $2s$ AOs for the second-row homonuclear diatomic molecules can be neglected at our level of discussion. However, for these same molecules, the $2s$ and $2p_z$ AOs both have σ symmetry and will mix if their energies are not greatly different. Because the energy difference between the $2s$ and $2p_z$ atomic orbitals increases in the sequence $\text{Li} \rightarrow \text{F}$, *s–p* mixing decreases for the second-row diatomic molecules in the order $\text{Li}_2, \text{B}_2, \dots, \text{O}_2, \text{F}_2$.

Are the contributions from the *s* and *p* AOs equally important in MOs that exhibit *s–p* mixing? The answer is no because the AO closest in energy to the resulting MO is the major contributor to the MO. Therefore, the $2s$ AO is the major contributor to the 2σ MO because the MO energy is closer to the $2s$ than to the $2p$ orbital energy. Applying the same reasoning, the $2p_z$ atomic orbital is the major contributor to the 3σ MO. The MOs used to describe chemical bonding in first- and second-row homonuclear diatomic molecules are shown in Table 12.1 in order of increasing MO energy from bottom to top. The AO that is the major contributor to the MO is shown in the last column, and the minor contribution is shown in parentheses. For the sequence of molecules $\text{H}_2 \rightarrow \text{N}_2$, the MO energy calculated using higher-level methods with extended basis sets increases in the sequence $1\sigma_g < 1\sigma_u^* < 2\sigma_g < 2\sigma_u^* < 1\pi_u < 3\sigma_g < 1\pi_g^* < 3\sigma_u^*$.

TABLE 12.1 Molecular Orbitals Used to Describe Chemical Bonding in Homonuclear Diatomic Molecules

MO Designation	Alternate	Character	Atomic Orbitals
$3\sigma_u^*$	$\sigma_u^*(2p_z)$	Antibonding	$2p_z$ ($2s$)
$1\pi_g^*$	$\pi_g^*(2p_x, 2p_y)$	Antibonding	$2p_x, 2p_y$
$1\pi_u$	$\pi_u(2p_x, 2p_y)$	Bonding	$2p_x, 2p_y$
$3\sigma_g$	$\sigma_g(2p_z)$	Bonding	$2p_z$ ($2s$)
$2\sigma_u^*$	$\sigma_u^*(2s)$	Antibonding	$2s$ ($2p_z$)
$2\sigma_g$	$\sigma_g(2s)$	Bonding	$2s$ ($2p_z$)
$1\sigma_u^*$	$\sigma_u^*(1s)$	Antibonding	$1s$
$1\sigma_g$	$\sigma_g(1s)$	Bonding	$1s$

Moving across the periodic table to O₂ and F₂, the relative order of the 1π_u and 3σ_g MOs is inverted. Note that the σ and π MOs generated from 2p AOs have different energies.

Figure 12.14 shows contour plots of the first few MOs for F₂ that are involved in bond formation obtained from a Hartree–Fock calculation. The 1σ_g^{*} and 1σ_u^{*} MOs are localized on the F atoms and have essentially zero overlap. For this reason, they are not involved in bond formation and are not depicted.

Let us now turn to the most important features of these MO contour plots. Notice in Figure 12.14 that MOs extend over the entire molecule, indicating that all electrons except for the 1s electrons are delocalized over both F atoms. Just as for the H₂⁺ molecule, the electron density is increased between the F atoms in bonding MOs and decreased between the F atoms in antibonding MOs. As might be expected from our studies of quantum-mechanical systems, the number of nodes in a MO increases with energy. All antibonding MOs have a nodal plane perpendicular to the internuclear axis midway between the atoms. The bonding and antibonding π MOs have a nodal plane containing the internuclear axis. The amplitude for all the antibonding σ MOs is zero midway between the atoms on the molecular axis and the wave function changes sign. In the next section, we introduce the concept of a molecular configuration in order to discuss trends in the periodic table of the elements in a more quantitative fashion.

12.6 ELECTRONIC STRUCTURE OF MANY-ELECTRON MOLECULES

To this point, our discussion has been largely qualitative in nature. The interaction of two AOs has been shown to give two MOs, and a framework of molecular orbitals has been introduced that can be used for many-electron diatomic molecules. To calculate properties of diatomic molecules such as the MO energies, the bond length, and the dipole moment, the Schrödinger equation must be solved numerically. As for many-electron atoms, the starting point for quantitative molecular calculations is the Hartree–Fock model. As the formulation of the model is more complex for molecules than for atoms, we refer the interested reader to Chapter 15 and to the book by Levine cited in Further Reading for additional details. As was discussed for many-electron atoms in Chapter 10, a crucial input for calculations based on the Hartree–Fock model is the expansion of the one-electron molecular orbitals ψ_j in a basis set of the N basis functions ϕ_i . A number of basis sets is available in commercially available computational chemistry software, allowing the MOs to be written in the form

$$\psi_j = \sum_{i=1}^N c_{ij} \phi_i \quad (12.30)$$

Although calculations using the Hartree–Fock model generally give sufficiently accurate values for bond lengths in diatomic molecules and bond angles in polyatomic molecules, accurate MO energy-level calculations require inclusion of electron correlation terms, as will be discussed in Chapter 15.

Once the MO energy levels have been calculated, a **molecular configuration** is obtained by putting two electrons in each MO, in order of increasing orbital energy, until all electrons have been accommodated, as was done using the Aufbau principle for many-electron atoms in Chapter 10. If the degeneracy of an energy level is greater than one, Hund's first rule, discussed in Chapter 11, is followed, and the electrons are placed in the MOs in such a way that the total number of unpaired electrons is maximized.

We next discuss the molecular configuration for the ground state of H₂. The MO energy diagram in Figure 12.15 shows the number and spin of the electrons rather than the magnitude and sign of the AO coefficients, as was the case in Figure 12.2. What can we say about the magnitude and sign of the AO coefficients for each of the MOs in Figure 12.15?

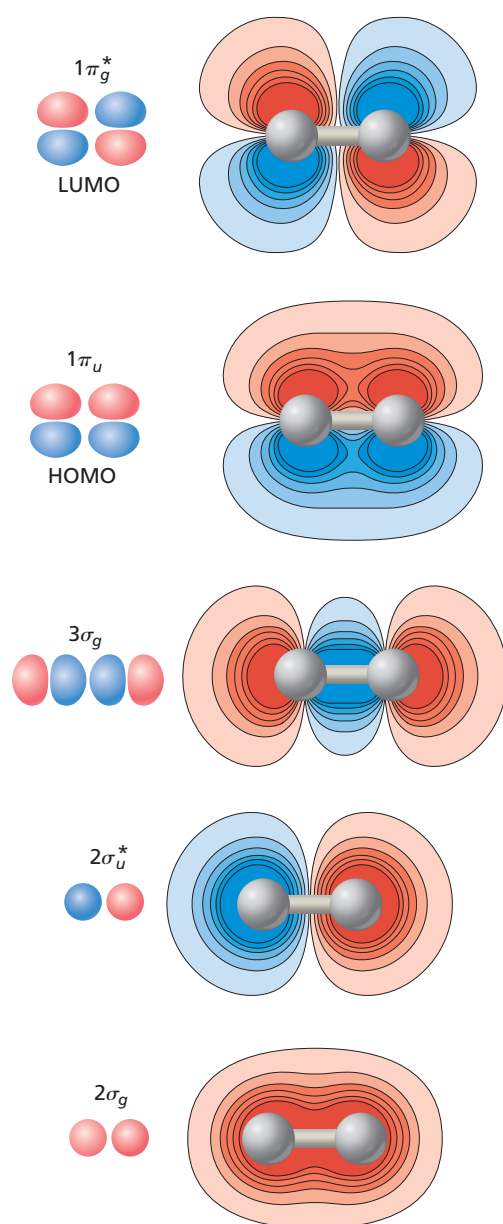


Figure 12.14
Contour plots of the most important MOs involved in bond formation for F₂. The primary AOs used to form each MO is indicated schematically. The highest energy occupied molecular orbital (HOMO) and lowest energy unoccupied molecular orbital (LUMO) are indicated. The energy of the MOs increases from bottom to top in the figure.

Concept

A molecular configuration is obtained by putting two electrons in each MO, in order of increasing orbital energy.

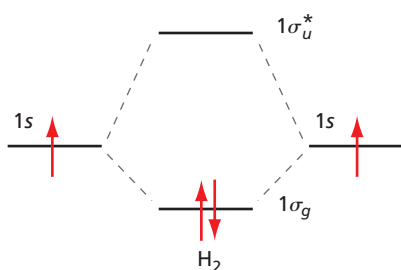


Figure 12.15

Atomic and molecular orbital energies and electron occupation for H_2 . Upward and downward-pointing arrows indicate α and β spins, respectively.

The interaction of 1s orbitals on each atom gives rise to a bonding and an antibonding MO as shown schematically in Figure 12.15. Each MO can hold two electrons of opposite spin. The configuration for ground state H_2 is $(1\sigma_g)^2$. We should consider two cautionary remarks about the interpretation of molecular orbital energy diagrams. First, just as for the many-electron atom, the total energy of a molecule is not the sum of the MO energies. Therefore, it is not always valid to draw conclusions about the stability or bond strength of a molecule solely on the basis of the orbital energy diagram. Second, the words *bonding* and *antibonding* give information about the relative signs of the AO coefficients in the MO, but they do not convey whether the electron is bound to the molecule. The total energy for any stable molecule is lowered by adding electrons to any orbital for which the energy is less than zero. For example, O_2^- is a stable species, even though the additional electron is placed in an antibonding MO.

For H_2 , both electrons are in the $1\sigma_g$ MO, which is lower in energy than the 1s AOs. Calculations show that the $1\sigma_u^*$ MO energy is greater than zero. In this case, the total energy is minimized by putting both electrons in the $1\sigma_g$ orbital and increased if electrons are additionally put into the $1\sigma_u^*$ as would be the case for H_2^- .

The preceding example used a single 1s orbital on each atom to form molecular orbitals. Now we discuss the molecules F_2 and N_2 , for which both *s* and *p* AOs contribute to the MOs. Combining n AOs generates n MOs, so combining the 1s, 2s, 2p_x, 2p_y, and 2p_z AOs on N and F generates 10 MOs for F_2 and N_2 . Although MOs with contributions from both the 1s and 2s AOs are in principle possible, mixing between these AOs does not occur for F_2 and N_2 because the AOs have very different energies. Mixing between the 2s and the 2p_x or 2p_y does not occur, because the net overlap is zero, as shown in Figure 12.13. We next consider mixing between the 2s and 2p_z AOs. For F_2 , 2s–2p mixing can be neglected because the 2s AO lies 21.6 eV in energy below the 2p AO. The F_2 MOs, in order of increasing energy, are $1\sigma_g < 1\sigma_u^* < 2\sigma_g < 2\sigma_u^* < 3\sigma_g < 1\pi_u = 1\pi_u^* < 1\pi_g = 1\pi_g^*$, and the configuration for F_2 is $(1\sigma_g)^2(1\sigma_u^*)^2(2\sigma_g)^2(2\sigma_u^*)^2(3\sigma_g)^2(1\pi_u)^2(1\pi_u^*)^2(1\pi_g)^2(1\pi_g^*)^2$. For this molecule, the 2σ MOs are quite well described by a single 2s AO on each atom, and the 3σ MOs are quite well described by a single 2p_z AO on each atom. Because the 2p_x and 2p_y AOs have a net zero overlap with each other, each of the doubly degenerate $1\pi_u$ and $1\pi_g^*$ MOs originates from a single 2p_x or 2p_y AO on each atom. Figure 12.16 shows a molecular orbital energy diagram for F_2 . Note that the $3\sigma_g$ and $3\sigma_u^*$ MOs have a greater energy separation than the $1\pi_u$ and $1\pi_g^*$ MOs. This energy separation is due to the overlap of the 2p_z AOs on the two F atoms being greater than the overlap of the 2p_x or 2p_y AOs.

For N_2 , the 2s AO lies below the 2p AO by only 12.4 eV, and in comparison to F_2 , s–p mixing is not negligible. The MOs, in order of increasing energy, are $1\sigma_g < 1\sigma_u^* < 2\sigma_g < 2\sigma_u^* < 1\pi_u = 1\pi_u^* < 3\sigma_g < 1\pi_g = 1\pi_g^*$, and the configuration is $(1\sigma_g)^2(1\sigma_u^*)^2(2\sigma_g)^2(2\sigma_u^*)^2(1\pi_u)^2(1\pi_u^*)^2(3\sigma_g)^2$. Because of 2s–2p mixing, the 2σ and 3σ MOs have significant contributions from both 2s and 2p_z AOs, with the

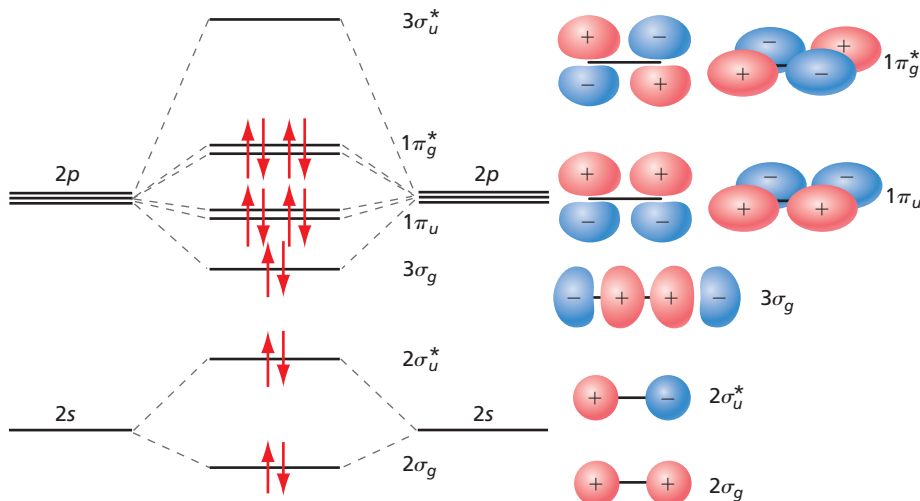
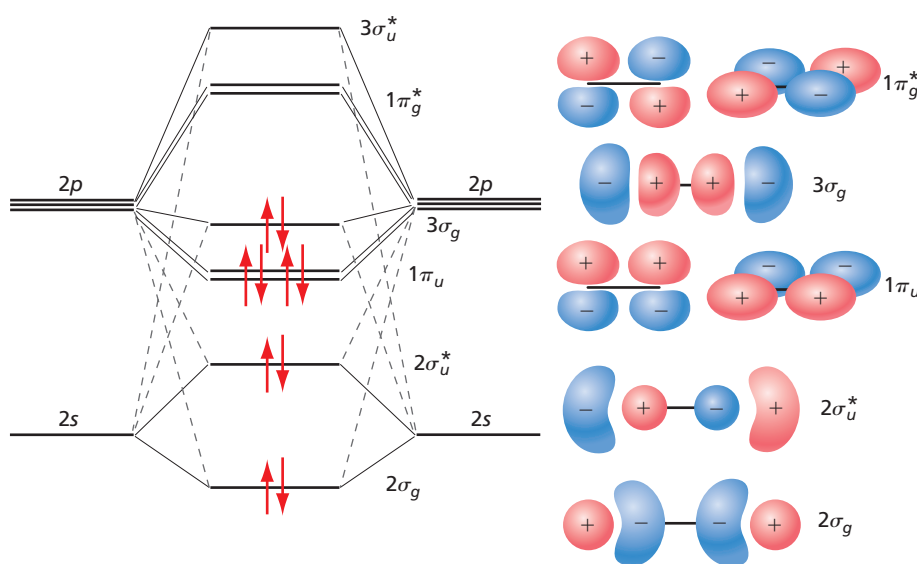


Figure 12.16

Schematic MO energy diagram for the valence electrons in F_2 . The degenerate *p* and π orbitals are shown slightly offset in energy. The dominant atomic orbital contributions to the MOs are shown as solid lines. Minor contributions due to *s*–*p* mixing have been neglected. The AOs that generate the MOs are schematically depicted on the right side of the figure. The $1\sigma_g$ and $1\sigma_u^*$ MOs are not shown.

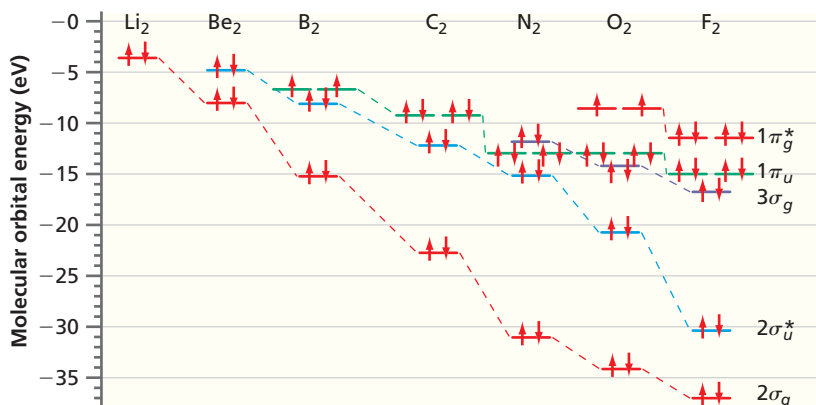
**Figure 12.17**

Schematic MO energy diagram for the valence electrons in N_2 . The degenerate p and π orbitals are shown slightly offset in energy. The dominant AO contributions to the MOs are shown as solid lines. Lesser contributions arising from $s-p$ mixing are shown as dashed lines. The AOs that generate the MOs are schematically depicted on the right side of the figure. The $1\sigma_g$ and $1\sigma_u^*$ MOs are not shown.

result that the $3\sigma_g$ MO is higher in energy than the $1\pi_u$ MO. A MO energy diagram for N_2 is shown in Figure 12.17. The shape of the 2σ and 3σ N_2 MOs schematically indicates $s-p$ mixing. The $2\sigma_g$ MO has more bonding character because the probability of finding the electron between the atoms is greater than it was without $2s-2p$ mixing. Applying the same reasoning, we find that the $2\sigma_u^*$ MO has become less antibonding in character and the $3\sigma_g$ MO has become less bonding in character for N_2 in comparison with F_2 . We can see from the overlap in the AOs that the triple bond in N_2 arises from electron occupation of the $3\sigma_g$ and the pair of $1\pi_u$ MOs.

This discussion of MO theory for H_2 , N_2 , and F_2 can be extended to all second-row homonuclear diatomic molecules. After the relative energies of the molecular orbitals are established from numerical calculations, the MOs are filled in the sequence of increasing energy, and the number of unpaired electrons for each molecule can be predicted. The results are shown in Figure 12.18. Using Hund's first rule, we see that both B_2 and O_2 are predicted to have two unpaired electrons; therefore, these molecules should have a net magnetic moment (they are paramagnetic), whereas all other homonuclear diatomics should have a zero net magnetic moment (they are diamagnetic). These predictions are in good agreement with experimental measurements, which provides strong support for the validity of the MO model.

Figure 12.18 also shows that the energy of each of the MOs decreases with increasing atomic number in this series. This is a result of the increase in the effective nuclear charge ζ with increasing atomic number across rows of the periodic table. The larger effective nuclear charge and the smaller atomic size lead to a lower AO energy, which in turn leads to a lower MO energy. However, the $3\sigma_g$ orbital energy falls more rapidly for this series than the $1\pi_u$ orbital. This occurs because of a number of factors, including the decrease of $2s-2p$ mixing from Li_2 to F_2 and the change in overlap of the AOs

**Figure 12.18**

Molecular orbital energy levels for occupied MOs of the second-row diatomic molecules. The $1\sigma_g$ and $1\sigma_u^*$ orbitals lie at much lower values of energy and are not shown.

Source: From calculations by E. R. Davidson, unpublished.

resulting from changes in the bond length and effective nuclear charge. As a result, an inversion occurs in the order of MO energies between the $1\pi_u$ and $3\sigma_g$ orbitals for O₂ and F₂ relative to the other molecules in this series.

12.7 BOND ORDER, BOND ENERGY, AND BOND LENGTH

Concept

Trends in bond order, bond energy and length, and vibrational force constant for homonuclear diatomic molecules can all be understood using qualitative molecular orbital theory.

Molecular orbital theory has demonstrated its predictive power by providing an explanation of the observed net magnetic moment in B₂ and O₂ and the absence of a net magnetic moment in the other second-row diatomic molecules. We now show that the theory can also provide an understanding of trends in the bond energy and the vibrational force constant for these molecules. Figure 12.19 shows data for these observables for the series H₂ → Ne₂. As the number of electrons in the diatomic molecule increases, the bond energy has a pronounced maximum for N₂ and a smaller maximum for H₂. The vibrational force constant shows the same trend. The bond length increases as the bond energy and force constant decrease in the series Be₂ → N₂, but it exhibits a more complicated trend for the first few molecules in this series. All of these data can be qualitatively understood using molecular orbital theory.

Consider the MO energy diagram for H₂ in Figure 12.15. For simplicity, we assume that the total energy of a molecule is proportional to the sum of the orbital energies. Because the bonding orbital is lower in energy than the atomic orbitals from which it was created, putting electrons into a bonding orbital leads to an energy lowering with

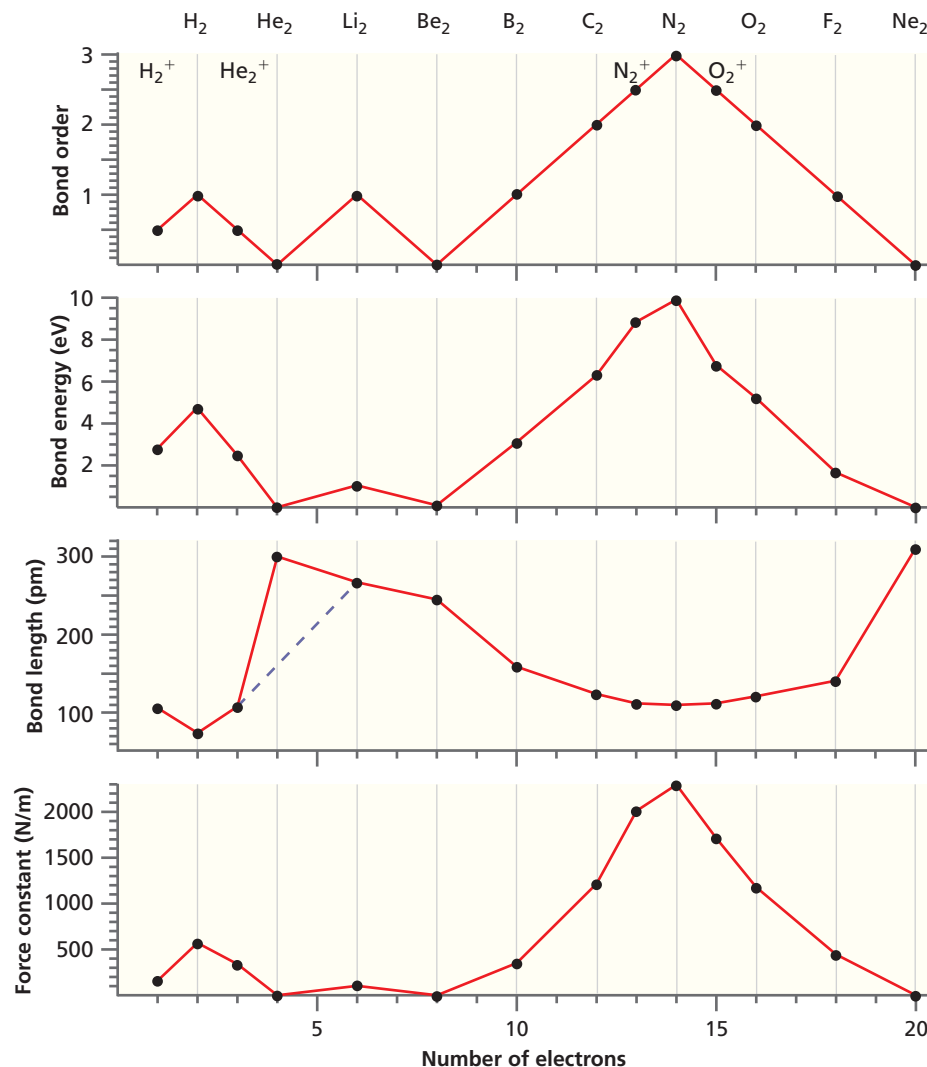


Figure 12.19
Bond energy, bond length, and vibrational force constant of the first 10 diatomic molecules as a function of the number of electrons in the molecule. The upper panel shows the calculated bond order for these molecules. The dashed line indicates the dependence of the bond length on the number of electrons if the He₂ data point is omitted.

respect to the atoms. This makes the molecule more stable than the separated atoms, which is necessary for chemical bond formation. Similarly, putting two electrons into each of the bonding and antibonding orbitals leads to a total energy that is greater than that of the separated molecules. Therefore, the molecule is unstable with respect to dissociation into two atoms. This result suggests that stable bond formation requires more electrons to be in bonding orbitals than in antibonding orbitals. We introduce the concept of **bond order**, which is defined as

$$\text{Bond order} = 1/2 [(\text{total bonding electrons}) - (\text{total antibonding electrons})]$$

This definition applies to homonuclear diatomic molecules and must be modified for heteronuclear diatomic molecules, as we will see in Section 12.8.

We expect the bond energy to be very small for a bond order of zero and to increase with increasing bond order. As shown in Figure 12.19, the bond order shows the same trend as the bond energies. The bond order also tracks the vibrational force constant very well. Again, we can explain the data by associating a stiffer bond with a higher bond order. This agreement is a good example of how a model, in this case molecular orbital theory, becomes validated and useful when it provides an understanding for different sets of experimental data. He_2 has an anomalous bond length because it is not a true chemical bond.

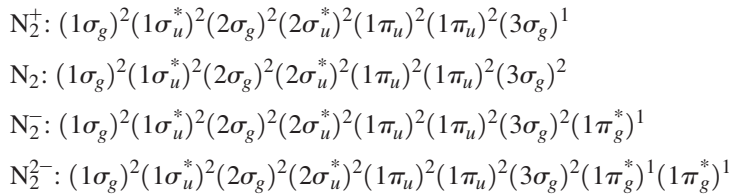
The relationship between the bond length and the number of electrons in the molecule is influenced both by the bond order and by the variation of the atomic radius with the effective nuclear charge. For a given atomic radius, the bond length is expected to decrease as the bond order increases. This trend is approximately followed for the series $\text{Be}_2 \rightarrow \text{N}_2$ in which the atomic radii are not constant but decrease steadily. The bond order increases from He_2^+ to Li_2 ; therefore, we might expect the bond length to decrease. This does not occur because the valence electron in Li is in the 2s rather than the 1s AO, which leads to an increase in the atomic radius. The correlation between bond order and bond length also breaks down for He_2 because the atoms are not chemically bonded. On balance, the trends shown in Figures 12.18 and 12.19 provide significant support for the concepts underlying molecular orbital theory.

EXAMPLE PROBLEM 12.3

Arrange the following in terms of increasing bond energy and bond length on the basis of their bond order: N_2^+ , N_2 , N_2^- , and N_2^{2-} .

Solution

The ground state configurations for these species are



In this series, the bond order is 2.5, 3, 2.5, and 2. Therefore, the bond energy is predicted to follow the order $\text{N}_2 > \text{N}_2^+, \text{N}_2^- > \text{N}_2^{2-}$ using the bond order alone. However, because of the extra electron in the antibonding $1\pi_g^*$ MO, the bond energy in N_2^- will be less than that in N_2^+ . Because bond lengths decrease as the bond strength increases, the bond length will follow the opposite order.

Looking back at what we have learned about homonuclear diatomic molecules, several important concepts stand out. Combining atomic orbitals on each atom to form molecular orbitals provides a way to generate molecular configurations for molecules. Although including many AOs on each atom (which is equivalent to using a larger basis set) is necessary to calculate accurate MO energies, important trends can be predicted using a minimal basis set of one or two AOs per atom. The symmetry of atomic

orbitals is important in predicting whether they contribute to a given molecular orbital. The concept of bond order allows us to understand why He_2 , Be_2 , and Ne_2 are not stable and why the bond in N_2 is so strong.

12.8 HETERONUCLEAR DIATOMIC MOLECULES

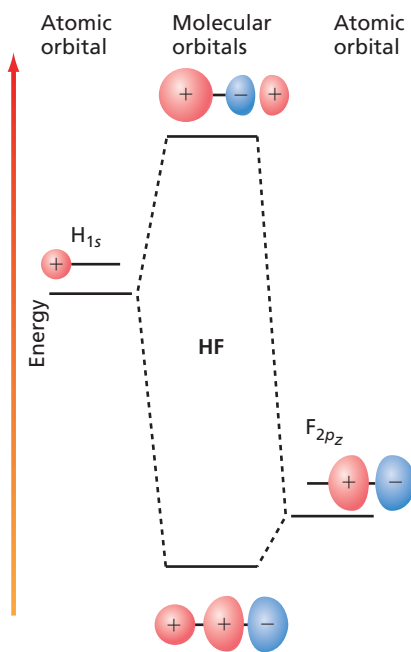
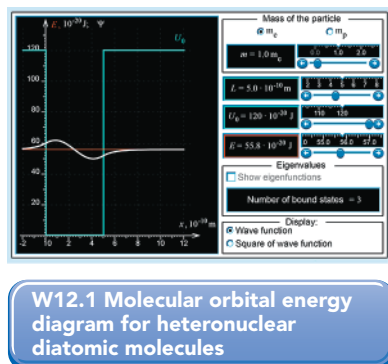


Figure 12.20

Molecular orbital energy diagram for a qualitative description of bonding in HF. The atomic orbitals are shown to the left and right, and the molecular orbitals are shown in the middle. Dashed lines connect the MO with the AOs from which it was constructed. Shaded circles have a diameter proportional to the coefficients c_{ij} . Red and blue shading signifies positive and negative signs of the AO amplitudes, respectively.

We can now extend the discussion of Section 12.1 on generating molecular orbitals to heteronuclear diatomic molecules for which the AO energies are not equal. For simplicity, we again consider only one AO on each atom. To be specific, consider HF and let ϕ_1 be a hydrogen 1s orbital and let ϕ_2 be a fluorine 2p_z orbital. The bonding and antibonding MOs have the form

$$\psi_1 = c_{1H}\phi_{H1s} + c_{1F}\phi_{F2p_z} \quad \text{and} \quad \psi_2 = c_{2H}\phi_{H1s} + c_{2F}\phi_{F2p_z} \quad (12.31)$$

where the coefficients are to be determined. The MOs ψ_1 and ψ_2 are the in-phase and out-of-phase combinations of the AOs, and have energies ε_1 and ε_2 , respectively. Evaluating the normalization integrals as in Equation (12.18) produces the result

$$(c_{1H})^2 + (c_{1F})^2 + 2c_{1H}c_{1F}S_{HF} = 1 \quad \text{and} \\ (c_{2H})^2 + (c_{2F})^2 + 2c_{2H}c_{2F}S_{HF} = 1 \quad (12.32)$$

To calculate ε_1 , ε_2 , c_{1H} , c_{2H} , c_{1F} , and c_{2F} , we need numerical values for H_{HH} , H_{FF} , H_{HF} , and S_{HF} . As discussed in Section 12.3, to a good approximation, H_{HH} and H_{FF} correspond to the first ionization energies of H and F, respectively, and fitting experimental data gives the approximate empirical relation $H_{HF} = -1.75 S_{HF} \sqrt{H_{HH}H_{FF}}$. To obtain numerical values for the coefficients in Equation (12.31), we assume that $S_{HF} = 0.30$. We know that $H_{HH} = -13.6 \text{ eV}$, and $H_{FF} = -18.6 \text{ eV}$, from which we determine that $H_{HF} = -8.35 \text{ eV}$. We are looking for trends rather than striving for accuracy, so these approximate values are sufficiently good for our purposes. Substituting these values in Equation (12.12) gives the MO energy levels shown next. Example Problem 12.4 shows how to obtain the corresponding values of the coefficients. The results are shown in Equation (12.33).

$$\begin{aligned} \varepsilon_1 &= -19.6 \text{ eV} & \psi_1 &= 0.34\phi_{H1s} + 0.84\phi_{F2p_z} \\ \varepsilon_2 &= -10.3 \text{ eV} & \psi_2 &= 0.99\phi_{H1s} - 0.63\phi_{F2p_z} \end{aligned} \quad (12.33)$$

Note that the magnitudes of the coefficients in the MOs are not equal as they were for H_2^+ . The coefficient of the lower-energy AO (F 2p_z) has the larger magnitude in the in-phase (bonding) MO and the smaller magnitude in the out-of-phase (antibonding) MO. The MO energy results for HF are shown in a molecular orbital energy diagram in Figure 12.20. The relative size of the AO coefficients are indicated by the size of the AO, and the sign of the coefficient is indicated by the color of the symbol.

EXAMPLE PROBLEM 12.4

Calculate c_{2H} and c_{2F} for the antibonding HF MO for which $\varepsilon_2 = -10.3 \text{ eV}$. Calculate c_{1H} and c_{1F} for the HF bonding MO for which $\varepsilon_1 = -19.6 \text{ eV}$. Assume that $S_{HF} = 0.30$.

Solution

We first obtain the result $H_{HF} = -1.75 S_{HF} \sqrt{H_{HH}H_{FF}} = -8.35 \text{ eV}$. We then calculate c_{1H}/c_{1F} and c_{2H}/c_{2F} by substituting the values for ε_1 and ε_2 in the first equation in Equation (12.10)

$$c_{2H}(H_{HH} - \varepsilon_2) + c_{2F}(H_{HF} - \varepsilon_2 S_{HF}) = 0.$$

$$\text{For } \varepsilon_2 = -10.3 \text{ eV}, c_{2H}(-13.6 + 10.3) + c_{2F}(-8.35 + 0.30 \times 10.3) = 0$$

$$\frac{c_{2H}}{c_{2F}} = -1.58$$

Using this result in the normalization equation $c_{2H}^2 + c_{2F}^2 + 2c_{2H}c_{2F}S_{HF} = 1$

$$c_{2H} = 0.99, c_{2F} = -0.63, \text{ and } \psi_2 = 0.99\phi_{H1s} - 0.63\phi_{F2p_z}$$

$$\text{For } \varepsilon_1 = -19.6 \text{ eV}, c_{1H}(-13.6 + 19.6) + c_{1F}(-8.35 + 0.3 \times 19.6) = 0$$

$$\frac{c_{1H}}{c_{1F}} = 0.41$$

Using this result in the normalization equation $c_{1H}^2 + c_{1F}^2 + 2c_{1H}c_{1F}S_{HF} = 1$

$$c_{1H} = 0.34, c_{1F} = 0.84 \text{ and } \psi_1 = 0.34\phi_{H1s} + 0.84\phi_{F2p_z}$$

Just as for H_2^+ , in the bonding MO, the coefficients of the AOs have the same sign (in-phase). In the antibonding MO, they have the opposite sign (out-of-phase). However, because the AO energies are not equal, the magnitude of the coefficient of the lower-energy AO is *larger* in the bonding orbital and *smaller* in the antibonding orbital.

The relative magnitude of the coefficients of the AOs provides information about the charge distribution in the molecule, within the framework of the following simple model. Consider an electron in the HF bonding MO described by $\psi_1 = 0.34\phi_{H1s} + 0.84\phi_{F2p_z}$. Because of the association made in the first postulate between $|\psi|^2$ and probability, the individual terms in $\int \psi_1^* \psi_1 d\tau = (c_{1H})^2 + (c_{1F})^2 + 2c_{1H}c_{1F}S_{HF} = 1$ can be interpreted in the following way. We associate $(c_{1H})^2 = 0.12$ with the probability of finding the electron around the H atom, $(c_{1F})^2 = 0.71$ with the probability of finding the electron around the F atom, and $2c_{1H}c_{1F}S_{HF} = 0.17$ with the probability of finding the electron shared by the F and H atoms. We divide the shared probability equally between the atoms. This gives the probabilities of $(c_{1H})^2 + c_{1H}c_{1F}S_{HF} = 0.21$ on the H atom and $(c_{1F})^2 + c_{1H}c_{1F}S_{HF} = 0.79$ for finding the electron on the F atom. This result is reasonable given the known electronegativities of F and H. A more accurate Hartree–Fock calculation using a 28-member basis set predicts a charge of +0.48 and −0.48 on the H and F atoms, respectively. These calculated charges generate a dipole moment of 2.03 debye (1 debye = 3.34×10^{-30} Cm), which is in good agreement with the experimental value of 1.91 debye.

The method of assigning charge that has been described was originally suggested by Robert Mulliken. Although this method is reasonable, there is no unique way to distribute the electron charge in a MO among atoms because the charge on an atom is not a quantum-mechanical observable. For a pictorial justification of this assertion, see Figure 15.23. Note, that the charge transfer is in the opposite direction for the antibonding MO. We find that the shared probability has a positive sign for a bonding orbital and a negative sign for an antibonding orbital. This is a useful criterion for distinguishing between bonding and antibonding MOs.

The results for HF show that the bonding MO has a greater amplitude on F, which has the lower-energy AO. In other words, the bonding MO is more localized on F than on H. We generalize this result to a hypothetical molecule HX where the AO energy of X lies significantly lower than that of H by calculating ε_1 , c_{1H} , and c_{1X} for different AO energies of X. The results are shown in Table 12.2, where $H_{HH} = -13.6 \text{ eV}$ and $S_{HX} = 0.30$.

Note that as the X AO energy becomes more negative, the X AO coefficient → 1 and the H AO coefficient → 0 in the bonding MO. It is also seen that the MO energy approaches the lower AO energy as the X AO energy becomes more negative, which means that the MO is essentially identical to the AO. This result shows that although we

Concept

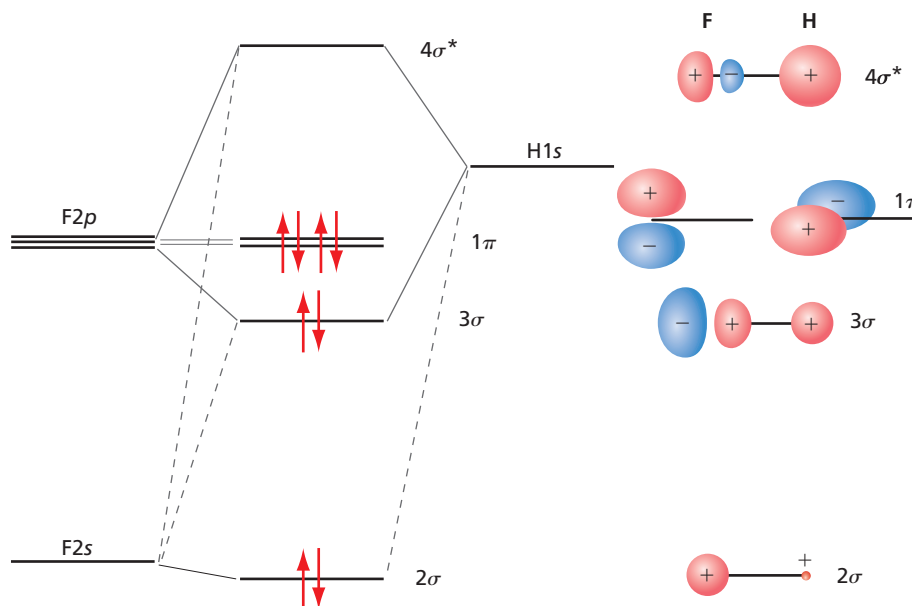
Although atomic charges are not quantum mechanical observables, reasonable models exist that allow their calculation.

TABLE 12.2 AO Coefficients and MO Energies for Different Values of H_{xx}

H_{xx} (eV)	c_{1H}	c_{1X}	ε_1 (eV)
−18.6	0.345	0.840	−19.9
−23.6	0.193	0.925	−24.1
−33.6	0.055	0.982	−33.7
−43.6	0.0099	1.00	−43.6

Figure 12.21

Schematic energy diagram showing the relationship between atomic and molecular orbital energy levels for valence electrons in HF. The degenerate p and π orbitals are shown slightly offset in energy. The dominant atomic orbital contributions to the MOs are shown as solid lines. Lesser contributions are shown as dashed lines. The MOs are depicted to the right of the figure. We assign the 1s electrons on F to the 1σ MO, which is localized on the F atom.



have assumed that MOs are delocalized over the molecule, a MO formed from AOs that differ substantially in energy is largely localized on the atom with the lower AO energy.

Now, let us turn to nomenclature specifically for MOs for heteronuclear diatomic molecules. Because the two atoms are dissimilar, the u and g symmetries do not apply as inversion interchanges the nuclei. However, the MOs will still have either σ or π symmetry. Therefore, the MOs on a heteronuclear diatomic molecule are numbered differently than for the molecules Li₂–N₂:

Homonuclear	$1\sigma_g$	$1\sigma_u^*$	$2\sigma_g$	$2\sigma_u^*$	$1\pi_u$	$3\sigma_g$	$1\pi_g^*$	$3\sigma_u^*$
Heteronuclear	1σ	2σ	3σ	4σ	1π	5σ	2π	6σ

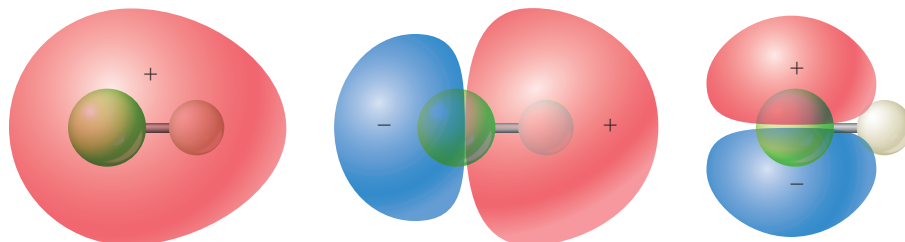
It is customary to omit the $*$ symbol, which indicates out-of-phase AOs for heteronuclear diatomic molecules. A common alternate numbering system is to assign the 1σ MO to the lowest-energy valence MO rather than including, for example, the 1s electrons on F, which are localized on the F atom.

We again consider HF, though this time more quantitatively. To begin, we construct MOs using the 1s AO on H and the 2s and 2p_z AOs on F rather than just one AO on each atom, as depicted in Figure 12.20. The revised molecular orbital energy diagram for HF is shown in Figure 12.21. The eight valence electrons corresponding to the $1\sigma^2 2\sigma^2 3\sigma^2 1\pi^4$ molecular configuration are entered in the appropriate energy levels.

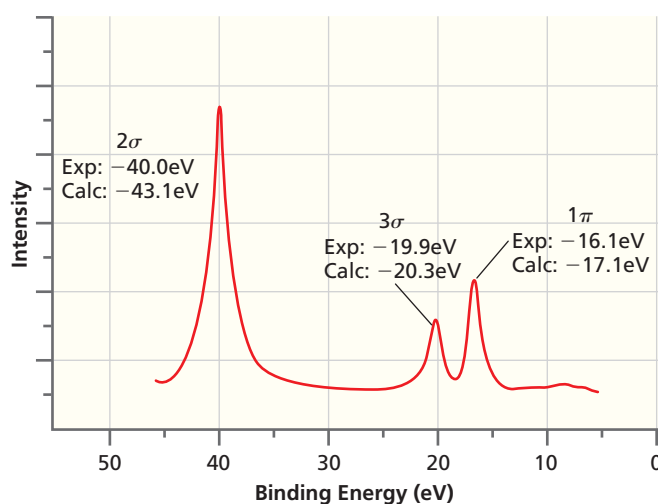
The AOs on the two atoms that give rise to the MOs are shown on the right side of the diagram, with the size of the orbital proportional to its coefficient in the MO. Numerical calculations show that the 1σ electrons are almost completely localized on the F atom. The 1π electrons are completely localized on the F atom because the 2p_x and 2p_y orbitals on F have a zero net overlap with the 1s orbital on H. Electrons in MOs localized on a single atom are referred to as **nonbonding electrons**. For HF, the highest energy occupied molecular orbital (HOMO) is nonbonding and the bond can be attributed to the 2σ MO. The mixing of 2s and 2p AOs in the 3σ and 4σ MOs changes the electron distribution in the HF molecule when compared with a homonuclear diatomic molecule. The 3σ MO has less bonding character, and the 4σ MO has less antibonding character. Depictions of the 2σ , 3σ , and 1π MOs obtained in calculations using a larger basis set are shown in Figure 12.22.

Concept

Electrons in MOs localized on a single atom are referred to as nonbonding electrons.

**Figure 12.22**

The 2σ , 3σ , and 1π MOs for HF are shown from left to right.

**Figure 12.23**

Intensity of photoelectron spectroscopy signal versus electron binding energy. Peaks are observed at energies that correlate well with calculated MO energy levels.

Source: Adapted from Banna et al., *Journal of Chemical Physics*, 61 (1974): 4780–4786.

As expected, in the 2σ bonding orbital the electron density is much greater on the more electronegative fluorine than on the hydrogen. However, in the antibonding 4σ orbital, this polarity is reversed. As you will see in the end-of-chapter problems, the estimated dipole moment is smaller in the excited state than in the ground state.

The definition given for bond order in Section 12.7 must be modified for heteronuclear diatomic molecules where the delocalized electrons are not equally shared by the two atoms. Note that the 2σ MO is largely localized on the F atom, so that it has no bonding character, the 3σ MO is not totally bonding, and the 1π MOs are nonbonding and completely localized on the F atom. Therefore, the total bond order is approximately one.

The MO energies can be experimentally determined using photoelectron spectroscopy, as was depicted for atoms in Figure 11.18. The MO energy is determined from the kinetic energy of the ejected electrons using Koopmans' theorem (see Section 10.5). An example of the results obtained from such a measurement for HF is shown in Figure 12.23. The 2σ level has an energy of -40.0 eV, and the corresponding values for the 3σ and 1π MOs are -19.9 eV and -16.1 eV. For more details, see the reference to Banna et al. in Further Reading. Also shown in Figure 12.23 are MO energy values calculated using the Hartree–Fock method. Notice that the agreement between experimental and calculated values is good.

12.9 THE MOLECULAR ELECTROSTATIC POTENTIAL

As discussed in Section 12.8, the charge on an atom in a molecule is not a quantum-mechanical observable; consequently, atomic charges cannot be assigned uniquely. However, we know that the electron charge is not uniformly distributed in a polar molecule. For example, the region around the oxygen atom in H_2O has a net negative charge, whereas the region around the hydrogen atoms has a net positive charge. How can this nonuniform charge distribution be discussed? To do so, we introduce the **molecular electrostatic potential**, which is the electrical potential experienced by a test charge at various points in the molecule.

The molecular electrostatic potential is calculated by considering separately the contribution of the valence electrons and the atomic nuclei. Consider the nuclei first. For a point charge of magnitude q , the electrostatic potential $\phi(r)$ at a distance r from the charge, is given by

$$\phi(r) = \frac{q}{4\pi\epsilon_0 r} \quad (12.34)$$

Concept

The molecular electrostatic potential is useful in describing the charge distribution of the valence electrons in a molecule.

Therefore, the contribution to the molecular electrostatic potential from the atomic nuclei is given by

$$\phi_{nuclei}(x_1, y_1, z_1) = \sum_i \frac{q_i}{4\pi\epsilon_0 r_i} \quad (12.35)$$

where q_i is the atomic number of nucleus i , and r_i is the distance of nucleus i from the observation point with the coordinates (x_1, y_1, z_1) . The sum extends over all atoms in the molecule.

The electrons in the molecule can be considered as a continuous charge distribution with a density at a point with the coordinates (x, y, z) that is related to the n -electron wave function by

$$\rho(x, y, z) = -e \int \dots \int (\psi(x, y, z; \dots; x_n, y_n, z_n))^2 \times dx_1 dy_1 dz_1 \dots dx_n dy_n dz_n \quad (12.36)$$

The integration is over the position variables of all n electrons. Combining the contributions of the nuclei and the electrons, the molecular electrostatic potential is given by

$$\phi(x_1, y_1, z_1) = \sum_i \frac{q_i}{4\pi\epsilon_0 r_i} - \iiint \frac{\rho(x, y, z)}{4\pi\epsilon_0 r_e} dx dy dz \quad (12.37)$$

where r_e is the distance of an infinitesimal volume element of electron charge from the observation point with the coordinates (x_1, y_1, z_1) .

The molecular electrostatic potential must be calculated numerically using the Hartree–Fock method or other methods discussed in Chapter 15. To visualize the polarity in a molecule, it is convenient to display a contour of constant electron density around the molecule and then display the values of the molecular electrostatic potential on the density contour using a color scale, as shown for HF in Figure 12.24. Negative values of the electrostatic potential, shown in red, occur near atoms to which electron charge transfer occurs. For HF, this is the region around the fluorine atom. Positive values of the molecular electrostatic potential, shown in blue, occur around atoms from which electron transfer occurs, as for the hydrogen atom in HF.

The calculated molecular electrostatic potential function identifies regions of a molecule that are either electron rich or depleted in electrons. We can use this function to predict regions of a molecule that are susceptible to nucleophilic or electrophilic attack as in enzyme–substrate reactions. The molecular electrostatic potential is particularly useful because it can also be used to obtain a set of atomic charges that is more reliable than the Mulliken model discussed in Section 12.8. This is done by initially choosing a set of atomic charges and calculating an approximate molecular electrostatic potential around a molecule using Equation (12.35). These atomic charges are varied systematically, subject to the constraint that the total charge is zero for a neutral molecule, until optimal agreement is obtained between the approximate and the accurate molecular electrostatic potential calculated from Equation (12.37). The atomic charges obtained in computational chemistry software calculated in this way are discussed in Chapter 15.

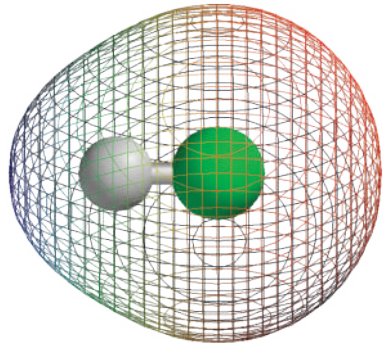


Figure 12.24

Surface grid of constant electron density for the HF molecule. The fluorine atom is shown in green. The color shading on the grid indicates the value of the molecular electrostatic potential. Red and blue correspond to negative and positive values, respectively.

VOCABULARY

- π symmetry
- σ symmetry
- antibonding molecular orbital
- antisymmetric wave function
- atomic orbital (AO)
- bond energy
- bond order
- bonding molecular orbital
- Born–Oppenheimer approximation
- delocalization

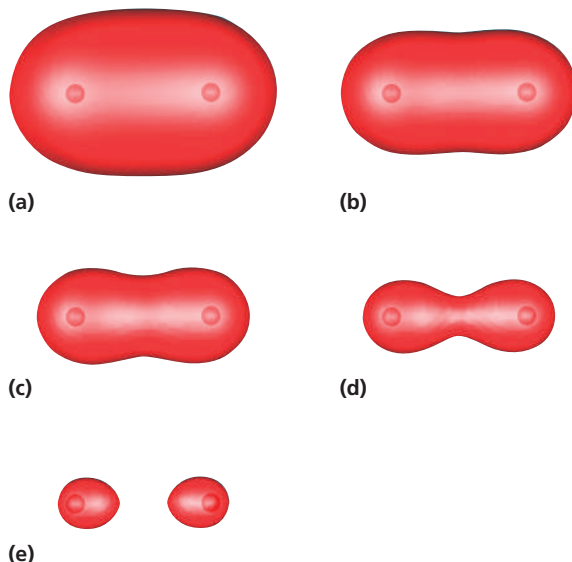
- delocalized
- g symmetry
- LCAO-MO model
- localization
- molecular configuration
- molecular electrostatic potential
- molecular orbital (MO)
- molecular orbital energy diagram
- molecular wave function
- nonbonding electrons
- overlap integral
- secular determinant
- secular equations
- $s-p$ mixing
- symmetric wave function
- symmetry operation
- u symmetry
- variational parameter

KEY EQUATIONS

Equation	Significance of Equation	Equation Number
$\begin{vmatrix} H_{aa} - \varepsilon & H_{ab} - \varepsilon S_{ab} \\ H_{ab} - \varepsilon S_{ab} & H_{bb} - \varepsilon \end{vmatrix} = 0$	This condition on the secular determinant allows AO coefficients to have a solution other than $c_a = c_b = 0$	12.11
$\varepsilon_1 = \frac{H_{aa} + H_{ab}}{1 + S_{ab}} \quad \text{and} \quad \varepsilon_2 = \frac{H_{aa} - H_{ab}}{1 - S_{ab}}$	Energy levels of two MOs formed by combining one AO on each atom of a diatomic molecule	12.13
$\phi_{H1s} = \frac{1}{\sqrt{\pi}} \left(\frac{\zeta}{a_0} \right)^{3/2} e^{-\zeta r/a_0}$	Hydrogen 1s orbital with variational parameter ζ	12.16
$\psi_g = c_g(\phi_{H1s_a} + \phi_{H1s_b})$ $\psi_u = c_u(\phi_{H1s_a} - \phi_{H1s_b})$	MOs formed by combining H 1s AOs on each atom in a homonuclear diatomic molecule	12.17
$\langle E_{\text{potential}} \rangle = -2 \langle E_{\text{kinetic}} \rangle$	Virial theorem	12.27
$\psi_j = \sum_{i=1}^N c_{ij} \phi_i$	Expansion of molecular orbital in a basis set	12.30
$\phi(x_1, y_1, z_1) = \sum_i \frac{q_i}{4\pi\varepsilon_0 r_i} - \iiint \frac{\rho(x, y, z)}{4\pi\varepsilon_0 r_e} dx dy dz$	Definition of molecular electrostatic potential	12.37

CONCEPTUAL PROBLEMS

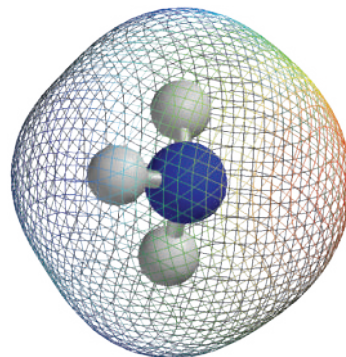
Q12.1 The following images show contours of constant electron density for H_2 calculated using the methods described in Chapter 15. The values of electron density are (a) 0.10, (b) 0.15, (c) 0.20, (d) 0.25, (e) 0.30 electron/ a_0^3 .



- a. Explain why the apparent size of the H_2 molecule as approximated by the volume inside the contour varies in the sequence a–e.
- b. Notice the neck that forms between the two hydrogen atoms in contours c and d. What does neck formation tell you about the relative density in the bonding region and in the region near the nuclei?

- c. Explain the shape of the contours in image e.
- d. Estimate the electron density in the bonding region midway between the H atoms by estimating the value of the electron density at which the neck disappears.

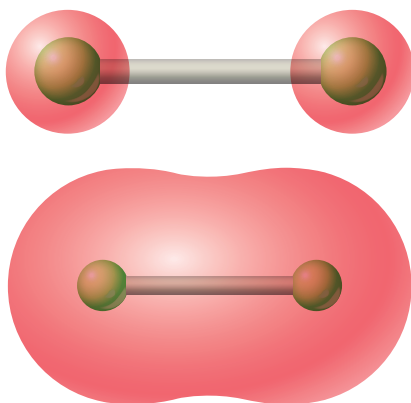
Q12.2 Consider the molecular electrostatic potential map for the NH_3 molecule shown here. Is hydrogen (shown as a white sphere) an electron acceptor or an electron donor in this molecule?



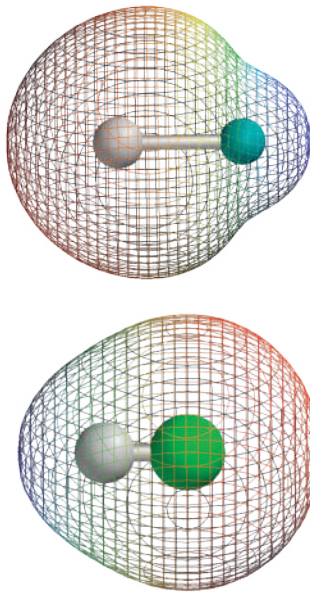
Q12.3 Give examples of AOs for which the overlap reaches its maximum value only as the internuclear separation approaches zero in a diatomic molecule. Also give examples of AOs for which the overlap goes through a maximum value and then decreases as the internuclear separation approaches zero.

Q12.4 Why is it reasonable to approximate H_{11} and H_{22} by the appropriate ionization energy of the corresponding neutral atom?

Q12.5 Identify the molecular orbitals for F_2 in the images shown here in terms of the two designations discussed in Section 12.5.



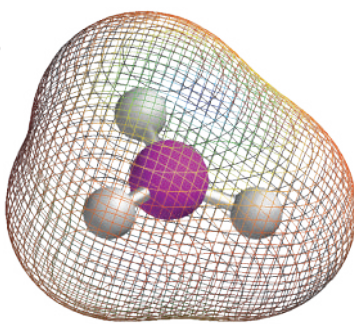
Q12.6 The molecular electrostatic potential maps for LiH and HF are shown here. Does the apparent size of the hydrogen atom (shown as a white sphere) tell you whether it is an electron acceptor or an electron donor in these molecules?



Q12.7 For H_2^+ , explain why H_{aa} is the total energy of an undisturbed hydrogen atom separated from a bare proton by the distance R .

Q12.8 Distinguish between the following concepts used to describe chemical bond formation: basis set, minimal basis set, atomic orbital, molecular orbital, and molecular wave function.

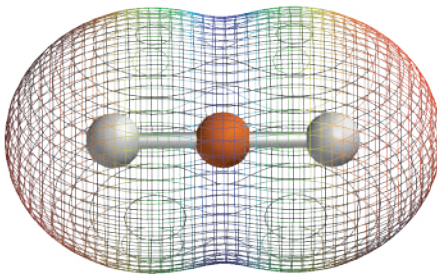
Q12.9 Consider the molecular electrostatic potential map for the BH_3 molecule shown here. Is the hydrogen atom (shown as a white sphere) an electron acceptor or an electron donor in this molecule?



Q12.10 Using Figures 12.10 and 12.11, explain why $\Delta\psi_g^2 < 0$ and $\Delta\psi_u^2 > 0$ outside of the bonding region of H_2^+ .

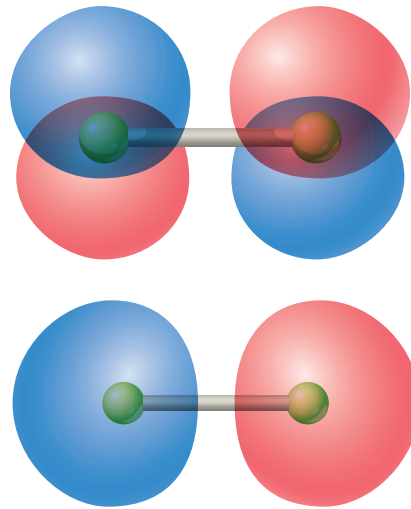
Q12.11 Consider the molecular electrostatic potential map for the BeH_2 molecule shown here. Is the hydrogen atom

(shown as a white sphere) an electron acceptor or an electron donor in this molecule?



Q12.12 Why are MOs on heteronuclear diatomic molecules not labeled with g and u subscripts?

Q12.13 Identify the molecular orbitals for F_2 in the images shown here in terms of the two designations discussed in Section 12.5. The molecular axis is the z axis, and the y axis is tilted slightly out of the plane of the image.



Q12.14 What is the justification for stating that, in expanding MOs in terms of AOs, the equality $\psi_j(1) = \sum_{i=1}^{\infty} c_{ij}\phi_i(1)$ can in principle be satisfied?

Q12.15 Why are the magnitudes of the coefficients c_a and c_b in the H_2^+ wave functions ψ_g and ψ_u equal?

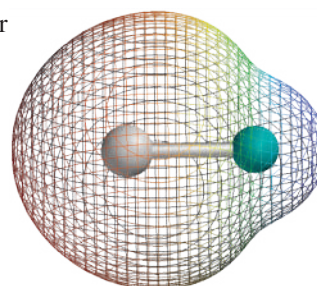
Q12.16 Explain why $s-p$ mixing is more important in Li_2 than in F_2 .

Q12.17 Justify the Born–Oppenheimer approximation based on vibrational frequencies and electron relaxation times.

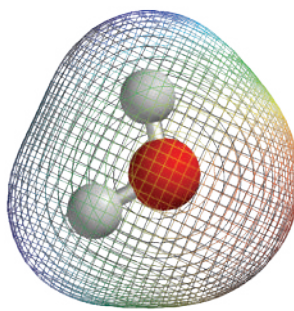
Q12.18 Why can you conclude that the energy of the antibonding MO in H_2^+ is raised more than the energy of the bonding MO is lowered?

Q12.19 Does the total energy of a molecule increase or decrease when an electron is put in an antibonding orbital?

Q12.20 Consider the molecular electrostatic potential map for the LiH molecule shown here. Is the hydrogen atom (shown as a white sphere) an electron acceptor or an electron donor in this molecule?



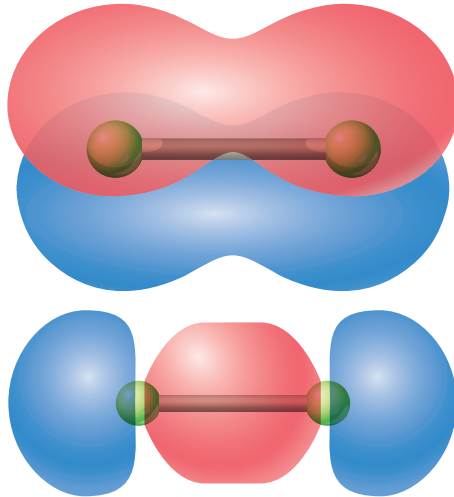
Q12.21 Consider the molecular electrostatic potential map for the H₂O molecule shown here. Is the hydrogen atom (shown as a white sphere) an electron acceptor or an electron donor in this molecule?



Q12.22 For the case of two H_{1s} AOs, the value of the overlap integral S_{ab} is never exactly zero. Explain this statement.

Q12.23 If there is a node in ψ_u , is the electron in this wave function really delocalized? How does it get from one side of the node to the other?

Q12.24 Identify the molecular orbitals for F₂ in the images shown here in terms of the two designations discussed in Section 12.5. The molecular axis is the z axis, and the y axis is tilted slightly out of the plane of the image.



Q12.25 By considering each term in

$$K = \int \phi_{H1s_b}^* \left(\frac{e^2}{4\pi\epsilon_0 r_b} \right) \phi_{H1s_a} d\tau$$

and

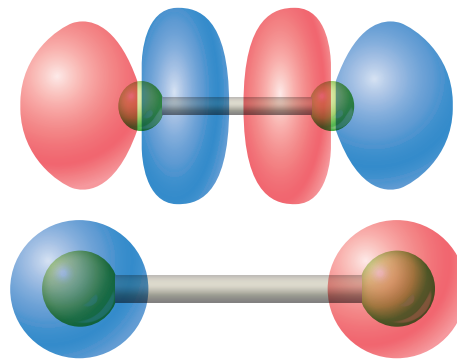
$$J = \int \phi_{H1s_a}^* \left(\frac{e^2}{4\pi\epsilon_0 r_b} \right) \phi_{H1s_a} d\tau$$

explain why the values of J and K are positive for H₂⁺.

Q12.26 Why do we neglect the bond length in He₂ when discussing the trends shown in Figure 12.19?

Q12.27 Explain why the nodal structures of the 1σ_g MOs in H₂ and F₂ differ.

Q12.28 Identify the molecular orbitals for F₂ in the images shown here in terms of the two designations discussed in Section 12.5.



Q12.29 Would the properties of the H₂⁺ molecule change if the red and blue contours in Figure 12.8 were interchanged?

NUMERICAL PROBLEMS

Section 12.1

P12.1 Using ζ as a variational parameter in the normalized function $\psi_{H1s} = 1/\sqrt{\pi}(\zeta/a_0)^{3/2}e^{-\zeta r/a_0}$ allows one to vary the size of the orbital. Show this by calculating the probability of finding the electron inside a sphere of radius a_0 for different values of ζ using the standard integral

$$\int x^2 e^{-ax} dx = -e^{-ax} \left(\frac{2}{a^3} + 2 \frac{x}{a^2} + \frac{x^2}{a} \right)$$

- a. Obtain an expression for the probability as a function of ζ .
- b. Evaluate the probability for $\zeta = 1.5, 2.5$, and 3.5 .

P12.2 The overlap integral for ψ_g and ψ_u as defined in Section 12.3 is given by

$$S_{ab} = e^{-\zeta R/a_0} \left(1 + \zeta \frac{R}{a_0} + \frac{1}{3} \zeta^2 \frac{R^2}{a_0^2} \right)$$

Plot S_{ab} as a function of R/a_0 for $\zeta = 0.8, 1.0$, and 1.2 . Estimate the value of R/a_0 for which $S_{ab} = 0.4$ for each of these values of ζ .

Section 12.2

P12.3 Follow the procedure outlined in Section 12.3 to determine c_u in Equation (12.17).

Section 12.3

P12.4 Show that calculating E_u in the manner described by Equation (12.7) gives the result $E_u = (H_{aa} - H_{ab})/(1 - S_{ab})$.

Section 12.5

P12.5 Arrange the following in terms of decreasing bond energy and bond length: O_2^+ , O_2 , O_2^- , and O_2^{2-} .

P12.6 Predict the bond order in the following species:

- a. N_2^+
- b. Li_2^+
- c. O_2^-
- d. H_2^-
- e. C_2^+

P12.7 What is the electron configuration corresponding to O_2 , O_2^- , and O_2^+ ? What do you expect the relative order of bond strength to be for these species? Which, if any, have unpaired electrons?

P12.8 Evaluate the energy for the two MOs generated by combining two H_{1s} AOs. Use Equation (12.13) and carry out the calculation for $S_{12} = 0.15$, 0.30 , and 0.45 to mimic the effect of decreasing the atomic separation in the molecule. Use the parameters $H_{11} = H_{22} = -13.6$ eV and $H_{12} = -1.75S_{12}\sqrt{H_{11}H_{22}}$. Explain the trend that you observe in the results.

P12.9 Calculate the bond order in each of the following species. Which of the species in parts a–d do you expect to have the shorter bond length?

- a. Li_2 or Li_2^+
- b. C_2 or C_2^+
- c. O_2 or O_2^+
- d. F_2 or F_2^-

Section 12.6

P12.10 Make a sketch of the highest occupied molecular orbital (HOMO) for the following species:

- a. N_2^+
- b. Li_2^+
- c. O_2^-
- d. H_2^-
- e. C_2^+

Calculate the bond order of each molecule.

Section 12.7

P12.11 Calculate the bond order in each of the following species. Predict which of the two species in the following pairs has the higher vibrational frequency:

- a. Li_2 or Li_2^+
- b. C_2 or C_2^+
- c. O_2 or O_2^+
- d. F_2 or F_2^-

P12.16 A Hartree–Fock calculation using the minimal basis set of the $1s$, $2s$, $2p_x$, $2p_y$, and $2p_z$ AOs on each of N and O generated the energy eigenvalues and AO coefficients listed in the accompanying table.

a. Designate the MOs in the accompanying table as σ or π symmetry and as bonding or antibonding. Assign the MOs to the following images, in which the O atom is red. The molecular axis is the z axis. In doing so, keep the following criteria in mind:

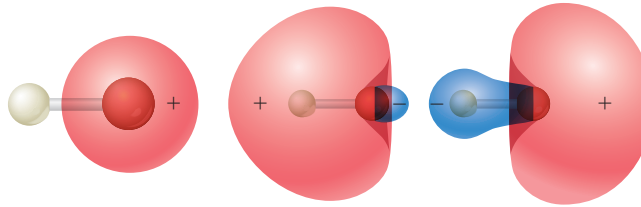
MO	$\varepsilon(\text{eV})$	$c_{\text{N}1s}$	$c_{\text{N}2s}$	$c_{\text{N}2p_z}$	$c_{\text{N}2p_x}$	$c_{\text{N}2p_y}$	$c_{\text{O}1s}$	$c_{\text{O}2s}$	$c_{\text{O}2p_z}$	$c_{\text{O}2p_x}$	$c_{\text{O}2p_y}$
3	-41.1	-0.13	+0.39	+0.18	0	0	-0.20	+0.70	+0.18	0	0
4	-24.2	-0.20	0.81	-0.06	0	0	0.16	-0.71	-0.30	0	0
5	-18.5	0	0	0	0	0.70	0	0	0	0	0.59
6	-15.2	+0.09	-0.46	+0.60	0	0	+0.05	-0.25	-0.60	0	0
7	-15.0	0	0	0	0.49	0	0	0	0	0.78	0
8	-9.25	0	0	0	0	0.83	0	0	0	0	-0.74

Section 12.8

P12.12 Sketch a molecular orbital energy diagram for CO and place the electrons in the levels appropriate for the ground state. The AO ionization energies are $O2s$: 32.3 eV; $O2p$: 15.8 eV; $C2s$: 19.4 eV; and $C2p$: 10.9 eV. The MO energies follow the sequence (from lowest to highest) 1σ , 2σ , 3σ , 4σ , 1π , 5σ , 2π , 6σ . Connect each MO level with the level of the major contributing AO on each atom.

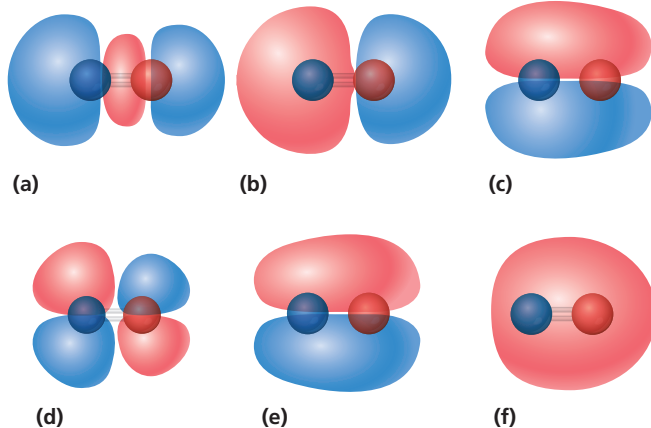
P12.13 Calculate the value for the coefficients of the AOs in Example Problem 12.4 for $S_{12} = 0.45$. How are they different from the values calculated in that problem for $S_{12} = 0.3$? Can you offer an explanation for the changes?

P12.14 Images of molecular orbitals for LiH calculated using the minimal basis set are shown below. In these images, the smaller atom is H. The H $1s$ AO has a lower energy than the Li $2s$ AO. The energy of the MOs is (left to right) -63.9 eV, -7.92 eV, and +2.14 eV. Prepare a molecular orbital diagram for this molecule, associate the MOs with the images, and designate the MOs in the images below as filled or empty. Which MO is the HOMO? Which MO is the lowest energy unoccupied molecular orbital (LUMO)? Do you expect the dipole moment in this molecule to have the negative end on H or Li?



P12.15 The ionization energy of CO is greater than that of NO. Explain this difference based on the electron configuration of these two molecules.

- If AOs of the same type on the two atoms have the same sign, they are in phase; if they have the opposite sign, they are out of phase.
- Energy increases with the number of nodes.
- If the coefficients of the s and p_z AOs are zero, the MO has π symmetry.
- If the coefficients of the p_x and p_y AOs are zero, the MO has σ symmetry.



- b.** Explain why MOs 5 and 7 do not have the same energy. Why is the energy of MO 5 lower than that of MO 7?

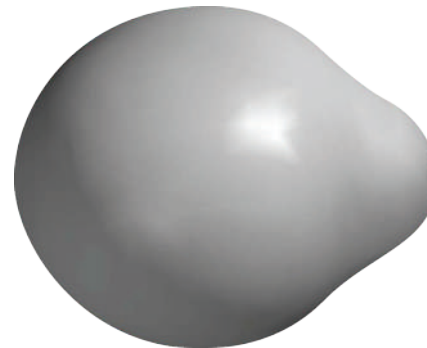
P12.17 Using the method of Mulliken, calculate the probabilities of finding an electron involved in the chemical bond on the H and F atoms for the bonding and antibonding MOs for Problem 12.13.

P12.18 Explain the difference in the appearance of the MOs in Problem P12.14 with those for HF. Based on the MO energies, do you expect LiH^+ to be stable? Do you expect LiH^- to be stable?

P12.19 Calculate the dipole moment of HF for the bonding MO in Equation (12.33). Use the method outlined in Section 12.8 and the results of Example Problem 12.4 to calculate the charge on each atom. The bond length in HF is 91.7 pm. The experimentally determined dipole moment of ground-state HF is 1.91 Debye, where 1 Debye = 3.33×10^{-30} C m.

Compare your result with this value. Does the simple theory give a reliable prediction of the dipole moment?

P12.20 A surface displaying a contour of the total charge density in LiH is shown here. What is the relationship between this surface and the MOs displayed in Problem P12.14? Why does this surface closely resemble one of the MOs?



P12.21 Sketch the molecular orbital energy diagram for the radical OH based on what you know about the corresponding diagram for HF. How will the diagrams differ? Characterize the HOMO and LUMO as antibonding, bonding, or nonbonding.

P12.22 The bond dissociation energies of the species NO, CF^- , and CF^+ follow the trend $\text{CF}^+ > \text{NO} > \text{CF}^-$. Explain this trend using MO theory.

P12.23 Evaluate the energy for the two MOs generated by combining a $\text{H}1s$ and a $\text{F}2p$ AO. Use Example Problem 12.4 and carry out the calculation for $S_{HF} = 0.075$, 0.18, and 0.40 to mimic the effect of increasing the atomic separation in the molecule. Use the parameters $H_{11} = -13.6$ eV, $H_{22} = -18.6$ eV, and $H_{12} = -1.75S_{12}\sqrt{H_{11}H_{22}}$. Explain the trend that you observe in the results.

P12.24 The expressions $(c_{11})^2 + c_{11}c_{21}S_{12}$ and $(c_{12})^2 + c_{11}c_{21}S_{12}$ for the probability of finding an electron on the H and F atoms in HF, respectively, were derived in Section 12.8. Use your results from Problem P12.23 and these expressions to calculate the probability of finding an electron in the bonding orbital on the F atom for $S_{HF} = 0.075$, 0.18, and 0.40. Explain the trend shown by these results.

COMPUTATIONAL PROBLEMS

More detailed instructions on carrying out these calculations using Spartan Physical Chemistry are found at:
<https://www.pearsonhighered.com/chemistryresources/>

C12.1 According to Hund's rules, the ground state of O_2 should be a triplet because the last two electrons are placed in a doubly degenerate set of π MOs. Calculate the energy of the singlet and triplet states of O_2 using the B3LYP method and the 6-31G* basis set. Does the singlet or triplet have the lower energy? Both states will be populated if the energy difference $\Delta E \sim k_B T$. For which temperature is this the case?

C12.2 If the ground state of oxygen is a diradical, you might think that O_2 would dimerize to form square planar O_4 to achieve a molecule in which all electrons are paired. Optimize the geometry and calculate the energies of triplet O_2 and

singlet O_4 using the B3LYP method and the 6-31G* basis set. Do you predict O_4 to be more or less stable than 2O_2 molecules? Use a nonplanar shape in building your O_4 molecule. Is the geometry optimized molecule planar or nonplanar?

C12.3 O_6 might be more stable than O_4 because the bond angle is larger, leading to less steric strain. Optimize the geometry and compare the energy of O_6 with 1.5 times the energy of O_4 using the B3LYP method and the 6-31G* basis set. Is O_6 more stable than O_4 ? Use a nonplanar shape in building your O_6 molecule. Is the geometry optimized molecule planar or nonplanar?

C12.4 In a LiF crystal, both the Li and F are singly ionized species. Optimize the geometry and calculate the charge on Li and F in a single LiF molecule using the B3LYP method and the 6-31G* basis set. Are the atoms singly ionized? Compare the value of the bond length with the distance between Li⁺ and F⁻ ions in the crystalline solid.

C12.5 Does LiF dissociate into neutral atoms or into Li⁺ and F⁻? Answer this question by comparing the energy difference between reactants and products for the reactions $\text{LiF}(g) \rightarrow \text{Li}(g) + \text{F}(g)$ and $\text{LiF}(g) \rightarrow \text{Li}^+(g) + \text{F}^-(g)$ using the B3LYP method and the 6-31G* basis set.

C12.6 Calculate Hartree–Fock MO energy values for HF using the MP2 method and the 6-31G* basis set. Make a molecular energy diagram to scale omitting the lowest energy MO. Why can you neglect this MO? Characterize the other MOs as bonding, antibonding, or nonbonding.

C12.7 a. Based on the molecular orbital energy diagram in Problem C12.6, would you expect triplet neutral HF in which an electron is promoted from the 1π to the $4\sigma^*$ MO to be more or less stable than singlet HF?

b. Calculate the equilibrium bond length and total energy for singlet and triplet HF using the MP2 method and the 6-31G* basis set. Using the frequency as a criterion, are both stable molecules? Compare the bond lengths and vibrational frequencies.

c. Calculate the bond energy of singlet and triplet HF by comparing the total energies of the molecules with the total energy of F and H. Are your results consistent with the bond lengths and vibrational frequencies obtained in part (b)?

C12.8 Computational chemistry allows you to carry out calculations for hypothetical molecules that do not exist in order to see trends in molecular properties. Calculate the charge on the atoms in singlet HF and in triplet HF for which the bond length is fixed at 10% greater than the bond length for singlet HF. Are the trends that you see consistent with those predicted by Figure 12.21? Explain your answer.

WEB-BASED SIMULATIONS, ANIMATIONS, AND PROBLEMS

Simulations, animations, and homework problem worksheets can be accessed at www.pearsonhighered.com/advchemistry

W12.1 Two atomic orbitals are combined to form two molecular orbitals. The energy levels of the molecular orbitals and the coefficients of the atomic orbitals in each

MO are calculated by varying the relative energy of the AOs and the overlap, S_{12} , using sliders.

FURTHER READING

Baird, N. C. “The Chemical Bond Revisited.” *Journal of Chemical Education* 63 (1986): 660–664.

Banna, M., Mills, B., Davis, D., and Shirley, D. “X-ray Photoemission Molecular Orbitals of Hydrogen Fluoride and the Fluorinated Methanes.” *Journal of Chemical Physics* 61 (1974): 4780–4786.

Bock, H., and Mollère, P. “Photoelectron Spectra: An Experimental Approach to Teaching Molecular Orbital Models.” *Journal of Chemical Education* 51 (1974): 506–514.

Harrison, J., and Lawson, D. “Some Observations on Molecular Orbital Theory.” *Journal of Chemical Education* 82 (2005): 1205–1209.

Levine, I. N. *Quantum Chemistry*, 7th Edition, Pearson, Boston, 2014.

McQuarrie, D. A., *Mathematical Methods for Scientists and Engineers*, University Science Books, Sausalito, 2003.

Snow, R., and Bills, J. “The Pauli Principle and Electronic Repulsion in Helium.” *Journal of Chemical Education* 51 (1974): 585–586.

Willis, C. “Orbital Energy Levels in Molecular Hydrogen.” *Journal of Chemical Education* 65 (1988): 418–422.

Wind, H. “Electron Energy for H₂⁺ in the Ground State.” *Journal of Chemical Physics* 42 (1965): 2371–2373.

Molecular Structure and Energy Levels for Polyatomic Molecules

WHY is this material important?

We extend the discussion of chemical bonding to larger molecules, conjugated molecules, aromatic molecules, and solids. Polyatomic molecules are common and important in many subfields of chemistry and related sciences, and insight into the character of bonding in these molecules is critical to understanding their behavior.

WHAT are the most important concepts and results?

Both localized and delocalized bonding models have their advantages in discussing chemical bonding in molecules. Delocalized bonding involving molecular orbitals is the most useful approach in carrying out quantitative computational chemical calculations.

WHAT would be helpful for you to review for this chapter?

It would be helpful to review the material on chemical bonding in diatomic molecules in Chapter 12.

13.1 LEWIS STRUCTURES AND THE VSEPR MODEL

In Chapter 12, we discussed chemical bonding and the electronic structure of diatomic molecules. Molecules with more than two atoms introduce a new aspect to our discussion of chemical bonding, namely, bond angles. In this chapter, the discussion of bonding is expanded to include the structure of small molecules. This will allow us to answer questions such as “Why is the bond angle 104.5° in H_2O and 92.2° in H_2S ?”. The most straightforward answer to this question is that the angles 104.5° and 92.2° in H_2O and in H_2S minimize the total energy of these molecules. As will be shown in Chapter 15, numerical quantum-mechanical calculations of bond angles are in very good agreement with experimentally determined values. This result confirms that the approximations made in the calculation are valid and that bond angles in molecules for which there are no data can be calculated with confidence. An interpretation of the numerical calculations is required to provide an understanding about *why* a bond angle of 104.5° minimizes the energy for H_2O , whereas a bond angle of 92.2° minimizes the energy for H_2S .

Results from calculations can be used to formulate useful qualitative theoretical models. For example, Walsh’s Rules, which are discussed in Section 13.5, predict how the bond angle in a class of molecules H_2X , with X representing O, S, Se, or Te, depends on X. Gaining a qualitative understanding of why small molecules have a particular structure is the primary goal of this chapter.

- 13.1 Lewis Structures and the VSEPR Model
- 13.2 Describing Localized Bonds Using Hybridization for Methane, Ethene, and Ethyne
- 13.3 Constructing Hybrid Orbitals for Nonequivalent Ligands
- 13.4 Using Hybridization to Describe Chemical Bonding
- 13.5 Predicting Molecular Structure Using Qualitative Molecular Orbital Theory
- 13.6 How Different Are Localized and Delocalized Bonding Models?
- 13.7 Molecular Structure and Energy Levels from Computational Chemistry
- 13.8 Qualitative Molecular Orbital Theory for Conjugated and Aromatic Molecules: The Hückel Model
- 13.9 From Molecules to Solids
- 13.10 Making Semiconductors Conductive at Room Temperature

Concept

Models for chemical bonding can be classified as localized or delocalized.

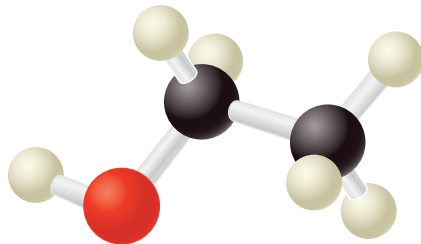


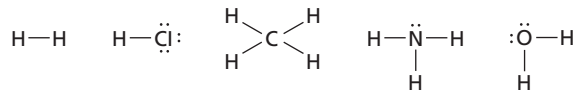
Figure 13.1
A ball-and-stick model depiction of ethanol.

Molecular structure is addressed from two different vantage points. The most significant difference between these points of view is their description of the electrons in a molecule as being localized, as in the valence bond (VB) model, or delocalized, as in the molecular orbital (MO) model. As discussed in Chapter 12, MO theory is based on electron orbitals that are delocalized over the entire molecule. By contrast, explanation and depiction of chemical bonding in terms of localized bonds and lone electron pairs are given by a **Lewis structure**, such as that for molecular fluorine, which is represented as $\ddot{\text{F}}-\ddot{\text{F}}$. These two models seem to be irreconcilable at first glance. However, as shown in Section 13.6, each model can be reformulated in the language of the other.

We will first discuss molecular structure using **localized bonding models**. We do so because there is a long tradition in chemistry of describing chemical bonds in terms of the interaction between neighboring atoms. A great deal was known about the thermochemical properties, stoichiometry, and structure of molecules before the advent of quantum mechanics. For instance, scientists knew that a set of two atom bond enthalpies could be extracted from experimental measurements. Using these bond enthalpies, we can calculate the enthalpy of formation of molecules with reasonable accuracy as the sum of the bond enthalpies associated with the reactants minus the sum of the bond enthalpies for the product. Using another example, the bond length between two specific atoms, O—H, is found to be nearly the same in many different compounds. As discussed in Chapter 8, the characteristic vibrational frequency of a group such as —OH is largely independent of the composition of the rest of the molecule. Results such as these give strong support for the idea that a molecule can be described by a set of coupled but nearly independent chemical bonds between adjacent atoms. The molecule can be assembled by linking these chemical bonds.

Figure 13.1 shows how a structural formula is used to describe ethanol. This structural formula provides a pictorial statement of a localized bonding model. However, a picture like this raises a number of questions. Do the sticks in a ball and stick model have any reality? Localized bonding models imply that bonding electrons are localized between adjacent atoms. However, we know from studying the particle in the box, the hydrogen atom, and many-electron atoms that localizing electrons results in a high energy cost. We also know that it is not possible to distinguish one electron from another, so does it make sense to assign some electrons in F_2 to lone pairs and others to the bond? At first glance, a localized model of bonding seems to be at odds with what we have learned about quantum mechanics. Yet, the preceding discussion provides credibility for a local model of chemical bonding. Comparing and contrasting the localized and delocalized models of chemical bonding and molecular structure is a major theme of this chapter.

A useful place to start a discussion of localized bonding is with Lewis structures, which emphasize the pairing of electrons as the basis for chemical bond formation. Bonds are shown as connecting lines, and electrons not involved in the bonds are indicated by dots. Lewis structures for a few representative small molecules are shown here:



Lewis structures are useful in understanding the stoichiometry of a molecule and in emphasizing the importance of nonbonding electron pairs, also called **lone pairs**. Lewis structures are less useful in predicting the geometrical structure of molecules.

Concept

The valence shell electron pair repulsion (VSEPR) model provides a qualitative rationalization of molecular structures using the Lewis concepts of localized bonds and lone pairs.

The **valence shell electron pair repulsion (VSEPR) model** provides a qualitative rationalization of molecular structures using the Lewis concepts of localized bonds and lone pairs. The basic assumptions of the model can be summarized in the following statements about a central atom that may have lone pairs and is also bonded to several atomic ligands:

- The ligands and lone pairs around a central atom act as if they repel one another. They adopt an arrangement in three-dimensional space that maximizes their angular separation.
- A lone pair occupies more angular space than a ligand.

- The amount of angular space occupied by a ligand decreases as its electronegativity increases and increases as the electronegativity of the central atom increases.
- A multiply bonded ligand occupies more angular space than a singly bonded ligand.

As Figure 13.2 shows, the structure of a large number of molecules can be understood using the VSEPR model. For example, the decrease in the bond angle in the molecules CH₄, NH₃, and H₂O can be explained on the basis of the greater angular space occupied by lone pairs than by ligands. The tendency of lone pairs to maximize their angular separation also explains why XeF₂ is linear, SO₂ is bent, and IF₄⁻ is planar. However, in some cases the model is inapplicable or does not predict the correct structure. For instance, the radical CH₃, which has an unpaired electron, is planar and, therefore, does not display the structure predicted by the VSEPR model. Alkaline earth dihalides such as CaF₂ and SrCl₂ are angular rather than linear, as predicted by the VSEPR model. SeF₆²⁻ and TeCl₆²⁻ are octahedral even though they each have a lone pair in addition to the six ligands. This result indicates that lone pairs do not always exert an influence on molecular shape. In addition, lone pairs do not play as strong a role as the model suggests in transition metal complexes. Example Problem 13.1 demonstrates how to use the VSEPR guidelines.

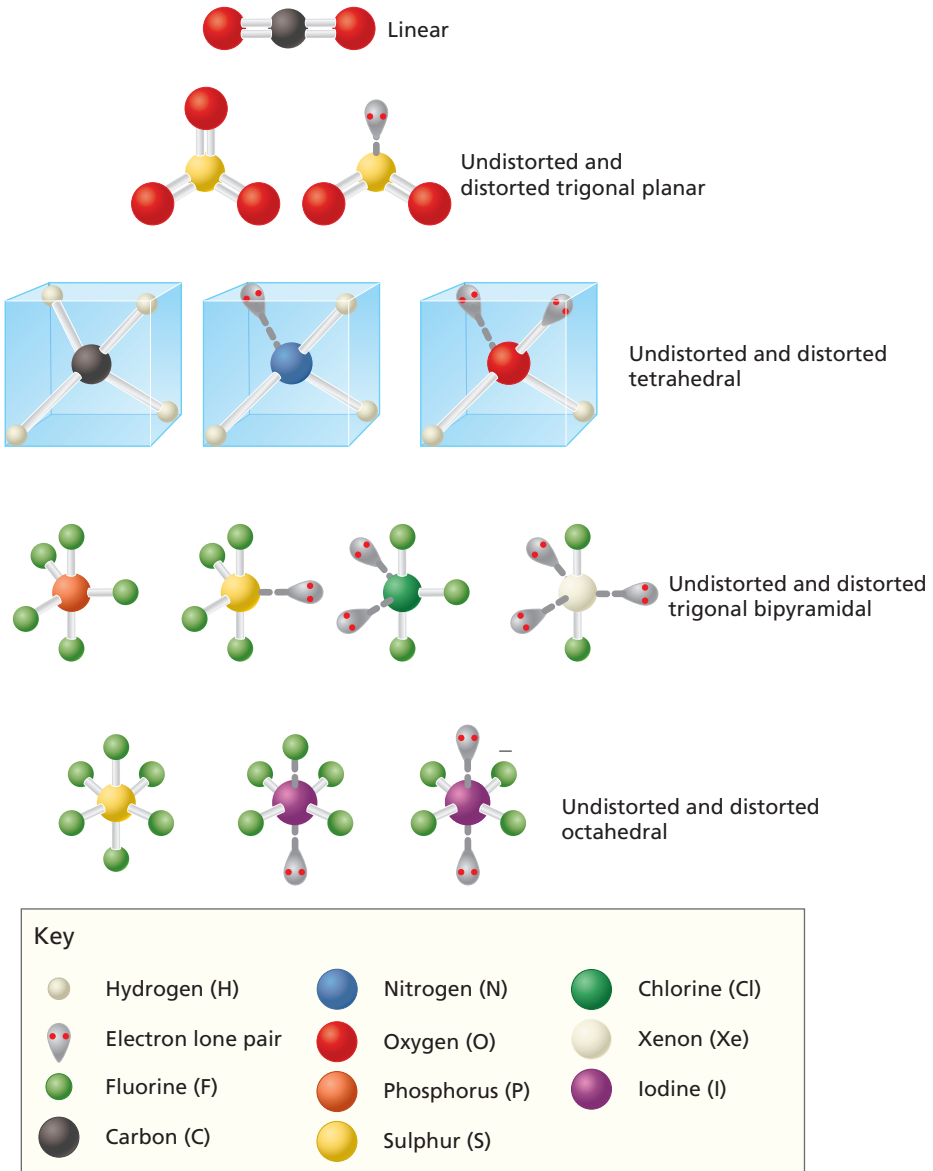


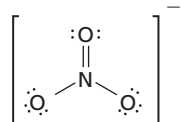
Figure 13.2
Examples of correctly predicted molecular shapes using the VSEPR model.

EXAMPLE PROBLEM 13.1

Using the VSEPR model, predict the shape of NO_3^- and OCl_2 .

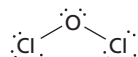
Solution

The following Lewis structure shows one of the three resonance structures of the nitrate ion:



Because the central nitrogen atom has no lone pairs and the three oxygens are equivalent, the nitrate ion should be planar with a 120° bond angle. This is the observed structure.

The Lewis structure for OCl_2 is



The central oxygen atom is surrounded by two ligands and two lone pairs. The ligands and lone pairs are described by a distorted tetrahedral arrangement, leading to a bent molecule. The VSPER model predicts that the bond angle is less than the tetrahedral angle of 109.5° . The observed bond angle is 111° .

13.2 DESCRIBING LOCALIZED BONDS USING HYBRIDIZATION FOR METHANE, ETHENE, AND ETHYNE

Concept

In the valence bond model, atomic orbitals (AOs) on the same atom are combined to generate a set of directed orbitals in a process called hybridization.

As discussed earlier, the VSEPR model is useful in predicting the shape of a wide variety of molecules. Although the rules used in its application do not specifically use the vocabulary of quantum mechanics, **valence bond (VB) theory** does use the concept of localized orbitals to explain molecular structure. In the VB model, atomic orbitals (AOs) on the same atom are combined to generate a set of directed orbitals in a process called **hybridization**. The combined orbitals are referred to as **hybrid orbitals**. The hybrid orbitals are assumed to contribute independently to the electron density and to the energy of the molecule, as much as possible, because this allows the assembly of the molecule out of separate and largely independent parts. This requires the set of hybrid orbitals to be orthogonal.

How is hybridization used to describe molecular structure? Consider the sequence of molecules methane, ethene, and ethyne. From previous chemistry courses, we know that carbon in these molecules is characterized by the sp^3 , sp^2 , and sp hybridizations, respectively. What is the functional form of localized orbitals associated with these different hybridizations? Let us construct the hybrid orbitals for ethene to illustrate the procedure.

To model the three σ bonds in ethene, the carbon AOs are hybridized to the configuration $1s^2 2p_y^1(\psi_a)^1(\psi_b)^1(\psi_c)^1$ rather than to the configuration $1s^2 2s^2 2p^2$, which is appropriate for an isolated carbon atom. The orbitals ψ_a , ψ_b , and ψ_c are the wave functions that are used in a valence bond model for the three σ bonds in ethene. We next formulate ψ_a , ψ_b , and ψ_c in terms of the $2s$, $2p_x$, and $2p_z$ AOs on carbon.

The three sp^2 -hybrid orbitals ψ_a , ψ_b , and ψ_c must satisfy the geometry shown schematically in Figure 13.3. The orbitals lie in the xz plane and are oriented at 120° to one another. The appropriate linear combination of carbon AOs is

$$\begin{aligned}\psi_a &= c_1 \phi_{2p_z} + c_2 \phi_{2s} + c_3 \phi_{2p_x} \\ \psi_b &= c_4 \phi_{2p_z} + c_5 \phi_{2s} + c_6 \phi_{2p_x} \\ \psi_c &= c_7 \phi_{2p_z} + c_8 \phi_{2s} + c_9 \phi_{2p_x}\end{aligned}\tag{13.1}$$

How can c_1 through c_9 be determined? A few aspects of the chosen geometry simplify the task of determining the coefficients. Because the $2s$ orbital is spherically symmetrical, it will contribute equally to each of the hybrid orbitals. Therefore, $c_2 = c_5 = c_8$. Furthermore, these three coefficients must satisfy the equation $\sum_i (c_{2s,i})^2 = 1$, where the subscript $2s$ refers to the $2s$ AO. This summation equation states that all of the $2s$ contributions to the hybrid orbitals must be accounted for. We choose $c_2 < 0$ in the preceding equations to make the $2s$ orbital

$$\psi_{200}(r) = \frac{1}{\sqrt{32\pi}} \left(\frac{1}{a_0} \right)^{3/2} \left(2 - \frac{r}{a_0} \right) e^{-r/2a_0}$$

have a positive amplitude in the bonding region. (For graphs of the $2s$ AO amplitude versus r , see Figures 9.5 and 9.6.) Therefore, we conclude that

$$c_2 = c_5 = c_8 = -\frac{1}{\sqrt{3}}$$

From the orientation of the orbitals seen in Figure 13.3, $c_3 = 0$ because ψ_a is oriented on the z axis. Because the hybrid orbital points along the positive z axis, $c_1 > 0$. We can also conclude that $c_4 = c_7$, that both are negative, and that $-c_6 = c_9$ with $c_9 > 0$. Based on these considerations, Equation (13.1) simplifies to

$$\begin{aligned} \psi_a &= c_1 \phi_{2p_z} - \frac{1}{\sqrt{3}} \phi_{2s} \\ \psi_b &= c_4 \phi_{2p_z} - \frac{1}{\sqrt{3}} \phi_{2s} - c_6 \phi_{2p_x} \\ \psi_c &= c_4 \phi_{2p_z} - \frac{1}{\sqrt{3}} \phi_{2s} + c_6 \phi_{2p_x} \end{aligned} \quad (13.2)$$

As shown in Example Problem 13.2, the remaining unknown coefficients can be determined by normalizing and orthogonalizing ψ_a , ψ_b , and ψ_c .

EXAMPLE PROBLEM 13.2

Determine the three unknown coefficients in Equation (13.2) by normalizing and orthogonalizing the hybrid orbitals.

Solution

We first normalize ψ_a . Terms such as $\int \phi_{2p_x}^* \phi_{2p_z} d\tau$ and $\int \phi_{2s}^* \phi_{2p_x} d\tau$ do not appear in the following equations because all AOs are orthogonal to one another. Evaluation of the integrals is simplified because the individual AOs are normalized.

$$\begin{aligned} \int \psi_a^* \psi_a d\tau &= (c_1)^2 \int \phi_{2p_z}^* \phi_{2p_z} d\tau + \left(-\frac{1}{\sqrt{3}} \right)^2 \int \phi_{2s}^* \phi_{2s} d\tau = 1 \\ &= (c_1)^2 + \frac{1}{3} = 1 \end{aligned}$$

which informs us that $c_1 = \sqrt{2/3}$. Orthogonalizing ψ_a and ψ_b , we obtain

$$\begin{aligned} \int \psi_a^* \psi_b d\tau &= c_4 \sqrt{\frac{2}{3}} \int \phi_{2p_z}^* \phi_{2p_z} d\tau + \left(-\frac{1}{\sqrt{3}} \right)^2 \int \phi_{2s}^* \phi_{2s} d\tau = 0 \\ &= c_4 \sqrt{\frac{2}{3}} + \frac{1}{3} = 0 \quad \text{and} \end{aligned}$$

$$c_4 = -\sqrt{\frac{1}{6}}$$

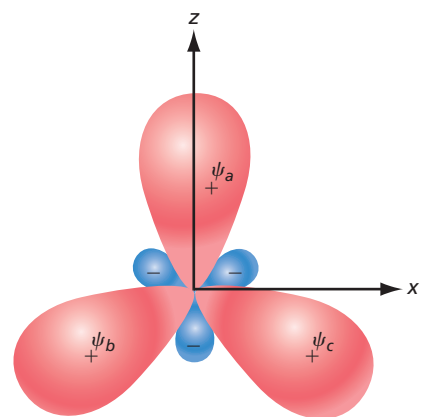


Figure 13.3

Geometry of the sp^2 -hybrid orbitals used in Equation (13.1). In this and in most of the figures in this chapter, we use a “slimmed down” picture of hybrid orbitals to separate individual orbitals. A more correct form for $s-p$ hybrid orbitals is shown in Figure 13.5.

Normalizing ψ_b , we obtain

$$\begin{aligned}\int \psi_b^* \psi_b d\tau &= \left(-\frac{1}{\sqrt{6}}\right)^2 \int \phi_{2p_z}^* \phi_{2p_z} d\tau \\ &\quad + \left(-\frac{1}{\sqrt{3}}\right)^2 \int \phi_{2s}^* \phi_{2s} d\tau + (-c_6)^2 \int \phi_{2p_x}^* \phi_{2p_x} d\tau \\ &= (c_6)^2 + \frac{1}{3} + \frac{1}{6} = 1 \quad \text{and} \\ c_6 &= +\frac{1}{\sqrt{2}}\end{aligned}$$

We have chosen the positive root so that the coefficient of ϕ_{2px} in ψ_b is negative. Using these results, the normalized and orthogonal set of hybrid orbitals is

$$\begin{aligned}\psi_a &= \sqrt{\frac{2}{3}} \phi_{2p_z} - \frac{1}{\sqrt{3}} \phi_{2s} \\ \psi_b &= -\frac{1}{\sqrt{6}} \phi_{2p_z} - \frac{1}{\sqrt{3}} \phi_{2s} - \frac{1}{\sqrt{2}} \phi_{2p_x} \\ \psi_c &= -\frac{1}{\sqrt{6}} \phi_{2p_z} - \frac{1}{\sqrt{3}} \phi_{2s} + \frac{1}{\sqrt{2}} \phi_{2p_x}\end{aligned}$$

Note that ψ_c is normalized and orthogonal to ψ_a and ψ_b .

How can the 2s and 2p character of the hybrids be quantified? Because the sum of the squares of the coefficients for each hybrid orbital equals 1, the p and s character of the hybrid orbital can be calculated. The fraction of 2p character in ψ_b is $1/6 + 1/2 = 2/3$. The fraction of 2s character is $1/3$. Because the ratio of the 2p to 2s character is 2:1, we refer to sp^2 hybridization.

How do we know that these hybrid orbitals are oriented with respect to one another as shown in Figure 13.3? Because ψ_a has no component of the $2p_x$ orbital, it must lie on the z axis, corresponding to a value of zero for the polar angle θ . To demonstrate that the ψ_b orbital is oriented as shown, we find its maximum value with respect to the variable θ , which is measured from the z axis.

EXAMPLE PROBLEM 13.3

Demonstrate that the hybrid orbital ψ_b has the orientation shown in Figure 13.3.

Solution

To carry out this calculation, we need to explicitly include the θ dependence of the $2p_x$ and $2p_z$ orbitals from Chapter 9. In doing so, we set the azimuthal angle ϕ , discussed in Section 9.4, equal to zero:

$$\begin{aligned}\frac{d\psi_b}{d\theta} &= \left[\frac{1}{\sqrt{32\pi}} \left(\frac{\zeta}{a_0} \right)^{3/2} e^{-\zeta r/2a_0} \right] \\ &\times \frac{d}{d\theta} \left(-\frac{1}{\sqrt{6}} \frac{\zeta r}{a_0} \cos \theta - \frac{1}{\sqrt{3}} \left[2 - \frac{\zeta r}{a_0} \right] - \frac{1}{\sqrt{2}} \frac{\zeta r}{a_0} \sin \theta \right) = 0\end{aligned}$$

which simplifies to

$$\frac{1}{\sqrt{6}} \sin \theta - \frac{1}{\sqrt{2}} \cos \theta = 0 \quad \text{or} \quad \tan \theta = \sqrt{3}$$

This value for $\tan \theta$ is satisfied by $\theta = 60^\circ$ and 240° . Applying the condition that $d^2\psi_b/d\theta^2 < 0$ for the maximum, we conclude that $\theta = 240^\circ$ corresponds to the maximum and $\theta = 60^\circ$ corresponds to the minimum. Similarly, it can be shown that ψ_c has its maximum value at 120° and a minimum at 300° .

TABLE 13.1 C—C Bond Types

Carbon—Carbon Single Bond Types	σ Bond Hybridization	s-to-p Ratio	Angle between Equivalent σ Bonds ($^{\circ}$)	Carbon—Carbon Single Bond Length (pm)
$\geqslant \text{C} - \text{C} \leqslant$	sp^3	1:3	109.4	154
$\geqslant \text{C} - \text{C} \leqslant$	sp^2	1:2	120	146
$\equiv \text{C} - \text{C} \equiv$	sp	1:1	180	138

Example Problem 13.3 shows that sp^2 hybridization generates three equivalent hybrid orbitals that are separated by an angle of 120° . By following the procedure outlined earlier, it can be shown that the set of orthonormal sp -hybrid orbitals that are oriented 180° apart is

$$\begin{aligned}\psi_a &= \frac{1}{\sqrt{2}}(-\phi_{2s} + \phi_{2p_z}) \\ \psi_b &= \frac{1}{\sqrt{2}}(-\phi_{2s} - \phi_{2p_z})\end{aligned}\quad (13.3)$$

and that the set of tetrahedrally oriented orthonormal hybrid orbitals for sp^3 hybridization that are oriented 109.4° apart is

$$\begin{aligned}\psi_a &= \frac{1}{2}(-\phi_{2s} + \phi_{2p_x} + \phi_{2p_y} + \phi_{2p_z}) \\ \psi_b &= \frac{1}{2}(-\phi_{2s} - \phi_{2p_x} - \phi_{2p_y} + \phi_{2p_z}) \\ \psi_c &= \frac{1}{2}(-\phi_{2s} + \phi_{2p_x} - \phi_{2p_y} - \phi_{2p_z}) \\ \psi_d &= \frac{1}{2}(-\phi_{2s} - \phi_{2p_x} + \phi_{2p_y} - \phi_{2p_z})\end{aligned}\quad (13.4)$$

By combining s and p orbitals, at most four hybrid orbitals can be generated. To describe bonding around a central atom with coordination numbers greater than four, d orbitals need to be included in forming the hybrids. Although hybrid orbitals with d character are not discussed in this book, the principles used in constructing them are the same as those outlined earlier.

The properties of C—C single bonds depend on the hybridization of the carbon atoms, as shown in Table 13.1. The most important conclusion that can be drawn from this table for the discussion in the next section is that increasing the s character in $s-p$ hybrids increases the bond angle. Note also that the C—C single bond length becomes shorter as the s character of the hybridization increases and that the C—C single bond energy increases as the s character of the hybridization increases.

13.3 CONSTRUCTING HYBRID ORBITALS FOR NONEQUIVALENT LIGANDS

In the preceding section, the construction of hybrid orbitals for equivalent ligands was considered. However, in general, molecules contain nonequivalent ligands as well as nonbonding lone pairs of electrons. How can hybrid orbitals be constructed for such molecules if the bond angles are not known? By considering the experimentally determined structures of a wide variety of molecules, Henry Bent formulated the following guidelines:

- Central atoms that obey the octet rule can be classified into three structural types. Central atoms that are surrounded by a combination of four single bonds or electron pairs are to a first approximation described by a tetrahedral geometry and sp^3

Concept

Bent's guidelines are useful in constructing hybrid orbitals for nonequivalent ligands.

Concept

Bent's rule states that atomic *s* character concentrates in hybrid orbitals directed toward electropositive ligands and that *p* character concentrates in hybrid orbitals directed toward electronegative ligands.

hybridization. Central atoms that form one double bond and a combination of two single bonds or electron pairs are to a first approximation described by a trigonal planar geometry and sp^2 hybridization. Central atoms that form two double bonds or one triple bond and either a single bond or an electron pair are to a first approximation described by a linear geometry and sp hybridization.

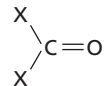
- The presence of different ligands is taken into account by assigning a different hybridization to all nonequivalent ligands and lone pairs. The individual hybridization is determined by the electronegativity of each ligand. A nonbonding electron pair can be considered to be electropositive or, equivalently, to have a small electronegativity. **Bent's rule** states that atomic *s* character concentrates in hybrid orbitals directed toward electropositive ligands and that *p* character concentrates in hybrid orbitals directed toward electronegative ligands. Example Problem 13.4 demonstrates how Bent's rule is applied.

We now apply these guidelines to H_2O . The oxygen atom in H_2O is to a first approximation described by a tetrahedral geometry and sp^3 hybridization. However, because the H atoms are more electronegative than the electron pairs, the *p* character of the hybrid orbitals directed toward the hydrogen atoms will be greater than that of sp^3 hybridization. Because Table 13.1 shows that increasing the *p* character decreases the bond angle, Bent's rule says that the H—O—H bond angle will be less than 109.4° . Note that the effect of Bent's rule is the same as the effect of the VSEPR rules listed in Section 13.1. However, the hybridization model provides a basis for the VSEPR rules.

Although useful in predicting bond angles, Bent's rule is not quantitative. To make it predictive, a method is needed to assign a hybridization to a specific combination of two atoms that is independent of the other atoms in the molecule. Several authors have developed methods that meet this need; see, for example, the reference to Root in Further Reading.

EXAMPLE PROBLEM 13.4

- Use Bent's rule to decide if the X—C—X bond angle in F_2CO is larger or smaller than in H_2CO .



- Use Bent's rule to estimate whether the H—C—H bond angle in FCH_3 and $ClCH_3$ differs from 109.5° .

Solution

- To first order, the carbon atom exhibits sp^2 hybridization. Because F is more electronegative than H, the hybridization of the C—F ligand contains more *p* character than does the C—H ligand. Therefore, the F—C—F bond angle will be smaller than the H—C—H bond angle.
- For both FCH_3 and $ClCH_3$, H is more electropositive than the halogen atom, so that the C—H bonds have greater *s* character than the C-halogen bond. This makes the H—C—H bond angle greater than 109.5° in both molecules.

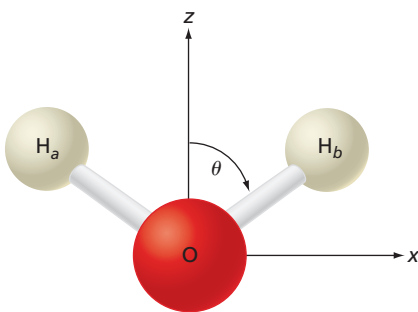


Figure 13.4

Coordinate system used to generate the hybrid orbitals on the oxygen atom that are suitable for describing the structure of H_2O .

To test the predictions of Bent's rule, the hybrid orbitals for water are constructed using the known bond angle, and their individual hybridizations are determined. Constructing the lone pair orbitals is left as an end-of-chapter problem. The valence electron configuration of the water molecule can be written in the form $1s_{\text{oxygen}}^2(\psi_{OH})^2(\psi_{OH})^2(\psi_{\text{lone pair}})^2(\psi_{\text{lone pair}})^2$. Each ψ_{OH} and $\psi_{\text{lone pair}}$ describes localized hybrid orbitals. From the known geometry, the two bonding orbitals are oriented at 104.5° with respect to one another, as shown in Figure 13.4. Starting with this input, how do we construct ψ_{OH} and $\psi_{\text{lone pair}}$ from the atomic orbitals on hydrogen and oxygen? To describe the H_2O molecule, a pair of orthogonal equivalent *s*—*p* hybrids, called ψ_a and ψ_b , is constructed on the oxygen atom. The calculation is initially carried out for an arbitrary bond angle.

The hybrid orbitals are described by

$$\begin{aligned}\psi_a &= N \left[(\cos \theta) \phi_{2p_z} + (\sin \theta) \phi_{2p_x} - \alpha \phi_{2s} \right] \\ \psi_b &= N \left[(\cos \theta) \phi_{2p_z} - (\sin \theta) \phi_{2p_x} - \alpha \phi_{2s} \right]\end{aligned}\quad (13.5)$$

where N is a normalization constant and α is the ratio of the amplitudes of the $2s$ and $2p$ orbitals.

To derive Equation (13.5), visualize ϕ_{2p_x} and ϕ_{2p_z} as vectors along the x and z directions. Because the $2s$ orbital has one radial node, the $2s$ orbital coefficient in Equation (13.5) is negative, which generates a positive amplitude at the position of the H atom. The two hybrid orbitals are orthogonal only if

$$\begin{aligned}\int \psi_a^* \psi_b d\tau &= N^2 \int \left[(\cos \theta) \phi_{2p_z}^* + (\sin \theta) \phi_{2p_x}^* - \alpha \phi_{2s}^* \right] \\ &\quad \times \left[(\cos \theta) \phi_{2p_z} - (\sin \theta) \phi_{2p_x} - \alpha \phi_{2s} \right] d\tau \\ &= N^2 \left[\cos^2 \theta \int \phi_{2p_z}^* \phi_{2p_z} d\tau - \sin^2 \theta \int \phi_{2p_x}^* \phi_{2p_x} d\tau + \alpha^2 \int \phi_{2s}^* \phi_{2s} d\tau \right] = 0\end{aligned}\quad (13.6)$$

Terms such as $\int \phi_{2p_x}^* \phi_{2p_z} d\tau$ and $\int \phi_{2s}^* \phi_{2p_x} d\tau$ do not appear in this equation because all the atomic orbitals are orthogonal to one another. Because each of the AOs is normalized, Equation (13.6) reduces to

$$\begin{aligned}N^2 [\cos^2 \theta - \sin^2 \theta + \alpha^2] &= N^2 [\cos 2\theta + \alpha^2] = 0 \quad \text{or} \\ \cos 2\theta &= -\alpha^2\end{aligned}\quad (13.7)$$

In simplifying this equation, we have used the identity $\cos^2 x - \sin^2 y = \cos(x + y) \cos(x - y)$. Because $\alpha^2 > 0$, $\cos 2\theta < 0$ and the bond angle $180^\circ \geq 2\theta \geq 90^\circ$. What has this calculation shown? We have demonstrated that it is possible to create two hybrid orbitals separated by a bonding angle in this angular range simply by varying the relative contributions of the $2s$ and $2p$ orbitals to the hybrid.

The hybrid orbitals in Equation (13.5) are not specific to a particular molecule other than that the two atoms that bond to the central oxygen atom are identical. We now calculate the value of α that generates the correct bond angle in H_2O . Calculating α by substituting the known value $\theta = 52.25^\circ$ in Equation (13.7), we find that the unnormalized hybrid orbitals that describe bonding in water are

$$\begin{aligned}\psi_a &= N [0.61 \phi_{2p_z} + 0.79 \phi_{2p_x} - 0.50 \phi_{2s}] \\ \psi_b &= N [0.61 \phi_{2p_z} - 0.79 \phi_{2p_x} - 0.50 \phi_{2s}]\end{aligned}\quad (13.8)$$

EXAMPLE PROBLEM 13.5

Normalize the hybrid orbitals given in Equation (13.8).

Solution

$$\begin{aligned}\int \psi_a^* \psi_a d\tau &= N^2 (0.61)^2 \int \phi_{2p_z}^* \phi_{2p_z} d\tau \\ &\quad + N^2 (0.79)^2 \int \phi_{2p_x}^* \phi_{2p_x} d\tau + N^2 (0.50)^2 \int \phi_{2s}^* \phi_{2s} d\tau = 1\end{aligned}$$

Other terms do not contribute because the atomic orbitals are orthogonal to one another.

$$\int \psi_a^* \psi_a d\tau = N^2 (0.61)^2 + N^2 (0.79)^2 + N^2 (0.50)^2 = 1.25 N^2 = 1$$

$$N = 0.89$$

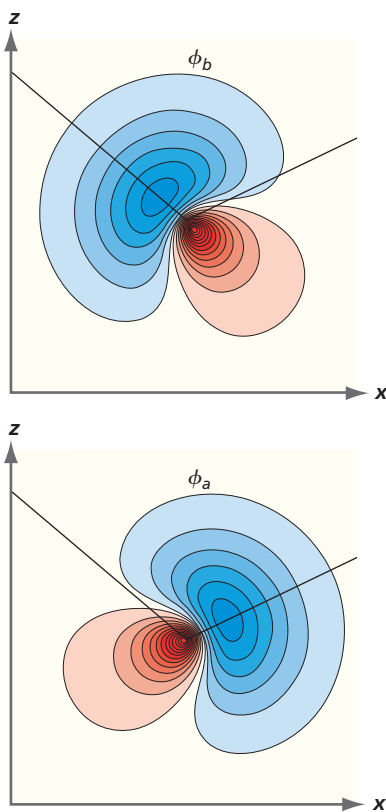


Figure 13.5
Directed hybrid bonding orbitals for H_2O . The black lines show the bond angle and orbital orientation. Positive and negative amplitudes are shown as red and blue, respectively. Darker colors indicate larger values for the magnitude of the amplitude.

Using the result of Example Problem 13.5, we can write the normalized hybrid orbitals as follows:

$$\begin{aligned}\psi_a &= 0.55 \phi_{2p_z} + 0.71 \phi_{2p_x} - 0.45 \phi_{2s} \\ \psi_b &= 0.55 \phi_{2p_z} - 0.71 \phi_{2p_x} - 0.45 \phi_{2s}\end{aligned}\quad (13.9)$$

Because the sum of the squares of the coefficients for each hybrid orbital equals 1, we can calculate their p and s character. The fraction of $2p$ character is $(0.55)^2 + (0.71)^2 = 0.80$. The fraction of $2s$ character is $(-0.45)^2 = 0.20$. Therefore, the hybridization of the bonding hybrid orbitals is described as sp^4 . These hybrid orbitals have more p character than the first approximation sp^3 , as predicted by Bent's rule.

The two hybrid orbitals are shown in Figure 13.5. Note that each of the directed hybrid orbitals lies along one of the bonding directions and has little amplitude along the other bonding direction. These hybrid orbitals could be viewed as the basis for the line connecting bonded atoms in the Lewis structure for water. Figure 13.5 shows a realistic representation of the hybrid orbitals to compare with the “slimmed down” version of Figure 13.3.

This calculation for H_2O illustrates how to construct bonding hybrid orbitals with a desired relative orientation. To this point, the energetics of this process have not been discussed. In many-electron atoms, the $2p$ orbital energy is greater than that for the $2s$ orbital. How can these orbitals be mixed in all possible proportions without putting energy into the atom? To create the set of occupied hybrid orbitals on an isolated ground state oxygen atom would indeed require energy; however, the subsequent formation of bonds to the central atom lowers the energy, leading to an overall decrease in the energy of the molecule relative to the isolated atoms after bond formation. In the language of the hybridization model, the energy cost of promoting the electrons from the $1s^2 2s^2 2p^4$ configuration to the $1s^2 \psi_c^2 \psi_d^2 \psi_a^1 \psi_b^1$ configuration is more than offset by the energy gained in forming two O—H bonds. Keep in mind that the individual steps in the formation of the H_2O molecule, such as promotion of the O atom, followed by the creation of O—H bonds, are only an aid in describing the formation of H_2O , rather than a series of actual events. The language of the hybridization model should not be taken too literally because neither the promotion process nor hybrid orbitals are observables, and it is important to distinguish between a model and reality. The reality of orbitals is discussed in Section 13.6 in more detail.

13.4 USING HYBRIDIZATION TO DESCRIBE CHEMICAL BONDING

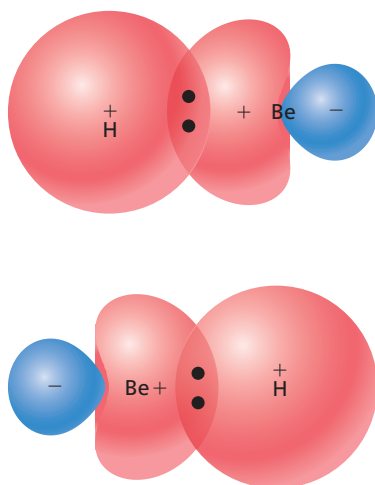


Figure 13.6
Bonding in BeH_2 using two sp -hybrid orbitals on Be. The two Be—H hybrid bonding orbitals are shown separately.

By using the hybridization model to create local bonding orbitals, the concepts inherent in Lewis structures can be given a quantum-mechanical basis. As an example, consider BeH_2 , which is not observed as an isolated molecule because it forms a solid through polymerization of BeH_2 units stabilized by hydrogen bonds. We consider only a single BeH_2 unit. Be has the configuration $1s^2 2s^2 2p^0$, and because it has no unpaired electrons, it is not obvious how bonding to the H atoms can be explained in the Lewis model. In the VB model, the $2s$ and $2p$ orbitals are hybridized to create bonding hybrids on the Be atom. Because the bond angle is known to be 180° , two equivalent and orthogonal sp -hybrid orbitals are constructed as given by Equation (13.3). This allows Be to be described as $1s^2(\psi_a)^1(\psi_b)^1$. In this configuration, Be has two unpaired electrons and, therefore, the hybridized atom is divalent. The orbitals are depicted schematically in Figure 13.6. To make a connection to Lewis structures, the bonding electron pair is placed in the overlap region between the Be and H orbitals as indicated by the dots. In reality, the bonding electron density is distributed over the entire region in which the orbitals have a nonzero amplitude. We will return to BeH_2 in Section 13.6 where we will compare localized and delocalized bonding models for this molecule.

The most important use of the hybridization model in chemistry is in describing bonding in molecules containing carbon. Figure 13.7 depicts valence bond

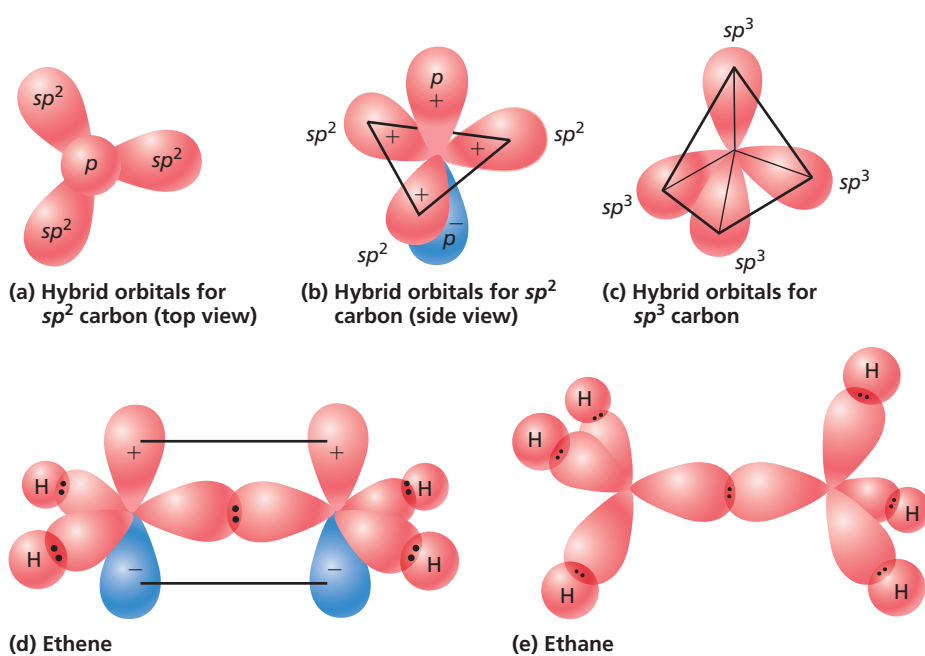


Figure 13.7
Hybrid bonding orbitals for ethene and ethane compounds.

hybridization in ethene and ethane. For ethene, each carbon atom is promoted to the $1s^2 2p_y^1 (\psi_a)^1 (\psi_b)^1 (\psi_c)^1$ configuration before forming four C—H σ bonds, a C—C σ bond, and a C—C π bond. The maximal overlap between the p orbitals to create a π bond in ethene occurs when all atoms lie in the same plane. The double bond is made from one σ and one π bond. For ethane, each carbon atom is promoted to the $1s^2 (\psi_a)^1 (\psi_b)^1 (\psi_c)^1 (\psi_d)^1$ configuration before forming six C—H σ bonds and a C—C σ bond.

In summarizing this discussion of hybridization, we emphasize the positive aspects of the model and point out some of its shortcomings. The main usefulness of hybridization is that it is an easily understandable model with considerable predictive power using, for instance, Bent's rule. It retains the main features of Lewis structures in describing local orthogonal bonds between adjacent atoms in terms of electron pairing, and it justifies Lewis structures in the language of quantum mechanics. Hybridization also provides a theoretical basis for the VSEPR rules.

Hybridization also offers more than a useful framework for understanding bond angles in molecules. Because the $2s$ AO is lower in energy than the $2p$ level in many-electron atoms, the electronegativity of a hybridized atom increases with increasing s character. Therefore, the hybridization model predicts that an sp -hybridized carbon atom is more electronegative than an sp^3 -hybridized carbon atom. Evidence for this effect is that the positive end of the dipole moment in $N\equiv C—Cl$ is on the Cl atom. We conclude that the carbon atom in the cyanide group is more electronegative than a chlorine atom. Because increased s character leads to shorter bond lengths, and because shorter bonds generally have a greater bond strength, the hybridization model provides a correlation of s character and bond strength.

The hybridization model also has a few shortcomings. For known bond angles, the hybridization can be calculated as was done for ethane and H_2O . However, semi-empirical prescriptions must be used to estimate the s and p character of a hybrid orbital for a molecule in the absence of structural information. It is also more straightforward to construct an appropriate hybridization for symmetric molecules such as methane than for molecules with electron lone pairs and several different ligands bonded to the central atom. Additionally, the depiction of bonding hybrids in Figure 13.7 seems to imply that the electron density is highly concentrated along the bonding directions. This is not true, as can be seen by looking at the realistic representation of hybrid orbitals in Figure 13.5. Finally, the conceptual formalism used in creating hybrid orbitals—in particular, promotion followed by hybridization—assumes much more detail than can be verified by experiments.

13.5 PREDICTING MOLECULAR STRUCTURE USING QUALITATIVE MOLECULAR ORBITAL THEORY

Concept

Molecular orbital theory assumes that electrons involved in bonding are delocalized over the molecule.

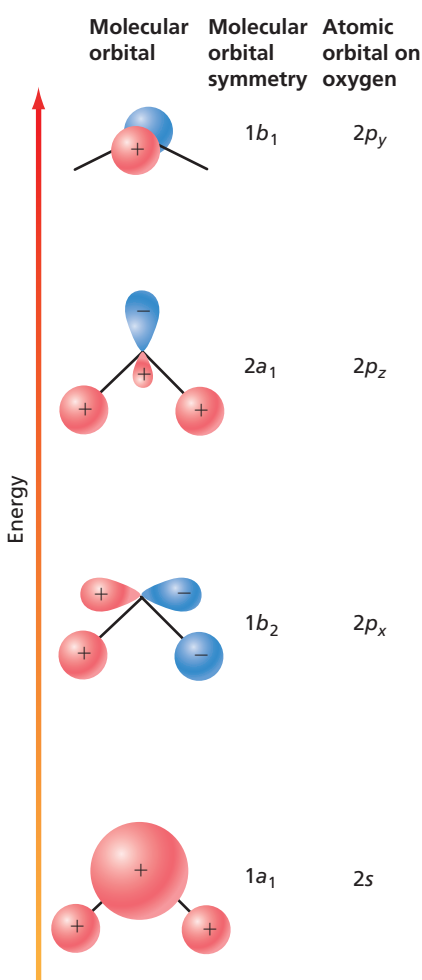


Figure 13.8

Valence molecular orbitals occupied in the ground state of water in order of increasing orbital energy. In the left column, the MOs are depicted in terms of the AOs from which they are constructed. The second column gives the MO symmetry, and the third column lists the dominant AO orbital on the oxygen atom.

We now consider a **delocalized bonding model** of the chemical bond. Molecular orbital theory approaches the structure of molecules quite differently than local models of chemical bonding. The electrons involved in bonding are assumed to be delocalized over the molecule. Each one-electron molecular orbital σ_j is expressed as a linear combination of atomic orbitals such as $\sigma_j(k) = \sum_i c_{ij} \phi_i(k)$, which refers to the j th molecular orbital for electron k . The many-electron wave function ψ is written as a Slater determinant in which the individual entries are the $\sigma_j(k)$.

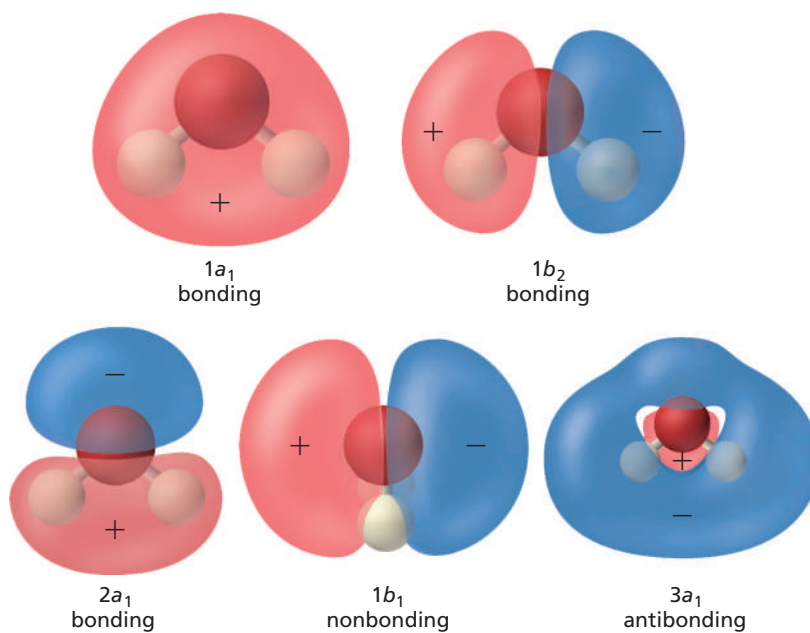
In quantitative molecular orbital theory, which will be discussed in Chapter 15, structure emerges naturally as a result of solving the Schrödinger equation and determining the atomic positions for which the energy has its minimum value. Although this concept can be formulated in a few words, carrying out this procedure is a complex exercise in numerical computing. In this section, our focus is on a more qualitative approach that conveys the spirit of molecular orbital theory but that can be written down without extensive mathematics.

To illustrate this approach, we use qualitative molecular orbital (MO) theory to understand the bond angle in triatomic molecules of the type H_2A , where A is one of the atoms in the sequence $Be \rightarrow O$, and show that a qualitative picture of the optimal bond angle can be obtained by determining how the energy of the individual occupied molecular orbitals varies with the bond angle. In doing so, we assume that the total energy of the molecule is proportional to the sum of the orbital energies. This assumption can be justified, although we do not do so here. Experimentally, we know that BeH_2 is a linear molecule and H_2O has a bond angle of 104.5° . How can this difference be explained using MO theory?

The minimal basis set used here to construct the MOs consists of the $1s$ orbitals on each of the H atoms and the $1s$, $2s$, $2p_x$, $2p_y$, and $2p_z$ orbitals on atom A . Seven MOs can be generated using these seven AOs. We omit the two lowest MOs generated from the $1s$ oxygen AO from the following discussion because the corresponding electrons are localized on the oxygen atom. Water has eight valence electrons that occupy four of the five remaining MOs. The occupied valence MOs for water are shown in Figure 13.8 in terms of the AOs from which they are constructed. The MOs are labeled according to their symmetry with respect to a set of rotation and reflection operations that leave the water molecule unchanged. We will discuss the importance of molecular symmetry in constructing MOs from AOs at some length in Chapter 15. However, in the present context it is sufficient to think of these designations simply as labels.

How do we order these MOs with respect to energy? Recall that orbital energy increases with the number of nodes for the particle in the box, the harmonic oscillator, and the H atom. We also know that the lower the AO energies, the lower the MO energy will be. Because the oxygen $2s$ AO is lower in energy than the $2p$ AOs, the MO with no nodes designated $1a_1$ in Figure 13.8 is expected to have the lowest energy of all possible valence MOs. The next higher MOs involve $2p$ AOs on the O atom and the $1s$ AO on the H atoms.

The three oxygen $2p$ orbitals are oriented differently with respect to the plane containing the H atoms. As a result, the MOs that they generate are quite different in energy. Assume that the H_2O molecule lies in the xz plane with the z axis bisecting the $H-O-H$ angle as shown in Figure 13.4. The $1b_2$ MO, generated using the $2p_x$ AO, and the $2a_1$ MO, generated using the $2p_z$ AO, each have no nodes in the $O-H$ region and, therefore, have binding character. However, because each has one node, both MOs have a higher energy than the $1a_1$ MO. Calculations show that the MO generated using the $2p_x$ AO has a lower orbital energy than that generated using the $2p_z$ AO. Note that some $s-p$ mixing has been incorporated in the $2a_1$ and $3a_1$ MO generated from the $2s$ and $2p_z$ AO. Having discussed the MOs formed using the $2p_x$ and $2p_z$ AOs, we turn to the $2p_y$ AO. The $2p_y$ orbital has no net overlap with the H atoms and gives rise to the $1b_1$ nonbonding MO that is localized on the O atom. Because this MO is not stabilized through interaction with the H $1s$ AOs, it has the highest energy of all the

**Figure 13.9**

The first five valence molecular orbitals for H_2O . The $1b_1$ and $3a_1$ MOs are the HOMO and LUMO, respectively. Note that the $1b_1$ MO is the AO corresponding to the nonbonding $2p_y$ electrons on oxygen. The plane of the molecule has been rotated for the $1b_1$ MO to better display the nodal structure.

occupied MOs. Numerically calculated molecular orbitals, including the $3a_1$ LUMO, are depicted in Figure 13.9.

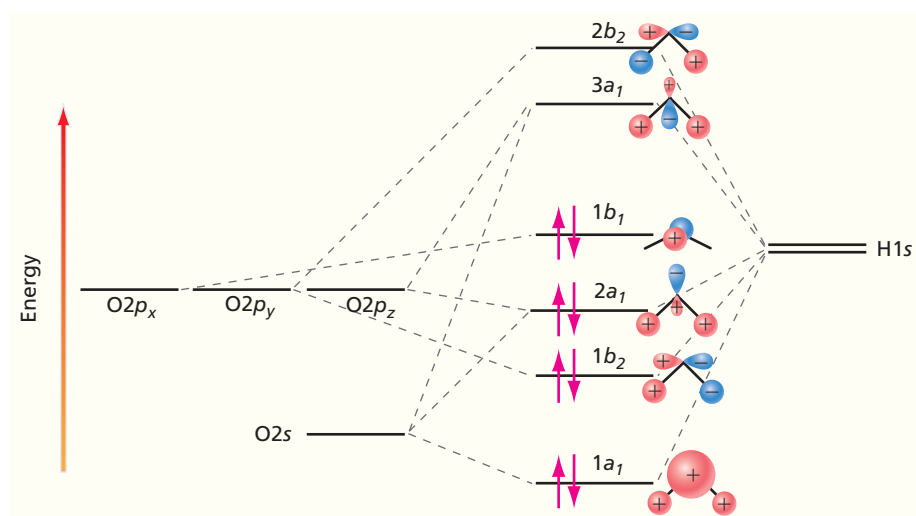
The preceding discussion about the relative energy of the MOs for H_2O is sufficient to allow us to draw the MO energy diagram shown in Figure 13.10. The MO energy levels in this figure are drawn for the experimentally observed bond angle of 105.4° , but the energy levels vary with 2θ , as shown in Figure 13.11, in what is known as a **Walsh correlation diagram**. It is important to understand the trends shown in Figure 13.11 that are discussed in the next few paragraphs because the variation of the MO energies with angle is ultimately responsible for BeH_2 being linear and H_2O being bent.

How does the $1a_1$ energy vary with 2θ ? The overlap between the s orbitals on A and H is independent of 2θ , but as this angle decreases from 180° , the overlap between the H atoms increases. This stabilizes the molecule and, therefore, the $1a_1$ energy decreases. By contrast, the overlap between the $2p_y$ orbital and the H $1s$ orbitals is a maximum at 180° and, therefore, the $1b_2$ energy increases as 2θ decreases. Because the effect of the H—H overlap on the $1a_1$ energy is a secondary effect, the $1b_2$ energy falls more rapidly with increasing 2θ than the $1a_1$ energy increases.

We now consider the $2a_1$ and $1b_1$ energies. The $2p_y$ and $2p_z$ orbitals are nonbonding and degenerate for a linear H_2A molecule. However, as 2θ decreases from 180° , the

Concept

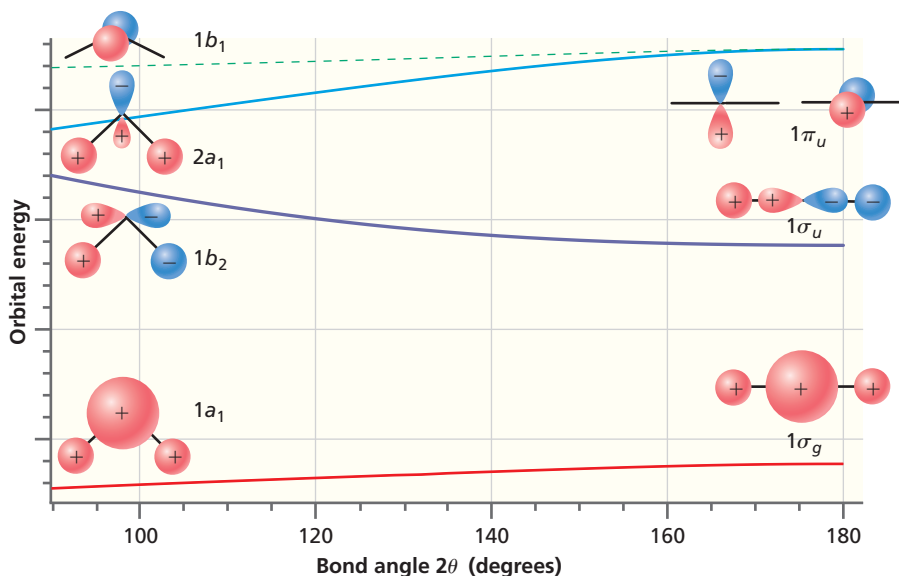
A Walsh correlation diagram depicts how molecular orbital energies change with bond angle.

**Figure 13.10**

Molecular orbital energy-level diagram for H_2O at its equilibrium geometry.

Figure 13.11

Schematic variation of molecular orbital energies for water as a function of bond angle. The symbols used on the left to describe the MOs are based on symmetry considerations and are valid for $2\theta < 180^\circ$. This nomenclature is discussed in Chapter 16.



O $2p_z$ orbital has a net overlap with the H 1s AOs and has increasingly more bonding character. Therefore, the $2a_1$ MO energy decreases as 2θ decreases from 180° . The $1b_1$ MO remains nonbonding as 2θ decreases from 180° , but electron repulsion effects lead to a slight decrease of the MO energy. These variations in the MO energies are depicted in Figure 13.11.

The MO energy diagram of Figure 13.10 is equally valid for H₂A molecules, with A being second-period elements other than oxygen. Consider the molecules BeH₂ and H₂O. BeH₂ has four valence electrons that are placed in the two lowest-lying valence MOs, $1a_1$ and $1b_2$. Because the $1b_2$ orbital energy decreases with increasing 2θ more than the $2a_1$ orbital energy increases, the total energy of the molecule is minimized if $2\theta = 180^\circ$. This qualitative argument predicts that BeH₂, as well as any other four-valence electron H₂A molecule, is linear and has the valence electron configuration $(1\sigma_g)^2(1\sigma_u)^2$. Note that the description of H₂A in terms of σ MOs with *g* or *u* symmetry applies only to a linear molecule, whereas a description in terms of $1a_1$ and $1b_2$ applies to all bent molecules.

We now consider H₂O, which has eight valence electrons. In this case, the lowest four MOs are doubly occupied. At what angle is the total energy of the molecule minimized? For water, the decrease in the energy of the $1a_1$ and $2a_1$ MOs as 2θ decreases more than offsets the increase in energy for the $1b_2$ MO. Therefore, H₂O is bent rather than linear and has the valence electron configuration $(1a_1)^2(1b_2)^2(2a_1)^2(1b_1)^2$. The degree of bending depends on how rapidly the energy of the MOs changes with angle. Numerical calculations for water using this approach predict a bond angle that is very close to the experimental value of 104.5° . These examples for BeH₂ and H₂O and Example Problem 13.6 illustrate how qualitative MO theory can be used to predict bond angles.

EXAMPLE PROBLEM 13.6

Predict the equilibrium shape of H₃⁺, LiH₂, and NH₂ using qualitative MO theory.

Solution

H₃⁺ has two valence electrons and is bent as predicted by the variation of the $1a_1$ MO energy with angle as shown in Figure 13.11. LiH₂ or any molecule of the type H₂A with four electrons is predicted to be linear. NH₂ has one electron fewer than H₂O and, using the same reasoning as for water, is bent.

13.6 HOW DIFFERENT ARE LOCALIZED AND DELOCALIZED BONDING MODELS?

Molecular orbital theory and hybridization-based valence bond theory have been developed using delocalized and localized bonding, respectively. These models approach the chemical bond from very different starting points. However, it is instructive to compare the molecular wave functions generated by these models using BeH₂ as an example. We have already discussed BeH₂ using hybridization in Section 13.4 and now formulate its many-electron wave function using the MO model. To minimize the size of the determinant in Equation (13.11), we assume that the Be 1s electrons are not delocalized over the molecule. With this assumption, BeH₂ has the configuration (1s_{Be})²(1σ_g)²(1σ_u)². On the basis of the symmetry requirements posed on the MOs by the linear geometry (see Chapter 16), the two lowest energy MOs are

$$\begin{aligned}\sigma_g &= c_1(\phi_{H1sA} + \phi_{H1sB}) + c_2\phi_{Be2s} \\ \sigma_u &= c_3(\phi_{H1sA} - \phi_{H1sB}) - c_4\phi_{Be2p_z}\end{aligned}\quad (13.10)$$

The many-electron determinantal wave function that satisfies the Pauli requirement is

$$\psi(1, 2, 3, 4) = \frac{1}{\sqrt{4!}} \begin{vmatrix} \sigma_g(1)\alpha(1) & \sigma_g(1)\beta(1) & \sigma_u(1)\alpha(1) & \sigma_u(1)\beta(1) \\ \sigma_g(2)\alpha(2) & \sigma_g(2)\beta(2) & \sigma_u(2)\alpha(2) & \sigma_u(2)\beta(2) \\ \sigma_g(3)\alpha(3) & \sigma_g(3)\beta(3) & \sigma_u(3)\alpha(3) & \sigma_u(3)\beta(3) \\ \sigma_g(4)\alpha(4) & \sigma_g(4)\beta(4) & \sigma_u(4)\alpha(4) & \sigma_u(4)\beta(4) \end{vmatrix}\quad (13.11)$$

Each entry in the determinant is an MO multiplied by a spin function.

We now use a property of a determinant that you will prove in the end-of-chapter problems for a 2 × 2 determinant, namely,

$$\begin{vmatrix} a & c \\ b & d \end{vmatrix} = \begin{vmatrix} a & \gamma a + c \\ b & \gamma b + d \end{vmatrix}\quad (13.12)$$

This equation states that one can add a column of the determinant multiplied by an arbitrary constant γ to another column *without changing the value of the determinant*. For reasons that will become apparent shortly, we replace the MOs σ_g and σ_u with the new MOs $\sigma' = \sigma_g + (c_1/c_3)\sigma_u$ and $\sigma'' = \sigma_g - (c_1/c_3)\sigma_u$. These hybrid MOs are related to the AOs by

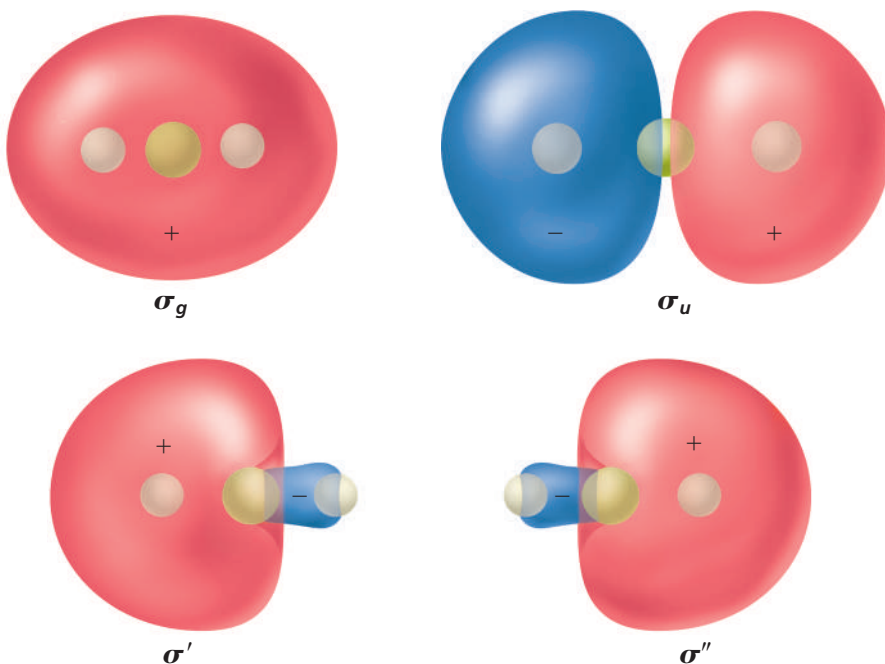
$$\begin{aligned}\sigma' &= 2c_1\phi_{H1sA} + \left(c_2\phi_{Be2s} - \frac{c_1c_4}{c_3}\phi_{Be2p_z} \right) \\ \sigma'' &= 2c_1\phi_{H1sB} + \left(c_2\phi_{Be2s} + \frac{c_1c_4}{c_3}\phi_{Be2p_z} \right)\end{aligned}\quad (13.13)$$

Transforming from σ_g and σ_u to σ' and σ'' requires two steps similar to the one in Equation (13.12). Note that with this transformation, ϕ_{H1sB} no longer appears in σ' and ϕ_{H1sA} no longer appears in σ'' . Because of the property of determinants cited earlier, neither $\psi(1, 2, 3, 4)$ —nor any molecular observable—will be affected by this change in the MOs. Therefore, the configurations (1s_{Be})²(1σ_g)²(1σ_u)² and (1s_{Be})²[1σ_g + (c₁/c₃)1σ_u]²[1σ_g − (c₁/c₃)1σ_u]² are completely equivalent, and no experiment can distinguish between them.

Why have we made this particular change? Equation (13.13) and Figure 13.12 show that the new MOs σ' and σ'' are localized bonding MOs, one combining the 1s orbital on H_A with an s-p hybrid AO on Be, and the other combining the 1s orbital on H_B with an s-p hybrid AO on Be. In other words, the two delocalized MOs σ_g and σ_u have been transformed into two localized MOs *without changing the molecular wave function* $\psi(1, 2, 3, 4)$. This result can be generalized to the statement that for any

Figure 13.12

Schematic representation of the delocalized molecular orbitals σ_g and σ_u and the localized bonding orbitals σ' and σ'' .



Concept

Except for open shell molecules and conjugated or aromatic molecules, delocalized MOs can be transformed into localized orbitals.

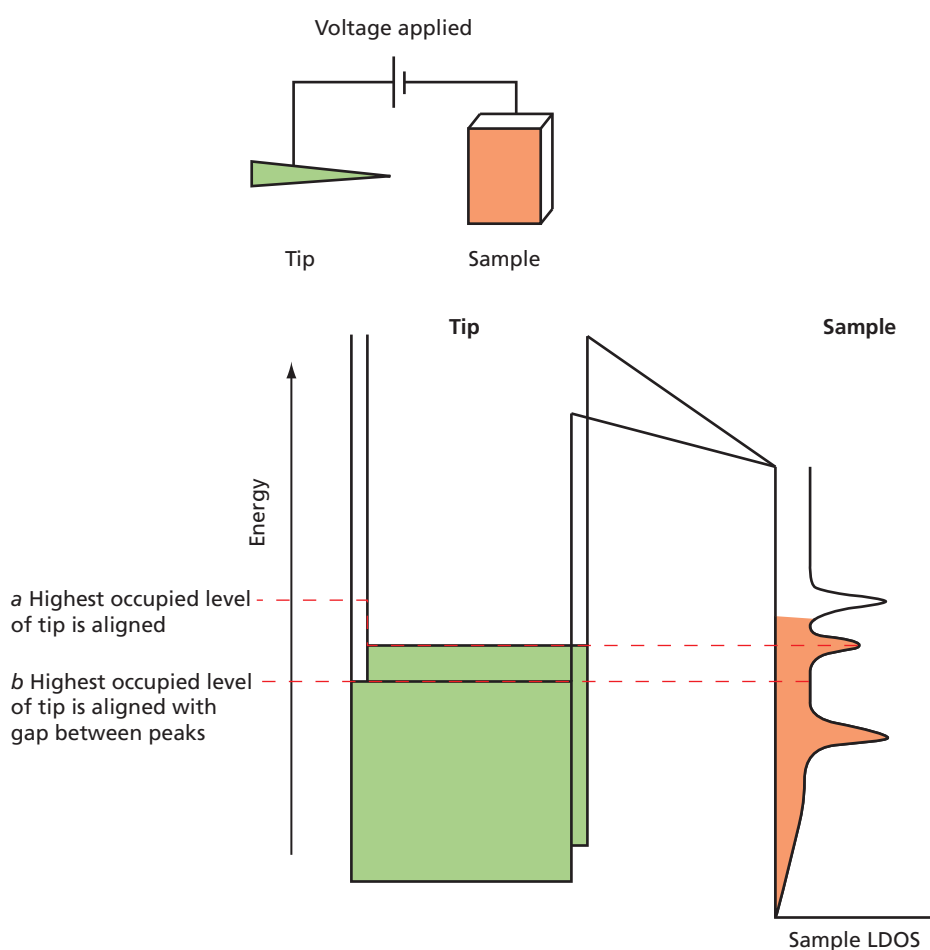
closed-shell molecular configuration, the set of delocalized MOs can be transformed into a set of localized orbitals predominantly involving two neighboring atoms. Such a transformation is not possible for open-shell molecules or conjugated and aromatic molecules in which at least some of the electrons are delocalized over the molecule.

As the BeH₂ example shows, the distinction between localized and delocalized orbitals is not as clear-cut as it seemed to be at the beginning of this chapter. Working with σ' and σ'' has some disadvantages because they are not eigenfunctions of the total energy operator. This means that we cannot assign orbital energies to these functions or draw energy-level diagrams as can be done for the delocalized MOs that are solutions to the molecular Hartree–Fock equations. Additionally, computational algorithms used to solve the Schrödinger equation are more efficient when formulated in terms of delocalized MOs than for localized orbitals. Because of these advantages, delocalized rather than localized MOs are generally used to calculate wave functions and energy levels in molecules.

The preceding discussion implies that there is no unique set of one-electron MOs for a molecule and raises the question “How ‘real’ are the molecular orbitals depicted in this and the previous chapter?” It is useful to distinguish between observables and elements of a model that are not amenable to measurement. Although a many-electron wave function $\psi(1, \dots, n)$ cannot be determined experimentally, electron density is proportional to $\sum_i |\psi_i(1, \dots, n)|^2$ and can be measured using techniques such as X-ray diffraction. Because of the summation over all occupied orbitals, X-ray diffraction does not give information directly about individual MOs.

Although individual one-electron MOs are also not amenable to direct measurement, experimental measurements can be made that strongly reflect the spatial distribution of the true many-electron wave function over a molecule for a given energy. An example is the use of scanning tunneling microscopy to measure the variation of the tunneling current over a molecule for different values of the energy of the tunneling electrons. The principle of the measurement is shown in Figure 13.13.

As discussed in Section 5.6, the difference between the highest occupied energy levels in the tip and sample can be varied by applying a voltage between the two elements of the scanning tunneling microscope (STM). With the voltage polarity shown in Figure 13.13, the tunneling current flows from the surface to the tip, both of which are metals. As discussed in Section 5.4, a metal is characterized by a continuum of states in the conduction band. If a molecule with discrete energy levels is adsorbed on the surface, the number of states at a given energy, called the local density of states, has a multipeaked structure, where the peaks correspond to the discrete MO energy levels. Tunneling occurs into the highest occupied level in the tip, and the tunneling

**Figure 13.13**

Principles of scanning tunneling spectroscopy. A voltage applied between the tip and sample aligns different energy levels of the molecule adsorbed on the surface with the highest occupied energy level in the tip. Scanning of the tip over the molecule gives an image of the local density of states in the molecule at a fixed energy corresponding to the fixed voltage. To a good approximation, this is the magnitude of the MO, as shown for case (a), the HOMO. If an appropriate voltage with the reverse polarity is applied, tunneling from the tip to the empty states of the sample can occur and the LUMO can be imaged.

current is proportional to the local density of states. If the highest occupied level of the tip is aligned with a peak in the local density of states of the adsorbed molecule as shown in case *a* of Figure 13.13, scanning of the tip over the molecule will give an image of the magnitude of the molecular orbital corresponding to the peak energy. However, if the highest occupied level of the tip is aligned with a gap between peaks in the local density of states of the adsorbed molecule as shown in case *b* of Figure 13.13, scanning of the tip over the molecule will give an image of the geometry of the molecule because the density of states on the metal surface is approximately constant over the region being scanned.

Figure 13.14 shows the results of carrying out the experiment just described on individual pentacene molecules separated from a copper surface by an atomically thin layer of NaCl. This ultrathin insulator layer prevents coupling between the electronic states of pentacene with the delocalized states of the metal. In the preceding discussion, we have assumed that the density of states in the tip has no influence on the measurement. Figure 13.14 shows results for two tip configurations: a bare metal tip and a tip terminated in a single pentacene molecule. Although the general features of the results are similar for both tips, the details differ. A comparison of the results obtained with the pentacene terminated tip with calculations using density functional theory (see Chapter 15) for a gas phase pentacene molecule shows very good agreement between the calculated and observed HOMO and LUMO probability densities.

What does this experiment tell us about the reality of molecular orbitals? Adsorption of the molecule on the surface is necessary to immobilize it. This weak “bonding” influences the electronic structure of the pentacene. Additionally, the local density of states in the tip and surface influence the results, so that the images shown in Figure 13.14 are not exact images of the HOMO and LUMO probability densities for an isolated pentacene molecule. However, the high degree of correspondence between the calculation and experimental results implies that orbital approximation that leads to the picture of one-electron MOs is valid in this case. Because the HOMO and LUMO are occupied by the π electrons in this aromatic molecule, a delocalized model is necessary for their description.

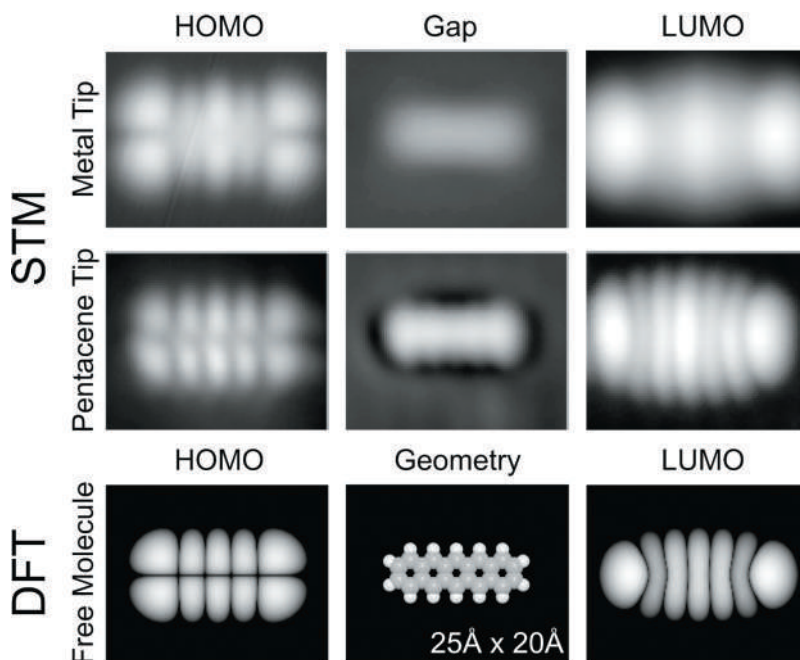
Concept

Using scanning tunneling spectroscopy, the local density of states in a molecule can be imaged experimentally.

Figure 13.14

Images of the local density of states of a pentacene molecule adsorbed on a copper surface. The images are shown in the first two rows of columns one and three. Calculated probability densities for the HOMO and LUMO are shown in the third row. The first two rows of the middle column show results obtained in an energy gap for which the local density of states for pentacene are negligible.

Source: Adapted from Repp et al., *Physical Review Letters*, 94(2), (2005).



These experimental results do not contradict the assertion made in Section 6.6 that it is not possible to reconstruct a wave function from experimental results because at most only the magnitude of the wave function can be determined.

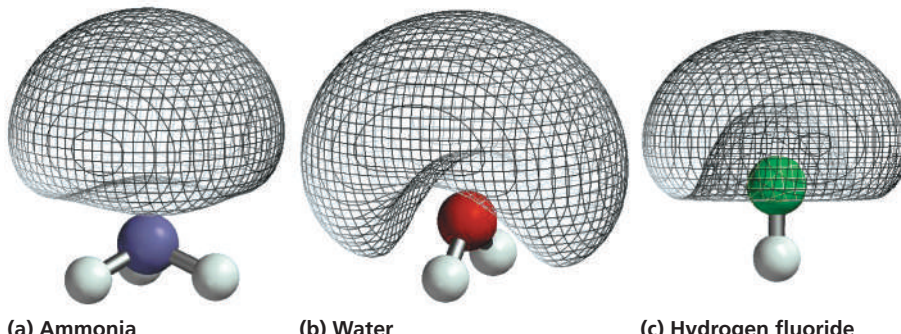
13.7 MOLECULAR STRUCTURE AND ENERGY LEVELS FROM COMPUTATIONAL CHEMISTRY

Concept

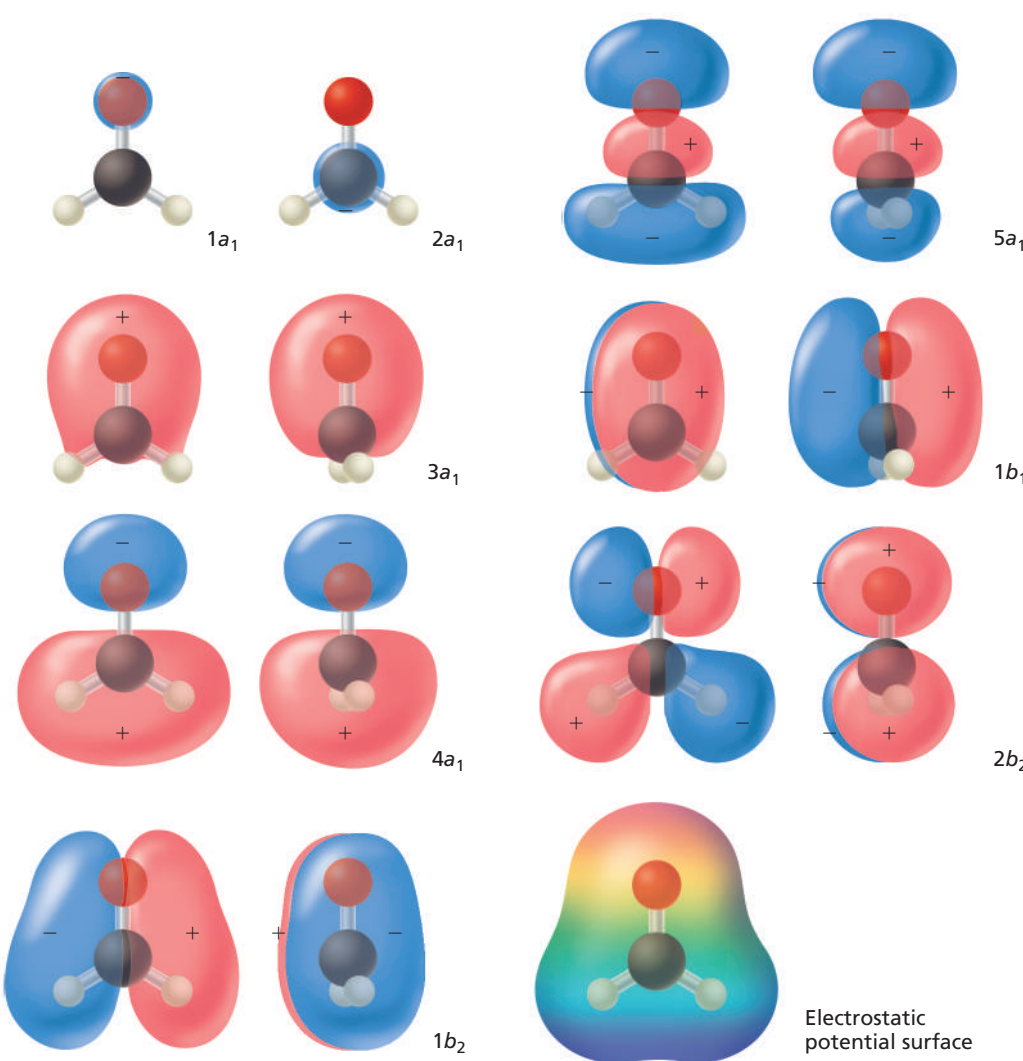
Accurate numerical quantum mechanical calculations on small molecules can be carried out quickly on personal computers, eliminating the need for simplified qualitative bonding models.

Solving the Schrödinger equation analytically is possible only for one-electron atoms and molecules. Molecular orbitals and energy levels for many-electron atoms and molecules must be obtained using numerical methods to solve the Schrödinger equation. Fortunately, readily available software can be used to solve structures for small molecules such as those discussed in this chapter on standard personal computers in less than a minute. Inexpensive or free versions of such software are available. Currently, there is little need for chemists and other scientists to use oversimplified, nonquantitative models that were developed before the advent of computers. The methods and approximations that are commonly used today, as well as the accuracy of these calculations, are discussed in detail in Chapter 15. Here, we present a few results from computational chemistry that support topics discussed in Chapters 12 and 13.

Lewis structures represent bonding and lone pair electrons differently. Can this picture be supported by rigorous calculations? Figure 13.15 shows negative electrostatic potential surfaces for molecules that Lewis structures would assign one, two, and three lone pairs. Notice that the shape and extent of the surfaces are consistent with the number of lone pairs as well as their distribution in space to minimize repulsive interactions.

**Figure 13.15**

Electrostatic potential surfaces. The diagrams are for (a) ammonia, (b) water, and (c) hydrogen fluoride. The lobes correspond to regions of negative charge and support the concept of localized lone pairs.

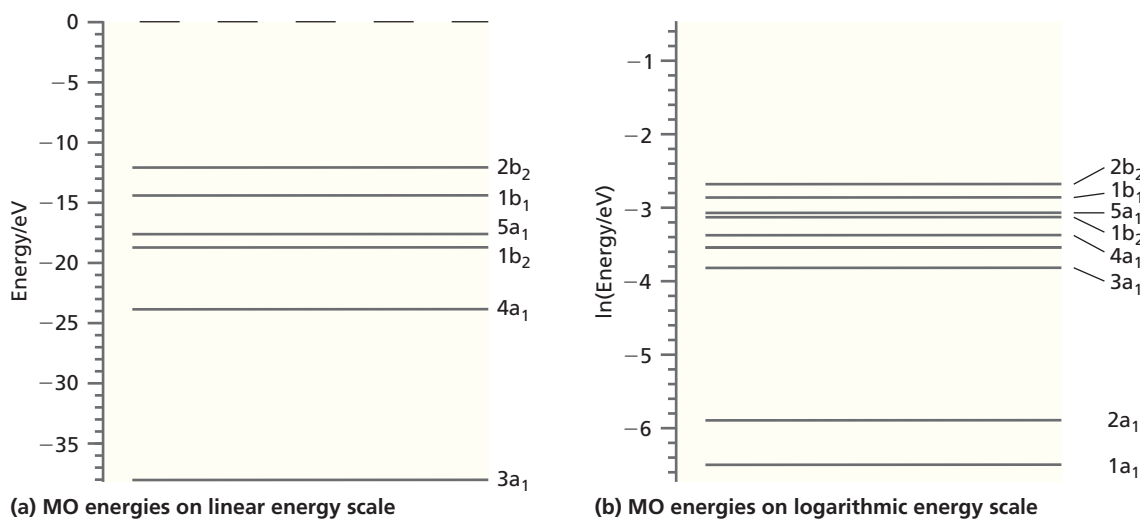
**Figure 13.16**

Symmetry-adapted molecular orbitals for formaldehyde. For all but the localized MOs, two perpendicular orientations of the molecule are shown.

The last image shows a charge density contour enclosing 90% of the electron charge with a superimposed electrostatic potential map in which red and blue correspond to negative and positive regions of the molecule.

Figure 13.16 shows calculated symmetry-adapted MOs for the eight occupied MOs on formaldehyde, which has 16 electrons. The MO designations indicate whether the MO changes its sign when the molecule undergoes a rotation about a symmetry axis or a reflection in a symmetry plane. This topic is discussed further in Chapter 16. For the discussion in this chapter, consider the MO designations as labels.

Next, we interpret the individual MOs in a localized bonding framework. The order of the occupied MOs from lowest to highest energy is $1a_1$, $2a_1$, $3a_1$, $4a_1$, $1b_2$, $5a_1$, $1b_1$, and $2b_2$. The $1a_1$ MO is localized on O and corresponds to the $1s$ AO. The $2a_1$ MO is localized on C and corresponds to the $1s$ AO. Note that although these two MOs were assumed to be delocalized over the molecule, the calculation shows that they are localized as expected for core electrons. The next lowest MO, designated $3a_1$, has contributions from the O $2s$ and C $2s$ AOs and a small contribution from the H atoms. This MO contributes to bonding in the C—O region. Participation of the $2p$ electrons is first observed in the $4a_1$ MO. It has contributions from the C sp^2 hybrid AO directed in the negative x direction toward the H atoms and the $2p_x$ lone pair on O. This MO is bonding in the C—H regions and antibonding in the C—O region. The $1b_2$ MO has contributions from the $2p_y$ lone pair AO on O, mixing in-phase with C—H bonding orbitals formed from $2p_y$ on C and the out-of-phase combination of H $1s$ AOs. This MO is bonding in both the C—O and C—H regions. The $5a_1$ MO has contributions from the $2p_x$ lone pair on O, which mixes in phase with the sp^2 hybrid AOs on C. These hybrid orbitals are directed toward the H atoms. This MO is bonding in both the C—O and C—H regions. The $1b_1$ MO represents a π bond in the C—O region. Because the net overlap with the H $1s$ AOs is zero, there is no contribution from the H atoms to this

**Figure 13.17**

Molecular orbital energy levels for formaldehyde. (a) Formaldehyde valence MO energy levels shown on a linear energy scale. Because the 1a₁ and 2a₁ MO levels plot well off the area shown in the diagram (−560.2 and −308.7 eV, respectively), they are not shown. (b) All MO energy levels shown on a logarithmic energy scale. Values were obtained from an MP2 calculation using the 6-31G* basis set (see Chapter 15).

MO. This MO is bonding in the C—O region and nonbonding in the C—H regions. The 2b₂ MO is the HOMO. It is the antibonding version of the 1b₂ MO. The 2p_y lone pair AO on O interacts in an antibonding fashion with the C—H bonds that are formed from the 2p_y AO on C and the out-of-phase combination of H 1s AOs. This MO is nonbonding in CO and bonding in CH regions.

We can also interpret these MOs by focusing on the C=O group. The lone pair electrons on the oxygen atoms can be most directly associated with the 2b₂ (HOMO) and also with the 4a₁ and 5a₁ MOs. The π bond of the C=O group is associated with the 1b₁ MO.

The electrons in the 3a₁, 1b₂, 5a₁ and 1b₁ MOs all contribute to bonding in the C—O region, whereas the 4a₁ MO decreases the bond order because of its antibonding character. The electrons in the 4a₁, 1b₂, 5a₁, and 2b₂ MOs all contribute to bonding in the C—H region.

The charges on the individual atoms calculated as discussed in Section 12.8 are H: −0.064, C: +0.60, O: −0.47, and the calculated dipole moment is 2.35 debye, which compares well with the measured value of 2.33 debye. The MO energy levels are shown in Figure 13.17. As AOs from three types of atoms are involved, it is not possible to draw lines linking the MO energy levels to AO energy levels as was done for diatomic molecules. The HOMO energy level should correspond to the first ionization energy. The calculated value is 12.0 eV, and the measured value is 11 eV. The accuracy of these and other calculated quantities depends significantly on the computational model used, as will be discussed in Chapter 15.

13.8 QUALITATIVE MOLECULAR ORBITAL THEORY FOR CONJUGATED AND AROMATIC MOLECULES: THE HÜCKEL MODEL

The molecules in the preceding sections can be discussed using either a localized or a delocalized model of chemical bonding. This is not the case for conjugated and aromatic molecules, in which a delocalized model must be used. **Conjugated molecules** such as 1,3-butadiene have a planar carbon backbone with alternating single and double bonds. Butadiene has single and double bond lengths of 147 and 134 pm, respectively. The single bonds are shorter than the single bond length in ethane (154 pm), which suggests that a delocalized π network is formed. Such a delocalized network can be modeled in terms of the coupling between sp^2 -hybridized carbon atoms in a σ-bonded carbon backbone. The lowering of the total energy that can be attributed to the formation of the π network is responsible for the reduced reactivity of conjugated molecules compared to molecules with isolated double bonds.

Aromatic molecules are a special class of conjugated molecules. They are based on ring structures that are particularly stable in chemical reactions. The presence of “closed

"circuits" of mobile electrons is required for a molecule to be designated as aromatic. Because such currents imply electron delocalization, bonding in aromatic molecules cannot be explained by electron pairing in localized bonds. For example, benzene has six C—C bonds of equal length, 139 pm, a value between the single and double bond lengths in 1,3-butadiene. This suggests that the six π electrons are distributed over all six carbon atoms. Therefore, a delocalized model is required to discuss aromatic molecules.

Erich Hückel formulated a useful application of qualitative MO theory to calculate the energy levels of the delocalized π electrons in conjugated and aromatic molecules. Despite its simplicity, the **Hückel model** correctly predicts the stabilization that arises from delocalization and predicts which of many possible cyclic polyenes will be aromatic. In the Hückel model, the π network of MOs can be treated separately from the σ network of the carbon backbone. The Hückel model uses hybridization and the localized valence bond model to describe the σ -bonded skeleton and MO theory to describe the delocalized π electrons.

In the Hückel theory, the p atomic orbitals that combine to form π MOs are treated separately from the sp^2 σ -bonded carbon backbone. For the four-carbon π network in butadiene, the π MO can be written in the form

$$\psi_{\pi} = c_1\phi_{2p_z1} + c_2\phi_{2p_z2} + c_3\phi_{2p_z3} + c_4\phi_{2p_z4} \quad (13.14)$$

As was done in Section 12.1, the variational method is used to calculate the coefficients that give the lowest energy for the four MOs that result from combining four AOs. We obtain the following secular equations:

$$\begin{aligned} c_1(H_{11} - \varepsilon S_{11}) + c_2(H_{12} - \varepsilon S_{12}) + c_3(H_{13} - \varepsilon S_{13}) + c_4(H_{14} - \varepsilon S_{14}) &= 0 \\ c_1(H_{21} - \varepsilon S_{21}) + c_2(H_{22} - \varepsilon S_{22}) + c_3(H_{23} - \varepsilon S_{23}) + c_4(H_{24} - \varepsilon S_{24}) &= 0 \\ c_1(H_{31} - \varepsilon S_{31}) + c_2(H_{32} - \varepsilon S_{32}) + c_3(H_{33} - \varepsilon S_{33}) + c_4(H_{34} - \varepsilon S_{34}) &= 0 \\ c_1(H_{41} - \varepsilon S_{41}) + c_2(H_{42} - \varepsilon S_{42}) + c_3(H_{43} - \varepsilon S_{43}) + c_4(H_{44} - \varepsilon S_{44}) &= 0 \end{aligned} \quad (13.15)$$

Similar to the discussion in Chapter 12, integrals of the type H_{aa} are called Coulomb integrals, integrals of the type H_{ab} are called resonance integrals, and integrals of the type S_{ab} are called overlap integrals. Rather than evaluate these integrals, in the Hückel model thermodynamic and spectroscopic data obtained from different conjugated molecules are used to obtain their values. Because it relies on both theoretical and experimental input, the Hückel model is a **semi-empirical theory**.

In the Hückel model, the Coulomb and resonance integrals are assumed to be the same for all conjugated hydrocarbons and are given the symbols α and β , respectively, where α is the negative of the ionization energy of the $2p$ orbital, and β , which is negative, is usually left as an adjustable parameter. Do not confuse this notation with spin up and spin down. The secular determinant (discussed in Chapter 12) used to obtain the MO energies and the coefficients of the AOs for 1,3-butadiene is

$$\begin{vmatrix} H_{11} - \varepsilon S_{11} & H_{12} - \varepsilon S_{12} & H_{13} - \varepsilon S_{13} & H_{14} - \varepsilon S_{14} \\ H_{21} - \varepsilon S_{21} & H_{22} - \varepsilon S_{22} & H_{23} - \varepsilon S_{23} & H_{24} - \varepsilon S_{24} \\ H_{31} - \varepsilon S_{31} & H_{32} - \varepsilon S_{32} & H_{33} - \varepsilon S_{33} & H_{34} - \varepsilon S_{34} \\ H_{41} - \varepsilon S_{41} & H_{42} - \varepsilon S_{42} & H_{43} - \varepsilon S_{43} & H_{44} - \varepsilon S_{44} \end{vmatrix} \quad (13.16)$$

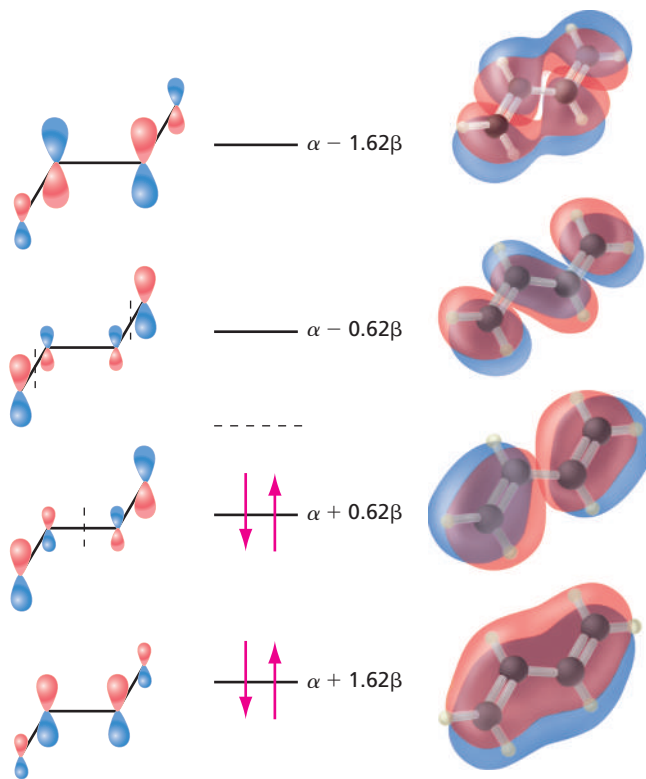
Several simplifying assumptions are made in the Hückel model to make it easier to solve secular determinants. The first is $S_{ii} = 1$ and $S_{ij} = 0$ unless $i = j$. This is a rather drastic simplification because if the overlap between adjacent atoms were zero, no bond formation would occur. It is also assumed that $H_{ij} = \beta$ if i and j are on adjacent C atoms, $H_{ij} = \alpha$ if $i = j$, and $H_{ij} = 0$ otherwise. Setting $H_{ij} = 0$ for nonadjacent carbon atoms is equivalent to stating that the primary interaction is between the neighboring $2p_z$ orbitals. The result of the simplifying assumptions is that all elements of the determinant that are more than one position removed from the diagonal are zero for noncyclic polyenes.

Concept

The Hückel model is a qualitative model for understanding electron delocalization in conjugated and aromatic molecules.

Figure 13.18

Energy levels and molecular orbitals for butadiene in the Hückel approximation. The sizes of the $2p_z$ AOs in the left column are proportional to their coefficients in the MO. Calculated MOs (see text) are shown in the right column. Red and blue lobes refer to positive and negative amplitudes, respectively. The vertical dashed lines indicate nodal planes.



With these assumptions, the secular determinant for butadiene reduces to

$$\begin{vmatrix} \alpha - \varepsilon & \beta & 0 & 0 \\ \beta & \alpha - \varepsilon & \beta & 0 \\ 0 & \beta & \alpha - \varepsilon & \beta \\ 0 & 0 & \beta & \alpha - \varepsilon \end{vmatrix} = 0 \quad (13.17)$$

As shown in Example Problem 13.7, this determinant has the solutions for the π orbital energies shown in Figure 13.18.

Let us consider several of the results shown in Figure 13.18. First, the coefficients of the AOs in the different MOs are not the same. Second, a pattern of nodes is seen that is identical to the other quantum-mechanical systems that have been solved. The ground state has no nodes perpendicular to the plane of the molecule, and successively higher MOs have an increasing number of nodes. Recall that nodes correspond to regions in which the probability of finding the electron is zero. Because the nodes appear between the carbon atoms, they add an antibonding character to the MO, which increases the MO energy.

EXAMPLE PROBLEM 13.7

Solve the secular determinant for butadiene to obtain the MO energies.

Solution

The 4×4 secular determinant can be expanded to yield (see Math Essential 9) the following equation:

$$\begin{aligned} & \begin{vmatrix} \alpha - \varepsilon & \beta & 0 & 0 \\ \beta & \alpha - \varepsilon & \beta & 0 \\ 0 & \beta & \alpha - \varepsilon & \beta \\ 0 & 0 & \beta & \alpha - \varepsilon \end{vmatrix} \\ &= (\alpha - \varepsilon) \begin{vmatrix} \alpha - \varepsilon & \beta & 0 \\ \beta & \alpha - \varepsilon & \beta \\ 0 & \beta & \alpha - \varepsilon \end{vmatrix} - \beta \begin{vmatrix} \beta & \beta & 0 \\ 0 & \alpha - \varepsilon & \beta \\ 0 & \beta & \alpha - \varepsilon \end{vmatrix} \end{aligned}$$

$$\begin{aligned}
 &= (\alpha - \varepsilon)^2 \begin{vmatrix} \alpha - \varepsilon & \beta \\ \beta & \alpha - \varepsilon \end{vmatrix} - \beta(\alpha - \varepsilon) \begin{vmatrix} \beta & \beta \\ 0 & \alpha - \varepsilon \end{vmatrix} - \beta^2 \begin{vmatrix} \alpha - \varepsilon & \beta \\ \beta & \alpha - \varepsilon \end{vmatrix} + \beta^2 \begin{vmatrix} 0 & \beta \\ 0 & \alpha - \varepsilon \end{vmatrix} \\
 &= (\alpha - \varepsilon)^4 - (\alpha - \varepsilon)^2\beta^2 - (\alpha - \varepsilon)^2\beta^2 - (\alpha - \varepsilon)^2\beta^2 + \beta^4 \\
 &= (\alpha - \varepsilon)^4 - 3(\alpha - \varepsilon)^2\beta^2 + \beta^4 = \frac{(\alpha - \varepsilon)^4}{\beta^4} - \frac{3(\alpha - \varepsilon)^2}{\beta^2} + 1 = 0
 \end{aligned}$$

This equation can be written in the form of a quadratic equation:

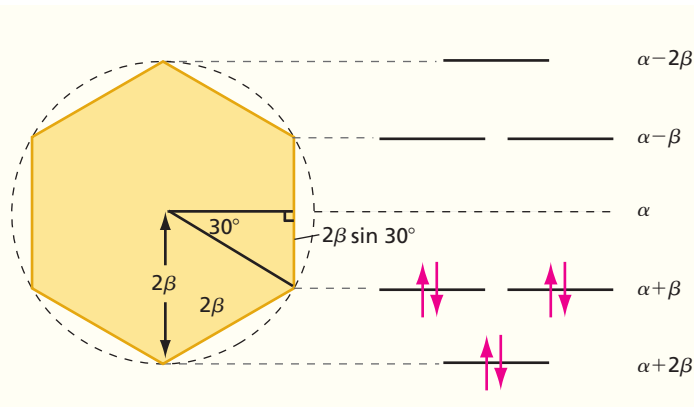
$$\frac{(\alpha - \varepsilon)^2}{\beta^2} = \frac{3 \pm \sqrt{5}}{2}$$

which has the four solutions $\varepsilon = \alpha \pm 1.62\beta$ and $\varepsilon = \alpha \pm 0.62\beta$.

The effort required to obtain the energy levels and the AO coefficients for a monocyclic polyene can be greatly simplified by using the following geometrical construction: inscribe a regular polygon with the shape of the polyene in a circle of radius 2β with one vertex of the polygon pointing directly downward. Draw a horizontal line at each point for which the polygon touches the circle. These lines correspond to the energy levels, with the center of the circle corresponding to the energy α . This method is illustrated in Example Problem 13.8.

EXAMPLE PROBLEM 13.8

Use the inscribed polygon method to calculate the Hückel MO energy levels for benzene.



Solution

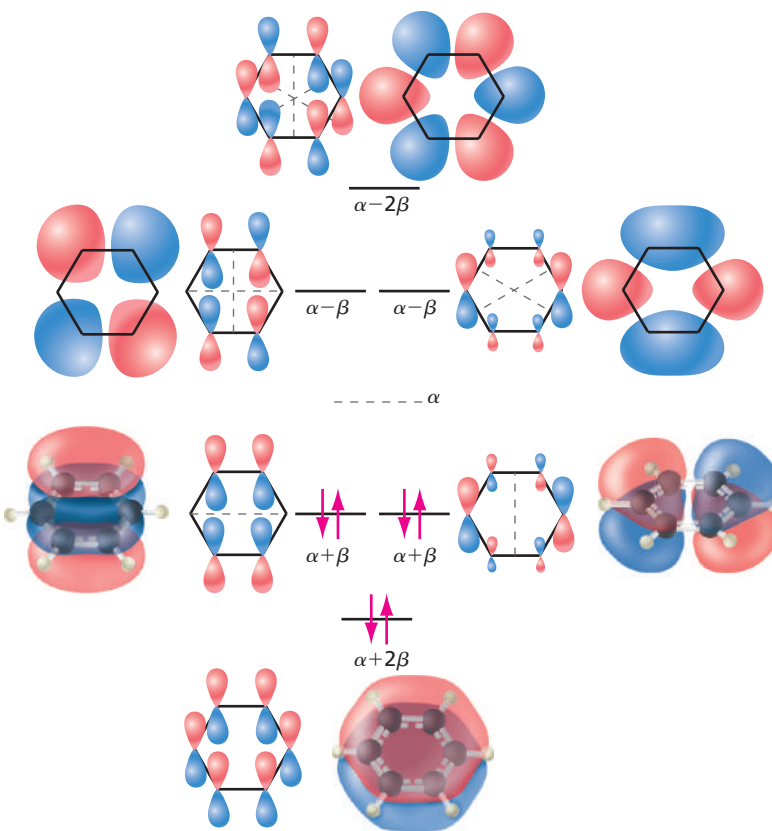
The geometrical construction shows that the energy levels are $\alpha + 2\beta$, $\alpha + \beta$, $\alpha - \beta$, and $\alpha - 2\beta$. The sum of the orbital energies for the six π electrons is $6\alpha + 8\beta$.

The benzene MOs and their energies are shown in Figure 13.19. Note that the energy levels for $\alpha + \beta$ and $\alpha - \beta$ are doubly degenerate. As was the case for butadiene, the lowest MO has no nodes perpendicular to the molecular plane, and the energy of the MO increases with the number of additional nodal planes. The average orbital energy of a π electron in benzene is

$$\frac{1}{6}[2(\alpha + 2\beta) + 4(\alpha + \beta)] = \alpha + 1.33\beta$$

Figure 13.19

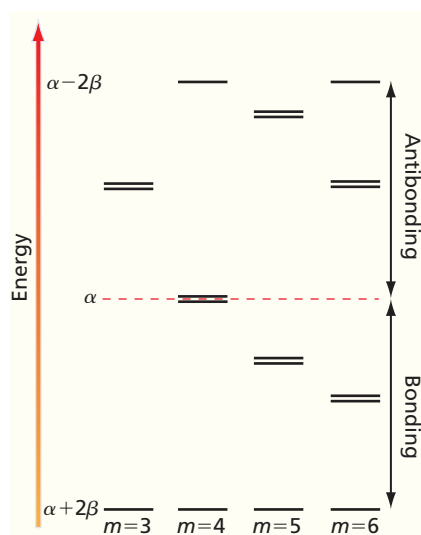
Energy levels and molecular orbitals for benzene in the Hückel approximation. The sizes of the $2p_z$ AOs are proportional to their coefficients in the MO. Calculated MOs (see text) are shown in a three-dimensional perspective for the filled MOs and as an on-top view for the unfilled MOs. Red and blue lobes refer to positive and negative amplitudes. Thin dashed lines indicate nodal planes.



The energy levels for the smaller monocyclic polyenes ($\text{CH})_m$, where m is the number of π bonded carbons, exhibit the pattern shown in Figure 13.20. The energy value α separates the bonding and antibonding MOs.

This figure provides a justification for the following **Hückel rules** for a monocyclic conjugated system with $N \pi$ electrons:

- If $N = 4n + 2$, where n is an integer $0, 1, 2, \dots$, the molecule is stabilized through the π delocalization network.
- If $N = 4n + 1$ or $4n + 3$, the molecule is a free radical.
- If $N = 4n$, the molecule has two unpaired electrons and is very reactive.

**Figure 13.20**

Energy of π molecular orbitals for cyclic polyenes described by the formula $(\text{CH})_m$ with $m = 3$ to 6 bonded carbons. The doubly degenerate pairs are shown slightly separated in energy for clarity.

The justification for these rules can be understood from Figure 13.20. For each cyclic polyene, the lowest energy level is nondegenerate and has the energy $\alpha + 2\beta$. All other levels are doubly degenerate, with the exception of the highest level if m is even. The maximum stabilization is attained if $N = 4n + 2$, because all π electrons are paired and in bonding orbitals for which $\varepsilon < \alpha$. For $n = 1$, six π electrons correspond to the maximal stabilization. Benzene, for which $m = 6$, is an example of this case. Next consider benzene with one fewer or one more π electron. Because $N = 5$ or 7, both species are radicals because the highest occupied energy level is not filled, and both are less stable than benzene. What happens to a system of maximum stabilization if two electrons are removed? Because all energy levels, except the lowest (and if m is even, the highest), are doubly degenerate, each of the degenerate levels has an occupancy of one for $N = 4n$, and the molecule is a diradical.

These rules can be used to make useful predictions. For example, C_3H_3 , which is formed from cyclopropene by the removal of one H atom, should be more stable as $\text{C}_3\text{H}_3^+(\text{N} = 2)$ than as neutral $\text{C}_3\text{H}_3(\text{N} = 3)$ or $\text{C}_3\text{H}_3^-(\text{N} = 4)$. Undistorted cyclobutadiene ($N = 4$) with four π electrons will be a diradical and, therefore, very reactive. The maximum stabilization for C_5H_5 is for $N = 6$, as is seen in Figure 13.20. Therefore, C_5H_5^- is predicted to be more stable than C_5H_5 or C_5H_5^+ . These predictions have been verified by experiment and show that the Hückel model has considerable predictive power, despite its significant approximations.

At present, the Hückel model is primarily useful for explaining the $4n + 2$ rule. Readily available computational chemistry software can rapidly calculate MOs and their corresponding energy levels on personal computers, making the determination of α and β from experimental data unnecessary. The MOs shown in Figures 13.18 and 13.19 were obtained with computational chemistry software using the B3LYP method of density functional theory and the 6-31G* basis set (see Chapter 15).

Having introduced the Hückel model, we now discuss the **resonance stabilization energy** that arises in aromatic compounds through the presence of closed circuits of mobile electrons. No unique method is available for calculating this stabilization energy. However, a reasonable way to determine this energy is to compare the π network energy of the cyclic polyene with that of a linear polyene that consists of alternating double and single bonds with the same number and arrangement of hydrogen atoms. In some cases, this may be a hypothetical molecule whose π network energy can be calculated using the method outlined earlier. As has been shown by L. Schaad and B. Hess [*Journal of Chemical Education* 51 (1974): 640–643], meaningful results for the resonance stabilization energy can be obtained only if the reference molecule is similar in all aspects except one: it is a linear polyene rather than a cyclic polyene. For benzene, the reference molecule has the total π energy $6\alpha + 7.608\beta$. From Figure 13.20, note that the corresponding value for benzene is $6\alpha + 8\beta$. Therefore, the resonance stabilization energy per π electron in benzene is $(8.000\beta - 7.608\beta)/6 = 0.065\beta$. By considering suitable reference compounds, Schaad and Hess calculated the resonance stabilization energy for a large number of compounds, some of which are shown in Figure 13.21.

Figure 13.21 indicates that benzene and benzocyclobutadiene have the greatest resonance delocalization energy, as described in the previous paragraph. Molecules with negative values for the resonance stabilization energy are predicted to be more stable as linear polyenes than as cyclic polyenes and are referred to as **antiaromatic molecules**. Note that these calculations only provide information on the π network energy and that the total energy of the molecule is assumed to be proportional to the sum of the occupied π orbital energies. We have also ignored the possible effect of strain energy that arises if the C—C—C bonding angles are significantly different from 120° , which is optimal for sp^2 hybridization. For example, cyclobutadiene, for which the bond angle is 90° , has an appreciable strain energy associated with the σ -bonded backbone, which

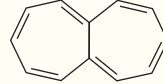
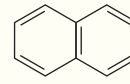
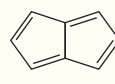
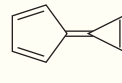
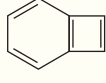
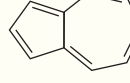
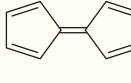
	Benzene 0.065		Heptalene −0.004
	Naphthalene 0.055		Pentalene −0.018
	Calicene 0.043		Benzocyclobutadiene 0.065
	Azulene 0.023		Fulvalene −0.033
	Fulvene −0.002		Cyclobutadiene −0.268

Figure 13.21
Resonance delocalization energy per π electron for selected cyclic polyenes. The values are units of β .

destabilizes the molecule relative to a linear polyene. A ranking of the degree of aromaticity based on experimental data such as thermochemistry, reactivity, and chemical shifts using nuclear magnetic resonance spectroscopy (see Chapter 17) is in good agreement with the predictions of the Hückel model if the appropriate reference molecule is used to calculate the resonance stabilization energy.

Although the examples used in this section to illustrate aromaticity are planar compounds, this is not a requirement for aromaticity. Sandwich compounds such as ferrocene, as well as the fullerenes, also show aromatic behavior. For these molecules, the closed circuits of mobile electrons extend over all three dimensions. These calculations for conjugated and aromatic molecules show the power of the Hückel model in obtaining useful results with minimal computational effort and without evaluating any integrals or even using numerical values for α and β . Fewer simplifying assumptions are made in the extended Hückel model, which treats the σ and π electrons similarly.

13.9 FROM MOLECULES TO SOLIDS

Concept

In solids, discrete MO energy levels are replaced by continuous energy bands that are separated by band gaps.

The Hückel model is also useful for understanding the energy levels in a solid, which can be thought of as a giant molecule. In discussing the application of the particle in the box model to solids in Chapter 5, we learned that a solid has an energy spectrum that has both continuous and discrete aspects. Within a range of energies called a band, the energy spectrum is continuous. However, the energy bands are separated by **band gaps** in which no quantum states are allowed. The Hückel model (Figure 13.22) is useful in developing an understanding of how this energy spectrum is generated.

Consider a one-dimensional chain of atoms in which π bonds are formed. Combining N $2p_x$ atomic orbitals creates the same number of π MOs as was seen for ethene, butadiene, and benzene. Hückel theory predicts that the difference in energy between the lowest- and highest-energy MO depends on the length of the conjugated chain but approaches the value 4β as the chain becomes infinitely long. All N energy levels still must lie in the range between $\alpha + 2\beta$ and $\alpha - 2\beta$. Therefore, as $N \rightarrow \infty$, the spacing between adjacent levels becomes vanishingly small, and the energy spectrum becomes continuous, generating a band.

The wave functions of the long one-dimensional chain are schematically indicated in Figure 13.23. At the bottom of the band, all AOs are in phase (fully bonding), but at the top of the band, the AOs on adjacent atoms are out of phase (fully antibonding). At energies near the middle of the band, the nodal spacing is intermediate between N and one atomic spacing, making the state partially bonding. The energy versus distance curves from Figure 12.4 can be applied to the one-dimensional chain. This has been done in Figure 13.23. For a two-atom solid (diatomic molecule), the wave function is either fully bonding or fully antibonding. For a long chain, all possible wave functions between fully bonding and fully antibonding are possible. Therefore, the entire energy range indicated by the space between the totally bonding and totally antibonding curves in Figure 13.23 is allowed.

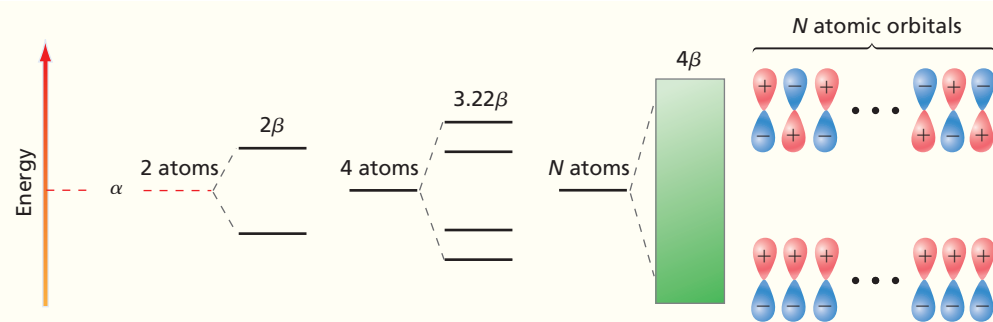


Figure 13.22

Molecular orbitals generated in an atom chain using the Hückel model. As N becomes very large, the energy spectrum becomes continuous. The energy range of the MOs is shown in units of β .

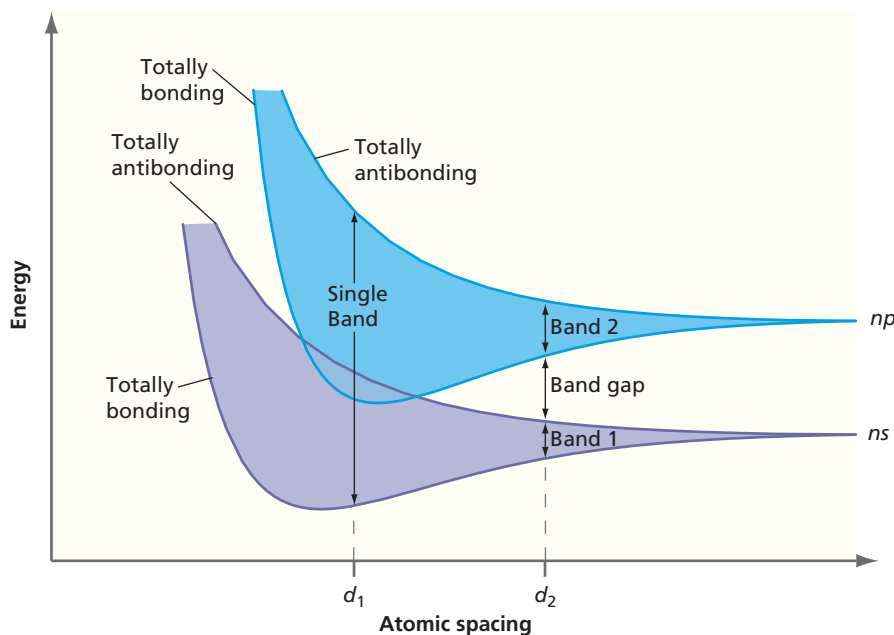


Figure 13.23

Bands generated from two different atomic orbitals on a very large number of atoms in a one-dimensional solid. For each of the ns and np AOs, the lower curve corresponds to the fully bonding case, and the upper curve corresponds to the fully antibonding case. The shading between the two curves indicates that all possible cases between fully bonding and fully antibonding can occur, so that all energies in the shaded area are allowed. The width in energy of the band of the allowed states depends on the atomic spacing. For the equilibrium spacing indicated by d_1 , the two AO bands overlap and all energy values between the top and bottom arrowheads are allowed. This is not true for larger spacing d_2 , for which the allowed energies lie in two bands separated by a band gap.

Let us now consider a specific example that demonstrates the contrasts among a conductor, a semiconductor, and an insulator. In solids, separate bands are generated from different AOs, such as the $3s$ and $3p$ AOs on Mg. If there is sufficient overlap between AOs to generate bonding, the bands are wide in energy. If this is not the case, the bands are narrow in energy. Magnesium, with the $[Ne]3s^2$ atomic configuration, has two $3s$ valence electrons that occupy a band generated from the overlap of the $3s$ electrons on neighboring Mg atoms. Because N Mg atoms generate N MOs, each of which can be doubly occupied, the $2N$ Mg valence electrons completely fill the $3s$ -generated band (lower band in Figure 13.23). If there were a gap between this and the next-highest band (upper band in Figure 13.23), which is generated from the $3p$ electrons, Mg would be an insulator. This situation corresponds to the atomic spacing d_2 . However, in this case, the $3s$ and $3p$ bands overlap, corresponding to the atomic spacing d_1 . As a result, the unoccupied states in the overlapping bands are only infinitesimally higher in energy than the highest filled state. For this reason, Mg is a conductor.

If there is a gap between a completely filled band and the empty band of next higher energy, the solid is either an insulator or a semiconductor. The distinction between a semiconductor and an insulator is the width of the energy gap. If $E_{gap} \gg kT$ at temperatures below the melting point of the solid, the material is an insulator. Diamond is an insulator even at very high temperatures because it has a large band gap. However, if at elevated temperatures $E_{gap} \sim k_B T$, the Boltzmann distribution [Equation (2.2)] predicts that it will be easy to promote an electron from the filled valence band to the empty conduction band. In this case, the highest filled state is infinitesimally lower in energy than the lowest unfilled state, and the solid is a conductor. Silicon and germanium are called semiconductors because they behave like insulators at low temperatures and like conductors at higher temperatures.

Concept

Semiconductors behave like insulators at low temperatures and like conductors at high temperatures.

13.10 MAKING SEMICONDUCTORS CONDUCTIVE AT ROOM TEMPERATURE

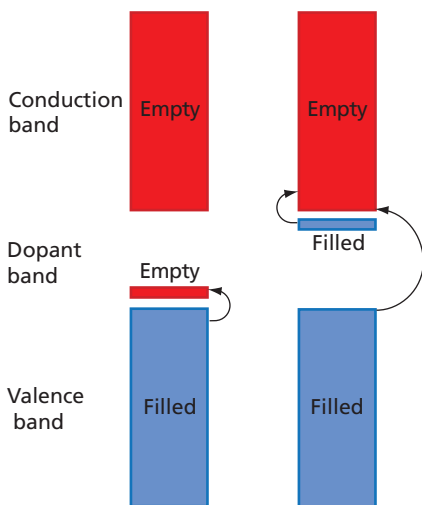


Figure 13.24

Modification of silicon band structure generated by introduction of dopants. The excitation that leads to conduction is from the valence band to the dopant band (*p*-type), as shown on the left, or dopant band to conduction band (*n*-type), as shown on the right, rather than across the Si band gap as indicated by the right-most curved arrow. Occupied and unoccupied bands are indicated by blue and red coloring, respectively. Energy increases vertically in the figure.

Concept

Introducing dopants into semiconductors allows them to conduct electricity at room temperature.

In its pure state, silicon is conductive to an appreciable extent only at temperatures greater than 900 K because it has a band gap of 1.1 eV. Yet computers and other devices that are based on silicon technology function at room temperature. For this to happen, these devices must transmit electrical currents at 300 K. What enables silicon to be conductive at such low temperatures? The key to changing the properties of Si is the introduction of other atoms that occupy Si sites in the silicon crystal structure. The introduction of these foreign atoms in the Si crystal lattice is called **doping**. An elemental substance used as foreign atoms in doping is referred to as the **dopant**.

Silicon is normally doped using atoms such as boron or phosphorus, which have one fewer or one more valence electron than silicon, respectively. Typically, the dopant concentration is on the order of a few parts per million relative to the Si concentration. How does this make Si conductive at lower temperatures? The Coulomb potential associated with the phosphorus atoms overlaps with the Coulomb potentials of the neighboring Si atoms, and the valence electrons of the P atom become delocalized throughout the crystal and form a separate band as discussed in Section 5.4. Because P has one more valence electron than Si, this band is only partially filled. As indicated in Figure 13.24, this band is located ~0.04 eV below the bottom of the empty conduction band. Electrons can be thermally excited from the dopant band to populate the empty Si conduction band. Importantly, it is the 0.04 eV rather than the Si band gap of 1.1 eV that must be comparable to $k_B T$ to produce delocalized electrons in the conduction band. Therefore, phosphorus-doped silicon is conductive at 300 K, where $k_B T \approx 0.04$ eV. Because the dominant charge carriers are negative, one refers to an *n*-type semiconductor.

Boron can be introduced as a dopant at a ppm concentration. The Si crystal site that a boron atom occupies has one valence electron fewer than the neighboring sites and acts like a positive charge, which is referred to as a hole. The hole is delocalized throughout the lattice and acts similar to a mobile positive charge because electrons from adjacent Si atoms can fill it, leaving the B atom with an extra negative charge while the hole jumps from Si to Si atom. In this case, the empty dopant band is located ~0.045 eV above the top of the filled valence band. Thermal excitations of electrons from the filled valence band into the empty dopant band make the *p*-type semiconductor conductive. Because the dominant charge carriers in this case are positive, one refers to a *p*-type semiconductor.

For both *n*-type and *p*-type semiconductors, the activation energy to promote charge carriers and to induce conduction is much less than the Si band gap. The modifications to the Si **band structure** introduced by dopants are illustrated in Figure 13.24.

VOCABULARY

antiaromatic molecules	doping	resonance stabilization energy
aromatic molecules	Hückel model	semi-empirical theory
band gap	Hückel rules	<i>sp</i> , <i>sp</i> ² , and <i>sp</i> ³ hybridization
band structure	hybrid orbital	valence bond (VB) theory
Bent's rule	hybridization	valence shell electron pair repulsion (VSEPR) model
conjugated molecules	Lewis structure	Walsh correlation diagram
delocalized bonding model	localized bonding model	
dopant	lone pair	

KEY EQUATIONS

Equation	Significance of Equation	Equation Number
$\psi_a = \sqrt{\frac{2}{3}}\phi_{2p_z} - \frac{1}{\sqrt{3}}\phi_{2s}$		
$\psi_b = -\frac{1}{\sqrt{6}}\phi_{2p_z} - \frac{1}{\sqrt{3}}\phi_{2s} - \frac{1}{\sqrt{2}}\phi_{2p_x}$	sp^2 hybrid orbitals	Example Problem 13.2
$\psi_c = -\frac{1}{\sqrt{6}}\phi_{2p_z} - \frac{1}{\sqrt{3}}\phi_{2s} + \frac{1}{\sqrt{2}}\phi_{2p_x}$		
$\psi_a = \frac{1}{\sqrt{2}}(-\phi_{2s} + \phi_{2p_z})$		
$\psi_b = \frac{1}{\sqrt{2}}(-\phi_{2s} - \phi_{2p_z})$	sp hybrid orbitals	13.3
$\psi_a = \frac{1}{2}(-\phi_{2s} + \phi_{2p_x} + \phi_{2p_y} + \phi_{2p_z})$		
$\psi_b = \frac{1}{2}(-\phi_{2s} - \phi_{2p_x} - \phi_{2p_y} + \phi_{2p_z})$		
$\psi_c = \frac{1}{2}(-\phi_{2s} + \phi_{2p_x} - \phi_{2p_y} - \phi_{2p_z})$	sp^3 hybrid orbitals	13.4
$\psi_d = \frac{1}{2}(-\phi_{2s} - \phi_{2p_x} + \phi_{2p_y} - \phi_{2p_z})$		

CONCEPTUAL PROBLEMS

Q13.1 Why is it unclear whether a material is a semiconductor or an insulator?

Q13.2 How do the values of the AO coefficients in an MO differ for a delocalized and a localized bond?

Q13.3 What experimental evidence can you cite in support of the hypothesis that the electronegativity of a hybridized atom increases with increasing s character?

Q13.4 Explain why all possible wave functions between the fully bonding and the fully antibonding are possible for the bands shown in Figure 13.23.

Q13.5 On the basis of what you know about the indistinguishability of electrons and the difference between the wave functions for bonding electrons and lone pairs, discuss the validity and usefulness of the Lewis structure for the fluorine molecule.

Q13.6 What evidence can you find in Table 13.1 that C—C sp bonds are stronger than sp^3 bonds?

Q13.7 How is it possible that a semiconductor would become metallic if the nearest neighbor spacing could be changed sufficiently?

Q13.8 Why are localized and delocalized models equally valid for describing bonding in closed-shell molecules? Why can experiments not distinguish between these models?

Q13.9 The hybridization model assumes that atomic orbitals are recombined to prepare directed orbitals that have the bond

angles appropriate for a given molecule. What aspects of the model can be tested by experiments, and what aspects are conjectures that are not amenable to experimental verification?

Q13.10 Why can localized orbitals not be represented in an MO energy diagram?

Q13.11 In using the sum of the occupied MO energies to predict the bond angle in H_2A molecules, the total energy of the molecule is assumed to be proportional to the sum of the occupied MO energies. This assumption can be justified. Do you expect this sum to be greater than or smaller than the total energy? Justify your answer.

Q13.12 In explaining molecular structure, the MO model uses the change in MO energy with bond angle. Explain why the decrease in energy of the $1a_1$ and $2a_1$ MOs as 20° decreases more than offsets the increase in energy for the $1b_2$ MO for water.

Q13.13 What is the in-plane amplitude of the wave functions describing the π network in the conjugated molecules shown in Figures 13.18 and 13.19?

Q13.14 What is the rationale for setting $H_{ij} = 0$ for nonadjacent atoms in the Hückel model?

Q13.15 A cyclic polyene is known to be nonplanar. Are the MO energy levels of this molecule well described by the Hückel model? Justify your answer.

NUMERICAL PROBLEMS

Section 13.1

P13.1 Use the VSEPR method to predict the structures of the following:

- a. PCl₅
- b. SO₂
- c. XeF₂
- d. PCl₆⁻

P13.2 Use the VSEPR method to predict the structures of the following:

- a. PF₃
- b. CO₂
- c. BrF₅
- d. SO₃²⁻

Section 13.2

P13.3 Use the method described in Example Problem 13.3 to show that the *sp*-hybrid orbitals $\psi_a = 1/\sqrt{2}(-\phi_{2s} + \phi_{2p_z})$ and $\psi_b = 1/\sqrt{2}(-\phi_{2s} - \phi_{2p_z})$ are oriented 180° apart.

P13.4 Use the formula $\cos 2\theta = -\alpha^2$ and the method in Section 13.2 to derive the formulas $\psi_a = 1/\sqrt{2}(-\phi_{2s} + \phi_{2p_z})$ and $\psi_b = 1/\sqrt{2}(-\phi_{2s} - \phi_{2p_z})$ for two *sp* hybrid orbitals directed 180° apart. Show that these hybrid orbitals are orthogonal.

P13.5 Show that two of the set of four equivalent orbitals appropriate for *sp*³ hybridization,

$$\psi_a = \frac{1}{2}(-\phi_{2s} + \phi_{2p_x} + \phi_{2p_y} + \phi_{2p_z}) \quad \text{and}$$

$$\psi_b = \frac{1}{2}(-\phi_{2s} - \phi_{2p_x} - \phi_{2p_y} + \phi_{2p_z})$$

are orthogonal.

P13.6 Show that the water hybrid bonding orbitals given by $\psi_a = 0.55\phi_{2p_z} + 0.71\phi_{2p_y} - 0.45\phi_{2s}$ and $\psi_b = 0.55\phi_{2p_z} - 0.71\phi_{2p_y} - 0.45\phi_{2s}$ are orthogonal.

Section 13.3

P13.7 Use the framework described in Section 13.3 to construct normalized hybrid bonding orbitals on the central oxygen in O₃ that are derived from 2s and 2p atomic orbitals. The bond angle in ozone is 116.8°.

P13.8 In P13.6 you showed that the water hybrid bonding orbitals are orthogonal. Derive two mutually orthogonal hybrid orbitals for the lone pairs on oxygen in H₂O, each of which is orthogonal to σ_a and σ_b by following these steps:

- a. Start with the following formulas for the lone pair orbitals

$$\psi_c = d_1\phi_{2p_z} + d_2\phi_{2p_y} + d_3\phi_{2s} + d_4\phi_{2p_x},$$

$$\psi_d = d_5\phi_{2p_z} + d_6\phi_{2p_y} + d_7\phi_{2s} + d_8\phi_{2p_x}$$

Use symmetry conditions to determine d_2 and d_4 , and to determine the ratio of d_3 to d_7 and of d_4 to d_8 .

- b. To determine the unknown coefficients, use the condition that the sum of the squares of the coefficients over all hybrid orbitals and lone pair orbital is equal to one.

P13.9 In P13.7, the hybrid bonding orbitals for ozone were derived. Use the framework described in Section 13.3 to construct normalized hybrid lone pair orbitals on the central oxygen in O₃ that are derived from 2s and 2p atomic orbitals. The bond angle in ozone is 116.8°.

P13.10 Using your results from P13.6,

- a. Calculate the *s* and *p* character of the water lone pair hybrid orbitals
- b. Show that the lone pair orbitals are orthogonal to each other and to the hybrid bonding orbitals.

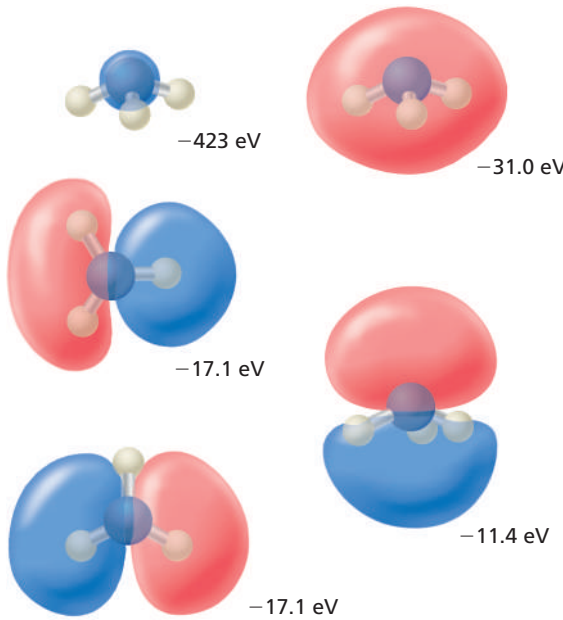
P13.11 *s-p* hybridization on each Ge atom in planar *trans*-digermane has been described as *sp*^{1.5} for the Ge—Ge sigma bond and *sp*^{1.8} for the Ge—H bond. Suppose that the Ge lone electron (in terms of Lewis-dot valence electrons) is in an *sp*^{*n*} hybrid orbital, where *n* is the hybrid *p* character. The three in-plane *s-p* hybrid orbitals on germanium must be normalized and mutually orthogonal. Assume that the molecule lies in the *xz* plane with the Ge-Ge bond on the *z* axis. Express the hybrid orbitals as linear combinations of the *p* and *s* AOs and calculate the coefficients. Use these values to calculate *n*.

P13.12 *s-p* hybridization on each Ge atom in planar *trans*-digermane has been described as *sp*^{1.5} for the Ge—Ge sigma bond and *sp*^{1.8} for the Ge—H bond. Calculate the H—Ge—Ge bond angle based on this information. Note that the *4p_x* and *4p_y* orbitals are proportional to $\cos \theta$ and $\sin \theta$, respectively, and use the coefficients determined in P13.11 to solve this problem.

Section 13.5

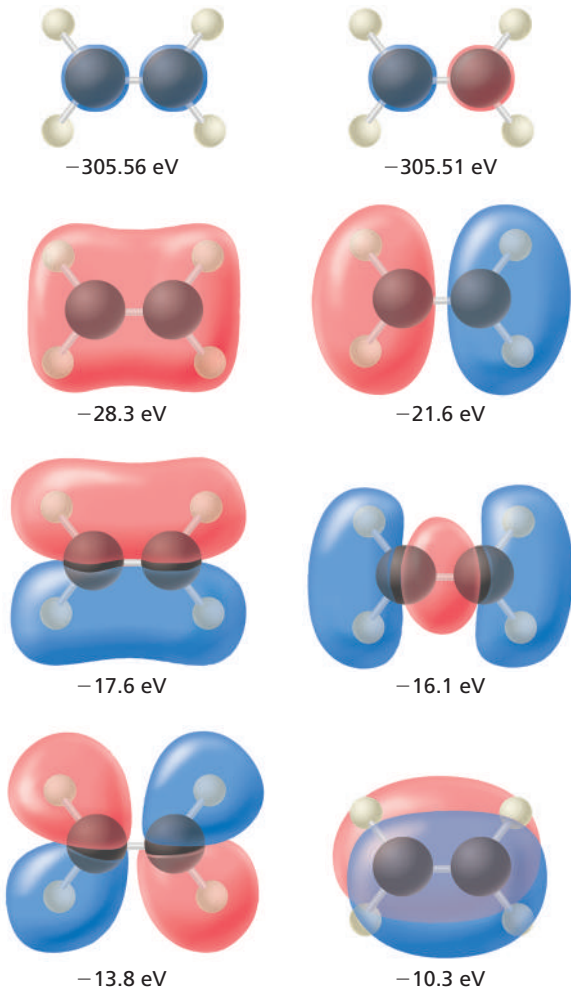
P13.13 Predict which of the bent molecules, BH₂ or NH₂, should have the larger bond angle on the basis of the Walsh correlation diagram in Figure 13.11. Explain your answer.

P13.14 The occupied MOs and MO energies of ammonia are shown in the accompanying figure. Indicate which AOs are most important for each MO and indicate the relative phases of the AOs. Classify the MOs as localized or delocalized, and bonding, nonbonding, or antibonding.

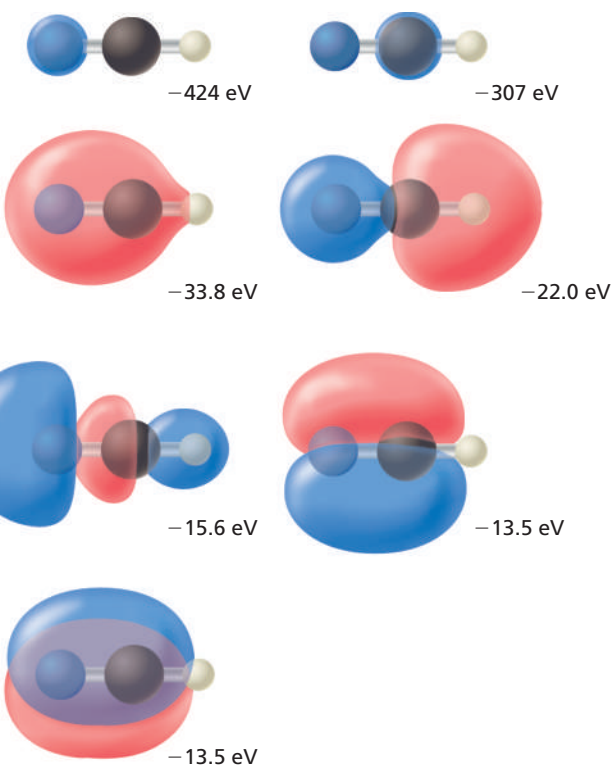


P13.15 Predict whether the ground state or the first excited state of CH_2 should have the larger bond angle on the basis of the Walsh correlation diagram shown in Figure 13.11. Explain your answer.

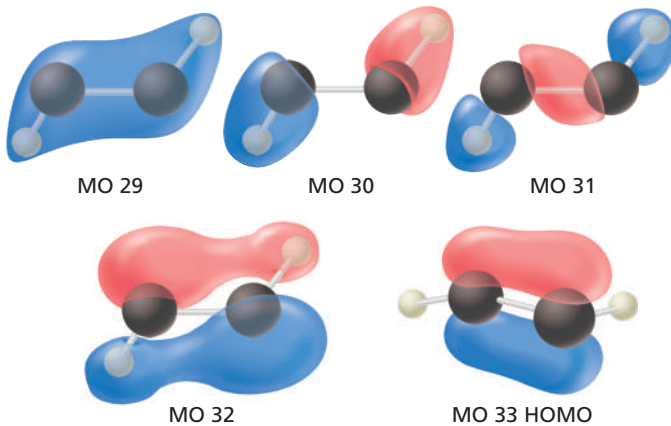
P13.16 The occupied MOs and MO energies of ethene are shown in the accompanying figure. Indicate which AOs are most important in each MO and indicate the relative phases of the AOs. Classify the MOs as localized or delocalized, σ or π bonds, and bonding, nonbonding, or antibonding.



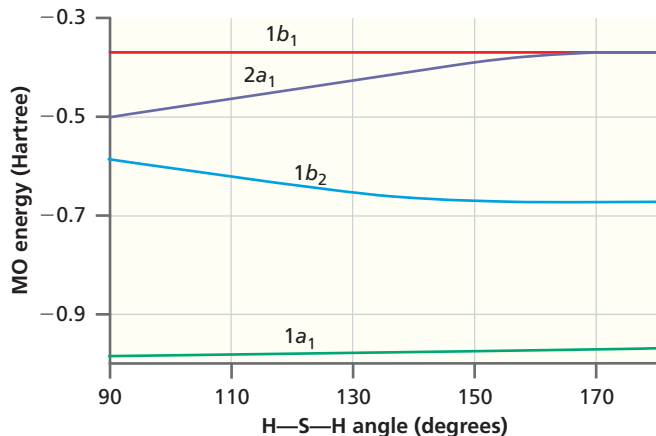
P13.17 The occupied MOs and MO energies of hydrogen cyanide are shown in the accompanying figure in the right column. Indicate which AOs are most important in each MO and indicate the relative phases of the AOs. Classify the MOs as localized or delocalized, σ or π bonds, and bonding, nonbonding, or antibonding.



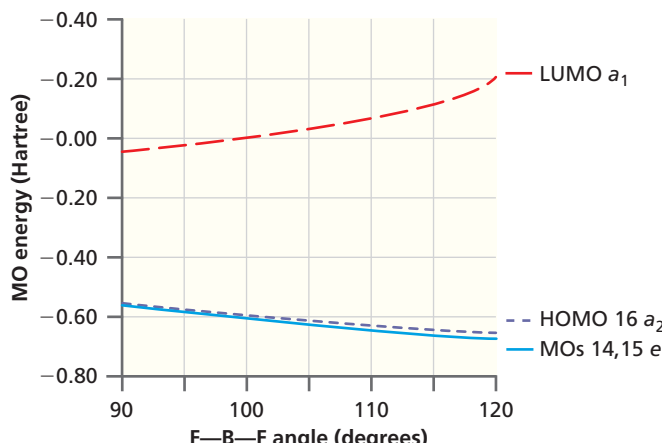
P13.18 One of the low-energy structures of digermane, Ge_2H_2 , is ethene-like. The accompanying Lewis-dot structure is one of three Lewis-dot resonant forms. The order of the $\text{Ge}—\text{Ge}$ bond has been described as numerically between two and three. A bond order greater than two relies on the lone electrons participating in bonding. The five highest-energy occupied valence molecular orbitals are shown below. Classify the MOs as localized or delocalized, σ or π bonds, and bonding, nonbonding, or antibonding.



P13.19 The energy of the occupied valence MOs of H₂S is shown in the accompanying figure as a function of the H—S—H bond angle. Compare this diagram to the analogous diagram, Figure 13.11, for H₂O. Explain, based on the MO diagram, why H₂S is bent and why its bond angle (92°) is smaller than the bond angle in water. For comparison, also offer a bond-angle explanation based on hybridization rather than on the MO diagram.



P13.20 The diagram below shows the energies of valence molecular orbitals of boron trifluoride. The energies of three occupied orbitals (the a_2 HOMO and doubly degenerate e orbitals) are shown. The energy of the unoccupied LUMO is also shown. The angle on the abscissa is the F—B—F bond angle. Based on the MO diagram, is boron trifluoride planar or pyramidal? Which structure does the VSEPR model predict?



P13.21 Predict whether LiH₂⁺ and NH₂[−] should be linear or bent based on the Walsh correlation diagram in Figure 13.11. Explain your answers.

Section 13.6

P13.22 Show that the determinantal property

$$\begin{vmatrix} a & c \\ b & d \end{vmatrix} = \begin{vmatrix} a & \gamma a + c \\ b & \gamma b + d \end{vmatrix}$$

used in the discussion of localized and delocalized orbitals in Section 13.6 is correct.

P13.23 Are the localized bonding orbitals in Equation (13.13) defined by

$$\sigma' = 2c_1\phi_{H1sA} + \left(c_2\phi_{Be2s} - \frac{c_1c_4}{c_3}\phi_{Be2p_z} \right) \text{ and}$$

$$\sigma'' = 2c_1\phi_{H1sB} + \left(c_2\phi_{Be2s} + \frac{c_1c_4}{c_3}\phi_{Be2p_z} \right)$$

orthogonal? Answer this question by evaluating the integral $\int (\sigma')^* \sigma'' d\tau$.

Section 13.8

P13.24 Use the geometrical construction shown in Example Problem 13.8 to derive the π electron MO levels for cyclobutadiene. What is the total π energy of the molecule? How many unpaired electrons will the molecule have?

P13.25 Determine the AO coefficients for the lowest energy Hückel π MO for butadiene.

P13.26 Use the geometrical construction shown in Example Problem 13.8 to derive the π electron MO levels for the cyclopentadienyl radical. What is the total π energy of the molecule? How many unpaired electrons will the molecule have?

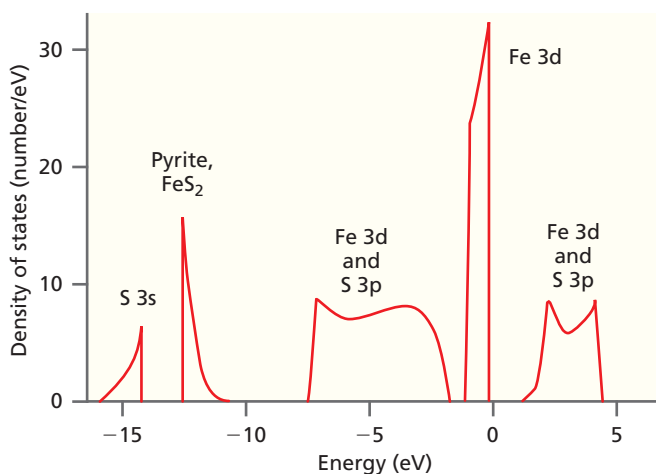
P13.27 The allyl cation CH₂=CH—CH₂⁺ has a delocalized π network that can be described by the Hückel method. Derive the MO energy levels of this species and place the electrons in the levels appropriate for the ground state. Using the butadiene MOs as an example, sketch what you would expect the MOs to look like. Classify the MOs as bonding, antibonding, or nonbonding.

P13.28 Write down and solve the secular determinant for the π system of ethylene in the Hückel model. Determine the coefficients for the $2p_z$ AOs on each of the carbons and make a sketch of the MOs. Characterize the MOs as bonding and antibonding.

P13.29 Use the geometrical construction shown in Example Problem 13.8 to derive the energy levels of the cycloheptatrienyl cation. What is the total π energy of the molecule? How many unpaired electrons will the molecule have? Would you expect this species, the neutral species, or the anion to be aromatic? Justify your answer.

Section 13.9

P13.30 The density of states (DOS) of pyrite, crystalline FeS₂, as calculated by Eyert et al., *Physical Review B* 55 (1998): 6350 is shown below. The highest occupied energy level corresponds to zero energy. Based on the DOS, is pyrite an insulator, a conductor, or a semiconductor? The melting point of pyrite is 1444 K. Also, how does the DOS support the localized-bonding view that some iron valence orbitals are nonbonding?



COMPUTATIONAL PROBLEMS

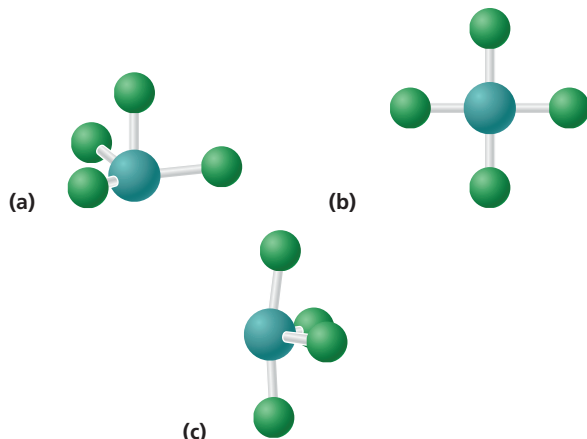
More detailed instructions on carrying out these calculations using Spartan Physical Chemistry are found at:
<https://www.pearsonhighered.com/chemistryresources/>

C13.1 Calculate the bond angles in NH_3 and in NF_3 using the density functional method with the B3LYP functional and the 6-31G* basis set. Compare your result with literature values. Do your results agree with the predictions of the VSEPR model and Bent's rule?

C13.2 Calculate the bond angles in H_2O and in H_2S using the density functional method with the B3LYP functional and the 6-31G* basis set. Compare your result with literature values. Do your results agree with the predictions of the VSEPR model and Bent's rule?

C13.3 Calculate the bond angle in ClO_2 using the density functional method with the B3LYP functional and the 6-31G* basis set. Compare your result with literature values. Does your result agree with the predictions of the VSEPR model?

C13.4 SiF_4 has four ligands and one lone pair on the central S atom. Which of the following structures do you expect to be the equilibrium form based on a calculation using the density functional method with the B3LYP functional and the 6-31G* basis set? In (a) the structure is a trigonal bipyramidal, (b) is a square planar structure, and (c) is a see-saw structure.



Section 13.10

P13.31 Use the Boltzmann distribution to answer parts (a) and (b):

- Calculate the ratio of electrons at the bottom of the conduction band to those at the top of the valence band for pure Si at 300. K. The Si band gap is 1.1 eV.
- Calculate the ratio of electrons at the bottom of the conduction band to those at the top of the dopant band for P-doped Si at 300. K. The top of the dopant band lies 0.040 eV below the bottom of the Si conduction band.

C13.5 Calculate the bond angles in singlet BeH_2 , doublet NH_2 , and singlet BH_2 using the Hartree–Fock method and the 6-31G* basis set. Explain your results using the Walsh diagram of Figure 13.11.

C13.6 Calculate the bond angle in singlet LiH_2^+ using the Hartree–Fock method and the 6-31G* basis set. Can you explain your results using the Walsh diagram of Figure 13.11? (Hint: Determine the calculated bond lengths in the LiH_2^+ molecule.)

C13.7 Calculate the bond angle in singlet and triplet CH_2 and doublet CH_2^+ using the Hartree–Fock method and the 6-31G* basis set. Can you explain your results using the Walsh diagram of Figure 13.11?

C13.8 Calculate the bond angle in singlet NH_2^+ , doublet NH_2 , and singlet NH_2^- using the Hartree–Fock method and the 6-31G* basis set. Can you explain your results using the Walsh diagram of Figure 13.11?

C13.9 How essential is coplanarity to conjugation? Answer this question by calculating the total energy of butadiene using the Hartree–Fock method and the 6-31G* basis set for dihedral angles of 0, 45, and 90 degrees. Calculate the energy difference in kJ mol^{-1} between planar 1,3-butadiene and the two twisted structures. Which costs more energy, rotation by 45° around the C1-C2 or the C2-C3 bond? Why?

C13.10 Calculate the equilibrium structures for singlet and triplet formaldehyde using the density functional method with the B3LYP functional and the 6-311 + G** basis set. Choose (a) planar and (b) pyramidal starting geometries. Calculate vibrational frequencies for both starting geometries. Are any of the frequencies imaginary? Explain your results.

C13.11 Calculate the equilibrium structure for Cl_2O using the density functional method with the B3LYP functional and the 6-31G* basis set. Obtain an infrared spectrum and activate the normal modes. What are the frequencies corresponding to the symmetric stretch, the asymmetric stretch, and the bending modes?

C13.12 Calculate the equilibrium structures for PF_3 using the density functional method with the B3LYP functional and the 6-31G* basis set. Obtain an infrared spectrum and activate the normal modes. What are the frequencies corresponding to the symmetric stretch, the symmetric deformation, the degenerate stretch, and the degenerate deformation modes?

C13.13 Calculate the equilibrium structures for C_2H_2 using the density functional method with the B3LYP functional and the 6-31G* basis set. Obtain an infrared spectrum and activate the normal modes. What are the frequencies corresponding to the symmetric C—H stretch, the antisymmetric C—H stretch, the C—C stretch, and the two bending modes?

C13.14 Calculate the structure of $\text{N}\equiv\text{C}-\text{Cl}$ using the density functional method with the B3LYP functional and the 6-31G* basis set. Which is more electronegative, the Cl or the cyanide group? What result of the calculation did you use to answer this question?

FURTHER READING

Gillespie, R. “Teaching Geometry with the VSEPR Model.” *Journal of Chemical Education* 81 (2004): 298–304.

Lindmark, A. “Who Needs Lewis Structures to Get VSEPR Geometries?” *Journal of Chemical Education* 87 (2010): 487–491.

Pisanty, A. “The Electronic Structure of Graphite: A Chemist’s Introduction to Band Theory.” *Journal of Chemical Education* 68 (1991): 804–808.

Repp, J., Meyer, G., Stojkovic, S., Gourdon, A., and Joachim, C. “Molecules on Insulating Films: Scanning-Tunneling

Microscopy Imaging of Individual Molecular Orbitals.” *Physical Review Letters* 94, no. 2 (2005) 026803-1–026803-4.

Root, D. M., Landis, C., and Cleveland, T. “Valence Bond Concepts Applied to the Molecular Mechanics Description of Molecular Shapes. 1. Application to Nonhypervalent Molecules of the P-Block.” *Journal of the American Chemical Society* 115 (1993): 4201–4209.

Electronic Spectroscopy

Why is this material important?

Electronic spectroscopy involves visible and UV photon absorption and emission. Such large energy changes in a molecule can lead to changes in the structure and chemical reactivity of the molecules. Electronic spectroscopy is used to identify molecules, to determine small concentrations of chemical impurities in drinking water, to probe the dynamics of biomolecules in solution, and to study the folding of biomolecules.

What are the most important concepts and results?

The only strong selection rule in electron spectroscopy is $\Delta S = 0$. A molecule can have a number of excited singlet and triplet states. Vibrational transitions that occur together with electronic transitions are governed by the Franck–Condon factors rather than the $\Delta n = \pm 1$ dipole selection rule. The excited state can relax to the ground state through a combination of fluorescence, internal conversion, intersystem crossing, and phosphorescence. Fluorescence is very useful in analytical chemistry and can be used to detect as little as 2×10^{-13} mol/L of a strongly fluorescing species. Ultraviolet photoemission can be used to obtain information about the orbital energies of molecules. Linear and circular dichroism spectroscopy can be used to determine the secondary and tertiary structure of biomolecules in solution.

What would be helpful for you to review for this chapter?

It would be helpful to review the material in Chapter 8 on the absorption of light.

14.1 THE ENERGY OF ELECTRONIC TRANSITIONS

In Chapter 8, spectroscopy and the basic concepts relevant to transitions between energy levels of a molecule were introduced. Recall that the energy spacing between rotational levels is much smaller than the spacing between vibrational levels. Extending this comparison to electronic states, $\Delta E_{\text{electronic}} \gg \Delta E_{\text{vibrational}} \gg \Delta E_{\text{rotational}}$. Whereas rotational and vibrational transitions are induced by microwave and infrared radiation, electronic transitions are induced by visible and ultraviolet (UV) radiation. Just as an absorption spectrum in the infrared exhibits both rotational and vibrational transitions, an absorption spectrum in the visible and UV range exhibits a number of electronic transitions, and a specific electronic transition will include vibrational and rotational fine structure.

Electronic excitations are responsible for giving color to the objects we observe because the human eye is sensitive to light only in the limited range of wavelengths in which some electronic transitions occur. Reflected light is observed if an object is opaque and transmitted light is observed if an object is transparent. Transmitted and reflected light complement the absorbed light. For example, a leaf is green because chlorophyll absorbs in the blue (450 nm) and red (650 nm) regions of the visible light spectrum.

- 14.1 The Energy of Electronic Transitions
- 14.2 Molecular Term Symbols
- 14.3 Transitions between Electronic States of Diatomic Molecules
- 14.4 The Vibrational Fine Structure of Electronic Transitions in Diatomic Molecules
- 14.5 UV-Visible Light Absorption in Polyatomic Molecules
- 14.6 Transitions among the Ground and Excited States
- 14.7 Singlet–Singlet Transitions: Absorption and Fluorescence
- 14.8 Intersystem Crossing and Phosphorescence
- 14.9 Fluorescence Spectroscopy and Analytical Chemistry
- 14.10 Ultraviolet Photoelectron Spectroscopy
- 14.11 Single-Molecule Spectroscopy
- 14.12 Fluorescent Resonance Energy Transfer
- 14.13 Linear and Circular Dichroism
- 14.14 (Supplemental Section)
Assigning + and – to Σ Terms of Diatomic Molecules

Electronic excitations can be detected (at a limited resolution) without the aid of a spectrometer because the human eye is a very sensitive detector of radiation. At a wavelength of 500 nm, the human eye can detect light intensity that is lower than sunlight on a bright day by a factor of 10^6 . This sensitivity corresponds to as few as 500 photons per second incident on an area of 1 mm².

Because the electronic spectroscopy of a molecule is directly related to its energy levels, which are in turn determined by its structure and chemical composition, UV-visible spectroscopy provides a useful qualitative tool for identifying molecules. In addition, for a given molecule, electronic spectroscopy can be used to determine electron energy levels in molecules. However, the UV and visible photons that initiate an electronic excitation perturb a molecule far more than rotational or vibrational excitation. For example, the bond length in electronically excited states of O₂ is as much as 30% longer than that in the ground state. Whereas in its ground state, formaldehyde is a planar molecule, it is pyramidal in its lowest two excited states. As might be expected from such changes in structure, the chemical reactivity of excited-state species can be quite different from the reactivity of the ground state molecule.

14.2 MOLECULAR TERM SYMBOLS

We begin our discussion of electronic excitations by introducing **molecular term** symbols, which describe the electronic states of molecules in the same way that atomic term symbols describe atomic electronic states. The following discussion is restricted to diatomic molecules. Although a quantitative discussion of electronic spectroscopy requires knowledge of molecular term symbols, electronic spectroscopy can be discussed at a qualitative level without discussing molecular term symbols. To do so, move directly to Section 14.4.

Concept

The component of **L** and **S** along the molecular axis and **S** are the only good quantum numbers to specify individual states for diatomic molecules.

The component of **L** and **S** along the molecular axis (M_L and M_S), which is chosen to be the *z* axis, and **S** are the only good quantum numbers (see Section 11.1) by which to specify individual states in diatomic molecules. Therefore, term symbols for molecules are defined using these quantities. As for atoms, only unfilled subshells need to be considered to obtain molecular term symbols. Just as for atoms, the quantum numbers m_{li} and m_{si} can be added to generate M_L and M_S for the molecule because they are scalars rather than vectors. The addition process is described by the equations

$$M_L = \sum_{i=1}^n m_{li} \quad \text{and} \quad M_S = \sum_{i=1}^n m_{si} \quad (14.1)$$

in which m_{li} and m_{si} are the *z* components of orbital and spin angular momentum for the *i*th electron in its molecular orbital and the summation is over unfilled subshells. As discussed in Chapter 12, the molecular orbitals of diatomic molecules have either σ symmetry, in which the orbital is unchanged by rotation around the molecular axis, or π symmetry, in which the MO has a nodal plane passing through the molecular axis. For a σ orbital, $m_l = 0$, whereas for a π orbital, $m_l = \pm 1$. Note that the $m_l = 0$ value does not occur for a π MO because this value corresponds to the $2p_z$ AO, which forms a σ MO. M_S is calculated from the individual spin angular momentum vector components $m_{si} = \pm 1/2$ in the same way for molecules as for atoms (see Chapter 11). The allowed values of the quantum numbers S and L can be calculated from $-L \leq M_L \leq L$ and $-S \leq M_S \leq S$ to generate a molecular term symbol of the form $^{2S+1}\Lambda$, where $\Lambda = |M_L|$. For molecules, the following symbols are used for different Λ values to avoid confusion with atomic terms:

Λ	0	1	2	3	
Symbol	Σ	Π	Δ	Φ	(14.2)

Concept

Different symbols are used to designate atomic and molecular terms.

A *g* or *u* right subscript is added to the molecular term symbol for homonuclear diatomic molecules as illustrated in Example Problem 14.1. Because heteronuclear diatomic molecules do not possess an inversion center, they do not have *g* or *u* symmetry. This formalism will become clearer with a few examples.

EXAMPLE PROBLEM 14.1

What is the molecular term symbol for the H₂ molecule in its ground state? In its first two excited states?

Solution

In the ground state, the H₂ molecule is described by the (1σ_g)² configuration. For both electrons, $m_l = 0$. Therefore, $\Lambda = 0$, and we are dealing with a Σ term. Because of the Pauli principle, one electron has $m_s = +1/2$ and the other has $m_s = -1/2$. Therefore, $M_S = 0$, and it follows that $S = 0$. It remains to be determined whether the MO has *g* or *u* symmetry. Each term in the antisymmetrized MO is of the form $\sigma_g \times \sigma_g$ (see Section 12.6). Recall that the products of two even or odd functions is even, and the product of an odd and an even function is odd. Therefore, the product of two *g* functions is a *g* function, and the ground state of the H₂ molecule is ${}^1\Sigma_g$.

After promotion of an electron, the configuration is (1σ_g)¹(1σ_u^{*})¹, and because the electrons are in separate MOs, this configuration leads to both **singlet states** and **triplet states**. Again, because $m_l = 0$ for both electrons, we are dealing with a Σ term. Because the two electrons are in different MOs, $m_s = \pm 1/2$ for each electron, giving m_s values of $-1/2$, 0 (twice), and $+1/2$. This is consistent with $S = 1$ and $S = 0$. Because the product of a *u* and a *g* function is a *u* function, both singlet and triplet states are *u* functions. Therefore, the first two excited states are described by the terms ${}^3\Sigma_u$ and ${}^1\Sigma_u$. Using Hund's first rule, we conclude that the triplet state is lower in energy than the singlet state.

In a more complete description, an additional superscript + or - is added to Σ terms only, depending on whether the antisymmetrized molecular wave function changes sign (-) or remains unchanged (+) in a reflection through any plane containing the molecular axis. The assignment of + or - to the terms is an advanced topic that is discussed in Supplemental Section 14.14. For our purposes, the following guidelines are sufficient for considering the ground state of second-row homonuclear diatomic molecules:

- If all MOs are filled, + applies.
- If all partially filled MOs have σ symmetry, + applies.
- For partially filled MOs of π symmetry (for example, B₂ and O₂), if Σ terms arise, the triplet state is associated with -, and the singlet state is associated with +.

These guidelines do not apply to excited states. We conclude that the term corresponding to the (π^{*})² ground state configuration of O₂ (see Figure 12.18) is designated by ${}^3\Sigma_g^-$. The other terms that arise from the ground state configuration are discussed in Example Problem 14.2.

EXAMPLE PROBLEM 14.2

Determine the possible molecular terms for O₂, which has the following configuration: (1σ_g)²(1σ_u^{*})²(2σ_g)²(2σ_u^{*})²(3σ_g)²(1π_u)²(1π_u^{*})²(1π_g^{*})¹

Solution

Only the last two electrons contribute to nonzero net values of M_L and M_S because the other subshells are filled. The various possibilities for combining the orbital and spin angular momenta of these two electrons in a way consistent with the Pauli principle are given in the following table. The Λ values are determined as discussed for atomic terms in Chapter 11. Because $M_L \leq L$, the first two entries in the table belong to a Δ term. Because $M_S = 0$ for both entries, it is a ${}^1\Delta$ term. Of the remaining four entries, two have $|M_S| = 1$, corresponding to a triplet term. One of the two other entries with $M_S = 0$ must also belong to this term. Because $M_L = 0$ for all four entries, it is a ${}^3\Sigma$ term. The remaining entry corresponds to a ${}^1\Sigma$ term.

m_{l1}	m_{l2}	$M_L = m_{l1} + m_{l2}$	m_{s1}	m_{s2}	$M_S = m_{s1} + m_{s2}$	Term
1	1	2	+1/2	-1/2	0	$\left. \right\} {}^1\Delta$
-1	-1	-2	+1/2	-1/2	0	
1	-1	0	+1/2	+1/2	1	$\left. \right\} {}^3\Sigma$
1	-1	0	-1/2	-1/2	-1	
1	-1	0	+1/2	-1/2	0	$\left. \right\} {}^1\Sigma, {}^3\Sigma$
1	-1	0	-1/2	+1/2	0	

The next task is the assignment of the *g* or *u* label to these molecular terms. Because both of the electrons are in an MO of *g* symmetry, the overall symmetry of the term will be *g* in all cases.

The + and - symbols are assigned in Supplemental Section 14.14. There we will show that the singlet term is ${}^1\Sigma_g^+$ and the triplet term is ${}^3\Sigma_g^-$. By Hund's first rule, the ${}^3\Sigma_g^-$ term is lowest in energy and is the ground state. Experimentally, the ${}^1\Delta_g$ and ${}^1\Sigma_g^+$ terms are found to lie 0.98 and 1.62 eV higher in energy, respectively, than the ground state.

In terms of arrows indicating the spin orientations, the allowed combinations of m_l and m_s in the table can be represented in a shorthand notation by

$$\begin{aligned}
 & (1\sigma_g)^2 (1\sigma_u^*)^2 (2\sigma_g)^2 (2\sigma_u^*)^2 (3\sigma_g)^2 (1\pi_u)^2 (1\pi_u^*)^2 (1\pi_g^*)^1 (1\pi_g)^1 \\
 & (\uparrow\downarrow) (\uparrow\downarrow) (\uparrow\downarrow) (\uparrow\downarrow) (\uparrow\downarrow) (\uparrow\downarrow) (\uparrow\downarrow) (\uparrow) (\downarrow) \quad {}^1\Sigma_g^+, {}^1\Delta_g \\
 & \left. \left[\begin{array}{cccccccccc} (1\sigma_g)^2 (1\sigma_u^*)^2 (2\sigma_g)^2 (2\sigma_u^*)^2 (3\sigma_g)^2 (1\pi_u)^2 (1\pi_u^*)^2 (1\pi_g^*)^1 (1\pi_g)^1 \\ (\uparrow\downarrow) (\uparrow\downarrow) (\uparrow\downarrow) (\uparrow\downarrow) (\uparrow\downarrow) (\uparrow\downarrow) (\uparrow\downarrow) (\uparrow) (\uparrow) \\ (\uparrow\downarrow) (\uparrow\downarrow) (\uparrow\downarrow) (\uparrow\downarrow) (\uparrow\downarrow) (\uparrow\downarrow) (\uparrow\downarrow) (\uparrow) (\downarrow) \\ + \\ (\uparrow\downarrow) (\uparrow\downarrow) (\uparrow\downarrow) (\uparrow\downarrow) (\uparrow\downarrow) (\uparrow\downarrow) (\uparrow\downarrow) (\downarrow) (\uparrow) \\ (\uparrow\downarrow) (\uparrow\downarrow) (\uparrow\downarrow) (\uparrow\downarrow) (\uparrow\downarrow) (\uparrow\downarrow) (\uparrow\downarrow) (\downarrow) (\downarrow) \end{array} \right] \right\} {}^3\Sigma_g^-
 \end{aligned}$$

Note that this notation with arrows pointing up and down to indicate α and β spins is inadequate because it is not possible to represent the different values of m_{l1} and m_{l2} .

Concept

A molecular configuration specifies which molecular orbitals are occupied.

On the basis of this discussion, the **molecular configuration** and the ground state terms for the first-row homonuclear diatomic molecules are listed in Table 14.1. The procedure for heteronuclear diatomic molecules is similar, but it differs in that the numbering of the MOs is different and the *g* and *u* symmetries do not apply.

TABLE 14.1 Terms for Ground State Second-Row Diatomic Molecules

Molecule	Electron Configuration	Ground State Term
H_2^+	$(1\sigma_g)^1$	${}^2\Sigma_g^+$
H_2	$(1\sigma_g)^2$	${}^1\Sigma_g^+$
He_2^+	$(1\sigma_g)^2 (1\sigma_u^*)^1$	${}^2\Sigma_u^+$
Li_2	$(1\sigma_g)^2 (1\sigma_u^*)^2 (2\sigma_g)^2$	${}^1\Sigma_g^+$
B_2	$(1\sigma_g)^2 (1\sigma_u^*)^2 (2\sigma_g)^2 (2\sigma_u^*)^2 (1\pi_u)^1 (1\pi_u^*)^1$	${}^3\Sigma_g^-$
C_2	$(1\sigma_g)^2 (1\sigma_u^*)^2 (2\sigma_g)^2 (2\sigma_u^*)^2 (1\pi_u)^2 (1\pi_u^*)^2$	${}^1\Sigma_g^+$
N_2^+	$(1\sigma_g)^2 (1\sigma_u^*)^2 (2\sigma_g)^2 (2\sigma_u^*)^2 (1\pi_u)^2 (1\pi_u^*)^2 (3\sigma_g)^1$	${}^2\Sigma_g^+$
N_2	$(1\sigma_g)^2 (1\sigma_u^*)^2 (2\sigma_g)^2 (2\sigma_u^*)^2 (1\pi_u)^2 (1\pi_u^*)^2 (3\sigma_g)^2$	${}^1\Sigma_g^+$
O_2^+	$(1\sigma_g)^2 (1\sigma_u^*)^2 (2\sigma_g)^2 (2\sigma_u^*)^2 (3\sigma_g)^2 (1\pi_u)^2 (1\pi_u^*)^2 (1\pi_g^*)^1$	${}^2\Pi_g$
O_2	$(1\sigma_g)^2 (1\sigma_u^*)^2 (2\sigma_g)^2 (2\sigma_u^*)^2 (3\sigma_g)^2 (1\pi_u)^2 (1\pi_u^*)^2 (1\pi_g^*)^1 (1\pi_g^*)^1$	${}^3\Sigma_g^-$
F_2	$(1\sigma_g)^2 (1\sigma_u^*)^2 (2\sigma_g)^2 (2\sigma_u^*)^2 (3\sigma_g)^2 (1\pi_u)^2 (1\pi_u^*)^2 (1\pi_g^*)^2$	${}^1\Sigma_g^+$

14.3 TRANSITIONS BETWEEN ELECTRONIC STATES OF DIATOMIC MOLECULES

Diatom molecules have the most easily interpretable electronic spectra because the spacing between the various rotational-vibrational-electronic states is sufficiently large to allow individual states to be resolved. Potential energy curves for the five lowest lying bound states of O₂ are shown in Figure 14.1. Vibrational energy levels are indicated schematically in the figure, but rotational levels are not shown. Note that the lowest four states all dissociate to give two ground state ³P oxygen atoms, whereas the highest energy state shown dissociates to give one ³P and one ¹D oxygen atom. The letter X before ³ Σ_g^- indicates that the term symbol refers to the ground state. Electronic states of higher energy are designated by A, B, C, . . . if they have the same multiplicity, $2S + 1$, as the ground state, and a, b, c, . . . if they have a different multiplicity.

The bond length of excited-state molecules is generally greater and the binding energy generally less than that for the ground state. This is the case because the excited states generally have a greater antibonding character than the ground states. The decrease in bond order leads to a smaller bond energy, a larger bond length, and a lower vibrational frequency for the excited-state species. You will address the fact that the bond lengths for the first two excited states are similar to that for the ground state in the end-of-chapter questions.

Although a symbol such as ³ Σ_g^- completely describes the quantum state for a ground state O₂ molecule, it is also useful to associate a molecular configuration with the state. Starting with a configuration makes it easier to visualize a transition in terms of promoting an electron from an occupied to an unoccupied level. To what configurations do the excited states shown in Figure 14.1 correspond? The $X^3\Sigma_g^-$, $a^1\Delta_g$, and $b^1\Sigma_g^+$ states all belong to the ground state configuration $(1\sigma_g)^2(1\sigma_u^*)^2(2\sigma_g)^2(2\sigma_u^*)^2(3\sigma_g)^2(1\pi_u)^2(1\pi_u^*)^1(1\pi_g^*)^1$ but are associated with different M_L and M_S values as was shown in Example Problem 14.2. The $A^3\Sigma_u^+$ and $B^3\Sigma_u^-$ states are associated with the $(1\sigma_g)^2(1\sigma_u^*)^2(2\sigma_g)^2(2\sigma_u^*)^2(3\sigma_g)^2(1\pi_u)^1(1\pi_u^*)^2(1\pi_g^*)^2$ configuration. Keep in mind that although a molecular term can be associated with a configuration, in general, several molecular terms are generated from the same configuration.

Spectroscopy involves transitions between molecular states. What selection rules govern transitions between different electronic states? The selection rules for molecular electronic transitions are most well defined for lower molecular weight diatomic molecules in which spin-orbit coupling is not important. This is the case if the atomic number of the atoms, Z, is less than 40. For these molecules, the selection rules are

$$\Delta\Lambda = 0 \text{ or } \pm 1, \text{ and } \Delta S = 0 \quad (14.3)$$

Recall that Λ is the component of the total orbital angular momentum \mathbf{L} along the molecular axis. The value $\Delta\Lambda = 0$ applies to a $\Sigma \leftrightarrow \Sigma$ transition, and $\Delta\Lambda = \pm 1$ applies to $\Sigma \leftrightarrow \Pi$ transitions. Further selection rules are associated with the $+/-$ and g/u parities. For homonuclear diatomic molecules, $u \leftrightarrow g$ transitions are allowed, but $u \leftrightarrow u$ and $g \leftrightarrow g$ transitions are forbidden. The transitions $\Sigma^- \leftrightarrow \Sigma^-$ and $\Sigma^+ \leftrightarrow \Sigma^+$ are allowed, but $\Sigma^+ \leftrightarrow \Sigma^-$ transitions are forbidden. All of these selection rules can be derived by calculating the transition dipole element defined in Section 8.5.

With these selection rules in mind, we consider the possible transitions among the states shown in Figure 14.1 for O₂. The $X^3\Sigma_g^- \rightarrow a^1\Delta_g$ and $X^3\Sigma_g^- \rightarrow b^1\Sigma_g^+$ transitions are forbidden because of the $\Delta S = 0$ selection rule and because $g \leftrightarrow g$ transitions are forbidden. The $X^3\Sigma_g^- \rightarrow A^3\Sigma_u^+$ transition is forbidden because $\Sigma^+ \leftrightarrow \Sigma^-$ transitions are forbidden. Therefore, the lowest allowed transition originating from the ground state is $X^3\Sigma_g^- \rightarrow B^3\Sigma_u^-$. Absorption from the ground state into various vibrational levels of the $B^3\Sigma_u^-$ excited state occurs in a band between 175 and 200 nm wavelengths. An interesting consequence of these selection rules is that if transitions from the ground state to the first two excited states were allowed, O₂ would absorb light in the visible part of the spectrum, and Earth's atmosphere would not be transparent.

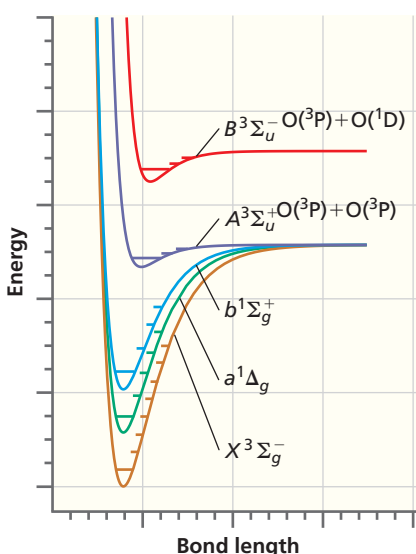


Figure 14.1

Potential energy curves for the ground state of O₂ and for the four lowest excited states. The spectroscopic designation of the states is explained in the text. Horizontal lines in the potential energy curves schematically indicate vibrational levels for each state.

Concept

The main selection rules for electronic transitions in light diatomic molecules are $\Delta\Lambda = 0$ or ± 1 , and $\Delta S = 0$.

If sufficient energy is taken up by the molecule, dissociation can occur through the pathway



The maximum wavelength consistent with this reaction is 242 nm. This reaction is an example of a **photodissociation** reaction. This particular reaction is of great importance in the stratosphere because it is the only significant pathway for forming the atomic oxygen needed for ozone production through the reaction



where M designates a gas-phase spectator species that absorbs the energy released in the O_3 formation reaction. Because O_3 absorbs UV radiation strongly in the 220 to 350 nm range, it plays a vital role in filtering out UV radiation from the sunlight incident on the planet. The ozone layer, located in the stratosphere 10–50 km above Earth’s surface, absorbs 97–99% of the high-frequency ultraviolet solar light, which is light that is potentially damaging to life on Earth.

14.4 THE VIBRATIONAL FINE STRUCTURE OF ELECTRONIC TRANSITIONS IN DIATOMIC MOLECULES

Each of the molecular bound states shown in Figure 14.1 has well-defined vibrational and rotational energy levels. As discussed in Chapter 8, changes in the vibrational state can occur together with a change in the rotational state. Similarly, the vibrational and rotational quantum numbers can change during electronic excitation. We next discuss the vibrational excitation and de-excitation associated with electronic transitions but do not discuss the associated rotational transitions. We will see that the $\Delta n = \pm 1$ selection rule for vibrational transitions within a given electronic state does not hold for transitions between two electronic states.

What determines Δn in a vibrational transition between electronic states? This question can be answered by looking more closely at the **Born–Oppenheimer approximation**, which was introduced in Chapter 12. This approximation states that the total wave function for the molecule can be factored into two parts. The part that depends only on the position of the nuclei ($\mathbf{R}_1, \dots, \mathbf{R}_m$) is associated with vibration of the molecule. The second part depends only on the position of the electrons ($\mathbf{r}_1, \dots, \mathbf{r}_n$) at a fixed position of all the nuclei. This part describes electron “motion” in the molecule:

$$\begin{aligned} \psi(\mathbf{r}_1, \dots, \mathbf{r}_n, \mathbf{R}_1, \dots, \mathbf{R}_m) &= \psi^{\text{electronic}}(\mathbf{r}_1, \dots, \mathbf{r}_n, \mathbf{R}_1^{\text{fixed}}, \dots, \mathbf{R}_m^{\text{fixed}}) \\ &\times \phi^{\text{vibrational}}(\mathbf{R}_1, \dots, \mathbf{R}_m) \end{aligned} \quad (14.6)$$

As discussed in Section 8.5, the spectral line corresponding to an electronic and vibrational transition (initial \rightarrow final) has a measurable intensity only if the value of the transition dipole moment is different from zero:

$$\mu^{\text{fi}} = \int \psi_f^*(\mathbf{r}_1, \dots, \mathbf{r}_n, \mathbf{R}_1, \dots, \mathbf{R}_m) \hat{\mu} \psi_i(\mathbf{r}_1, \dots, \mathbf{r}_n, \mathbf{R}_1, \dots, \mathbf{R}_m) d\tau \neq 0 \quad (14.7)$$

The superscripts and subscripts f and i refer to the final and initial states in the transition. In Equation (14.7), the dipole moment operator $\hat{\mu}$ is given by

$$\hat{\mu} = -e \sum_{j=1}^n \mathbf{r}_j \quad (14.8)$$

where the summation is over the positions of the electrons.

Because the total wave function can be written as a product of electronic and vibrational parts, Equation (14.7) becomes

$$\begin{aligned}\mu^{fi} &= \int (\phi_f^{vibrational}(\mathbf{R}_1, \dots, \mathbf{R}_m))^* \phi_i^{vibrational}(\mathbf{R}_1, \dots, \mathbf{R}_m) d\tau \\ &\quad \times \int (\psi_f^{electronic}(\mathbf{r}_1, \dots, \mathbf{r}_n, \mathbf{R}_1^{fixed}, \dots, \mathbf{R}_m^{fixed}))^* \hat{\mu} \psi_i^{electronic}(\mathbf{r}_1, \dots, \mathbf{r}_n, \mathbf{R}_1^{fixed}, \dots, \mathbf{R}_m^{fixed}) d\tau \\ &= S_{ol} \int \psi_f^*(\mathbf{r}_1, \dots, \mathbf{r}_n, \mathbf{R}_1^{fixed}, \dots, \mathbf{R}_m^{fixed}) \hat{\mu} \psi_i(\mathbf{r}_1, \dots, \mathbf{r}_n, \mathbf{R}_1^{fixed}, \dots, \mathbf{R}_m^{fixed}) d\tau\end{aligned}\quad (14.9)$$

We have introduced the subscript *ol* on *S* to indicate overlap as a means of distinguishing it from the spin quantum number. Note that the first of the two product integrals in Equation (14.9) represents the overlap *S* between the vibrational wave functions in the ground and excited states. The magnitude of the square of this integral for a given transition is known as the **Franck–Condon factor** and is a measure of the expected intensity of an electronic transition. The Franck–Condon factor replaces the selection rule $\Delta n = \pm 1$ obtained for pure vibrational transitions derived in Section 8.4 as a criterion for the intensity of a transition:

$$S_{ol}^2 = \left| \int (\phi_f^{vibrational})^* \phi_i^{vibrational} d\tau \right|^2 \quad (14.10)$$

The **Franck–Condon principle** states that transitions between electronic states correspond to vertical lines on an energy versus internuclear distance diagram. The basis of this principle is that electronic transitions occur on a timescale that is very short compared to the vibrational period of a molecule. Therefore, the atoms do not move during the transition. As Equation (14.9) shows, the intensity of a vibrational-electronic transition is governed by the overlap between the final and initial vibrational wave functions at fixed values of the internuclear distances. Is it necessary to consider all vibrational levels in the ground state as an initial state for an electronic transition? As discussed in Chapter 8, nearly all molecules in the ground state have the vibrational quantum number $n = 0$, for which the maximum amplitude of the wave function is at the equilibrium bond length. As shown in Figure 14.2, vertical transitions predominantly occur from this ground vibrational state to several vibrational states in the upper electronic state.

How does the Franck–Condon principle determine the n values in the excited state that give the most intense spectral lines? The most intense electronic transitions are to vibrational levels in the upper electronic state that have the largest overlap with the ground vibrational level in the lower electronic state. As shown in Figures 7.9 and 7.10, the vibrational wave functions have their largest amplitude near the R value at which the energy level meets the potential curve, because this corresponds to the classical turning point. For the example shown in Figure 14.2, the overlap $|\int (\phi_f^{vibrational})^* \phi_i^{vibrational} d\tau|$ is greatest between the $n = 0$ vibrational state of the ground electronic state and the $n = 4$ vibrational state of the excited electronic state. Although this transition has the maximum overlap and generates the most intense spectral line, other states close in energy to the most probable state will also give rise to spectral lines. Their intensity is lower because *S* is smaller.

The fact that a number of vibrational transitions are observed in an electronic transition is very useful in obtaining detailed information about both the ground electronic state potential energy surface and that of the electronic state to which the transition occurs. For example, vibrational transitions are observed in the electronic spectra of O₂ and N₂, although neither of these molecules absorbs energy in the infrared region of the electromagnetic spectrum. Because multiple vibrational peaks are often observed in electronic spectra, the bond strength of the molecule in excited states can be determined by fitting the observed frequencies of the transitions to a model potential such as the Morse potential discussed in Section 8.3. Because the excited state can also correspond to a photodissociation product, electronic spectroscopy can be used to determine the vibrational force constant and bond energy of highly reactive species such as the CN radical that cannot be studied with conventional infrared absorption techniques.

For the example shown in Figure 14.2, the molecule will exhibit a discrete energy spectrum in the visible or UV region of the spectrum. However, for some conditions,

Concept

The Franck–Condon factor replaces the selection rule $\Delta n = \pm 1$ obtained for pure vibrational transitions as a criterion for the intensity of a transition.

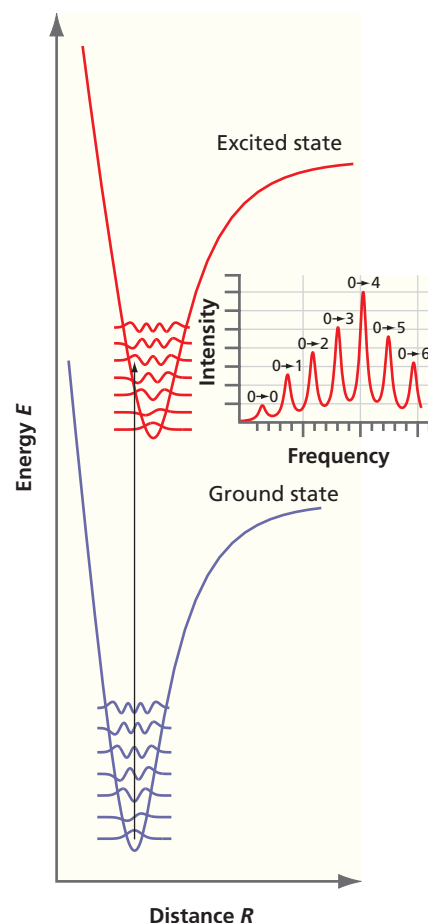
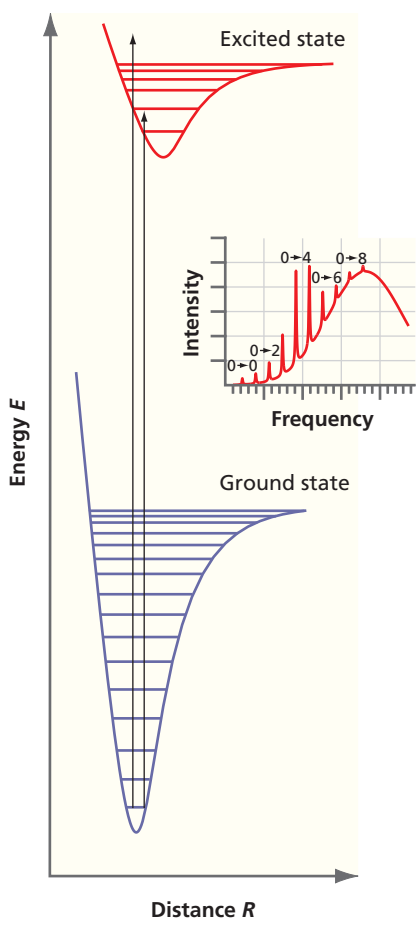


Figure 14.2
Relationship between energy and bond length for two electronic states. Only the lowest vibrational energy levels and the corresponding wave functions are shown. The vertical line shows the most probable transition predicted by the Franck–Condon principle. The inset shows the relative intensities of different vibrational lines in an absorption spectrum for the potential curves shown.

**Figure 14.3**

Discrete and continuous spectra produced by excitation. For absorption from the ground vibrational state of the ground electronic state to the excited electronic state, a discrete energy spectrum is observed for an incident light frequency $\nu < E/h$. A continuous spectrum is observed for higher frequencies.

the electronic absorption spectrum for a diatomic molecule is continuous. A continuous spectrum is observed if the photon energy is sufficiently high that excitation occurs to an unbound region of an excited state. This is illustrated in Figure 14.3. In this case, a discrete energy spectrum is observed for low photon energy and a continuous energy spectrum is observed for incident light frequencies $\nu > E/h$, where E corresponds to the energy of the transition to the highest bound state in the excited state potential. A purely continuous energy spectrum at all energies is observed if the excited state is a nonbinding state, such as that corresponding to the first excited state for H_2^+ .

The preceding discussion briefly summarizes the most important aspects of the electronic spectroscopy of diatomic molecules. In general, the vibrational energy levels for these molecules are sufficiently far apart that individual transitions can be resolved. We will next consider polyatomic molecules, for which this is not usually the case.

14.5 UV-VISIBLE LIGHT ABSORPTION IN POLYATOMIC MOLECULES

Many rotational and vibrational transitions are possible if an electronic transition occurs in polyatomic molecules. Large molecules have large moments of inertia, and as Equation (8.22) shows, this leads to closely spaced rotational energy levels. A large molecule may have ~ 1000 rotational levels in an interval of 1 cm^{-1} . For this reason, individual spectral lines overlap and broad bands are often observed in UV-visible absorption spectroscopy. This is schematically indicated in Figure 14.4. An electronic transition in an atom gives a sharp line. An electronic transition in a diatomic molecule has additional structure resulting from vibrational and rotational transitions that can often be resolved into individual peaks. However, the many rotational and vibrational transitions possible in a polyatomic molecule generally overlap, giving rise to a broad, nearly featureless band. This overlap makes it difficult to extract information on the initial and final states involved in an electronic transition in polyatomic molecules. In addition, there are no good angular momentum quantum numbers for triatomic and larger molecules. Therefore, the main selection rule that applies is $\Delta S = 0$, together with selection rules based on the symmetry of the initial and final states.

The number of transitions observed can be reduced dramatically by obtaining spectra at temperatures low enough that most of the molecules are in the ground vibrational state and only a few rotational states are populated. Low-temperature spectra for individual molecules can be obtained either by embedding the molecule of interest in a solid rare gas matrix at cryogenic temperatures or by expanding gaseous He that contains the molecules of interest in dilute concentration through a nozzle into a vacuum. The He gas as well as the molecules of interest are cooled to very low temperatures in the expansion.

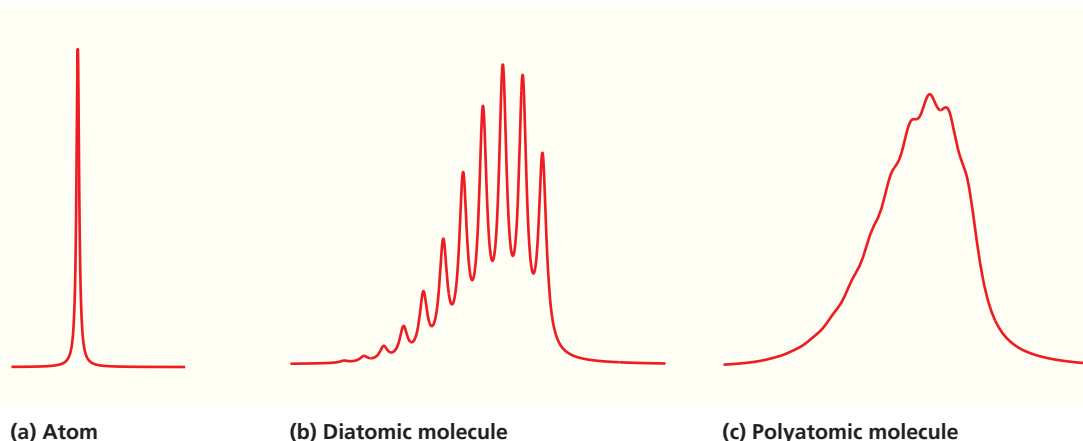


Figure 14.4
Intensity of absorption in a small part of the UV-visible range of the electromagnetic spectrum. Schematic spectra are shown for (a) an atom, (b) a diatomic molecule, and (c) a polyatomic molecule.

An example of the elimination of spectral congestion through such a gas expansion is shown for CF_3NO in Figure 14.5. The temperature of 20 K is reached by simply expanding the 300 K gas mixture into a vacuum using a molecular beam apparatus.

The concept of chromophores is particularly useful for discussing the electronic spectroscopy of polyatomic molecules. As discussed in Chapter 8, characteristic vibrational frequencies are associated with neighboring atoms, such as $-\text{OH}$ in molecules. Similarly, the absorption of UV and visible light in molecules can be understood by visualizing the molecule as including polyatomic units, such as $-\text{C}=\text{C}-$ or $-\text{O}-\text{H}$, that are called chromophores. A **chromophore** is a chemical entity that forms part of a molecule and that absorbs radiation at nearly the same wavelength in different molecular environments. Common chromophores in electronic spectroscopy are $-\text{C}=\text{C}-$, $-\text{C}=\text{O}$, $-\text{C}\equiv\text{N}$, or $-\text{C}=\text{S}$ groups. Each chromophore has one or several characteristic absorption frequencies in the UV, and the UV absorption spectrum of the molecule, to a first approximation, can be thought of as arising from the sum of the absorption spectra of its chromophores. The wavelengths and absorption strengths associated with specific chromophores are discussed next.

In a localized bonding model, an absorption band in an electronic spectrum can be associated with a specific chromophore. Whereas in atomic spectroscopy the selection rule $\Delta S = 0$ is strictly obeyed, in molecular spectroscopy one finds instead that spectral lines for transitions corresponding to $\Delta S = 0$ are much stronger than those for which this condition is not fulfilled. It is useful to quantify what is meant by strong and weak absorption. If I_0 is the incident light intensity at the frequency of interest and I_t is the intensity of transmitted light, the dependence of I_t/I_0 on the concentration c and the path length l is described by **Beer's law**:

$$\log\left(\frac{I_t}{I_0}\right) = -\varepsilon lc \quad (14.11)$$

The **molar extinction coefficient** ε is a measure of the strength of the transition. It is independent of path length and concentration and is characteristic of the chromophore and wavelength. The **integral absorption coefficient**, $A = \int \varepsilon(\nu) d\nu$, is a measure of the probability that an incident photon will be absorbed in a specific electronic transition. Looking at this integral more closely, we see that the integration over the spectral line includes associated vibrational and rotational transitions. Also, the terms A and ε depend on frequency. Values for ε , measured at the maximum intensity of the spectral line ε_{max} , have been tabulated for many chromophores. Some characteristic values for spin-allowed transitions are given in Table 14.2.

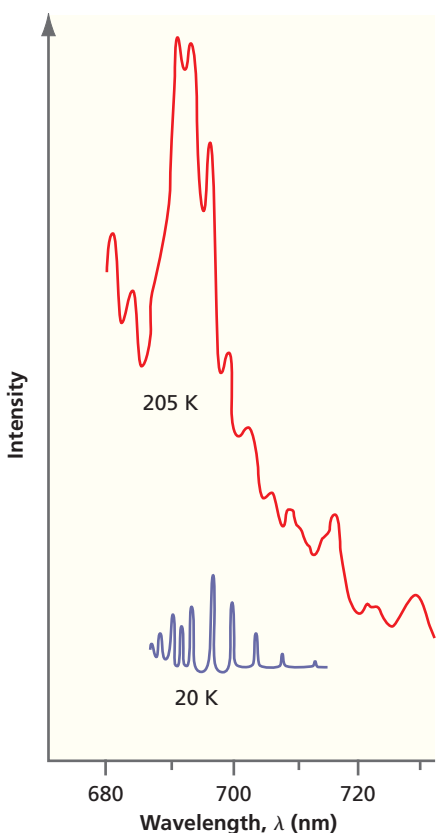


Figure 14.5

Small portion of absorption spectra of CF_3NO . The spectra were obtained at 205 K and 20 K. The low-temperature experiments used expansion of a dilute mixture of CF_3NO in He through a nozzle into a vacuum. At 205 K, the molecule absorbs throughout the frequency range, and individual transitions cannot be resolved. At 20 K, very few rotational and vibrational states are populated, and individual spectral features are observed.
Source: Adapted from B. DeKoven, K. Fung, D. Levy, L. Hoffland and K. Spears, *Journal of Chemical Physics* 74 (1981): 4755–4764.

TABLE 14.2 Characteristic Parameters for Common Chromophores

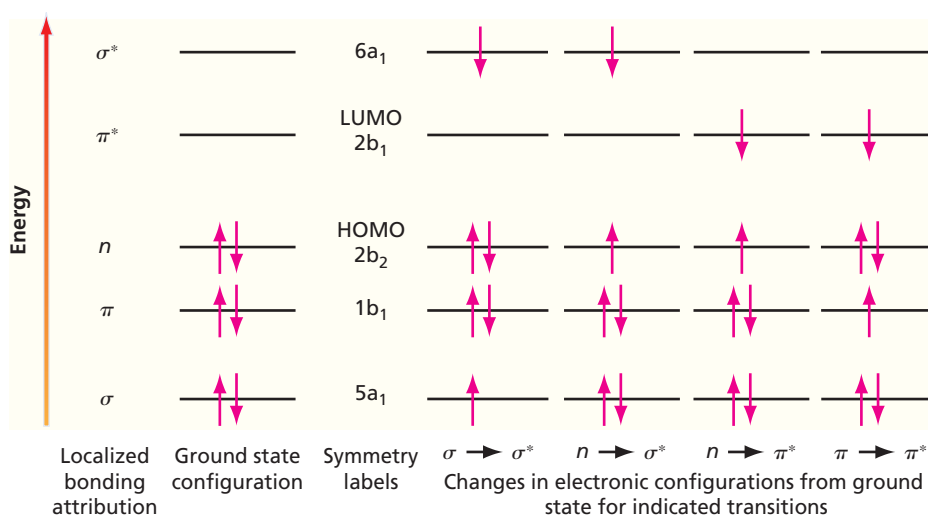
Chromophore	Transition	λ_{max} (nm)	ε_{max} ($\text{dm}^3 \text{ mol}^{-1} \text{ cm}^{-1}$)
$\text{N}=\text{O}$	$n \rightarrow \pi^*$	660	200
$\text{N}=\text{N}$	$n \rightarrow \pi^*$	350	100
$\text{C}=\text{O}$	$n \rightarrow \pi^*$	280	20
	$\pi \rightarrow \pi^*$	190	200
NO_2	$n \rightarrow \pi^*$	270	20
C_6H_6 (benzene)	$\pi \rightarrow \pi^*$	260	200
$\text{C}=\text{N}$	$n \rightarrow \pi^*$	240	150
$\text{C}=\text{C}-\text{C}=\text{O}$	$\pi \rightarrow \pi^*$	220	2×10^5
$\text{C}=\text{C}-\text{C}=\text{C}$	$\pi \rightarrow \pi^*$	220	2×10^5
$\text{S}=\text{O}$	$n \rightarrow \pi^*$	210	1.5×10^3
$\text{C}=\text{C}$	$\pi \rightarrow \pi^*$	180	1×10^3
$\text{C}-\text{C}$	$\sigma \rightarrow \sigma^*$	<170	1×10^3
$\text{C}-\text{H}$	$\sigma \rightarrow \sigma^*$	<170	1×10^3

Concept

The strength of absorption at a given wavelength is described by the Beers–Lambert law.

Figure 14.6

Lowest energy transitions between electronic energy levels in formaldehyde. Ground state configuration and relevant MO energy levels, symmetry labels, and localized bonding attributions. The four columns on the right show the changes in electronic configurations from the ground state for the transitions indicated below each column.



In Table 14.2, note the large enhancement of ϵ_{\max} displayed by conjugated bonds. As a general rule, values for ϵ_{\max} between 10 and $5 \times 10^4 \text{ dm}^3 \text{ mol}^{-1} \text{ cm}^{-1}$ for spin-allowed transitions ($\Delta S = 0$) and between 1×10^{-4} and $1 \text{ dm}^3 \text{ mol}^{-1} \text{ cm}^{-1}$ for singlet-triplet transitions ($\Delta S = 1$) are typical. Therefore, the attenuation of light passing through a sample that results from singlet-triplet transitions will be smaller by a factor of $\sim 10^4$ to 10^7 than the attenuation from singlet-singlet transitions. This illustrates that in an absorption experiment, transitions for which $\Delta S = 1$ are not completely forbidden if spin-orbit coupling is not negligible; however, these transitions are typically too weak to be of much importance. However, as discussed in Section 14.8, singlet-triplet transitions are important for phosphorescence.

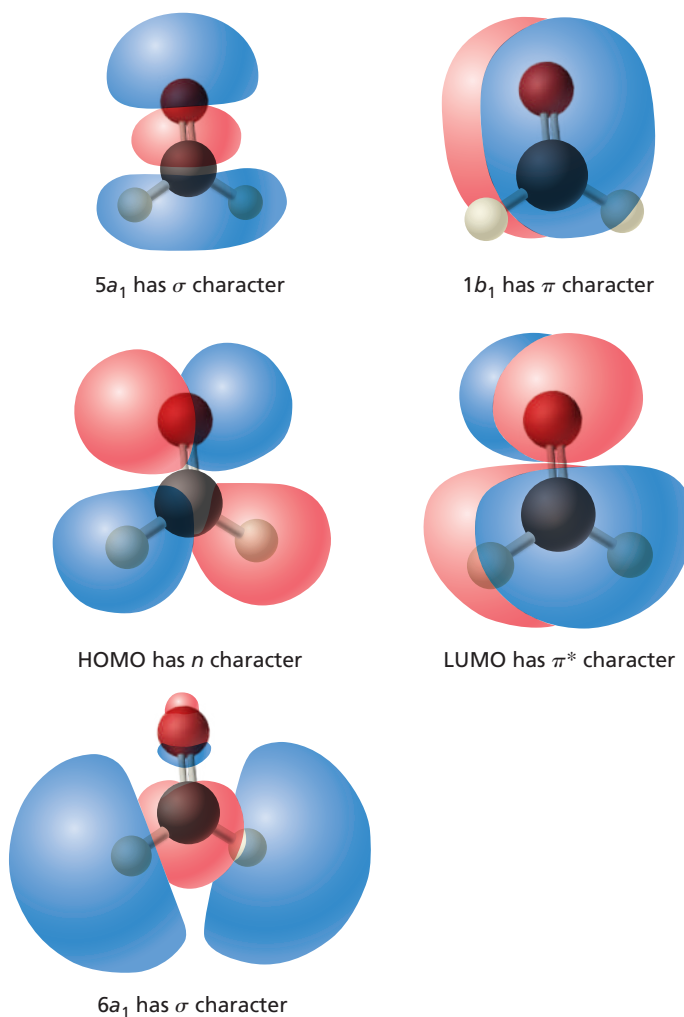
Concept

Changes in the electronic configuration of a molecule in an electronic transition can be described by localized or delocalized bonding models.

To make this discussion of chromophores more specific, we consider the electronic absorption spectroscopy of formaldehyde from both a localized and a delocalized perspective. Figure 14.6 shows an overview of possible electronic transitions in formaldehyde. Recall from Section 13.6 that because localized orbitals are not eigenfunctions of the total energy operator, they cannot be associated with orbital energies. Therefore, Figure 14.6 displays the delocalized MOs in an MO energy diagram. However, the contributions from localized bonds can be seen in the MOs that are depicted in Figure 14.7, as we next discuss in this section. The $5a_1$ MO has σ character with the $2p_z$ AO visible in the C=O region as well as σ character in the C—H bonds. The $1b_1$ MO depicts a π bond arising from an in-phase combination of the $2p_x$ AOs on C and O. The HOMO has nonbonding or n character with the lone pair in the $2p_y$ oxygen AO clearly visible. The LUMO depicts an antibonding π^* bond arising from an out-of-phase combination of the $2p_x$ AOs on the C and O atoms. The $6a_1$ MO shows σ bonds in both the C—O and C—H regions, and, because nodes are present in the C—H and C—O bonds, this MO is antibonding in character.

Recall from Section 14.4 that the strength of electronic transitions is determined by the Franck–Condon factor, which in turn depends on the overlap between the wave functions corresponding to the initial and final states of the transition. The overlap for the $\pi \rightarrow \pi^*$ transition in formaldehyde is between two wave functions that have their maximum amplitudes displaced from the molecular plane. The overlap for the $n \rightarrow \pi^*$ transition in formaldehyde is between two wave functions, one of which has zero amplitude in the molecular plane, whereas the other has its maximum amplitude in the molecular plane. Therefore, we expect the $\pi \rightarrow \pi^*$ transition in formaldehyde to be much stronger than the $n \rightarrow \pi^*$ transition. This is confirmed by the values for ϵ_{\max} in Table 14.2. In general, the intensity of $\sigma \rightarrow \sigma^*$ is weak, which is expected for formaldehyde from the small overlap between the $5a_1$ and $6a_1$ wave functions.

To this point, our discussion has focused on the formaldehyde. More generally, $\pi \rightarrow \pi^*$ transitions require multiple bonds and occur in alkenes, alkynes, and aromatic compounds. The $n \rightarrow \pi^*$ transitions require both a nonbonding electron pair and multiple bonds and occur in molecules containing carbonyls, thiocarbonyls, nitro, azo, and imine groups and in unsaturated halocarbons. The $\sigma \rightarrow \sigma^*$ transitions are observed in many molecules, particularly in alkanes, in which none of the other transitions is possible.

**Figure 14.7**

Molecular orbitals corresponding to the energy levels in Figure 14.6. Dominant localized bonding character is indicated for each MO.

14.6 TRANSITIONS AMONG THE GROUND AND EXCITED STATES

We will next generalize the preceding discussion for formaldehyde to an arbitrary molecule. What transitions can take place among ground and excited states? Consider the energy levels for such a molecule shown schematically in the Jablonski diagram in Figure 14.8. The ground state is, in general, a singlet state, and the excited states can be either singlet or triplet states. We include only one excited singlet and triplet state in addition to the ground state and consider the possible transitions among these states. The restriction is justified because an initial excitation to higher-lying states will rapidly decay to the lowest-lying state of the same multiplicity through a process called internal conversion, which is discussed later. The diagram also includes vibrational levels associated with each of the electronic levels. Rotational levels are omitted to simplify the diagram. The fundamental rule governing transitions is that all transitions must conserve energy and angular momentum. Energy can also be conserved by transferring energy between a molecule and its surroundings.

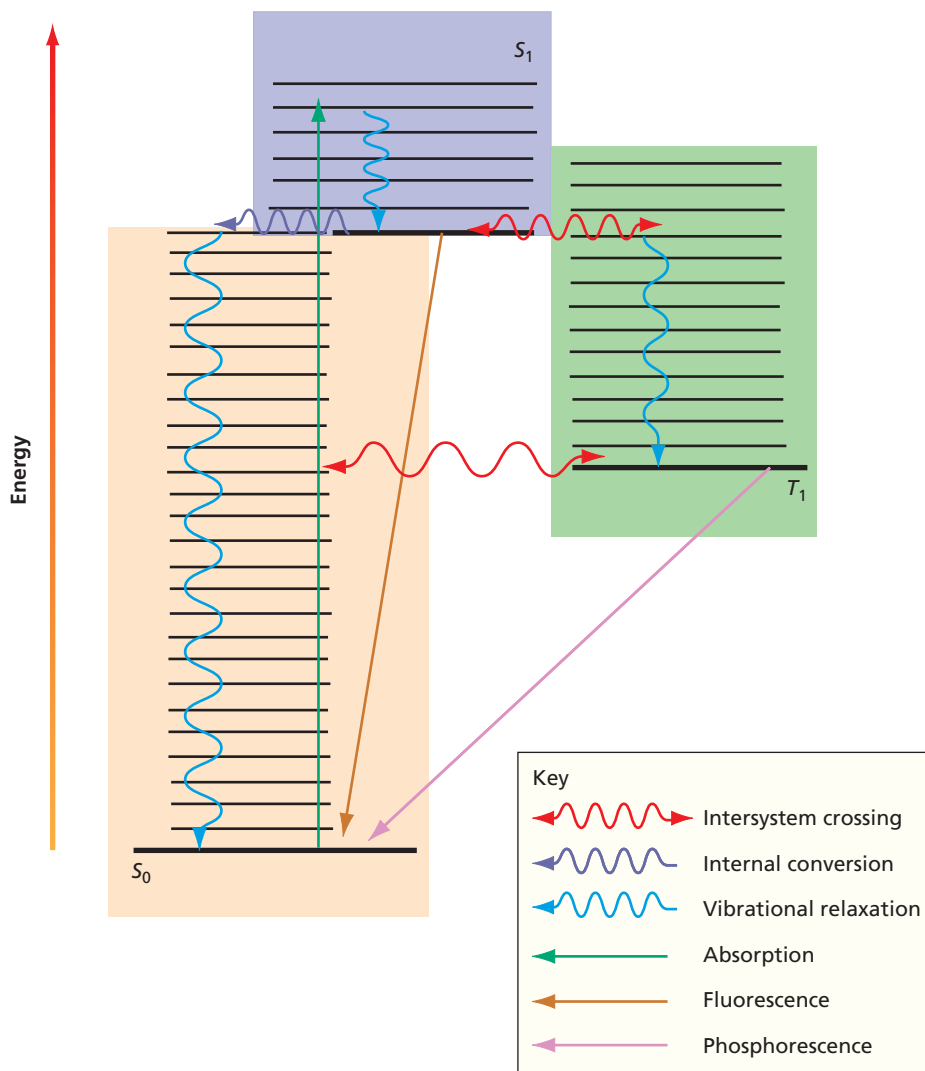
Four types of transitions are indicated in Figure 14.8. **Radiative transitions**, in which a photon is absorbed or emitted, are indicated by solid lines. **Nonradiative transitions**, in which energy is transferred between different degrees of freedom of a molecule or to the surroundings, are indicated by blue wavy vertical lines. **Internal conversion** occurs without a change in energy between states of the same multiplicity and is shown as a horizontal wavy line. An **intersystem crossing** differs from an internal conversion in that a change in multiplicity ($\Delta S \neq 0$) occurs. The pathway by which a molecule in an excited state decays to the ground state depends on the rates of a number of competing processes. In the next two sections, these processes are discussed individually.

Concept

A transition between ground and excited states can be categorized as a radiative transition, a nonradiative transition, an internal conversion, or an intersystem crossing.

Figure 14.8

A Jablonski diagram for depicting various photophysical processes. In the diagram, S_0 is the ground electronic singlet state, S_1 is the first excited singlet state, and T_1 is the first excited triplet state. Radiative processes are indicated by the straight lines. The nonradiative processes of intersystem crossing, internal conversion, and vibrational relaxation are indicated by the wavy lines.



14.7 SINGLET-SINGLET TRANSITIONS: ABSORPTION AND FLUORESCENCE

Assume that a molecule in the ground state S_0 absorbs a photon and is excited to the state S_1 . The excited-state molecule in S_1 can return to the ground state S_0 through a radiative transition or through nonradiative transitions involving collisions with other molecules. What determines which of these two pathways will be followed? An isolated excited-state molecule (for instance, in interstellar space) cannot exchange energy with other molecules through collisions and, therefore, nonradiative transitions (other than an isoenergetic, internal, electronic-to-vibrational energy transfer) will not occur. However, excited-state molecules in a crystal, in solution, or in a gas undergo frequent collisions with other molecules in which they lose energy and return to the lowest vibrational state of S_1 through vibrational relaxation. This process generally occurs much faster than a radiative transition directly from a vibrationally excited state in S_1 to a vibrational state in S_0 . Once in the lowest vibrational state of S_1 , either of three events can occur. The molecule can undergo several types of transitions, including: (1) a radiative transition to a vibrational state in S_0 in a process called **fluorescence**; or (2) a nonradiative transition to an excited vibrational state of S_0 through internal conversion; or (3) a nonradiative transition to an excited vibrational state of T_1 through intersystem crossing. Intersystem crossing violates the $\Delta S = 0$ selection rule and, therefore, occurs at a very low rate in comparison with the other processes depicted in Figure 14.8.

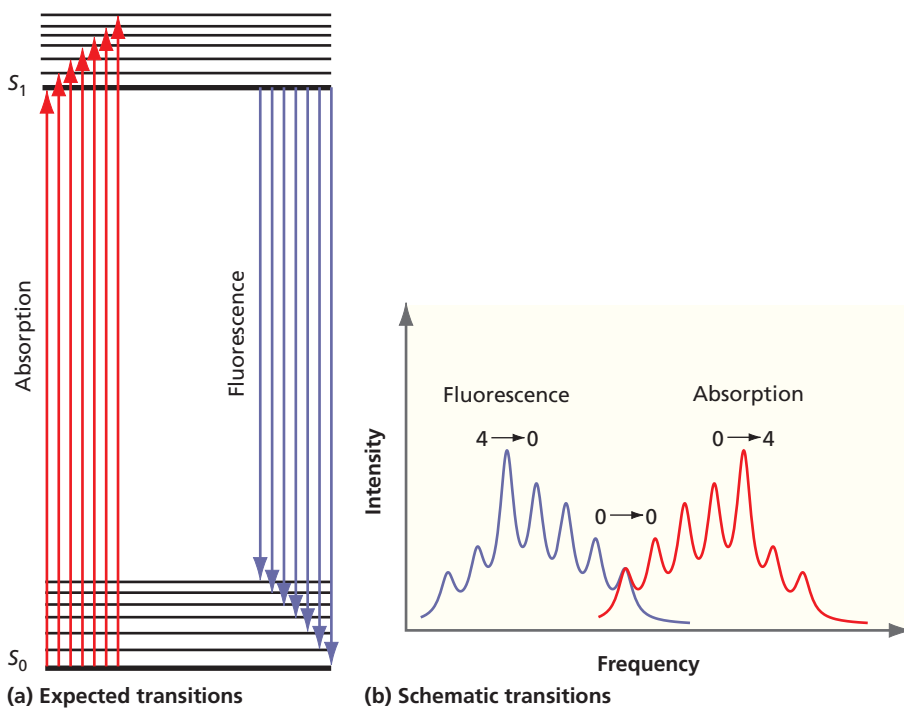
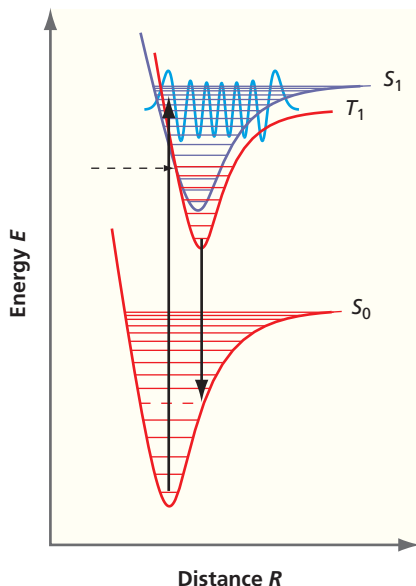
**Figure 14.9**

Illustration of absorption and fluorescence bands expected if vibrational relaxation is rapid relative to fluorescence. The relative intensities of individual transitions within the absorption and fluorescence bands are determined by the Franck–Condon principle. The diagrams show (a) expected transitions and (b) schematic spectra. Note the symmetry displayed by the absorption and fluorescence bands and spectra.

Concept

As a result of the vibrational relaxation, the fluorescence spectrum is shifted to lower energies relative to the absorption spectrum.

**Figure 14.10**

Depiction of process giving rise to phosphorescence for a diatomic molecule. Absorption from S_0 leads to a population of excited vibrational states in S_1 . The molecule has a finite probability of making a transition to an excited vibrational state of T_1 if it has the same structure in both states and if there are vibrational levels of the same energy in both states. The dashed arrow indicates the coincidence of vibrational energy levels in T_1 and S_1 . For reasons of clarity, only the lowest vibrational levels in T_1 are shown. The initial excitation to S_1 occurs to a vibration state of maximum overlap with the ground state of S_0 as indicated by the blue vibrational wave function.

14.8 INTERSYSTEM CROSSING AND PHOSPHORESCENCE

Although intersystem crossing between singlet and triplet electronic states is forbidden by the $\Delta S = 0$ selection rule, the probability of this happening is high for many molecules. The probability of intersystem crossing transitions is enhanced by two factors: a very similar molecular structure in the excited singlet and triplet states, and a strong spin-orbit coupling, which allows the spin flip associated with a singlet–triplet transition to occur. The processes involved in phosphorescence are illustrated in a simplified fashion in Figure 14.10 for a diatomic molecule.

Imagine that a molecule is excited from S_0 to S_1 . This is a dipole-allowed transition, so it has a high probability of occurring. Through collisions with other molecules, the excited-state molecule loses vibrational energy and decays to the lowest vibrational state of S_1 . As shown in Figure 14.10, the potential energy curves can overlap such that an excited vibrational state in S_1 can have the same energy as an excited vibrational state in T_1 . In this case, the molecule has the same structure and energy in both singlet and triplet states. In Figure 14.10, this occurs for $n = 4$ in the state S_1 . If the spin-orbit coupling is strong enough to initiate a spin flip, the molecule can cross over to the triplet state without a change in geometry or energy. Through vibrational relaxation, it will rapidly relax to the lowest vibrational state of T_1 . At this point, it can no longer make a transition back to S_1 because the ground vibrational state of T_1 is lower than any state in S_1 .

However, from the ground vibrational state of T_1 , the molecule can decay radiatively to the ground state in the dipole transition forbidden process called **phosphorescence**.

Concept

The probability for a $T_1 \rightarrow S_0$ phosphorescence transition is generally much lower than for fluorescence.

This is not a high-probability event because nonradiative processes involving collisions between molecules or with the walls of the reaction vessel can compete effectively with phosphorescence. Therefore, the probability for a $T_1 \rightarrow S_0$ phosphorescence transition is generally much lower than for fluorescence. The ratio usually lies in the range of 10^{-2} to 10^{-5} . The relative probabilities of fluorescence and phosphorescence if collisional relaxation can occur is determined by the lifetime of the excited state. Fluorescence is an allowed transition, and the excited-state lifetime is short, typically less than 10^{-8} s. By contrast, phosphorescence is a forbidden transition and the excited-state lifetime is typically longer than 10^{-6} s. On this timescale, collisional relaxation has a high probability.

Fluorescence can be induced using broadband radiation or highly monochromatic laser light. Fluorescence spectroscopy is well suited for detecting very small concentrations of a chemical species if the wavelength of the emission lies in the visible-UV part of the electromagnetic spectrum where there is little background signal near room temperature. As shown in Figure 14.9, relaxation to lower vibrational levels within the excited electronic state has the consequence that the fluorescence signal occurs at a longer wavelength than the light used to create the excited state. Therefore, the contribution of the incident radiation to the background at the wavelength used to detect the fluorescence is very small.

14.9 FLUORESCENCE SPECTROSCOPY AND ANALYTICAL CHEMISTRY

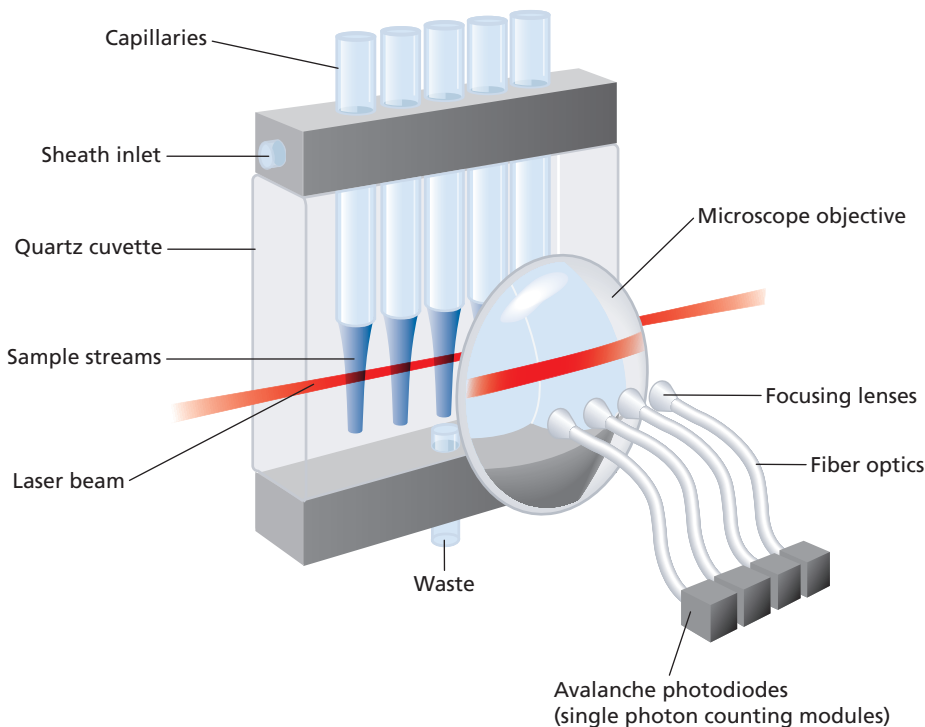
Concept

Fluorescence spectroscopy was used to sequence the human genome.

We will now describe a particularly powerful application of fluorescence spectroscopy, namely, the sequencing of the human genome. The goal of the human genome project was to determine the sequence of the four bases, A, C, T, and G, in DNA that encode all the genetic information necessary for propagating the human species. A sequencing technique based on laser-induced fluorescence spectroscopy that has been successfully used in this effort can be considered as consisting of three parts.

In the first part, a section of DNA is cut into small lengths of 1000 to 2000 base pairs using mechanical shearing. Each of these pieces is replicated to create many copies, and these replicated pieces are put into a solution with a mixture of the four bases, A, C, T, and G. A reaction is set in motion that leads to the strands growing in length through replication. A small fraction of each of the A, C, T, and G bases in solution that are incorporated into the pieces of DNA has been modified in two ways. The modified base terminates the replication process. It also contains a dye chosen to fluoresce strongly at a known wavelength. The initial segments continue to grow if they incorporate unmodified bases, and they no longer grow if they incorporate one of the modified bases. As a result of these competing processes involving the incorporation of modified or unmodified bases, a large number of partial replicas of the whole DNA are created, each of which is terminated in the base that has a fluorescent tag built into it. The ensemble of these partial replicas contains all possible lengths of the original DNA segment that terminate in the particular base chosen for modification. If the lengths of these segments can be measured, then the positions of the particular base in the DNA segment can be determined.

In the second part of the sequencing technique, the lengths of the partial replicas are measured using capillary electrophoresis coupled with detection using laser-induced fluorescence spectroscopy. In this method, a solution containing the partial replicas is passed through a glass capillary filled with a gel. An electrical field along the capillary causes the negatively charged DNA partial replicas to travel down the column with a speed that depends inversely on their length. Because of the different migration speeds, a separation in length occurs as the partial replicas pass through the capillary. At the end of the capillary, the partial replicas emerge from the capillary into a buffer solution that flows past the capillary, forming a sheath. The flow pattern of the buffer solution is carefully controlled to achieve a focusing of the emerging stream containing the partial replicas to a diameter somewhat smaller than the inner diameter of the capillary. A schematic diagram of such a sheath flow cuvette electrophoresis apparatus is shown in Figure 14.11. An array of capillaries is used rather than a single capillary in order to obtain the multiplexing advantage of carrying out several experiments in parallel.

**Figure 14.11**

Schematic diagram of the application of fluorescence spectroscopy in the sequencing of the human genome. The individual components of the apparatus described in the text are indicated.

Source: Adapted from Norman Dovichi, Development of DNA Sequencer. *Science* 285 (1999): 1016.

The final part of the sequencing procedure is to measure the time that each of the partial replicas spent in transit through the capillary, which determines its length, and to identify the terminating base. The latter task is accomplished by means of laser-induced fluorescence spectroscopy. A narrow beam of visible laser light is passed through all the capillaries in series. Because of the very dilute solutions involved, the attenuation of the laser beam by each successive capillary is very small. The fluorescent light emitted from each of the capillaries is directed to light-sensing photodiodes by means of a microscope objective and individual focusing lenses. A rotating filter wheel between the microscope objective and the focusing lenses allows a discrimination to be made among the four different fluorescent dyes with which the bases were tagged. The sensitivity of the system shown in Figure 14.11 is 130 ± 30 molecules in the volume illuminated by the laser, which corresponds to a concentration of 2×10^{-13} mol/L! This extremely high sensitivity is a result of coupling the sensitive fluorescence technique to a sample cell designed with a very small sampling volume. Matching the laser beam diameter to the sample size and reducing the size of the cuvette result in a significant reduction in background noise. Commercial versions of this approach utilizing 96 parallel capillaries played a major part in the first phase of the sequencing of the human genome. For more details, see the reference to Dovichi in Further Reading.

14.10 ULTRAVIOLET PHOTOELECTRON SPECTROSCOPY

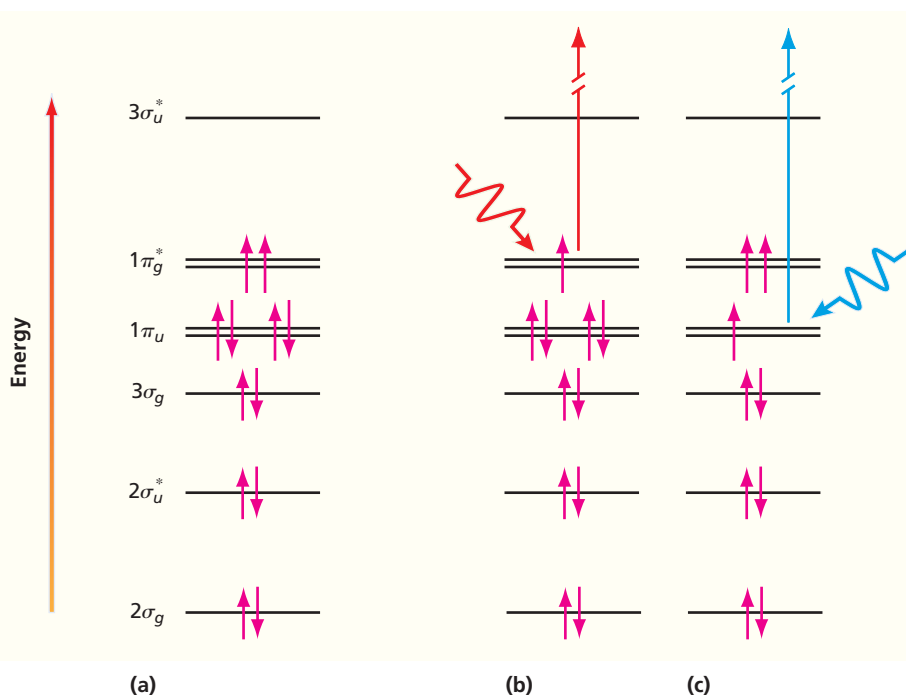
Spectroscopy in general, and electronic spectroscopy in particular, provides information on the energy difference between the initial and final states rather than the energy levels involved in the transition. However, the energy of both occupied and unoccupied molecular orbitals is of particular interest to chemists. Information at this level of detail cannot be obtained directly from a UV absorption spectrum because only a difference between energy levels is measured. However, information about the orbitals involved in the transition can be extracted from an experimentally obtained spectrum using a model. For example, the molecular orbital model described in Chapter 12 can be used to calculate the orbital energy levels for a molecule. With these results, an association can be made between energy-level differences calculated from observed spectral peaks and differences in the orbital energy levels obtained from the model.

Concept

Combining the results of UV absorption and UV photoelectron spectroscopy can provide information on the energies of occupied and unoccupied molecular orbitals.

Figure 14.12

Molecular orbital diagrams demonstrating principles of UV photoelectron spectroscopy. The ground state molecular orbital diagram of O_2 is shown in (a). An incident UV photon can eject an electron from one of the occupied MOs, generating an O_2^+ ion and an unbound electron whose kinetic energy can be measured as shown in (b) and (c) for two different MOs. Electrons ejected from different MOs will differ in their kinetic energy.



Of all the possible forms of electronic spectroscopy, **UV photoelectron spectroscopy** comes closest to the goal of directly identifying the orbital energy level from which an electronic transition originates. What is the principle of this spectroscopy? As in the photoelectric effect discussed in Chapter 1, an incident photon of sufficiently high energy ejects an electron from one of the filled valence orbitals of the molecule, creating a positive ion as shown in Figure 14.12, using O_2 as an example. The kinetic energy of the ejected electron is related to the total energy required to form the positive ion via **photoionization**,

$$E_{kinetic} = h\nu - \left[E_f + \left(n_f + \frac{1}{2} \right) h\nu_{vibration} \right] \quad (14.12)$$

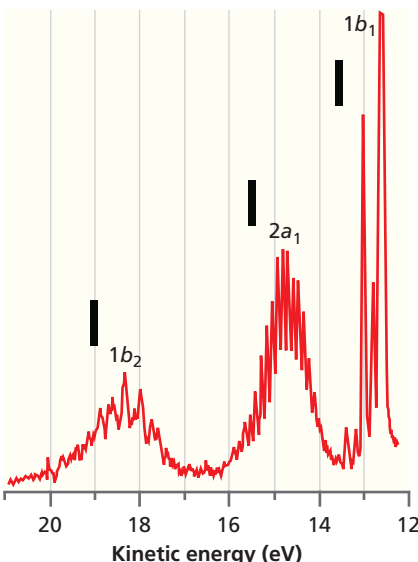
where E_f is the energy of the cation, which is formed by the removal of the electron, in its ground state. Equation (14.12) takes vibrational excitation of the cation into account, which by conservation of energy leads to a lower kinetic energy for the photoejected electron. Because, in general, either the initial or final state is a radical, a delocalized MO model must be used to describe UV photoelectron spectroscopy.

Under the assumptions to be discussed next, the measured value of $E_{kinetic}$ can be used to obtain the energy of the orbital $\epsilon_{orbital}$ from which the electron originated. The energy of the cation, E_f , which can be determined directly from a photoelectron spectrum, is equal to $\epsilon_{orbital}$ if the following assumptions are valid:

- The nuclear positions are unchanged in the transition (Born–Oppenheimer approximation).
- The orbitals for the atom and ion are the same (**frozen orbital approximation**). This assumes that the electron distribution is unchanged in the ion, even though the ion has one fewer electron.
- The total electron correlation energy in the molecule and ion is the same.

The association of E_f with $\epsilon_{orbital}$ for the neutral molecule under these assumptions is known as **Koopmans' theorem**. In comparing spectra obtained for a large number of molecules with high-level numerical calculations, the measured and calculated orbital energies commonly differ by approximately 1 to 3 eV. The difference results primarily from the last two assumptions not being entirely satisfied.

This discussion suggests that a photoelectron spectrum consists of a series of peaks, each of which can be associated with a particular molecular orbital of the molecule. Figure 14.13 shows a photoelectron spectrum obtained for gas-phase water molecules

**Figure 14.13**

UV photoelectron spectrum of gas-phase H_2O . Three groups of peaks are visible, each of which is associated with the water MOs discussed in Chapter 13. The structure within each group results from vibrational excitation of the cation formed in the photoionization process. The vertical bars show calculated values for the molecular orbital energies.

Source: Adapted from C. R. Brundle and D. W. Turner. High resolution molecular photoelectron spectroscopy II. Water and deuterium oxide, *Proceedings of the Royal Society A*. 307 (1968): 27–36.

for a photon energy $h\nu = 21.8$ eV, corresponding to a strong UV emission peak from a helium discharge lamp. Each of the three groups of peaks can be associated with a particular molecular orbital of H_2O , and the approximately equally spaced peaks within a group correspond to vibrational excitations of the cation formed in the photoionization process. The vertical lines indicate the calculated MO energies obtained from an MP2 calculation (see Chapter 15). It is seen that the agreement between experimental and calculated values is good.

14.11 SINGLE-MOLECULE SPECTROSCOPY

Spectroscopic measurements are generally carried out in a sample cell in which a very large number of the molecules of the compound of interest, called an ensemble, are present. In general, the local environment of the molecules in an ensemble is not identical, which leads to inhomogeneous broadening of an absorption line as discussed in Section 8.9. Figure 14.14 shows how a broad absorption band arises if the corresponding narrow bands for individual molecules in the ensemble are slightly shifted in frequency because of variations in the immediate environment of a molecule.

Clearly, more information is obtained from the spectra of the individual molecules than from the inhomogeneously broadened band. The “true” absorption spectrum for an individual molecule is observed only if the number of molecules in the volume being sampled is very small, such as in the bottom spectrum in Figure 14.14.

Single-molecule spectroscopy is particularly useful in understanding the structural-functional relationship of biomolecules. The structure of a biomolecule can be discussed in terms of primary, secondary, tertiary, and quaternary structure. The **primary structure** refers to the linear order of amino acids in a polypeptide sequence. The term **secondary structure** refers to the local conformation of a part of the polypeptide. Two common secondary structures of polypeptides are the α -helix and the β -sheet as shown in Figure 14.15. **Tertiary structure** refers to the overall three-dimensional folding of a single-chain protein. If multiply folded proteins combine to form a larger stable multimeric complex, the **quaternary structure** is the structure of the larger complex.

Keep in mind that the conformation of a biomolecule in solution is not static. Collisions with solvent and other solute molecules continuously change the energy and the conformation of each biomolecule with time. What are the consequences of such conformational changes for an enzyme? Because the activity is intimately linked to structure, conformational changes lead to fluctuations in activity, making an individual enzyme molecule alternately active and inactive as a function of time. Spectroscopic measurements carried out on an ensemble of enzyme molecules give an average over all possible conformations and hence over all possible activities for the enzyme. Such measurements are of limited utility in understanding how structure and chemical activity are related. As we will show in the next section, single-molecule spectroscopy can provide a view at a resolution beyond the ensemble limit and gives information on the possible conformations of biomolecules and on the timescales on which transitions to different conformations take place.

To carry out single-molecule spectroscopy, the number of molecules in the sampling volume must be reduced to approximately one. How is a spectrum of individual biomolecules in solution obtained? Only molecules in the volume that is both illuminated by the light source and imaged by the detector contribute to the measured spectrum. For this number to be approximately one, a laser focused to a small diameter is used to excite the molecules of interest, and a confocal microscope is used to collect the photons emitted in fluorescence from a small portion of the much larger cylindrical volume of the solution illuminated by the laser. In a confocal microscope, the sampling volume is at one focal point, and the detector is behind a pinhole aperture located at the other focal point of the microscope imaging optics. Because photons that originate outside of a volume of approximately $1 \mu\text{m} \times 1 \mu\text{m} \times 1 \mu\text{m}$ centered at the focal point are not imaged on the pinhole aperture, they cannot reach the detector. Therefore, the volume sampled by the detector is much smaller than the volume illuminated by the laser. To ensure that no more than a few molecules are likely to be present in the sampling volume,

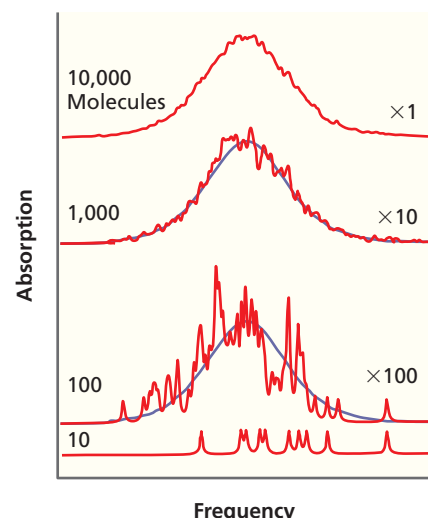


Figure 14.14

Peak width as a function of number of molecules in sample. The absorption spectrum of an individual molecule is narrow, but the peak occurs over a range of frequencies for molecules in different local environments, as shown in the lowest curve for 10 molecules in the sampling volume. As the number of molecules in the sampling volume is increased, the observed peak shows inhomogeneous broadening and is characteristic of the ensemble average (purple curves) rather than of an individual molecule.

Concept

Single molecule spectroscopy can eliminate the heterogeneous broadening observed in ensemble-averaged spectroscopy techniques.

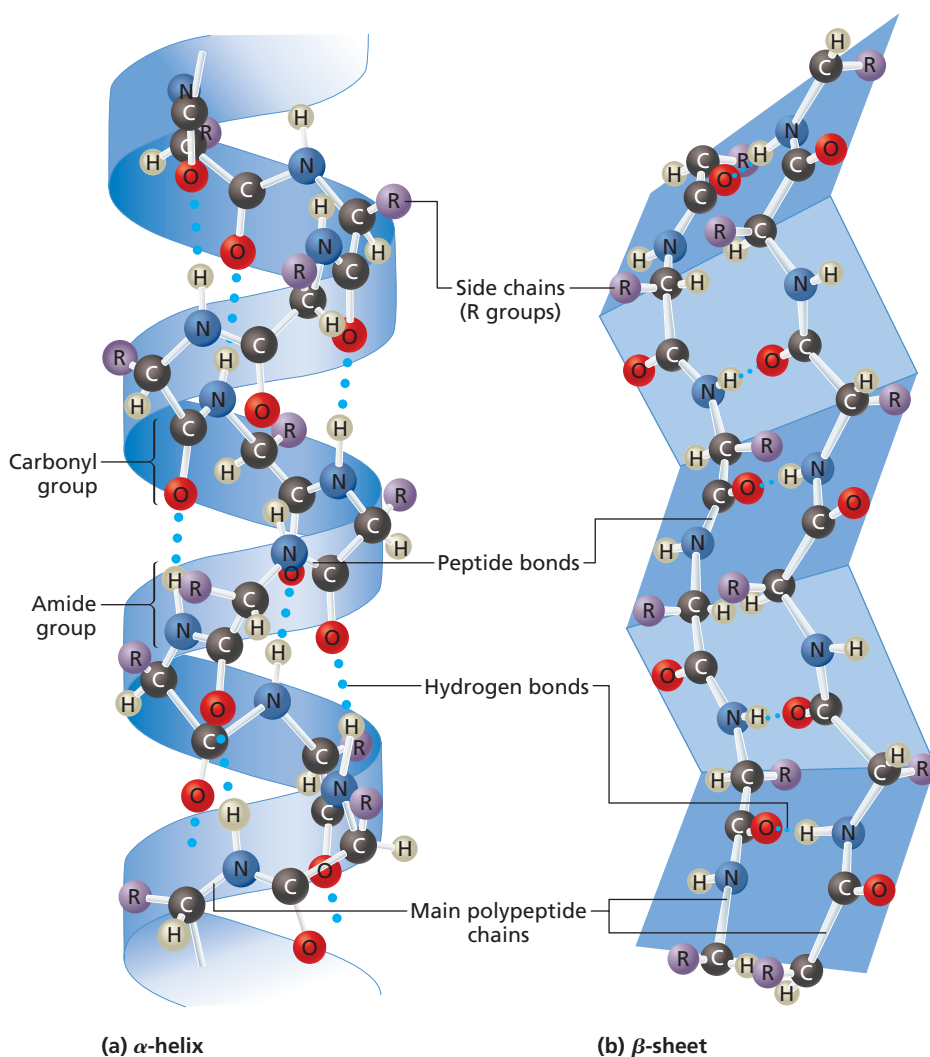


Figure 14.15

Two common secondary structures of polypeptides. The (a) α -helix and (b) β -sheet are two important forms in which proteins occur in aqueous solutions. In both structures, hydrogen bonds form between imino ($-\text{NH}-$) groups and carbonyl groups.

the concentration of the biomolecule must be less than $\sim 1 \times 10^{-6}$ M. Fluorescence spectroscopy is well suited for single-molecule studies because, as discussed in Section 14.8, vibrational relaxation in the excited state ensures that the emitted photons have a lower frequency than the photons used to excite the molecule. Therefore, optical filters can be used to ensure that scattered laser light or photons from Raman scattering outside of sampling volume do not reach the detector. If the molecules being investigated are immobilized in a film or gel, they can also be investigated using the same experimental techniques.

14.12 FLUORESCENT RESONANCE ENERGY TRANSFER

Fluorescent Resonance Energy Transfer (FRET) is a form of single-molecule spectroscopy that has proved to be very useful in studying biochemical systems. An electronically excited molecule can lose energy by either radiative or nonradiative events, as discussed in Section 14.6. We refer to the molecule that loses energy as the **donor** and the molecule that gains the energy as the **acceptor**. Recall from Section 14.7 that vibrational relaxation

in the excited donor shifts the donor emission spectrum to shorter wavelengths relative to the absorption spectrum. If the emission spectrum of the donor overlaps the absorption spectrum of the acceptor, as shown in Figure 14.16, then **resonance energy transfer** can occur, as shown in Figure 14.17. Under resonance conditions, the energy transfer from the donor to the acceptor can proceed with a high efficiency.

The probability for resonant energy transfer is strongly dependent on the distance r between the donor and acceptor. Theodor Förster showed that the rate at which resonant energy transfer occurs decreases as the sixth power of the donor-acceptor distance, as shown in the relationship

$$k_{ret} = \frac{1}{\tau_D^{\circ}} \left(\frac{R_0}{r} \right)^6 \quad (14.13)$$

In Equation (14.13), τ_D° is the lifetime of the donor in its excited state and R_0 , the critical Förster radius, which is the distance at which the resonance transfer rate and the rate for spontaneous decay of the excited state donor are equal. Both of these quantities can be determined experimentally. The sensitive dependence of the resonance energy transfer on the donor-acceptor distance makes it possible to use FRET as a spectroscopic ruler to measure donor-acceptor distances in the 1–10 nm range.

FRET can be used to investigate both protein structure and the interactions between proteins and binding partners. Using chemical synthesis techniques, a donor can be placed at different positions in a biomolecule. Investigators can then measure the FRET efficiency between each of these different donor labels with an acceptor conjugated to a binding partner. Because the efficiency of resonance energy transfer depends sensitively on the distance between the donor and acceptor, a comparison of the FRET efficiency for different donor positions allows the relative distances between the acceptor and the different donor positions to be measured. Because the positions of the donor sites are known, this allows the mapping of the acceptor position. An example is shown in Figure 14.18 for a complex between a protein, Rep, and its DNA substrate. Rep belongs to a family of proteins called helicases, which bind to DNA and separate the annealed strands of the double helix. The green space-filling clusters on the protein structure on the left indicate the different donor positions along the surface of Rep, and the comb-shaped structure with a red circle represents the acceptor-labeled DNA substrate. The relative FRET efficiencies for each donor site and the substrate are shown by the red bars. From these values, the relative donor-acceptor distances can be determined using Equation (14.13). These data support an acceptor position marked by the red sphere adjacent to the protein structure on the right and provide information on how DNA is bound by Rep. For details, see the reference to Rasnik et al. in Further Reading.

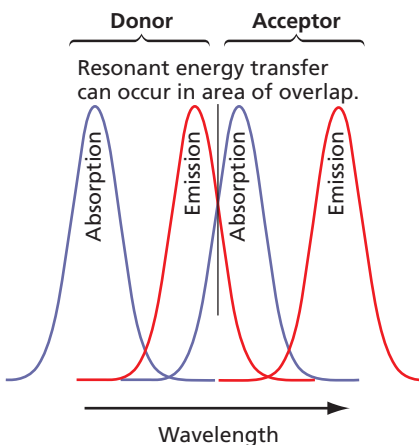


Figure 14.16

Criterion for resonance energy transfer. The blue and red curves show the range in wavelength over which absorption (respectively) occur for the donor and acceptor molecules. Note that emission occurs at longer wavelengths than absorption as discussed in Section 14.7. If the emission band for the donor overlaps the absorption band for the acceptor, resonant energy transfer can occur.

Concept

FRET can be used to investigate both protein structure and the interactions between proteins and binding partners.

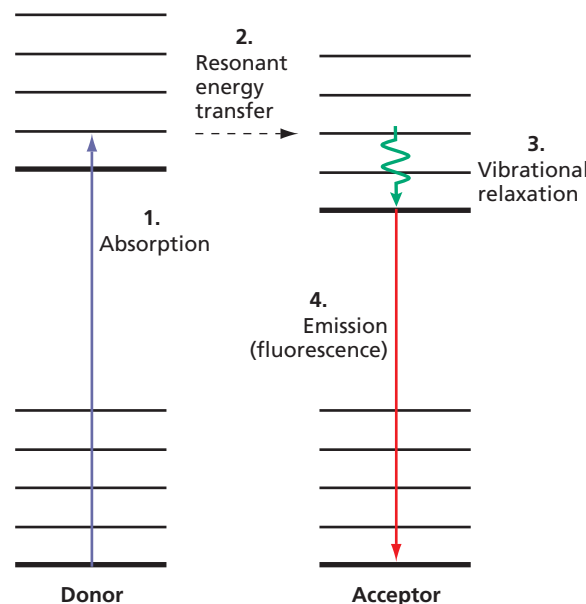
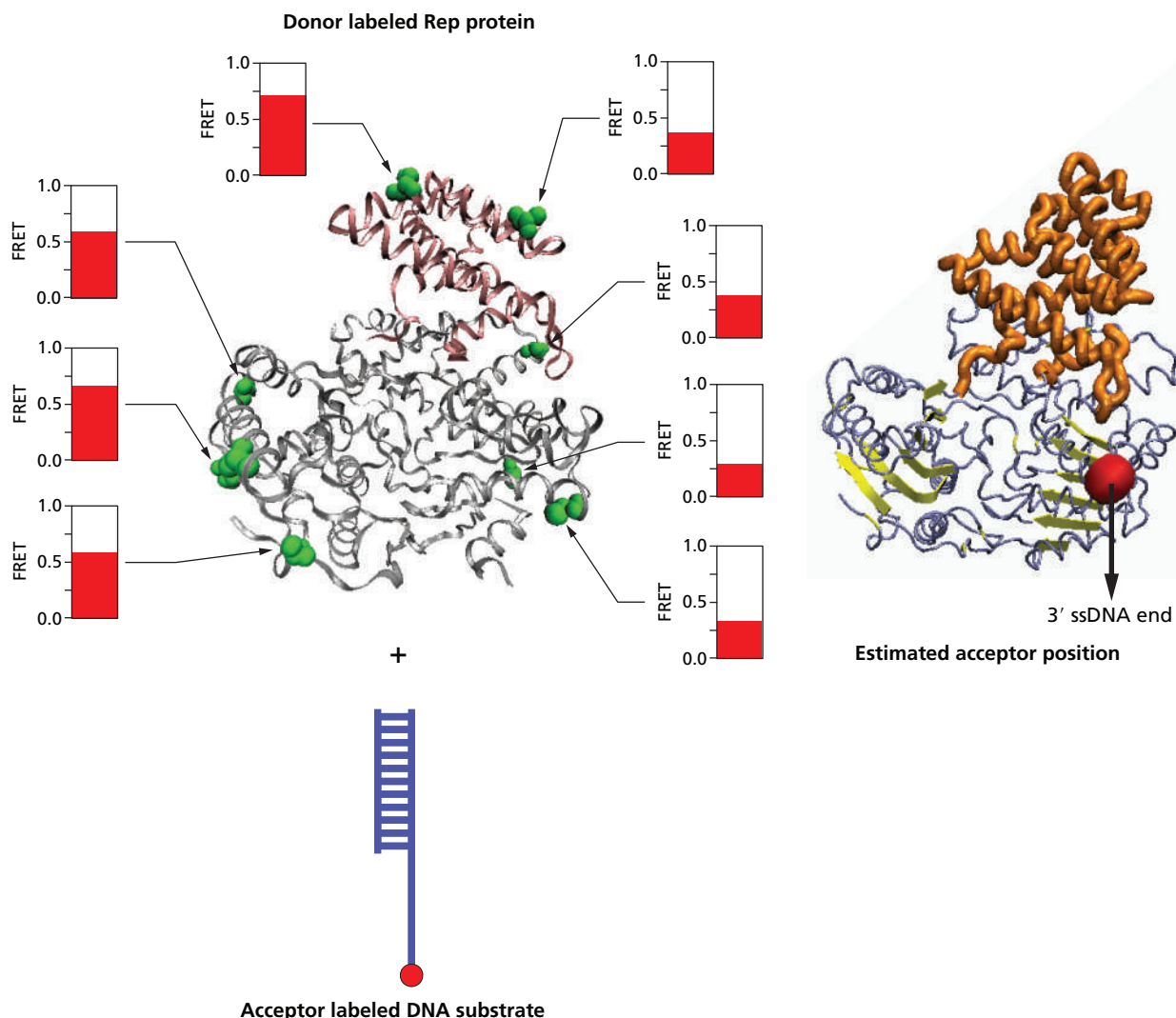


Figure 14.17

Individual events in FRET-based fluorescence spectroscopy. After absorption of a photon by the donor molecule (1), resonant transfer to an excited state of the acceptor molecule at the same energy occurs (2). Rapid vibrational relaxation (3) occurs to the lowest vibration state in the excited acceptor state. The final step (4) is fluorescence to the ground state of the acceptor with the emission of a photon. Note that because of vibrational relaxation in the excited acceptor state, the wavelength of the emitted light is longer than that of the absorbed light. This shift allows the use of optical filters to detect acceptor emission in the presence of scattered light from the laser used to excite the donor.

**Figure 14.18**

Application of FRET in determining tertiary structure of proteins. The green complexes correspond to several different donor positions in a Rep-DNA complex. The relative FRET efficiency for each donor position (red bars) relative to the acceptor (red complex in the lower right of the figure) is measured. The relative donor-acceptor distances can be determined using Equation (14.13). Figure courtesy of Taekjip Ha.

Concept

Linear and circular dichroism are particularly useful in providing information on the secondary structure of biomolecules.

14.13 LINEAR AND CIRCULAR DICHROISM

Because the structure of molecules is closely linked to their reactivity, it is a goal of chemists to understand the structure of molecules. This is a major challenge for biomolecules because the larger the molecule, the more challenging it is to determine the structure. However, several spectroscopic techniques are available that allow us to determine aspects of the molecular structure of biomolecules. Linear and circular dichroism are particularly useful in providing information on the secondary structure of biomolecules. It should be noted, however, that these techniques do not determine the positions of all atoms in the molecule.

As discussed in Section 8.1, light is a transverse electromagnetic wave that interacts with molecules through a coupling of the electric field \mathbf{E} of the light wave to the permanent or transient dipole moment μ of the molecule. Both \mathbf{E} and μ are vectors, and in classical physics the strength of the interaction is proportional to the scalar product $\mathbf{E} \cdot \mu$. For a transition between two states of a molecule, the intensity of the spectral line is proportional to $\mathbf{E} \cdot \mu^{fi}$, where the **transition dipole moment** is defined by

$$\mu^{fi} = \int \psi_f^*(\tau) \mu(\tau) \psi_i(\tau) d\tau \quad (14.14)$$

In Equation (14.14), $d\tau$ is the infinitesimal three-dimensional volume element, and ψ_i and ψ_f refer to the initial and final states in the transition in which a photon is absorbed

or emitted. The spatial orientation of μ^{fi} is determined by the direction of motion of electron charge that occurs in the transition. We show the orientation of μ^{fi} for an excitation of the amide group, which is the building block for the backbone of a polypeptide for a given $\pi \rightarrow \pi^*$ transition in Figure 14.20.

Many biomolecules have a long rod-like shape and can be oriented by embedding them in a film and then stretching the film. For such a sample, the molecule and therefore μ^{fi} has a well-defined orientation in space. The electric field \mathbf{E} can also be oriented in a plane with any desired orientation using a polarization filter, in which **linearly polarized light** is produced, as shown in Figure 14.19.

If the plane of polarization is varied with respect to the molecular orientation, the measured absorbance A will vary. It has a maximum value if \mathbf{E} and μ^{fi} are parallel, and it is zero if \mathbf{E} and μ^{fi} are perpendicular. In **linear dichroism spectroscopy**, the variation of the absorbance with the orientation of plane-polarized light relative to the sample is measured. Linear dichroism spectroscopy is primarily useful in determining the direction of μ^{fi} for an ensemble of oriented molecules whose secondary structure is not known. One measures the absorbance, A , with \mathbf{E} parallel and perpendicular to the molecular axis. The difference $A_{\parallel} - A_{\perp}$ relative to the absorbance for randomly polarized light is the quantity of interest.

We illustrate the application of linear dichroism spectroscopy in determining the secondary structure of a polypeptide in the following discussion. The amide groups shown in Figure 14.20 interact with one another because of their close spacing, and the interaction can give rise to a splitting of the transition into two separate peaks. The orientation of μ^{fi} for each peak depends on the polypeptide secondary structure. For the case of an α -helix, a transition near 208 nm with μ^{fi} parallel to the helix axis and a transition near 190 nm with μ^{fi} perpendicular to the helix axis is predicted from theory. Figure 14.21 shows the absorbance for randomly polarized light and $A_{\parallel} - A_{\perp}$ for a polypeptide. The data show that $A_{\parallel} < A_{\perp}$ for the transition near 190 nm and that $A_{\parallel} > A_{\perp}$ near 208 nm. This shows that the secondary structure of this polypeptide is an α -helix. By contrast, the absorption for randomly polarized light gives no structural information.

Because molecules must be oriented in space for spectroscopists to perform linear dichroism spectroscopy, the technique cannot be used for biomolecules in a static solution. For solutions, circular dichroism spectroscopy is widely used to obtain secondary structural information. In this type of spectroscopy, circularly polarized light, which is depicted in Figure 14.22, is passed through the solution.

Biomolecules are optically active, meaning that they do not possess a center of inversion. For an optically active molecule, the absorption for circularly polarized light in which the direction of rotation is clockwise (R) differs from that in which the direction of rotation is counterclockwise (L). This difference in A can be expressed as a difference in the extinction coefficient ε .

$$\Delta A(\lambda) = A_L(\lambda) - A_R(\lambda) = [\varepsilon_L(\lambda) - \varepsilon_R(\lambda)]lc = \Delta \varepsilon lc \quad (14.15)$$

In Equation (14.15), l is the path length in the sample cell and c is the concentration. In practice, the difference between $A_L(\lambda)$ and $A_R(\lambda)$ is usually expressed as the molar residual ellipticity, which is the shift in the phase angle θ between the components of the circularly polarized light in the form

$$\theta = 2.303 \times (A_L - A_R) \times 180/(4\pi) \text{ degrees} \quad (14.16)$$

Circular dichroism can only be observed if ε is nonzero and is usually observed in the visible part of the light spectrum.

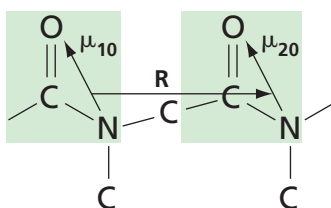


Figure 14.20
Amide bonds (indicated by shaded area) in a polypeptide chain. The strength of the dipole–dipole interaction between the N—O dipoles designated by μ_{10} and μ_{20} depends on their separation, designated by R .

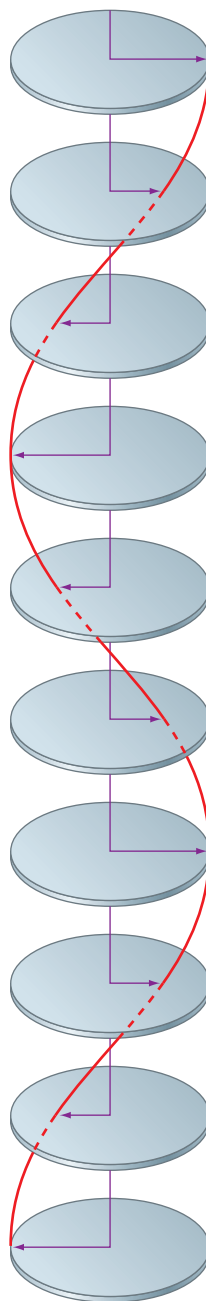
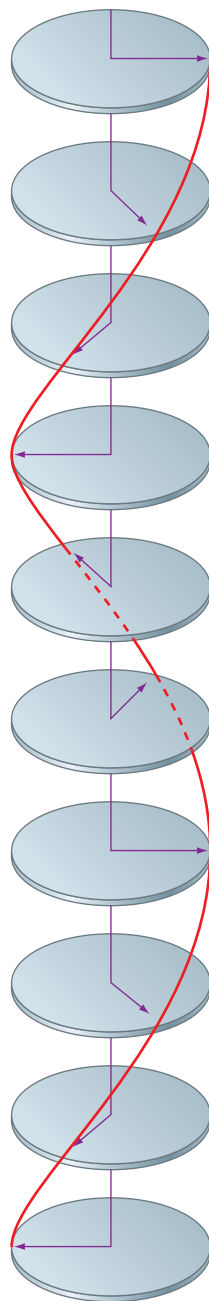


Figure 14.19

Depiction of linearly polarized light. The discs represent slices perpendicular to the propagation of a light wave. The arrows in successive images indicate the direction of the electric field vector as a function of time or distance. For linearly polarized light, the amplitude of the electric field vector changes periodically, but is confined to the plane of polarization.

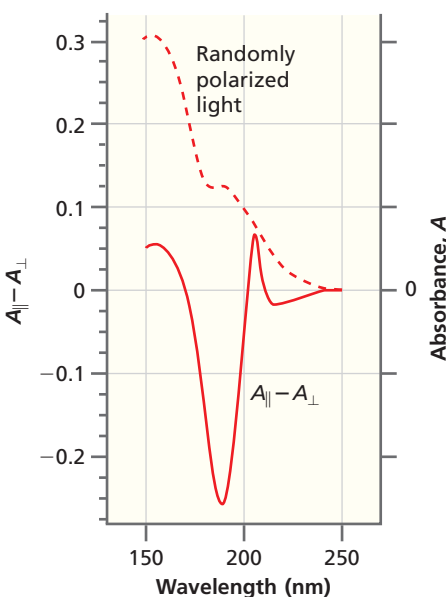
**Figure 14.22**

Depiction of circularly polarized light. The discs represent slices perpendicular to the propagation of a light wave. The arrows in successive images indicate the direction of the electric field vector as a function of time or distance. For circularly polarized light, the amplitude of the electric field vector is constant, but its plane of polarization undergoes a periodic variation.

Figure 14.21

Absorbance for randomly polarized light and $A_{\parallel} - A_{\perp}$ for a polypeptide. The absorbance A for randomly polarized light (dashed line) and $A_{\parallel} - A_{\perp}$ (solid line) are shown as a function of the wavelength for an oriented film of poly(γ -ethyl-L-glutamate), which has an α -helix secondary structure.

Source: Adapted from data from J. Brahms et al., Application of a New Modulation Method for Linear Dichroism Studies of Oriented Biopolymers in the Vacuum Ultraviolet, *Proceedings of the National Academy of Sciences USA* 60 (1968): 1130.

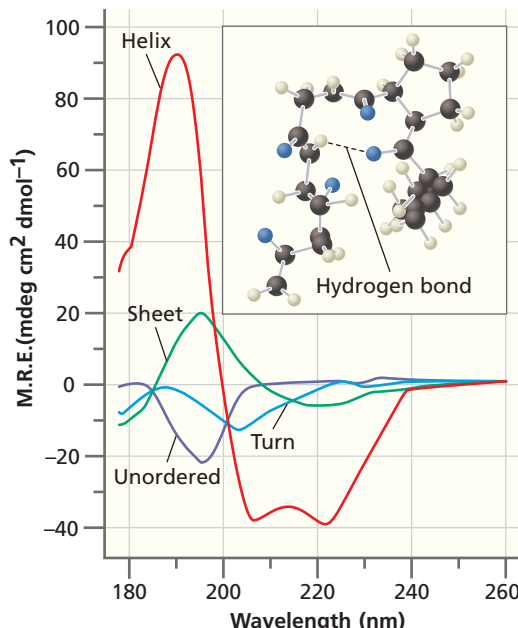


As in the case of linear dichroism, $\Delta A(\lambda)$ for a given transition is largely determined by the secondary structure and is much less sensitive to other aspects of the conformation. A discussion of how $\Delta A(\lambda)$ depends on the secondary structure is beyond the level of this textbook, but it can be shown that common secondary structures such as the α -helix, the β -sheet, a single turn, and a random coil have a distinctly different $\varepsilon(\lambda)$ dependence, as shown in Figure 14.23. In this range of wavelengths, the absorption corresponds to $\pi \rightarrow \pi^*$ transitions of the amide group.

The absorbance curves for the different secondary structures in Figure 14.23 are sufficiently different that the extracted $\Delta \varepsilon(\lambda)$ curve obtained for a protein of unknown secondary structure in solution can be expressed in the form

$$\Delta \varepsilon_{\text{observed}}(\lambda) = \sum_i F_i \Delta \varepsilon_i(\lambda) \quad (14.17)$$

where $\Delta \varepsilon_i(\lambda)$ is the curve corresponding to one of the possible secondary structures of the biomolecule and F_i is the fraction of the peptide chromophores in that particular secondary structure. A best fit of the data to Equation (14.17) using widely available software allows a determination of the F_i to be made.

**Figure 14.23**

Mean residual ellipticity θ as a function of wavelength for biomolecules with different secondary structures. Because the curves for common secondary structures are distinctly different, circular dichroism spectra can be used to determine the secondary structure for optically active molecules. The inset shows the hydrogen bonding between different amide groups that generates different secondary structures.

Source: Adapted from John T. Pelton, Secondary Considerations, *Science* 291: 2175–2176, March 16, 2001.

Figure 14.24 shows the results of an application of circular dichroism in determining the secondary structure of α -synuclein bound to unilamellar phospholipid vesicles, which were used as a model for cell membranes. α -synuclein is a small soluble protein of 140–143 amino acids that is present in high concentration in presynaptic nerve terminals. A mutation in this protein has been linked to Parkinson disease, and it is believed to be a precursor in the formation of extracellular plaques in Alzheimer disease.

As can be seen by comparing the spectra in Figure 14.24 with those of Figure 14.23, the conformation of α -synuclein in solution is that of a random coil. However, upon binding to unilamellar phospholipid vesicles, the circular dichroism spectrum is dramatically changed and is characteristic of an α -helix. These results show that the binding of α -synuclein requires a change in its secondary structure. This change can be understood from the known sequence of amino acids in the protein. By forming an α -helix, the polar and nonpolar groups in the protein are shifted to opposite sides of the helix. This allows the polar groups to associate with the acidic phospholipids, leading to a stronger binding than would be the case for a random coil.

SUPPLEMENTAL SECTION

14.14 ASSIGNING + AND - TO Σ TERMS OF DIATOMIC MOLECULES

In this section, we will illustrate how the + and – symmetry designations are applied to Σ terms for homonuclear diatomic molecules. More complete discussions appear in the references to Levine, and to Karplus and Porter in Further Reading.

Recall that only partially filled MOs need to be considered in generating term symbols from a molecular configuration. The + and – designations refer to the change in sign of the molecular wave function on reflection in a plane that contains the molecular axis. If there is no change in sign, the + designation applies; if the wave function does change sign, the – designation applies. In the simplest case, all MOs are filled or the unpaired electrons are all in σ MOs. For such states, the + sign applies because there is no change in the sign of the wave function as a result of the reflection operation, as can be seen in Figure 14.25.

We next discuss molecular terms that do not fit into these categories, using O_2 as an example. The configuration for ground state O_2 is $(1\sigma_g)^2(1\sigma_u^*)^2(2\sigma_g)^2(2\sigma_u^*)^2(3\sigma_g)^2(1\pi_u)^2(1\pi_u^*)^2(1\pi_g^*)^1(1\pi_g^*)^1$, where we associate the partially filled MOs with the out-of-phase combinations of the $2p_x$ and $2p_y$ AOs as shown in Figure 14.26. Because filled MOs can be ignored, O_2 has a $(\pi^*)^2$ configuration, with one electron on each of the two degenerate π^* MOs. Recall that, in general, a configuration gives rise to several quantum states. Because the two electrons are in different $1\pi_g^*$ MOs, all six combinations of ± 1 for m_l and $\pm 1/2$ for m_s are possible. For example, the Σ terms for which $M_L = m_{l1} + m_{l2} = 0$ occur as singlet and triplet terms. To satisfy the Pauli exclusion principle, the overall wave function (which is a product of spin and spatial parts) must be antisymmetric in the exchange of two electrons.

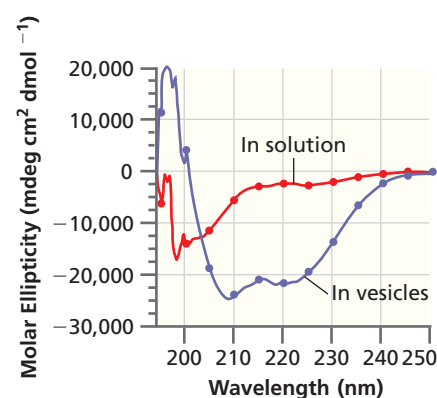


Figure 14.24

Molar ellipticity is shown as a function of the wavelength for α -synuclein. The molar ellipticity is shown for α -synuclein in solution (red circles) and for α -synuclein bound to unilamellar phospholipid vesicles (blue circles).

Source: Adapted from W. Sean Davidson et al., Stabilization of α -Synuclein Secondary Structure upon Binding to Synthetic Membranes, *The Journal of Biological Chemistry*, 273 (16): 9443–9449, April 1998.

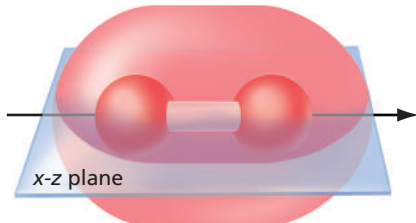


Figure 14.25

Reflection of a σ molecular orbital in a plane passing through the molecular axis. This geometrical arrangement leaves the wave function unchanged.

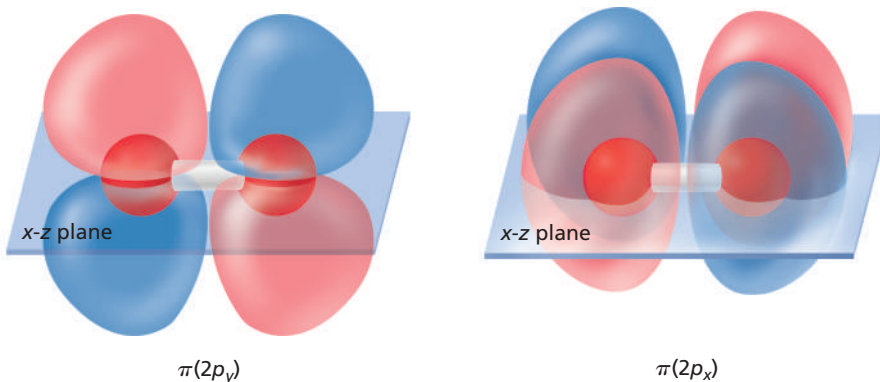


Figure 14.26

Depiction of two degenerate $1\pi_g^*$ wave functions.

However, just as the $2p_x$ and $2p_y$ AOs are not eigenfunctions of the operator \hat{L}_z , as discussed in Chapter 7, the MOs depicted in Figure 14.26 are not eigenfunctions of the operator \hat{L}_z . To discuss the assignment of + and – to molecular terms, we can only use wave functions that are eigenfunctions of \hat{L}_z . In the cylindrical coordinates appropriate for a diatomic molecule, $\hat{L}_z = -i\hbar(\partial/\partial\phi)$, where ϕ is the angle of rotation around the molecular axis, and the eigenfunctions of this operator have the form $\psi(\phi) = Ae^{-i\Lambda\phi}$, as shown in Section 7.4. We cannot depict these complex functions because this requires a six-dimensional space rather than the three-dimensional space required to depict real functions.

The O₂ molecule has a $(\pi^*)^2$ configuration, and antisymmetric molecular wave functions can be formed either by combining symmetric spatial functions with antisymmetric spin functions or vice versa. All possible combinations are shown in the following equations. The subscript +1 or –1 on the spatial function indicates the value of m_l .

$$\begin{aligned}\psi_1 &= \pi_{+1}\pi_{+1}(\alpha(1)\beta(2) - \beta(1)\alpha(2)) \\ \psi_2 &= \pi_{-1}\pi_{-1}(\alpha(1)\beta(2) - \beta(1)\alpha(2)) \\ \psi_3 &= (\pi_{+1}\pi_{-1} + \pi_{-1}\pi_{+1})(\alpha(1)\beta(2) - \beta(1)\alpha(2)) \\ \psi_4 &= (\pi_{+1}\pi_{-1} - \pi_{-1}\pi_{+1})\alpha(1)\alpha(2) \\ \psi_5 &= (\pi_{+1}\pi_{-1} - \pi_{-1}\pi_{+1})(\alpha(1)\beta(2) + \beta(1)\alpha(2)) \\ \psi_6 &= (\pi_{+1}\pi_{-1} - \pi_{-1}\pi_{+1})\beta(1)\beta(2)\end{aligned}$$

As shown in Section 11.2, the first three wave functions are associated with singlet states, and the last three are associated with triplet states. Because $\Lambda = |M_L|$, ψ_1 and ψ_2 belong to a Δ term, and ψ_3 through ψ_6 belong to Σ terms.

Finally, we determine how these six wave functions are changed on reflection through a plane containing the molecular axis. As shown in Figure 14.27, reflection through such a plane changes the rotation angle $+\phi$ into $-\phi$. As a consequence, for each eigenfunction of \hat{L}_z , $Ae^{-i\Lambda\phi}$ is transformed into $Ae^{+i\Lambda\phi}$, which is equivalent to changing the sign of M_L . Therefore, $\pi_{+1} \rightarrow \pi_{-1}$ and $\pi_{-1} \rightarrow \pi_{+1}$. Note that reflection does not change the sign of the wave function for ψ_1 through ψ_3 because $(-1) \times (-1) = 1$. Therefore, the plus sign applies and the term corresponding to ψ_3 is ${}^1\Sigma_g^+$. However, reflection does change the sign of the wave function for ψ_4 through ψ_6 because $(-1) \times (+1) = -1$; therefore, the minus sign applies. Because these three wave functions belong to a triplet term, the term symbol is ${}^3\Sigma_g^-$. A similar analysis can be carried out for other configurations.

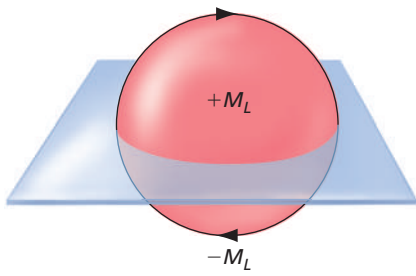


Figure 14.27

The rotation angle ϕ is transformed into $-\phi$ through reflection in a plane that contains the molecular axis. This operation is equivalent to changing $+M_L$ into $-M_L$.

VOCABULARY

- acceptor
- Beer's law
- Born–Oppenheimer approximation
- chromophore
- donor
- fluorescence
- Franck–Condon factor
- Franck–Condon principle
- frozen orbital approximation
- integral absorption coefficient
- internal conversion

- intersystem crossing
- Koopmans' theorem
- linear dichroism spectroscopy
- linearly polarized light
- molar extinction coefficient
- molecular configuration
- molecular term
- nonradiative transition
- phosphorescence
- photodissociation
- photoionization
- primary structure
- quaternary structure
- radiative transition
- resonance energy transfer
- secondary structure
- $\sigma \rightarrow \sigma^*$ transitions
- singlet state
- tertiary structure
- transition dipole moment
- triplet state
- UV photoelectron spectroscopy

KEY EQUATIONS

Equation	Significance of Equation	Equation Number
$M_L = \sum_{i=1}^n m_{li}$ and $M_S = \sum_{i=1}^n m_{si}$	Good quantum numbers for diatomic molecules	14.1
$S_{ol}^2 = \left \int (\phi_f^{\text{vibrational}})^* \phi_i^{\text{vibrational}} d\tau \right ^2$	Franck–Condon factor determines the intensity of electronic transitions	14.10
$\log\left(\frac{I_t}{I_0}\right) = -\epsilon lc$	Beer's law relates decrease in light intensity upon passing through sample to concentration, path length, and molar extinction coefficient	14.11
$E_{\text{kinetic}} = h\nu - \left[E_f + \left(n_f + \frac{1}{2} \right) h\nu_{\text{vibration}} \right]$	Kinetic energy of ejected electron in UV photoelectron spectroscopy	14.12
$k_{\text{ret}} = \frac{1}{\tau_D^\circ} \left(\frac{R_0}{r} \right)^6$	Rate constant for resonant energy transfer	14.13
$\mu^{fi} = \int \psi_f^*(\tau) \mu(\tau) \psi_i(\tau) d\tau$	Transition dipole moment determines intensity of electronic transition	14.14

CONCEPTUAL PROBLEMS

Q14.1 Predict the number of unpaired electrons and the ground state term for the following molecules:

- a. BO b. LiO

Q14.2 How can FRET provide information about the tertiary structure of a biological molecule in solution?

Q14.3 Photoionization of a diatomic molecule produces a singly charged cation. An electronic spectrum will show vibrational transitions as discussed in Section 14.4. For the molecules listed here, calculate the bond order of the neutral molecule and the lowest energy cation. For which of the molecules do you expect the $n = 0 \rightarrow n' = 1$ vibrational peak to have a higher intensity than the $n = 0 \rightarrow n' = 0$ vibrational peak? The term n refers to the vibrational quantum number in the ground state, and n' refers to the vibrational quantum number in the excited state.

- a. H₂ b. O₂ c. F₂ d. NO

Q14.4 What would the intensity versus frequency plot in Figure 14.9 look like if fluorescence were fast with respect to internal conversion?

Q14.5 What aspect of the confocal microscope makes single-molecule spectroscopy in solutions possible?

Q14.6 Explain why the fluorescence and absorption groups of peaks in Figure 14.9 are shifted and show mirror symmetry for idealized symmetrical ground state and excited-state potentials.

Q14.7 The rate of fluorescence is higher than that for phosphorescence. Can you explain this fact?

Q14.8 Can linear dichroism spectroscopy be used for molecules in a static solution or in a flowing solution? Explain your answer.

Q14.9 Predict the number of unpaired electrons and the ground-state term for the following:

- a. NO b. CO

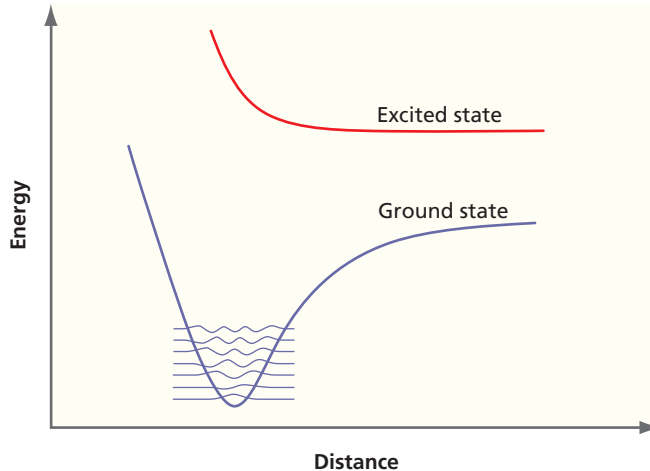
Q14.10 How many distinguishable states belong to the following terms:

- a. ${}^1\Sigma_g^+$ b. ${}^3\Sigma_g^-$ c. ${}^2\Pi$ d. ${}^2\Delta$

Q14.11 Explain why the spectator species M in Equation (14.5) is needed to make the reaction proceed.

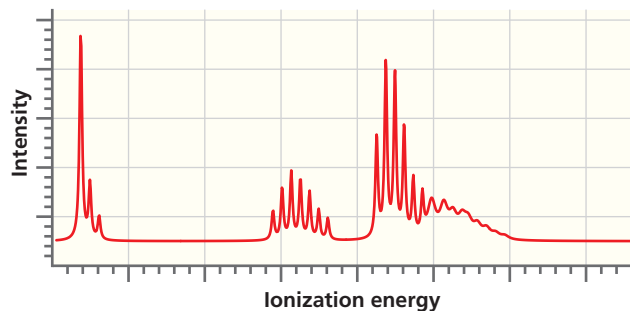
Q14.12 Because internal conversion is in general very fast, the absorption and fluorescence spectra are shifted in frequency, as shown in Figure 14.9. This shift is crucial in making fluorescence spectroscopy capable of detecting very small concentrations. Can you explain why?

Q14.13 What do you expect the electronic spectrum to look like for the ground and excited states shown here?



Q14.14 Why are the spectra of individual molecules in the bottom trace of Figure 14.14 shifted in frequency?

Q14.15 Suppose you obtain the UV photoelectron spectrum shown here for a gas-phase molecule. Each of the groups corresponds to a cation produced by ejecting an electron from a different MO. What can you conclude about the bond length of the cations in the three states formed relative to the ground state neutral molecule? Use the relative intensities of the individual vibrational peaks in each group to answer this question.



Q14.16 The ground state of O_2^+ is $X^2\Pi_g$, and the next few excited states, in order of increasing energy, are $a^4\Pi_u$, $A^2\Pi_u$, $b^1\Sigma_g^+$, $A^3\Sigma_u^+$, $B^3\Sigma_u^-$, and $c^4\Sigma_u^-$. On the basis of selection rules, which of the excited states can be accessed from the ground state by absorption of UV light?

Q14.17 The relative intensities of vibrational peaks in an electronic spectrum are determined by the Franck–Condon factors. How would the potential curve for the excited state in Figure 14.2 need to be shifted along the distance axis for the $n = 0 \rightarrow n' = 0$ transition to have the highest intensity?

Q14.18 Calculate the bond order for O_2 in the $X^3\Sigma_g^-$, $a^1\Delta_g$, $b^1\Sigma_g^+$, $A^3\Sigma_u^+$, and $B^3\Sigma_u^-$ states. Arrange these states in order of increasing bond length on the basis of bond order. Do your results agree with the potential energy curves shown in Figure 14.1? For which of the molecules do you expect the $n = 0 \rightarrow n' = 1$ vibrational peak to have a higher intensity than the $n = 0 \rightarrow n' = 0$ vibrational peak? The term n refers to the vibrational quantum number in the ground state, and n' refers to the vibrational quantum number in the excited state.

Q14.19 How can circular dichroism spectroscopy be used to determine the secondary structure of a biomolecule?

Q14.20 What does the word resonance in FRET refer to?

Q14.21 In a simple model used to analyze UV photoelectron spectra, the orbital energies of the neutral molecule and the cation formed by ejection of an electron are assumed to be the same. In fact, some relaxation occurs to compensate for the reduction in the number of electrons by one. Would you expect the orbital energies to increase or decrease in the relaxation? Explain your answer.

NUMERICAL PROBLEMS

Section 14.3

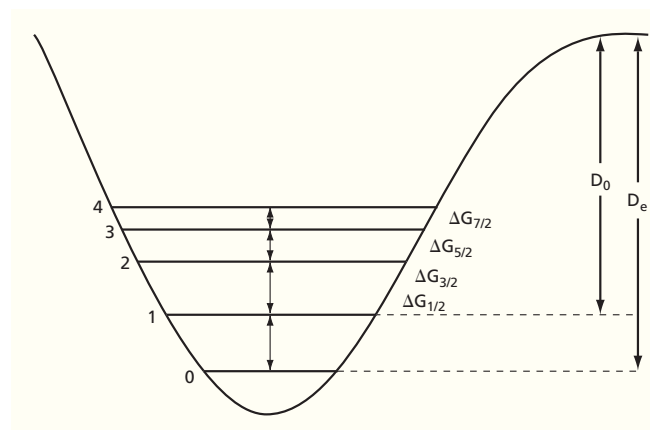
P14.1 Determine if the following transitions are allowed or forbidden:

- $^3\Pi_u \rightarrow ^3\Sigma_g^-$
- $^1\Sigma_g^+ \rightarrow ^1\Pi_g$
- $^3\Sigma_g^- \rightarrow ^3\Pi_g$
- $^1\Pi_g \rightarrow ^1\Delta_u$

P14.2 The ground electronic state of O_2 is $^3\Sigma_g^-$, and the next two highest energy states are $^1\Delta_g$ (7918 cm^{-1}), and $^1\Sigma_g^+$ (13195 cm^{-1}), where the value in parentheses is the energy of the state relative to the ground state.

- Determine the excitation wavelength required for a transition between the ground state and the first two excited states.
- Are these transitions allowed? Why or why not?

P14.3 When vibrational transitions are observed in electronic absorption spectrum, these transitions can be used to determine dissociation energies. Specifically, a Birge–Sponer plot is constructed in which the energy difference between successive vibrational transitions n and $n + 1$ ($\Delta G_{n+1/2}$) is plotted against the vibrational level (see the accompanying figure). Note that G does not refer to the Gibbs energy in this context.



The central idea behind the approach is that the dissociation energy is equal to the sum of these energy differences from $n = 0$ to the dissociation limit:

$$D_0 = \Delta G_{1/2} + \Delta G_{3/2} + \Delta G_{5/2} + \dots = \sum_{n=0}^{n_{diss}} \Delta G_{n+1/2}$$

- For the ground state of I_2 the following values for ΔG versus n were determined (*Journal of Chemical Physics*, 32, 738 [1960]):

n	$\Delta G \text{ (cm}^{-1}\text{)}$
0	213.31
1	212.05
2	210.80
3	209.66
4	208.50
5	207.20
6	205.80
7	204.55
8	203.18
9	201.93
10	199.30
11	198.05
12	196.73
13	195.36
14	194.36
15	192.73
16	191.31
17	189.96
18	188.47
19	187.07

If the potential function can be described by a Morse potential (Equation 8.5), ΔG will be a linear function of $n + \frac{1}{2}$. Construct a Birge–Sponer plot (ΔG versus $n + \frac{1}{2}$) using the above data, and using best fit to a straight line determine the value of n where $\Delta G = 0$. This is the I_2 ground state vibrational level at dissociation.

- b.** The area under the Birge–Sponer plot is equal to the dissociation energy, D_0 . This area can be determined by summing the ΔG values from $n = 0$ to n at dissociation (determined in part a). Perform this summation to determine D_0 for ground state I_2 . You can also integrate the best fit equation to determine D_0 .

P14.4 Birge–Sponer plots are generally made using ΔG for n values numerically distant from the dissociation limit. If the data include n values close to the dissociation limit, deviations from a linear relationship between ΔG and n are observed. Taking these deviations into account allows a more accurate determination of the n value corresponding to dissociation and D_0 to be made. A student determined the following values for ΔG versus n for the ground state of H_2 :

n	$\Delta G \text{ (cm}^{-1}\text{)}$
0	4133
1	3933
2	3733
3	3533
4	3233
5	3000
6	2733
7	2533
8	2267
9	2000
10	1733
11	1400
12	1067
13	633

- Construct a Birge–Sponer plot (ΔG versus $n + \frac{1}{2}$) using the above data, and fit the data assuming a linear relationship between ΔG and n . Determine the value of n where $\Delta G = 0$. This is the H_2 ground state vibrational level at dissociation.
- The area under the Birge–Sponer plot is equal to the dissociation energy, D_0 . This area can be determined by summing the ΔG values from $n = 0$ to n at dissociation (determined in part a). Perform this summation to determine D_0 for ground state I_2 . You can also integrate your best fit expression $\Delta G(n)$ from zero to the n value corresponding to dissociation. Compare your result with the value shown in Table 8.3.
- Determine the value of n where $\Delta G = 0$ and determine D_0 assuming a quadratic relationship between ΔG and n , $\Delta G = a + b(n + 1/2) + c(n + 1/2)^2$. Which fit gives better agreement with the value for D_0 shown in Table 8.3?

P14.5 Electronic spectroscopy of the Hg–Ar van der Waals complex was performed to determine the dissociation energy of the complex in the first excited state (C. J. K. Quayle et al., *Journal of Chemical Physics* 99 (1993): 9608). As described in P14.3, the following data regarding ΔG versus n were obtained:

n	$\Delta G \text{ (cm}^{-1}\text{)}$
1	37.2
2	34
3	31.6
4	29.2
5	26.8

- Construct a Birge–Sponer plot (ΔG versus $n + \frac{1}{2}$) using the above data, and using a best fit to a straight line determine the value of n where $\Delta G = 0$. This is the vibrational level at dissociation in the excited state. $\Delta G_{1/2}$ can also be determined from the plot.
- The area under the Birge–Sponer plot is equal to the dissociation energy, D_0 , for this van der Waals complex in the excited state. The area can be determined by summing the ΔG values from $n = 0$ to n at dissociation [determined in part (a)]. You can also integrate the best fit equation to determine D_0 .

Section 14.4

P14.6 Consider a diatomic molecule for which the bond force constant in the ground and excited electronic states is the same, but the equilibrium bond length is shifted by an amount δ in the excited state relative to the ground state. For this case, the vibrational wave functions for the $n = 0$ state are:

$$\psi_{g,0} = \left(\frac{\alpha}{\pi}\right)^{1/4} e^{-\frac{1}{2}\alpha r^2}, \psi_{e,0} = \left(\frac{\alpha}{\pi}\right)^{1/4} e^{-\frac{1}{2}\alpha(r-\delta)^2}, \alpha = \sqrt{\frac{k\mu}{\hbar^2}}$$

Calculate the Franck–Condon factor for the 0–0 transition for this molecule by evaluating the following expression:

$$\left| \int_{-\infty}^{\infty} \psi_{g,0}^* \psi_{e,0} dr \right|^2$$

In evaluating this expression, the following integral will be useful:

$$\int_{-\infty}^{\infty} e^{-ax^2 - bx} dx = \left(\frac{\pi}{a}\right)^{1/2} e^{\frac{b^2}{4a}} \quad (a > 0).$$

P14.7 One method for determining Franck–Condon factors between the $n = 0$ vibrational state of the ground electronic state and the n_{th} vibrational level of an electronic excited state is (note change to lower-case delta for consistency with the previous problem):

$$FC_{0-n} = \frac{1}{n!} \left(\frac{\delta^2}{2} \right)^n \exp \left(-\frac{\delta^2}{2} \right)$$

where δ is the dimensionless displacement of the excited state relative to the ground state and can be related to atomic displacements through:

$$\delta = \left(\frac{\mu\omega}{\hbar} \right)^{1/2} (r_e - r_g)$$

- a. Determine the Franck–Condon factors for $n = 0$ to $n = 5$ when $\delta = 0.20$ corresponding to the excited-state potential surface being slightly displaced from that of the ground state.
- b. How would you expect the Franck–Condon factors to change if the excited-state displacement increases to $\delta = 2.0$? Verify your expectation by calculating the Franck–Condon factors from $n = 0$ to $n = 5$ for this displacement.

Section 14.7

P14.8 Ozone (O_3) has absorptivity at 300. nm of $0.000500 \text{ torr}^{-1} \text{ cm}^{-1}$. In atmospheric chemistry, the amount of ozone in the atmosphere is quantified using the Dobson unit (DU), where 1 DU is equivalent to a 10^{-2} -mm-thick layer of ozone at 1 atm and 273.15 K.

- a. Calculate the absorbance of the ozone layer at 300. nm for a typical coverage of 300. DU.
- b. Seasonal stratospheric ozone depletion results in a decrease in ozone coverage to values as low as 120. DU. Calculate the absorbance of the ozone layer at this reduced coverage.

In each part, also calculate the transmission from absorbance using Beer's law.

Section 14.12

P14.9 Green fluorescent protein (GFP) and variants of this protein have been developed for *in vivo* FRET studies (B. Pollok and R. Heim, *Trends in Cell Biology* 9 [1999] 57). Two variants of GFP, cyan fluorescent protein (CFP) and yellow fluorescent protein (YFP), form a FRET pair where $R_0 = 4.72 \text{ nm}$. The excited-state lifetime of the CFP donor in the absence of YFP is 2.7 ns.

- a. At what distance will the rate of energy transfer be equal to the excited-state decay rate for isolated CFP (which is also equal to the inverse of the excited-state lifetime)?
- b. Determine the distance at which the energy transfer rate will be five times the excited-state decay rate.

P14.10 Structural changes in proteins have been measured using FRET with the amino acid tryptophan as the donor and dansyl as the acceptor where dansyl is attached to the protein through addition to amino acids with aliphatic amine groups such as lysine. For this pair $R_0 = 2.1 \text{ nm}$, and the excited state lifetime of tryptophan is $\sim 1.0 \text{ ns}$. Determine the rate of energy transfer for $r = 0.50, 1.0, 2.0, 3.0, \text{ and } 5.0 \text{ nm}$.

P14.11 Assume that a FRET donor-acceptor pair is composed of the fluorescent dyes Alexa Fluor 488 (excited-state lifetime of 4.1 ns) and Alexa Fluor 594. For this FRET pair $R_0 = 5.4 \text{ nm}$. The distance between the FRET pair ranges from 2.0 nm to 12.5 nm for the biomolecule of interest. Calculate the variation in the energy transfer rate for $r = 2.0, 7.0, \text{ and } 12.0 \text{ nm}$.

FURTHER READING

Brundle, C. R., and Turner, D. W. High resolution molecular photoelectron spectroscopy II. Water and deuterium oxide. *Proceedings of the Royal Society A*, 307 (1968): 27–36.

Campbell, M. “A Systematic Method for Determining Molecular Term Symbols for Diatomic Molecules Using Uncoupled-States Orbital Diagrams.” *Journal of Chemical Education* 73 (1996): 749–751.

Carrick, P., Curl, R. F., Dawes, M., Koester, E., Murray, K. K., Petri, M., and Richnow, M. L. “The OH Stretching Fundamental of Methanol.” *Journal of Molecular Structure* 223 (June 1990): 171–184.

Dovichi, N. “Development of DNA Sequencer.” *Science* 285 (1999): 1016.

Dunbrack, R., Jr. “Calculation of Franck–Condon Factors for Undergraduate Quantum Chemistry.” *Journal of Chemical Education* 63 (1986): 953–955.

Karplus, M. and Porter, R., *Atoms & Molecules*, Menlo Park: Benjamin Cummings (1970).

Levine, I. N. *Quantum Chemistry* (7th ed.). Boston: Pearson, 2014.

Pazhani, Y., Horn, A., Grado, L., and Kugel, J. “Evaluating the Relationship between FRET Changes and Distance Changes Using DNA Length and Restriction Enzyme Specificity.” *Journal of Chemical Education* 93 (2016): 383–385.

Qiao, L. Xiao, H., Heald, S., Bowden, M., Varga, T., Exarhos, G., et al. “The Impact of Crystal Symmetry on the Electronic Structure and Functional Properties of Complex Lanthanum Chromium Oxides.” *Journal of Materials Chemistry C* 1 (2013): 4527–4535.

Rasnik, I., McKinney, S., and Ha, T. “Surfaces and Orientations: Much to FRET about?” *Accounts of Chemical Research* 38 (2005): 542–548.

Weiss, S. “Measuring Conformational Dynamics of Biomolecules by Single Molecule Fluorescence Spectroscopy.” *Nature Structural Biology*, 7 (2000): 724–729.

Wright, J., and Zielinski, T. “Franck–Condon Factors and Their Use in Undergraduate Quantum Mechanics.” *Journal of Chemical Education* 76 (1999): 1367–1373.

Computational Chemistry

Warren J. Hehre, CEO, Wavefunction, Inc.

To the memory of Sir John Pople, 1925–2004

WHY is this material important?

Although the Schrödinger equation can easily be formulated for atoms and molecules, it cannot be solved exactly for any atom or molecule that has more than one electron. Therefore, numerical methods are essential in obtaining properties such as molecular orbital (MO) energy levels, bond lengths, bond angles, and thermodynamic quantities such as bond energy. This chapter discusses the trade-off between accuracy and cost in computational chemistry calculations as well as the underlying theoretical models on which calculations are based.

WHAT are the most important concepts and results?

The starting point of computational chemistry calculations is the Hartree–Fock model, which neglects electron correlation. For many applications, this model generates sufficiently accurate values of bond lengths and bond angles. However, to obtain thermodynamic information such as bond dissociation energies, reaction enthalpies, or activation energies, theoretical models that take correlation into account, such as density functional theory or Møller–Plesset theory, must be used.

WHAT would be helpful for you to review for this chapter?

It would be helpful to review the material in Chapters 10 and 12 on the Hartree–Fock model.

15.1 THE PROMISE OF COMPUTATIONAL CHEMISTRY

Calculations on molecules based on quantum mechanics, once a mere novelty, are now poised to complement experiments as a means to uncover and explore new chemistry. The most important reason for this is that the theories underlying the calculations have now evolved to the point at which a variety of important quantities, among them molecular equilibrium structure and reaction energetics, can be obtained with sufficient accuracy to actually be of use. Also important are the spectacular advances in computer hardware that have been made during the past decade. Taken together, this means that good theories can now be routinely applied to real systems. Finally, current computer software can be easily and productively used with little special training.

In making these quantum-mechanics calculations, however, significant obstacles remain. For one, the chemist is confronted with many choices to make and few guidelines on how to make these choices. The fundamental problem is that the mathematical

- 15.1 The Promise of Computational Chemistry
- 15.2 Potential Energy Surfaces
- 15.3 Hartree–Fock Molecular Orbital Theory: A Direct Descendant of the Schrödinger Equation
- 15.4 Properties of Limiting Hartree–Fock Models
- 15.5 Theoretical Models and Theoretical Model Chemistry
- 15.6 Moving Beyond Hartree–Fock Theory
- 15.7 Gaussian Basis Sets
- 15.8 Selection of a Theoretical Model
- 15.9 Graphical Models
- 15.10 Conclusion

equations that arise from the application of quantum mechanics to chemistry—and that ultimately govern molecular structure and properties—cannot be solved analytically. Approximations need to be made to generate equations that can actually be solved. Severe approximations may lead to methods that can be widely applied but may not yield accurate information. Less severe approximations may lead to methods that are more accurate but too costly to apply routinely. In short, no one method of calculation is likely to be ideal for all applications, and the ultimate choice of specific methods rests on a balance between accuracy and cost. We equate cost with the computational time required to carry out the calculation.

This chapter is designed to guide the student past the point of merely thinking about quantum mechanics as one of several components of a physical chemistry course and to instead have the student use quantum mechanics to address real chemical problems. The chapter starts with the many-electronic Schrödinger equation and then outlines the approximations that need to be made to transform this equation into what is now commonly known as Hartree–Fock theory. In the spirit of emphasizing the concepts rather than the theoretical framework, mathematical descriptions of the theoretical models discussed appear in boxes. A detailed understanding of this framework, however desirable, is not necessary to apply quantum mechanics to chemistry.

A focus on the limitations of Hartree–Fock theory leads to ways to improve on it and to a range of practical quantum-chemical models. A few of these models are examined in detail, and their performance and cost are discussed. Finally, a series of graphical techniques is presented to portray the results of quantum-chemical calculations. Aside from its practical focus, what sets this chapter apart from the remainder of this textbook is the problems. None of these are of the pencil-and-paper type; instead they require use of a quantum-chemical program¹ on a digital computer. For the most part, the problems are open ended (as is an experimental laboratory), meaning that the student is free to explore. Problems that use the quantum-chemical models under discussion are referenced throughout the chapter. It is strongly recommended that problems be worked out as they are presented, before proceeding to the next section.

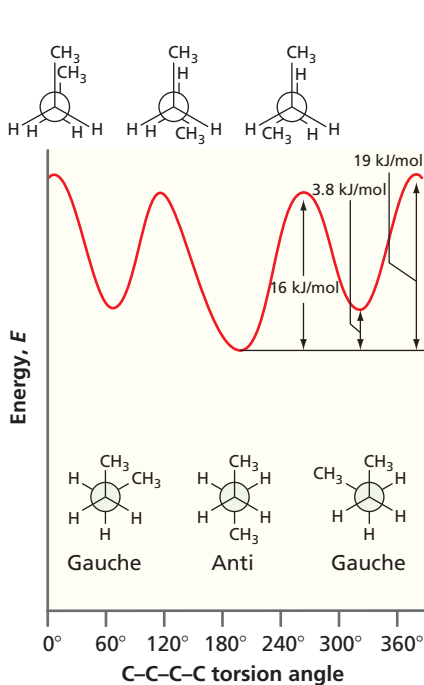
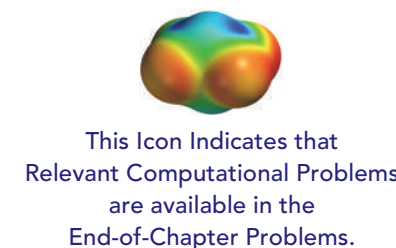


Figure 15.1

Energy of *n*-butane as a function of the C-C-C-C torsion angle. The torsion angle is the reaction coordinate.

15.2 POTENTIAL ENERGY SURFACES

Chemists are familiar with the plot of energy versus the torsion angle that involves the central carbon–carbon bond in *n*-butane. Figure 15.1 reveals three energy minima, corresponding to staggered structures, and three energy maxima, corresponding to eclipsed structures. One of the minima is given by a torsion angle of 180° (the so-called *anti* structure), and it is lower in energy and distinct from the other two minima with torsion angles of approximately 60° and 300° (so-called *gauche* structures), which are identical. Similarly, one of the energy maxima corresponding to a torsion angle of 0° is distinct from the other two maxima with torsion angles of approximately 120° and 240°, which are identical.

Eclipsed forms of *n*-butane are not stable molecules; instead they correspond only to hypothetical structures between *anti* and *gauche* minima. Thus, any sample of *n*-butane is made up of only two distinct compounds, *anti* *n*-butane and *gauche* *n*-butane. The relative abundance of the two compounds as a function of temperature is given by the Boltzmann distribution (see the discussion in Section 2.1).

The important geometrical coordinate in the example of Figure 15.1 can be clearly identified as a torsion involving one particular carbon–carbon bond. More generally,

¹The problems have been designed with the capabilities of the Student Edition of the Spartan molecular modeling program in mind. Other programs that allow equilibrium and transition-state geometry optimization, conformational searching, energy, property, and graphical calculations using Hartree–Fock, and density functional and MP2 models can also be used. The only exceptions are problems P15.1–P15.4 that appear early in the chapter before calculation models have been fully introduced. These problems make use of precalculated Spartan files that are available to students at www.pearsonhighered.com/advchemistry.

the important coordinate will be some combination of bond distances and angles and will be referred to simply as the **reaction coordinate**. This leads to a general type of plot in which energy is plotted as a function of the reaction coordinate. Diagrams such as this are commonly referred to as **reaction coordinate diagrams** or **potential energy surfaces** and provide essential connections between important chemical observables—structure, stability, reactivity, and selectivity—and energy.

15.2.1 Potential Energy Surfaces and Molecular Structure

The positions of the energy minima along the reaction coordinate indicate the equilibrium structures of the reactants and products as shown in Figure 15.2. Similarly, the position of the energy maximum defines the transition state. For example, where the reaction involves *gauche* *n*-butane transforming to the more stable *anti* conformer, the reaction coordinate may be thought of as a simple torsion about the central carbon–carbon bond. The individual reactant, transition-state, and product structures are depicted in terms of this coordinate in Figure 15.3.

On one hand, equilibrium structure can be determined from experiments as long as the molecule can be prepared and is sufficiently long lived to be subject to measurement. On the other hand, the structure of a transition state cannot be established from measurement. This is because a sufficiently large population of molecules of the transition state does not exist long enough to make measurements of sufficient precision.

Both equilibrium and transition-state structure can be determined from calculations. The former requires a search for an energy minimum on a potential energy surface, whereas the latter requires a search for an energy maximum along the reaction coordinate (and a minimum along each of the remaining coordinates). To see what is actually involved, the qualitative picture provided earlier must be replaced by a rigorous mathematical treatment. Reactants, products, and transition states are all stationary points on the potential energy diagram. In the one-dimensional case (the reaction coordinate diagram, such as that shown in Figure 15.2), this means that the first derivative of the potential energy, V , with respect to the reaction coordinate is zero:

$$\frac{dV}{dR} = 0 \quad (15.1)$$

The same must be true in dealing with a many-dimensional potential energy diagram (a potential energy surface). Here all partial derivatives of the energy with respect to each of the $3N - 6$ (N atoms) independent geometrical coordinates (R_i) are zero:

$$\frac{\partial V}{\partial R_i} = 0 \quad i = 1, 2, \dots, 3N - 6 \quad (15.2)$$

In the one-dimensional case, reactants and products are energy minima and are characterized by a positive second energy derivative:

$$\frac{d^2V}{dR^2} > 0 \quad (15.3)$$

The transition state is an energy maximum and is characterized by a negative second energy derivative:

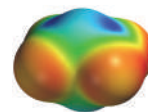
$$\frac{d^2V}{dR^2} < 0 \quad (15.4)$$

In the many-dimensional case, each independent coordinate, R_i , gives rise to $3N - 6$ second derivatives:

$$\frac{\partial^2V}{\partial R_i R_1}, \frac{\partial^2V}{\partial R_i R_2}, \frac{\partial^2V}{\partial R_i R_3}, \dots, \frac{\partial^2V}{\partial R_i R_{3N-6}} \quad (15.5)$$

Concept

Minima in potential energy surfaces correspond to equilibrium structures and maxima correspond to transition states.



Problem P15.1

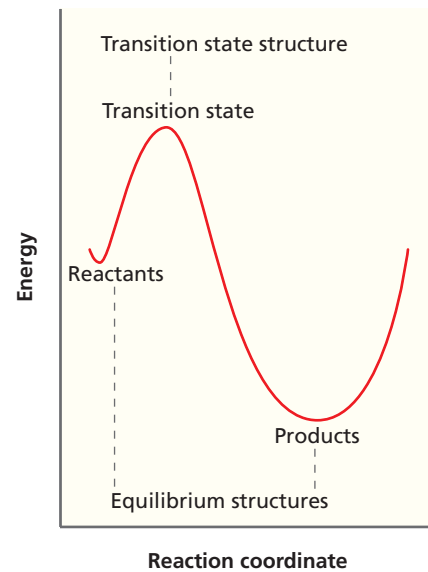


Figure 15.2

A generic reaction coordinate diagram. Energy is plotted as a function of the reaction coordinate. Reactants and products correspond to minima, and the transition state corresponds to a maximum along the path.

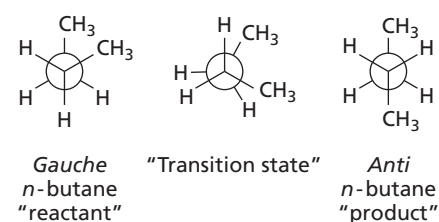


Figure 15.3

The structure of the reactant, product, and transition state in the “reaction” of *gauche* *n*-butane to *anti* *n*-butane.

This leads to a matrix of second derivatives (the so-called Hessian):

$$\begin{bmatrix} \frac{\partial^2 V}{\partial R_1^2} & \frac{\partial^2 V}{\partial R_1 \partial R_2} & \cdots \\ \frac{\partial^2 V}{\partial R_2 \partial R_1} & \frac{\partial^2 V}{\partial R_2^2} & \cdots \\ \cdots & \cdots & \cdots \\ \cdots & \cdots & \frac{\partial^2 V}{\partial R_{3N-6}^2} \end{bmatrix} \quad (15.6)$$

In this form, it is not possible to state whether any given coordinate corresponds to an energy minimum, an energy maximum, or neither. This would be possible if the matrix of Equation 15.6 were diagonal. Therefore, the original set of structural coordinates (R_i) is replaced by a new set of coordinates (ξ_i), which leads to a matrix of second derivatives that is diagonal:

$$\begin{bmatrix} \frac{\partial^2 V}{\partial \xi_1^2} & 0 & \cdots & 0 \\ 0 & \frac{\partial^2 V}{\partial \xi_2^2} & \cdots & 0 \\ \cdots & \cdots & \cdots & \cdots \\ 0 & 0 & \cdots & \frac{\partial^2 V}{\partial \xi_{3N-6}^2} \end{bmatrix} \quad (15.7)$$

The ξ_i are unique and referred to as **normal coordinates**. Stationary points for which all second derivatives (in normal coordinates) are positive are energy minima:

$$\frac{\partial^2 V}{\partial \xi_i^2} > 0 = 1, 2, \dots, 3N - 6 \quad (15.8)$$

These correspond to equilibrium forms (reactants and products). Stationary points for which all but one of the second derivatives are positive are so-called (first-order) saddle points and may correspond to transition states. If they do, the coordinate for which the second derivative is negative is referred to as the reaction coordinate (ξ_p):

$$\frac{\partial^2 V}{\partial \xi_p^2} < 0 \quad (15.9)$$

15.2.2 Potential Energy Surfaces and Vibrational Spectra

The vibrational frequency for a diatomic molecule A-B is given by Equation (15.10) as discussed in Section 7.1:

$$\nu = \frac{1}{2\pi} \sqrt{\frac{k}{\mu}} \quad (15.10)$$

In this equation, k is the force constant, which is in fact the second energy derivative of the potential energy, V , with respect to the bond length, R , at its equilibrium position

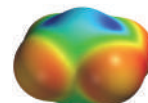
$$k = \frac{d^2 V(R)}{dR^2} \quad (15.11)$$

and μ is the reduced mass,

$$\mu = \frac{m_A m_B}{m_A + m_B} \quad (15.12)$$

where m_A and m_B are masses of atoms A and B.

Polyatomic systems are treated in a similar manner. Here, the force constants are the elements in the diagonal representation of the Hessian [Equation (15.7)]. Each vibrational mode is associated with a particular motion of atoms away from their equilibrium positions on the potential energy surface. Low frequencies correspond to motions in shallow regions of the surface, whereas high frequencies correspond to motions in steep regions. Note that one of the elements of the Hessian for a transition state will be a negative number, meaning that the corresponding frequency will be imaginary [the square root of a negative number as in Equation (15.10)]. This normal coordinate refers to motion along the reaction coordinate.



Problems P15.2–P15.3

15.2.3 Potential Energy Surfaces and Thermodynamics

The relative stability of reactant and product molecules is indicated on the potential energy surface by their energies. The thermodynamic state functions internal energy, U , and enthalpy, H , can be obtained from the energy of a molecule calculated by quantum mechanics, as discussed in Section 15.8.4.

The most common case, as depicted in Figure 15.4, is the one in which energy is released in the reaction. This kind of reaction is said to be **exothermic**, and the difference in stabilities of reactant and product is simply the enthalpy difference ΔH . For example, the reaction of *gauche* *n*-butane to *anti* *n*-butane is exothermic, and $\Delta H = -3.8 \text{ kJ/mol}$ as shown in Figure 15.1.

Thermodynamic principles inform us that if we wait long enough, the amount of products in an exothermic reaction will be greater than the amount of reactants. The actual ratio of the number of molecules of products (n_{products}) to reactants ($n_{\text{reactants}}$) also depends on the temperature and follows from the Boltzmann distribution:

$$\frac{n_{\text{products}}}{n_{\text{reactants}}} = \exp\left[-\frac{E_{\text{products}} - E_{\text{reactants}}}{k_B T}\right] \quad (15.13)$$

where E_{products} and $E_{\text{reactants}}$ are the energies per molecule of the products and reactants, respectively, T is the temperature, and k_B is the Boltzmann constant. The Boltzmann distribution reveals the relative amounts of the products and reactants at equilibrium. Even small energy differences between major and minor products lead to large product ratios, as shown in Table 15.1. The product formed in greatest abundance is that with the lowest energy, irrespective of the reaction pathway. In this case, the product is referred to as the **thermodynamic product** and the reaction is said to be **thermodynamically controlled**.

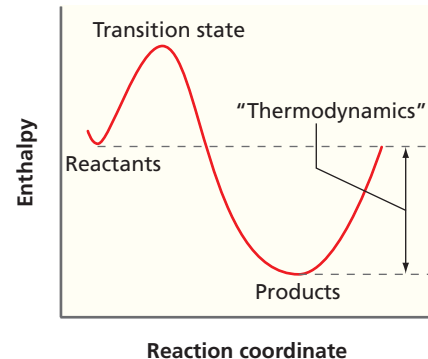


Figure 15.4

Energy difference between reactants and products determines the “thermodynamics” of a reaction.

TABLE 15.1 Ratio of Major to Minor Product as a Function of the Energy Difference between These Products

Energy Difference kJ/mol	Major: Minor (at Room Temperature)
2	~80:20
4	~90:10
8	~95:5
12	~99:1

15.2.4 Potential Energy Surfaces and Kinetics

A potential energy surface also reveals information about the rate at which a reaction occurs. The difference in energy between reactants and the transition state as shown in Figure 15.5 determines the kinetics of the reaction. The absolute reaction rate depends both on the concentrations of the reactants, $[A]^a, [B]^b, \dots$, where a, b, \dots are typically integers or half integers, and a quantity k' , called the **rate constant**:

$$\text{Rate} = k'[A]^a[B]^b[C]^c\dots \quad (15.14)$$

The rate constant is given by the Arrhenius equation and depends on the temperature:

$$k' = A \exp\left[-\frac{(E_{\text{transition state}} - E_{\text{reactants}})}{k_B T}\right] \quad (15.15)$$

Here, $E_{\text{transition state}}$ and $E_{\text{reactants}}$ are the energies per molecule of the transition state and the reactants, respectively. Note that the rate constant and the overall rate do not depend on the energies of reactants and products, but only on the difference in energies between reactants and the transition state. This difference is commonly referred to as

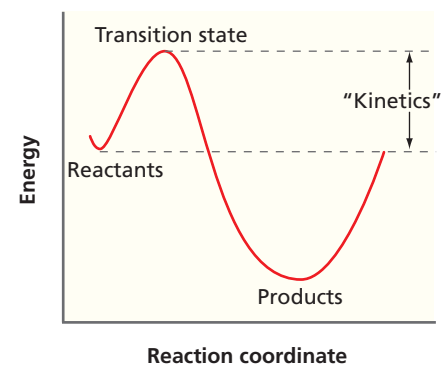


Figure 15.5

The energy difference between the reactants and transition state determines the rate of a reaction.

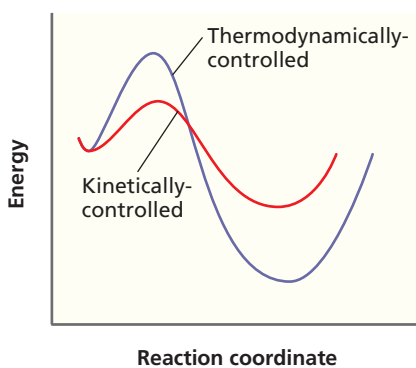
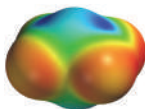


Figure 15.6

Two different pathways passing through different transition states. The path in red is followed for a kinetically-controlled reaction, whereas the path in purple is followed for a thermodynamically controlled reaction. The reaction coordinate differs for the two pathways.



Problem P15.4

the **activation energy** and is usually given the symbol ΔE^\ddagger . Other factors such as the likelihood of encounters between molecules and the effectiveness of these encounters in promoting reactions are taken into account by way of the **preexponential factor**, A , which is generally assumed to have the same value for reactions involving a single set of reactants forming different products or for reactions involving closely related reactants.

In general, the lower the activation energy, the faster the reaction. In the limit $\Delta E^\ddagger = 0$, the reaction rate will be limited entirely by how rapidly the molecules can move. Such limiting reactions are known as **diffusion-controlled reactions**. The product formed in greatest amount in a kinetically-controlled reaction is that proceeding via the lowest energy transition state, irrespective of whether or not this is the thermodynamically stable product. For example, a **kinetically-controlled reaction** will proceed along the red pathway in Figure 15.6, and the product formed is different from that corresponding to equilibrium in the system. The **kinetic product** ratio shows a dependence on activation energy differences that is analogous to that of Equation (15.13) with $E_{\text{transition state}}$ in place of E_{product} .

15.3 HARTREE-FOCK MOLECULAR ORBITAL THEORY: A DIRECT DESCENDANT OF THE SCHRÖDINGER EQUATION

The Schrödinger equation is deceptive in that, although it is remarkably easy to write down for any collection of nuclei and electrons, it has proven to be insolvable except for the one-electron case (the hydrogen atom). This situation was elaborated as early as 1929 by Paul Dirac, one of the early founders of quantum mechanics:

The underlying physical laws necessary for the mathematical theory of a large part of physics and the whole of chemistry are thus completely known, and the difficulty is only that the exact application of these laws leads to equations much too complicated to be solvable.

P. A. M. Dirac, 1902–1984

To realize a practical quantum-mechanical theory, it is necessary to make three approximations to the general multinuclear, multielectron Schrödinger equation:

$$\hat{H}\Psi = E\Psi \quad (15.16)$$

where E is the total energy of the system and Ψ is the n -electron wave function that depends both on the identities and positions of the nuclei and on the total number of electrons. The Hamiltonian \hat{H} provides the recipe for specifying the kinetic and potential energies for each of the particles:

$$\begin{aligned} \hat{H} = & -\frac{\hbar^2}{2m_e} \sum_i \nabla_i^2 - \frac{\hbar^2}{2} \sum_A \frac{1}{M_A} \nabla_A^2 - \frac{e^2}{4\pi\epsilon_0} \sum_i \sum_A \frac{Z_A}{r_{iA}} \\ & + \frac{e^2}{4\pi\epsilon_0} \sum_i \sum_j \frac{1}{r_{ij}} + \frac{e^2}{4\pi\epsilon_0} \sum_A \sum_B \frac{Z_A Z_B}{R_{AB}} \end{aligned} \quad (15.17)$$

where Z_A is the nuclear charge, M_A is the mass of nucleus A , m_e is the mass of the electron, R_{AB} is the distance between nuclei A and B , r_{ij} is the distance between electrons i and j , r_{iA} is the distance between electron i and nucleus A , ϵ_0 is the permittivity of free space, and \hbar is the Planck constant divided by 2π.

The first approximation takes advantage of the fact that nuclei move much more slowly than do electrons. We assume that the nuclei are stationary from the perspective of the electrons (see Section 12.2), which is known as the **Born–Oppenheimer approximation**. This assumption leads to a nuclear kinetic energy term in Equation (15.17), the second

Concept

In the Born–Oppenheimer approximation, it is assumed that the nuclei are stationary from the perspective of the electrons.

term, which is zero, and a nuclear–nuclear coulombic energy term, the last term, which is constant. This line of reasoning leads to the **electronic Schrödinger equation**:

$$\hat{H}^{el}\Psi^{el} = E^{el}\Psi^{el} \quad (15.18)$$

$$\hat{H}^{el} = -\frac{\hbar^2}{2m_e} \sum_i^{electrons} \nabla_i^2 - \frac{e^2}{4\pi\epsilon_0} \sum_i^{electrons} \sum_A^{nuclei} \frac{Z_A}{r_{iA}} + \frac{e^2}{4\pi\epsilon_0} \sum_j^{electrons} > \sum_i^{electrons} \frac{1}{r_{ij}} \quad (15.19)$$

The (constant) nuclear–nuclear Coulomb energy, the last term in Equation (15.17), needs to be added to E^{el} to include the total energy. Note that nuclear mass does not appear in the electronic Schrödinger equation. To the extent that the Born–Oppenheimer approximation is valid, this means that isotope effects on molecular properties must have a different origin.

Equation (15.18), as with Equation (15.16), is insolvable for the general (many-electron) case, and further approximations need to be made. The most obvious next step is to assume that electrons move independently of each other, which is what is done in the **Hartree–Fock approximation**. In practice, this can be accomplished by assuming that individual electrons are confined to functions called spin orbitals, χ_i . Each of the N electrons experiences the presence of an average field consisting of all other ($N - 1$) electrons. To ensure that the total (many-electron) wave function Ψ is antisymmetric upon interchange of electron coordinates, it is written in the form of a single determinant called the **Slater determinant** (see Section 10.3):

$$\Psi = \frac{1}{\sqrt{n!}} \begin{vmatrix} \chi_1(1) & \chi_2(1) & \dots & \chi_n(1) \\ \chi_1(2) & \chi_2(2) & \dots & \chi_n(2) \\ \dots & \dots & \dots & \dots \\ \chi_1(n) & \chi_2(n) & \dots & \chi_n(n) \end{vmatrix} \quad (15.20)$$

Individual electrons are represented by different rows in the determinant, which means that interchanging the coordinates of two electrons is equivalent to interchanging two rows in the determinant and multiplying its value by -1 . Spin orbitals are the product of spatial functions or molecular orbitals, ψ_i , and spin functions, α or β . The fact that there are only two kinds of spin functions (α and β) leads to the conclusion that two electrons at most may occupy a given molecular orbital. Were a third electron to occupy the orbital, two rows in the determinant would be the same, as was shown in Section 10.3. Therefore, the value of the determinant would be zero. Thus, the notion that electrons are paired is a consequence of the Hartree–Fock approximation through use of a determinant for the wave function. The set of molecular orbitals leading to the lowest energy is obtained by a process referred to as a **self-consistent-field (SCF) procedure**, which was discussed in Section 10.5 for atoms and in Section 13.1 for molecules.

The Hartree–Fock approximation leads to a set of differential equations, the **Hartree–Fock equations**, each involving the coordinates of a single electron. Although they can be solved numerically, it is advantageous to introduce an additional approximation in order to transform the Hartree–Fock equations into a set of algebraic equations. The basis for this approximation is the expectation that the one-electron solutions for many-electron molecules will closely resemble the one-electron wave functions for the hydrogen atom. After all, molecules are made up of atoms, so why should molecular solutions not be made up of atomic solutions? As discussed in Section 13.2, the molecular orbitals ψ_i are expressed as linear combinations of a basis set of prescribed functions known as basis functions, ϕ :

$$\psi_i = \sum_{\mu}^{basis functions} c_{\mu i} \phi_{\mu} \quad (15.21)$$

In this equation, the coefficients $c_{\mu i}$ are the (unknown) molecular orbital coefficients. Because the ϕ are usually centered at the nuclear positions, they are referred to as atomic orbitals, and Equation (15.21) is called the **linear combination of atomic orbitals (LCAO) approximation**. Note that in the limit of a complete (infinite) basis set, the LCAO approximation is exact at the Hartree–Fock level.

Concept

In the Hartree–Fock approximation, it is assumed that the electrons move independently of one another.

Concept

The many-electron wave function is written in the form of a Slater determinant to satisfy the Pauli principle.

Concept

To reduce computation time, molecular orbitals are expressed as a linear combination of atomic orbitals.

MATHEMATICAL FORMULATION OF THE HARTREE–FOCK METHOD

The Hartree–Fock and LCAO approximations, taken together and applied to the electronic Schrödinger equation, lead to a set of matrix equations now known as the **Roothaan–Hall equations**:

$$\mathbf{Fc} = \varepsilon \mathbf{Sc} \quad (15.22)$$

where \mathbf{c} are the unknown molecular orbital coefficients [see Equation (15.21)], ε are orbital energies, \mathbf{S} is the overlap matrix, and \mathbf{F} is the Fock matrix, which is analogous to the Hamiltonian in the Schrödinger equation:

$$F_{\mu\nu} = H_{\mu\nu}^{\text{core}} + J_{\mu\nu} - K_{\mu\nu} \quad (15.23)$$

where H^{core} is the so-called core Hamiltonian, the elements of which are given by

$$H_{\mu\nu}^{\text{core}} = \int \phi_\mu(1) \left[-\frac{\hbar^2}{2m_e} \nabla^2 - \frac{e^2}{4\pi\varepsilon_0} \sum_A^{\text{nuclei}} \frac{Z_A}{r_{1A}} \right] \phi_\nu(1) d\tau \quad (15.24)$$

Coulomb and exchange elements are given by:

$$J_{\mu\nu} = \sum_{\lambda}^{\text{basis functions}} \sum_{\sigma} P_{\lambda\sigma}(\mu\nu|\lambda\sigma) \quad (15.25)$$

$$K_{\mu\nu} = \frac{1}{2} \sum_{\lambda}^{\text{basis functions}} \sum_{\sigma} P_{\lambda\sigma}(\mu\lambda|\nu\sigma) \quad (15.26)$$

where \mathbf{P} is called the density matrix, the elements of which involve a product of two molecular orbital coefficients summed over all occupied molecular orbitals (the number of which is simply half the total number of electrons for a closed-shell molecule):

$$P_{\lambda\sigma} = 2 \sum_i^{\text{occupied molecular orbitals}} c_{\lambda i} c_{\sigma i} \quad (15.27)$$

and $(\mu\nu|\lambda\sigma)$ are two-electron integrals, the number of which increases as the fourth power of the number of basis functions. Therefore, the cost of a calculation rises rapidly with the size of the basis set:

$$(\mu\nu|\lambda\sigma) = \iint \phi_\mu(1) \phi_\nu(1) \left[\frac{1}{r_{12}} \right] \phi_\lambda(2) \phi_\sigma(2) d\tau_1 d\tau_2 \quad (15.28)$$

Methods resulting from solution of the Roothaan–Hall equations are called **Hartree–Fock models**. The corresponding energy in the limit of a complete basis set is called the **Hartree–Fock energy**.

15.4 PROPERTIES OF LIMITING HARTREE–FOCK MODELS

As discussed earlier in Section 10.5, total energies obtained from limiting (complete basis set) Hartree–Fock calculations will be too large (positive). This can be understood by recognizing that the Hartree–Fock approximation leads to replacement of instantaneous interactions between individual pairs of electrons with a picture in which each electron interacts with a charge cloud formed by all other electrons. The loss of flexibility causes electrons to get in each other's way to a greater extent than would actually be the case, leading to an overall electron repulsion energy that is too large and, hence, a total energy that is too large. The direction of the error in the total energy is also a direct consequence of the fact that Hartree–Fock models are variational. The limiting Hartree–Fock energy must be larger than (or at best equal to) the energy that would result from the solution of the exact Schrödinger equation.

Concept

The limiting Hartree–Fock energy must be larger than (or at best equal to) the energy that would result from the solution of the exact Schrödinger equation.

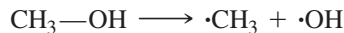
The difference between the limiting Hartree–Fock energy and the exact Schrödinger energy is called the **correlation energy**. The term *correlation* stems from the idea that the motion of one electron necessarily adjusts to or correlates with the motions of all other electrons. Any restriction on the freedom of electrons to move independently will, therefore, reduce their ability to correlate with other electrons.

The magnitude of the correlation energy may be quite large in comparison with typical bond energies or reaction energies. However, a major part of the total correlation energy may be insensitive to molecular structure, and Hartree–Fock models, which provide an incomplete account of correlation, may provide acceptable accounts of the energy change in some types of chemical reactions. It is also commonly the case that other properties, such as equilibrium structures and dipole moments, are less influenced by correlation effects than are total energies. The sections that follow explore to what extent these conclusions are valid.

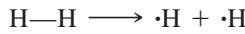
It is important to realize that calculations cannot actually be carried out at the Hartree–Fock limit. Presented here under the guise of limiting Hartree–Fock quantities are the results of calculations performed with a relatively large and flexible basis set, specifically the 6-311+G** basis set. (Basis sets are discussed at length in Section 15.7.) Although such a treatment leads to total energies that are greater than actual limiting Hartree–Fock energies by several tens to several hundreds of kilojoules per mole (depending on the size of the molecule), it is expected that errors in relative energies, as well as in structures, vibrational frequencies, and properties such as dipole moments, will be much smaller.

15.4.1 Reaction Energies

The most easily understood problem with limiting Hartree–Fock models is uncovered in comparisons of calculated **homolytic bond dissociation** energies with experimentally determined values. In such a reaction, a bond is broken leading to two radicals, for example, in methanol:



As seen from the data in Table 15.2, Hartree–Fock dissociation energies are too small. In fact, limiting Hartree–Fock calculations suggest an essentially zero O—O bond energy in hydrogen peroxide and a negative F—F “bond energy” in the fluorine molecule! Something is seriously wrong. To see what the problem is, consider the analogous bond dissociation reaction in the hydrogen molecule:



On the one hand, each of the hydrogen atoms that comprise the product contains only a single electron, and its energy is given exactly by the (limiting) Hartree–Fock model. On the other hand, the reactant contains two electrons, and, according to the variation principle, its energy must be too high (too positive). Therefore, the bond dissociation energy must be too low (too negative). To generalize, because the products of a homolytic bond dissociation reaction will contain one fewer electron pair than the reactant, the products would be expected to have lower correlation energy. The correlation energy associated with an electron pair is greater than that for a separated pair of electrons.

Concept

The difference between the limiting Hartree–Fock energy and the exact Schrödinger energy is called the correlation energy.

Concept

Hartree–Fock calculations do not give accurate values for homolytic bond dissociation energies because the correlation energy differs between reactants and products.

TABLE 15.2 Homolytic Bond Dissociation Energies (kJ/mol)

Molecule (bond)	Hartree–Fock Limit	Experiment	Δ
$\text{CH}_3\text{—CH}_3 \longrightarrow \cdot\text{CH}_3 + \cdot\text{CH}_3$	276	406	-130
$\text{CH}_3\text{—NH}_2 \longrightarrow \cdot\text{CH}_3 + \cdot\text{NH}_2$	238	389	-151
$\text{CH}_3\text{—OH} \longrightarrow \cdot\text{CH}_3 + \cdot\text{OH}$	243	410	-167
$\text{CH}_3\text{—F} \longrightarrow \cdot\text{CH}_3 + \cdot\text{F}$	289	477	-188
$\text{NH}_2\text{—NH}_2 \longrightarrow \cdot\text{NH}_2 + \cdot\text{NH}_2$	138	289	-151
$\text{HO—OH} \longrightarrow \cdot\text{OH} + \cdot\text{OH}$	-8	230	-238
$\text{F—F} \longrightarrow \cdot\text{F} + \cdot\text{F}$	-163	184	-347

TABLE 15.3 Relative Energies of Structural Isomers (kJ/mol)

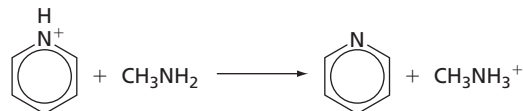
Reference Compound	Isomer	Hartree–Fock Limit	Experiment	Δ
Acetonitrile	Methyl isocyanide	88	88	0
Acetaldehyde	Oxirane	134	113	21
Acetic acid	Methyl formate	71	75	-4
Ethanol	Dimethyl ether	46	50	-4
Propyne	Allene	8	4	4
	Cyclopropene	117	92	25
Propene	Cyclopropane	42	29	13
1,3-Butadiene	2-Butyne	29	38	-9
	Cyclobutene	63	46	17
	Bicyclo[1.1.0]butane	138	109	29

The poor results seen for homolytic bond dissociation reactions do not necessarily carry over into other types of reactions as long as the total number of electron pairs is maintained. A good example is found in energy comparisons among structural isomers (see Table 15.3). Although bonding may be quite different among isomers (for example, one single and one double bond in propene versus three single bonds in cyclopropane), the total number of bonds is the same in reactants and products:



The errors noted here are an order of magnitude less than those found for homolytic bond dissociation reactions, although in some of the comparisons they are still quite large, in particular where small-ring compounds are compared with (unsaturated) acyclics, such as the comparison between propene and cyclopropane.

The performance of limiting Hartree–Fock models for reactions involving even more subtle changes in bonding is better still. For example, the data in Table 15.4 show calculated energies of protonation of nitrogen bases relative to the energy of protonation of methylamine as a standard (for example, pyridine relative to methylamine).



The results are in reasonable accord with their respective experimental values as shown in Table 15.4.

TABLE 15.4 Proton Affinities of Nitrogen Bases Relative to the Proton Affinity of Methylamine (kJ/mol)

Base	Hartree–Fock Limit	Experiment	Δ
Ammonia	-50	-38	-12
Aniline	-25	-10	-15
Methylamine	0	0	—
Dimethylamine	29	27	2
Pyridine	29	29	0
Trimethylamine	50	46	4
Diazabicyclooctane	75	60	15
Quinuclidine	92	75	17

15.4.2 Equilibrium Geometries

As with the example of homolytic bond disassociation above, systematic discrepancies between calculated and experimental values are also noted in comparisons involving limiting Hartree–Fock and experimental equilibrium structures. We will explore two sets of comparisons. The first set is illustrated in Table 15.5 and involves the structures of the hydrogen molecule, lithium hydride, methane, ammonia, water, and hydrogen fluoride, whereas examples of the second set are provided in Table 15.6 and involve AB bond distances in two-heavy-atom hydrides, H_mABH_n . Most evident is the fact that, aside from lithium hydride, all calculated bond distances are shorter than experimental values. In the case of bonds with hydrogen, the magnitude of the error increases with the electronegativity of the heavy atom. In the case of the two-heavy-atom hydrides, the error increases substantially when two electronegative elements are involved in the bond. Thus, although errors in bond distances for methylamine, methanol, and methyl fluoride are fairly small, those for hydrazine, hydrogen peroxide, and fluorine molecule are much larger. The reason (1) for the trend of limiting Hartree–Fock bond distances

TABLE 15.5 Bond distances in One-Heavy-Atom Hydrides (Å)

Molecule	Geometrical Parameter	Hartree–Fock Limit	Experiment	Δ
H_2	$r(HH)$	0.736	0.742	-0.006
LiH	$r(LiH)$	1.607	1.596	+0.011
CH_4	$r(CH)$	1.083	1.092	-0.009
NH_3	$r(NH)$	1.000	1.012	-0.012
	$\angle(HNH)$	107.9	106.7	-1.2
H_2O	$r(OH)$	0.943	0.958	-0.015
	$\angle(HOH)$	106.4	104.5	+1.9
HF	$r(FH)$	0.900	0.917	-0.017

TABLE 15.6 Bond Distances in Two Heavy Atom Hydrides (Å)

Molecule (Bond)	Hartree–Fock Limit	Experiment	Δ
Ethane ($H_3C—CH_3$)	1.527	1.531	-0.004
Methylamine ($H_3C—NH_2$)	1.453	1.471	-0.018
Methanol ($H_3C—OH$)	1.399	1.421	-0.022
Methyl fluoride ($H_3C—F$)	1.364	1.383	-0.019
Hydrazine ($H_2N—NH_2$)	1.412	1.449	-0.037
Hydrogen peroxide ($HO—OH$)	1.388	1.452	-0.064
Fluorine (F—F)	1.330	1.412	-0.082
Ethylene ($H_2C=CH_2$)	1.315	1.339	-0.024
Formaldimine ($H_2C=NH$)	1.247	1.273	-0.026
Formaldehyde ($H_2C=O$)	1.178	1.205	-0.027
Diimide ($NH=NH$)	1.209	1.252	-0.043
Oxygen ($O=O$)	1.158	1.208	-0.050
Acetylene ($HC\equiv CH$)	1.185	1.203	-0.018
Hydrogen cyanide ($HC\equiv N$)	1.124	1.153	-0.029
Nitrogen ($N\equiv N$)	1.067	1.098	-0.031

TABLE 15.7 Symmetric Stretching Frequencies in Diatomic and Small Polyatomic Molecules (cm^{-1})

Molecule	Hartree–Fock Limit	Experiment	Δ
Lithium fluoride	927	914	13
Fluorine	1224	923	301
Lithium hydride	1429	1406	23
Carbon monoxide	2431	2170	261
Nitrogen	2734	2360	374
Methane	3149	3137	12
Ammonia	3697	3506	193
Water	4142	3832	310
Hydrogen fluoride	4490	4139	351
Hydrogen	4589	4401	188

being shorter than experimental values and the reason (2) that lithium hydride is an exception will become evident when we examine how Hartree–Fock models can be extended to treat electron correlation in Section 15.6.

15.4.3 Vibrational Frequencies

Concept

Vibrational frequencies calculated with the Hartree–Fock method are larger than experimental values.

A few comparisons of limiting Hartree–Fock and experimental symmetric stretching frequencies for diatomic and small polyatomic molecules are provided in Table 15.7. (Note that the experimentally measured frequencies have been corrected for anharmonic behavior before being compared with calculated harmonic frequencies.) The systematic error in equilibrium bond distances for limiting Hartree–Fock models (calculated distances are shorter than experimental lengths) seems to be parallel to a systematic error in stretching frequencies (calculated frequencies are larger than experimental frequencies). This is not unreasonable: too short a bond implies too strong a bond, which translates to a value for frequency that is too large. Note, however, that homolytic bond dissociation energies from limiting Hartree–Fock models are actually smaller (not larger) than experimental values, an observation that might imply that frequencies should be smaller (not larger) than experimental values. The reason for the apparent contradiction is that the Hartree–Fock model does not dissociate to the proper limit of two radicals as a bond is stretched.

15.4.4 Dipole Moments

Electric dipole moments for a few simple molecules from limiting Hartree–Fock calculations are compared with experimental moments in Table 15.8. The calculations reproduce the overall ordering of dipole moments. Although the sample is too small to

TABLE 15.8 Electric Dipole Moments (debye)

Molecule	Hartree–Fock Limit	Experiment	Δ
Methylamine	1.5	1.31	0.2
Ammonia	1.7	1.47	0.2
Methanol	1.9	1.70	0.2
Hydrogen fluoride	2.0	1.82	0.2
Methyl fluoride	2.2	1.85	0.3
Water	2.2	1.85	0.3

generalize, the calculated values are consistently larger than the corresponding experimental quantities. This might seem to be at odds with the notion that limiting Hartree–Fock bond lengths in these same molecules are smaller than experimental distances (which would imply that dipole moments should be smaller than experimental values). We address this issue later in Section 15.8.8.

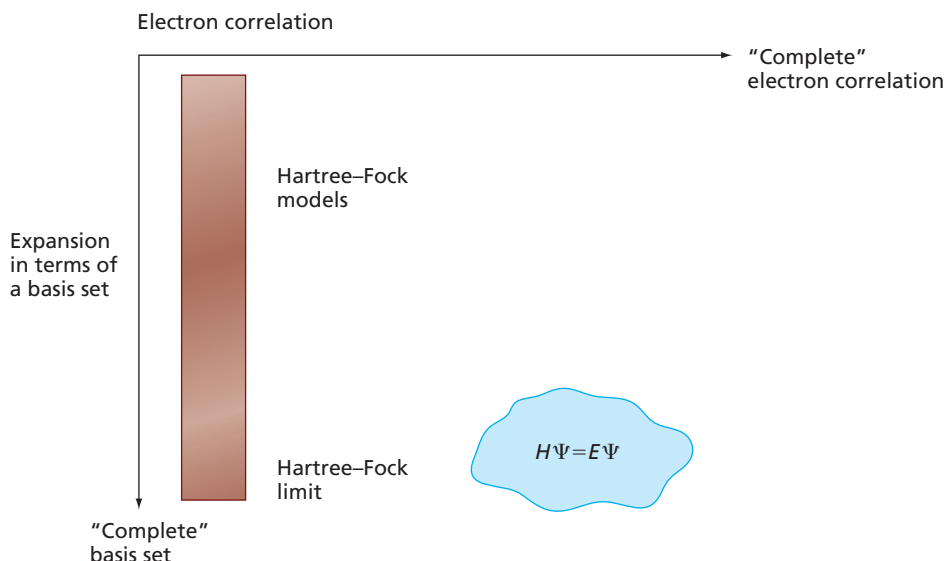
15.5 THEORETICAL MODELS AND THEORETICAL MODEL CHEMISTRY

As discussed in the preceding section, limiting Hartree–Fock models do not provide results that are identical to experimental results. This is, of course, a direct consequence of the Hartree–Fock approximation, which replaces instantaneous interactions between individual electrons by interactions between a particular electron and the average field created by all other electrons. As a consequence of this approximation, electrons get in each other's way to a greater extent than they actually do. This leads to an overestimation of the electron–electron repulsion energy and too high a total energy.

At this point, it is instructive to introduce the idea of a **theoretical model**. For our specific purpose, a theoretical model is a detailed recipe that begins with the electronic Schrödinger equation and ends with a useful scheme. Furthermore, the notion that any given theoretical model necessarily leads to a set of results, which we will refer to as a **theoretical model chemistry**, confirms the choice and application of the approximations. At the outset, we might anticipate that the less severe the approximations that make up a particular theoretical model, the closer will be its results to experiment. The terms *theoretical model* and *theoretical model chemistry* were introduced by Sir John Pople, who in 1998 received the Nobel Prize in chemistry for his work in bringing quantum chemistry into widespread use.

All possible theoretical models may be viewed in the context of the two-dimensional diagram shown in Figure 15.7. The horizontal axis relates the extent to which the motions of electrons in a many-electron system are independent of each other or, alternately, the degree to which electron correlation is taken into account. At the extreme left are Hartree–Fock models. The vertical axis designates the basis set, which is used to represent the individual molecular orbitals. At the top is a so-called minimal basis set, which involves the fewest possible functions discussed in Section 15.7.1, whereas at the very bottom is the hypothetical complete basis set. The bottom of the column of Hartree–Fock models (at the far left) is called the Hartree–Fock limit.

Proceeding all the way to the right in Figure 15.7 (electron correlation fully taken into account) and then all the way to the bottom (both complete basis set and electron correlation taken into account) on this diagram is functionally equivalent to solving



Concept

The accuracy of quantum mechanical calculations of energy and structure depends on the size of the basis set and the extent to which electron correlation is taken into account.

Figure 15.7

Accuracy of a calculation shown as a function of electron correlation and size of basis set. The blue field represents both a complete basis set and electron correlation taken into account, which is functionally equivalent to solving the Schrödinger equation exactly.

the Schrödinger equation exactly—something that, as stated earlier, cannot be realized. Note, however, that starting from some position on the diagram (that is, some level of treatment of electron correlation and some assumptions for the basis set), if moving down and to the right produces no significant change in a particular property of interest, then we can reasonably conclude that further motion would also not result in change in this property. In effect, this would signal that the exact solution has been achieved.

To the extent that it is possible, any theoretical model should satisfy a number of conditions. Most importantly, it should yield a unique energy, among other molecular properties, given only the kinds and positions of the nuclei, the total number of electrons, and the number of unpaired electrons. A model should not appeal in any way to chemical intuition. Also important is that, if at all possible or practical, the magnitude of the error of the calculated energy should increase roughly in proportion to molecular size; that is, the model should be **size consistent**. Only then is it reasonable to anticipate that reaction energies can be properly described. Less important, but highly desirable, is that the model energy should represent a bound to the exact energy; that is, the model should be **variational**. Finally, a model needs to be practical; that is, able to be applied not only to very simple or idealized systems, but also to problems that are actually of interest. Were this not an issue, then it would not be necessary to move beyond the Schrödinger equation itself.

Hartree–Fock models, which have previously been discussed, are well defined and yield unique properties. They are both size consistent and variational. Most importantly, Hartree–Fock models are presently applicable to molecules consisting of 50 to 100 or more atoms. We have already seen that limiting Hartree–Fock models also provide excellent descriptions of a number of important chemical observables, most important among them being equilibrium molecular structure and the energies of some kinds of reactions. We shall see in Section 15.8 that “practical” Hartree–Fock models are also quite successful in similar situations.

15.6 MOVING BEYOND HARTREE–FOCK THEORY

We next discuss improvements to the Hartree–Fock model that have the effect of moving down and to the right in Figure 15.7. Because these improvements increase the cost of a calculation, it is important to ask if they are necessary for a given calculation. This question must be answered by determining the extent to which the value of the observable of interest has the desired accuracy. Sections 15.8.1 through 15.8.11 explicitly address this question for a number of important observables, among them equilibrium structures, reaction energies, and dipole moments.

Two fundamentally different approaches for moving beyond Hartree–Fock theory have received widespread attention. The first increases the flexibility of the Hartree–Fock wave function (associated with the electronic ground state) by combining it with wave functions corresponding to various excited states. The second introduces an explicit term in the Hamiltonian to account for the interdependence of electron motions.

Solution of the Roothaan–Hall equations results in a set of molecular orbitals, each of which is doubly occupied,² and a set of higher-energy unoccupied molecular orbitals. The number of occupied molecular orbitals is equal to half of the number of electrons for closed-shell molecules, whereas the number of unoccupied molecular orbitals depends on the choice of basis set. Typically, this number is much larger than the number of occupied molecular orbitals, and for the hypothetical case of a complete basis set it is infinite. The unoccupied molecular orbitals play no part in establishing the Hartree–Fock energy nor any ground-state properties obtained from Hartree–Fock models. They are, however, the basis for models that move beyond Hartree–Fock theory.

²This is valid for the vast majority of molecules. Radicals have one singly occupied molecular orbital, and the oxygen molecule has two singly occupied molecular orbitals.

15.6.1 Configuration Interaction Models

It can be shown that in the limit of a complete basis set, the energy resulting from the optimum linear combination of the ground state electronic configuration (that obtained from Hartree–Fock theory) and all possible excited-state electronic configurations formed by promotion of one or more electrons from occupied to unoccupied molecular orbitals is the same as would result from solution of the full many-electron Schrödinger equation. An example of such a promotion is shown in Figure 15.8.

This result, referred to as **full configuration interaction**, while interesting, is of no practical value simply because the number of excited-state electronic configurations is infinite. Practical configuration interaction models may be realized first by assuming a finite basis set and then by restricting the number of excited-state electronic configurations included in the mixture. Because of these two restrictions, the final energy is not the same, as would result from solution of the exact Schrödinger equation. Operationally, what is required is first to obtain the Hartree–Fock wave function and then to write a new wave function as a sum, the leading term of which, Ψ_0 , is the Hartree–Fock wave function, and remaining terms, Ψ_s , are wave functions derived from the Hartree–Fock wave function by electron promotions:

$$\Psi = a_0 \Psi_0 + \sum_{s>0} a_s \Psi_s \quad (15.29)$$

The unknown linear coefficients, a_s , are determined by solving Equation (15.30):

$$\sum_s (H_{st} - E\delta_{st}) a_s = 0 \quad (15.30)$$

where the matrix elements are given by

$$H_{st} = \int \dots \int \Psi_s \hat{H} \Psi_t d\tau_1 d\tau_2 \dots d\tau_n \quad (15.31)$$

The lowest energy wave function obtained from solution of Equation (15.30) corresponds to the energy of the electronic ground state.

One approach for limiting the number of electron promotions is referred to as the **frozen core approximation**. In effect, this method eliminates any promotions from molecular orbitals that correspond essentially to (combinations of) inner-shell or core electrons. Although the total contribution to the energy arising from inner-shell promotions is not insignificant, experience suggests that this contribution is nearly identical for the same types of atoms in different molecules. A more substantial approximation is to limit the number of promotions based on the total number of electrons involved—that is, **single-electron promotions**, **double-electron promotions**, and so on. Configuration interaction based on single-electron promotions only, the so-called **CIS (Configuration Interaction Single) method**, leads to no improvement of the (Hartree–Fock) energy or wave function. The simplest procedure to use that actually leads to improvement over Hartree–Fock is the so-called **CID (Configuration Interaction Double) method**, which is restricted to double-electron promotions:

$$\Psi_{CID} = a_0 \Psi_0 + \sum_{i<j}^{\text{occ}} \sum_{a<b}^{\text{unocc}} a_{aij}^{ab} \Psi_{ij}^{ab} \quad (15.32)$$

A somewhat less restricted recipe, the so-called CISD (Configuration Interaction Single and Double) method, considers both single- and double-electron promotions:

$$\Psi_{CISD} = a_0 \Psi_0 + \sum_i^{\text{occ}} \sum_a^{\text{unocc}} a_i^a \Psi_i^a + \sum_{i<j}^{\text{occ}} \sum_{a<b}^{\text{unocc}} \sum_{a<b}^{\text{occ}} \sum_{a<b}^{\text{unocc}} a_{ij}^{ab} \Psi_{ij}^{ab} \quad (15.33)$$

Solution of Equation (15.30) for either CID or CISD methods is practical for reasonably large systems. Both methods are obviously well defined, and they are variational. However, neither method (or any limited configuration interaction method) is size consistent. This can easily be seen by considering the CISD description of a two-electron system. As an example, see the configuration of a helium atom in Figure 15.9, which

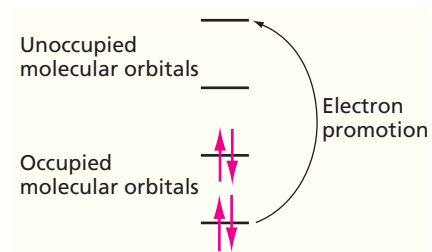


Figure 15.8

Electron promotion from occupied to unoccupied molecular orbitals.

Concept

Configuration interaction models take electron correlation into account by including excited-state electron configurations.

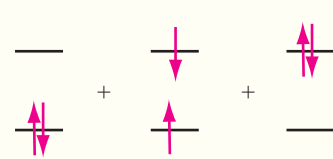
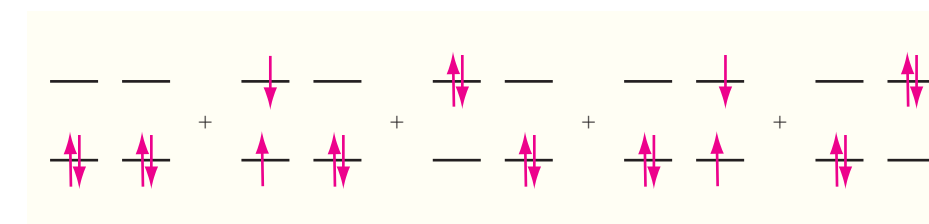


Figure 15.9

The CISD description of He.

Figure 15.10

The CISD description of He_2 restricted to one- and two-electron promotions.



uses only two basis functions and which leads to one occupied and one unoccupied molecular orbital. In this case, the CISD description for the isolated atom is exact (within the confines of the basis set), meaning that all possible electron promotions have been explicitly considered. Similarly, the description of two helium atoms treated independently is exact.

Next consider the corresponding CISD treatment of two helium atoms together but at infinite separation, as shown in Figure 15.10. This description is not exact because three- and four-electron promotions have not been taken into account. Thus, the calculated energies of two helium atoms treated separately and two helium atoms at infinite separation will be different. Size consistency is a very important attribute for any quantum-chemical model, and its absence for any practical configuration interaction models makes them much less appealing than they otherwise might be.

15.6.2 Møller–Plesset Models

Concept

Møller–Plesset models take electron correlation into account using perturbation theory.

Practical size-consistent alternatives to configuration interaction models are **Møller–Plesset models**. Of particular utility is the second-order Møller–Plesset model (MP2). Møller–Plesset models are based on the recognition that, while the Hartree–Fock wave function Ψ_0 and ground state energy E_0 are approximate solutions to the Schrödinger equation, they are exact solutions to an analogous problem involving the Hartree–Fock Hamiltonian, \hat{H}_0 , in place of the exact Hamiltonian, \hat{H} . If the Hartree–Fock wave function Ψ and energy are, in fact, very close to the exact wave function and ground state energy E , the exact Hamiltonian can then be written in the following form:

$$\hat{H} = \hat{H}_0 + \lambda \hat{V} \quad (15.34)$$

In Equation (15.34), \hat{V} is a small perturbation and λ is a dimensionless parameter. Using perturbation theory, the exact wave function and energy are expanded in terms of the Hartree–Fock wave function and energy to produce the following equations:

$$E = E^{(0)} + \lambda E^{(1)} + \lambda^2 E^{(2)} + \lambda^3 E^{(3)} + \dots \quad (15.35)$$

$$\Psi = \Psi_0 + \lambda \Psi^{(1)} + \lambda^2 \Psi^{(2)} + \lambda^3 \Psi^{(3)} + \dots \quad (15.36)$$

MATHEMATICAL FORMULATION OF MØLLER–PLESSET MODELS

Substituting the expansions of Equations (15.34) to (15.36) into the Schrödinger equation and gathering terms in λ^n yield

$$\hat{H}_0 \Psi_0 = E^{(0)} \Psi_0 \quad (15.37a)$$

$$\hat{H}_0 \Psi^{(1)} + \hat{V} \Psi_0 = E^{(0)} \Psi^{(1)} + E^{(1)} \Psi_0 \quad (15.37b)$$

$$\hat{H}_0 \Psi^{(2)} + \hat{V} \Psi^{(1)} = E^{(0)} \Psi^{(2)} + E^{(1)} \Psi^{(1)} + E^{(2)} \Psi_0 \quad (15.37c)$$

...

Multiplying each of the Equations (15.37) by Ψ_0 and integrating over all space yields the following expression for the n th-order Møller–Plesset (MP n) energy:

$$E^{(0)} = \int \dots \int \Psi_0 \hat{H}_0 \Psi_0 d\tau_1 d\tau_2 \dots d\tau_n \quad (15.38a)$$

$$E^{(1)} = \int \dots \int \Psi_0 \hat{V} \Psi_0 d\tau_1 d\tau_2 \dots d\tau_n \quad (15.38b)$$

$$E^{(2)} = \int \dots \int \Psi_0 \hat{V} \Psi^{(1)} d\tau_1 d\tau_2 \dots d\tau_n \quad (15.38c)$$

...

In this framework, the Hartree–Fock energy is the sum of the zero- and first-order Møller–Plesset energies:

$$E^{(0)} + E^{(1)} = \int \dots \int \Psi_0 (\hat{H}_0 + \hat{V}) \Psi_0 d\tau_1 d\tau_2 \dots d\tau_n \quad (15.39)$$

The first correction, $E^{(2)}$, can be written as follows:

$$E^{(2)} = \sum_{i < j}^{\text{molecular orbitals}} \sum_{a < b}^{\text{occ}} \sum_{a < b}^{\text{unocc}} \frac{[(ij||ab)]^2}{(\varepsilon_a + \varepsilon_b - \varepsilon_i - \varepsilon_j)} \quad (15.40)$$

where ε_i and ε_j are energies of occupied molecular orbitals, and ε_a and ε_b are energies of unoccupied molecular orbitals. The integrals $(ij||ab)$ over filled (i and j) and empty (a and b) molecular orbitals account for changes in electron–electron interactions as a result of electron promotion,

$$(ia||jb) = -(ib|ja) \quad (15.41)$$

in which the integrals $(ij|ab)$ and $(ib|ja)$ involve molecular orbitals rather than basis functions; for example,

$$(ia|jb) = \int \psi_i(1) \psi_a(1) \left[\frac{1}{r_{12}} \right] \psi_j(2) \psi_b(2) d\tau_1 d\tau_2 \quad (15.42)$$

The two integrals are related by a simple transformation,

$$(ij|ab) = \sum_{\mu} \sum_{\nu}^{\text{basis functions}} \sum_{\lambda} \sum_{\sigma} c_{\mu i} c_{\nu j} c_{\lambda a} c_{\sigma b} (\mu\nu|\lambda\sigma) \quad (15.43)$$

where $(\mu\nu|\lambda\sigma)$ are given by Equation (15.28).

The MP2 model is well defined and leads to unique results. As mentioned previously, MP2 is size consistent, although (unlike configuration interaction models) it is not variational. Therefore, the calculated energy may be lower than the exact value.

15.6.3 Density Functional Models

The second approach for moving beyond the Hartree–Fock model is now commonly known as **density functional theory**. It is based on the availability of an exact solution for an idealized many-electron problem, specifically an electron gas of uniform density. The part of this solution that relates only to the exchange and correlation contributions is extracted and then directly incorporated into a self-consistent-field (SCF) formalism much like Hartree–Fock formalism. Because the new exchange and correlation terms derive from idealized problems, density functional models, unlike configuration interaction and Møller–Plesset models, do not limit to the exact solution of the Schrödinger equation. In a sense, they are empirical in that they incorporate external data (the form of the solution of the idealized problem). What makes density functional models of great interest is their significantly lower computation cost than either configuration interaction or Møller–Plesset models. For his discovery, leading up to the development of practical density functional models, Walter Kohn was awarded the Nobel Prize in chemistry in 1998.

Concept

Density functional models include electron correlation, yet have a similar computational cost to Hartree–Fock calculations.

The Hartree–Fock energy may be written as a sum of the kinetic energy, E_T , the electron–nuclear potential energy, E_V , and coulombic, E_J , and exchange, E_K , components of the electron–electron interaction energy:

$$E^{HF} = E_T + E_V + E_J + E_K \quad (15.44)$$

The first three of these terms also appear in density functional models, whereas the Hartree–Fock exchange energy is replaced by a so-called exchange-correlation energy, E_{XC} , the form of which follows from the solution of the idealized electron gas problem:

$$E^{DFT} = E_T + E_V + E_J + E_{XC} \quad (15.45)$$

Except for E_T , all components depend on the total electron density, $\rho(\mathbf{r})$:

$$\rho(\mathbf{r}) = 2 \sum_i^{\text{orbitals}} |\psi_i(\mathbf{r})|^2 \quad (15.46)$$

The ψ_i are orbitals, strictly analogous to molecular orbitals in Hartree–Fock theory.

MATHEMATICAL FORMULATION OF DENSITY FUNCTIONAL THEORY

Within a finite basis set (analogous to the LCAO approximation for Hartree–Fock models), the components of the density functional energy, E^{DFT} , can be written as follows:

$$E_T = \sum_{\mu}^{\text{basis functions}} \sum_{\nu}^{\text{basis functions}} \int \phi_{\mu}(\mathbf{r}) \left[-\frac{\hbar^2 e^2}{2m_e} \nabla^2 \right] \phi_{\nu}(\mathbf{r}) d\mathbf{r} \quad (15.47)$$

$$E_V = \sum_{\mu}^{\text{basis functions}} \sum_{\nu}^{\text{basis functions}} P_{\mu\nu} \sum_A^{\text{nuclei}} \int \phi_{\mu}(\mathbf{r}) \left[-\frac{Z_A e^2}{4\pi\epsilon_0 |\mathbf{r} - \mathbf{R}_A|} \right] \phi_{\nu}(\mathbf{r}) d\mathbf{r} \quad (15.48)$$

$$E_J = \frac{1}{2} \sum_{\mu}^{\text{basis functions}} \sum_{\nu}^{\text{basis functions}} \sum_{\lambda}^{\text{basis functions}} \sum_{\sigma}^{\text{basis functions}} P_{\mu\nu} P_{\lambda\sigma} (\mu\nu|\lambda\sigma) \quad (15.49)$$

$$E_{XC} = \int f(\rho(\mathbf{r}), \nabla\rho(\mathbf{r}), \dots) d\mathbf{r} \quad (15.50)$$

where Z is the nuclear charge, $|\mathbf{r} - \mathbf{R}_A|$ is the distance between the nucleus and the electron density, \mathbf{P} is the density matrix [Equation (15.27)], and the symbols $(\mu\nu|\lambda\sigma)$ indicate two-electron integrals [Equation (15.28)]. The $f(\rho(\mathbf{r}), \nabla\rho(\mathbf{r}), \dots)$ is the so-called exchange-correlation functional, which depends on the electron density. In the simplest form of the theory, it is obtained by fitting the density produced from the idealized electron gas problem to a function. Better models result from also fitting the gradient of the density. Minimizing E^{DFT} with respect to the unknown orbital coefficients yields a set of matrix equations, the Kohn–Sham equations, analogous to the Roothaan–Hall equations [Equation (15.22)]:

$$\mathbf{Fc} = \varepsilon \mathbf{Sc} \quad (15.51)$$

Here the elements of the Hartree–Fock matrix are given by

$$F_{\mu\nu} = H_{\mu\nu}^{\text{core}} + J_{\mu\nu} - F_{\mu\nu}^{XC} \quad (15.52)$$

and are defined analogously to Equations (15.25) and (15.26), respectively, and \mathbf{F}^{XC} is the exchange-correlation part, the form of which depends on the particular exchange-correlation functional used. Note that substitution of the Hartree–Fock exchange, \mathbf{K} , for \mathbf{F}^{XC} yields the Roothaan–Hall equations.

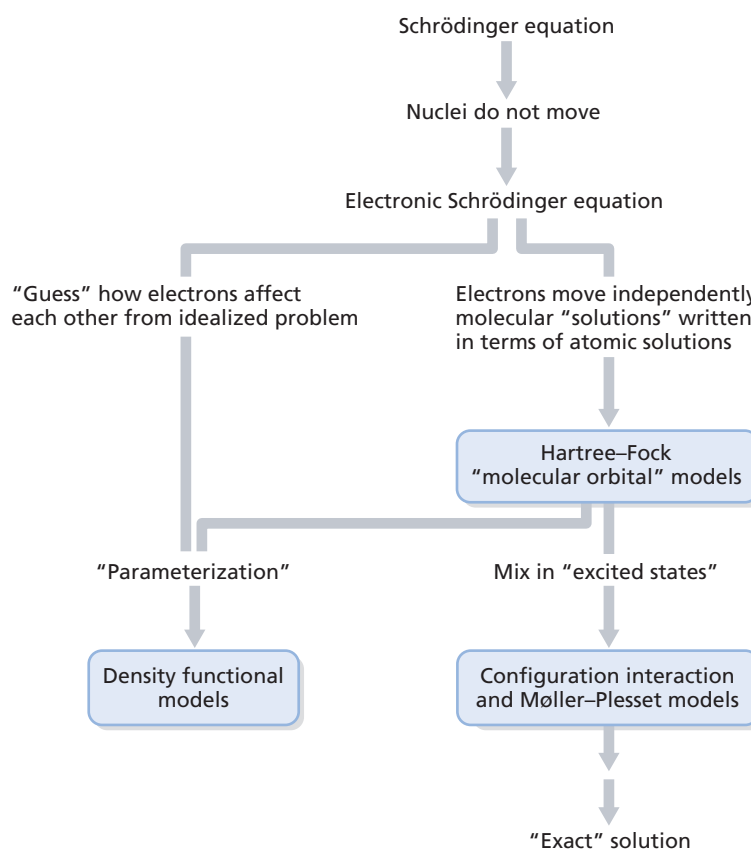


Figure 15.11
Schematic diagram showing how quantum-chemical models are related to one another.

Density functional models are well defined and yield unique results. They are neither size consistent nor variational. Note that if the exact exchange-correlation functional had been known for the problem at hand (rather than only for the idealized many-electron gas problem), then the density functional approach would be exact. Although better forms of such functionals are constantly being developed, at present there is no systematic way to improve the functional to achieve an arbitrary level of accuracy.

15.6.4 Overview of Quantum-Chemical Models

An overview of quantum-chemical models, starting with the Schrödinger equation and including Hartree–Fock models, configuration interaction and Møller–Plesset models, and density functional models, is provided in Figure 15.11.

15.7 GAUSSIAN BASIS SETS

The LCAO approximation requires the use of a basis set made up of a finite number of well-defined functions centered on each atom. The obvious choice for the functions are those corresponding closely to the exact solution of the hydrogen atom—that is, a polynomial in the Cartesian coordinates multiplying an exponential in r . However, the use of these functions is not cost effective, and early numerical calculations were carried out using nodeless **Slater-type orbitals** (STOs), defined by

$$\phi(r, \theta, \phi) = \frac{(2\zeta/a_0)^{n+1/2}}{[(2n)!]^{1/2}} r^{n-1} e^{-\zeta r/a_0} Y_l^m(\theta, \phi) \quad (15.53)$$

The symbols n , m , and l denote the usual quantum numbers, and ζ is the effective nuclear charge. Use of these so-called Slater functions was entertained seriously in the

Concept

Gaussian basis sets are widely used in quantum chemical calculations because they reduce computational cost.

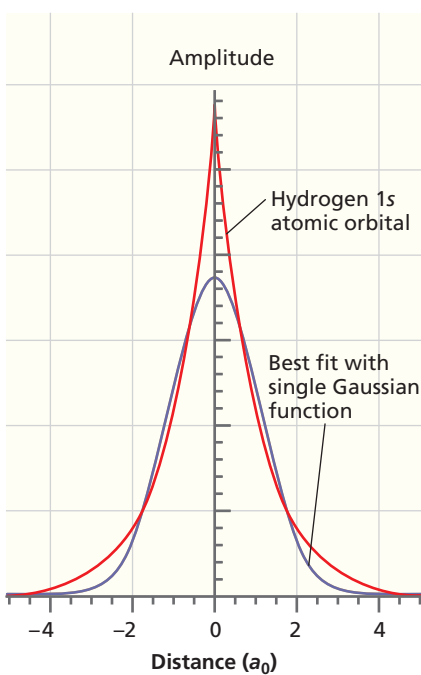


Figure 15.12
Comparison of the hydrogen atom 1s atomic orbital (red curve) with a single Gaussian function (purple curve). Note that the AO has a cusp at the nucleus, whereas the Gaussian function has zero slope at the nucleus. Note also that the Gaussian function falls off more rapidly with distance because of the r^2 dependence in the exponent.

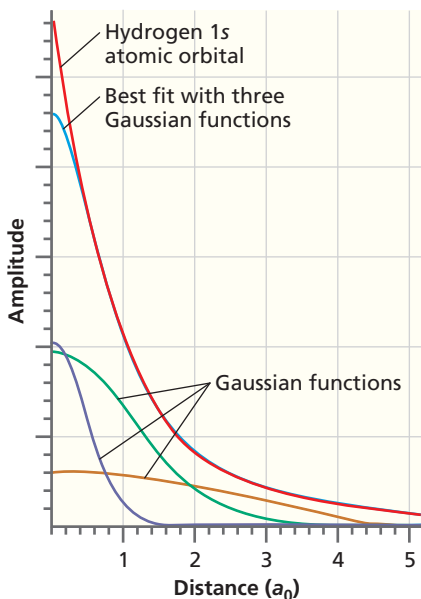


Figure 15.13
Hydrogen atom 1s atomic orbital (red curve) fit with three Gaussian functions with different α values (green, brown, and purple curves). Both the α values and the coefficients multiplying the Gaussian functions are optimized in the best fit function, shown in blue.

years immediately following the introduction of the Roothaan–Hall equations, but was soon abandoned because they led to integrals that are difficult, if not impossible, to evaluate analytically. Further work showed that the cost of calculations can be further reduced if the AOs are expanded in terms of **Gaussian functions**, which have the form

$$g_{ijk}(r) = N x^i y^j z^k e^{-\alpha r^2} \quad (15.54)$$

In this equation, x , y , and z are the position coordinates measured from the nucleus of an atom; i , j , and k are nonnegative integers, and α is an orbital exponent. An s -type function (zeroth order Gaussian) is generated by setting $i = j = k = 0$; a p -type function (first-order Gaussian) is generated if one of i , j , and k is 1 and the remaining two are 0; and a d -type function (second-order Gaussian) is generated by all combinations that give $i + j + k = 2$. Note that this recipe leads to six rather than five d -type functions, but appropriate combinations of these six functions give the usual five d -type functions and a sixth function that has s symmetry.

Gaussian functions lead to integrals that are easily evaluated. With the exception of so-called semi-empirical models, which do not actually entail evaluation of large numbers of difficult integrals, all practical quantum-chemical models now make use of Gaussian functions.

Given the different radial dependence of STOs and Gaussian functions, it is not obvious at first glance that Gaussian functions are appropriate choices for AOs. Figure 15.12 shows a comparison of the two functional forms. The solution to this problem is to approximate the STO by a linear combination of Gaussian functions having different α values, rather than by a single Gaussian function. For example, a best fit to a 1s-type STO using three Gaussian functions is shown in Figure 15.13. We can see that, although the region near the nucleus is not fit well, in the bonding region beyond $0.5 a_0$, the fit is very good. The fit near the nucleus can be improved by using more Gaussian functions.

In practice, instead of taking individual Gaussian functions as members of the basis set, a normalized linear combination of Gaussian functions with fixed coefficients is constructed to provide a best fit to an AO. The value of each coefficient is optimized either by seeking minimum atom energies or by comparing calculated and experimental results for “representative” molecules. These linear combinations are called **contracted functions**. The contracted functions become the elements of the basis set. Although the coefficients in the contracted functions are fixed, the coefficients $c_{\mu i}$ in Equation (15.21) are variable and are optimized in the solution of the Schrödinger equation.

15.7.1 Minimal Basis Sets

Although there is no limit to the number of functions that can be placed on an atom, there is a minimum number. The minimum number is the number of functions required to hold all the electrons of the atom while still maintaining its overall spherical nature. This simplest representation or **minimal basis set** involves a single (1s) function for hydrogen and helium, a set of five functions (1s, 2s, 2p_x, 2p_y, 2p_z) for lithium to neon, and a set of nine functions (1s, 2s, 2p_x, 2p_y, 2p_z, 3s, 3p_x, 3p_y, 3p_z) for sodium to argon. Note that although 2p functions are not occupied in the lithium or beryllium atoms (and 3p functions are not occupied in the sodium or magnesium atoms), they are needed to provide proper descriptions of the bonding in molecular systems. For example, the bonding in a molecule such as lithium fluoride involves electron donation from a lone pair on fluorine to an appropriate (p-type) empty orbital on lithium (back bonding) as shown in Figure 15.14.

Of the minimal basis sets that have been devised, perhaps the most widely used and extensively documented is the **STO-3G basis set**. Here, each of the basis functions is expanded in terms of three Gaussian functions, where the values of the Gaussian exponents and the linear coefficient have been determined by least squares as best fits to Slater-type (exponential) functions.

The STO-3G basis set and all minimal basis sets have two obvious shortcomings. The first shortcoming is that all basis functions are either themselves spherical or come in sets that, when taken together, describe a sphere. This means that atoms with spherical molecular environments or nearly spherical molecular environments will be better described than atoms with aspherical environments. This suggests that comparisons

among different molecules will be biased in favor of those incorporating the most spherical atoms. The second shortcoming follows from the fact that basis functions are atom centered. This restricts their ability to describe electron distributions between nuclei, which are a critical element of chemical bonds. Minimal basis sets such as STO-3G are primarily of historical interest and have largely been replaced in practical calculations by split-valence basis sets and polarization basis sets, which have been formulated to address these two shortcomings. These latter two basis sets are discussed in the following two subsections.

15.7.2 Split-Valence Basis Sets

The first shortcoming of a minimal basis set, namely, a bias toward atoms with spherical environments, can be addressed by providing two sets of valence basis functions: an inner set, which is more tightly held, and an outer set, which is more loosely held. The iterative process leading to solution of the Roothaan–Hall equations adjusts the balance of the two parts independently for the three Cartesian directions, by adjusting the individual molecular orbital coefficients. For example, the proper linear combination to produce a molecular orbital suitable for σ bonding might involve a large coefficient (σ_{inner}) multiplying the inner basis function (in the σ direction) and a small coefficient (σ_{outer}) multiplying the outer basis function, whereas that to produce a molecular orbital suitable for π bonding might involve a small coefficient (π_{inner}) multiplying the inner basis function and a large coefficient (π_{outer}) multiplying the outer basis function as shown in Figure 15.15. The fact that the three Cartesian directions are treated independently of each other means that the atom (in the molecule) may be nonspherical.

A **split-valence basis set** represents core atomic orbitals by one set of functions and valence atomic orbitals by two sets of functions, $1s$, $2s^i$, $2p_x^i$, $2p_y^i$, $2p_z^i$, $2s^o$, $2p_x^o$, $2p_y^o$, $2p_z^o$ for lithium to neon and $1s$, $2s$, $2p_x$, $2p_y$, $2p_z$, $3s^i$, $3p_x^i$, $3p_y^i$, $3p_z^i$, $3s^o$, $3p_x^o$, $3p_y^o$, $3p_z^o$ for sodium to argon. Note that the valence $2s$ ($3s$) functions are also split into inner (superscript i) and outer (superscript o) components and that hydrogen atoms are also represented by inner and outer valence ($1s$) functions. Among the simplest split-valence basis sets are 3-21G and 6-31G. Each core atomic orbital in the 3-21G basis set is expanded in terms of three Gaussian functions, whereas basis functions representing inner and outer components of valence atomic orbitals are expanded in terms of two and one Gaussian functions, respectively. The 6-31G basis sets are similarly constructed, with core orbitals represented in terms of six Gaussian functions and valence orbitals split into three and one Gaussian components. Expansion coefficients and Gaussian exponents for 3-21G and 6-31G basis sets have been determined by Hartree–Fock energy minimization on atomic ground states.

15.7.3 Polarization Basis Sets

The second shortcoming of a minimal (or split-valence) basis set, namely, that the basis functions are centered on atoms rather than between atoms, can be addressed by providing d -type functions on main-group elements (where the valence orbitals are of

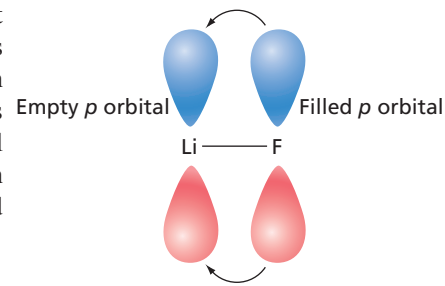


Figure 15.14

2p orbitals must be included in the Li basis set to allow back bonding.

Concept

Split-valence basis sets can model non-spherical electron distributions around atoms.

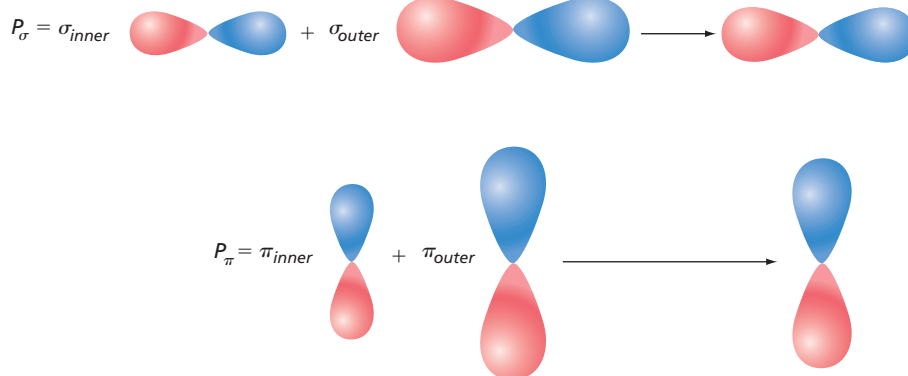


Figure 15.15

Properties of a split-valence basis set.

A split-valence basis set provides a way to allow the electron distribution about an atom to be nonspherical. Only one of the three atomic orbitals oriented along the x , y , and z directions is shown. Because the proportions of the inner and outer orbitals can be different along the three directions, the resulting charge distribution can be nonspherical.

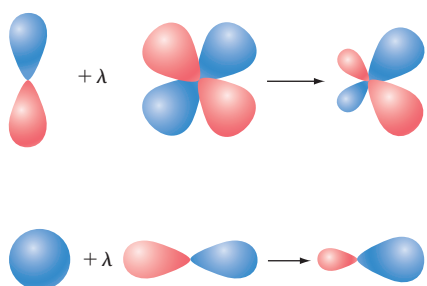


Figure 15.16
Polarization functions shift the center of the electron distribution to the bonding region between atoms.

Concept

Polarization basis sets can model electron distributions that are shifted to the bonding region between atoms.

s and *p* type) and (optionally) *p*-type functions on hydrogen (where the valence orbital is of *s* type). This allows displacement of electron distributions away from the nuclear positions, as depicted in Figure 15.16.

The inclusion of **polarization functions** can be thought about either in terms of hybrid orbitals (for example, *pd* and *sp* hybrids) or alternatively a Taylor series expansion of a function (*d* functions are the first derivatives of *p* functions and *p* functions are the first derivatives of *s* functions). Although the first way of thinking is quite familiar to chemists (Pauling hybrids), the second offers the advantage of knowing what steps might be taken next to effect further improvement—that is, adding second and third derivatives.

Among the simplest polarization basis sets is 6-31G*, constructed from 6-31G by adding a set of *d*-type polarization functions written in terms of a single Gaussian for each heavy (nonhydrogen) atom. A set of six second-order Gaussian functions is added in the case of 6-31G*. Gaussian exponents for polarization functions have been chosen to give the lowest energies for representative molecules. Polarization of the *s* orbitals on hydrogen atoms is necessary for an accurate description of the bonding in many systems (particularly those in which hydrogen is a bridging atom). The 6-31G** basis set is identical to 6-31G*, except that it also provides three *p*-type polarization functions for hydrogen.

15.7.4 Basis Sets Incorporating Diffuse Functions

Calculations involving anions, such as absolute acidity calculations and calculations of molecules in excited states and of UV absorption spectra, often pose special problems. This is because the highest energy electrons for such species may only be loosely associated with specific atoms (or pairs of atoms). In these situations, basis sets may need to be supplemented by **diffuse functions**, which decrease in value slowly with distance from the nucleus. Examples of diffuse functions are diffuse *s*- and *p*-type functions on heavy (nonhydrogen) atoms (designated with a plus sign as in 6-31+G* and 6-31+G**). It may also be desirable to provide hydrogens with diffuse *s*-type functions (designated by two plus signs as in 6-31++G* and 6-31++G**).

15.8 SELECTION OF A THEORETICAL MODEL

By now, it should be apparent to the reader that many different models are available and useful in describing molecular structure, reaction energies, and other properties. All of these models ultimately stem from the electronic Schrödinger equation, and they differ from each other both in the manner in which they treat electron correlation and in the nature of the atomic basis set. Each distinct combination (a theoretical model) leads to a scheme with its own particular characteristics (a theoretical model chemistry).

Hartree–Fock models may be seen as the parent model in that they treat electron correlation in the simplest possible manner, replacing, in effect, instantaneous electron–electron interactions with average interactions. Despite their simplicity, Hartree–Fock models have proven to be remarkably successful in a large number of situations and remain a mainstay of computational chemistry.

As discussed earlier, models that incorporate electron correlation can be broadly divided into two categories. The first category includes density functional models, which provide an explicit empirical term in the Hamiltonian to account for electron correlation. The second category includes configuration interaction and Møller–Plesset models, which start from the Hartree–Fock description and then optimally mix together wave functions corresponding to the ground and various excited states. Each of these models exhibits its own particular characteristics. Models that incorporate electron correlation are collectively known as **correlated models**.

Of course, no single theoretical model is likely to be ideal for all applications. A great deal of effort has been expended defining the limits of different models and judging the degree of success and the pitfalls of each. Most simply, success depends on the ability of a model to consistently reproduce known (experimental) data. This assumes that reliable experimental data are available or, at least, that errors in the data have been quantified. These include data on the structures and conformations (shapes) of stable

molecules, the enthalpies of chemical reactions (thermodynamics), and on such properties as vibrational frequencies (infrared spectra) and dipole moments. Quantum-mechanical models may also be applied to high-energy molecules (reactive intermediates) for which reliable experimental data may be difficult to obtain, and to reaction transition states, which may not even be directly observed, much less characterized. Although no experimental transition-state structures are available with which to compare the results of the calculations, experimental kinetic data may be interpreted to provide information about activation energies. As an alternative, transition-state structures can instead be compared with the results of high-level quantum-chemical calculations.

The level of a quantum-chemical model depends on the problem under investigation. A model also needs to be practical for the task at hand. The nature and size of the system needs to be taken into account, as do the available computational resources and the experience and patience of the practitioner. Practical models usually share one feature in common, which is they are not likely to be the highest level of calculation possible. Compromise is almost always an essential component of model selection.

Oddly enough, the main problem faced by those who wish to apply computational chemistry techniques to investigate chemistry is not the lack of suitable models, but rather the excess of models. Quite simply, there are too many choices. In this spirit, consideration from this point on will be limited to just four theoretical models: Hartree–Fock models with 3-21G split-valence and 6-31G* polarization basis sets, the B3LYP/6-31G* density functional model, and the MP2/6-31G* model. Although all of these models can be routinely applied to molecules of considerable size, they differ by two orders of magnitude in the amount of computer time they require. Thus, it is quite important to know where the less time-consuming models perform satisfactorily and where the more time-consuming models are needed. Note that although this set of models has been successfully applied to a wide range of chemical problems, some problems may require more accurate and more time-consuming models.

It is difficult to quantify the overall computation time of a calculation because it depends not only on the specific system and task at hand, but also on the sophistication of the computer program, the computational power available, and the experience of the user. For molecules of moderate size (for example, 10 atoms other than H), the HF/6-31G*, B3LYP/6-31G*, and MP2/6-31G* models are expected to exhibit overall computation times in a ratio of roughly 1:1.5:10. The HF/3-21G model requires a one-third to one-half of the computation time required by the corresponding HF/6-31G* model, whereas the computation time of Hartree–Fock, B3LYP, and MP2 models with basis sets larger than 6-31G* increase roughly as the cube (HF and B3LYP) and the fifth power (MP2) of the total number of basis functions. Structure optimizations and frequency calculations are typically an order of magnitude more time consuming than energy calculations, and the ratio will increase with increasing complexity (number of independent geometrical variables) of the system. Transition state structure optimizations are likely to be even more time consuming than equilibrium structure optimizations, owing primarily to a poorer initial guess of the structure.

Only a few calculated properties are examined in this discussion, including equilibrium bond distances, reaction energies, conformational energy differences, and dipole moments. Comparisons between the results of the calculations and experimental data are few for each of these, but sufficient to establish meaningful trends.

15.8.1 Equilibrium Bond Distances

A comparison of calculated and experimentally determined carbon–carbon bond distances in hydrocarbons is provided in Table 15.9. Whereas errors in measured bond distances are typically on the order of $\pm 0.02 \text{ \AA}$, experimental data for hydrocarbons and other small molecules presented here are more precise, and comparisons with the results of calculations to 0.01 \AA are meaningful. In terms of mean absolute error, all four models perform admirably. The B3LYP/6-31G* and MP2/6-31G* models perform better than the two Hartree–Fock models, owing largely to a sizable systematic error in carbon–carbon double-bond lengths in the Hartree–Fock models. With one exception, Hartree–Fock double-bond lengths are shorter than experimental distances.

Concept

The optimal level of a practical quantum mechanical model depends on the size and nature of the problem and the available computational resources.

TABLE 15.9 Bond Distances in Hydrocarbons (Å)

Bond	Hydrocarbon	Hartree–Fock 3-21G	Hartree–Fock 6-31G*	B3LYP 6-31G*	MP2 6-31G*	Experiment
C—C	But-1-yne-3-ene	1.432	1.439	1.424	1.429	1.431
	Propyne	1.466	1.468	1.461	1.463	1.459
	1,3-Butadiene	1.479	1.467	1.458	1.458	1.483
	Propene	1.510	1.503	1.502	1.499	1.501
	Cyclopropane	1.513	1.497	1.509	1.504	1.510
	Propane	1.541	1.528	1.532	1.526	1.526
	Cyclobutane	1.543	1.548	1.553	1.545	1.548
	Cyclopropene	1.282	1.276	1.295	1.303	1.300
C=C	Allene	1.292	1.296	1.307	1.313	1.308
	Propene	1.316	1.318	1.333	1.338	1.318
	Cyclobutene	1.326	1.322	1.341	1.347	1.332
	But-1-yne-ene	1.320	1.322	1.341	1.344	1.341
	1,3-Butadiene	1.320	1.323	1.340	1.344	1.345
	Cyclopentadiene	1.329	1.329	1.349	1.354	1.345
Mean absolute error		0.011	0.011	0.006	0.007	—

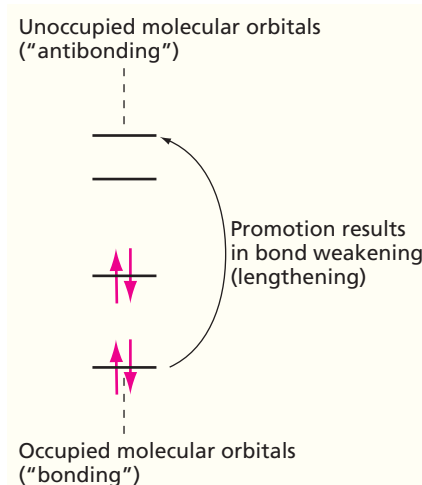


Figure 15.17
Promotion of electrons to unfilled orbitals reduces bond strength and leads to bond lengthening.

This is easily rationalized. Treatment of electron correlation (for example, in the MP2 model) involves the promotion of electrons from occupied molecular orbitals (in the Hartree–Fock wave function) to unoccupied molecular orbitals. Because occupied molecular orbitals are (generally) net bonding in character and because unoccupied molecular orbitals are (generally) net antibonding in character, any promotions should result in bond weakening (lengthening) as illustrated in Figure 15.17. This in turn suggests that bond lengths from limiting Hartree–Fock models are necessarily shorter than exact values. Apparently, Hartree–Fock models with 3-21G and 6-31G* basis set are close enough to the limit for this behavior to be seen.

Consistent with such an interpretation, B3LYP/6-31G* and MP2/6-31G* double-bond lengths do not show a systematic trend and are both smaller and larger than experimental values.

Similar comments can be made regarding CN and CO bond distances (Table 15.10). In terms of mean absolute error, the performance of the B3LYP/6-31G* and MP2/6-31G* models is similar to that previously noted for CC bonds in hydrocarbons, but the two Hartree–Fock models do not fare as well. Note that although bond distances from the HF/6-31G* model are constantly smaller than measured values, in accord with the picture presented for hydrocarbons, HF/3-21G bond lengths do not show such a trend. It appears that the 3-21G basis set is not large enough to closely mirror the Hartree–Fock limit in this instance. Most bond distances obtained from the B3LYP/6-31G* and MP2/6-31G* models are actually slightly larger than experimental distances. (The CN bond length in formamide is the only significant exception.) Bond lengthening from the corresponding (6-31G* basis set) Hartree–Fock model is a direct consequence of treatment of electron correlation.

In summary, all four models discussed in this section (see results in Table 15.10) provide a plausible account of equilibrium bond lengths. Similar comments also apply to bond angles and more generally to the structures of larger molecules.

15.8.2 Finding Equilibrium Structures

As discussed in detail at the beginning of this chapter, an equilibrium structure is a point on a multidimensional potential energy surface for which all first energy derivatives with respect to the individual geometrical coordinates are zero, and for which the

TABLE 15.10 Bond Distances in Molecules with Heteroatoms (Å)

Bond	Hydrocarbon	Hartree–Fock		B3LYP	MP2	Experiment
		3-21G	6-31G*	6-31G*	6-31G*	
C—N	Formamide	1.351	1.349	1.362	1.362	1.376
	Methyl isocyanide	1.432	1.421	1.420	1.426	1.424
	Trimethylamine	1.471	1.445	1.456	1.455	1.451
	Aziridine	1.490	1.448	1.473	1.474	1.475
	Nitromethane	1.497	1.481	1.499	1.488	1.489
C—O	Formic acid	1.350	1.323	1.347	1.352	1.343
	Furan	1.377	1.344	1.364	1.367	1.362
	Dimethyl ether	1.435	1.392	1.410	1.416	1.410
	Oxirane	1.470	1.401	1.430	1.439	1.436
Mean absolute error		0.017	0.018	0.005	0.005	—

diagonal representation of the matrix of second energy derivatives has all positive elements. In simple terms, an equilibrium structure corresponds to the bottom of a well on the overall potential energy surface.

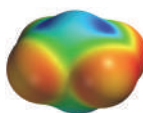
Not all equilibrium structures correspond to (kinetically) stable molecules. This means that not all equilibrium structures will correspond to detectable (let alone characterizable) molecules. Stability also implies that the well is deep enough to preclude the molecule from being transformed into other molecules. Equilibrium structures that clearly exist but cannot be detected easily are commonly referred to as **reactive intermediates**.

Structure optimization does not guarantee that the final structure will have a lower energy than any other structure of the same molecular formula. All that it guarantees is that the structure will correspond to a local minimum; in other words, a structure with lower energy than similar structures. However, the resulting structure may still not be the lowest energy structure possible for the molecule. Other local minima that are lower in energy may exist and be accessible via low-energy rotations about single bonds or puckering of rings (see Figure 15.1). The full collection of local minima are referred to as **conformers**. Identifying the lowest energy conformer or global minimum requires repeated structure optimization starting with a different initial structure as discussed in Section 15.8.6.

Identifying an equilibrium structure is not as difficult a chore as it might first appear. For one, chemists know a great deal about what molecules look like and can usually provide an excellent starting structure. Also, optimization to a minimum is an important task in many fields of science and engineering, and very good algorithms exist with which to accomplish it.

Structure optimization is an iterative process. The energy and energy gradient (first derivatives with respect to all geometrical coordinates) are calculated for the initial structure, and this information is then used to project a new structure. This process needs to continue until the lowest energy or optimized structure is reached. Three criteria must be satisfied before a structure is accepted as optimized. First, successive structure changes must not lower the energy by more than a specified (small) value. Second, the energy gradient must closely approach zero. Third, successive iterations must not change any geometrical parameter by more than a specified (small) value.

In principle, structure optimization carried out in the absence of symmetry must produce a local energy minimum. However, the imposition of symmetry may result in a structure that is not an energy minimum. The most conservative tactic is always to optimize structure in the absence of symmetry. If this is not practical, and if there is any doubt that the symmetrical structure corresponds to an energy minimum, then it is always possible to verify that the structure located corresponds to a local minimum by calculating vibrational frequencies for the final (optimized) structure. These should all be real numbers. The presence of an imaginary frequency indicates that the corresponding coordinate is not an energy minimum.



Problems P15.5–P15.12

TABLE 15.11 Homolytic Bond Dissociation Energies (kJ/mol)

Bond Dissociation Reaction	Hartree–Fock 3-21G	B3LYP 6-31G*	MP2 6-31G*	Experiment
$\text{CH}_3\text{—CH}_3 \rightarrow \cdot\text{CH}_3 + \cdot\text{CH}_3$	285	293	406	414
$\text{CH}_3\text{—NH}_2 \rightarrow \cdot\text{CH}_3 + \cdot\text{NH}_2$	247	243	372	385
$\text{CH}_3\text{—OH} \rightarrow \cdot\text{CH}_3 + \cdot\text{OH}$	222	247	402	410
$\text{CH}_3\text{—F} \rightarrow \cdot\text{CH}_3 + \cdot\text{F}$	247	289	473	477
$\text{NH}_2\text{—NH}_2 \rightarrow \cdot\text{NH}_2 + \cdot\text{NH}_2$	155	142	293	305
$\text{HO—OH} \rightarrow \cdot\text{OH} + \cdot\text{OH}$	13	0	226	230
$\text{F—F} \rightarrow \cdot\text{F} + \cdot\text{F}$	-121	-138	176	159
Mean absolute error	190	186	9	2
				—

15.8.3 Reaction Energies

Reaction energy comparisons are divided into three parts: bond dissociation energies, energies of reactions relating structural isomers, and relative proton affinities. Bond dissociation reactions are the most disruptive because they lead to a change in the number of electron pairs. Structural isomer comparisons maintain overall electron pair count but swap bonds of one kind for those of another. Relative proton affinity comparisons are least disruptive in that they maintain the numbers of each kind of formal chemical bond and lead only to subtle changes in the molecular environment.

A comparison of homolytic bond dissociation energies based on calculation and on experimental thermochemical data is provided in Table 15.11. Hartree–Fock models with the 3-21G and 6-31G* basis set turn in a very poor performance, paralleling the poor performance of limiting Hartree–Fock models (see the discussion in Section 15.4.1). Bond energies are far too small, consistent with the fact that the total correlation energy for the radical products is smaller than that for the reactant due to a decrease in the number of electron pairs. B3LYP/6-31G* and especially MP2/6-31G* models fare much better (results for the latter are well inside the experimental error bars).

Without doubt, two of the most commonly asked questions relating to thermochemistry are: “Which of several possible structural isomers is most stable?” and “What are the relative energies of any reasonable alternatives?” The ability to successfully choose the lowest energy isomer and at least rank the energies of higher energy isomers is essential to the success of any model. A few comparisons of this kind are found in Table 15.12.

TABLE 15.12 Relative Energies Isomer—Reference Compound of Structural Isomers (kJ/mol)

Reference Compound	Isomer	Hartree–Fock		B3LYP	MP2	
		3-21G	6-31G*	6-31G*	6-31G*	Experiment
Acetonitrile	Methyl isocyanide	88	100	113	121	88
Acetaldehyde	Oxirane	142	130	117	113	113
Acetic acid	Methyl formate	54	54	50	59	75
Ethanol	Dimethyl ether	25	29	21	38	50
Propyne	Allene	13	8	-13	21	4
	Cyclopropene	167	109	92	96	92
Propene	Cyclopropane	59	33	33	17	29
1,3-butadiene	2-Butyne	17	29	33	17	38
	Cyclobutane	75	54	50	33	46
	Bicyclo [1.1.0] butane	192	126	117	88	109
Mean absolute error		32	13	12	15	—

TABLE 15.13 Proton Affinities of Nitrogen Bases Relative to the Proton Affinity of Methylamine (kJ/mol)

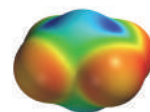
Base	Hartree–Fock 3-21G	B3LYP 6-31G*	MP2 6-31G*	Experiment
Ammonia	-42	-46	-42	-38
Aniline	-38	-17	-21	-10
Methylamine	0	0	0	0
Dimethylamine	29	29	25	27
Pyridine	17	29	25	29
Trimethylamine	46	46	38	46
Diazabicyclooctane	67	71	59	60
Quinuclidine	79	84	75	75
Mean absolute error	8	5	4	—

In terms of mean absolute error, three of the four models provide similar results. The HF/3-21G model is inferior. None of the models is consistent with the standard that would make it a useful reliable replacement for experimental data (<5 kJ/mol). More detailed comparisons provide insight into the shortcomings of these models. For example, Hartree–Fock models consistently disfavor small-ring cyclic structures over their unsaturated cyclic isomers, whereas neither the B3LYP/6-31G* nor the MP2/6-31G* method shows a consistent preference.

The final comparison (Table 15.13) is between proton affinities of a variety of nitrogen bases and that of methylamine as a standard; that is,



This type of comparison is important not only because proton affinity (basicity) is an important property in its own right, but also because it typifies property comparisons among sets of closely related compounds. The experimental data derive from equilibrium measurements in the gas phase and are accurate to ± 4 kJ/mol. In terms of mean absolute error, all four models turn in similar and respectable accounts over what is a considerable range (>100 kJ/mol) of experimental proton affinities. The HF/3-21G model is clearly the poorest performer, owing primarily to underestimation of the proton affinities of aniline and pyridine.



Problems P15.13–P15.16

15.8.4 Energies, Enthalpies, and Gibbs Energies

Quantum-chemical calculations account for reaction thermochemistry by combining the energies of reactant and product molecules at 0 K. Additionally, the residual energy of vibration (the so-called zero point energy discussed in Sections 7.3 and 8.3) is ignored. On the other hand, experimental thermochemical comparisons are most commonly based on enthalpies or Gibbs energies of 1 mol of real (vibrating) molecules at some finite temperature (typically 298.15 K). The connection between the various quantities involves the mass, equilibrium structure, and set of vibrational frequencies for each of the molecules in the reaction. Calculating thermodynamic quantities is straightforward but, because it requires frequencies and consumes significant computation time, it is performed only where necessary.

We start with two familiar thermodynamic relationships:

$$\Delta G = \Delta H - T\Delta S \quad (15.55)$$

$$\Delta H = \Delta U + \Delta(PV) \approx \Delta U \quad (15.56)$$

where G is the Gibbs energy, H is the enthalpy, S is the entropy, U is the internal energy, and T , P , and V are the temperature, pressure, and volume, respectively. For most cases,

the $\Delta(PV)$ term can be ignored, which implies that $\Delta U = \Delta H$ at 0 K. Three steps are required to obtain ΔG , the first two to relate the quantum-mechanical energy at 0 K to the internal energy at 298 K and the third to calculate the Gibbs energy.

- Correction of the internal energy for finite temperature.* The change in internal energy from 0 K to a finite temperature, T , $\Delta U(T)$, is given by

$$\Delta U(T) = \Delta U_{trans}(T) + \Delta U_{rot}(T) + \Delta U_{vib}(T) \quad (15.57)$$

$$\Delta U_{trans}(T) = \frac{3}{2}RT \quad (15.58)$$

$$\Delta U_{rot}(T) = \frac{3}{2}RT \text{ (RT for a linear molecule)} \quad (15.59)$$

$$\Delta U_{vib}(T) = U_{vib}(T) - U_{vib}(0\text{ K}) = N_A \sum_i^{\nu_i} \frac{h\nu_i}{e^{h\nu_i/kT} - 1} \quad (15.60)$$

The ν_i are vibrational frequencies, N_A is Avogadro's number, and R , k , and h are the gas constant, the Boltzmann constant, and the Planck constant, respectively.

- Correction for zero point vibrational energy.* The zero point vibrational energy, $U_{vib}(0)$, of n moles of a molecule at 0 K is given by

$$U_{vib}(0) = nN_A E_{zero\ point} = \frac{1}{2}nN_A \sum_i^{\nu_i} h\nu_i \quad (15.61)$$

This calculation also requires knowledge of the vibrational frequencies.

- Entropy.* The absolute entropy, S , of n moles of a molecule may be written as a sum of terms:

$$S = S_{trans} + S_{rot} + S_{vib} + S_{el} - nR[\ln(nN_A) - 1] \quad (15.62)$$

$$S_{trans} = nR \left[\frac{3}{2} + \ln \left(\left(\frac{nRT}{P} \right) \left(\frac{2\pi mkT}{h^2} \right)^{3/2} \right) \right] \quad (15.63)$$

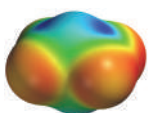
$$S_{rot} = nR \left[\frac{3}{2} + \ln \left(\left(\frac{\sqrt{\pi}}{\sigma} \right) \left(\frac{kT}{hcB_A} \right)^{1/2} \left(\frac{kT}{hcB_B} \right)^{1/2} \left(\frac{kT}{hcB_C} \right)^{1/2} \right) \right] \quad (15.64)$$

$$S_{vib} = nR \sum_i \left[\left(\frac{\mu_i}{e^{\mu_i} - 1} \right) + \ln \left(\frac{1}{1 - e^{-\mu_i}} \right) \right] \quad (15.65)$$

$$S_{el} = nR \ln g_0 \quad (15.66)$$

In these equations, m is the molecular mass, B_i is the rotational constant, σ is the symmetry number, $\mu_i = h\nu_i/kT$, c is the speed of light, and g_0 is the degeneracy of the electronic ground state (normally equal to one).

Note that molecular structure enters into the rotational entropy through B and that the vibrational frequencies enter into the vibrational entropy. The translational entropy cancels in a (mass) balanced reaction, and the electronic entropy is usually zero because for most molecules $g_0 = 1$. Note also that the expression provided for the vibrational contribution to entropy approaches infinity as the vibrational frequency approaches zero. This is clearly wrong and has its origin in the use of the linear harmonic oscillator approximation to derive the expression. Unfortunately, low-frequency modes are the major contributors to the vibrational entropy, and caution must be exercised when using the preceding formulas for the case of frequencies below approximately 300 cm^{-1} . In this case, the molecular partition function must be evaluated term by term rather than assuming the classical limit.



Problem P15.17

15.8.5 Conformational Energy Differences

Rotation around single bonds may give rise to rotational isomers (conformers). Because bond rotation is almost always a very low-energy process, this means that more than one conformer may be present at equilibrium. For example, *n*-butane exists as a mixture of

anti and *gauche* conformers, as shown in Figures 15.1 and 15.18. The same reasoning carries over to molecules incorporating flexible rings, where conformer interconversion may be viewed in terms of a process involving restricted rotation about the bonds in the ring.

Knowledge of the conformer of lowest energy and, more generally, the distribution of conformers is important because many molecular properties depend on detailed molecular shape. For example, whereas *gauche n*-butane is a polar molecule (albeit very weakly polar), *anti n*-butane is nonpolar, and the value of the dipole moment for an actual sample of *n*-butane would depend on how much of each species was actually present.

Experimentally, a great deal is known about the conformational preferences of molecules in the solid state (from X-ray crystallography). Far less is known about the conformations of isolated (gas-phase) molecules, although there are sufficient data to allow gross assessment of practical quantum-chemical models. Experimental conformational energy differences are somewhat more scarce, but accurate data are available for a few very simple (two-conformer) systems. Comparison of these data with the results of calculations for hydrocarbons is provided in Table 15.14. These are expressed in terms of the energy of the high-energy conformer relative to that of the low-energy conformer.

All models correctly assign the ground state conformer in all molecules. In terms of mean absolute error, the MP2/6-31G* model provides the best description of conformational energy differences and the HF/6-31G* model the worst description. Hartree–Fock models consistently overestimate differences (the sole exception is for the *trans/gauche* energy difference in 1,3-butadiene from the 3-21G model), in some cases by large amounts (nearly 5 kJ/mol for the *equatorial-axial* energy difference in *tert*-butylcyclohexane from the 3-21G model). Correlated models also typically (but not always) overestimate energy differences, but the magnitudes of the errors are much smaller than those seen for Hartree–Fock models.

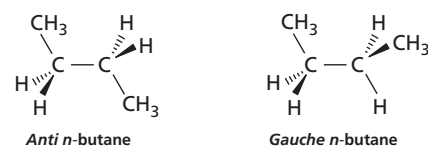
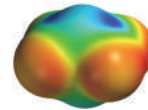


Figure 15.18

Structures of two *n*-butane conformers.



Problems P15.18–P15.20

15.8.6 Determining Molecular Shape

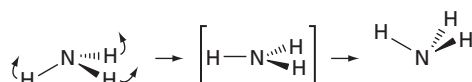
Many molecules can (and do) exist in more than one shape, arising from different arrangements around single bonds and flexible rings. The problem of identifying the lowest energy conformer (or the complete set of conformers) in simple molecules such as *n*-butane and cyclohexane is straightforward but rapidly becomes difficult as the number of conformational degrees of freedom increases, owing simply to the large number of arrangements that need to be examined. For example, a systematic search on a molecule with N single bonds and step size of $360^\circ/M$, would need to examine M^N conformers. For a molecule with three single bonds and a step size of $120^\circ (M = 3)$, this leads to 27 conformers; for a molecule with eight single bonds, more than 6500 conformers would need to be considered. It is clear that it will not always be possible to

TABLE 15.14 Conformational Energy in Hydrocarbons (kJ/mol)

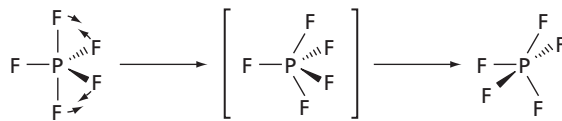
Hydrocarbon	Low-Energy/ High-Energy Conformer	Hartree–Fock 3-21G	Hartree–Fock 6-31G*	B3LYP 6-31G*	MP2 6-31G*	Experiment
<i>n</i> -Butane	<i>anti/gauche</i>	3.3	4.2	3.3	2.9	2.80
1-Butene	<i>skew/cis</i>	3.3	2.9	1.7	2.1	0.92
1,3-Butadiene	<i>trans/gauche</i>	11.3	13.0	15.1	10.9	12.1
Cyclohexane	<i>chair/twist-boat</i>	27.2	28.5	26.8	27.6	19.7–25.9
Methylcyclohexane	<i>equatorial/axial</i>	7.9	9.6	8.8	7.9	7.32
<i>tert</i> -Butylcyclohexane	<i>equatorial/axial</i>	27.2	25.5	22.2	23.4	22.6
<i>cis</i> -1,3-	<i>equatorial/axial</i>	26.4	27.2	25.1	23.8	23.0
Dimethylcyclohexane						
Mean absolute error		1.9	2.3	1.3	0.9	—

Figure 15.19

Inversion of NH_3 leads to its mirror image.

**Figure 15.20**

Pseudorotation leads to exchange of *equatorial* and *axial* positions at a trigonal bipyramidal phosphorus center.

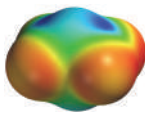


look everywhere, and sampling techniques will need to replace systematic procedures for complex molecules. The most common of these are so-called Monte Carlo methods (which randomly sample different conformations) and molecular dynamics techniques (which follow motion among different conformers in time).

15.8.7 Alternatives to Bond Rotation

Single-bond rotation (including restricted bond rotation in flexible rings) is the most common mechanism for conformer interconversion, but it is by no means the only mechanism. At least two other processes are known: inversion and pseudorotation. Inversion is normally associated with pyramidal nitrogen or phosphorus and involves a planar (or nearly planar) transition state, as in, for example, ammonia, as shown in Figure 15.19. Note that the starting and ending molecules are mirror images. Were the nitrogen to be bonded to three different groups and were the nitrogen lone pair to be counted as a fourth group, inversion would result in a change in chirality at this center. Pseudorotation, which is depicted in Figure 15.20, is normally associated with trigonal bipyramidal phosphorus and involves a square-based-pyramidal transition state. Note that pseudorotation interconverts *equatorial* and *axial* positions on phosphorus.

On one hand, both inversion of pyramidal nitrogen and pseudorotation around trigonal bipyramidal phosphorus are very low-energy processes ($<20\text{--}30\text{ kJ/mol}$) and generally proceed rapidly at 298 K. On the other hand, inversion of pyramidal phosphorus is more difficult (100 kJ/mol) and is inhibited at 298 K.



Problem P15.21

15.8.8 Dipole Moments

Calculated dipole moments for a selection of diatomic and small polyatomic molecules are compared with experimental values in Table 15.15. The experimental data cover a wide spectrum of molecules, from carbon monoxide, which is close to being nonpolar, to lithium fluoride, which is close to being fully ionic. All models provide a good

TABLE 15.15 Dipole Moments in Diatomic and Small Polyatomic Molecules (debyes)

Molecule	Hartree–Fock 3-21G	Hartree–Fock 6-31G*	B3LYP 6-31G*	MP2 6-31G*	Experiment
Carbon monoxide	0.4	0.3	0.1	0.2	0.11
Ammonia	1.8	1.9	1.9	2.0	1.47
Hydrogen fluoride	2.2	2.0	1.9	1.9	1.82
Water	2.4	2.2	2.1	2.2	1.85
Methyl fluoride	2.3	2.0	1.7	1.9	1.85
Formaldehyde	2.7	2.7	2.2	2.3	2.34
Hydrogen cyanide	3.0	3.2	2.9	3.0	2.99
Lithium hydride	6.0	6.0	5.6	5.8	5.83
Lithium fluoride	5.8	6.2	5.6	5.9	6.28
Mean absolute error	0.3	0.2	0.2	0.1	—

overall account of this range. In terms of mean absolute error, the HF/3-21G model fares worst and the MP2/6-31G* model fares best, but the differences are not large. Note that dipole moments from the two Hartree–Fock models are consistently larger than experimental values, the only exception being for lithium fluoride. This is in accord with the behavior of the limiting Hartree–Fock model (see previous discussion in Section 15.4.4) and may now easily be rationalized. Recognize that electron promotion from occupied to unoccupied molecular orbitals (either implicit or explicit in all electron correlation models) transfers electrons from “where they are” (negative regions) to “where they are not” (positive regions), as illustrated in Figure 15.21. In formaldehyde, for example, the lowest energy promotion is from a nonbonded lone pair localized on oxygen into a π^* orbital principally concentrated on carbon. As a result, electron correlation acts to reduce overall charge separation and to reduce the dipole moment in comparison with the Hartree–Fock value. This explanation is supported by the fact that dipole moments from correlated (B3LYP/6-31G* and MP2/6-31G*) calculations are not consistently larger than experimental values.

15.8.9 Atomic Charges: Real or Fictional?

Charges are part of the everyday language of chemistry and, aside from structures and energies, are the most commonly demanded quantities from quantum-chemical calculations. Charge distributions not only assist chemists in assessing overall molecular structure and stability, but they also inform them about the chemical reactions that molecules can undergo. Consider, for example, the two resonance structures that a chemist would draw for acetate anion, CH_3CO_2^- , as shown in Figure 15.22. This figure indicates that the two CO bonds are equivalent and should be intermediate in length between single and double linkages, and that the negative charge is evenly distributed on the two oxygens. Taken together, these two observations suggest that the acetate ion is delocalized and therefore particularly stable.

Despite their obvious utility, atomic charges are not measurable properties, nor can they be determined uniquely from calculations. Although the total charge on a molecule (the total nuclear charge and the sum of the charges on all of the electrons) is well defined, and although overall charge distribution may be inferred from such observables as the dipole moment, it is not possible to assign discrete atomic charges. To do this would require accounting both for the nuclear charge and for the charge of any electrons uniquely associated with the particular atom. Although it is reasonable to assume that the nuclear contribution to the total charge on an atom is simply the atomic number, it is not at all obvious how to partition the total electron distribution by atoms. Consider, for example, the electron distribution for the heteronuclear diatomic molecule hydrogen fluoride, shown in Figure 15.23. Here, the surrounding contour is a particular electron density surface that, for example, corresponds to a van der Waals surface and encloses a large fraction of the total electron density. In this picture, the surface has been drawn to suggest that more electrons are associated with fluorine than with hydrogen. This is entirely reasonable, given the known polarity of the molecule—that is, $\delta^+\text{H}—\text{F}\delta^-$, as observed experimentally by the direction of its dipole moment. It is, however, not at all apparent how to divide this surface between the two nuclei. Are any of the divisions shown in Figure 15.23 better than the others? No! Atomic charges are not molecular properties, and it is not possible to provide a unique definition. We

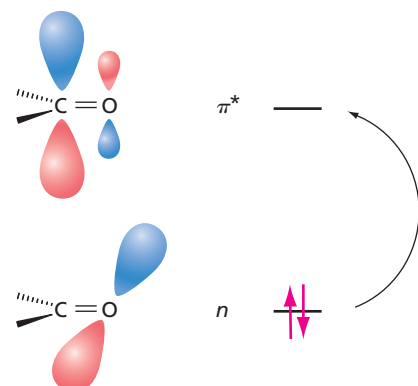


Figure 15.21

An example of electron promotion from occupied to unoccupied molecular orbitals. Accounting for electron correlation involves excitations such as the $n \rightarrow \pi^*$ transition in formaldehyde, which moves charge from oxygen to carbon and reduces the dipole moment in the carbonyl group.



Figure 15.22

The two Lewis structures of the acetate ion.

Concept

Atomic charges are not molecular properties, and it is not possible to provide a unique definition.

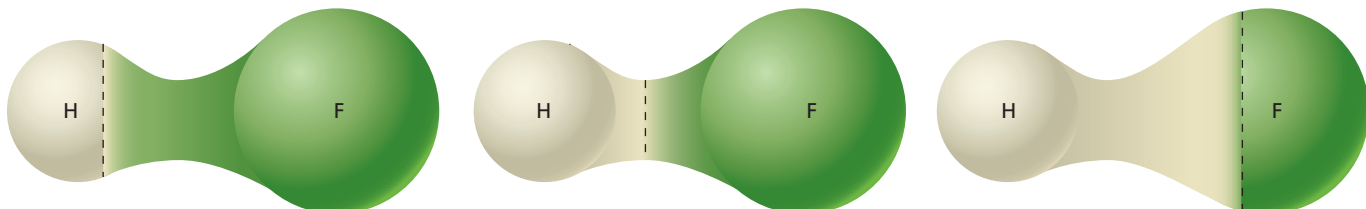


Figure 15.23

Three different ways of partitioning the electrons in hydrogen fluoride between hydrogen and fluorine.

can calculate (and measure using X-ray diffraction) molecular charge distributions, which are the number of electrons in a particular volume of space, but it is not possible to uniquely partition them among the atomic centers.

Despite the obvious problem with their definition, atomic charges are still useful, and several recipes have been formulated to calculate them. The simplest of these, now referred to as **Mulliken population analysis**, was discussed in Section 12.8. This analysis provides a procedure for estimating partial atomic charges based on calculations that involve linear combination of atomic orbitals, as described in more detail next.

MATHEMATICAL DESCRIPTION OF MULLIKEN POPULATION ANALYSIS

Mulliken population analysis starts from the definition of the electron density, $\rho(\mathbf{r})$, in the framework of the Hartree–Fock model:

$$\rho(\mathbf{r}) = \sum_{\mu}^{\text{basis functions}} \sum_{\nu}^{\text{basis functions}} P_{\mu\nu} \phi_{\mu}(\mathbf{r}) \phi_{\nu}(\mathbf{r}) \quad (15.67)$$

where $P_{\mu\nu}$ is an element of the density matrix [see Equation (15.27)], and the summations are carried out over all atom-centered basis functions, ϕ_{μ} . Summing over basis functions and integrating over all space leads to an expression for the total number of electrons, n :

$$\begin{aligned} \int \rho(\mathbf{r}) d\mathbf{r} &= \sum_{\mu}^{\text{basis functions}} \sum_{\nu}^{\text{basis functions}} P_{\mu\nu} \int \phi_{\mu}(\mathbf{r}) \phi_{\nu}(\mathbf{r}) d\mathbf{r} \\ &= \sum_{\mu}^{\text{basis functions}} \sum_{\nu}^{\text{basis functions}} P_{\mu\nu} S_{\mu\nu} = n \end{aligned} \quad (15.68)$$

where $S_{\mu\nu}$ are elements of the overlap matrix:

$$S_{\mu\nu} = \int \phi_{\mu}(\mathbf{r}) \phi_{\nu}(\mathbf{r}) d\mathbf{r} \quad (15.69)$$

Analogous expressions can be constructed for correlated models. The important point is that it is possible to equate the total number of electrons in a molecule to a sum of products of density matrix and overlap matrix elements as follows:

$$\sum_{\mu}^{\text{basis functions}} \sum_{\nu}^{\text{basis functions}} P_{\mu\nu} S_{\mu\nu} = \sum_{\mu}^{\text{basis functions}} P_{\mu\mu} + 2 \sum_{\mu \neq \nu}^{\text{basis functions}} P_{\mu\nu} S_{\mu\nu} = n \quad (15.70)$$

It is reasonable (but not necessarily correct) to assign any electrons associated with a particular diagonal element, $\mu\mu$, to that atom on which the basis function ϕ_{μ} is located. It is also reasonable to assign electrons associated with off-diagonal elements, $\mu\nu$, where both ϕ_{μ} and ϕ_{ν} reside on the same atom, to that atom. However, it is not apparent how to partition electrons from density matrix elements, $\mu\nu$, where ϕ_{μ} and ϕ_{ν} reside on different atoms. Mulliken provided such a method, which assigns each atom half of the total, which is very simple but completely arbitrary! According to Mulliken's scheme, the gross electron population, q_{μ} , for basis function ϕ_{μ} is given by:

$$q_{\mu} = P_{\mu\mu} + \sum_{\nu}^{\text{basis functions}} P_{\mu\nu} S_{\mu\nu} \quad (15.71)$$

Atomic electron populations, q_A , and atomic charges, Q_A , follow, where Z_A is the atomic number of atom A:

$$q_A = \sum_{\mu}^{\text{basis functions on atom A}} q_{\mu} \quad (15.72)$$

$$Q_A = Z_A - q_A \quad (15.73)$$

An entirely different approach to providing atomic charges is the following: fit the value of some property, which has been calculated based on the exact wave function, with that obtained from representation of the electronic charge distribution in terms of a collection of atom-centered charges. One choice of property is the **electrostatic potential**, ε_p . This represents the energy of interaction of a unit positive charge at some point in space, p , with the nuclei and the electrons of a molecule:

$$\varepsilon_p = \sum_A^{nuclei} \frac{Z_A e^2}{4\pi\epsilon_0 R_{Ap}} - \frac{e^2}{4\pi\epsilon_0} \sum_{\mu}^{basis functions} \sum_{\nu} P_{\mu\nu} \int \frac{\phi_{\mu}(\mathbf{r})\phi_{\nu}(\mathbf{r})}{r_p} d\mathbf{r} \quad (15.74)$$

Z_A are atomic numbers, $P_{\mu\nu}$ are elements of the density matrix, and R_{Ap} and r_p are distances separating the point charges from the nuclei and electrons, respectively. The first summation is over nuclei, and the second pair of summations is over basis functions.

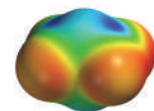
Operationally, electrostatic-fit charges are obtained by first defining a grid of points surrounding the molecule, then calculating the electrostatic potential at each of these grid points, and finally providing a best (least-squares) fit of the potential at the grid points to an approximate electrostatic potential, ε_p^{approx} , based on replacing the nuclei and electron distribution by a set of atom-centered charges, Q_A , subject to overall charge balance:

$$\varepsilon_p^{approx} = \sum_A^{nuclei} \frac{e^2 Q_A}{4\pi\epsilon_0 R_{Ap}} \quad (15.75)$$

The lack of uniqueness of the procedure is a consequence of the selection of the grid points.

Concept

Electrostatic potential is a property that can be calculated and gives information on the charge distribution in a molecule.



Problem P15.22

15.8.10 Transition-State Geometries and Activation Energies

Quantum-chemical calculations need not be limited to the description of the structures and properties of stable molecules—that is, molecules that can actually be observed and characterized experimentally. The calculations may as easily be applied to molecules that are highly reactive (reactive intermediates) and, even more interesting, to transition states, which cannot be observed, let alone characterized. However, activation energies can be inferred from experimental kinetic data. The complete absence of experimental data on transition-state structures complicates assessment of the performance of different models. However, it is possible to get around this by assuming that some particular (high-level) model yields reasonable structures for the transition state and then to compare the results of the other models with this standard. For our discussion, we have selected the MP2/6-311+G** model as the standard.

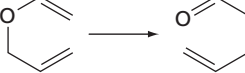
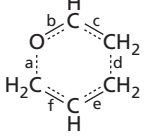
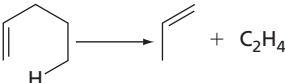
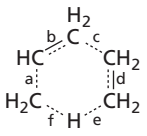
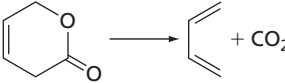
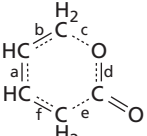
The most conspicuous difference between the structure data presented in Table 15.16 and previous comparisons, which involved equilibrium bond distances, is the much larger variation among different models. This variation should not come as a surprise. Transition states represent a compromise situation in which some bonds are being broken while others are being formed, and the potential energy surface around the transition state would be expected to be flat, meaning that large changes in structure are expected to lead only to small changes in the energy. In terms of mean absolute deviations from the standard, all models give reasonable results, but the MP2/6-31G* model produced the best results and the two Hartree–Fock models fared the worst. In terms of individual comparisons, the largest deviations among different models correspond to making and breaking single bonds. In such situations, the potential energy surface is expected to be quite flat.

As discussed in Section 15.2.4, an experimental activation energy can be obtained from the temperature dependence of the measured reaction rate by way of the Arrhenius equation, Equation (15.15). This result first requires that a rate law be postulated [Equation (15.14)]. Association of the activation energy with the difference in energies between reactants and transition state (as obtained from quantum-chemical calculations) requires the further assumption that all reacting molecules pass through the transition state. In effect, this implies that all reactants have the same energy or that none of the reactants has energy in excess of that needed to reach the transition state. This is the essence of transition-state theory.

Concept

Activation energies for chemical reactions can be determined from calculations of the structures and energies of reactants and transition states.

TABLE 15.16 Key Bond Distances in Transition States for Organic Reactions (Å)

Reaction/Transition State	Bond Length	Hartree–Fock		B3LYP	MP2	
		3-21G	6-31G*	6-31G*	6-31G*	6-311+G**
	a	1.88	1.92	1.90	1.80	1.80
	b	1.29	1.26	1.29	1.31	1.30
	c	1.37	1.37	1.38	1.38	1.39
	d	2.14	2.27	2.31	2.20	2.22
	e	1.38	1.38	1.38	1.39	1.39
	f	1.39	1.39	1.40	1.41	1.41
	a	1.40	1.40	1.42	1.43	1.43
	b	1.37	1.38	1.39	1.39	1.39
	c	2.11	2.12	2.11	2.02	2.07
	d	1.40	1.40	1.41	1.41	1.41
	e	1.45	1.45	1.48	1.55	1.53
	f	1.35	1.36	1.32	1.25	1.25
	a	1.39	1.38	1.40	1.40	1.40
	b	1.37	1.37	1.38	1.38	1.38
	c	2.12	2.26	2.18	2.08	2.06
	d	1.23	1.22	1.24	1.25	1.24
	e	1.88	1.74	1.78	1.83	1.83
	f	1.40	1.43	1.42	1.41	1.41
Mean absolute deviation from MP2/6-311+G**		0.05	0.05	0.03	0.01	—

Absolute activation energies for a small series of organic reactions are provided in Table 15.17. As with transition-state structures, results from the practical models are compared with those of the standard, MP2/6-311+G**. Overall, the performance of Hartree–Fock models is very poor. In most cases, the activation energies are overestimated by large amounts. This is not surprising in view of previous comparisons involving homolytic bond dissociation energies (see Table 15.11), which were too small. The argument that might be given here is that a transition state is typically more tightly bound than the reactants, meaning that correlation effects will be greater. The B3LYP/6-31G* and MP2/6-31G* perform much better and lead to errors (relative to the standard) that are comparable to those previously noted for reaction energy comparisons.

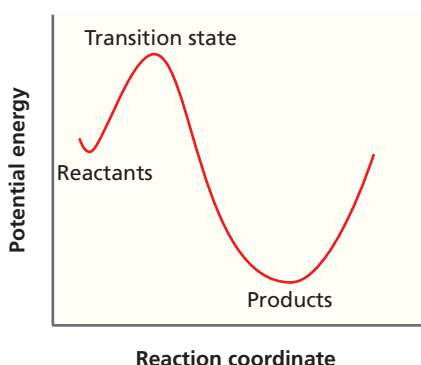


Figure 15.24
Generic potential energy surface in one dimension. The potential energy surface for a reaction is typically represented by a one-dimensional representation of the energy as a function of the reaction coordinate.

15.8.11 Finding a Transition State

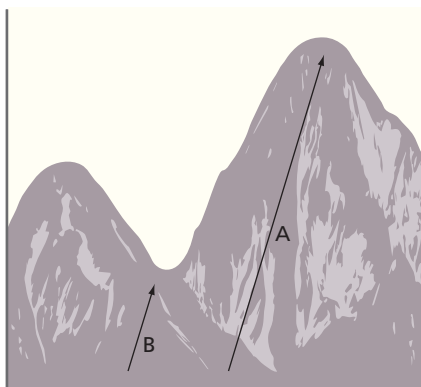
The usual picture of a chemical reaction in terms of a one-dimensional potential energy (or reaction coordinate) diagram is shown in Figure 15.24. The vertical axis corresponds to the energy of the system, and the horizontal axis (reaction coordinate) corresponds to the structure of the system. The starting point on the diagram (reactants) is an energy minimum, as is the ending point (products). Motion along the reaction coordinate is assumed to be continuous and to pass through a single-energy maximum called the transition state. As described in Section 15.2.1, a transition state on a real many-dimensional potential energy surface corresponds to a point that is actually an energy minimum in all but one dimension and an energy maximum along the reaction coordinate. The obvious analogy is to the crossing of a mountain range, the goal of which is simply to get from one side of the range to the other side with minimal effort.

TABLE 15.17 Absolute Activation Energies for Organic Reactions (kJ/mol)

Reaction	Hartree–Fock 3-21G	B3LYP 6-31G*	MP2 6-31G*	MP2 6-311+G**	Experiment
$\text{CH}_3\text{NC} \longrightarrow \text{CH}_3\text{CN}$	238	192	172	180	172
$\text{HCO}_2\text{CH}_2\text{CH}_3 \longrightarrow \text{HCO}_2\text{H} + \text{C}_2\text{H}_4$	259	293	222	251	234
	192	238	142	117	109
	176	205	121	109	105
	126	167	84	50	38
	314	356	243	251	230
$\text{HCNO} + \text{C}_2\text{H}_2 \longrightarrow \text{2-methylfuran}$	105	146	50	33	38
	230	247	163	159	142
	176	197	151	155	142
	247	251	167	184	172
	205	205	92	105	92
Mean absolute deviation from MP2/6-311+G**	71	100	17	13	—

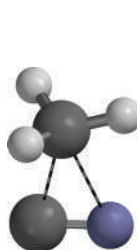
Crossing over the top of a “mountain” (pathway A), which corresponds to crossing through an energy maximum on a (two-dimensional) potential energy surface, accomplishes the goal, as shown in Figure 15.25. However, it is not likely to be the chosen pathway. This is because less effort (energy) will be expended by going through a “pass” between two “mountains” (pathway B), a maximum in one dimension but a minimum in the other dimension. This is referred to as a saddle point and corresponds to a transition state.

A single molecule may have many transition states (some corresponding to real chemical reactions and others not), and merely finding a transition state does not guarantee that it is *the* transition state, implying that it is at the top of the lowest energy pathway that smoothly connects reactants and products. Although it is possible to verify the smooth connection of reactants and products, it will generally not be possible to know with complete certainty that what has been identified as the transition state is in fact the lowest energy structure over which the reaction might proceed, or whether in fact the actual reaction proceeds over a transition state that is not the lowest energy structure.

**Figure 15.25**

A reaction in two dimensions is analogous to crossing a mountain range.

Pathway A, which crosses over the top of a mountain, requires more effort to traverse than pathway B, which crosses through a pass between two mountains.

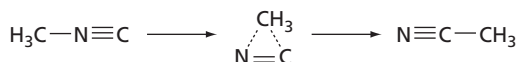
**Figure 15.26**

Calculated transition state for the isomerization of methyl isocyanide to acetonitrile. The calculated transition state is consistent with a three-membered ring in the reaction scheme shown.

**Figure 15.27**

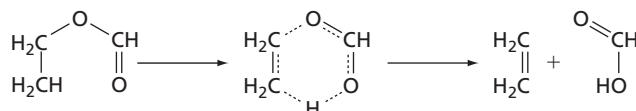
Calculated transition state in the pyrolysis of ethyl formate. The calculated transition state is consistent with a six-membered ring in the reaction scheme shown.

The fact that transition states, as with the reactants and products of a chemical reaction, correspond to well-defined structures indicates that they can be fully characterized from calculation. However, this is one area where the results of calculation cannot be tested, except with reference to chemical intuition. For example, it is reasonable to expect that the transition state for the unimolecular isomerization of methyl isocyanide to acetonitrile takes the form of a three-membered ring,



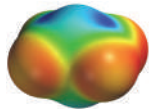
in accord with the structure actually calculated, which is shown in Figure 15.26.

It is also reasonable to expect that the transition state for pyrolysis of ethyl formate leading to formic acid and ethylene will take the form of a six-membered ring:



This expectation agrees with the result of the calculation, as shown in Figure 15.27.

15.9 GRAPHICAL MODELS

**Problems P15.23–P15.25**

In addition to numerical quantities (bond lengths and angles, energies, dipole moments, and so on), quantum-chemical calculations furnish a wealth of information that is best displayed in the form of images. Among the results of calculations that have proven to be of value are the molecular orbitals themselves, the electron density, and the electrostatic potential. These can all be expressed as three-dimensional functions of the coordinates. One way to display them on a two-dimensional video screen (or on a printed page) is to define a surface of constant value, a so-called isosurface or, more simply, an isosurface:

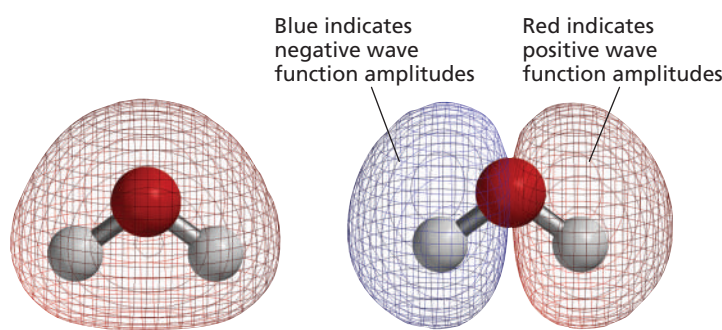
$$f(x, y, z) = \text{constant} \quad (15.76)$$

The value of the constant may be chosen to reflect a particular physical observable of interest, such as the “size” of a molecule in the case of display of electron density.

15.9.1 Molecular Orbitals

As discussed in detail in Section 15.3, molecular orbitals, ψ , are written in terms of linear combinations of basis functions, ϕ , which are centered on the individual nuclei:

$$\psi_i = \sum_{\mu}^{\text{basis functions}} c_{\mu i} \phi_{\mu} \quad (15.21)$$

**Figure 15.28**

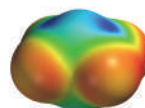
Molecular orbitals that can be identified with the O—H bonds in water. In this and subsequent diagrams, the color scheme for atoms follows that outlined in Figure 13.2. The red surface indicates positive wave function amplitudes, and the blue surface indicates negative wave function amplitudes. For a more detailed discussion of these MOs, see Section 13.5.

Although it is tempting to associate a molecular orbital with a particular bond, this is generally inappropriate. Molecular orbitals are generally delocalized over the entire molecule, whereas bonds are normally associated with a pair of atoms. Also, molecular orbitals, unlike bonds, display the symmetry of the molecule. For example, the equivalence of the two OH bonds in water is revealed by the two molecular orbitals best describing OH bonding as shown in Figure 15.28.

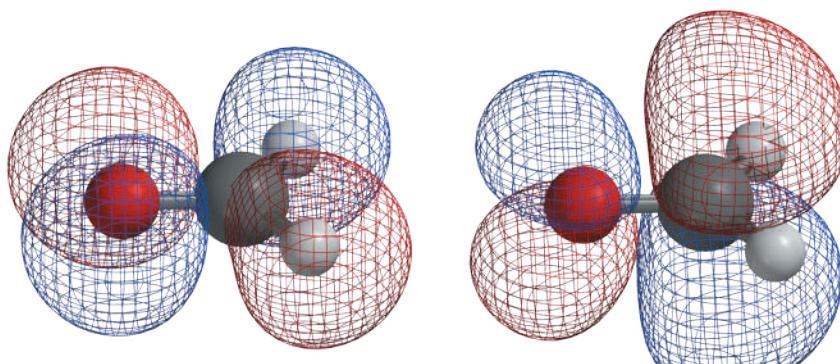
Molecular orbitals, in particular, the highest energy occupied molecular orbital (the HOMO) and the lowest energy unoccupied molecular orbital (the LUMO), are often quite familiar to chemists. The former holds the highest energy (most available) electrons and should be subject to attack by electrophiles, whereas the latter provides the lowest energy space for additional electrons and should be subject to attack by nucleophiles. For example, the HOMO in formaldehyde is in the heavy-atom plane of the molecule, indicating that attack by an electrophile, such as a proton, will occur here, as shown in Figure 15.29, whereas the LUMO is out of plane on the carbonyl carbon, consistent with the known nucleophilic chemistry.

15.9.2 Orbital Symmetry Control of Chemical Reactions

In the 1960s, Woodward and Hoffmann, building on the earlier ideas of Fukui, first clearly pointed out how the symmetries of the HOMO and LUMO (together referred to as the **frontier molecular orbitals**) could be used to rationalize why some chemical reactions proceed easily whereas others do not. For example, the fact that the HOMO in *cis*-1,3-butadiene is able to interact favorably with the LUMO in ethene suggests that the two molecules should readily combine in a concerted manner to form cyclohexene in a process called Diels–Alder cycloaddition. This process is depicted in Figure 15.30. On the other hand, interaction between the HOMO on one ethene and the LUMO on another ethene is not favorable, as illustrated in Figure 15.31, and concerted addition to form cyclobutane would not be expected. Reactions that are allowed or forbidden because of orbital symmetry have been collected under what is now known as the Woodward–Hoffmann rules. For their work, Hoffmann and Fukui shared the Nobel Prize in chemistry in 1981.



Problems P15.26–P15.31



(a) The highest energy occupied molecular orbital (HOMO)-electrophilic attack most likely.

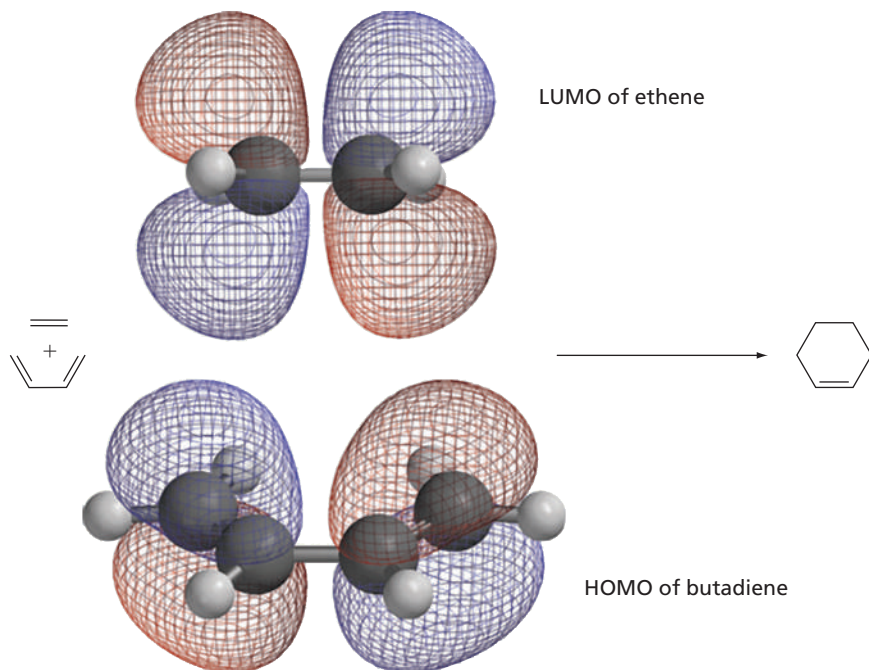
(b) The lowest energy unoccupied molecular orbital (LUMO)-nucleophilic attack most likely.

Figure 15.29

The highest energy occupied molecular orbital (HOMO) and the lowest energy unoccupied molecular orbital (LUMO) for formaldehyde. The HOMO (a) and LUMO (b) identify regions where electrophilic and nucleophilic attack, respectively, are likely to occur.

Figure 15.30

Cyclohexene formation via the Diels–Alder cycloaddition process. The HOMO of butadiene (bottom) is able to interact with the LUMO of ethene (top), resulting in cycloaddition, in agreement with experiment.



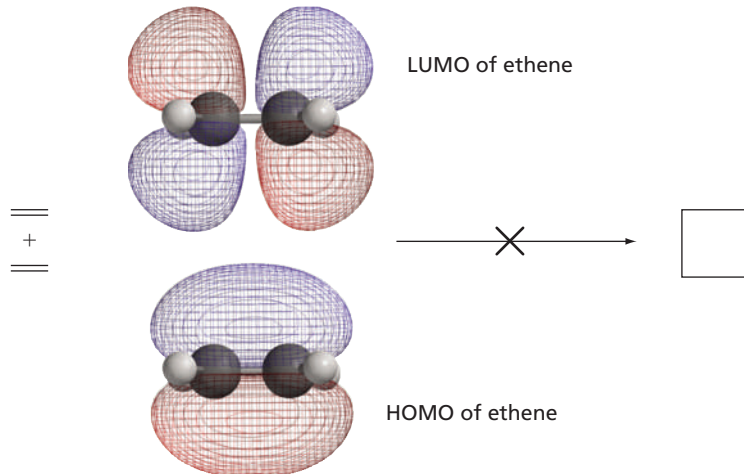
15.9.3 Electron Density

Electron density, $\rho(\mathbf{r})$, is a function of the coordinates \mathbf{r} , defined such that $\rho(\mathbf{r}) d\mathbf{r}$ is the number of electrons inside a small volume $d\mathbf{r}$. X-ray diffraction experiments measure electron density. Electron density $\rho(\mathbf{r})$ is written in terms of a sum of products of basis functions, ϕ_μ :

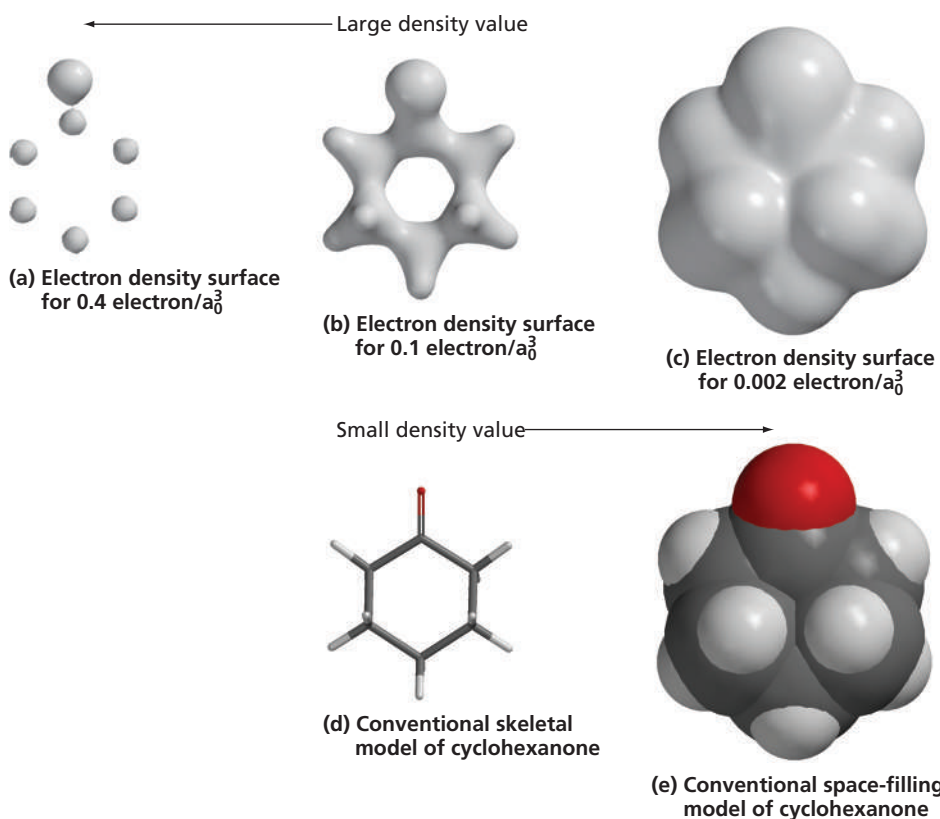
$$\rho(\mathbf{r}) = \sum_{\mu}^{\text{basis functions}} \sum_{v} P_{\mu v} \phi_{\mu}(\mathbf{r}) \phi_v(\mathbf{r}) \quad (15.77)$$

where $P_{\mu v}$ are elements of the density matrix [Equation (15.27)]. Electron density can be portrayed in terms of a surface (an **electron density surface**) with the size and shape of the surface being given by the value of density, such as in cyclohexanone in Figure 15.32.

Depending on the particular density value, isodensity surfaces can serve to locate atoms (Figure 15.32a), to delineate chemical bonds (Figure 15.32b), or to indicate overall molecular size and shape (Figure 15.32c). The regions of highest electron density surround the heavy (nonhydrogen) atoms in a molecule. This is the basis of X-ray crystallography, which locates atoms by identifying regions of high electron density.

**Figure 15.31**

The HOMO of ethene (bottom) is not able to interact with the corresponding LUMO (top). This inability to interact suggests that cycloaddition is not likely to occur, in agreement with experiment.

**Figure 15.32**

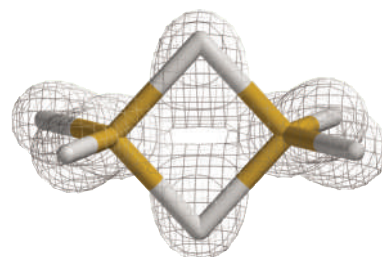
Electron density surfaces for cyclohexanone. These surfaces correspond to three different values of the electron density: (a) 0.4 electron/ a_0^3 , (b) 0.1 electrons/ a_0^3 , and (c) 0.002 electrons/ a_0^3 . The isodensity surfaces in the top row can serve to locate atoms (a), to delineate chemical bonds (b), or to indicate overall molecular size and shape (c). Conventional (d) skeletal and (e) space-filling models appear below the two electron density surfaces with the smallest values.

Also interesting are regions of lower electron density. For example, a 0.1 electrons/ a_0^3 isodensity surface for cyclohexanone conveys essentially the same information as a conventional skeletal structure model (compare images in b and d in Figure 15.32); that is, it depicts the locations of bonds. A surface of 0.002 electrons/ a_0^3 provides a good fit to conventional space-filling models and, hence, serves to portray overall molecular size and shape (compare images in c and e in Figure 15.32). As is the case with the space-filling model, this definition of molecular size is completely arbitrary (except that it closely matches experimental data on how closely atoms fit together in crystalline solids). A single parameter, namely, the value of the electron density at the surface, has replaced the set of atomic radii used for space-filling models. These latter two electron density surfaces are examined in more detail in the following section.

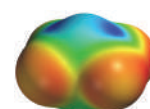
15.9.4 Where Are the Bonds in a Molecule?

An electron density surface can be employed to reveal the location of bonds in a molecule. Of course, chemists routinely employ a variety of tactics to depict chemical bonding, ranging from pencil sketches (Lewis structures) to physical models such as the familiar ball-and-stick models available in kits. The most important advantage of electron density surfaces is that they can be applied to elucidate bonding and not only to portray bonding in cases where the location of bonds is known. For example, the electron density surface for diborane, B_2H_6 , (Figure 15.33) clearly shows a molecule with very little electron density concentrated between the two boron atoms. This fact suggests that the appropriate Lewis structure of the two shown in Figure 15.34 is the one that lacks a boron–boron bond, rather than the one that shows the two borons directly bonded.

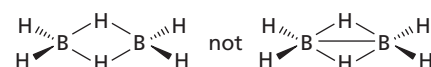
Another important application of electron density surfaces is to the description of the bonding in transition states. An example is the pyrolysis of ethyl formate, leading to formic acid and ethylene, which is illustrated in Figure 15.35. The electron density surface offers clear evidence of a **late transition state**, meaning that the CO bond is nearly fully cleaved and the migrating hydrogen is more tightly bound to oxygen (as in the product) than to carbon (as in the reactant).

**Figure 15.33**

An electron density surface for diborane. The image shows that there is no boron–boron bond.



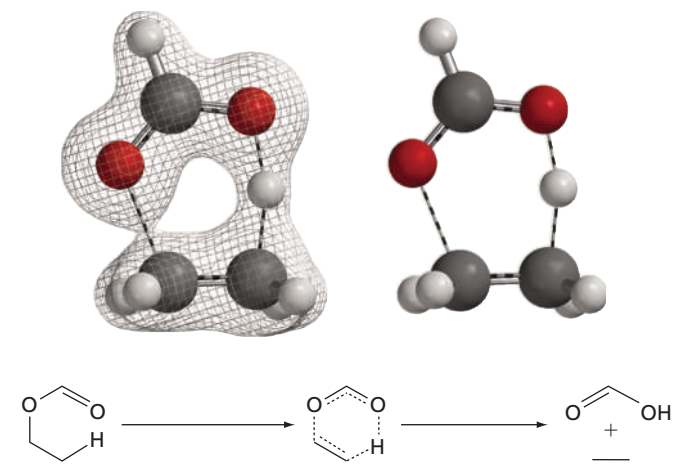
Problem P15.32

**Figure 15.34**

Two possible Lewis structures of diborane. These structures differ in that only one has a boron–boron bond.

Figure 15.35

An electron density structure for the transition state in the pyrolysis of ethyl formate. The images in the top row show a six-membered ring consistent with the conventional Lewis picture. The reaction scheme is shown in the bottom row.

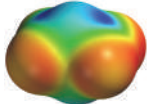


15.9.5 How Big Is a Molecule?

The size of a molecule can be defined according to the amount of space that it occupies in a liquid or solid. The so-called space-filling or CPK model has been formulated to portray molecular size, based on fitting experimental data to a set of atomic radii (one for each atom type). Although this simple model is remarkably satisfactory overall, some problematic cases do arise, in particular for atoms that may adopt different oxidation states, such as Fe^0 in $\text{Fe}(\text{CO})_5$ compared with Fe^{II} in FeCl_4^{2-} .

Because the electrons—not the underlying nuclei—dictate overall molecular size, electron density provides an alternate measure of how much space molecules actually occupy. Unlike space-filling models, electron density surfaces respond to changes in the chemical environment and allow atoms to adjust their sizes in response to different environments. An extreme example concerns the size of hydrogen in main-group hydrides.

As seen in Figure 15.36, electron density surfaces reveal that the hydrogen in lithium hydride is much larger than that in hydrogen fluoride, consistent with the fact that the former serves as a base (hydride donor), whereas the latter serves as an acid (proton donor). Hydrogen sizes in beryllium hydride, borane, methane, ammonia, and water are intermediate and parallel the ordering of the electronegativities of the heavy atom.

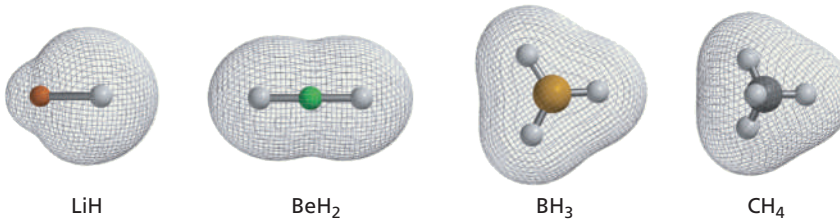


Problems P15.33–P15.34

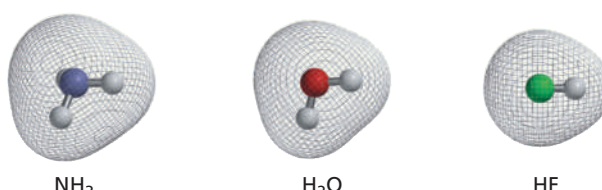
15.9.6 Electrostatic Potential

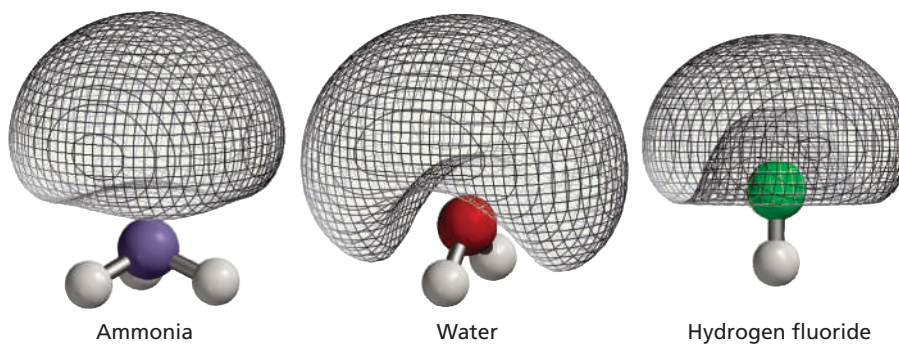
Electrostatic potential, ε_p , is defined as the energy of interaction of a positive point charge located at p with the nuclei and electrons of a molecule:

$$\varepsilon_p = \sum_A \frac{Z_A e^2}{4\pi\varepsilon_0 R_{Ap}} - \frac{e^2}{4\pi\varepsilon_0} \sum_{\mu}^{\text{basis functions}} \sum_{\nu}^{} P_{\mu\nu} \int \frac{\phi_{\mu}(\mathbf{r})\phi_{\nu}(\mathbf{r})}{r_p} d\mathbf{r} \quad (15.74)$$

**Figure 15.36**

Electron density surfaces for hydrides of lithium to fluorine.



**Figure 15.37**

Electrostatic potential surfaces for ammonia, water, and hydrogen fluoride. These types of images are useful for depicting lone pairs.

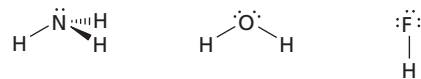
Notice that electrostatic potential represents a balance between repulsion of the point charge by the nuclei (first summation) and attraction of the point charge by the electrons (second summation). $P_{\mu\nu}$ are elements of the density matrix [see Equation (15.27)], and the ϕ are atomic basis functions.

15.9.7 Visualizing Lone Pairs

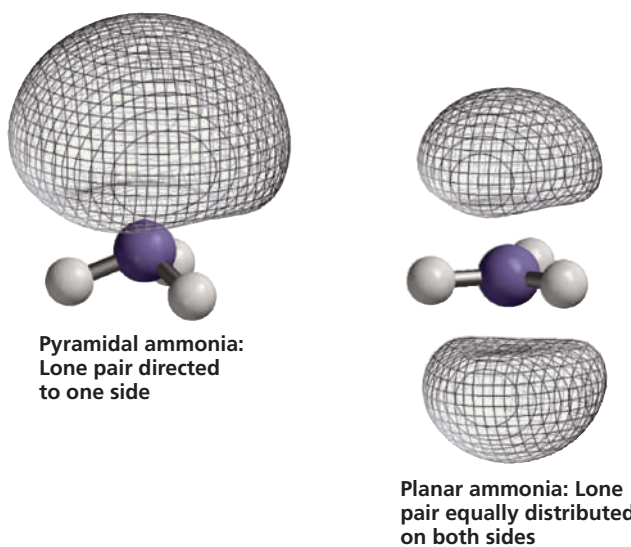
The octet rule dictates that each main-group atom in a molecule will be surrounded by eight valence electrons. These electrons can either be involved in bonds (two electrons for a single bond, four electrons for a double bond, six electrons for a triple bond), or they can remain with the atom as a nonbonded or lone pair of electrons. Although one cannot actually see bonds, you can see their consequence on the atoms to which bonds are made. On this basis, lone pairs would seem to be completely invisible because there are no telltale atoms. However, the fact that the electrons in lone pairs should be highly accessible suggests another avenue. Regions of space around a molecule where the potential is negative suggest an excess of electrons. To the extent that lone pairs represent electron-rich environments, they should be revealed by electrostatic potential surfaces. A good example is provided by negative electrostatic potential surfaces for ammonia, water, and hydrogen fluoride, as shown in Figure 15.37.

The electron-rich region in ammonia is in the shape of a lobe pointing in the fourth tetrahedral direction, whereas that in water takes the form of a crescent occupying two tetrahedral sites. At first glance, the electrostatic potential surface for hydrogen fluoride is nearly identical to that in ammonia. Closer inspection reveals that rather than pointing away from the fluorine (as it points away from ammonia), the surface encloses the atom. All in all, these three surfaces are entirely consistent with conventional Lewis structures for the three hydrides shown in Figure 15.38.

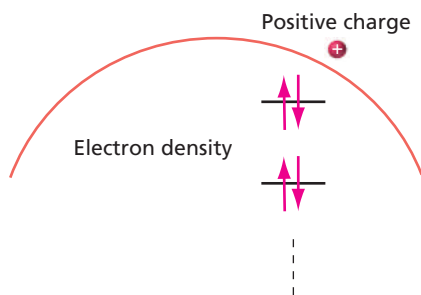
A related comparison between electrostatic potential surfaces for ammonia in both the observed pyramidal and unstable trigonal planar structures is shown in Figure 15.39.

**Figure 15.38**

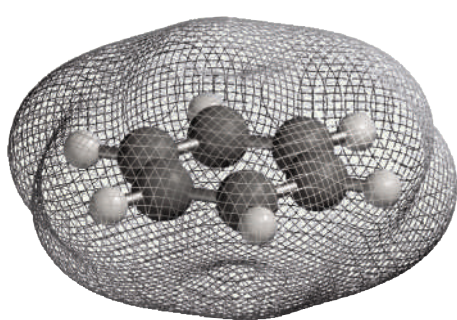
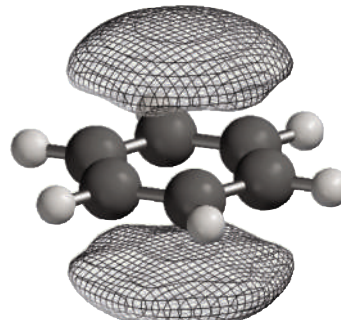
Lewis structures for ammonia, water, and hydrogen fluoride.

**Figure 15.39**

Electrostatic potential surfaces comparing pyramidal and planar ammonia. The images show that the lone pair of electrons is directed to one side of pyramidal ammonia but is equally distributed on both sides of planar ammonia.

**Figure 15.40**

Depiction of an electrostatic potential map. An electrostatic potential map shows the value of the electrostatic potential at all locations on a surface of electron density (corresponding to overall size and shape).

**(a) Density surface****(b) Negative electrostatic potential surface****Figure 15.41**

Two graphic depictions of benzene. The diagrams show (a) an electron density surface and (b) a negative electrostatic potential surface for benzene.

As previously mentioned, the former depicts a lobe pointing in the fourth tetrahedral direction, and the electrostatic potential surface for the planar trigonal arrangement shows two equal out-of-plane lobes. This is, of course, consistent with the fact that pyramidal ammonia has a dipole moment (with the negative end pointing in the direction of the lone pair), whereas planar ammonia does not have a dipole moment.

15.9.8 Electrostatic Potential Maps

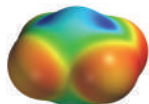
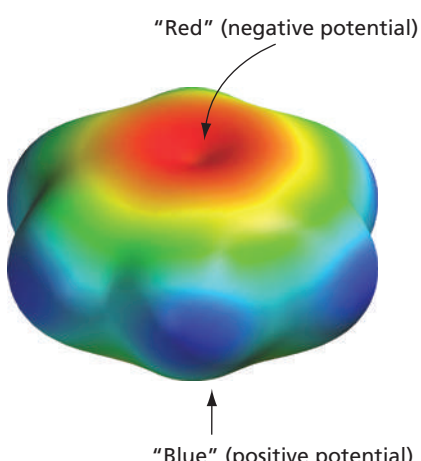
Graphical models need not be restricted to portraying a single quantity. Additional information can be presented in terms of a property map on top of an isosurface, where different colors can be used to portray different property values. Most common are maps on electron density surfaces. Here the surface can be used to designate overall molecular size and shape, and colors can be used to represent the value of some property at various locations on the surface. The most commonly used property map is the **electrostatic potential map**, schematically depicted in Figure 15.40. This gives the value of the electrostatic potential at locations on a particular surface, most commonly a surface of electron density corresponding to overall molecular size.

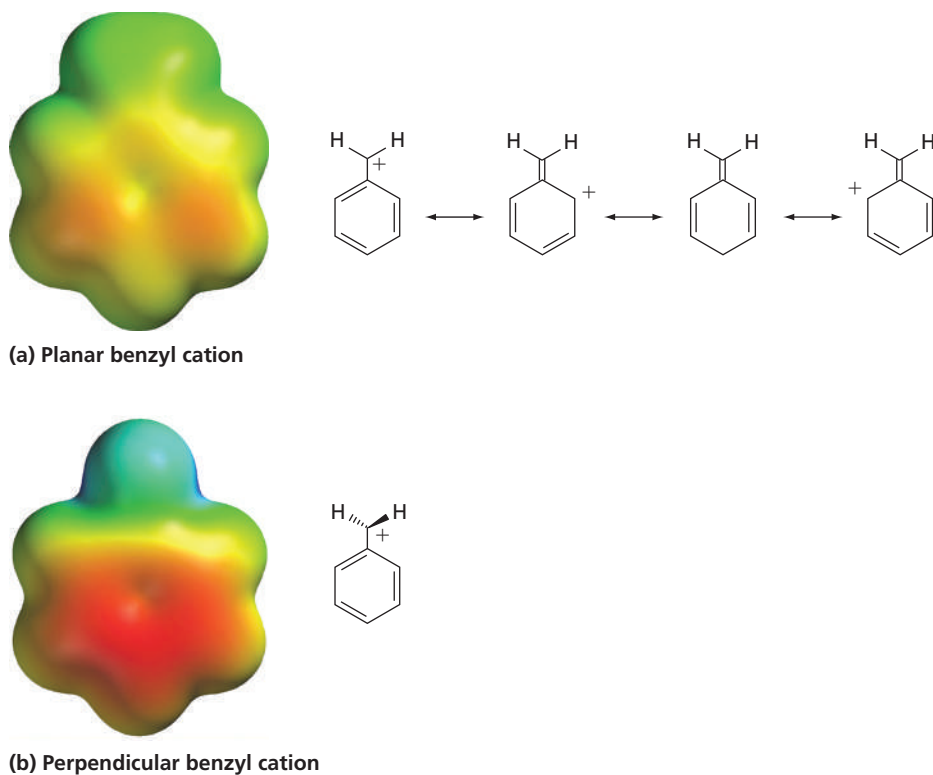
To see how an electrostatic potential map (and by implication any property map) is constructed, first consider both a density surface and a particular (negative) electrostatic potential surface for benzene, as shown in Figure 15.41. Both of these surfaces convey structure. The density surface reveals the size and shape of benzene, and the negative electrostatic potential surface delineates in which regions surrounding benzene a particular (negative) electrostatic potential will be felt.

Next, consider making a map of the value of the electrostatic potential on the density surface (an electrostatic potential map), using colors to designate values of the potential. This leaves the density surface unchanged (insofar as it represents the size and shape of benzene), but replaces the gray-scale image (conveying only structural information) with a color image (conveying the value of the electrostatic potential *in addition to* structure). An electrostatic map for benzene is presented in Figure 15.42. Red represents large negative values of potential, whereas blue represents large positive values. Orange, yellow, and green represent intermediate values of the potential. Note that the π system is red, consistent with the (negative) potential surface previously shown.

Electrostatic potential maps are used for myriad purposes other than rapidly conveying which regions of a molecule are likely to be electron rich and which are likely to be electron poor. For example, they can be used to distinguish between molecules in which charge is localized from those where it is delocalized.

Compare the electrostatic potential maps in Figure 15.43 for the planar (top) and perpendicular (bottom) structures of the benzyl cation. The latter reveals a heavy concentration of positive charge (blue color) on the benzylic carbon and perpendicular to the plane of the ring. This is consistent with the notion that only a single Lewis

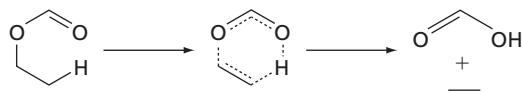
**Problem P15.35****Figure 15.42**
An electrostatic potential map of benzene.

**Figure 15.43**

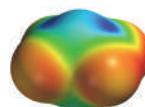
An electrostatic potential map for the benzyl cation. (a) The planar benzyl cation shows delocalization of positive charge, whereas in (b) the perpendicular benzyl cation shows charge localization. Note that in (a) multiple Lewis structures can be drawn to represent the structure, whereas in (b) only one Lewis structure is possible.

structure can be drawn. Planar benzyl cation, however, shows no such buildup of positive charge on the benzylic carbon, but rather delocalization onto *ortho* and *para* ring carbons, consistent with the fact that several Lewis structures can be drawn.

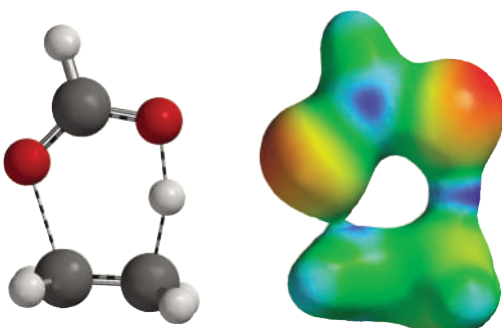
Electrostatic potential maps can also be employed to characterize transition states in chemical reactions. A good example is pyrolysis of ethyl formate (leading to formic acid and ethylene):



Here, the electrostatic potential map shown in Figure 15.44 (based on an electron density surface appropriate to identify bonds) clearly shows that the hydrogen atom being transferred (from carbon to oxygen) is positively charged; that is, it is an electrophile.



Problems P15.36–P15.37

**Figure 15.44**

An electrostatic potential map is useful in depicting the charge distribution in the transition state for the pyrolysis of ethyl formate.

15.10 CONCLUSION

Quantum-chemical calculations are rapidly becoming a viable alternative to experiments as a means to investigate chemistry. Continuing rapid advances in computer hardware and software technology will only further this trend and lead to even wider adoption among mainstream chemists. Calculations are already able to properly account for molecular structure and energetics, among other important quantities. Perhaps most intriguing is the ability of the calculations to deal with highly reactive molecules, which may be difficult to synthesize, and with reaction transition states, which cannot be observed at all. In this regard, calculations open up entirely new avenues for chemical research.

Quantum-chemical calculations do have limitations. Most conspicuous of these is the trade-off between accuracy and cost. Practical-quantum chemical models do not always yield results that are sufficiently accurate to actually be of value, and models that are capable of yielding accurate results may not yet be practical for the system of interest. Second, a number of quantities important to chemists cannot yet be routinely and reliably obtained from calculations. The most important limitation, however, is that, for the most part, calculations apply strictly to isolated molecules (gas phase), whereas much if not most chemistry is carried out in solution. Practical models that take solvent into account are being developed and tested to determine their accuracy and limitations.

The prognosis is very bright. In the next 20 or so years (for the research or industry careers of the students now reading this book), chemists and allied scientists and engineers will have at their disposal a whole range of powerful tools for exploring and understanding chemistry, just as previous generations were given technologies such as the laser to exploit. It is all part of the natural evolution of the science.

VOCABULARY

activation energy	full configuration interaction	rate constant
Born–Oppenheimer approximation	Gaussian functions	reaction coordinate
CID method	Hartree–Fock approximation	reaction coordinate diagrams
CIS method	Hartree–Fock energy	reactive intermediates
conformer	Hartree–Fock equations	Roothaan–Hall equations
contracted functions	Hartree–Fock model	self-consistent-field (SCF) procedure
correlated models	homolytic bond dissociation	size consistent
correlation energy	kinetic product	single-electron promotions
density functional theory	kinetically-controlled reaction	Slater determinant
diffuse functions	late transition state	Slater-type orbitals
diffusion-controlled reactions	linear combination of atomic orbitals (LCAO) approximation	split-valence basis set
double-electron promotions	minimal basis set	STO-3G basis set
electron density surface	Møller–Plesset models	theoretical model
electronic Schrödinger equation	Mulliken population analysis	theoretical model chemistry
electrostatic potential	normal coordinates	thermodynamic product
electrostatic potential map	polarization functions	thermodynamically controlled
exothermic	potential energy surface	variational
frontier molecular orbitals	preexponential factor	
frozen core approximation		

KEY EQUATIONS

Equation	Significance of Equation	Equation Number
$\hat{H}^{el}\Psi^{el} = E^{el}\Psi^{el}$	Electronic Schrödinger equation	15.18
$\hat{H}^{el} = -\frac{\hbar^2}{2m_e} \sum_i \nabla_i^2 - \frac{e^2}{4\pi\epsilon_0} \sum_i \text{electrons nuclei} \frac{Z_A}{r_{iA}} + \frac{e^2}{4\pi\epsilon_0} \sum_j \text{electrons electrons} \sum_i \frac{1}{r_{ij}}$	Electronic Schrödinger equation	15.19
$\psi_i = \sum_{\mu} \text{basis functions} c_{\mu i} \phi_{\mu}$	Molecular orbitals are expanded in basis sets to facilitate calculations	15.21
$g_{ijk}(r) = N x^i y^j z^k e^{-\alpha r^2}$	Definition of Gaussian functions on which most practical basis sets are based	15.54
$\epsilon_p = \sum_A \frac{\text{nuclei } Z_A e^2}{4\pi\epsilon_0 R_{Ap}} - \frac{e^2}{4\pi\epsilon_0} \sum_{\mu} \text{basis functions} \sum_{\nu} P_{\mu\nu} \int \frac{\phi_{\mu}(\mathbf{r})\phi_{\nu}(\mathbf{r})}{r_p} d\mathbf{r}$	Definition of electrostatic potential	15.74

CONCEPTUAL PROBLEMS

Q15.1 Why is it not possible to determine by experimental methods the structure of a transition state on a potential energy surface?

Q15.2 What is a saddle point on a potential energy surface, and what can it correspond to if the potential energy surface describes a chemical reaction?

Q15.3 What is the Born–Oppenheimer approximation, and why is it justified?

Q15.4 What is the fundamental assumption made in the Hartree–Fock approximation?

Q15.5 Why are total energies calculated in the Hartree–Fock limit too large?

Q15.6 Define the term *correlation energy*.

Q15.7 Why are bond distances calculated in the Hartree–Fock limit systematically too small?

Q15.8 What does it mean to say that a theoretical model is variational?

Q15.9 Why are Gaussian basis sets more widely used in computational chemistry rather than Slater-type orbitals?

Q15.10 What is an advantage of using split valence basis sets?

Q15.11 What is an advantage of using polarization basis sets?

NUMERICAL PROBLEMS

P15.1 The assumption that the reaction mechanism in transforming from *gauche* to *anti* *n*-butane is a simple torsion is an oversimplification because other geometrical changes no doubt also occur during rotation around the carbon–carbon bond, such as changes in bond lengths and angles. Examine the energy profile for *n*-butane (“*n*-butane” on the precalculated Spartan file) and plot the change in distance of the central CC bond and CCC bond angle as a function of the torsion angle. Are the bond length and bond angle nearly identical or significantly different (>0.02 Å and $>2^\circ$) for the two equilibrium forms of *n*-butane? Are the two parameters nearly identical or significantly different between the *anti* form and either or both of the transition states? Explain your results.

P15.2 Ammonia provides a particularly simple example of the dependence of vibrational frequencies on the atomic masses and of the use of vibrational frequencies to distinguish between a stable molecule and a transition state. First examine the vibrational spectrum of pyramidal ammonia (“ammonia” on the pre-calculated Spartan file). Then answer the following questions.

a. How many vibrational frequencies are there? How does this number relate to the number of atoms? Are all frequencies

real numbers, or are one or more imaginary numbers? Describe the motion associated with each frequency and characterize each as being primarily bond stretching, angle bending, or a combination of the two. Is bond stretching or angle bending lower in energy? Do the stretching motions each involve a single NH bond, or do they involve combinations of two or three bonds?

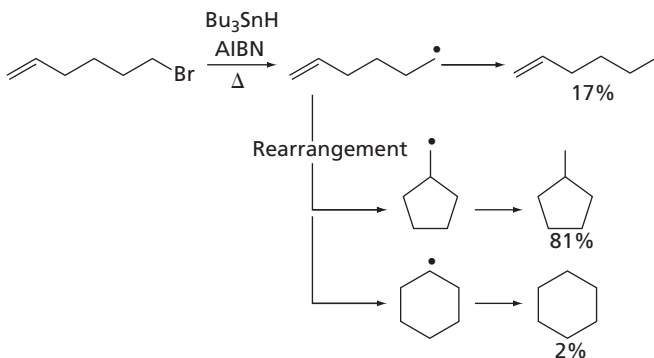
b. Next, consider changes to the vibrational frequencies of ammonia as a result of substituting deuterium atoms for hydrogen atoms (“perdeuteroammonia” on the pre-calculated Spartan file). Are the frequencies in ND_3 larger, smaller, or unchanged relative to those in NH_3 ? Are any changes greater for motions that are primarily bond stretching or motions that are primarily angle bending?

c. Finally, examine the vibrational spectrum of an ammonia molecule that has been constrained to a planar structure (“planar ammonia” on the Spartan download). Are all the frequencies real numbers? If not, describe the motions associated with any imaginary frequencies and relate them to the corresponding motion(s) in the pyramidal equilibrium form.

P15.3 The presence of the carbonyl group in a molecule is easily confirmed by an intense line in the infrared spectrum around 1700 cm^{-1} that corresponds to the $\text{C}=\text{O}$ stretching vibration. Locate this line in the calculated infrared spectrum of acetone (“acetone” on the precalculated Spartan file) and note its position in the overall spectrum (relative to the positions of the other lines) and the intensity of the absorption.

- Speculate why this line is a reliable diagnostic for carbonyl functionality.
- Examine the lowest frequency and then the highest frequency modes for acetone. Describe the associated atomic motion in each mode.

P15.4 Chemists recognize that the cyclohexyl radical is likely to be more stable than the cyclopentylmethyl radical, because they know that six-membered rings are more stable than five-membered rings and, more importantly, that secondary radicals are more stable than primary radicals. However, much important chemistry is not controlled by what is most stable (thermodynamics) but rather by what forms most readily (kinetics). For example, loss of bromine from 6-bromo-hexene leading initially to hex-5-enyl radical, results primarily in product from cyclopentylmethyl radical.



The two possible interpretations for the experimental result are that the reaction is thermochemically controlled but that our understanding of radical stability is wrong or, conversely, that the reaction is kinetically controlled.

- First, see if you can rule out the first possibility. Examine structures and total energies for cyclohexyl and cyclopentylmethyl radicals (“cyclohexyl and cyclopentylmethyl radicals” on the precalculated Spartan file). Which radical, cyclohexyl or cyclopentylmethyl, is more stable (lower in energy)? Is the energy difference large enough such that only the more stable radical is likely to be observed? (Recall that at room temperature an energy difference of 12 kJ/mol corresponds to a product ratio of >99:1.) Do you conclude that ring closure is under thermodynamic control?
- The next objective is to establish which ring closure, to cyclohexyl radical or to cyclopentylmethyl radical, is predicted; that is, which product, cyclohexane or methylcyclopentane, is the kinetic product? Examine structures and total energies for the transition states for the two ring closures (“to cyclohexyl and cyclopentylmethyl radicals” on the Spartan download). Which radical, cyclohexyl or cyclopentylmethyl, is lower in energy?

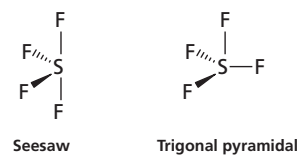
- Consider the following relationships between transition-state energy difference, ΔE^\ddagger , and the ratio of major to minor (kinetic) products, calculated from the Boltzmann distribution:

$\Delta E^\ddagger(\text{kJ/mol})$	Major : Minor (room temperature)
4	~90:10
8	~95:5
12	~99:1

What is the approximate ratio of products suggested by the calculations? How does this compare with what is observed? Do you conclude that ring closure is under kinetic control?

P15.5 Valence state electron pair repulsion (VSEPR) theory was formulated to anticipate the local geometry about an atom in a molecule (see discussion in Section 14.1). All that is required to predict the molecular structure is the number of electron pairs surrounding the atom, broken down into bonded pairs and nonbonded (lone) pairs. For example, the carbon in carbon tetrafluoride is surrounded by four electron pairs, all of them occupied in CF bonds, whereas the sulfur in sulfur tetrafluoride is surrounded by five electron pairs, four of which are occupied in SF bonds, with the fifth being a lone pair.

VSEPR theory is based on two simple rules. The first is that electron pairs (either lone pairs or bonds) will seek to avoid each other as much as possible. Thus, two electron pairs will lead to a linear structure, three pairs to a trigonal planar structure, four pairs to a tetrahedral structure, five pairs to a trigonal bipyramidal structure, and six pairs to an octahedral structure. Although this knowledge is sufficient to assign a structure for a molecule such as carbon tetrafluoride (tetrahedral), it is not sufficient to specify the structure of a molecule such as sulfur tetrafluoride. Does the lone pair assume an *equatorial* position on the trigonal bipyramidal leading to a seesaw structure, or an *axial* position leading to a trigonal pyramidal structure?



The second rule, that lone pairs occupy more space than bonds, clarifies the situation. The seesaw structure in which the lone pair is 90° to two of the SF bonds and 120° to the other two bonds is preferable to the trigonal pyramidal structure in which three bonds are 90° to the lone pair.

Although VSEPR theory is easy to apply, its results are strictly qualitative and often of limited value. For example, although the model tells us that sulfur tetrafluoride adopts a seesaw structure, it does not reveal whether the trigonal pyramidal structure (or any other structure) is an energy minimum, and if it is, what its energy is relative to the seesaw form. Also, it has little to say when more than six electron pairs are present. For example, VSEPR theory tells us that xenon hexafluoride is not octahedral, but it does not tell us what structure the molecule actually assumes. Hartree–Fock molecular orbital calculations provide an alternative.

- a. Optimize the structure of SF₄ in a seesaw structure (C_{2v} symmetry) using the HF/3-21G model and calculate vibrational frequencies (the infrared spectrum). This calculation is necessary to verify that the energy is at a minimum. Next, optimize the structure of SF₄ in a trigonal pyramidal structure and calculate its vibrational frequencies. Is the seesaw structure an energy minimum? What leads you to your conclusion?

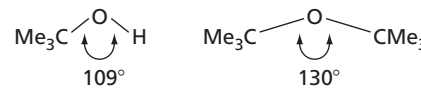
Is it lower in energy than the corresponding trigonal pyramidal structure in accordance with VSEPR theory? What is the energy difference between the two forms? Is it small enough that both might actually be observed at room temperature? Is the trigonal pyramidal structure an energy minimum?

- b. Optimize the atomic structure of XeF₆ in an octahedral structure (O_h symmetry) using the HF/3-21G model and calculate vibrational frequencies. Next, optimize XeF₆ in a structure that is distorted from octahedral (preferably a structure with C₁ symmetry) and calculate its vibrational frequencies. Is the octahedral form of XeF₆ an energy minimum? What leads you to your conclusion? Does distortion lead to a stable structure of lower energy?

P15.6 A description of the geometric structure of carbon in ethane, ethene, and acetylene is as follows: In ethane, each carbon is surrounded by four atoms in a roughly tetrahedral structure; in ethene, each carbon is surrounded by three atoms in a trigonal planar structure, and; in acetylene, each carbon is surrounded by two atoms in a linear structure. These structures can be rationalized by suggesting that the valence 2s and 2p orbitals of carbon are able to combine to produce four equivalent sp³ hybrids directed toward the four corners of a tetrahedron, or three equivalent sp² hybrids directed toward the corners of an equilateral triangle with a p orbital left over, or two equivalent sp hybrids directed along a line with two p orbitals “left over” and available for ethane, ethene, and acetylene, respectively. The 2p atomic orbitals extend farther from carbon than the 2s orbital. Therefore, sp³ hybrids will extend farther than sp² hybrids, which in turn will extend farther than sp hybrids. As a consequence, bonds made with sp³ hybrids should be longer than those made with sp² hybrids, which should in turn be longer than those made with sp hybrids. Considering this background information, answer the following questions;

- a. Obtain equilibrium structures for ethane, ethene, and acetylene using the HF/6-31G* model. Is the ordering in CH bond lengths what you expect on the basis of the hybridization arguments? Using the CH bond length in ethane as a standard, what is the percent reduction in CH bond lengths in ethene? In acetylene?
- b. Obtain equilibrium structures for cyclopropane, cyclobutane, cyclopentane, and cyclohexane using the HF/6-31G* model. Are the CH bond lengths in each of these molecules consistent with their incorporating sp³-hybridized carbons? Note any exceptions.
- c. Obtain equilibrium structures for propane, propene, and propyne using the HF/6-31G* model. Is the ordering of bond lengths the same as that observed for the CH bond lengths in ethane, ethene, and acetylene? Are the percent reductions in bond lengths from the standard (propane) similar ($\pm 10\%$) to those seen for ethene and acetylene (relative to ethane)?

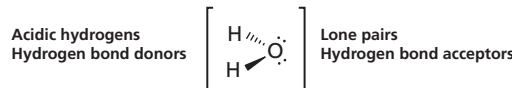
P15.7 The bond angle about oxygen in alcohols and ethers is typically quite close to tetrahedral (109.5°) but opens up significantly in response to extreme steric crowding, such as in comparing *tert*-butyl alcohol to di-*tert*-butyl ether:



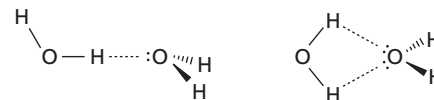
This is entirely consistent with the notion that although lone pairs occupy space, they can be “squeezed” to relieve crowding. Another way to relieve unfavorable steric interactions (without changing the position of the lone pairs) is to increase the CO bond distance.

- a. Build *tert*-butyl alcohol and di-*tert*-butyl ether and optimize the structure of each using the HF/6-31G* model. Are the calculated bond angles involving oxygen in accord with the values given earlier, in particular with regard to the observed increase in bond angle? Do you see any lengthening of the CO bond in the ether over that in the alcohol? If not, or if the effect is very small (<0.01 Å), speculate why not.
- b. Next, consider the analogous trimethylsilyl compounds Me₃SiOH and Me₃SiOSiMe₃. Calculate their equilibrium structures using the HF/6-31G* model. Point out any similarities and any differences between the calculated structures of these compounds and their *tert*-butyl analogues. In particular, do you see any widening of the bond angle involving oxygen in response to increased steric crowding? Do you see lengthening of the SiO bond in the ether over that of the alcohol? If not, rationalize what you do see.

P15.8 Water contains two acidic hydrogens that can act as hydrogen bond donors and two lone pairs that can act as hydrogen bond acceptors:



Given that all are tetrahedrally disposed around oxygen, this suggests two reasonable structures for the hydrogen-bonded dimer of water, (H₂O)₂, one with a single hydrogen bond and one with two hydrogen bonds:

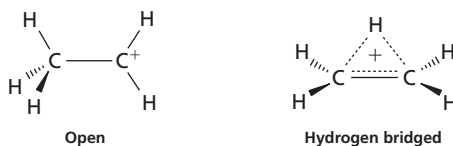


Whereas the second seems to make better use of the attributes of water, in doing so, it imposes geometrical restrictions on the dimer.

Build the two dimer structures. Take into account that the hydrogen bond distance (O · · · H) is typically on the order of 2 Å. Optimize the structure of each using the HF/6-31G* model and, following this, calculate vibrational frequencies.

Which structure, singly or doubly hydrogen bonded, is more stable? Is the other (higher-energy) structure also an energy minimum? Explain how you reached your conclusion. If the dimer with the single hydrogen bond is more stable, speculate what this has told you about the geometric requirements of hydrogen bonds. Based on your experience with water dimers, suggest a “structure” for liquid water.

P15.9 For many years, a controversy raged concerning the structures of so-called electron-deficient molecules, that is, molecules with insufficient electrons to make normal two-atom, two-electron bonds. Typical is the ethyl cation, C_2H_5^+ , formed from protonation of ethene.



Is the molecule best represented as an open Lewis structure with a full positive charge on one of the carbons, or as a hydrogen-bridged structure in which the charge is dispersed onto several atoms? Build both open and hydrogen-bridged structures for ethyl cation. Optimize the structure of each using the B3LYP/6-31G* model and calculate vibrational frequencies. Which structure is lower in energy, the open or hydrogen-bridged structure? Is the higher-energy structure an energy minimum? Explain your answer.

P15.10 One of the most powerful advantages of quantum-chemical calculations compared with experiments is their ability to deal with any molecular system, stable or unstable, real or imaginary. Consider as an example the legendary (but imaginary) kryptonite molecule. Its very name gives us a formula, KrO_2^- , and the fact that this species is isoelectronic with the known linear molecule, KrF_2 , suggests that it too should be linear.

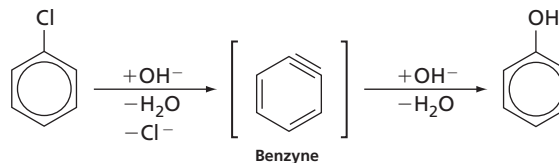
- Build KrF_2 as a linear molecule ($\text{F}—\text{Kr}—\text{F}$), optimize its structure using the HF/6-31G* model, and calculate vibrational frequencies. Is the calculated KrF bond distance close to the experimental value (1.89 \AA)? Does the molecule prefer to be linear, or does it want to bend? Explain how you reached this conclusion.
- Build KrO_2^- as a linear molecule (or as a bent molecule if the preceding analysis has shown that KrF_2 is not linear), optimize its structure using the HF/6-31G* model, and calculate vibrational frequencies. What is the structure of KrO_2^- ?

P15.11 Discussion of the VSEPR model in Section 14.1 suggested a number of incorrect structural predictions. Examples of such failures include applications to the structures of CaF_2 and SrCl_2 , which (according to the VSEPR model) should be linear but which are apparently bent. Other examples of such failure are SeF_6^{2-} and TeCl_6^{2-} , which should not be octahedral (according to the VSEPR model) but apparently are. Are these really failures of the model, or do the discrepancies lie with the fact that the experimental structures correspond to the solid rather than the gas phase (isolated molecules)?

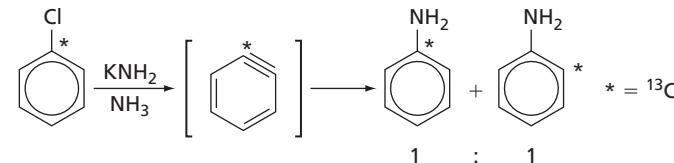
- Obtain equilibrium structures for linear CaF_2 and SrCl_2 and also calculate vibrational frequencies (infrared spectra). Use the HF/3-21G model, which has proven to be quite successful in describing the structures of main-group inorganic molecules. Are the linear structures for CaF_2 and SrCl_2 energy minima? Elaborate. If one or both are not, repeat your optimization starting with a bent structure.
- Obtain equilibrium structures for octahedral SeF_6^{2-} and TeCl_6^{2-} and also calculate vibrational frequencies. Use the HF/3-21G model. Are the octahedral structures for SeF_6^{2-}

and TeCl_6^{2-} energy minima? Elaborate. If one or both are not, repeat your optimization starting with distorted structures (preferably with C_1 symmetry).

P15.12 Benzyne has long been implicated as an intermediate in nucleophilic aromatic substitution, as shown in the following example:



Although the structure of benzyne has yet to be conclusively established, the results of a ^{13}C labeling experiment leave little doubt that two (adjacent) positions on the ring are equivalent:



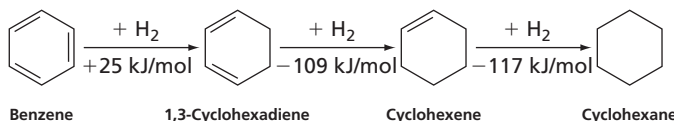
There is a report, albeit controversial, that benzyne has been trapped in a low-temperature matrix and its infrared spectrum recorded. Furthermore, a line in the spectrum at 2085 cm^{-1} has been assigned to the stretching mode of the incorporated triple bond.

Optimize the structure of benzyne using the HF/6-31G* model and calculate vibrational frequencies. For reference, perform the same calculations on 2-butyne. Locate the $\text{C}\equiv\text{C}$ stretching frequency in 2-butyne and determine an appropriate scaling factor to bring it into agreement with the corresponding experimental frequency (2240 cm^{-1}). Then, identify the vibration corresponding to the triple-bond stretch in benzyne and apply the same scaling factor to this frequency. Finally, plot the calculated infrared spectra of both benzyne and 2-butyne.

Does your calculated structure for benzyne incorporate a fully formed triple bond? Compare your answer with the bond in 2-butyne as a standard. Locate the vibrational motion in benzyne corresponding to the triple-bond stretch. Is the corresponding (scaled) frequency significantly different ($>100 \text{ cm}^{-1}$) from the frequency assigned in the experimental investigation? If it is, are you able to locate any frequencies from your calculation that would fit with the assignment of a benzyne mode at 2085 cm^{-1} ? Elaborate. Does the calculated infrared spectrum provide further evidence for or against the experimental observation? (Hint: Look at the intensity of the triple-bond stretch in 2-butyne.)

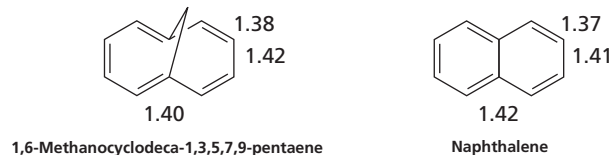
P15.13 All chemists know that benzene is unusually stable; that is, it is an aromatic compound. They are also well aware that many other similar molecules are stabilized by aromaticity to some extent and, more often than not, can recognize aromatic molecules as those with delocalized bonding. What most chemists are unable to do, however, is “put a number” on the aromatic stabilization afforded benzene or to quantify aromatic stabilization among different molecules. This is not to say that methods have not been proposed (for a discussion see Section 13.8), but rather that these methods have rarely been applied to real molecules.

Assigning a value to aromatic stabilization is actually quite straightforward. Consider a hypothetical reaction in which a molecule of hydrogen is added to benzene to yield 1,3-cyclohexadiene. Next, consider analogous hydrogenation reactions of 1,3-cyclohexadiene (leading to cyclohexene) and of cyclohexene (leading to cyclohexane):



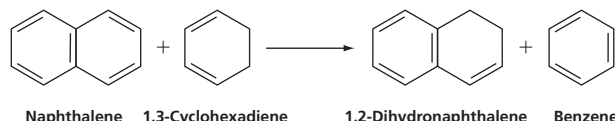
Addition of H₂ to benzene trades an H—H bond and a C—C π bond for two C—H bonds, but in so doing destroys the aromaticity. In contrast, H₂ addition to either 1,3-cyclohexadiene or cyclohexene trades the same bonds but does not result in any loss of aromaticity (there is nothing to lose). Therefore, the difference in the heats of hydrogenation (134 kJ/mol referenced to 1,3-cyclohexadiene and 142 kJ/mol referenced to cyclohexene) is a measure of the aromaticity of benzene.

Reliable quantitative comparisons require accurate experimental data (heats of formation). These will generally be available only for very simple molecules and will almost never be available for novel interesting compounds. As a case in point, consider to what extent, if any, the 10 π -electron molecule 1,6-methanocyclodeca-1,3,5,7,9-pentaene (“bridged naphthalene”) is stabilized by aromaticity. Evidence provided by the X-ray crystal structure suggests a fully delocalized π system. The 10 carbons that make up the base are very nearly coplanar, and all CC bonds are intermediate in length between normal single and double linkages, just as they are in naphthalene:



Calculations provide a viable alternative to experiment for thermochemical data. Although absolute hydrogenation energies may be difficult to describe with currently practical models, hydrogenation energies relative to a closely related standard compound are much easier to describe accurately. In this case, the natural standard is benzene.

- a. Optimize the structures of benzene, 1,3-cyclohexadiene, naphthalene, and 1,2-dihydronaphthalene using the HF/6-31G* model. Evaluate the energy of the following reaction, relating the energy of hydrogenation of naphthalene to that of benzene (as a standard):

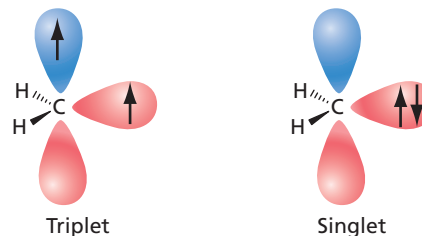


On the basis of relative hydrogenation energies, would you conclude that naphthalene is stabilized (by aromaticity) to about the same extent as is benzene or to a lesser or greater extent? Try to explain your result.

- b. Optimize the structures of 1,6-methanocyclodeca-1,3,5,7,9-pentaene and its hydrogenation product using the HF/6-31G* model. Evaluate the energy of hydrogenation relative to that of naphthalene. On the basis of relative hydrogenation energies, would you say that the bridged naphthalene is stabilized to about the same extent as is naphthalene or to a lesser or greater extent? Try to explain your result.

P15.14 Singlet and triplet carbenes exhibit different properties and show markedly different chemical behavior. For example, a singlet carbene will add to a *cis*-disubstituted alkene to produce only *cis*-disubstituted cyclopropane products (and to a *trans*-disubstituted alkene to produce only *trans*-disubstituted cyclopropane products), whereas a triplet carbene will add to produce a mixture of *cis* and *trans* products.

The origin of the difference lies in the fact that triplet carbenes are biradicals (or diradicals) and exhibit chemical behavior similar to that exhibited by radicals, whereas singlet carbenes incorporate both a nucleophilic site (a low-energy unfilled molecular orbital) and an electrophilic site (a high-energy filled molecular orbital); for example, for singlet and triplet methylene:

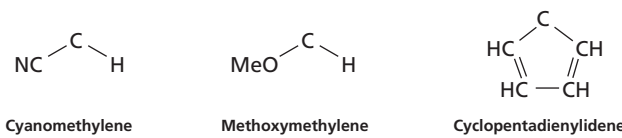


It should be possible to take advantage of what we know about stabilizing radical centers as opposed to stabilizing empty orbitals, and use that knowledge to design carbenes that will either be singlets or triplets. Additionally, it should be possible to state with confidence that a specific carbene of interest will either be a singlet or a triplet and, thus, to anticipate its chemical behavior.

The first step is to pick a model and then to establish the error in the calculated singlet–triplet energy separation in methylene where the triplet is known experimentally to be approximately 42 kJ/mol lower in energy than the singlet. This can then be applied as a correction for calculated singlet–triplet separations in other systems.

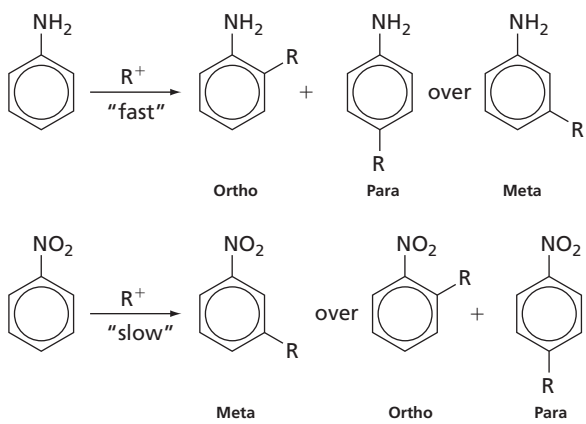
- a. Optimize the structures of both the singlet and triplet states of methylene using both Hartree–Fock and B3LYP density functional models with the 6-31G* basis set. Which state (singlet or triplet) is found to be lower energy according to the HF/6-31G* calculations? Is the singlet or the triplet unduly favored at this level of calculation? Rationalize your result. (*Hint:* Triplet methylene contains one fewer electron pair than singlet methylene.) What energy correction needs to be applied to calculated singlet–triplet energy separations? Which state (singlet or triplet) is found to be lower energy according to the B3LYP/6-31G* calculations? What energy correction needs to be applied to calculated energy separations?

- b. Proceed with either the HF/6-31G* or B3LYP/6-31G* model, depending on which leads to better agreement for the singlet–triplet energy separation in methylene. Optimize singlet and triplet states for cyanomethylene, methoxymethylene, and cyclopentadienylidene:

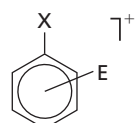


Apply the correction obtained in the previous step to estimate the singlet–triplet energy separation in each. For each of the three carbenes, assign the ground state as singlet or triplet. Relative to hydrogen (in methylene), has the cyano substituent in cyanomethylene and the methoxy substituent in methoxymethylene led to favoring of the singlet or the triplet? Rationalize your result by first characterizing cyano and methoxy substituents as π donors or π acceptors, and then speculating about how a donor or acceptor would stabilize or destabilize singlet and triplet methylene. Has incorporation into a cyclopentadienyl ring led to increased preference for a singlet or triplet ground state (relative to the preference in methylene)? Rationalize your result. (Hint: Count the number of π electrons associated with the rings in both singlet and triplet states.)

P15.15 Electron-donating groups on benzene promote electrophilic aromatic substitution and lead preferentially to so-called *ortho* and *para* products over *meta* products, whereas electron-withdrawing groups retard substitution and lead preferentially to *meta* products (over *ortho* and *para* products), such as for electrophilic alkylation:

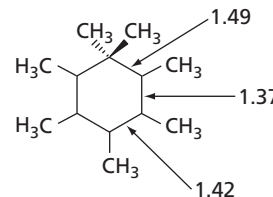


We can expect the first step in the substitution to be addition of the electrophile, leading to a positively charged adduct:



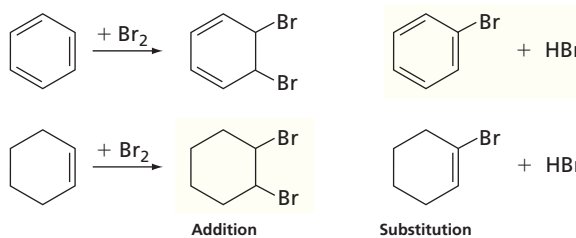
So-called benzenium ions have been characterized spectroscopically, and X-ray crystal structures for several are known. Will the stabilities of benzenium ion intermediates anticipate product distribution?

- a. Optimize the structures of benzene, aniline, and nitrobenzene using the HF/3-21G model. You will need their energies to ascertain the relative reactivities of the three substituted benzenes. Also, optimize the structure of the benzenium ion using the HF/3-21G model. A good guess is a planar six-membered ring containing five sp^2 carbons and an sp^3 carbon with bond distances between sp^2 carbons intermediate in length between those of single and double bonds. It should have C_{2v} symmetry. In terms of ring bond distances, how does your calculated structure compare with the experimental X-ray structure of heptamethylbenzenium ion?



- b. Optimize the structures of methyl cation adducts of benzene, aniline (*meta* and *para* isomers only), and nitrobenzene (*meta* and *para* isomers only) using the HF/3-21G model. Use the calculated structure of the parent benzenium ion as a template. Which isomer, *meta* or *para*, of the aniline adduct is more stable? Which isomer of the nitrobenzene adduct is more stable? Considering only the lower-energy isomer for each system, put the binding energies of methyl cation adducts of benzene, aniline, and nitrobenzene in order. That is, $E(\text{substituted benzene methyl cation adduct}) - E(\text{substituted benzene}) - E(\text{methyl cation})$. You will need to calculate the energy of the methyl cation using the HF/3-21G model. Which aromatic compound should be most reactive? Which should be least reactive? Taken as a whole, do your results provide support for the involvement of benzenium ion adducts in electrophilic aromatic substitution? Explain.

P15.16 Aromatic molecules such as benzene typically undergo substitution when reacted with an electrophile such as Br_2 , whereas alkenes such as cyclohexene most commonly undergo addition:



What is the reason for the change in preferred reaction in moving from the alkene to the arene? Use the Hartree–Fock 6-31G* model to obtain equilibrium structures and energies for reactants and products of both addition and substitution reactions of both cyclohexene and benzene (four reactions in total). Assume *trans* addition products (1,2-dibromocyclohexane and 5,6-dibromo-1,3-cyclohexadiene). Use your calculated

energies for the reactants and products to determine the change in energy in all four reactions. Is your result consistent with what is actually observed? Are all four reactions exothermic? If one or more are not exothermic, provide a rationale as to why.

P15.17 Evaluate the difference between change in energy at 0 K in the absence of zero point vibration and both change in enthalpy and in free energy for real molecules at 298 K. Consider both a unimolecular isomerization that does not lead to a net change in the number of molecules and a thermal decomposition reaction that leads to an increase in the number of molecules.

- a. Calculate ΔU , $\Delta H(298)$, and $\Delta G(298)$ for the following isomerization reaction:



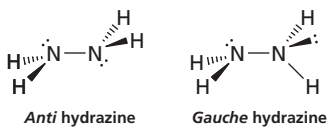
Obtain equilibrium structures for both methyl isocyanide and acetonitrile using the B3LYP/6-31G* density functional model. Do the calculated values for ΔU and ΔH (298) differ significantly (by more than 10%)? If so, is the difference due primarily to the temperature correction or to the inclusion of zero point energy (or to a combination of both)? Is the calculated value for ΔG (298) significantly different from that of ΔH (298)?

- b. Repeat your analysis (again using the B3LYP/6-31G* model) for the following pyrolysis reaction:



Do these two reactions provide a similar or a different picture as to the importance of relating experimental thermochemical data to calculated ΔG values rather than ΔU values? If different, explain your result.

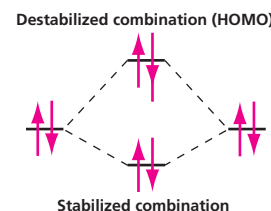
P15.18 Hydrazine would be expected to adopt a conformation in which the NH bonds stagger. There are two likely candidates, one with the lone pairs on nitrogen *anti* to each other and the other with the lone pairs *gauche*:



On the basis of the same arguments made in VSEPR theory (electron pairs take up more space than bonds) you might expect that *anti* hydrazine would be the preferred structure.

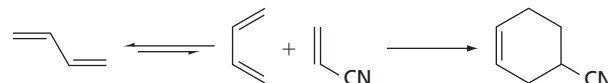
- a. Obtain energies for the *anti* and *gauche* conformers of hydrazine using the HF/6-31G* model. Which is the more stable conformer? Is your result in line with what you expect from VSEPR theory?

You can rationalize your result by recognizing that when electron pairs interact they form combinations, one of which is stabilized (relative to the original electron pairs) and one of which is destabilized. The extent of destabilization is greater than that of stabilization, implying that overall interaction of two electron pairs is unfavorable energetically:



- b. Measure the energy of the highest occupied molecular orbital (the HOMO) for each of the two hydrazine conformers. This corresponds to the higher-energy (destabilized) combination of electron pairs. Which hydrazine conformer (*anti* or *gauche*) has the higher HOMO energy? Is this also the higher-energy conformer? If so, is the difference in HOMO energies comparable to the difference in total energies between the conformers?

P15.19 Diels–Alder cycloaddition of 1,3-butadiene with acrylonitrile requires that the diene be in a *cis* (or *cis*-like) conformation:



In fact, 1,3-butadiene exists primarily in a *trans* conformation. In contrast, the *cis* conformer is approximately 9 kJ/mol less stable than, and separated from, the *trans* conformer by a low-energy barrier. At room temperature, only approximately 5% of butadiene molecules will be in a *cis* conformation. Clearly, rotation into a *cis* conformation is required before reaction can proceed.

Conduct a search for a substituted 1,3-butadiene that actually prefers to exist in a *cis* (or *cis*-like) conformation as opposed to a *trans* conformation. The only restriction you need to be aware of is that the diene needs to be electron rich in order to be reactive. Restrict your search to alkyl and alkoxy substituents as well as halogen. Use the HF/3-21G model. Report your successes and provide rationales.

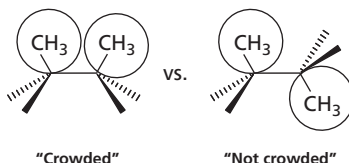
P15.20 The energy of rotation about a single bond is a periodic function of the torsion angle, ϕ , and is, therefore, appropriately described in terms of a truncated Fourier series, the simplest acceptable form of which is given by

$$\begin{aligned} V(\phi) &= \frac{1}{2}V_1(1 - \cos \phi) + \frac{1}{2}V_2(1 - \cos 2\phi) \\ &\quad + \frac{1}{2}V_3(1 - \cos 3\phi) \\ &= V_1(\phi) + V_2(\phi) + V_3(\phi) \end{aligned}$$

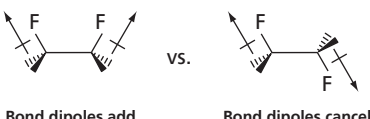
Here, V_1 is the onefold component (periodic in 360°), V_2 is the twofold component (periodic in 180°), and V_3 is the threefold component (periodic in 120°).

A Fourier series is an example of an orthogonal polynomial, meaning that the individual terms that comprise it are independent of each other. It should be possible, therefore, to dissect a complex rotational energy profile into a series of N -fold components and to interpret each of these components independent of all others. The one-fold component is quite

easy to rationalize. For example, the onefold term for rotation about the central bond in *n*-butane no doubt reflects the crowding of methyl groups,



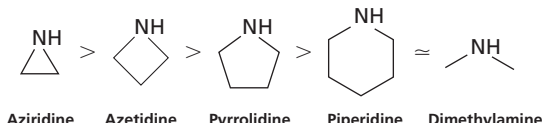
whereas the onefold term in 1,2-difluoroethane probably reflects differences in electrostatic interactions as represented by bond dipoles:



The threefold component represents the difference in energy between eclipsed and staggered arrangements about a single bond. However, the twofold component is perhaps the most interesting of the three and is what concerns us here. It relates to the difference in energy between planar and perpendicular arrangements.

Optimize the structure of dimethyl peroxide (CH_3OOCH_3) subject to the COOC dihedral angle being held at 0° , 20° , 40° , ..., 180° (10 optimizations in total). Use the B3LYP/6-31G* density functional model. Construct a plot of energy versus dihedral angle and fit this to a three-term Fourier series. Does the Fourier series provide a good fit to your data? If so, what is the dominant term? Rationalize it. What is the second most important term? Rationalize your result.

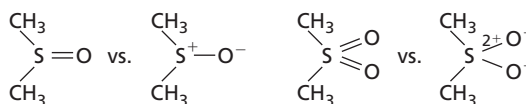
P15.21 Pyramidal inversion in the cyclic amine aziridine is significantly more difficult than inversion in an acyclic amine, such as requiring 80 kJ/mol compared with 23 kJ/mol in dimethylamine according to HF/6-31G* calculations. One plausible explanation is that the transition state for inversion needs to incorporate a planar trigonal nitrogen center, which is obviously more difficult to achieve in aziridine, for which one bond angle is constrained to a value of approximately 60° , than it is in dimethylamine. Such an interpretation suggests that the barriers to inversion in the corresponding four- and five-membered ring amines (azetidine and pyrrolidine) should also be larger than normal and that the inversion barrier in the six-membered ring amine (piperidine) should be quite close to that for the acyclic.



Optimize the structures of aziridine, azetidine, pyrrolidine, and piperidine using the HF/6-31G* model. Starting from these optimized structures, provide guesses at the respective inversion transition states by replacing the tetrahedral nitrogen center with a trigonal center. Obtain transition states using the same Hartree–Fock model and calculate inversion barriers. Calculate vibrational frequencies to verify that you have actually located the appropriate inversion transition states.

Do the calculated inversion barriers follow the order suggested in the preceding figure? If not, which molecule(s) appear to be anomalous? Rationalize your observations by considering other changes in structure from the amine to the transition state.

P15.22 Molecules such as dimethylsulfoxide and dimethylsulfone can either be represented as *hypervalent*, that is, with more than the normal complement of eight valence electrons around sulfur, or as *zwitterions*, in which sulfur bears a positive charge:



Atomic charges obtained from quantum-chemical calculations can help to decide which representation is more appropriate.

- Obtain equilibrium structures for dimethylsulfide, $(\text{CH}_3)_2\text{S}$, and dimethylsulfoxide using the HF/3-21G model and obtain charges at sulfur based on fits to the electrostatic potential. Is the charge on sulfur in dimethylsulfoxide about the same as that on sulfur in dimethylsulfide (normal sulfur), or has it increased by one unit, or is it somewhere between? Would you conclude that dimethylsulfoxide is best represented as a hypervalent molecule, as a zwitterion, or something between? See if you can support your conclusion with other evidence (structures, dipole moments, and so on).
- Repeat your analysis for dimethylsulfone. Compare your results for the charge at sulfur to those for dimethylsulfide and dimethylsulfoxide.

P15.23 Hydroxymethylene has never been observed, although it is believed to be an intermediate both in (1) the photofragmentation of formaldehyde to hydrogen and to carbon monoxide,



and in (2) the photodimerization of formaldehyde in an argon matrix:



Does hydroxymethylene actually exist? To have a chance “at life,” it must be separated from both its rearrangement product (formaldehyde) and its dissociation product (hydrogen and carbon monoxide) by a sizable energy barrier (>80 kJ/mol). Of course, it must also actually be a minimum on the potential energy surface.

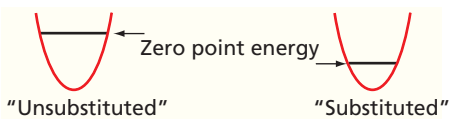
- First, calculate the energy difference between formaldehyde and hydroxymethylene and compare your result to the indirect experimental estimate of 230 kJ/mol. Try two different models, B3LYP/6-31G* and MP2/6-31G*. Following calculation of the equilibrium structure for hydroxymethylene, obtain vibrational frequencies. Is hydroxymethylene an energy minimum? How do you know? Is the energy difference inferred from experiment reasonably well reproduced with one or both of the two models?

- b.** Proceed with the model that gives the better energy difference and try to locate transition states both for isomerization of hydroxymethylene to formaldehyde and for dissociation to hydrogen and carbon monoxide. Be certain to calculate vibrational frequencies for the two transition states. On the basis of transition states you have located, would you expect that both isomerization and dissociation reactions are available to hydroxymethylene? Explain. Do both suggest that hydroxymethylene is in a deep enough energy well to actually be observed?

P15.24 The three vibrational frequencies in H_2O (1595, 3657, and 3756 cm^{-1}) are all much larger than the corresponding frequencies in D_2O (1178, 1571, and 2788 cm^{-1}). This follows from the fact that vibrational frequency is given by the square root of a (mass-independent) quantity, which relates to the curvature of the energy surface at the minima, divided by a quantity that depends on the masses of the atoms involved in the motion.

As discussed in Section 15.8.4, vibrational frequencies enter into both terms required to relate the energy obtained from a quantum-chemical calculation (stationary nuclei at 0 K) to the enthalpy obtained experimentally (vibrating nuclei at finite temperature), as well as the entropy required to relate enthalpies to free energies. For the present purpose, focus is entirely on the so-called zero point energy term—that is, the energy required to account for the latent vibrational energy of a molecule at 0 K.

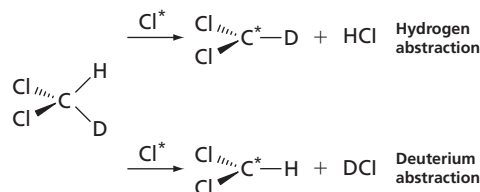
The zero point energy is given simply as the sum over individual vibrational energies (frequencies). Thus, the zero point energy for a molecule in which isotopic substitution has resulted in an increase in mass will be reduced from that in the unsubstituted molecule:



A direct consequence of this is that enthalpies of bond dissociation for isotopically substituted molecules (light to heavy) are larger than those for unsubstituted molecules.

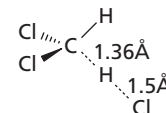
- a.** Perform B3LYP/6-31G* calculations on HCl and on its dissociation products, a chlorine atom and a hydrogen atom. Following structure optimization on HCl, calculate the vibrational frequency for both HCl and DCl and evaluate the zero point energy for each. In terms of a percentage of the total bond dissociation energy, what is the change noted in going from HCl to DCl?

d_1 -Methylene chloride can react with chlorine atoms in either of two ways: by hydrogen abstraction (producing HCl) or by deuterium abstraction (producing DCl):



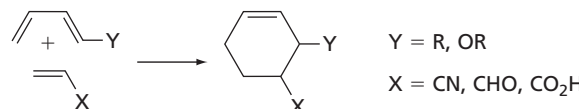
Which pathway is favored on the basis of thermodynamics, and which is favored on the basis of kinetics?

- b.** Obtain the equilibrium structure for dichloromethyl radical using the B3LYP/6-31G* model. Also, obtain vibrational frequencies for both the unsubstituted and the deuterium-substituted radical and calculate zero point energies for the two abstraction pathways (you already have zero point energies for HCl and DCl). Which pathway is favored on the basis of thermodynamics? What would you expect the (thermodynamic) product ratio to be at room temperature?
- c.** Obtain the transition state for hydrogen abstraction from methylene chloride using the B3LYP/6-31G* model. A reasonable guess is shown here:

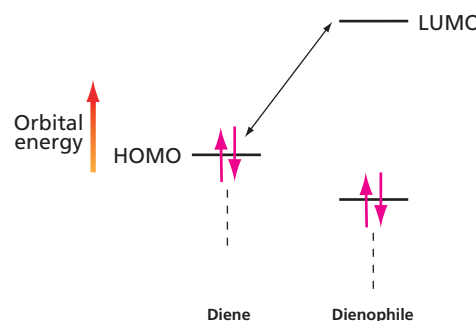


Calculate vibrational frequencies for the two possible structures with one deuterium and evaluate the zero point energies for these two structures. (For the purpose of zero point energy calculation, ignore the imaginary frequency corresponding to the reaction coordinate.) Which pathway is favored on the basis of kinetics? Is it the same or different from the thermodynamic pathway? What would you expect the (kinetic) product ratio to be at room temperature?

P15.25 Diels–Alder reactions commonly involve electron-rich dienes and electron-deficient dienophiles, as shown here:

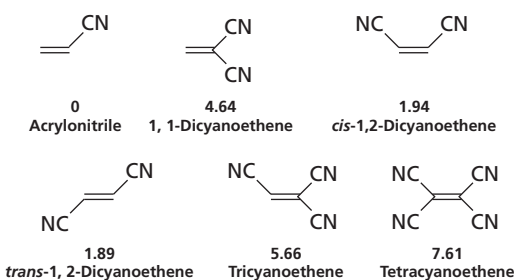


The rate of these reactions generally increases with the π -donor ability of the diene substituent, Y, and with the π -acceptor ability of the dienophile substituent, X. The usual interpretation is that electron donors will push up the energy of the HOMO on the diene and that electron acceptors will push down the energy of the LUMO on the dienophile, as illustrated here:



The resulting decrease in the HOMO–LUMO gap leads to a stronger interaction between diene and dienophile and to a decrease in the activation barrier.

- a. Obtain equilibrium structures for acrylonitrile, 1,1-dicyanoethylene, *cis*- and *trans*-1,2-dicyanoethylene, tricyanoethylene, and tetracyanoethylene using the HF/3-21G model.



Plot the LUMO energy for each dienophile versus the log of the observed relative rate for its addition to cyclopentadiene (listed below the structures in the preceding figure). Is there a reasonable correlation between LUMO energy and relative rate?

- b. Obtain transition-state structures for Diels–Alder cycloadditions of acrylonitrile and cyclopentadiene and tetracyanoethylene and cyclopentadiene using the HF/3-21G model. Also obtain a structure for cyclopentadiene. Calculate activation energies for the two reactions.

How does the calculated difference in activation energies compare with the experimental difference (based on a value of 7.61 for the difference in the log of the rates and assuming 298 K)?

- P15.26** It is well known that cyanide acts as a “carbon” and not a “nitrogen” nucleophile in S_N2 reactions, as shown in this example:

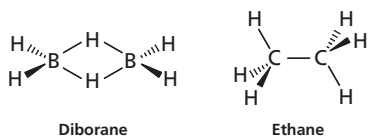


How can this behavior be rationalized with the notion that nitrogen is in fact more electronegative than carbon and, therefore, would be expected to hold any excess electrons?

- a. Optimize the structure of cyanide using the HF/3-21G model and examine the HOMO. Describe the shape of the HOMO of cyanide. Is it more concentrated on carbon or nitrogen? Does it support the picture of cyanide acting as a carbon nucleophile? If so, explain why your result is not at odds with the relative electronegativities of carbon and nitrogen. Why does iodide leave following nucleophilic attack by cyanide on methyl iodide?

- b. Optimize the structure of methyl iodide using the HF/3-21G model and examine the LUMO. Describe the shape of the LUMO of methyl iodide. Does it anticipate the loss of iodide following attack by cyanide? Explain.

- P15.27** At first glance, the structure of diborane would seem unusual. Why should the molecule not assume the same atomic structure as ethane, which after all has the same number of heavy atoms and the same number of hydrogens?



The important difference between the two molecules is that diborane has two fewer electrons than ethane and is not able to make the same number of bonds. In fact, it is ethene that has the same number of electrons, to which diborane is structurally related.

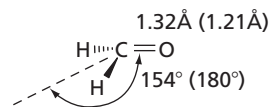
Obtain equilibrium structures for both diborane and ethene using the HF/6-31G* model and display the six valence molecular orbitals for each. Associate each valence orbital in ethene with its counterpart in diborane. Focus on similarities in the structure of the orbitals and not on their position in the lists of orbitals. To which orbital in diborane does the π orbital in ethene (the HOMO) best relate? How would you describe this orbital in diborane? Is it B—B bonding, B—H bonding, or both?

- P15.28** Molecular orbitals are most commonly delocalized throughout the molecule and exhibit distinct bonding or antibonding character. Loss of an electron from a specific molecular orbital from excitation by light or by ionization would, therefore, be expected to lead to distinct changes in bonding and changes in molecular structure.

- a. Obtain equilibrium structures for ethene, formaldimine, and formaldehyde using the HF/6-31G* model and display the highest occupied and lowest unoccupied molecular orbitals (HOMO and LUMO, respectively) for each. What would happen to the structure around carbon (remain planar versus pyramidalize), to the C=X bond length, and (for formaldimine) to the C=NH bond angle if an electron were to be removed from the HOMO of ethene, formaldimine, and formaldehyde?
- b. Obtain equilibrium structures for radical cations of ethene, formaldimine, and formaldehyde using the HF/6-31G* model. Are the calculated structures of these species, in which an electron has been removed from the corresponding neutral molecule, in line with your predictions based on the shape and nodal structure of the HOMO?
- c. Unoccupied molecular orbitals are also delocalized and also show distinct bonding or antibonding character. Normally, this is of no consequence. However, were these orbitals to become occupied (from excitation or from capture of an electron), then changes in molecular structure would also be expected. What would happen to the structure around carbon, to the C=X bond length, and (for formaldimine) to the C=NH bond angle, if an electron were to be added to the LUMO of ethene, formaldimine, and formaldehyde?
- d. Obtain equilibrium structures for the radical anions of ethene, formaldimine, and formaldehyde using the HF/6-31G* model. Are the calculated structures of these species, in which an electron has been added to the corresponding neutral molecule, in line with your predictions based on the shape and nodal structure of the LUMO?

The first excited state of formaldehyde (the so-called $n \rightarrow \pi^*$ state) can be thought of as arising from the promotion of one electron from the HOMO (in the ground state of formaldehyde) to the LUMO. The experimental equilibrium structure of the molecule shows lengthening of

the CO bond and a pyramidal carbon (ground state values are shown in parentheses):



- e. Rationalize this experimental result on the basis of what you know about the HOMO and LUMO in formaldehyde and your experience with calculations on the radical cation and radical anion of formaldehyde.

P15.29 BeH_2 is linear, whereas CH_2 with two additional electrons and H_2O with four additional electrons are both bent to a similar degree. Could these changes in structure have been anticipated by examining the shapes of the bonding molecular orbitals?

- a. Perform a series of structure optimizations on BeH_2 with the bond angle constrained at 90° , 100° , 110° , ..., 180° (10 optimizations in total). Use the HF/6-31G* model. Plot the total energy, along with the HOMO and LUMO energies versus bond angle. Also, display the HOMO and LUMO for one of your structures of intermediate bond angle.

Does the energy of the HOMO of BeH_2 increase (more positive) or decrease in transitioning from a bent to a linear structure, or does it remain constant, or is the energy at a minimum or maximum somewhere between? Would this result have been anticipated by examining the shape and nodal structure of the HOMO?

Does the energy of the LUMO of BeH_2 increase or decrease with increase in bond angle, or does it remain constant, or is the energy at a minimum or maximum somewhere between? Rationalize your result by reference to the shape and nodal structure of the LUMO. What do you anticipate would happen to the atomic structure of BeH_2 as electrons are added to the LUMO? Take a guess at the structure of BH_2^+ (one electron added to the LUMO) and singlet CH_2 (two electrons added to the LUMO).

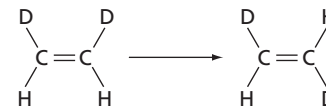
- b. Optimize the structures of (singlet) BH_2^+ and singlet CH_2 using the HF/6-31G* model. Are the results of the quantum-chemical calculations in line with your qualitative arguments?
- c. Perform a series of structure optimizations on singlet CH_2 with the bond angle constrained to 90° , 100° , 110° , ..., 180° . Plot the total energy as a function of the angle as well as the HOMO and LUMO energies.

Display the LUMO for some intermediate structure. Does the plot of HOMO energy versus angle in CH_2 mirror the plot of LUMO energy versus angle in BeH_2 ? Rationalize your answer. Does the energy of the LUMO in CH_2 increase, decrease, or remain constant with increase in bond angle (or is it at a minimum or maximum somewhere between)? Is the change in LUMO energy smaller, larger, or about the same as the change in the energy of the HOMO over the same range of bond angles? Rationalize these two observations by reference to the shape and nodal

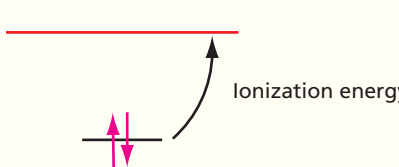
structure of the LUMO. What do you anticipate would happen to the atomic structure of CH_2 as electrons are added to the LUMO? Take a guess at the structure of NH_2^+ (one electron added to the LUMO) and H_2O (two electrons added to the LUMO).

- d. Optimize the structures of NH_2^+ and H_2O using the HF/6-31G* model. Are the results of the quantum-chemical calculations in line with your qualitative arguments?

P15.30 Most olefins assume planar (or nearly planar) structures. This ensures maximum overlap between p orbitals and maximum π -bond strength. Any distortion away from planarity should reduce orbital overlap and bond strength. In principle, π -bond strength can be determined experimentally, by measuring the activation energy required for *cis-trans* isomerization, such as in *cis*-1,2-dideuteroethylene:



Another measure of π -bond strength, at least π -bond strength relative to a standard, is the energy required to remove an electron from the π orbital, or the ionization energy as in the accompanying diagram:

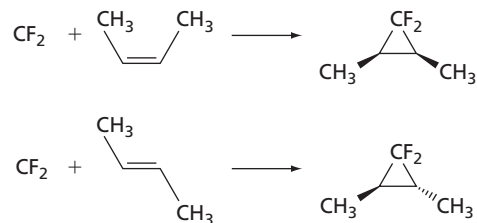


Nonplanar olefins might be expected to result from incorporation of a *trans* double bond into a small ring. Small-ring cycloalkenes preferentially form *cis* double bonds. The smallest *trans* cycloalkene to have been isolated is cyclooctene, which is known experimentally to be approximately 39 kJ/mol less stable than *cis*-cyclooctene. Is this a measure of reduction in π bond strength?

Optimize the structures of both *cis*- and *trans*-cyclooctene using the HF/3-21G model. (First, examine the possible conformers available to each of the molecules.) Finally, calculate and display the HOMO for each molecule.

Is the double bond in *trans*-cyclooctene significantly distorted from its ideal planar structure? If so, would you characterize the distortion as puckering of the double-bond carbons or as twisting around the bond, or both? Does the HOMO in *trans*-cyclooctene show evidence of distortion? Elaborate. Is the energy of the HOMO in *trans*-cyclooctene significantly higher (less negative) than that in *cis*-cyclooctene? How does the energy difference compare to the experimentally measured difference in ionization potentials between the two isomers (0.29 eV)? How does the difference in HOMO energies (ionization potentials) relate to the calculated (measured) difference in isomer energies?

P15.31 Singlet carbenes add to alkenes to yield cyclopropanes. Stereochemistry is maintained, indicating that *cis*- and *trans*-substituted alkenes produce *cis*- and *trans*-substituted cyclopropanes, respectively; for example:



This maintenance of stereochemistry implies that the two σ bonds are formed more or less simultaneously, without the intervention of an intermediate that would allow *cis-trans* isomerization.

Locate the transition state for addition of singlet difluorocarbene and ethene using the HF/3-21G model and, following this, calculate vibrational frequencies. When completed, verify that you have in fact found a transition state and that it appears to be on the way to the correct product.

What is the orientation of the carbene relative to ethene in your transition state? Is it the same orientation as adopted in the product (1,1-difluorocyclopropane)? If not, what is the reason for the difference? (*Hint:* Consider that the π electrons on ethylene need to go into a low-lying unoccupied molecular orbital on the carbene. Build difluorocarbene and optimize its geometry using the HF/3-21G model and display the LUMO.)

P15.32 Additional information about the mechanism of the ethyl formate pyrolysis reaction can be obtained by replacing the static picture with a movie, that is, an animation along the reaction coordinate. Access “ethyl formate pyrolysis” (on the Spartan download) and examine the change in electron density as the reaction proceeds. Do hydrogen migration and CO bond cleavage appear to occur in concert, or is one leading the other?

P15.33 Do related molecules with the same number of electrons occupy the same amount of space, or are other factors (beyond electron count) of importance when dictating overall size requirements? Obtain equilibrium structures for methyl anion, ammonia, and hydronium cation using the HF/6-31G* model and compare electron density surfaces corresponding to enclosure of 99% of the total electron density. Do the three molecules occupy the same amount of space? If not, why not?

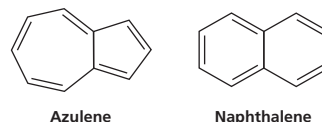
P15.34 Lithium provides a very simple example of the effect of oxidation state on overall size. Perform HF/6-31G* calculations on lithium cation, lithium atom, and lithium anion, and compare the three electron density surfaces corresponding to enclosure of 99% of the total electron density. Which is smallest? Which is largest? How does the size of lithium relate to the number of electrons? Which surface most closely resembles a conventional space-filling model? What, if anything does this communicate to you about the kinds of molecules that were used to establish the space-filling radius for lithium?

P15.35 A surface for which the electrostatic potential is negative delineates regions in a molecule that are subject to

electrophilic attack. It can help you to rationalize the widely different chemical behavior of molecules that are structurally similar.

Optimize the structures of benzene and pyridine using the HF/3-21G model and examine electrostatic potential surfaces corresponding to -100 kJ/mol . Describe the potential surface for each molecule. Use it to rationalize the following experimental observations: (1) Benzene and its derivatives undergo electrophilic aromatic substitution far more readily than do pyridine and its derivatives; (2) protonation of perdeuterobenzene (C_6D_6) leads to loss of deuterium, whereas protonation of perdeuteropyridine (C_5D_5N) does not lead to loss of deuterium; and (3) benzene typically forms π -type complexes with transition metals, whereas pyridine typically forms σ -type complexes.

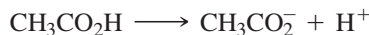
P15.36 Hydrocarbons are generally considered to be nonpolar or weakly polar at best, characterized by dipole moments that are typically only a few tenths of a debye. For comparison, dipole moments for molecules of comparable size with heteroatoms are commonly several debyes. One recognizable exception is azulene, which has a dipole moment of 0.8 debye. The structure of azulene is compared with that of its nonpolar isomer naphthalene in the accompanying diagram:



Azulene Naphthalene

Optimize the structure of azulene using the HF/6-31G* model and calculate an electrostatic potential map. For reference, perform the same calculations on naphthalene. Display the two electrostatic potential maps side by side and on the same (color) scale. According to its electrostatic potential map, is one ring in azulene more negative (relative to naphthalene as a standard) and one ring more positive? If so, which is which? Is this result consistent with the direction of the dipole moment in azulene? Rationalize your result. (*Hint:* Count the number of π electrons.)

P15.37 Chemists know that nitric and sulfuric acids are strong acids and that acetic acid is a weak acid. They would also agree that ethanol is at best a very weak acid. Acid strength is described directly by the energetics of deprotonation (heterolytic bond dissociation); for example, for acetic acid:



As written, this is a highly *endothermic* process because not only is a bond broken but two charged molecules are created from the neutral acid. It occurs readily in solution only because the solvent acts to disperse charge.

Acid strength can be calculated simply as the difference in energy between the acid and its conjugate base (the energy of the proton is 0). In fact, acid strength comparisons among closely related systems, such as carboxylic acids, are described quite well with practical quantum-chemical models. This is consistent with the ability of the same models to correctly account for relative base strengths (see discussion in Section 15.8.3).

Another possible measure of acid strength is the degree of positive charge on the acidic hydrogen as measured by the electrostatic potential. It is reasonable to expect that the more positive the potential in the vicinity of the hydrogen, the more easily it will dissociate and the stronger the acid. This kind of measure, were it to prove successful, offers an advantage over the calculation of reaction energy in that only the acid (and not the conjugate base) needs to be considered.

- a. Obtain equilibrium structures for nitric acid, sulfuric acid, acetic acid, and ethanol using the HF/3-21G model, and compare electrostatic potential maps. Be certain to choose the same (color) scale for the four acids. For which acid is the electrostatic potential in the vicinity of (the acidic)

hydrogen most positive? For which is it least positive? Do electrostatic potential maps provide a qualitatively correct account of the relative acid strength of these four compounds?

- b. Obtain equilibrium structures for several of the carboxylic acids found in the following table using the HF/3-21G model and display an electrostatic potential map for each.

“Measure” the most positive value of the electrostatic potential associated with the acidic hydrogen in each of these compounds and plot this against experimental pK_a (given in the preceding table). Is there a reasonable correlation between acid strengths and electrostatic potential at hydrogen in this closely related series of acids?

Acid	pK_a	Acid	pK_a
<chem>Cl3CCO2H</chem>	0.7	<chem>HCO2H</chem>	3.75
<chem>HO2CCCO2H</chem>	1.23	<chem>trans-ClCH=CHCO2H</chem>	3.79
<chem>Cl2CHCO2H</chem>	1.48	<chem>C6H5CO2H</chem>	4.19
<chem>NCCH2CO2H</chem>	2.45	<chem>p-ClC6H4CH=CHCO2H</chem>	4.41
<chem>ClCH2CO2H</chem>	2.85	<chem>trans-CH3CH=CHCO2H</chem>	4.70
<chem>trans-HO2CCH=CHCO2H</chem>	3.10	<chem>CH3CO2H</chem>	4.75
<chem>p-HO2CC6H4CO2H</chem>	3.51	<chem>(CH3)3CCO2H</chem>	5.03

FURTHER READING

Geerlings, P., De Proft, F., and Langenaeker, W. “Conceptual Density Functional Theory.” *Chemical Reviews* 103 (2003): 1793–1873.

Levine, I. *Quantum Chemistry* (7th ed.). Boston: Pearson, 2014.

Matito, E., Duran, M., and Solà, M. “A Novel Exploration of the Hartree–Fock Homolytic Bond Dissociation Problem in the Hydrogen Molecule by Means of Electron Localization Measures.” *Journal of Chemical Education* 83 (2006): 1243–1248.

Olsson, L., and Kloo, L. “Electron Pairing, Repulsion, and Correlation: A Simplistic Approach.” *Journal of Chemical Education* 81 (2004): 138–141.

Summerfeld, J., Beltrane, G., and Loeser, J. “A Simple Model for Understanding Electron Correlation Methods.” *Journal of Chemical Education* 76 (1999): 1430–1438.

This page intentionally left blank

MATH ESSENTIAL 10: Working with Matrices

A matrix is an array of numbers, functions, or operators arranged in rows and columns. Matrices have a wide variety of applications in mathematics, physical sciences, computer sciences, and other fields.

ME10.1 DEFINITION OF A MATRIX

An $n \times m$ matrix is an array of numbers, functions, or operators enclosed by parentheses that can undergo mathematical operations such as addition and multiplication with one another. A 3×3 matrix is shown in Equation (ME10.1).

$$\mathbf{M} = \begin{pmatrix} 1 & 2 & 1 \\ 3 & 0 & -1 \\ -1 & -1 & 2 \end{pmatrix} \quad (\text{ME10.1})$$

The elements of a matrix are designated by the indices of their row and column, M_{rc} . For the matrix in Equation (ME 10.1), $M_{32} = -1$. Diagonal matrices are matrices for which only the diagonal elements are nonzero,

$$\mathbf{D} = \begin{pmatrix} 1 & 0 & 0 \\ 0 & 3 & 0 \\ 0 & 0 & 2 \end{pmatrix} \quad (\text{ME10.2})$$

Matrices need not be square, and the simplest matrices are column and row matrices, such as those shown in Equation (ME 10.3).

$$\mathbf{R} = \begin{pmatrix} 1 & 2 & 0 & -1 \end{pmatrix} \quad \mathbf{C} = \begin{pmatrix} 5 \\ -2 \\ 1 \\ 1 \end{pmatrix} \quad (\text{ME10.3})$$

A square ($n \times n$) matrix in which all the entries are numbers can be associated with a single number, the determinant of that matrix, as discussed in Math Essential 9. Operations such as addition and multiplication can be carried out with matrices, as will be discussed below. Before describing these operations, we illustrate the usefulness of matrices in the following example.

ME10.2 REPRESENTING REFLECTION IN TERMS OF A MATRIX

Consider a vector \mathbf{A} in the x - y plane. How can the operation in which \mathbf{A} is reflected across the x axis, resulting in the vector \mathbf{B} , be represented in terms of matrices?

We can describe this transformation, shown in Figure ME10.1, in the following equations in terms of the coordinates of \mathbf{A} and \mathbf{B} .

$$\begin{aligned} x_B &= 1 \times x_A + 0 \times y_A \\ y_B &= 0 \times x_A - 1 \times y_A \end{aligned} \quad (\text{ME10.4})$$

ME10.1 Definition of a Matrix

ME10.2 Representing Reflection in Terms of a Matrix

ME10.3 Multiplication of Two Matrices

ME10.4 Addition of Two Matrices

ME10.5 The Identity Matrix

ME10.6 The Inverse Matrix

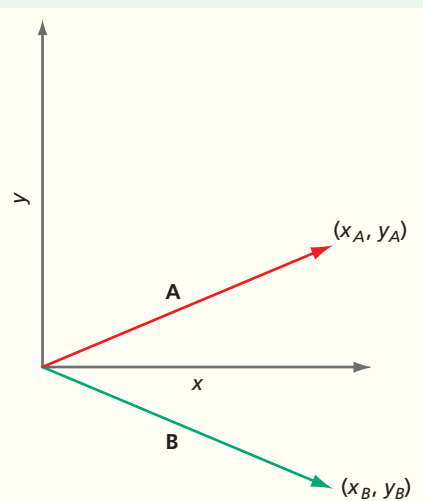


Figure ME10.1

Vector \mathbf{A} in the x - y plane is reflected across the x axis.

If we represent vectors \mathbf{A} and \mathbf{B} by column vectors,

$$\mathbf{A} = \begin{pmatrix} x_A \\ y_A \end{pmatrix} \quad \mathbf{B} = \begin{pmatrix} x_B \\ y_B \end{pmatrix} \quad (\text{ME10.5})$$

And the reflection operator by the matrix

$$\mathbf{R} = \begin{pmatrix} 1 & 0 \\ 0 & -1 \end{pmatrix} \quad (\text{ME10.6})$$

We can describe the reflection operation by

$$\mathbf{B} = \mathbf{R} \times \mathbf{A} \quad \text{or} \quad \begin{pmatrix} x_B \\ y_B \end{pmatrix} = \begin{pmatrix} 1 & 0 \\ 0 & -1 \end{pmatrix} \begin{pmatrix} x_A \\ y_A \end{pmatrix} \quad (\text{ME10.7})$$

ME10.3 MULTIPLICATION OF TWO MATRICES

In Equation (ME10.7), we implicitly defined the multiplication process for matrices. Two matrices \mathbf{D} and \mathbf{E} can be multiplied to generate matrix \mathbf{F} if the number of columns in the matrix to the left of the multiplication symbol is equal to the number of rows in the matrix to the right of the multiplication symbol. The element of the product matrix F_{rc} is given by Equation (ME10.8):

$$F_{rc} = \sum D_{r,ci} E_{ri,c} \quad (\text{ME10.8})$$

This equation is illustrated pictorially in Equation (ME10.9) for the multiplication of two 5×5 matrices.

$$\begin{aligned} \mathbf{F} = \mathbf{D} \times \mathbf{E} &= \begin{pmatrix} \cdot & \cdot & \cdot & \cdot & \cdot \\ \cdot & \cdot & \cdot & \cdot & \cdot \\ D_{31} & D_{32} & D_{33} & D_{34} & D_{35} \\ \cdot & \cdot & \cdot & \cdot & \cdot \\ \cdot & \cdot & \cdot & \cdot & \cdot \end{pmatrix} \begin{pmatrix} \cdot & \cdot & E_{13} & \cdot & \cdot \\ \cdot & \cdot & E_{23} & \cdot & \cdot \\ \cdot & \cdot & E_{33} & \cdot & \cdot \\ \cdot & \cdot & E_{43} & \cdot & \cdot \\ \cdot & \cdot & E_{53} & \cdot & \cdot \end{pmatrix} \\ &= \begin{pmatrix} \cdot & \cdot & \cdot & \cdot & \cdot \\ \cdot & \cdot & \cdot & \cdot & \cdot \\ \cdot & \cdot & F_{33} & \cdot & \cdot \\ \cdot & \cdot & \cdot & \cdot & \cdot \\ \cdot & \cdot & \cdot & \cdot & \cdot \end{pmatrix} \end{aligned} \quad (\text{ME10.9})$$

In this case, the element F_{33} is given by

$$F_{33} = D_{31}E_{13} + D_{32}E_{23} + D_{33}E_{33} + D_{34}E_{43} + D_{35}E_{53} \quad (\text{ME10.10})$$

Using this rule, Equation (ME10.7) describing the reflection becomes

$$\begin{pmatrix} x_B \\ y_B \end{pmatrix} = \begin{pmatrix} 1 & 0 \\ 0 & -1 \end{pmatrix} \begin{pmatrix} x_A \\ y_A \end{pmatrix} = \begin{pmatrix} x_A \\ -y_A \end{pmatrix} \quad (\text{ME10.11})$$

For 2×2 matrices, multiplication takes the following form.

$$\mathbf{AB} = \begin{pmatrix} a_{11} & a_{12} \\ a_{21} & a_{22} \end{pmatrix} \begin{pmatrix} b_{11} & b_{12} \\ b_{21} & b_{22} \end{pmatrix} = \begin{pmatrix} a_{11}b_{11} + a_{12}b_{21} & a_{11}b_{12} + a_{12}b_{22} \\ a_{21}b_{11} + a_{22}b_{21} & a_{21}b_{12} + a_{22}b_{22} \end{pmatrix} \quad (\text{ME10.12})$$

Using numerical examples,

$$\begin{pmatrix} 2 & 1 \\ -3 & 4 \end{pmatrix} \begin{pmatrix} 1 & 6 \\ 2 & -1 \end{pmatrix} = \begin{pmatrix} 4 & 11 \\ 5 & -22 \end{pmatrix} \text{ and } \begin{pmatrix} 1 & 6 \\ 2 & -1 \end{pmatrix} \begin{pmatrix} 1 \\ -1 \end{pmatrix} = \begin{pmatrix} -5 \\ 3 \end{pmatrix} \quad (\text{ME10.13})$$

ME10.4 ADDITION OF TWO MATRICES

Addition of two matrices is accomplished by adding each of the individual elements of the two matrices. Only matrices that have the same number of rows and columns can be added.

$$\begin{pmatrix} 2 & 1 \\ -3 & 4 \end{pmatrix} + \begin{pmatrix} 1 & 6 \\ 2 & -1 \end{pmatrix} = \begin{pmatrix} 3 & 7 \\ -1 & 3 \end{pmatrix}$$

ME10.5 THE IDENTITY MATRIX

We extend this discussion to the transformation of vectors in three dimensions and specifically consider rotation about the z axis. As we show in Example Problem 16.2, the transformation matrix is given by the 3×3 matrix \mathbf{R}_z as

$$\mathbf{R}_z = \begin{pmatrix} \cos \theta & -\sin \theta & 0 \\ \sin \theta & \cos \theta & 0 \\ 0 & 0 & 1 \end{pmatrix} \quad (\text{ME10.14})$$

Note that this matrix is not diagonal because rotation about the z axis mixes the x and y components of the original vector. However, the zeros in the first two elements of the third column and row and the presence of the number one in the lower right corner of the matrix shows that the z coordinate is unaffected by the rotation.

One special matrix, the identity matrix designated \mathbf{I} , deserves additional mention. The identity matrix corresponds to an operation in which nothing is changed. The matrix that corresponds to the transformation $(x_1, y_1, z_1) \rightarrow (x_1, y_1, z_1)$ is expressed in equation form as

$$\begin{aligned} x_2 &= x_1 + 0y_1 + 0z_1 \\ y_2 &= 0x_1 + y_1 + 0z_1 \\ z_2 &= 0x_1 + 0y_1 + z_1 \end{aligned} \quad (\text{ME10.15})$$

and is represented by the identity matrix $\mathbf{I} = \begin{pmatrix} 1 & 0 & 0 \\ 0 & 1 & 0 \\ 0 & 0 & 1 \end{pmatrix}$. The identity matrix is a

special case of a diagonal matrix. In the identity matrix of order $n \times n$, all the diagonal elements have the value one and the off-diagonal elements are 0.

ME10.6 THE INVERSE MATRIX

The operation that results from the sequential operation of two individual operations represented by the matrices \mathbf{A} and \mathbf{B} is the product of the matrices: $\mathbf{C} = \mathbf{AB}$. An interesting case illustrating this relationship is counterclockwise rotation through an angle θ followed by clockwise rotation through the same angle. The second operation corresponds to rotation by $-\theta$. Because $\cos(-\theta) = \cos \theta$ and $\sin(-\theta) = -\sin \theta$, the rotation matrix for $-\theta$ must be

$$\mathbf{R}_{-z} = \begin{pmatrix} \cos \theta & \sin \theta & 0 \\ -\sin \theta & \cos \theta & 0 \\ 0 & 0 & 1 \end{pmatrix} \quad (\text{ME10.16})$$

Because the sequential operations leave the vector unchanged, it must be the case that $\mathbf{R}_z\mathbf{R}_{-z} = \mathbf{R}_{-z}\mathbf{R}_z = \mathbf{I}$. We verify that the first of these relations is obeyed below.

$$\begin{aligned}
 \mathbf{R}_z\mathbf{R}_{-z} &= \begin{pmatrix} \cos \theta & -\sin \theta & 0 \\ \sin \theta & \cos \theta & 0 \\ 0 & 0 & 1 \end{pmatrix} \begin{pmatrix} \cos \theta & \sin \theta & 0 \\ -\sin \theta & \cos \theta & 0 \\ 0 & 0 & 1 \end{pmatrix} \\
 &= \begin{pmatrix} \cos^2 \theta + \sin^2 \theta + 0 & \sin \theta \cos \theta - \sin \theta \cos \theta + 0 & 0 \\ \sin \theta \cos \theta - \sin \theta \cos \theta + 0 & \cos^2 \theta + \sin^2 \theta + 0 & 0 \\ 0 & 0 & 1 \end{pmatrix} \\
 &= \begin{pmatrix} 1 & 0 & 0 \\ 0 & 1 & 0 \\ 0 & 0 & 1 \end{pmatrix}
 \end{aligned} \tag{ME10.17}$$

Any matrix \mathbf{B} that satisfies the relationship $\mathbf{AB} = \mathbf{BA} = \mathbf{I}$ is called the inverse matrix of \mathbf{A} and is designated \mathbf{A}^{-1} . Inverse matrices play an important role in solving a set of simultaneous equations and in eigenvalue problems such as finding the energies of a set of molecular orbitals that is a linear combination of atomic orbitals. In general, calculating inverse matrices is labor intensive and is best done using mathematical software.

Molecular Symmetry and an Introduction to Group Theory

WHY is this material important?

Recognizing molecular symmetry greatly simplifies a number of problems in quantum chemistry.

WHAT are the most important concepts and results?

Invoking molecular symmetry simplifies decisions as to which atomic orbitals contribute to molecular orbitals, understanding the origin of spectroscopic selection rules, identifying the normal modes of vibration for a molecule, and determining if a particular molecular vibration is infrared active, Raman active, or both. Also, the combination of group theory and quantum mechanics provides a powerful tool for understanding the consequences of molecular symmetry.

WHAT would be helpful for you to review for this chapter?

It would be helpful to review the material on the chemical bond in Chapter 13.

16.1 SYMMETRY ELEMENTS, SYMMETRY OPERATIONS, AND POINT GROUPS

An individual molecule has an inherent symmetry based on the spatial arrangement of its atoms. For example, after a rotation of benzene by 60° about an axis that is perpendicular to the plane of the molecule and that passes through the center of the molecule, the molecule cannot be distinguished from the original configuration. Solid benzene in a crystalline form has additional symmetry that arises from the way in which individual benzene molecules are arranged in the crystal structure. These symmetry elements are essential in discussing diffraction of X rays. However, in this chapter, the focus is on the symmetry of an individual molecule.

Why is molecular symmetry useful to chemists? The symmetry of a molecule determines a number of important properties. For example, CF_4 has no dipole moment, but H_2O has a dipole moment because of the symmetry of these molecules. All molecules have vibrational modes. However, the number of vibrational modes that are infrared and Raman active and the degeneracy of a given vibrational frequency depend on molecular symmetry. Symmetry also determines the selection rules for transitions between states of the molecule in all forms of spectroscopy, and symmetry determines which atomic orbitals contribute to a given molecular orbital.

The focus in this chapter is on applying the predictive power of group theory to problems of interest in quantum chemistry, rather than on formally developing the

- 16.1 Symmetry Elements, Symmetry Operations, and Point Groups
- 16.2 Assigning Molecules to Point Groups
- 16.3 The H_2O Molecule and the C_{2v} Point Group
- 16.4 Representations of Symmetry Operators, Bases for Representations, and the Character Table
- 16.5 The Dimension of a Representation
- 16.6 Using the C_{2v} Representations to Construct Molecular Orbitals for H_2O
- 16.7 Symmetries of the Normal Modes of Vibration of Molecules
- 16.8 Selection Rules and Infrared versus Raman Activity
- 16.9 (Supplemental Section) Using the Projection Operator Method to Generate MOs That Are Bases for Irreducible Representations

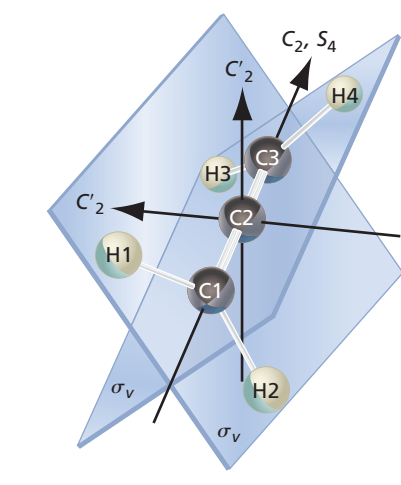
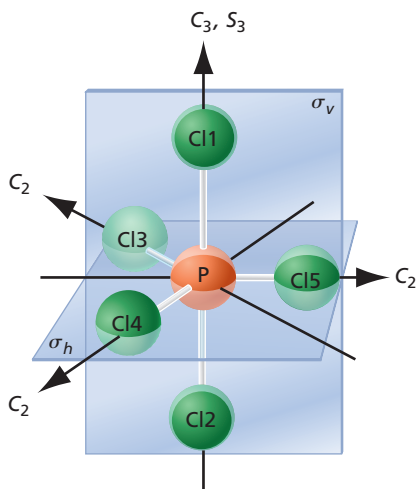
(a) Allene (CH_2CCH_2)(b) PCl_5

Figure 16.1 Examples of symmetry elements. The symmetry elements are shown for (a) allene (CH_2CCH_2) and (b) PCl_5 . Only one of the three σ_v planes for PCl_5 is shown in (b).

mathematical framework behind group theory. Therefore, results from group theory that are needed for specific applications are introduced without their derivations. These results are highlighted in shaded text boxes. Readers who wish to see these results derived or discussed in more detail may pursue the references to Carter and Kettle in Further Reading. **Group theory** is a powerful formal method for analyzing abstract and physical systems in which symmetry is present, and it has surprising importance in physics, especially quantum mechanics. In Sections 16.1 through 16.5, the essentials of group theory that are needed to address problems of chemical interest are discussed. With a working knowledge of reducible and irreducible representations and character tables, several applications of group theory to chemistry are presented in the rest of the chapter. In Section 16.6, group theory is used to construct molecular orbitals (MOs) that incorporate the symmetry of the molecule under consideration from atomic orbitals (AOs). In Section 16.7, we discuss the normal modes for the vibration of molecules, and in Section 16.8, we show that symmetry determines whether a given vibrational mode of a molecule is infrared or Raman active. We will also show that symmetry determines the number of normal modes that have the same vibrational frequency.

We begin our discussion of molecular symmetry by describing symmetry elements and symmetry operations. **Symmetry elements** are geometric entities such as axes, planes, or points with respect to which operations can be carried out. **Symmetry operations** are actions with respect to the symmetry elements that leave the molecule in a configuration that cannot be distinguished from the original configuration. There are only five different types of symmetry elements for an isolated molecule, although a molecule may require several elements of each type— n -fold rotation axes, n -fold rotation-reflection axes, or mirror planes—to fully define its symmetry. These elements and operations are listed in Table 16.1. Operators are indicated by a caret above the symbol.

Whereas other symmetry elements generate a single operation, C_n and S_n axes generate n operations. We choose the direction of rotation to be counterclockwise. However, if rotation is carried through consistently, either direction can be used. Examples of these symmetry elements are illustrated in Figure 16.1 for allene and PCl_5 . Consider first the following symmetry elements for allene shown in Figure 16.1a:

- A rotation of $360^\circ/2 = 180^\circ$ about the C_2 **rotation axes** passing through the carbon atoms leaves the molecule in a position that is indistinguishable from its initial position.
- A rotation of $360^\circ/4 = 90^\circ$ about the twofold axis discussed in the previous point, followed by a reflection through a plane perpendicular to the axis that passes through the central carbon atom, also leaves the allene molecule unchanged. The combined operation is called an S_4 fourfold **rotation-reflection axis**. This S_4 axis and the C_2 rotation axis of the previous bullet are collinear.
- Two additional C_2 rotation axes exist in this molecule. Both pass through the central carbon atom (C_2). Consider the two planes shown in Figure 16.1a. One contains H_1 and H_2 , and the other contains H_3 and H_4 . The two C_2 axes bisect the angle between the two planes and, therefore, are perpendicular to one another.
- The molecule contains two mirror planes, as shown. Because they contain the main twofold axis, which is referred to as the vertical axis, they are designated with σ_v .

TABLE 16.1 Symmetry Elements and Their Corresponding Operations

Symmetry Elements	Symmetry Operations
E	Identity
C_n	n -Fold rotation axis
σ	Mirror plane
i	Inversion center
S_n	n -Fold rotation-reflection axis
\hat{E}	leaves molecule unchanged
$\hat{C}_n, \hat{C}_n^2, \dots, \hat{C}_n^n$	rotate about axis by $360^\circ/n$ 1, 2, ..., n times (indicated by superscript)
$\hat{\sigma}$	reflect through the mirror plane
\hat{i}	$(x, y, z) \rightarrow (-x, -y, -z)$
\hat{S}_n	rotate about axis by $360^\circ/n$, and reflect through a plane perpendicular to the axis.

Next, consider the PCl_5 molecule, shown in Figure 16.1b, which has the following symmetry elements:

- A threefold rotation axis C_3 that passes through Cl1, Cl2, and the central P atom.
- A **mirror plane**, σ_h , that passes through the centers of the three equatorial Cl atoms. Reflection through this plane leaves the equatorial Cl atoms in their original location and exchanges the axial Cl atoms.
- Three C_2 axes that pass through the central P atom and one of the equatorial Cl atoms.
- Three mirror planes, σ_v , that contain Cl1, Cl2, and P as well as one of Cl3, Cl4, or Cl5.

Only one of the planes alluded to in the final bullet point is shown in Figure 16.1b. As we will see in Section 16.2, allene and PCl_5 can each be assigned to a group on the basis of symmetry elements of the molecule.

What is the relationship between symmetry elements, the symmetry operators, and the group? A set of symmetry elements forms a **group** if the following statements are true about their corresponding operators:

- The successive application of two operators is equivalent to one of the operations of the group. This guarantees that the group is closed.
- An **identity operator**, \hat{E} , exists that commutes with any other operator and leaves the molecule unchanged. Although this operator seems trivial, it plays an important role in linking other members of a group, as we will see later. The identity operator has the property that $\hat{A}\hat{E} = \hat{E}\hat{A} = \hat{A}$ where \hat{A} is an arbitrary element of the group.
- The group contains an **inverse operator** for each element in the group. If \hat{B}^{-1} is the inverse operator of \hat{B} , then $\hat{B}\hat{B}^{-1} = \hat{B}^{-1}\hat{B} = \hat{E}$. If $\hat{A} = \hat{B}^{-1}$, then $\hat{A}^{-1} = \hat{B}$. In addition, $\hat{E} = \hat{E}^{-1}$. Successive operations are carried from right to left.
- The operators are **associative**, meaning that $\hat{A}(\hat{B}\hat{C}) = (\hat{A}\hat{B})\hat{C}$.

The groups of interest in this chapter are called **point groups** because the set of symmetry elements intersects in a point or set of points. To utilize the power of group theory in chemistry, molecules are assigned to point groups on the basis of the symmetry elements characteristic of the particular molecule. Each point group has its own set of symmetry elements and corresponding operations. We will work with several of these groups in more detail in the following sections.

Concept

Symmetry elements include rotation axes, mirror planes, rotation-reflection axes, identity, and an inversion center. Each symmetry element has a corresponding operator.

16.2 ASSIGNING MOLECULES TO POINT GROUPS

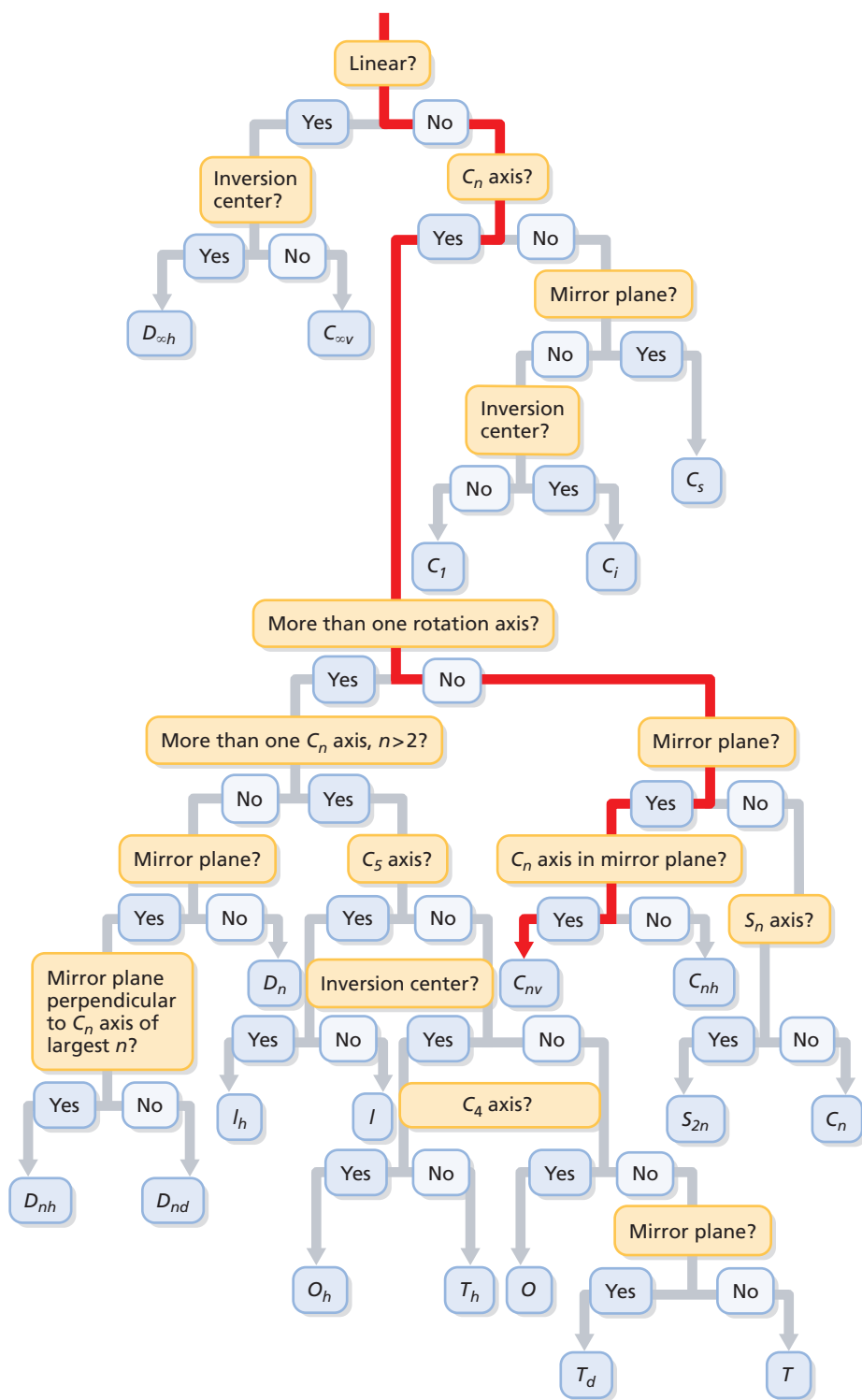
How is the point group to which a molecule belongs determined? The assignment is made using the logic diagram of Figure 16.2. To illustrate the use of this logic diagram, we will consider how NF_3 , CO_2 , and AuCl_4^- are assigned to specific point groups. In doing so, it is useful to first identify the major symmetry elements. After a tentative assignment of a point group is made based on these symmetry elements, it is necessary to verify that the other symmetry elements of that group are also present in the molecule. We start at the top of the diagram and follow the branching points.

NF_3 is a pyramidal molecule that has a threefold axis (C_3) passing through the N atom and a point in the plane of the F atoms that is equidistant from all three F atoms. NF_3 has no other rotation axes. The molecule has three mirror planes in which the C_3 axis, the N atom, and one F atom lie. These planes are perpendicular to the line connecting the other two fluorine atoms. Because the C_3 axis lies in the mirror plane, we conclude that NF_3 belongs to the C_{3v} group. The pathway through the logic diagram of Figure 16.2 is shown as a red line.

Carbon dioxide is a linear molecule with an **inversion center**, which is a point (also known as a *center of symmetry*) through which each atom in the molecule, located at coordinates $(+x, +y, +z)$, is related to another atom of the same element located

Figure 16.2

Logic diagram for assigning molecules to point groups. The red line indicates how NF_3 is assigned to the C_{3v} point group.



at coordinates $(-x, -y, -z)$. These symmetry characteristics uniquely specify CO_2 as belonging to the $D_{\infty h}$ group. The ∞ appears rather than the subscript n because any rotation about the molecular axis leaves the molecule unchanged.

AuCl_4^- is a square planar complex with a C_4 axis. It has C_2 axes perpendicular to the C_4 axis, but no other C_n axis with $n > 2$. It has mirror planes, one of which is perpendicular to the C_4 axis. Therefore, this complex belongs to the D_{4h} group. Trace the paths through the logic diagram for these molecules to see if you would have made the same assignments.

These examples illustrate how a given molecule can be assigned to a point group, but they have only utilized a few of the symmetry operations of a given group. A number

TABLE 16.2 Selected Point Groups and Their Elements

Point Group	Symmetry Elements	Example Molecule
C _s	E, σ	BFClBr (planar)
C ₂	E, C ₂	H ₂ O ₂
C _{2v}	E, C ₂ , σ _v , σ' _v	H ₂ O
C _{3v}	E, C ₃ , C ₃ ² , 3σ _v	NF ₃
C _{∞v}	E, C _∞ , ∞σ _v	HCl
C _{2h}	E, C ₂ , σ _h	<i>trans</i> -C ₂ H ₂ F ₂
D _{2h}	E, C ₂ , C' ₂ , C'' ₂ , σ _h , σ' _v , σ'' _v , i	C ₂ F ₄
D _{3h}	E, C ₃ , C ₃ ² , 3C ₂ , S ₃ , S ₃ ² , σ _h , 3σ _v	SO ₃
D _{4h}	E, C ₄ , C ₄ ² , C ₂ , 2C' ₂ , 2C'' ₂ , i, S ₄ , S ₄ ² , σ _h , 2σ' _v , 2σ'' _v	XeF ₄
D _{6h}	E, C ₆ , C ₆ ⁵ , C ₃ , C ₃ ² , C ₂ , 3C' ₂ , 3C'' ₂ , i, S ₃ , S ₃ ² , S ₆ , S ₆ ⁵ , σ _h , 3σ' _v , 3σ'' _v	C ₆ H ₆ (benzene)
D _{∞h}	E, C _∞ , S _∞ , ∞C ₂ , ∞σ _v , σ' _h , i	H ₂ , CO ₂
T _d	E, 4C ₃ , 4C ₃ ² , 3C ₂ , 3S ₄ , 3S ₄ ³ , 6σ _v	CH ₄
O _h	E, 4C ₃ , 4C ₃ ² , 6C ₂ , 3C ₄ , 3C ₂ , i, 3S ₄ , 3S ₄ ³ , 4S ₆ , 4S ₆ ⁵ , 3σ _h , 6σ' _v	SF ₆

of point groups applicable to small molecules are listed in Table 16.2. All symmetry elements of the group are listed. Note that several groups have different categories or **classes** of symmetry elements such as C_n and σ , which are indicated by single and double primes. Classes are defined in Section 16.3.

The preceding discussion of the symmetry elements of a group has been of a general nature. In the following section, we discuss the symmetry elements of the C_{2v} group, to which water belongs, in greater detail.

16.3 THE H₂O MOLECULE AND THE C_{2v} POINT GROUP

To gain practice in working with the concepts introduced in the preceding section, we next consider a specific molecule, express the symmetry operators mathematically, and show that the symmetry elements form a group. We do so by representing the operators as matrices and showing the requirements that the elements of any group must meet for this particular group.

Figure 16.3 shows all symmetry elements for the water molecule. By convention, the rotation axis of highest symmetry (principal rotation axis), C_2 , is oriented along the z axis. The C_2 axis passes through the O atom. The molecule has two mirror planes oriented at 90° to one another, and their line of intersection is the C_2 axis. Because the mirror planes contain the principal rotation axis, the symmetry planes are referred to as vertical planes and designated by the subscript v . Mirror planes perpendicular to the principal rotation axis are referred to as horizontal and are designated by the subscript h . The water molecule does not contain a horizontal mirror plane. The molecule lies in the plane designated σ' , and the second mirror plane, designated σ_v , bisects the H—O—H bond angle. As shown in Example Problem 16.1, these two mirror planes belong to different classes and, therefore, have different symbols.

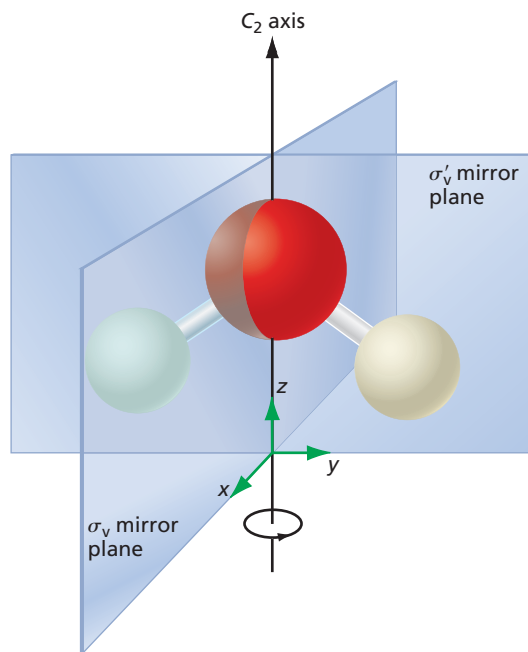
Symmetry elements that belong to the same class can be transformed into one another by other symmetry operations of the group. For example, the operators \hat{C}_n , \hat{C}_n^2 , ..., \hat{C}_n^n belong to the same class.

Concept

Symmetry elements that can be transformed into one another by symmetry operations of the group belong to the same class.

Figure 16.3

Water molecule shown with its symmetry elements. Convince yourself that the two mirror planes are in different classes.

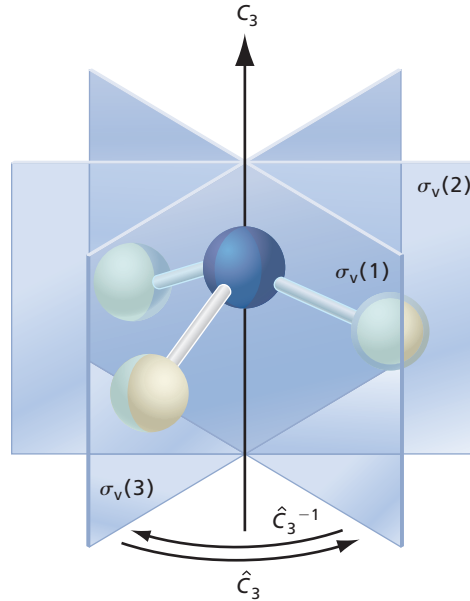


EXAMPLE PROBLEM 16.1

- Are the three mirror planes for the NF_3 molecule in the same or in different classes?
- Are the two mirror planes for H_2O in the same or in different classes?

Solution

- NF_3 belongs to the C_{3v} group, which contains the rotation operators \hat{C}_3 , $\hat{C}_3^2 = (\hat{C}_3)^{-1}$, and $\hat{C}_3^3 = \hat{E}$ and the vertical mirror planes $\hat{\sigma}_v(1)$, $\hat{\sigma}_v(2)$, and $\hat{\sigma}_v(3)$. These operations and elements are illustrated by this figure:



We see that \hat{C}_3 converts $\sigma_v(1)$ to $\sigma_v(3)$, and $\hat{C}_3^2 = (\hat{C}_3)^{-1}$ converts $\sigma_v(1)$ to $\sigma_v(2)$. Therefore, all three mirror planes belong to the same class.

- Figure 16.3 shows that neither the \hat{C}_2 nor the \hat{E} operation converts σ_v to σ'_v . Therefore, these two mirror planes are in different classes.

Using the logic diagram of Figure 16.2, we conclude that H_2O belongs to the C_{2v} group. This point group is given the shorthand notation C_{2v} because it has a C_2 axis and

vertical mirror planes. The C_{2v} group has four symmetry elements: the identity element, a C₂ rotation axis, and two mutually perpendicular mirror planes. The corresponding operators are the identity operator \hat{E} and the operators \hat{C}_2 , $\hat{\sigma}$, and $\hat{\sigma}'$.

To understand how these operators act, we must introduce mathematical representations of the operators and then carry out the operations. To do so, the operators of the C_{2v} group are represented by 3 × 3 matrices, which act on a vector in three-dimensional space. See Math Essential 10 for an introduction to working with matrices.

Consider the effect of the symmetry operators on an arbitrary vector $\mathbf{r} = (x_1, y_1, z_1)$, originating at the intersection of the mirror planes and the C₂ axis. The vector \mathbf{r} is converted to the vector (x_2, y_2, z_2) through the particular symmetry operation. We begin with a counterclockwise rotation by the angle θ about the z axis. As Example Problem 16.2 shows, the transformation of the components of the vector is described by Equation (16.1):

$$\begin{pmatrix} x_2 \\ y_2 \\ z_2 \end{pmatrix} = \begin{pmatrix} \cos \theta & -\sin \theta & 0 \\ \sin \theta & \cos \theta & 0 \\ 0 & 0 & 1 \end{pmatrix} \begin{pmatrix} x_1 \\ y_1 \\ z_1 \end{pmatrix} \quad (16.1)$$

EXAMPLE PROBLEM 16.2

Show that a rotation about the z axis can be represented by the matrix

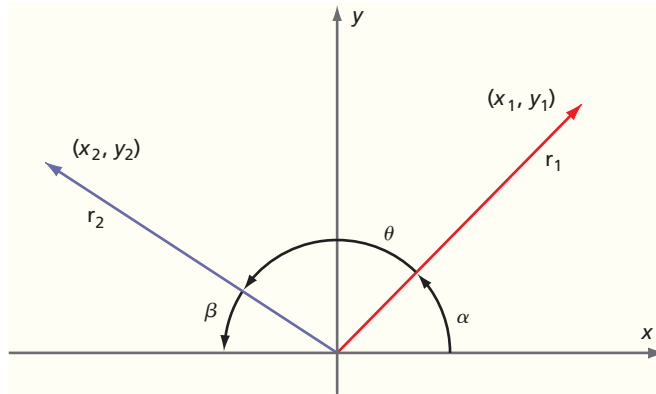
$$\begin{pmatrix} \cos \theta & -\sin \theta & 0 \\ \sin \theta & \cos \theta & 0 \\ 0 & 0 & 1 \end{pmatrix}$$

Show that for a rotation of 180° this matrix takes the form

$$\begin{pmatrix} -1 & 0 & 0 \\ 0 & -1 & 0 \\ 0 & 0 & 1 \end{pmatrix}$$

Solution

The z coordinate is unchanged in a rotation about the z axis, so we need only consider the vectors $\mathbf{r}_1 = (x_1, y_1)$ and $\mathbf{r}_2 = (x_2, y_2)$ in the xy plane. These equations can be derived from the following figure:



$$\theta = 180^\circ - \alpha - \beta$$

$$x_1 = r \cos \alpha, \quad y_1 = r \sin \alpha$$

$$x_2 = -r \cos \beta, \quad y_2 = r \sin \beta$$

Using the identities $\cos(\phi \pm \delta) = \cos \phi \cos \delta \mp \sin \phi \sin \delta$ and $\sin(\phi \pm \delta) = \sin \phi \cos \delta \pm \cos \phi \sin \delta$, x_2 and y_2 can be expressed in terms of θ and α .

$$\begin{aligned} x_2 &= -r \cos \beta = -r \cos(180^\circ - \alpha - \theta) \\ &= r \sin 180^\circ \sin(-\theta - \alpha) - r \cos 180^\circ \cos(-\theta - \alpha) \\ &= r \cos(-\theta - \alpha) = r \cos(\theta + \alpha) = r \cos \theta \cos \alpha - r \sin \theta \sin \alpha \\ &= x_1 \cos \theta - y_1 \sin \theta \end{aligned}$$

Using the same procedure, it can be shown that $y_2 = x_1 \sin \theta + y_1 \cos \theta$.

Concept

Matrices provide a convenient representation of symmetry operators.

The coordinate z is unchanged in the rotation, so that $z_2 = z_1$. The three equations

$$\begin{aligned}x_2 &= x_1 \cos \theta - y_1 \sin \theta \\y_2 &= x_1 \sin \theta + y_1 \cos \theta \quad \text{and} \\z_2 &= z_1\end{aligned}$$

can be expressed in the matrix form

$$\begin{pmatrix} x_2 \\ y_2 \\ z_2 \end{pmatrix} = \begin{pmatrix} \cos \theta & -\sin \theta & 0 \\ \sin \theta & \cos \theta & 0 \\ 0 & 0 & 1 \end{pmatrix} \begin{pmatrix} x_1 \\ y_1 \\ z_1 \end{pmatrix}$$

Because $\cos(180^\circ) = -1$ and $\sin(180^\circ) = 0$, the matrix for 180° rotation around the z axis takes the form

$$\begin{pmatrix} -1 & 0 & 0 \\ 0 & -1 & 0 \\ 0 & 0 & 1 \end{pmatrix}$$



The effect of the four operators, \hat{E} , \hat{C}_2 , $\hat{\sigma}_v$, and $\hat{\sigma}'_v$ on \mathbf{r} can also be deduced from Figure 16.4. Convince yourself, using Example Problem 16.1 and Figure 16.4, that the symmetry operators of the C_{2v} group have the following effect on the vector (x, y, z) :

$$\hat{E} \begin{pmatrix} x \\ y \\ z \end{pmatrix} \Rightarrow \begin{pmatrix} x \\ y \\ z \end{pmatrix}, \quad \hat{C}_2 \begin{pmatrix} x \\ y \\ z \end{pmatrix} \Rightarrow \begin{pmatrix} -x \\ -y \\ z \end{pmatrix}, \quad \hat{\sigma}_v \begin{pmatrix} x \\ y \\ z \end{pmatrix} \Rightarrow \begin{pmatrix} x \\ -y \\ z \end{pmatrix}, \quad \hat{\sigma}'_v \begin{pmatrix} x \\ y \\ z \end{pmatrix} \Rightarrow \begin{pmatrix} -x \\ y \\ z \end{pmatrix} \quad (16.2)$$

Given these results, the operators \hat{E} , \hat{C}_2 , $\hat{\sigma}'_v$, and $\hat{\sigma}_v'$ can be described by the following 3×3 matrices:

$$\hat{E}: \begin{pmatrix} 1 & 0 & 0 \\ 0 & 1 & 0 \\ 0 & 0 & 1 \end{pmatrix} \quad \hat{C}_2: \begin{pmatrix} -1 & 0 & 0 \\ 0 & -1 & 0 \\ 0 & 0 & 1 \end{pmatrix} \quad \hat{\sigma}_v: \begin{pmatrix} 1 & 0 & 0 \\ 0 & -1 & 0 \\ 0 & 0 & 1 \end{pmatrix} \quad \hat{\sigma}'_v: \begin{pmatrix} -1 & 0 & 0 \\ 0 & 1 & 0 \\ 0 & 0 & 1 \end{pmatrix} \quad (16.3)$$

Equation (16.3) gives a formulation of the symmetry operators as 3×3 matrices. Do these operators satisfy the requirements listed in Section 16.1 for the corresponding elements to form a group? We begin answering this question by showing in Example Problem 16.3 that the successive application of two operators is equivalent to applying one of the four operators.

EXAMPLE PROBLEM 16.3

Evaluate $\hat{C}_2 \hat{\sigma}_v$ and $\hat{C}_2 \hat{C}_2$. What operation is equivalent to the two sequential operations?

Solution

$$\hat{C}_2 \hat{\sigma}_v = \begin{pmatrix} -1 & 0 & 0 \\ 0 & -1 & 0 \\ 0 & 0 & 1 \end{pmatrix} \begin{pmatrix} 1 & 0 & 0 \\ 0 & -1 & 0 \\ 0 & 0 & 1 \end{pmatrix} = \begin{pmatrix} -1 & 0 & 0 \\ 0 & 1 & 0 \\ 0 & 0 & 1 \end{pmatrix} = \hat{\sigma}'_v$$

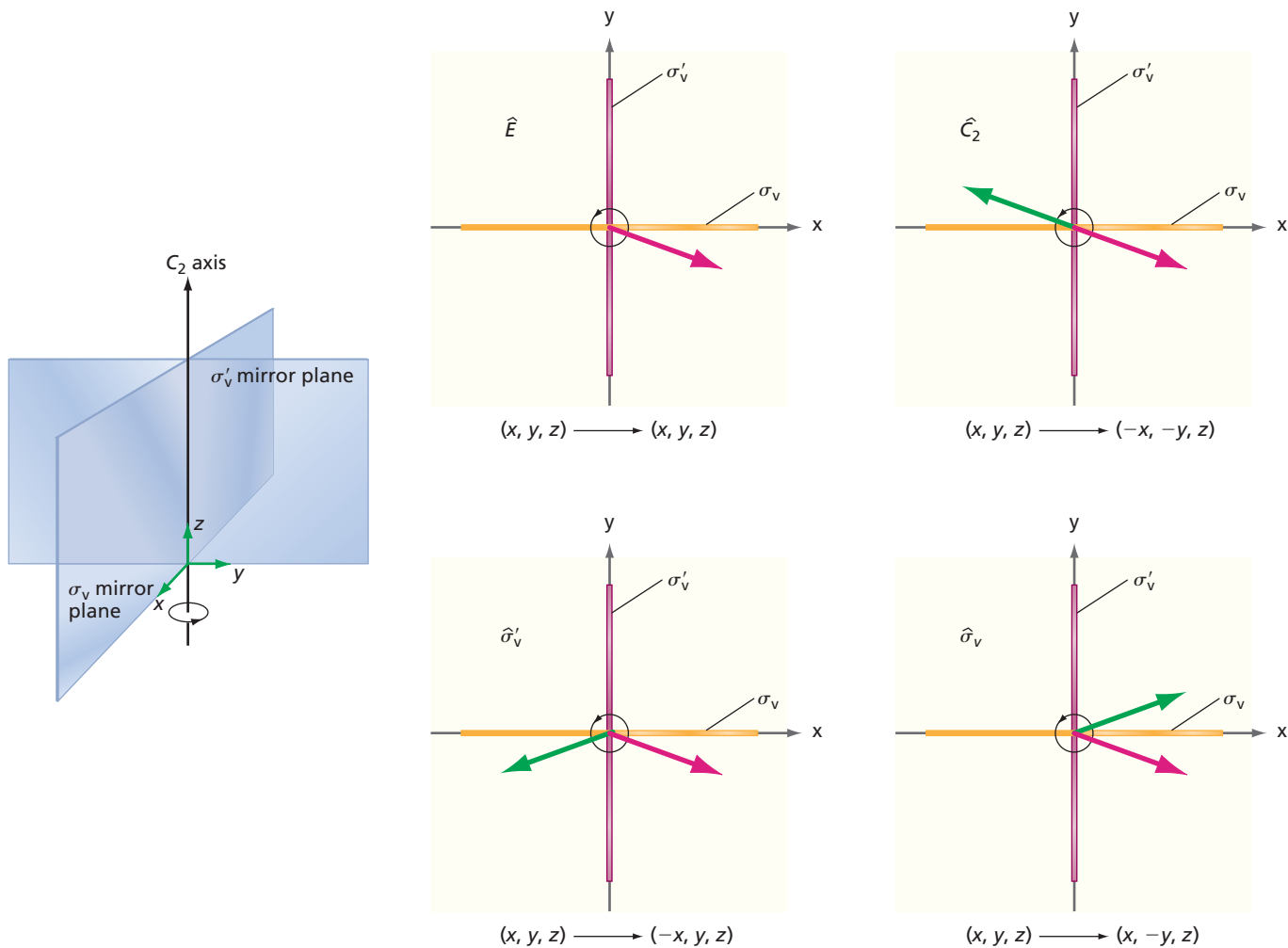
$$\hat{C}_2 \hat{C}_2 = \begin{pmatrix} -1 & 0 & 0 \\ 0 & -1 & 0 \\ 0 & 0 & 1 \end{pmatrix} \begin{pmatrix} -1 & 0 & 0 \\ 0 & -1 & 0 \\ 0 & 0 & 1 \end{pmatrix} = \begin{pmatrix} 1 & 0 & 0 \\ 0 & 1 & 0 \\ 0 & 0 & 1 \end{pmatrix} = \hat{E}$$

Concept

The product of two operators is another operator of the point group.

We see that the product of the two operators is another operator of the group.



**Figure 16.4**

Schematic illustration of the effect of the four symmetry operations of the C_{2v} group on an arbitrary vector (x, y, z). The symmetry elements are shown on the left. Because z is unchanged through any of the operations, it is sufficient to determine the changes in xy coordinates through the symmetry operations. This is shown on the right side of the figure viewed along the C_2 axis. The wide lines along the x and y axis represent the σ_v and σ'_v mirror planes, respectively. The red vector is transformed into the green vector in each case.

By repeating the procedure from Example Problem 16.3 with all possible combinations of operators, Table 16.3 can be generated. This table shows that, as required, the result of any two successive operations is another of these four symmetry operations. The table also shows that $\hat{C}_2\hat{C}_2 = \hat{\sigma}_v\hat{\sigma}'_v = \hat{\sigma}'_v\hat{\sigma}_v = \hat{E}$. Each operator has an inverse operator in the group, and in this particular case, each operator is its own inverse operator. The operations are also associative, which can be shown by evaluating an arbitrary combination of three operators such as $\hat{\sigma}_v(\hat{C}_2\hat{\sigma}'_v) - (\hat{\sigma}_v\hat{C}_2)\hat{\sigma}'_v$. If the operators are associative, this expression will equal zero. Using the multiplication table to evaluate the products in parentheses in the following equation, the result is

$$\hat{\sigma}_v(\hat{C}_2\hat{\sigma}'_v) - (\hat{\sigma}_v\hat{C}_2)\hat{\sigma}'_v = \hat{\sigma}_v\hat{\sigma}_v - \hat{\sigma}'_v\hat{\sigma}'_v = \hat{E} - \hat{E} = 0 \quad (16.4)$$

Convince yourself that any other combination of three operators will give the same result. We have now shown that the four symmetry elements characteristic of the water molecule satisfy the requirements of a group.

In this section, it was useful to express the operators of the C_{2v} group as 3 × 3 matrices in order to generate the group multiplication table. It turns out that these operators can be expressed in many different ways. This important topic is discussed in the following section.

TABLE 16.3 Multiplication Table for Operators of the C_{2v} Group

Second Operation	\hat{E}	\hat{C}_2	$\hat{\sigma}_v$	$\hat{\sigma}'_v$
\hat{E}	\hat{E}	\hat{C}_2	$\hat{\sigma}_v$	$\hat{\sigma}'_v$
\hat{C}_2	\hat{C}_2	\hat{E}	$\hat{\sigma}'_v$	$\hat{\sigma}_v$
$\hat{\sigma}_v$	$\hat{\sigma}_v$	$\hat{\sigma}'_v$	\hat{E}	\hat{C}_2
$\hat{\sigma}'_v$	$\hat{\sigma}'_v$	$\hat{\sigma}_v$	\hat{C}_2	\hat{E}

16.4 REPRESENTATIONS OF SYMMETRY OPERATORS, BASES FOR REPRESENTATIONS, AND THE CHARACTER TABLE

Concept

Symmetry operators can be represented by numbers that obey the multiplication table of the group.

The matrices derived in the previous section are called **representations** of that group, meaning that the multiplication table of the group can be reproduced with the matrices. For the C_{2v} group, the symmetry operators can be represented by numbers, and these numbers obey the multiplication table of a group. How can the operators of the C_{2v} group be represented by numbers? Surprisingly, each operation can be represented by either the number +1 or -1 and the multiplication table is still satisfied. As shown later, this is far from a trivial result. You will show in the end-of-chapter problems that the following four sets of +1 and -1, denoted Γ_1 through Γ_4 , each satisfy the C_{2v} multiplication table and, therefore, are individual representations of the C_{2v} group:

Representation	E	C_2	σ_v	σ'_v
Γ_1	1	1	1	1
Γ_2	1	1	-1	-1
Γ_3	1	-1	1	-1
Γ_4	1	-1	-1	1

Other than the trivial set in which the value zero is assigned to all operators, no other set of numbers satisfies the multiplication table. The fact that a representation of the group can be constructed using only the numbers +1 and -1 means that 1×1 matrices are sufficient to describe all operations of the C_{2v} group. This conclusion can also be reached by noting that all four 3×3 matrices derived in the previous section are diagonal, meaning that x , y , and z each transform independently of the other two coordinates.

It is useful to regard the set of numbers for an individual representation as a row vector, which we designate Γ_1 through Γ_4 for the C_{2v} group. Each group has an infinite number of different representations. For example, had we considered a Cartesian coordinate system at the position of each atom in water, we could have used 9×9 matrices to describe the operators. However, a much smaller number of representations, called **irreducible representations**, play a fundamental role in group theory. The irreducible representations are the matrices of smallest dimension that obey the multiplication table of the group. We cite the following theorem from group theory:

Concept

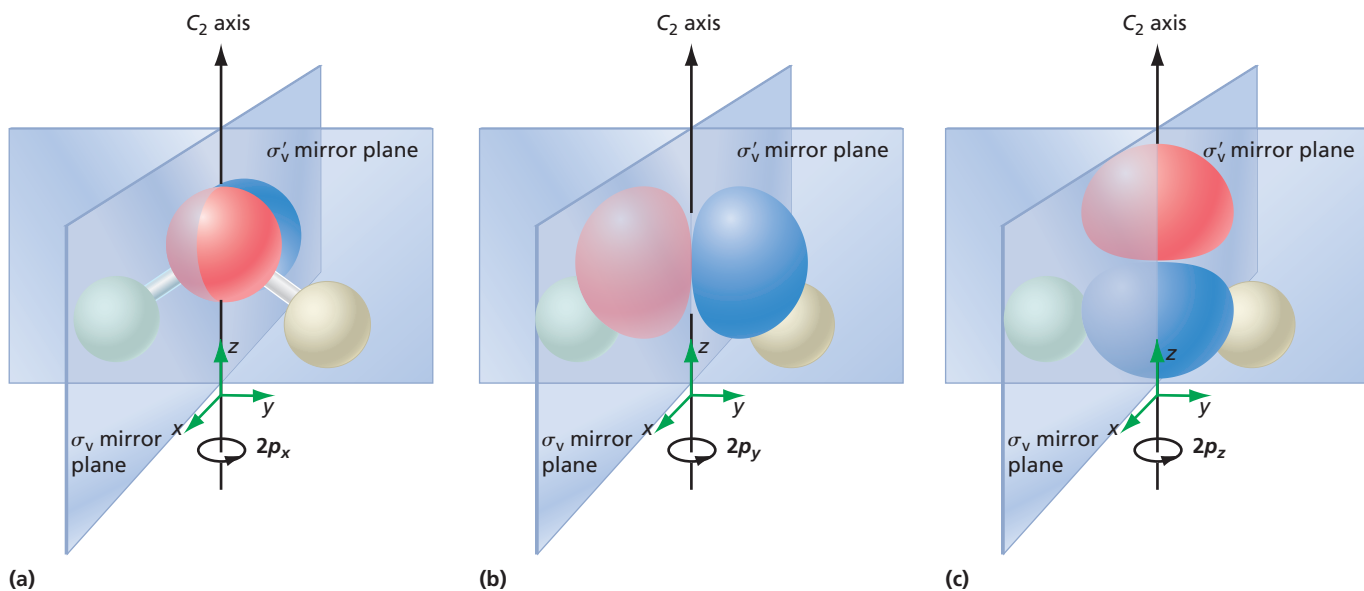
Irreducible representations are the matrices of smallest dimension that obey the multiplication table of the group.

A group has as many irreducible representations as it has classes of symmetry elements.

Irreducible representations play a central role in discussing molecular symmetry. We explore irreducible representations in greater depth in the next section.

Because the C_{2v} group has four classes of symmetry elements, only four different irreducible representations of this group are possible. This is an important result that we will return to in Section 16.5. The usefulness of these representations in quantum chemistry can be seen by considering the effect of symmetry operations on the oxygen AOs in H_2O . Consider the three different $2p$ atomic orbitals on the oxygen atom shown in Figure 16.5.

How are the three oxygen $2p$ orbitals transformed under the symmetry operations of the C_{2v} group? Numbers are assigned to the transformation of the $2p$ orbitals in the following way. If the sign of each lobe is unchanged by the operation, +1 is assigned to the transformation. If the sign of each lobe is changed, -1 is assigned to the transformation. These are the only possible outcomes for the symmetry operations of the C_{2v} group. Consider the $2p_z$ AO first. Figure 16.5c shows that the sign of each lobe remains the same after each operation. Therefore, we assign +1 to each operation. For the $2p_x$ AO in Figure 16.5a, the \hat{C}_2 rotation and the $\hat{\sigma}'_v$ reflection change the sign of each lobe, but the sign of each lobe is unchanged after the \hat{E} and $\hat{\sigma}_v$ operations. Therefore, we

**Figure 16.5**

The three p orbitals on the oxygen atom transform differently under the symmetry operations of the C_{2v} group. The orbitals and symmetry elements are shown for (a) $2p_x$, (b) $2p_y$ and (c) $2p_z$.

assign $+1$ to the \hat{E} and $\hat{\sigma}_v$ operators and -1 to the \hat{C}_2 and $\hat{\sigma}'_v$ operators. Similarly, for the $2p_y$ AO in Figure 16.5b, we assign $+1$ to the \hat{E} and $\hat{\sigma}'_v$ operators and -1 to the \hat{C}_2 and $\hat{\sigma}_v$ operators. Note that if you arrange the numbers $+1$ and -1 obtained separately for the $2p_z$, $2p_x$, and $2p_y$ orbitals in the order \hat{E} , \hat{C}_2 , $\hat{\sigma}_v$, and $\hat{\sigma}'_v$, the sequences that we have just derived are identical to the first, third, and fourth representations for the C_{2v} group.

Because each of the $2p_z$, $2p_x$, and $2p_y$ AOs can be associated with a different representation, each of these AOs **forms a basis** for one of the representations. Had we considered an unoccupied $3d_{xy}$ AO on the oxygen, we would have found that it forms a basis for the second representation. In the nomenclature used in group theory, one says that an AO, or any other function, **belongs to a particular representation** if it forms a basis for that representation. To this point, we have shown that 3×3 matrices, an appropriate set of the numbers $+1$ and -1 , and the AOs of oxygen all form a basis for the C_{2v} point group.

The information on the possible irreducible representations discussed can be assembled in a form known as a **character table**. Each point group has its unique character table. The character table for the C_{2v} group is as follows:

	E	C_2	σ_v	σ'_v			
A_1	1	1	1	1	z	x^2, y^2, z^2	$2p_z(O)$
A_2	1	1	-1	-1	R_z	xy	$3d_{xy}(O)$
B_1	1	-1	1	-1	x, R_y	xz	$2p_x(O)$
B_2	1	-1	-1	1	y, R_x	yz	$2p_y(O)$

Much of the information in this character table was derived to make the origin of the individual entries clear. However, this task is not necessary, because character tables for point groups in this standard format are widely accessible; they are listed in Appendix A.

The character table is the single most important result of group theory for chemists. Therefore, the structure and individual entries in the character table are now discussed in detail. The leftmost column in a character table shows the symbol for each irreducible representation. By convention, a representation that is symmetric ($+1$) with respect to rotation about the principal axis, C_2 in this case, is given the symbol A . A representation that is antisymmetric (-1) with respect to rotation about the principal axis is given the symbol B . Subscript 1 is used for representations that are symmetric, and subscript 2 is used for representations that are antisymmetric with respect to a C_2 axis perpendicular to the principal axis. If such an axis is not an element of the group, the symmetry with respect to a vertical mirror plane, $\hat{\sigma}_v$ in this case, is used. The representation in which all entries are $+1$ is called the **totally symmetric representation**. Every group has a totally symmetric representation.

Concept

Coordinates, functions of coordinates, and rotation axes can all form a basis for a given representation of a group.

Concept

Useful information on the possible irreducible representations of a group are shown in a character table.

The next section of the table (columns 2 through 5) has an entry for each operation of the group in each representation. These entries are called **characters**. The right section of the table (columns 6 through 8) shows several of the many possible bases for each representation. Column 6 shows bases in terms of the three Cartesian coordinates and rotations about the three axes. Column 8 shows the AOs on the oxygen atom that can be used as bases for the different representations; note that this column is not usually shown in character tables. It is shown here because we will work further with this set of **basis functions**. The information in this column can be inferred from the previous two columns as the p_x , p_y , and p_z AOs transform as x , y , and z , respectively. Similarly, the d_z^2 , d_{xy} , d_{yz} , $d_{x^2-y^2}$, and d_{xy} AOs transform as their subscript indices. The s AOs are a basis for A_1 because of their spherical symmetry. Next consider columns 6 and 7 in this section, which have entries based on the x , y , and z coordinates and rotations about the axes designated R_x , R_y , and R_z . We show later that the R_z rotation and the different coordinate combinations are bases for the indicated representations.

How can it be shown that the indicated functions are bases for the four irreducible representations? Equation (16.2) shows that the effect of any of the C_{2v} operators on the components x , y , and z of an arbitrary three-dimensional vector are $x \rightarrow \pm x$, $y \rightarrow \pm y$, and $z \rightarrow z$. Because z does not change sign under any of the operators, all characters for the representation have the value +1. Therefore, z is a basis for the A_1 representation. Similarly, because x^2 , y^2 , and z^2 do not change under any of the operations, these functions are also bases for the A_1 representation. Equation (16.2) also shows that the product $xy \rightarrow xy$ for \hat{E} and \hat{C}_2 and $xy \rightarrow -xy$ for $\hat{\sigma}_v$ and $\hat{\sigma}'_v$. Therefore, the product xy is a basis for the A_2 representation. Because z does not change sign under any operation, xz and yz transform as x and y . Therefore, Equation (16.2) shows that the functions x and xz are bases for the B_1 representation, and y and yz are bases for the B_2 representation.

Example Problem 16.1 demonstrated that in the operation R_z (C_2 in this case), $x \rightarrow -x$, $y \rightarrow -y$, and $z \rightarrow z$. Therefore, the product xy is unchanged because $xy \rightarrow (-x)(-y) = xy$. This shows that both R_z and xy are bases for the A_2 representation. We will not prove that R_x and R_y are bases for the B_1 and B_2 representations, but the procedure to do so is the same as for the other representations. As we saw in Section 16.3, the rotation operators are three-dimensional matrices. Therefore, in contrast to the coordinate bases, the rotation operators are bases for **reducible representations** because their dimension is greater than one.

As shown earlier, all irreducible representations of the C_{2v} group are one dimensional. However, it is useful to consider reducible representations for this group such as R_x , R_y , and R_z , all of which are three dimensional, to visualize how individual operators act on an arbitrary vector. Some of the groups discussed in this chapter also have irreducible representations whose dimensionality is two or three. Therefore, before we begin to work on problems of chemical interest using character tables, it is necessary to discuss the dimensionality of irreducible representations.

16.5 THE DIMENSION OF A REPRESENTATION

The bases for the different representations of the C_{2v} group include either x or y or z , but not a linear combination of two coordinates such as $x + y$. This is the case because under any transformation $(x, y, z) \rightarrow (x', y', z')$, x' is only a function of x as opposed to being a function of x and y or x and z or x , y , and z . Similar statements can be made for y' and z' . As a consequence, all of the matrices that describe the operators for the C_{2v} group have a diagonal form, as shown in Equation (16.3).

The matrix generated by two successive operations of diagonal matrices, which is denoted by $\hat{R}''' = \hat{R}'\hat{R}''$, is also a diagonal matrix whose elements are given by

$$\hat{R}_{ii}''' = \hat{R}'_{ii}\hat{R}''_{ii} \quad (16.5)$$

The **dimension of a representation** is defined as the size of the matrix used to represent the symmetry operations. As discussed earlier, the matrices of Equation (16.3) form a three-dimensional representation of the C_{2v} group. However, because all of the matrices are diagonal, the 3×3 matrix operations can be reduced to three 1×1 matrix

operations, which consist of the numbers +1 and -1. Therefore, the three-dimensional reducible representation of Equation (16.3) can be reduced to three one-dimensional representations.

Point groups can also have two-dimensional and three-dimensional irreducible representations. If x' and/or $y' = f(x, y)$ for a representation, then the basis will be (x, y) and the dimension of that irreducible representation is two. At least one of the matrices representing the operators will have the form

$$\begin{pmatrix} a & b & 0 \\ c & d & 0 \\ 0 & 0 & e \end{pmatrix}$$

in which entries a through e are in general nonzero. If x' and/or y' and/or $z' = f(x, y, z)$ the dimension of the representation is three and at least one of the operators will have the form

$$\begin{pmatrix} a & b & c \\ d & e & f \\ g & h & j \end{pmatrix}$$

in which entries a through j are in general nonzero.

How does one know how many irreducible representations a group has and what their dimension is? The following result of group theory is used to answer this question:

The dimension of the different irreducible representations, d_j , and the **order of the group**, h , defined as the number of symmetry elements in the group, are related by the equation

$$\sum_{j=1}^N d_j^2 = h \quad (16.6)$$

This sum is over the irreducible representations of the group.

Because every point group contains the one-dimensional totally symmetric representation, at least one of the $d_j = 1$. We apply this formula to the C_{2v} representations. This group has four elements, and all belong to different classes. Therefore, there are four different irreducible representations. The only set of nonzero integers that satisfies the equation

$$d_1^2 + d_2^2 + d_3^2 + d_4^2 = 4 \quad (16.7)$$

is $d_1 = d_2 = d_3 = d_4 = 1$. We conclude that all of the irreducible representations of the C_{2v} group are one dimensional. Because a 1×1 matrix cannot be reduced to one of lower dimensionality, all one-dimensional representations are irreducible.

For the C_{2v} group, the number of irreducible representations is equal to the number of elements and classes. More generally, the number of irreducible representations is equal to the number of classes for any group. Recall that all operators generated from a single symmetry element and successive applications of other operators of the group belong to the same class. For example, consider NF_3 , which belongs to the C_{3v} group. As shown in Example Problem 16.1, the C_3 and C_3^2 rotations of the C_{3v} group belong to the same class. The three σ_v mirror planes also belong to the same class because the second and third planes are generated from the first by applying \hat{C}_3 and \hat{C}_3^2 . Therefore, the C_{3v} group has six elements but only three classes.

We next show that the C_{3v} point group has one representation that is not one dimensional. Using the result from Example Problem 16.2, we see that the matrix that describes a 120° rotation is

$$\hat{C}_3 = \begin{pmatrix} \cos \theta & -\sin \theta & 0 \\ \sin \theta & \cos \theta & 0 \\ 0 & 0 & 1 \end{pmatrix} = \begin{pmatrix} -1/2 & -\sqrt{3}/2 & 0 \\ \sqrt{3}/2 & -1/2 & 0 \\ 0 & 0 & 1 \end{pmatrix} \quad (16.8)$$

The other operators in this group have a diagonal form. The \hat{C}_3 operator does not have a diagonal form, and \hat{C}_3 acting on the vector (x, y, z) mixes x and y . However, z' depends

Concept

Point groups can have one-, two- and three-dimensional irreducible representations.

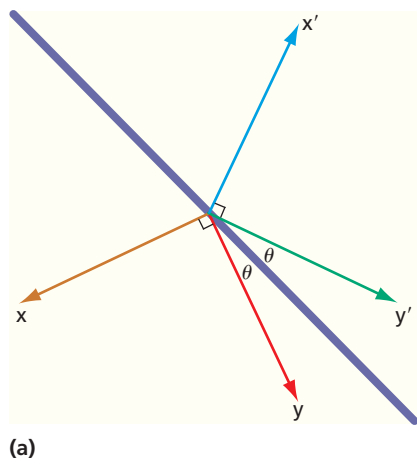
only on z and not on x or y . Therefore, it is possible to reduce the 3×3 matrix operator for \hat{C}_3 into separate irreducible 2×2 and 1×1 matrix operators. We conclude that the C_{3v} point group contains a two-dimensional irreducible representation. Example Problem 16.4 shows how to determine the number and dimension of the remaining irreducible representations for the C_{3v} group.

EXAMPLE PROBLEM 16.4

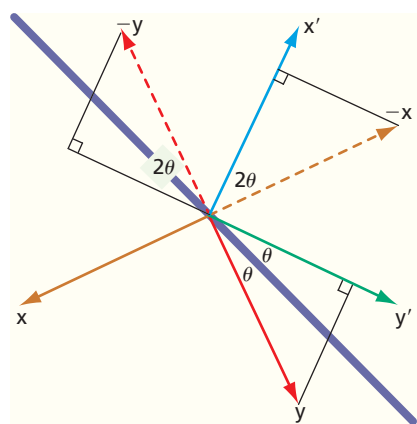
The C_{3v} group has the elements \hat{E} , \hat{C}_3 , and \hat{C}_3^2 and three σ_v mirror planes. How many different irreducible representations does this group have, and what is the dimensionality of each irreducible representation?

Solution

The order of the group is the number of elements, so $h = 6$. The number of representations is the number of classes. As discussed earlier, \hat{C}_3 and \hat{C}_3^2 belong to one class, and the same is true of the three σ_v reflections. Although the group has six elements, it has only three classes. Therefore, the group has three irreducible representations. The equation $l_1^2 + l_2^2 + l_3^2 = 6$ is solved to find the dimension of the representations, and one of the values must be 1. The only possible solution is $l_1 = l_2 = 1$ and $l_3 = 2$. We see that the C_{3v} group contains one two-dimensional representation and two one-dimensional representations.



(a)



(b)

Figure 16.6
Schematic depiction of the transformation of x - y coordinates effected by reflection through a mirror plane, σ , containing the z axis. (a) The x - y coordinate system for which the y axis is rotated by θ relative to the mirror plane is reflected through the mirror plane (purple line). This operation generates the x' - y' coordinate system. (b) The geometry used to derive Equation (16.9) is shown.

To gain practice in working with irreducible representations of more than one dimension, the matrices for the individual operations that describe the two-dimensional representation in the C_{3v} group are derived next. Example Problem 16.2 shows how to set up the matrices for rotation operators. Figure 16.6 shows how the x - y coordinate system is transformed by a mirror plane, σ .

The values x' and y' are related to x and y by

$$\begin{aligned} x' &= -x \cos 2\theta - y \sin 2\theta \\ y' &= -x \sin 2\theta + y \cos 2\theta \end{aligned} \quad (16.9)$$

Equation (16.9) is used to evaluate the 2×2 matrices for the mirror planes $\hat{\sigma}$, $\hat{\sigma}'$, and $\hat{\sigma}''$ at 0 , $\pi/3$, and $2\pi/3$, and Equation (16.1) is used to evaluate the 2×2 matrices for \hat{C}_3 and \hat{C}_3^2 . The resulting operators for the two-dimensional representation of the C_{3v} group are shown in Equation (16.10). Remember that $\hat{\sigma}$, $\hat{\sigma}'$, and $\hat{\sigma}''$ all belong to the one class, as do \hat{C}_3 and \hat{C}_3^2 .

$$\begin{aligned} \hat{E} &= \begin{pmatrix} 1 & 0 \\ 0 & 1 \end{pmatrix} \\ \hat{\sigma} &= \begin{pmatrix} -\cos 0 & -\sin 0 \\ -\sin 0 & \cos 0 \end{pmatrix} = \begin{pmatrix} -1 & 0 \\ 0 & 1 \end{pmatrix} \\ \hat{\sigma}' &= \begin{pmatrix} -\cos(2\pi/3) & -\sin(2\pi/3) \\ -\sin(2\pi/3) & \cos(2\pi/3) \end{pmatrix} = \begin{pmatrix} 1/2 & \sqrt{3}/2 \\ \sqrt{3}/2 & -1/2 \end{pmatrix} \\ \hat{\sigma}'' &= \begin{pmatrix} -\cos(4\pi/3) & -\sin(4\pi/3) \\ -\sin(4\pi/3) & \cos(4\pi/3) \end{pmatrix} = \begin{pmatrix} 1/2 & -\sqrt{3}/2 \\ -\sqrt{3}/2 & -1/2 \end{pmatrix} \\ \hat{C}_3 &= \begin{pmatrix} \cos(2\pi/3) & -\sin(2\pi/3) \\ \sin(2\pi/3) & \cos(2\pi/3) \end{pmatrix} = \begin{pmatrix} -1/2 & -\sqrt{3}/2 \\ \sqrt{3}/2 & -1/2 \end{pmatrix} \\ \hat{C}_3^2 &= \begin{pmatrix} \cos(4\pi/3) & -\sin(4\pi/3) \\ \sin(4\pi/3) & \cos(4\pi/3) \end{pmatrix} = \begin{pmatrix} -1/2 & \sqrt{3}/2 \\ -\sqrt{3}/2 & -1/2 \end{pmatrix} \end{aligned} \quad (16.10)$$

How is the character table for the C_{3v} group constructed? In particular, how are characters assigned to the two-dimensional representation, which is generally called E ?

(Do not confuse this symbol for a two-dimensional representation with the operator \hat{E} .)

The following theorem of group theory is used:

Concept

The character for an operator in a representation of dimension greater than one is given by the sum of the diagonal elements of the matrix.

The character for an operator in a representation of dimension greater than one is given by the sum of the diagonal elements of the matrix.

Using this rule, we see that the character of $\hat{\sigma}$, $\hat{\sigma}'$, and $\hat{\sigma}''$ is 0 and that the character of \hat{C}_3 and \hat{C}_3^2 is -1 . As expected, the character of all elements in a class is the same. Recall also that every group has a totally symmetric representation in which all characters are $+1$.

Because the C_{3v} group contains three classes, it must have three irreducible representations. We enter the information that we obtained earlier for A_1 and E in the following partially completed character table. All of the symmetry operators of a class are grouped together in a character table. For example, in the following listing, the elements C_3 and C_3^2 are listed as $2C_3$ to make the notation compact.

	E	$2C_3$	$3\sigma_v$
A_1	1	1	1
?	a	b	c
E	2	-1	0

The characters a , b , and c can be obtained as shown in Example Problem 16.5. We use another result from group theory:

If the set of characters associated with a representation of the group is viewed as a vector, $\Gamma_i = \chi_i(\hat{R}_j)$, with one component for each element of the group, the following condition holds:

$$\Gamma_i \Gamma_k = \sum_{j=1}^h \chi_i(\hat{R}_j) \chi_k(\hat{R}_j) = h \delta_{ik}, \quad \text{where } \delta_{ik} = 0 \text{ if } i \neq k \text{ and } 1 \text{ if } i = k \quad (16.11)$$

Or, equivalently, $\Gamma_i \Gamma_k = \chi_i(\hat{R}_j) \cdot \chi_k(\hat{R}_j) = h \delta_{ik}$. The sum is over all elements of the group.

EXAMPLE PROBLEM 16.5

Determine the unknown coefficients a , b , and c for the preceding partially completed character table and assign the appropriate symbol to the irreducible representation.

Solution

From Example Problem 16.4, we know that the unknown representation is one dimensional. From Equation (16.11), we know that the $\chi_i(\hat{R}_j)$ for different values of the index i are orthogonal. Therefore,

$$\begin{aligned} \chi_? \cdot \chi_{A_1} &= a + b + b + c + c + c = a + 2b + 3c = 0 \\ \chi_? \cdot \chi_E &= 2a - b - b = 2a - 2b = 0 \end{aligned}$$

We could also have taken the sum over classes and multiplied each term by the number of elements in the class, because all elements in a class have the same character. We also know that $a = 1$ because it is the character of the identity operator. Solving the equations gives the results of $b = 1$ and $c = -1$. Because the character of C_3 is $+1$, and the character of σ_v is -1 , the unknown representation is designated A_2 . Table 16.4 shows the completed C_{3v} character table.

Note that the two-dimensional basis functions occur in pairs. You will be asked to verify that z and R_z are bases for the A_1 and A_2 representations, respectively, in the end-of-chapter problems.

TABLE 16.4 The C_{3v} Character Table

	E	$2C_3$	$3\sigma_v$		
A_1	1	1	1	z	$x^2 + y^2, z^2$
A_2	1	1	-1	R_z	
E	2	-1	0	$(x, y), (R_x, R_y)$	$(x^2 - y^2, xy), (xz, yz)$

16.6 USING THE C_{2v} REPRESENTATIONS TO CONSTRUCT MOLECULAR ORBITALS FOR H_2O

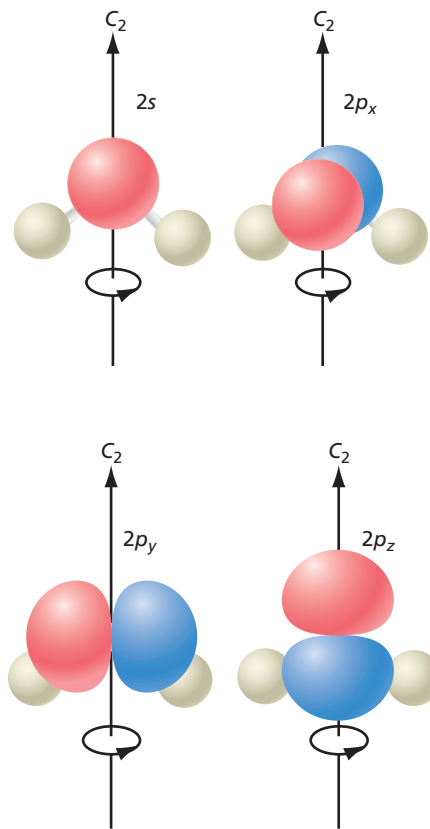


Figure 16.7

Depiction of the oxygen atomic orbitals that will be considered as contributors to the molecular orbital formed using $\phi_+ = \phi_{H1sA} + \phi_{H1sB}$.

Concept

Symmetry-adapted MOs are of central importance in quantum chemistry.

A number of aspects of group theory have been discussed in the preceding sections. In particular, the structure of character tables, which for chemists are the most important result of group theory, has been explained. We now illustrate the usefulness of character tables to solve a problem of chemical interest, namely, the construction of MOs that incorporate the symmetry of a molecule. Why is this necessary?

To answer this question, consider the relationship among the total energy operator, the molecular wave functions ψ_j , and the symmetry of the molecule. A molecule that has undergone one of its symmetry operations, \hat{A} , is indistinguishable from the original molecule. Therefore, \hat{H} must also be unchanged under this and any other symmetry operation of the group because the total energy of the molecule is the same in any of its equivalent positions. If this is the case, then \hat{H} belongs to the totally symmetric representation.

Because the order of applying \hat{H} and \hat{A} to the molecule is immaterial, it follows that \hat{H} and \hat{A} commute. Therefore, as discussed in Chapter 6, eigenfunctions of \hat{H} can be found that are simultaneously eigenfunctions of \hat{A} and of all other operators of the group. These **symmetry-adapted MOs** are of central importance in quantum chemistry. In this section, we illustrate how to generate symmetry-adapted MOs from AOs. Not all AOs contribute to a particular symmetry-adapted MO. Invoking the symmetry of a molecule produces a set of MOs consisting of fewer AOs than would have been obtained had the molecular symmetry been neglected.

Consider a specific example. Which of the AOs on oxygen contribute to the symmetry-adapted MOs on water? We begin by asking which of the four oxygen valence AOs can be combined with the hydrogen AOs to form symmetry-adapted MOs. All possible combinations are shown in Figure 16.7. In order to take the symmetry of the water molecule into account, the hydrogen AOs will appear as in-phase or out-of-phase combinations. Consider first the in-phase combination, $\phi_+ = \phi_{H1sA} + \phi_{H1sB}$.

The overlap integral S_{+j} between the orbital ϕ_+ and an oxygen ϕ_j is defined by

$$S_{+j} = \int \phi_+^* \phi_j \, d\tau \quad (16.12)$$

Only the oxygen AOs that have a nonzero overlap with the hydrogen AOs are useful in forming chemical bonds. Because S_{+j} is just a number, it cannot change upon applying any of the operators of the C_{2v} group to the integral. In other words, S_{+j} belongs to the A_1 representation. The same must be true of the integrand; therefore, the integrand must also belong to the A_1 representation. If ϕ_+ belongs to one representation and ϕ_j belongs to another, what can be concluded about the symmetry of the direct product $\phi_+ \cdot \phi_j$? A result of group theory is used to answer this question:

The character for an operator \hat{R} (\hat{E} , \hat{C}_2 , $\hat{\sigma}_v$, or $\hat{\sigma}'_v$ for the C_{2v} group) of the direct product of two representations is given by

$$\chi_{product}(\hat{R}) = \chi_i(\hat{R}) \chi_j(\hat{R}) \quad (16.13)$$

For example, if ϕ_+ belongs to A_2 , and ϕ_j belongs to B_2 , $\Gamma_{product}$ can be calculated from the $\chi_{product}$ terms as follows:

$$\begin{aligned}\Gamma_{product} &= \chi_{A_2} \cdot \chi_{B_2} = [1 \times 1 \quad 1 \times (-1) \quad (-1) \times (-1) \quad (-1) \times 1] \\ &= (1 \quad -1 \quad 1 \quad -1)\end{aligned}\quad (16.14)$$

Looking at the C_{2v} character table, we can see that the direct product $A_2 \cdot B_2$ belongs to B_1 .

How is this result useful in deciding which of the oxygen AOs contribute to the symmetry-adapted water MOs? Because the integrand must belong to the A_1 representation, each character of the representation of $\phi_+^* \phi_j$ must be equal to one. We thus conclude that

$$\sum_{k=1}^h \chi_+(\hat{R}_k) \chi_j(\hat{R}_k) = h \quad (16.15)$$

However, according to Equation (16.11), this equation is never satisfied if the two representations to which the orbitals belong, denoted + and j , are different. We conclude that *the overlap integral between two combinations of AOs is nonzero only if the combinations belong to the same representation.*

Using this result, which of the oxygen AOs in Figure 16.7 form symmetry-adapted MOs with the combination $\phi_+ = \phi_{H1sA} + \phi_{H1sB}$? The orbital ϕ_+ is unchanged by any of the symmetry operators, so it must belong to the A_1 representation. The $2s$ AO on oxygen is spherically symmetrical, so that it transforms as $x^2 + y^2 + z^2$. As the C_{2v} character table shows, the $2s$ AO belongs to the A_1 representation, as does the $2p_z$ orbital. By contrast, the $2p_x$ and $2p_y$ AOs on oxygen belong to the B_1 and B_2 representations, respectively. Therefore, only the oxygen $2s$ and $2p_z$ AOs belong to the same irreducible representation as ϕ_+ , and only these AOs will contribute to MOs involving ϕ_+ . The AOs on the hydrogen atoms can be combined in the symmetric, $\phi_+ = \phi_{H1sA} + \phi_{H1sB}$, and antisymmetric, $\phi_- = \phi_{H1sA} - \phi_{H1sB}$, forms, as shown in Figure 16.8. The combinations of the $2s$ AO and $2p_z$ oxygen AO with $\phi_+ = \phi_{H1sA} + \phi_{H1sB}$ result in the $1a_1$, the $2a_1$, and the $3a_1$, MOs for water shown in Figure 16.9. We now have an explanation for the nomenclature introduced in Figures (14.6) and (14.7) for the symmetry-adapted water MOs. The term a_1 refers to the particular irreducible representation of the C_{2v} group, and the integer 1, 2, . . . , refers to the lowest, next lowest, . . . , energy MO belonging to the A_1 representation.

Concept

The overlap integral between two combinations of AOs is nonzero only if the combinations belong to the same representation.

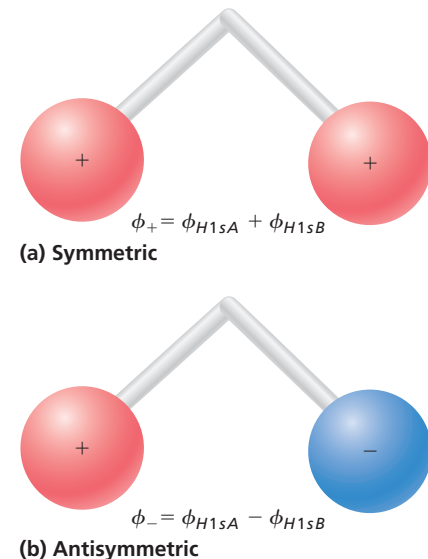


Figure 16.8

Combinations of atomic orbitals on hydrogen atoms. The figures show the (a) symmetric and (b) antisymmetric combinations.

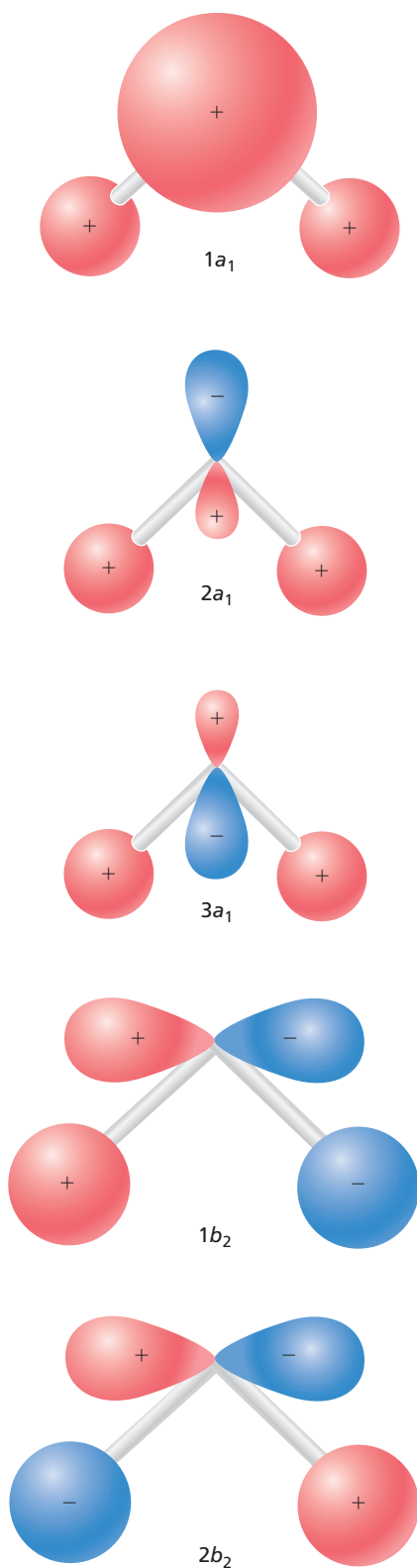
EXAMPLE PROBLEM 16.6

Which of the oxygen AOs shown in Figure 16.7 will participate in forming symmetry-adapted water MOs with the antisymmetric combination of hydrogen AOs defined by $\phi_- = \phi_{H1sA} - \phi_{H1sB}$?

Solution

The antisymmetric combination of the H AOs is given by $\phi_- = \phi_{H1sA} - \phi_{H1sB}$, shown in Figure 16.8b. By considering the C_{2v} operations shown in Figure 16.4, convince yourself that the characters for the different operations are $\hat{E}:+1$, $\hat{C}_2:-1$, $\hat{C}_v:-1$, and $\hat{\sigma}_v':+1$. Therefore, ϕ_- belongs to the B_2 representation. Of the valence oxygen AOs, only the $2p_y$ orbital belongs to the B_2 representation. Therefore, the only symmetry adapted MOs formed from ϕ_- and the $2s$ and $2p$ orbitals that have a nonzero overlap among the AOs are the MOs denoted $1b_2$ and $2b_2$, which are shown in Figure 16.9. This nomenclature indicates that they are the lowest and next lowest energy MOs of B_2 symmetry.

We now make an important generalization of the result just obtained. The same symmetry considerations used for the overlap integral apply in evaluating integrals of the type $H_{ab} = \int \psi_a^* \hat{H} \psi_b d\tau$. As shown in Chapters 12 and 13, such integrals appear whenever the total energy is calculated. The value of H_{ab} is zero unless $\psi_a^* \hat{H} \psi_b$ belongs to the A_1 representation. Because \hat{H} belongs to the A_1 representation, H_{ab} will be zero unless ψ_a and ψ_b belong to the same representation (not necessarily the A_1 representation). Only then will the integrand $\psi_a^* \hat{H} \psi_b$ contain the A_1 representation. This important result is of great help in evaluating entries in a secular determinant such as those encountered in Chapter 12.

**Figure 16.9**

Water molecular orbitals formed from the symmetric and antisymmetric combinations of the hydrogen atomic orbitals.

In the preceding discussion, symmetry-adapted MOs for H₂O were generated from AOs that belong to the different irreducible representations of the C_{2v} group in an ad hoc manner. In Supplemental Section 16.9, we will discuss a powerful method, called the projection operator method, that allows the symmetry-adapted MOs to be constructed for arbitrary molecules.

16.7 SYMMETRIES OF THE NORMAL MODES OF VIBRATION OF MOLECULES

The vibrational motions of individual atoms in a molecule might appear to be chaotic and independent of one another. However, the selection rules for infrared vibrational and Raman spectroscopy are characteristic of the normal modes of a molecule, which can be described in the following way. In a normal mode vibration, each atom is displaced from its equilibrium position by a vector that can (but is not restricted to) lie along the bond direction (for example, in a bending mode). The directions and magnitudes of the displacements are not the same for all atoms. The following points summarize the motion of atoms in the normal modes:

- During a vibrational period, the center of mass of the molecule remains fixed and all atoms in the molecule undergo in-phase periodic motion about their equilibrium positions.
- All atoms in a molecule reach their minimum and maximum amplitudes at the same time.
- These collective motions are called **normal modes**, and the frequencies are called the **normal mode frequencies**.
- The frequencies measured in vibrational spectroscopy are the normal mode frequencies.
- All normal modes are independent in the harmonic approximation, meaning that excitation of one normal mode does not transfer vibrational energy into another normal mode.
- Any seemingly random motion of the atoms in a molecule can be expressed as a linear combination of the normal modes of that molecule.

How many normal modes does a molecule have? An isolated atom has three translational degrees of freedom; therefore, a molecule consisting of n atoms has $3n$ degrees of freedom. Three of these are translations of the molecule and are not of interest here. A nonlinear molecule with n atoms has three degrees of rotational freedom, and the remaining $3n - 6$ internal degrees of freedom correspond to normal modes of vibration. Because a linear molecule has only two degrees of rotational freedom, it has $3n - 5$ normal modes of vibration. For a diatomic molecule, there is only one vibrational mode, and the motion of the atoms is directed along the bond. In the harmonic approximation,

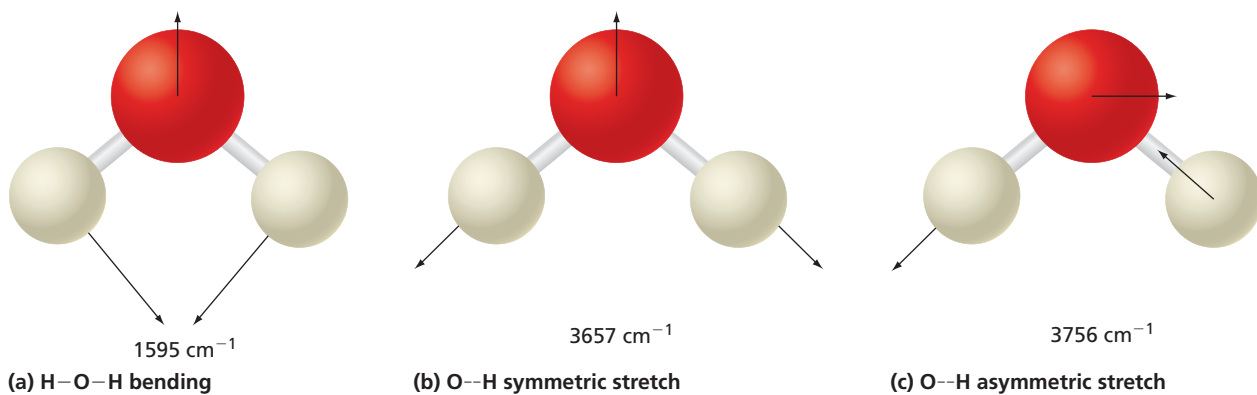
$$V(x) = \frac{1}{2}kx^2 = \frac{1}{2}\left(\frac{d^2V}{dx^2}\right)x^2$$

where x is the displacement from the equilibrium position in the center of mass coordinates. For a molecule with N vibrational degrees of freedom, the potential energy is given by

$$V(q_1, q_2, \dots, q_N) = \frac{1}{2}\sum_{i=1}^N \sum_{j=1}^N \frac{\partial^2 V}{\partial q_i \partial q_j} q_i q_j \quad (16.16)$$

where each q_i designates an individual normal mode displacement. Classical mechanics allows us to find a new set of vibrational coordinates $Q_j(q_1, q_2, \dots, q_N)$ that simplify Equation (16.16) to the form

$$V(Q_1, Q_2, \dots, Q_N) = \frac{1}{2}\sum_{i=1}^N \left(\frac{\partial^2 V}{\partial Q_i^2}\right) Q_i^2 \quad (16.17)$$

**Figure 16.10**

The normal modes of H_2O are depicted, with the vectors indicating atomic displacements (not to scale). Experimentally observed frequencies are indicated below each diagram.

The $Q_j(q_1, q_2, \dots, q_N)$ are known as the **normal coordinates** of the molecule. This transformation has significant advantages in describing vibrational motion. Because there are no cross terms of the type $Q_i Q_j$ in the potential energy, the vibrational modes are independent in the harmonic approximation, meaning that

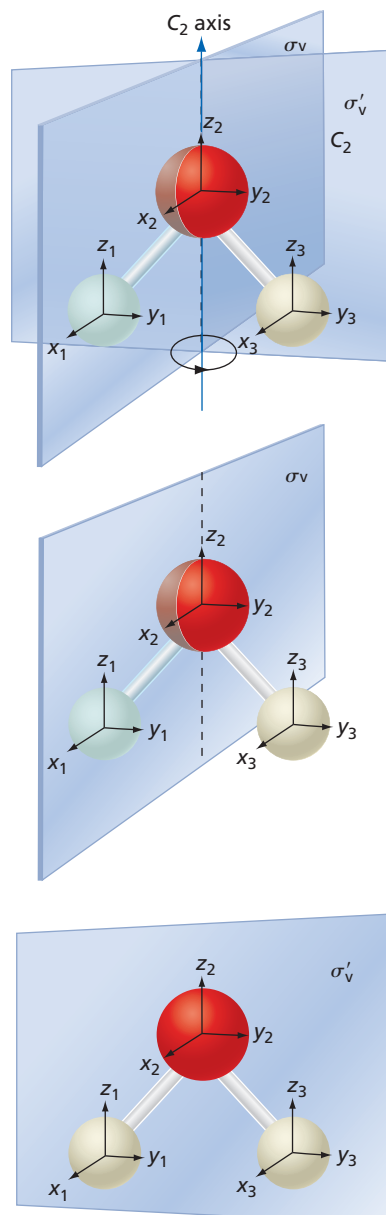
$$\psi_{vibrational}(Q_1, Q_2, \dots, Q_N) = \psi_1(Q_1)\psi_2(Q_2)\dots\psi_N(Q_N) \quad \text{and} \\ E_{vibrational} = \sum_{i=1}^N \left(n_i + \frac{1}{2} \right) \hbar \nu_i \quad (16.18)$$

Because of the transformation to normal coordinates, each of the normal modes contributes independently to the energy, and the vibrational motions of different normal modes are not coupled, consistent with the properties in the first paragraph of this section. Finding the normal modes is a nontrivial but straightforward exercise that can be done most easily using numerical methods. The calculated normal modes of H_2O are shown in Figure 16.10. The arrows show the displacement of each atom at a given time. After half the vibrational period, each arrow has the same magnitude, but the direction is opposite to that shown in the figure. We will not carry out a normal mode calculation but will instead focus on the symmetry properties of the normal modes.

Just as the $2p$ atomic orbitals on the oxygen atom belong to individual representations of the C_{2v} group, the normal modes of a molecule belong to individual representations. The next task is to identify the symmetry of the three different normal modes of H_2O . To do so, a coordinate system is set up at each atom and a matrix representation formed that is based on the nine x , y , and z coordinates of the atoms in the molecule. Figure 16.11 illustrates the geometry under consideration.

Consider the C_2 operation. By visualizing the motion of the coordinate systems on the three atoms, convince yourself that the individual coordinates are transformed as follows under this operation.

$$\begin{pmatrix} x_1 \\ y_1 \\ z_1 \\ x_2 \\ y_2 \\ z_2 \\ x_3 \\ y_3 \\ z_3 \end{pmatrix} \Rightarrow \begin{pmatrix} -x_3 \\ -y_3 \\ z_3 \\ -x_2 \\ -y_2 \\ z_2 \\ -x_1 \\ -y_1 \\ z_1 \end{pmatrix} \quad (16.19)$$

**Figure 16.11**

Transformations of coordinate systems centered on the atoms in water. Each coordinate system is considered a separate entity under symmetry operations of the C_{2v} group.

You can also convince yourself that the 9×9 matrix that describes this transformation is

$$\hat{C}_2 = \begin{pmatrix} 0 & 0 & 0 & 0 & 0 & 0 & -1 & 0 & 0 \\ 0 & 0 & 0 & 0 & 0 & 0 & 0 & -1 & 0 \\ 0 & 0 & 0 & 0 & 0 & 0 & 0 & 0 & 1 \\ 0 & 0 & 0 & -1 & 0 & 0 & 0 & 0 & 0 \\ 0 & 0 & 0 & 0 & -1 & 0 & 0 & 0 & 0 \\ 0 & 0 & 0 & 0 & 0 & 1 & 0 & 0 & 0 \\ -1 & 0 & 0 & 0 & 0 & 0 & 0 & 0 & 0 \\ 0 & -1 & 0 & 0 & 0 & 0 & 0 & 0 & 0 \\ 0 & 0 & 1 & 0 & 0 & 0 & 0 & 0 & 0 \end{pmatrix} \quad (16.20)$$

Note that this matrix has a simple structure. It consists of identical 3×3 subunits shown in boxes. More importantly, the diagonal elements of the subunits lie along the diagonal of the 9×9 matrix only if the atom is not shifted to another position through the transformation. Because H atoms 1 and 3 exchange places under the C_2 operation, they do not contribute to the character of the operator, which is the sum of the diagonal elements of the matrix. This result leads to the following guidelines for calculating the character of each element of the group in the 9×9 matrix representation:

- If the atom remains in the same position under the transformation and the sign of x , y , or z is not changed, the value +1 is associated with each unchanged coordinate.
- If the sign of x , y , or z is changed, the value -1 is associated with each changed coordinate.
- If the coordinate system is exchanged with the position of another coordinate system, the value zero is associated with each of the three coordinates.
- Recall that only the diagonal elements contribute to the character. Therefore, only atoms that are not shifted by an operation contribute to the character.

This procedure is applied to the water molecule. Because nothing changes under the E operation, the character of \hat{E} is 9. Under the rotation of 180° , the two H atoms are interchanged, so that none of the six coordinates contributes to the character of the \hat{C}_2 operator. On the oxygen atom, $x \rightarrow -x$, $y \rightarrow -y$, and $z \rightarrow z$. Therefore, the character of \hat{C}_2 is -1. For the $\hat{\sigma}_v$ operation, the H atoms are again interchanged so that they do not contribute to the character of $\hat{\sigma}_v$. On the oxygen atom, $x \rightarrow x$, $y \rightarrow -y$, and $z \rightarrow z$. Therefore, the character of $\hat{\sigma}_v$ is +1. For the $\hat{\sigma}'_v$ operation, on the H atoms, $x \rightarrow -x$, $y \rightarrow y$, and $z \rightarrow z$, so that the two H atoms contribute 2 to the $\hat{\sigma}'_v$ character. On the oxygen atom, $x \rightarrow -x$, $y \rightarrow y$, and $z \rightarrow z$ so that the O atom contributes +1 to the $\hat{\sigma}'_v$ character. Therefore, the total character of $\hat{\sigma}'_v$ is +3. These considerations show that the reducible representation formed using the coordinate systems on the three atoms as a basis is

$$\begin{array}{cccc} E & C_2 & \sigma_v & \sigma'_v \\ \hline 9 & -1 & 1 & 3 \end{array} \quad (16.21)$$

This is a reducible representation because it is a nine-dimensional representation, whereas all irreducible representations of the C_{2v} group are one dimensional. To use this result to characterize the symmetry of the normal modes of water, it is necessary to decompose this reducible representation into the irreducible representations that it contains, as follows:

The general method for decomposing a reducible representation into its irreducible representations utilizes the vector properties of the representations introduced in Section 16.3. Take the scalar product between the reducible representation $\Gamma_{\text{reducible}}(\hat{R}_j)$ and each of the irreducible representations $\Gamma_i(\hat{R}_j)$ in turn, and divide by the order of the group. The result of this procedure is a positive

integer n_i that is the number of times each representation appears in the irreducible representation. This statement is expressed by the equation

$$n_i = \frac{1}{h} \Gamma_i \Gamma_{reducible} = \frac{1}{h} \chi_i(\hat{R}_j) \cdot \chi_{reducible}(\hat{R}_j) = \frac{1}{h} \sum_{j=1}^h \chi_i(\hat{R}_j) \chi_{reducible}(\hat{R}_j),$$

for $i = 1, 2, \dots, N$ (16.22)

We calculate the contribution of the individual irreducible representations to this reducible presentation using Equation (16.22):

$$\begin{aligned} n_{A_1} &= \frac{1}{h} \sum_{j=1}^h \chi_{A_1}(\hat{R}_j) \chi_{reducible}(\hat{R}_j) = \frac{1 \times 9 + 1 \times (-1) + 1 \times 1 + 1 \times 3}{4} = 3 \\ n_{A_2} &= \frac{1}{h} \sum_{j=1}^h \chi_{A_2}(\hat{R}_j) \chi_{reducible}(\hat{R}_j) = \frac{1 \times 9 + 1 \times (-1) + (-1) \times 1 + (-1) \times 3}{4} = 1 \\ n_{B_1} &= \frac{1}{h} \sum_{j=1}^h \chi_{B_1}(\hat{R}_j) \chi_{reducible}(\hat{R}_j) = \frac{1 \times 9 + (-1) \times (-1) + 1 \times 1 + (-1) \times 3}{4} = 2 \\ n_{B_2} &= \frac{1}{h} \sum_{j=1}^h \chi_{B_2}(\hat{R}_j) \chi_{reducible}(\hat{R}_j) = \frac{1 \times 9 + (-1) \times (-1) + (-1) \times 1 + 1 \times 3}{4} = 3 \end{aligned} \quad (16.23)$$

This calculation shows that $\Gamma_{reducible} = 3A_1 + A_2 + 2B_1 + 3B_2$. However, not all of these representations describe vibrational normal modes. The translation of the molecules along the x , y , and z axes as well as their rotation about the same axes must be separated out to obtain the representations of the vibrational normal modes. This can be done by subtracting the representations belonging to x , y , and z as well as to R_x , R_y , and R_z . Representations for these degrees of freedom can be determined from the C_{2v} character table. Eliminating them gives the representations of the three vibrational modes as

$$\begin{aligned} \Gamma_{reducible} &= 3A_1 + A_2 + 2B_1 + 3B_2 - (B_1 + B_2 + A_1) - (B_2 + B_1 + A_2) \\ &= 2A_1 + B_2 \end{aligned} \quad (16.24)$$

This calculation has shown that the symmetry of the H_2O molecule dictates the symmetry of the normal modes. Of the three normal modes, one belongs to B_2 and two belong to A_1 . The normal mode calculations outlined here give the modes shown in Figure 16.10.

How can these modes be assigned to different irreducible representations of the C_{2v} group? The arrows on each atom in Figure 16.10 show the direction and magnitude of the displacement at a given time. All displacement vectors are reversed after half a period. If the set of displacement vectors is to be a basis for a representation, they must transform as the characters of the particular representation. Consider first the 1595-cm^{-1} normal mode. The direction and magnitude of each vector are unaffected by each of the operations E , C_2 , σ_v , and $\hat{\sigma}'_v$. Therefore, this mode must belong to the A_1 representation. The same is true of the 3657-cm^{-1} normal mode. By contrast, the displacement vector on the O atom is reversed upon carrying out the C_2 operation for the 3756-cm^{-1} normal mode. Because the H atoms are interchanged, their displacement vectors do not contribute to the character of the C_2 operation, which is -1 . Therefore, this mode must belong to either the B_1 or B_2 representations. Which of these is appropriate can be decided by examining the effect of the $\hat{\sigma}'_v$ operation on the individual displacement vectors. Because the vectors lie in the mirror plane, they are unchanged in the reflection, corresponding to a character of $+1$. Therefore, the 3756-cm^{-1} normal mode belongs to the B_2 representation.

The water molecule is small enough that the procedure described can be carried out without a great deal of effort. For larger molecules, the effort is significantly greater, but the normal modes and the irreducible representations to which they belong can be calculated using widely available quantum chemistry software. Many of these programs allow an animation of the vibration to be displayed, which is helpful in assigning

Concept

The normal modes of vibration for a molecule belong to different irreducible representations of the point group corresponding to the molecule.

the dominant motion to a stretch or a bend. Normal mode animations for several molecules are explored in the Web-based problems of Chapter 8 and in the computational problems for Chapter 13.

16.8 SELECTION RULES AND INFRARED VERSUS RAMAN ACTIVITY

We next show that the selection rule for infrared absorption spectroscopy, $\Delta n = +1$, can be derived using group theory. More importantly, we show that for allowed transitions, $\Gamma_{\text{reducible}}$ as calculated in the previous section must contain the A_1 representation. As discussed in Section 8.3, for most molecules, only the $n = 0$ vibrational state is populated to a significant extent at 300 K. The molecule can be excited to a state with $n_j > 0$ through the absorption of infrared energy if the dipole matrix element satisfies the condition given by

$$\mu_{Q_j}^{m \leftarrow 0} = \left(\frac{\partial \mu}{\partial Q_j} \right) \int \psi_m^*(Q_j) \hat{\mu}(Q_j) \psi_0(Q_j) dQ_j \neq 0,$$

where $j = \text{one of } 1, 2, \dots, 3N - 6$ (16.25)

We have modified Equation (8.6), which is applicable to a diatomic molecule, to the more general case of a polyatomic molecule and expressed the position variable in terms of the normal coordinate. To simplify the mathematics, the electric field is oriented along the normal coordinate. From Chapter 7, ψ_0 , ψ_1 , and ψ_2 are given by

$$\begin{aligned} \psi_0(Q_j) &= \left(\frac{\alpha_j}{\pi} \right)^{1/4} e^{-(\alpha_j Q_j^2)/2} \\ \psi_1(Q_j) &= \left(\frac{4\alpha_j^3}{\pi} \right)^{1/4} Q_j e^{-(\alpha_j Q_j^2)/2} \\ \psi_2(Q_j) &= \left(\frac{\alpha_j}{4\pi} \right)^{1/4} (2\alpha_j Q_j^2 - 1) e^{-(\alpha_j Q_j^2)/2} \end{aligned} \quad (16.26)$$

and the dipole moment operator is given by

$$\hat{\mu}(Q_j) = \mu_e + \left[\left(\frac{\partial \mu}{\partial Q_j} \right) Q_j + \dots \right]$$

where μ_e is the static dipole moment. Higher terms are neglected in the harmonic approximation.

For what final states ψ_f will Equation (16.25) for the transition dipole moment be satisfied? Section 16.6 demonstrated that for the integral to be nonzero, the integrand $\psi_m^*(Q_j) \mu(Q_j) \psi_0(Q_j)$ must belong to the A_1 representation. The C_{2v} character table shows that Q_j^2 is a basis for this representation, so the integrand must be a function of Q_j^2 only. We know that ψ_0 is an even function of Q_j , $\psi_0(Q_j) = \psi_0(-Q_j)$ and that μ is an odd function of Q_j , $\mu(Q_j) = -\mu(-Q_j)$. Under what condition will the integrand be an even function of Q_j ? It will be an even function only if ψ_m^* is an odd function of Q_j , $\psi_m^*(Q_j) = f(Q_j)$. Because of this restriction, $n = 0 \rightarrow n = 1$ is an allowed transition, but $n = 0 \rightarrow n = 2$ is not allowed in the dipole approximation. This same conclusion was reached in Section 8.4, using a different line of reasoning.

Concept

For a normal mode to be infrared active, it must have x , y , or z as a basis.

Concept

For a normal mode to be Raman active, it must have x^2 , y^2 , z^2 , xy , yz , or xz as a basis.

The preceding discussion addressed the selection rule but not the symmetry requirements for the normal modes that satisfy Equation (16.25). Because $\hat{\mu}(Q_j) = f(Q_j)$ transforms as x , y , or z and $\psi_0(Q_j) = f(Q_j^2)$ transform as x^2 , y^2 , or z^2 , $\psi_m(Q_j)$ must transform as x , y , or z , in order for $\psi_m^*(Q_j) \mu(Q_j) \psi_0(Q_j)$ to transform as x^2 , y^2 , or z^2 . This provides the requirement that a normal mode is infrared active; it must have x , y , or z as a basis. For H_2O , this means that the normal modes must belong to A_1 , B_1 , or B_2 . Because, as shown in Equation (16.24), the three normal modes belong to A_1 and B_2 , we conclude that all are infrared active. As discussed in more advanced textbooks, normal modes of a molecule are Raman active if the bases of the representation to which the normal mode belongs are the x^2 , y^2 , z^2 , xy , yz , or xz functions. By looking

at the C_{2v} character table, we can see that all three normal modes of water are Raman active. It is not generally the case that all normal modes are both infrared and Raman active for a molecule.

Based on this discussion, recall the infrared absorption spectrum for CH_4 shown in Figure 8.10. Although CH_4 has $3n - 6 = 9$ normal modes, only two peaks are observed. Methane belongs to the T_d point group, and an analysis equivalent to that which led to Equation (16.24) shows that

$$\Gamma_{\text{reducible}} = A_1 + E + 2T_2 \quad (16.27)$$

The dimensions of the representations are one for A_1 , two for E , and three for T_2 . Therefore, all nine normal modes are accounted for. An examination of the character table for the T_d group shows that only the T_2 representations have x , y , or z as a basis. Therefore, only six of the nine normal modes of methane are infrared active. Why are only two peaks observed in the spectrum? The following result of group theory is used:

All normal modes that belong to a particular representation have the same frequency.

Concept

All normal modes that belong to a particular representation have the same frequency.

Therefore, each of the T_2 representations has three degenerate vibrational frequencies. For this reason, only two vibrational frequencies are observed in the infrared absorption spectrum of CH_4 shown in Figure 8.10. However, each frequency corresponds to three distinct but degenerate normal modes.

SUPPLEMENTAL SECTION

16.9 USING THE PROJECTION OPERATOR METHOD TO GENERATE MOs THAT ARE BASES FOR IRREDUCIBLE REPRESENTATIONS

In Section 16.6, symmetry-adapted MOs for H_2O were generated from AOs that belong to the different irreducible representations of the C_{2v} group in an ad hoc manner. We next discuss a powerful method, called the **projection operator method**, that allows the same end to be achieved for arbitrary molecules. The method is applied to ethene, which belongs to the D_{2h} point group.

The symmetry elements for ethene and the D_{2h} character table are shown in Table 16.5 and Figure 16.12. Aside from the identity element, the group contains three C_2 axes and three mirror planes, all of which form separate classes, as well as an inversion center. Irreducible representations in groups with an inversion center have the subscript g or u denoting that they are symmetric (+1) or antisymmetric (-1) with respect to the inversion center.

Concept

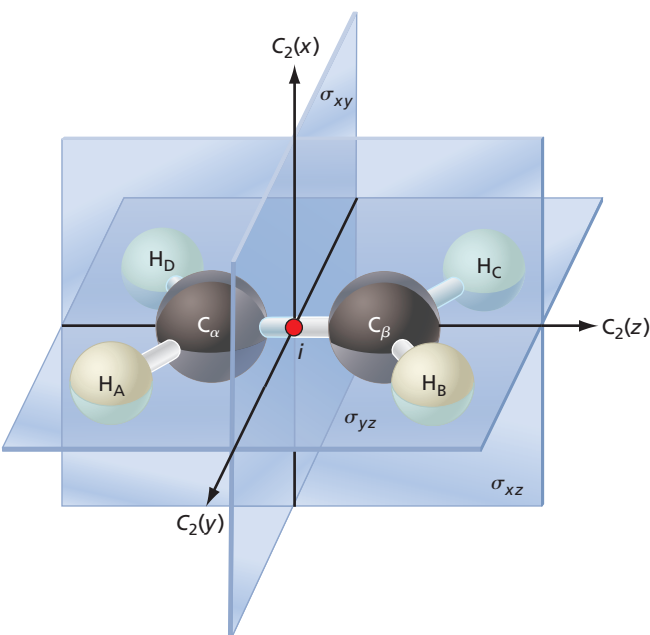
The projection operator method can be used to generate MOs that are bases for irreducible representations.

TABLE 16.5 Character Table for the D_{2h} Point Group

	E	$C_2(z)$	$C_2(y)$	$C_2(x)$	i	$\sigma(xy)$	$\sigma(xz)$	$\sigma(yz)$	
A_g	1	1	1	1	1	1	1	1	x^2, y^2, z^2
B_{1g}	1	1	-1	-1	1	1	-1	-1	R_z xy
B_{2g}	1	-1	1	-1	1	-1	1	-1	R_y xz
B_{3g}	1	-1	-1	1	1	-1	-1	1	R_x yz
A_u	1	1	1	1	-1	-1	-1	-1	
B_{1u}	1	1	-1	-1	-1	-1	1	1	z
B_{2u}	1	-1	1	-1	-1	1	-1	1	y
B_{3u}	1	-1	-1	1	-1	1	1	-1	x

Figure 16.12

Symmetry elements of D_{2h} group shown for ethene. The symbol i at the intersection of the C_2 axes indicates the inversion center. The molecule lies in the yz plane.



Next consider how the individual H atoms are affected by the symmetry operations of the group. Convince yourself that the result of applying a symmetry operation to the molecule shifts the atom H_A as listed here:

\hat{E}	$\hat{C}_2(z)$	$\hat{C}_2(y)$	$\hat{C}_2(x)$
$H_A \rightarrow H_A$	$H_A \rightarrow H_D$	$H_A \rightarrow H_B$	$H_A \rightarrow H_C$
\hat{i}	$\hat{\sigma}(xy)$	$\hat{\sigma}(xz)$	$\hat{\sigma}(yz)$
$H_A \rightarrow H_C$	$H_A \rightarrow H_B$	$H_A \rightarrow H_D$	$H_A \rightarrow H_A$

(16.28)

Next consider the atom C_α and follow the same procedure used earlier for the $2s$, $2p_x$, $2p_y$, and $2p_z$ AOs. Convince yourself that the results shown in Table 16.6 are correct. These results are used to generate symmetry-adapted MOs for ethene using the method described here:

The following procedure, based on the projection operator method, can be used to generate a symmetry-adapted MO from AOs that forms a basis for a given representation. The recipe consists of the following steps:

- Choose an AO on an atom and determine into which AO it is transformed by each symmetry operator of the group.
- Multiply the AO of the transformed species by the character of the operator in the representation of interest for each symmetry operator.
- The resulting linear combination of these AOs forms a MO that is a basis for that representation.

The use of the projection operator method is illustrated in the following two example problems.

TABLE 16.6 Effect of Symmetry Operations on the Carbon Atom Orbitals

	\hat{E}	$\hat{C}_2(z)$	$\hat{C}_2(y)$	$\hat{C}_2(x)$	\hat{i}	$\hat{\sigma}(xy)$	$\hat{\sigma}(xz)$	$\hat{\sigma}(yz)$
$2s$	$C_\alpha \rightarrow C_\alpha$	$C_\alpha \rightarrow C_\alpha$	$C_\alpha \rightarrow C_\beta$	$C_\alpha \rightarrow C_\beta$	$C_\alpha \rightarrow C_\beta$	$C_\alpha \rightarrow C_\beta$	$C_\alpha \rightarrow C_\alpha$	$C_\alpha \rightarrow C_\alpha$
$2p_x$	$C_\alpha \rightarrow C_\alpha$	$C_\alpha \rightarrow -C_\alpha$	$C_\alpha \rightarrow -C_\beta$	$C_\alpha \rightarrow C_\beta$	$C_\alpha \rightarrow -C_\beta$	$C_\alpha \rightarrow C_\beta$	$C_\alpha \rightarrow C_\alpha$	$C_\alpha \rightarrow -C_\alpha$
$2p_y$	$C_\alpha \rightarrow C_\alpha$	$C_\alpha \rightarrow -C_\alpha$	$C_\alpha \rightarrow C_\beta$	$C_\alpha \rightarrow -C_\beta$	$C_\alpha \rightarrow -C_\beta$	$C_\alpha \rightarrow C_\beta$	$C_\alpha \rightarrow -C_\alpha$	$C_\alpha \rightarrow C_\alpha$
$2p_z$	$C_\alpha \rightarrow C_\alpha$	$C_\alpha \rightarrow C_\alpha$	$C_\alpha \rightarrow -C_\beta$	$C_\alpha \rightarrow -C_\beta$	$C_\alpha \rightarrow -C_\beta$	$C_\alpha \rightarrow -C_\beta$	$C_\alpha \rightarrow C_\alpha$	$C_\alpha \rightarrow C_\alpha$

EXAMPLE PROBLEM 16.7

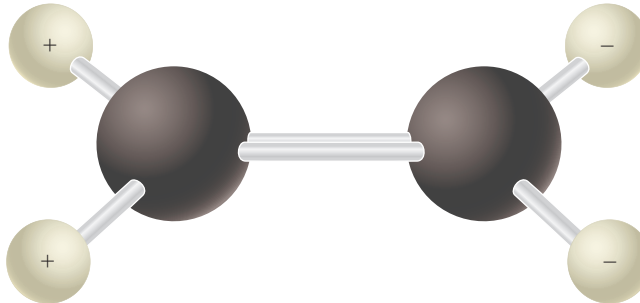
Form a linear combination of the H atomic orbitals in ethene that is a basis for the B_{1u} representation. Show that there is no combination of the H atomic orbitals in ethene that is a basis for the B_{3u} representation.

Solution

We take ϕ_{H_A} as the initial orbital, and multiply the AO into which ϕ_{H_A} is transformed by the character of the B_{1u} representation for each operator and sum these terms. The result is

$$\begin{aligned}\psi_{B_{1u}}^H &= 1 \times \phi_{H_A} + 1 \times \phi_{H_D} - 1 \times \phi_{H_B} - 1 \times \phi_{H_C} - 1 \times \phi_{H_C} \\ &\quad + -1 \times \phi_{H_B} + 1 \times \phi_{H_D} + 1 \times \phi_{H_A} \\ &= \phi_{H_A} + \phi_{H_D} - \phi_{H_B} - \phi_{H_C} - \phi_{H_B} + \phi_{H_D} + \phi_{H_A} \\ &= 2(\phi_{H_A} - \phi_{H_B} - \phi_{H_C} + \phi_{H_D})\end{aligned}$$

This molecular wave function has not yet been normalized. Pictorially, this combination looks like this:



Follow the same procedure to generate the linear combination for the B_{3u} representation:

$$\phi_{B_{3u}}^H = \phi_{H_A} - \phi_{H_D} - \phi_{H_B} + \phi_{H_C} - \phi_{H_C} + \phi_{H_B} + \phi_{H_D} - \phi_{H_A} = 0$$

This result shows that there is no linear combination of the H AOs that is a basis for B_{3u} .

EXAMPLE PROBLEM 16.8

Use the same procedure as in Example Problem 16.7 to form a linear combination of the C atomic orbitals in ethene that is a basis for the B_{1u} representation.

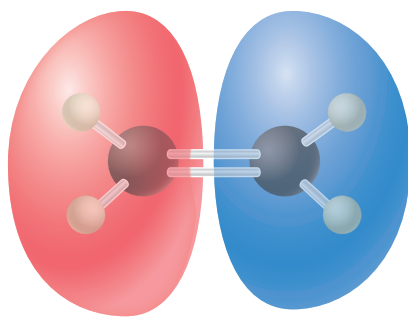
Solution

Follow the same procedure outlined in Example Problem 16.7 and apply it to each of the carbon valence AOs:

$$\begin{aligned}2s: & 1 \times \phi_{C_\alpha} + 1 \times \phi_{C_\alpha} - 1 \times \phi_{C_\beta} - 1 \times \phi_{C_\beta} - 1 \times \phi_{C_\beta} - 1 \times \phi_{C_\beta} \\ & + 1 \times \phi_{C_\alpha} + 1 \times \phi_{C_\alpha} = 4\phi_{C_\alpha} - 4\phi_{C_\beta} \\ 2p_x: & 1 \times \phi_{C_\alpha} - 1 \times \phi_{C_\alpha} + 1 \times \phi_{C_\beta} - 1 \times \phi_{C_\beta} + 1 \times \phi_{C_\beta} - 1 \times \phi_{C_\beta} \\ & + 1 \times \phi_{C_\alpha} - 1 \times \phi_{C_\alpha} = 0 \\ 2p_y: & 1 \times \phi_{C_\alpha} - 1 \times \phi_{C_\alpha} - 1 \times \phi_{C_\beta} + 1 \times \phi_{C_\beta} + 1 \times \phi_{C_\beta} - 1 \times \phi_{C_\beta} \\ & - 1 \times \phi_{C_\alpha} + 1 \times \phi_{C_\alpha} = 0 \\ 2p_z: & 1 \times \phi_{C_\alpha} + 1 \times \phi_{C_\alpha} + 1 \times \phi_{C_\beta} + 1 \times \phi_{C_\beta} + 1 \times \phi_{C_\beta} + 1 \times \phi_{C_\beta} \\ & + 1 \times \phi_{C_\alpha} + 1 \times \phi_{C_\alpha} = 4\phi_{C_\alpha} + 4\phi_{C_\beta}\end{aligned}$$

This result shows that the appropriate linear combination of carbon AOs to construct the symmetry-adapted MO that is a basis for the B_{1u} representation is

$$\psi_{B_{1u}}^C = c_1(\phi_{C_{2s\alpha}} - \phi_{C_{2s\beta}}) + c_2(\phi_{C_{2p_z\alpha}} + \phi_{C_{2p_z\beta}})$$

**Figure 16.13**

The ethene molecular orbital that is a basis of the B_{1u} representation.

Combining the results of the last two example problems, we find that the symmetry-adapted MO that includes AOs on all atoms and is also a representation of the B_{1u} representation is

$$\psi_{B1u} = c_1(\phi_{C_{2s\alpha}} - \phi_{C_{2s\beta}}) + c_2(\phi_{C_{2p_{z\alpha}}} + \phi_{C_{2p_{z\beta}}}) + c_3(\phi_{H_A} - \phi_{H_B} - \phi_{H_C} + \phi_{H_D})$$

An image of this molecular orbital is shown in Figure 16.13.

The values of the AO coefficients in the MOs cannot be obtained from symmetry considerations, but we can determine which coefficients are zero, equal in magnitude, and equal or opposite in sign. For the case of interest, c_1 through c_3 must be determined in a variational calculation in which the total energy of the molecule is minimized. Note that without taking symmetry into consideration, 12 coefficients would have been required to specify the wave function (one AO on each H and four AOs on each C). We see that forming the symmetry-adapted MO significantly reduces the number of coefficients required in the calculation from 12 to just 3. This example shows the simplification of the molecular wave function that is obtained by forming symmetry-adapted MOs.

VOCABULARY

associative
basis function
belongs to a particular representation
character
character table
class
dimension of a representation
forms a basis
group
group theory

identity operator
inverse operator
inversion center
irreducible representation
mirror plane
normal coordinate
normal mode
normal mode frequency
order of the group
point group

projection operator method
reducible representation
representation
rotation axis
rotation-reflection axis
symmetry elements
symmetry operations
symmetry-adapted MO
totally symmetric representation

KEY EQUATIONS

Equation	Significance of Equation	Equation Number
$\sum_{j=1}^N d_j^2 = h$	Relation between dimensions of different irreducible representations and order of a group	16.6
$\Gamma_i \Gamma_k = \sum_{j=1}^h \chi_i(\hat{R}_j) \chi_k(\hat{R}_j) = h \delta_{ik}$, where $\delta_{ik} = 0$ if $i \neq k$ and 1 if $i = k$	Set of characters associated with different representations of a group can be viewed as a vector. All such vectors are mutually orthogonal.	16.11
$\chi_{product}(\hat{R}) = \chi_i(\hat{R}) \chi_j(\hat{R})$	Definition of the character for an operator \hat{R} of the direct product of two representations.	16.13
$n_i = \frac{1}{h} \Gamma_i \Gamma_{reducible} = \frac{1}{h} \chi_i(\hat{R}_j) \cdot \chi_{reducible}(\hat{R}_j) = \frac{1}{h} \sum_{j=1}^h \chi_i(\hat{R}_j) \chi_{reducible}(\hat{R}_j)$	General method for decomposing a reducible representation into its irreducible representations.	16.22

CONCEPTUAL PROBLEMS

Q16.1 Can a molecule with an inversion center have a dipole moment? Give an example of a molecule with this symmetry element and explain your reasoning.

Q16.2 Which of the three normal modes of H_2O in Figure 16.10 is best described as a bending mode? Does the bond angle remain unchanged in any of the modes? Which requires less energy, bond bending or bond stretching?

Q16.3 Why does the list of elements for the D_{6h} group in Table 16.2 not list the elements C_6^2 , C_6^3 , and C_6^4 ?

Q16.4 Why does the list of elements for the D_{6h} group in Table 16.2 not list the elements S_6^2 , S_6^3 , and S_6^4 ?

Q16.5 How are quantum-mechanical calculations in the LCAO-MO model simplified through the construction of symmetry-adapted MOs?

Q16.6 Some symmetry operations can be carried out physically using a ball-and-stick model of a molecule, and others can only be imagined. Give two examples of each category.

Q16.7 Why does the C_{3v} group have a two-dimensional irreducible representation? Answer this question by referring to the form of the matrices that represent the operations of the group.

Q16.8 Can NH_3 have molecular orbitals that are triply degenerate in energy?

Q16.9 Can a molecule with an inversion center be superimposed on its mirror image without disassembly and reassembly

and therefore be chiral? Give an example of a molecule with this symmetry element and explain your reasoning.

Q16.10 Why are all one-dimensional representations irreducible?

Q16.11 What is the difference between a symmetry element and a symmetry operation?

Q16.12 Can a molecule with D_{2h} symmetry have a dipole moment? Give an example of a molecule with this symmetry and explain your reasoning.

Q16.13 Can a molecule with C_{3h} symmetry have a dipole moment? Give an example of a molecule with this symmetry and explain your reasoning.

Q16.14 Explain why only two peaks are observed in the infrared spectrum of methane, although six of the nine normal modes are infrared active.

Q16.15 Explain why the overlap integral between two combinations of AOs is nonzero only if the combinations belong to the same representation.

NUMERICAL PROBLEMS

Section 16.1

P16.1 Show that a molecule with an inversion center implies the presence of an S_2 element.

P16.2 XeF_4 belongs to the D_{4h} point group with the following symmetry elements: E , C_4 , C_4^2 , C_2 , C'_2 , C''_2 , i , S_4 , S_4^2 , σ_h , $2\sigma_v'$, and $2\sigma_v''$. Make a drawing similar to Figure 16.1 showing these elements.

P16.3 CH_4 belongs to the T_d point group with the following symmetry elements: E , $4C_3$, $4C_3^2$, $3C_2$, $3S_4$, $3S_4^3$, and $6\sigma_v$. Make a drawing similar to Figure 16.1 showing these elements.

Section 16.2

P16.4 Use the logic diagram of Figure 16.2 to determine the point group for the planar molecule *trans*-HBrC=CBrH. Indicate your decision-making process as was done in the text for NH_3 .

P16.5 Use the logic diagram of Figure 16.2 to determine the point group for allene. Indicate your decision-making process as was done in the text for NH_3 .

P16.6 Use the logic diagram of Figure 16.2 to determine the point group for the planar molecule *cis*-HBrC=CClH. Indicate your decision-making process as was done in the text for NH_3 .

P16.7 Use the logic diagram of Figure 16.2 to determine the point group for PCl_5 . Indicate your decision-making process as was done in the text for NH_3 .

P16.8 Use the logic diagram of Figure 16.2 to determine the point group for CH_3Cl . Indicate your decision-making process as was done in the text for NH_3 .

P16.9 Show that a molecule with a C_n axis cannot have a dipole moment perpendicular to the axis.

P16.10 Show that the presence of a C_2 axis and a mirror plane perpendicular to the rotation axis implies the presence of a center of inversion.

Section 16.3

P16.11 Use the 3×3 matrices for the C_{2v} group in Equation (16.3) to verify the group multiplication table for the following successive operations:

a. $\hat{\sigma}_v \hat{\sigma}'_v$ b. $\hat{\sigma}_v \hat{C}_2$ c. $\hat{C}_2 \hat{C}_2$

P16.12 Use the 3×3 matrices for the C_{2v} group in Equation (16.3) to verify the associative property for the following successive operations:

a. $\hat{\sigma}_v (\hat{\sigma}'_v \hat{C}_2) = (\hat{\sigma}_v \hat{\sigma}'_v) \hat{C}_2$
b. $(\hat{\sigma}_v \hat{E}) \hat{C}_2 = \hat{\sigma}_v (\hat{E} \hat{C}_2)$

P16.13 Use the method illustrated in Example Problem 16.2 to generate a 3×3 matrix for the following:

- a. \hat{C}_6 operator
b. \hat{S}_4 operator
c. \hat{i} operator

P16.14 Use the 2×2 matrices of Equation (16.10) to derive the multiplication table for the C_{3v} group.

Section 16.4

P16.15 The D_3 group has the following classes: E , $2C_3$, and $3C_2$. How many irreducible representations does this group have, and what is the dimensionality of each?

Section 16.5

P16.16 Show that z is a basis for the A_1 representation and that R_z is a basis for the A_2 representation of the C_{3v} group.

P16.17 Consider the function $f(x, y) = xy$ integrated over a square region in the x - y plane centered at the origin.

- a. Draw contours of constant f values (positive and negative) in the plane and decide whether the integral can have a nonzero value.
- b. Use the information that the square has D_{4h} symmetry and determine to which representation the integrand belongs. Decide whether the integral can have a nonzero value from this information.

P16.18 The C_{4v} group has the following classes: E , $2C_4$, C_2 , $2\sigma'_v$ and $2\sigma''_v$. How many irreducible representations does this group have, and what is the dimensionality of each?

Section 16.7

P16.19 To determine the symmetry of the normal modes of methane, an analysis of the transformation of individual coordinate systems on the five atoms is carried out, as shown in Figure 16.11 for H_2O . After the rotational and translational representations are removed, the following reducible representation $\chi_{\text{reducible}}$ is obtained for the vibrational modes:

E	$8C_3$	$3C_2$	$6C_4$	$6\sigma_v$
9	0	1	-1	3

Using the character table for the T_d group, verify that $\Gamma_{\text{reducible}} = A_1 + E + 2T_2$.

P16.20 Decompose the following reducible representation into irreducible representations of the C_{2v} group:

E	C_2	σ_v	σ'_v
4	0	0	0

P16.21 Decompose the following reducible representation into irreducible representations of the C_{3v} group:

E	$2C_3$	$3\sigma_v$
5	2	-1

Section 16.8

P16.22 Methane belongs to the T_d group. The reducible representation for the vibrational modes is $\Gamma_{\text{reducible}} = A_1 + E + 2T_2$.

- a. Show that the A_1 and T_2 representations are orthogonal to each other and to the other representations in the table.
- b. What is the symmetry of each of the vibrational modes that gives rise to Raman activity? Are any of the Raman active modes degenerate in energy?

P16.23 Assume that a central atom in a molecule has ligands with C_{4v} symmetry. Decide by evaluating the appropriate transition dipole element if the transition $p_x \rightarrow p_z$ is allowed with the electric field in the z direction.

P16.24 Benzene, C_6H_6 , belongs to the D_{6h} group. The reducible representation for the vibrational modes is

$$\begin{aligned}\Gamma_{\text{reducible}} = & 2A_{1g} + A_{2g} + A_{2u} + 2B_{1u} + 2B_{2g} \\ & + 2B_{2u} + E_{1g} + 3E_{1u} + 4E_{2g} + 2E_{2u}\end{aligned}$$

- a. How many vibrational modes does benzene have?
- b. How many of these modes are infrared active, and to which representation do they belong?
- c. Which of the infrared active modes are degenerate in energy, and what is the degeneracy for each?
- d. How many of these modes are Raman active, and to which representation do they belong?
- e. Which of the Raman active modes are degenerate in energy, and what is the degeneracy for each?
- f. Which of the infrared modes are also Raman active?

P16.25 NH_3 belongs to the C_{3v} group. The reducible representation for the vibrational modes is $\Gamma_{\text{reducible}} = 2A_1 + 2E$.

- a. How many vibrational modes does NH_3 have?
- b. How many of these modes are infrared active, and to which representation do they belong?
- c. Are any of the infrared active modes degenerate in energy?
- d. How many of these modes are Raman active, and to which representation do they belong?
- e. Are any of the Raman active modes degenerate in energy?
- f. How many modes are both infrared and Raman active?

FURTHER READING

Brown, R. "Melting Point and Molecular Symmetry." *Journal of Chemical Education* 77 (2000): 724–731.

Carter, R. L. *Molecular Symmetry and Group Theory*. New York: Wiley, 1998.

Cass, M., Rzepa, H., Rzepa, D., and Williams, C. "The Use of the Free, Open-Source Program Jmol to Generate an Interactive Web Site to Teach Molecular Symmetry." *Journal of Chemical Education* 82 (2005): 1736–1740.

Coleman, W., and Fedosky, E. "Teaching Molecular Symmetry with JCE WebWare." *Journal of Chemical Education* 82 (2005): 1741–1743.

Coleman, W., and Fedosky, E. "An Interactive Computer Program to Help Students Learn Molecular Symmetry Elements and Operations." *Journal of Chemical Education* 84 (2007): 1551–1552.

Kettle, S. F. A. *Symmetry and Structure: Readable Group Theory for Chemists* (3d ed.). New York: Wiley, 2007.

Levine, I. N. *Quantum Chemistry* (7th ed.). Boston: Pearson, 2014.

Myrick, M., Colavita, P., Greer, A., Long, B., and Andreatta, D. "Use of Molecular Symmetry to Describe Pauli Principle Effects on the Vibration–Rotation Spectroscopy of $CO_2(g)$." *Journal of Chemical Education* 81 (2004): 379–382.

Nuclear Magnetic Resonance Spectroscopy

WHY is this material important?

Nuclear magnetic resonance is arguably the most important spectroscopic technique in the chemist's arsenal because it relates directly to the structure of molecules of interest. Its application ranges from characterizing newly synthesized small molecules to large biological macromolecules such as proteins and nucleic acids.

WHAT are the most important concepts and results?

Most atoms in the periodic table have magnetic nuclei in high enough natural abundance to allow NMR to be applied to almost every compound. The nuclear magnetic moment serves as a reporter for nuclear position and dynamics. Structure determination depends on different types of magnetic couplings between neighboring nuclei, such as scalar and dipolar coupling, which can be analyzed in terms of the local structure of a molecule.

WHAT would be helpful for you to review for this chapter?

It would be helpful to review the material in Chapter 7 on angular momentum.

17.1 INTRINSIC NUCLEAR ANGULAR MOMENTUM AND MAGNETIC MOMENT

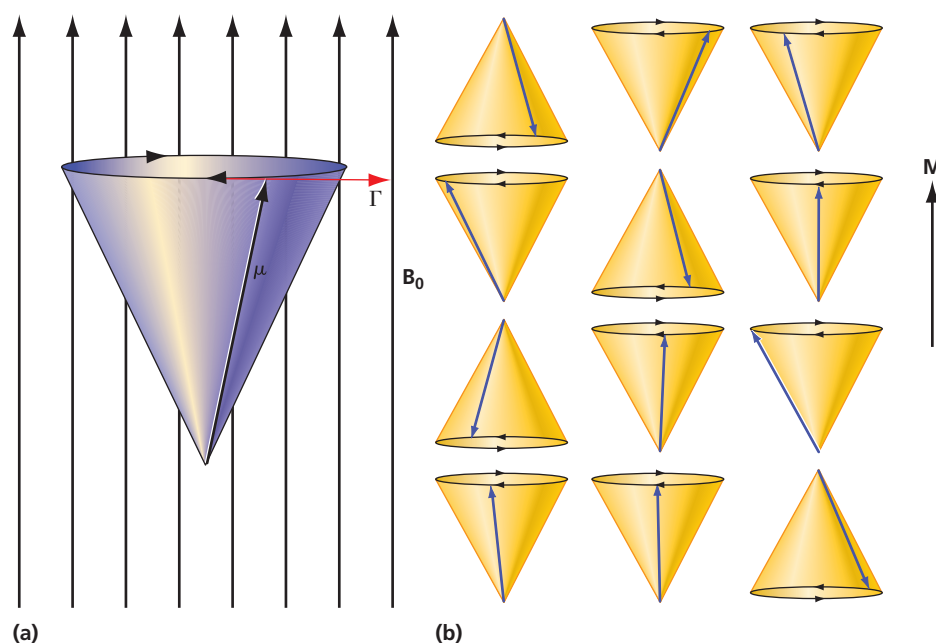
Nuclear magnetic resonance (NMR) is arguably the most important spectroscopic technique used by chemists in their work. This is due to a combination of several factors that make NMR an excellent tool for molecular structure determination: (1) nuclear magnetic moments are localized within the confines of atomic nuclei—that is, within diameters of the order of a few fm, which allows for exquisite spatial resolution only limited by the vibrational motion of the atoms in a molecule. (2) Interactions between neighboring magnetic nuclei enrich the NMR spectrum and allow for the accurate determination of distances (dipolar coupling) and dihedral angles (J -coupling). This analytical capability leads to applications in structure analysis of very large biomolecules such as proteins and nucleic acids. (3) The energy of interaction between the tiny nuclear magnetic moment and its environment is very small, on the order of 0.2 J/mol. Consequently, the nuclear magnetic moment acts as a true observer of the molecular structure and dynamics without interfering with the system. (4) Nuclear spins occur in almost all molecules; hence, NMR can be applied to almost any system of chemical interest.

The small magnitude of the nuclear magnetic moment results in a low inherent sensitivity. However, more than 70 years of scientific and technical advances have pushed the envelope and have made NMR an indispensable tool not only in chemistry but in other natural sciences as well. Pulsed NMR has harnessed the multiplex advantage

- 17.1 Intrinsic Nuclear Angular Momentum and Magnetic Moment
- 17.2 The Nuclear Zeeman Effect
- 17.3 The Chemical Shift
- 17.4 Spin-Spin Coupling and Multiplet Splittings
- 17.5 Spin Dynamics
- 17.6 Pulsed NMR Spectroscopy
- 17.7 Two-Dimensional NMR
- 17.8 Solid-State NMR
- 17.9 Dynamic Nuclear Polarization
- 17.10 Magnetic Resonance Imaging

Figure 17.1

Precession of individual spins and their magnetic moments leads to a macroscopic magnetization (a) Precession of an individual nuclear spin about the magnetic field direction for an α spin. (b) The magnetization vector \mathbf{M} resulting from summing the individual spin magnetic moments (yellow cones) is oriented parallel to the magnetic field. It has no transverse component.



inherent in Fourier transform spectroscopy to allow for efficient spectrum acquisition, and the multidimensional pulse techniques discussed in Section 17.7 have allowed scientists to disentangle complex nuclear coupling networks and have paved the way for structure determination of large molecules of biological interest. Modern probe development has made solids accessible to high-resolution NMR through magic angle spinning, as will be discussed in Section 17.8, and high- T_c superconducting probes¹ led to dramatic advances in sensitivity. Modern magnet technology has pushed accessible NMR frequencies beyond 1 GHz, which translates into enhanced sensitivity and spectral resolution, and dynamic nuclear polarization (DNP) has overcome the Boltzmann limit for NMR sensitivity, as will be discussed in Section 17.9.

Each nucleus with a spin also has a magnetic moment that serves as the “handle” used in NMR spectroscopy to unlock information about the atom. The word *spin* suggests a particle spinning about its own axis. That picture, however, is incorrect and cannot explain the spin and magnetic moment of the fundamental particles that comprise an atom. Spin has to be regarded as a relativistic quantum effect that confers angular momentum to particles.

Nuclear spin is analyzed with the same mathematical treatment as other quantum-mechanical angular momenta such as electron spin and orbital angular momentum (see Chapter 7). It is represented by a vector \mathbf{I} with length $|\mathbf{I}| = \sqrt{I(I+1)}\hbar$, which may be projected on a spatial quantization axis with a corresponding magnetic quantum number $m_I = -I, -I+1, \dots, +I$. The quantization axis, customarily denoted by \mathbf{z} , is usually provided by an external magnetic field, \mathbf{B}_0 . Projected along this axis, the allowed values of angular momentum are $I_z = m_I\hbar$. The position of the spin in the x and y direction is undetermined because \hat{I}_x and \hat{I}_y do not commute with \hat{I}_z . The spin precesses about the z axis on the surface of a cone, as illustrated in the vector diagram in Figure 17.1. Experimentally, only the projection of the spin along the z axis is observed.

Nuclear spins can assume integer and half-integer quantum numbers ranging from $I = 0$ to $9/2$ for stable isotopes. Nucleons couple their spin, which leads to a range of possibilities for the ground state nuclear spin. As a result, nuclei with equal even numbers of protons and neutrons will show zero nuclear spin as observed, for example,

¹These probes incorporate RF coils made from high- T_c superconducting materials that are cooled below the superconducting phase transition temperature. They feature much lower losses than conventional radio-frequency coils and therefore provide a higher signal-to-noise ratio for the NMR experiment.

TABLE 17.1 Dependence of Nuclear Spin Quantum Numbers on Nucleon Composition

Mass Number	Proton Number	Neutron Number	Spin I	Examples
Even	Even	Even	0	^{12}C , ^{16}O
	Odd	Odd	1, 2, ...	$^2\text{H}(1)$, $^{14}\text{N}(1)$
Odd	Even	Odd	1/2, 3/2, ...	$^{13}\text{C}(1/2)$, $^{17}\text{O}(5/2)$
	Odd	Even	1/2, 3/2, ...	$^1\text{H}(1/2)$, $^{15}\text{N}(1/2)$, $^{31}\text{P}(1/2)$

in ^{12}C and ^{16}O . Table 17.1 provides an overview of how the spin quantum numbers are related to the number of nucleons in the nucleus. For most questions of interest to chemists, it is customary to view the nuclear spin as an inherent and unique property for a given nucleus.

Nuclear spin operators have the same commutation relationships as those for electron spin (see Section 7.6). For a spin 1/2 nucleus such as ^1H , there are only two spatial orientations for the spin, which are customarily designated (1) α for “spin up,” for which $\mathbf{I} \cdot \mathbf{z} > 0$ and \mathbf{I} is parallel to \mathbf{z} , and (2) β for “spin down” where $\mathbf{I} \cdot \mathbf{z} < 0$, for which \mathbf{I} is antiparallel to \mathbf{z} . This nomenclature is similar to that for the electron, which could lead to confusion but emphasizes the fact that mathematically both spin systems are treated the same way. The corresponding eigenvalues are given by the relations:

$$\begin{aligned}\hat{I}^2\alpha &= \frac{1}{2}\left(\frac{1}{2} + 1\right)\hbar^2\alpha; & \hat{I}_z\alpha &= +\frac{1}{2}\hbar\alpha \\ \hat{I}^2\beta &= \frac{1}{2}\left(\frac{1}{2} + 1\right)\hbar^2\beta; & \hat{I}_z\beta &= -\frac{1}{2}\hbar\beta\end{aligned}\quad (17.1)$$

As for the electron, a spin-carrying nucleus has an associated magnetic moment. The composite nature of the nuclear spin leads to anomalous magnetic moments that are unique for each nucleus and are reflected in the nuclear g -factor g_N , which may be considered as an empirical “fudge factor” that is different for each nucleus and relates the spin vector \mathbf{I} with the magnetic moment vector $\boldsymbol{\mu}$ given by

$$\boldsymbol{\mu} = g_N \frac{e}{2m_{\text{proton}}} \mathbf{I} = \frac{g_N \beta_N}{\hbar} \mathbf{I} = \gamma \mathbf{I} \quad (17.2)$$

In the SI system of units, $\boldsymbol{\mu}$ has units of ampere \times (meter) 2 = joule/tesla, and \mathbf{I} has units of joule \times second. In Equation (17.2), the quantity $\beta_N = e\hbar/(2m_{\text{proton}})$, which has the value $5.0507866 \times 10^{-27}$ J/T, is called the **nuclear magneton**, and $\gamma = g_N \beta_N / \hbar$ is termed the **gyromagnetic ratio**. Because m_{proton} is greater than m_e by a factor of 1837, the nuclear magnetic moment is much smaller than the electron magnetic moment for the same spin quantum number and similar g -factors. Values of these quantities for the nuclei most commonly used in NMR spectroscopy are shown in Table 17.2.

TABLE 17.2 Parameters for NMR-Active Nuclei and the Free Electron

Species	Isotopic Abundance (%)	Spin Quantum Number	g-Factor, g_N (or g_e)	Gyromagnetic Ratio $\gamma [10^7 \text{ rad}/(\text{T} \cdot \text{s})]$
^1H	99.985	1/2	5.5854	26.75
^{13}C	1.108	1/2	1.4042	6.73
^{31}P	100	1/2	2.2610	10.84
^2H	0.015	1	0.8574	4.11
^{14}N	99.63	1	0.4036	1.93
free electron		1/2	-2.00231930436182	1.760859644×10^4

17.2 THE NUCLEAR ZEEMAN EFFECT

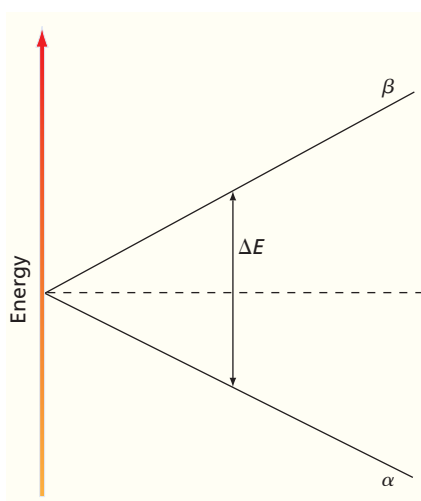


Figure 17.2

Energy of a nuclear spin $I = 1/2$ in an external magnetic field.

Concept

A quantum-mechanical spin experiences spatial quantization in a magnetic field. For a spin 1/2 nucleus, only two spin orientations are allowed.

NMR spectroscopy is usually performed by placing a sample of interest into an external magnetic field. In this section, we consider how this field interacts with the nuclear spin and its associated magnetic moment and how the field strength and the temperature of the sample affect the NMR experiment. When an external magnetic field, \mathbf{B}_0 , is applied to a system that contains nuclear spins, their magnetic moments couple to \mathbf{B}_0 , which slightly alters the total energy due to the magnetic energy contribution

$$E = -\mu \cdot \mathbf{B}_0 = -\gamma m \hbar B_0 \quad (17.3)$$

A classical magnetic moment μ in an external field \mathbf{B}_0 may assume any orientation. However, a quantum-mechanical spin experiences spatial quantization, as shown in Figure 17.1; hence, only specific orientations are observed, which produces discrete magnetic energies for the corresponding nuclei. For the case of a spin 1/2 nucleus such as ^1H , we expect only two spin orientations, denoted α and β , with distinct energy levels (see Figure 17.2) as follows:

$$E_{\alpha, \beta} = -\left(\pm \frac{1}{2}\right) g_N \beta_N B_0 = -\left(\pm \frac{1}{2}\right) \gamma \hbar B_0 \quad (17.4)$$

This energetic splitting in an external magnetic field is known as the **Zeeman effect**. Even though these energy levels are discrete, their values depend continuously on the strength of the external magnetic field.

Because the nuclear magnetic moment vector μ usually points in the same direction as the spin vector \mathbf{I} , spin down (β) is greater in energy than spin up (α). There are a few exceptions to this rule, for which the directions of μ and \mathbf{I} are antiparallel; for example, $g_N < 0$ for ^{15}N . Note that, in the absence of a magnetic field, the energy levels of α and β are degenerate.

Even though the x and y components of the magnetic moment vector are undetermined, μ is clearly not parallel to the z axis (see Figure 17.1) because, if that were the case, then the x and y components of the magnetic moment vector would be precisely known to be zero. A magnetic moment that is not parallel to the magnetic field experiences a torque that deflects the magnetic moment in a direction perpendicular to both μ and \mathbf{B}_0 according to the cross product:

$$\Gamma = \mu \times \mathbf{B}_0 \quad (17.5)$$

This torque leads to a movement of the magnetic moment vector μ on the surface of a cone about the magnetic field direction (see Figure 17.1a). This motion is called **precession** and is analogous to the motion of a spinning top in a gravitational field. The precession of individual spins and their magnetic moments is shown in Figure 17.1b. In NMR spectroscopy, one deals with a finite volume that contains many individual spins. Therefore, it is useful to define the **macroscopic magnetic moment \mathbf{M}** , which is the vector sum of the individual magnetic moments, $\mathbf{M} = \sum_i \mu_i$. Whereas classical mechanics is not appropriate for describing individual nuclear magnetic moments, it is useful for describing the behavior of \mathbf{M} . In Figure 17.1, all the individual yellow cones representing different μ_z have the same magnitude for their z component, but their transverse components are randomly distributed in the x - y plane. Therefore, in a macroscopic sample containing on the order of Avogadro's number of nuclear spins, the transverse component of \mathbf{M} is zero at equilibrium. We conclude that \mathbf{M} points along the z axis, which corresponds to the field direction.

The frequency with which an individual magnetic moment precesses about the magnetic field direction is given by

$$\nu_0 = \frac{\gamma B_0}{2\pi} \quad \text{or} \quad \omega_0 = 2\pi\nu_0 = \gamma B_0 \quad (17.6)$$

and is called the **Larmor frequency**. It increases linearly with the magnetic field and has characteristic values for different nuclei according to their unique gyromagnetic ratios. It is also the frequency required for the electromagnetic radiation to induce a

Concept

An individual magnetic moment precesses about the magnetic field direction at the Larmor frequency.

transition between adjacent energy levels of the spin system for which the selection rule $\Delta m_I = \pm 1$ is obeyed. This can be seen by calculating the energy difference between the β - and α -states for ^1H . This so-called **resonance condition** is given by

$$\begin{aligned}\Delta E &= E_\beta - E_\alpha = \left\{ -\left(-\frac{1}{2} \right) \gamma \hbar B_0 \right\} - \left\{ -\left(+\frac{1}{2} \right) \gamma \hbar B_0 \right\} \\ &= \gamma \hbar B_0 = \hbar \omega_0 = h\nu_0 \\ \nu_0 &= \frac{\gamma B_0}{2\pi}, \quad \omega_0 = \gamma B_0\end{aligned}\tag{17.7}$$

For instance, ^1H has a resonance frequency of 500 MHz at a field of approximately 12 T. As shown in Example Problem 17.1, the energy separation of these two levels is very small compared to $k_B T$ at room temperature. This makes the energy absorption difficult to detect and is the principal reason for the low sensitivity typically encountered in NMR experiments.

EXAMPLE PROBLEM 17.1

- Calculate the two possible energies of the ^1H nuclear spin in a uniform magnetic field of 5.50 T.
- Calculate the energy ΔE absorbed in making a transition from the α to the β state. If a transition is made between these levels by the absorption of electromagnetic radiation, what region of the spectrum is used?
- Calculate the relative population difference of these two states in equilibrium at 300 K.

Solution

- The two energies are given by

$$\begin{aligned}E_{\alpha,\beta} &= -\left(\pm \frac{1}{2} \right) g_N \beta_N B_0 \\ &= \mp \frac{1}{2} \times 5.5854 \times (5.051 \times 10^{-27} \text{ J/T}) \times 5.50 \text{ T} = \mp 7.76 \times 10^{-26} \text{ J}\end{aligned}$$

- The energy difference is given by

$$\Delta E = 2(7.76 \times 10^{-26} \text{ J}) = 1.55 \times 10^{-25} \text{ J}$$

$$\nu = \frac{\Delta E}{h} = \frac{1.55 \times 10^{-25} \text{ J}}{6.626 \times 10^{-34} \text{ Js}} = 2.34 \times 10^8 \text{ s}^{-1}$$

This is in the range of frequencies called radio frequencies (RF).

- The relative population difference of the two states is given by

$$\begin{aligned}\frac{n_\beta}{n_\alpha} &= \exp\left(-\frac{E_\beta - E_\alpha}{k_B T}\right) = \exp\left(-\frac{2(7.76 \times 10^{-26} \text{ J})}{(1.381 \times 10^{-23} \text{ J/K})(300 \text{ K})}\right) \\ &= 0.999963 \\ \frac{n_\alpha - n_\beta}{n_\alpha + n_\beta} &\approx \frac{(1 - 0.999963)n_\alpha}{2n_\alpha} = 1.9 \times 10^{-5}\end{aligned}$$

From this result, we see that the populations of the two states are the same to within a few parts per million (ppm).

The solution to part (c) of Example Problem 17.1 shows that because $\Delta E \ll k_B T$, the population of both states is approximately equal; that is, $n_\alpha \approx n_\beta$. This result has important consequences for implementing NMR spectroscopy. As we learned in Section 8.2, if a two-level system is exposed to resonant radiation, the rates of upward

and downward transitions depend on the population of the two states. Here they are almost equal to each other. Therefore, only a very small fraction of the nuclear spins contributes to the NMR signal. More generally, the energy absorbed is proportional to the product of ΔE and $\Delta n = n_\alpha - n_\beta$. The population difference between the two resonant states is usually expressed in terms of the so-called **spin polarization**, P , which is related to the NMR signal intensity. P depends on the macroscopic magnetization and is a measure of NMR detectability. It is normally given in %:

$$P = \frac{n_\alpha - n_\beta}{n_\alpha + n_\beta} \times 100\% \quad (17.8)$$

For a spin system in thermodynamic equilibrium with its environment, the population difference is determined by Boltzmann statistics (see Section 2.1), which allows the spin polarization to be expressed as a function of the external magnetic field and temperature, as shown in Equation (17.9):

$$\begin{aligned} \frac{n_\beta}{n_\alpha} &= \exp\left(-\frac{E_\beta - E_\alpha}{k_B T}\right) = \exp\left(-\frac{\gamma\hbar B_0}{k_B T}\right) \\ n_\beta &= n_\alpha \exp\left(-\frac{\gamma\hbar B_0}{k_B T}\right) \\ P &= \frac{n_\alpha - n_\beta}{n_\alpha + n_\beta} = \frac{1 - \exp\left(-\frac{\gamma\hbar B_0}{k_B T}\right)}{1 + \exp\left(-\frac{\gamma\hbar B_0}{k_B T}\right)} = \tanh\left(\frac{\gamma\hbar B_0}{2k_B T}\right) \end{aligned} \quad (17.9)$$

NMR experiments are sometimes carried out when the spin system is deliberately prepared far from equilibrium. In these situations, the spin polarization is still defined by Equation (17.8) but cannot be calculated by Equation (17.9). Instead, one has to carefully determine the population numbers n_α and n_β from experiment. Sometimes a spin system will undergo population inversion, in which $n_\alpha < n_\beta$, which leads to a negative spin polarization and results in an emissive NMR signal rather than an absorptive one. An important application of nonequilibrium NMR is the DNP effect, which leads to improved experimental sensitivity and is discussed further in Section 17.9.

P in Equation (17.9) is plotted in Figure 17.3 and shows the dependence of the spin polarization on the ratio of ΔE to $k_B T$. When $\Delta E/(k_B T) \gg 1$, which implies a

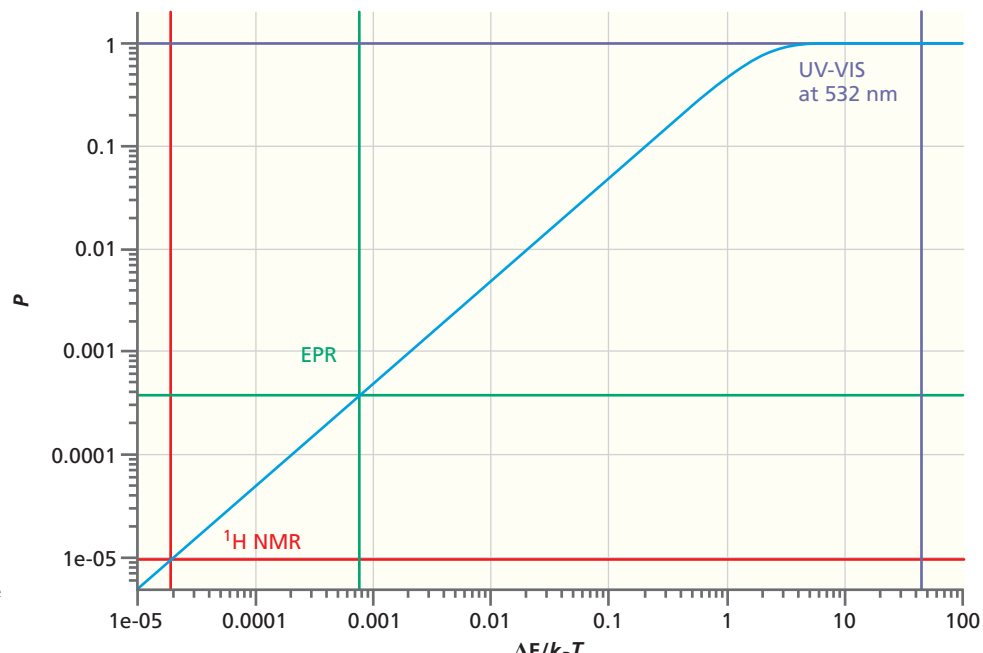


Figure 17.3

Plot of polarization of a two-level system as a function of the ratio of the energy gap and the thermal energy according to Equation (17.9).

very high external magnetic field or very low temperatures, the polarization approaches unity, or 100%. At high temperature and low field, $\Delta E/(k_B T) \rightarrow 0$, however, the polarization approaches zero because the two states will become equally populated. The vertical lines in Figure 17.3 indicate the value of the polarization for ^1H NMR at 5.50 T (see Example Problem 17.1a), for electron paramagnetic resonance (EPR) of a free electron, and for comparison a UV-VIS (ultraviolet-visible light) experiment on a two-level system at 532 nm. Because $\Delta E = \gamma \hbar B_0$ is such a small energy compared to the thermal energy, $k_B T$, at room temperature the spin polarization is only on the order of 19 ppm for ^1H at 5.5 T, as shown in Example Problem 17.1c. This value is almost two orders of magnitude smaller than the polarization for EPR, its electron magnetic resonance sibling.

To improve this sensitivity problem for samples in thermodynamic equilibrium, two different strategies may be pursued: (1) increase the external magnetic field, and (2) decrease the temperature. Both options are useful in solving chemical problems but are limited in their impact on sensitivity. Lowering the temperature also comes at the cost of freezing liquid samples. This leads to significant line broadening, which intrinsically lowers the spectral resolution. High resolution can be recovered in solid-state NMR (ssNMR) by spinning the sample about an axis oriented at the magic angle with respect to the external magnetic field direction, a technique that is further discussed in Section 17.8.

If no more information than that outlined in the preceding paragraphs could be obtained with this technique, NMR spectroscopy would simply be an expensive tool for quantitatively analyzing the elemental composition of compounds. However, two important aspects make it very useful for obtaining additional chemical information at the molecular level. The first of these aspects is that the magnetic field in Equation (17.4) is not the applied external field, but rather the local field present at the location of the nuclear spin. As we will see, the local field at a magnetic moment is influenced by the electron distribution on the atom of interest as well as by the electron distribution on nearby atoms. This difference between the external and local magnetic fields is the origin of the chemical shift. The H atoms in methane and chloroform have a different Larmor frequency because of this chemical shift. The origin of the chemical shift is discussed in Section 17.3. The second important aspect is that individual magnetic dipoles interact with one another. This leads to a splitting of the energy levels of a two-spin system and the appearance of multiplet spectra in NMR. As discussed in Section 17.4, the multiplet structure of a NMR resonance absorption provides direct structural information about the molecule.

17.3 THE CHEMICAL SHIFT

The power of NMR spectroscopy becomes apparent when considering the effect of the environment on the resonance condition [Equation (17.7)], which is called the **chemical shift**. Chemical shifts are induced by the external magnetic field and are generally small corrections to the resonance condition in which the local magnetic field, $\mathbf{B}_{\text{local}}$, at the position of a nucleus is slightly shifted to lower (diamagnetic shift, $\sigma > 0$) or higher (paramagnetic shift, $\sigma < 0$) values compared to the external field \mathbf{B}_0 :

$$\mathbf{B}_{\text{local}} = (1 - \sigma)\mathbf{B}_0 \quad (17.10)$$

The effect is called diamagnetic when the local field is opposed to the external field and paramagnetic when it is aligned with the external field. Chemical shifts can be divided into several categories, local and remote diamagnetic and paramagnetic shifts, isotropic and anisotropic in nature, as well as other sources of chemical shift that are not of molecular origin (such as the Knight shift induced by conduction electrons in nuclei of metals).

A conceptually simple way to look at chemical shifts is to consider them as a response of the electrons surrounding the nucleus to the presence of the external field \mathbf{B}_0 . A **diamagnetic response** for which the **shielding constant** $\sigma > 0$ can then be explained by ring currents in the electron orbitals surrounding the nucleus that are induced by the external field \mathbf{B}_0 . As illustrated in Figure 17.4, these ring currents cause

Concept

At room temperature the spin polarization is only on the order of 19 ppm for ^1H at 5.5 T.

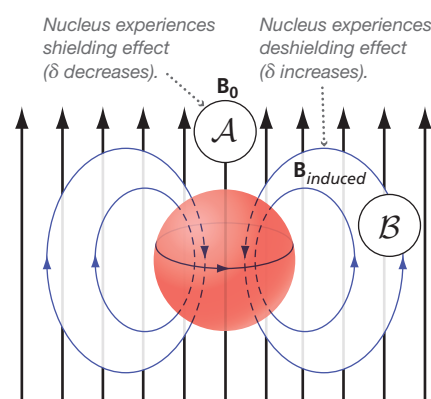


Figure 17.4

Illustration of the origin of ring currents. The shaded spherical volume represents a negatively charged continuous charge distribution such as in filled s orbitals near a nucleus. When placed in a magnetic field, the distribution will circulate, as indicated by the horizontal orbit. This distribution creates a ring current in a plane perpendicular to the external magnetic field direction. The motion will induce a magnetic field at the center of the distribution that opposes the external field ($\sigma > 0$). This classical picture is not strictly applicable at the atomic level, but the outcome is the same as a rigorous quantum-mechanical treatment. For locations labeled \mathcal{A} and \mathcal{B} , a nucleus in region \mathcal{A} experiences a shielding effect (δ decreases), whereas a nucleus in region \mathcal{B} experiences a deshielding effect (δ increases). See text for discussion.

Concept

The local field at a magnetic moment is influenced by the electron distribution on the atom of interest as well as by the electron distribution on nearby atoms. This difference between the external and local magnetic fields is the origin of the chemical shift.

a magnetic dipole field that will oppose the external field at the position of the nucleus. The local diamagnetic contribution is primarily caused by electrons in spherically symmetric orbitals (*s* orbitals) in close vicinity to the nucleus. Because the induced field lowers the local field compared to the external field, the resonance frequency for the nucleus is slightly lower as well ($\Delta\nu < 0$), leading to the following correction to the resonance condition:

$$\nu = \frac{\gamma(1 - \sigma)B_0}{2\pi} \quad \text{or} \quad \omega = \gamma(1 - \sigma)B_0$$

$$\Delta\nu = \nu - \nu_0 = \frac{\gamma(1 - \sigma)B_0}{2\pi} - \frac{\gamma B_0}{2\pi} = -\frac{\sigma\gamma B_0}{2\pi} \quad (17.11)$$

Local paramagnetic contributions with $\sigma < 0$ are due to currents involving electrons in *p*-orbitals requiring low-lying excited states. Because the chemical shift is proportional to the external magnetic field, it is convenient to express it in terms of a dimensionless parameter, δ :

$$\delta = \frac{(\nu - \nu_{\text{ref}})}{\nu_{\text{ref}}} \times 10^6 = \frac{(\sigma_{\text{ref}} - \sigma)}{(1 - \sigma_{\text{ref}})} \times 10^6 \approx (\sigma_{\text{ref}} - \sigma) \times 10^6 \quad (17.12)$$

Concept

Comparing a chemical shift to a reference compound ensures that the chemical shift has the same value on different NMR spectrometers with different magnetic fields.

The factor 10^6 scales the numerical value of δ to a convenient size, allowing it to be expressed in terms of parts per million. Because the frequency shift relative to the reference is scaled by the reference frequency, δ does not depend on B_0 . This dimensionless parameter is a molecular property unique to a given nucleus in a compound and allows one to directly compare experimental results from many different NMR spectrometers with different magnetic field strengths. Because δ becomes smaller with increasing σ , just like the actual resonance frequency, it is effectively a “deshielding” parameter. For ^1H and ^{13}C NMR, the reference compound to which the value of $\delta = 0$ is assigned is $(\text{CH}_3)_4\text{Si}$ (tetramethylsilane, TMS), because this molecule is inert and soluble in most organic solvents. TMS provides single, strong NMR lines for both ^1H and ^{13}C nuclei and has the added advantage that both nuclei are strongly shielded, putting their resonance frequency lower than most other protons and ^{13}C nuclei in a sample and making $\delta > 0$ for most cases. It is customary to plot NMR spectra on a δ scale with increasing values from right to left—that is, more shielded nuclei to the right and more de-shielded ones to the left.

Concept

The chemical shift for ^1H depends on the functional group containing the H atom.

Figure 17.5 illustrates the observed ranges of δ for protons in different types of chemical compounds. For example, the chemical shift for the OH group in alcohols is quite different from the chemical shift for H atoms in a methyl group. It also shows that the range in observed chemical shifts for a class of compounds can be quite large, as is seen for the aromatic alcohols. A quantitative understanding of these shifts requires

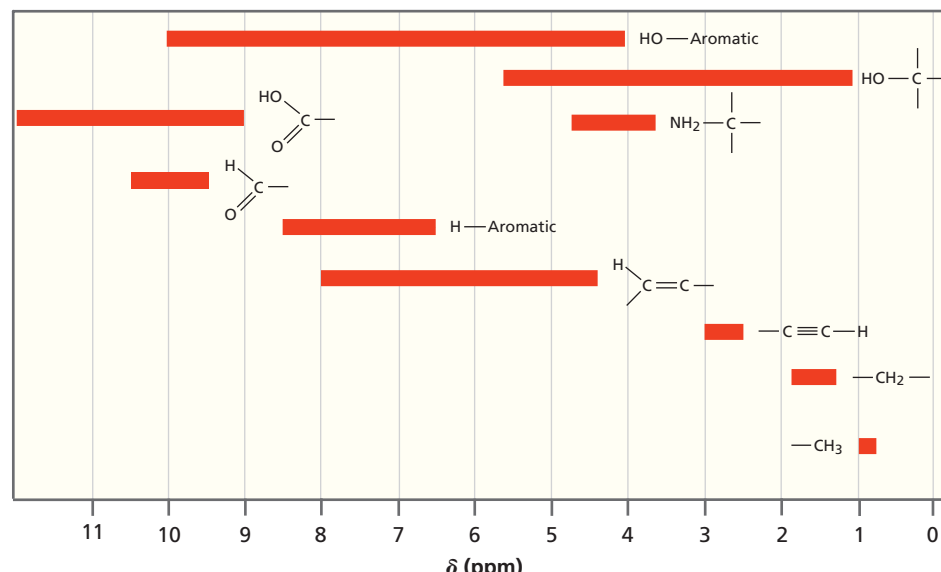
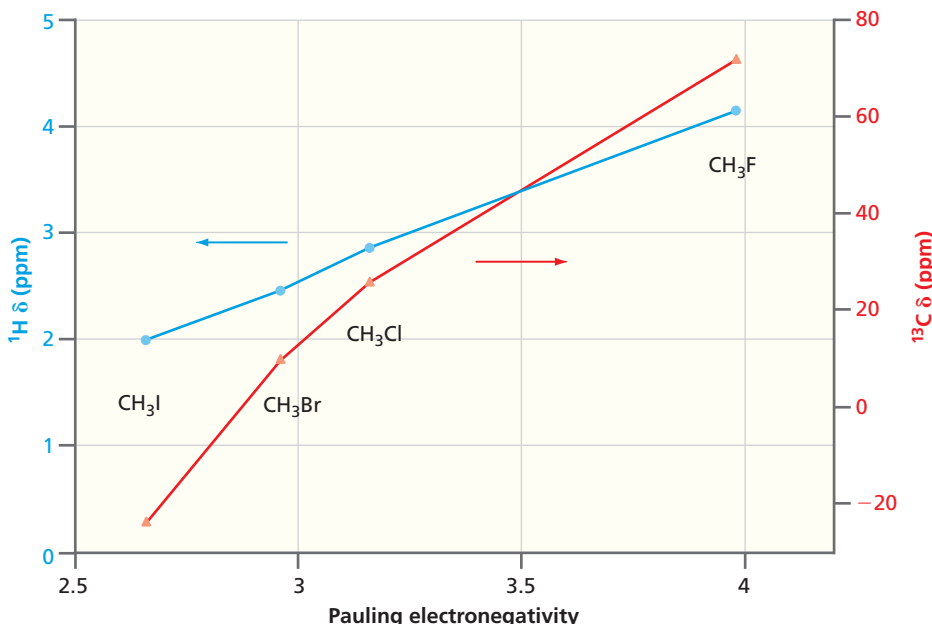


Figure 17.5

Chemical shifts δ as defined by Equation (17.12) for ^1H in different classes of chemical compounds. Extensive compilations of chemical shifts are available in the chemical literature.

**Figure 17.6**

Correlation of δ with the Pauling electronegativity of the halogen in methyl halides. ${}^1\text{H}$ chemical shifts are shown in blue circles and ${}^{13}\text{C}$ chemical shifts in red triangles.

the consideration of many factors, and numerical values can now be well predicted using quantum-chemical calculations. Conceptually, two factors are responsible for the major part of the chemical shift: the electronegativity and the induced magnetic field of a neighboring group at the position of the nucleus of interest. This leads us from considering only atoms and local effects to considering groups of atoms in molecules and remote effects.

Recall that the local diamagnetic chemical shift depends strongly on the electron density near the nucleus. The larger the electron density, the larger the shielding constant and the smaller the deshielding parameter δ . If a neighboring group increases in electronegativity, the electron density on the probe nucleus decreases, leading to smaller σ and larger δ . This is readily demonstrated in the methyl halides, which show an almost linear correlation between δ and the Pauling electronegativity of the substituent. Figure 17.6 shows this correlation for both ${}^1\text{H}$ and ${}^{13}\text{C}$ nuclei. The range of this effect is limited to about three or four bond lengths, as can be shown by considering the chemical shifts in 1-chlorobutane. In this molecule, δ for the ${}^1\text{H}$ on the CH_2 group closest to the Cl is almost 3 ppm larger than the ${}^1\text{H}$ on the terminal CH_3 group, which has nearly the same δ as in propane.

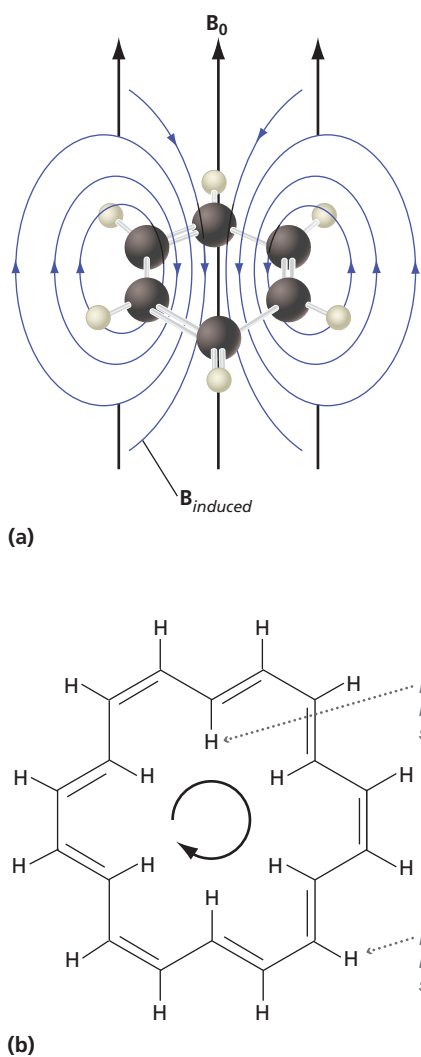
As Figure 17.4 illustrates, the effect of a magnetic dipole field at a location other than its center depends on the geometry and is therefore **anisotropic**, which implies different strengths of interaction in different directions. Depending on where a probe nucleus is located relative to the charge distribution that gives rise to the magnetic moment, it may experience a diamagnetic or a paramagnetic shift of its local magnetic field. Consider, for example, the locations labeled \mathcal{A} and \mathcal{B} in Figure 17.4. A nucleus in region \mathcal{A} experiences a shielding effect (δ decreases), whereas a nucleus in region \mathcal{B} experiences a deshielding effect (δ increases). The z component of the induced magnetic dipole field at any position in space can be calculated with the formula

$$B_z = \frac{\mu_0 |\boldsymbol{\mu}|}{4\pi |\mathbf{r}|^3} (3 \cos^2 \theta - 1) \quad (17.13)$$

In this equation, μ_0 is the vacuum permeability, $\boldsymbol{\mu}$ is the induced magnetic moment due to the ring currents of the charge distribution, \mathbf{r} is the distance vector between the origin (location of the magnetic dipole moment $\boldsymbol{\mu}$) and the nucleus of interest, and θ is the polar angle between the z axis and \mathbf{r} . Note that the induced field falls off rapidly with distance. Depending on whether $3 \cos^2 \theta > 1$ or $3 \cos^2 \theta < 1$, B_z will add to or subtract from the external applied magnetic field at the point (r, θ) and therefore deshield or shield a nucleus at that position. If the electron cloud that gives rise to the magnetic moment is spherical and therefore isotropic as in the example in Figure 17.4,

Concept

Two factors are responsible for the major part of the chemical shift: the electronegativity and the induced magnetic field of a neighboring group at the position of the nucleus of interest.

**Figure 17.7**

Ring currents in planar aromatic ring systems (a) The induced magnetic field generated by a ring current in benzene. Note that inside the ring the induced field is opposed to the external field, whereas outside the ring it is parallel to the external field. This leads to a paramagnetic shift for the ring protons. (b) 18-Annulene provides a confirmation of this model because δ has the opposite sign for interior and exterior ^1H and shows a diamagnetic shift for the protons inside the ring. δ for an exterior ^1H of 18-annulene is +9.3, and that for an interior ^1H is -3.0 ppm.

the shielding and deshielding effects on neighboring nuclei are averaged out by rapid tumbling of the molecule in a liquid. This effect occurs for other anisotropic magnetic interactions as well and will be considered further in Sections 17.4 and 17.8. However, if the charge distribution that leads to ring currents is not spherical, it will not completely average out and lead to a remote diamagnetic or paramagnetic shielding contribution. Striking examples of such behavior are the filled π molecular orbitals in the triple bond in acetylene or the delocalized π -orbitals in an aromatic ring such as benzene. When the $\text{C}\equiv\text{C}$ triple bond is aligned with the external field, a strong ring current will be observed; that is, the induced anisotropic magnetic moment has a large magnitude along the bond axis. This magnetic moment is very small for cases in which the bond axis is oriented perpendicular to the external field. Similarly, an aromatic ring system has a strong anisotropy and will lead to strong ring currents when its plane is perpendicular to the external magnetic field, whereas these currents are negligible when the magnetic field is oriented in the plane of the ring (see Figure 17.7). The effect is called **neighboring group anisotropy** and is observed in many molecules. This remote shielding effect is usually small (except for aromatic neighboring groups) and will not lead to significant line-broadenings in liquid state NMR. However, it leads to spectral broadening in solid-state NMR, as discussed in Section 17.8.

Before concluding our discussion of the chemical shift, we briefly mention the important topic of nuclear equivalency. Two atoms of the same kind are called chemically equivalent if they have the same connectivity within a molecule and their nuclei find themselves in identical electronic environments. Chemically equivalent atoms are usually connected by molecular symmetry, but one should also bear in mind that in the liquid or gas phase chemical groups can usually rotate freely about single bonds, which may lead to an averaging effect that will impose chemical equivalency on some nuclei, such as protons in a freely rotating methyl group. Chemical equivalency of two nuclei means that their chemical shifts are identical. However, accidental overlap of the NMR signals of chemically inequivalent nuclei is also possible. It is often observed in the protons of phenyl rings, which are strongly shielded by the ring currents in the conjugated π -bonds in the ring, yet are not chemically equivalent based on symmetry. In the next section, in which we will look at intramolecular nuclear spin coupling, we will consider nuclear equivalency in greater detail.

The discussion in this section has provided a brief introduction to the origin of the chemical shift in NMR spectroscopy. For ^1H , the range of observed values for δ among different chemical compounds is about 10 ppm. For nuclei in atoms that can exhibit both paramagnetic and diamagnetic behavior, δ can vary over a much wider range.

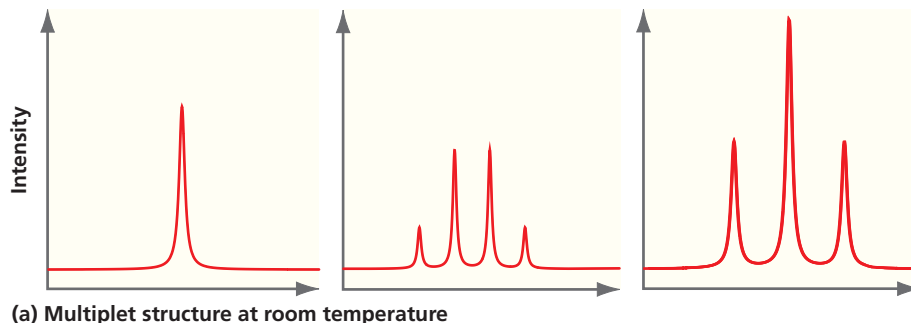
For example, δ for ^{19}F can vary by 1000 ppm for different chemical compounds. Vast libraries of ^1H NMR spectra for different compounds have been assembled and provide chemists with a valuable tool for identifying chemical compounds on the basis of chemical shifts in their NMR spectra.

17.4 SPIN-SPIN COUPLING AND MULTIPLLET SPLITTINGS

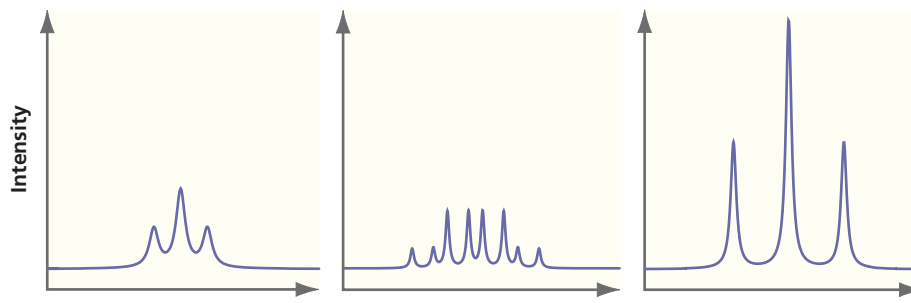
Although the chemical shift with its multitude of environmental effects discussed in the previous section is an extremely valuable tool to investigate molecular structure, it is not the only source of information available in NMR spectra. In this section, we discuss how neighboring nuclear spins affect each other by magnetic coupling through molecular bonds or through space.

We have noted that chemical shift effects are field-induced, which means they scale linearly with an applied magnetic field. However, another source of local field differences arises from the interaction of magnetic moments with neighboring nuclear spins. Local fields originating from neighboring nuclear magnetic moments are present even in the absence of an external magnetic field. However, as the orientation of the probe spin A and its neighbor X are both spatially quantized in the external field, the contribution of the magnetic moments of adjacent nuclear spins to the local field of A is discrete, which leads to a splitting of the NMR line of A into several lines called a **multiplet**. This multiplet structure is a sensitive indicator of the presence, number, and identity of any neighboring spin X and therefore is extremely important for understanding molecular structure using NMR. In this section, we will examine the physical mechanisms for the various forms of this so-called **spin–spin coupling** and consider several instructive examples.

For example, what might one expect the ^1H spectrum of ethanol to look like? A good guess is that each group of chemically equivalent protons resonates in a separate frequency range, one corresponding to the methyl group, another to the methylene group, and the third to the OH group. The OH proton is most strongly deshielded (largest δ) because it is directly bound to the electronegative oxygen atom. The H chemical shift for the OH group is ~ 5 ppm. Because the methylene group is closer to the electronegative OH group, its protons are more deshielded and appear at larger values of δ (near 3.5 ppm) than the methyl protons, which are found near 1 ppm. Furthermore, we expect that the areas of the peaks have the ratio 1:2:3 for the OH:CH₂:CH₃ groups because the NMR signal is proportional to the number of contributing nuclei. A simulated NMR spectrum for ethanol is shown in Figure 17.8. Starting with the spectrum in an aprotic solvent in which the OH-proton is not readily exchanged [Figure 17.8(b)], which prevents its spectral features from being averaged out, we note that the methyl and the OH protons are split into a triplet of lines with a characteristic intensity ratio of 1:2:1, whereas the methylene proton signal is split into eight lines, a so-called doublet of a quartet with an intensity ratio of 1:3 between the two outermost lines on both sides and the four inner lines. When measuring the molecule in the presence of small amounts of water (a protic solvent) and at higher temperature, the OH proton lines collapse into a single line, whereas the methylene doublet of a quartet becomes a quartet, yet still with a 1:3 intensity ratio between the outer and inner lines. The methyl proton triplet remains unchanged [Figure 17.8(a)].



(a) Multiplet structure at room temperature



(b) Multiplet structure observed at lower temperature in an aprotic solvent

Concept

The contribution of the magnetic moments of adjacent nuclear spins to the local field of A is discrete, which leads to a splitting of the NMR line of A into several lines called a multiplet.

Figure 17.8

Simulated NMR spectrum for ethanol. Intensity (vertical axis) is shown as a function of frequency. (a) Multiplet structure at room temperature with H_2O . (b) Multiplet structure observed at lower temperature than in (a) and in an aprotic solvent such as dimethylsulfoxide (i.e., without rapid proton exchange at the OH group). The different portions of the spectrum are not to scale but have the relative areas discussed in the text.

Multiplet splittings arise as a result of spin–spin interactions among different nuclei. To understand the observed multiplet structure for ethanol, we first consider the case of two distinguishable noninteracting spins, for example, one methyl and one methylene proton, and label them with index 1 and 2, respectively. At a later point, we will extend the discussion to the interaction of more than two spins. Because the methyl protons are more shielded than the methylene protons, $\sigma_1 > \sigma_2$. The quantum-mechanical energy operator describing the Zeeman splitting is given by

$$\hat{H} = -\gamma B_0(1 - \sigma_1)\hat{I}_{z_1} - \gamma B_0(1 - \sigma_2)\hat{I}_{z_2} \quad (17.14)$$

The spin eigenfunctions for this operator expressed in terms of the α - β nomenclature for spin-up and spin-down states are the products of the individual spin eigenfunctions along the z axis and are as follows:

$$\begin{aligned}\psi_1 &= \alpha(1)\alpha(2) \\ \psi_2 &= \beta(1)\alpha(2) \\ \psi_3 &= \alpha(1)\beta(2) \\ \psi_4 &= \beta(1)\beta(2)\end{aligned}\quad (17.15)$$

Using the properties of the spin operators in Equation (17.1), the following energy eigenvalues are obtained by applying the energy operator in Equation (17.14) on the wave functions in Equation (17.15):

$$\begin{aligned}E_1 &= -\gamma B_0 \hbar \left(1 - \frac{\sigma_1 + \sigma_2}{2}\right) \\ E_2 &= -\frac{\gamma B_0 \hbar}{2}(\sigma_1 - \sigma_2) \\ E_3 &= \frac{\gamma B_0 \hbar}{2}(\sigma_1 - \sigma_2) \\ E_4 &= \gamma B_0 \hbar \left(1 - \frac{\sigma_1 + \sigma_2}{2}\right)\end{aligned}\quad (17.16)$$

as shown in Example Problem 17.2. This energy-level diagram is shown in Figure 17.9.

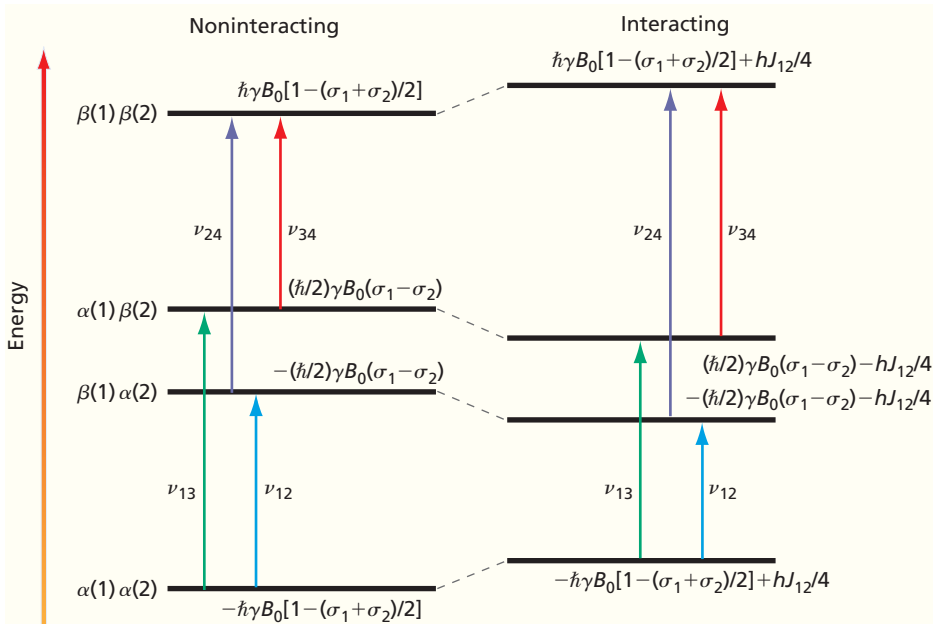


Figure 17.9

Energy-level diagrams for two inequivalent protons. Energy levels for two noninteracting spins and allowed transitions between these levels are shown on the left. The same information is shown on the right for interacting spins. Splitting between levels 2 and 3 and the energy shifts of all four levels for interacting spins are greatly magnified to emphasize spin–spin interactions.

EXAMPLE PROBLEM 17.2

Show that the total nuclear energy eigenvalue for the wave function $\psi_2 = \beta(1)\alpha(2)$ is

$$E_2 = -\gamma B_0 \hbar (\sigma_1 - \sigma_2)/2$$

Solution

$$\begin{aligned}\hat{\mathcal{H}}\psi_2 &= [-\gamma B_0(1 - \sigma_1)\hat{I}_{z_1} - \gamma B_0(1 - \sigma_2)\hat{I}_{z_2}]\beta(1)\alpha(2) \\ &= -\gamma B_0(1 - \sigma_1)\alpha(2)\hat{I}_{z_1}\beta(1) + [-\gamma B_0(1 - \sigma_2)]\beta(1)\hat{I}_{z_2}\alpha(2) \\ &= \frac{\hbar}{2}\gamma B_0(1 - \sigma_1)\beta(1)\alpha(2) - \frac{\hbar}{2}\gamma B_0(1 - \sigma_2)\beta(1)\alpha(2) \\ &= -\frac{\gamma\hbar B_0}{2}(\sigma_1 - \sigma_2)\beta(1)\alpha(2) = E_2\psi_2\end{aligned}$$

For allowed NMR transitions, the selection rules are $\Delta m_I = \pm 1$, which indicates that one of the two spins will have to flip up or down. Four transitions between the four levels are allowed, as shown in Figure 17.9. In the noninteracting case, this leads to only two signals that appear at two distinct frequencies according to the different chemical shifts:

$$\begin{aligned}\nu_{12} = \nu_{34} &= \frac{E_2 - E_1}{h} = \frac{E_4 - E_3}{h} = \frac{\gamma B_0}{2\pi}(1 - \sigma_1) \\ \nu_{13} = \nu_{24} &= \frac{E_3 - E_1}{h} = \frac{E_4 - E_2}{h} = \frac{\gamma B_0}{2\pi}(1 - \sigma_2)\end{aligned}\quad (17.17)$$

We next consider the case of interacting spins. Because each of the nuclear spins acts like a small bar magnet, spins interact with one another through spin–spin coupling. There are two different types of spin–spin coupling: (1) through-space vectorial dipole coupling, which is important in the NMR of solids (see Section 17.8), and (2) through-bond, or scalar coupling. Dipolar coupling can be treated similarly to the way we treated the remote anisotropic chemical shift in the previous section. The local magnetic field differences generated by dipolar coupling average out in liquid-state NMR (see discussion below). In contrast, scalar coupling does not change with the orientation of the molecule in the external field, and therefore does not cancel out during rapid tumbling of the molecule. It leads to an up- or down-shift of the resonance frequency. The effect is usually small compared to the chemical shift and decreases with distance between the two nuclei. However, it is responsible for the multiplet splitting shown in Figure 17.8. Unless the two nuclei have very similar chemical shifts, or the molecule has a large number of ^1H (as in the case of proteins), multiplets on nonequivalent nuclei tend not to overlap, making analysis of the NMR spectra of small molecules straightforward. The energy operator for the scalar coupling contribution is given by the scalar product of the two nuclear spin operators:

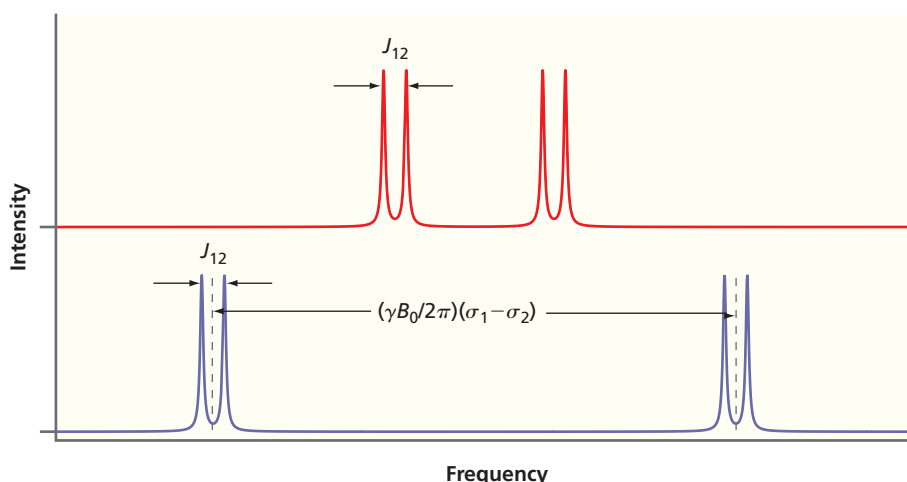
$$\hat{\mathcal{H}}_J = \frac{\hbar}{\hbar^2} J_{12} \hat{\mathbf{I}}_1 \cdot \hat{\mathbf{I}}_2 \quad (17.18)$$

In this equation, the parameter J_{12} is the coupling constant, which measures the strength of the coupling between the two magnetic moments. The factor \hbar/\hbar^2 is included to ensure that the units of J_{12} are in frequency units, s^{-1} . Because the interaction energy hJ_{12} is orders of magnitude smaller than the Zeeman splitting, its energy operator can be considered to be a small perturbation of the Zeeman energy operator in Equation (17.14), which allows us to apply an approximation called perturbation theory to calculate the energy shifts in the basis of the unperturbed spin functions, $\alpha(i)$ and $\beta(i)$. Without further proof, the energy correction for the four states in Equation (17.15) can be calculated using Equation (17.18) as

$$\begin{aligned}\Delta E_j &= \iint \psi_j^* \hat{\mathcal{H}}_J \psi_j d\tau_1 d\tau_2 = \frac{\hbar}{\hbar^2} J_{12} \iint \psi_j^* \hat{\mathbf{I}}_1 \cdot \hat{\mathbf{I}}_2 \psi_j d\tau_1 d\tau_2 \\ &= \frac{\hbar}{\hbar^2} J_{12} \iint \psi_j^* \hat{I}_{z_1} \cdot \hat{I}_{z_2} \psi_j d\tau_1 d\tau_2 = hm_1 m_2 J_{12}\end{aligned}\quad (17.19)$$

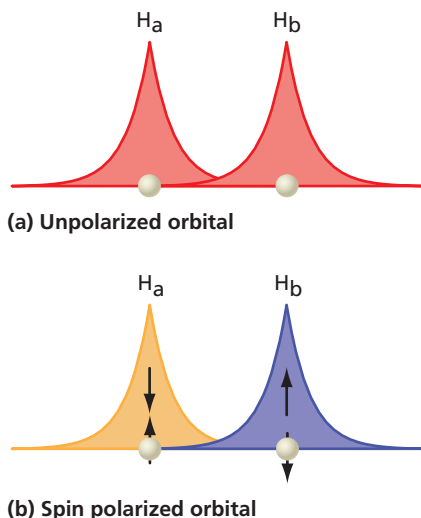
Figure 17.10

Splitting of a system of two interacting spins into doublets for two values of B_0 . The same system of two nuclei in two different magnetic fields. B_0 for the lower spectrum is significantly greater than that for the upper spectrum. Spacing within the doublet is independent of magnetic field strength, but spacing of the doublets increases linearly with B_0 .



In this equation, the indices 1 and 2 on the magnetic quantum numbers m refer to nuclei 1 and 2. In our example of two coupling protons, $m_I = \pm 1/2$, which leads to a negative sign for ΔE in Equation (17.19) for cases in which the two spins are antiparallel and point in opposite direction and ΔE is positive for cases in which they are parallel. The corrections to the resonance frequencies in Equation (17.17) are therefore:

$$\begin{aligned}\nu_{12} &= \frac{\gamma B_0}{2\pi}(1 - \sigma_1) - \frac{J_{12}}{2} \\ \nu_{34} &= \frac{\gamma B_0}{2\pi}(1 - \sigma_1) + \frac{J_{12}}{2} \\ \nu_{13} &= \frac{\gamma B_0}{2\pi}(1 - \sigma_2) - \frac{J_{12}}{2} \\ \nu_{24} &= \frac{\gamma B_0}{2\pi}(1 - \sigma_2) + \frac{J_{12}}{2}\end{aligned}\quad (17.20)$$

**Figure 17.11**

Schematic illustration of how spin polarized orbitals facilitate scalar coupling between nuclear spins. Nuclei are represented by gray spheres. The shaded areas represent the s orbitals surrounding the nuclei. (a) Unpolarized orbitals without coupling between the nuclei. (b) Spin polarized orbitals illustrating coupling between the nuclear spins. The upper and lower arrows indicate the electron and nuclear spins, respectively.

When $J_{12} > 0$ the energy levels for parallel spins are increased but for the case of antiparallel spins, as indicated in Figure 17.9, they are decreased. We see that the two frequencies of the noninteracting case have now become four frequencies for two interacting spins. Because we only considered two coupled nuclei, the noninteracting signals have been split into two doublets, as shown in Figure 17.10. Note that the first term in the expressions in Equation (17.20) is dependent on the external magnetic field B_0 because it represents the Zeeman effect, whereas the second term is independent of the magnetic field and reflects only the spin–spin interaction. This illustrates one of the advantages of higher magnetic fields for NMR: higher fields result in a better separation of multiplets for nuclei with different chemical shifts and therefore a higher resolution in spectra with many nuclei, such as proteins or nucleic acids.

Scalar or J coupling is transmitted through electrons in chemical bonds. Figure 17.11 illustrates how two nuclei (H_a and H_b) may couple through local electron orbitals that overlap with each other by a mechanism that is termed *spin polarization* and should not be confused with the same term describing population differences between spin states (which was discussed in Section 17.2). Figure 17.11a shows the unpolarized case in the absence of nuclear spins. Because the electrons in both s -type orbitals on nuclei H_a and H_b are paired, they remain unpolarized. A nuclear spin on H_a (in α orientation in Figure 17.11b) will polarize the electrons in the orbital in its vicinity, promoting an excess of β electron spin because antiparallel nuclear and electron spin orientations are energetically favored. This polarization effect on the electrons cannot happen within an isolated filled molecular orbital but needs the admixture of low-lying empty excited state orbitals. The polarization also must be offset by an opposite polarization elsewhere in the molecule to ensure that the overall net polarization of the electrons remains zero. The effect is transmitted to the neighboring nuclei via the orbital overlap of s -atomic orbitals in the bond between the atoms. An excess of

α polarization is created in the orbital near nucleus H_b, which lowers the energy of the β nuclear spin at that position because of the antiparallel arrangement of nuclear and electron spins. A well-shielded nuclear spin can still sense the spin orientation of its neighbors through this interaction. Because the effect is weak and other factors favor molecular orbitals without polarization, the degree of spin polarization is very small. However, it is sufficient to account for the parts per million changes in the frequency of NMR transitions in multiplets.

In our simple example of two coupled protons, we assumed a positive coupling constant, $J_{12} > 0$. However, the sign and magnitude of the spin–spin coupling cannot easily be predicted in more complicated cases without very accurate molecular wave functions and detailed knowledge of low-lying excited states necessary to promote spin polarization. Because the sign of the coupling constant does not affect the structure of the resulting multiplets, its knowledge is not essential for structural determinations. The magnitude of J diminishes rapidly with increasing distance between the spin pair. The 280 Hz coupling constant in H₂ is among the largest known. Other one-bond coupling constants such as between a hydrogen bonded to a carbon, $^1J_{\text{CH}}$, are in the range 100–250 Hz and depend on the amount of *s*-character in the hybridization of the carbon. In the series ethane, ethene, ethyne, the increasing *s*-character of the hybrid orbital of carbon, sp^3 , sp^2 , and sp , that participates in the CH bond leads to increasing J coupling constants of 125, 157, and 250 Hz, respectively. Two-bond proton–proton couplings, $^2J_{\text{HH}}$, are smaller and vary within a range of –25 to +45 Hz with large substituent effects. Although even smaller, with only approximately 20 Hz, the most useful spin–spin couplings are 3-bond couplings of vicinal protons (on neighboring heteroatoms), such as $^3J_{\text{HH}}$ in H—C—C—H fragments. They vary with the dihedral torsion angle θ , according to the **Karplus relation**:

$$^3J = A + B \cos \theta + C \cos^2 \theta \quad (17.21)$$

and provide useful information regarding the backbone conformation of amino acid chains, which depend on the dihedral angle between the amide and C _{α} protons of the peptide bond. The main structural protein folding motifs, α -helices and β -sheets, have characteristic H—N—C _{α} —H dihedral angles of approximately -120° and 180° , respectively.¹ The parameters A , B , and C are empirically derived constants that depend on the atoms present. Four-bond couplings are generally very small (that is, less than 1 Hz), but exceptions occur, for example, when spin–spin coupling is mediated by an extended π -electron chain.

Not all NMR peaks are split into multiplets. To understand this observation, it is important to distinguish between **chemically equivalent nuclei** and **magnetically equivalent nuclei**. Consider the two molecules shown in Figure 17.12. In both cases, the two H atoms and the two F atoms are chemically equivalent. The nuclei of chemically equivalent atoms are also magnetically equivalent *only* if the interactions that they experience with other nuclei of nonzero spin are identical. Because the two F nuclei in CH₂F₂ are equidistant from each H atom, the two H—F couplings, $^2J_{\text{HF}}$, are identical and the ¹H are magnetically equivalent, and no multiplet splitting is observed. However, in CH₂CF₂ the $^2J_{\text{HF}}$ are different because the spacing between a H and each F nucleus is different. Therefore, the ¹H nuclei in this molecule are magnetically inequivalent, and a multiplet splitting is observed. Multiplet splitting only arises through the interaction of magnetically inequivalent nuclei and therefore is not observed in the reference compound for chemical shifts, (CH₃)₄Si.

Until now, we have only considered spin–spin coupling between a pair of spins, A and X , which leads to doublet splittings of lines of both nuclei centered at their respective chemical shifts by a frequency difference $\Delta\nu = J_{\text{AX}}$. Of course, this does not explain the triplet or quartet splittings observed for ethanol (seen in Figure 17.8), which arise as a result of the coupling of more than two nuclei. We will now consider a more complex situation with the coupling of three distinct spin-1/2 nuclei labeled A , M , and X . The two coupling constants to consider for the probe nucleus are J_{AM} and J_{AX} , and let us assume that $J_{\text{AM}} > J_{\text{AX}}$. The effect of these couplings can be visualized by

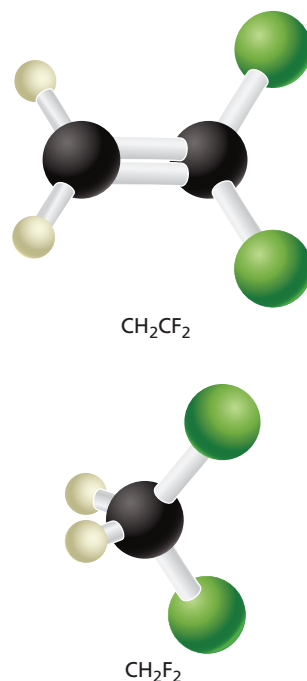


Figure 17.12

Illustration of chemical versus magnetically equivalency. The H atoms in CH₂CF₂ are chemically equivalent but magnetically inequivalent. The H atoms in CH₂F₂ are chemically and magnetically equivalent.

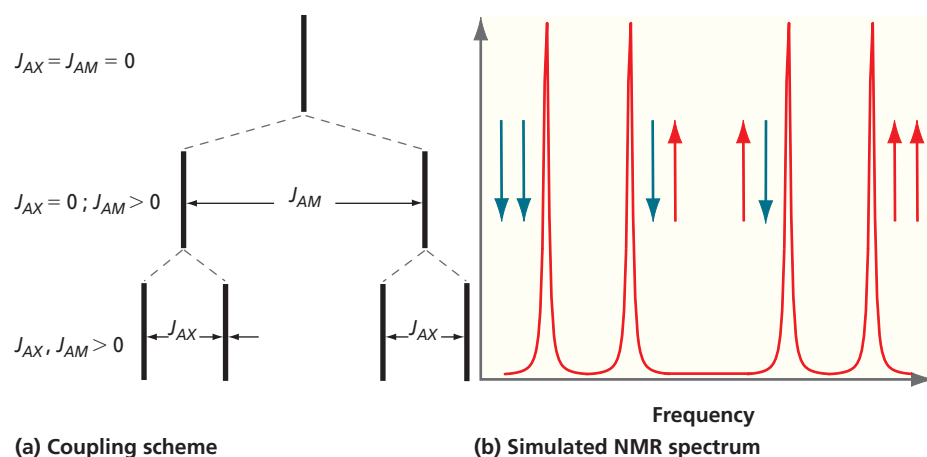
Concept

Not all NMR peaks are split into multiplets. To understand this observation, it is important to distinguish between chemically equivalent nuclei and magnetically equivalent nuclei.

¹These angles should not be confused with the torsional angle ϕ normally quoted for protein structures.

Figure 17.13

Coupling scheme and expected NMR spectrum for spin A coupled to spins M and X with different coupling constants J_{AX} and J_{AM} . The vertical axis shows the signal intensity.

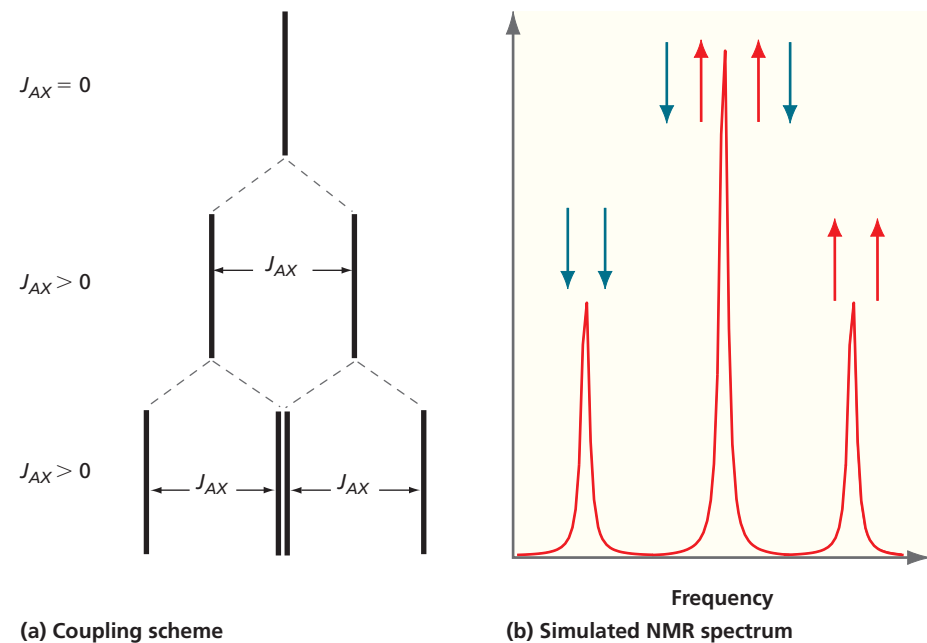


turning on the couplings individually, as indicated in Figure 17.13. The result is that each of the lines in the doublet that arises from turning on the interaction J_{AM} is again split into a second doublet when the interaction J_{AX} is turned on.

The four resonance frequencies can be obtained using similar approximations as for Equation (17.20):

$$\nu_A = \frac{\gamma B_0}{2\pi} (1 - \sigma_A) - \sum_{K=M,X} J_{AK} m_A m_K \quad (17.22)$$

A special case occurs when A and M are magnetically equivalent, so that $J_{AM} = J_{AX}$. Because the middle two lines for the AMX case now overlap at the same frequency, the doublet of doublets converts into a triplet with an unequal 1:2:1 line intensity ratio. This is the so-called AX_2 pattern shown in Figure 17.14. Such a spectrum is observed for both the OH proton (in aprotic solvent) and the methyl protons in ethanol, both of which couple to the two magnetically equivalent methylene protons via a 3-bond interaction.

**Figure 17.14**

Analysis of the AX_2 pattern. (a) Coupling scheme and (b) expected NMR spectrum for spin A coupled to two spins X. In this case, there is only one coupling constant J_{AX} . The closely spaced lines in the lower part of (a) actually coincide, though they are shown separated to make their origin clear. The vertical axis in (b) shows the signal intensity.

EXAMPLE PROBLEM 17.3

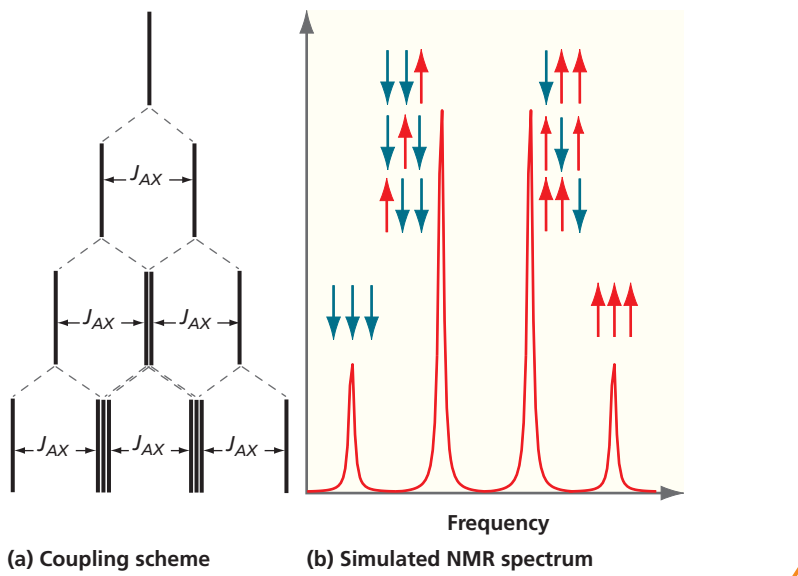
Using the same reasoning as that applied to the AX_2 case, predict the NMR spectrum for an AX_3 spin system and give the resonance frequencies for the probe nucleus A. Such a spectrum is observed for methylene protons in the ethanol molecule in which the coupling is with the methyl group hydrogens.

Solution

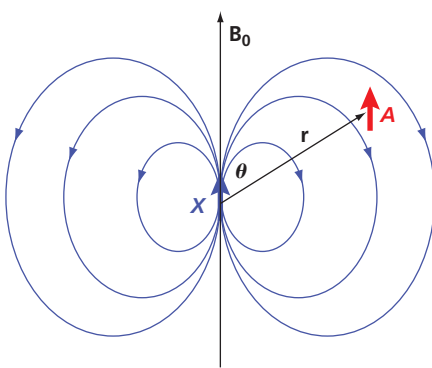
The resonance frequencies are obtained as above from Equation (17.22) by extending the sum to the third X nucleus:

$$\nu_A = \frac{\gamma B_0}{2\pi} (1 - \sigma_A) - \sum_{j=1}^3 J_{AX_j} m_A m_{X_j}$$

Turning on each of the interactions in sequence results in the following diagram in which significant line overlap occurs because only one coupling constant is present in this system. The ratio of line intensities is given as 1:3:3:1. These results can be generalized to the rule that if a ${}^1\text{H}$ nucleus has n equivalent ${}^1\text{H}$ neighbors, its NMR spectral line will be split into $n + 1$ peaks. The relative intensity of these peaks is provided by the coefficients in the expansion of $(1 + x)^n$, the binomial expression.



Having discussed spin–spin coupling, we are now in a position to fully understand the spectra of ethanol, shown in Figure 17.8, in protic and aprotic solvents. In aprotic solvent, the OH proton is a triplet owing to the presence of two magnetically equivalent methylene protons three bonds away. The methyl protons are too distant to have any meaningful coupling with the OH proton. Each of the three methyl protons experiences the same scalar coupling effect with the two methylene protons and therefore shows a triplet splitting. The methylene protons experience the most complex splitting pattern because both neighbors, the OH proton and the methyl group, are only three bonds away. Because they are not magnetically equivalent, the coupling strengths are different, with the OH proton providing a somewhat larger coupling constant. This leads to an eight-line multiplet with a 1:3 intensity ratio between the two outermost lines on either side of the spectrum and the four inner lines. Switching the couplings on sequentially, one can see that this pattern is a doublet of a quartet. No accidental line overlap is present beyond the AX_3 quartet. When ethanol is placed in a protic solvent at room temperature, the OH proton exchanges rapidly with the solvent, which averages out the effect of its scalar coupling with neighboring nuclei. Essentially, the respective J goes to zero. This reduces the triplet of the OH proton to a singlet and the doublet of quartets of the methylene protons to a quartet that arises solely from the coupling with the three methyl protons.

**Figure 17.15**

Dipolar coupling between two spin magnetic moments A and X in an external magnetic field. The correction to the local field at the position of nucleus A depends on the angle θ , which in turn depends on the orientation of the molecule (containing the two nuclei) with respect to the external field.

We now turn our attention to the **dipolar spin–spin coupling** mechanism. Dipolar spin–spin coupling is the magnetic coupling of two nuclear spins through space. This mechanism is responsible for spectral broadening in ssNMR but does not lead to multiplet splittings in the liquid state because it is usually averaged out by rapid tumbling. However, dipolar spin–spin coupling is relevant to liquid-state NMR because it is the main spin relaxation mechanism (discussed in more detail in Section 17.5). Consider the magnetic dipole moments of a pair of spin-1/2 nuclei of different kind, labeled A and X , that interact with each other through space, as illustrated in Figure 17.15, which is similar to that discussed previously for the remote chemical shift (see Figure 17.4), except that in this case the local magnetic field correction that probe nucleus A experiences originates from the spin magnetic moment of its neighboring nucleus, X . Again, whether the correction is paramagnetic or diamagnetic (increases or decreases the external field) depends on the position of nucleus X relative to nucleus A and the external magnetic field. In a fixed geometry, that is, in the solid state, the resonance frequency of nucleus A becomes dependent on the orientation of the molecule with respect to the magnetic field.

The local field contribution from the magnetic moment of X in the z direction at the location of nucleus A can be calculated semiclassically as

$$B_{X_z} = -\left(\frac{\mu_0}{4\pi}\right) \frac{\gamma_X \hbar m_X}{|\mathbf{r}_{AX}|^3} (1 - 3 \cos^2 \theta) \quad (17.23)$$

Its contribution to the energy operator [Equation (17.14)] can again be treated as a perturbation and calculated separately using the Zeeman basis functions [Equations (17.15)]. It takes the simple form:

$$\begin{aligned} \hat{\mathcal{H}}_d &= -\left(\frac{\hbar}{\hbar^2}\right) d (3 \cos^2 \theta - 1) \mathbf{I}_{X_z} \cdot \mathbf{I}_{A_z} \\ d &= \left(\frac{\mu_0}{4\pi}\right) \frac{\gamma_A \gamma_X}{|\mathbf{r}_{AX}|^3} \end{aligned} \quad (17.24)$$

where the parameter d is used to denote the dipolar spin–spin coupling constant. It decays with the third power of the distance between the two spins, a property that can be used to measure distances between neighboring spins. Considering just the A spin, we can determine the following two possible transition frequencies with X in the α or β state:

$$\nu_A = \frac{\gamma B_0}{2\pi} (1 - \sigma_A) \pm \frac{d}{2} (3 \cos^2 \theta - 1) \quad (17.25)$$

Depending on the value of the polar angle θ , the resonance frequency of nucleus A shifts lower (diamagnetic) or higher (paramagnetic). This effect leads to line-broadening in ssNMR, as we will further explore in Section 17.8. In low-viscosity liquids, the rapid tumbling of the molecules changes the angle θ randomly over its entire range during the NMR experiment, and the frequency shifts are therefore averaged out, allowing for the observation of narrow NMR lines. However, the effect still manifests itself in the dynamic behavior of the nuclear spins, which is explored further in Section 17.5.

17.5 SPIN DYNAMICS

In the preceding sections, we discussed the energetic splittings of the quantized states of nuclear spins in various environments and how they affect the appearance of an NMR spectrum. However, nuclear spins are dynamic. They interact with each other and with their environment in a time-dependent fashion that has implications for how NMR spectra are measured and provides further information that can be used in building structural and dynamic models for a system of interest. In this section, we focus on the way the time-dependent magnetic field component of the RF interacts with the nuclear magnetization. We will also discuss different forms of relaxation of nuclear spins and the nuclear Overhauser effect.

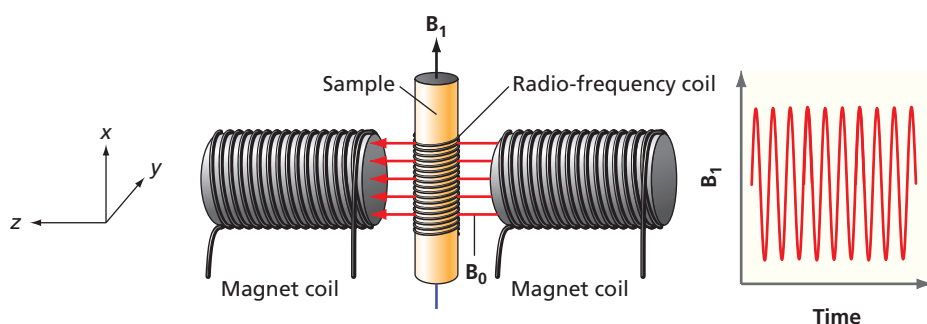


Figure 17.16

Schematic diagram of the NMR experiment showing the static field and the RF field coil. The coordinate system on the left refers to the vector model in which the z axis is parallel to the external magnetic field, \mathbf{B}_0 , and the magnetic field component of the RF field, \mathbf{B}_1 , is lined up with the x axis. The magnetic field oscillates rapidly with time, as seen in the graph to the right of the figure.

To understand the way nuclear spins react to resonant RF pulses, it is helpful to introduce the **vector model** of nuclear magnetization. This model describes the macroscopic magnetization vector \mathbf{M} within a Cartesian coordinate system in which the z axis is lined up with the external magnetic field direction. The x and y axes represent the plane in which the magnetization vector precesses about the z axis. We already alluded to this model earlier (see Figure 17.1). We remind ourselves that when the spin system is in thermal equilibrium with its environment its macroscopic magnetic moment vector \mathbf{M} is oriented parallel to the external magnetic field vector \mathbf{B}_0 because this will minimize the magnetic contribution to the energy [Equation (17.3)].

In order to induce transitions between the α -level and β -level of the nuclear spin system, the selection rules for magnetic dipole transitions dictate that the directions of the two relevant magnetic field vectors, \mathbf{B}_0 , the external magnetic field, and \mathbf{B}_1 , the oscillating magnetic field vector of the resonant RF field, have to be perpendicular to each other. In practice, this condition is achieved by orienting the excitation (and detection) coils perpendicular to the external magnetic field in the x - y plane, as shown in Figure 17.16.

In this arrangement, the \mathbf{B}_1 field is linearly polarized and points along the x axis in the laboratory coordinate system. It can be decomposed into two counterrotating vector components that represent a clockwise and counterclockwise circularly polarized RF field, as illustrated in Figure 17.17. When the oscillation frequency equals the

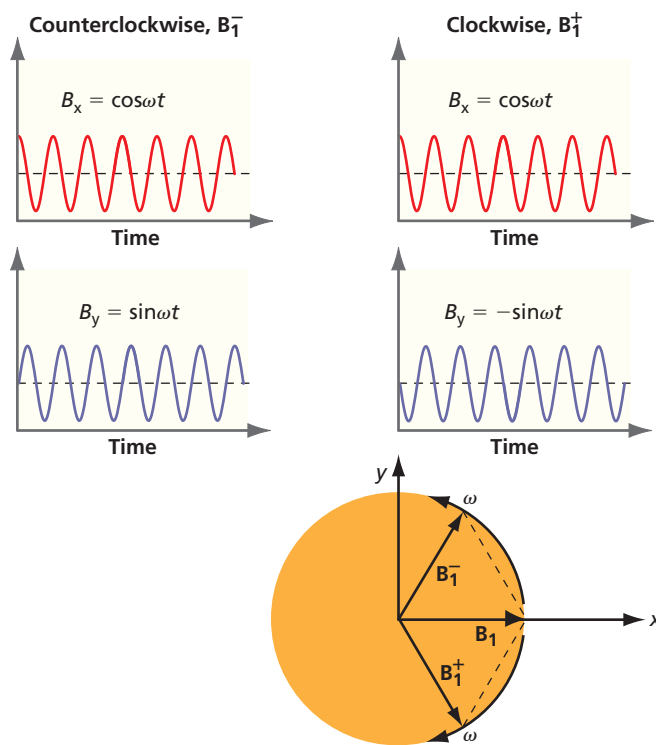


Figure 17.17

A linearly polarized oscillating field, \mathbf{B}_1 , can be decomposed into a superposition of two circularly polarized waves, \mathbf{B}_1^+ and \mathbf{B}_1^- , rotating in opposite directions. \mathbf{B}_1 oscillates along the x axis. It is decomposed into a clockwise and counterclockwise rotating component by addition of an oscillating field along the y axis that is phase-shifted by 90° . Note that the y component of the two circularly polarized fields \mathbf{B}_1^+ and \mathbf{B}_1^- are out of phase by 180° and therefore cancel each other out completely. Adding \mathbf{B}_1^+ and \mathbf{B}_1^- together recovers \mathbf{B}_1 .

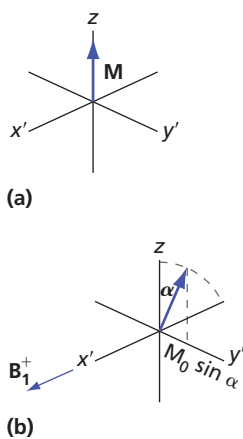


Figure 17.18

Effect of a resonant electromagnetic RF field on the magnetization in the rotating frame vector model. (a) The equilibrium magnetization is aligned along the z axis. (b) The resonant RF field is turned on with its magnetic field component \mathbf{B}_1^+ pointing along the x' axis. This induces a torque on the nuclear spins and produces a precession about the \mathbf{B}_1^+ field direction in the y' - z plane. When \mathbf{B}_1^+ is turned off, the magnetization has undergone a rotation in the y' - z plane described by the tip angle α [see Equation (17.26)]. Based on J. Keeler, Understanding NMR Spectroscopy, Chapter 3, Figs. 3.4 and 3.7.

Concept

In order to visualize the dynamic processes that occur during resonant RF pulses or spin relaxation in which the spin system returns to thermal equilibrium, it is useful to transform the coordinate system into the so-called rotating frame of reference.

Larmor frequency, $\omega = \omega_0$, the electromagnetic field is in resonance with the nuclear spins and will induce transitions. However, only the clockwise rotating component will effectively couple to the magnetization because both rotate with the same sense and frequency around the z axis and can therefore couple effectively. The component that rotates counterclockwise will have a negligible effect.

In order to visualize the dynamic processes that occur during resonant RF pulses or spin relaxation in which the spin system returns to thermal equilibrium, it is useful to transform the coordinate system into the so-called **rotating frame** of reference. Instead of looking at the magnetization in the laboratory coordinate system with the axes x , y , and z , the observer rotates about the z axis along with the circularly polarized magnetic field of the resonant RF wave, denoted \mathbf{B}_1^+ (see Figure 17.17). It leads to considerable simplifications in the visualization and interpretation of the dynamic motion of the macroscopic magnetization vector because \mathbf{M} rotates in the same direction with the same angular velocity and appears to stand still in the rotating frame if the RF field is in resonance with the nuclear spin. Because the rotation is about the z axis, the transformed z' axis is identical to the z axis, whereas the transformed x' and y' axes follow the rotational motion of \mathbf{B}_1^+ in the x - y plane. A by-product of this transformation is that the external magnetic field vanishes in the rotating frame and \mathbf{B}_1^+ (in our case applied along the x' axis) is the only magnetic field that can exert a torque on the magnetization vector. It will now rotate \mathbf{M} away from its equilibrium position along z by an angle α in the y' - z plane, as shown in Figure 17.18.

The so-called *tip angle* α is proportional to the strength of the \mathbf{B}_1 field and the time interval Δt during which the RF field is applied to the spin system. It also depends on the gyromagnetic ratio because the torque depends on the magnitude of the magnetic moment of the spin. The expression for the tip angle is as follows:

$$\alpha = \frac{\gamma_N B_1 \Delta t}{2} \quad (17.26)$$

The factor of 2 in Equation (17.26) arises because only half of the \mathbf{B}_1 field strength is present in the circularly polarized field, \mathbf{B}_1^+ , that induces the transition. Both \mathbf{B}_1 and Δt are experimental parameters under the control of the NMR spectroscopist. Matching them to the γ_N of the nucleus of interest allows the creation of RF pulses with specific tip angles, such as 90° or 180° as in the famous Hahn echo discussed in Section 17.6. Keeping a strong \mathbf{B}_1 field applied to the sample for long time intervals leads to a rotation of the magnetization in the y' - z plane by multiple periods, the so-called Rabi oscillation with the frequency ω_1 . It describes the precession of \mathbf{M} about the \mathbf{B}_1^+ field. The Rabi frequency is given by the following expression:

$$\omega_1 = \frac{\gamma_N B_1}{2} \quad (17.27)$$

In practice, the dependency of the Rabi frequency on B_1 allows one to measure the B_1 field strength in a given NMR probe. A NMR probe is the part of the spectrometer that contains the sample and allows one to irradiate it with RF. The NMR probe also contains the detection coils and in some instruments, signal preamplifiers. Rabi oscillations are damped over time because of the energetic losses between the spins and their environment, which are due to **relaxation** processes and are important for the experimental observation of NMR transitions and for the understanding of spin dynamics.

Consider the following thought experiment: You rapidly place a system of chemically equivalent ^1H spins from zero magnetic field into an NMR magnet and attempt to measure its spectrum. At zero field, the two spin states α and β are degenerate and have equal population. If there is no spin relaxation, the equal population of the two states will persist even after the sample is placed into the NMR magnet, which produces zero intensity of the NMR spectrum. At this point, the spin system is not in thermodynamic equilibrium with its environment because there are too many spins in state β . As all natural systems do, the ^1H spins will tend to achieve equilibrium over time by transitioning the excess β population to the ground state α . This process is called **spin-lattice relaxation** (SLR) because the spin system will dump its excess

energy by heating the “lattice,” which is a general term for the matter surrounding the nuclei. This relaxation process is usually exponential in time. The rate at which it proceeds is related to a characteristic time constant, called T_1 , which is determined by the strength of the coupling of the spin system with its environment and therefore is system-dependent. Therefore, the polarization, and with it the macroscopic magnetization, build up over time starting from zero and approach the equilibrium polarization exponentially according to

$$P(t) = P_{\text{eq}} \left\{ 1 - \exp\left(-\frac{t}{T_1}\right) \right\}$$

$$M_z(t) = M_{\text{eq}} \left\{ 1 - \exp\left(-\frac{t}{T_1}\right) \right\} \quad (17.28)$$

which is depicted in Figure 17.19. This relaxation behavior is expected to occur for situations in which the polarization is perturbed from its equilibrium value, which can be initiated by sudden events such as field jumps (a sudden change in magnetic field, as in our thought experiment), temperature jumps, and chemical reactions, but most notably excitation of the nuclear spin system by RF pulses used in the NMR experiment. Typical T_1 relaxation times for protons in water range between hundreds of milliseconds to several seconds. T_1 relaxation is also referred to as *longitudinal relaxation*.

What are the mechanisms leading to T_1 relaxation? Spontaneous emission can be excluded as it depends on the third power of the energy gap, which is extremely small for NMR compared to other spectroscopic techniques. Collisions between molecules, though numerous, are ineffective as well because the nuclear spins remain aligned with the external magnetic field and not with the molecular orientation. However, anisotropic magnetic interactions, such as the dipolar interaction discussed in the preceding section, have a profound influence on the magnetic energy levels of a nucleus as the molecule tumbles freely in solution. Although the effect on the actual spectrum is averaged out, the constant and random jumps of the local magnetic field, induced, for example, by the dipolar field of a neighboring nucleus, has a strong dynamic effect on the probe spin and its magnetic moment and therefore causes SLR.

As it turns out, SLR is not the only type of relaxation for a spin system. When an ensemble of spins is in thermodynamic equilibrium, its macroscopic magnetization vector \mathbf{M} is aligned with the external magnetic field along the z axis. However, this does not need to be the case when the system is far from equilibrium. In fact, we will see later

Concept

A spin system approaches equilibrium by exchanging energy with neighboring molecules in a process called spin-lattice relaxation that has the characteristic time T_1 .

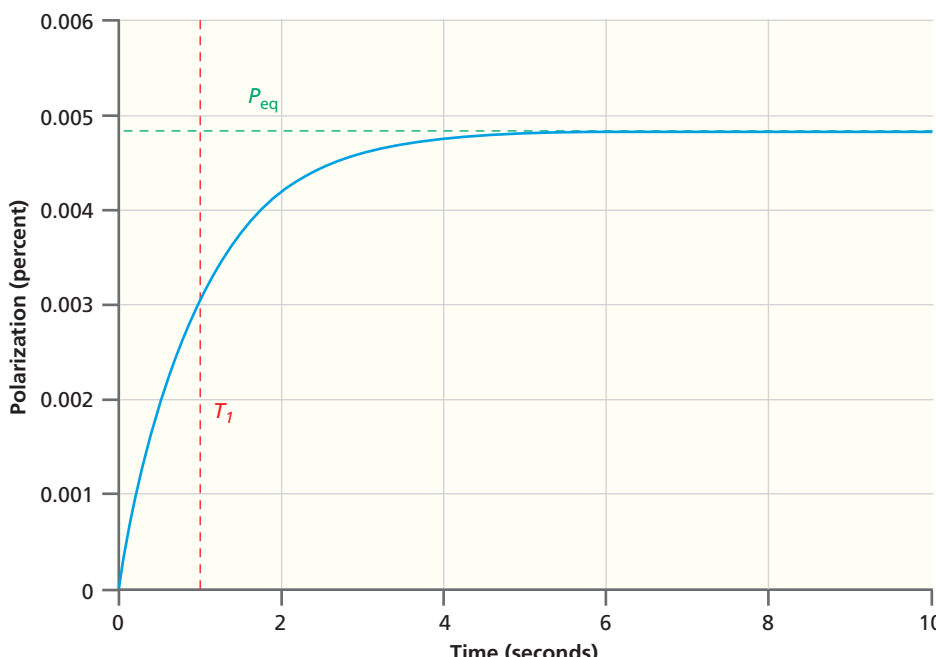


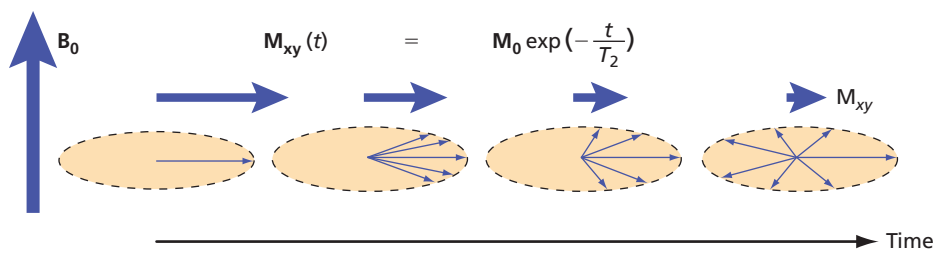
Figure 17.19
Exponential relaxation of the spin polarization P . The experiment begins with a polarization value of zero, indicating complete saturation, and ends with the equilibrium value as determined by the Boltzmann population. The characteristic time constant T_1 in this example is 1 s. The equilibrium polarization was calculated according to Equation (17.28) for proton spins at room temperature in a field of 14.1 T, which is used in a 600 MHz spectrometer.

Figure 17.20

Depiction of the loss of transverse magnetization in the x - y plane over time due to dephasing of individual spin packets from each other. The magnetization vector \mathbf{M}_{xy} represents the vector sum over individual magnetization vectors that precess about the z axis (parallel to \mathbf{B}_0), with slightly different angular velocities due to slightly different local magnetic fields at the location of each nucleus.

Note that the vector that appears to stay in place belongs to spin packets that precess exactly with the reference frequency of the rotating frame.

Source: Adapted from: <http://mriquestions.com/what-is-t2.html>.



that its component perpendicular to the z direction, called the *transverse component*, is critical to detecting the NMR signal. Hence, there is a so-called transverse or spin-spin relaxation mechanism (T_2 relaxation) that will decrease the macroscopic magnetization vector perpendicular to z , \mathbf{M}_{xy} , by dephasing individual magnetic moments in the x - y plane (see Figure 17.20).

Unlike T_1 relaxation, pure T_2 relaxation does not involve energy exchange between the spin system and its environment. Rather, differences in the local field of the nuclei (for example, inhomogeneity of the external magnetic field) as well as random processes that suddenly change the orientation and precession frequency of the spins in the x - y plane will lead to a decrease in \mathbf{M}_{xy} . For a two-level system, the process can be described by an exponential law with a characteristic time constant T_2 :

$$\mathbf{M}_{xy}(t) = \mathbf{M}_0 \exp\left(-\frac{t}{T_2}\right) \quad (17.29)$$

One distinguishes between homogeneous and inhomogeneous T_2 relaxation. The inhomogeneous contribution, T_2^{inh} , deals with processes that lead to transverse dephasing of \mathbf{M}_{xy} , which can be reversed by a spin echo (see Section 17.6) because the precession frequency of a given spin in the ensemble does not change over time. This situation is depicted in Figure 17.20 in which each spin packet keeps its unique precession frequency over time. Small differences between the local magnetic field and the external magnetic field lead to small deviations of the resonance frequency of each spin from the frequency of the instrument, which is used as the reference frequency of the rotating frame. These deviations in turn lead to the dephasing effect. It is often caused by external field inhomogeneities, which has led to the term *inhomogeneous T_2* .

On the other hand, T_2^{hom} applies to events that lead to changes in the spin precession frequency around the z axis with a loss of phase coherence between spins. Such events are due to molecular processes, such as collisions that lead to spin-exchange, so-called flip-flop processes, or diffusion of molecules between regions of differing external fields. These processes occur randomly, and the resulting loss of phase coherence accumulates over time and is irreversible. Measurement of homogeneous relaxation can give insights into the make-up and dynamic behavior of a sample at the molecular level. In practice, T_2^{inh} is often much shorter than T_2^{hom} and therefore dominates transverse relaxation. We will see in Section 17.6 how T_2^{hom} can be determined in the presence of a dominant T_2^{inh} with the so-called spin-echo experiment. The observed transverse relaxation time as defined in Equation (17.30) is a composite of both contributions:

$$\frac{1}{T_2} = \frac{1}{T_2^{\text{inh}}} + \frac{1}{T_2^{\text{hom}}} \quad (17.30)$$

Of course, both transverse and longitudinal relaxation processes will be active at the same time. Hence, a macroscopic magnetization vector in the x - y plane will not only decrease in-plane but eventually increase and align along the z axis. T_1 relaxation is therefore effectively a form of T_2 relaxation. When T_1 relaxation is the only T_2 process present, $T_2 = 2T_1$. Hence, we have to incorporate T_1 relaxation in Equation (17.30), as follows:

$$\frac{1}{T_2} = \frac{1}{T_2^{\text{inh}}} + \frac{1}{T_2^{\text{hom}}} + \frac{1}{2T_1} \quad (17.31)$$

Concept

Spin-spin relaxation decreases the macroscopic magnetization component perpendicular to the external field by dephasing individual magnetic moments with a characteristic time T_2 .

How is the rate of relaxation of \mathbf{M} related to the NMR linewidth? In discussing this issue, it is useful to view the experiment from two vantage points, time and frequency. The macroscopic magnetization vector precessing about the z axis in the x - y plane gives rise to the induction signal in the NMR coils. On one hand, a long-lived \mathbf{M}_{xy} will show a narrow line after Fourier transformation of the data because essentially only one frequency component (the Larmor frequency of the spins) contributes to its motion. On the other hand, if \mathbf{M}_{xy} decays quickly via spin–spin relaxation effects, the line becomes broadened owing to the admixture of additional frequencies necessary to describe the decay. This broadening is a fundamental relationship that governs all forms of spectroscopy and can be expressed in terms of a simple inverse relationship between linewidth and relaxation time,

$$\frac{\Delta\nu}{\Delta t} \approx \frac{1}{T_2}$$

(17.32)

Nuclear magnetic resonance spectra in solids are broad—that is, $\Delta\nu$ is large—because T_2 is small. This observation can be explained by the multitude of long-range dipolar couplings with other nuclei in a sample, which leads to a very small homogeneous T_2 . On the other hand, these couplings are averaged out in a liquid sample, which allows for a much narrower linewidth because of a longer T_2 . In the limit of very fast motional averaging, T_2 is determined by T_1 relaxation, which also becomes less efficient because even though the random jumps in the local magnetic field due to tumbling become faster and more frequent they also become smaller in amplitude.

The lifetime of the excited state in NMR spectroscopy can be significantly changed relative to the preceding discussion if the spins are strongly coupled to their surroundings. For example, this occurs if a proton on a tumbling molecule in solution undergoes a chemical exchange between two different sites. Consider the proton exchange reaction for ethanol:



The exchange decreases the lifetime of the excited state, or T_1 , leading to a broadening of the NMR peak. These peaks become significantly broader only if the site exchange time is in the range of 10^{-4} to 10 s, for this is the timescale of typical NMR experiments. This effect is referred to as **motional broadening**.

For significantly faster exchange, only a single sharp peak is observed, an effect referred to as **motional narrowing**. Motional narrowing is observed for ethanol at room temperature or warmer because the exchange occurs on a timescale faster than 10^{-4} s. For this reason, the portion of the ethanol NMR spectrum shown in Figure 17.8 corresponding to the OH proton is a singlet (rather than a triplet), and the CH_2 hydrogen signal is a quartet rather than a doublet of quartets.

Until now, we have only considered relaxation of an isolated spin ensemble that exchanges energy with its immediate environment. However, we know from Section 17.3 that spins can couple both through bond and through space over significant distances. This leads to an important phenomenon, the **nuclear Overhauser effect** (NOE), named after the physicist Albert Overhauser who discovered it, initially in metals, in 1953. It is exploited in modern NMR for the structure analysis of large biomolecules, as we will see in Section 17.7. We can understand the NOE with the example of two inequivalent proton spins, I and S , which have slightly different resonance frequencies and are separated by less than 5 Å. At this distance, through-space dipolar coupling is appreciable in strength. For simplicity, we assume that both spins have no (through-bond) scalar coupling and therefore the solution NMR spectrum will consist of two narrow lines without multiplet splitting. The NOE predicts that for dipolar coupled nuclei the signal of one of the spins, I , is affected when the signal of the other, S , is saturated by strong RF irradiation. Saturation of the S spin means that its α and β states become equally populated, making its NMR signal disappear. The signal of the I spin may be enhanced, weakened, or even inverted (become negative). How can this effect be explained? Dipolar coupling with a coupling parameter d in Equation (17.25) on the order of 1 kHz is strong enough for the magnetic moments of the two nuclei to affect each other.

Concept

If protons on a tumbling molecule undergo a chemical exchange between two different sites, the NMR peaks can either become broadened or narrowed, depending on the time scale of the exchange reaction.

Concept

The nuclear Overhauser effect predicts that for dipolar coupled nuclei, the signal of one of the spins is increased or decreased if the signal of the other spin is saturated by strong RF irradiation.

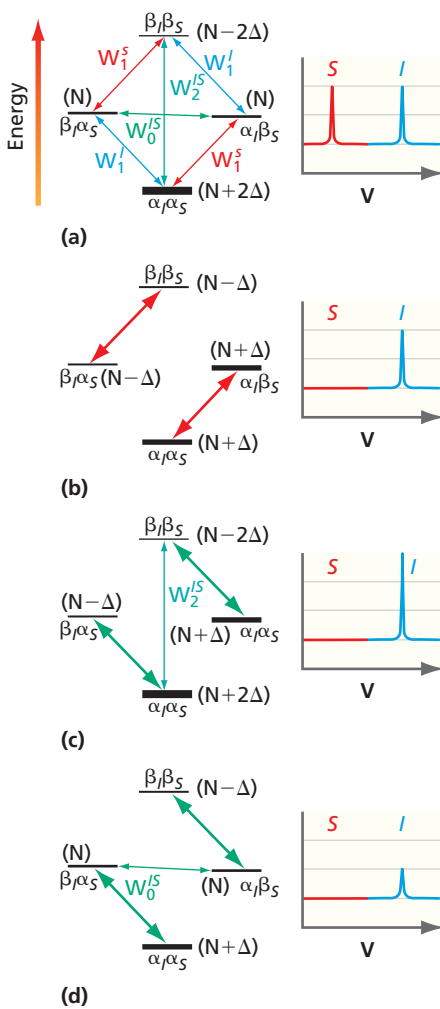


Figure 17.21

Energy diagrams with relaxation pathways and NMR spectra illustrating the NOE effect. The left side of the figure shows the energy-level diagram for two spins I and S coupled by dipolar coupling with various relaxation pathways, as explained in the text. The right side shows the corresponding NMR spectra of the two spins whose intensities depend on the population differences shown between the corresponding levels on the left. (a) Spin system in equilibrium. (b) The levels of spin S are saturated with strong RF irradiation indicated by bold red arrows. (c) Case where the cross-relaxation pathway W_2^{IS} dominates. The double-headed green arrows indicate the transitions of the I spins that are affected by the saturation of the S spins. (d) Same as (c) but with the cross-relaxation pathway W_0^{IS} dominating.

The NOE does not depend on the frequency shifts predicted by Equation (17.25) but instead relies on subtle relaxation effects called **cross relaxation** that are caused by the coupling. The principle is illustrated in Figure 17.21.

The energy-level diagrams in Figure 17.21 contain four individual states characterized by the four combinations of α and β orientations for the two nuclear spins, I and S . Note the similarity with the energy-level diagram in Figure 17.9a. The energy levels are labeled with the α and β states of the two spins (spin type indicated with subscript). The population of the four levels is indicated by the thickness of the horizontal lines as well as an approximate population number in parentheses, N for the two middle levels, $N + 2\Delta$ for the lowest level, and $N - 2\Delta$ for the highest level approximating a Boltzmann distribution. There are four allowed ($\Delta m_{I,S} = \pm 1$) NMR transitions between these states along the single-quantum pathways W_1^{IS} , leading to two distinct NMR peaks, one for I and one for S (shown on the right side of the figure). Spin-lattice relaxation, as discussed earlier in the section, occurs along those same pathways irrespective of the presence of dipolar coupling between both spins. However, the diagram also depicts two cross-relaxation pathways, indicated by W_0^{IS} and W_2^{IS} , that are only present when the two spins experience appreciable dipolar coupling. W_0^{IS} describes a flip-flop process in which a spin flip of I is coupled to a flip of S in the opposite direction (a flop). Because the sum of the spin quantum numbers does not change and the change in energy is minimal, this is a zero-quantum process.

This process is not an allowed radiative transition and hence will not be observed in the NMR spectrum. However, it is a relaxation pathway that may change the populations of the $\beta_I\alpha_S$ and $\alpha_I\beta_S$ levels. It is effective because of the chaotic random motion of the molecule and the dipolar interaction over short distances that leads to a correlation of the fluctuating local fields experienced by both spins at the same time. The same argument can be made for W_2^{IS} , which describes a double flip transition (simultaneous spin flips). Again, this latter transition is not an allowed radiative transition and will not manifest in the spectrum. Rather, it is a relaxation pathway that is induced by the correlation of fluctuating local fields. Because it corresponds to a double-quantum transition and requires a much larger amount of energy to be absorbed from or delivered to the environment compared to the zero-quantum transition, this transition depends differently on molecular motion. For slow-tumbling molecules, which result from high viscosity, large molecules, or both, W_0^{IS} dominates over W_2^{IS} . The opposite is true for fast-tumbling motion (that is, low-viscosity solvents, or small molecules, or both).

In order to observe the NOE, one has to saturate (or invert) one of the transitions. Figure 17.21b illustrates changes in the spin polarization between the four levels that occur when the S spins become saturated. This is done by a strong resonant RF field, which averages the population numbers of the levels it connects. $\beta_I\alpha_S$ loses the amount Δ from its population, which gets added to $\beta_I\beta_S$ for an equal population of $N - \Delta$ of these two levels. The same happens to the other two, $\alpha_I\alpha_S$ and $\alpha_I\beta_S$, except that here the equalized population number turns out to be $N + \Delta$ because $\alpha_I\alpha_S$ started out with more, $N + 2\Delta$. At this point, the signal of the S spins is quenched because of the equal population of its two-level systems. The signal of the I spins remains unchanged despite the population changes of all four states because the population numbers of both of its two-level systems were moved up or down by the same amount, leaving the difference at 2Δ , the same as during equilibrium. To observe a change in the I -spin polarization, cross relaxation has to take effect. The case in which W_2^{IS} dominates is shown in part (c). It applies to fast-tumbling molecules. Because of cross relaxation, $\beta_I\beta_S$ loses population (up to Δ), preferentially to $\alpha_I\alpha_S$. This loss leads to an enhancement of the population differences for I -spin transitions (indicated by double-headed green arrows) of as much as three Δ and an increase of its spectrum by as much as 50%, as depicted by the blue spectrum on the right that has increased in intensity compared to the ones in (a) and (b). In the case of slow-tumbling molecules for which W_0^{IS} dominates cross relaxation, $\beta_I\alpha_S$ and $\alpha_I\beta_S$ tend to equilibrate their population. As much as one Δ is moved from $\alpha_I\beta_S$ to $\beta_I\alpha_S$. This leads to a reduction of the population differences for I -spin transitions to approximately one Δ and a reduction of its spectral intensity by as much as 50%. Of course the experiment can also be conducted the other way, whereby the I spins are saturated and the S spins probed.

Depending on the relative magnitude of the zero- and double-quantum coherence (W_0 and W_2) cross-relaxation rates, the NOE is either positive (intensity enhancement) or negative (intensity reduction) and is quantified by the parameter η , which is defined as

$$\eta = \frac{I - I_0}{I_0} \quad (17.34)$$

where I is the signal intensity of the I spins when the S spins are saturated and I_0 is the signal intensity of the I spins when the S spins are in equilibrium. One can show that η is related to the relaxation rates in the following way:

$$\eta = \frac{W_2^{IS} - W_0^{IS}}{2W_1^I + W_2^{IS} + W_0^{IS}} \cdot \frac{\gamma_S}{\gamma_I} \quad (17.35)$$

The gyromagnetic ratios of the I spin and S spin, which may differ from each other, are included in this equation. It is possible to observe NOE between different types of spins as long as there is appreciable dipolar coupling between them. Note that W_1^S is missing from the equation because it gets overpowered by the strong RF field, saturating the S spins. W_1^I appears with a factor of 2 because it is effective along two relaxation pathways. Overall, W_2 and W_0 , and with them the NOE, depend on the inverse sixth power of internuclear distance and are therefore only observed for nuclei in close proximity to each other. This makes NOE an excellent tool for identifying close contacts between nuclei in different parts of large biomolecules and for developing distance constraints that can be used to build structural models (see Section 17.7).

17.6 PULSED NMR SPECTROSCOPY

When NMR was first developed in the mid-1940s, spectra were acquired by continuous wave (cw) methods. To cover the required spectral range, one would sweep the external magnetic field while irradiating the sample with a fixed radio frequency, the same way that cw EPR spectroscopy is still predominantly done today. However, technological advances have transformed the field to utilizing pulsed RF excitation while keeping the external magnetic field fixed, in combination with time-resolved signal detection and the use of the **Fourier transform** (FT). In this section we will discuss how RF pulses affect the magnetization vector, how the detection of its precession in the time domain leads to the NMR spectrum, and how multiple RF pulses can be combined to extract useful information about the spin system.

The key to understanding pulsed magnetic resonance techniques is the realization that RF pulses are not monochromatic but contain a range of frequencies. This can be seen by considering the Fourier transform of an RF pulse of duration τ_p at a carrier frequency ω_c . The mathematical description of the resulting electromagnetic wave in both the time and frequency domain is given by:

$$B_1(t) = \begin{cases} B_1 \cos(\omega_c t) & \text{for } |t| \leq \frac{\tau_p}{2} \\ 0 & \text{for } |t| > \frac{\tau_p}{2} \end{cases}$$

$$B_1(\omega) = \int_{-\infty}^{\infty} B_1(t) \exp(-i\omega t) dt = B_1 \int_{-\tau_p/2}^{\tau_p/2} \cos(\omega_c t) \exp(-i\omega t) dt$$

$$= B_1 \left(\frac{\sin\left[\frac{(\omega_c - \omega)\tau_p}{2}\right]}{(\omega_c - \omega)} + \frac{\sin\left[\frac{(\omega_c + \omega)\tau_p}{2}\right]}{(\omega_c + \omega)} \right) \approx B_1 \left(\frac{\sin\left[\frac{(\omega_c - \omega)\tau_p}{2}\right]}{(\omega_c - \omega)} \right) \quad (17.36)$$

Concept

The advantage of using RF pulses is that the full NMR spectrum can be excited with a single pulse if the frequency width of the spectrum is narrow enough to fit within the envelope of the power spectrum of the pulse.

Figure 17.22 shows a plot for a pulse of monochromatic radiation of duration τ_p and a frequency spectrum of the pulse as described by the function in Equation (17.36). On the frequency axis, the amplitude of B_1 decreases as the function $\sin(x)/x$ where x represents the deviation from the carrier frequency, ω_c . The carrier frequency is placed at the center of the power spectrum of the pulse. Hence, spins whose NMR lines are off center will not experience the same B_1 amplitude at their particular Larmor frequency, and their turning angle α and Rabi frequency ω_1 are smaller than those for spins with NMR lines in the center of the distribution. However, the amplitude distribution of the pulse is somewhat flat-topped, so that transitions at frequencies in the vicinity of ω_c will be excited just as effectively as those whose Larmor frequency exactly matches ω_c . The advantage of using RF pulses is that the full NMR spectrum can be excited with a single pulse if the frequency width of the spectrum is narrow enough to fit within the envelope of the power spectrum of the pulse. For proton NMR, this basic so-called hard pulse has a duration of the order of 8 to 13 μs on most instruments. Such pulses effectively cover a frequency range of $1/(4\tau_p)$, which is usually sufficient to excite the full proton spectrum.

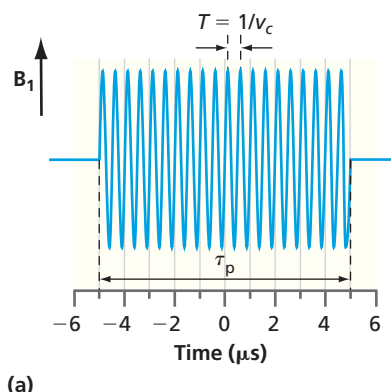
EXAMPLE PROBLEM 17.4

Calculate the frequency coverage in Hz for a hard RF pulse with a duration of 8 μs , a typical pulse length used in proton NMR.

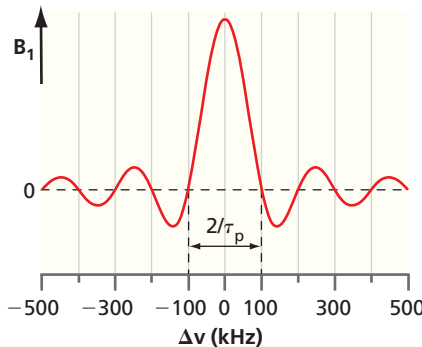
Solution:

$$\Delta\nu = \frac{1}{4\tau_p} = \frac{1}{4(8 \mu\text{s})} = 31,250 \text{ Hz}$$

This result tells us that a hard RF pulse will have a frequency coverage of approximately 30 kHz. The central half of it is in the flat-topped region covering the range of typical NMR spectra (see Figure 17.22b).



(a)



(b)

Figure 17.22

Fourier transform of a short RF pulse. (a) A burst of monochromatic radiation of duration τ_p . (b) Power spectrum of the pulse in (a), described by the function in Equation (17.36) shifted by ν_c (the zero value corresponds to the carrier frequency ν_c).

As explained in the previous section, the effect of an RF pulse on a spin system can be described by the vector model in the rotating frame shown in Figure 17.18. Note that relaxation during the duration of a resonant RF pulse is usually neglected because the pulse duration is short compared to the relaxation times T_1 and T_2 . The time-dependent motion of the magnetization vector \mathbf{M} is described by the so-called Bloch equations, which can be expressed in the rotating frame and allow the inclusion of relaxation effects as well as the effects of cw or pulsed RF fields. See the citations in Further Reading for a discussion of the Bloch equations.

Assuming the spin system to be in thermal equilibrium before the RF pulse, its magnetization vector will be aligned along the z axis and have an initial value M_0 as calculated from the Boltzmann population of the two states:

$$M_0 = \gamma_N \hbar (n_\alpha - n_\beta) = g_N \mu_K (n_\alpha - n_\beta) = \chi_m B_0 \quad (17.37)$$

The nuclear g -factor, g_N , magneton, μ_K , and gyromagnetic ratio, γ (here with index N to indicate its dependence on the type of nucleus considered), have been introduced in Section 17.1. The magnetic susceptibility, χ_m , is a dimensionless constant that relates the magnetization to the applied magnetic field. It depends on the gyromagnetic ratio, the total number of spins, and the temperature through the spin polarization, as noted in Equation (17.9).

The \mathbf{B}_1^\dagger -field of the RF pulse is aligned along the x' axis in the rotating frame and will rotate the magnetization vector through the $y'-z$ plane with the Rabi frequency, ω_1 , according to

$$\begin{aligned} M_z &= M_0 \cos(\omega_1 t) \\ q &= M_0 \sin(\omega_1 t) \end{aligned} \quad (17.38)$$

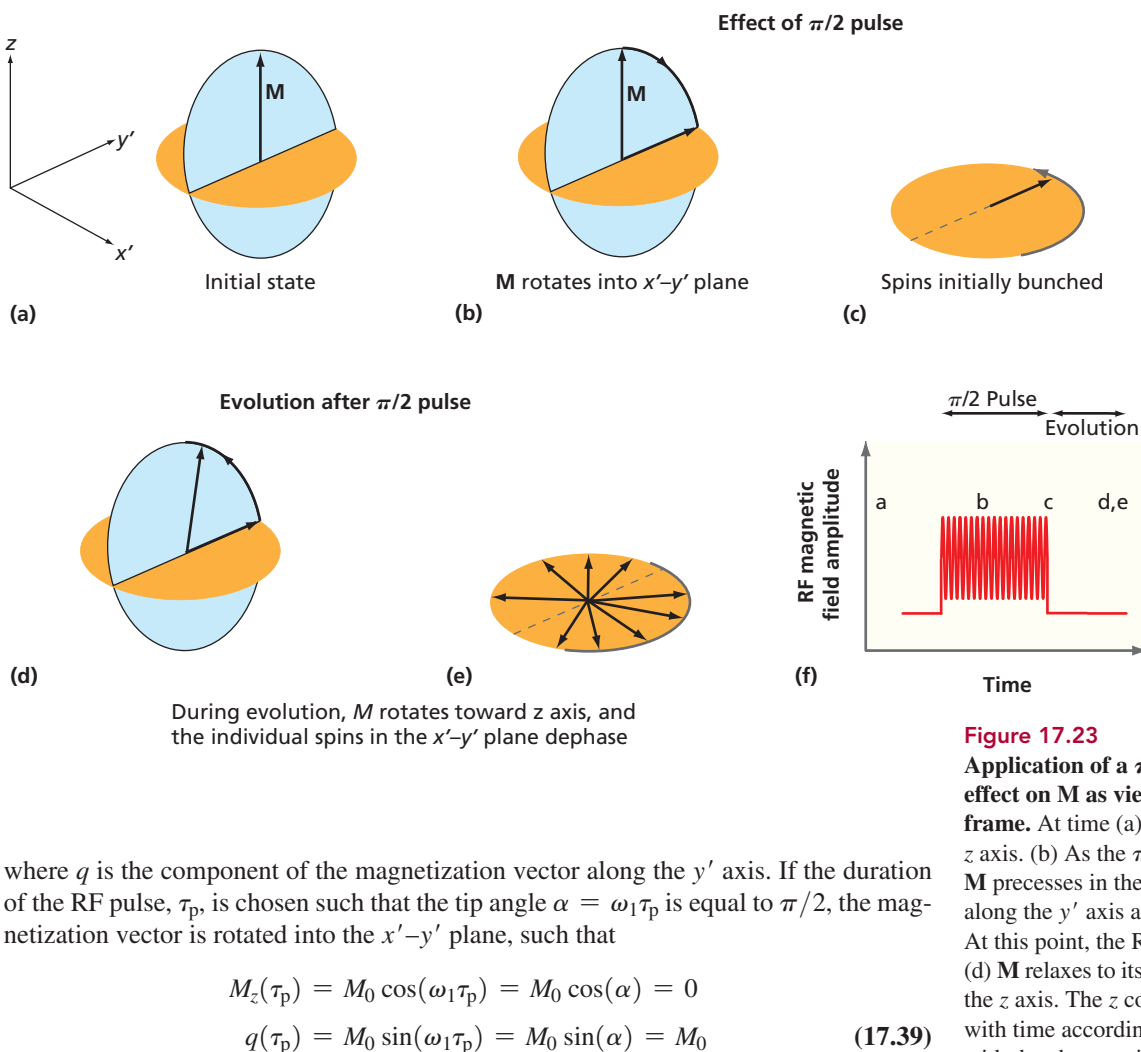


Figure 17.23

Application of a $\pi/2$ RF pulse and the effect on \mathbf{M} as viewed from the rotating frame. At time (a), \mathbf{M} points along the z axis. (b) As the $\pi/2$ pulse is applied, \mathbf{M} precesses in the y' - z plane and points along the y' axis as shown for time (c). At this point, the RF pulse is turned off. (d) \mathbf{M} relaxes to its initial orientation along the z axis. The z component increases with time according to Equation (17.28) with the characteristic relaxation time T_1 . (e) Simultaneously, the transverse component of \mathbf{M} decays in the x' - y' plane with the relaxation time T_2 as the individual spins dephase. (f) Plot of RF magnetic field amplitude with time.

where q is the component of the magnetization vector along the y' axis. If the duration of the RF pulse, τ_p , is chosen such that the tip angle $\alpha = \omega_1\tau_p$ is equal to $\pi/2$, the magnetization vector is rotated into the x' - y' plane, such that

$$\begin{aligned} M_z(\tau_p) &= M_0 \cos(\omega_1\tau_p) = M_0 \cos(\alpha) = 0 \\ q(\tau_p) &= M_0 \sin(\omega_1\tau_p) = M_0 \sin(\alpha) = M_0 \end{aligned} \quad (17.39)$$

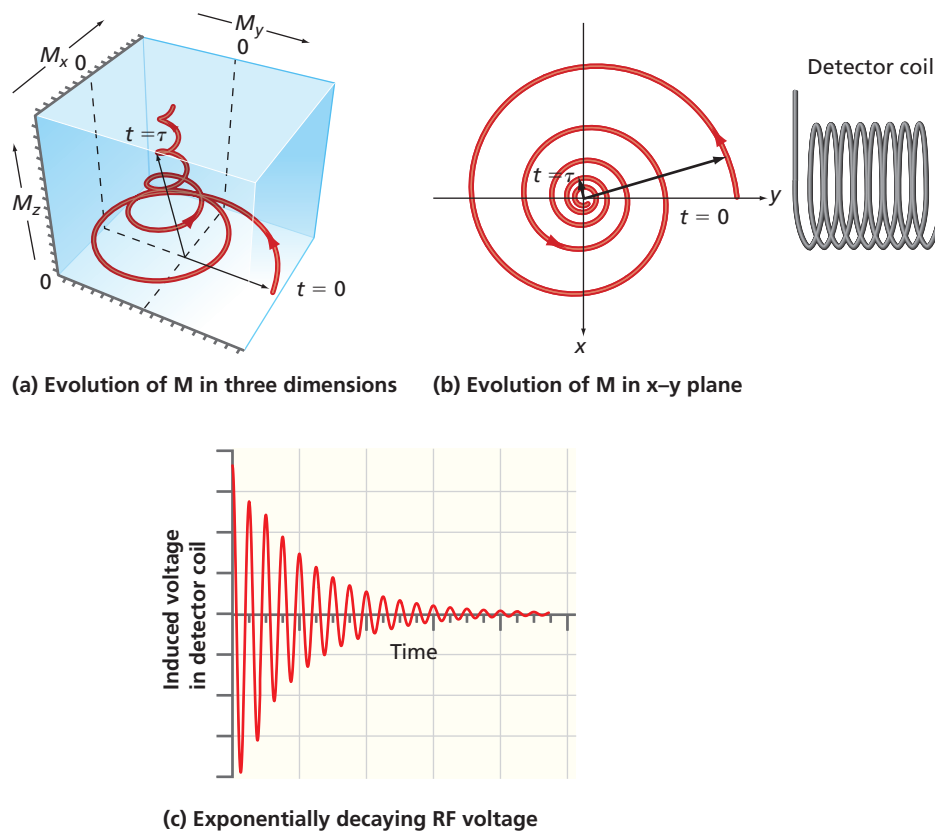
The effect of the $\pi/2$ pulse on the magnetization in the rotating frame is visualized in Figure 17.23a, b, and c. After the magnetization vector of the nuclear spin system has been prepared in the x' - y' plane by the $\pi/2$ -pulse, it enters the evolution period during which both longitudinal and transversal relaxation occur (see Figure 17.23d and e). The magnetization of those spins that are exactly on resonance with the carrier frequency ω_c will stay aligned with the y' axis in the rotating frame until longitudinal relaxation moves it back along the z axis. However, for spin packets I with a slightly different Larmor frequency, a frequency offset $\Omega_I = \omega_I - \omega_0$ will be observed in the rotating frame, with the effect that those spin packets will slowly precess about the z axis with the frequency Ω_I . This motion can be described by the following equation in which p_I and q_I represent the magnetization along the x' and y' axis, respectively. The index I refers to a given spin packet I with a particular frequency offset Ω_I .

$$\begin{aligned} p_I(t) &= M_I \cos(\Omega_I t) \\ q_I(t) &= M_I \sin(\Omega_I t) \end{aligned} \quad (17.40)$$

Note that Ω_I is the difference of the Larmor frequency of the spins in question and the RF frequency and can be positive or negative, corresponding to right- or left-handed precession about the z axis in the rotating frame. In a sample with many of these spin packets with different Ω_I offsets, the overall magnetization vector starts to dephase (see Figures 17.20 and 17.23e). The time dependence of this dephasing process is given by T_2 of Equation (17.31). Longitudinal relaxation of course will also realign the spins along the z axis over time. This behavior of the macroscopic magnetization is described by Equation (17.41) and is summarized in Figure 17.24, as viewed in the laboratory coordinate system. In the rotating frame, the macroscopic magnetization now describes

Figure 17.24

Evolution of the magnetization vector \mathbf{M} in three dimensions and M_{xy} as a function of time. The evolution of M_{xy} with time as seen in (a) and (b) leads to an exponentially decaying induced RF voltage in the detector coil (c).



a damped oscillatory motion in the x' - y' plane, whereas the z component increases with a rate constant of $1/T_1$, as shown in the following equations:

$$\begin{aligned} p(t) &= M_0 \exp\left(\frac{-t}{T_2}\right) \cos\{\Omega_I t\} \\ q(t) &= M_0 \exp\left(\frac{-t}{T_2}\right) \sin\{\Omega_I t\} \\ M_z(t) &= M_0 \left[1 - \exp\left(\frac{-t}{T_1}\right) \right] \end{aligned} \quad (17.41)$$

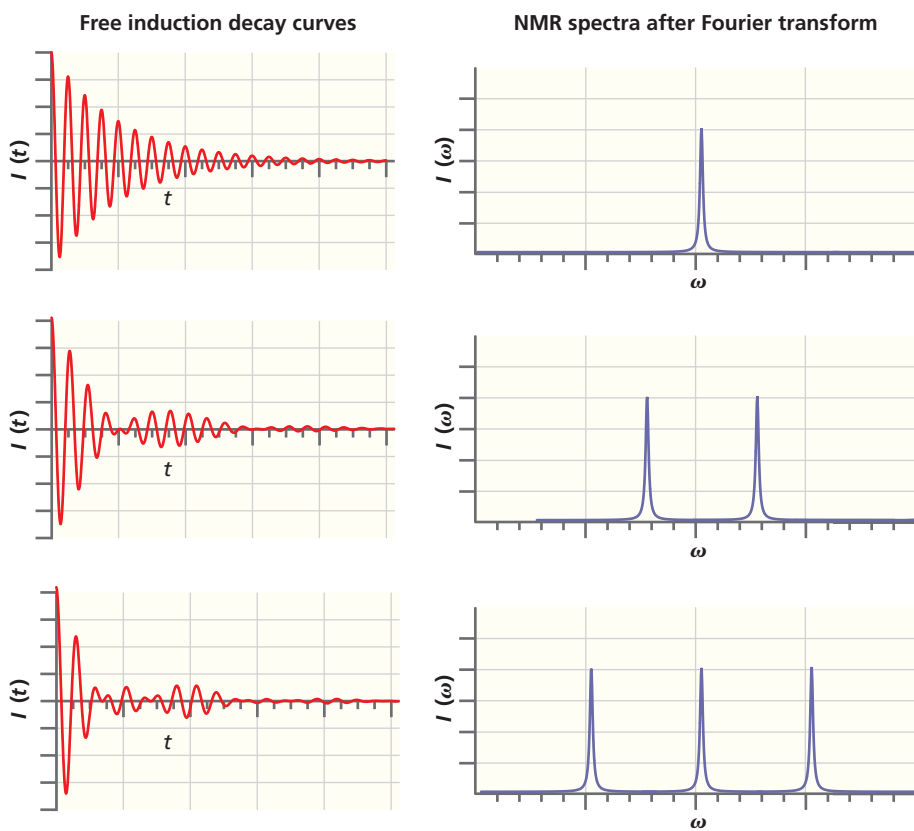
Note that it is the magnetization component in the x - y plane that is measured by the instrument. It is customary to express this time-dependent part of the magnetization vector as a complex quantity,

$$M_+ = p + iq \quad (17.42)$$

The transient decay of M_{xy} is known as the **free induction decay** (FID). The origin of the FID is shown in Figure 17.24, and an example is presented in Figure 17.24c. In FID, *free* refers to the absence of an RF field during its acquisition after the preparation pulse; *induction* refers to the oscillating voltage generated by magnetic induction in the NMR detection coil; and *decay* refers to the fact that the oscillation is enveloped by an approximately exponential decay function with the characteristic relaxation time T_2 . The NMR spectrum of the nuclear spin system that gave rise to the FID can be recovered by performing the complex Fourier transformation on its time evolution:

$$I(\omega) = \int_{-\infty}^{\infty} M_+(t) \exp(-i\omega t) dt \quad (17.43)$$

$I(\omega)$ is therefore also a complex quantity. Its real part represents the absorption of the NMR line on the frequency axis, which is usually used for analysis. Individual NMR

**Figure 17.25**

Examples of FIDs and corresponding spectra. Free induction decay curves on the left for one, two, and three equal-amplitude frequency components (shown in top, middle, and bottom rows, respectively). The NMR spectra on the right represent the Fourier transform of the free induction decay curves.

lines are best described by the Lorentzian lineshape function because it is derived from the Fourier transform of an exponentially decaying FID signal, as given by

$$g_L(\omega) = \frac{T_2^{\text{hom}}/\pi}{1 + [T_2^{\text{hom}}(\omega - \omega_0)]^2} \quad (17.44)$$

Of course, a typical sample will exhibit a complicated spectrum generated by multiple spin packets, each with a different local field. Examples of FIDs and their corresponding spectra are shown in Figure 17.25. The presence of additional spin packets leads to additional frequencies, similar to what can be experienced acoustically when two instruments are tuned. When they are slightly off-resonance, a low-frequency oscillation of their combined amplitude is observed, which is called *beating* and is produced by the time oscillation between constructive and destructive interference of the two waves. It should be noted that the spectrum recovered in the Fourier transform of the FID extends to negative and positive frequencies. The zero point of this spectrum is simply the carrier frequency of the experiment, ω_c , and the true spectrum can be reconstructed by shifting it by that frequency. However, NMR spectra are usually depicted as difference spectra based on an internal standard (see discussion in Section 17.3).

FT-NMR has several important advantages over conventional cw NMR, specifically:

- 1. The multiplex advantage:** This advantage is inherent to most Fourier transform (FT) techniques such as Fourier transform infrared (FTIR) spectroscopy (see Chapter 8). All lines in a given spectral region (approximately 32,000 Hz for an 8 μs RF pulse) are detected simultaneously, whereas in cw NMR the field is swept and only one spin packet is detected at a time. The full spectrum must be acquired by a relatively slow scan. There is an obvious time savings at work when the full spectrum can be collected after a single pulse. This advantage is especially powerful for systems with relatively short T_1 relaxation times because rapid repetitions of the experiment and signal averaging result in improved signal-to-noise ratio.
- 2. Time resolution:** A single FT spectrum can be recorded in less than a ms. This allows for time sampling a spin system evolving in time, such as during a chemical reaction. It allows the detection and investigation of kinetics well into the sub-ms time regime.

Concept

Fourier-transform NMR has several advantages over slowly sweeping the RF frequency:

1. The entire spectrum can be obtained using a single RF pulse.
2. An NMR spectrum can be obtained with high time resolution.
3. T_1 and T_2 can be measured directly.
4. Multi-pulse experiments can be designed to measure the structure of molecules in solution.

3. **Efficient relaxation time measurement:** T_1 and T_2 can be measured directly from the response of specialized pulse experiments rather than by extraction from convoluted lineshapes or saturation behavior.
4. **Multidimensional experiments:** When using multiple time evolution periods in specially designed multi-pulse experiments, one can pull the magnetic interactions between different nuclei apart and measure their distances in space. This has led to the use of NMR in the structure determination of large biomolecules (proteins, nucleic acids) and will be separately discussed in the following section.

In Section 17.5, it was explained that T_2 relaxation could be subdivided into a homogeneous and an inhomogeneous part. A spectrum dominated by homogeneous relaxation determined by the intrinsic lifetime of the upper state usually shows Lorentzian lineshapes [see Equation (17.44)]. These lines are much narrower than inhomogeneously broadened lines that are composed of many overlapping homogeneous lines. Inhomogeneous broadening can arise from magnetic field inhomogeneities across the sample volume but may also be inherent to the sample when very small interactions lead to many closely spaced and overlapping signals. The functional form of the lineshape of an inhomogeneous line is commonly Gaussian where the argument of the exponent depends on the negative square of the frequency offset:

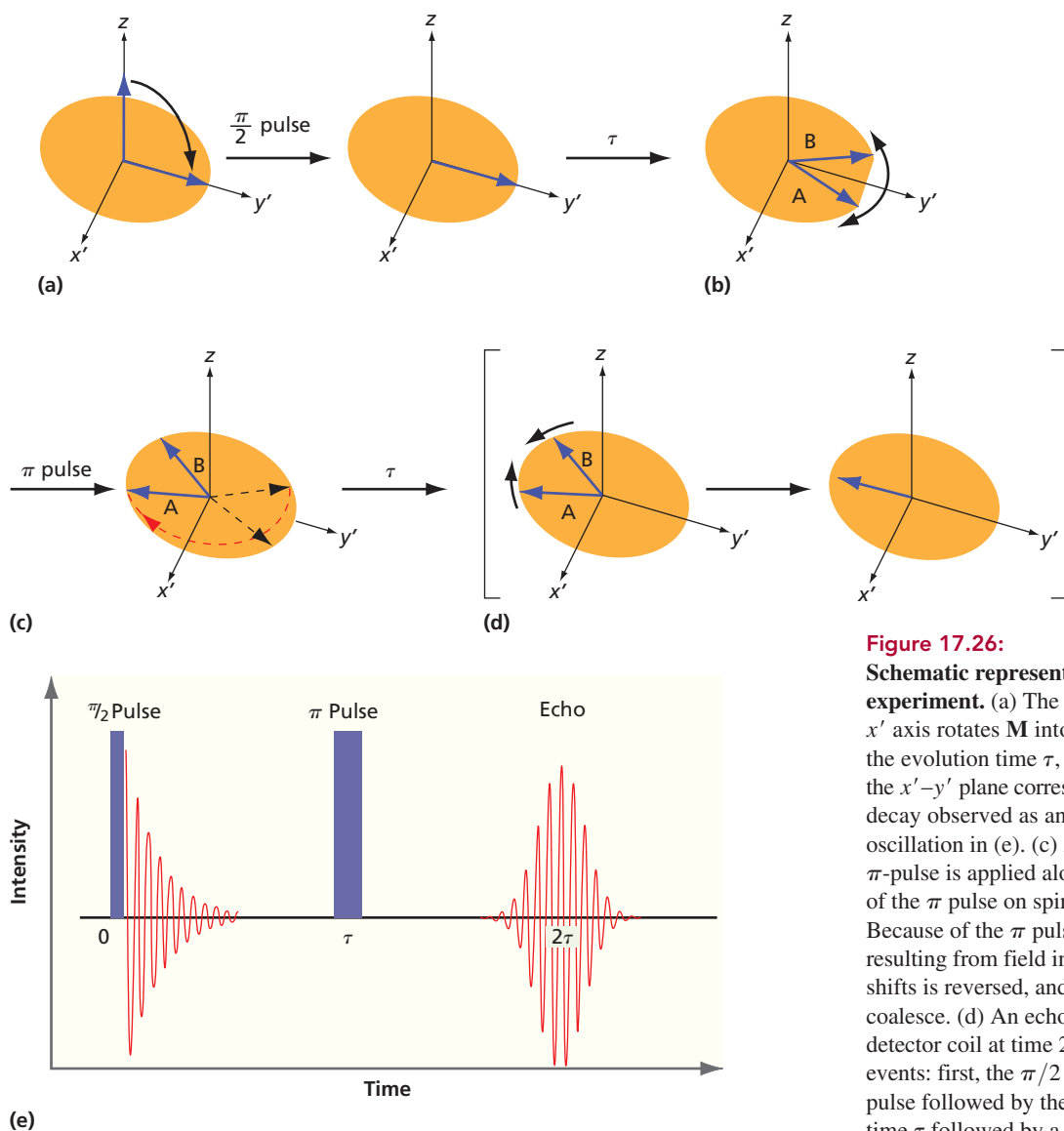
$$g_G(\omega) = \frac{T_2^{\text{inh}}}{\sqrt{2\pi}} \exp\left(-\frac{[T_2^{\text{inh}}(\omega_0 - \omega)]^2}{2}\right) \quad (17.45)$$

The lineshape determines the decay envelope of the FID, which is Gaussian as well because it falls off with $\exp(-t^2)$. However, it is usually approximated by an exponential decay with the time constant T_2^{inh} . One is often interested in T_2^{hom} because it contains the fundamental relaxation interactions of a sample rather than T_2^{inh} , which is often due to experimental artifacts. T_2^{hom} can be measured and distinguished from the inhomogeneous decay with the help of the **spin echo** experiment. This experiment utilizes two RF pulses that are separated by a time τ (see Figure 17.26). The spin echo appears as a macroscopic magnetization at the time 2τ after the first pulse even though by that time the FIDs of both pulses have vanished because T_2^{inh} is usually much shorter than T_2^{hom} .

A spin echo can be used to collect all those spins together that have lost their phase owing to the inhomogeneous phase memory loss (which is reversible). Figure 17.27 illustrates this with the picture of runners on a track. At a certain time after the start, the runners have dephased as a result of different individual speeds or different lengths of the track. At a signal, they all turn around and reverse their track. If their speed stays constant, they will all rephase when they pass the original starting line to form an echo. Normally, when you shout in a canyon, the echo will be weaker than your original sound. This is the case with the runners in the race, too, as some of them will experience irreversible phase loss when they bump into obstacles or into each other. When we apply the π pulse, which reverses the direction, not all of the spins will rephase to form the echo. The longer the time between the start and the reversal pulse, the fewer the spins that will rephase. This irreversible loss of phase memory corresponds to the homogeneous T_2^{hom} (also called T_m in solids). This illustration suggests an easy way to measure the homogeneous T_2^{hom} . One measures the intensity of the echo as a function of the time delay τ between the start and the reversal pulse. The resulting echo intensity is then plotted against a time axis for which the variable is 2τ . It will exhibit an exponential decay according to

$$I(2\tau) = I(0) \exp\left(\frac{-2\tau}{T_2^{\text{hom}}}\right) \quad (17.46)$$

$I(0)$ is the intensity of the signal after the magnetization has first been flipped into the x' - y' plane, such as immediately after the first $\pi/2$ pulse. Note that in most cases the echo is approximately composed of two back-to-back mirror images of the FID of the spin system because the spins rephase and dephase again as they form the echo for which the rephasing and dephasing are due to the same inhomogeneous spectral distribution of the spin packets (see Figure 17.26). In honor of its inventor, Erwin Hahn, the $\pi/2 - \tau - \pi$ pulse sequence is called the *Hahn echo*.

**Figure 17.26:**

Schematic representation of the spin echo experiment. (a) The $\pi/2$ pulse applied along the x' axis rotates \mathbf{M} into the x' - y' plane. (b) During the evolution time τ , the spin packets dephase in the x' - y' plane corresponding to the free induction decay observed as an exponentially decaying oscillation in (e). (c) After the evolution time, a π -pulse is applied along the x' axis. The effect of the π pulse on spin A is shown by the red arc. Because of the π pulse, the fanning-out process resulting from field inhomogeneities and chemical shifts is reversed, and the A and B spins start to coalesce. (d) An echo will be observed in the detector coil at time 2τ . (e) The time sequence of events: first, the $\pi/2$ pulse shown as a rectangular pulse followed by the FID during the evolution time τ followed by a rectangular π pulse, and finally the echo with its increasing and decreasing time envelope of the oscillating magnetization.

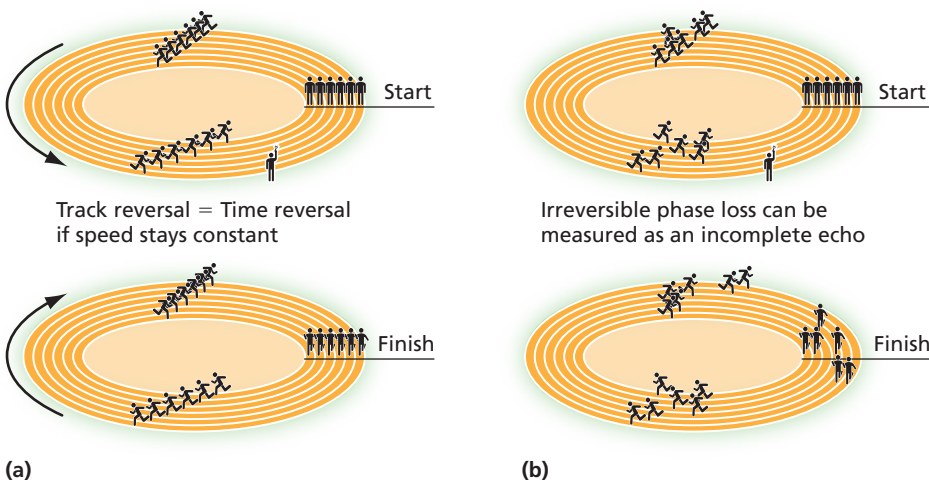
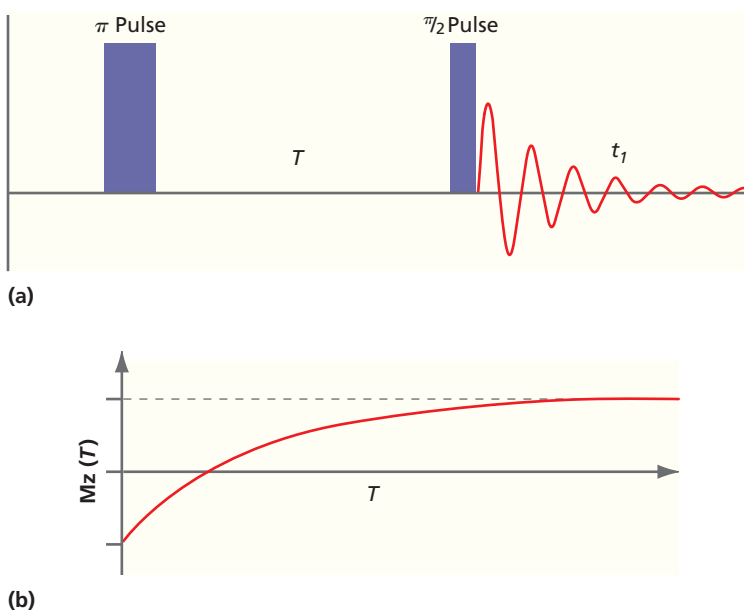
**Figure 17.27**

Illustration of the spin echo with runners on a track. See text for explanation.

Figure 17.28

Inversion recovery experiment. (a) The pulse sequence is composed of a π inversion pulse followed by a $\pi/2$ pulse and FID detection. (b) Time dependence of the intensity of the FID as a function of the delay time T .

Source: Adapted from Malcolm Levitt's 'Spin Dynamics: basics of nuclear magnetic resonance'; 2nd ed. (2000) and Ray H. Hashemi, William G. Bradley, Christopher J. Lisanti text book 'MRI The Basics', 3rd ed. (2010).



A different pulse sequence may be used to experimentally determine the longitudinal (spin-lattice) relaxation time T_1 . Here, one first creates a nonequilibrium polarization (along the z axis) and then measures its time-dependent recovery into equilibrium. This is usually done with a π pulse that inverts the polarization along the z direction. The recovery of the equilibrium spin polarization is probed by bringing the leftover magnetization into the x' - y' plane after a time delay T . Usually, a simple $\pi/2$ pulse followed by the monitoring of the resulting FID is used, as shown in Figure 17.28.

For small delay times between the inversion pulse and the detection sequence, the phase of the FID is reversed because the magnetization has been inverted (points into the negative z direction). At very long times, the magnetization comes back to its positive equilibrium value. The resulting transient function can be simulated by

$$I(T) = I_0 \left\{ 1 - 2 \exp\left(-\frac{T}{T_1}\right) \right\} \quad (17.47)$$

and T_1 can be extracted by fitting the data to this functional form. The superposition of different species may lead to a multiexponential behavior of the inversion-recovery curve, which may be used for identifying different chemical species.

17.7 TWO-DIMENSIONAL NMR

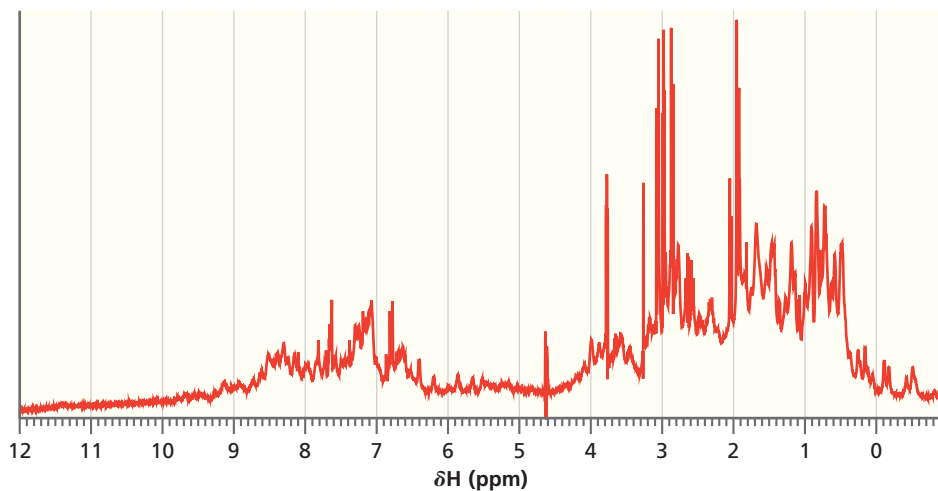
One of the most important modern applications of NMR is the structure determination of large biomolecules, such as proteins and nucleic acids, in solution. This section discusses two multi-pulse experiments that are fundamental to these applications.

NMR structure determination is principally based on dipolar coupling and the NOE, which yields distance constraints between specific nuclei. Once a large set of such distance constraints has been obtained experimentally, they are used for model building, which requires triangulation between the locations of different spins. This is done both for like spins (homonuclear) and unlike spins (heteronuclear). Protons are the most abundant magnetic nuclei in large macromolecules and therefore of prime importance in structure determination. The one-dimensional (1D) NMR spectrum of a protein cannot be analyzed as easily as our initial example ethanol because many lines overlap even when high magnetic fields are employed. The challenge is therefore to separate and assign NMR lines that cannot be resolved such as, for example, in the 1D NMR spectrum of a 17,000 amu polypeptide shown in Figure 17.29.

The correlations between different nuclear spins can be measured by carefully designed multi-pulse NMR experiments and are usually quantified and visualized by

Concept

NMR structural determination is based on dipolar coupling and the nuclear Overhauser effect.

**Figure 17.29**

One-dimensional ^1H NMR spectrum of a small protein in aqueous solution. The protein has a molecular weight of approximately 17,000 amu. The large number of overlapping broad peaks precludes the assignment of peaks and a structural determination on the basis of a single spectrum.

Source: Published by permission of Rachel Klevit, University of Washington.

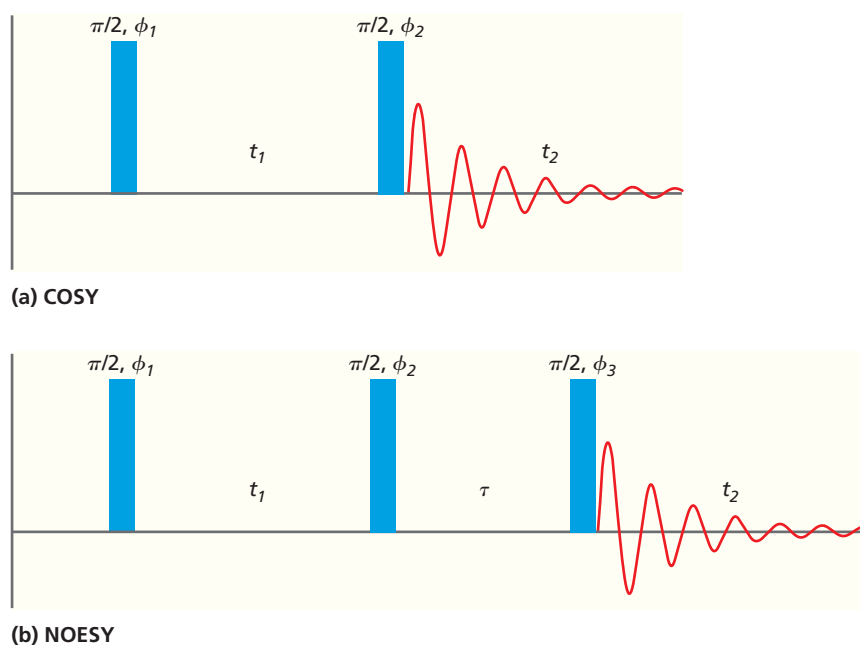
cross peaks in a two-dimensional (2D) NMR spectrum, as will be explained below. Almost all these experiments have four distinct temporal parts: (1) A preparation period that consists of one or more tailored RF pulses to create detectable magnetization in the x' - y' plane. (2) An evolution period without pulses in which the magnetic moments are allowed to precess freely in the external magnetic field. (3) A mixing period during which additional RF pulses are delivered to the sample in order to transfer the magnetization between nuclei to detect special or through-bond connections between them. (4) Finally, a detection period that is designed to transform the evolved magnetization into an observable NMR signal as a function of time.

Two important 2D experiments for structure analysis are COSY (correlation spectroscopy) and NOESY (NOE spectroscopy, pronounced *nosy*). In their most basic forms they can be performed with relatively few pulses as shown in Figure 17.30.

The COSY sequence consists of an initial $\pi/2$ pulse in the preparation period, followed by an evolution period t_1 . This time is varied in subsequent experiments and serves as one of the time variables of the 2D spectrum. After the evolution time t_1 , a second $\pi/2$ pulse excites the sample. This represents the mixing period during which time magnetization is transferred to ^1H nuclei 2–3 bonds away. After the mixing pulse, the FID of the sample is detected during the detection time period, t_2 , which serves as the second time variable of the 2D spectrum. The experiments start with zero time delay t_1 between the two pulses and the full FID during t_2 is recorded. Then the spin

Concept

Two important 2D experiments for structure analysis are COSY and NOESY. In their most basic forms they can be performed with relatively few pulses as shown in Figure 17.30.

**Figure 17.30**

Two-dimensional experiments for structural analysis. (a) COSY and (b) NOESY 2D NMR pulse sequences in their simplest form. The rectangles indicate RF pulses with $\pi/2$ tip angles and different phase relationships indicated by the letter ϕ indexed by the pulse number. These phase angles can be used to discriminate between different FIDs and echoes that are generated by any of the pulses and to select the FID of the last pulse evolving along the time period t_2 as the main observable of interest. t_2 is the second time dimension of the 2D data set, whereas t_1 is the first dimension. It describes the temporal separation of the first two pulses and has to be stepped through a range of values from zero to a maximum value limited by the homogeneous T_2 relaxation time. The time delay τ in the NOESY experiment is chosen for optimal buildup of the NOE effect, usually of the order of 50 ms. Adapted from <https://www.chemie.uni-hamburg.de/nmr/insensitive/tutorial/en.lproj>.

system is allowed to return to equilibrium. When the next spectrum is recorded, the evolution period, t_1 , is incremented by a small additional time interval Δt . The second FID is placed next to the first one into a two-dimensional memory array. The sequence is then repeated numerous times. Each time t_1 changes by an additional Δt until the full 2D spectrum is built up. The data are now contained in a 2D digital array in which each data point represents an amplitude of the voltage recorded in the detection coil at two specific time points, t_1 and t_2 . The t_2 axis is easier to understand because it represents the time axis of the FID signal, which is an interferogram of the NMR spectrum of the spin packets that are oscillating and decaying in the $x'-y'$ plane of the rotating frame.

It has to be kept in mind that the spectrum encoded in these FIDs is not a simple absorption spectrum of the sample because the spins are not in equilibrium at the time the second RF pulse hits them. In fact, they have been prepared in a state of coherent superposition by the first pulse, followed by a variable time delay that allowed any couplings between different spin packets to modulate their initial coherence. This history affects the population of the individual spin states at the time of the detection pulse. As a result, the spectra encoded in these FIDs contain positive (absorption) and negative (emission) signals that become visible after the data set is Fourier transformed along the t_2 axis. Moreover, these spectra are modulated along the second axis, t_1 , by the precession frequencies of the spin packets, creating a second interferogram of the Fourier-transformed spectra along t_1 . An additional Fourier transform of the spectra along the t_1 axis will reveal the spectral components along the frequency axis ω_1 and generate correlated spectra that show diagonal peaks (peaks at the same frequency in both axes) and cross peaks (peaks that have different frequencies in the two axes). The diagonal peaks contain little information apart from that already given in the 1D NMR spectrum. It is the cross peaks that are of interest as they convey information about spin packets at one resonance frequency ω_1 coupling to other spin packets at resonance frequency ω_2 (see Figure 17.31).

In both cases (COSY and NOESY), the preparation is done with a single $\pi/2$ pulse that places the M_z magnetization into the $x'-y'$ -plane. This pulse is followed by an evolution period t_1 , which is varied in the 2D experiment, and after Fourier transform along this axis will produce the first frequency axis of the 2D spectrum. The mixing phase is different for the two experiments. For COSY, it consists of another $\pi/2$ pulse that transfers magnetization to a nucleus 2–3 bonds away. This magnetization is subsequently detected in the t_2 dimension. The NOESY experiment has two $\pi/2$ pulses separated by a constant time τ that allows for cross relaxation to occur and the NOE effect to build up. Finally, in both experiments the detection period t_2 occurs after the last $\pi/2$ pulse, which places the magnetization of interest into the $x'-y'$ plane. Fourier transform along t_2 generates the second frequency axis of the 2D spectrum. The diagonal peak at (ω_1, ω_1) in the 2D COSY spectrum in Figure 17.31 represents an NMR signal of a nucleus I with resonance frequency ω_1 , which was excited by the first pulse and then evolves in the $x'-y'$ plane. If it does not couple to a spin packet with a different resonance frequency, the evolution and mixing period will leave the coherence at the same transition frequency, ω_1 , during the detection period. In other words, the interferogram along t_1 of the signal measured during t_2 only contains the ω_1 frequency component leading to the diagonal peak at (ω_1, ω_1) after the 2D Fourier transform of the data. On the other hand, a cross peak at (ω_1, ω_2) shows that during the mixing period coherence is transferred from the original transition at ω_1 to a different one at ω_2 . Hence, we know that the two spins with resonance frequencies ω_1 and ω_2 couple magnetically through 2 or 3 bonds and therefore have to be in close proximity to each other. Usually, one finds both diagonal and cross peaks in the same 2D spectrum, as seen in Figure 17.31.

Figure 17.32 illustrates the COSY experiment for a coupled IS -spin system. Scalar coupling between both spins leads to a doublet splitting as illustrated by the two doublet signals in (i). For simplicity, the system does not begin in Boltzmann equilibrium but in a state in which the S spins have been saturated and show no magnetization along the z axis, as illustrated by the relative populations of the four states in (j). The only magnetization present at the start of the experiment (a) comes from the doublet of spin I . The first $\pi/2$ pulse flips this magnetization into the $x'-y'$ plane where it starts to

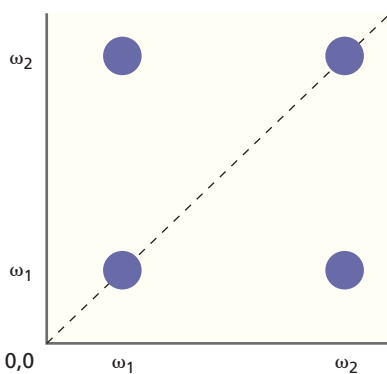


Figure 17.31

Two-dimensional correlation spectra. The diagram shows two diagonal peaks at (ω_1, ω_1) and (ω_2, ω_2) as well as two cross peaks at (ω_1, ω_2) and (ω_2, ω_1) as they appear in 2D COSY spectra.

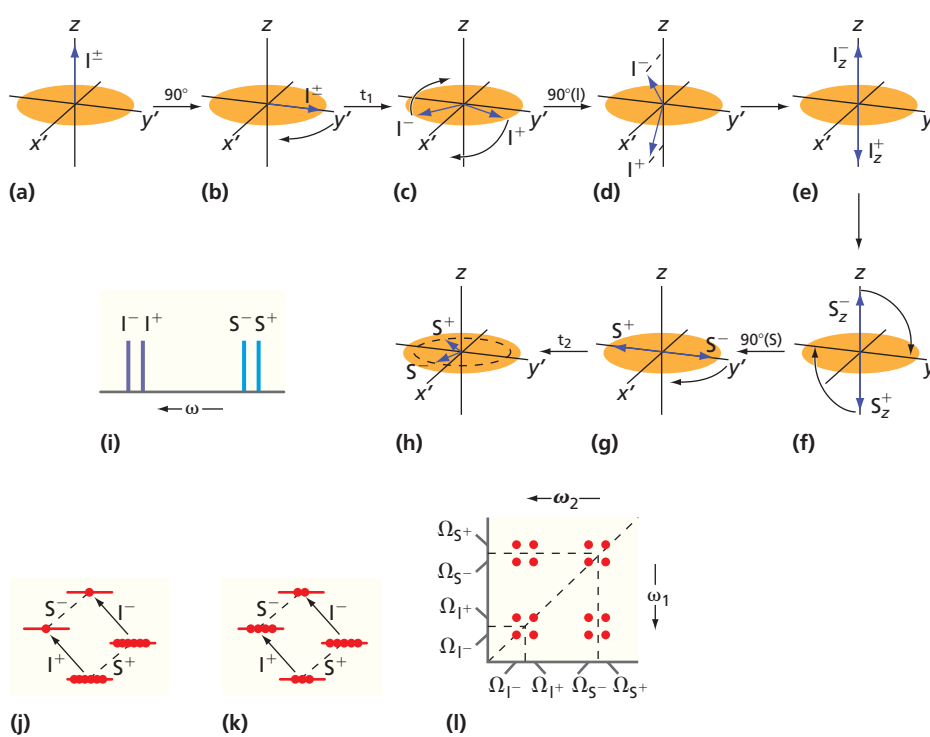


Figure 17.32

Vector model for a coupled spin system, IS , undergoing the COSY pulse sequence. (a) Spin packets I^{\pm} aligned along the z axis. (b) After the first $\pi/2$ pulse, the magnetization is flipped into the $x'-y'$ plane. (c) During the variable evolution time t_1 the two spin packets dephase. (d) The second $\pi/2$ pulse flips the magnetization from the $x'-y'$ plane into the $x'-z$ plane. (e) Same as (d) but with the x' components omitted for clarity. (f) The z magnetization of the S spins, which has been modulated by the changes in the population of the I spins. (g) The second $\pi/2$ pulse flips the z magnetization of the S spins into the $x'-y'$ plane. (h) The S spins start to precess and relax during the detection time t_2 . (i) 1D spectrum of the coupled spin system. The superscripts + and - refer to the spin state (α and β , respectively) of the other spin. (j) Populations of the four energy levels of the coupled spin system at the beginning of the experiment with the S spins saturated. (k) Populations of the four energy levels immediately after the second $\pi/2$ pulse. (l) 2D COSY spectrum after Fourier transform in both axes.

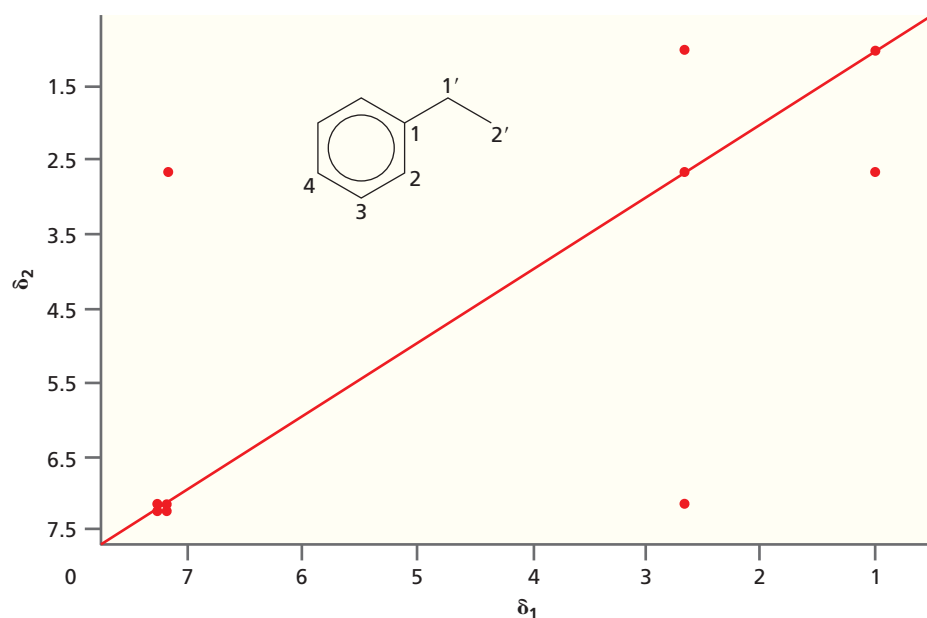
Source: Based on Hore, P. J. *Nuclear Magnetic Resonance*, Oxford Chemistry Primers.

precess (b). During the evolution time t_1 both spin packets dephase and separate from each other according to their different resonance frequencies, Ω_{I+} and Ω_{I-} (c). We now consider first the effect of the second $\pi/2$ pulse on the two spin packets I^{\pm} (d). Their magnetization vectors get rotated by 90° from the $x'-y'$ plane into the $x'-z$ plane. What had been their y' component before the pulse now has become their z component after the pulse. The x' components are omitted in (e) for clarity. The new z components correspond to changes in the populations of the four states that were induced by the evolution and mixing periods (k). The transition labeled I^- still reflects an absorption event because the lower-energy state has higher population than the upper one. However, the transition I^+ reflects an emission event because its upper-energy state has a higher population than the lower one. This situation is indicated in (e) by the magnetization for the I^- spin packet pointing in positive z direction for absorption, whereas that of the I^+ spin packet points in negative z direction for emission. In (k), one can see that these changes in population numbers have had an impact on the transitions for the S -spin packets, S^{\pm} . S^- is now polarized in absorption, while S^+ is in emission. Because the second $\pi/2$ pulse is a hard pulse that also excites the S spins, their magnetization is flipped into the $x'-y'$ plane concurrently with the I^{\pm} spins being flipped into the $x'-z$ plane (f and g). After the second $\pi/2$ pulse, the magnetization in the $x'-y'$ plane continues to evolve while inducing the FID, which is being observed in the experiment. Contributions to this signal arise from the S^{\pm} spin packets (h) as well as from residual transversal magnetization from leftover I^{\pm} spins that are not shown in the figure. As explained before, the full 2D COSY data set is built up by FID signals detected along t_2 while varying the length of the evolution time period t_1 incrementally. 2D Fourier transform of this data set leads to the 2D COSY spectrum (l).

In order to observe cross peaks in 2D COSY spectra, it is important that the two spin packets, I^{\pm} , significantly dephase during the evolution time t_1 . This requires scalar couplings that are sufficiently strong and that usually limits the application of COSY to 3-bond couplings or shorter distances. The main objective of the COSY experiment is to discover the network of scalar couplings and make spectral assignments. An example of a 2D COSY spectrum of ethyl benzene is shown in Figure 17.33. One can see cross peaks for each of the 3-bond couplings, and one 4-bond coupling, that is, for the proton pairs on the carbon positions (1', 2'), (1', 2), and among the protons on the benzene ring. There is no cross peak between the protons on 2' and the ones on the benzene ring because they are too far apart to couple strongly.

Figure 17.33

Simulated 2D COSY experiment on ethylbenzene. The simulation used the NMR web service at <http://www.nmrdb.org>. The most shielded protons with $\delta \approx 1.5$ ppm are on the methyl group at position 2'. The methylene protons at 1' are less shielded with $\delta \approx 2.6$ ppm, whereas the protons on the benzene ring at positions 2, 3, and 4 are strongly deshielded and cluster around a chemical shift near 7.4 ppm. Cross peaks are visible between protons that are up to 4 bond lengths away. This is seen for the methyl and methylene groups at (1.5, 2.6) ppm and (2.6, 1.5) ppm and for the methylene protons and the protons at position 2 at (2.6, 7.4) ppm and (7.4, 2.6) ppm.

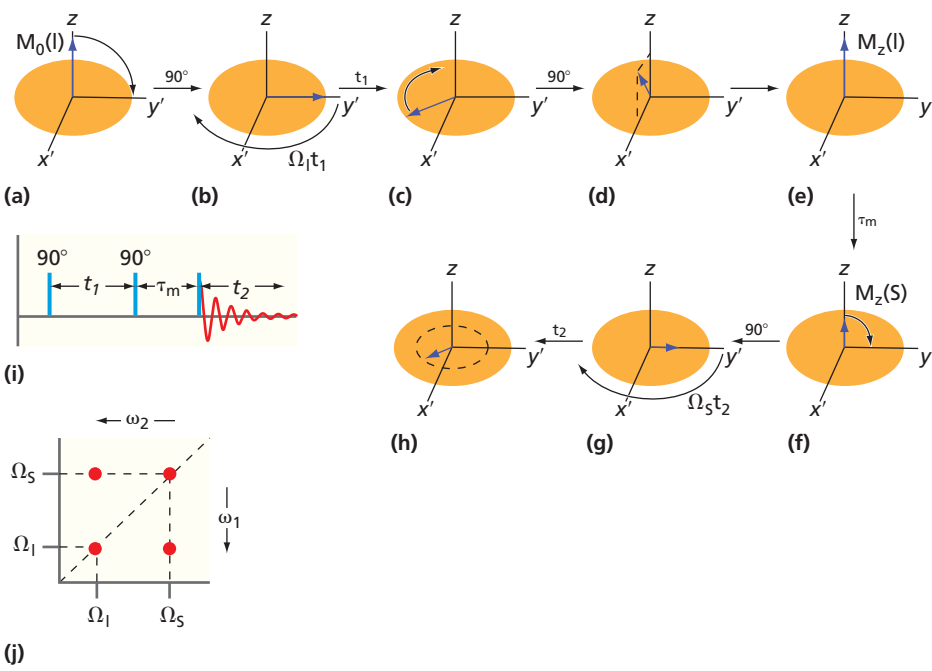
**Figure 17.34**

Vector diagram of an *IS* spin pair with dipolar coupling during the NOESY experiment. (a) Equilibrium magnetization of the *I* spins along the *z* axis. (b) After the initial $\pi/2$ pulse the magnetization of the *I* spins is flipped into the *x'*-*y'* plane. (c) With completion of the evolution period t_1 , the *y'* magnetization has precessed with its offset frequency Ω_I . (d) After the second $\pi/2$ pulse, the *y'* component of the magnetization is flipped back along the *z* axis, whereas the *x'* component remains in the plane. (e) Same picture as (d) but with the transversal part of the magnetization omitted for clarity. (f) After the mixing time τ_m , cross relaxation leads to the development of NOE enhancement or reduction of the population of *S* spins. (g) The last $\pi/2$ pulse brings the magnetization of the *S* spins into the *x'*-*y'* plane. (h) The *S* spins oscillate with their characteristic resonance offset frequency ω_S and decay due to T_2 relaxation to produce the FID. (i) Pulse scheme for the 2D NOESY experiment with FID. (j) The 2D spectrum after the data set has undergone 2D Fourier transform.

Source: Based on Hore, P. J. *Nuclear Magnetic Resonance*, Oxford Chemistry Primers.

Whereas the 2D COSY experiment is useful for the analysis of scalar couplings, the 2D NOESY experiment focuses on through-space dipolar couplings and allows one to derive a network of distance constraints between nuclei in large biomolecules. Typically, one performs both experiments on the same sample to get the benefit of the analysis of both types of couplings. The principle of the NOESY experiment with a pair of dipolar coupled (but not *J* coupled) spins *I* and *S* is demonstrated in Figure 17.34.

The 2D NOESY experiment is very similar to the 2D COSY experiment. However, instead of a 2-pulse sequence, the 2D NOESY experiment uses three $\pi/2$ pulses. The sequence of events depicted in Figure 17.34 begins with the spins in equilibrium and their magnetization vector aligned with the *z* axis (Figure 17.34a). Only the magnetization of the *I* spins is depicted here, but the same applies for that of the *S* spins. In Figure 17.34b, the first $\pi/2$ pulse flips the magnetization into the *x'*-*y'* plane along the *y'* axis where it begins to precess with the offset frequency Ω_I , the difference between the Larmor frequency of the *I* spins and the carrier frequency of the instrument (Figure 17.34c). The modulation of the magnetization of the *I* spins, which will ultimately lead to the NOE effect, happens again during the evolution period t_1 , which



starts out at zero and is increased in steps of Δt for each subsequent scan of the 2D data set. For each increment of t_1 , the experiment takes a snapshot of the progress of the I -spin magnetization precessing and relaxing in the $x'-y'$ plane. In Figure 17.34d, after completion of the evolution period t_1 , the second $\pi/2$ pulse rotates the magnetization vector by 90° from the $x'-y'$ plane into the $x'-z$ plane. Any remaining y' magnetization has now been turned into z magnetization. The x' magnetization remains unaffected and will continue to precess in the $x'-y'$ plane after the second pulse. However, it is not of interest and has been omitted from Figure 17.34e for clarity.

At this point, the I spins are in a nonequilibrium state in which their polarization depends on the product of Ω_I and t_1 , that is, the angle of precession during the evolution period. In Figure 17.34f, cross relaxation within the four-level system (see Figure 17.21) will now affect the spin polarization of the S spins during the mixing time τ_m , leading to enhancement or reduction of their z magnetization. The duration of τ_m is usually of the order of 50 ms to several hundreds of ms and may have to be optimized for the molecule under study. Note that the NOE encodes the resonance frequency of the I spins, Ω_I , on the magnetization of the S spins during the mixing time. This leads to the cross peaks between I and S spins in the final spectrum. In Figure 17.34g, the last $\pi/2$ pulse brings the magnetization of the S spins into the $x'-y'$ plane where they will precess with their characteristic offset frequency Ω_S (Figure 17.34h) and will induce a FID signal during the time period t_2 (Figure 17.34i). Note that τ_m stays constant throughout the experiment, while t_1 is being incremented. In Figure 17.34j, the 2D data set is ordered along the two variable time axes t_1 and t_2 , then Fourier transformed along both axes. Cross peaks appear when dipolar coupling is present and induces the NOE during the mixing phase.

The simple 2D NMR techniques explained in this section were initially developed and validated with relatively small structures such as the bovine pancreatic trypsin inhibitor protein (BPTI), with 58 amino acid residues and a molecular weight of only 6.5 kDa. The original study led to the Nobel Prize in 2002 for Kurt Wüthrich of the ETH Zürich. These 2D NMR techniques are often used in combination with each other as COSY allows one to follow the bond network, whereas NOESY allows one to find neighbors that couple through space. Continued advances in NMR, such as development of higher field-frequency spectrometers, isotopic labeling, and more complex multipulse techniques that help sort out some of the spectral congestion observed in larger proteins, have led to impressive advances and have allowed the structural determination of proteins and protein aggregates with molecular weights of hundreds of kDa, such as the mitochondrial Ca^{2+} uniporter, a large membrane protein that consists of five subunits and regulates calcium uptake in mitochondria. Currently, the RCSB Protein Databank, an online depository for protein structures, hosts almost 12,000 protein structures solved by NMR based on these techniques. A more detailed discussion of using 2-D methods to determine structures can be found in the citations listed in Further Reading.

17.8 SOLID-STATE NMR

In Section 17.4, we discussed dipolar coupling between neighboring spins and how that affects the local field of an observer spin, which depends on the orientation of the distance vector between the two spins and the external magnetic field. The dipolar coupling leads to a shift in the resonance frequency of the observer spin according to the dipolar coupling energy operator (Equation 17.24). In solid-state NMR, the shift is not averaged out by rapid tumbling of the molecules, and one finds broad, unresolved spectra with much overlap that dramatically reduce their apparent information content. The resulting powder NMR spectrum is composed of the contributions of many spin pairs in the ensemble that are randomly oriented with respect to the polar angle θ and the azimuthal angle φ in the laboratory coordinate system averaging over the full space angle. It shows the characteristic *Pake doublet* pattern visible in Figure 17.35. In this figure, the intense edges of the spectrum result from the contributions when $\theta = 90^\circ$ and the local field correction is diamagnetic, whereas the weaker outer edges result from the contributions of $\theta = 0^\circ$ and the correction is paramagnetic. The center of the spectrum is at the unperturbed position of nucleus A. The observation of a Pake pattern

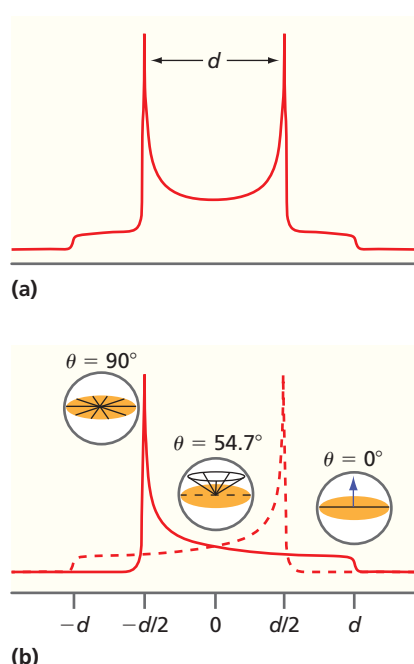


Figure 17.35

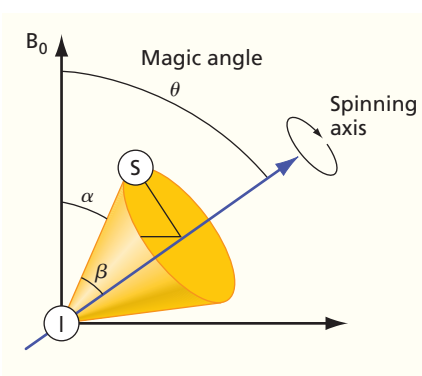
Solid-state NMR spectrum of a nucleus experiencing dipolar interaction with a different nucleus. (a) NMR spectrum of nucleus A plotted on a frequency axis scaled by the dipolar parameter d that describes the dipolar coupling with nucleus X. The spectrum shows the Pake pattern observed in a powder (or frozen solution) sample. Note that the frequency axis is zeroed at the resonance of the uncoupled nucleus A. (b) The spectrum is composed of two signals corresponding to the X spin in the α or β state. The points with maximum intensity correspond to $\theta = 90^\circ$ where the distance vector assumes a perpendicular orientation with respect to the external magnetic field direction. The smallest number of AX pairs have their internuclear vector parallel to the external field ($\theta = 0^\circ$) and constitute the low-intensity signal at the extreme frequency positions. At the so-called magic angle of $\theta = 54.7^\circ$, the dipolar coupling is zero. Although we have focused on nucleus A as the “reporter nucleus,” the same effect is observed for nucleus X. Typical values of d are larger than the scalar couplings and longer in range. Consider the case of a ^1H nucleus coupling to a ^{13}C nucleus, $d = 8950$ Hz at a distance $r_{\text{CH}} = 1.5$ Å, 472 Hz at 4 Å, and 30.2 Hz at 10 Å. Finally, it should be noted that in the solid state, the dipolar coupling between magnetically equivalent nuclei will not cancel out.

Source: Based on Laws, D. D. et al., *Angew. Chem. Int. Ed.* 41 (2002): 3096–3129.

Figure 17.36

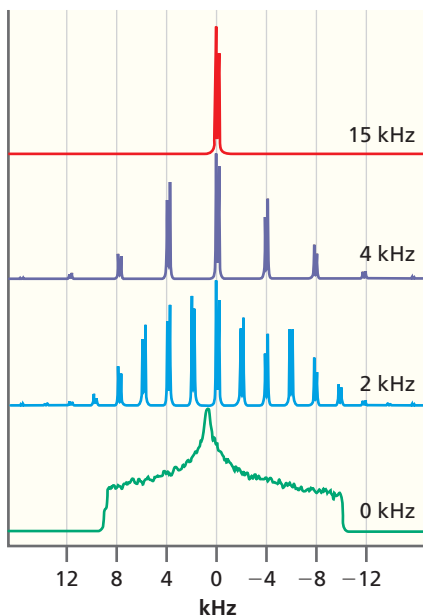
Vector diagram illustrating magic angle spinning. A sample containing two dipolar coupled spins I and S , randomly oriented at an angle α with respect to the external magnetic field, is rapidly spun about an axis set at the magic angle θ relative to the external field.

Source: Based on Matsuoka, S. et al., *Chem. Commun.*, (2009), 5664–5675.



Concept

In solid-state NMR, dipolar coupling is not averaged out by rapid tumbling of the molecules, and magic angle spinning is used to simulate the averaging effect of tumbling in liquids.

**Figure 17.37**

The ^{13}C NMR spectrum of a powder in which the unit cell contains a molecule with two inequivalent $-\text{C}=\text{O}$ groups.

The green spectrum in the bottom panel shows the anisotropically broadened solid-state spectrum. The 15-kHz spectrum (red) shows only two sharp peaks in the center that can be attributed to the two chemically inequivalent $-\text{C}=\text{O}$ groups. The remaining spectra are obtained at different spinning frequencies. The spinning sidebands seen at 2 kHz (light blue) and 4 kHz (dark blue) are experimental artifacts that arise if the spinning frequency is not sufficiently high.

Source: Published by permission of Gary Drobny, University of Washington.

In an ssNMR experiment allows the immediate determination of the dipolar coupling constant d from the separation between the two strong edges. The two outer edges are separated by $2d$. Note that the signal intensity at the zero position in Figure 17.35 arises from an orientation in which the polar angle $\theta = 54.7^\circ$, which reduces the dipolar contribution in Equation (17.25) to zero because $3 \cos^2 \theta - 1 = 0$. This specific polar angle is termed the *magic angle*.

The spectroscopic information about scalar coupling is not lost; rather, it is just hidden beneath the broadened solid-state lines and must be recovered by suitable experimental means. To achieve recovery, one has to simulate the averaging effect of tumbling in liquids. One very successful approach is called **magic angle spinning (MAS)**. The magic angle θ is defined by the relationship

$$(3 \cos^2 \theta - 1) = 0 \\ \theta = 54.7356^\circ \quad (17.48)$$

When the polar angle between the vector connecting the two spins and the external magnetic field (defining the laboratory z axis) becomes equal to the magic angle, the dipolar coupling energy in Equation (17.24) “magically” becomes zero. This condition zeros out the dipolar contribution to the resonance frequency given as the second term in Equation (17.25). To achieve this condition for all random molecular orientations, the sample is rotated (spun) about an axis oriented at the magic angle with respect to the external field (see Figure 17.36). This configuration leads to all vectors between any pair of nuclei to assume an averaged orientation along the rotation axis.

The distance vector between any pair of spins in the sample (e.g., the spin pair IS in Figure 17.36), originally oriented at a random angle α , is now spinning on the surface of a cone with apex angle 2β , for which $\beta = \theta - \alpha$. The cone is aligned along the rotor axis. If the rotation is fast enough compared to the duration of the NMR experiment, the orientation of the distance vector between the two spins is averaged out to the magic angle, canceling out all anisotropic contributions to the NMR spectrum and recovering narrow lines. However, so-called spinning sidebands may appear in the NMR spectrum on the low- and high-frequency side at multiples of the spinning frequency (see Figure 17.37). These sidebands are sometimes used to trace out the ssNMR lineshapes in order to infer information about the underlying anisotropic couplings between the nuclear spins. However, when this is not desired, spinning frequencies higher than the ssNMR linewidths are used to remove these sidebands altogether.

Solid-state nuclear magnetic resonance has seen a dramatic development since magic angle spinning was introduced in the late 1950s by E. Raymond Andrew. Not only is it possible to recover narrow lines from solid samples to obtain chemical shift information about the nuclei in a sample but modern multidimensional NMR pulse sequences have been adapted to ssNMR, which allows study of the molecular structure and dynamics of molecules of interest. ssNMR is particularly useful to obtain microscopic structural information about disordered solids such as glasses or polymers. However, it also allows the study of diffusion of liquids through porous solids, including nanoporous materials.

17.9 DYNAMIC NUCLEAR POLARIZATION

As noted in Section 17.2, NMR is rather insensitive owing to the small resonance energies coupled with usually unfavorable Boltzmann population differences. As Figure 17.3 illustrates, the spin polarization of ^1H NMR at room temperature is of the order of 10^{-5} . Therefore, large sample concentrations in NMR experiments are needed, which are sometimes difficult to achieve. To address this problem so-called hyperpolarization schemes have been developed to prepare nuclear spin systems in highly polarized non-equilibrium states with orders of magnitude higher signal intensities. **Dynamic nuclear polarization** (DNP) is one such method and grew out of the original work by Albert Overhauser in 1953. The fundamental idea behind this method is to couple electron spins with the surrounding nuclei and to transfer their much higher equilibrium spin polarization to the nuclei. A number of different DNP schemes have been developed for liquid and solid samples.

Given the same external field and temperature, the equilibrium population difference between the α and β spin states [see Equation (17.9)] of the electron spin in a free radical is approximately 658 times larger than that of a proton spin owing to the much higher gyromagnetic ratio of the electron spin, as shown in the following computations:

$$P = \tanh\left(\frac{\gamma\hbar B_0}{2k_B T}\right) \approx \left(\frac{\gamma\hbar B_0}{2k_B T}\right)$$

$$\frac{P_e}{P_n} \approx \frac{\gamma_e}{\gamma_n} = \frac{1.760859644 \times 10^{11} \text{ s}^{-1}}{2.675221900 \times 10^8 \text{ s}^{-1}} \approx 658 \quad (17.49)$$

In liquids, the so-called Overhauser mechanism is active and can be understood using a simple energy-level scheme in which an electron spin is coupled to a nuclear spin (both spin-1/2), as seen in Figure 17.38. Note that this four-level scheme is very similar to the one used earlier in the discussion of the NOE (see Figure 17.21). The main difference between the two diagrams is that one of the nuclear spins has been replaced with an electron spin. This makes the energy difference between the levels drastically different because electron spin transitions (labeled with W_e in Figure 17.38) occur in the microwave range of electromagnetic radiation; that is, their photon energies are two to three orders of magnitude greater than those of the nuclear transitions (labeled with W_n) that occur in the RF range.

In this scheme, the relaxation of the population of a given level can be calculated by considering both single-quantum relaxation rates for the electron and nuclear spins, W_e and W_n , respectively, as well as the zero- and double-quantum cross-relaxation rates, W_0 and W_2 . By setting up the rate equations for the various relaxation processes for the four states, one arrives at a very similar result for DNP enhancement as was seen for NOE enhancement [see Equation (17.35)]. The DNP effect on the nuclei is obtained by saturating the electron spin transition. Experimentally, this is done by irradiating the sample with high-intensity microwave radiation at the resonance frequency of the electron spins. As was the case for NOE, the cross-relaxation rates W_0 and W_2 are the important ingredients and require efficient dipolar coupling between the electron spin and the nuclear spin. This in turn requires spatial proximity because dipolar coupling trails off with the sixth power of the distance. Under steady-state conditions, the DNP enhancement of the NMR spectra of nearby nuclear spins can be estimated by the following equation:

$$\frac{\Delta N_I}{\Delta N_I^{\text{eq}}} = 1 - \frac{W_2 - W_0}{2W_n + W_2 + W_0} \cdot \frac{2W_n + W_2 + W_0}{2W_n + W_2 + W_0 + W_I} \cdot \frac{(\Delta N_S - \Delta N_S^{\text{eq}})}{\Delta N_S^{\text{eq}}} \cdot \frac{|\gamma_S|}{|\gamma_I|}$$

$$= 1 - \rho_{fs} \frac{|\gamma_S|}{|\gamma_I|} = E \quad (17.50)$$

In this equation, E is the NMR signal enhancement upon saturation of the EPR transition. ΔN_I is the population difference of the nuclear spin levels under DNP conditions, whereas ΔN_I^{eq} is the equilibrium population difference. A similar notation for the electron spin is indicated with the subscript S . The relaxation rates W_i are those given in Figure 17.38, except for W_I , which represents the rate of any additional nuclear spin

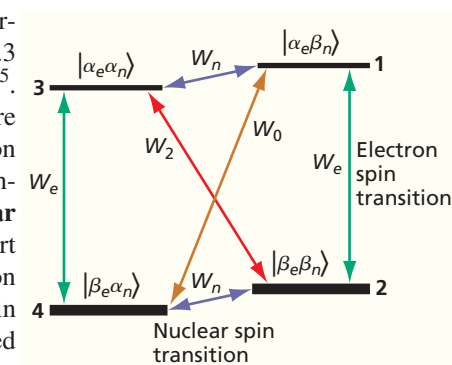


Figure 17.38

Energy-level diagram for a coupled system of an electron spin-1/2 and a nuclear spin-1/2 in an external magnetic field. The electron spin-1/2 is indexed with e , and the nuclear spin-1/2 is indexed with n . The single quantum relaxation rate constants for both spins are indicated by W_e and W_n . The cross-relaxation rate constant W_0 corresponds to a flip-flop process whereby one spin flips and the other one flops. The index 0 indicates that this is a zero-quantum transition. In the double-quantum transition, both spins flip or flop together, and its relaxation rate constant is indicated by W_2 . The thickness of the energy levels indicates the Boltzmann population of the corresponding states. The energy levels are not to scale.

Source: Based on van Bentum et al., *J. Mag. Res.* 264 (2016): 59–67.

Concept

Dynamic nuclear polarization can be used to prepare nuclear spin systems in highly polarized non-equilibrium states with orders of magnitude higher signal intensities.

relaxation mechanism active in the system other than dipolar relaxation. The parameters ρ , f , and s are called the coupling, leakage, and saturation factors, respectively, and are defined by:

$$\begin{aligned}\rho &= \frac{W_2 - W_0}{2W_n + W_2 + W_0} \\ f &= \frac{2W_n + W_2 + W_0}{2W_n + W_2 + W_0 + W_1} \\ s &= \frac{(\Delta N_S - \Delta N_S^{\text{eq}})}{\Delta N_S^{\text{eq}}}\end{aligned}\quad (17.51)$$

Among these parameters, the coupling factor is the most important one. It represents the difference between the two cross-relaxation rate constants W_2 and W_0 normalized by all electron spin-induced relaxation mechanisms. At room temperature in nonviscous solvents, the possible values for ρ range from $+0.5$ to -1.0 when cross relaxation is induced by only dipolar interactions between the two spins. The coupling factor depends on the molecular tumbling rate given by the inverse rotational correlation time, and the distance between the electron and nuclear spins. The leakage factor f represents the ratio of the nuclear spin relaxation rates due to the dipolar or scalar coupling with the electron spin scaled by the sum of all possible nuclear relaxation rates. The leakage factor therefore ranges in value between 0 and 1, with $f = 1$ when nuclear relaxation is induced solely by scalar or dipolar coupling and $f = 0$ when nuclear relaxation is completely independent of the presence of the electron spin and no DNP effect may be observed.

In general, the leakage factor is a function of the concentration of the free radical species that are added to the solution to induce the DNP effect. The saturation factor depends on the difference in the electron spin polarization from equilibrium in the presence of saturating microwave radiation. It also depends sensitively on the number of EPR lines of the radical used. For example, a typical nitroxide radical has three distinct hyperfine lines. When only one is saturated, the saturation factor is one-third of the maximum possible s_{max} . Rapid electron spin exchange in concentrated nitroxide solutions is mediated through frequent collisions of nitroxide molecules and will merge the three lines and make it possible to achieve the full $s_{\text{max}} \approx 1$.

Finally, the quotient of the gyromagnetic ratios of electron and proton spins is 658 as given in Equation (17.49). Therefore, the NMR signal enhancement E for protons under ideal conditions (only dipolar coupling without leakage and full saturation) is at most 659. This can potentially lead to a time-saving factor of 434,000 for a solution NMR experiment because signal acquisition times for a given signal-to-noise ratio scale with the inverse square of the signal enhancement. Because the coupling factor depends largely on molecular parameters such as rotational correlation times, average distance between nuclear and electron spins, the maximum enhancement factor depends on the molecular systems used. In low magnetic fields (~ 0.3 T), enhancements on the order of 200 have been observed. As was noted before, high magnetic fields confer a resolution advantage on NMR that makes it desirable to scale DNP up to high fields. Unfortunately, the Overhauser mechanism predicts smaller efficiencies at high fields, although enhancement factors on the order of 40 have been reported for 3.4 T.

EXAMPLE PROBLEM 17.5

Calculate the maximum possible NMR signal enhancement and time-saving factor for ^{13}C nuclei.

Solution:

$$\begin{aligned}E &= 1 - \rho fs \frac{|\gamma_e|}{|\gamma_{^{13}\text{C}}|} \\ &= 1 - (-1.0)(1.0)(1.0) \frac{1.760859644 \times 10^{11} \text{ s}^{-1}}{6.7262 \times 10^7 \text{ s}^{-1}} = 1 + 2617.9 \approx 2619\end{aligned}$$

The maximum time-saving factor is 6.9×10^6 , the square of the calculated E .

There are other polarization transfer mechanisms that can be exploited for DNP, mostly in the solid state. The *solid effect* depends on the coupling of an electron and a nuclear spin leading to an energy-level scheme as seen in Figure 17.38. The DNP effect is generated by irradiating the normally forbidden zero- or double-quantum transitions that become partially allowed by the hyperfine-induced mixing of the spin states.

The *cross effect* depends on the presence of two electron spins that couple to a nuclear spin with broad EPR lines for which the matching condition

$$\omega_I = \omega_{S1} - \omega_{S2} \quad (17.52)$$

is met. Here, ω_I is the nuclear Larmor frequency, and ω_{S1} and ω_{S2} are the electron Larmor frequencies of the two electron spins, which differ from each other and are dependent on the orientation of the magnetic field relative to the molecular axes. The cross effect requires a bi-radical to be introduced and yields somewhat better NMR enhancements in ssNMR than the solid effect.

Other nuclear hyperpolarization schemes have also been described in the literature and have found numerous applications. For example, hyperpolarized ^{129}Xe is used in magnetic resonance imaging of the lung. The use of para-hydrogen as a source of hyperpolarized protons has led to better understanding of hydrogenation catalysts. Chemically induced dynamic nuclear polarization (CIDNP), particularly photochemical CIDNP experiments, have been used to study protein folding. The field of hyperpolarized NMR is vital and growing because of its potential to deliver important structural and dynamic information about molecules of interest in all areas of science using nuclear spins as localized and sensitive probes.

17.10 MAGNETIC RESONANCE IMAGING

An important application of NMR spectroscopy is its use in imaging solids as well as biological tissue. In the health sciences, **magnetic resonance imaging (MRI)** has proved to be the most powerful and least invasive technique for obtaining information on soft tissue, such as internal organs in humans. The protons in water molecules are used in medical MRI because they are the most abundant protons in soft tissue. How is the spatial resolution needed for imaging obtained using NMR?

For imaging, a **magnetic field gradient** is superimposed onto the constant external magnetic field that permeates the sample. In this way, the resonance frequency of a given spin depends not only on the identity of the spin (e.g., ^1H or ^{13}C), but also on its position relative to the laboratory frame of reference in which the field gradient is applied. Figure 17.39 illustrates how the addition of a field gradient to the constant magnetic field allows the spatial mapping of spins to be carried out. Imagine a sphere and a cube containing $^1\text{H}_2\text{O}$ immersed in a background that contains no spin-active nuclei. In the absence of the field gradient, all spins in the structures resonate at the same frequency, giving rise to a single-proton NMR peak. However, with the field gradient present, each volume element of the structure along the gradient has a different resonance frequency. The intensity of the NMR peak at each frequency is proportional to the total number of spins in the 2D slice perpendicular to the gradient. A plot of the NMR peak intensity versus field strength gives a projection of the volume of the structures along each of the three gradient directions. With three scans corresponding to orthogonal gradient directions, the three-dimensional structure of the specimen can be reconstructed.

The particular usefulness of NMR for imaging biological samples relies on how different experimental observables can be used to create contrast in an image. These properties include the relaxation times T_1 and T_2 , as well as chemical shifts and flow rates. The relaxation time offers the most useful contrast mechanism. The relaxation times T_1 and T_2 for water can vary in biological tissues from 0.1 s to several seconds. The more strongly bound water is to a biological membrane, the greater the change in its relaxation time relative to freely tumbling water molecules. For example, the brain can be imaged with high contrast because the relaxation times of ^1H in gray matter, white matter, and spinal fluid are quite different. In some cases, contrast agents have to be injected into the body to obtain higher-quality images. These agents typically consist of paramagnetic molecules that reduce the nuclear relaxation times by dipolar coupling.

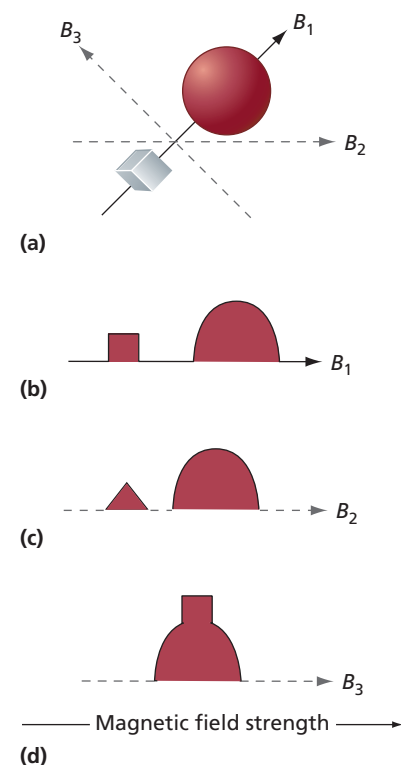


Figure 17.39

Illustration of how the addition of a field gradient to the constant magnetic field allows spatial mapping of spins.

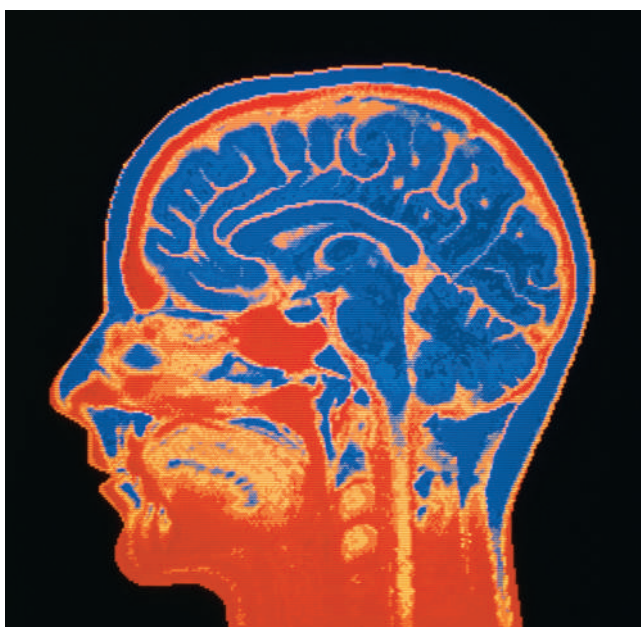
(a) Two structures are shown, along with the three indicated gradient directions along which NMR spectra are obtained. The external magnetic field \mathbf{B}_0 may be applied in one of these three perpendicular directions. In each case, spins within a thin volume slice perpendicular to the gradient resonate at the same frequency. This leads to a spectrum that is a projection of the volumes onto the gradient axis. Image reconstruction techniques originally developed for X-rays can be used to determine the three-dimensional structure. (b – d) NMR spectra that would be observed along the \mathbf{B}_1 , \mathbf{B}_2 , and \mathbf{B}_3 directions indicated in part (a).

Concept

In the health sciences, magnetic resonance imaging (MRI) has proved to be the most powerful and least invasive technique for obtaining information on soft tissue, such as internal organs in humans.

Figure 17.40

NMR image of a human head. The section shown is from a noninvasive scan of the patient's head. The contrast has its origin in the dependence of the relaxation time on the strength of binding of water molecules to different biological tissues.
Source: M. Kulyk/Science Source



Significant development efforts are being devoted to finding nontoxic contrast agents with relatively short retention times in the body. Data acquisition methods have been developed to enhance the signal amplitude for a particular range of relaxation times, enabling the contrast to be optimized for the problem of interest. Figure 17.40 shows an NMR image of a human head.

Concept

Chemical shift imaging can be used to localize metabolic processes and to follow signal transmission in the brain through chemical changes that occur at nerve synapses.

Chemical shift imaging can be used to localize metabolic processes and to follow signal transmission in the brain through chemical changes that occur at nerve synapses. One variation of flow imaging is based on the fact that it takes times that are several multiples of T_1 for the local magnetization to achieve its equilibrium value. If, for instance, blood flows into the region under investigation on shorter timescales, it will not have the full magnetization of the spins that have been exposed to the field for much longer times. In such a case, the $^1\text{H}_2\text{O}$ proton spins in the blood experience a phase shift compared to the surrounding ^1H spins which can be visualized by phase-sensitive imaging techniques.

NMR imaging also has many applications in materials science. Examples include the measurement of the chemical cross-link density in polymers, the appearance of heterogeneities in elastomers such as rubber through vulcanization or aging, and the diffusion of solvents into polymers. Voids and defects in ceramics and the porosity of ceramics can be detected by nondestructive NMR imaging.

VOCABULARY

anisotropic
chemical shift
chemical shift imaging
chemically equivalent nuclei
cross relaxation
diamagnetic response
dipolar spin–spin coupling
dynamic nuclear polarization
Fourier transform
free induction decay (FID)
gyromagnetic ratio
Karplus relation

Larmor frequency
macroscopic magnetic moment \mathbf{M}
magic angle spinning
magnetically equivalent nuclei
magnetic field gradient
magnetic resonance imaging (MRI)
motional broadening
motional narrowing
multiplet
neighboring group anisotropy
nuclear magneton
nuclear Overhauser effect (NOE)

precession
relaxation
resonance condition
rotating frame
shielding constant
spin echo
spin-lattice relaxation
spin polarization
spin–spin coupling
vector model
Zeeman effect

KEY EQUATIONS

Equation	Significance of Equation	Equation Number
$\mu = g_N \frac{e}{2m_{\text{proton}}} \mathbf{I} = \frac{g_N \beta_N}{\hbar} \mathbf{I} = \gamma \mathbf{I}$	Relationship between magnetic moment to spin and gyromagnetic ratio	17.2
$E = -\mu \cdot \mathbf{B}_0 = -\gamma m_I \hbar B_0$	Energy of spin in magnetic field and spatial quantization	17.3
$\Delta E = E_\beta - E_\alpha = \gamma \hbar B_0 = \hbar \omega_0 = h\nu$		
$\nu_0 = \frac{\gamma B_0}{2\pi}, \quad \omega_0 = \gamma B_0$	NMR resonance condition	17.7
$\delta = \frac{(\nu - \nu_{\text{ref}})}{\nu_{\text{ref}}} \times 10^6 \approx (\sigma_{\text{ref}} - \sigma) \times 10^6$	Definition of chemical shift	17.12
$B_z = \frac{\mu_0 \mu }{4\pi \mathbf{r} ^3} (3 \cos^2 \theta - 1)$	z component of magnetic moment, key to dipolar coupling between spins	17.13
$\alpha = \frac{\gamma_N B_1 \Delta t}{2}$	Tip angle for a spin exposed to a resonant RF pulse	17.26
$\omega_1 = \frac{\gamma_N B_1}{2}$	Rabi frequency	17.27
$\Delta\nu \approx \frac{1}{\Delta t}$ $\Delta t = T_2$	Relationship between linewidth and relaxation time	17.32
$\eta = \frac{I - I_0}{I_0}$	DNP enhancement parameter	17.34
$(3 \cos^2 \theta - 1) = 0$ $\theta = 54.7356^\circ$	Definition of the magic angle in ssNMR	17.48

CONCEPTUAL PROBLEMS

Q17.1 Why can the signal loss that results from spin dephasing, which is caused by magnetic field inhomogeneities and chemical shift, be recovered in the spin echo experiment?

Q17.2 Why do neighboring groups lead to a net induced magnetic field at a given spin in a molecule in the solid state, but not for the same molecule in solution?

Q17.3 Why is it useful to define the chemical shift relative to a reference compound as follows?

$$\delta = \frac{(\nu - \nu_{\text{ref}})}{\nu_{\text{ref}}} \cdot 10^6$$

Q17.4 What is the advantage of a 2D NMR experiment compared with a 1D NMR experiment?

Q17.5 Why do magnetic field inhomogeneities of only a few parts per million pose difficulties in NMR experiments?

Q17.6 Why does NMR lead to a higher contrast in the medical imaging of soft tissues than X-ray techniques?

Q17.7 Why is the multiplet splitting for coupled spins independent of the static magnetic field?

Q17.8 Under what conditions does the H atom on the OH group lead to a multiplet splitting of the methyl hydrogens of ethanol?

Q17.9 Why are the multiplet splittings in Figure 17.10 not dependent on the static magnetic field?

Q17.10 Redraw Figure 17.2a for β spins. What is the direction of precession for the spins and for the macroscopic magnetic moment?

Q17.11 Why is the measurement time in NMR experiments reduced by using Fourier transform techniques?

Q17.12 Order the molecules CH_3I , CH_3Br , CH_3Cl , and CH_3F in terms of increasing chemical shift for ${}^1\text{H}$. Explain your answer.

Q17.13 Explain why $T_1 \geq T_2/2$.

Q17.14 Explain why two magnetic fields, a static field and a radio-frequency field, are needed to carry out NMR experiments. Why must the two field directions be perpendicular?

Q17.15 Explain the difference in the mechanism that gives rise to through-space dipole–dipole coupling and through-bond coupling.

Q17.16 In order to visualize the NOE effect for a sample, NOE difference spectra are usually taken, that is, spectra with and without RF pumping of a signal of interest. Explain why this is a useful approach and describe what type of information is contained in the NOE difference spectrum.

Q17.17 Explain why it is generally not possible to infer T_2^{hom} from the decay of a simple FID.

Q17.18 Explain why it is generally not possible to infer T_2^{hom} from the linewidth of a NMR spectrum.

Q17.19 Identify the preparation, evolution, mixing, and detection periods in the 2D NOESY experiment.

Q17.20 Explain why transitions along the relaxation paths W_1 in Figure 17.21 are called single-quantum transitions.

Q17.21 Explain why transitions along the relaxation paths W_0 and W_2 in Figure 17.21 are called zero- and double-quantum transitions, respectively.

Q17.22 Explain why the NOE effect can be used for distance measurements between nuclei.

NUMERICAL PROBLEMS

P17.1 Predict the number of chemically shifted ^1H peaks and the multiplet splitting of each peak that you would observe for diethyl ether. Justify your answer.

P17.2 For a fixed frequency of the radio-frequency field, ^1H , ^{13}C , and ^{31}P will be in resonance at different values of the static magnetic field. Calculate the value of \mathbf{B}_0 for these nuclei to be in resonance if the radio-frequency field has a frequency of 600 MHz.

P17.3 The nuclear spin operators can be represented as 2×2 matrices, and α and β can be represented as column vectors in the form

$$\alpha = \begin{pmatrix} 1 \\ 0 \end{pmatrix} \quad \text{and} \quad \beta = \begin{pmatrix} 0 \\ 1 \end{pmatrix}$$

Given that

$$\hat{I}_x = \frac{\hbar}{2} \begin{pmatrix} 0 & 1 \\ 1 & 0 \end{pmatrix}, \quad \hat{I}_y = \frac{\hbar}{2} \begin{pmatrix} 0 & -i \\ i & 0 \end{pmatrix}, \quad \text{and} \quad \hat{I}_z = \frac{\hbar}{2} \begin{pmatrix} 1 & 0 \\ 0 & -1 \end{pmatrix}$$

and

$$\hat{I}^2 = \frac{3\hbar^2}{4} \begin{pmatrix} 1 & 0 \\ 0 & 1 \end{pmatrix}$$

show that

$$\hat{I}^2\alpha = \frac{3\hbar^2}{4}\alpha, \quad \hat{I}^2\beta = \frac{3\hbar^2}{4}\beta, \quad \hat{I}_z\alpha = \frac{\hbar}{2}\alpha \quad \text{and} \quad \hat{I}_z\beta = -\frac{\hbar}{2}\beta$$

P17.4 Using the matrix representation of the operators and spin eigenfunctions (see the preceding problem), show that the relationships listed in Equation (17.17) are obtained when the Hamilton operator, as defined by Equation (17.14), is applied to the wavefunctions defined in Equation (17.15). Assume noninteracting spins.

P17.5 Carry out the calculations in Problem 17.4 under the assumption of interacting spins for which the Hamilton operator for scalar coupling given in Equation (17.18) applies in addition to the one in Equation (17.14).

P17.6 Using your result from the previous problems, show that there are four possible transitions between the energy

levels of two interacting spins and that the frequencies are given by Equation (17.20):

$$\begin{aligned} v_{12} &= \frac{\gamma B_0}{2\pi} (1 - \sigma_1) - \frac{J_{12}}{2} \\ v_{34} &= \frac{\gamma B_0}{2\pi} (1 - \sigma_1) + \frac{J_{12}}{2} \\ v_{13} &= \frac{\gamma B_0}{2\pi} (1 - \sigma_2) - \frac{J_{12}}{2} \\ v_{24} &= \frac{\gamma B_0}{2\pi} (1 - \sigma_2) + \frac{J_{12}}{2} \end{aligned}$$

P17.7 Predict the number of chemically shifted ^1H peaks and the multiplet splitting of each peak that you would observe for bromoethane. Justify your answer.

P17.8 A 250 MHz ^1H spectrum of a compound shows two peaks. The frequency of one peak is 510 Hz higher than that of the reference compound (tetramethylsilane), and the second peak is at a frequency 170 Hz lower than that of the reference compound. What chemical shift should be assigned to these two peaks?

P17.9 Predict the number of chemically shifted ^1H peaks and the multiplet splitting of each peak that you would observe for 1,1,1,2-tetrachloroethane. Justify your answer.

P17.10 Predict the number of chemically shifted ^1H peaks and the multiplet splitting of each peak that you would observe for 1,1,2,2-tetrachloroethane. Justify your answer.

P17.11 Predict the number of chemically shifted ^1H peaks and the multiplet splitting of each peak that you would observe for nitroethane. Justify your answer.

P17.12 Predict the number of chemically shifted ^1H peaks and the multiplet splitting of each peak that you would observe for nitromethane. Justify your answer.

P17.13 Predict the number of chemically shifted ^1H peaks and the multiplet splitting of each peak that you would observe for 1,1,2-trichloroethane. Justify your answer.

P17.14 Using the spin operators as defined in Problem 17.3, show that none of the pairs of spin operators, \hat{I}_x , \hat{I}_y , \hat{I}_z , commute with each other.

P17.15 Using the spin operators as defined in Problem 17.3, show that each of the spin operators, \hat{I}_x , \hat{I}_y , \hat{I}_z , commutes with \hat{I}^2 .

P17.16 Predict the number of chemically shifted ^1H peaks and the multiplet splitting of each peak that you would observe for 1-chloropropane. Justify your answer.

P17.17 Assume that the $\pi/2$ pulse of a 600 MHz NMR spectrometer is tuned at $8.0 \mu\text{s}$. Calculate the strength of the B_1 field for proton spins under these conditions.

P17.18 Assume that the $\pi/2$ pulse of a 600 MHz NMR spectrometer is tuned at $8.0 \mu\text{s}$. Calculate the Rabi frequency for proton spins under these conditions.

P17.19 A 500 MHz ^1H NMR spectrometer needs to be used to carry out experiments on ^{13}C . Calculate the carrier frequency necessary for the ^{13}C experiment given that the external magnetic field remains the same.

P17.20 At the end of 2017, the highest field superconducting magnet with a projected field strength of 32 T will be commissioned at the National High Magnetic Field Laboratory in Tallahassee, Florida. Its coils are built with high- T_c superconducting wires. Calculate the spin polarization achievable for ^1H NMR at room temperature with the nuclear spins at equilibrium at this field.

P17.21 Calculate the spin polarization achievable for an EPR experiment on a free radical with spin-1/2 in an external magnetic field of 24 T at a temperature of 4.2 K.

P17.22 Calculate the gain in proton spin polarization at room temperature for each increase in external magnetic field of 1.0 T. Hint: You may use a Taylor expansion of the polarization as defined in Equation (17.9) with the assumption that the argument of the tanh function is very small.

P17.23 At a magnetic field strength of 1.5 T, proton NMR relaxation times in human blood at 37°C were observed to be 330 and 1200 ms for T_2 and T_1 , respectively. Calculate T_2^{inh} assuming that it dominates the transverse relaxation rate.

P17.24 An inversion recovery experiment was performed on two different proton peaks in a sample. The zero-crossing of the NMR signal was observed at 0.20 and 0.45 s after the inversion pulse. Give an estimate of the T_1 relaxation times for the two signals.

P17.25 In a spin echo experiment, the following data were measured for the intensity I of the echo as a function of pulse delay time τ . Estimate T_2^{hom} graphically.

τ/s	0.1	0.2	0.3	0.4	0.5	0.6	0.7	0.8	0.9
I	97.5	59.1	35.9	21.8	13.2	8.00	4.86	2.94	1.78

P17.26 In an experiment by Denysenkov et al., published in *Phys. Chem. Chem. Phys.* 12 (2010) 5786–5790, the enhancement factor $\varepsilon = \rho fs|\gamma_S|/|\gamma_H|$ on water protons using 40 mM of Fremy's salt, a stable nitroxide radical for protons, was observed to be -29 when a high-power gyrotron was used to pump the EPR transition of the radical at 260 GHz. The leakage factor was observed to be 0.94, and theoretical calculations led to a coupling factor of -0.072 . Calculate the saturation that could be achieved under the experimental conditions.

FURTHER READING

Bain, A. D., Fletcher, D. A., and Hazendonk, P. "What Is a Transition?" *Concepts in Magnetic Resonance* 10 (1998): 85–95.

Dingley, A. J., Cordier, F., and Grzesiek, S. "An Introduction to Hydrogen Bond Scalar Couplings." *Concepts in Magnetic Resonance* 13 (2001): 103–127.

Hore, Peter. *Nuclear Magnetic Resonance* (2nd ed.). New York: Oxford University Press, 2015.

Goldenberg, D. P. *Principles of NMR Spectroscopy*. Mill Valley, CA: University Science Press, 2016.

Keeler, James. *Understanding NMR Spectroscopy* (2nd ed.). Hoboken, NJ: Wiley, 2010.

Zivkovic, A., Bandolik, J. J., Skerhut, A. J., Coesfeld, C., Zivkovic, N., Raos, M., and Stark, H. "Introducing Students to NMR Methods Using Low-Field ^1H NMR Spectroscopy to Determine the Structure and the Identity of Natural Amino Acids." *Journal of Chemical Education* 94 (2017): 115–120.

This page intentionally left blank

Point Group Character Tables

A.1 THE NONAXIAL GROUPS

C_1	E
A	1

C_s	E	σ_h		
A'	1	1	x, y, R_z	x^2, y^2, z^2, xy
A''	1	-1	z, R_x, R_y	yz, xz

C_i	E	i		
A_g	1	1	R_x, R_y, R_z	$x^2, y^2, z^2, xy, xz, yz$
A_u	1	-1	x, y, z	

A.2 THE C_n GROUPS

C_2	E	C_2		
A	1	1	z, R_z	x^2, y^2, z^2, xy
B	1	-1	x, y, R_x, R_y	yz, xz

C_4	E	C_4	C_2	C_4^3		
A	1	1	1	1	z, R_z	$x^2 + y^2, z^2$
B	1	-1	1	-1		$x^2 - y^2, xy$
E	$\begin{cases} 1 & i \\ 1 & -i \end{cases}$	$\begin{cases} -1 & -i \\ -1 & i \end{cases}$			$(x, y), (R_x, R_y)$	(yz, xz)

A.3 THE D_n GROUPS

D_2	E	$C_2(z)$	$C_2(y)$	$C_2(x)$		
A	1	1	1	1		x^2, y^2, z^2
B_1	1	1	-1	-1	z, R_z	xy
B_2	1	-1	1	-1	y, R_y	xz
B_3	1	-1	-1	1	x, R_x	yz

D_3	E	$2C_3$	$3C_2$		
A_1	1	1	1		$x^2 + y^2, z^2$
A_2	1	1	-1	z, R_z	
E	2	-1	0	$(x, y), (R_x, R_y)$	$(x^2 - y^2, xy), (xz, yz)$

D_4	E	$2C_4$	$C_2 (= C_4^2)$	$2C'_2$	$2C''_2$		
A_1	1	1	1	1	1		$x^2 + y^2, z^2$
A_2	1	1	1	-1	-1	z, R_z	
B_1	1	-1	1	1	-1		$x^2 - y^2$
B_2	1	-1	1	-1	1		xy
E	2	0	-2	0	0	$(x, y), (R_x, R_y)$	(xz, yz)

D_5	E	$2C_5$	$2C_5^2$	$5C_2$		
A_1	1	1	1	1		$x^2 + y^2, z^2$
A_2	1	1	1	-1	z, R_z	
E_1	2	$2 \cos 72^\circ$	$2 \cos 144^\circ$	0	$(x, y), (R_x, R_y)$	(xz, yz)
E_2	2	$2 \cos 144^\circ$	$2 \cos 72^\circ$	0		$(x^2 - y^2, xy)$

D_6	E	$2C_6$	$2C_3$	C_2	$3C'_2$	$3C''_2$	
A_1	1	1	1	1	1	1	
A_2	1	1	1	1	-1	-1	z, R_z
B_1	1	-1	1	-1	1	-1	
B_2	1	-1	1	-1	-1	1	
E_1	2	1	-1	-2	0	0	$(x, y), (R_x, R_y)$
E_2	2	-1	-1	2	0	0	

A.4 THE C_{nv} GROUPS

C_{2v}	ε	C_2	$\sigma_v(xz)$	$\sigma'_v(yz)$		
A_1	1	1	1	1	z	x^2, y^2, z^2
A_2	1	1	-1	-1	R_z	xy
B_1	1	-1	1	-1	x, R_y	xz
B_2	1	-1	-1	1	y, R_x	yz

C_{3v}	E	$2C_3$	$3\sigma_v$		
A_1	1	1	1	z	$x^2 + y^2, z^2$
A_2	1	1	-1	R_z	
E	2	-1	0	$(x, y), (R_x, R_y)$	$(x^2 - y^2, xy), (xz, yz)$

C_{4v}	E	$2C_4$	C_2	$2\sigma_v$	$2\sigma_d$		
A_1	1	1	1	1	1	z	$x^2 + y^2, z^2$
A_2	1	1	1	-1	-1	R_z	
B_1	1	-1	1	1	-1		$x^2 - y^2$
B_2	1	-1	1	-1	1		xy
E	2	0	-2	0	0	$(x, y), (R_x, R_y)$	(xz, yz)

C_{5v}	E	$2C_5$	$2C_5^2$	$5\sigma_v$		
A_1	1	1	1	1	z	$x^2 + y^2, z^2$
A_2	1	1	1	-1	R_z	
E_1	2	$2 \cos 72^\circ$	$2 \cos 144^\circ$	0	$(x, y), (R_x, R_y)$	(xz, yz)
E_2	2	$2 \cos 144^\circ$	$2 \cos 72^\circ$	0		$(x^2 - y^2, xy)$

C_{6v}	E	$2C_6$	$2C_3$	C_2	$3\sigma_v$	$3\sigma_d$		
A_1	1	1	1	1	1	1	z	$x^2 + y^2, z^2$
A_2	1	1	1	1	-1	-1	R_z	
B_1	1	-1	1	-1	1	-1		
B_2	1	-1	1	-1	-1	1		
E_1	2	1	-1	-2	0	0	$(x, y), (R_x, R_y)$	(xz, yz)
E_2	2	-1	-1	2	0	0		$(x^2 - y^2, xy)$

A.5 THE C_{nh} GROUPS

C_{2h}	E	C_2	i	σ_h		
A_g	1	1	1	1	R_z	x^2, y^2, z^2, xy
B_g	1	-1	1	-1	R_x, R_y	xz, yz
A_u	1	1	-1	-1	z	
B_u	1	-1	-1	1	x, y	

C_{4h}	E	C_4	C_2	C_4^3	i	S_4^3	σ_h	S_4	
A_g	1	1	1	1	1	1	1	1	R_z
B_g	1	-1	1	-1	1	-1	1	-1	
E_g	$\begin{cases} 1 & i \\ 1 & -i \end{cases}$	$\begin{cases} -1 & -i \\ -1 & i \end{cases}$	$\begin{cases} 1 & 1 \\ 1 & -1 \end{cases}$	$\begin{cases} -i & -1 \\ -i & 1 \end{cases}$	$\begin{cases} 1 & i \\ 1 & -i \end{cases}$	$\begin{cases} -1 & -1 \\ -1 & 1 \end{cases}$	$\begin{cases} -i & i \\ i & -i \end{cases}$	$\begin{cases} (R_x, R_y) \\ (xz, yz) \end{cases}$	
A_u	1	1	1	1	-1	-1	-1	-1	z
B_u	1	-1	1	-1	-1	1	-1	1	
E_u	$\begin{cases} 1 & i \\ 1 & -i \end{cases}$	$\begin{cases} -1 & -i \\ -1 & i \end{cases}$	$\begin{cases} -i & -1 \\ -i & 1 \end{cases}$	$\begin{cases} 1 & 1 \\ 1 & -1 \end{cases}$	$\begin{cases} -i & i \\ i & -i \end{cases}$	$\begin{cases} 1 & -1 \\ -1 & 1 \end{cases}$	$\begin{cases} (x, y) \\ (x, y) \end{cases}$		

A.6 THE D_{nh} GROUPS

D_{2h}	E	$C_2(z)$	$C_2(y)$	$C_2(x)$	i	$\sigma(xy)$	$\sigma(xz)$	$\sigma(yz)$		
A_g	1	1	1	1	1	1	1	1		x^2, y^2, z^2
B_{1g}	1	1	-1	-1	1	1	-1	-1	R_z	xy
B_{2g}	1	-1	1	-1	1	-1	1	-1	R_y	xz
B_{3g}	1	-1	-1	1	1	-1	-1	1	R_x	yz
A_u	1	1	1	1	-1	-1	-1	-1		
B_{1u}	1	1	-1	-1	-1	-1	1	1	z	
B_{2u}	1	-1	1	-1	-1	1	-1	1	y	
B_{3u}	1	-1	-1	1	-1	1	1	-1	x	

D_{3h}	E	$2C_3$	$3C_2$	σ_h	$2S_3$	$3\sigma_v$		
A'_1	1	1	1	1	1	1		$x^2 + y^2, z^2$
A'_2	1	1	-1	1	1	-1	R_z	
E'	2	-1	0	2	-1	0	(x, y)	$(x^2 - y^2, xy)$
A''_1	1	1	1	-1	-1	-1		
A''_2	1	1	-1	-1	-1	1	z	
E''	2	-1	0	-2	1	0	(R_x, R_y)	(xz, yz)

D_{4h}	E	$2C_4$	C_2	$2C'_2$	$2C''_2$	i	$2S_4$	σ_h	$2\sigma_v$	$2\sigma_d$		
A_{1g}	1	1	1	1	1	1	1	1	1	1		$x^2 + y^2, z^2$
A_{2g}	1	1	1	-1	-1	1	1	1	-1	-1	R_z	
B_{1g}	1	-1	1	1	-1	1	-1	1	1	-1		$x^2 - y^2$
B_{2g}	1	-1	1	-1	1	1	-1	1	-1	1		xy
E_g	2	0	-2	0	0	2	0	-2	0	0	(R_x, R_y)	(xz, yz)
A_{1u}	1	1	1	1	1	-1	-1	-1	-1	-1		
A_{2u}	1	1	1	-1	-1	-1	-1	-1	1	1	z	
B_{1u}	1	-1	1	1	-1	-1	1	-1	-1	1		
B_{2u}	1	-1	1	-1	1	-1	1	-1	1	-1		
E_u	2	0	-2	0	0	-2	0	2	0	0	(x, y)	

D_{6h}	E	$2C_6$	$2C_3$	C_2	$3C'_2$	$3C''_2$	i	$2S_3$	$2S_6$	σ_h	$3\sigma_d$	$3\sigma_v$		
A_{1g}	1	1	1	1	1	1	1	1	1	1	1	1		$x^2 + y^2, z^2$
A_{2g}	1	1	1	1	-1	-1	1	1	1	1	-1	-1	R_z	
B_{1g}	1	-1	1	-1	1	-1	1	-1	1	-1	1	-1		
B_{2g}	1	-1	1	-1	-1	1	1	-1	1	-1	-1	1		
E_{1g}	2	1	-1	-2	0	0	2	1	-1	-2	0	0	(R_x, R_y)	(xz, yz)
E_{2g}	2	-1	-1	2	0	0	2	-1	-1	2	0	0		$(x^2 - y^2, xy)$
A_{1u}	1	1	1	1	1	1	-1	-1	-1	-1	-1	-1		
A_{2u}	1	1	1	1	-1	-1	-1	-1	-1	-1	1	1	z	
B_{1u}	1	-1	1	-1	1	-1	-1	1	-1	1	-1	1		
B_{2u}	1	-1	1	-1	-1	1	-1	1	-1	1	1	-1		
E_{1u}	2	1	-1	-2	0	0	-2	-1	1	2	0	0	(x, y)	
E_{2u}	2	-1	-1	2	0	0	-2	1	1	-2	0	0		

D_{8h}	E	$2C_8^3$	$2C_8$	$2C_4$	C_2	$4C'_2$	$4C''_2$	i	$2S_8^3$	$2S_8$	$2S_4$	σ_h	$4\sigma_d$	$4\sigma_v$		
A_{1g}	1	1	1	1	1	1	1	1	1	1	1	1	1	1	$x^2 + y^2, z^2$	
A_{2g}	1	1	1	1	1	-1	-1	1	1	1	1	1	-1	-1	R_z	
B_{1g}	1	-1	-1	1	1	1	-1	1	-1	-1	1	1	1	-1		
B_{2g}	1	-1	-1	1	1	-1	1	1	-1	-1	1	1	-1	1		
E_{1g}	2	$\sqrt{2}$	$-\sqrt{2}$	0	-2	0	0	2	$\sqrt{2}$	$-\sqrt{2}$	0	-2	0	0	(R_x, R_y)	(xz, yz)
E_{2g}	2	0	0	-2	2	0	0	2	0	0	-2	2	0	0		$(x^2 - y^2, xy)$
E_{3g}	2	$-\sqrt{2}$	$\sqrt{2}$	0	-2	0	0	2	$-\sqrt{2}$	$\sqrt{2}$	0	-2	0	0		
A_{1u}	1	1	1	1	1	1	1	-1	-1	-1	-1	-1	-1	-1		
A_{2u}	1	1	1	1	1	-1	-1	-1	-1	-1	-1	-1	1	1	z	
B_{1u}	1	-1	-1	1	1	1	-1	-1	1	1	-1	-1	-1	-1	1	
B_{2u}	1	-1	-1	1	1	-1	1	-1	1	1	-1	-1	1	-1		
E_{1u}	2	$\sqrt{2}$	$-\sqrt{2}$	0	-2	0	0	-2	$-\sqrt{2}$	$\sqrt{2}$	0	2	0	0	(x, y)	
E_{2u}	2	0	0	-2	2	0	0	-2	0	0	2	-2	0	0		
E_{3u}	2	$-\sqrt{2}$	$\sqrt{2}$	0	-2	0	0	-2	$\sqrt{2}$	$-\sqrt{2}$	0	2	0	0		

A.7 THE D_{nd} GROUPS

D_{2d}	E	$2S_4$	C_2	$2C'_2$	$2\sigma_d$		
A_1	1	1	1	1	1		$x^2 + y^2, z^2$
A_2	1	1	1	-1	-1	R_z	
B_1	1	-1	1	1	-1		$x^2 - y^2$
B_2	1	-1	1	-1	1	z	xy
E	2	0	-2	0	0	$(x, y), (R_x, R_y)$	(xz, yz)

D_{3d}	E	$2C_3$	$3C_2$	i	$2S_6$	$3\sigma_d$		
A_{1g}	1	1	1	1	1	1		$x^2 + y^2, z^2$
A_{2g}	1	1	-1	1	1	-1	R_z	
E_g	2	-1	0	2	-1	0	(R_x, R_y)	$(x^2 - y^2, xy), (xz, yz)$
A_{1u}	1	1	1	-1	-1	-1		
A_{2u}	1	1	-1	-1	-1	1	z	
E_u	2	-1	0	-2	1	0	(x, y)	

D_{4d}	E	$2S_8$	$2C_4$	$2S_8^3$	C_2	$4C'_2$	$4\sigma_d$		
A_1	1	1	1	1	1	1	1		$x^2 + y^2, z^2$
A_2	1	1	1	1	1	-1	-1	R_z	
B_1	1	-1	1	-1	1	1	-1		
B_2	1	-1	1	-1	1	-1	1	z	
E_1	2	$\sqrt{2}$	0	$-\sqrt{2}$	-2	0	0	(x, y)	
E_2	2	0	-2	0	2	0	0		$(x^2 - y^2, xy)$
E_3	2	$-\sqrt{2}$	0	$\sqrt{2}$	-2	0	0	(R_x, R_y)	(xz, yz)

D_{6d}	E	$2S_{12}$	$2C_6$	$2S_4$	$2C_3$	$2S_{12}^5$	C_2	$6C'_2$	$6\sigma_d$		
A_1	1	1	1	1	1	1	1	1	1		$x^2 + y^2, z^2$
A_2	1	1	1	1	1	1	1	-1	-1	R_z	
B_1	1	-1	1	-1	1	-1	1	1	-1		
B_2	1	-1	1	-1	1	-1	1	-1	1	z	
E_1	2	$\sqrt{3}$	1	0	-1	$-\sqrt{3}$	-2	0	0	(x, y)	
E_2	2	1	-1	-2	-1	1	2	0	0		$(x^2 - y^2, xy)$
E_3	2	0	-2	0	2	0	-2	0	0		
E_4	2	-1	-1	2	-1	-1	2	0	0		
E_5	2	$-\sqrt{3}$	1	0	-1	$\sqrt{3}$	-2	0	0	(R_x, R_y)	(xz, yz)

A.8 THE CUBIC GROUPS

T_d	E	$8C_3$	$3C_2$	$6S_4$	$6\sigma_d$		
A_1	1	1	1	1	1		$x^2 + y^2 + z^2$
A_2	1	1	1	-1	-1		
E	2	-1	2	0	0		$(2z^2 - x^2 - y^2, x^2 - y^2)$
T_1	3	0	-1	1	-1	(R_x, R_y, R_z)	
T_2	3	0	-1	-1	1	(x, y, z)	(xy, xz, yz)

O	E	$8C_3$	$3C_2 (= C_4^2)$	$6C_4$	$6C_2$		
A_1	1	1	1	1	1		$x^2 + y^2 + z^2$
A_2	1	1	1	-1	-1		
E	2	-1	2	0	0		$(2z^2 - x^2 - y^2, x^2 - y^2)$
T_1	3	0	-1	1	-1	$(R_x, R_y, R_z), (x, y, z)$	
T_2	3	0	-1	-1	1		(xy, xz, yz)

O_h	E	$8C_3$	$6C_2$	$6C_4$	$3C_2 (= C_4^2)$	i	$6S_4$	$8S_6$	$3\sigma_h$	$6\sigma_d$		
A_{1g}	1	1	1	1	1	1	1	1	1	1		$x^2 + y^2 + z^2$
A_{2g}	1	1	-1	-1	1	1	-1	1	1	-1		
E_g	2	-1	0	0	2	2	0	-1	2	0		$(2z^2 - x^2 - y^2, x^2 - y^2)$
T_{1g}	3	0	-1	1	-1	3	1	0	-1	-1	(R_x, R_y, R_z)	
T_{2g}	3	0	1	-1	-1	3	-1	0	-1	1		(xz, yz, xy)
A_{1u}	1	1	1	1	1	-1	-1	-1	-1	-1		
A_{2u}	1	1	-1	-1	1	-1	1	-1	-1	1		
E_u	2	-1	0	0	2	-2	0	1	-2	0		
T_{1u}	3	0	-1	1	-1	-3	-1	0	1	1	(x, y, z)	
T_{2u}	3	0	1	-1	-1	-3	1	0	1	-1		

A.9 THE GROUPS $C_{\infty v}$ AND $D_{\infty h}$ FOR LINEAR MOLECULES

$C_{\infty v}$	E	$2C_\infty^\Phi$	\dots	$\infty\sigma_v$		
$A_1(\Sigma^+)$	1	1		1	z	$x^2 + y^2, z^2$
$A_2(\Sigma^-)$	1	1	\dots	-1	R_z	
$E_1(\Pi)$	2	$2 \cos \Phi$	\dots	0	$(x, y), (R_x, R_y)$	(xz, yz)
$E_2(\Delta)$	2	$2 \cos 2\Phi$	\dots	0		$(x^2 - y^2, xy)$
$E_3(\Phi)$	2	$2 \cos 3\Phi$	\dots	0		
\dots	\dots	\dots	\dots	\dots		

Credits

Cover

Stephen Yates

Frontmatter

Page viii: Thomas Engel.

Chapter 1

Page 25: Adapted from D. S. Kaufman et al., *The Journal of Chemical Physics*, Vol. 86, 3682 (1987).

Chapter 3

Page 73: Library of Congress Prints and Photographs Division (LC-DIG-ds-00175).

Chapter 5

Page 106: Courtesy of Johnson, Kevin. “The Thermal Decomposition and Desorption Mechanism of Ultra-Thin Oxide on Silicon Studied by Scanning Tunneling Microscopy.” PhD thesis. Page 108: Adapted from Giessibl, *Reviews of Modern Physics* 75 (2003): 949. Page 109: Republished with permission of American Assn for the Advancement of Science, from “The Chemical Structure of a Molecule Resolved by Atomic Force Microscopy”, Gross et al., *Science* Vol. 325, Issue 5944 (1110–14), 2009; permission conveyed through Copyright Clearance Center, Inc. Page 110: Adapted from Zuev et al., *Science* 299 (2003): 867–870.

Page 112: Adapted from Michalat et al., *Science* 307 (2005): 538. Page 113: Republished with permission of American Assn. for the Advancement of Science, from “Water-Soluble Quantum Dots for Multiphoton Fluorescence Imaging in Vivo”, Larson et al., *Science* Vol. 300, Issue 5624 (1434–36), 2003; permission conveyed through Copyright Clearance Center, Inc.

Page 113: Reprinted by permission from Macmillan Publishers Ltd: Nature Biotechnology, Near-infrared fluorescent type II quantum dots for sentinel lymph node mapping, Kim et al., *Nature Biotechnology* 22(1), (2004): 93–97.

Chapter 6

Page 124: The Niels Bohr Archive, Copenhagen. Page 133: Adapted from D. V. Strekalov et al., *Physical Review Letters* 74, 3600–3603, 1995. Copyright 1995 by the American Physical Society. <http://link.aps.org/doi/10.1103/PhysRevLett.74.3600>.

Chapter 10

Page 243: Calculated from data in E. Clementi and C. Roetti. “Roothaan-Hartree-Fock Atomic Wavefunctions: Basis Functions and Their Coefficients for Ground and Certain Excited States of Neutral and Ionized Atoms, $Z \leq 54$.” *Atomic Data and Nuclear Data Tables* 14 (1974): 177. Page 243: Calculated from data in E. Clementi and C. Roetti. “Roothaan-Hartree-Fock Atomic Wavefunctions: Basis Functions and Their Coefficients for Ground and Certain Excited States of Neutral and Ionized Atoms, $Z \leq 54$.” *Atomic Data and Nuclear Data Tables* 14 (1974): 177. Page 244: Calculated from data in E. Clementi and C. Roetti. “Roothaan-Hartree-Fock Atomic Wavefunctions: Basis Functions and Their Coefficients for Ground and Certain Excited States of Neutral and Ionized Atoms, $Z \leq 54$.” *Atomic Data and Nuclear Data Tables* 14 (1974): 177. Page 244: Calculated from data in E. Clementi and C. Roetti. “Roothaan-Hartree-Fock Atomic Wavefunctions: Basis Functions and Their Coefficients for Ground and Certain Excited States of Neutral and Ionized Atoms, $Z \leq 54$.” *Atomic Data and Nuclear Data Tables* 14 (1974): 177.

Chapter 11

Page 278: Photo courtesy of Pacific Northwest National Laboratory. © Liang et al., Electrochemical Society Proceedings Volume 2001-5. 125–133. Reproduced by permission of the Electrochemical Society, Inc. Page 279: Adapted from L. Qiao et al., *Journal of Materials Chemistry C*, 1 (2013): 4527–4535.

Chapter 12

Page 293: Based on Wind, *Journal of Chemical Physics* 42 (1965): 2371. **Page 301:** From calculations by E. R. Davidson, unpublished. **Page 307:** Adapted from Banna et al., *Journal of Chemical Physics*, 61 (1974): 4780–4786. **Page 313:** Warren Hehre.

Chapter 13

Page 332: Reprinted with permission from Molecules on Insulating Films: Scanning-Tunneling Microscopy Imaging of Individual Molecular Orbitals as follows: Repp, Jascha; Meyer, Gerhard; Stojkovic, Sladjana M.; Gourdon, Andre; Joachim, Christian, *Physical Review Letters* (2005), 94(2), 026803. Copyright 2011 by the American Physical Society.

Chapter 14

Page 357: Adapted from B. DeKoven, K. Fung, D. Levy, L. Hofflad and K. Spears, *Journal of Chemical Physics* 74 (1981): 4755–4764. **Page 363:** Adapted from Norman Dovichi, Development of DNA Sequencer. *Science* 285 (1999): 1016.

Page 364: Adapted from C. R. Brundle and D. W. Turner. High resolution molecular photoelectron spectroscopy II. Water and deuterium oxide, *Proceedings of the Royal Society A*. 307 (1968): 27–36. **Page 368:** Dr. Taekjip Ha. **Page 370:** Adapted from data from J. Brahms et al., Application of a New Modulation Method for Linear Dichroism Studies of Oriented Biopolymers in the Vacuum Ultraviolet. *Proceedings of the National Academy of Sciences USA* 60 (1968): 1130. **Page 370:** Adapted from John T. Pelton, Secondary Considerations, *Science* 291: 2175–2176, March 16, 2001. Copyright © 2001, The American Association for the Advancement of Science. Reprinted with permission from AAAS. **Page 371:** Adapted from W. Sean Davidson, et al., Stabilization of a-Synuclein Secondary Structure upon Binding to Synthetic Membranes, *The Journal of Biological Chemistry*, 273 (16): 9443–9449, April 1998.

Chapter 17

Page 486: Based on J. Keeler, Understanding NMR Spectroscopy, Chapter 3, Figs. 3.4 and 3.7. **Page 488:** Adapted from: <http://mriquestions.com/what-is-t2.html>. **Page 498:** Adapted from Malcolm Levitt's 'Spin Dynamics: basics of nuclear magnetic resonance'; 2nd ed. (2000) and Ray H. Hashemi, William G. Bradley, Christopher J. Lisanti text book 'MRI The Basics', 3rd ed. (2010). **Page 499:** Published by permission of Rachel Klevit, University of Washington. **Page 499:** Adapted from <https://www.chemie.uni-hamburg.de/nmr/insensitive/tutorial/en.lproj>. **Page 501:** Based on Hore, P. J. *Nuclear Magnetic Resonance*, Oxford Chemistry Primers. **Page 502:** Based on Hore, P. J. *Nuclear Magnetic Resonance*, Oxford Chemistry Primers. **Page 503:** Based on D. D. Laws et al., *Ange. Chemi. Int. Ed.* 41 (2002): 3096–3129. **Page 504:** Based on S. Matsuoka et al., *Chem. Commun.*, (2009): 5664–5675. **Page 504:** Published by permission of Gary Drobny, University of Washington. **Page 505:** Based on van Bentum et al., *J. of Mag. Res.* 264 (2016): 59–67. **Page 508:** M. Kulyk/Science Source.

Index

Note: An *f* following a page number indicates a figure. A *t* indicates a table.

Symbols

- Δ (molecular term symbols), 350–352, 352*t*
- Λ (molecular term symbols), 350–352, 352*t*
- Σ (molecular term symbols), 350–352, 352*t*
- assigning + and – in diatomic molecules, 371–372, 371*f*, 372*f*
- $\sigma\text{-}\sigma^*$ transitions chromophores, 358, 358*f*, 359*f*
- Φ (molecular term symbols), 350–352, 352*t*

A

- Absorption, 174–175, 174*f*
 - Beer’s law, 357–358, 357*ft*, 358*f*, 359*f*
 - chromophores, 357–358, 357*ft*, 358*f*, 359*f*
 - integral absorption coefficient, 357–358, 357*ft*, 358*f*, 359*f*
 - linearly polarized light, 369–371, 369*f*, 370*f*, 371*f*
 - molar extinction coefficient, 357–358, 357*ft*, 358*f*, 359*f*
 - singlet-singlet transitions, 360–361
- UV-visible light absorption, polyatomic molecules, 356–358, 357*ft*, 358*f*, 359*f*
- Absorption spectroscopy. *See* Infrared absorption spectroscopy; Spectroscopy
- Absorption spectrum, 171–172, 172*f*.
 - See also* Spectroscopy
- Acceleration
 - angular acceleration (α), 148–149, 149*f*
 - harmonic oscillator, classic, 144–147, 144*f*, 146*f*
 - rigid rotor, 148–149, 149*f*
- Acceptor molecule, 366–367, 367*f*, 368*f*
- Activation energy, 109, 110*f*, 381–382, 381*f*, 382*f*
- computational chemistry, 409–412, 410*t*, 411*t*, 412*f*

- AES (Auger electron spectroscopy), 277–279, 277*f*, 278*f*, 279*f*
- AFM (atomic force microscope), 104–109, 105*f*, 106*f*, 108*f*, 109*f*
- Amplification threshold, 275–276, 275*f*, 276*f*
- Amplitude, waves, 50–51, 51*f*
 - harmonic oscillator, quantum-mechanical, 152–154, 153*f*
- Andrew, E. Raymond, 504
- Angular acceleration (α), 148–149, 149*f*
- Angular frequency, 50
 - harmonic oscillator, classic, 146–147, 146*f*
- Angular momentum, 149. *See also L*(orbital angular momentum); Orbital angular momentum; S (spin angular momentum); Spin angular momentum
 - configuration energy and, 259–266, 259*f*, 260*f*, 262*f*, 263*t*, 264*t*
 - electron spin, 235–236
 - good quantum numbers, 257–259, 258*f*, 259*f*
 - intrinsic nuclear angular momentum, 467–469, 468*f*, 469*f*
 - quantization of, 159–161
 - quantum-mechanical rotation, 157, 185
 - spatial quantization, 164–165, 165*f*
 - spin-orbit coupling, 266–267, 266*f*
 - total angular momentum, 266–267, 266*f*
 - vector model of angular momentum, 165, 165*f*
- Angular motion, rigid rotor, 147–149, 148*f*, 149*f*
- Angular velocity (ω), 148–149, 149*f*
- Anharmonic potential, 176–177, 177*f*
- Anisotropic magnetic interactions, 476, 476*f*
- Antiaromatic molecules, 339–340
- Antibonding molecular orbitals, 293–294, 293*f*, 294*f*, 298, 300
 - ψ_g and ψ_u wave functions for hydrogen, 294–297, 294*f*, 295*f*, 296*f*
- Antiparallel spin, 259–260, 259*f*, 260*f*
- Anti-Stokes frequency, 195–196, 195*f*
- Anti-structure
 - conformational energy differences, 404–405, 405*f*
 - potential energy surface computations, 378–382, 378*f*, 379*f*, 381*ft*, 382*f*
- Antisymmetric wave function, 236–238, 291
- AO. *See* Atomic orbitals (AOs)
- Aromatic molecules, 334–335
 - Hückel model, 334–340, 336*f*, 338*f*, 339*f*
 - resonance stabilization energy, 339–340, 339*f*
- Associative, 441
- Atom. *See also* Hydrogen (H) atom
 - atomic size and orbital energy, 244–245, 244*f*, 245
 - Bohr model of, 29–32, 29*f*, 30*f*, 31*f*, 32*f*
 - electron affinity, 246–247, 246*f*
 - electron configuration, 237–238
 - electron indistinguishability, 236–238
 - electron spin, 235–236
 - good quantum numbers, 257–259, 258*f*, 259*f*
 - many-electron atoms, overview, 232–235, 234*f*
 - Pauli principle, 237
 - periodic table trends, 247–249, 248*f*, 249*f*
 - shell model, 209, 224–225, 224*f*
- Atomic absorption spectroscopy, 269–272, 272*f*
- Atomic charge calculations, 407–409, 407*f*
- Atomic emission spectroscopy, 269–272, 272*f*
- Atomic force microscope (AFM), 104–109, 105*f*, 106*f*, 108*f*, 109*f*
- Atomic orbitals (AOs), 287. *See also* Hydrogen (H) atom; Orbitals
 - heteronuclear diatomic molecules, 304–307, 304*f*, 306*f*, 307*f*
 - hybrid orbitals, 318–321, 319*f*, 321*t*
 - hydrogen molecule, 289–291, 289*f*, 290*f*

- Atomic orbitals (*continued*)
 molecular orbital energy diagram, 288–289, 289f
 molecular orbitals, generation of, 285–289, 288f, 289f
 projection operator method, 461–464, 461t, 462ft, 464f
 solids, energy spectrum and band gaps, 340–341, 340f, 341f
s–p mixing, diatomic molecules, 298–299, 298t, 299f
 spherical harmonic functions, 161–164, 163f, 164f
 symmetry elements, operations, and point groups, 439–441, 440f
 symmetry-adapted MOs, 454–456, 454f, 455f, 456f
- Atomic spectra, 29–32, 29f, 30f, 31f, 32f
- Atomic spectroscopy, 267–269, 269f
 absorption spectroscopy, 269–272, 272f
 analytical techniques based on, 269–272, 272f
 Auger electron spectroscopy, 277–279, 277f, 278f, 279f
 Doppler effect, 272–273, 272f
 emission spectroscopy, 269–272, 272f
 Grotrian diagram, 269, 269f
 helium-neon laser, 273–276, 274f, 275f, 276f
 X-ray photoelectron spectroscopy, 277–279, 277f, 278f, 279f
- Aufbau principle, 246–247, 246ft
- Auger electron spectroscopy (AES), 277–279, 277f, 278f, 279f
- Average value (postulate 4) of measurement, 70–73, 71f, 72f, 73f, 87–89
- Axial conformation, 405–406, 406f
- B**
- Balmer series, 268
- Band gaps, 99f, 100, 100f, 340–341, 340f, 341f
- Band structure, 99–100, 99f, 100f, 342, 342f
- Barrier width, tunneling through, 103–104, 103f, 104f
- Bases for representations, 448–450, 449f
 projection operator method, 461–464, 461t, 462ft, 464f
- Basis functions, 241, 450
- Beer–Lambert Law, 180–181
- Beer's Law, 357–358, 357ft, 358f, 359f
- Belongs to a representation, 449–450, 449f
- Bent's rule, 321–324, 322f, 324f
- Binding energy. *See also* Bond energy
 chemical shift, 278–279, 279f
 diatomic molecules, 294, 307, 307f
 excited state molecules, 353
 work function, 23
- Binnig, Gerd, 104
- Bioanalytic methods, fluorescence, 112–113, 112f, 113f
- Biomolecules
 DNA sequencing, fluorescence spectroscopy, 362–363, 363f
 Fluorescent Resonance Energy Transfer (FRET), 366–367, 367f, 368f
 linear and circular dichroism, 368–371, 369f, 370f, 371f
 single-molecule spectroscopy, 365–366, 366f
 two-dimensional NMR, 498–503, 499f, 500f, 501f, 502f
- Bit, 134–135
- Blackbody radiation, 21–22, 21f, 22f
- Blackbody spectral density function, 174–175, 174f
- Bloch equations, 492
- Bohr, Niels, 30, 123–124, 124f
- Bohr model of atoms, 29–32, 29f, 30f, 31f, 32f, 123–124, 124f
- Bohr radius, 211
- Boltzmann constant, 46–47
- Boltzmann distribution, 46–49, 49f
- Bond angles
 antiaromatic molecules, 339–340
- Bent's rule, 321–324, 322f, 324f
- diatomic molecules, electronic state transitions, 353–354, 353f
- equilibrium geometries, 387–388, 387t, 388t
- equilibrium structures, 400–401, 401t
- hybridization and bonding descriptions, 324–325, 324f, 325f
- Lewis structures, 315–316, 316f
- localized vs. delocalized bonding models, 329–332, 330f, 331f, 332f
- potential energy surface computations, 378–382, 378f, 379f, 381ft, 382f
- qualitative molecular orbital theory, 326–328, 326f, 327f, 328f
- VSEPR (valence shell electron pair repulsion) model, 316–318, 317f
- Walsh correlation diagram, 327–328, 328f
- Bond dissociation reactions, 402–403, 402t, 403t
- Bond energy, 176, 286. *See also* Binding energy
 bonding and antibonding molecular orbitals, 293–294, 293f, 294f
 C–C single bonds, 321
 diatomic molecules, electronic state transitions, 353–354, 353f
 diatomic molecules, molecular constant values, 178, 178t
 electronic spectroscopy, uses of, 355–356, 355f, 356f
 molecular orbital theory, 302–304, 302f
 molecular orbitals generation of, 285–289, 288f, 289f
 Morse potential calculations, 177–178, 177f
- Bond length
 molecular orbital theory, 302–304, 302f
 transition-state geometries, 409–412, 410t, 411t, 412f
- Bond order, 303
 molecular orbital theory, 302–304, 302f
- Bond rotation alternatives, 406, 406f
- Bonding molecular orbitals, 293–294, 293f, 294f, 300
 ψ_g and ψ_u wave functions for hydrogen, 294–297, 294f, 295f, 296f
- Born–Oppenheimer approximation, 286, 382–383
 electronic transitions, vibrational fine structure, 354–356, 355f, 356f
 hydrogen molecule, 289–290, 289f, 290f
- Boron, semiconductors, 342, 342f
- Boundary conditions, 79
 quantum-mechanical rotation, 156–157, 156f
- Brackett series, 268
- C**
- C_{2v} point group and water, 443–447, 444f, 447ft
- molecular orbital representations, 454–456, 454f, 455f, 456f
- Capillary electrophoresis, 362–363, 363f

- Carbon bonds
activation energies, organic reactions, 409–412, 410*t*, 411*t*, 412*f*
antiaromatic molecules, 339–340
aromatic molecules, 334–335
bond types, orbital hybridization and, 321, 321*t*
equilibrium bond distances, 399–400, 400*t*
Hückel model, 334–340, 336*f*, 338*f*, 339*f*
hybridization, bonding descriptions and, 324–325, 324*f*, 325*f*
organic compounds, transition-state geometries, 409–412, 410*t*, 411*t*, 412*f*
projection operator method, molecular symmetry, 461–464, 461*t*, 462*f*, 464*f*
resonance stabilization energy, 339–340, 339*f*
- Carbon (C), chemical shift, 474–475, 474*f*, 475*f*
- Carbon dioxide
greenhouse gases, 179–180, 180*f*
vibrational spectra data, 182–184, 182*f*, 183*f*, 184*f*
- Catalysts, tunneling and chemical reactions, 109, 110*f*
- Cavity ringdown spectroscopy, 181
- Center of symmetry, 441–443, 442*f*, 443*t*
- Center-of-mass coordinates, 144, 144*f*
harmonic oscillator, classic, 144–147, 144*f*, 146*f*
rigid rotor, 147–148, 148*f*
- Centrifugal potential, 211, 211*f*
- Centripetal acceleration, 148–149, 149*f*
- Character table, 448–450, 449*f*
 C_{2v} representations and molecular orbitals of water, 454–456, 454*f*, 455*f*, 456*f*
projection operator method, 461–464, 461*t*, 462*f*, 464*f*
- Characters, 450
 C_{2v} representations and molecular orbitals of water, 454–456
dimension of representation, 452–453
projection operator method, 461–464, 461*t*, 462*f*, 464*f*
- Charge distribution
heteronuclear diatomic molecules, 304–307, 304*f*, 306*f*, 307*f*
- molecular electrostatic potential, 307–308, 308*f*
molecular orbitals, generation of, 285–289, 288*f*, 289*f*
- Chemical bond. *See also* Bond angles; Bond energy
equilibrium bond distances, 399–400, 400*t*
equilibrium geometries, 387–388, 387*t*, 388*t*
homolytic bond dissociation, 385–386, 385*t*, 386*t*
molecular bond, graphical model, 415–416, 415*f*, 416*f*
reaction energy calculations, 402–403, 402*t*, 403*t*
vibrational frequency calculations, 388, 388*t*
- Chemical bond, diatomic molecules
antibonding orbital designation, 298
bond order, energy, and length, 302–304, 302*f*
bonding and antibonding molecular orbitals, 293–294, 293*f*, 294*f*
energy of molecular wave function, g and u symmetry, 291–294, 293*f*, 294*f*
generating molecular orbitals, 285–289, 288*f*, 289*f*
heteronuclear molecules, 304–307, 304*f*, 306*f*, 307*f*
homonuclear molecules, 297–299, 297*f*, 298*f*, 299*f*
hydrogen molecule, 289–291, 289*f*, 290*f*
LCAO-MO model, 287
many-electron molecules, 299–302, 300*f*, 301*f*
molecular electrostatic potential, 307–308, 308*f*
variational parameter, 290–291
 ψ_g and ψ_u wave functions for hydrogen, 294–297, 294*f*, 295*f*, 296*f*
- Chemical bond, polyatomic molecules
antiaromatic molecules, 339–340
aromatic molecules, 334–335
Bent's rule, 321–324, 322*f*, 324*f*
computational modeling, 332–334, 332*f*, 333*f*, 334*f*
conjugated molecules, 334–335
Hückel model, 334–340, 336*f*, 338*f*, 339*f*
- hybrid orbitals for nonequivalent ligands, 321–324, 322*f*, 324*f*
hybridization, bonding descriptions and, 324–325, 324*f*, 325*f*
hybridization, valence bond theory, 318–321, 319*f*, 321*t*
Lewis structures, 315–316, 316*f*
localized vs. delocalized bonding models, 329–332, 330*f*, 331*f*, 332*f*
molecular orbital theory, 326–328, 326*f*, 327*f*, 328*f*
resonance stabilization energy, 339–340, 339*f*
solids, energy spectrum and band gaps, 340–341, 340*f*, 341*f*
Walsh correlation diagram, 327–328, 328*f*
- Chemical equivalency, 476
- Chemical reactions
rate, potential energy surfaces and, 381–382, 381*f*, 382*f*
rate, transition-state geometries and activation energy, 409–412, 410*t*, 411*t*, 412*f*
reaction coordinate, 378–382, 378*f*, 379*f*, 381*f*, 382*f*
reaction coordinate diagrams, 378–382, 378*f*, 379*f*, 381*f*, 382*f*
reaction energy calculations, 402–403, 402*t*, 403*t*
tunneling and, 109, 110*f*
- Chemical shift, 278–279, 279*f*, 473–476, 473*f*, 474*f*, 475*f*, 476*f*
- Chemical shift imaging, 508, 508*f*
- Chemically equivalent nuclei, 481, 481*f*
- Chemically induced nuclear polarization (CIDNP), 507
- Chromophore, 357–358, 357*f*, 358*f*, 359*f*
- CID (Configuration Interaction Double) method, 391–392, 391*f*, 392*f*
- CIDNP (chemically induced nuclear polarization), 507
- Circular dichroism spectroscopy, 369–371, 369*f*, 370*f*, 371*f*
- CIS (Configuration Interaction Single) method, 391–392, 391*f*, 392*f*
- Classic waves, 49–54, 50*f*, 51*f*, 52*f*
- Classical nondispersive wave equations, 49–54, 50*f*, 51*f*, 52*f*
- Classically forbidden region, 96

Clebsch–Gordan series, 261–264, 263*t*, 264*t*
 Coherent photon emission, 175
 Coherent photon source, 175, 273
 helium-neon laser, 273–276, 274*f*, 275*f*, 276*f*
 Commutation relations, 119–121
 Commutator, 120–121, 123
 Commute, 120–121
 Completeness, 59–60, 60*f*
 Complex conjugate, 58–59
 Computational chemistry, 377–378
 atomic charge, 407–409, 407*f*
 bond rotation alternatives, 406, 406*f*
 bonds in a molecule, graphical model, 415–416, 415*f*, 416*f*
 configuration interaction models, 391–392, 391*f*, 392*f*
 conformational energy differences, 404–405, 405*f*
 contracted functions, 396
 density functional models, 393–395, 395*f*
 diffuse functions, 398, 398*f*
 dipole moments, 388–389, 388*t*, 406–407, 407*f*
 double-electron promotions, 391–392, 391*f*, 392*f*
 electron density, graphical models, 414–415, 415*f*
 electrostatic potential, 409
 electrostatic potential, graphical model, 416–417, 417*f*
 electrostatic potential map, 418–419, 418*f*, 419*f*
 energies, enthalpies, Gibbs energies, 403–404
 equilibrium bond distances, 399–400, 400*t*
 equilibrium geometries, 387–388, 387*t*, 388*t*
 equilibrium structures, 400–401, 401*t*
 frozen core approximation, 391–392, 391*f*, 392*f*
 Gaussian basis sets, 395–398, 396*f*, 397*f*, 398*f*
 Hartree–Fock, Schrödinger equation and, 382–384
 Hartree–Fock models, properties of limiting, 384–389, 385*t*, 386*t*, 387*t*, 388*t*

Hartree–Fock theory, moving beyond, 390
 LCAO (linear combination of atomic orbitals) approximations, 383
 lone pair visualization, graphical model, 417–418, 417*f*, 418*f*
 minimal basis sets, 396–397, 397*f*
 molecular orbitals, graphical models, 412–413, 413*f*
 molecular shape, determining, 405–406, 406*f*
 molecular size, graphical model, 416, 416*f*
 Møller–Plesset models, 392–393
 Mulliken population analysis, 408–409
 orbital symmetry control, graphical models, 413, 413*f*, 414*f*
 polarization basis sets, 397–398, 398*f*
 potential energy surfaces, 378–382, 378*f*, 379*f*, 381*f*, 382*f*
 reaction energies, 385–386, 385*t*, 386*t*, 402–403, 402*t*, 403*t*
 Roothaan–Hall equations, 384
 single-electron promotions, 391–392, 391*f*, 392*f*
 split-valence basis set, 397, 397*f*
 STO-3G basis set, 396–397, 397*f*
 theoretical model selection, overview of, 398–399
 theoretical models and theoretical model chemistry, 389–390, 389*f*
 transition-state geometries and activation energy, 409–412, 410*t*, 411*t*, 412*f*
 vibrational frequencies, 388, 388*t*
 Computational models, molecular structure, 332–334, 332*f*, 333*f*, 334*f*
 Conduction band, 99–100, 99*f*, 100*f*
 Conductors, 98–100, 99*f*, 100*f*
 semiconductors, 341–342, 341*f*, 342*f*
 Configuration, 237–238, 259, 259*t*
 degeneracy of term, 261
 Hund’s rules, 265–266
 molecular configuration, 299–302, 300*f*, 301*f*
 multiplicity, 261
 orbital and spin angular momentum, 259–266, 259*f*, 260*f*, 262*f*, 263*t*, 264*t*
 paired and unpaired electrons, 260, 260*f*
 parallel and antiparallel spin, 259–260, 259*f*, 260*f*
 singlet and triplet states, 260, 260*f*
 spin-orbit coupling and levels, 266–267, 266*f*
 term generation and assignment, 261–264, 263*t*, 264*t*
 term symbol, 261
 Configuration Interaction Double (CID) method, 391–392, 391*f*, 392*f*
 Configuration interaction models, 391–392, 391*f*, 392*f*
 Configuration Interaction Single (CIS) method, 391–392, 391*f*, 392*f*
 Conformational energy differences, 404–405, 405*f*
 Conformers, 401, 401*t*
 energy differences, 404–405, 405*f*
 molecular shape, determining, 405–406, 406*f*
 Conjugated molecules, 334
 Hückel model, 334–340, 336*f*, 338*f*, 339*f*
 Constructive interference, 51
 Continuous energy spectrum, 46–49, 49*f*, 146
 free particles, 78
 Continuous function, 68
 Contracted functions, 396
 Core electrons, 96–97, 97*f*
 Correlated models, 398–399
 Correlation energy, 247
 Correlation spectroscopy (COSY), 499–503, 499*f*, 500*f*, 501*f*, 502*f*
 Correspondence principle, 81–83, 82*f*
 Coulomb integral, 335
 Coulomb potential, 211, 211*f*
 shell model of atom, 224–225, 224*f*
 Coupling factors, 506–507
 Cross effect, 507
 Cross relaxation, 490, 490*f*, 506–507

D

d orbital. *See also* Configuration; Molecular orbitals (MOs); Terms Aufbau principle, 246–247, 246*f*
 Hartree–Fock self-consistent field model, 241–247, 241*f*, 242*f*, 243*f*, 244*f*, 245*t*, 246*f*
 periodic table trends, Hartree–Fock and, 247–249, 248*f*, 249*f*

- quantization of angular momentum, 159–161
- radial probability distribution function, 219–223, 220*f*, 223*f*
- Schrödinger equation, hydrogen atom, 217–219, 217*f*, 218*f*, 219*f*
- shell model, validity of, 224–225, 224*f*
- spherical harmonic functions, 161–164, 163*f*, 164*f*
- Data encryption, 135
- Davisson, Clinton, 25
- de Broglie, Louis, 24
- de Broglie relation, 24–25, 25*f*
- Decay, free induction, 494
- Decay length, 103–104, 103*f*, 104*f*
- Degeneracy, 47, 84
- benzene molecular orbitals, 337–338, 338*f*
 - Clebsch–Gordan series, 261–265, 263*t*, 264*t*
 - configurations, terms, levels, and states, 259*f*
 - diatomic molecules, 371
 - energy diagrams, 306*f*
 - energy-level spectrum calculations, 156, 159
 - hydrogen atom, 215
 - molecular configuration, 299–302, 300*f*, 301*f*
 - molecular symmetry and, 439, 461
 - population inversion, 273
 - rotational energy, 186
 - of term, 261
 - vibrational spectra, 182
 - vibrational transitions, 188
 - water molecule, 327
- X-ray photoelectron spectroscopy, 279
- Degenerate, defined, 84
- Delocalization, 97–98, 97*f*, 98*t*, 286
- Hückel model, 334–340, 336*f*, 338*f*, 339*f*
 - ψ_g and ψ_u wave functions for hydrogen, 295–297, 295*f*, 296*f*
- Delocalized bonding model, 326–328, 326*f*, 327*f*, 328*f*
- localized vs. delocalized bonding models, 329–332, 330*f*, 331*f*, 332*f*
- Density functional theory, 393–395, 395*f*
- Dephasing effect, 488, 488*f*
- Deshielding effect, 475–476, 476*f*
- Destructive interference, 51
- Determinants
- antisymmetric wave functions, 237–238
 - Hückel model, 335
 - localized vs. delocalized bonding models, 329–332, 330*f*, 331*f*, 332*f*
- Deterministic outcome, 72–73
- Diamagnetic response, 473–476, 473*f*, 474*f*, 475*f*, 476*f*
- Diamond, as insulator, 100
- Diatomc molecules
- antibonding orbital designation, 298
 - bond order, energy, and length, 302–304, 302*f*
 - bonding and antibonding molecular orbitals, 293–294, 293*f*, 294*f*
 - dipole moment calculations, 406–407, 407*f*
 - electronic state transitions, 353–354, 353*f*
 - electronic transitions, vibrational fine structure, 354–356, 355*f*, 356*f*
 - energy of molecular wave function, *g* and *u* symmetry, 291–294, 293*f*, 294*f*
 - heteronuclear molecules, 304–307, 304*f*, 306*f*, 307*f*
 - homonuclear molecules, 297–299, 297*f*, 298*f*, 299*f*
 - hydrogen molecule, 289–291, 289*f*, 290*f*
 - LCAO-MO model, 287
 - many-electron molecule structure, 299–302, 300*f*, 301*f*
 - molecular electrostatic potential, 307–308, 308*f*
 - molecular orbitals, generation of, 285–289, 288*f*, 289*f*
 - molecular term symbols, 350–352, 352*t*
 - variational parameter, 290–291
 - vibrational frequency, 380–381
 - ψ_g and ψ_u wave functions for hydrogen, 294–297, 294*f*, 295*f*, 296*f*
- Diffraction, 25
- Diffraction, double slit, 26–29, 27*f*, 28*f*
- Diffuse functions, 398, 398*f*
- Diffusion-controlled reactions, 382, 382*f*
- Dimension of representation, 450–454, 452*f*, 454*t*
- Dipolar coupling
- nuclear magnetic resonance (NMR) spectroscopy, 467
 - solid-state NMR, 503–504, 503*f*, 504*f*
- Dipolar spin-spin coupling, 484, 484*f*
- Dipole approximations, 179
- atomic spectroscopy, 267–269, 269*f*
 - heteronuclear diatomic molecules, 304–307, 304*f*, 306*f*, 307*f*
- Dipole moment. *See also* Transition dipole moment (μ^{fi})
- atomic charge calculations, 407–409, 407*f*
 - computational chemistry, 406–407, 407*f*
 - dipolar spin-spin coupling, 484, 484*f*
 - Hartree–Fock calculations, 388–389, 388*t*
 - permanent and dynamic, 173, 173*f*
 - polarizability, 194–196, 195*f*
- Dirac, Paul, 382
- Discrete energy spectrum, 46
- Dissociation energy, 385–386, 385*t*, 386*t*
- Distance, harmonic oscillator, classic, 144–147, 144*f*, 146*f*
- DNA (deoxyribonucleic acid) studies
- fluorescence spectroscopy, 362–363, 363*f*
- Fluorescent Resonance Energy Transfer (FRET), 367, 367*f*, 368*f*
- two-dimensional NMR, 498–503, 499*f*, 500*f*, 501*f*, 502*f*
- DNP (dynamic nuclear polarization), 505–507, 505*f*
- Donor molecule, 366–367, 367*f*, 368*f*
- Dopant, 342, 342*f*
- Doping, 342, 342*f*
- Doppler broadening, 273, 274–276, 275*f*
- Doppler effect, 272–273, 272*f*
- Doppler linewidth, 275–276, 275*f*
- Doppler shift, 272–273, 272*f*
- Double bonds
- aromatic molecules, 334–335
 - Bent’s rule, 321–324, 322*f*, 324*f*
 - conjugated molecules, 334
 - equilibrium bond differences, 399
 - homolytic bond dissociation, 386
 - hybridization, bond descriptions, 325
 - lone pairs, 417
- Double flip transition, 490

Double-electron promotions, 391–392, 391*f*, 392*f*
 Doublet state, 261
 Dynamic dipole moment, 173, 173*f*
 Dynamic nuclear polarization (DNP), 468, 505–507, 505*f*

E

Effective nuclear charge, 234–235
 ionization, 247
 shielding and, 245
 Effective potential, 211, 211*f*
 Eigenfunctions, 56–57. *See also*
 Schrödinger equation
 commutation, 120–121
 complete sets, 59–60, 60*f*
 H atom eigenfunctions, 213
 many-electron atoms, 232–235, 234*f*, 239–240
 orbital approximation, 234–235, 234*f*
 orthogonality of, 57–59
 spherical harmonic functions, 161–164, 163*f*, 164*f*
 spin–spin coupling, 478–479
 total energy, Schrödinger equation, 211–217, 212*f*, 217*f*
 total molecular energy, 287
 variational method, 239–240
 Eigenvalues, 56–57
 good quantum numbers, 257–259, 258*f*, 259*f*
 many-electron atoms, 232–235, 234*f*, 239–240
 total energy, Schrödinger equation, 211–217, 212*f*, 217*f*
 total molecular energy, 287
 variational method, 239–240
 Einstein, Albert, 23, 73, 132
 Electric field, electromagnetic spectrum, 173, 173*f*
 Electromagnetic spectrum, 171–172, 172*f*. *See also* Atomic spectroscopy; Rotational spectroscopy; Vibrational spectroscopy
 pi (π) electrons, 97–98, 97*f*, 98*t*
 spectroscopy, overview, 171–173, 172*f*, 173*f*
 Electron(s). *See also* Atomic spectroscopy; Hydrogen (H) atom
 atomic spectra and Bohr model of atom, 29–32, 29*f*, 30*f*, 31*f*, 32*f*

binding energy, work function and, 23
 Born–Oppenheimer approximation, 286, 382–383
 conductors, insulators, and semiconductors, 98–100, 99*f*, 100*f*
 configuration, 237–238, 259, 259*t*
 (See also Configuration)
 core electrons, 96–97, 97*f*
 delocalization and localization, 295–297, 295*f*, 296*f*
 delocalized bonding model, 326–328, 326*f*, 327*f*, 328*f*
 diffraction, double slit, 26–29, 27*f*, 28*f*
 effective nuclear charge, 234–235
 Hartree–Fock self-consistent field model, 241–247, 241*f*, 242*f*, 243*f*, 244*f*, 245*t*, 246*f*
 indistinguishability, 236–238
 Koopman’s theory, 246–247, 246*f*
 lone pairs, 316
 lone pairs, graphical models, 417–418, 417*f*, 418*f*
 magnetic moment, 122
 many-electron atoms, overview, 232–235, 234*f*
 mean free path, 277
 nonbonding electrons, 306–307, 306*f*, 307*f*
 paired and unpaired electrons, 260, 260*f*
 Pauli principle, 237
 periodic table trends, Hartree–Fock and, 247–249, 248*f*, 249*f*
 photoelectric effect, 22–24, 22*f*, 23*f*
 photon-assisted transitions, 174–175, 174*f*
 pi (π)-bonded network, 97–98, 97*f*, 98*t*
 radial probability distribution function, 219–223, 220*f*, 223*f*
 terms, 259, 259*t* (See also Terms)
 valence electrons, 96–97, 97*f*
 ψ_g and ψ_u wave functions for hydrogen, 294–297, 294*f*, 295*f*, 296*f*
 Electron affinity, 246–247, 246*f*
 Electron correlation, 234–235
 Electron density
 bond location, 415, 415*f*
 chemical shift, 475–476, 475*f*
 density functional theory, 393–395
 diatomic molecules, 299, 307, 308
 electrostatic potential, 308, 308*f*
 electrostatic potential maps, 418–419, 418*f*, 419*f*
 graphical model, 412, 414–415, 415*f*
 indistinguishability, 236
 molecular size and, 416, 416*f*
 Mulliken population analysis, 408
 polyatomic molecules, 318, 324, 325, 330
 probability density and, 295
 scanning tunneling microscope (STM), 109, 109*f*
 Electron density surface, 414–415, 415*f*
 Electron spin, 122, 235–236
 Electronegativity, 248–249, 248*f*, 249*f*
 Electron-electron repulsion term, 234–235, 234*f*
 Electronic charge. *See also* Electrostatic potential
 delocalization and localization of electrons, 295–297, 295*f*, 296*f*
 Electronic Schrödinger equation, 383
 Electronic spectroscopy
 Beer’s Law, 357–358, 357*f*, 358*f*, 359*f*
 chromophores, 357–358, 357*f*, 358*f*, 359*f*
 diatomic molecules, electronic state transitions, 353–354, 353*f*
 diatomic molecules, vibrational fine structure of transitions, 354–356, 355*f*, 356*f*
 energy of electronic transitions, 349–350
 fluorescence spectroscopy, 362–363, 363*f*
 Fluorescent Resonance Energy Transfer (FRET), 366–367, 367*f*, 368*f*
 Franck–Condon principle, 355–356, 355*f*, 356*f*
 integral absorption coefficient, 357–358, 357*f*, 358*f*, 359*f*
 internal conversion, 359, 360*f*
 intersystem crossing, 359, 360*f*
 intersystem crossing and phosphorescence, 361–362, 361*f*
 linear and circular dichroism, 368–371, 369*f*, 370*f*, 371*f*
 molar extinction coefficient, 357–358, 357*f*, 358*f*, 359*f*
 molecular term symbols, 350–352, 352*t*

- molecular term symbols, Σ terms + and – assignment, 371–372, 371*f*, 372*f*
- nonradiative transitions, 359, 360*f*
- polyatomic molecules, UV-visible light absorption, 356–358, 357*f*, 358*f*, 359*f*
- radiative transitions, 359, 360*f*
- resonance energy transfer, 367, 367*f*, 368*f*
- single-molecule spectroscopy, 365–366, 366*f*
- singlet-singlet transitions, absorption and fluorescence, 360–361
- UV photoelectron spectroscopy, 363–365, 364*f*
- Electronic state transitions. *See also* Electronic spectroscopy
- diatomic molecules, 353–354, 353*f*
- donor and acceptor molecules, 366–367, 367*f*, 368*f*
- Franck–Condon factor, 355–356, 355*f*, 356*f*
- Franck–Condon principle, 355–356, 355*f*, 356*f*
- integral absorption coefficient, 357–358, 357*f*, 358*f*, 359*f*
- internal conversion, 359, 360*f*
- intersystem crossing, 359, 360*f*
- intersystem crossing and phosphorescence, 361–362, 361*f*
- molar extinction coefficient, 357–358, 357*f*, 358*f*, 359*f*
- nonradiative transitions, 359, 360*f*
- radiative transitions, 359, 360*f*
- resonance energy transfer, 367, 367*f*, 368*f*
- singlet-singlet transitions, absorption and fluorescence, 360–361
- UV photoelectron spectroscopy, 363–365, 364*f*
- vibrational fine structure, 354–356, 355*f*, 356*f*
- Electrophoresis, 362–363, 363*f*
- Electrostatic potential, 409
- graphical model, 416–417, 417*f*
- map of, graphical models, 418–419, 418*f*, 419*f*
- molecular potential, 307–308, 308*f*
- molecular potential, computational modeling of, 332–334, 332*f*, 333*f*, 334*f*
- Emission spectrum, 171–172, 172*f*. *See also* Spectroscopy
- Energy
- activation energy, 109, 110*f*
 - blackbody radiation, 21–22
 - computational chemistry, 403–404
 - computational modeling, 332–334, 332*f*, 333*f*, 334*f*
 - continuous energy spectrum, 46
 - correlation energy, 247
 - degeneracy, 47
 - discrete energy spectrum, 46
 - ground state, 98
 - photoelectric effect, 22–24, 22*f*, 23*f*
 - solids, energy spectrum and band gaps, 340–341, 340*f*, 341*f*
 - variational theorem, 239–240
 - zero point, 211
- Energy band, 99–100, 99*f*, 100*f*
- Energy gap, 99*f*, 100, 100*f*
- Energy levels, defined, 48–49, 49*f*
- Energy spectrum, 180–184, 181*f*, 182*f*, 183*f*, 184*f*
- Ensemble, 365
- Entangled states, 132–135, 133*f*
- Enthalpy, computational chemistry, 403–404
- Enzymes
- molecular electrostatic potential, 308
 - single-molecule spectroscopy, 365–366, 366*f*
- Equatorial conformation, 405–406, 406*f*
- Equilibrium, photon-assisted transitions and, 174–175, 174*f*
- Equilibrium bond distance calculations, 399–400, 400*t*
- Equilibrium geometries, 387–388, 387*t*, 388*t*
- Equilibrium structures, 400–401, 401*t*
- Ethane, hybridization bonding description, 324–325, 324*f*, 325*f*
- Ethene
- hybrid orbitals, 318–321, 319*f*, 321*t*
 - hybridization, bonding description and, 324–325, 324*f*, 325*f*
- Ethyne, hybrid orbitals, 318–321, 319*f*, 321*t*
- Euler relation, 53
- Excited state transitions, types of, 359, 360*f*. *See also* Electronic state transitions
- Exothermic reactions, 381, 381*f*
- Expansion coefficient, 71
- Expectation value, 70–73, 71*f*, 72*f*, 73*f*
- particles in a box, 87–89
- External magnetic field, chemical shift, 473–476, 473*f*, 474*f*, 475*f*, 476*f*
- F**
- FID (free induction decay), 494
- two-dimensional NMR, 499–503, 499*f*, 500*f*, 501*f*, 502*f*
- Finite depth box, 95–96, 95*f*, 96*f*
- Flip transitions, 490
- Flop transition, 490
- Fluorescence, 112, 112*f*, 360–361, 362
- single-molecule spectroscopy, 365–366, 366*f*
- Fluorescence spectroscopy, 362–363, 363*f*
- single-molecule spectroscopy, 365–366, 366*f*
- Fluorescent Resonance Energy Transfer (FRET), 366–367, 367*f*, 368*f*
- Force
- harmonic oscillator, classic, 144–147, 144*f*, 146*f*
 - rigid rotor, 148–149, 149*f*
- Force constant (*k*), 144
- rotational-vibrational spectrum effects, 187, 187*f*
- Forms a basis, 449–450, 449*f*
- Fourier sine and cosine series, 59–60, 60*f*
- Fourier transform (FT), 192–194, 193*f*, 194*f*
- Fourier transform (FT)-NMR, 495–496
- pulsed NMR spectroscopy, 491–498, 493*f*, 494*f*, 495*f*, 497*f*, 498*f*
- Fourier transform infrared spectroscopy (FTIR), 190–194, 191*f*, 192*f*, 193*f*, 194*f*
- Fourier transform spectroscopy, 468
- Franck–Condon factor, 355–356, 355*f*, 356*f*
- Franck–Condon principle, 355–356, 355*f*, 356*f*
- Free induction decay (FID), 494
- two-dimensional NMR, 499–503, 499*f*, 500*f*, 501*f*, 502*f*
- Free particles, 77–78

Frequency

angular frequency, 50, 146–147, 146*f*
 Fourier transform, 192–194, 193*f*, 194*f*
 harmonic oscillator, classic, 145–147,
 146*f*
 harmonic oscillator, quantum-
 mechanical, 151
 helium-neon lasers, 275–276, 275*f*,
 276*f*
 interferogram, 191–192, 191*f*, 192*f*
 Larmor frequency, 470–471
 Michelson interferometer, 190–192,
 191*f*, 192*f*
 molar absorption coefficient, 181–182,
 182*t*
 normal mode frequencies, 456–460,
 456*f*, 457*f*
 photoelectric effect, 22–24, 22*f*, 23*f*
 potential energy surfaces, 380–381
 Rayleigh, Stokes, and anti-Stokes
 frequencies, 195–196, 195*f*
 spectral density, 21–22, 21*f*, 22*f*
 spectroscopy, transition rates and
 frequency, 196–200, 199*f*, 200*f*
 wave function, 50

Frequency of oscillation (ν), defined, 151

FRET (Fluorescent Resonance Energy Transfer), 366–367, 367*f*, 368*f*

Frontier molecular orbitals, 413, 413*f*,
 414*f*

Frozen core approximation, 391–392,
 391*f*, 392*f*

Frozen orbital approximation, 364–365,
 364*f*

FTIR (Fourier transform infrared spectroscopy), 190–194, 191*f*, 192*f*,
 193*f*, 194*f*

Full configuration interaction, 391–392,
 391*f*, 392*f*

Fullerenes, 340

G

g symmetry, 290–291
 homonuclear diatomic molecules,
 297–299, 297*f*, 298*ft*, 299*f*
 molecular term symbols, 350–352, 352*t*
 molecular wave function energy,
 291–294, 293*f*, 294*f*
 Gamma rays, electromagnetic spectrum,
 172*ft*

Gauche structure

conformational energy differences,
 404–405, 405*f*
 potential energy surface computations,
 378–382, 378*f*, 379*f*, 381*ft*, 382*f*
 Gaussian basis sets, 395–398, 396*f*,
 397*f*, 398*f*
 contracted functions, 396
 diffuse functions, 398, 398*f*
 Hartree–Fock calculations, 241–243,
 242*f*
 minimal basis sets, 396–397, 397*f*
 polarization basis sets, 397–398, 398*f*
 split-valence basis set, 397, 397*f*
 STO-3G basis set, 396–397, 397*f*
 Gaussian functions, 396, 396*f*
 Gene sequencing, fluorescence
 spectroscopy, 362–363, 363*f*
 Germer, Lester, 25
 Gibbs energy, computational chemistry,
 403–404
 Global warming, 179–180, 180*f*
 Good quantum numbers, 257–259,
 258*f*, 259*f*. *See also L* (orbital
 angular momentum); *S* (spin angular
 momentum)
 spin-orbit coupling, 266–267, 266*f*

Graphical models

- bonds in a molecule, 415–416, 415*f*,
 416*f*
- electron density, 414–415, 415*f*
- electrostatic potential, 416–417, 417*f*
- electrostatic potential maps, 418–419,
 418*f*, 419*f*
- lone pair visualization, 417–418, 417*f*,
 418*f*
- molecular orbitals, 412–413, 413*f*
- molecular size, 416, 416*f*
- orbital symmetry control of reactions,
 413, 413*f*, 414*f*
- Greenhouse gases, 179–180, 180*f*
- Grotian diagram, 269, 269*f*
- Ground state, 98
- diatomic molecules, electronic state
 transitions, 353–354, 353*f*
- excited state transitions, types of, 359,
 360*f*
- Hartree–Fock self-consistent field
 model, 241–247, 241*f*, 242*f*, 243*ft*,
 244*f*, 245*t*, 246*ft*
- helium, electron configuration,
 237–238

molecular hydrogen, 299–302, 300*f*,
 301*f*

molecular term symbols, 351–352, 352*t*
 periodic table trends, Hartree–Fock
 and, 247–249, 248*f*, 249*f*

Group, 441. *See also Point groups*

Group frequencies, 175

Group theory, 440

assigning molecules to point groups,
 441–443, 442*f*, 443*t*

C_{2v} point group and water, 443–447,
 444*f*, 447*ft*

C_{2v} representations and molecular
 orbitals of water, 454–456, 454*f*,
 455*f*, 456*f*

dimension of representation, 450–454,
 452*f*, 454*t*

elements, operations, and point
 groups, 439–441, 440*ft*

order of the group, 451

projection operator method, 461–464,
 461*t*, 462*ft*, 464*f*

representations, bases, and character
 table, 448–450, 449*f*

selection rules, infrared vs. Raman
 activity, 460–461

symmetry of normal modes of
 vibration, 456–460, 456*f*, 457*f*

Gyromagnetic ratio, 469, 492

Larmor frequency, 470–471

H

Hahn, Erwin, 496

Hahn echo, 496–498, 497*f*

Hamiltonian operators, 69, 382, 390

Hard pulse, 492

Harmonic oscillator. *See also Spherical*
 harmonic functions
 classical, 143–147, 144*f*, 146*f*
 quantum-mechanical, 149–154, 150*f*,
 153*f*

Harmonic potential, 176

Hartree–Fock approximation, 383–384

Hartree–Fock energy, 384

Hartree–Fock equations, 383–384

Hartree–Fock models, 384

correlation energy, 384–389, 385*t*,
 386*t*, 387*t*, 388*t*

dipole moments, 388–389, 388*t*

equilibrium geometries, 387–388,
 387*t*, 388*t*

- reaction energies, 385–386, 385*t*, 386*t*
vibrational frequencies, 388, 388*t*
- Hartree–Fock self-consistent field model, 239, 240–247, 241*f*, 242*f*, 243*f*, 244*f*, 245*t*, 246*f*
correlation energy, 247
effective nuclear charge, 245, 245*t*
electron-electron repulsion, 242–243
homonuclear diatomic molecules, 297–299, 297*f*, 298*f*, 299*f*
many-electron molecule structure, 299–302, 300*f*, 301*f*
radial distribution function, 243–245, 243*f*, 244*f*
Schrödinger equation and, 382–384
- Heisenberg uncertainty principle, 124–127, 125*f*
standard deviation and, 128–130, 130*f*
- Heisenberg, Werner, 32
- Helium (He) atom
electron indistinguishability, 236–238
electron spin, 235–236
- Hartree–Fock self-consistent field model, 241–247, 241*f*, 242*f*, 243*f*, 244*f*, 245*t*, 246*f*
many-electron atoms, overview, 232–235, 234*f*
- Helium-neon laser, 273–276, 274*f*, 275*f*, 276*f*
- Hermite polynomials, 150
- Hermitian operators, 69
- Hess, B., 339
- Hessian, 380
- Heterostructure, 110
- Holes, 264
- HOMO (highest energy occupied molecular orbital), 306–307, 306*f*, 307*f*, 331–332, 332*f*
graphical models, 413, 413*f*, 414*f*
- Homogeneous relaxation, 488, 488*f*
- Homolytic bond dissociation, 385–386, 385*t*, 386*t*, 402–403, 402*t*, 403*t*
- Homonuclear diatomic molecules, 297–299, 297*f*, 298*f*, 299*f*
- Hückel, Erich, 335
- Hückel model, 334–340, 336*f*, 338*f*, 339*f*
- Hückel rules, 338–340, 339*f*
- Human genome sequencing, spectroscopy and, 362–363, 363*f*
- Hund, Friedrich, 265
- Hund’s rules, 265–266
many-electron molecules, 301–302, 301*f*
- Huygen’s construction, 26
- Hybrid orbitals, 318–321, 319*f*, 321*t*
- Hybridization, 318–321, 319*f*, 321*t*
Bent’s rule, 321–324, 322*f*, 324*f*
bonding descriptions and, 324–325, 324*f*, 325*f*
carbon-hydrogen bonds, coupling constants, 481
localized vs. delocalized bonding models, 329–332, 330*f*, 331*f*, 332*f*
model shortcomings, 325
orbitals of nonequivalent ligands, 321–324, 322*f*, 324*f*
polarization functions, 398
- Hydrocarbons
bond distances, 399–400, 400*t*
chemical shift, 474–475, 474*f*, 475*f*
conformation energy, 405, 405*t*
Hückel model, 334–340, 336*f*, 338*f*, 339*f*
ring currents, 476, 476*f*
transition-state geometries and activation energy, 409–412, 410*t*, 411*t*, 412*f*
- Hydrogen (H) atom. *See also* Water bonding and antibonding molecular orbitals, 293–294, 293*f*, 294*f*
chemical shift, 474–475, 474*f*, 475*f*
diatomic molecules, chemical bond, 289–291, 289*f*, 290*f*
energy level diagram with transitions, 217, 217*f*
energy of molecular wave function, *g* and *u* symmetry, 291–294, 293*f*, 294*f*
good quantum numbers, 257–259, 258*f*, 259*f*
molecular orbitals, generation of, 285–289, 288*f*, 289*f*
orbitals, 213, 217–219, 217*f*, 218*f*, 219*f*
radial probability distribution function, 219–223, 220*f*, 223*f*
Rydberg constant for hydrogen, 217
- Schrödinger equation, formulation of, 209–210
- Schrödinger equation, solving of, 210–211, 211*f*
- shell model, validity of, 224–225, 224*f*
- total energy eigenvalues and eigenfunctions, 211–217, 212*f*, 217*f*
 ψ_g and ψ_u wave functions, 294–297, 294*f*, 295*f*, 296*f*
- Hyperpolarization schemes, 505–507, 505*f*
- I**
- Identity operator, 441
- Imaging, quantum dots and, 113, 113*f*
- Incoherent photon emission, 175
- Incoherent photon source, 175, 273
- Indistinguishability, 236–238
- Individual measurement, 71
particles in a box, 87–89
- Inelastic mean free path, 277
- Infrared absorption spectroscopy, 180–184, 181*f*, 182*f*, 183*f*, 184*f*
- Fourier transform infrared spectroscopy (FTIR), 190–194, 191*f*, 192*f*, 193*f*, 194*f*
- Michelson interferometer, 190–192, 191*f*, 192*f*
- molar absorption coefficient, 180–181
- monochromator, 181
- Raman spectroscopy, 194–196, 195*f*
selection rules, infrared vs. Raman activity, 460–461
- Infrared (IR) radiation
electromagnetic spectrum, 172*f*
photon energy, 187
- Inhomogeneous broadening, 200, 200*f*
- Inhomogeneous relaxation, 488, 488*f*
- Insulators, 98–100, 99*f*, 100*f*
semiconductors and, 341–342, 341*f*, 342*f*
- Integral absorption coefficient, 357–358, 357*f*, 358*f*, 359*f*
- Integrals
Coulomb integral, 335
overlap integral, 287, 288*f*, 335
resonance integral, 335
- Interference, waves, 51
- Interferogram, 191–192, 191*f*, 192*f*
- Internal conversions, 359, 360*f*
singlet-singlet transitions, 360–361
- Intersystem crossing, 359, 360*f*
phosphorescence and, 361–362, 361*f*
singlet-singlet transitions, 360–361
- Intrinsic electron spin, 235–236
- Intrinsic linewidth, 199–200, 200*f*

Intrinsic nuclear angular momentum, 467–469, 468*f*, 469*t*
 Inverse operator, 441
 Inversion center, 441–443, 442*f*, 443*t*
 Ionization
 atomic charge calculations, 407–409, 407*f*
 finite depth box, 95–96, 95*f*, 96*f*
 Hückel model, 335
 periodic table trends, Hartree–Fock and, 247–249, 248*f*, 249*f*
 photoionization, 364–365, 364*f*
 Ionization energy, 245–247, 246*f*
 periodic table trends, Hartree–Fock and, 247–249, 248*f*, 249*f*
 IR. *See* Infrared (IR) radiation
 Irreducible representations, 448–450, 449*f*, 458–460
 projection operator method, 461–464, 461*t*, 462*f*, 464*f*
 IS spin system, COSY and NOESY experiment, 499*f*, 500–503, 500*f*, 501*f*, 502*f*
 Isomers, rotational
 conformational energy differences, 404–405, 405*f*
 molecular shape, determining, 405–406, 406*f*
 transition state calculations, 412, 412*f*
 Isomers, structural
 reaction energies, 386, 386*t*, 402–403, 402*t*, 403*t*
 transition state calculations, 412, 412*f*

J

J (scalar)-coupling, NMR spectroscopy, 467, 479–480, 480*f*
 Jablonski diagram, 359, 360*f*

K

Karplus relation, 481
 Kinetic energy
 Born–Oppenheimer approximation, 286
 commutation relations, 120–121
 harmonic oscillator, classic, 144, 144*f*, 146–147, 146*f*
 hydrogen molecules, charge distribution and, 295*f*, 296–297, 296*f*
 photoelectric effect, 22–24, 22*f*, 23*f*
 photoionization, 364–365, 364*f*

quantum-mechanical harmonic oscillator, 152–154, 153*f*
 rigid rotor, classical, 147–149, 148*f*, 149*f*
 viral theorem, 214
 Kinetic product, 382, 382*f*
 Kinetically-controlled reactions, 382, 382*f*
 Kinetics, reaction
 potential energy surfaces and, 381–382, 381*f*, 382*f*
 transition-state geometries and activation energy, 409–412, 410*t*, 411*t*, 412*f*
 Kohn, Walter, 393
 Koopmans’ theorem, 246–247, 246*f*, 364–365, 364*f*

L

L (orbital angular momentum)
 atomic spectroscopy, overview, 267–269, 269*f*
 Clebsch–Gordan series, 261–264, 263*t*, 264*t*
 configuration energy, 259–266, 259*f*, 260*f*, 262*f*, 263*t*, 264*t*
 good quantum numbers, 257–259, 258*f*, 259*f*
 molecular term symbols, 350–352, 352*t*
 spin-orbit coupling and levels, 266–267, 266*f*
 Larmor frequency, 470–471, 486, 493
 Lasers, 273
 atomic spectroscopy, overview, 267–269, 269*f*
 fluorescence spectroscopy, 362–363, 363*f*
 helium-neon laser, 273–276, 274*f*, 275*f*, 276*f*
 single-molecule spectroscopy, 365–366, 366*f*
 Lasing transition, 275–276, 275*f*, 276*f*
 Late transition state, 415–416, 415*f*, 416*f*
 LCAO (linear combination of atomic orbitals) approximations, 383–384
 LCAO-MO model, 287
 hydrogen molecule, 289–291, 289*f*, 290*f*
 Leakage factors, 506–507

Levels, spin-orbit coupling, 266–267, 266*f*
 Lewis structures, 315–316, 316*f*
 Ligands
 hybrid orbitals for nonequivalent ligands, 321–324, 322*f*, 324*f*, 325
 VSEPR (valence shell electron pair repulsion) model, 316–318, 317*f*
 Light energy. *See also* Atomic spectroscopy; Spectroscopy
 atomic spectra and Bohr model of atom, 29–32, 29*f*, 30*f*, 31*f*, 32*f*
 de Broglie relation, 24–25, 25*f*
 diffraction, double slit, 26–29, 27*f*, 28*f*
 electromagnetic spectrum, 172*f*, 173, 173*f*
 fluorescence, 112, 112*f*
 photoelectric effect, 22–24, 22*f*, 23*f*
 pi (π) electrons, 97–98, 97*f*, 98*t*
 Linear combination of atomic orbitals (LCAO) approximations, 383–384
 Linear dichroism, 368–371, 369*f*, 370*f*, 371*f*
 Linear dichroism spectroscopy, 369–371, 369*f*, 370*f*, 371*f*
 Linearly polarized light, 369, 369*f*
 Local magnetic field
 chemical shift, 473–476, 473*f*, 474*f*, 475*f*, 476*f*
 Local realism, 132
 Localization, 295–297, 295*f*, 296*f*
 localized vs. delocalized bonding models, 329–332, 330*f*, 331*f*, 332*f*
 Localized bonding models, 316–318, 317*f*
 Lone pairs, 316–318, 317*f*
 visualization, graphical models, 417–418, 417*f*, 418*f*
 Lowest energy unoccupied molecular orbital (LUMO), 413, 413*f*, 414*f*
 LUMO (lowest energy unoccupied molecular orbital), 413, 413*f*, 414*f*
 Lyman series, 268

M

Macroscopic magnetic moment (M), 470–473, 470*f*, 472*f*
 spin polarization, 472–473, 472*f*
 Magic angle spinning (MAS), 468, 504, 504*f*
 Magnesium, semiconductors and, 341

- Magnetic field
chemical shift, 473–476, 473*f*, 474*f*, 475*f*, 476*f*
nuclear Zeeman effect, 470–473, 470*f*, 472*f*
- Magnetic field gradient, 507–508, 507*f*, 508*f*
- Magnetic moment, 122, 467–469, 468*f*, 469*t*
anisotropic magnetic interactions, 476, 476*f*
dipolar spin-spin coupling, 484, 484*f*
electron spin, 235–236
gyromagnetic ratio, 469
multiplet splitting, NMR, 476–484, 477*f*, 478*f*, 480*f*, 481*f*, 482*f*, 484*f*
nuclear magneton, 469
nuclear spin dynamics, 484–491, 485*f*, 486*f*, 487*f*, 488*f*, 490*f*
nuclear Zeeman effect, 470–473, 470*f*, 472*f*
spin-orbit coupling, 266–267, 266*f*
spin-spin coupling, 476–484, 477*f*, 478*f*, 480*f*, 481*f*, 482*f*, 484*f*
- Magnetic moment, macroscopic (M), 470–473, 470*f*, 472*f*
- Magnetic resonance imaging (MRI), 507–508, 507*f*, 508*f*
- Magnetic susceptibility, 492
- Magnetically equivalent nuclei, 481, 481*f*
- Magnetization (M) vector. *See also* Nuclear magnetic resonance (NMR) spectroscopy
free induction decay (FID), 494
pulsed NMR, 491–498, 493*f*, 494*f*, 495*f*, 497*f*, 498*f*
- Magneton, 492
- MAS (magic angle spinning), 468, 504, 504*f*
- Mass
center-of-mass coordinates, 144–147, 144*f*, 146*f*
harmonic oscillator, classic, 144–147, 144*f*, 146*f*
reduced mass (μ), 144–147, 144*f*, 146*f*
- MBE (molecular beam epitaxy)
technique, 110–112, 111*f*, 112*f*
- Mean free path, inelastic, 277
- Measured linewidth, 199–200, 200*f*
- Measurement process, 73
commutation relations, 119–121
- Heisenberg uncertainty principle, 124–127, 125*f*
- Heisenberg uncertainty principle, standard deviations, 128–130, 130*f*
- Stern–Gerlach experiment, 121–124, 121*f*, 122*f*, 123*f*, 124*f*
- Methane
hybrid orbitals, 318–321, 319*f*, 321*t*
vibrational spectra data, 182–184, 182*f*, 183*f*, 184*f*
- Michelson interferometer, 190–192, 191*f*, 192*f*
- Microscopes
atomic force microscope (AFM), 104–109, 105*f*, 106*f*, 108*f*, 109*f*
scanning tunneling microscope (STM), 104–109, 105*f*, 106*f*, 108*f*, 109*f*
- Microwaves
electromagnetic spectrum, 172*f*
photon energy, 187
- Minimal basis sets, 396–397, 397*f*
- Mirror plane, 440*f*, 441
- M_L orbital angular momentum
good quantum numbers, 257–259, 258*f*, 259*f*
term generation and assignment, 262–264, 263*t*, 264*t*
- MO. *See* Molecular orbitals (MOs)
- Molar absorption coefficient, 180–181
- Molar extinction coefficient, 357–358, 357*f*, 358*f*, 359*f*
- Molecular beam epitaxy (MBE) technique, 110–112, 111*f*, 112*f*
- Molecular configuration, 299–302, 300*f*, 301*f*, 352, 352*t*
diatomic molecules, electronic state transitions, 353–354, 353*f*
- Molecular electrostatic potential, 307–308, 308*f*
- Molecular orbital energy diagram, 288–289, 289*f*
heteronuclear diatomic molecules, 304–307, 304*f*, 306*f*, 307*f*
Walsh correlation diagram, 327–328, 328*f*
- Molecular orbital (MO) model, 316
- Molecular orbital theory, qualitative, 326–328, 326*f*, 327*f*, 328*f*. *See also* Hartree–Fock self-consistent field model
- Hückel model, 334–340, 336*f*, 338*f*, 339*f*
- localized vs. delocalized bonding models, 329–332, 330*f*, 331*f*, 332*f*
- Walsh correlation diagram, 327–328, 328*f*
- Molecular orbitals (MOs), 287. *See also* Molecular symmetry
antibonding molecular orbitals, 293–294, 293*f*, 294*f*, 298, 300
bond order, energy, and length, 302–304, 302*f*
bonding molecular orbitals, 293–294, 293*f*, 294*f*, 300
computational modeling, 332–334, 332*f*, 333*f*, 334*f*
 C_{2v} representations and molecular orbitals of water, 454–456, 454*f*, 455*f*, 456*f*
energy diagram, 288–289, 289*f*
energy of molecular wave function, g and u symmetry, 291–294, 293*f*, 294*f*
frontier molecular orbitals, 413, 413*f*, 414*f*
generation from atomic orbitals, 285–289, 288*f*, 289*f*
graphical models, 412–413, 413*f*
heteronuclear diatomic molecules, 304–307, 304*f*, 306*f*, 307*f*
highest energy occupied molecular orbital (HOMO), 306–307, 306*f*, 307*f*
- homonuclear diatomic molecules, 297–299, 297*f*, 298*f*, 299*f*
- hybrid orbitals, 318–321, 319*f*, 321*t*
- hybrid orbitals for nonequivalent ligands, 321–324, 322*f*, 324*f*
- hydrogen molecule, 289–291, 289*f*, 290*f*
- LCAO-MO model, 287
- many-electron molecule structure, 299–302, 300*f*, 301*f*
- nonbonding electrons, 306–307, 306*f*, 307*f*
- $\pi(\pi)$ symmetry, 297–299, 297*f*, 298*f*, 299*f*
- σ symmetry, 297–299, 297*f*, 298*f*, 299*f*
- solids, energy spectrum and band gaps, 340–341, 340*f*, 341*f*
- $s-p$ mixing, 298–299, 298*f*, 299*f*
- symmetry-adapted MOs, 454–456, 454*f*, 455*f*, 456*f*
- ψ_g and ψ_u wave functions for hydrogen, 294–297, 294*f*, 295*f*, 296*f*

- Molecular shape, determining, 405–406, 406*f*
- Molecular size, graphical model, 416, 416*f*
- Molecular structure. *See also* Nuclear magnetic resonance (NMR) spectroscopy
- potential energy surface computations, 378–382, 378*f*, 379*f*, 381*ft*, 382*f*
 - transition-state geometries and activation energy, 409–412, 410*t*, 411*t*, 412*f*
- Molecular symmetry
- assigning molecules to point groups, 441–443, 442*f*, 443*t*
 - C_{2v} point group and water, 443–447, 444*f*, 447*ft*
 - C_{2v} representations and molecular orbitals of water, 454–456, 454*f*, 455*f*, 456*f*
 - dimension of representation, 450–454, 452*f*, 454*t*
 - elements, operations, and point groups, 439–441, 440*ft*
 - normal modes of vibration, 456–460, 456*f*, 457*f*
 - order of the group, 451
 - projection operator method, 461–464, 461*t*, 462*ft*, 464*f*
 - representations, bases, and character table, 448–450, 449*f*
 - selection rules, infrared *vs.* Raman activity, 460–461
- Molecular term
- configuration and, 353
 - singlet states, 351
 - symbols for, 350–352, 352*t*
 - triplet states, 351
 - Σ terms, assigning + and – in diatomic molecules, 371–372, 371*f*, 372*f*
- Molecular wave function, 286
- Molecules. *See* Diatomic molecules; Polyatomic molecules
- Møller–Plesset models, 392–393
- Moment of inertia, 149
- rotational-vibrational spectrum effects, 187, 187*f*
- Momentum. *See also* Angular momentum; Orbital angular momentum; Spin angular momentum
- commutation relations, 120–121
- de Broglie relation, 24–25, 25*f*
- Heisenberg uncertainty principle, 124–127, 125*f*
- Heisenberg uncertainty principle, standard deviations, 128–130, 130*f*
- measurement of, 88–89
- quantization of angular momentum, 159–161
- rigid rotor, 148–149, 149*f*
- Monochromator, 181
- Morse potential, 176–177, 177*f*
- harmonic oscillator, quantum-mechanical, 150, 150*f*
- Motional broadening, 489
- Motional narrowing, 489
- MRI (magnetic resonance imaging), 507–508, 507*f*, 508*f*
- M_S spin angular momentum
- good quantum numbers, 257–259, 258*f*, 259*f*
 - term generation and assignment, 262–264, 263*t*, 264*t*
- Mulliken, Robert, 248
- Mulliken population analysis, 408–409
- Multiplet splitting, NMR, 476–484, 477*f*, 478*f*, 480*f*, 481*f*, 482*f*, 484*f*
- Multiplex advantage, 190
- Multiplicity, 261
- N**
- Neighboring group anisotropy, 476, 476*f*
- Neon, helium-neon laser, 273–276, 274*f*, 275*f*, 276*f*
- Newton's Second Law of Motion, 144–147, 144*f*, 146*f*
- Nitrogen bases, bond energies, 386, 386*t*
- NMR. *See* Nuclear magnetic resonance (NMR) spectroscopy
- Nodal surfaces, 219, 219*f*
- Nodes, waves, 80
- NOESY (NOE spectroscopy), 499, 502–503, 502*f*
- Nonbonding electrons, 306–307, 306*f*, 307*f*
- Bent's rule, 321–324, 322*f*, 324*f*
- Noncommuting operators, 124–127, 125*f*
- Nonradiative transitions, 359, 360–361, 360*f*
- Normal coordinates, 380, 456*f*, 457–460, 457*f*
- Normal mode frequencies, 456–460, 456*f*, 457*f*, 461
- Normal modes, 183–184, 183*f*, 184*f*, 456–460, 456*f*, 457*f*
- Normalization, wave function, 68
- Normalization constant, 151
- Normalized functions, 58–59
- Nuclear equivalency, 476
- Nuclear g-factor, 492
- Nuclear magnetic moment, 467–469, 468*f*, 469*t*. *See also* Nuclear magnetic resonance (NMR) spectroscopy
- gyromagnetic ratio, 469
- nuclear magneton, 469
- Zeeman effect, 470–473, 470*f*, 472*f*
- Nuclear magnetic resonance (NMR) spectroscopy, 172. *See also* Spectroscopy
- chemical shift, 473–476, 473*f*, 474*f*, 475*f*, 476*f*
 - chemically equivalent nuclei, 481, 481*f*
 - cross relaxation, 490, 490*f*
 - dipolar spin-spin coupling, 484, 484*f*
 - dynamic nuclear polarization (DNP), 505–507, 505*f*
 - Fourier transform (FT)-NMR, 495–496
 - intrinsic nuclear angular momentum and magnetic moment, 467–469, 468*f*, 469*t*
 - Karplus relation, 481
 - magic angle spinning, 504, 504*f*
 - magnetic resonance imaging (MRI), 507–508, 507*f*, 508*f*
 - magnetically equivalent nuclei, 481, 481*f*
 - motional broadening and narrowing, 489
 - multiplet splitting, 476–484, 477*f*, 478*f*, 480*f*, 481*f*, 482*f*, 484*f*
 - neighboring group anisotropy, 476, 476*f*
 - nuclear Overhauser effect (NOE), 489–490, 490*f*
 - nuclear Zeeman effect, 470–473, 470*f*, 472*f*
 - pulsed NMR, 467–468, 491–498, 493*f*, 494*f*, 495*f*, 497*f*, 498*f*
 - relaxation and linewidth, 489–491, 490*f*
 - resonance condition, 471
 - solid-state NMR, 503–504, 503*f*, 504*f*
 - spin dynamics, 484–491, 485*f*, 486*f*, 487*f*, 488*f*, 490*f*

- spin echo, 496–498, 497*f*
 spin polarization, 472–473, 472*f*
 spin-lattice relaxation (SLR), 486–488
 spin-spin coupling, 476–484, 477*f*,
 478*f*, 480*f*, 481*f*, 482*f*, 484*f*
 transverse component, 487–488, 488*f*
 two-dimensional NMR, 498–503,
 499*f*, 500*f*, 501*f*, 502*f*
 Nuclear magneton, 469
 Nuclear Overhauser effect (NOE),
 489–490, 490*f*
 Nuclear spin, 468–469, 468*f*, 469*t*
 Nuclear-nuclear repulsion
 bonding and antibonding molecular
 orbitals, 293–294, 293*f*, 294*f*
 Born–Oppenheimer approximation,
 286
 hydrogen molecule, 289–290, 289*f*,
 290*f*
 Nucleic acids
 fluorescence spectroscopy, 362–363,
 363*f*
 Fluorescent Resonance Energy
 Transfer (FRET), 367, 367*f*, 368*f*
 two-dimensional NMR, 498–503,
 499*f*, 500*f*, 501*f*, 502*f*
 Nucleons, 468–469, 468*f*, 469*t*
 Nucleus. *See also* Hydrogen (H) atom;
 Nuclear magnetic resonance (NMR)
 spectroscopy
 Born–Oppenheimer approximation,
 286, 382–383
 chemically equivalent nuclei, 481,
 481*f*
 magnetically equivalent nuclei, 481,
 481*f*
 molecular electrostatic potential,
 307–308, 308*f*
 molecular wave function, 286
 orbital energy and atomic size,
 244–245, 244*f*, 245
 shielding, nuclear charge and, 245
 spin dynamics, NMR, 484–491, 485*f*,
 486*f*, 487*f*, 488*f*, 490*f*
 ψ_g and ψ_u wave functions for hydro-
 gen, 294–297, 294*f*, 295*f*, 296*f*
- O**
- Observable, Schrödinger equation,
 56–57
 Octahedral structures, 317, 317*f*
- One-dimensional box, 79–83, 79*f*, 80*f*,
 81*f*, 82*f*
 One-electron orbitals, 234–235, 234*f*
 Operator, Hamiltonian, 69
 Operator, Hermitian, 69
 Operator, Schrödinger equation, 56–57
 Optical resonator, 273–276, 274*f*
 Optoelectronics, 113
 Orbital angular momentum. *See also* L
 (orbital angular momentum)
 atomic spectroscopy, overview,
 267–269, 269*f*
 configuration energy and, 259–266,
 259*f*, 260*f*, 262*f*, 263*t*, 264*t*
 good quantum numbers, 257–259,
 258*f*, 259*f*
 Hund’s rules, 265, 266
 Orbital approximation, 234–235, 234*f*
 Orbital energy, 234–235, 234*f*
 atomic number and, 244–245, 244*f*, 245
 Aufbau principle, 246–247, 246*f*
 Hartree–Fock self-consistent field
 model, 245–247, 246*f*
 heteronuclear diatomic molecules,
 304–307, 304*f*, 306*f*, 307*f*
 molecular configuration, 299–302,
 300*f*, 301*f*
 Orbital symmetry control of reactions,
 413, 413*f*, 414*f*
 Orbitals. *See also* Atomic orbitals
 (AOs); Hydrogen (H) atom; Molecu-
 lar orbitals (MOs)
 Aufbau principle, 246–247, 246*f*
 computational modeling, 332–334,
 332*f*, 333*f*, 334*f*
 configuration (*See* Configuration)
 configuration, occupied orbitals, 259,
 259*t*
 defined, 159
 electron indistinguishability, 236–238
 frozen orbital approximation,
 364–365, 364*f*
 H atom orbitals, defined, 213
 Hartree–Fock self-consistent field
 model, 241–247, 241*f*, 242*f*, 243*f*,
 244*f*, 245*t*, 246*f*
 hybrid orbitals, 318–321, 319*f*, 321*t*
 hydrogen atom, overview of, 217–
 219, 217*f*, 218*f*, 219*f*
 ionization energy, 245–247, 246*f*
 many-electron atoms, overview,
 232–235, 234*f*
- molecular orbitals, generation of,
 285–289, 288*f*, 289*f*
 Pauli Principle, 237–238
 periodic table trends, Hartree–Fock
 and, 247–249, 248*f*, 249*f*
 quantization of angular momentum,
 159–161, 185
 radial probability distribution function,
 219–223, 220*f*, 223*f*
 shell model, validity of, 224–225, 224*f*
 shells and subshells, 238
 spherical harmonic functions,
 161–164, 163*f*, 164*f*
 terms, 259, 259*t* (*See also* Terms)
 UV photoelectron spectroscopy,
 363–365, 364*f*
 viral theorem, 214
 Order of the group, 451
 Organic reactions, transition-state
 geometries and activation energy,
 409–412, 410*t*, 411*t*, 412*f*
 Orthogonality, 57–59
 Orthonormal hybrid orbitals, 321, 321*t*
 Orthonormal sets, 58–59, 71
 Oscillatory behavior, 144. *See also*
 Spherical harmonic functions
 harmonic oscillator, classical,
 143–147, 144*f*, 146*f*
 harmonic oscillator, quantum-
 mechanical, 149–154, 150*f*, 153*f*
 Overhauser, Albert, 505
 Overhauser mechanism, 505–507, 505*f*
 Overlap, 287, 288*f*
 Overlap integral, 287, 288*f*, 335
 Overlap of wave functions, 99*f*, 100, 100*f*
 Overtone, 176–177, 177*f*, 181
 Oxygen. *See* Water
 Ozone, photodissociation and, 354
- P**
- P branch, infrared absorption spectrum,
 188–189, 189*f*, 190*f*
 p orbital. *See also* Configuration;
 Molecular orbitals (MOs); Terms
 Aufbau principle, 246–247, 246*f*
 Hartree–Fock self-consistent field
 model, 241–247, 241*f*, 242*f*, 243*f*,
 244*f*, 245*t*, 246*f*
 Hückel model, 334–335
 many-electron atoms, overview,
 232–235, 234*f*

- p* orbital (*continued*)
 periodic table trends, Hartree–Fock and, 247–249, 248*f*, 249*f*
 quantization of angular momentum, 159–161
 radial probability distribution function, 219–223, 220*f*, 223*f*
 Schrödinger equation, hydrogen atom, 217–219, 217*f*, 218*f*, 219*f*
 shell model, validity of, 224–225, 224*f*
sp hybridization, 318–321, 319*f*, 321*t*
 spherical harmonic functions, 161–164, 163*f*, 164*f*
 water molecule, 324, 324*f*
- Paired electrons, 260, 260*f*
 Pake doublet, 503–504, 503*f*, 504*f*
 Parallel spin, 259–260, 259*f*, 260*f*
 Particle in a box
 conductors, insulators, and semiconductors, 98–100, 99*f*, 100*f*
 finite depth box, 95–96, 95*f*, 96*f*
 hydrogen atom, energy diagram, 211–212, 212*f*
 one-dimensional box, 79–83, 79*f*, 80*f*, 81*f*, 82*f*
 quantum-mechanical postulates and, 84–89
 three-dimensional box thought experiment, 130–132, 131*f*
 traveling waves and energy barriers, 100–102, 101*f*, 102*f*
 trial wave function Φ , 239–240
 tunneling through a barrier, 103–104, 103*f*, 104*f*
 two- and three-dimensional boxes, 83–84
- Particles
 free particles, 77–78
 system descriptions, 45–49, 49*f*
 understanding particles, postulates and, 84–89
- Paschen series, 268
 Pauli, Wolfgang, 237
 Pauli principle, 237, 261
 Period, wave function, 50
 Periodic table trends
 Hartree–Fock self-consistent field model, 247–249, 248*f*, 249*f*
 homonuclear diatomic molecules, 298–299, 298*t*, 299*f*
 Permanent dipole moment, 173, 173*f*
 Perturbation theory, 392–393
- Pfund series, 268
 Phase, wave function, 50, 51*f*
 Phosphorescence, 361–362, 361*f*
 Phosphorus, semiconductors, 342, 342*f*
 Photodissociation, 354
 Photoelectric effect, 22–24, 22*f*, 23*f*
 Photoionization, 364–365, 364*f*
 Photons. *See also* Atomic spectroscopy; Electronic spectroscopy; Spectroscopy
 coherent photon emission, 175
 coherent photon source, 273
 defined, 23
 electromagnetic spectrum, 172*f*
 electron transition processes, 174–175, 174*f*
 fluorescence, 112, 112*f*
 incoherent photon emission, 175
 incoherent photon source, 273
 UV photoelectron spectroscopy, 363–365, 364*f*
- Pi (π) symmetry
 chromophores, 358, 358*f*, 359*f*
 heteronuclear diatomic molecules, 306–307, 306*f*, 307*f*
 homonuclear diatomic molecules, 297–299, 297*f*, 298*f*, 299*f*
 Hückel model, 334–335, 338–340
 molecular term symbols, 350–352, 352*t*
 Pi (π) electrons, movement in a box, 97–98, 97*f*, 98*t*
 Pi (π)-bonded network, 97–98, 97*f*, 98*t*
- Planck, Max, 21–22
 Planck constant (h), 21–22
 Plane waves, 50, 50*f*, 78
 Point groups, 441
 assigning molecules to, 441–443, 442*f*, 443*t*
 C_{2v} point group and water, 443–447, 444*f*, 447*f*
 C_{2v} representations and molecular orbitals of water, 454–456, 454*f*, 455*f*, 456*f*
 dimension of representation, 450–454, 452*f*, 454*t*
 order of the group, 451
 projection operator method, 461–464, 461*t*, 462*f*, 464*f*
 representations, bases, and character table, 448–450, 449*f*
- selection rules, infrared vs. Raman activity, 460–461
 symmetry of normal modes of vibration, 456–460, 456*f*, 457*f*
 Polarity, molecular electrostatic potential, 307–308, 308*f*
 Polarizability, 194–196, 195*f*
 Polarization
 CIDNP (chemically induced nuclear polarization), 507
 dynamic nuclear polarization (DNP), 505–507, 505*f*
 spin polarization, NMR spectroscopy, 480–481
 Polarization basis sets, 397–398, 398*f*
 Polarization functions, 398, 398*f*
 Polarized light, linearly, 369, 369*f*
 Polyatomic molecules
 antiaromatic molecules, 339–340
 aromatic molecules, 334–335
 Bent's rule, 321–324, 322*f*, 324*f*
 computational modeling, 332–334, 332*f*, 333*f*, 334*f*
 conjugated molecules, 334
 dipole moment calculations, 406–407, 407*f*
 Hückel model, 334–340, 336*f*, 338*f*, 339*f*
 hybrid orbitals for nonequivalent ligands, 321–324, 322*f*, 324*f*
 hybridization, bonding descriptions and, 324–325, 324*f*, 325*f*
 hybridization, valence bond theory and, 318–321, 319*f*, 321*t*
 Lewis structure and VSEPR model, 315–318, 316*f*, 317*f*
 localized vs. delocalized bonding models, 329–332, 330*f*, 331*f*, 332*f*
 molecular orbital theory, 326–328, 326*f*, 327*f*, 328*f*
 resonance stabilization energy, 339–340, 339*f*
 solids, energy spectrum and band gaps, 340–341, 340*f*, 341*f*
 UV-visible light absorption, 356–358, 357*f*, 358*f*, 359*f*
 vibrational frequency, 380–381
 Walsh correlation diagram, 327–328, 328*f*
- Pople, Sir John, 389
 Population inversion, 273–276, 274*f*, 275*f*, 276*f*

Postulates. *See* Quantum-mechanical postulates
 Potential energy
 barriers, traveling waves and, 100–102, 101*f*, 102*f*
 conductors, insulators, and semiconductors, 98–100, 99*f*, 100*f*
 electron-electron repulsion term, 234–235
 harmonic oscillator, classic, 144, 144*f*, 146–147, 146*f*
 harmonic oscillator, quantum-mechanical, 150, 150*f*, 152–154, 153*f*
 hydrogen molecules, charge distribution and, 295*f*, 296–297, 296*f*
 quantum-mechanical rotation, 155–156
 rigid rotor, 148
 viral theorem, 214
 Potential energy surface computations, 378–382, 378*f*, 379*f*, 381*ft*, 382*f*
 Precession, 470–473, 470*f*, 472*f*
 Preexponential factor, 382, 382*f*
 Primary structure, 365–366, 366*f*
 Probabilistic outcome, 72
 Probability
 Heisenberg uncertainty principle, 124–127, 125*f*
 particle reflections, 101–102, 102*f*
 particle transmission, traveling waves, 101–102, 102*f*
 particles in a box, 84–86
 radial probability distribution function, 219–223, 220*f*, 223*f*
 of resonance energy transfer, 367, 367*f*, 368*f*
 wave function and, 67–68, 68*f*
 Probability density, 81
 finite depth box, 96
 harmonic oscillator, quantum-mechanical, 153–154, 153*f*
 radial distribution function and, 222–223, 223*f*
 spherical harmonic functions, 161–164, 163*f*, 164*f*
 ψ_g and ψ_u wave functions for hydrogen, 294–297, 294*f*, 295*f*, 296*f*
 Projection operator method, 461–464, 461*ft*, 462*ft*, 464*f*
 Protein structure, two-dimensional NMR, 498–503, 499*f*, 500*f*, 501*f*, 502*f*

Protons. *See also* Hydrogen (H) atom
 Born–Oppenheimer approximation, 286, 289
 chemical shift, 474, 476
 diatomic molecules, 286, 289, 289*f*, 292, 293, 296
 dynamic nuclear polarization, 505, 506, 507
 magnetic resonance imaging (MRI), 507, 508
 NMR peaks, effect on, 489
 NMR spin-spin coupling and multiplet splitting, 477–478, 477*f*, 478*f*, 480, 481, 482, 483
 nuclear spin, 468–469, 469*t*
 proton affinity and reaction energies, 386, 386*t*, 402, 403, 403*f*
 pulsed NMR spectroscopy, 492
 spin dynamics, 487, 489
 tunneling microscopy, 107
 two-dimensional NMR, 498, 501, 502*f*
 as wave-particle, 20
 Pulsed NMR spectroscopy, 491–498, 493*f*, 494*f*, 495*f*, 497*f*, 498*f*
 Pumping transition, 276, 276*f*

Q

Qualitative molecular orbital theory, 326–328, 326*f*, 327*f*, 328*f*. *See also* Hartree–Fock self-consistent field model
 Hückel model, 334–340, 336*f*, 338*f*, 339*f*
 localized vs. delocalized bonding models, 329–332, 330*f*, 331*f*, 332*f*
 Quanta, defined, 20
 Quantitized, defined, 80
 Quantization, defined, 20
 Quantum computers, 132–135, 133*f*
 Quantum dots, 110–113, 111*f*, 112*f*, 113*f*
 Quantum mechanics
 atomic spectra and Bohr model of atom, 29–32, 29*f*, 30*f*, 31*f*, 32*f*
 blackbody radiation, 21–22, 21*f*, 22*f*
 de Broglie relation, 24–25, 25*f*
 diffraction by double slit, 26–29, 27*f*, 28*f*
 history of, 20
 importance of, 19–20
 photoelectric effect, 22–24, 22*f*, 23*f*
 system descriptions with, 45–49, 49*f*

Quantum number, 80–83
 Quantum well devices, 111–113, 111*f*, 112*f*, 113*f*
 Quantum wells structure, 110–113, 111*f*, 112*f*, 113*f*
 Quantum-mechanical analog of position, 81
 Quantum-mechanical harmonic oscillator, 149–154, 150*f*, 153*f*
 Quantum-mechanical operator complete sets, 59–60, 60*f*
 orthogonality of, 57–59
 Quantum-mechanical postulates
 postulate 1, wave function and probability, 67–68, 68*f*, 84–86
 postulate 2, every observable has an operator, 69
 postulate 3, individual measurement results, 69–70, 87–89
 postulate 4, expectation value, 70–73, 71*f*, 72*f*, 73*f*, 87–89
 postulate 5, evolution in time, 73
 understanding particles in a box, 84–89
 Quantum-mechanical waves
 time-dependent Schrödinger equation, 55
 time-independent Schrödinger equation, 54–55
 Quartet state, 261
 Quaternary structure, 365–366, 366*f*
 Qubit, 135

R

r, electron position, molecular wave function, overview, 286
 R, nucleus position, molecular wave function, 286
 R branch, infrared absorption spectrum, 188–189, 189*f*, 190*f*
 Rabi frequency, 486, 492
 Rabi oscillation, 486
 Radial distribution function, 222–223, 223*f*
 shell model of atom, 224–225, 224*f*
 Radial function, Schrödinger equation, solving of, 210–211, 211*f*
 Radial probability distribution function, 219–223, 220*f*, 223*f*
 Hartree–Fock radial functions, 243, 243*f*

- Radians, 148
- Radiation, blackbody, 21–22, 21*f*, 22*f*
- Radiative transitions, 359, 360*f*
singlet-singlet transitions, 360–361
- Radio frequencies (RF). *See also*
Nuclear magnetic resonance (NMR)
spectroscopy
- pulsed NMR spectroscopy, 491–498,
493*f*, 494*f*, 495*f*, 497*f*, 498*f*
- two-dimensional NMR, 498–503,
499*f*, 500*f*, 501*f*, 502*f*
- Radio waves, electromagnetic spectrum, 172*ft*
- Radius, radians, 148–149, 149*f*
- Raman microscope (microprobe), 196
- Raman spectroscopy, 182, 188–189,
194–196, 195*f*
- selection rules, infrared *vs.* Raman
activity, 460–461
- symmetry of normal modes of
vibration, 456–460, 456*f*, 457*f*
- Random phase angle, 27
- Rate constant, potential energy surfaces
and, 381–382, 381*f*, 382*f*
- Rayleigh frequency, 195–196, 195*f*
- Reaction coordinate, 378–382, 378*f*,
379*f*, 381*ft*, 382*f*
- Reaction coordinate diagrams, 378–382,
378*f*, 379*f*, 381*ft*, 382*f*
- Reaction energy calculations, 402–403,
402*t*, 403*t*
- Reaction rate
potential energy surfaces and,
381–382, 381*f*, 382*f*
- transition-state geometries and activation
energy, 409–412, 410*t*, 411*t*,
412*f*
- Reactive intermediates, 401, 401*t*
- transition-state geometries, 409–412,
410*t*, 411*t*, 412*f*
- Realism, local, 132
- Reduced mass (μ), 144, 144*f*
harmonic oscillator, classic, 144–147,
144*f*, 146*f*
- rigid rotor, 148, 148*f*, 149
- spectroscopy, diatomic molecules,
178, 380
- spectroscopy, hydrogen atom, 217,
268
- Reducible representations, 450,
458–460
- Reflection probability, 101–102, 102*f*
- Relaxation, 486–488
coupling factor, 506–507
- cross relaxation, 490, 490*f*
- NMR linewidth, 489–491, 490*f*
- Representations, 448–450, 449*f*
 C_{2v} representations and molecular
orbitals of water, 454–456, 454*f*,
455*f*, 456*f*
- dimension of representation, 450–454,
452*f*, 454*t*
- order of the group, 451
- projection operator method, 461–464,
461*t*, 462*ft*, 464*f*
- Repulsion forces
atomic spectroscopy, 259, 259*f*, 261,
265, 266*f*
- bonding and antibonding molecular
orbitals, 293–294, 293*f*, 294*f*
- Born–Oppenheimer approximation, 286–287
- electron correlation, 234
- electron-electron repulsion term,
234
- electrostatic potential, 417
- ground state, 247
- hydrogen molecule, 289–290, 289*f*,
290*f*, 292, 293, 293*f*
- many-electron atoms, 239, 241, 242,
246, 247
- polyatomic molecules, 328
- VSEPR (valence shell electron pair
repulsion) model, 316–318, 317*f*
- Resonance condition, 471
- Resonance energy transfer, 367, 367*f*,
368*f*
- Resonance integral, 335
- Resonance stabilization energy,
339–340, 339*f*
- Resonator modes, 274–276, 274*f*
- Right-hand rule, 149, 149*f*
- Rigid rotor, 147–149, 148*f*, 149*f*
with electric field, 185, 185*f*
- rotational constant, 178, 186
- Ring currents, 473–476, 473*f*, 474*f*,
475*f*, 476, 476*f*
- Rohrer, Heinrich, 104
- Roothaan–Hall equations, 384, 390
- Rotating frame, 486, 486*f*, 493–494
- Rotation axes, 440–441, 440*f*
- Rotational constant, 178, 186
- Rotational isomers
conformational energy differences,
404–405, 405*f*
- molecular shape, determining,
405–406, 406*f*
- Rotational motion
Born–Oppenheimer approximation, 286
- conformational energy differences,
404–405, 405*f*
- diatomic molecules, electronic state
transitions, 353–354, 353*f*
- electronic transitions, energy of,
349–350
- quantization of angular momentum,
159–161
- quantum-mechanical rotation,
154–157, 156*f*, 157*f*
- quantum-mechanical rotation, three
dimensions, 157–159
- rigid rotor, classical, 147–149, 148*f*,
149*f*
- rigid rotor, with electric field, 185, 185*f*
- rotational constant, 178, 186
- spatial quantization, 164–165, 165*f*
- spherical harmonic functions,
161–164, 163*f*, 164*f*
- in two dimensions, 155
- Rotational spectroscopy, 184–189,
185*f*, 186*f*, 187*ft*, 188*f*, 189*f*, 190*f*
- absorption peaks, number of, 187
- electron transition processes,
174–175, 174*f*
- Raman spectroscopy, 194–196, 195*f*
- rotational-vibrational spectrum
effects, 187–189, 187*f*, 189*f*, 190*f*
- spectroscopy, overview, 171–173,
172*ft*, 173*f*
- Rotation-reflection axis, 440–441, 440*f*
- Rotor, rigid, 147–149, 148*f*, 149*f*
- Rutherford, Ernest, 29, 209
- Rydberg constant, 30, 268
- Rydberg constant for hydrogen, 217

S

- s* orbital. *See also* Configuration;
Molecular orbitals (MOs); Terms
- Aufbau principle, 246–247, 246*ft*
- Hartree–Fock self-consistent field
model, 241–247, 241*f*, 242*f*, 243*ft*,
244*f*, 245*t*, 246*ft*

- Hückel model, 334–335
many-electron atoms, overview, 232–235, 234*f*
periodic table trends, Hartree–Fock and, 247–249, 248*f*, 249*f*
quantization of angular momentum, 159–161
radial probability distribution function, 219–223, 220*f*, 223*f*
Schrödinger equation, hydrogen atom, 217–219, 217*f*, 218*f*, 219*f*
shell model, validity of, 224–225, 224*f*
sp hybridization, 318–321, 319*f*, 321*t*
spherical harmonic functions, 161–164, 163*f*, 164*f*
water molecule, 324, 324*f*
- S* (spin angular momentum)
atomic spectroscopy, overview, 267–269, 269*f*
Clebsch–Gordan series, 261–264, 263*t*, 264*t*
configuration energy and, 259–266, 259*f*, 260*f*, 262*f*, 263*t*, 264*t*
good quantum numbers, 257–259, 258*f*, 259*f*
molecular term symbols, 350–352, 352*t*
spin-orbit coupling and levels, 266–267, 266*f*
s symmetry, molecular wave function energy, 291–294, 293*f*, 294*f*
Sandwich compounds, 340
Saturation factors, 506–507
Scalar (*J*) coupling, NMR spectroscopy, 479–480, 480*f*
Scanning electron microscopy (SEM), 278, 278*f*
Scanning tunneling microscope (STM), 104–109, 105*f*, 106*f*, 108*f*, 109*f*, 330–332, 331*f*, 332*f*
SCF (self-consistent-field) procedure, 383
Schaad, L., 339
Schrödinger, Erwin, 132
Schrödinger equation, 54–55. *See also* Quantum-mechanical postulates
electron spin, 235–236
electron-electron repulsion term, 234–235, 234*f*
electronic Schrödinger equation, 383
finite depth box, 95–96, 95*f*, 96*f*
- formulation of, 209–210
free particles, 77–78
Hartree–Fock molecular orbital theory and, 382–384
Hartree–Fock self-consistent field model, 241–247, 241*f*, 242*f*, 243*f*, 244*f*, 245*t*, 246*f*
hydrogen atom orbitals, 217–219, 217*f*, 218*f*, 219*f*
many electron atoms and, 232–235, 234*f*
molecular wave function, 286
operators, observables, eigenfunctions, and eigenvalues, 55–57
particle in a one-dimensional box, 79–83, 79*f*, 80*f*, 81*f*, 82*f*
quantum-mechanical harmonic oscillator, 150–151
quantum-mechanical rotation, 155–157
quantum-mechanical rotation, three dimensions, 157–159
shell model of atom, validity of, 224–225, 224*f*
solving for hydrogen atom, 210–211, 211*f*
spherical harmonic functions, 161–164, 163*f*, 164*f*
total energy eigenvalues and eigenfunctions, 211–217, 212*f*, 217*f*
two and three dimensional boxes, 83–84
variational method and, 239–240
Second Law of Motion, harmonic oscillator, classic, 144–147, 144*f*, 146*f*
Secondary structure, 365–366, 366*f*
Secular determinant, 288
Hückel model, 335
Secular equations, 288
Selection rules, 173
atomic spectroscopy, 267–269, 269*f*
diatomic molecules, electronic state transitions, 353–354
diatomic molecules, spectroscopy, 187, 188
electronic state transitions, 353
helium-neon laser, 273, 276
infrared vs. Raman activity, 460–461
NMR transitions, 479, 485
origin of, 178–180, 179*f*, 180*f*
Raman spectroscopy, 194
- symmetry of normal modes of vibration, 439, 456–460, 456*f*, 457*f*
transition dipole moment, 198
Self-consistent-field (SCF) procedure, 383
SEM (scanning electron microscopy), 278, 278*f*
Semiclassical description, 164–165, 165*f*
Semiconductors, 98–100, 99*f*, 100*f*, 340–342, 340*f*, 341*f*, 342*f*
MBE (molecular beam epitaxy) technique, 111–113, 111*f*, 112*f*, 113*f*
Semi-empirical theory, 335
Separation of variables, 83–84
quantum-mechanical rotation, 155–157, 156*f*, 157*f*
Shell, defined, 238
Shell model, 209–210, 224–225, 224*f*
Shielding constant (σ), 473–476, 473*f*, 474*f*, 475*f*, 476*f*
Shielding effect, 475–476, 476*f*
Shor's algorithm, 135
Sidebands, spinning, 504, 504*f*
Sigma (σ) symmetry
chromophores, 358, 358*f*, 359*f*
heteronuclear diatomic molecules, 306–307, 306*f*, 307*f*
homonuclear diatomic molecules, 297–299, 297*f*, 298*f*, 299*f*
Hückel model, 334–335
molecular term symbols, 350–352, 352*t*
sp hybridization, 318–321, 319*f*, 321*t*
Silicon semiconductors, 341–342, 341*f*, 342*f*
Single-electron promotions, 391–392, 391*f*, 392*f*
Single-molecule spectroscopy, 365–366, 366*f*
Fluorescent Resonance Energy Transfer (FRET), 366–367, 367*f*, 368*f*
Singlet state, 260, 260*f*, 261, 351
Singlet-singlet transitions, absorption and fluorescence, 360–361
Single-value function, 68
Size consistent model, 390
Slater determinants, 237–238, 383
Hartree–Fock self-consistent field model, 241–247, 241*f*, 242*f*, 243*f*, 244*f*, 245*t*, 246*f*

- Slater-type orbitals (STOs), 395–396, 396*f*
- SLR (spin-lattice relaxation), 486–488, 490, 490*f*
- Solid effect, 507
- Solids, energy spectrum and band gaps, 340–341, 340*f*, 341*f*
- Solid-state NMR, 503–504, 503*f*, 504*f*
- sp* hybridization, 318–321, 319*f*, 321*t*
- Hückel model, 334–335
- s-p* mixing, 298–299, 298*t*, 299*f*
- Spatial quantization, 164–165, 165*f*
- Spectral density, 21–22, 21*f*, 22*f*
- Spectral lines
- atomic spectroscopy and, 268–269, 269*f*
 - series determination, 268–269, 269*f*
- Spectroscopists, 172
- Spectroscopy, 171–173, 172*f*, 173*f*.
- See also* Atomic spectroscopy; Electronic spectroscopy; Nuclear magnetic resonance (NMR) spectroscopy
- absorption, 174–175, 174*f*
- atomic spectra and Bohr model of atom, 29–32, 29*f*, 30*f*, 31*f*, 32*f*
- Auger electron spectroscopy, 277–279, 277*f*, 278*f*, 279*f*
- COSY (correlation spectroscopy), 499–503, 499*f*, 500*f*, 501*f*, 502*f*
- fluorescence spectroscopy, 362–363, 363*f*
- Fluorescent Resonance Energy Transfer (FRET), 366–367, 367*f*, 368*f*
- Fourier transform infrared spectroscopy (FTIR), 190–194, 191*f*, 192*f*, 193*f*, 194*f*
- infrared absorption spectroscopy, 180–184, 181*f*, 182*f*, 183*f*, 184*f*
- inhomogeneous broadening, 200, 200*f*
- interferogram, 191–192, 191*f*, 192*f*
- linewidth, intrinsic and measured, 199–200, 200*f*
- Michelson interferometer, 190–192, 191*f*, 192*f*
- molar absorption coefficient, 180–181
- monochromator, 181
- multiplex advantage, 190
- normal modes of vibration, 183–184, 183*f*, 184*f*
- pi (π) electrons, 97–98, 97*f*, 98*f*
- polarizability, 194–196, 195*f*
- Raman spectroscopy, 182, 194–196, 195*f*
- Rayleigh, Stokes, and anti-Stokes frequencies, 195–196, 195*f*
- rotational spectroscopy, 184–189, 185*f*, 186*f*, 187*f*, 188*f*, 189*f*, 190*f*
- scanning tunneling spectroscopy, 330–332, 331*f*, 332*f*
- selection rules, origin of, 178–180, 179*f*, 180*f*
- single-molecule spectroscopy, 365–366, 366*f*
- spontaneous emission, 174–175, 174*f*
- stimulated emission, 174–175, 174*f*
- transition rate and frequency, 196–200, 199*f*, 200*f*
- UV photoelectron spectroscopy, 363–365, 364*f*
- vibrational spectroscopy, overview of, 175–178, 175*t*, 177*f*, 178*t*
- X-ray photoelectron spectroscopy, 277–279, 277*f*, 278*f*, 279*f*
- Spherical harmonic functions, 161–164, 163*f*, 164*f*
- defined, 158
- hydrogen atom total energy, 215–216
- quantum-mechanical rotation, three dimensions, 158–159
- Spherical waves, 50, 50*f*
- Spin, nuclear, 468–469, 468*f*, 469*t*
- Spin angular momentum, 235–236. *See also* *S* (spin angular momentum)
- atomic spectroscopy, overview, 267–269, 269*f*
- configuration energy and, 259–266, 259*f*, 260*f*, 262*f*, 263*t*, 264*t*
- good quantum numbers, 257–259, 258*f*, 259*f*
- Hückel model, 335
- Hund's rules, 265, 266
- paired and unpaired electrons, 260, 260*f*
- parallel and antiparallel spin, 259–260, 259*f*, 260*f*
- singlet and triplet states, 260, 260*f*
- Spin dynamics, 484–491, 485*f*, 486*f*, 487*f*, 488*f*, 490*f*
- Spin echo, 496–498, 497*f*
- Spin flip, 361–362, 361*f*
- Spin polarization, 472–473, 472*f*
- Spin polarization, NMR spectroscopy, 480–481
- Spin variable, 236
- Spin-echo experiment, 488
- Spin-lattice relaxation (SLR), 486–488, 490, 490*f*
- Spinning sidebands, 504, 504*f*
- Spin-orbit coupling, 266–267, 266*f*
- intersystem crossing and phosphorescence, 361–362, 361*f*
- Spin-spin coupling, 476–484, 477*f*, 478*f*, 480*f*, 481*f*, 482*f*, 484*f*
- dipolar spin-spin coupling, 484, 484*f*
- Split-valence basis set, 397, 397*f*
- Spontaneous emission, 174–175, 174*f*
- Standard deviations, 128–130, 130*f*
- Standing waves, 52
- Stationary states, 52
- Stern–Gerlach experiment, 121–124, 121*f*, 122*f*, 123*f*, 124*f*
- Stimulated emission, 174–175, 174*f*
- STM (scanning tunneling microscope), 104–109, 105*f*, 106*f*, 108*f*, 109*f*, 330–332, 331*f*, 332*f*
- STO-3G basis set, 396–397, 397*f*
- Stokes frequency, 195–196, 195*f*
- STOs (Slater-type orbitals), 395–396, 396*f*
- Structural isomers
- bond energies, 386, 386*t*
 - reaction energies, 402–403, 402*t*, 403*t*
- Subshell, 238
- Superconducting loops, 135
- Superposition state, 71, 73, 135
- Symmetric wave function, 236–238, 291
- Symmetry elements, 439–441, 440*f*
- assigning molecules to point groups, 441–443, 442*f*, 443*t*
- C_{2v} point group and water, 443–447, 444*f*, 447*f*
- dimension of representation, 450–454, 452*f*, 454*t*
- order of the group, 451
- projection operator method, 461–464, 461*t*, 462*f*, 464*f*
- representations, bases, and character table, 448–450, 449*f*
- Symmetry operations, 297–299, 297*f*, 298*f*, 299*f*, 439–441, 440*f*
- C_{2v} point group and water, 443–447, 444*f*, 447*f*
- dimension of representation, 450–454, 452*f*, 454*t*

projection operator method, 461–464, 461*t*, 462*f*, 464*f*
representations, bases, and character table, 448–450, 449*f*
Symmetry-adapted MOs, 454–456, 454*f*, 455*f*, 456*f*

T

Taylor–Maclaurin series, 22
Teleportation, 132–135, 133*f*
Temperature (*T*)
Boltzmann distribution, 47
spectral density, 21–22, 21*f*, 22*f*
spin polarization and, 472–473, 472*f*
UV-visible light absorption, polyatomic molecules, 356–358, 357*f*, 358*f*, 359*f*
Term symbol, 261
Terms, 259, 259*t*
degeneracy of term, 261
generation and assignment of, 261–264, 263*t*, 264*t*
Hund’s rules, 265, 266
multiplicity, 261
spin-orbit coupling and levels, 266–267, 266*f*
term symbols, 261
Tertiary structure, 365–366, 366*f*
Tetrahedral structures, 317, 317*f*, 321, 321
Bent’s rule, 321–324, 322*f*, 324*f*
Tetramethylsilane (TMS), 474
Theoretical model chemistry, 389–390, 389*f*
Theoretical models, 389–390, 389*f*
selection of overview, 398–399
Thermodynamic product, 381, 381*f*
Thermodynamically controlled, 381, 381*f*
Thermodynamics, potential energy surfaces and, 381, 381*f*
Three-dimensional boxes, 83–84
thought experiment, 130–132, 131*f*
understanding particles, postulates and, 84–89
Three-dimensional space
quantization of angular momentum, 159–161
quantum-mechanical rotation, 157–159
spatial quantization, 164–165, 165*f*

Time
harmonic oscillator, classic, 145–147, 146*f*
harmonic oscillator, quantum-mechanical, 153–154, 153*f*
Time-dependent Schrödinger equation, 55, 73
free particles, 77–78
traveling waves and energy barriers, 101–102, 101*f*, 102*f*
Time-independent Schrödinger equation, 54–55
Tip angle, 486, 486*f*
TMS (tetramethylsilane), 474
Torsion angle, 378–379, 378*f*
Total angular momentum (*J*), 266–267, 266*f*
atomic spectroscopy, overview, 267–269, 269*f*
Total energy operator, quantum-mechanical rotation, 154–157, 156*f*, 157*f*
Totally symmetric representation, 449–450, 449*f*
Transition dipole moment (μ^{fi}), 178, 368–371, 369*f*, 370*f*, 371*f*
diatomic molecules, electronic state transitions, 353–354
selection rules, 178–180, 179*f*, 180*f*
Transition metals, orbital energy, 247
Transition-state geometries, calculations of, 409–412, 410*t*, 411*t*, 412*f*
Transmission probability, 101–102, 102*f*
Transverse component, 487–488, 488*f*
Traveling waves, 52
potential energy barriers and, 100–102, 101*f*, 102*f*
Trial wave function Φ , 239–240
Trigonal planar structures, 317, 317*f*
Bent’s rule, 321–324, 322*f*, 324*f*
Triple bonds
Bent’s rule, 321–324, 322*f*, 324*f*
chemical shift, 476
electronic structure, 301
visualizing lone pairs, 417
Triplet state, 260, 260*f*, 261, 351
Tunneling, 103–104, 103*f*, 104*f*
atomic force microscope (AFM), 104–109, 105*f*, 106*f*, 108*f*, 109*f*
in chemical reactions, 109, 110*f*
scanning tunneling microscope (STM), 104–109, 105*f*, 106*f*, 108*f*, 109*f*

Two-dimensional boxes, 83–84
understanding particles, postulates and, 84–89
Two-dimensional NMR, 498–503, 499*f*, 500*f*, 501*f*, 502*f*

U

u symmetry, 290–291
homonuclear diatomic molecules, 297–299, 297*f*, 298*f*, 299*f*
molecular term symbols, 350–352, 352*t*
Ultraviolet (UV) light. *See also* Electronic spectroscopy
absorption in polyatomic molecules, 356–358, 357*f*, 358*f*, 359*f*
electronic transitions, energy of, 349–350
greenhouse gases and, 179–180, 180*f*
ozone, 354
pi (π) electrons, 97–98, 97*f*, 98*f*
UV photoelectron spectroscopy, 363–365, 364*f*
Ultraviolet (UV) radiation, electromagnetic spectrum, 172*f*
Uncertainty principle, Heisenberg, 124–127, 125*f*
Unpaired electrons, 260, 260*f*
UV photoelectron spectroscopy, 363–365, 364*f*

V

Valence band, 99–100, 99*f*, 100*f*
Valence bond (VB) theory, 316
hybridization, 318–321, 319*f*, 321*t*
Valence electrons, 96–97, 97*f*
Bent’s rule, 322
conductors, insulators, and semiconductors, 98–100, 99*f*, 100*f*
delocalized electrons, 286
effective nuclear charge, 245
electron spin, 235
heteronuclear diatomic molecules, 306, 306*f*
Hückel model, 334–340, 336*f*, 338*f*, 339*f*
localized vs. delocalized bonding models, 329–332, 330*f*, 331*f*, 332*f*
many-electron atoms, overview, 232–235, 234*f*

Valence electrons (*continued*)
many-electron molecules, 299–302, 300f, 301f
molecular electrostatic potential, 307–308, 308f
molecular orbitals, generation of, 285–289, 288f, 289f
periodic table trends, 249
qualitative molecular orbital theory, 326–328, 326f, 327f, 328f
semiconductors, 340–342, 341f, 342f
visualizing lone pairs, 417

Valence shell electron pair repulsion (VSEPR) model, 316–318, 317f

Variational method, 239–240

Variational model, 390

Variational parameter, 290

Variational theorem, 239–240

Vector model, nuclear magnetization, 485–491, 485f, 486f, 487f, 488f, 490f

Vector model of angular momentum, 165, 165f

Vectorial dipole coupling, NRM spectroscopy, 479

Velocity
angular velocity (ω), 148–149, 149f
harmonic oscillator, quantum-mechanical, 152–154, 153f
rigid rotor, 148–149, 149f
wave function, 50

Vibration
Born–Oppenheimer approximation, 286
diatomic molecules, electronic state transitions, 353–354, 353f
diatomic molecules, vibrational fine structure of transitions, 354–356, 355f, 356f
electronic transitions, energy of, 349–350
group frequencies, 175
harmonic oscillator, classical, 143–147, 144f, 146f
harmonic oscillator, quantum-mechanical, 149–154, 150f, 153f
intersystem crossing and phosphorescence, 361–362, 361f
normal modes, 183–184, 183f, 184f
potential energy surfaces, 380–381
symmetry of normal modes of vibration, 456–460, 456f, 457f
Vibrational energy levels, 48–49, 49f

Vibrational force constant, electronic spectroscopy, uses of, 355–356, 355f, 356f
Vibrational frequency calculations, 388, 388t
Vibrational spectroscopy
absorption peaks, number of, 187
anharmonic potential, 176–177, 177f
bond energy, 176, 178, 178t
electron transition processes, 174–175, 174f
Fourier transform infrared spectroscopy (FTIR), 190–194, 191f, 192f, 193f, 194f
group frequencies, 175
harmonic potential, 176
infrared absorption spectroscopy, 180–184, 181f, 182f, 183f, 184f
Morse potential, 176–177, 177f
normal modes of vibration, 183–184, 183f, 184f
overview of, 175–178, 175t, 177f, 178t
Raman spectroscopy, 194–196, 195f
rotational-vibrational spectrum, 187–189, 187f, 189f, 190f
selection rules, 179
selection rules, infrared vs. Raman activity, 460–461
spectroscopy, overview, 171–173, 172f, 173f
symmetry of normal modes of vibration, 456–460, 456f, 457f
Virial theorem, 214, 295f, 296–297, 296f
Virtual state, 195–196, 195f
Visible light. *See also* Electronic spectroscopy
absorption in polyatomic molecules, 356–358, 357f, 358f, 359f
electromagnetic spectrum, 172f
electronic transitions, energy of, 349–350
pi (π) electrons, 97–98, 97f, 98t
VSEPR (valence shell electron pair repulsion) model, 316–318, 317f

W

Walsh correlation diagram, 327–328, 328f
Walsh's rules, 315

Water
Bent's rule, 321–324, 322f, 324f
bond angle, qualitative molecular orbital theory, 326–328, 326f, 327f, 328f
 C_{2v} point group and water, 443–447, 444f, 447f
 C_{2v} representations and molecular orbitals, 454–456, 454f, 455f, 456f
symmetry of normal modes of vibration, 456–460, 456f, 457f
Walsh correlation diagram, 327–328, 328f

Wave behavior, particles, 24–25, 25f.
See also Quantum-mechanical postulates
classical nondispersive wave equations, 49–54, 50f, 51f, 52f
standing waves, 52
stationary states, 52
time-dependent Schrödinger equation, 55
time-independent Schrödinger equation, 54–55
traveling waves, 52

Wave fronts, 50, 50f

Wave functions, 50. *See also* Quantum-mechanical postulates
antisymmetric wave function, 236–238, 291
electron indistinguishability, 236–238
g symmetry, 290–291
LCAO-MO model, 287, 290
localized vs. delocalized bonding models, 329–332, 330f, 331f, 332f
molecular wave function, 286
nodes, 80
normalization, 68
overlap of, 99f, 100, 100f
Pauli principle, 237
probability and, 67–68, 68f
quantum-mechanical harmonic oscillator, 150, 150f
Schrödinger equation, solving of, 210–211, 211f
Slater determinants, 237–238
sp hybridization, 318–321, 319f, 321f
superposition state, 71
symmetric wave function, 236–238, 291
trial wave function Φ , 239–240
u symmetry, 290–291

variational method, 239–240
 ψ_g and ψ_u wave functions for hydrogen, 294–297, 294*f*, 295*f*, 296*f*
Wave number, units of, 172
Wave vector, 50, 81
Wavelength
 de Broglie relation, 24–25, 25*f*
 diffraction, 25
 diffraction, double slit, 26–29, 27*f*,
 28*f*
 fluorescence, 112, 112*f*
Michelson interferometer, 190–192,
 191*f*, 192*f*

molar absorption coefficient, 181
wave function, 50, 51*f*
Wave-particle duality, 20. *See also*
 Quantum-mechanical postulates
 atomic spectra and Bohr model of
 atom, 29–32, 29*f*, 30*f*, 31*f*, 32*f*
 classical nondispersive wave equations,
 49–54, 50*f*, 51*f*, 52*f*
 system descriptions with quantum
 mechanics, 45–49, 49*f*
Weighted average, 71
Work function, 23, 104
Wüthrich, Kurt, 503

X

X-ray photoelectron spectroscopy
 (XPS), 277–279, 277*f*, 278*f*, 279*f*
X-rays, electromagnetic spectrum, 172*ft*

Z

Zeeman effect, 470–473, 470*f*, 472*f*
Zero point energy, 80–83, 211
finite depth box, 96
quantum-mechanical harmonic
 oscillator, 151, 153*f*, 154
quantum-mechanical rotation, 157

This page intentionally left blank

Values of Selected Physical Constants

Constant	Symbol	Value
Atomic mass constant	amu	$1.660\ 538921 \times 10^{-27}\ \text{kg}$
Avogadro's constant	N_A	$6.022\ 140\ 857 \times 10^{23}\ \text{mol}^{-1}$
Bohr magneton	$\mu_B = e\hbar/2m_e$	$9.274\ 009994 \times 10^{-24}\ \text{J T}^{-1}$
Bohr radius	$a_0 = 4\pi\epsilon_0\hbar^2/m_e e^2$	$5.291\ 772\ 1067 \times 10^{-11}\ \text{m}$
Boltzmann constant	k_B	$1.380\ 6410 \times 10^{-23}\ \text{J K}^{-1}$ $0.695\ 03476\ \text{cm}^{-1}\ \text{K}^{-1}$
Electron rest mass	m_e	$9.109\ 38356 \times 10^{-31}\ \text{kg}$
Faraday constant	F	$9.648533289 \times 10^4\ \text{C mol}^{-1}$
Gravitational constant	G	$6.67408 \times 10^{-11}\ \text{m}^3\ \text{kg}^{-1}\ \text{s}^{-2}$
Standard acceleration of gravity	G_n	$9.80665\ \text{m s}^{-2}$
Molar gas constant	R	$8.3144598\ \text{J K}^{-1}\ \text{mol}^{-1}$ $0.083\ 144621\ \text{dm}^3\ \text{bar K}^{-1}\ \text{mol}^{-1}$ $0.082\ 0578\ \text{dm}^3\ \text{atm K}^{-1}\ \text{mol}^{-1}$
Molar volume, ideal gas (1 bar, 0°C)		$22.710953\ \text{L mol}^{-1}$
Molar volume, ideal gas (1 atm, 0°C)		$22.413968\ \text{L mol}^{-1}$
Nuclear magneton	$\mu_N = e\hbar/2m_p$	$5.050\ 78353 \times 10^{-27}\ \text{J T}^{-1}$
Permittivity of vacuum	ϵ_0	$8.854\ 187\ 817 \times 10^{-12}\ \text{C}^2\ \text{J}^{-1}\ \text{m}^{-1}$
Planck constant	h	$6.626\ 069934 \times 10^{-34}\ \text{J s}$
	\hbar	$1.054\ 571726 \times 10^{-34}\ \text{J s}$
Proton charge	e	$1.602\ 176\ 565 \times 10^{-19}\ \text{C}$
Proton magnetogyric ratio	γ_p	$2.675\ 221\ 28 \times 10^8\ \text{s}^{-1}\ \text{T}^{-1}$
Proton rest mass	m_p	$1.672\ 621\ 777 \times 10^{-27}\ \text{kg}$
Rydberg constant for infinite nuclear mass	$R_\infty = m_e e^4 / 8\epsilon_0^2 h^2$	$2.179\ 8736 \times 10^{-18}\ \text{J}$ $109\ 73731.568\ 539\ \text{m}^{-1}$
Rydberg constant for H	R_H	$109677.581\ \text{cm}^{-1}$
Speed of light in vacuum	c	$2.99\ 792\ 458 \times 10^8\ \text{m s}^{-1}$
Stefan-Boltzmann constant	$\sigma = 2\pi^5 k_B^4 / 15h^3 c^2$	$5.670\ 373 \times 10^{-8}\ \text{J m}^{-2}\ \text{K}^{-4}\ \text{s}^{-1}$

SI Prefixes

Fraction	Prefix	Symbol	Fraction	Prefix	Symbol
10^{-1}	deci	d	10	deca	da
10^{-2}	centi	c	10^2	hecto	h
10^{-3}	milli	m	10^3	kilo	k
10^{-6}	micro	μ	10^6	mega	M
10^{-9}	nano	n	10^9	giga	G
10^{-12}	pico	p	10^{12}	tera	T
10^{-15}	femto	f	10^{15}	peta	P
10^{-18}	atto	a	10^{18}	exa	E

Greek Alphabet

Alpha	A	α	Iota	I	ι	Rho	P	ρ
Beta	B	β	Kappa	K	κ	Sigma	Σ	σ
Gamma	Γ	γ	Lambda	Λ	λ	Tau	T	τ
Delta	Δ	δ	Mu	M	μ	Upsilon	Υ	υ
Epsilon	E	ε	Nu	N	ν	Phi	Φ	ϕ
Zeta	Z	ζ	Xi	Ξ	ξ	Chi	X	χ
Eta	H	η	Omicron	O	\o	Psi	Ψ	ψ
Theta	Θ	θ	Pi	Π	π	Omega	Ω	ω

Conversion Table for Units

Length

meter (SI unit)	m	
centimeter	cm	$= 10^{-2} \text{ m}$
ångström	Å	$= 10^{-10} \text{ m}$
micron	μ	$= 10^{-6} \text{ m}$

Volume

cubic meter (SI unit)	m^3	
liter	L	$= \text{dm}^3 = 10^{-3} \text{ m}^3$

Mass

kilogram (SI unit)	kg	
gram	g	$= 10^{-3} \text{ kg}$
metric ton	t	$= 1000 \text{ kg}$

Energy

joule (SI unit)	J	
erg	erg	$= 10^{-7} \text{ J}$
rydberg	Ry	$= 2.179\,87 \times 10^{-18} \text{ J}$
electron volt	eV	$= 1.602\,176\,565 \times 10^{-19} \text{ J}$
inverse centimeter	cm^{-1}	$= 1.986\,455\,684 \times 10^{-23} \text{ J}$
calorie (thermochemical)	Cal	$= 4.184 \text{ J}$
liter atmosphere	l atm	$= 101.325 \text{ J}$

Pressure

pascal (SI unit)	Pa	
atmosphere	atm	$= 101325 \text{ Pa}$
bar	bar	$= 10^5 \text{ Pa}$
torr	Torr	$= 133.322 \text{ Pa}$
pounds per square inch	psi	$= 6.894\,757 \times 10^3 \text{ Pa}$

Power

watt (SI unit)	W	
horsepower	hp	$= 745.7 \text{ W}$

Angle

radian (SI unit)	rad	
degree	\circ	$= \frac{2\pi}{360} \text{ rad} = \left(\frac{1}{52.295\,78}\right) \text{ rad}$

Electrical dipole moment

C m (SI unit)		
debye	D	$= 3.335\,64 \times 10^{-30} \text{ C m}$

Masses and Natural Abundances for Selected Isotopes

Nuclide	Symbol	Mass (amu)	Percent Abundance
H	¹ H	1.0078	99.985
	² H	2.0140	0.015
He	³ He	3.0160	0.00013
	⁴ He	4.0026	100
Li	⁶ Li	6.0151	7.42
	⁷ Li	7.0160	92.58
B	¹⁰ B	10.0129	19.78
	¹¹ B	11.0093	80.22
C	¹² C	12 (exact)	98.89
	¹³ C	13.0034	1.11
N	¹⁴ N	14.0031	99.63
	¹⁵ N	15.0001	0.37
O	¹⁶ O	15.9949	99.76
	¹⁷ O	16.9991	0.037
	¹⁸ O	17.9992	0.204
F	¹⁹ F	18.9984	100
P	³¹ P	30.9738	100
S	³² S	31.9721	95.0
	³³ S	32.9715	0.76
	³⁴ S	33.9679	4.22
Cl	³⁵ Cl	34.9688	75.53
	³⁷ Cl	36.9651	24.4
Br	⁷⁹ Br	79.9183	50.54
	⁸¹ Br	80.9163	49.46
I	¹²⁷ I	126.9045	100

Main groups		Main groups																			
group	period	1	2	3	4	5	6	7	8	9	10	11	12	13	14	15	16	17	18		
		H 1.0079	He 4.003	Li 6.941	Be 9.012	Mg 22.99	Ca 40.08	Sc 44.96	V 50.94	Cr 52.00	Mn 54.94	Fe 55.85	Co 58.93	Ni 58.68	Cu 63.55	Zn 65.39	Ge 72.61	As 74.92	Se 78.95	Br 79.90	Kr 83.80
		Na 22.99	Ca 40.08	Sc 44.96	V 50.94	Cr 52.00	Mn 54.94	Fe 55.85	Co 58.93	Ni 58.68	Cu 63.55	Zn 65.39	Ge 72.61	As 74.92	Se 78.95	Br 79.90	Kr 83.80				
		Rb 85.47	Sr 87.62	Y 88.91	Zr 91.22	Nb 92.91	Mo 95.94	Tc (96)	Ru 101.07	Rh 102.91	Pd 106.42	Ag 107.87	Cd 112.41	In 114.82	Sn 118.71	Sb 121.76	Te 127.80	I 126.90	Xe 131.29		
		Cs 132.91	Ba 137.33	La 138.91	Hf 178.49	Ta 180.95	W 183.84	Re 186.21	Os 190.23	Ir 193.22	Pt 195.08	Au 196.97	Hg 200.59	Tl 204.38	Pb 207.2	Bi 208.98	At (209)	Rn (222)			
		Fr (223)	Ra (226)	Ac (227)	Rf (261)	D_b (262)	Sg (263)	H_s (265)	M_t (266)	D_s (271)	Rg (272)	C_n (285)	N_h (286)	F_l (289)	L_v (289)	M_c (289)	T_s (293)	O_g (294)			
		Lanthanides	Ce 140.12	Pr 140.91	Nd 144.24	Pm (145)	Sm 150.36	Eu 151.96	Gd 157.25	Tb 158.93	Dy 162.50	Ho 164.93	Er 167.26	Tm 168.93	Yb 173.04	Lu 174.97					
		Actinides	Th 232.04	Pa 231.04	U 237	Np (244)	Pu (244)	Am (243)	Cm (243)	Bk (247)	Cf (251)	Md (257)	Es (258)	Fm (257)	No (259)	Lr (262)					

Answers to Selected Numerical Problems

Chapter 1

- P1.2** At 1350. K, 1.11×10^{-3} J m $^{-3}$; At 6000. K, 0.981 J m $^{-3}$
- P1.3** -0.0369 for $T = 5000.$ K; -0.130 for 1500. K and -0.933 for 300. K
- P1.4** $\lambda_{\max} = 4.26 \times 10^{-6}$ m at 675 K., 2.50×10^{-6} m at 1150. K., and 4.64×10^{-7} m at 6200. K
- P1.5** 3.89×10^{26} W
- P1.6** 1.30×10^5 J s $^{-1}$; 0.0475 m
- P1.7** 8.18×10^{15} ; 2.27×10^{-19} J; 7.06×10^5 m s $^{-1}$
- P1.9** a) 1.26×10^{15} s $^{-1}$; b) 5.87×10^5 m s $^{-1}$
- P1.10** $\Delta v_{H_2} = 1.13$ m s $^{-1}$; $\frac{\Delta v}{v} = 4.55 \times 10^{-4}$
- P1.11** $\lambda = 1.00 \times 10^4$ nm; 793 m s $^{-1}$; $\lambda = 500.$ nm; 3.55×10^3 m s $^{-1}$; $\lambda = 100.$ nm; 7.93×10^3 m s $^{-1}$; and $\lambda = 0.100$ nm; 2.51×10^5 m s $^{-1}$
 $T = 959$ K for $\lambda = 1.00 \times 10^4$ nm. The results for 500. nm, 100. nm and 0.100 nm are 1.92×10^4 K, 9.59×10^4 K, and 9.59×10^7 K
- P1.12** 0.0467 m s $^{-1}$
- P1.13** 0.152 m s $^{-1}$
- P1.14** 25 K for He; 2.6 K for Ar
- P1.15** $v = 5.82 \times 10^6$ m s $^{-1}$; $E_{kinetic} = 1.54 \times 10^{-17}$ J
- P1.16** 1.26×10^{-10} m for H₂ at 200. K; 5.93×10^{-11} m for H₂ at 900. K; 2.83×10^{-11} m for Ar at 200. K; 1.33×10^{-11} m for Ar at 900. K
- P1.17** 4.31 cm
- P1.18** 16.7 V
- P1.19** 0.992 nm; 2.18×10^{14} s $^{-1}$
- P1.20** 5.08×10^{20}
- P1.21** 6.23×10^{18} s $^{-1}$
- P1.22** 3.50×10^7 J s $^{-1}$; 7.71×10^{17}

Chapter 2

- P2.3** $x_0 = 0.796$ m and $t_0 = -5.50 \times 10^{-4}$ s
- P2.6** a) $\sqrt{13} \exp(-0.588i)$
 $\phi = -0.588 + 2\pi = 5.70$ radians;
b) 4; c) $\frac{1}{\sqrt{2}} \exp(-0.785i)$
 $\phi = -0.785 + 2\pi = 5.50$ radians;
d) $5 \exp(1.571i)$; e) $2\sqrt{5} \exp(-1.107i)$
 $\phi = -1.107 + 2\pi = 5.18$ radians
- P2.7** a) $0.707 + 2.92i$; b) $2.48 + 1.36i$; c) $5e^{5.36i}$; d) $\sqrt{13}e^{0.983i}$

P2.15 $\frac{n_2}{n_1}(220.\text{ K}) = 1.76$; $\frac{n_2}{n_1}(875\text{ K}) = 1.94$;
 $\frac{n_{12}}{n_1}(220.\text{ K}) = 0.0334$; $\frac{n_{12}}{n_1}(875\text{ K}) = 2.73$

- P2.21** for $n_2/n_1 = 0.150$ $T = 93.0$ K;
for $n_2/n_1 = 0.900$ $T = 302$ K

- P2.30** a) $r = \sqrt{14}$; $\theta = 1.30$ radians; b) $x = 2.12$;
 $y = 3.67$; $z = 4.24$

Chapter 4

- P4.7** a) 5.92; b) 15.8; c) 0.502
- P4.8** 5.50×10^{-6} m
- P4.9** 8.4×10^{35}
- P4.10** 1.64×10^{-37} J; 3.96×10^{-17}
- P4.11** 4.5×10^{-9} m
- P4.14** a) 0.052; b) 0.0084
- P4.17** a) 8.32×10^{10} ; b) 1.48×10^{-31} J; c) 3.60×10^{-11}
- P4.24** 4.92×10^{-21} J; 0.073
- P4.28** 3.51×10^{-20} m
- P4.32** 2.29×10^{17} s $^{-1}$; 1.00×10^{-10} m

Chapter 5

- P5.1** 119 nm
- P5.2** 368 nm
- P5.3** b) 4.76×10^{-20} J, 1.86×10^{-19} J, and 3.95×10^{-19} J
- P5.4** 8.7×10^2 K for Si; 4.3×10^3 K for diamond
- P5.6** $R = 0.11$; $T = 0.89$
- P5.7** copper: 2.8×10^6 A/m 2 ; STM: 1.0×10^9 A/m 2

Chapter 6

- P6.14** c) $\pm 2.59 \times 10^{-2}$ m
- P6.17** $p = 3.64 \times 10^{-24}$ kg m s $^{-1}$; 0.0182
- P6.18** 5.28 eV
- P6.20** $\Delta x = 1.94 \times 10^{-33}$ m

Chapter 7

- P7.1** 2.56×10^{-32} J; 6.23×10^{-12}
- P7.2** a) 3.572 pm from the Cl atom;
b) 48.35 pm from the O atom
- P7.4** vibration 8.96×10^{13} s $^{-1}$; rotation: 6.35×10^{11} s $^{-1}$
- P7.5** 2294 N m $^{-1}$; 7.48×10^{-3} m
- P7.8** 1.75×10^{13} s $^{-1}$; 1.71×10^{-6} m
- P7.10** 517 kg s $^{-2}$; 1.98 kg

P7.12 a) 2.21 N m^{-1} ; b) $9.94 \times 10^{-34} \text{ J}$; c) $2.23 \times 10^{-5} \text{ J}$;
d) 1.12×10^{28}

P7.13 $2.97 \times 10^{-20} \text{ J}$; 997 m s^{-1}

P7.14 a) $4.11 \times 10^{-20} \text{ J}$; b) $1.24 \times 10^{14} \text{ s}^{-1}$

P7.15 for Br_2 $\frac{N_{n=1}}{N_{n=0}} = 0.212$; $\frac{N_{n=2}}{N_{n=0}} = 0.0450$; 1015 K

$$\text{For D}_2 \frac{N_{n=1}}{N_{n=0}} = 3.20 \times 10^{-7};$$

$$\frac{N_{n=2}}{N_{n=0}} = 1.03 \times 10^{-13}; 9.79 \times 10^3 \text{ K}$$

P7.20 for $n = 0$, 0.0158 ; for $n = 1$, 0.0274 ; for $n = 2$, 0.0354

P7.23 a) $E_{rot} = 4.22 \times 10^{-21} \text{ J}$; $\frac{E_{rot}}{k_B T} = 1.02$;

$$E_{vib} = 2.16 \times 10^{-20} \text{ J}; \frac{E_{vib}}{k_B T} = 5.20;$$

$$\text{b)} T_{rot} = 8.23 \times 10^{-13} \text{ s}; T_{vib} = 1.53 \times 10^{-14} \text{ s}; 53.5$$

P7.24 0.0842

P7.27 b) 9.27×10^{-3} ; c) 9.27×10^{-3}

P7.28 $8.33 \times 10^{-22} \text{ J}$

P7.29 $\frac{n_0}{n_0} = 1$; $\frac{n_5}{n_0} = 3.55$; $\frac{n_{10}}{n_0} = 0.332$;

$$\frac{n_{20}}{n_0} = 5.42 \times 10^{-6}$$

P7.30 $\frac{E_{J=5}}{kT} = 2.01$; $\frac{E_{J=10}}{kT} = 7.37$; $\frac{E_{J=20}}{kT} = 28.2$

P7.32 a) $E = 0, 7.68 \times 10^{-23} \text{ J}, 2.30 \times 10^{-22} \text{ J}, 4.61 \times 10^{-22} \text{ J}, 7.68 \times 10^{-22} \text{ J}$ for $J = 0, 1, 2, 3, 4$

b) $E = 0, 3.84 \times 10^{-23} \text{ J}, 1.54 \times 10^{-22} \text{ J}, 3.46 \times 10^{-22} \text{ J}, 6.15 \times 10^{-22} \text{ J}$ for $J = 0, 1, 2, 3, 4$

P7.33 $\mu = 1.63 \times 10^{-27} \text{ kg}$; $I = 2.65 \times 10^{-47} \text{ kg m}^2$;
 $|\mathbf{L}| = 2.58 \times 10^{-34} \text{ J s}$; $E = 1.26 \times 10^{-21} \text{ J}$

P7.36 $\theta = 0.955$ and $\pi - 0.955$ radians or 54.7 and 125.3 degrees.

Chapter 8

P8.1 a) $E_0 = 4.06 \times 10^{-20} \text{ J}$, $E_1 = 1.19 \times 10^{-19} \text{ J}$,
 $E_2 = 1.94 \times 10^{-19} \text{ J}$, $E_3 = 2.65 \times 10^{-19} \text{ J}$;
b) $\nu_{0 \rightarrow 1} = 1.18 \times 10^{14} \text{ s}^{-1}$,
 $\nu_{0 \rightarrow 2} = 2.31 \times 10^{14} \text{ s}^{-1}$, $\nu_{0 \rightarrow 3} = 3.38 \times 10^{14} \text{ s}^{-1}$
Error($\nu_{0 \rightarrow 2}$) = -2.43% ; Error($\nu_{0 \rightarrow 3}$) = -5.00%

P8.2 208 N m^{-1} , $1.24 \times 10^{-13} \text{ s}$

P8.3 $E_0^{HH} = 8.74 \times 10^{-20} \text{ J}$, $E_0^{DD} = 6.19 \times 10^{-20} \text{ J}$,
 $\frac{E_0^{HH} - E_0^{DD}}{k_B T} = 6.19$

P8.4 For H_2 at $250. \text{ K}$, $\frac{n_1}{n_0} = 9.97 \times 10^{-12}$

For H_2 at $1250. \text{ K}$, $\frac{n_1}{n_0} = 6.31 \times 10^{-3}$

For H_2 at $250. \text{ K}$, $\frac{n_2}{n_0} = 9.94 \times 10^{-23}$

For H_2 at $1250. \text{ K}$, $\frac{n_2}{n_0} = 3.98 \times 10^{-5}$

For Br_2 at $250. \text{ K}$, $\frac{n_1}{n_0} = 0.154$

For B_2 at $1250. \text{ K}$, $\frac{n_1}{n_0} = 0.688$

For Br_2 at $250. \text{ K}$, $\frac{n_2}{n_0} = 0.0236$

For Br_2 at $1250. \text{ K}$, $\frac{n_2}{n_0} = 0.473$

P8.6 $3.25 \times 10^{-19} \text{ J}$

P8.7 $\frac{\nu_D}{\nu_H} = 0.935$

P8.8 $4.75 \times 10^{12} \text{ s}^{-1}$, $1.57 \times 10^{-21} \text{ J}$

P8.9 $1.13 \times 10^{13} \text{ s}^{-1}$, $8.82 \times 10^{-14} \text{ s}$, 0.0234 eV

P8.10 $D_e = 1.738 \times 10^{-18} \text{ J}$, $D_0 = 1.716 \times 10^{-18} \text{ J}$

P8.12 $E_1 = 4.30 \times 10^{-20} \text{ J}$

$E_2 = 1.25 \times 10^{-19} \text{ J}$

$E_3 = 2.01 \times 10^{-19} \text{ J}$

$E_4 = 2.72 \times 10^{-19} \text{ J}$

$E_5 = 3.37 \times 10^{-19} \text{ J}$

$E_6 = 3.96 \times 10^{-19} \text{ J}$

$E_7 = 4.50 \times 10^{-19} \text{ J}$

$E_8 = 4.98 \times 10^{-19} \text{ J}$

$E_9 = 5.40 \times 10^{-19} \text{ J}$

$E_{10} = 5.78 \times 10^{-19} \text{ J}$

$E_{11} = 6.08 \times 10^{-19} \text{ J}$

$E_{12} = 6.34 \times 10^{-19} \text{ J}$

$E_{13} = 6.54 \times 10^{-19} \text{ J}$

$E_{14} = 6.68 \times 10^{-19} \text{ J}$

$E_{15} = 6.77 \times 10^{-19} \text{ J}$

$E_{16} = 6.80 \times 10^{-19} \text{ J}$

P8.16 a) 0.105

b) 12.5

P8.31 a) 3.2 cm ; b) 0.74 cm

P8.32 20%

P8.33 $4.7 \times 10^5 \text{ cm}$ for CH_3CCl_3 ; $2.1 \times 10^2 \text{ cm}$ for CFC-14

P8.34 $r = 116.227 \text{ pm}$ and $R = 156.014 \text{ pm}$

P8.35 $2.32121 \times 10^{-10} \text{ m}$

P8.37 0.4370 cm^{-1} ; $2.620 \times 10^{10} \text{ s}^{-1}$

P8.38 $1.284 \times 10^{-10} \text{ m}$ for $n = 0$ and $1.344 \times 10^{-10} \text{ m}$ for $n = 3$. $1.275 \times 10^{-10} \text{ m}$ assuming that B does not depend on n .

P8.40 $1.596 \times 10^{-10} \text{ m}$

P8.41 $1.401 \times 10^{-46} \text{ kg m}^2$; $6.837 \times 10^{-34} \text{ J s}$;
 $1.668 \times 10^{-21} \text{ J}$; $\frac{E_J}{k_B T} = 0.4052$

P8.43 $109.8 \times 10^{-12} \text{ m}$

P8.44 $7.89 \times 10^{-34} \text{ J s}$

P8.45 $109.8 \times 10^{-12} \text{ m}$

Chapter 9

- P9.1** Most energetic: $\tilde{\nu} = 109,678 \text{ cm}^{-1}$ for the Lyman series, 27419.5 cm^{-1} for the Balmer series, and 12186.4 cm^{-1} for the Paschen series.
 Least energetic: $\tilde{\nu} = 82258.5 \text{ cm}^{-1}$ for the Lyman series, and 15233.1 cm^{-1} for the Balmer series, and 5331.57 cm^{-1} for the Paschen series.
- P9.4** $E_H = -2.179 \times 10^{-18} \text{ J}$,
 $E_{He^+} = -8.717 \times 10^{-18} \text{ J}$,
 $E_{Li^{2+}} = -19.61 \times 10^{-18} \text{ J}$,
 $E_{Be^{3+}} = -34.87 \times 10^{-18} \text{ J}$
- P9.5b** The probability evaluated at $r = 0.250 a_0 = 1.44 \times 10^{-2}$. The probability evaluated at $r = 2.25 a_0 = 0.826$. The probability evaluated at $r = 5.50 a_0 = 0.999$.
- P9.10** $I_H = 2.179 \times 10^{-18} \text{ J}$; $I_{He^+} = 8.717 \times 10^{-18} \text{ J}$;
 $I_{Li^{2+}} = 1.961 \times 10^{-17} \text{ J}$; $I_{Be^{3+}} = 3.487 \times 10^{-17} \text{ J}$
- P9.16** 1.66
- P9.22** 0.385
- P9.23** 0.323
- P9.29** a) 148 kg m^{-3} ; b) $4.0 \times 10^{17} \text{ kg m}^{-3}$;
 c) 0.0808 kg m^{-3}
- P9.33** 0.92, 0.062, and 2.8×10^{-3} at $0.50 a_0$, $3.0 a_0$, and $5.0 a_0$ respectively

Chapter 10

- P10.3** 54.7° and 125.3°
- P10.11** 0.14 eV ; 1.77×10^{-3}
- P10.12** $-3.923 \times 10^{-18} \text{ J}$
- P10.13** $1.764 \times 10^{-11} \text{ m}$

Chapter 11

- P11.23** Lyman $\lambda = 121.569 \text{ nm}$; 102.574 nm ; 97.2553 nm ;
 91.1768 nm
 Balmer $\lambda = 656.473 \text{ nm}$; 486.276 nm ; 434.175 nm ;
 364.707 nm
 Paschen $\lambda = 1875.64 \text{ nm}$; 1282.17 nm ; 1094.12 nm ;
 820.591 nm
- P11.24** most energetic $2.17872 \times 10^{-18} \text{ J}$; 109678 cm^{-1} ;
 $3.28813 \times 10^{15} \text{ s}^{-1}$; 9117.63 nm
 Least energetic $1.63404 \times 10^{-18} \text{ J}$; 82258.2 cm^{-1} ;
 $2.4661 \times 10^{15} \text{ s}^{-1}$; 121.568 nm
- P11.25** $\nu_H = 3.08255 \times 10^{15} \text{ s}^{-1}$; $\nu_T = 3.08367 \times 10^{15} \text{ s}^{-1}$
- P11.27** 3.4 eV
- P11.30** ${}^1P_1 \rightarrow {}^1S_0$: 3.86×10^{-8} ; ${}^2P_{3/2} \rightarrow {}^2S_{1/2}$: 8.67×10^{-5} ;
 ${}^2P_{1/2} \rightarrow {}^2S_{1/2}$: 4.65×10^{-5}
- P11.31** $E({}^3p \, {}^2P_{1/2}) = 3.369 \times 10^{-19} \text{ J} = 2.103 \text{ eV}$
 $E({}^3p \, {}^2P_{3/2}) = 3.373 \times 10^{-19} \text{ J} = 2.105 \text{ eV}$
 $E({}^4s \, {}^2S_{1/2}) = 5.048 \times 10^{-19} \text{ J} = 3.150 \text{ eV}$
 $E({}^5s \, {}^2S_{1/2}) = 6.597 \times 10^{-19} \text{ J} = 4.118 \text{ eV}$

$$E({}^3d \, {}^2D_{3/2}) = 5.797 \times 10^{-19} \text{ J} = 3.618 \text{ eV}; \\ E({}^4d \, {}^2D_{3/2}) = 6.869 \times 10^{-19} \text{ J} = 4.287 \text{ eV}$$

$$\mathbf{P11.33} \quad E({}^4p \, {}^2P) = 6.015 \times 10^{-19} \text{ J} = 3.754 \text{ eV}; \\ E({}^5s \, {}^2S) = 6.597 \times 10^{-19} \text{ J} = 4.117 \text{ eV}$$

$$\mathbf{P11.34} \quad 200 \text{ K}: 3.65; 1000 \text{ K}: 4.70$$

$$\mathbf{P11.35} \quad \Delta\nu = 1.70 \times 10^9 \text{ s}^{-1}; \frac{\Delta\nu}{\nu} = 3.33 \times 10^{-6}$$

$$\mathbf{P11.36} \quad 39 \text{ eV}$$

$$\mathbf{P11.37} \quad \frac{I}{I_0} = 0.39; \theta = 44^\circ$$

Chapter 12

$$\mathbf{P12.1} \quad 0.577 \text{ for } \zeta = 1.5; \quad 0.875 \text{ for } \zeta = 2.5; \\ 0.970 \text{ for } \zeta = 3.5$$

$$\mathbf{P12.2} \quad S_{ab} \text{ has the value of 0.4 at } R/a_0 = 3.44, 2.75, \text{ and} \\ 2.30 \text{ for } \zeta = 0.8, 1.0, \text{ and } 1.2, \text{ respectively.}$$

$$\mathbf{P12.8} \quad S_{12} = 0.15: -14.9 \text{ eV}, -11.8 \text{ eV}; \\ S_{12} = 0.30: -16.0 \text{ eV}, -9.23 \text{ eV}; \\ S_{12} = 0.45: -16.8 \text{ eV}, -5.25 \text{ eV}$$

$$\mathbf{P12.13} \quad c_{2H} = 1.1; c_{2F} = -0.82; c_{1H} = 0.39; c_{1F} = 0.76$$

$$\mathbf{P12.17} \quad \text{bonding MO: 0.28 on H and 0.72 on F; antibonding} \\ \text{MO: 0.72 on H and 0.28 on F}$$

$$\mathbf{P12.19} \quad 2.60 \text{ D}$$

$$\mathbf{P12.23} \quad S_{12} = 0.0075: -13.4 \text{ eV}, -18.7 \text{ eV}; \\ S_{12} = 0.18: -12.4 \text{ eV}, -19.1 \text{ eV}; \\ S_{12} = 0.40: -7.65 \text{ eV}, -20.1 \text{ eV}$$

$$\mathbf{P12.24} \quad S_{12} = 0.0075; P_F = 0.97; S_{12} = 0.18; P_F = 0.88; \\ S_{12} = 0.40; P_F = 0.74$$

Chapter 13

$$\mathbf{P13.8} \quad \psi_c = -0.45\phi_{2p_z} - 0.55\phi_{2s} + 0.71\phi_{2p_x}; \\ \psi_d = -0.45\phi_{2p_z} - 0.55\phi_{2s} - 0.71\phi_{2p_x}$$

$$\mathbf{P13.9} \quad \psi_{ep} = -0.7884\phi_{2p_z} - 0.615\phi_{2s}$$

$$\mathbf{P13.10} \quad \text{a) } s \text{ character } 0.30; p \text{ character } 0.70$$

$$\mathbf{P13.11} \quad 3.1$$

$$\mathbf{P13.12} \quad 127^\circ$$

$$\mathbf{P13.25} \quad c_1 = 0.3715; c_2 = 0.602; c_3 = 0.602; c_4 = 0.3715$$

$$\mathbf{P13.29} \quad E_\pi = 6\alpha + 9\beta$$

$$\mathbf{P13.31} \quad 3.35 \times 10^{-18}; \text{ b) } 0.213$$

Chapter 14

$$\mathbf{P14.2} \quad 1.263 \mu\text{m}; 757.86 \text{ nm}$$

$$\mathbf{P14.4} \quad 17$$

$$\mathbf{P14.5} \quad 15; 325 \text{ cm}^{-1}.$$

$$\mathbf{P14.8} \quad \text{a) } 0.114, 89.2\%; \text{ b) } 0.0456, 95.5\%$$

$$\mathbf{P14.9} \quad \text{a) } 4.72 \text{ nm}; \text{ b) } 3.60 \text{ nm}$$

$$\mathbf{P14.10} \quad 0.5 \text{ nm}: 5.5 \times 10^{12} \text{ s}^{-1}; 1.0 \text{ nm}: 8.6 \times 10^{10}; \\ 2.0 \text{ nm}: 1.3 \times 10^9; 3.0 \text{ nm}: 1.2 \times 10^8; \\ 5.0 \text{ nm}: 5.5 \times 10^6$$

$$\mathbf{P14.11} \quad 2.0 \text{ nm}: 9.4 \times 10^{10} \text{ s}^{-1}; 7.0 \text{ nm}: 5.1 \times 10^7; \\ 12.0 \text{ nm}: 2.0 \times 10^6$$

Chapter 17

P17.2 14.1 T; 56.0 T; 34.8 T

P17.8 2.04 ppm; -0.68 ppm

P17.17 1.5 mT

P17.18 1.96×10^5 rad/s; 31 Hz

P17.19 126 MHz

P17.20 1.097×10^{-4}

P17.21 0.99908

P17.22 3.4×10^{-6}

P17.23 383 ms

P17.24 0.29 s; 0.65 s

P17.25 0.400 s

P17.26 0.65

A visual, conceptual and contemporary approach to the fascinating field of Physical Chemistry guides students through core concepts with visual narratives and connections to cutting-edge applications and research.

The fourth edition of *Quantum Chemistry & Spectroscopy* includes many changes to the presentation and content at both a global and chapter level. These updates have been made to enhance the student learning experience and update the discussion of research areas.

Mastering™ Chemistry, with a new enhanced Pearson eText, has been significantly expanded to include a wealth of new end-of-chapter problems from the 4th edition, new self-guided, adaptive Dynamic Study Modules with wrong answer feedback and remediation, and the new Pearson eText which is mobile friendly.



Please visit us at www.pearson.com for more information. To order any of our products, contact our customer service department at (800) 824-7799, or (201) 767-5021 outside of the U.S., or visit your campus bookstore.

www.pearson.com